International Journal of
Molecular Sciences

Special Issue Reprint

Molecular Classification of Human Cancer

Diagnosis and Treatment

Edited by
William Cho

mdpi.com/journal/ijms

MDPI

Molecular Classification of Human Cancer: Diagnosis and Treatment

Molecular Classification of Human Cancer: Diagnosis and Treatment

Guest Editor

William Cho

MDPI

Basel • Beijing • Wuhan • Barcelona • Belgrade • Novi Sad • Cluj • Manchester

Guest Editor
William Cho
Department of Clinical
Oncology
Queen Elizabeth Hospital
Hong Kong
China

Editorial Office
MDPI AG
Grosspeteranlage 5
4052 Basel, Switzerland

This is a reprint of the Special Issue, published open access by the journal *International Journal of Molecular Sciences* (ISSN 1422-0067), freely accessible at: https://www.mdpi.com/journal/ijms/special_issues/huaman_cancer.

For citation purposes, cite each article independently as indicated on the article page online and as indicated below:

Lastname, A.A.; Lastname, B.B. Article Title. *Journal Name* **Year**, *Volume Number*, Page Range.

ISBN 978-3-7258-8373-8 (Hbk)
ISBN 978-3-7258-8374-5 (PDF)
https://doi.org/10.3390/books978-3-7258-8374-5

© 2026 by the authors. Articles in this reprint are Open Access and distributed under the Creative Commons Attribution (CC BY) license. The reprint as a whole is distributed by MDPI under the terms and conditions of the Creative Commons Attribution-NonCommercial-NoDerivs (CC BY-NC-ND) license (https://creativecommons.org/licenses/by-nc-nd/4.0/).

Contents

About the Editor . . . . . **ix**

Preface . . . . . **xi**

Salvador J. Diaz-Cano
Pathological Bases for a Robust Application of Cancer Molecular Classification
Reprinted from: *Int. J. Mol. Sci.* **2015**, *16*, 8655–8675,
https://doi.org/10.3390/ijms16048655 . . . . . **1**

Qianling Liu, Jie Jin, Jianming Ying, Mengkui Sun, Yun Cui, Lian Zhang, et al.
Frequent Epigenetic Suppression of Tumor Suppressor Gene Glutathione Peroxidase 3 by Promoter Hypermethylation and Its Clinical Implication in Clear Cell Renal Cell Carcinoma
Reprinted from: *Int. J. Mol. Sci.* **2015**, *16*, 10636–10649,
https://doi.org/10.3390/ijms160510636 . . . . . **22**

Ying-Yu Kuo, Wai-Tim Jim, Liang-Cheng Su, Chi-Jung Chung, Ching-Yu Lin, Chieh Huo, et al.
Caffeic Acid Phenethyl Ester Is a Potential Therapeutic Agent for Oral Cancer
Reprinted from: *Int. J. Mol. Sci.* **2015**, *16*, 10748–10766,
https://doi.org/10.3390/ijms160510748 . . . . . **36**

Razmik Mirzayans, Bonnie Andrais, April Scott, Ying W. Wang, Robert H. Weiss and David Murray
Spontaneous γH2AX Foci in Human Solid Tumor-Derived Cell Lines in Relation to p21WAF1 and WIP1 Expression
Reprinted from: *Int. J. Mol. Sci.* **2015**, *16*, 11609–11628,
https://doi.org/10.3390/ijms160511609 . . . . . **55**

Zewu Li, Xin Zhang, Yongmei Yang, Sanhui Yang, Zhaogang Dong, Lutao Du, et al.
Periostin Expression and Its Prognostic Value for Colorectal Cancer
Reprinted from: *Int. J. Mol. Sci.* **2015**, *16*, 12108–12118,
https://doi.org/10.3390/ijms160612108 . . . . . **75**

Yin-Jie Su, Jin Yu, Ya-Qin Huang and Jin Yang
Circulating Long Noncoding RNA as a Potential Target for Prostate Cancer
Reprinted from: *Int. J. Mol. Sci.* **2015**, *16*, 13322–13338,
https://doi.org/10.3390/ijms160613322 . . . . . **86**

Nikolaos Kourkoumelis, Ioannis Balatsoukas, Violetta Moulia, Aspasia Elka, Georgios Gaitanis and Ioannis D. Bassukas
Advances in the *in Vivo* Raman Spectroscopy of Malignant Skin Tumors Using Portable Instrumentation
Reprinted from: *Int. J. Mol. Sci.* **2015**, *16*, 14554–14570,
https://doi.org/10.3390/ijms160714554 . . . . . **103**

Dueng-Yuan Hueng, Wen-Chiuan Tsai, Hsin-Ying Clair Chiou, Shao-Wei Feng, Chin Lin, Yao-Feng Li, et al.
DDX3X Biomarker Correlates with Poor Survival in Human Gliomas
Reprinted from: *Int. J. Mol. Sci.* **2015**, *16*, 15578–15591,
https://doi.org/10.3390/ijms160715578 . . . . . **120**

Shiyan Yan, Yuqin Wang, Meimei Chen, Guangming Li and Jiangao Fan
Deregulated SLC2A1 Promotes Tumor Cell Proliferation and Metastasis in Gastric Cancer
Reprinted from: *Int. J. Mol. Sci.* **2015**, *16*, 16144–16157,
https://doi.org/10.3390/ijms160716144 . . . . . **134**

Yu-Jen Wu, Choo-Aun Neoh, Chia-Yu Tsao, Jui-Hsin Su and Hsing-Hui Li
Sinulariolide Suppresses Human Hepatocellular Carcinoma Cell Migration and Invasion by InhibitingMatrix Metalloproteinase-2/-9 through MAPKs and PI3K/Akt Signaling Pathways
Reprinted from: *Int. J. Mol. Sci.* **2015**, *16*, 16469–16482,
https://doi.org/10.3390/ijms160716469 . . . . . **148**

Pier Vitale Nuzzo, Alessandra Rubagotti, Francesca Argellati, Antonio Di Meglio, Elisa Zanardi, Linda Zinoli, et al.
Prognostic Value of Preoperative Serum Levels of Periostin (PN) in Early Breast Cancer (BCa)
Reprinted from: *Int. J. Mol. Sci.* **2015**, *16*, 17181–17192,
https://doi.org/10.3390/ijms160817181 . . . . . **162**

Lisha Qi, Wangzhao Song, Zhiyong Liu, Xiulan Zhao, Wenfeng Cao and Baocun Sun
Wnt3a Promotes the Vasculogenic Mimicry Formation of Colon Cancer via Wnt/β-Catenin Signaling
Reprinted from: *Int. J. Mol. Sci.* **2015**, *16*, 18564–18579,
https://doi.org/10.3390/ijms160818564 . . . . . **174**

Filippo Lococo, Massimiliano Paci, Cristian Rapicetta, Teresa Rossi, Valentina Sancisi, Luca Braglia, et al.
Preliminary Evidence on the Diagnostic and Molecular Role of Circulating Soluble EGFR in Non-Small Cell Lung Cancer
Reprinted from: *Int. J. Mol. Sci.* **2015**, *16*, 19612–19630,
https://doi.org/10.3390/ijms160819612 . . . . . **190**

Xin Zhang, Qingshan You, Xiaolei Zhang and Xiangmei Chen
SOCS3 Methylation Predicts a Poor Prognosis in HBV Infection-Related Hepatocellular Carcinoma
Reprinted from: *Int. J. Mol. Sci.* **2015**, *16*, 22662–22675,
https://doi.org/10.3390/ijms160922662 . . . . . **209**

Sally Temraz, Deborah Mukherji and Ali Shamseddine
Dual Inhibition of MEK and PI3K Pathway in KRAS and BRAF Mutated Colorectal Cancers
Reprinted from: *Int. J. Mol. Sci.* **2015**, *16*, 22976–22988,
https://doi.org/10.3390/ijms160922976 . . . . . **223**

Fei Zhang, Zhiyong Wang, Yanling Fan, Qiao Xu, Wei Ji, Ran Tian and Ruifang Niu
Elevated STAT3 Signaling-Mediated Upregulation of MMP-2/9 Confers Enhanced Invasion Ability in Multidrug-Resistant Breast Cancer Cells
Reprinted from: *Int. J. Mol. Sci.* **2015**, *16*, 24772–24790,
https://doi.org/10.3390/ijms161024772 . . . . . **236**

Yoo Jin Lee and Byoung Kuk Jang
The Role of Autophagy in Hepatocellular Carcinoma
Reprinted from: *Int. J. Mol. Sci.* **2015**, *16*, 26629–26643,
https://doi.org/10.3390/ijms161125984 . . . . . **255**

Byeong Mo Kim, Yunkyung Hong, Seunghoon Lee, Pengda Liu, Ji Hong Lim, Yong Heon Lee, et al.
Therapeutic Implications for Overcoming Radiation Resistance in Cancer Therapy
Reprinted from: *Int. J. Mol. Sci.* **2015**, *16*, 26880–26913,
https://doi.org/10.3390/ijms161125991 . . . . . **270**

Dan Zi, Zhi-Wei Zhou, Ying-Jie Yang, Lin Huang, Zun-Lun Zhou, Shu-Ming He, et al.
Danusertib Induces Apoptosis, Cell Cycle Arrest, and Autophagy but Inhibits Epithelial to Mesenchymal Transition Involving PI3K/Akt/mTOR Signaling Pathway in Human Ovarian Cancer Cells
Reprinted from: *Int. J. Mol. Sci.* **2015**, *16*, 27228–27251,
https://doi.org/10.3390/ijms161126018 . . . . . **304**

Dagmara Jaworska, Wojciech Król and Ewelina Szliszka
Prostate Cancer Stem Cells: Research Advances
Reprinted from: *Int. J. Mol. Sci.* **2015**, *16*, 27433–27449,
https://doi.org/10.3390/ijms161126036 . . . . . **328**

Paola Maroni, Paola Bendinelli, Daniele Morelli, Lorenzo Drago, Alessandro Luzzati, Giuseppe Perrucchini, et al.
High SPARC Expression Starting from Dysplasia, Associated with Breast Carcinoma, Is Predictive for Bone Metastasis without Enhancement of Plasma Levels
Reprinted from: *Int. J. Mol. Sci.* **2015**, *16*, 28108–28122,
https://doi.org/10.3390/ijms161225997 . . . . . **345**

Lianzhi Dai, Luhua Zhuang, Bingchang Zhang, Fen Wang, Xiaolei Chen, Chun Xia and Bing Zhang
DAG/PKCδ and IP3/Ca^{2+}/CaMK IIβ Operate in Parallel to Each Other in PLCγ1-Driven Cell Proliferation and Migration of Human Gastric Adenocarcinoma Cells, through Akt/mTOR/S6 Pathway
Reprinted from: *Int. J. Mol. Sci.* **2015**, *16*, 28510–28522,
https://doi.org/10.3390/ijms161226116 . . . . . **360**

Jielai Yang, Dongdong Cheng, Shumin Zhou, Bin Zhu, Tu Hu and Qingcheng Yang
Overexpression of X-Box Binding Protein 1 (XBP1) Correlates to Poor Prognosis and Up-Regulation of PI3K/mTOR in Human Osteosarcoma
Reprinted from: *Int. J. Mol. Sci.* **2015**, *16*, 28635–28646,
https://doi.org/10.3390/ijms161226123 . . . . . **373**

Irene Vanni, Simona Coco, Anna Truini, Marta Rusmini, Maria Giovanna Dal Bello, Angela Alama, et al.
Next-Generation Sequencing Workflow for NSCLC Critical Samples Using a Targeted Sequencing Approach by Ion Torrent PGM™ Platform
Reprinted from: *Int. J. Mol. Sci.* **2015**, *16*, 28765–28782,
https://doi.org/10.3390/ijms161226129 . . . . . **385**

Wen-Shih Huang, Jen-Tsung Yang, Chien-Chang Lu, Shun-Fu Chang, Cheng-Nan Chen, Yu-Ping Su and Ko-Chao Lee
Fulvic Acid Attenuates Resistin-Induced Adhesion of HCT-116 Colorectal Cancer Cells to Endothelial Cells
Reprinted from: *Int. J. Mol. Sci.* **2015**, *16*, 29370–29382,
https://doi.org/10.3390/ijms161226174 . . . . . **403**

Kang Li, Jianxiang Liu, Mei Tian, Gang Gao, Xuesong Qi, Yan Pan, et al.
CHMP4C Disruption Sensitizes the Human Lung Cancer Cells to Irradiation
Reprinted from: *Int. J. Mol. Sci.* **2016**, *17*, 18,
https://doi.org/10.3390/ijms17010018 . . . . . **416**

Sergey V. Gudkov, Natalya Yu. Shilyagina, Vladimir A. Vodeneev and Andrei V. Zvyagin
Targeted Radionuclide Therapy of Human Tumors
Reprinted from: *Int. J. Mol. Sci.* **2016**, *17*, 33,
https://doi.org/10.3390/ijms17010033 . . . . . **428**

Bao-Jun Ren, Zhi-Wei Zhou, Da-Jian Zhu, Yong-Le Ju, Jin-Hao Wu, Man-Zhao Ouyang, et al.
Alisertib Induces Cell Cycle Arrest, Apoptosis, Autophagy and Suppresses EMT in HT29 and Caco-2 Cells
Reprinted from: *Int. J. Mol. Sci.* **2016**, *17*, 41,
https://doi.org/10.3390/ijms17010041 . . . . . **447**

Xu-Yan Li, Wen-Jun Zhai and Chun-Bo Teng
Notch Signaling in Pancreatic Development
Reprinted from: *Int. J. Mol. Sci.* **2016**, *17*, 48,
https://doi.org/10.3390/ijms17010048 . . . . . **481**

Agnieszka Klupczynska, Agata Swiatly, Joanna Hajduk, Jan Matysiak, Wojciech Dyszkiewicz, Krystian Pawlak and Zenon J. Kokot
Identification of Serum Peptidome Signatures of Non-Small Cell Lung Cancer
Reprinted from: *Int. J. Mol. Sci.* **2016**, *17*, 410,
https://doi.org/10.3390/ijms17040410 . . . . . **500**

Li Zhou, Jin Hao, Yue Yuan, Rui Peng, Honglian Wang, Dongsheng Ni, et al.
EIYMNVPV Motif is Essential for A1CF Nucleus Localization and A1CF (-8aa) Promotes Proliferation of MDA-MB-231 Cells via Up-Regulation of *IL-6*
Reprinted from: *Int. J. Mol. Sci.* **2016**, *17*, 811,
https://doi.org/10.3390/ijms17060811 . . . . . **517**

About the Editor

William Cho

William Cho, 3rd Top Scientist in Mainland (Oncology), is a distinguished biomedical scientist whose career has significantly advanced global clinical cancer research. For decades, he has contributed to both research discovery and clinical application to improve therapeutic outcomes. Prof Cho's professional standing is reflected in numerous fellowships: Fellow of the Institute of Biomedical Science (UK) since 1998; Fellow of the Hong Kong Institute of Medical Laboratory Sciences and the Hong Kong Society of Molecular Diagnostic Sciences since 2003; and Chartered Scientist (UK Science Council) since 2004. Prof Cho's multidisciplinary work spans molecular biology, genomics, immunology, bioinformatics, and Chinese medicine, with emphasis on cancer biomarkers, proteomics, non-coding RNA, extracellular vesicles, and novel anti-cancer therapeutics. His biomarker studies in lung cancer, nasopharyngeal carcinoma, breast cancer, and colorectal cancer have informed personalised treatment strategies. Prof Cho has published over 750 SCI peer-review articles in journals including *Annals of Oncology*, *The Lancet Oncology*, *Molecular Cancer*, *PNAS*, and *Journal of Thoracic Oncology*, with over 45,000 citations and an H-index of 120. Since 2017 he has been named on Stanford University's list of the world's top 2% scientists, and in 2023 and 2024 he was recognised as a Highly Cited Researcher by Clarivate Analytics, an honour awarded to fewer than 7,000 scholars worldwide, making him one of very few within the Hospital Authority to attain this recognition. Prof Cho is also a prolific author of over 40 academic books held by libraries of renowned universities, including *Resistance to Anti-CD20 Antibodies and Approaches for Their Reversal* (Academic Press) and Springer Nature volumes such as *An Omics Perspective on Cancer Research and the Evidence-based Anticancer Complementary and Alternative Medicine* series, through which he has advanced evidence-based traditional Chinese medicine globally.

Preface

The recognition that human cancers are not monolithic entities but rather diverse collections of molecularly distinct diseases has fundamentally transformed oncologic research and clinical practice. This Special Issue, "Molecular Classification of Human Cancer: Diagnosis and Treatment", was conceived to capture the depth and breadth of this transformation, providing a platform for disseminating cutting-edge knowledge that bridges molecular discovery and patient care.

The focus of this Reprint is the integration of molecular profiling into the classification, diagnosis, and treatment of human cancers. Its scope encompasses a wide array of technological approaches including genomics, microRNA analysis, proteomics, epigenetics, and next-generation sequencing, applied across multiple tumor types such as breast, lung, colorectal, gastric, and hematologic malignancies. The primary aim is to assemble a collection of original research contributions and comprehensive review articles that demonstrate how molecular subtyping facilitates more accurate prognosis, predicts therapeutic response, and guides rational treatment selection in the era of precision medicine.

The motivation for compiling this scientific work stems from the limitations of traditional histopathology, which often fails to capture the underlying biological heterogeneity driving variable clinical outcomes. As targeted therapies proliferate, the ability to identify which patients will benefit from which treatment has become paramount. Molecular classification addresses this need by uncovering actionable drivers and resistance mechanisms, thereby facilitating individualized therapeutic strategies. Additionally, the emergence of technologies such as liquid biopsy and single-cell sequencing has opened new avenues for dynamic disease monitoring.

This Reprint is addressed to oncologists, molecular pathologists, translational researchers, laboratory scientists, and residents in oncology and molecular medicine. It is a valuable resource for anyone seeking to understand how molecular taxonomy is reshaping cancer care and how these insights are driving improvements in patient outcomes through more precise diagnosis and individualized treatment strategies. We hope this collection serves as both a reference and an inspiration for future breakthroughs in the fight against cancer.

William Cho
Guest Editor

Int. J. Mol. Sci. **2015**, *16*, 8655-8675; doi:10.3390/ijms16048655

OPEN ACCESS
International Journal of
Molecular Sciences
ISSN 1422-0067
www.mdpi.com/journal/ijms

Review

Pathological Bases for a Robust Application of Cancer Molecular Classification

Salvador J. Diaz-Cano

King's Health Partners, Cancer Studies, King's College Hospital-Viapath, Denmark Hill, London SE5-9RS, UK; E-Mail: sdiaz-cano@nhs.net; Tel.: +44-20-3299-3041; Fax: +44-20-3299-3670

Academic Editor: William Chi-shing Cho

Received: 28 January 2015 / Accepted: 7 April 2015 / Published: 17 April 2015

Abstract: Any robust classification system depends on its purpose and must refer to accepted standards, its strength relying on predictive values and a careful consideration of known factors that can affect its reliability. In this context, a molecular classification of human cancer must refer to the current gold standard (histological classification) and try to improve it with key prognosticators for metastatic potential, staging and grading. Although organ-specific examples have been published based on proteomics, transcriptomics and genomics evaluations, the most popular approach uses gene expression analysis as a direct correlate of cellular differentiation, which represents the key feature of the histological classification. RNA is a labile molecule that varies significantly according with the preservation protocol, its transcription reflect the adaptation of the tumor cells to the microenvironment, it can be passed through mechanisms of intercellular transference of genetic information (exosomes), and it is exposed to epigenetic modifications. More robust classifications should be based on stable molecules, at the genetic level represented by DNA to improve reliability, and its analysis must deal with the concept of intratumoral heterogeneity, which is at the origin of tumor progression and is the byproduct of the selection process during the clonal expansion and progression of neoplasms. The simultaneous analysis of multiple DNA targets and next generation sequencing offer the best practical approach for an analytical genomic classification of tumors.

Keywords: molecular pathology; cancer; neoplasm; classification; analytical genomic classification of tumors; genomic pathology; cancer cell biology

1. Introduction

A general definition of neoplasm like "cellular disease characterized by abnormal growth regulatory mechanisms" is descriptive and difficult to apply routinely, working definitions being required. The introduction of new markers has improved the diagnostic precision, but can potentially result in big changes in prevalence and uncertainties for particular lesions. The current WHO classifications of tumors incorporate new developments based on pathology and genetics, the leading criteria still being morphological; in this context, molecular findings complement the histological evaluation without replacing it. Additionally, any new definition should be validated against the accepted standard (specificity/sensitivity), should improve patient's management, and should provide a biologic meaning for its application. The first requirement is typically met by the initial design, and the second condition would be expected in any successful implementation. The third criterion is harder to put into practice, but any new definition should be biologically meaningful and would incorporate core elements in tumor biology (in particular genetic and kinetic correlates) [1–5]. These elements need to be included in a score system. Examples include the PAX8/PPARγ fusion gene described in follicular thyroid carcinomas and adenomas or RET/PTC fusion genes reported in papillary thyroid carcinomas and Hashimoto's thyroiditis. Molecular findings are contributing to a better understanding and classification of neoplasms [6–8]. The proposal, to classify neoplasms based only on the identification of one molecular abnormality, is naïve, especially considering that neoplasms require several mutations to reach the no-return point during the malignant transformation [4,5,9,10]. This approach raises fundamental issues in tumor classification and terminology that would need further considerations. Any classification is an organization in domains by hierarchical groups, according to features generalizable to the members of the groups. Classifications are important because class properties are shared among the members of a class, and because members of a class inherit the properties of their ancestors. The classification process must also be differentiated from terms like identification, discrimination, taxonomy, and ontology that cause considerable confusion among pathologists and cancer researchers. Identification is the act of placing something into its correct slot within an existing classification. Discrimination is finding features that separate members of a group according to expected variations in group behavior, the so-called prognostic factors such as grading and staging. A taxonomy is a complete listing of all the members of a classification, and an ontology is a rule-based grouping of some portion of a taxonomy.

2. General Features of Tumor Classification: Current Status

A classification has certain properties that distinguish it from other ways of organizing data. Any classification tries to encapsulate all knowledge related to a domain, but much of the current work in the molecular classification of tumors is identification, and discriminant analysis disguised as classification. It is impossible to create a molecular classification of tumors based solely on the separation of tumors by variations of molecular markers. Clustering by variation only identifies differences among tumors and is not sufficient to establish a classification. Classification is the process of showing that certain differences reliably distinguish the members of a group from the members of all other groups and that these differences apply to the group's hierarchical descendants. In a modern

classification, the elements of the classification serve as annotation keys and are capable of relating all data to the classification, incorporating molecular pathways that will be used as targets for new, non-toxic chemotherapeutic agents. There have been early successes with tumors sensitive to the inhibition of tyrosine kinases (gastrointestinal stromal tumors (GIST) and chronic myelogenous leukemia) with imatinib [11]. Both these tumors derive from non-endodermal/ectodermal embryonic layers, suggesting that molecular pathways (hence targets for chemotherapy) may be class-dependent.

Reliable classification systems require a careful use of internationally accepted nomenclature based on differentiation-developmental system that represents the current gold standard. The main criteria used in tumor classification are founded in tissue differentiation and developmental biology [4,9,10,12,13], which result in a system that gives several advantages: assign tumors to unique positions within the classification, avoiding the problem of multiple embryologic derivatives that can be present within one organ; provide a cell developmental stage that is usually reproduced by the differentiation process; give relevant behavioral information, such as the likely metastatic dissemination via lymphatics for epithelial neoplasms and by hematogenous spread of mesenchymal neoplasms; correlate closely with modern molecular analysis of tumors (sarcomas and lymphomas are frequently characterized by simple fusion genes, carcinomas and melanomas cannot be marked by a single genetic abnormality, and primitive blastomas share similar markers regardless of the organ of origin). For these reasons, the classification nomenclature used internationally is based on this terminology. However, current tumor classifications are site or organ system specific, often based on medical disciplines rather than biologic principles, appear redundant when subclassifications are merged and have problems analyzing heterogeneous biological data. Several fundamental issues in tumor classification exemplify the growing rift between morphologic and molecular approaches to tumor classification [9,10,14,15]: (1) intratumor heterogeneity and morpho-functional changes associated with tumor progression; (2) the distinction between loss of differentiation during progression and primary lack of differentiation; (3) the molecular properties shared by morphologically disparate tumors with or without a common developmental lineage; (4) the grouping of tumors based on shared cellular functions; (5) the separation of epithelial and non-epithelial tumors; (6) the distinction between germ cell tumors and pluripotent tumors of non-germ cell origin; and (7) the problem of re-classifying morphologically identical but clinically distinct subsets of tumors. If a tumor lacks a morphologic or molecular feature at one point in its development and gains it at a later point, the element cannot determine a new class of tumor. If a tumor has a good prognosis at one point (e.g., before it has metastasized) and a bad prognosis later (e.g., after it has metastasized), then prognostic features associated with metastasis cannot be used to determine a new class of tumor.

The differentiation-developmental classification of neoplasms makes basic assumptions, including: morphologic and molecular features of tumors will both fall sensibly into classes determined by tumor cell lineage; pathways with molecular alterations producing a tumor phenotype will tend to operate in all tumors of a developmental class; and morphologic properties associated with the altered pathway will be visible for all class members. It would therefore be sensible to keep the advantages of morphological classifications, complementing it with biological concepts and measurable features provided by molecular analysis, in particular those coming from genomic evaluations (multigene analysis highlights cooperative genetic interactions) [9,10]. Our understanding of embryologic lineage has changed very little over the past half century, and a classification based on differentiation and

developmental biology permits tumors to be assigned to well-defined classes. Somatic DNA has lineage-specific epigenetic modifications that occur throughout development [16–20], opening the avenue for measurable and definable patterns of epigenetic modifications (e.g., methylation) as key informative features for the developmental lineage of tumors. Kho and coworkers [13] have developed a method that projects gene expression profiles of tumors onto a mouse developmental sequence. Human medulloblastoma most closely matched the gene expression profile of postnatal day five mouse cerebella. Although this study examined only a few tumors, it described a method that allows any human tumor to be matched against a library of gene expression profiles collected from normal tissues at different stages of development.

Because classifications are hypotheses about the fundamental nature of a knowledge domain, the foundational assumptions of any classification must be continually evaluated and challenged. In this scenario, the role of pathologists is essential as the best link to accomplish a robust, reliable and biologically founded classification of neoplasms. The pathologist prepares, describes and diagnoses the tissue samples; organizes and integrates the available information (demographic, clinical, and ancillary techniques); and identifies enriched tissue samples for more reliable molecular results by microdissection techniques. In all cases, the clinicopathologic annotations used by the molecular biologist are generated in whole or in part by surgical pathologists. It has been noted that, "the pathologist's understanding of anatomic, physiologic, biochemical, immune, and other underlying factors that drive mechanisms of tissue responses to noxious agents turns a bewildering array of gene expression data into focused research programs" [21].

3. Key Cellular and Molecular Processes to Incorporate in a Robust Classification

Biologically, neoplasms develop through acquisition of capabilities that involve tumor cell aspects and microenvironment interactions [9,22,23]. The unrestricted growth observed in neoplasms is generally due to a stepwise accumulation of cooperative genetic alterations in oncogenes and tumor-suppressor genes, the number being more important than the order of changes; [24] the evidence available suggest that 5–7 genetic alterations are required for clinically detectable tumors, correlating with morphological progression in some locations. These capabilities are not equally relevant at different stages during tumorigenesis, as highlighted by careful morphological evaluations. The markers should be selected considering the ability to test and the marker role during tumor initiation and promotion. Tumor promotion markers would be more relevantly assessed during progression, which needs to be defined on clear clinical and morphological grounds. The main tumorigenesis molecular pathways must be evaluated according to the acquired capabilities: self-maintained replication (cell cycle dysregulation), extended cell survival (cell cycle arrest, apoptosis dysregulation, and replicative lifespan), genetic instability (chromosomal and microsatellite), changes in chromatin, transcription and epigenetics, mobilization of cellular resources, and modified microenvironment interactions (tumor cells, stromal cells, extracellular, endothelium) [9]. All these aspects must finally be integrated into the mechanisms of tumor initiation (including clonality) and progression. The knowledge of these pathways in each acquired capability is also essential to plan any sensible molecular evaluation of neoplasms (Figure 1): It will allow a marker selection based on biological features and it will allow a precise range of surrogate/secondary markers to validate the results. In addition, some pathways are

mutually exclusive (*i.e.*, RAS and B-RAF mutations or EGFR and RAS analyses) and have to be evaluated simultaneously.

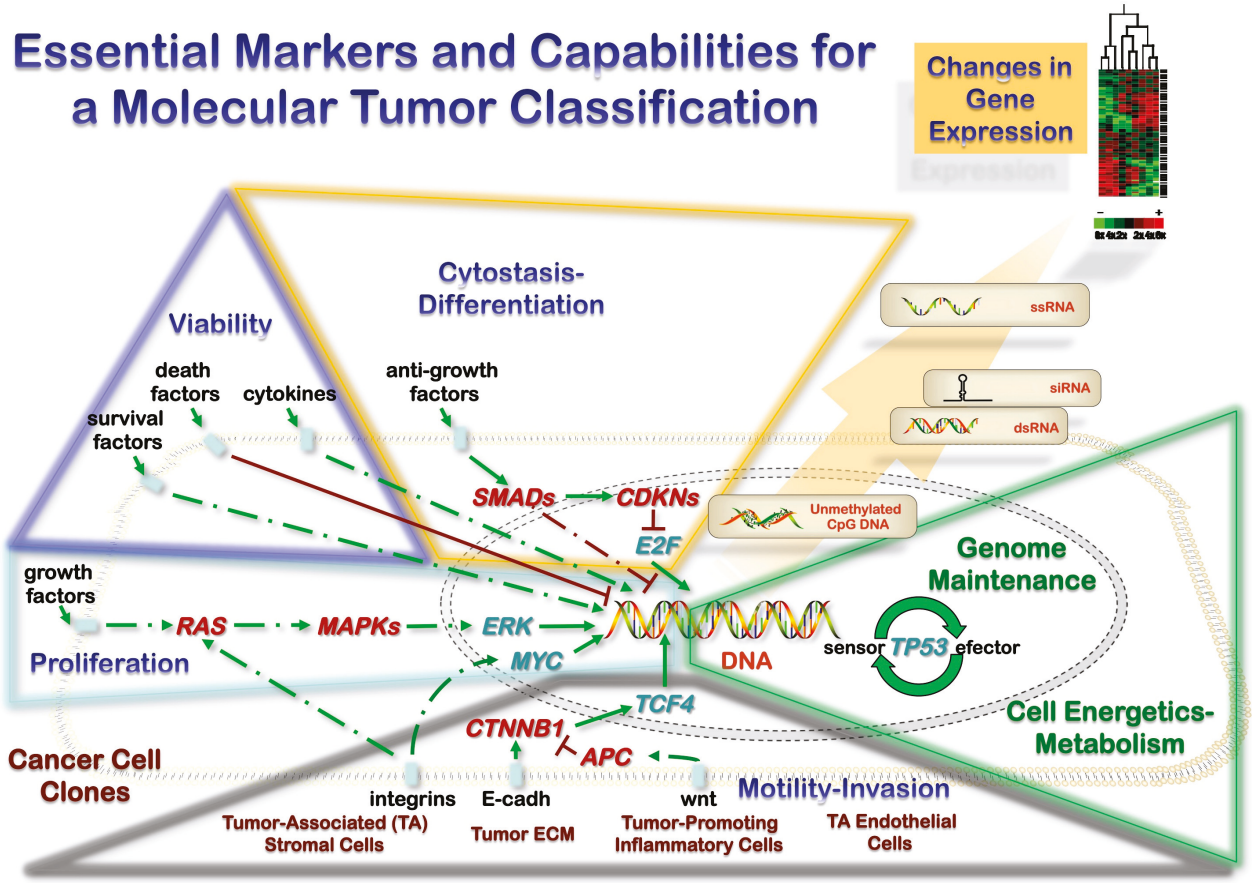

Figure 1. Malignant tumors are heterogeneous biological structures comprising cancer cell clones along with tumor-associated components necessary for maintaining the autonomous growth (stromal cells, extracellular matrix, inflammatory cells and endothelial cells). This heterotypic biology is self-maintained by acquired capabilities that promote both endless growth (proliferation, expanded cell survival or viability, resistance to cytostasis, and motility/invasion) and progression (evasion of genome maintenance, and appropriate cell energetics-metabolism). Cooperative genetic alterations in these pathways are common in cancer at different levels (DNA sequence, chemical modifications of DNA and gene expression), and their combinations can serve as elements of a molecular classification. However, as these combinations are not always pathognomonic and there is an additional complexity of gene expression (intercellular RNA transfer in heterotopic biology, RNA degradation), multitargeted simultaneous DNA analysis would be the most promising way to improve our current pathological neoplasm classification.

Molecular markers and pathways should be selected based on biological criteria comprising key features of tumorigenesis: heterotypic biology including microenvironment interactions and their role in mutagenesis (as key aspects of activation/suppression of gene function) and metastatic potential, along with the gene expression deregulations and their role in differentiation. These elements then need to be integrated with a sensible molecular test requirement and score system for practical implementation.

3.1. Heterotypic Tumor Biology: Tumor Cells-Microenvironment Interactions

Normal cells survive and grow within defined environmental niches and are subjected to microenvironmental control. Outside of their particular niche, the tissue environment is hostile to normal cells. Since they lack necessary cell autonomous survival signals, normal cells will not survive an inappropriate microenvironment [25]. Detachment-induced cell death (anoikis) has been proposed as the mechanism preventing normal cells from leaving their original environment and seeding at inappropriate locations [9]. In order to evade local tissue control and avoid anoikis during tumor development and progression, malignant cells start interacting with the surrounding ECM [26]. A bidirectional relationship is initiated by tumor cells and its surrounding stroma as a first step to invasive growth on metastatic spreading. Stromal changes sustaining tumor progression include modifications of the ECM composition, activation of fibroblasts, myoepithelial cells, and the recruitment of pericytes or smooth muscle cells and immune and inflammatory cells [27].

Human tumors arise from single cells that have accumulated the necessary number and types of heritable alterations. Each such cell leads to dysregulated growth and eventually the formation of a tumor. Despite their monoclonal origin, at the time of diagnosis most tumors show a striking amount of intratumor heterogeneity in all measurable phenotypes; the evolutionary dynamics of heterogeneity arising from exponential expansion of a tumor cell population, in which heritable alterations confer random fitness changes to cells [28]. Classical multistage modeling of tumorigenesis evolves through the processes of local proliferative lesions (tumor initiation and promotion or selection), and acquisition of invasion-metastatic potential (tumor progression). Broadly speaking, tumor development consists of the selective (clonal) expansion of altered cells to form focal lesions [3,29]. Within this definition, the process of promotion is mainly a quantitative phenomenon (many cells arising from a single cell), while no qualitative changes are necessarily implied. However, these latter properties are lost during tumor progression, which is typically characterized by increasing levels of tumor cell heterogeneity resulting in dominant qualitative changes [5,30], generating distinct cellular subclones with different phenotypes. Such a background represents the landscape for the full deployment of tumor progression.

These two distinctive processes, the mainly *quantitative* process of tumor promotion and the intrinsically *qualitative* process of tumor progression, are driven by two distinct microenvironments: the tissue and the tumor microenvironments [31–33]. The tissue microenvironment specifically refers to the local environment surrounding altered cells during their selective clonal expansion to form focal proliferative lesions. Conversely, the tumor microenvironment describes the unique biological milieu that emerges inside focal proliferative lesions as a consequence of their altered growth pattern [31–33]. Such new biological niche is characterized by a tissue architecture, which is not developmentally programmed and is bound to pose significant challenges for cell survival, due to altered/inadequate supply of oxygen and nutrients. This in turn can lead to biochemical and metabolic alterations that can profoundly impact on the fate of the cell populations inside focal lesions [34].

Given that altered cells can be selected in a tissue microenvironment which is otherwise growth-inhibitory to surrounding counterparts, a relevant question pertains to the biochemical and molecular basis of such phenotypic resistance. Blagosklonny has proposed the existence of two broad types of resistance [35]: (I) Non-oncogenic resistance relates to changes in drug metabolism and/or uptake, such that the rarely altered cell can withstand toxicity compared to the rest of the population in

that tissue. Such phenotypic resistance would still translate into the clonal growth of that rare cell, but no increased risk of neoplastic disease would be implied [35]; (II) The oncogenic resistance is linked to the inability of the cell to sense or repair DNA damage and/or to activate effector mechanisms leading to cell cycle arrest and/or cell death. As a result, the affected cell is susceptible to acquire a "mutator phenotype", *i.e.*, the tendency to undergo a cascade of further mutations [9,36–38].

The mutator phenotype has been linked with a defect in mismatch repair (MMR) genes so that a cascade of mutations occurs in cancer-related genes. To justify the onset of a mutator phenotype in "sporadic cancers" (which are in fact the vast majority) we have to revisit some theories of carcinogenesis and their evidence base [1,39]. In sporadic cancers, the origin of the mutator phenotype has been attributed to chance, or to mutagens that selectively affect specific genes similar to MMR genes, or to a combination of the two. However, MMR is apparently mutated only in a minority of cases: For example, colon cancers characterized by the presence of microsatellites (MIN) are a small minority compared to cancers characterized by chromosome instability (CIN), whose onset has not yet been attributed to the failure of any particular gene repair such as MMR [37,38]. To explain the most common type of lesions that are found in nonhereditary cancers, chromosome aberrations, and CIN, we have to explain how the mutator phenotype originates. In addition, a fundamental concept emerging recently is that mutations or instability are irrelevant if there is not a *microenvironmental change* that selects the cells carrying such mutations.

Cell replication is the primary source of cellular stress. On one hand, continuous proliferation results in telomere attrition and reduced stability of chromosome ends, which activate the cycle of chromosomal fusion-bridge-breakage and a higher incidence of translocations such as expression of chromosomal instability (CIN). On the other hand, nucleotide mismatches are introduced by DNA polymerase and will accumulate in DNA regions with repetitive sequences, such as microsatellites; this is the primary reason for microsatellite instability (MSI), a finding more frequently detected in tissues with higher proliferation. CIN and MSI have been described as two alternative pathways to cancer [9,38]. CIN is defined as the ability of a cell to gain and lose chromosomes and is a feature of many types of cancer. Conversely, microsatellite instability is related to a defect in the DNA mismatch repair machinery (MSI cancers).

The net result of CIN is the deregulation of chromosome number (aneuploidy) and an enhanced rate of loss of heterozygosity, which is an important mechanism of inactivation of tumor suppressor genes. Cytogenetic studies of bladder, lung and colon tumors have shown that karyotype complexity, cell ploidy, and the number of structural changes found were closely associated with tumor grade and stage. It has been suggested that different environmental carcinogens can induce distinct forms of genetic instability [40]. The available data demonstrate that exposure to particular carcinogens can indeed select for tumor cells with distinct types of genetic instability and *vice versa*. These data offer potential clues to one of the remaining unsolved problems in cancer research, the relationship between environmental factors and the genetic abnormalities that affect the tumorigenesis.

Chronic inflammation promotes tumor onset and development through nonimmune and immune mechanisms. The nonimmune mechanisms include the following: (I) the production of reactive oxygen species (ROS) such as peroxynitrites, which cause DNA mutations that contribute to genetic instability and the proliferation of malignant cells [41]; (II) the production of proangiogenic factors such as

vascular endothelial growth factor (VEGF), which promote tumor neovascularization [42]; and (III) the production of matrix metalloproteases, which facilitate invasion and metastasis [43].

3.2. Microenvironment and Metastasis

Cancer is a systemic disease: malignant tumors shed large numbers of cells into the blood and lymph vessels, some of them developing in distant sites into metastases. Moreover, distant metastasis is responsible for the majority of cancer-related deaths, and, therefore, understanding the underlying biological mechanisms of it is of primary importance. The invasion/metastasis capability is closely related with cell motility and requires the cytoskeleton as a critical component, which is also essential during mitoses. As malignancy criteria are mainly related to the phenotype of actively proliferating cells, it not surprising that metastatic deposits genetically match well-differentiated areas of primary neoplasms, and that invasive areas (periphery of solid organ neoplasms and deep compartment of luminal organ tumors) show lower cellular turnover and higher incidence of genetic abnormalities [38,39,44–46]. These factors need attention when planning the evaluation of intratumoral heterogeneity and would include: detailed specification of sampling (intratumoral location, number of samples), combined evaluation of kinetic and genetic features to assess selective process, analysis of pathways at several steps to avoid confounding factors (redundancy and pleiotropism) [5,9,47]. These biological foundations will enable a better therapeutic design, using the heterogeneity to improve patient's management.

According to a traditional model of tumor development, tissue constraints constitute a significant evolutionary bottleneck in cancer evolution; thus, the acquisition of metastatic ability is considered to be the final step in tumor development, contingent on the acquisition of all of the other hallmarks of cancer [9,22,23]. This model implies that metastatic tumors should be genetically similar to the bulk of primary tumor cells.

Many studies that compared the genetic composition of primary tumors and secondary metastatic sites have found very close clonal relationships between the two in the majority of cases [48–50]. Similarly, analysis of gene expression profiles revealed very similar patterns between primary tumors and metastatic sites, a scenario highly unlikely for genetically divergent clones [51–53]. Another prediction from the linear model of tumor progression is that different metastases should display close clonal relationships among each other. Indeed, this prediction is supported by a recent study that compared the genetic composition of anatomically distinct metastatic lesions in 29 prostate cancer patients using SNP arrays and CGH [54]. In all cases, different metastatic lesions from the same patients demonstrated close clonal relationships, signifying monoclonal origin [54]. This demonstration of monoclonality of metastatic cancers is especially impressive given that primary prostate cancers are frequently multifocal [55], and show substantial intra-tumor genetic heterogeneity [55,56].

While the evidence of the close genetic relationship between primary and metastatic tumors is compelling, some cases display dramatic divergence, challenging the model where acquisition of metastasis is considered to be the last step of tumor progression. Radically different patterns of allelic losses, indicative of a high degree of genetic divergence, have been reported in primary tumors and lymph node metastases in prostate cancers [49], and between primary tumors and asynchronous metastases in breast cancers [50]. Highly divergent clonal evolution was also evident in a subset of

cases in CGH studies of primary tumors *versus* lymph node metastases in breast cancers and of primary tumors *versus* metastatic tumors in renal cell carcinomas [48]. A recent report, comparing sequences of primary tumors and metastases in lobular breast cancers, revealed multiple mutations present only in metastases and several other mutations with increased frequency in metastatic sites [57]. Some of these genetic changes result in a higher incidence of apoptosis of tumor cells of dormant metastases (more than threefold higher) [58]. These data show that metastases remain dormant when tumor cell proliferation is balanced by an equivalent rate of cell death and suggest that angiogenesis inhibitors control metastatic growth by indirectly increasing apoptosis in tumor cells.

3.3. Gene Expression: Transfer of Genetic Material and Sequence-Independent Modifications

Gene expression analysis is becoming a useful tool for a better definition of neoplasms at diagnostic, prognostic and predictive levels. The identification of predictive markers of these features will help classifying neoplasms and stratifying patients for better management. However, the nature and biological meaning of these gene expression markers is not always clear: origin of the tested RNA, mechanism of RNA transference, utility for subclassification of neoplastic lesions. Gene expression analysis is becoming a useful tool for a better definition of neoplasms at diagnostic, prognostic and predictive levels [59–63]. The gene expression signature also reflects the *metastatic potential* in both cell lines and tumor samples [64–68]. First, the expression profile of low metastatic subline is distinct from that of the high metastatic subline. Metastases of the low metastatic subline closely resembled the pattern of the low metastatic primary tumor and did not "switch over" to the high metastatic gene expression profile. Thus, heterogeneity exists in this cell line/tumor, but may not be apparent as the signature reflects the majority of the tumor cells. The low metastatic subline is capable of spawning metastases, albeit at a lower rate, and its gene expression profile is therefore of significant interest. Second, the gene expression profile of the sublines as *in vitro* cultures is very distinct from the same sublines as primary tumors. While the primary tumors are a mixture of tumor cells and heterogeneous host cells (stromal cells, endothelial cells, among others), the contribution of these cells to the observed gene expression profiles should be minimal. Thus, the differences are thought to reflect changes in the tumor cells in response to the *in vivo* microenvironment. Third, comparable numbers of genes were "turned on" and "turned off" in the more highly metastatic tissues. We think about metastasis as the acquisition of traits, but the data remind us to pay equal attention to the loss of growth and differentiation-controlling genes. Many of the differentially expressed genes fall into the category of "usual suspects" for metastasis.

Cancer cells communicate with the environment through delivery of surface proteins, release of soluble factors (growth factors and cytokines), and sophisticated nano vesicles (exosomes) for the establishment of invasive tumor growth. A central question in molecular studies is to determine the *cellular origin of the target mRNA*. Two biological aspects are essential for this process: how the tumor mRNA gets there and the functionality of this mRNA. The answers to these questions are most relevant in locations where the tumor cells are scanty and the expression profile support higher tumor cell load [69]. *Membrane vesicles* derived from both tumor and host cells have recently been recognized as new candidates for critical roles in the promotion of tumor growth and metastasis [70]. The transfer of membrane components between donor and acceptor cells has been described

"trogocytosis" (from Greek "trogo", meaning "gnaw" or "bite"). Two forms of membrane transfer (trogocytosis) have been described: via nanotubes or membrane vesicles [71]. The biogenesis of membrane vesicles fundamentally distinguishes exosomes from shedding microvesicles and apoptotic blebs. The biologic heterogeneity of intraepithelial and invasive malignancies is well known at the morphologic, kinetic and genetic levels, an issue that has not been addressed in this paratumoral gene expression analysis and should warrant future studies. The gene expression markers should be evaluated in the appropriate biological context. Gene expression profiles are determined by a gene regulatory network comprising regulatory core of genes represented most prominently by transcription factors and miRNAs, which influence the expression of other genes, and a periphery of effector genes that are regulated but not regulating [72,73]. Most studies do not differentiate between these two essential groups, which can also be useful in selecting surrogate markers for a given condition [9,72]. There is a general concept to keep in mind during the analysis of gene expression: the amount of information is overwhelming, and the number of variables included in the studies significantly outnumbers the cases. In this scenario, the significant variables can be the result of a statistical selection rather than the expression of a biologically important process for a particular neoplasm. Relevant variables frequently include genes of the general metabolic activation associated with the neoplastic transformation [9,23], rather than tissue- or differentiation-specific gene variables.

Epigenetic dysregulation is central to cancer development and progression [74]. The best-known epigenetic marker is DNA methylation. This dysregulation includes hypomethylation leading to oncogene activation and chromosomal instability, hypermethylation and tumor suppressor gene silencing, and chromatin modification acting directly, and cooperatively with methylation changes, to modify gene expression [75]. The initial finding of global hypomethylation of DNA in human tumors was soon followed by the identification of hypermethylated tumor-suppressor genes, and then, more recently, the discovery of inactivation of microRNA (miRNA) genes by DNA methylation.

3.4. Molecular Test Scoring System for Practical Implementation

The application of these biologic concepts in oncologic pathology leads to consider the molecular testing requirements (Molecular Test Score System) for a reliable implementation, which cover biological effects (1–3), molecular pathway (4, 5), biological validation (6–8), and technical validation (9, 10) (Figure 2) [9].

Currently, the most efficient way to achieve this goal, is by genomic approach and multi-target analysis like that provided by next generation sequencing. This multi-target analysis also complies with the multistep process widely accepted during tumorigenesis and is further supported by the need for multiple cooperative mutations in neoplasms [3–5,9,10,46,76]. Although organ-specific examples have been published based on proteomics, transcriptomics and genomics evaluations, the most common approach uses gene expression analysis as a direct correlate of cellular differentiation, which represents the key feature of the histological classification. RNA is a labile molecule that varies significantly according with the preservation protocol, its transcription reflect the adaptation of the tumor cells to the microenvironment, it can be passed through mechanisms of intercellular transference of genetic information (exosomes), and it is exposed to epigenetic modifications. More robust classifications should be based on stable molecules, at the genetic level represented by DNA to

improve reliability, and its analysis must deal with the concept of intratumoral heterogeneity, which is at the origin of tumor progression and is the byproduct of the selection process during the clonal expansion and progression of neoplasms.

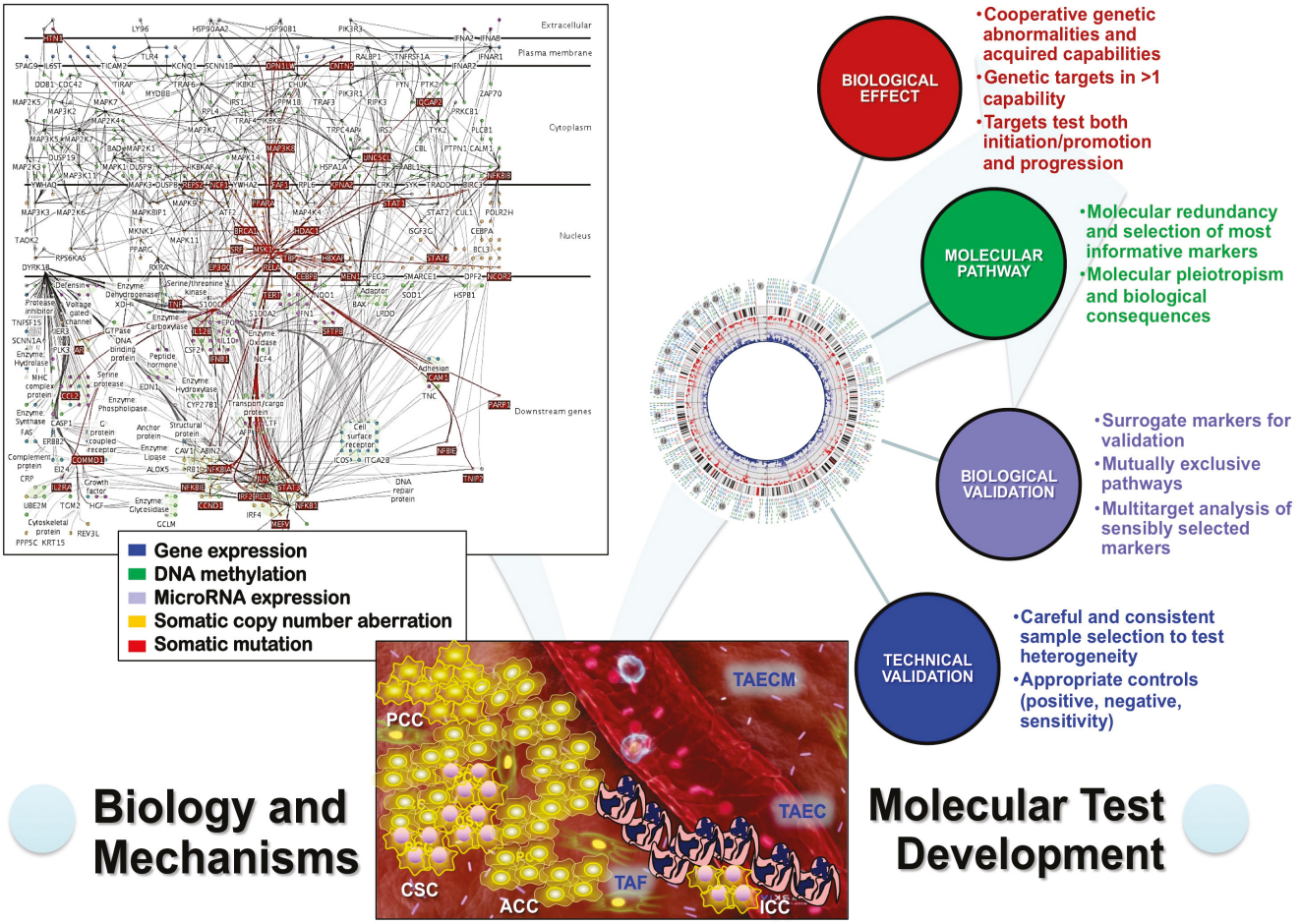

Figure 2. Multitarget genomic analysis of malignancies must consider the heterotypic nature of neoplasms of both cancer cells (cancer stem cells CSC, proliferating cancer cells PCC, arrested cancer cells ACC, and invasive cancer cells ICC) and tumor-associated (TA) components (fibroblasts TAF, endothelial cells TAEC, and extracellular matrix TAECM). Any comprehensive study need to address biological aspects and mechanisms of tumor genetic alterations to explain the natural history of a given neoplasm, provide essential prognostic information and predict response to therapy. The genetic alterations should be characterized at the cellular level (extracellular, plasma membrane, cytoplasm, nucleus or downstream genes) and molecular level (gene expression, methylation, microRNA, copy number aberrations and mutations). Any tests developed for this evaluation must follow a careful assessment of biological effects, pathways involved, biological validation and technical validation. In practice, the most promising approach fulfilling these criteria is the next generation sequencing.

4. Analytical Genomic Classification of Tumors (AGCT)

An analytical genomic classification of tumors (AGCT) must be based on multiple informative features covering general characteristics of hierarchical class and instances, epidemiologic features from the pathways highlighted by inherited cancer syndromes, and the etiopathogenic features from experimental pathology (Table 1).

Table 1. Proposed requirements for independent classes in AGCT (Analytical Genomic Classification of Tumors).

General Features	Specific Features
A classification is a hierarchical grouping	Each group is defined by the greatest number of informative features that can apply to every instance of the class.
	Nomenclature should refer to differentiation/developmental terms internationally accepted.
	Every instance of the knowledge domain must fit the classification.
	Every instance and class must have exactly one slot in the classification.
	Instances of one class cannot migrate to a different class but must remain in the same class or a subclass of the same class.
	Instances and classes are separable from other instances and classes by informative features.
	All new findings of subpopulations of tumors can be considered candidate function to characterize a class and distinguish the class from other classes.
	Subclasses inherit the properties (shared informative features) of their ancestor classes.
Familial syndromes and epidemiologic features	Prevalence of the disease should be significantly higher in those carrying the genetic abnormalities (if familial model exists).
Animal models of the genetic abnormality–Etiopathogenic features	Marker gene should be more commonly abnormally expressed in animals with the disease than in controls without the disease when all risk factors are held constant.
	Incidence of the disease should be significantly higher in those animals with the abnormal gene than in those not exposed.
	A spectrum of preinvasive changes should follow the expression of the abnormal gene along a logical biologic gradient from mild to severe in the grading during neoplastic transformation (in particular for epithelial malignancies).
	Elimination or modification of the putative gene or of the vector carrying it should decrease the incidence of the disease.

A multi-target genome-wide approach warrants the simultaneous evaluation of several pathways controlling the acquired capabilities that characterize neoplasms and cancers. It needs a detailed computational bioinformatics to distinguish the driver from passenger genetic alterations, along with a quantitative analysis to assess the proportion of mutated tumor cells and copy number variation. The aim of the study should be the evaluation of affected genes and the genetic mechanisms involved in their activation/inactivation. Once candidate molecules (*i.e.*, genes, proteins, and other macromolecules or patterns of these molecules) are found to associate with a particular tumor variant, the pathologist gets a second chance to determine if a morphologic pattern correlates with the molecular property. Examples of both point mutations and translocations have been reported.

Most GISTs have a *KIT* mutation that results in Kit protein overexpression [11,77]. Some GIST tumors lacking *KIT* mutations have a mutation in the platelet-derived growth-factor receptor alpha gene [78]. Sakurai and coworkers have examined GIST tumors that stain negatively for CD117, a marker for Kit protein overexpression. Many of these tumors have mutations in platelet-derived growth-factor receptor alpha gene and a distinctive histo-morphology characterized by myxoid epithelioid tumor cells and tumor infiltration by mast cells [79]. This newly recognized subtype of GIST involved the morphologic re-examination of the tumors following a molecular discovery. Secretory carcinoma of the breast is an uncommon variant of breast cancer that occurs most frequently in young women. It is characterized by the ETV6-NTRK3 fusion gene [80,81]. The search and discovery of this molecular marker was accomplished through asynchronous contributions from three biomedical realms: (1) pathologists, who defined the morphologic subset of breast carcinoma known as secretory carcinoma of breast; (2) oncologists who validated the clinically distinct features of the tumor; and (3) molecular biologists who discovered the translocation that characterized the tumor. This fusion gene is not unique for secretory carcinomas of the breast it has also been identified in radiation-induced carcinomas [82–84].

However, the molecular component should resolve several seemingly intractable problems. As the number of molecular pathways controlling cell-specific functions altered during the neoplastic transformation is limited, pathways will be shared by different classes of neoplasms and are not type-specific. Mutations in genes of the chromatin remodeling pathway have been described in various types of neoplasms such as malignant rhabdoid tumors [85], atypical teratoid/rhabdoid tumors of the brain [86–88] and hypercalcemic type of ovarian small cell carcinomas [6–8]; these mutations target closely related genes SMARCA and SMARCB that regulate this pathway, which is not particular of these neoplasms: SMARCB1 homozygous deletions have been found in epithelioid sarcoma and a subset of myoepithelial carcinomas [87]. Cytogenetic abnormalities and gene alterations in tumors co-occur with other anomalies, and the complex state of molecular abnormalities in tumors make it very difficult to assign classes of tumor to a single type of genetic abnormality. In addition, these alterations could represent the cause or the by-product of the genetic instability associated with the neoplastic progression, both driver and carrier mutations coexisting in the heterogeneous built of neoplasms. In this context, it may be impossible to reach scientific consensus on complex sets of molecular signatures that define groups of tumors. As an example, balanced translocations play biologic roles in several tumors [12]. Although certain translocations are characteristic of individual tumors, it has proven difficult to generalize that translocations occur in any particular class of tumors. Certainly, characteristic tumor translocations occur more commonly in mesenchymal tumors [12], but such translocations have also been observed in thyroid carcinomas [89,90], prostate adenocarcinoma and precursors [91,92], secretory carcinoma of breast [81], and in midline (lung) carcinoma of children and young adults [93]. Some translocations are also shared by carcinomas and sarcomas, such as the balanced and unbalanced chromosome X; 17 translocations in both Xp11.2 renal cell carcinoma and alveolar soft part sarcoma, supporting a preference but not a necessity for the translocation to be balanced in the carcinoma and unbalanced in the sarcoma [94–96]. The notable exception, wherein a class of tumors is characterized by a set of translocations, is the Ewing's tumor family of tumors [97–99]. Translocations are tissue non-specific, occurring at a frequency related to the overall number of cytogenetic abnormalities found in tumors [100]. It can be noted that despite numerous projects aimed

at classifying tumors with gene expression profiles, no comprehensive classification based on this technology has emerged.

Much of what passes for neoplasm "classification" in the bioinformatics literature is actually the algorithmic ranking of expressed genes that can discriminate one tumor variant from another [101–105], but without precise pathogenetic or etiologic considerations for those changes [14]. Some classifications can be challenged more easily than others. A classification built on a set of continually changing parameters is constantly evolving and challenging to evaluate. This is certainly true of a molecular classification, because our knowledge of the field changes almost daily. A few years ago, it was safe to say that all recurrent balanced translocations were a phenomenon of mesenchymal tumors. New findings of recurrent balanced translocations in non-mesenchymal tumors have nullified this class assertion [100]. Morphologists once classified clear cell sarcoma as a type of malignant melanoma, based on finding melanosomes within tumor cells. Recent molecular classification of these tumors clearly distinguishes them from cutaneous melanoma. Clear cell sarcomas have characteristic EWS-AFT1 fusion transcript not found in cutaneous melanomas [106,107]. In addition, BRAF mutations, commonly found in cutaneous melanomas, are absent from clear cell sarcomas [108,109]. The rapid accumulation of new knowledge about the molecular characteristics of tumors can quickly change classifications built on morphology or molecular biology. Pathologists seem to be putting this tumor back into the mesenchymal class of neoplasms [110].

5. Conclusions

A scientifically sound classification of neoplasms will serve as a guide to prognostic stratification of patients and to selecting a new generation of cancer medications targeted to molecular pathways specific for particular classes of tumors. Without a robust scientific foundation to the tumor classification, biological measurements on individual tumor samples cannot be generalized to other tumors, and constitutive properties common to a class of tumors cannot be distinguished from uninformative data collected from complex and chaotic biological systems (Figure 1). Morphology, even in the post-genomic era, has enormous value in the realm of discovery of informative features that eventually would be pathogenic and etiologic if possible. Careful morphologic examination has discovered previously unrecognized features that are diagnostic for new tumors or new clinical variants of known tumors that have characteristic molecular profiles. For tumor classification, lineage, morphologic, and multi-target molecular informative features must fulfill minimal criteria for the class assignment, generation of testable hypotheses and verification of etiopathogenic features (Table 1). These elements must also consider the molecular test requirements (Molecular Test Score System) for a reliable implementation, which cover biological effects, molecular pathways, biological validation, and technical validation (Figure 2).

Conflicts of Interest

The author declares no conflict of interest.

References

1. Blanes, A.; Sanchez-Carrillo, J.J.; Diaz-Cano, S.J. Topographic molecular profile of pheochromocytomas: Role of somatic down-regulation of mismatch repair. *J. Clin. Endocrinol. Metab.* **2006**, *91*, 1150–1158.
2. Arif, S.; Blanes, A.; Diaz-Cano, S.J. Hashimoto's thyroiditis shares features with early papillary thyroid carcinoma. *Histopathology* **2002**, *41*, 357–362.
3. Baithun, S.I.; Naase, M.; Blanes, A.; Diaz-Cano, S.J. Molecular and kinetic features of transitional cell carcinomas of the bladder: Biological and clinical implications. *Virchows Arch. Int. J. Pathol.* **2001**, *438*, 289–297.
4. Diaz-Cano, S.J. Designing a molecular analysis of clonality in tumours. *J. Pathol.* **2000**, *191*, 343–344.
5. Pozo-Garcia, L.; Diaz-Cano, S.J. Clonal origin and expansions in neoplasms: Biologic and technical aspects must be considered together. *Am. J. Pathol.* **2003**, *162*, 353–355.
6. Foulkes, W.D.; Clarke, B.A.; Hasselblatt, M.; Majewski, J.; Albrecht, S.; McCluggage, W.G. No small surprise–small cell carcinoma of the ovary, hypercalcaemic type, is a malignant rhabdoid tumour. *J. Pathol.* **2014**, *233*, 209–214.
7. Jelinic, P.; Mueller, J.J.; Olvera, N.; Dao, F.; Scott, S.N.; Shah, R.; Gao, J.; Schultz, N.; Gonen, M.; Soslow, R.A.; *et al*. Recurrent SMARCA4 mutations in small cell carcinoma of the ovary. *Nat. Genet.* **2014**, *46*, 424–426.
8. Witkowski, L.; Carrot-Zhang, J.; Albrecht, S.; Fahiminiya, S.; Hamel, N.; Tomiak, E.; Grynspan, D.; Saloustros, E.; Nadaf, J.; Rivera, B.; *et al*. Germline and somatic SMARCA4 mutations characterize small cell carcinoma of the ovary, hypercalcemic type. *Nat. Genet.* **2014**, *46*, 438–443.
9. Diaz-Cano, S.J. General morphological and biological features of neoplasms: Integration of molecular findings. *Histopathology* **2008**, *53*, 1–19.
10. Diaz-Cano, S.J. Tumor heterogeneity: Mechanisms and bases for a reliable application of molecular marker design. *Int. J. Mol. Sci.* **2012**, *13*, 1951–2011.
11. Blay, J.-Y.; Bonvalot, S.; Casali, P.; Choi, H.; Debiec-Richter, M.; Dei Tos, A.P.; Emile, J.-F.; Gronchi, A.; Hogendoorn, P.C.W.; Joensuu, H.; *et al*. Consensus meeting for the management of gastrointestinal stromal tumors. Report of the GIST consensus conference of 20–21 march 2004, under the auspices of ESMO. *Ann. Oncol.* **2005**, *16*, 566–578.
12. Futreal, P.A.; Coin, L.; Marshall, M.; Down, T.; Hubbard, T.; Wooster, R.; Rahman, N.; Stratton, M.R. A census of human cancer genes. *Nat. Rev. Cancer* **2004**, *4*, 177–183.
13. Kho, A.T.; Zhao, Q.; Cai, Z.; Butte, A.J.; Kim, J.Y.H.; Pomeroy, S.L.; Rowitch, D.H.; Kohane, I.S. Conserved mechanisms across development and tumorigenesis revealed by a mouse development perspective of human cancers. *Genes Dev.* **2004**, *18*, 629–640.
14. Evans, A.S. Causation and disease: The henle-koch postulates revisited. *Yale J. Biol. Med.* **1976**, *49*, 175–195.
15. Berman, J.J. Tumor classification: Molecular analysis meets aristotle. *BMC Cancer* **2004**, *4*, 10.
16. Morgan, H.D.; Santos, F.; Green, K.; Dean, W.; Reik, W. Epigenetic reprogramming in mammals. *Hum. Mol. Genet.* **2005**, *14*, R47–R58.

17. Shiota, K.; Kogo, Y.; Ohgane, J.; Imamura, T.; Urano, A.; Nishino, K.; Tanaka, S.; Hattori, N. Epigenetic marks by DNA methylation specific to stem, germ and somatic cells in mice. *Genes Cells* **2002**, *7*, 961–969.
18. Allegrucci, C.; Thurston, A.; Lucas, E.; Young, L. Epigenetics and the germline. *Reproduction* **2005**, *129*, 137–149.
19. Esteller, M. Epigenetics provides a new generation of oncogenes and tumour-suppressor genes. *Br. J. Cancer* **2007**, *96*, R26–R30.
20. Ooi, S.L.; Henikoff, S. Germline histone dynamics and epigenetics. *Curr. Opin. Cell Biol.* **2007**, *19*, 257–265.
21. Boorman, G.A.; Anderson, S.P.; Casey, W.M.; Brown, R.H.; Crosby, L.M.; Gottschalk, K.; Easton, M.; Ni, H.; Morgan, K.T. Toxicogenomics, drug discovery, and the pathologist. *Toxicol. Pathol.* **2002**, *30*, 15–27.
22. Hanahan, D.; Weinberg, R.A. The hallmarks of cancer. *Cell* **2000**, *100*, 57–70.
23. Hanahan, D.; Weinberg, R.A. Hallmarks of cancer: The next generation. *Cell* **2011**, *144*, 646–674.
24. Kinzler, K.W.; Vogelstein, B. Lessons from hereditary colorectal cancer. *Cell* **1996**, *87*, 159–170.
25. Morrison, S.J.; Spradling, A.C. Stem cells and niches: Mechanisms that promote stem cell maintenance throughout life. *Cell* **2008**, *132*, 598–611.
26. Reddig, P.J.; Juliano, R.L. Clinging to life: Cell to matrix adhesion and cell survival. *Cancer Metastasis Rev.* **2005**, *24*, 425–439.
27. Tlsty, T.D.; Coussens, L.M. Tumor stroma and regulation of cancer development. *Annu. Rev. Pathol.* **2006**, *1*, 119–150.
28. Durrett, R.; Foo, J.; Leder, K.; Mayberry, J.; Michor, F. Intratumor heterogeneity in evolutionary models of tumor progression. *Genetics* **2011**, *188*, 461–477.
29. Diaz-Cano, S.J. Clonality studies in the analysis of adrenal medullary proliferations: Application principles and limitations. *Endocr. Pathol.* **1998**, *9*, 301–316.
30. Diaz-Cano, S.J.; Blanes, A.; Wolfe, H.J. Pcr techniques for clonality assays. *Diagn. Mol. Pathol.* **2001**, *10*, 24–33.
31. Laconi, E. The evolving concept of tumor microenvironments. *BioEssays News Rev. Mol. Cell. Dev. Biol.* **2007**, *29*, 738–744.
32. Laconi, E.; Doratiotto, S.; Vineis, P. The microenvironments of multistage carcinogenesis. *Semin. Cancer Biol.* **2008**, *18*, 322–329.
33. Laconi, E.; Sonnenschein, C. Cancer development at tissue level. *Semin. Cancer Biol.* **2008**, *18*, 303–304.
34. Huang, L.E.; Bindra, R.S.; Glazer, P.M.; Harris, A.L. Hypoxia-induced genetic instability—A calculated mechanism underlying tumor progression. *J. Mol. Med.* **2007**, *85*, 139–148.
35. Blagosklonny, M.V. Oncogenic resistance to growth-limiting conditions. *Nat. Rev.* **2002**, *2*, 221–225.
36. Breivik, J. The evolutionary origin of genetic instability in cancer development. *Semin. Cancer Biol.* **2005**, *15*, 51–60.
37. Bielas, J.H.; Loeb, L.A. Mutator phenotype in cancer: Timing and perspectives. *Environ. Mol. Mutagen.* **2005**, *45*, 206–213.

38. Blanes, A.; Diaz-Cano, S.J. Complementary analysis of microsatellite tumor profile and mismatch repair defects in colorectal carcinomas. *World J. Gastroenterol. WJG* **2006**, *12*, 5932–5940.
39. Rubio, J.; Blanes, A.; Sanchez-Carrillo, J.J.; Diaz-Cano, S.J. Microsatellite abnormalities and somatic down-regulation of mismatch repair characterize nodular-trabecular muscle-invasive urothelial carcinoma of the bladder. *Histopathology* **2007**, *51*, 458–467.
40. Bardelli, A.; Cahill, D.P.; Lederer, G.; Speicher, M.R.; Kinzler, K.W.; Vogelstein, B.; Lengauer, C. Carcinogen-specific induction of genetic instability. *Proc. Natl. Acad. Sci. USA* **2001**, *98*, 5770–5775.
41. Coussens, L.M.; Werb, Z. Inflammation and cancer. *Nature* **2002**, *420*, 860–867.
42. Ellis, L.M.; Hicklin, D.J. Vegf-targeted therapy: Mechanisms of anti-tumour activity. *Nat. Rev.* **2008**, *8*, 579–591.
43. Yang, L.; Huang, J.; Ren, X.; Gorska, A.E.; Chytil, A.; Aakre, M.; Carbone, D.P.; Matrisian, L.M.; Richmond, A.; Lin, P.C.; *et al*. Abrogation of TGFβ signaling in mammary carcinomas recruits Gr-1+CD11b+ myeloid cells that promote metastasis. *Cancer Cell* **2008**, *13*, 23–35.
44. Blanes, A.; Diaz-Cano, S.J. DNA and kinetic heterogeneity during the clonal evolution of adrenocortical proliferative lesions. *Hum. Pathol.* **2006**, *37*, 1295–1303.
45. Blanes, A.; Rubio, J.; Martinez, A.; Wolfe, H.J.; Diaz-Cano, S.J. Kinetic profiles by topographic compartments in muscle-invasive transitional cell carcinomas of the bladder: Role of TP53 and NF1 genes. *Am. J. Clin. Pathol.* **2002**, *118*, 93–100.
46. Diaz-Cano, S.J.; Blanes, A.; Rubio, J.; Matilla, A.; Wolfe, H.J. Molecular evolution and intratumor heterogeneity by topographic compartments in muscle-invasive transitional cell carcinoma of the urinary bladder. *Lab. Investig. J. Tech. Methods Pathol.* **2000**, *80*, 279–289.
47. Jimenez, J.J.; Blanes, A.; Diaz-Cano, S.J. Microsatellite instability in colon cancer. *N. Engl. J. Med.* **2003**, *349*, 1774–1776.
48. Bissig, H.; Richter, J.; Desper, R.; Meier, V.; Schraml, P.; Schaffer, A.A.; Sauter, G.; Mihatsch, M.J.; Moch, H. Evaluation of the clonal relationship between primary and metastatic renal cell carcinoma by comparative genomic hybridization. *Am. J. Pathol.* **1999**, *155*, 267–274.
49. Cheng, L.; Bostwick, D.G.; Li, G.; Wang, Q.; Hu, N.; Vortmeyer, A.O.; Zhuang, Z. Allelic imbalance in the clonal evolution of prostate carcinoma. *Cancer* **1999**, *85*, 2017–2022.
50. Kuukasjarvi, T.; Karhu, R.; Tanner, M.; Kahkonen, M.; Schaffer, A.; Nupponen, N.; Pennanen, S.; Kallioniemi, A.; Kallioniemi, O.P.; Isola, J. Genetic heterogeneity and clonal evolution underlying development of asynchronous metastasis in human breast cancer. *Cancer Res.* **1997**, *57*, 1597–1604.
51. Ramaswamy, S.; Ross, K.N.; Lander, E.S.; Golub, T.R. A molecular signature of metastasis in primary solid tumors. *Nat. Genet.* **2003**, *33*, 49–54.
52. Weigelt, B.; Glas, A.M.; Wessels, L.F.; Witteveen, A.T.; Peterse, J.L.; van't Veer, L.J. Gene expression profiles of primary breast tumors maintained in distant metastases. *Proc. Natl. Acad. Sci. USA* **2003**, *100*, 15901–15905.
53. Weigelt, B.; Hu, Z.; He, X.; Livasy, C.; Carey, L.A.; Ewend, M.G.; Glas, A.M.; Perou, C.M.; van't Veer, L.J. Molecular portraits and 70-gene prognosis signature are preserved throughout the metastatic process of breast cancer. *Cancer Res.* **2005**, *65*, 9155–9158.

54. Liu, W.; Laitinen, S.; Khan, S.; Vihinen, M.; Kowalski, J.; Yu, G.; Chen, L.; Ewing, C.M.; Eisenberger, M.A.; Carducci, M.A., *et al*. Copy number analysis indicates monoclonal origin of lethal metastatic prostate cancer. *Nat. Med.* **2009**, *15*, 559–565.
55. Ruijter, E.T.; van de Kaa, C.A.; Schalken, J.A.; Debruyne, F.M.; Ruiter, D.J. Histological grade heterogeneity in multifocal prostate cancer. Biological and clinical implications. *J. Pathol.* **1996**, *180*, 295–299.
56. Alvarado, C.; Beitel, L.K.; Sircar, K.; Aprikian, A.; Trifiro, M.; Gottlieb, B. Somatic mosaicism and cancer: A micro-genetic examination into the role of the androgen receptor gene in prostate cancer. *Cancer Res.* **2005**, *65*, 8514–8518.
57. Shah, S.P.; Morin, R.D.; Khattra, J.; Prentice, L.; Pugh, T.; Burleigh, A.; Delaney, A.; Gelmon, K.; Guliany, R.; Senz, J.; *et al*. Mutational evolution in a lobular breast tumour profiled at single nucleotide resolution. *Nature* **2009**, *461*, 809–813.
58. Holmgren, L.; O'Reilly, M.S.; Folkman, J. Dormancy of micrometastases: Balanced proliferation and apoptosis in the presence of angiogenesis suppression. *Nat. Med.* **1995**, *1*, 149–153.
59. Bornstein, S.R.; Hornsby, P.J. What can we learn from gene expression profiling for adrenal tumor management? *J. Clin. Endocrinol. Metab.* **2005**, *90*, 1900–1902.
60. Garber, M.E.; Troyanskaya, O.G.; Schluens, K.; Petersen, S.; Thaesler, Z.; Pacyna-Gengelbach, M.; van de Rijn, M.; Rosen, G.D.; Perou, C.M.; Whyte, R.I.; *et al*. Diversity of gene expression in adenocarcinoma of the lung. *Proc. Natl. Acad. Sci. USA* **2001**, *98*, 13784–13789.
61. Steeg, P.S. New insights into the tumor metastatic process revealed by gene expression profiling. *Am. J. Pathol.* **2005**, *166*, 1291–1294.
62. Van de Rijn, M.; Rubin, B.P. Gene expression studies on soft tissue tumors. *Am. J. Pathol.* **2002**, *161*, 1531–1534.
63. Van't Veer, L.J.; Paik, S.; Hayes, D.F. Gene expression profiling of breast cancer: A new tumor marker. *J. Clin. Oncol.* **2005**, *23*, 1631–1635.
64. Ouatas, T.; Salerno, M.; Palmieri, D.; Steeg, P.S. Basic and translational advances in cancer metastasis: Nm23. *J. Bioenerg. Biomembr.* **2003**, *35*, 73–79.
65. Salerno, M.; Ouatas, T.; Palmieri, D.; Steeg, P.S. Inhibition of signal transduction by the nm23 metastasis suppressor: Possible mechanisms. *Clin. Exp. Metastasis* **2003**, *20*, 3–10.
66. Steeg, P.S. Metastasis suppressors alter the signal transduction of cancer cells. *Nat. Rev.* **2003**, *3*, 55–63.
67. Steeg, P.S.; Ouatas, T.; Halverson, D.; Palmieri, D.; Salerno, M. Metastasis suppressor genes: Basic biology and potential clinical use. *Clin. Breast Cancer* **2003**, *4*, 51–62.
68. Wulfkuhle, J.D.; Paweletz, C.P.; Steeg, P.S.; Petricoin, E.F., III; Liotta, L. Proteomic approaches to the diagnosis, treatment, and monitoring of cancer. *Adv. Exp. Med. Biol.* **2003**, *532*, 59–68.
69. Diaz-Cano, S.J. Paratumoral gene expression profiles: Promising markers of malignancy in melanocytic lesions. *Br. J. Dermatol.* **2011**, *165*, 702–703.
70. Peinado, H.; Lavotshkin, S.; Lyden, D. The secreted factors responsible for pre-metastatic niche formation: Old sayings and new thoughts. *Semin. Cancer Biol.* **2011**, *21*, 139–146.
71. Gyorgy, B.; Szabo, T.G.; Pasztoi, M.; Pal, Z.; Misjak, P.; Aradi, B.; Laszlo, V.; Pallinger, E.; Pap, E.; Kittel, A.; *et al*. Membrane vesicles, current state-of-the-art: Emerging role of extracellular vesicles. *Cell Mol. Life Sci.* **2011**, *68*, 2667–2688.

72. Guo, Y.; Feng, Y.; Trivedi, N.S.; Huang, S. Medusa structure of the gene regulatory network: Dominance of transcription factors in cancer subtype classification. *Exp. Biol. Med.* **2011**, *236*, 628–636.
73. Guo, Z.; Wu, F.; Asplund, A.; Hu, X.; Mazurenko, N.; Kisseljov, F.; Ponten, J.; Wilander, E. Analysis of intratumoral heterogeneity of chromosome 3p deletions and genetic evidence of polyclonal origin of cervical squamous carcinoma. *Mod. Pathol.* **2001**, *14*, 54–61.
74. Esteller, M. Epigenetics in cancer. *N. Engl. J. Med.* **2008**, *358*, 1148–1159.
75. Feinberg, A.P. The epigenetics of cancer etiology. *Semin. Cancer Biol.* **2004**, *14*, 427–432.
76. Diaz-Cano, S.J. Molecular mechanisms in melanoma. *N. Engl. J. Med.* **2006**, *355*, 1395–1396.
77. Fletcher, C.D.M.; Berman, J.J.; Corless, C.; Gorstein, F.; Lasota, J.; Longley, B.J.; Miettinen, M.; O'Leary, T.J.; Remotti, H.; Rubin, B.P.; *et al*. Diagnosis of gastrointestinal stromal tumors: A consensus approach. *Hum. Pathol.* **2002**, *33*, 459–465.
78. Medeiros, F.; Corless, C.L.; Duensing, A.; Hornick, J.L.; Oliveira, A.M.; Heinrich, M.C.; Fletcher, J.A.; Fletcher, C.D.M. Kit-negative gastrointestinal stromal tumors: Proof of concept and therapeutic implications. *Am. J. Surg. Pathol.* **2004**, *28*, 889–894.
79. Sakurai, S.; Hasegawa, T.; Sakuma, Y.; Takazawa, Y.; Motegi, A.; Nakajima, T.; Saito, K.; Fukayama, M.; Shimoda, T. Myxoid epithelioid gastrointestinal stromal tumor (gist) with mast cell infiltrations: A subtype of gist with mutations of platelet-derived growth factor receptor alpha gene. *Hum. Pathol.* **2004**, *35*, 1223–1230.
80. Laé, M.; Fréneaux, P.; Sastre-Garau, X.; Chouchane, O.; Sigal-Zafrani, B.; Vincent-Salomon, A. Secretory breast carcinomas with ETV6-NTRK3 fusion gene belong to the basal-like carcinoma spectrum. *Mod. Pathol.* **2009**, *22*, 291–298.
81. Makretsov, N.; He, M.; Hayes, M.; Chia, S.; Horsman, D.E.; Sorensen, P.H.B.; Huntsman, D.G. A fluorescence *in situ* hybridization study of ETV6-NTRK3 fusion gene in secretory breast carcinoma. *Genes Chromosomes Cancer* **2004**, *40*, 152–157.
82. Leeman-Neill, R.J.; Kelly, L.M.; Liu, P.; Brenner, A.V.; Little, M.P.; Bogdanova, T.I.; Evdokimova, V.N.; Hatch, M.; Zurnadzy, L.Y.; Nikiforova, M.N.; *et al*. ETV6-NTRK3 is a common chromosomal rearrangement in radiation-associated thyroid cancer. *Cancer* **2014**, *120*, 799–807.
83. Qi, M.; Li, Y.; Liu, J.; Yang, X.; Wang, L.; Zhou, Z.; Han, B. Morphologic features of carcinomas with recurrent gene fusions. *Adv. Anat. Pathol.* **2012**, *19*, 417–424.
84. Skálová, A.; Vanecek, T.; Majewska, H.; Laco, J.; Grossmann, P.; Simpson, R.H.W.; Hauer, L.; Andrle, P.; Hosticka, L.; Branžovský, J.; *et al*. Mammary analogue secretory carcinoma of salivary glands with high-grade transformation: Report of 3 cases with the ETV6-NTRK3 gene fusion and analysis of TP53, β-catenin, EGFR, and CCND1 genes. *Am. J. Surg. Pathol.* **2014**, *38*, 23–33.
85. Versteege, I.; Sévenet, N.; Lange, J.; Rousseau-Merck, M.F.; Ambros, P.; Handgretinger, R.; Aurias, A.; Delattre, O. Truncating mutations of hSNF5/INI1 in aggressive paediatric cancer. *Nature* **1998**, *394*, 203–206.
86. Chen, F.; Becker, A.J.; LoTurco, J.J. Contribution of tumor heterogeneity in a new animal model of cns tumors. *Mol. Cancer Res.* **2014**, *12*, 742–753.

87. Le Loarer, F.; Zhang, L.; Fletcher, C.D.; Ribeiro, A.; Singer, S.; Italiano, A.; Neuville, A.; Houlier, A.; Chibon, F.; Coindre, J.-M.; *et al*. Consistent smarcb1 homozygous deletions in epithelioid sarcoma and in a subset of myoepithelial carcinomas can be reliably detected by fish in archival material. *Genes Chromosomes Cancer* **2014**, *53*, 475–486.
88. Vu-Han, T.-L.; Frühwald, M.C.; Hasselblatt, M.; Kerl, K.; Nagel, I.; Obser, T.; Oyen, F.; Siebert, R.; Schneppenheim, R. Identifying molecular markers for the sensitive detection of residual atypical teratoid rhabdoid tumor cells. *Cancer Genet.* **2014**, *207*, 390–397.
89. Vu-Phan, D.; Grachtchouk, V.; Yu, J.; Colby, L.A.; Wicha, M.S.; Koenig, R.J. The thyroid cancer PAX8-PPARG fusion protein activates Wnt/TCF-responsive cells that have a transformed phenotype. *Endocr. Relat. Cancer* **2013**, *20*, 725–739.
90. Ricarte-Filho, J.C.; Li, S.; Garcia-Rendueles, M.E.R.; Montero-Conde, C.; Voza, F.; Knauf, J.A.; Heguy, A.; Viale, A.; Bogdanova, T.; Thomas, G.A.; *et al.* Identification of kinase fusion oncogenes in post-chernobyl radiation-induced thyroid cancers. *J. Clin. Investig.* **2013**, *123*, 4935–4944.
91. Mackinnon, A.C.; Yan, B.C.; Joseph, L.J.; Al-Ahmadie, H.A. Molecular biology underlying the clinical heterogeneity of prostate cancer: An update. *Arch. Pathol. Lab. Med.* **2009**, *133*, 1033–1040.
92. Mehra, R.; Han, B.; Tomlins, S.A.; Wang, L.; Menon, A.; Wasco, M.J.; Shen, R.; Montie, J.E.; Chinnaiyan, A.M.; Shah, R.B. Heterogeneity of TMPRSS2 gene rearrangements in multifocal prostate adenocarcinoma: Molecular evidence for an independent group of diseases. *Cancer Res.* **2007**, *67*, 7991–7995.
93. Fournier, G.; Valeri, A.; Mangin, P.; Cussenot, O. Prostate cancer. Epidemiology. Risk factors. Pathology. *Ann. Urol.* **2004**, *38*, 187–206.
94. Hodge, J.C.; Pearce, K.E.; Wang, X.; Wiktor, A.E.; Oliveira, A.M.; Greipp, P.T. Molecular cytogenetic analysis for TFE3 rearrangement in Xp11.2 renal cell carcinoma and alveolar soft part sarcoma: Validation and clinical experience with 75 cases. *Mod. Pathol.* **2014**, *27*, 113–127.
95. Kobos, R.; Nagai, M.; Tsuda, M.; Merl, M.Y.; Saito, T.; Laé, M.; Mo, Q.; Olshen, A.; Lianoglou, S.; Leslie, C.; *et al*. Combining integrated genomics and functional genomics to dissect the biology of a cancer-associated, aberrant transcription factor, the ASPSCR1-TFE3 fusion oncoprotein. *J. Pathol.* **2013**, *229*, 743–754.
96. Ross, H.; Argani, P. Xp11 translocation renal cell carcinoma. *Pathology* **2010**, *42*, 369–373.
97. Gulley, M.L.; Kaiser-Rogers, K.A. A rational approach to genetic testing for sarcoma. *Diagn. Mol. Pathol.* **2009**, *18*, 1–10.
98. Machado, I.; Traves, V.; Cruz, J.; Llombart, B.; Navarro, S.; Llombart-Bosch, A. Superficial small round-cell tumors with special reference to the ewing's sarcoma family of tumors and the spectrum of differential diagnosis. *Semin. Diagn. Pathol.* **2013**, *30*, 85–94.
99. Riley, R.D.; Burchill, S.A.; Abrams, K.R.; Heney, D.; Sutton, A.J.; Jones, D.R.; Lambert, P.C.; Young, B.; Wailoo, A.J.; Lewis, I.J. A systematic review of molecular and biological markers in tumours of the ewing's sarcoma family. *Eur. J. Cancer* **2003**, *39*, 19–30.
100. Mitelman, F.; Johansson, B.; Mertens, F. Fusion genes and rearranged genes as a linear function of chromosome aberrations in cancer. *Nat. Genet.* **2004**, *36*, 331–334.

101. Ramaswamy, S.; Tamayo, P.; Rifkin, R.; Mukherjee, S.; Yeang, C.H.; Angelo, M.; Ladd, C.; Reich, M.; Latulippe, E.; Mesirov, J.P.; *et al*. Multiclass cancer diagnosis using tumor gene expression signatures. *Proc. Natl. Acad. Sci. USA* **2001**, *98*, 15149–15154.
102. Tsai, Y.-S.; Lin, C.-T.; Tseng, G.C.; Chung, I.-F.; Pal, N.R. Discovery of dominant and dormant genes from expression data using a novel generalization of snr for multi-class problems. *BMC Bioinform.* **2008**, *9*, 425.
103. Golub, T.R.; Slonim, D.K.; Tamayo, P.; Huard, C.; Gaasenbeek, M.; Mesirov, J.P.; Coller, H.; Loh, M.L.; Downing, J.R.; Caligiuri, M.A.; *et al*. Molecular classification of cancer: Class discovery and class prediction by gene expression monitoring. *Science* **1999**, *286*, 531–537.
104. Perez-Diez, A.; Morgun, A.; Shulzhenko, N. Microarrays for cancer diagnosis and classification. *Adv. Exp. Med. Biol.* **2007**, *593*, 74–85.
105. Statnikov, A.; Aliferis, C.F. Are random forests better than support vector machines for microarray-based cancer classification? *AMIA Annu. Symp. Proc.* **2007**, 686–690.
106. Brownlee, N.A.; Perkins, L.A.; Stewart, W.; Jackle, B.; Pettenati, M.J.; Koty, P.P.; Iskandar, S.S.; Garvin, A.J. Recurring translocation (10;17) and deletion (14q) in clear cell sarcoma of the kidney. *Arch. Pathol. Lab. Med.* **2007**, *131*, 446–451.
107. Rakheja, D.; Weinberg, A.G.; Tomlinson, G.E.; Partridge, K.; Schneider, N.R. Translocation (10;17)(q22;p13): A recurring translocation in clear cell sarcoma of kidney. *Cancer Genet. Cytogenet.* **2004**, *154*, 175–179.
108. Meis-Kindblom, J.M. Clear cell sarcoma of tendons and aponeuroses: A historical perspective and tribute to the man behind the entity. *Adv. Anat. Pathol.* **2006**, *13*, 286–292.
109. Panagopoulos, I.; Mertens, F.; Isaksson, M.; Mandahl, N. Absence of mutations of the braf gene in malignant melanoma of soft parts (clear cell sarcoma of tendons and aponeuroses). *Cancer Genet. Cytogenet.* **2005**, *156*, 74–76.
110. Covinsky, M.; Gong, S.; Rajaram, V.; Perry, A.; Pfeifer, J. EWS-ATF1 fusion transcripts in gastrointestinal tumors previously diagnosed as malignant melanoma. *Hum. Pathol.* **2005**, *36*, 74–81.

© 2015 by the authors; licensee MDPI, Basel, Switzerland. This article is an open access article distributed under the terms and conditions of the Creative Commons Attribution license (http://creativecommons.org/licenses/by/4.0/).

Int. J. Mol. Sci. **2015**, *16*, 10636-10649; doi:10.3390/ijms160510636

OPEN ACCESS
International Journal of
Molecular Sciences
ISSN 1422-0067
www.mdpi.com/journal/ijms

Article

Frequent Epigenetic Suppression of Tumor Suppressor Gene Glutathione Peroxidase 3 by Promoter Hypermethylation and Its Clinical Implication in Clear Cell Renal Cell Carcinoma

Qianling Liu [1], Jie Jin [1], Jianming Ying [2], Mengkui Sun [1], Yun Cui [1], Lian Zhang [1], Ben Xu [1], Yu Fan [1] and Qian Zhang [1,*]

[1] Department of Urology, Peking University First Hospital and Institute of Urology, National Research Center for Genitourinary Oncology, Beijing 100034, China; E-Mails: lqlbjmu@163.com (Q.L.); jinjie@vip.163.com (J.J.); wkdsmk@163.com (M.S.); cuiyunbjmu@163.com (Y.C.); hays0324@163.com (L.Z.); xuben123457890@163.com (B.X.); dantefanbmu@126.com (Y.F.)

[2] Department of Pathology, Cancer Institute and Cancer Hospital, Peking Union Medical College (PUMC), Chinese Academy of Medical Sciences, Beijing 100021, China; E-Mail: jmying@hotmail.com

* Author to whom correspondence should be addressed; E-Mail: zhangqian@bjmu.edu.cn or zhangqianbmu@vip.sina.com; Tel.: +86-10-8357-5100.

Academic Editor: William Chi-shing Cho

Received: 28 March 2015 / Accepted: 5 May 2015 / Published: 11 May 2015

Abstract: The goal of this study is to identify novel tumor suppressor genes silenced by promoter methylation in clear cell renal cell carcinoma (ccRCC) and discover new epigenetic biomarkers for early cancer detection. Reactive oxygen species (ROS) is a major cause of DNA damage that correlates with cancer initiation and progression. Glutathione peroxidase 3 (*GPX3*), the only known extracellular glycosylated enzyme of GPXs, is a major scavenger of ROS. *GPX3* has been identified as a tumor suppressor in many cancers. However, the role of *GPX3* in ccRCC remains unclear. This study aimed to investigate its epigenetic alteration in ccRCC and possible clinicopathological association. In our study, *GPX3* methylation and down-regulation were detected in 5 out of 6 ccRCC cell lines and the *GPX3* mRNA and protein expression level in ccRCC tumors was significantly lower than in adjacent non-malignant renal tissues ($p < 0.0001$). Treatment with 5-Aza-2'-deoxycytidine restored *GPX3* expression in ccRCC cells. Aberrant methylation was further detected in 77.1% (162/210) of RCC primary tumors, but only 14.6% (7/48) in adjacent non-malignant

renal tissues. *GPX3* methylation status was significantly associated with higher tumor nuclear grade ($p = 0.014$). Thus, our results showing frequent *GPX3* inactivation by promoter hypermethylation in ccRCC may reveal the failure in the cellular antioxidant system in ccRCC and may be associated with renal tumorigenesis. *GPX3* tumor specific methylation may serve as a biomarker for early detection and prognosis prediction of ccRCC.

Keywords: *GPX3*; reactive oxygen species; methylation; tumor suppress gene; clear cell renal cell carcinoma

1. Introduction

Clear cell Renal cell carcinoma (ccRCC) is the most lethal type of urological cancer due to its occult onset and resistance to chemotherapy and radiation. Although radical nephrectomy is effective to cure local and early ccRCCs, 30% of patients develop metastases after surgery [1]. Therefore, novel, specific biomarkers for early tumor detection and anti-tumor agents are urgently required.

It is well recognized that inactivation of tumor suppressor genes (TSGs) may lead to neoplastic changes. TSGs can be inactivated by both genetic and epigenetic mechanisms, such as point mutation, LOH, and promoter hypermethylation. Recently, multiple TSGs associated with promoter hypermethylation have been identified in ccRCC, such as *VHL*, *p16*, *RASSF1A*, *SPINT2* and *HOXB13* [2–5]. Our group has also identified some TSGs silenced by promoter methylation in ccRCC, including *DLC1*, *DLEC1* and *IRF8* [6–8]. These findings provide a new insight to probe the molecular mechanisms of ccRCC and to seek potential diagnostic and therapeutic target for ccRCC. However, most of these known TSGs have a relatively low frequency of methylation in ccRCC. Thus, further studies are needed to identify novel and specific methylation-sensitive tumor suppressor genes in ccRCC.

Increased reactive oxygen species（ROS）levels have been found in a broad range of tumor tissues (e.g., lung, breast, esophagus and liver) [9], indicating a role for ROS as a common cause of human cancers. Under normal circumstances, ROS play a role in signal transduction. However, accumulation of excess cellular ROS has been reported to induce increased DNA mutations that have been associated with increased carcinogenesis [10].

Normal cells have integrated antioxidative systems that protect cells from ROS-induced DNA damage and cell injury. Among these systems, the glutathione peroxidase family (GPXs) is a major antioxidative enzyme family that promotes the reduction of lipid peroxides, hydrogen peroxide and organic hydroperoxide by reduced glutathione [11]. *GPX3*, located on chromosome 5q32, is the only known extracellular glycosylated enzyme of GPXs that can use thioredoxin, glutaredoxin and glutathione as electron donors, to reduce a wide range of hydroperoxides [12,13]. It is a major scavenger of ROS produced during normal metabolism or after oxidative insult. *GPX3* mRNA is expressed in a variety of normal human tissues, including kidney, liver, breast, heart, lung, brain, and gastrointestinal tract, but the majority of plasma *GPX3* is kidney-derived [13,14]. Recently, downregulation of *GPX3* by promoter hypermethylation has been reported in multiple human cancers, such as prostate, gastric, esophageal, cervical, and bladder cancer [15–17], suggesting that *GPX3* serves as a tumor suppressor in these cancers. However, the role and the clinical implication of *GPX3* in ccRCC remain unclear.

In this study, we examined *GPX3* expression and promoter methylation status in ccRCC cell lines and primary tumors, analyzed the relationship between its methylation and clinicopathological features in patients with RCC.

2. Results

2.1. Methylation of the GPX3 Promoter Correlates with Its Downregulation in ccRCC Cell Lines

By Real-Time PCR, we detected for the first time that *GPX3* mRNA expression was downregulated in five out of six (83.3%) ccRCC cell lines compared with "normal" human embryonic kidney cell line (Hek293) and "normal" human proximal tubular cell line (HK-2) (Figure 1A). The region spanning the assumed promoter and exon 1 of *GPX3* is a typical CpG island and, thus, susceptible to epigenetic silencing. Therefore, we next explored the role of promoter methylation in silencing *GPX3* by methylation-specific PCR. Full or partial methylation was detected in five renal cancer cell lines (786-0, Caki-1, Osrc-2, Kert-3 and 769P), which showed downregulated *GPX3* expression, whereas only weak or no methylation was detected in the cell lines (Hek293 and HK-2) with *GPX3* expression (Figure 1A). To confirm MSP results, BGS was performed to identify methylation status of 14 CpG sites within the *GPX3* promoter. The bisulfite genomic sequencing results were consistent with those of methylation specific PCR in which high density methylated alleles were detected in *GPX3* downregulated 786-0, Caki-1, Kert-3 and Osrc-2 cell lines, while more unmethylated alleles were detected in Hek293 cell line and HK-2cell line (Figure 1B). These results indicated that promoter methylation was associated with the downregulation of *GPX3* in ccRCC cell lines.

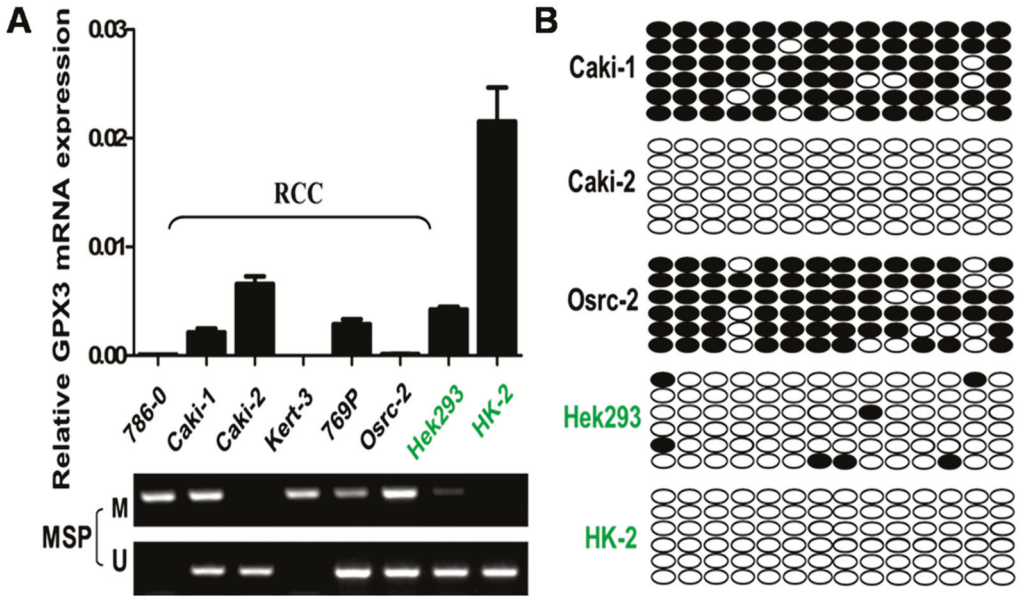

Figure 1. *GPX3* downregulation by promoter hypermethylation in ccRCC cell lines. (**A**) Detection of *GPX3* mRNA expression and methylation in a panel of ccRCC, Hek293, and HK-2 cell lines by real time RT-PCR and MSP. *M*, methylated. *U*, unmethylated; (**B**) Representative methylation analysis of individual CpG sites in the *GPX3* promoter by bisulfite genomic sequencing. Each row represents one bacterial clone with one circle symbolizing one CpG site. Filled ovals indicate methylated. Open ovals indicate unmethylated.

2.2. Pharmacological Demethylation Restored GPX3 Expression in ccRCC Cells

To explore whether promoter methylation directly mediates *GPX3* reduction in ccRCC, three methylated cell lines that showed downregulation of *GPX3* were treated with the DNA methyltransferase inhibitor 5-Aza-2'-deoxycytidine with or without the histone deacetylase inhibitor trichostatin A. Results showed that 5-Aza treatment could restore *GPX3* mRNA expression in ccRCC cells along with a decrease in methylated alleles, and the same results were observed in A + T treated-RCC cells (Figure 2A,B). Further detailed BGS methylation analysis for 786-0 and Osrc-2 before and after Aza treatment confirmed its demethylation (Figure 2C). To check if demethylation treatment also restored *GPX3* protein level, we performed an immunofluorescence assay, using antibody against *GPX3* in 786-0 cells. As shown in Figure 2D, there was a significant increase in the *GPX3* green immunofluorescence signal after 5-Aza and 5-Aza-TSA treatments as compared to DMSO control, suggesting that pharmacological demethylation can restore the *GPX3* protein expression in 786-0 cells. These results indicated that CpG methylation of the *GPX3* promoter directly led to its suppression in ccRCC cell lines.

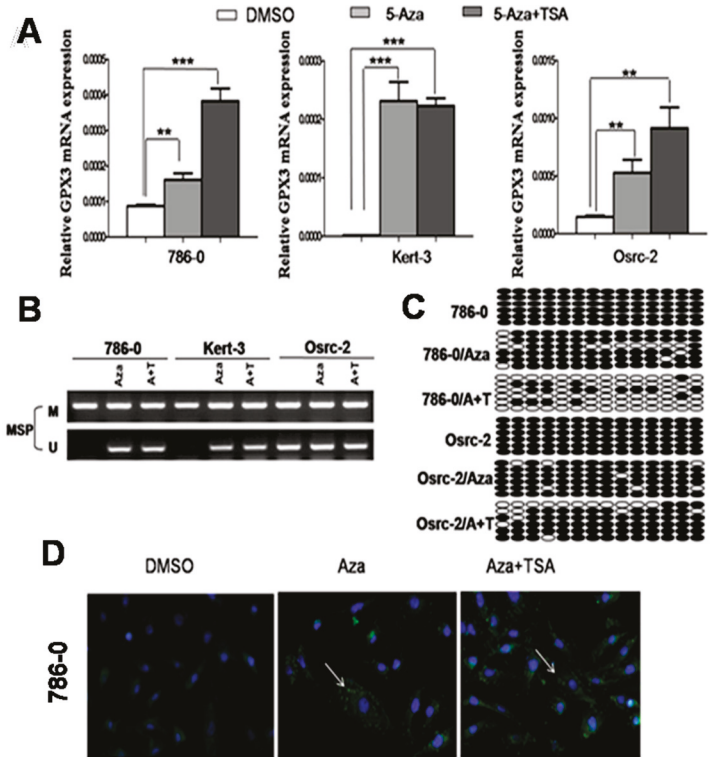

Figure 2. (**A**,**B**) Pharmalogic demethylation with 5-Aza alone or combined with trichostatin A (A + T) restored *GPX3* mRNA expression and induced its demethyation in ccRCC cell lines. ** $p < 0.01$; and *** $p < 0.001$; (**C**) BGS analysis of Aza and A + T treated 786-O and Osrc-2 ccRCC cells. Each row represents one bacterial clone with one circle symbolizing one CpG site. Filled ovals indicate methylated. Open ovals indicate unmethylated; (**D**) Immunofluorescence staining of *GPX3* protein in 786-O cells. Pharmalogic demethylation with 5-Aza alone or combined with trichostatin A (A + T) restored *GPX3* protein expression in 786-O cells. Green pellet in the cytoplasm represents positive staining (indicated by arrows).

2.3. GPX3 mRNA and Protein Expression Was Frequently Downregulated or Silenced in Primary ccRCC Tumor Tissues

We investigated mRNA expression of *GPX3* in 76 paired ccRCC tumor tissues and their adjacent non-tumor tissues using quantitative Real-Time PCR. As shown in Figure 3A, *GPX3* was significantly downregulated in renal tumors compared with their adjacent non-tumor tissues ($p < 0.0001$). We revealed consistently low levels of *GPX3* mRNA expression in 94.74% (72 of 76) of ccRCC samples. Moreover, there was a dramatic reduction in levels of *GPX3* in 40.79% (31/76) of the cases, with a 20-fold reduction compared with the normal samples (Figure 3A). Inhibition of *GPX3* in ccRCC was further confirmed at protein level by using immunohistochemical staining. We examined *GPX3* protein expression in 54 ccRCCs and paired adjacent non-tumor tissues. In adjacent non-tumor tissues, intense immunostaining for *GPX3* was observed in a cytoplasmic distribution (Figure 3B), whereas absent/weak immunostaining was detected in the cytoplasm of tumor tissues (Figure 3B). Out of 54 ccRCC tumor tissues, *GPX3* protein was negative in five (9.3%), weakly positive in 24 (44.4%), moderately positive in 17 (31.5%), and strongly positive in eight (14.8%) (Figure 3C). In contrast, out of 54 adjacent non-tumor tissues, *GPX3* protein was negative in 0, weakly positive in five (9.3%), moderately positive in 23 (42.6%), and strongly positive in 26 (48.1%) (Figure 3C). As shown in Figure 3C, statistical analysis of the immunohistochemical results revealed that protein expression of *GPX3* in ccRCC tumor tissues was significantly lower than in adjacent non-tumor tissues ($p < 0.0001$).

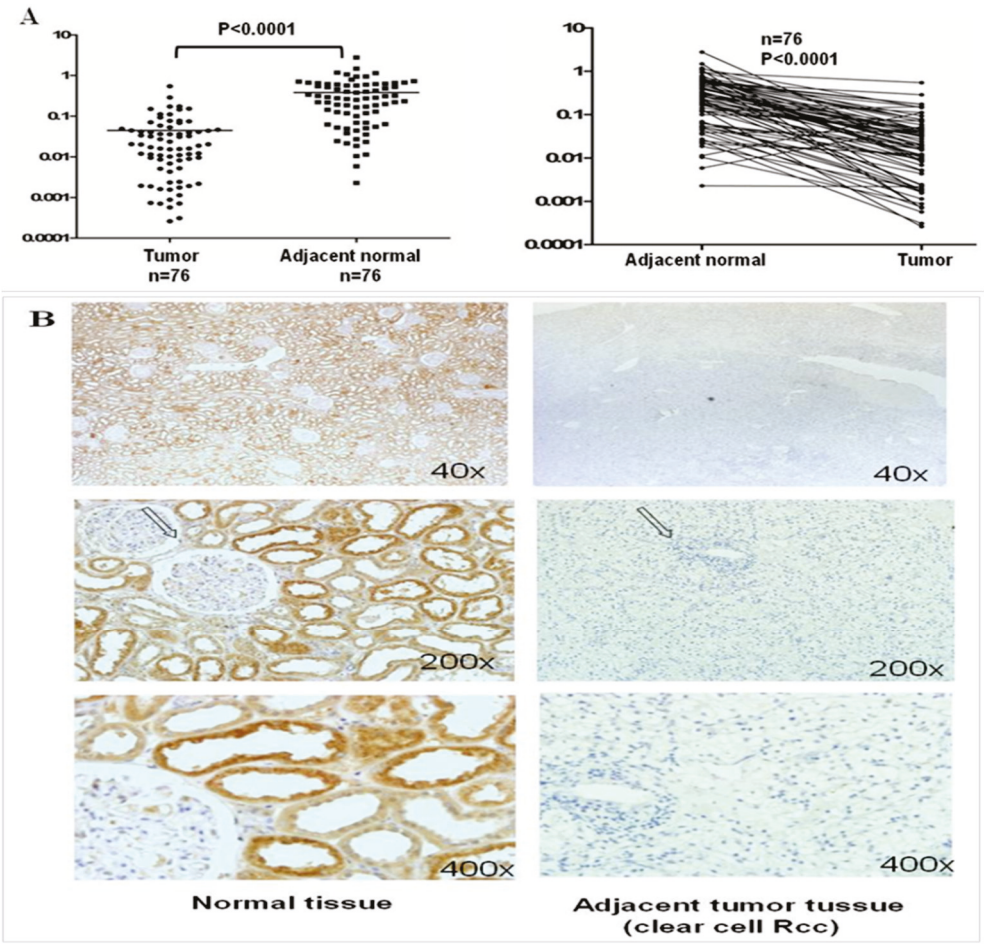

Figure 3. *Cont.*

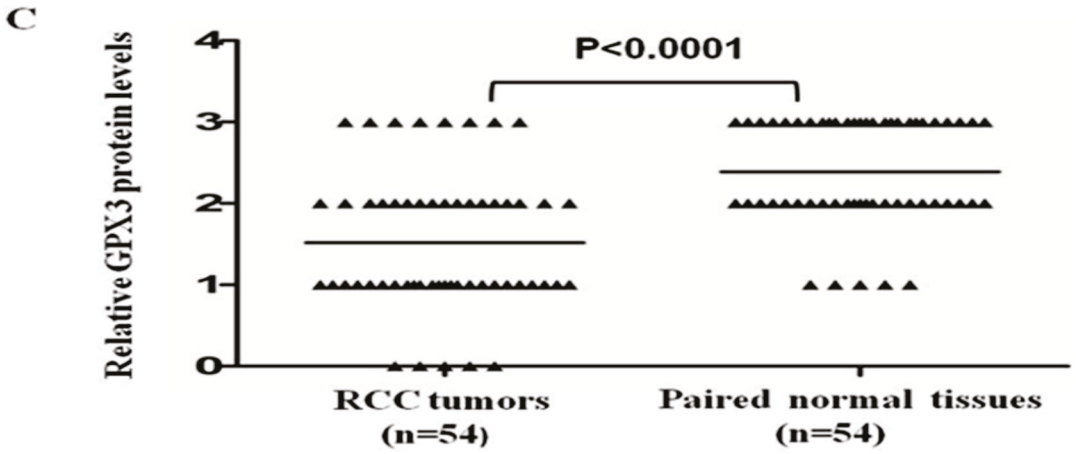

Figure 3. Expression pattern of *GPX3* in ccRCC. (**A**) Seventy-six paired ccRCC samples and adjacent non-tumor tissues were analyzed by real time RT-PCR for *GPX3* mRNA expression, which was significantly downregulated in ccRCC tumors as compared to adjacent non-tumor samples ($p < 0.0001$); (**B**) Representative immunohistochemical staining of a pair of ccRCC specimens and corresponding non-tumor tissue. In adjacent non-tumor tissues, intense immunostaining for *GPX3* was detected in a cytoplasmic distribution, whereas absent/weak immunostaining was observed in the cytoplasm of tumor tissues; The place of pictures taken in 400× was indicated by arrows; (**C**) Evaluation and statistical analysis of *GPX3* protein expression in 54 paired ccRCC samples and adjacent non-tumor tissues. *GPX3* protein expression was significantly downregulated in ccRCC samples compared to adjacent non-tumor tissues ($p < 0.0001$).

2.4. Frequent GPX3 Promoter Methylation in Primary RCC Tumors Is Associated with Poor Prognosis

We further examined *GPX3* methylation status in primary RCC samples and their adjacent non-tumor tissues. Results showed that *GPX3* methylation was detected in 77.1% (162/210) of RCC tumors, but only 14.6% (7/48) in adjacent non-malignant renal tissues, suggesting tumor-specific methylation of *GPX3* in RCC. Representative methylation status of *GPX3* in RCC primary tumors (T) and paired adjacent non-tumor tissues (N) are shown in Figure 4A. MSP results were confirmed by bisulfite genomic sequencing (Figure 4B). We also analyzed the correlation between *GPX3* methylation and clinicopathological features of patients with RCC. As shown in Table 1, *GPX3* methylation was significantly associated with higher tumor nuclear grade of RCC ($p = 0.014$), whereas no significant correlation was found between its methylation and gender, age, tumor location, TNM stage and histological type. In addition, our study also showed an increased percentage of GPX3 methylation in Stage 2 or higher tumors compared with Stage 1 patients (although this was not statistically significant). Collectively, these data indicate that *GPX3* methylation is a frequent event in pathogenesis of RCC and is associated with patient poor prognosis.

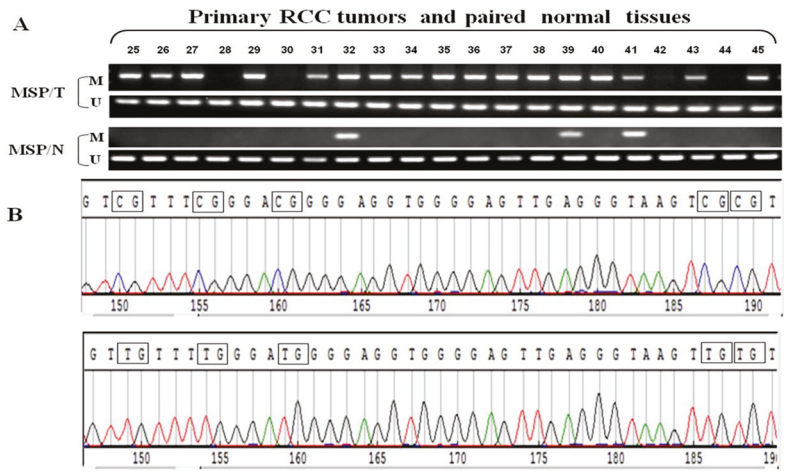

Figure 4. (**A**) Representative MSP results of *GPX3* methylation in RCC primary tumors (T) and paired adjacent non-tumor tissues (N). *M*, methylated; *U*, unmethylated; (**B**) Representative bisulfite genomic sequencing results of cloned BGS-PCR products. Methylated CpG sites will appear as CG during sequencing, while unmethylated CpG sites as TG.

Table 1. Association between GPX3 methylation and clinicopathological features of patients with RCC.

Clinicopathological Features	Number (n = 210)	GPX3 Methylation Status	p Value
		Methylated Unmethylated	
Overall	210	162 (77.1) 48 (22.9)	
Gender			
M	146	112 (76.7) 34 (23.3)	0.860
F	64	50 (78.1) 14 (21.9)	(Fisher's exact test)
Age			
<60 (median)	109	84 (77.1) 25 (22.9)	1.000
⩾60	101	78 (77.2) 23 (22.8)	(Fisher's exact test)
Side			
Rt	113	82 (72.6) 31 (27.4)	0.088
Lt	97	80 (82.5) 17 (17.5)	(Fisher's exact test)
TNM Classification			
pT1a	79	56 (70.9) 23 (29.1)	0.206
pT1b	72	60 (83.3) 12 (16.7)	(chi-square test)
pT2	17	15 (83.3) 2 (16.7)	
pT3	42	32 (76.2) 10 (23.8)	
Nuclear Grade			
G1	48	30 (62.5) 18 (37.5)	0.014 *
G2	135	108 (80.0) 27 (20.0)	(chi-square test)
G3	27	24 (88.9) 3 (11.1)	
Histological Type			
Clear cell Rcc	193	150 (77.7) 43 (23.3)	0.734
papillary Rcc	9	6 (66.7) 3 (33.3)	(chi-square test)
chromophobe Rcc	8	6 (75.0) 2 (25.0)	

* Significant difference.

3. Discussion

Recent studies have shown increased evidences demonstrating that reactive oxygen species (ROS) are a major cause of DNA damage that correlate with a wide range of human diseases including cancer. For instance, carcinoma cells utilize ROS to stimulate their proliferation, angiogenesis, migration, and escape of apoptotic mechanism [18]. In addition, ROS promote the motility and invasion of carcinoma cells by activating protein kinase-C (PKC) and the ERK/MAPK signaling pathways, thus increasing the risk of metastasis [19,20].

The glutathione peroxidases, a family of oxidation-reduction enzymes, play central roles in balancing the signaling, immunomodulatory and detrimental effects of ROS. *GPX3*, also named plasma glutathione peroxidase, is the only known selenocysteine-containing extracellular form of GPXs and accounts for nearly all of the glutathione peroxidase activity in plasma [21]. This peculiar feature makes *GPX3* an extremely important part, not only in GPXs family, but also among cellular antioxidant system, serving as a first line of defense against ROS prior to their entry into the cell.

GPX3 mRNA is expressed in a wide range of normal human tissues, however, downregulation of *GPX3* has been found in multiple human cancers, such as prostate, gastric, esophageal, cervical, and bladder cancer [15–17], suggesting its importance in human tumorigenesis. Yu, *et al.* reported that *GPX3* suppression in prostate cancer correlates with increased incidence of lymph node metastasis and poor clinical prognosis. Overexpression of *GPX3* in prostate cancer cell lines seemed to restrain tumor growth and metastasis through downregulation of c-met, a receptor tyrosine tumor transforming gene involved in a variety of cellular processes [17,22,23]. In addition, *GPX3* was found to increase apoptotic cell death by interacting directly with p53-induced gene 3 (*PIG3*) both *in vivo* and *in vitro* [24], suggesting a novel signaling pathway of *GPX3*-*PIG3* in the regulation of cell death in prostate cancer. Recently, a study in colitis-associated carcinoma reported that *GPX3*-deficient mice exhibited increased inflammation with redistribution towards pro-tumorigenic M2 macrophage subsets, increased proliferation, hyperactive WNT signaling, and increased DNA damage [25]. Knockdown of *GPX3* in the human colon cancer cell line Caco2 resulted in increased ROS production and DNA damage. These data supports a tumor suppressor role for *GPX3* via clearance of ROS and DNA damage that lead to tumor initiation and progression.

Plasma *GPX3* is mainly derived from kidney; however, in our study we found that expression of *GPX3* was significantly downregulated in primary renal tumors compared with their adjacent non-tumor tissues ($p < 0.0001$). This finding indicate that the function of *GPX3* is impaired in ccRCC, a consequence of which is likely to be an increased amount of ROS, which would induce DNA damage, driving the carcinogenic process of ccRCC.

As an alternative to genetic changes, hypermethylation of CpG rich promoter regions leading to consequent downregulation or silencing of TSGs is now recognized as an important mechanism for cancer initiation and progression. In addition to its biological relevance to malignant transformation, DNA methylation is one of the most promising biomarkers for early detection and prognosis assessments of human cancers. Recently, studies have shown a great number of aberrantly methylated TSGs in ccRCC. However, the frequencies of aberrant methylation of most classical TSGs, such as *VHL*, *p16*, *APC*, and *CDH1*, are less than 30% in ccRCC [2], indicating that these genes are probably not the major epigenetic targets for methylation silencing in ccRCC.

Downregulation of *GPX3* expression by promoter hypermethylation has been reported in 71.4% of esophageal squamous cell carcinoma, 83% of gastric cancer and 90% of prostate cancer [17,26,27], indicating its possible suppression by epigenetic change in ccRCC. To check this hypothesis, three methylated ccRCC cell lines that showed *GPX3* inactivation were treated with the hypomethylating agents. Consistent with our research expectations, *GPX3* expression was restored by demethylation treatment, suggesting that promoter methylation of *GPX3* directly led to its suppression in ccRCC cell lines. In addition, the combine treatment with TSA exerted additional stimulatory effect on GPX3 mRNA expression, suggesting that histone acetylation may also play some roles in the regulation of GPX3 in RCC. *GPX3* methylation was further detected in 77.1% (162/210) of RCC tumors, but only 14.6% (7/48) of adjacent non-malignant renal tissues, indicating that *GPX3* methylation is a tumor-specific event involved in tumorigenesis of RCC. Of note, we observed promoter hypermethylation and downregulation of *GPX3* in a small number of tumor-adjacent "normal" renal tissues. These tumor-adjacent "normal" samples, although histologically normal, they usually have some degree of changes at the molecular level. Therefore, our data suggest that promoter hypermethylation and *GPX3* suppression is possibly an early event in renal tumorigenesis. Moreover, *GPX3* hypermethylation was associated with higher nuclear grade, indicating its potential role as prognostic predictor of RCC. Similar results were noted for prostate cancer [27].

In summary, our results showing frequent *GPX3* inactivation by promoter hypermethylation in ccRCC may reveal the failure in the cellular antioxidant system, which is the first line of defense against detrimental ROS activity. In addition, this study provides new clinical implications of *GPX3* expression inactivation and promoter hypermethylation in ccRCC. First, as a tumor suppressor gene related to higher nuclear grade, *GPX3* suppression may have a negative influence on patients' clinical outcome, and detection of *GPX3* methylation may provide prognostic information on ccRCC, especially when TSG hypermethylation can be detected in patients' serum and urine samples, just like *RASSF1A*, tissue inhibitor of metalloproteinase-3 and *CDH1* methylation [28]. Second, *GPX3* may serve as a potential target for clinical intervention. Gene targeting therapy to enhance *GPX3* activity might be helpful in the prevention or treatment of ccRCC. *GPX3* expression is selenium dependent, since the existence of an opal stop codon in the mid section of the *GPX3* open reading frame, and thus selenium supplements in cancer treatment may augment expression of *GPX3* and could hold promise in suppressing tumor growth. Of course, further studies are urgently required to explore the functions of *GPX3* in renal tumorigenesis.

4. Experimental Section

4.1. Patients and Tissue Samples

All human primary RCCs and adjacent nonmalignant renal tissue were obtained from the urology department of Peking University First Hospital, Beijing, China, with patients' consent according to the university policy. All cases were collected from primary surgical resection with no prior history of RCC and adjuvant therapy. Pathological diagnosis was done and confirmed at the pathology department, Institute of Urology, Peking University First Hospital. The histopathology of tumors was classified by 2002 AJCC TNM stage and Fuhrman nuclear grade.

4.2. Cell Culture

Six RCC cell lines (786-O, Caki-1, CaKi-2, Kert-3, 769P and Osrc-2) were obtained from Cancer Research Institute of Beijing, Beijing University, China. Hek293 (a "normal" human embryonic kidney cell line) and HK-2 (a "normal" human proximal tubular cell line), which serve as the control cell lines for RCC, were purchased from American Type Culture Collection. They were routinely cultured in RPMI 1640 or DMEM medium supplemented with 10% fetal bovine serum (GIBCO Invitrogen, Carlsbad, CA, USA) and incubated in 5% CO_2 at 37 °C.

4.3. Drug Treatment

For 5-Aza-2'-deoxycytidine (Sigma, St. Louis, MO, USA) and Trichostatin A (TSA) (Sigma St. Louis, MO, USA) treatment, cell lines were grown in a 6-well plate and treated with 10 μM 5-Aza-2'-deoxycytidine for 72 h and subsequently with or without 100 nM trichostatin A for 24 h, as described previously [29]. Controlled cells were treated with an equivalent concentration of dimethyl sulfoxide.

4.4. Quantitative Real-Time PCR

Real-time PCR reactions were performed using GoTaq(R) qPCR Master Mix (Promega Biotech, Madison, WI, USA) according to the manufacturer's protocol on 7500 Fast Real-Time PCR System (ABI). The primers and PCR conditions are shown in Table 2. GAPDH was used as the housekeeping gene for loading control.

Table 2. Primer sequences used in this study.

Gene	Primer Sequence (5'-3')	Anneal. Temp. (°C)	No. of Cycles
Real Time			
GPX3 F	CTTCCTACCCTCAAGTATGTCCG	55	45
GPX3 R	GAGGTGGGAGGACAGGAGTTCTT		
GAPDH F	GGTGGTCTCCTCTGACTTCAACA	55	45
GAPDH R	GTTGCTGTAGCCAAATTCGTTGT		
MSP			
GPX3 m1	TATGTTATTGTCGTTTCGGGAC	59	40
GPX3 m2	GTCCGTCTAAAATATCCGACG		
GPX3 U1	TTTATGTTATTGTTGTTTTGGGATG	59	40
GPX3 U2	ATCCATCTAAAATATCCAACACTCC		
BGS			
GPX3 BGS F	GGAGTTAAAAGAGGAAGGG	58	40
GPX3 BGS R	CCCAACCACCTTTCAAAC		

4.5. Immunohistochemistry

Fifty-four paraffin-embedded tumor tissues and paired adjacent non-tumor tissues were analyzed using immunohistochemical Staining. Briefly, the sections were deparaffinized in xylene and rehydrated by transfer through graded concentrations of ethanol to distilled water, and endogenous peroxidase activity was blocked by incubation with 3% H_2O_2 for 15 min at room temperature. Then, sections were

submitted to antigen retrieval in a microwave (sodium citrate buffer, pH 6.0) for 10 min, naturally refrigerated to room temperature. Blocking was performed with 10% goat serum for 30 min at room temperature. All sections were incubated with mouse anti-*GPX3* monoclonal antibody (Clone 23B1, 1:100, Abcam, Cambridge, MA, USA), overnight at 4 °C, and then incubated with goat anti-mouse secondary antibody for 30 min at room temperature. After rinsing three times in PBS for 5 min each, the sections were incubated with DAB for 2 min, counterstained with hematoxylin for 3 min, dehydrated with gradient alcohol and transparentized with dimethylbenzene. Immunohistochemical expression of *GPX3* was examined via light microscopy. Tissues were graded on the following scale: 0, negative; 1, weakly positive; 2, moderately positive; 3, strongly positive.

4.6. Immunofluorescence

To check *GPX3* protein expression after demethylation treatment, we performed immunofluorescence staining against *GPX3* in 786-0. Cells were fixed with 4% paraformaldehyde for 15 min, followed by permeabilization with 0.1% Triton X-100 for 5 min. Then, after washing with PBS, the cells were blocked with goat serum for 30 min. For immunofluorescence, Cells were incubated with primary antibody against *GPX3* overnight at 4 °C followed by secondary goat anti-mouse antibody conjugated with FITC (1:200 dilution; Invitrogen, Carlsbad, CA, USA) at room temperature for 45 min. The nuclei were counterstained with DAPI (1 μg/mL; Roche, Indianapolis, IN, USA) and viewed under a fluorescence microscope.

4.7. Bisulfite Treatment and Methylation-Specific PCR

The bisulfite modification of purified genomic DNA was performed using an EpiTect Bisulfite Kit (Qiagen 59104, Hilden, Germany) following the manufacturer's instructions. Table 2 lists MSP primers and PCR conditions. MSP primers were examined previously for not amplifying any unbisulfited DNA and MSP products of several ccRCC cell lines were confirmed by direct sequencing, indicating that our MSP system was specific.

4.8. Bisulfite Genomic Sequencing

Bisulfite-treated DNA was amplified with primers specific for a fragment of the *GPX3* promoter CpG islands that contained 14 CpG sites. Table 2 lists BGS primers and PCR conditions. The PCR products were subcloned into the pEasy-T5 vector (Transgene, Beijing, China) and 5–8 colonies were randomly chosen and sequenced.

4.9. Statistical Analysis

Statistical analyses were tested using the 2-tailed *t*-test, Fisher exact test or chi-square test with $p < 0.05$ considered significant.

5. Conclusions

To our knowledge, we report for the first time that *GPX3* is frequently downregulated in renal tumors compared with their adjacent non-tumor tissues, indicating its role as a tumor suppressor.

Aberrant methylation was an important reason for the suppression of *GPX3* and may be associated with renal tumorigenesis. *GPX3* tumor specific methylation may serve as a potential biomarker for early detection and prognosis prediction of RCC, especially when *GPX3* hypermethylation can be detected in patients' serum and urine samples.

Acknowledgments

This study was supported by grants from National Natural Science Foundation (No. 81272290).

Author Contributions

Qianling Liu carried out the design of this research, analysis and interpretation of data, and drafted the original manuscript. Ben Xu and Yu Fan participated in the collection of data. Mengkui Sun and Yun Cui assisted in the tumor specimen acquisition. Jianming Ying and Lian Zhang assisted in the detailed materials and methods of this trial. Qian Zhang and Jie Jin conceived the study, reviewed all of the statistical analysis of the data, and revised the manuscript. All authors read and approved the final manuscript.

Abbreviations

Aza, 5-Aza-2'-deoxycytidine; BGS, bisulfite genomic sequencing; GPX3, glutathione peroxidase 3; LOH, loss of heterozygosity; MSP, methylation- specific PCR; PCR, polymerase chain reaction; RCC, renal cell carcinoma; ROS, reactive oxygen species; TSA, trichostatin A; TSG, tumor suppressor gene.

Conflicts of Interest

The authors declare no conflict of interest.

References

1. Thillai, K.; Allan, S.; Powles, T.; Rudman, S.; Chowdhury, S. Neoadjuvant and adjuvant treatment of renal cell carcinoma. *Expert Rev. Anticancer Ther.* **2012**, *12*, 765–776.
2. Sanz-Casla, M.T.; Maestro, M.L.; Del, B.V.; Zanna, I.; Moreno, J.; Vidaurreta, M.; Almansa, I.; Fernandez, C.; Blanco, J.; Maestro, C.; *et al*. Loss of heterozygosity and methylation of p16 in renal cell carcinoma. *Urol. Res.* **2003**, *31*, 159–162.
3. Morris, M.R.; Gentle, D.; Abdulrahman, M.; Maina, E.N.; Gupta, K.; Banks, R.E.; Wiesener, M.S.; Kishida, T.; Yao, M.; Teh, B.; *et al*. Tumor suppressor activity and epigenetic inactivation of hepatocyte growth factor activator inhibitor type 2/SPINT2 in papillary and clear cell renal cell carcinoma. *Cancer Res.* **2005**, *65*, 4598–4606.
4. Morrissey, C.; Martinez, A.; Zatyka, M.; Agathanggelou, A.; Honorio, S.; Astuti, D.; Morgan, N.V.; Moch, H.; Richards, F.M.; Kishida, T.; *et al*. Epigenetic inactivation of the RASSF1A 3p21.3 tumor suppressor gene in both clear cell and papillary renal cell carcinoma. *Cancer Res.* **2001**, *61*, 7277–7281.

5. Morris, M.R.; Ricketts, C.J.; Gentle, D.; McRonald, F.; Carli, N.; Khalili, H.; Brown, M.; Kishida, T.; Yao, M.; Banks, R.E.; *et al*. Genome-wide methylation analysis identifies epigenetically inactivated candidate tumour suppressor genes in renal cell carcinoma. *Oncogene* **2011**, *30*, 1390–1401.
6. Zhang, Q.; Ying, J.; Zhang, K.; Li, H.; Ng, K.M.; Zhao, Y.; He, Q.; Yang, X.; Xin, D.; Liao, S.K.; *et al*. Aberrant methylation of the 8p22 tumor suppressor gene DLC1 in renal cell carcinoma. *Cancer Lett.* **2007**, *249*, 220–226.
7. Zhang, Q.; Ying, J.; Li, J.; Fan, Y.; Poon, F.F.; Ng, K.M.; Tao, Q.; Jin, J. Aberrant promoter methylation of DLEC1, a critical 3p22 tumor suppressor for renal cell carcinoma, is associated with more advanced tumor stage. *J. Urol.* **2010**, *184*, 731–737.
8. Zhang, Q.; Zhang, L.; Li, L.; Wang, Z.; Ying, J.; Fan, Y.; Xu, B.; Wang, L.; Liu, Q.; Chen, G.; *et al*. Interferon regulatory factor 8 functions as a tumor suppressor in renal cell carcinoma and its promoter methylation is associated with patient poor prognosis. *Cancer Lett.* **2014**, *354*, 227–234.
9. Malins, D.C.; Polissar, N.L.; Gunselman, S.J. Progression of human breast cancers to the metastatic state is linked to hydroxyl radical-induced DNA damage. *Proc. Natl. Acad. Sci. USA* **1996**, *93*, 2557–2563.
10. Waris, G.; Ahsan, H. Reactive oxygen species: Role in the development of cancer and various chronic conditions. *J. Carcinog.* **2006**, *5*, 14.
11. Takebe, G.; Yarimizu, J.; Saito, Y.; Hayashi, T.; Nakamura, H.; Yodoi, J.; Nagasawa, S.; Takahashi, K. A comparative study on the hydroperoxide and thiol specificity of the glutathione peroxidase family and selenoprotein P. *J. Biol. Chem.* **2002**, *277*, 41254–41258.
12. Bjornstedt, M.; Xue, J.; Huang, W.; Akesson, B.; Holmgren, A. The thioredoxin and glutaredoxin systems are efficient electron donors to human plasma glutathione peroxidase. *J. Biol. Chem*. **1994**, *269*, 29382–29384.
13. Tham, D.M.; Whitin, J.C.; Kim, K.K.; Zhu, S.X.; Cohen, H.J. Expression of extracellular glutathione peroxidase in human and mouse gastrointestinal tract. *Am. J. Physiol.* **1998**, *275*, G1463–G1471.
14. Chu, F.F.; Esworthy, R.S.; Doroshow, J.H.; Doan, K.; Liu, X.F. Expression of plasma glutathione peroxidase in human liver in addition to kidney, heart, lung, and breast in humans and rodents, *Blood* **1992**, *79*, 3233–3238.
15. Chen, B.; Rao, X.; House, M.G.; Nephew, K.P.; Cullen, K.J.; Guo, Z. GPx3 promoter hypermethylation is a frequent event in human cancer and is associated with tumorigenesis and chemotherapy response. *Cancer Lett.* **2011**, *309*, 37–45.
16. Lee, O.J.; Schneider-Stock, R.; McChesney, P.A.; Kuester, D.; Roessner, A.; Vieth, M.; Moskaluk, C.A.; El-Rifai, W. Hypermethylation and loss of expression of glutathione peroxidase-3 in Barrett's tumorigenesis. *Neoplasia* **2005**, *7*, 854–861.
17. Yu, Y.P.; Yu, G.; Tseng, G.; Cieply, K.; Nelson, J.; Defrances, M.; Zarnegar, R.; Michalopoulos, G.; Luo, J.H. Glutathione peroxidase 3, deleted or methylated in prostate cancer, suppresses prostate cancer growth and metastasis. *Cancer Res.* **2007**, *67*, 8043–8050.
18. Storz, P. Reactive oxygen species in tumor progression. *Front. Biosci*. **2005**, *10*, 1881–1896.
19. Lo, I.C.; Shih, J.M.; Jiang, M.J. Reactive oxygen species and ERK 1/2 mediate monocyte chemotactic protein-1-stimulated smooth muscle cell migration. *J. Biomed. Sci.* **2005**, *12*, 377–388.

20. Wu, W.S. The signaling mechanism of ROS in tumor progression. *Cancer Metastasis Rev.* **2006**, *25*, 695–705.
21. Brigelius-Flohe, R.; Maiorino, M. Glutathione peroxidases. *Biochim. Biophys. Acta* **2013**, *1830*, 3289–3303.
22. Taulli, R.; Scuoppo, C.; Bersani, F.; Accornero, P.; Forni, P.E.; Miretti, S.; Grinza, A.; Allegra, P.; Schmitt-Ney, M.; Crepaldi, T.; *et al*. Validation of met as a therapeutic target in alveolar and embryonal rhabdomyosarcoma. *Cancer Res.* **2006**, *66*, 4742–4749.
23. Lutterbach, B.; Zeng, Q.; Davis, L.J.; Hatch, H.; Hang, G.; Kohl, N.E.; Gibbs, J.B.; Pan, B.S. Lung cancer cell lines harboring MET gene amplification are dependent on Met for growth and survival. *Cancer Res*. **2007**, *67*, 2081–2088.
24. Wang, H.; Luo, K.; Tan, L.Z.; Ren, B.G.; Gu, L.Q.; Michalopoulos, G.; Luo, J.H.; Yu, Y.P. p53-induced gene 3 mediates cell death induced by glutathione peroxidase 3. *J. Biol. Chem.* **2012**, *287*, 16890–16902.
25. Barrett, C.W.; Ning, W.; Chen, X.; Smith, J.J.; Washington, M.K.; Hill, K.E.; Coburn, L.A.; Peek, R.M.; Chaturvedi, R.; Wilson, K.T.; *et al*. Tumor suppressor function of the plasma glutathione peroxidase GPX3 in colitis-associated carcinoma. *Cancer Res.* **2013**, *73*, 1245–1255.
26. He, Y.; Wang, Y.; Li, P.; Zhu, S.; Wang, J.; Zhang, S. Identification of GPX3 epigenetically silenced by CpG methylation in human esophageal squamous cell carcinoma. *Dig. Dis. Sci.* **2011**, *56*, 681–688.
27. Peng, D.F.; Hu, T.L.; Schneider, B.G.; Chen, Z.; Xu, Z.K.; El-Rifai, W. Silencing of glutathione peroxidase 3 through DNA hypermethylation is associated with lymph node metastasis in gastric carcinomas. *PLoS ONE* **2012**, *7*, e46214.
28. Hoque, M.O.; Begum, S.; Topaloglu, O.; Jeronimo, C.; Mambo, E.; Westra, W.H.; Califano, J.A.; Sidransky, D. Quantitative detection of promoter hypermethylation of multiple genes in the tumor, urine, and serum DNA of patients with renal cancer. *Cancer Res.* **2004**, *64*, 5511–5517.
29. Ying, J.; Srivastava, G.; Hsieh, W.S.; Gao, Z.; Murray, P.; Liao, S.K.; Ambinder, R.; Tao, Q. The stress-responsive gene GADD45G is a functional tumor suppressor, with its response to environmental stresses frequently disrupted epigenetically in multiple tumors. *Clin. Cancer Res.* **2005**, *11*, 6442–6449.

© 2015 by the authors; licensee MDPI, Basel, Switzerland. This article is an open access article distributed under the terms and conditions of the Creative Commons Attribution license (http://creativecommons.org/licenses/by/4.0/).

Int. J. Mol. Sci. **2015**, *16*, 10748-10766; doi:10.3390/ijms160510748

OPEN ACCESS
International Journal of
Molecular Sciences
ISSN 1422-0067
www.mdpi.com/journal/ijms

Review

Caffeic Acid Phenethyl Ester Is a Potential Therapeutic Agent for Oral Cancer

Ying-Yu Kuo [1,2,3,†], Wai-Tim Jim [4,5,6,†], Liang-Cheng Su [1,†], Chi-Jung Chung [7], Ching-Yu Lin [1], Chieh Huo [1,8], Jen-Chih Tseng [1,3,9], Shih-Han Huang [1,8], Chih-Jen Lai [1], Bo-Chih Chen [1,3,9], Bi-Juan Wang [1,3,9], Tzu-Min Chan [10,11], Hui-Ping Lin [12], Wun-Shaing Wayne Chang [12], Chuang-Rung Chang [2] and Chih-Pin Chuu [1,13,14,15,*]

1 Institute of Cellular and System Medicine, National Health Research Institutes, Miaoli 35053, Taiwan; E-Mails: 034279@nhri.org.tw (Y.-Y.K.); liangcheng610@nhri.org.tw (L.-C.S.); cylin071@gmail.com (C.-Y.L.); s103080810@m103.nthu.edu.tw (C.H.); s100080826@m100.nthu.edu.tw (J.-C.T.); hshf7855@gmail.com (S.-H.H.); krad0127@gmail.com (C.-J.L.); s102080545@m102.nthu.edu.tw (B.-C.C.); bijuanwang1004@gmail.com (B.-J.W.)

2 Institute of Biotechnology, National Tsing Hua University, Hsinchu City 30013, Taiwan; E-Mail: crchang@life.nthu.edu.tw

3 College of Life Science, National Tsing Hua University, Hsinchu City 30013, Taiwan

4 Department of Pediatrics, Mackay Memorial Hospital, Taipei City 10449, Taiwan; E-Mail: waitim@ms1.mmh.org.tw

5 Department of Medicine, Mackay Medical College, New Taipei City 25245, Taiwan

6 Department of Early Childhood Care and Education, Mackay Junior College of Medicine, Nursing, and Management, New Taipei City 25245, Taiwan

7 Department of Health Risk Management, China Medical University, Taichung City 40402, Taiwan; E-Mail: cjchung@mail.cmu.edu.tw

8 Department of Life Sciences, National Central University, Taoyuan City 32001, Taiwan

9 Institute of Molecular and Cellular Biology, National Tsing Hua University, Hsinchu City 30013, Taiwan

10 Department of Medical Education and Research, China Medical University Beigang Hospital, Yunlin County 65152, Taiwan; E-Mail: ziv.j@yahoo.com.tw

11 Department of Medical Education and Research, Tainan Municipal An-Nan Hospital, China Medical University, Tainan City 70965, Taiwan

12 National Institute of Cancer Research, National Health Research Institutes, Miaoli 35053, Taiwan; E-Mails: diablofish@nhri.org.tw (H.-P.L.); wayne@nhri.org.tw (W.-S.W.C.)

13 Graduate Institute of Basic Medical Science and PhD Program for Aging, China Medical University, Taichung City 40402, Taiwan

14 Biotechnology Center, National Chung Hsing University, Taichung City 40227, Taiwan

[15] PhD Program in Environmental and Occupational Medicine, Kaohsiung Medical University, Kaohsiung City 80708, Taiwan

† These authors contributed equally to this work.

* Author to whom correspondence should be addressed; E-Mail: cpchuu@nhri.org.tw; Tel.: +886-37-246-166 (ext. 37300); Fax: +886-37-587-408.

Academic Editor: William Chi-shing Cho

Received: 4 March 2015 / Accepted: 6 May 2015 / Published: 12 May 2015

Abstract: Head and neck cancers, which affect 650,000 people and cause 350,000 deaths per year, is the sixth leading cancer by cancer incidence and eighth by cancer-related death worldwide. Oral cancer is the most common type of head and neck cancer. More than 90% of oral cancers are oral and oropharyngeal squamous cell carcinoma (OSCC). The overall five-year survival rate of OSCC patients is approximately 63%, which is due to the low response rate to current therapeutic drugs. In this review we discuss the possibility of using caffeic acid phenethyl ester (CAPE) as an alternative treatment for oral cancer. CAPE is a strong antioxidant extracted from honeybee hive propolis. Recent studies indicate that CAPE treatment can effectively suppress the proliferation, survival, and metastasis of oral cancer cells. CAPE treatment inhibits Akt signaling, cell cycle regulatory proteins, NF-κB function, as well as activity of matrix metalloproteinase (MMPs), epidermal growth factor receptor (EGFR), and Cyclooxygenase-2 (COX-2). Therefore, CAPE treatment induces cell cycle arrest and apoptosis in oral cancer cells. According to the evidence that aberrations in the EGFR/phosphoinositide 3-kinase (PI3K)/protein kinase B (Akt) signaling, NF-κB function, COX-2 activity, and MMPs activity are frequently found in oral cancers, and that the phosphorylation of Akt, EGFR, and COX-2 correlates to oral cancer patient survival and clinical progression, we believe that CAPE treatment will be useful for treatment of advanced oral cancer patients.

Keywords: oral cancer; caffeic acid phenethyl ester; Akt; MMP; NF-κB; cell proliferation; cell cycle arrest; apoptosis; metastasis

---

1. Introduction

Head and neck cancers include cancers evolved from the oral cavity, pharynx, larynx, paranasal sinuses and nasal cavity, and salivary glands. Head and neck cancers rank as the sixth most common cancer worldwide, affecting 650,000 people and causing 350,000 deaths per year [1,2]. Oral cancer is the most common type of head and neck cancer and caused 135,000 deaths worldwide in 2013 [3]. According to the Surveillance, Epidemiology, and End Results Program (SEER), the five-year survival

rate of oral cavity and pharynx cancer in the United States is 63%. The poor prognosis of oral and oropharyngeal squamous cell carcinoma (OSCC), which account for 90% of the oral cancers, is due to the low response rate to current therapeutic drugs [2,4].

Propolis (bee glue) is produced by honeybees through mixing the secretions of their hypopharyngeal glands with the digested product of resins collected from leaves, flowers, and tree barks, which is used to build honeybee hives [5]. Propolis protects honey bee hives against rain and is a very sticky substance that prevents insects, rodents, and robber bees from entering the hives [5]. Propolis also acts as a biocide to kill invasive bacteria, fungi, or even larvae [5]. Propolis is a natural medicine used for hundreds of years and is being sold as dietary supplements. Propolis has been reported to exhibit anti-bacterial, anti-viral, fungicidal, anti-oxidative, free radical scavenging, immuno-modulatory, and anti-cancer activities [5]. Clinical trials, animal models, and cell culture experiments indicated that treatment with propolis is beneficial in dental application [5,6], such as decreasing the dentinal hypersensitivity [7,8], defending the dental caries [6], decreasing the oral mucositis resulted from chemotherapy [9–11], fortifying the salivary gland function [12], reducing the xerostomia due to radiotherapy to salivary glands [12], preventing oral cancer [13], inhibiting plaque and having anti-inflammatory effects [14], increasing the periodontal ligament cell viability of avulsed teeth [15], stimulating wound healing in the dental pulp [16], acting as an analgesic [17], and as an antibacterial agent against oral pathogens [18–20], declining the quantity of Enterococcus faecalis in root canals [21], lessening gingivitis [22], reducing recurrent aphthous stomatitis (RAS) [23,24], protecting the oral mucosa [25], and promoting wound healing after surgeries in the oral cavity [14]. Propolis is a complex mixture of more than 300 different natural constituents including phenolic acid, terpenes, cinnamic acid, caffeic acid, aromatic aldehydes, alcohols, amino acids, fatty acids, vitamins (A, B1, B2, B3, and B7), esters, minerals, essential oils, and flavonoids (flavones, flavonols, and flavanones) [5]. The component of propolis varies according to the species of bees, the difference of geological region, and the different kinds of plants and flowers the bees collect, which makes it difficult to define the actual molecular mechanisms of the anti-cancer activity of propolis.

Caffeic acid phenethyl ester (CAPE) (Figure 1) is one of the most bioactive components extracted from honeybee hive propolis [26,27]. CAPE treatment exhibits anti-carcinogenic, anti-inflammatory, anti-viral, and immuno-modulatory properties [28]. Several recent studies indicate that CAPE treatment suppresses proliferation, survival, and invasion of human oral cancer cells. We therefore discuss the potential of using CAPE as a treatment for patients with oral cancer in this review article.

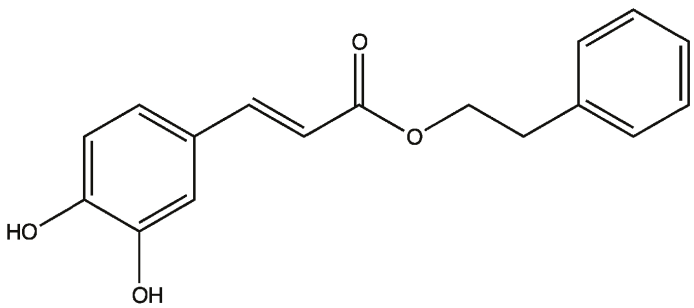

Figure 1. Structure of caffeic acid phenethyl ester (CAPE).

2. Oral Cancer

There are several types of oral cancers. The majority (>90%) of oral cancers are OSCC [2,4,29]. OSCCs arise in the oral cavity, oropharynx, larynx or hypopharynx and are characterized by poor prognosis and low survival rate [30]. The incidence and mortality rates worldwide of OSCC are approximately 5.9 and 3.3 per 100,000 persons per year, respectively [31]. Forty thousand OSCC cases were diagnosed and 8000 patients died from OSCC in the United States in 2012 [29,32]. The incidence of oral cancer is highest in Eastern and Southern Asia as well as central African countries and oral cancer accounts for 40%–50% of all malignancies in South and South-East Asian countries [33,34]. Environmental carcinogens, such as betel quid chewing, tobacco smoking, and alcohol drinking, have been identified as major risk factors for head and neck cancers [35]. According to the statistics of Taiwanese Department of Health, oral cancer ranks as the fourth most common cancer and the fifth leading cause of cancer death in Taiwanese males in 2012. The majority of oral cancer patients in Taiwan are regular users of betel quid [35]. Betal quid is a combination of betel leaf, areca nut, and slaked lime [35]. The cumulative effect of betel quid chewing, alcohol drinking, and tobacco smoking increases the risk of oral cancer up to 123-fold in Taiwanese patients [35].

3. Caffeic Acid Phenethyl Ester (CAPE) and Anticancer Effects

Caffeic acid phenethyl ester (CAPE) (Figure 1) is one of the main bioactive components extracted from honeybee hive propolis. CAPE is a strong antioxidant [26,27] and a lipophilic derivative of caffeic acid and a phenolic antioxidant structurally related to 3,4-dihydroxycinnamic acid. CAPE is a well-known NF-κB inhibitor [27]. CAPE treatment (50–80 μM) inhibits the activation of NF-κB via preventing the translocation of the p65 unit of NF-κB [27] and blocking the binding between NF-κB and DNA [27]. CAPE is an excellent anti-cancer agent. Treatment with CAPE inhibits the transformation of normal cells to cancer cells [36] as well as suppressing the proliferation of several human cancer cell lines, such as breast [37,38], prostate [39–42], lung [43,44], head and neck [45], cholangio [46], and cervical [47] cancer cells. Non-cancer human cells are much more resistant to CAPE treatment, indicating the potential selective cytotoxic effect against cancer cells of CAPE treatment [39,43,45,48]. CAPE treatment induces apoptosis or cell cycle arrest (G1 or G2/M) in different types of cancer cells [36,38,39,43,47,49–57]. CAPE treatment suppresses cancer cell movement and migration [58,59]. Oral administration or intraperitoneal (i.p.) injection of CAPE prevents cancer initiation, tumor growth, and cancer metastasis of colon, liver, and breast cancers [46,60–68] in animal models. CAPE is distributed extensively into animal tissues and is eliminated rapidly with a short half-life [69]. Intraperitoneal injection of CAPE at 10–30 mg/kg for seven days does not show toxic effects or affect the body weight of mice [65]. Additionally, CAPE treatment inhibits the proliferation of breast cancer stem cells [70]. CAPE treatments have also been shown to sensitize cancer cells to chemotherapeutic drugs and radiation treatment by inhibiting pathways that lead to treatment resistance as well as protecting important organs under chemotherapy and radiation treatments in animal models [71–81]. As CAPE exhibits very little or no toxic side effects, it is a potentially good candidate as a cancer therapeutic agent. Treatment with CAPE not only may suppress tumor growth in patients but also may protect patients from chemotherapy or radiation therapy.

4. Chemoprevention Effects of CAPE on Oral Cancer Cells

The epidermal growth factor receptor (EGFR), a receptor tyrosine kinase (RTK), is the cell-surface receptor for members of the epidermal growth factor (EGF) family. Elevated gene expression of EGFR has been reported to be associated with poor prognosis in OSCC [82,83]. Treatment with 5–30 μM CAPE dose-dependently suppresses the total abundance and phosphorylation of EGFR in breast cancer cells [37]. Cyclooxygenase (COX), including COX-1 and COX-2, is the enzyme responsible for the formation of the prostanoids. Cyclooxygenase-1 (COX-1) is present in most tissues, while Cyclooxygenase-2 (COX-2) is present at sites of inflammation. Both mRNA and protein level of COX-2 (also known as prostaglandin-endoperoxide synthase 2) are highly up-regulated in OSCC [84] and in high-risk premalignant oral lesions [85]. Up-regulation of COX-2 correlates to higher lymph node metastasis, faster cell proliferative activity, and worse survival rate in patients with oral carcinoma [86]. CAPE suppresses COX-2 activity with an IC_{50} of 6.3 nM in J774 macrophages [87]. Treatment with 35–70 μM of CAPE inhibits the activity and expression of COX-2 in human 1483 oral squamous carcinoma cells [88]. According to the facts that CAPE treatment is able to inhibit the activity and abundance of EGFR and COX-2, we believe that administration of CAPE can prevent and delay the development or progression of oral cancers.

5. Anticancer Activity Effects of CAPE on Oral Cancer Cells

TW2.6 is an OSCC cancer cell line established from the untreated primary squamous cell carcinoma of the buccal mucosa from a 48-year-old Taiwanese male patient with a betel quid chewing and tobacco smoking habit [4,89]. TW2.6 cells have morphological features of keratinocytes with a doubling time of 24 h [4,89]. CAPE treatment dose-dependently suppressed the cell proliferation and soft-agar colony formation of TW2.6 cells [4], confirming the anticancer activity of CAPE against oral cancer cells. CAPE treatment suppressed the survival and growth of several head and neck cancer cell lines. CAPE treatment suppressed the proliferation of oral submucosus fibroblast (OSF), neck metastasis of Gingiva carcinoma (GNM), tongue squamous cell carcinoma (TSCCa), oral squamous cell carcinoma (SAS) cell line, oral epidermoid carcinoma-Meng 1 (OEC-M1) cell line, and OSCC cell line TW2.6 [4,45,90] when being treated for as short as 24 h (Table 1). The SAS cell line is derived from a human squamous cell carcinoma developed from the primary lesion of a tongue carcinoma in a Japanese patient. SAS cell line has wild-type p53, high invasive potential, and high migration ability [45,91]. The OEC-M1 cell line is a human oral epidermoid carcinoma generated from the primary lesion of an oral carcinoma in a Taiwanese patient, which is a p53 mutant, resistant to retinoic acid treatment, and expresses smaller sized hypophosphorylated Rb proteins compared with normal cells [45,92]. Normal human oral fibroblast (NHOF) cells and buccal mucosal fibroblast (BF) cells were more resistant to CAPE treatment with an IC_{50} of 175 and 341 μM, respectively [45,90], (Table 1), indicating that CAPE exhibits selective suppressive effect on human oral cancer cells. The suppressive effect of CAPE accumulated over time. The IC_{50} of CAPE to suppress proliferation of TW2.6 cells was 72.1, 41.5, and 19.0 μM for 24, 48, and 96 h of treatment, respectively. Although the IC_{50} of CAPE seems to be relatively high as compared to other chemotherapy drugs, CAPE can be applied in

the form of topical cream or mouth rinsing solution. We believe that daily oral administration of CAPE for a week or longer is possible to cause regression of oral cancer cells.

Table 1. IC_{50} of CAPE for causing growth inhibition in non-malignant and cancerous human oral cell lines.

Human Oral Cell Lines	IC_{50} (μM)	Reference
Oral and oropharyngeal squamous cell carcinoma (OSCC) cell line TW2.6	72.1	[4]
Oral submucosus fibroblast (OSF)	90.6	[91]
Neck metastasis of Gingiva carcinoma (GNM)	101.0	[91]
Tongue squamous cell carcinoma (TSCCa)	120.9	[91]
Oral squamous cell carcinoma (SAS)	129.7	[45]
Oral epidermoid carcinoma-Meng 1 (OEC-M1)	159.2	[45]
Normal human oral fibroblast (NHOF)	175.0	[45]
Buccal mucosal fibroblast (BF)	341.0	[91]

5-Fluorouracil (also known as 5-FU) is a chemotherapy agent widely used for treating advanced head and neck cancer. 5-fluorouracil suppresses cancer cells by misincorporating fluoronucleotides into RNA and DNA as well as by inhibiting the nucleotide synthetic enzyme thymidylate synthase [93]. However, common undesired side effects of 5-fluorouracil include diarrhea, nausea, vomiting, mouth sores, poor appetite, watery eyes, photophobia, taste changes, metallic taste in mouth during infusion, and low blood counts. Co-treating TW2.6 cells with CAPE and 5-fluorouracil exhibited additive cell proliferation inhibition [4]. As the 5-fluorouracil is usually given as a topical cream or solution for oral cancer patients to form a thin coating at skin lesions, CAPE can be added into the 5-fluorouracil cream or solution for oral cancer treatment. Co-treatment of CAPE with 5-fluorouracil may decrease the uncomfortable syndromes or undesired side effects for patients using 5-fluorouracil.

6. Molecular Mechanism of Anticancer Activity of CAPE in Oral Cancer Cells

The PIK3CA oncogene is located at chromosome 3q26. Chromosome locus 3q26 is frequently amplified in OSCCs [94–97] and is associated with advanced stages as well as invasive and metastatic OSCC phenotypes [98–100]. Relatively high frequency of PIK3CA mutations was found in stage IV OSCC, suggesting that PI3K/Akt signaling may be involved in disease progression of OSCCs [101]. OSCC is relatively sensitive to radiotherapy, however, activated PI3K/Akt signaling enhances radiotherapy resistance in OSCC patients [102]. These findings suggested that PI3K/Akt signaling is a potential therapeutic target in OSCC patients. There are three mammalian isoforms of this enzyme, Akt1, Akt2, and Akt3 [103,104]. Two phosphorylation sites on Akt, threonine 308 and serine 473, regulate activity of Akt. Phosphorylation of Thr308 on Akt is activated by PDK1 [105,106], while phosphorylation of Ser473 on Akt is activated by mTOR kinase [107,108]. Phosphorylation of these two sites elevates activity of Akt. Akt regulates the phosphorylation of Gsk-3β Ser9, which in turn regulates the activity of Gsk-3β activity [109] as well as the abundance of β-catenin, cyclin D1, and cyclin E [108–110]. Forkhead box O1 (FOXO1) protein is a transcription factor that plays important roles in regulation of gluconeogenesis and glycogenolysis by insulin signaling. FOXO3a is a well-known tumor suppressor [111]. Recent studies suggest that FOXO1 is a tumor suppressor as well [112].

Phosphorylation of FOXO1 or FOXO3a by Akt inhibits their activity resulting in translocation of these proteins out of the nucleus [113]. Treatment with CAPE decreased protein abundance of signaling proteins involved in the Akt signaling pathway, including Akt, Akt1, Akt2, Akt3, phospho-Akt Ser473, phospho-Akt Thr308, Gsk3β, FOXO1, FOXO3a, phospho-FOXO1 Thr24, and phospho-FoxO3a Thr32 in Tw2.6 cells [4]. Overexpression of Akt1 or Akt2 in TW2.6 cells rescued growth inhibition caused by CAPE treatment [4], confirming that Akt is one of the main targets of CAPE in oral cancer cells.

The tumor microenvironment is the environment in which the cancer cell exists. The status of the surrounding blood vessels, immune cells, fibroblasts, stroma cells, hypoxia, signaling molecules, and the extracellular matrix (ECM) determine the conditions of the tumor microenvironment. CAPE treatment reduces the secretion of vascular endothelial growth factor (VEGF) through the inhibition of the ROS, PI3K and HIF-1α signaling pathways in human retinal pigment epithelial cells under hypoxic conditions [114]. Cancer metastasis is the major cause of cancer related death and involves the degradation of the ECM [115], which is regulated by the matrix metalloproteinases (MMPs) [116]. MMPs gene are expressed in response to stimulation by many pro-inflammatory cytokines such as TNF-α, interleukin (IL)-1β and IL-6. The activity of MMPs is regulated by several types of inhibitors, among them, tissue inhibitor of metalloproteinases (TIMPs) are the most important ones [117–119]. The balance between MMPs and TIMPs is responsible for the control of degradation of ECM proteins. MMP-2 and MMP-9 are the principal enzymes involved in the degradation of ECM [120,121] and both of these proteins have been reported to be overexpressed in oral cancers [122]. SCC-9 is a tumorigenic keratinocyte cell line cultured from human squamous cell carcinomas. CAPE treatment attenuates SCC-9 oral cancer cell migration and invasion at non-cytotoxic concentrations (0–40 μM) [123]. Western blot and gelatin zymography analysis indicates that CAPE down-regulated protein expression and enzymatic activity of MMP-2 [123]. CAPE exerts its inhibitory effects on MMP-2 expression and activity by up-regulating TIMP-2 and potently decreases migration by reducing focal adhesion kinase (FAK) phosphorylation and the activation of its downstream signaling molecules p38 mitogen-activated protein kinases (p38 MAPK) and c-Jun *N*-terminal kinases (JNKs) [123]. These data indicate that CAPE could potentially be used as a chemo-agent to prevent oral cancer metastasis and that the anticancer activity of CAPE is at least partially via regulation of the tumor microenvironment.

Nuclear factor kappa-B (NF-κB) is an important cell-survival signaling protein and plays a key role in regulating the cellular response to stress and the immune response to infection [124]. Dysregulation of NF-κB has been linked to cancer, inflammation, and autoimmune diseases [124]. NF-κB is one of the most important transcription factors for MMP-9 production [117,125,126]. High expression levels of NF-κB p65 and inhibitor of NF-κB kinase subunit alpha (IKKα) were found to correlate to invasiveness, metastasis, and anti-apoptotic activity of OSCC [127]. Oral cancer is associated with a high degree of local invasiveness [123]. CAPE treatment has been reported to suppress the activation of NF-κB induced by tumor necrosis factor (TNF) or inflammatory agents in a dose- and time-dependent manner [27]. CAPE prevents the translocation of the p65 subunit of NF-κB to the nucleus and delays nuclear factor of κ light polypeptide gene enhancer in B-cells inhibitor, alpha (IκBα) re-synthesis [27]. The effect of CAPE on inhibition of NF-κB binding to the DNA is target-specific [27]. Fifty μM or higher dosage of CAPE is an effective inhibitor of NF-κB activation in TW2.6 cells [4]. CAPE treatment (50 or 100 μM) suppress both the total abundance and the phosphorylation of NF-κB on Serine 536 [4].

Phosphorylation of NF-κB p65 at S536 is required for TNF-α-induced NF-κB activation [128]. Therefore, administration of CAPE can be a potential treatment for primary and metastatic OSCC by blocking the NF-κB survival pathway.

CAPE treatment decreased G1 cell population, increased G2/M cell population, and induced apoptosis in TW2.6 cells [4]. Skp2 is a member of the F-box protein family, which is responsible for ubiquitination and down-regulation of $p27^{Kip1}$ and other proteins [129,130]. Treatment with CAPE decreases protein abundance of Rb, phospho-Rb Ser807/811, Skp2, and cyclin D1, but increases cell cycle inhibitor $p27^{Kip}$ [4]. Rb is a tumor suppressor protein and is mutated or suppressed in several types of cancers [131]. Reduction in phosphorylation of Rb restricts cell proliferation by inhibiting activity of E2F transcriptional factors [132]. As the abundance of Rb is also suppressed by CAPE treatment in TW2.6 cells, the loss of Rb function may trigger either p53-dependent or p53-independent apoptosis [133]. Cyclin D1 is a protein encoded by *CCND1* gene and forms a complex with cyclin-dependent kinase 4 (CDK4) or CDK6. These complexes are essential for cell cycle G1/S transition [134]. Cyclin D1 interacts with Rb, and the expression of the *CCND1* gene is positively regulated by Rb [134]. Decline of phosphorylation of FOXO1 and FOXO3a caused by CAPE treatment elevates their tumor suppressor activity. Down-regulation of the protein level of Akt, phospho-Akt Ser473, phospho-Akt Thr308, Gsk3β, Skp2, phospho-Rb Ser807/811, phospho-FOXO1 Thr24, phospho-FOXO3a Thr32, and cyclin D1 coupled with the accumulation of $p27^{Kip1}$ protein likely contribute to the induction of G2/M cell cycle arrest and growth inhibition in TW2.6 oral cancer cells.

7. Conclusions

According to the above summaries in this review, there is strong evidence that CAPE treatment suppress proliferation, survival, metastasis, EGFR and COX-2 activity, PI3K-Akt signaling, and Skp2 in human oral cancer cells. We summarize the effects of CAPE treatment on different signaling proteins and the potential effect on cell survival, cell cycle, cell proliferation, and metastasis of oral cancer cells in Figure 2. The good bioavailability through the oral route, and the good historical safety profile of propolis, makes CAPE an ideal adjuvant agent for future oral cancer treatment. We believe that CAPE, being applied in the form of a topical cream or mouth rinsing solution, either alone or with 5-FU, can be a potentially effective treatment for patients with advanced oral cancer, targeting PI3K/Akt signaling, NF-κB, MMPs, and cell cycle regulatory proteins.

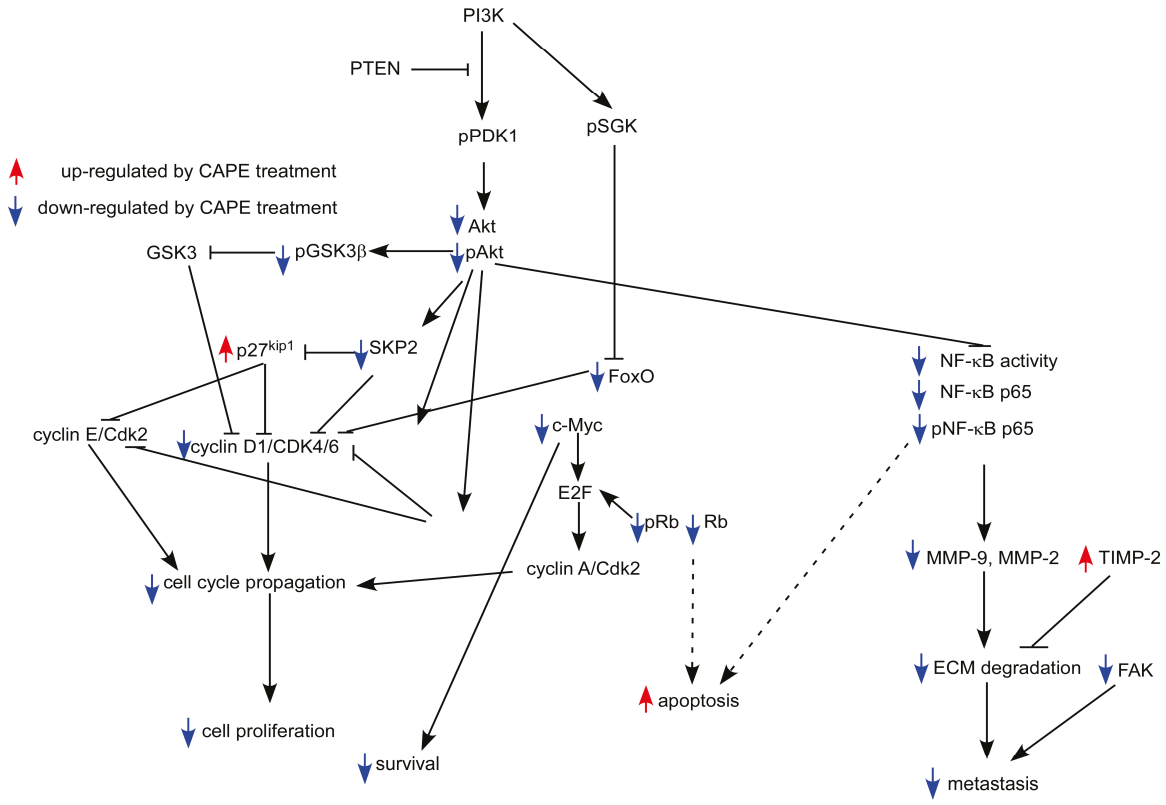

Figure 2. Putative model of anti-cancer effect of CAPE in human oral cancer cells. Protein abundance or activity being stimulated by CAPE treatment are labeled with red upward arrows, while those being suppressed by CAPE treatment are labeled with blue downward arrows. Arrows indicate activation of downstream signaling proteins, while bars mean inhibition of downstream signaling proteins. Dash lines indicated possible effects.

Acknowledgments

This study was supported by CS-103-PP-14 (National Health Research Institutes, NHRI), CA-103-SP-01 (Ministry of Health and Welfare), as well as MOST 103-2325-B-400-001, MOST 103-2321-B-400-016, and MOST 103-2633-B-400-002 (Ministry of Science and Technology) for Chih-Pin Chuu and MOST 103-2325-B-400-002 for Wun-Shaing Wayne Chang (Ministry of Science and Technology) in Taiwan. We thank the support from the Micro-Western Array core facility of NHRI.

Conflicts of Interest

The authors declare no conflict of interest.

This article is dedicated to our dear mentor, Dr. Shutsung Liao, Professor at the Ben May Department for Cancer Research of The University of Chicago. He passed away on July 20th 2014 at his Hyde Park home in Chicago. He was a member of the America Academy of Art & Science (USA) and of the Academia Sinica (Taiwan).

References

1. Argiris, A.; Karamouzis, M.V.; Raben, D.; Ferris, R.L. Head and neck cancer. *Lancet* **2008**, *371*, 1695–1709.
2. Mascolo, M.; Siano, M.; Ilardi, G.; Russo, D.; Merolla, F.; de Rosa, G.; Staibano, S. Epigenetic disregulation in oral cancer. *Int. J. Mol. Sci.* **2012**, *13*, 2331–2353.
3. GBD 2013 Mortality; Causes of Death Collaborators. Global, regional, and national age-sex specific all-cause and cause-specific mortality for 240 causes of death, 1990–2013: A systematic analysis for the Global Burden of Disease Study 2013. *Lancet* **2015**, *385*, 117–171.
4. Kuo, Y.Y.; Lin, H.P.; Huo, C.; Su, L.C.; Yang, J.; Hsiao, P.H.; Chiang, H.C.; Chung, C.J.; Wang, H.D.; Chang, J.Y.; *et al.* Caffeic acid phenethyl ester suppresses proliferation and survival of TW2.6 human oral cancer cells via inhibition of Akt signaling. *Int. J. Mol. Sci.* **2013**, *14*, 8801–8817.
5. Vagish Kumar, L.S. Propolis in dentistry and oral cancer management. *N. Am. J. Med. Sci.* **2014**, *6*, 250–259.
6. Parolia, A.; Kundabala, M.; Rao, N.N.; Acharya, S.R.; Agrawal, P.; Mohan, M.; Thomas, M. A comparative histological analysis of human pulp following direct pulp capping with Propolis, mineral trioxide aggregate and Dycal. *Aust. Dent. J.* **2010**, *55*, 59–64.
7. Mahmoud, A.S.; Almas, K.; Dahlan, A.A. The effect of propolis on dentinal hypersensitivity and level of satisfaction among patients from a university hospital Riyadh, Saudi Arabia. *Indian J. Dent. Res.* **1999**, *10*, 130–137.
8. Almas, K.; Mahmoud, A.; Dahlan, A. A comparative study of propolis and saline application on human dentin. A SEM study. *Indian J. Dent. Res.* **2001**, *12*, 21–27.
9. Abdulrhman, M.; Elbarbary, N.S.; Ahmed Amin, D.; Saeid Ebrahim, R. Honey and a mixture of honey, beeswax, and olive oil-propolis extract in treatment of chemotherapy-induced oral mucositis: A randomized controlled pilot study. *Pediatr. Hematol. Oncol.* **2012**, *29*, 285–292.
10. Tomazevic, T.; Jazbec, J. A double blind randomised placebo controlled study of propolis (bee glue) effectiveness in the treatment of severe oral mucositis in chemotherapy treated children. *Complement. Ther. Med.* **2013**, *21*, 306–312.
11. Noronha, V.R.; Araujo, G.S.; Gomes, R.T.; Iwanaga, S.H.; Barbosa, M.C.; Abdo, E.N.; Ferreira e Ferreira, E.; Viana Campos, A.C.; Souza, A.A.; Abreu, S.R.; *et al.* Mucoadhesive propolis gel for prevention of radiation-induced oral mucositis. *Curr. Clin. Pharmacol.* **2014**, *9*, 359–364.
12. Motallebnejad, M.; Abedi, S.M.; Seyedmajidi, M.; Moghadamnia, A.A.; Ashrafpour, M.; Salehi, M.; Moslemi, D.; Ghorbani, A. Evaluation of protective effect of propolis on parotid salivary glands in γ-irradiated rats. *J. Contemp. Dent. Prac.* **2014**, *15*, 8–11.
13. Cavalcante, D.R.; Oliveira, P.S.; Gois, S.M.; Soares, A.F.; Cardoso, J.C.; Padilha, F.F.; Albuquerque, R.L., Jr. Effect of green propolis on oral epithelial dysplasia in rats. *Braz. J. Otorhinolaryngol.* **2011**, *77*, 278–284.
14. Wieckiewicz, W.; Miernik, M.; Wieckiewicz, M.; Morawiec, T. Does propolis help to maintain oral health? *Evid. Based Complement. Altern. Med.* **2013**, *2013*, 351062.

15. Sanghavi, T.; Shah, N.; Parekh, V.; Singbal, K. Evaluation and comparison of efficacy of three different storage media, coconut water, propolis, and oral rehydration solution, in maintaining the viability of periodontal ligament cells. *J. Conserv. Dent.* **2013**, *16*, 71–74.
16. Bretz, W.A.; Chiego, D.J., Jr.; Marcucci, M.C.; Cunha, I.; Custodio, A.; Schneider, L.G. Preliminary report on the effects of propolis on wound healing in the dental pulp. *Z. Naturforsch. C* **1998**, *53*, 1045–1048.
17. Kamburoglu, K.; Ozen, T. Analgesic effect of Anatolian propolis in mice. *Agri* **2011**, *23*, 47–50.
18. Topcuoglu, N.; Ozan, F.; Ozyurt, M.; Kulekci, G. *In vitro* antibacterial effects of glass-ionomer cement containing ethanolic extract of propolis on *Streptococcus* mutans. *Eur. J. Dent.* **2012**, *6*, 428–433.
19. Kouidhi, B.; Zmantar, T.; Bakhrouf, A. Anti-cariogenic and anti-biofilms activity of Tunisian propolis extract and its potential protective effect against cancer cells proliferation. *Anaerobe* **2010**, *16*, 566–571.
20. Barrientos, L.; Herrera, C.L.; Montenegro, G.; Ortega, X.; Veloz, J.; Alvear, M.; Cuevas, A.; Saavedra, N.; Salazar, L.A. Chemical and botanical characterization of Chilean propolis and biological activity on cariogenic bacteria *Streptococcus* mutans and *Streptococcus* sobrinus. *Braz. J. Microbiol.* **2013**, *44*, 577–585.
21. Maekawa, L.E.; Valera, M.C.; Oliveira, L.D.; Carvalho, C.A.; Camargo, C.H.; Jorge, A.O. Effect of *Zingiber officinale* and propolis on microorganisms and endotoxins in root canals. *J. Appl. Oral Sci.* **2013**, *21*, 25–31.
22. Skaba, D.; Morawiec, T.; Tanasiewicz, M.; Mertas, A.; Bobela, E.; Szliszka, E.; Skucha-Nowak, M.; Dawiec, M.; Yamamoto, R.; Ishiai, S.; *et al.* Influence of the toothpaste with brazilian ethanol extract propolis on the oral cavity health. *Evid. Based Complement. Altern. Med.* **2013**, *2013*, 215391.
23. Preeti, L.; Magesh, K.; Rajkumar, K.; Karthik, R. Recurrent aphthous stomatitis. *J. Oral Maxillofac. Pathol.* **2011**, *15*, 252–256.
24. Samet, N.; Laurent, C.; Susarla, S.M.; Samet-Rubinsteen, N. The effect of bee propolis on recurrent aphthous stomatitis: A pilot study. *Clin. Oral Investig.* **2007**, *11*, 143–147.
25. Ozan, F.; Sumer, Z.; Polat, Z.A.; Er, K.; Ozan, U.; Deger, O. Effect of mouthrinse containing propolis on oral microorganisms and human gingival fibroblasts. *Eur. J. Dent.* **2007**, *1*, 195–201.
26. Bhimani, R.S.; Troll, W.; Grunberger, D.; Frenkel, K. Inhibition of oxidative stress in HeLa cells by chemopreventive agents. *Cancer Res.* **1993**, *53*, 4528–4533.
27. Natarajan, K.; Singh, S.; Burke, T.R., Jr.; Grunberger, D.; Aggarwal, B.B. Caffeic acid phenethyl ester is a potent and specific inhibitor of activation of nuclear transcription factor NF-κB. *Proc. Natl. Acad. Sci. USA* **1996**, *93*, 9090–9095.
28. Okutan, H.; Ozcelik, N.; Yilmaz, H.R.; Uz, E. Effects of caffeic acid phenethyl ester on lipid peroxidation and antioxidant enzymes in diabetic rat heart. *Clin. Biochem.* **2005**, *38*, 191–196.
29. Sharma, A.; Mendez, E.; Yueh, B.; Lohavanichbutr, P.; Houck, J.; Doody, D.R.; Futran, N.D.; Upton, M.P.; Schwartz, S.M.; Chen, C. Human papillomavirus-positive oral cavity and oropharyngeal cancer patients do not have better quality-of-life trajectories. *Otolaryngol. Head Neck Surg.* **2012**, *146*, 739–745.

30. Kelly, K.; Johnson-Obaseki, S.; Lumingu, J.; Corsten, M. Oncologic, functional and surgical outcomes of primary transoral robotic surgery for early squamous cell cancer of the oropharynx: A systematic review. *Oral Oncol.* **2014**, *50*, 696–703.
31. Ferlay, J.; Soerjomataram, I.; Dikshit, R.; Eser, S.; Mathers, C.; Rebelo, M.; Parkin, D.M.; Forman, D.; Bray, F. Cancer incidence and mortality worldwide: Sources, methods and major patterns in GLOBOCAN 2012. *Int. J. Cancer* **2015**, *136*, E359–E386.
32. Siegel, R.; Naishadham, D.; Jemal, A. Cancer statistics, 2012. *CA Cancer J. Clin.* **2012**, *62*, 10–29.
33. Petersen, P.E. Oral cancer prevention and control—The approach of the World Health Organization. *Oral Oncol.* **2009**, *45*, 454–460.
34. Johnson, N.W.; Jayasekara, P.; Amarasinghe, A.A. Squamous cell carcinoma and precursor lesions of the oral cavity: Epidemiology and aetiology. *Periodontology* **2011**, *57*, 19–37.
35. Chen, Y.J.; Chang, J.T.; Liao, C.T.; Wang, H.M.; Yen, T.C.; Chiu, C.C.; Lu, Y.C.; Li, H.F.; Cheng, A.J. Head and neck cancer in the betel quid chewing area: Recent advances in molecular carcinogenesis. *Cancer Sci.* **2008**, *99*, 1507–1514.
36. Nomura, M.; Kaji, A.; Ma, W.; Miyamoto, K.; Dong, Z. Suppression of cell transformation and induction of apoptosis by caffeic acid phenethyl ester. *Mol. Carcinog.* **2001**, *31*, 83–89.
37. Wu, J.; Omene, C.; Karkoszka, J.; Bosland, M.; Eckard, J.; Klein, C.B.; Frenkel, K. Caffeic acid phenethyl ester (CAPE), derived from a honeybee product propolis, exhibits a diversity of anti-tumor effects in pre-clinical models of human breast cancer. *Cancer Lett.* **2011**, *308*, 43–53.
38. Watabe, M.; Hishikawa, K.; Takayanagi, A.; Shimizu, N.; Nakaki, T. Caffeic acid phenethyl ester induces apoptosis by inhibition of NFκB and activation of Fas in human breast cancer MCF-7 cells. *J. Biol. Chem.* **2004**, *279*, 6017–6026.
39. Chuu, C.P.; Lin, H.P.; Ciaccio, M.F.; Kokontis, J.M.; Hause, R.J., Jr.; Hiipakka, R.A.; Liao, S.; Jones, R.B. Caffeic acid phenethyl ester suppresses the proliferation of human prostate cancer cells through inhibition of p70S6K and Akt signaling networks. *Cancer Prev. Res. (Phila)* **2012**, *5*, 788–797.
40. Lin, H.P.; Jiang, S.S.; Chuu, C.P. Caffeic acid phenethyl ester causes p21 induction, Akt signaling reduction, and growth inhibition in PC-3 human prostate cancer cells. *PLoS ONE* **2012**, *7*, e31286.
41. McEleny, K.; Coffey, R.; Morrissey, C.; Fitzpatrick, J.M.; Watson, R.W. Caffeic acid phenethyl ester-induced PC-3 cell apoptosis is caspase-dependent and mediated through the loss of inhibitors of apoptosis proteins. *BJU Int.* **2004**, *94*, 402–406.
42. Lin, H.P.; Lin, C.Y.; Liu, C.C.; Su, L.C.; Huo, C.; Kuo, Y.Y.; Tseng, J.C.; Hsu, J.M.; Chen, C.K.; Chuu, C.P. Caffeic Acid phenethyl ester as a potential treatment for advanced prostate cancer targeting Akt signaling. *Int. J. Mol. Sci.* **2013**, *14*, 5264–5283.
43. Chen, M.F.; Wu, C.T.; Chen, Y.J.; Keng, P.C.; Chen, W.C. Cell killing and radiosensitization by caffeic acid phenethyl ester (CAPE) in lung cancer cells. *J. Radiat. Res. (Tokyo)* **2004**, *45*, 253–260.
44. Lin, H.P.; Kuo, L.K.; Chuu, C.P. Combined treatment of curcumin and small molecule inhibitors suppresses proliferation of A549 and H1299 human non-small-cell lung cancer cells. *Phytother. Res.* **2011**, *26*, 122–126.

45. Lee, Y.T.; Don, M.J.; Hung, P.S.; Shen, Y.C.; Lo, Y.S.; Chang, K.W.; Chen, C.F.; Ho, L.K. Cytotoxicity of phenolic acid phenethyl esters on oral cancer cells. *Cancer Lett.* **2005**, *223*, 19–25.
46. Onori, P.; DeMorrow, S.; Gaudio, E.; Franchitto, A.; Mancinelli, R.; Venter, J.; Kopriva, S.; Ueno, Y.; Alvaro, D.; Savage, J.; *et al.* Caffeic acid phenethyl ester decreases cholangiocarcinoma growth by inhibition of NF-κB and induction of apoptosis. *Int. J. Cancer* **2009**, *125*, 565–576.
47. Hung, M.W.; Shiao, M.S.; Tsai, L.C.; Chang, G.G.; Chang, T.C. Apoptotic effect of caffeic acid phenethyl ester and its ester and amide analogues in human cervical cancer ME180 cells. *Anticancer Res.* **2003**, *23*, 4773–4780.
48. Usia, T.; Banskota, A.H.; Tezuka, Y.; Midorikawa, K.; Matsushige, K.; Kadota, S. Constituents of Chinese propolis and their antiproliferative activities. *J. Nat. Prod.* **2002**, *65*, 673–676.
49. Chen, Y.J.; Shiao, M.S.; Hsu, M.L.; Tsai, T.H.; Wang, S.Y. Effect of caffeic acid phenethyl ester, an antioxidant from propolis, on inducing apoptosis in human leukemic HL-60 cells. *J. Agric. Food Chem.* **2001**, *49*, 5615–5619.
50. Jin, U.H.; Song, K.H.; Motomura, M.; Suzuki, I.; Gu, Y.H.; Kang, Y.J.; Moon, T.C.; Kim, C.H. Caffeic acid phenethyl ester induces mitochondria-mediated apoptosis in human myeloid leukemia U937 cells. *Mol. Cell. Biochem.* **2008**, *310*, 43–48.
51. Lee, Y.J.; Kuo, H.C.; Chu, C.Y.; Wang, C.J.; Lin, W.C.; Tseng, T.H. Involvement of tumor suppressor protein p53 and p38 MAPK in caffeic acid phenethyl ester-induced apoptosis of C6 glioma cells. *Biochem. Pharmacol.* **2003**, *66*, 2281–2289.
52. Su, Z.Z.; Lin, J.; Grunberger, D.; Fisher, P.B. Growth suppression and toxicity induced by caffeic acid phenethyl ester (CAPE) in type 5 adenovirus-transformed rat embryo cells correlate directly with transformation progression. *Cancer Res.* **1994**, *54*, 1865–1870.
53. Lin, Y.H.; Chiu, J.H.; Tseng, W.S.; Wong, T.T.; Chiou, S.H.; Yen, S.H. Antiproliferation and radiosensitization of caffeic acid phenethyl ester on human medulloblastoma cells. *Cancer Chemother. Pharmacol.* **2006**, *57*, 525–532.
54. He, Y.J.; Liu, B.H.; Xiang, D.B.; Qiao, Z.Y.; Fu, T.; He, Y.H. Inhibitory effect of caffeic acid phenethyl ester on the growth of SW480 colorectal tumor cells involves β-catenin associated signaling pathway down-regulation. *World J. Gastroenterol.* **2006**, *12*, 4981–4985.
55. Kuo, H.C.; Kuo, W.H.; Lee, Y.J.; Lin, W.L.; Chou, F.P.; Tseng, T.H. Inhibitory effect of caffeic acid phenethyl ester on the growth of C6 glioma cells *in vitro* and *in vivo*. *Cancer Lett.* **2006**, *234*, 199–208.
56. Wang, D.; Xiang, D.B.; He, Y.J.; Li, Z.P.; Wu, X.H.; Mou, J.H.; Xiao, H.L.; Zhang, Q.H. Effect of caffeic acid phenethyl ester on proliferation and apoptosis of colorectal cancer cells *in vitro*. *World J. Gastroenterol.* **2005**, *11*, 4008–4012.
57. Xiang, D.; Wang, D.; He, Y.; Xie, J.; Zhong, Z.; Li, Z. Caffeic acid phenethyl ester induces growth arrest and apoptosis of colon cancer cells via the β-catenin/T-cell factor signaling. *Anticancer Drugs* **2006**, *17*, 753–762.

58. Shigeoka, Y.; Igishi, T.; Matsumoto, S.; Nakanishi, H.; Kodani, M.; Yasuda, K.; Hitsuda, Y.; Shimizu, E. Sulindac sulfide and caffeic acid phenethyl ester suppress the motility of lung adenocarcinoma cells promoted by transforming growth factor-β through Akt inhibition. *J. Cancer Res. Clin. Oncol.* **2004**, *130*, 146–152.
59. Weyant, M.J.; Carothers, A.M.; Bertagnolli, M.E.; Bertagnolli, M.M. Colon cancer chemopreventive drugs modulate integrin-mediated signaling pathways. *Clin. Cancer Res.* **2000**, *6*, 949–956.
60. Mahmoud, N.N.; Carothers, A.M.; Grunberger, D.; Bilinski, R.T.; Churchill, M.R.; Martucci, C.; Newmark, H.L.; Bertagnolli, M.M. Plant phenolics decrease intestinal tumors in an animal model of familial adenomatous polyposis. *Carcinogenesis* **2000**, *21*, 921–927.
61. Nagaoka, T.; Banskota, A.H.; Tezuka, Y.; Harimaya, Y.; Koizumi, K.; Saiki, I.; Kadota, S. Inhibitory effects of caffeic acid phenethyl ester analogues on experimental lung metastasis of murine colon 26-L5 carcinoma cells. *Biol. Pharm. Bull.* **2003**, *26*, 638–641.
62. Borrelli, F.; Izzo, A.A.; di Carlo, G.; Maffia, P.; Russo, A.; Maiello, F.M.; Capasso, F.; Mascolo, N. Effect of a propolis extract and caffeic acid phenethyl ester on formation of aberrant crypt foci and tumors in the rat colon. *Fitoterapia* **2002**, *73*, S38–S43.
63. Carrasco-Legleu, C.E.; Sanchez-Perez, Y.; Marquez-Rosado, L.; Fattel-Fazenda, S.; Arce-Popoca, E.; Hernandez-Garcia, S.; Villa-Trevino, S. A single dose of caffeic acid phenethyl ester prevents initiation in a medium-term rat hepatocarcinogenesis model. *World J. Gastroenterol.* **2006**, *12*, 6779–6785.
64. Carrasco-Legleu, C.E.; Marquez-Rosado, L.; Fattel-Fazenda, S.; Arce-Popoca, E.; Perez-Carreon, J.I.; Villa-Trevino, S. Chemoprotective effect of caffeic acid phenethyl ester on promotion in a medium-term rat hepatocarcinogenesis assay. *Int. J. Cancer* **2004**, *108*, 488–492.
65. Kudugunti, S.K.; Vad, N.M.; Ekogbo, E.; Moridani, M.Y. Efficacy of caffeic acid phenethyl ester (CAPE) in skin B16-F0 melanoma tumor bearing C57BL/6 mice. *Investig. New Drugs* **2011**, *29*, 52–62.
66. Liao, H.F.; Chen, Y.Y.; Liu, J.J.; Hsu, M.L.; Shieh, H.J.; Liao, H.J.; Shieh, C.J.; Shiao, M.S.; Chen, Y.J. Inhibitory effect of caffeic acid phenethyl ester on angiogenesis, tumor invasion, and metastasis. *J. Agric. Food Chem.* **2003**, *51*, 7907–7912.
67. Orsolic, N.; Knezevic, A.H.; Sver, L.; Terzic, S.; Basic, I. Immunomodulatory and antimetastatic action of propolis and related polyphenolic compounds. *J. Ethnopharmacol.* **2004**, *94*, 307–315.
68. Chung, T.W.; Moon, S.K.; Chang, Y.C.; Ko, J.H.; Lee, Y.C.; Cho, G.; Kim, S.H.; Kim, J.G.; Kim, C.H. Novel and therapeutic effect of caffeic acid and caffeic acid phenyl ester on hepatocarcinoma cells: Complete regression of hepatoma growth and metastasis by dual mechanism. *FASEB J.* **2004**, *18*, 1670–1681.
69. Wang, X.; Pang, J.; Maffucci, J.A.; Pade, D.S.; Newman, R.A.; Kerwin, S.M.; Bowman, P.D.; Stavchansky, S. Pharmacokinetics of caffeic acid phenethyl ester and its catechol-ring fluorinated derivative following intravenous administration to rats. *Biopharm. Drug Dispos.* **2009**, *30*, 221–228.
70. Omene, C.O.; Wu, J.; Frenkel, K. Caffeic acid phenethyl ester (CAPE) derived from propolis, a honeybee product, inhibits growth of breast cancer stem cells. *Investig. New Drugs.* **2012**, *30*, 1279–1288.

71. Akyol, S.; Ginis, Z.; Armutcu, F.; Ozturk, G.; Yigitoglu, M.R.; Akyol, O. The potential usage of caffeic acid phenethyl ester (CAPE) against chemotherapy-induced and radiotherapy-induced toxicity. *Cell Biochem. Funct.* **2012**, *30*, 438–443.
72. Yagmurca, M.; Erdogan, H.; Iraz, M.; Songur, A.; Ucar, M.; Fadillioglu, E. Caffeic acid phenethyl ester as a protective agent against doxorubicin nephrotoxicity in rats. *Clin. Chim. Acta* **2004**, *348*, 27–34.
73. Fadillioglu, E.; Oztas, E.; Erdogan, H.; Yagmurca, M.; Sogut, S.; Ucar, M.; Irmak, M.K. Protective effects of caffeic acid phenethyl ester on doxorubicin-induced cardiotoxicity in rats. *J. Appl. Toxicol.* **2004**, *24*, 47–52.
74. Irmak, M.K.; Fadillioglu, E.; Sogut, S.; Erdogan, H.; Gulec, M.; Ozer, M.; Yagmurca, M.; Gozukara, M.E. Effects of caffeic acid phenethyl ester and α-tocopherol on reperfusion injury in rat brain. *Cell Biochem. Funct.* **2003**, *21*, 283–289.
75. Iraz, M.; Ozerol, E.; Gulec, M.; Tasdemir, S.; Idiz, N.; Fadillioglu, E.; Naziroglu, M.; Akyol, O. Protective effect of caffeic acid phenethyl ester (CAPE) administration on cisplatin-induced oxidative damage to liver in rat. *Cell Biochem. Funct.* **2006**, *24*, 357–361.
76. Yilmaz, H.R.; Sogut, S.; Ozyurt, B.; Ozugurlu, F.; Sahin, S.; Isik, B.; Uz, E.; Ozyurt, H. The activities of liver adenosine deaminase, xanthine oxidase, catalase, superoxide dismutase enzymes and the levels of malondialdehyde and nitric oxide after cisplatin toxicity in rats: Protective effect of caffeic acid phenethyl ester. *Toxicol. Ind. Health* **2005**, *21*, 67–73.
77. Oktem, F.; Yilmaz, H.R.; Ozguner, F.; Olgar, S.; Ayata, A.; Uzare, E.; Uz, E. Methotrexate-induced renal oxidative stress in rats: The role of a novel antioxidant caffeic acid phenethyl ester. *Toxicol. Ind. Health* **2006**, *22*, 241–247.
78. Ozyurt, H.; Sogut, S.; Yildirim, Z.; Kart, L.; Iraz, M.; Armutcu, F.; Temel, I.; Ozen, S.; Uzun, A.; Akyol, O. Inhibitory effect of caffeic acid phenethyl ester on bleomycine-induced lung fibrosis in rats. *Clin. Chim. Acta* **2004**, *339*, 65–75.
79. Albukhari, A.A.; Gashlan, H.M.; El-Beshbishy, H.A.; Nagy, A.A.; Abdel-Naim, A.B. Caffeic acid phenethyl ester protects against tamoxifen-induced hepatotoxicity in rats. *Food Chem. Toxicol.* **2009**, *47*, 1689–1695.
80. Yildiz, O.G.; Soyuer, S.; Saraymen, R.; Eroglu, C. Protective effects of caffeic acid phenethyl ester on radiation induced lung injury in rats. *Clin. Investig. Med.* **2008**, *31*, E242–E247.
81. Chen, Y.J.; Liao, H.F.; Tsai, T.H.; Wang, S.Y.; Shiao, M.S. Caffeic acid phenethyl ester preferentially sensitizes CT26 colorectal adenocarcinoma to ionizing radiation without affecting bone marrow radioresponse. *Int. J. Radiat. Oncol. Biol. Phys.* **2005**, *63*, 1252–1261.
82. Chung, C.H.; Ely, K.; McGavran, L.; Varella-Garcia, M.; Parker, J.; Parker, N.; Jarrett, C.; Carter, J.; Murphy, B.A.; Netterville, J.; *et al.* Increased epidermal growth factor receptor gene copy number is associated with poor prognosis in head and neck squamous cell carcinomas. *J. Clin. Oncol.* **2006**, *24*, 4170–4176.
83. Temam, S.; Kawaguchi, H.; El-Naggar, A.K.; Jelinek, J.; Tang, H.; Liu, D.D.; Lang, W.; Issa, J.P.; Lee, J.J.; Mao, L. Epidermal growth factor receptor copy number alterations correlate with poor clinical outcome in patients with head and neck squamous cancer. *J. Clin. Oncol.* **2007**, *25*, 2164–2170.

84. Chan, G.; Boyle, J.O.; Yang, E.K.; Zhang, F.; Sacks, P.G.; Shah, J.P.; Edelstein, D.; Soslow, R.A.; Koki, A.T.; Woerner, B.M.; *et al.* Cyclooxygenase-2 expression is up-regulated in squamous cell carcinoma of the head and neck. *Cancer Res.* **1999**, *59*, 991–994.
85. Sudbo, J.; Ristimaki, A.; Sondresen, J.E.; Kildal, W.; Boysen, M.; Koppang, H.S.; Reith, A.; Risberg, B.; Nesland, J.M.; Bryne, M. Cyclooxygenase-2 (COX-2) expression in high-risk premalignant oral lesions. *Oral Oncol.* **2003**, *39*, 497–505.
86. Sakurai, K.; Urade, M.; Noguchi, K.; Hashitani, S.; Takaoka, K.; Segawa, E.; Kishimoto, H. Prognostic significance of cyclooxygenase-2 and DNA topoisomerase IIα expression in oral carcinoma. *Head Neck* **2007**, *29*, 1002–1009.
87. Rossi, A.; Ligresti, A.; Longo, R.; Russo, A.; Borrelli, F.; Sautebin, L. The inhibitory effect of propolis and caffeic acid phenethyl ester on cyclooxygenase activity in J774 macrophages. *Phytomedicine* **2002**, *9*, 530–535.
88. Michaluart, P.; Masferrer, J.L.; Carothers, A.M.; Subbaramaiah, K.; Zweifel, B.S.; Koboldt, C.; Mestre, J.R.; Grunberger, D.; Sacks, P.G.; Tanabe, T.; *et al.* Inhibitory effects of caffeic acid phenethyl ester on the activity and expression of cyclooxygenase-2 in human oral epithelial cells and in a rat model of inflammation. *Cancer Res.* **1999**, *59*, 2347–2352.
89. Kok, S.H.; Hong, C.Y.; Lin, S.K.; Lee, J.J.; Chiang, C.P.; Kuo, M.Y. Establishment and characterization of a tumorigenic cell line from areca quid and tobacco smoke-associated buccal carcinoma. *Oral Oncol.* **2007**, *43*, 639–647.
90. Lee, Y.J.; Liao, P.H.; Chen, W.K.; Yang, C.Y. Preferential cytotoxicity of caffeic acid phenethyl ester analogues on oral cancer cells. *Cancer Lett.* **2000**, *153*, 51–56.
91. Okumura, K.; Konishi, A.; Tanaka, M.; Kanazawa, M.; Kogawa, K.; Niitsu, Y. Establishment of high- and low-invasion clones derived for a human tongue squamous-cell carcinoma cell line SAS. *J. Cancer Res. Clin. Oncol.* **1996**, *122*, 243–248.
92. Kim, M.S.; Li, S.L.; Bertolami, C.N.; Cherrick, H.M.; Park, N.H. State of p53, Rb and DCC tumor suppressor genes in human oral cancer cell lines. *Anticancer Res.* **1993**, *13*, 1405–1413.
93. Longley, D.B.; Harkin, D.P.; Johnston, P.G. 5-fluorouracil: Mechanisms of action and clinical strategies. *Nat. Rev. Cancer* **2003**, *3*, 330–338.
94. Bockmuhl, U.; Schwendel, A.; Dietel, M.; Petersen, I. Distinct patterns of chromosomal alterations in high- and low-grade head and neck squamous cell carcinomas. *Cancer Res.* **1996**, *56*, 5325–5329.
95. Hashimoto, Y.; Oga, A.; Kawauchi, S.; Furuya, T.; Shimizu, N.; Nakano, T.; Imate, Y.; Yamashita, H.; Sasaki, K. Amplification of 3q26 approximately qter correlates with tumor progression in head and neck squamous cell carcinomas. *Cancer Genet. Cytogenet.* **2001**, *129*, 52–56.
96. Squire, J.A.; Bayani, J.; Luk, C.; Unwin, L.; Tokunaga, J.; MacMillan, C.; Irish, J.; Brown, D.; Gullane, P.; Kamel-Reid, S. Molecular cytogenetic analysis of head and neck squamous cell carcinoma: By comparative genomic hybridization, spectral karyotyping, and expression array analysis. *Head Neck* **2002**, *24*, 874–887.
97. Riazimand, S.H.; Welkoborsky, H.J.; Bernauer, H.S.; Jacob, R.; Mann, W.J. Investigations for fine mapping of amplifications in chromosome 3q26.3-28 frequently occurring in squamous cell carcinomas of the head and neck. *Oncology* **2002**, *63*, 385–392.

98. Okafuji, M.; Ita, M.; Hayatsu, Y.; Shinozaki, F.; Oga, A.; Sasaki, K. Identification of genetic aberrations in cell lines from oral squamous cell carcinomas by comparative genomic hybridization. *J. Oral Pathol. Med.* **1999**, *28*, 241–245.
99. Bockmuhl, U.; Schluns, K.; Schmidt, S.; Matthias, S.; Petersen, I. Chromosomal alterations during metastasis formation of head and neck squamous cell carcinoma. *Genes Chromosomes Cancer* **2002**, *33*, 29–35.
100. Woenckhaus, J.; Steger, K.; Werner, E.; Fenic, I.; Gamerdinger, U.; Dreyer, T.; Stahl, U. Genomic gain of PIK3CA and increased expression of p110α are associated with progression of dysplasia into invasive squamous cell carcinoma. *J. Pathol.* **2002**, *198*, 335–342.
101. Kozaki, K.; Imoto, I.; Pimkhaokham, A.; Hasegawa, S.; Tsuda, H.; Omura, K.; Inazawa, J. PIK3CA mutation is an oncogenic aberration at advanced stages of oral squamous cell carcinoma. *Cancer Sci.* **2006**, *97*, 1351–1358.
102. Bussink, J.; van der Kogel, A.J.; Kaanders, J.H. Activation of the PI3-K/AKT pathway and implications for radioresistance mechanisms in head and neck cancer. *Lancet Oncol.* **2008**, *9*, 288–296.
103. Coffer, P.J.; Jin, J.; Woodgett, J.R. Protein kinase B (c-Akt): A multifunctional mediator of phosphatidylinositol 3-kinase activation. *Biochem. J.* **1998**, *335*, 1–13.
104. Gonzalez, E.; McGraw, T.E., The Akt kinases: Isoform specificity in metabolism and cancer. *Cell Cycle* **2009**, *8*, 2502–2508.
105. Alessi, D.R.; James, S.R.; Downes, C.P.; Holmes, A.B.; Gaffney, P.R.; Reese, C.B.; Cohen, P. Characterization of a 3-phosphoinositide-dependent protein kinase which phosphorylates and activates protein kinase Bα. *Curr. Biol.* **1997**, *7*, 261–269.
106. Murugan, A.K.; Munirajan, A.K.; Tsuchida, N. Genetic deregulation of the PIK3CA oncogene in oral cancer. *Cancer Lett.* **2013**, *338*, 193–203.
107. Sarbassov, D.D.; Guertin, D.A.; Ali, S.M.; Sabatini, D.M. Phosphorylation and regulation of Akt/PKB by the rictor-mTOR complex. *Science* **2005**, *307*, 1098–1101.
108. Jacinto, E.; Facchinetti, V.; Liu, D.; Soto, N.; Wei, S.; Jung, S.Y.; Huang, Q.; Qin, J.; Su, B. SIN1/MIP1 maintains rictor-mTOR complex integrity and regulates Akt phosphorylation and substrate specificity. *Cell* **2006**, *127*, 125–137.
109. Li, M.; Wang, X.; Meintzer, M.K.; Laessig, T.; Birnbaum, M.J.; Heidenreich, K.A. Cyclic AMP promotes neuronal survival by phosphorylation of glycogen synthase kinase 3β. *Mol. Cell. Biol.* **2000**, *20*, 9356–9363.
110. Rossig, L.; Badorff, C.; Holzmann, Y.; Zeiher, A.M.; Dimmeler, S. Glycogen synthase kinase-3 couples AKT-dependent signaling to the regulation of p21Cip1 degradation. *J. Biol. Chem.* **2002**, *277*, 9684–9689.
111. Myatt, S.S.; Lam, E.W. The emerging roles of forkhead box (Fox) proteins in cancer. *Nat. Rev. Cancer* **2007**, *7*, 847–859.
112. Zhang, H.; Pan, Y.; Zheng, L.; Choe, C.; Lindgren, B.; Jensen, E.D.; Westendorf, J.J.; Cheng, L.; Huang, H. FOXO1 inhibits Runx2 transcriptional activity and prostate cancer cell migration and invasion. *Cancer Res.* **2011**, *71*, 3257–3267.

113. Brunet, A.; Bonni, A.; Zigmond, M.J.; Lin, M.Z.; Juo, P.; Hu, L.S.; Anderson, M.J.; Arden, K.C.; Blenis, J.; Greenberg, M.E. Akt promotes cell survival by phosphorylating and inhibiting a Forkhead transcription factor. *Cell* **1999**, *96*, 857–868.
114. Paeng, S.H.; Jung, W.K.; Park, W.S.; Lee, D.S.; Kim, G.Y.; Choi, Y.H.; Seo, S.K.; Jang, W.H.; Choi, J.S.; Lee, Y.M.; *et al.* Caffeic acid phenethyl ester reduces the secretion of vascular endothelial growth factor through the inhibition of the ROS, PI3K and HIF-1α signaling pathways in human retinal pigment epithelial cells under hypoxic conditions. *Int. J. Mol. Med.* **2015**, *35*, 1419–1426.
115. Stetler-Stevenson, W.G.; Liotta, L.A.; Kleiner, D.E., Jr., Extracellular matrix 6: Role of matrix metalloproteinases in tumor invasion and metastasis. *FASEB J.* **1993**, *7*, 1434–1441.
116. Egeblad, M.; Werb, Z. New functions for the matrix metalloproteinases in cancer progression. *Nat. Rev. Cancer* **2002**, *2*, 161–174.
117. Chou, Y.C.; Sheu, J.R.; Chung, C.L.; Chen, C.Y.; Lin, F.L.; Hsu, M.J.; Kuo, Y.H.; Hsiao, G. Nuclear-targeted inhibition of NF-κB on MMP-9 production by *N*-2-(4-bromophenyl) ethyl caffeamide in human monocytic cells. *Chem. Biol. Interact.* **2010**, *184*, 403–412.
118. Brew, K.; Dinakarpandian, D.; Nagase, H. Tissue inhibitors of metalloproteinases: Evolution, structure and function. *Biochim. Biophys. Acta* **2000**, *1477*, 267–283.
119. Bode, W.; Fernandez-Catalan, C.; Grams, F.; Gomis-Ruth, F.X.; Nagase, H.; Tschesche, H.; Maskos, K. Insights into MMP–TIMP interactions. *Ann. N. Y. Acad. Sci.* **1999**, *878*, 73–91.
120. Nelson, A.R.; Fingleton, B.; Rothenberg, M.L.; Matrisian, L.M. Matrix metalloproteinases: Biologic activity and clinical implications. *J. Clin. Oncol.* **2000**, *18*, 1135–1149.
121. Bjorklund, M.; Koivunen, E. Gelatinase-mediated migration and invasion of cancer cells. *Biochim. Biophys. Acta* **2005**, *1755*, 37–69.
122. Hong, S.D.; Hong, S.P.; Lee, J.I.; Lim, C.Y. Expression of matrix metalloproteinase-2 and -9 in oral squamous cell carcinomas with regard to the metastatic potential. *Oral Oncol.* **2000**, *36*, 207–213.
123. Peng, C.Y.; Yang, H.W.; Chu, Y.H.; Chang, Y.C.; Hsieh, M.J.; Chou, M.Y.; Yeh, K.T.; Lin, Y.M.; Yang, S.F.; Lin, C.W. Caffeic acid phenethyl ester inhibits oral cancer cell metastasis by regulating matrix metalloproteinase-2 and the mitogen-activated protein kinase pathway. *Evid. Based Complement. Altern. Med.* **2012**, *2012*, 732578.
124. Perkins, N.D. Integrating cell-signalling pathways with NF-κB and IKK function. *Nat. Rev. Mol. Cell Biol.* **2007**, *8*, 49–62.
125. Moon, S.K.; Cha, B.Y.; Kim, C.H. ERK1/2 mediates TNF-α-induced matrix metalloproteinase-9 expression in human vascular smooth muscle cells via the regulation of NF-κB and AP-1: Involvement of the ras dependent pathway. *J. Cell. Physiol.* **2004**, *198*, 417–427.
126. Bond, M.; Fabunmi, R.P.; Baker, A.H.; Newby, A.C. Synergistic upregulation of metalloproteinase-9 by growth factors and inflammatory cytokines: An absolute requirement for transcription factor NF-κB. *FEBS Lett.* **1998**, *435*, 29–34.
127. Nakayama, H.; Ikebe, T.; Beppu, M.; Shirasuna, K. High expression levels of nuclear factor κB, IκB kinase α and Akt kinase in squamous cell carcinoma of the oral cavity. *Cancer* **2001**, *92*, 3037–3044.

128. Hu, J.; Nakano, H.; Sakurai, H.; Colburn, N.H. Insufficient p65 phosphorylation at S536 specifically contributes to the lack of NF-κB activation and transformation in resistant JB6 cells. *Carcinogenesis* **2004**, *25*, 1991–2003.
129. Carrano, A.C.; Eytan, E.; Hershko, A.; Pagano, M. SKP2 is required for ubiquitin-mediated degradation of the CDK inhibitor p27. *Nat. Cell Biol.* **1999**, *1*, 193–199.
130. Tsvetkov, L.M.; Yeh, K.H.; Lee, S.J.; Sun, H.; Zhang, H. $p27^{Kip1}$ ubiquitination and degradation is regulated by the SCF^{Skp2} complex through phosphorylated Thr187 in p27. *Curr. Biol.* **1999**, *9*, 661–664.
131. Murphree, A.L.; Benedict, W.F. Retinoblastoma: Clues to human oncogenesis. *Science* **1984**, *223*, 1028–1033.
132. Chellappan, S.P.; Hiebert, S.; Mudryj, M.; Horowitz, J.M.; Nevins, J.R. The E2F transcription factor is a cellular target for the RB protein. *Cell* **1991**, *65*, 1053–1061.
133. Harbour, J.W.; Dean, D.C. Rb function in cell-cycle regulation and apoptosis. *Nat. Cell Biol.* **2000**, *2*, E65–E67.
134. Lew, D.J.; Dulic, V.; Reed, S.I. Isolation of three novel human cyclins by rescue of G1 cyclin (Cln) function in yeast. *Cell* **1991**, *66*, 1197–1206.

© 2015 by the authors; licensee MDPI, Basel, Switzerland. This article is an open access article distributed under the terms and conditions of the Creative Commons Attribution license (http://creativecommons.org/licenses/by/4.0/).

Int. J. Mol. Sci. **2015**, *16*, 11609-11628; doi:10.3390/ijms160511609

OPEN ACCESS
International Journal of
Molecular Sciences
ISSN 1422-0067
www.mdpi.com/journal/ijms

Article

Spontaneous γH2AX Foci in Human Solid Tumor-Derived Cell Lines in Relation to $p21^{WAF1}$ and WIP1 Expression

Razmik Mirzayans [1,*], Bonnie Andrais [1], April Scott [1], Ying W. Wang [1], Robert H. Weiss [2,3] and David Murray [1]

[1] Department of Oncology, University of Alberta, Cross Cancer Institute, Edmonton, AB T6G 1Z2, Canada; E-Mails: bonnie.andrais@albertahealthservices.ca (B.A.); april.scott@albertahealthservices.ca (A.S.); ywwang@ualberta.ca (Y.W.W.); david.murray5@albertahealthservices.ca (D.M.)

[2] Division of Nephrology, Department of Internal Medicine, University of California, Davis, CA 95616, USA; E-Mail: rhweiss@ucdavis.edu

[3] Department of Medicine, Mather VA Medical Center, Sacramento, CA 95655, USA

* Author to whom correspondence should be addressed; E-Mail: razmik.mirzayans@albertahealthservices.ca; Tel.: +1-780-432-8897; Fax: +1-780-432-8428.

Academic Editor: William Chi-shing Cho

Received: 15 April 2015 / Accepted: 15 May 2015 / Published: 20 May 2015

Abstract: Phosphorylation of H2AX on Ser139 (γH2AX) after exposure to ionizing radiation produces nuclear foci that are detectable by immunofluorescence microscopy. These so-called γH2AX foci have been adopted as quantitative markers for DNA double-strand breaks. High numbers of spontaneous γH2AX foci have also been reported for some human solid tumor-derived cell lines, but the molecular mechanism(s) for this response remains elusive. Here we show that cancer cells (e.g., HCT116; MCF7) that constitutively express detectable levels of $p21^{WAF1}$ (p21) exhibit low numbers of γH2AX foci (<3/nucleus), whereas p21 knockout cells (HCT116p21−/−) and constitutively low p21-expressing cells (e.g., MDA-MB-231) exhibit high numbers of foci (e.g., >50/nucleus), and that these foci are not associated with apoptosis. The majority (>95%) of cells within HCT116p21−/− and MDA-MB-231 cultures contain high levels of phosphorylated p53, which is localized in the nucleus. We further show an inverse relationship between γH2AX foci and nuclear accumulation of WIP1, an oncogenic phosphatase. Our studies suggest that: (i) p21 deficiency might provide a selective pressure for the emergence of

apoptosis-resistant progeny exhibiting genomic instability, manifested as spontaneous γH2AX foci coupled with phosphorylation and nuclear accumulation of p53; and (ii) p21 might contribute to positive regulation of WIP1, resulting in dephosphorylation of γH2AX.

Keywords: $p21^{WAF1}$; WIP1; γH2AX foci; p53; apoptosis

1. Introduction

Phosphorylation of the histone H2A variant H2AX on Ser139 is an important event in the cellular response to genotoxic agents that induce DNA double-strand breaks (DSBs) [1]. This phosphorylation can be mediated by different protein kinases, including ataxia telangiectasia mutated (ATM) and other members of the phosphatidylinositol 3-kinase (PI3K)-related family of protein kinases [2]. Hundreds of H2AX molecules in the chromatin surrounding a DSB are phosphorylated on this residue, which can be visualized as a distinct nuclear focus by immunofluorescence microscopy [3]. Ser139 phosphorylated H2AX molecules are referred to as γH2AX. The formation of these γH2AX foci around each DSB facilitates the recruitment of DNA repair and checkpoint signaling factors [1]. There is compelling evidence that DSBs provide the primary signal for H2AX phosphorylation [1]. Accordingly, the quantification of γH2AX foci has emerged as a widely-used marker of DSBs that are detected by the cell [1–6]. After repair of DSBs, dephosphorylation of γH2AX at Ser139 has been shown to be important in allowing restart of the cell cycle and the maintenance of cell homeostasis. This critical function is largely accomplished by wild-type p53-induced phosphatase 1 (WIP1, or PPM1D), a type 2C serine/threonine phosphatase [7–9].

Spontaneously high levels of γH2AX foci can occur in cells without exposure to exogenous stress. Apoptotic cell death [10,11] and replicative senescence [12–15], for example, are both associated with accumulation of DSBs, and, hence, γH2AX foci formation. Somewhat surprisingly, high numbers of γH2AX foci (e.g., 50 per nucleus) have also been observed in cells within proliferating cultures of some human solid tumor-derived cell lines. Yu *et al.* [16] examined 17 cell lines chosen randomly from the NCI-60 panel of cancer cell lines and observed that cell lines expressing mutant p53 or lacking p53 function showed a significantly higher number of γH2AX foci than cell lines expressing wild-type p53. The mechanism by which wild type p53 prevents the spontaneous H2AX phosphorylation remains largely speculative.

In the current study we tested the hypothesis that endogenous H2AX phosphorylation might be associated with constitutively low expression of $p21^{WAF1}$ (p21) and/or WIP1, both of which are transcriptionally activated by p53 and play major roles in the ATM-p53 pathway and maintenance of genomic stability (reviewed in [17]). The p21 protein was discovered in the early 1990's and was classified as a member of the CIP/KIP family of the cyclin-dependent kinase (CDK) inhibitors [18,19]. It binds to and inhibits the activity of cyclin/CDK complexes (e.g., CDK1, 2 and 4), thus effectively blocking cell cycle progression. Subsequently, p21 was described as a multifunctional, broad-acting protein with key roles not only in cell cycle regulation but also in DNA repair, transcription, apoptosis and senescence (reviewed in [17,20–22]). WIP1, on the other hand, dephosphorylates γH2AX and other DNA damage response proteins (e.g., ATM, p53, BAX), thereby suppressing apoptosis [17,23].

In view of these properties of p21 and WIP1, we reasoned that loss or constitutively low expression of p21 in human cancer cells might lead to genomic instability (e.g., DSBs), triggering spontaneous γH2AX foci formation, and that low expression of WIP1 might contribute to the persistence of such foci. We performed three sets of experiments to test our hypotheses: (i) studies with the HCT116 colon carcinoma cell line and its p21 knockout derivative (HCT116p21−/−); (ii) studies with breast cancer cell lines that differ with respect to *TP53* status, and hence constitutive p21 and WIP1 levels; and (iii) studies with the p53 wild-type MCF7 cell line in which WIP1 or p21 was suppressed by pharmacological and siRNA approaches. We demonstrate that high numbers of endogenous γH2AX foci correlate inversely with expression of both p21 and WIP1, and that these endogenous foci are not associated with cells undergoing apoptosis. Aside from providing a molecular basis for spontaneous γH2AX foci, our studies suggest that p21-deficiency (absence or constitutively low expression) in human solid tumor-derived cells might provide a selective pressure for the emergence of apoptosis-resistant progeny exhibiting genomic instability.

2. Results and Discussion

2.1. p21 Loss in HCT116 Cells Promotes Spontaneous Activation of a DNA Damage Response Pathway

The HCT116 colon carcinoma cell line expresses wild-type p53 and p21 proteins and responds to moderate doses of DNA-damaging agents by predominantly undergoing premature senescence [24–27]. The p21 protein is transcriptionally activated by p53 and contributes to the control of cell cycle checkpoints, DNA repair, transcription, apoptosis, and premature senescence [17,20–22]. In addition, studies with the parental HCT116 cell line and its p21 knockout derivative (HCT116p21−/−) have suggested a requirement of p21 in the negative regulation of p53 protein stability [28–32]. Endogenous p53 in HCT116p21−/− cells showed higher transcriptional activity [32] and phosphorylation at serines associated with p53 stability and nuclear localization [24,31,32] as compared to endogenous p53 in parental cells. These observations led Hill *et al.* [31] to conclude that HCT116p21−/− cells display a classical "stressed" phenotype. Consistent with this notion, these authors observed significantly higher levels of γH2AX in HCT116p21−/− cells than in parental cells when evaluated by immunoblot analysis. Whether high levels of γH2AX in HCT116p21−/− cells reflects nuclear foci was not reported.

We performed immunofluorescence staining with an antibody specific for the phosphorylation of Ser139 at the *C*-terminal region of H2AX and observed a remarkable difference between HCT116p21−/− and parental cultures in terms of spontaneous γH2AX foci. Representative immunofluorescence images are shown in Figure 1A, and averaged data from multiple experiments are presented in Figure 1B. For ease of comparison, cells were divided into three categories: cells with low numbers of foci (less than 3 per nucleus, as observed with normal human fibroblasts before exposure to genotoxic agents [4,33,34]), cells with moderate numbers of foci (between 3 and 10 per nucleus), and cells with high numbers of foci (greater than 10 per nucleus). Approximately 5% and 95% of the cells within HCT116p21−/− and parental cultures exhibited low (background) numbers of foci, respectively, whereas the majority (~95%) of cells within HCT116p21−/− cultures and only ~5% of cells within parental cultures contained moderate or high numbers of foci (Figure 1B).

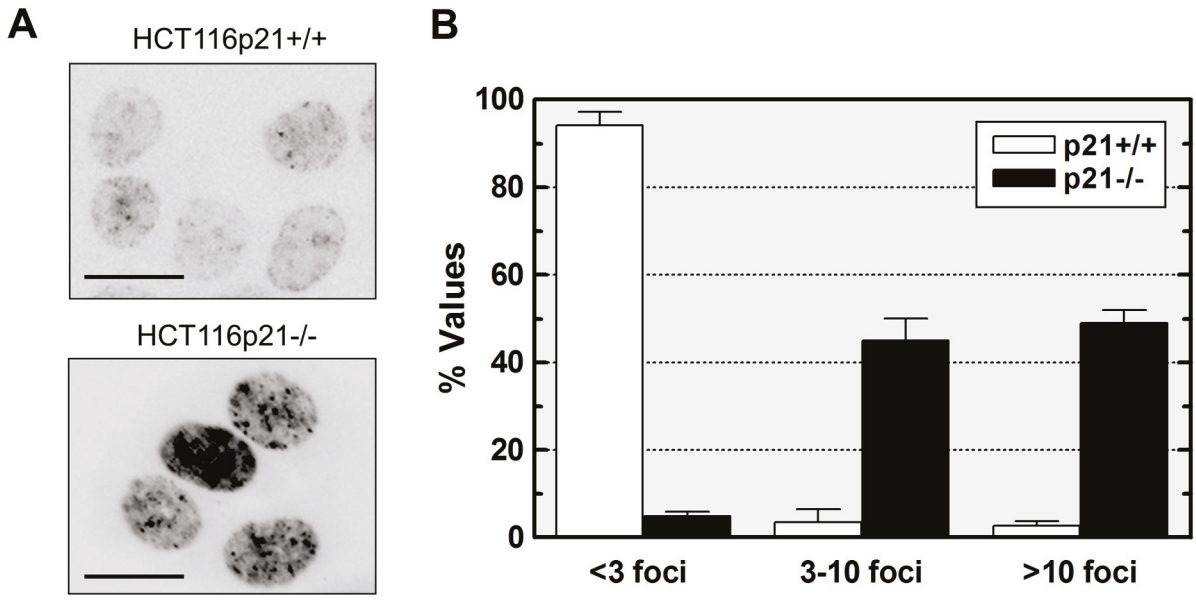

Figure 1. Influence of p21 loss on endogenous γH2AX foci in HCT116 cells. (**A**) Representative immunofluorescence images showing constitutive γH2AX foci in HCT116p21+/+ and HCT116p21−/− cultures; scale bar, 10 μm; (**B**) Comparison of these cultures for the proportion of cells with low/background (<3/nucleus), moderate (3–10/nucleus) and high (>10/nucleus) levels of foci. Bars, standard error (SE).

Given that the kinases (e.g., ATM) that phosphorylate H2AX in response to DSBs also typically phosphorylate p53, the presence of γH2AX foci in the majority of HCT116p21−/− cells suggests that these cells may also exhibit phosphorylation and nuclear accumulation of p53 in the absence of an exogenous DSB stimulus. Unfortunately the results in the literature on the influence of p21 loss on subcellular localization of p53 have been contradictory. Hill *et al.* [31] observed high levels of p53 in the nuclear fraction of HCT116p21−/− cells, whereas Peng *et al.* [35] reported the cytoplasmic sequestration of p53 in these cells. We therefore performed p53 immunostaining experiments to determine what proportion of cells within HCT116p21−/− cultures exhibit nuclear and/or cytoplasmic localization of p53. A small proportion (<5%) of HCT116p21−/− cells exhibited either cytoplasmic localization of p53 or did not express p53 at levels detectable by this assay (data not shown). The majority (>95%) of HCT116p21−/− cells, however, exhibited high levels of p53 in the absence of irradiation or other exogenous stress, and these p53 molecules were phosphorylated (e.g., at serines 15 and 46) and localized in the nucleus (Figure 2). Incubation of HCT116p21−/− cultures for 24 h with caffeine, an inhibitor of PI3K-like protein kinases [31], resulted in a marked decrease in the spontaneous phosphorylation and nuclear levels of p53 (Figure 2). Similar treatments with the PI3K-like protein kinase inhibitors wortmannin (10 μM) and LY294002 (20 μM) also suppressed nuclear p53 in HCT116p21−/− cells, although to a lesser extent than that seen with caffeine (data not shown). Unlike HCT116p21−/− cells, the majority (>80%) of parental HCT116 cells exhibited low levels and phosphorylation of constitutive p53 protein (Figure 2).

We conclude that loss of p21 in HCT116 cells promotes spontaneous activation of a DNA damage response pathway as evidenced by formation of γH2AX foci coupled with phosphorylation and nuclear accumulation of p53.

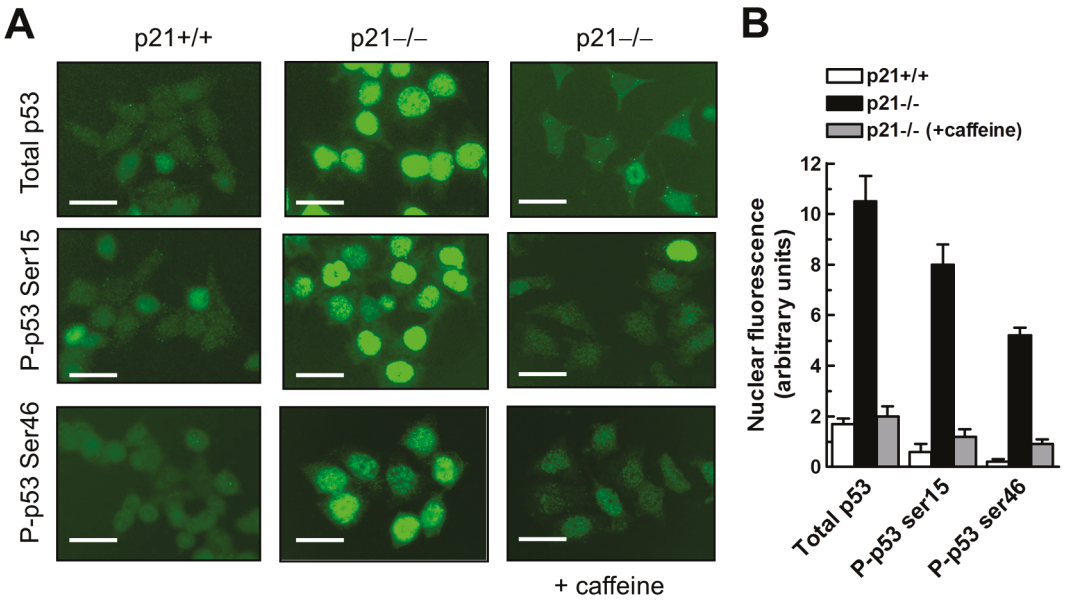

Figure 2. Immunofluorescence analysis of p53 protein levels and phosphorylation status in HCT116p21+/+ and HCT116p21−/− cultures before and after incubation with caffeine (4 mM; 24 h). (**A**) Representative images showing phosphorylation and nuclear localization of p53 in HCT116p21−/− cultures and suppression of these effects by caffeine; scale bar, 20 µm; (**B**) Densitometric evaluation of intensities of nuclear fluorescence staining. Bars, SE.

2.2. Loss of p21 in HCT116 Cells Is Associated with Accumulation of DNA Double-Strand Breaks (DSBs)

The presence of cells with high numbers of γH2AX foci within HCT116p21−/− cultures suggests the spontaneous accumulation of DNA DSBs. We used the neutral comet assay to further test this notion. In this assay, the appearance of a comet tail is presumed to reflect the presence of DSBs [36]. Representative comet images and measurement of the percentages of cells with a comet tail are shown in Figure 3. Exponentially growing HCT116p21−/− cultures contained a much higher (~8-fold) proportion of cells with DSBs than the parental cultures. However, it is important to note that the proportion of cells with DSBs (~40%) in HCT116p21−/− cultures was less than that of cells with >3 γH2AX foci (~95%).

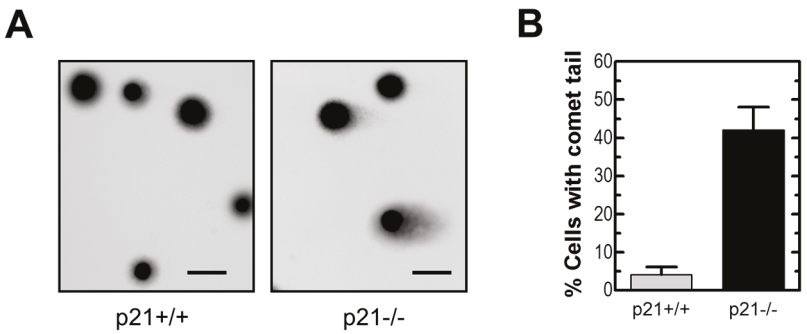

Figure 3. Neutral comet analysis of DSBs in HCT116p21+/+ and HCT116p21−/− cultures. Representative images (**A**) together with percentages of cells with DSBs (**B**) are presented. The mean (± SE) of the values obtained for four comet slides are shown in panel (**B**); at least 50 cells were analyzed for each slide. Scale bar, 10 µm.

2.3. Endogenous γH2AX Foci and DSBs in HCT116p21−/− Cells Are not Associated with Apoptosis

DNA DSBs can cause loss of colony-forming ability of different human cell types without triggering apoptosis. Studies with human fibroblast strains [37] and lung carcinoma cell lines [6] have shown that DSB-induced loss of clonogenicity predominantly reflects premature senescence, and that this response correlates with sustained upregulation of p21 in p53 wild-type cells and of $p16^{INK4a}$ (hereafter p16) in p53 mutated cells. The finding that DSBs are virtually non-apoptogenic in the fibroblast strains and cancer cell lines used in those studies is not surprising, given that both p21 [21] and p16 [38] are well known to suppress apoptosis. The HCT116 colon carcinoma cells, however, do not express p16 due to the presence of a frameshift mutation in one allele of the *INK4A* gene and hypermethylation of the promoter of the other allele [39]. Accordingly, loss of p21 function in these cells might be expected to render them highly sensitive to DSB-induced apoptosis. To test this possibility, exponentially growing HCT116p21−/− and parental cultures were evaluated by the Annexin V/flow cytometry, propidium iodide-exclusion, Hoechst 33258 staining, and BrdUrd immunofluorescence assays. The BrdUrd immunofluorescence assay was performed with cultures that were incubated for 24 h in the presence of BrdUrd (0.1 mM) to allow the selective incorporation of the analogue into the genome of replicating cells. The results are presented in Figure 4. Representative flow cytometric profiles and microscopic images are shown in panels A–C, and results from different experiments are averaged in panel D. There was no significant difference between HCT116p21−/− and parental cultures in terms of the proportion of Annexin V-positive (apoptotic) cells, propidium iodide-positive (nonviable) cells, and BrdUrd-positive (replicating) cells. Consistent with these observations, microscopic evaluation following Hoechst staining revealed the presence of <2% of cells with apoptotic morphology in both cultures.

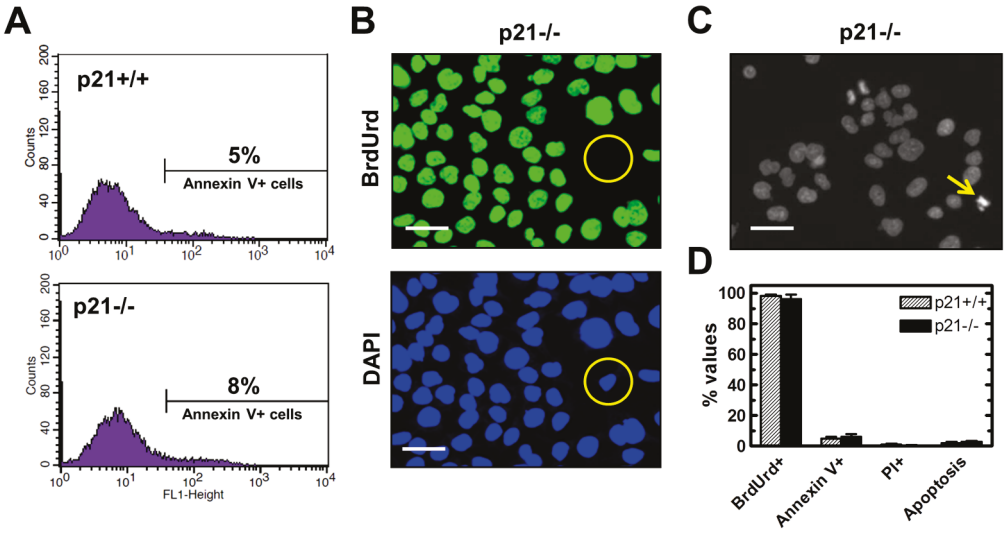

Figure 4. Comparison of HCT116p21+/+ and HCT116p21−/− cultures for apoptosis, viability and proliferation. (**A**) Flow cytometric evaluation of Annexin V-positive (apoptotic) cells; (**B**) Evaluation of replicating cells by the BrdUrd immunofluorescence assay. Circles mark a cell that did not exhibit DNA synthesis during the 24-h incubation period with BrdUrd; Scale bar, 20 μm; (**C**) Representative image of Hoechst 33258-stained HCT116p21−/− cells. The arrow marks a cell with apoptotic morphology; Scale bar, 20 μm; (**D**) Comparison of these cultures for the indicated parameters. Bars, SE. PI, propidium iodide.

These observations are compatible with a model in which the sustained absence of p21 function in p16-deficient cancers might create a strong selective pressure for the enrichment of cells exhibiting genomic instability coupled with resistance toward DSB-induced apoptosis.

2.4. Spontaneous γH2AX Foci in Mutant p53-Expressing Cell Lines in Relation to DSBs and Apoptosis

We next compared the breast cancer cell lines MCF7, MDA-MB-231 and MDA-MB-435s for γH2AX foci, DSBs, proliferation and apoptosis. MCF7 cells express wild-type p53, whereas MDA-MB-231 and MDA-MB-435s cells express mutant p53 [21,40], which is localized in the nucleus [21]; mutant p53 in MDA-MD-231 cells is phosphorylated on serine 15 in the absence of exogenous stress ([41,42] and Figure 5).

Immunofluorescence microscopy demonstrated the presence of moderate levels (between 3 and 10 per nucleus) or high levels (>10 per nucleus) of γH2AX foci in the majority (>80%) of cells within MDA-MB-231 and MDA-MB-435s cultures, but in only ~5% of cells within MCF7 cultures (Figure 6). The neutral comet assay also showed a higher proportion of cells with DSBs in MDA-MB-231 (~20%) and MDA-MB-435s (~30%) cultures than in MCF7 cultures (<5%) (data not shown). On the other hand, exponentially growing cultures of these three cell lines contained a similar proportion of apoptotic cells (<2%) and proliferating cells (>90%) (Figure 6C), indicating that spontaneous γH2AX foci and DSBs in the MDA-MB-231 and MDA-MB-435s cell lines are not associated with apoptosis.

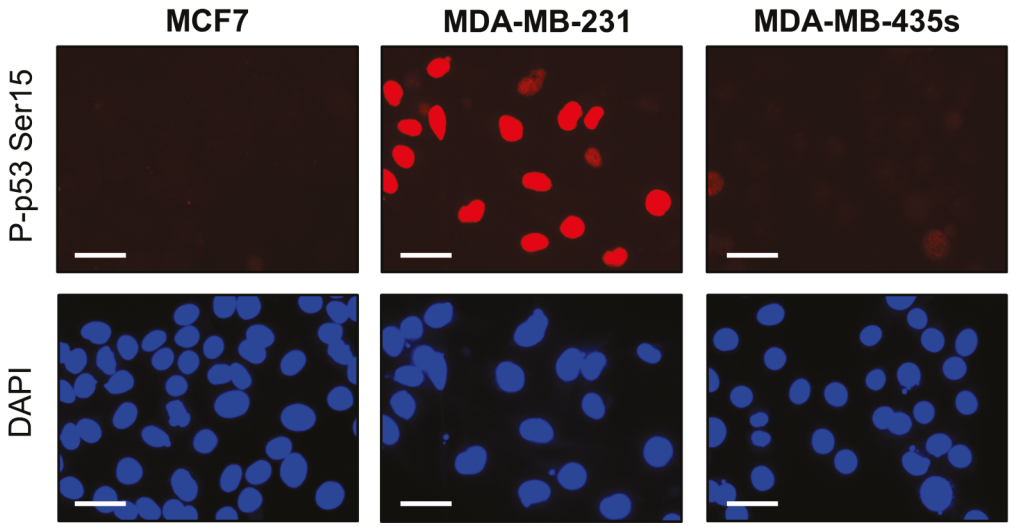

Figure 5. Serine 15-phosphorylated p53 protein levels in the indicated cancer cell lines. Scale bar, 20 µm.

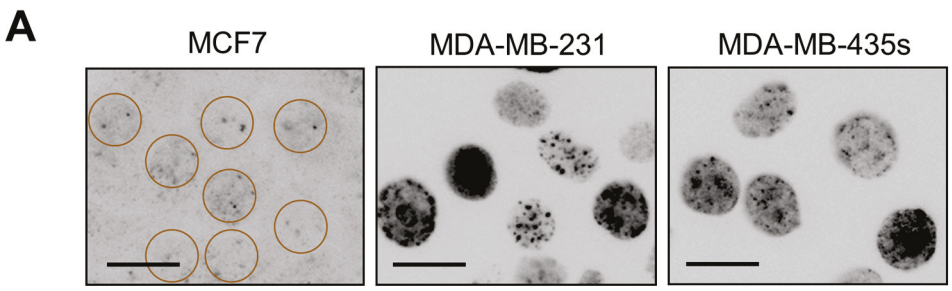

Figure 6. *Cont.*

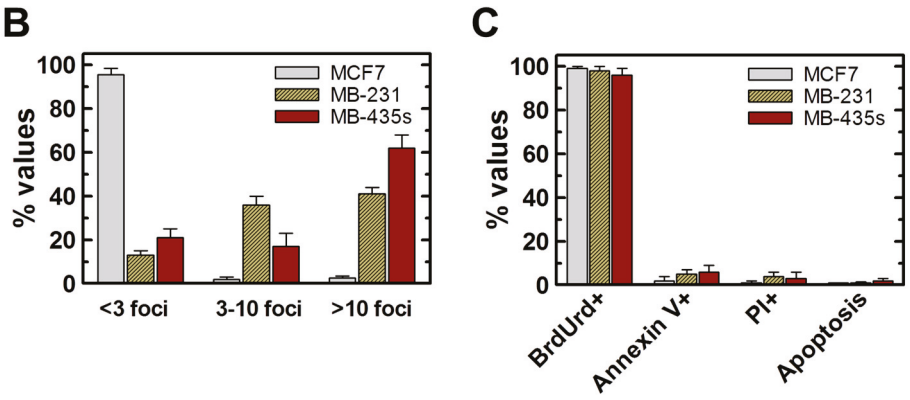

Figure 6. Spontaneous levels of γH2AX foci in the indicated breast cancer cell lines. (**A**) Immunofluorescence images showing constitutive γH2AX foci. Circles mark nuclei with low levels of foci; Scale bar, 10 μm; (**B**) Comparison of these cell lines for the proportion of cells exhibiting the indicated numbers of foci per nucleus. Bars, SE; (**C**) Comparison of these cultures for proliferation (BrdUrd incorporation), loss of viability (propidium iodide uptake) and apoptosis (Annexin V positive; apoptotic morphology). Bars, SE.

2.5. Inverse Correlation between γH2AX Foci and WIP1 Expression

Yu *et al.* [16] proposed that high endogenous levels of γH2AX foci in some cancer cell lines lacking wild-type p53 function might reflect chromatin instability, broadly defined. This conclusion was based on the observation that high numbers of γH2AX foci in the SW756 cervical carcinoma cell line were not associated with spontaneous DSBs when evaluated by the neutral comet assay. In the current study, we have shown that HCT116p21−/− cultures contain ~95% of cells with spontaneous γH2AX (Figure 1) but only ~40% of cells with DSBs (Figure 3). Similarly, the proportion of cells with γH2AX in MDA-MB-231 and MDA-MB435s cultures (Figure 6) was greater than that of cells with DSBs (data not shown). These results are consistent with the conclusion of Yu *et al.* [16] that factors in addition to DSBs might contribute to high endogenous levels of γH2AX foci in some cancer cell lines. We focused on WIP1, which is known to dephosphorylate γH2AX in response to ionizing radiation after DSBs are rejoined [9,17]. The results of immunofluorescence and immunoblotting experiments are presented in Figures 7 and 8, respectively. HCT116 and MCF7 cell lines that exhibit low (background) levels of γH2AX foci expressed detectable levels of constitutive WIP1, which was localized in the nucleus, whereas the three cell lines with high γH2AX foci levels (HCT116p21−/−, MDA-MB-231, and MDA-MB-435s) exhibited relatively low levels of WIP1.

We extended these studies to other cancer cell lines that express wild-type p53 (A549; SKNSH), mutant p53 (SUM159-PT; MDA-MB-648; BT20, SKBR3), or no p53 (SKOV3; HCT116 p53 knockout). Consistent with the observations reported above, wild-type p53-expressing cell lines contained low levels of γH2AX foci whereas cell lines lacking wild-type p53 function contained high levels of γH2AX foci (data not shown). Furthermore, levels of γH2AX foci in these cell lines correlated inversely with endogenous expression of both p21 and WIP1 (data not shown).

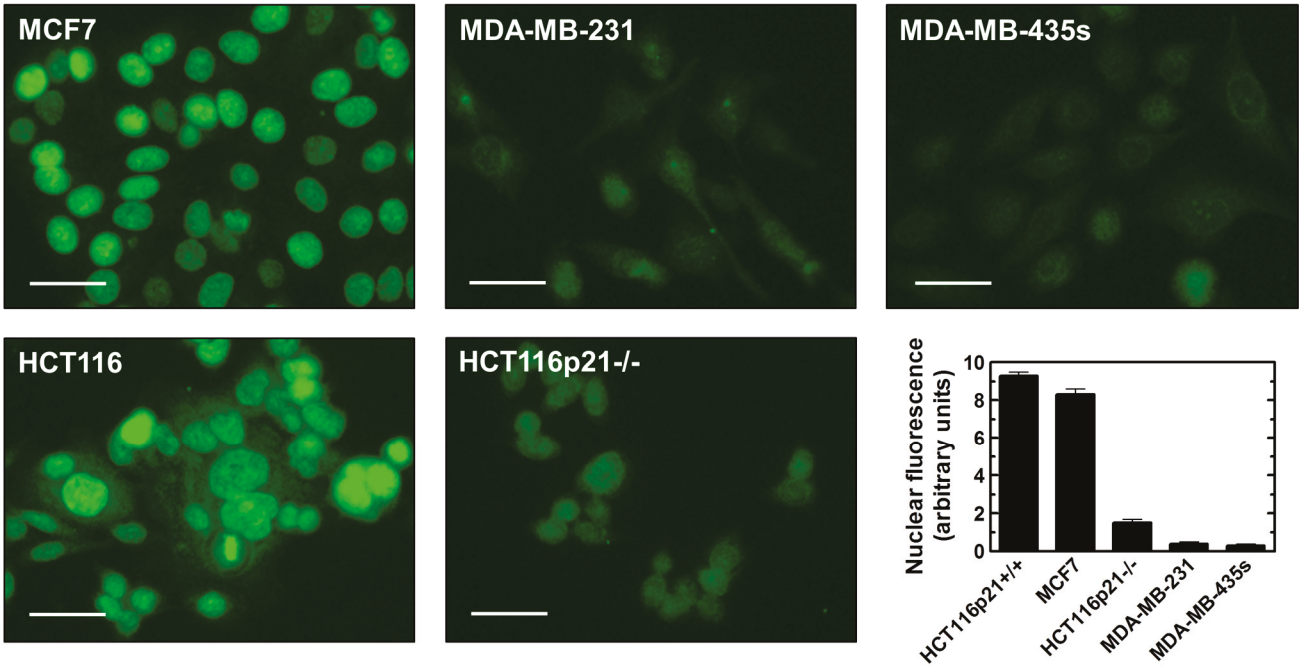

Figure 7. Immunofluorescence analysis of constitutive WIP1 protein levels in the indicated cell lines. Representative images together with densitometric evaluation of intensities of nuclear fluorescence staining are presented. Bars, SE. Scale bar, 20 μm.

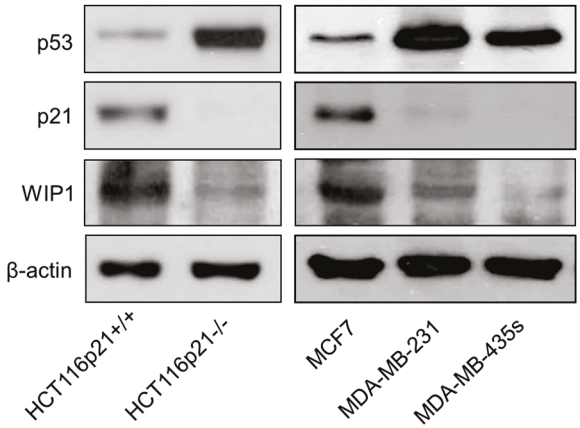

Figure 8. Immunoblot analysis of constitutive p53 (global), p21 and WIP1 protein levels in the indicated cell lines.

2.6. Influence of WIP1 Knockdown on γH2AX Foci

To determine whether phosphatase inhibition can, by itself, promote γH2AX foci formation, MCF7 cells were either treated with a phosphatase inhibitor (PhosSTOP) [43] or transfected with a WIP1 siRNA or a control siRNA [44] and then evaluated by γH2AX immunofluorescence. A 2-h treatment with PhosSTOP followed by incubation in fresh medium for 24 h resulted in γH2AX foci in the majority of the cells (Figure 9A,B). Similarly, transfection with WIP1 siRNA (50 nM) for 48 h resulted in lowering of nuclear WIP1 levels accompanied by γH2AX foci in the majority of the cells (Figure 9C,D). On the other hand, transfection with control siRNA had no influence on WIP1 levels and did not trigger γH2AX foci (Figure 9C,D).

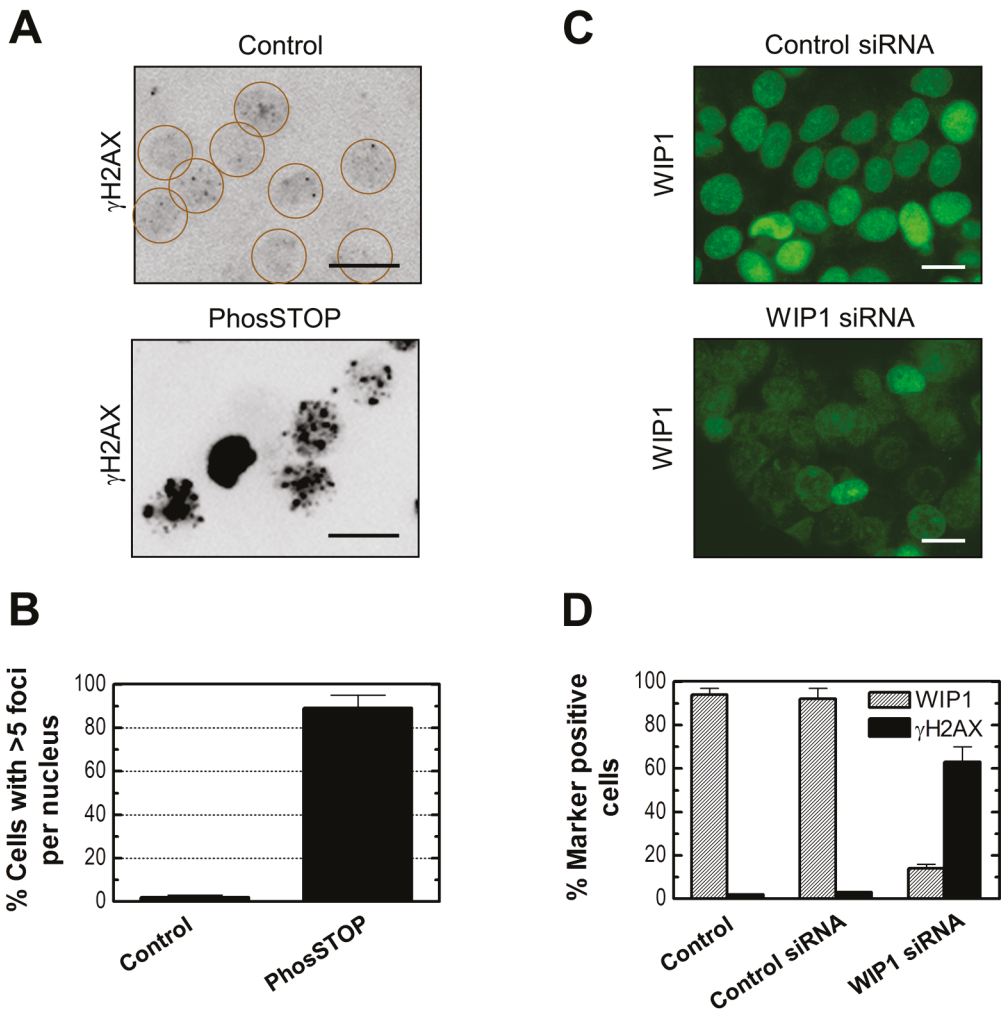

Figure 9. Influence of phosphatase inhibition by PhosSTOP or WIP1 siRNA on γH2AX foci in MCF7 cells. (**A**) Representative images showing presence of γH2AX foci after PhosSTOP treatment. Circles mark cells with low (background) levels of foci; Scale bar, 10 µm; (**B**) Proportion of cells with >5 γH2AX foci/nucleus for the indicated treatments. Bars, SE; (**C**) Representative images showing nuclear WIP1 levels after transfection with control siRNA or WIP1 siRNA; Scale bar, 10 µm; (**D**) Influence of transfection with the indicated siRNAs on the proportion of WIP1 positive cells (exhibiting strong nuclear staining) and γH2AX positive cells (exhibiting >5 γH2AX foci/nucleus); Bars, SE.

We also determined the effect of phosphatase inhibition on DSBs and cytotoxicity (data not shown). PhosSTOP treatment or transfection with WIP1 siRNA induced DSBs in only <5% of the cells when evaluated by the neutral comet assay. In addition, under these conditions we observed marginal (<5%) cytotoxicity when assessed by microscopic examination and immunofluorescence analysis after propidium iodide staining (loss of viability) and Hoechst 33258 staining (apoptotic morphology).

2.7. Influence of p21 Inhibition on γH2AX Foci and Nuclear Levels of WIP1 and p53

To determine whether p21 inhibition can promote γH2AX foci, we performed studies with MCF7 cells that were either treated with a pharmacological inhibitor of p21 (UC2288 [45] or high concentrations of the CDK/cyclin inhibitor roscovitine [46]), or were transfected with a p21 siRNA [47]. In contrast

to WIP1 inhibition, p21 inhibition under conditions typically used in published studies with other cell types resulted in significant cytotoxicity in MCF7 cultures. For example, a 48-h transfection with 50 nM p21 siRNA resulted in extensive cell detachment, whereas transfection with WIP1 siRNA under similar conditions elicited marginal (if any) effect (data not shown). Immunofluorescence analysis after propidium iodide and Hoechst 33258 staining indicated that virtually all detached cells had lost viability and a high proportion (~40%) exhibited apoptotic morphology (nuclear condensation and fragmentation) (data not shown).

We observed γH2AX foci in the majority (~70%) of MCF7 cells that remained adherent after treatment with roscovitine (Figure 10), treatment with UC2288 (data not shown), or transfection with p21 siRNA (data not shown). On the other hand, neutral comet assay demonstrated the presence of DSBs in only ~10% of these cells (Figure 10B and data not shown).

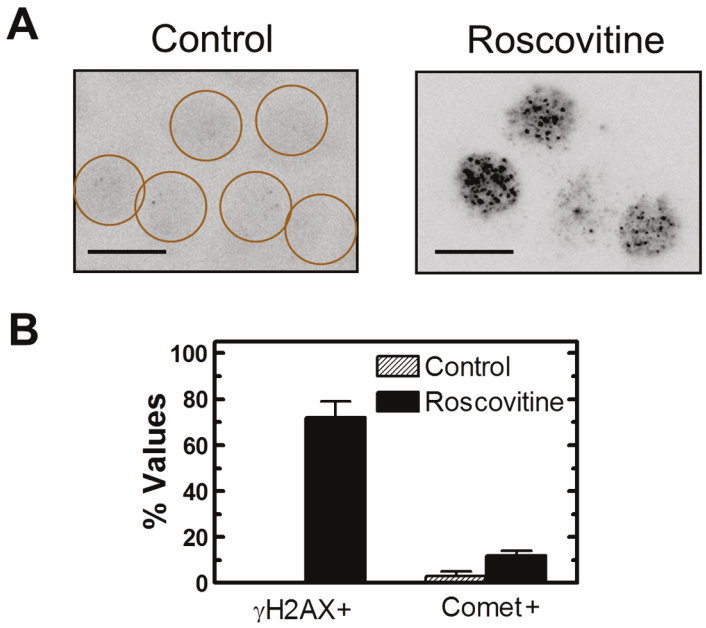

Figure 10. (**A**) Representative images showing the presence of γH2AX foci in MCF7 cells treated with roscovitine (40 μM) for 24 h. Circles mark cells with low (background) levels of foci; Scale bar, 10 μm; (**B**) Influence of roscovitine treatment on percentages of cells with γH2AX foci (exhibiting >5 foci/nucleus) and DSBs (exhibiting ≥10% fluorescence in comet tails). Bars, SE.

Roscovitine at 40 μM was less toxic than p21 siRNA and UC2288 when used under conditions required to diminish constitutive p21 protein levels in MCF7 cells. We, therefore, used roscovitine to determine the effect of p21 suppression on WIP1 and p53 protein levels. If p21 functions as a positive regulator of WIP1, as suggested by the studies reported above, then suppressing p21 should also lead to suppression of WIP1 (a negative regulator of p53) accompanied by upregulation of p53. The results of immunostaining and immunoblotting experiments are presented in Figure 11. Roscovitine treatment of MCF7 cells caused downregulation of both p21 and WIP1, but led to upregulation and nuclear localization of p53. We conclude that p21 does function as a positive regulator of WIP1 in this breast carcinoma cell line.

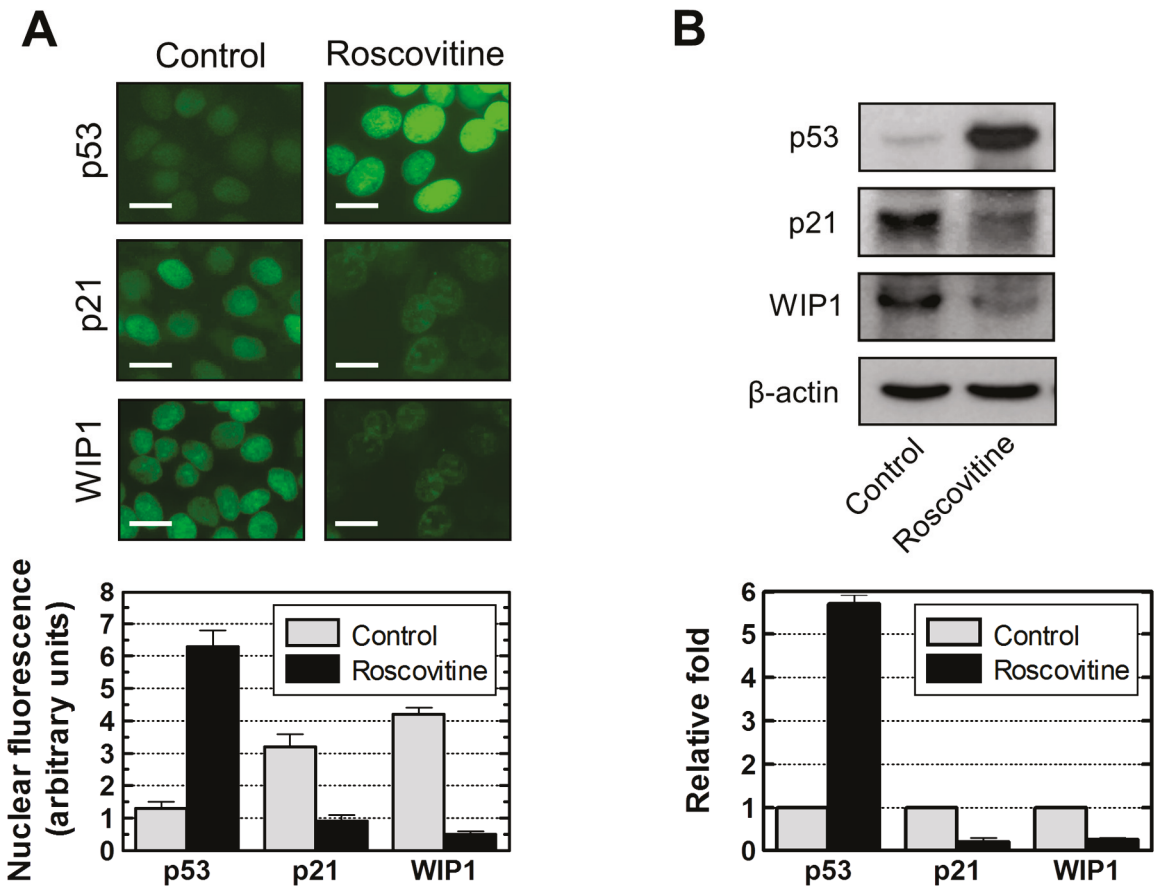

Figure 11. Influence of p21 downregulation by roscovitine (40 μM, 24 h) on p53 and WIP1 protein levels in MCF7 cells. (**A**) Immunofluorescence analysis of nuclear protein levels for control and roscovitine-treated cultures. The histograms for the indicated proteins were obtained from densitometric analysis of intensities of nuclear fluorescence staining from at least four coverslips; over 100 cells were evaluated for each coverslip. Bars, SE; Scale bar, 10 μm; (**B**) Immunoblot analysis of global protein levels before and after roscovitine treatment. The histograms for each protein were obtained from densitometric analysis of the band, normalized to actin, from at least three independent immunoblots. Bars, SE.

3. Experimental Section

3.1. Cells and Cell Culture

The human colon carcinoma cell line HCT116, which is known to activate the p53-p21 axis after DNA damage, and a p21 homozygous knockout derivative of this cell line (HCT116p21−/−) were generous gifts of Dr. Bert Vogelstein (Johns Hopkins University, Baltimore, MD, USA). All other cancer cell lines used in the present study were purchased from the American Type Culture Collection (Rockville, MD, USA). Cells were cultured as monolayers in DMEM/F12 nutrient medium supplemented with 10% (*v*/*v*) fetal bovine serum as described [25]. All cultures were free of *Mycoplasma* contamination.

3.2. Antibodies

Antibodies to p53 (DO-1), p21, WIP1, and β-actin were purchased from Santa Cruz Biotechnology (Santa Cruz, CA, USA). An antibody to bromodeoxyuridine (BrdUrd) was purchased from Becton Dickson (San Jose, CA, USA). A phosphospecific antibody to γH2AX (Ser139) was purchased from Cedarlane Laboratories (Hornby, ON, Canada). Phosphospecific antibodies to Ser15 and Ser46 of human p53 were purchased from Cell Signaling (Beverly, MA, USA). Alexa Fluor 488 antibodies (goat anti-mouse IgG and donkey anti-rabbit IgG) were purchased from Molecular Probes (Eugene, OR, USA).

3.3. Immunoblot and Immunofluorescence Techniques

Global levels of specific proteins were evaluated by immunoblotting as described [48]. Protein, γ-H2AX, and BrdUrd immunofluorescence assays were performed as described [49].

3.4. siRNA-Mediated Gene Silencing Analysis

Transfection with siRNA targeting WIP1 (D-004554-01; Thermo Scientific Dharmacon; Chicago, IL, USA), p21 (SC37007; Santa Cruz), or control siRNA (D-001210-01; Thermo Scientific) was performed using published protocols [50,51]. In a pilot experiment we compared different transfection reagents and found transfection using Lipofectamine 2000 (Invitrogen, Carlsbad, CA, USA) to yield reproducible results. Cells were incubated with the Lipofectamine 2000 transfection mixture containing siRNA sequences for 48 h and then analyzed by immunofluorescence microscopy.

3.5. Neutral Comet Assay

DSBs were quantified using a commercial neutral comet kit (Cell Signaling Technology, Beverly, MA, USA) as described [4]. DSB frequencies were determined from the percentage of total fluorescence in the comet tail as described [4]. Cells exhibiting ≥10% fluorescence in comet tail were scored as positive [4].

3.6. Annexin V/Flow Cytometry Analysis

Apoptosis was evaluated by the Annexin V/flow cytometry assay as described [49].

3.7. Propidium Iodide-Exclusion Assay

Cell viability was evaluated by the propidium iodide (PI)-exclusion assay as described [37].

4. Conclusions

High levels of spontaneous γH2AX foci that arise in certain human cancer cell lines have been postulated to reflect DNA replication stress, telomere dysfunction, and chromatin instability [13,16,52–55]. In this report, we have demonstrated an inverse relationship between γH2AX foci and expression of both p21 and WIP1 in proliferating cultures of the panel of cancer cell lines that we examined. Our

findings are consistent with the known properties of p21 and WIP1. In addition to its pivotal role in activating cell cycle checkpoints, downregulating apoptosis and inducing premature senescence, the p21 protein is recruited by γH2AX to DSB sites in genomic DNA [56–59] and promotes the replication-coupled repair of DSBs [59]. Loss or constitutively low expression of p21 would result in diminished ability to effect replication-coupled DSB rejoining as compared to wild-type cells expressing "normal" levels of p21, and low expression of WIP1 would result in γH2AX foci persisting for long times after rejoining of DSBs, which would be visualized as spontaneous γH2AX foci. In support of this model, down-regulating/inhibiting either WIP1 or p21 in MCF7 cells resulted in accumulation of γH2AX foci in the absence of exogenous stress.

Induction of WIP1 in response to genotoxic stress is mediated by p53-dependent and -independent mechanisms in human cancer cells [44]. Our current results suggest that p21 might function as a positive regulator of WIP1 independent of wild-type p53 activity. This conclusion is based on the findings that: (i) p21 knockout HCT116 cells express constitutively low levels of WIP1 despite the spontaneous phosphorylation and nuclear accumulation of (wild-type) p53 when compared to parental cells; and (ii) down-regulating p21 in MCF7 cells results in low expression of WIP1 but nuclear accumulation of (wild-type) p53. Given that WIP1 is a key negative regulator of p53 [17,60,61] and apoptotic cell death [23], our results suggest that one mechanism by which p21 might exert its inhibitory effects on p53 and apoptosis might be through regulating WIP1, at least in these widely used cancer cell lines.

As illustrated in Figure 12, our findings suggest a novel role for p21 in the response of solid tumor-derived cell lines to genotoxic stress (e.g., spontaneous DSBs); namely, its ability to form a regulatory loop with WIP1 and hence potentially contribute to dephosphorylation of p53, γH2AX, and probably other key participants in the DNA damage surveillance network. Thus, our findings add to the complexity of p21 functions and lend credence to the cautionary note made by us [17] and Warfel and El-Deiry [20] that a greater insight into the molecular and biological consequences associated with p21 loss is crucial to determining whether modulating p53–p21 signaling might be a promising approach for the treatment of certain types of cancers. Towards this end, further studies are warranted to determine: (i) the generality of our observations (*i.e.*, interplay between p53, p21 and WIP1) in different types of non-transformed and cancerous cells; and (ii) whether p21-mediated WIP1 regulation occurs at the transcriptional, post-transcriptional, or post-translational level.

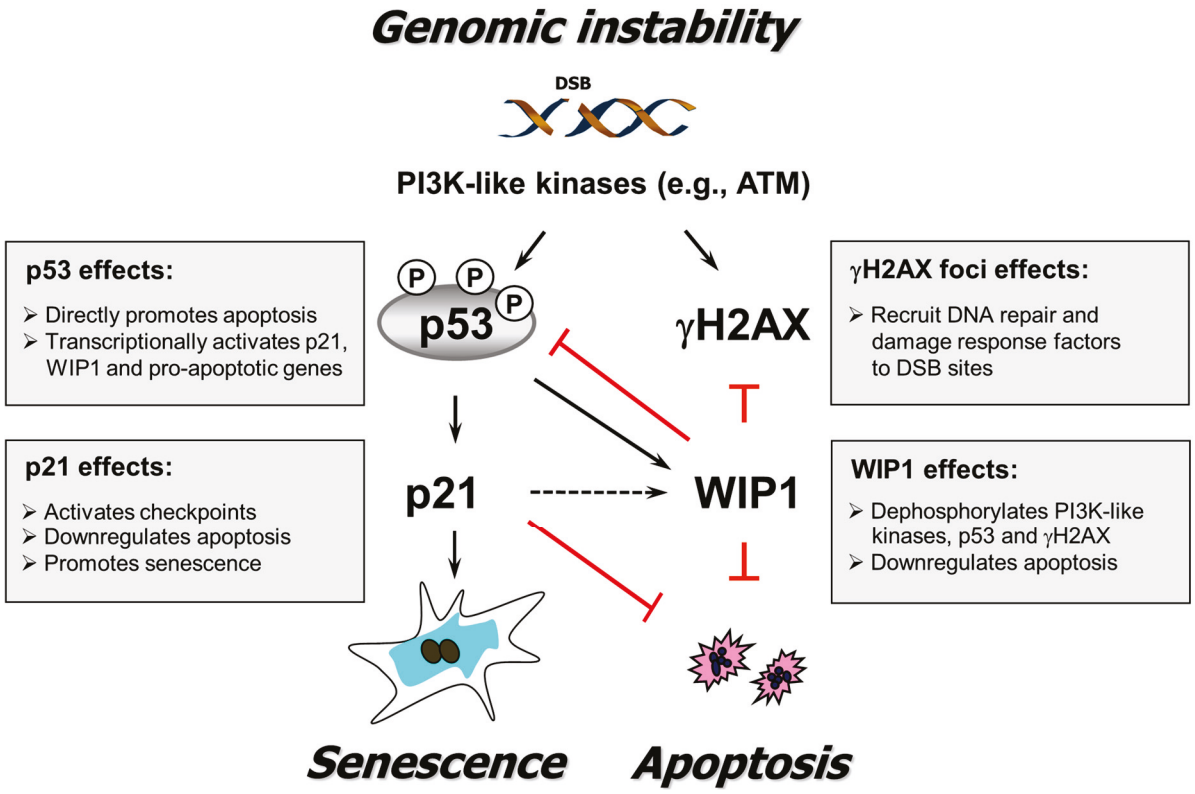

Figure 12. A schematic of the relationship between p53 signaling, γH2AX foci, DSB repair, and biological outcomes triggered by genotoxic stress (e.g., spontaneous DSBs) supported by the current study. Solid arrows indicate stimulation and T-shaped lines indicate inhibition. The dotted arrow indicates positive regulation of WIP1 by p21 suggested by studies reported herein. Some known functions of p53, p21, WIP1, and γH2AX are indicated (for details, consult [17]).

Acknowledgments

This work was supported by the Canadian Breast Cancer Foundation-Prairies/North West Territories Chapter.

Author Contributions

Razmik Mirzayans designed and planned the study, analyzed results, interpreted data, and wrote the manuscript. Bonnie Andrais, April Scott, Ying W. Wang performed experiments. Robert H. Weiss provided small molecule inhibitors and communicated inhibitor-related knowledge. David Murray interpreted data and edited the manuscript. All authors reviewed the manuscript.

Conflicts of Interest

The authors declare no conflict of interest.

References

1. Fernandez-Capetillo, O.; Lee, A.; Nussenzweig, M.; Nussenzweig, A. H2AX: The histone guardian of the genome. *DNA Repair* **2004**, *3*, 959–967.
2. Podhorecka, M.; Skladanowski, A.; Bozko, P. H2AX phosphorylation: Its role in DNA damage response and cancer therapy. *J. Nucleic Acids* **2010**, *2010*, 920161.
3. Pilch, D.R.; Sedelnikova, O.A.; Redon, C.; Celeste, A.; Nussenzweig, A.; Bonner, W.M. Characteristics of γ-H2AX foci at DNA double-strand breaks sites. *Biochem. Cell Biol.* **2003**, *81*, 123–129.
4. Mirzayans, R.; Severin, D.; Murray, D. Relationship between DNA double-strand break rejoining and cell survival after exposure to ionizing radiation in human fibroblast strains with differing ATM/p53 status: Implications for evaluation of clinical radiosensitivity. *Int. J. Radiat. Oncol. Biol. Phys.* **2006**, *66*, 1498–1505.
5. Kuo, L.J.; Yang, L.X. Gamma-H2AX—A novel biomarker for DNA double-strand breaks. *In Vivo* **2008**, *22*, 305–309.
6. Wang, M.; Morsbach, F.; Sander, D.; Gheorghiu, L.; Nanda, A.; Benes, C.; Kriegs, M.; Krause, M.; Dikomey, E.; Baumann, M.; *et al*. EGF receptor inhibition radiosensitizes NSCLC cells by inducing senescence in cells sustaining DNA double-strand breaks. *Cancer Res.* **2011**, *71*, 6261–6269.
7. Macůrek, L.; Lindqvist, A.; Voets, O.; Kool, J.; Vos, H.R.; Medema, R.H. WIP1 phosphatase is associated with chromatin and dephosphorylates γH2AX to promote checkpoint inhibition. *Oncogene* **2010**, *29*, 2281–2291.
8. Moon, S.H.; Lin, L.; Zhang, X.; Nguyen, T.A.; Darlington, Y.; Waldman, A.S.; Lu, X.; Donehower, L.A. Wild-type p53-induced phosphatase 1 dephosphorylates histone variant γ-H2AX and suppresses DNA double strand break repair. *J. Biol. Chem.* **2010**, *285*, 12935–22947.
9. Cha, H.; Lowe, J.M.; Li, H.; Lee, J.S.; Belova, G.I.; Bulavin, D.V.; Fornace, A.J., Jr. WIP1 directly dephosphorylates γ-H2AX and attenuates the DNA damage response. *Cancer Res.* **2010**, *70*, 4112–4122.
10. Rogakou, E.P.; Nieves-Neira, W.; Boon, C.; Pommier, Y.; Bonner, W.M. Initiation of DNA fragmentation during apoptosis induces phosphorylation of H2AX histone at serine 139. *J. Biol. Chem.* **2000**, *275*, 9390–9395.
11. Mukherjee, B.; Kessinger, C.; Kobayashi, J.; Chen, B.P.; Chen, D.J.; Chatterjee, A.; Burma, S. DNA-PK phosphorylates histone H2AX during apoptotic DNA fragmentation in mammalian cells. *DNA Repair* **2006**, *5*, 575–590.
12. Di Fagagna, F.A.; Reaper, P.M.; Clay-Farrace, L.; Fiegler, H.; Carr, P.; von Zglinicki. T.; Saretzki, G.; Carter, N.P.; Jackson, S.P. A DNA damage checkpoint response in telomere-initiated senescence. *Nature* **2003**, *426*, 194–198.
13. Sedelnikova, O.A.; Horikawa, I.; Zimonjic, D.B.; Popescu, N.C.; Bonner, W.M.; Barrett, J.C. Senescing human cells and ageing mice accumulate DNA lesions with unrepairable double-strand breaks. *Nat. Cell Biol.* **2004**, *6*, 168–170.
14. Von Zglinicki, T.; Saretzki, G.; Ladhoff, J.; di Fagagna, F.A.; Jackson, S.P. Human cell senescence as a DNA damage response. *Mech. Ageing Dev.* **2005**, *126*, 111–117.

15. Di Fagagna, F.A. Living on a break: Cellular senescence as a DNA-damage response. *Nat. Rev. Cancer* **2008**, *8*, 512–522.
16. Yu, T.; MacPhail, S.H.; Banáth, J.P.; Klokov, D.; Olive, P.L. Endogenous expression of phosphorylated histone H2AX in tumors in relation to DNA double-strand breaks and genomic instability. *DNA Repair* **2006**, *5*, 935–946.
17. Mirzayans, R.; Andrais, B.; Scott, A.; Wang, Y.W.; Murray, D. Ionizing radiation-induced responses in human cells with differing *TP53* status. *Int. J. Mol. Sci.* **2013**, *14*, 22409–22435.
18. Harper, J.W.; Adami, G.R.; Wei, G.N.; Keyomarsi, K.; Elledge, S.J. The p21 CDK-interacting protein CIP1 is a potent inhibitor of G1 cyclin-dependent kinases. *Cell* **1993**, *75*, 805–816.
19. Xiong, Y.; Hannon, G.J.; Zhang, H.; Casso, D.; Kobayashi, R.; Beach, D. p21 is a universal inhibitor of cyclin kinases. *Nature* **1993**, *366*, 701–704.
20. Warfel, N.A.; El-Deiry, W.S. $p21^{WAF1}$ and tumourigenesis: 20 years after. *Curr. Opin. Oncol*. **2013**, *25*, 52–58.
21. Mirzayans, R.; Andrais, B.; Scott, A.; Murray, D. New insights into p53 signaling and cancer-cell response to DNA damage: Implications for cancer therapy. *J. Biomed. Biotechnol.* **2012**, *2012*, 170325.
22. Kreis, N.N.; Louwen, F.; Yuan, J. Less understood issues: p21 CIP1 in mitosis and its therapeutic potential. *Oncogene* **2015**, *34*, 1758–1767.
23. Song, J.Y.; Ryu, S.H.; Cho, Y.M.; Kim, Y.S.; Lee, B.M.; Lee, S.W.; Choi, J. WIP1 suppresses apoptotic cell death through direct dephosphorylation of BAX in response to γ-radiation. *Cell Death Dis.* **2013**, *4*, e744.
24. Han, Z.; Wei, W.; Dunaway, S.; Darnowski, J.W.; Calabresi, P.; Sedivy, J.; Hendrickson, E.A.; Balan, K.V.; Pantazis, P.; Wyche, J.H. Role of p21 in apoptosis and senescence of human colon cancer cells treated with camptothecin. *J. Biol. Chem.* **2002**, *277*, 17154–17160.
25. Mirzayans, R.; Scott, A.; Cameron, M.; Murray, D. Induction of accelerated senescence following exposure to ionizing radiation in human solid tumor-derived cell lines expressing wild-type *TP53*. *Radiat. Res.* **2005**, *163*, 53–62.
26. Sohn, D.; Essmann, F.; Schulze-Osthoff, K.; Jänicke, R.U. p21 blocks irradiation-induced apoptosis downstream of mitochondria by inhibition of cyclin-dependent kinase-mediated caspase-9 activation. *Cancer Res.* **2006**, *66*, 11254–11262.
27. Sliwinska, M.A.; Mosieniak, G.; Wolanin, K.; Babik, A.; Piwocka, K.; Magalska, A.; Szczepanowska, J.; Fronk, J.; Sikora, E. Induction of senescence with doxorubicin leads to increased genomic instability of HCT116 cells. *Mech. Ageing Dev*. **2009**, *130*, 24–32.
28. Javelaud, D.; Besançon, F. Inactivation of $p21^{WAF1}$ sensitizes cells to apoptosis *via* an increase of both $p14^{ARF}$ and p53 levels and an alteration of the Bax/Bcl-2 ratio. *J. Biol. Chem.* **2002**, *277*, 37849–37954.
29. Wani, M.A.; Wani, G.; Yao, J.; Zhu, Q.; Wani, A.A. Human cells deficient in p53 regulated $P21^{WAF1/CIP1}$ expression exhibit normal nucleotide excision repair of UV-induced DNA damage. *Carcinogenesis* **2002**, *23*, 403–410.
30. Broude, E.V.; Swift, M.E.; Vivo, C.; Chang, B.D.; Davis, B.M.; Kalurupalle, S.; Blagosklonny, M.V.; Roninson, I.B. $P21^{WAF1/CIP1/SDI1}$ mediates retinoblastoma protein degradation. *Oncogene* **2007**, *26*, 6954–6958.

31. Hill, R.; Leidal, A.M.; Madureira, P.A.; Gillis, L.D.; Waisman, D.M.; Chiu, A.; Lee, P.W. Chromium-mediated apoptosis: Involvement of DNA-dependent protein kinase (DNA-PK) and differential induction of p53 target genes. *DNA Repair* **2008**, *7*, 1484–1499.
32. Ferrandiz, N.; Martin-Perez, J.; Blanco, R.; Donertas, D.; Weber, A.; Eilers, M.; Dotto, P.; Delgado, M.D.; Leon, J. HCT116 cells deficient in $P21^{WAF1}$ are hypersensitive to tyrosine kinase inhibitors and adriamycin through a mechanism unrelated to p21 and dependent on p53. *DNA Repair* **2009**, *8*, 390–399.
33. Marti, T.M.; Hefner, E.; Feeney, L.; Natale, V.; Cleaver, J.E. H2AX phosphorylation within the G1 phase after UV irradiation depends on nucleotide excision repair and not DNA double strand breaks. *Proc. Natl. Acad. Sci. USA* **2006**, *103*, 9891–9896.
34. Anderson, D.; Andrais, B.; Mirzayans, R.; Siegbahn, E.A.; Fallone, B.G.; Warkentin, B. Comparison of two methods for measuring H2AX nuclear fluorescence as a marker of DNA damage in cultured human cells: Applications for microbeam radiation therapy. *J. Instrum.* **2013**, *8*, C06008.
35. Pang, L.Y.; Scott, M.; Hayward, R.L.; Mohammed, H.; Whitelaw, C.B.; Smith, G.C.; Hupp, T.R. $p21^{WAF1}$ is component of a positive feedback loop that maintains the p53 transcriptional program. *Cell Cycle* **2011**, *10*, 932–950.
36. Wojewódzka, M.; Buraczewska, I.; Kruszewski, M. A modified neutral comet assay: Elimination of lysis at high temperature and validation of the assay with anti-single-stranded DNA antibody. *Mutat. Res.* **2002**, *518*, 9–20.
37. Mirzayans, R.; Andrais, B.; Scott, A.; Paterson, M.C.; Murray, D. Single-cell analysis of $p16^{INK4a}$ and $p21^{WAF1}$ expression suggests distinct mechanisms of senescence in normal human and Li-Fraumeni Syndrome fibroblasts. *J. Cell. Physiol.* **2010**, *223*, 57–67.
38. Mirzayans, R.; Andrais, B.; Hansen, G.; Murray, D. Role of $p16^{INK4A}$ in replicative senescence and DNA damage-induced premature senescence in p53-deficient human cells. *Biochem. Res. Int.* **2012**, *2012*, 951574.
39. Myohanen, S.K.; Baylin, S.B.; Herman, J.G. Hypermethylation can selectively silence individual $P16^{INK4a}$ alleles in neoplasia. *Cancer Res.* **1998**, *58*, 591–593.
40. Haldar, S.; Negrini, M.; Monne, M.; Sabbioni, S.; Croce, C.M. Down-regulation of Bcl-2 by p53 in breast cancer cells. *Cancer Res.* **1994**, *54*, 2095–2097.
41. Ramljak, D.; Romanczyk, L.J.; Metheny-Barlow, L.J.; Thompson, N.; Knezevic, V.; Galperin, M.; Ramesh, A.; Dickson, R.B. Pentameric procyanidin from *Theobroma cacao* selectively inhibits growth of human breast cancer cells. *Mol. Cancer Ther.* **2005**, *4*, 537–546.
42. Chai, Y.; Lee, H.J.; Shaik, A.A.; Nkhata, K.; Xing, C.; Zhang, J.; Jeong, S.J.; Kim, S.H.; Lu, J. Penta-*O*-galloyl-β-D-glucose induces G1 arrest and DNA replicative *S*-phase arrest independently of cyclin-dependent kinase inhibitor 1A, cyclin-dependent kinase inhibitor 1B and P53 in human breast cancer cells and is orally active against triple negative xenograft growth. *Breast Cancer Res.* **2010**, *12*, R67.
43. Morohaku, K.; Hoshino, Y.; Sasada, H.; Sato, E. Incorporation of phosphatase inhibitor in culture prompts growth initiation of isolated non-growing oocytes. *PLoS ONE* **2013**, *8*, e77533.

44. Park, J.Y.; Song, J.Y.; Kim, H.M.; Han, H.S.; Seol, H.S.; Jang, S.J.; Choi, J. p53-Independent expression of wild-type p53-induced phosphatase 1 (WIP1) in methylmethane sulfonate-treated cancer cell lines and human tumors. *Int. J. Biochem. Cell Biol.* **2012**, *44*, 896–904.
45. Wettersten, H.I.; Hee, H.S.; Li, C.; Shiu, E.Y.; Wecksler, A.T.; Hammock, B.D.; Weiss, R.H. A novel p21 attenuator which is structurally related to sorafenib. *Cancer Biol. Ther.* **2013**, *14*, 278–285.
46. Park, J.Y.; Park, S.H.; Weiss, R.H. Disparate effects of roscovitine on renal tubular epithelial cell apoptosis and senescence: Implications for autosomal dominant polycystic kidney disease. *Am. J. Nephrol.* **2009**, *29*, 509–515.
47. Braun, F.; Bertin-Ciftci, J.; Gallouet, A.S.; Millour, J.; Juin, P. Serum-nutrient starvation induces cell death mediated by Bax and Puma that is counteracted by p21 and unmasked by Bcl-x(L) inhibition. *PLoS ONE* **2011**, *6*, e23577.
48. Mirzayans, R.; Pollock, S.; Scott, A.; Gao, C.Q.; Murray, D. Metabolic labeling of human cells with tritiated nucleosides results in activation of the ATM-dependent p53 signaling pathway and acceleration of DNA repair. *Oncogene* **2003**, *22*, 5562–5571.
49. Mirzayans, R.; Scott, A.; Andrais, B.; Pollock, S.; Murray, D. Ultraviolet light exposure triggers nuclear accumulation of $p21^{WAF1}$ and accelerated senescence in human normal and nucleotide excision repair-deficient fibroblast strains. *J. Cell. Physiol.* **2008**, *215*, 55–67.
50. Xu, L.F.; Ni, J.Y.; Sun, H.L.; Chen, Y.T.; Wu, Y.D. Effects of hypoxia-inducible factor-1α silencing on the proliferation of CBRH-7919 hepatoma cells. *World J. Gastroenterol.* **2013**, *19*, 1749–1759.
51. Giovannini, C.; Baglioni, M.; Toaldo, M.B.; Ventrucci, C.; d'Adamo, S.; Cipone, M.; Chieco, P.; Gramantieri, L.; Bolondi, L. Notch3 inhibition enhances sorafenib cytotoxic efficacy by promoting GSK3b phosphorylation and p21 down-regulation in hepatocellular carcinoma. *Oncotarget* **2013**, *4*, 1618–1631.
52. Celeste, A.; Petersen, S.; Romanienko, P.J.; Fernandez-Capetillo, O.; Chen, H.T.; Sedelnikova, O.A.; Reina-San-Martin, B.; Coppola, V.; Meffre, E.; Difilippantonio, M.J.; *et al*. Genomic instability in mice lacking histone H2AX. *Science* **2002**, *296*, 922–927.
53. Bartkova, J.; Horejsi, Z.; Koed, K.; Kramer, A.; Tort, F.; Zieger, K.; Guldberg, P.; Sehested, M.; Nesland, J.M.; Lukas, C.; *et al*. DNA damage response as a candidate anti-cancer barrier in early human tumorigenesis. *Nature* **2005**, *434*, 864–870.
54. Gorgoulis, V.G.; Vassiliou, L.V.; Karakaidos, P.; Zacharatos, P.; Kotsinas, A.; Liloglou, T.; Venere, M.; Ditullio, R.A., Jr.; Kastrinakis, N.G.; Levy, B.; *et al*. Activation of the DNA damage checkpoint and genomic instability in human precancerous lesions. *Nature* **2005**, *434*, 907–913.
55. Warters, R.L.; Adamson, P.J.; Pond, C.D.; Leachman, S.A. Melanoma cells express elevated levels of phosphorylated histone H2AX foci. *J. Investig. Dermatol.* **2005**, *124*, 807–817.
56. Perucca, P.; Cazzalini, O.; Mortusewicz, O.; Necchi, D.; Savio, M.; Nardo, T.; Stivala, L.A.; Leonhardt, H.; Cardoso, M.C.; Prosperi, E. Spatiotemporal dynamics of p21CDKN1A protein recruitment to DNA-damage sites and interaction with proliferating cell nuclear antigen. *J. Cell Sci.* **2006**, *119*, 1517–1527.
57. Tobias, F.; Durante, M.; Taucher-Scholz, G.; Jakob, B. Spatiotemporal analysis of DNA repair using charged particle radiation. *Mutat. Res.* **2010**, *704*, 54–60.

58. Koike, M.; Yutoku, Y.; Koike, A. Accumulation of p21 proteins at DNA damage sites independent of p53 and core NHEJ factors following irradiation. *Biochem. Biophys. Res. Commun.* **2011**, *412*, 39–43.
59. Mauro, M.; Rego, M.A.; Boisvert, R.A.; Esashi, F.; Cavallo, F.; Jasin, M.; Howlett, N.G. p21 promotes error-free replication-coupled DNA double-strand break repair. *Nucleic Acids Res.* **2012**, *40*, 8348–8360.
60. Lu, X.; Nannenga, B.; Donehower, L. A. PPM1D dephosphorylates CHK1 and p53 and abrogates cell cycle checkpoints. *Genes Dev.* **2005**, *19*, 1162–1174.
61. Batchelor, E.; Mock, C.S.; Bhan, I.; Loewer, A.; Lahav, G. Recurrent initiation: A mechanism for triggering p53 pulses in response to DNA damage. *Mol. Cell* **2008**, *9*, 277–289.

© 2015 by the authors; licensee MDPI, Basel, Switzerland. This article is an open access article distributed under the terms and conditions of the Creative Commons Attribution license (http://creativecommons.org/licenses/by/4.0/).

Int. J. Mol. Sci. **2015**, *16*, 12108-12118; doi:10.3390/ijms160612108

OPEN ACCESS
International Journal of
Molecular Sciences
ISSN 1422-0067
www.mdpi.com/journal/ijms

Article

Periostin Expression and Its Prognostic Value for Colorectal Cancer

Zewu Li [1], Xin Zhang [1], Yongmei Yang [1], Sanhui Yang [2], Zhaogang Dong [1], Lutao Du [1], Lili Wang [1] and Chuanxin Wang [1,*]

[1] Department of Clinical Laboratory, Qilu Hospital, Shandong University, Jinan 250012, China; E-Mails: lizwlgs@yeah.net (Z.L.); zhangxin21@126.com (X.Z.); yymxx@126.com (Y.Y.); dongzg790828@gmail.com (Z.D.); dulutao1984@163.com (L.D.); wanglili808@163.com (L.W.)

[2] Department of General Surgery, Qilu Hospital, Shandong University, Jinan 250012, China; E-Mail: yangsanhui1234@163.com

* Author to whom correspondence should be addressed; E-Mail: cxwang@sdu.edu.cn; Tel.: +86-531-8216-6801; Fax: +86-531-8692-7544.

Academic Editor: William Chi-shing Cho

Received: 28 March 2015 / Accepted: 8 May 2015 / Published: 27 May 2015

Abstract: Integrin is important for cell growth, invasion and metastasis, which are frequently observed in malignant tumors. The periostin (POSTN) gene encodes the ligand for integrin, one of the key focal adhesion proteins contributing to the formation of a structural link between the extracellular matrix and integrins. High expression levels of the POSTN gene are correlated with numerous human malignancies. We examined POSTN protein in colorectal cancer specimens from 115 patients by strictly following up using immunohistochemistry. Cytoplasm immunohistochemical staining showed POSTN protein expression in colorectal cancers. The positive expression rate of POSTN protein (59.13%, 68/115) in colorectal cancers was significantly higher than that in adjacent normal colon mucosa (0.47%, 11/109). POSTN over-expression in colorectal cancers was positively correlated with tumor size, differentiation, lymph node metastasis, serosal invasion, clinical stage and five-year survival rates. Further analysis showed that patients with advanced stage colorectal cancer and high POSTN expression levels had lower survival rates than those with early stage colorectal cancer and low POSTN expression levels. Overall, our results showed that POSTN played an important role in the progression of colorectal cancers.

Keywords: colorectal cancer; POSTN; immunohistochemistry; survival analysis

1. Introduction

Colorectal cancer (CRC) is one of the most common malignancies worldwide, with about 1.2 million new cases and 608,700 deaths every year [1]. Colorectal carcinogenesis is a multistep process involving apoptosis, differentiation and survival mechanisms [2]. About half of the individuals with locally advanced CRC can be cured by surgery and multimodal treatment. Because traditional methods do not allow precise prediction of prognosis for the patients after surgical removal of the primary tumor, there is an urgent need for biomarkers capable of distinguishing patients with poor or good prognoses [3]. Although current novel monoclonal antibody-based therapies have improved the prognosis of colorectal cancer patients, a significant proportion of patients still die from the disease, and the clinical outcome and prognosis of colorectal cancer patients remains poor [4,5]. Consequently, to provide better treatment strategies, there is an urgent need to further understand the precise molecular mechanism of CRC and to identify new prognostic biomarkers and therapeutic targets for colorectal cancer.

Periostin (POSTN), a member of the fasciclin domain or osteoblast-specific factor 2 (OSF-2) family of proteins, contains a signal peptide coding sequence (*N*-terminal) and four repeat structures (RDS). Each repeat structure has two fasciclin I domains that are highly conserved to a type of cell-cell adhesion protein expressed in the insect nervous system [6,7]. It is secreted mainly by osteoblasts and their precursor cells in the periosteum and the periodontal membrane, and can promote the proliferation and differentiation of osteoblasts and periosteai bone precursor cells for aggregation and adhesion [6]. POSTN functions as a multidomain adaptor protein that integrates multiple signals such as cell surface receptors, integrins and growth factors [8]. Through these protein-protein interactions, it regulates a variety of physiological processes including cell motility, metastasis, matrix organization, tissue remolding, cell proliferation and survival [9]. Recently, it has been revealed that POSTN is overexpressed in various human cancers [10], including neuroblastoma [11], as well as head and neck [12], nasopharyngeal [13], thyroid [14], oral [15], breast [16] and ovarian cancers [9]. Bao *et al.* have reported that in CRC, periostin potently promotes metastatic growth of colon cancer by augmenting cell survival via the Akt/PKB pathway [17]. More recently, Wu *et al.* have demonstrated that periostin is related to the liver metastasis of CRC and may be a potential target for CRC [18]. However, the clinical-pathological implications of POSTN in CRC are lacking.

To investigate its prognostic value, we selected 115 cases of colorectal cancer and investigated the expression of POSTN by immunohistochemical staining. Our data showed that POSTN was frequently upregulated in colorectal cancers. These findings suggest that POSTN might be a predictor for poor prognosis in patients with colorectal cancer.

2. Results

2.1. POSTN Protein Is Over-Expressed in Colorectal Cancer

Immunohistochemical staining revealed that the POSTN protein had a cytoplasmic expression pattern in colorectal cancer cells (Figure 1). A low level of POSTN protein expression was detected in 93.13% (108/115) of colorectal cancer cells, which was significantly higher than in adjacent normal colon mucosa (31.30%, 36/115) cells. Similarly, a high level of POSTN protein expression was detected in 59.13% (68/115) of colorectal cancers cells, which was significantly higher than that in adjacent normal colon mucosa (10.47%, 11/109) ($p < 0.01$).

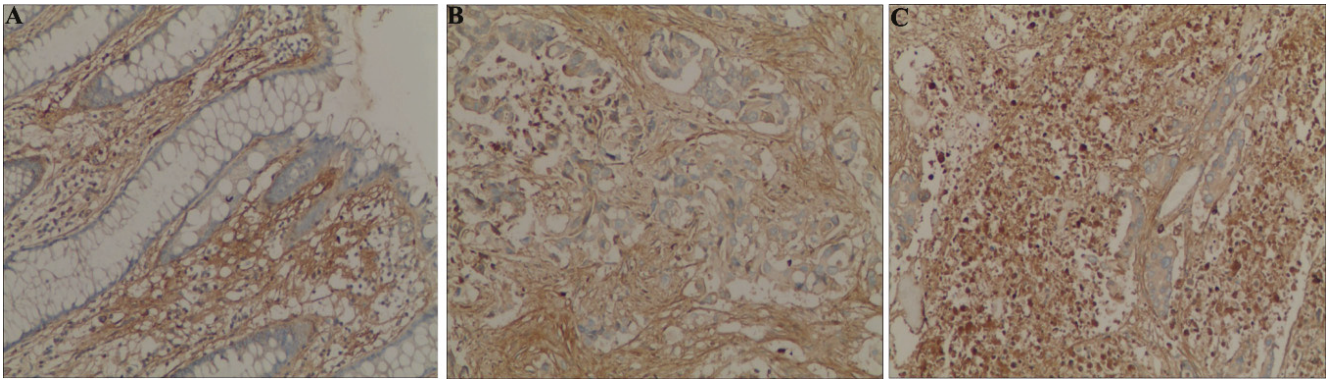

Figure 1. Immunohistochemical staining of POSTN protein in colorectal cancer and normal mucosa cells (original magnification, ×200). (**A**) POSTN is negative in normal colorectal mucosa; (**B**) Low levels of POSTN expression in colorectal cancer cells; and (**C**) High levels of POSTN expression in colorectal cancer cells.

2.2. Relationship between Clinical-Pathological Characteristics and POSTN Expression in Colorectal Cancer Tissues

To evaluate the relationship between POSTN protein expression and colorectal cancer progression, we further evaluated the correlation between POSTN expression and clinical-pathological characteristics. The data presented in Table 1 show that a high level of POSTN protein expression was significantly correlated with tumor size ($p = 0.014$), differentiation ($p = 0.01$), lymph nodes metastasis ($p = 0.006$), serosal invasion ($p = 0.0003$) and TNM stages ($p = 0.0002$). However, the over expression of POSTN protein was not related to gender, age or tumor location. Taken together, these results suggest that a high level of POSTN expression might be related to colorectal cancer progression.

Table 1. POSTN expression and clinical-pathological characteristics in colorectal cancer patients (n = 115).

Characteristic	No. of Cases	High Expression Cases (%)	OR (95% CI)	p Value
Gender			1.451 (0.594–3.539)	0.412
Male	90	55 (61.11%)		
Female	25	13 (52%)		
Age (years old)			0.669 (0.329–1.359)	0.265
<53	59	29 (49.15%)		
≥53	56	39 (69.64%)		
Location			0.520 (0.244–1.109)	0.089
Colon	60	31 (51.67%)		
Rectum	55	37 (67.27%)		
Tumor size (cm)			0.384 (0.177–0.830)	0.014
<5	60	29 (48.33%)		
≥5	55	39 (70.90%)		
Differentiation			0.370 (0.172–0.797)	0.010
Well	52	24 (46.15%)		
Poorly	63	44 (69.84%)		
Serosal invasion			0.237 (0.106–0.529)	0.0003
−	60	26 (43.33%)		
+	55	42 (76.36%)		
Lymph node metastasis			0.335 (0.152–0.736)	0.006
−	63	30 (47.62%)		
+	52	38 (73.07%)		
Stage			0.226 (0.010–0.510)	0.0002
I–IIA	62	27 (43.55%)		
IIB–IV	53	41 (77.36%)		

2.3. Correlation between POSTN Levels and Patient Survival

To further demonstrate the importance of high POSTN expression in the prognosis of colorectal cancer progression, we analyzed the correlations between POSTN expression and factors associated with the aggressiveness of colorectal cancer. The cumulative 5-year overall survival rate was 59.13%, and the 5-year cumulative probability of survival for patients with high levels of POSTN expression (45.6%) was significantly lower than that for patients with low levels of POSTN expression (78.7%) (p = 0.001, Figure 2A). In addition, the results of Kaplan-Meier analysis and log-rank test showed that survival time was also associated with serosal invasion (p = 0.014, Figure 2B), lymph nodes metastasis (p < 0.001, Figure 2C) and tumor stage (p = 0.01, Figure 2D).

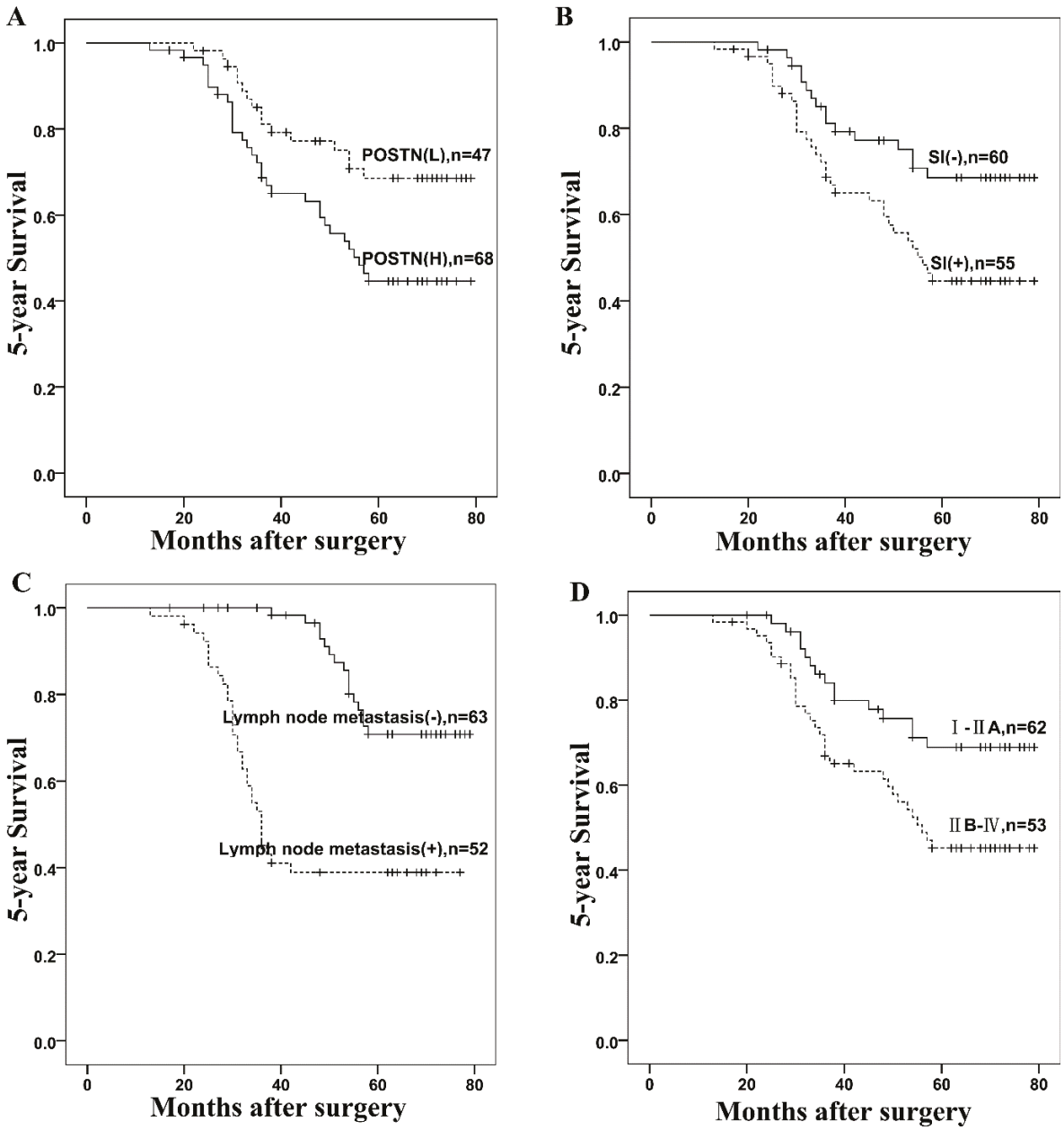

Figure 2. Kaplan-Meier analysis of five-year survival rates in 115 colorectal cancer patients according to (**A**) POSTN expression (p = 0.022); (**B**) Serosal invasion (SI) (p < 0.001); (**C**) Lymph nodes metastasis (p < 0.001); and (**D**) TNM stage (p < 0.001). Vertical bars represent censored patients.

2.4. Univariate and Multivariate Cox Analysis for Prognosis of Patients with Colorectal Cancer

Using univariate analysis, we found statistically significant correlations between overall survival and POSTN level, serosal invasion, lymph nodes metastasis and tumor stage (Table 2). We found that lymph nodes metastasis (p < 0.001) and POSTN expression (p = 0.044) were prognostic factors for overall survival rates (Table 3).

Table 2. Univariate survival analyses of various factors in patients with colorectal cancer.

Factors	B	SE	Wald	HR	95% CI		*p* Value
					Low	Upper	
Age	0.253	0.292	0.75	0.777	0.438	1.376	0.386
Gender	0.159	0.345	0.212	1.172	0.596	2.303	0.645
Tumor size	0.139	0.292	0.225	1.149	0.648	2.035	0.635
Location	0.149	0.292	0.261	1.161	0.655	2.057	0.609
Differentiation	0.174	0.295	0.349	0.84	0.471	1.498	0.555
Serosal invasion	0.736	0.308	5.708	0.51	0.262	0.876	0.017
Lymph node metastasis	1.363	0.311	19.268	3.909	2.127	7.185	<0.001
Tumor stage	0.784	0.313	6.259	0.457	0.247	1.844	0.012
POSTN	1.17	0.357	10.71	3.222	1.599	6.492	0.001

B: Coefficient; SE: stand error; HR: hazard ratio.

Table 3. Multivariant survival analyses of various factors in patients with colorectal cancer.

Factors	B	SE	Wald	HR	95% CI		*p* Value
					Low	Upper	
Lymph node metastasis	1.125	0.321	12.319	3.08	1.643	5.774	<0.001
Serosal invasion	0.279	0.372	0.564	0.756	0.365	1.568	0.453
Tumor stage	0.279	0.479	0.543	0.756	0.401	0.36	1.59
POSTN	0.705	0.381	3.427	2.023	0.959	4.266	0.044

3. Discussion

Periostin, also called osteoblast-specific factor 2, is a 93.3-kD secreted protein and can promote integrin dependent cell adhesion and motility [19,20]. Periostin-activated signaling pathways promote cellular survival, angiogenesis and resistance to hypoxia induced cell death. Additionally, periostin is upregulated in response to the stress of hypoxia in the human A549 non-small cell lung cancer cell line and in rat pulmonary arterial smooth muscle cells (PASMCs) [17,21]. It has been frequently reported lately that POSTN is overexpressed in various types of human malignant tumors. For instance, Qiu *et al.* have reported that periostin is a hypoxia-response gene and mediates a cross talk between GC and endothelial cells under hypoxia, partially through the regulation of VEGF expression [22]. Wong *et al*. have shown that POSTN may be a biomarker of the esophageal tumor microenvironment that can be used to detect pre neoplastic lesions [23]. Lee *et al.* have found that mesenchymal stem cell-derived TGFBI and periostin play key roles in tumorigenesis by stimulating adhesion of prostate cancer cells [24]. Increase in COMP and periostin expression and decrease in VAP-1 expression in prostate have been shown to be associated with aggressive prostate cancer [25]. Periostin expression has also been correlated with the increase of Gleason score and the aggressiveness of prostate diseases [26]. However, the downregulation of POSTN mRNA is significantly related to high grade bladder cancer [27,28]. Furthermore, Kanno *et al*. have demonstrated that POSTN has biphasic effects on the migration of pancreatic carcinoma [29]. These results suggest that POSTN may have different functions for different pathological types of cancer, and POSTN expression level and its relationship with prognosis in colorectal cancer have not been elucidated.

In the present study, we performed immunohistochemical staining of POSTN protein and survival data analyses in colorectal cancer cells and their adjacent normal tissue counterparts in 115 cases. We found that the expression levels of the POSTN oncoprotein were significantly higher in colorectal cancers than in adjacent normal tissues. These findings indicated that POSTN potentially played important roles in the progression of colorectal cancer. Results of previous studies have also provided some indirect evidence. For example, circulating periostin may help identify patients with more aggressive colorectal cancer [30]. Because POSTN may be present at higher levels in immature cells than in differentiated counterparts, it can also aid in gauging the differentiation potential of tumor cells. Liu *et al*. [31] have reported that periostin is a nicotine target gene in gastric cancer and play roles in gastric cancer cell growth, invasion, drug resistance, and EMT facilitated by nicotine. Lee *et al.* [32] have shown that the periostin-integrin signaling regulates breast cancer progression at multiple levels in tumor cells and the tumor microenvironment. Also, they reported that DNA aptamers targeting periostin can be used to inhibit breast cancer progression. Xu *et al.* have found that periostin is an independent prognostic factor for breast cancer or a potential target for breast cancer [33]. Combined evaluation of CTHRC1 and periostin can serve as a potential marker for breast cancer bone metastasis [34]. These results indicate that POSTN may be an attractive molecular target for therapy.

Here we demonstrated that high POSTN expression was associated with serosal invasion, lymph node metastasis, tumor size and differentiation, which were crucial histological features associated with poor prognosis in colorectal cancer. However, the high expression level of POSTN was not correlated with gender, age or tumor location. Colorectal cancer exhibiting serosal invasion and lymph nodes metastasis had low five-year survival rates. Of particular interest, high POSTN expression was an independent hazard factor in colorectal cancer. These findings suggested that POSTN facilitated not only serosal invasion and lymph node metastasis, but also aggressive cancer behavior, resulting in poor prognosis. Importantly, we found that colorectal cancer with high POSTN expression was correlated with late-stage tumors. To further verify our findings, the sample size will be increased in our future studies.

4. Experimental Section

4.1. Patients and Sample Collection

A total of 133 CRC patients who underwent radical resection for CRC in the Department of General Surgery, Qilu Hospital of Shandong University between May 2007 and November 2009 were recruited for this study. Of these subjects, 18 patients were excluded because of incomplete follow-up data and 7 patients were excluded because of statistically insignificant distant metastases. The remaining 115 patients had not received preoperative adjuvant therapy and were deemed eligible for the study. All patient data were obtained from clinical and pathologic records, including age, gender, location, tumor size, differentiation, serosal invasion, lymph node metastasis and clinical stage. The tumor location was categorized as colonic in 60 cases and rectal in 55 cases. Staging was evaluated according to the TNM classification of carcinoma of the colon and rectum. From these 115 tumor tissues, 62 were TNM stage I–IIA, which was considered early stage; and 53 samples were stage IIB–IV, an advanced stage according to the Union for International Cancer Control 7th Edition criteria and the

World Health Organization classification [35]. Of the 115 cases, 52 were well-differentiated and 63 were poorly differentiated cancers. The resected tumor tissues and paired adjacent non-cancerous tissues (at least 5 cm away from the tumor margin) were collected. This study was approved by the ethics committee of the Qilu Hospital of Shandong University and written informed consent was obtained from each patient or legal representative.

4.2. Follow up

The patients were followed up every 3–6 mo after the operation till December 2014, with a median follow-up period of 61 mo (range 13–79 mo). Overall survival (OS) was defined as the period from surgery to death or the end of the study. All data, including physical examination, laboratory results and computed tomography, were collected from hospital records or by patient interviews.

4.3. Immunohistochemistry for POSTN in Paraffin-Embedded Tissues

Immunohistochemical analysis was performed using periostin antibody (Santa Cruz Biotechnology, Santa Cruz, CA, USA). Paraffin-embedded CRC tissues were sliced as 5-μm sections, baked at 65 °C for 2 h, and deparaffinized using standard procedures. After antigen retrieval and washing with Tris buffer, the POSTN primary antibody was incubated with the slides and the expression of POSTN was reviewed after development with a peroxidase-conjugated goat anti-rabbit antibody (Zhongshan Golden Bridge Biotechnology, Beijing, China) following the manufacturer's guidelines.

4.4. Evaluation of Immunohistochemical Staining

To avoid discrepancies, a final score was obtained by reassessment on a double-headed microscope. Briefly, the immunostaining for POSTN was semi-quantitatively scored as "−" (negative, no or less than 5% positive cells), "+" (5%–25% weak positive cells), "++" (26%–50% positive cells) and "+++" (more than 50% positive cells). Immunoreactivity was evaluated according to the staining intensity (0: negative, 1: weak, 2: moderate, 3: strong). The total immunoreactive score was calculated as the sum of staining intensity score and the percentage of positive tumor cells score, and graded as follows: −, 0 to 1; +, 2 to 3; ++, 4 to 5; and +++, 6 to 7. POSTN expression level was denoted as high expression ("++" and "+++") and low expression ("−" and "+").

4.5. Statistical Analysis

Statistical analyses were performed using the SPSS 18.0 software (SPSS Inc., Chicago, IL, USA). Correlation between POSTN expression and clinical-pathological characteristics were evaluated by Chi-square test and Fisher's exact tests. The survival rates after tumor removal were calculated by the Kaplan-Meier method, and differences in survival curves were analyzed by the Log-rank tests. Multivariate survival analysis was performed on all the significant characteristics measured by univariate survival analysis (gender, age, tumor size, differentiation, lymph node metastasis, serosal invasion, tumor stage, and POSTN expression) through the Cox proportional hazard regression model. Difference with $p < 0.05$ was considered statistically significant.

5. Conclusions

In summary, we identified POSTN as a potential biomarker for the evaluation of tumor progression. POSTN expression was commonly seen in cases with poor prognostic factors of colorectal cancer, leading to lymph node metastasis, advanced stage, serosal invasion and reduced survival time. Similar results with an increased sample size would support POSTN as an independent prognostic marker for colorectal cancer. However, further studies are needed to support this hypothesis.

Acknowledgments

This study was supported by the National Natural Science Foundation of China (Grant Nos 81271916 and 81301506), and the Development of Science and Technology Project of Shandong Province (2014GSF118016).

Author Contributions

Conceived and designed the experiments: Chuanxin Wang, Zewu Li, Yongmei Yang; Performed the experiments: Zewu Li, Zhaogang Dong; Analyzed the data: Zewu Li; Contributed reagents/materials/analysis tools: Xin Zhang, Sanhui Yang, Lili Wang; Wrote the paper: Zewu Li, Xin Zhang; Development of methodology: Lutao Du; Study supervision: Lutao Du.

Conflicts of Interest

The authors declare no conflict of interest.

References

1. Jemal, A.; Bray, F.; Center, M.M.; Ferlay, J.; Ward, E.; Forman, D. Global cancer statistics. *CA Cancer J. Clin.* **2011**, *61*, 69–90.
2. Calvert, P.M.; Frucht, H. The genetics of colorectal cancer. *Ann. Intern. Med.* **2002**, *137*, 603–612.
3. Weitz, J.; Koch, M.; Debus, J.; Hohler, T.; Galle, P.R.; Buchler, M.W. Colorectal cancer. *Lancet* **2005**, *365*, 153–165.
4. Goldman, E.; Fisher, J.L. Discrepancies in cancer mortality estimates. *Arch. Med. Res.* **2006**, *37*, 548–551.
5. Duffy, M.J.; Lamerz, R.; Haglund, C.; Nicolini, A.; Kalousova, M.; Holubec, L.; Sturgeon, C. Tumor markers in colorectal cancer, gastric cancer and gastrointestinal stromal cancers: European group on tumor markers 2014 guidelines update. *Int. J. Cancer.* **2014**, *134*, 2513–2522.
6. Litvin, J.; Selim, A.H.; Montgomery, M.O.; Lehmann, K.; Rico, M.C.; Devlin, H.; Bednarik, D.P.; Safadi, F.F. Expression and function of periostin-isoforms in bone. *J. Cell. Biochem.* **2004**, *92*, 1044–1061.
7. Zhu, S.; Barbe, M.F.; Amin, N.; Rani, S.; Popoff, S.N.; Safadi, F.F.; Litvin, J. Immunolocalization of periostin-like factor and periostin during embryogenesis. *J. Histochem. Cytochem.* **2008**, *56*, 329–345.

8. Norris, R.A.; Damon, B.; Mironov, V.; Kasyanov, V.; Ramamurthi, A.; Moreno-Rodriguez, R.; Trusk, T.; Potts, J.D.; Goodwin, R.L.; Davis, J.; *et al.* Periostin regulates collagen fibrillogenesis and the biomechanical properties of connective tissues. *J. Cell. Biochem.* **2007**, *101*, 695–711.
9. Gillan, L.; Matei, D.; Fishman, D.A.; Gerbin, C.S.; Karlan, B.Y.; Chang, D.D. Periostin secreted by epithelial ovarian carcinoma is a ligand for $\alpha_v\beta_3$ and $\alpha_v\beta_3$ integrins and promotes cell motility. *Cancer Res.* **2002**, *62*, 5358–5364.
10. Ruan, K.; Bao, S.; Ouyang, G. The multifaceted role of periostin in tumorigenesis. *Cell. Mol. Life Sci.* **2009**, *66*, 2219–2230.
11. Sasaki, H.; Sato, Y.; Kondo, S.; Fukai, I.; Kiriyama, M.; Yamakawa, Y.; Fuji, Y. Expression of the periostin mrna level in neuroblastoma. *J. Pediatr. Surg.* **2002**, *37*, 1293–1297.
12. Kudo, Y.; Ogawa, I.; Kitajima, S.; Kitagawa, M.; Kawai, H.; Gaffney, P.M.; Miyauchi, M.; Takata, T. Periostin promotes invasion and anchorage-independent growth in the metastatic process of head and neck cancer. *Cancer Res.* **2006**, *66*, 6928–6935.
13. Chang, Y.; Lee, T.C.; Li, J.C.; Lai, T.L.; Chua, H.H.; Chen, C.L.; Doong, S.L.; Chou, C.K.; Sheen, T.S.; Tsai, C.H. Differential expression of osteoblast-specific factor 2 and polymeric immunoglobulin receptor genes in nasopharyngeal carcinoma. *Head Neck* **2005**, *27*, 873–882.
14. Puppin, C.; Fabbro, D.; Dima, M.; di Loreto, C.; Puxeddu, E.; Filetti, S.; Russo, D.; Damante, G. High periostin expression correlates with aggressiveness in papillary thyroid carcinomas. *J. Endocrinol.* **2008**, *197*, 401–408.
15. Siriwardena, B.S.; Kudo, Y.; Ogawa, I.; Kitagawa, M.; Kitajima, S.; Hatano, H.; Tilakaratne, W.M.; Miyauchi, M.; Takata, T. Periostin is frequently overexpressed and enhances invasion and angiogenesis in oral cancer. *Br. J. Cancer* **2006**, *95*, 1396–1403.
16. Shao, R.; Bao, S.; Bai, X.; Blanchette, C.; Anderson, R.M.; Dang, T.; Gishizky, M.L.; Marks, J.R.; Wang, X.F. Acquired expression of periostin by human breast cancers promotes tumor angiogenesis through up-regulation of vascular endothelial growth factor receptor 2 expression. *Mol. Cell. Biol.* **2004**, *24*, 3992–4003.
17. Ouyang, G.; Liu, M.; Ruan, K.; Song, G.; Mao, Y.; Bao, S. Upregulated expression of periostin by hypoxia in non-small-cell lung cancer cells promotes cell survival via the Akt/PKB pathway. *Cancer Lett.* **2009**, *281*, 213–219.
18. Wu, G.; Wang, X.; Zhang, X. Clinical implications of periostin in the liver metastasis of colorectal cancer. *Cancer Biother. Radiopharm.* **2013**, *28*, 298–302.
19. Horiuchi, K.; Amizuka, N.; Takeshita, S.; Takamatsu, H.; Katsuura, M.; Ozawa, H.; Toyama, Y.; Bonewald, L.F.; Kudo, A. Identification and characterization of a novel protein, periostin, with restricted expression to periosteum and periodontal ligament and increased expression by transforming growth factor β. *J. Bone Miner. Res.* **1999**, *14*, 1239–1249.
20. Takeshita, S.; Kikuno, R.; Tezuka, K.; Amann, E. Osteoblast-specific factor 2: Cloning of a putative bone adhesion protein with homology with the insect protein fasciclin I. *Biochem. J.* **1993**, *294*, 271–278.
21. Li, P.; Oparil, S.; Feng, W.; Chen, Y.F. Hypoxia-responsive growth factors upregulate periostin and osteopontin expression via distinct signaling pathways in rat pulmonary arterial smooth muscle cells. *J. Appl. Physiol.* **2004**, *97*, 1550–1558; discussion 1549.

22. Qiu, F.; Shi, C.H.; Zheng, J.; Liu, Y.B. Periostin mediates the increased pro-angiogenic activity of gastric cancer cells under hypoxic conditions. *J. Biochem. Mol. Toxicol.* **2013**, *27*, 364–369.
23. Wong, G.S.; Habibollahi, P.; Heidari, P.; Lee, J.S.; Klein-Szanto, A.J.; Waldron, T.J.; Gimotty, P.; Nakagawa, H.; Taylor, P.R.; Wang, T.C.; *et al.* Optical imaging of periostin enables early endoscopic detection and characterization of esophageal cancer in mice. *Gastroenterology* **2013**, *144*, 294–297.
24. Lee, M.J.; Heo, S.C.; Shin, S.H.; Kwon, Y.W.; Do, E.K.; Suh, D.S.; Yoon, M.S.; Kim, J.H. Oncostatin M promotes mesenchymal stem cell-stimulated tumor growth through a paracrine mechanism involving periostin and TGFBI. *Int. J. Biochem. Cell Biol.* **2013**, *45*, 1869–1877.
25. Chen, J.; Xi, J.; Tian, Y.; Bova, G.S.; Zhang, H. Identification, prioritization, and evaluation of glycoproteins for aggressive prostate cancer using quantitative glycoproteomics and antibody-based assays on tissue specimens. *Proteomics* **2013**, *13*, 2268–2277.
26. Tian, Y.; Choi, C.H.; Li, Q.K.; Rahmatpanah, F.B.; Chen, X.; Kim, S.R.; Veltri, R.; Chia, D.; Zhang, Z.; Mercola, D.; *et al.* Overexpression of periostin in stroma positively associated with aggressive prostate cancer. *PLoS ONE* **2015**, *10*, e0121502.
27. Kim, C.J.; Yoshioka, N.; Tambe, Y.; Kushima, R.; Okada, Y.; Inoue, H. Periostin is down-regulated in high grade human bladder cancers and suppresses *in vitro* cell invasiveness and *in vivo* metastasis of cancer cells. *Int. J. Cancer* **2005**, *117*, 51–58.
28. Kim, C.J.; Isono, T.; Tambe, Y.; Chano, T.; Okabe, H.; Okada, Y.; Inoue, H. Role of alternative splicing of periostin in human bladder carcinogenesis. *Int. J. Oncol.* **2008**, *32*, 161–169.
29. Kanno, A.; Satoh, K.; Masamune, A.; Hirota, M.; Kimura, K.; Umino, J.; Hamada, S.; Satoh, A.; Egawa, S.; Motoi, F.; *et al.* Periostin, secreted from stromal cells, has biphasic effect on cell migration and correlates with the epithelial to mesenchymal transition of human pancreatic cancer cells. *Int. J. Cancer* **2008**, *122*, 2707–2718.
30. Ben, Q.W.; Zhao, Z.; Ge, S.F.; Zhou, J.; Yuan, F.; Yuan, Y.Z. Circulating levels of periostin may help identify patients with more aggressive colorectal cancer. *Int. J. Oncol.* **2009**, *34*, 821–828.
31. Liu, Y.; Liu, B.A. Enhanced proliferation, invasion, and epithelial-mesenchymaltransition of nicotine-promoted gastric cancer by periostin. *World J. Gastroenterol*. **2011**, *17*, 2674–2680.
32. Lee, Y.J.; Kim, I.S.; Park, S.A.; Kim, Y.; Lee, J.E.; Noh, D.Y.; Kim, K.T.; Ryu, S.H.; Suh, P.G. Periostin-binding DNA aptamer inhibits breast cancer growth and metastasis. *Mol. Ther.* **2013**, *21*, 1004–1013.
33. Xu, D.; Xu, H.; Ren, Y.; Liu, C.; Wang, X.; Zhang, H.; Lu, P. Cancer stem cell-related gene periostin: A novel prognostic marker for breast cancer. *PLoS ONE* **2012**, *7*, e46670.
34. Kharaishvili, G.; Cizkova, M.; Bouchalova, K.; Mgebrishvili, G.; Kolar, Z.; Bouchal, J. Collagen triple helix repeat containing 1 protein, periostin and versican in primary and metastatic breast cancer: An immunohistochemical study. *J. Clin. Pathol.* **2011**, *64*, 977–982.
35. Hamilton, S.R.; Aaltonen, L.A. *World Health Organization Classification of Tumours-Pathology & Genetics Tumors of the Digestive System*; IARC Press: Lyon, France, 2000.

© 2015 by the authors; licensee MDPI, Basel, Switzerland. This article is an open access article distributed under the terms and conditions of the Creative Commons Attribution license (http://creativecommons.org/licenses/by/4.0/).

Int. J. Mol. Sci. **2015**, *16*, 13322-13338; doi:10.3390/ijms160613322

OPEN ACCESS
International Journal of
Molecular Sciences
ISSN 1422-0067
www.mdpi.com/journal/ijms

Review

Circulating Long Noncoding RNA as a Potential Target for Prostate Cancer

Yin-Jie Su [1], Jin Yu [2], Ya-Qin Huang [2] and Jin Yang [2,*]

[1] Trainee Brigade, the Third Military Medical University, Chongqing 400038, China; E-Mail: yinjiesu@tmmu.edu.cn

[2] Department of Cell Biology, the Third Military Medical University, Chongqing 400038, China; E-Mails: yujin100@aliyun.com (J.Y.); hyq808024@163.com (Y.-Q.H.)

* Author to whom correspondence should be addressed; E-Mail: jinyang@tmmu.edu.cn; Tel./Fax: +86-23-6875-2251.

Academic Editor: William Chi-shing Cho

Received: 27 March 2015 / Accepted: 2 June 2015 / Published: 11 June 2015

Abstract: Prostate cancer is considered the second most common visceral malignancy in men in Western countries. Its emergence is largely due to the coordination of a malignant network, and long noncoding RNA has been recently demonstrated to play a critical role in prostate carcinogenesis. The aberrant expression of long noncoding RNA in prostate cancer patients is strongly associated with diagnosis, risk stratification and carcinogenesis, information that provides new insight into the complicated intracellular milieu of prostate cancer. This review focuses mainly on literature evidence for the role of long noncoding RNA in prostate cancer, which may suggest novel strategies for its prognosis, diagnosis and clinical treatment.

Keywords: long noncoding RNA; prostate cancer; biomarker; therapeutic target

1. Introduction

Prostate cancer is considered to be the second most common visceral malignancy in men in Western countries [1,2]. According to the Cancer Statistics report in 2014, there will be an estimated 233,000 new cases, representing 27% of all cancer cases, and an estimated 29,480 deaths, representing 10% of cancer-related deaths among American men [3]. Prostate cancer is more likely to affect older people

than younger people, and 60% of new cases are diagnosed in patients older than 60 years of age. Most diagnoses are made in the terminal stage due to the lack of specific and sensitive methods for early prostate cancer screening [4,5]. Although pathological biopsy is considered the gold standard for cancer diagnosis, the invasiveness and risk of adverse effects limit its clinical use. Hence, there is a significant need to develop a noninvasive assay.

Serum prostate specific antigen (PSA) has been widely used as the optimal conventional serum marker for prostate cancer in the clinical setting, especially as a marker for initial diagnosis, as it can predict cancer risk and treatment outcome [6]. According to the literature, approximately 240,000 individuals are diagnosed with prostate cancer in the United States annually; however, fewer than 15% eventually die, which has been largely attributed to the widespread application of PSA testing and the effective treatment of early-stage prostate cancer [1,7–10]. Although PSA testing has positively influenced the diagnosis and treatment of prostate cancer, significantly decreasing the prostate cancer-related mortality rate [7–11], it has drawbacks that have negatively affected certain men. For example, PSA is specific to the prostate but not to prostate cancer. PSA can be elevated in some benign situations, such as prostatic hyperplasia [12] and prostatitis [13], and PSA levels can change frequently and inconsistently depending on the patient's condition. Additionally, serum PSA levels are not specifically correlated with malignancy. According to certain studies, the morbidity of more than a quarter of patients with localized prostate cancer is closely related to unnecessary overtreatment and the missed diagnosis of life-threatening cancer [14–18]. Therefore, the shortcomings of the PSA test highlight its insufficiency and risks in prostate cancer detection. Thus, the development of new and effective methods is urgently needed for clinical prostate cancer screening.

Long noncoding RNAs constitute a large proportion of noncoding transcripts that contain more than 200 nucleotides, and they have recently emerged as a new player in cancer biology [19]. Previously considered to be transcriptional noise, long noncoding RNAs have now been demonstrated to play a key role in carcinogenesis [20,21]. In cancer, the aberrant expression of long noncoding RNAs contributes to the development and progression of cancer by influencing proliferation, metastasis, self-renewal, survival and apoptosis through either transcriptional or post-transcriptional regulation. These aberrantly expressed long noncoding RNAs can be detected in circulating cancer cells and in the serum and urine of cancer patients, and they exhibit specific expression patterns at various stages of cancer and in various tissues. Thus, the evidence suggests that long noncoding RNA may serve as an effective biomarker for cancer detection [22]. In this review, we not only focus on the role of long noncoding RNAs in prostate cancer diagnosis but also discuss their biological behaviors in prostate cancer.

2. Long Noncoding RNAs as Potential Prognostic Markers for Detecting Prostate Cancer

2.1. Single Biomarker Tests

Neoplastic transcriptomes are more complex than previously believed. Along with the dysregulation of protein coding genes and small noncoding RNAs, misexpression of long noncoding RNAs has also proven to be a central contributor to carcinogenesis. Considering that long noncoding RNAs are detectable at the serum/urine level and exhibit specific expression levels at various stages of prostate cancer, selecting a long noncoding RNA as a prostate cancer biomarker would be a breakthrough in

clinical prostate cancer screening. In 1999, Bussemakers and colleagues first reported $DD3^{PCA3}$, a long noncoding RNA, as a potential diagnostic biomarker for prostate cancer [23]. They found that $DD3^{PCA3}$ is a unique, polyadenylated, atypical, alternatively spliced noncoding RNA that is extremely specific to the prostate, with amplification in 18 different normal human prostate tissues. Moreover, in a cohort of 56 patients with prostatic tumors, 53 patients over-expressed this RNA in prostatic tumor tissue compared with non-neoplastic prostatic tissue from the same patient. To further explore the promising role of $DD3^{PCA3}$ in prostate cancer detection, the level of $DD3^{PCA3}$ in the urine of patients with varying stages of prostate cancer was assessed. Researchers found that by examining the level of $DD3^{PCA3}$ in 201 urine samples, the overall sensitivity, specificity and positive and negative predictive values for detecting prostate cancer were 82%, 76%, 67% and 87%, respectively, compared with the values for urinary PSA of 98%, 5%, 40% and 83%, respectively [24]. Among 108 patients with a PSA level >3 ng/mL, there were only 24 individuals who had prostate cancer confirmed by a biopsy, whereas 16 of the 24 patients were positive for $DD3^{PCA3}$ [25]. These data indicate that $DD3^{PCA3}$ may be a superior biomarker to *PSA* in prostate cancer detection. First, $DD3^{PCA3}$ is a prostate-specific gene and is particularly over-expressed in more than 95% of prostate cancers. Second, the $DD3^{PCA3}$ test exhibits a higher specificity than the conventional PSA test because $DD3^{PCA3}$ levels do not change constantly or rely on the patient's condition. Moreover, the $DD3^{PCA3}$ scores predict prostatic malignancy more accurately than PSA, which could potentially reduce the number of unnecessary biopsies, overtreatment and the rate of missed diagnoses [25–28].

Recent reports have demonstrated that a novel long noncoding RNA is also involved in prostate cancer detection. Metastasis associated lung adenocarcinoma transcript 1 (*MALAT1*) was used to predict metastasis and survival in patients with early-stage non-small cell lung cancer [29]. Ren *et al.* found that its derived mini-RNA (*MD-miniRNA*) can be used in a novel approach to detect human prostate cancer [30]. The serum *MD-miniRNA* levels were significantly elevated in a cohort of 196 patients compared with non-prostate cancer patients. At a cut-off of 867.8 copies/mL plasma, the sensitivity and specificity between prostate cancer patients and non-prostate cancer patients were 58.6% and 84.8%, respectively, and the sensitivity and specificity between positive and negative biopsies were 43.5% and 81.6%, respectively. Additionally, Wang *et al.* reported that the *MALAT1* model would prevent approximately 30.2%–46.5% of unnecessary biopsies in patients with serum PSA levels of 4–10 ng/mL [31]. Moreover, Ren *et al.* quantitatively measured the expression of *MALAT1* by real-time PCR in prospectively collected urine samples and found that *MALAT1* expression was closely associated with the Gleason score and tumor size [32]. Thus, these data indicated that *MALAT1* is a promising biomarker for prostate cancer detection.

Additionally, other long noncoding RNAs have also been identified as potential tools for the risk stratification of patients with prostate cancer. *PCAT-18* (prostate cancer-associated noncoding RNA transcript 18), a long noncoding RNA, was recently discovered by RNA sequencing; *PCAT-18* exhibits a highly specific expression pattern in prostate cancer. This gene is specifically expressed in prostate tissue and is up-regulated in prostate cancer compared with other benign and malignant tissues. Similar to the aforementioned long noncoding RNAs, *PCAT-18* can be detected in plasma, and its expression incrementally increases as prostate cancer progresses from localized to metastatic disease. These results implicate *PCAT-18* as a potential biomarker for metastatic prostate cancer [33]. A similar study was conducted by Sun *et al.* in 1997 [34], who found that *PTI-1* (prostate tumor inducing gene-1) is

differentially expressed in the blood in patients with prostate cancer *versus* those with benign prostatic hypertrophy or a normal prostate and that serum PTI-1 levels can predict the tumor volume, though there was only one cancer cell present in 10^8 *PTI-1*-negative cells. This study indicated that PTI-1 represents a sensitive marker for prostate cancer progression. Unlike other serum/urine-based biomarkers, *SChLAP1* (second chromosome locus associated with prostate-1; also called *LINC00913*), second chromosome locus associated with prostate-1, was identified as a tissue-based biomarker of clinical outcome after radical prostatectomy in patients with localized prostate cancer [35]. *SChLAP1* expression increased with prostate cancer progression, and a high level of *SChLAP1* was associated with poor outcome among patients with clinically localized prostate cancer after radical prostatectomy.

2.2. Multi-Biomarker Tests

Although the abovementioned long noncoding RNAs are promising predictive tools for cancer detection, their accuracy is not better than that of a biopsy. The specificity and sensitivity of $DD3^{PCA3}$, *MALAT1*, and *EN2* (engrailed homeobox 2) are 82% and 76%, 58.6% and 84.8%, and 66% and 88.2%, respectively. Other long noncoding RNAs are not 100% accurate for risk stratification and do not predict the clinical outcome of prostate cancer patients. Additionally, Lee and colleagues found that $DD3^{PCA3}$ was not detected in all of the tested samples from patients with prostate cancer [36]. There remains a discrepancy between these biomarkers and the actual clinicopathological features of these patients, which can lead to unnecessary overtreatment and missed diagnoses of life-threatening cancer. To reduce these insufficiencies and the risks of depending on a single biomarker, multivariate prostate cancer biomarker tests should be developed. For example, the limitation of $DD3^{PCA3}$ as a biomarker can be improved by combining it with other molecular markers, such as the *TMPRSS2-ERG* fusion gene (the transmembrane protease, serine 2 gene and the v-ets erythroblastosis virus E26 oncogene homolog (avian) gene) [37]. The ability of the expression pattern of nine prostate-related genes to predict prostate cancer was evaluated in a cohort of 106 patients who underwent prostatectomies [38]. The quantification of the nine prostate-related genes (*AibZIP*, *D-GPCR*, *EZH2*, *PCA3*, *PDEF*, *prostein*, *PSA*, *PSCA*, and *TRPM8*) by real-time PCR and the receiver operating characteristic (ROC) analysis of their expression for risk stratification revealed that PCA3 was the best single marker with the highest area under the curve (AUC = 0.85), whereas a multivariable logistic regression model (*EZH2*, *PCA3*, *prostein*, and *TRPM8*) showed even greater predictability than PCA3 alone, with an AUC of 0.9. Moreover, Lee *et al.* identified six long noncoding RNAs (*AK024556*, *XLOC_007697*, *LOC100287482*, *XLOC_005327*, *XLOC_008559*, and *XLOC_009911*) that were significantly up-regulated in all the prostate cancer patient urine samples compared with the normal urine samples [36]. Therefore, the above data indicate the potential utility of these long noncoding RNAs in a multi-biomarker method to successfully distinguish cancerous from normal tissues.

2.3. Long Noncoding RNAs and Gene Variance in Prostate Cancer

Analysis of the differences in genetic variance between populations has always been considered as a method for the risk stratification of diseases. Long noncoding RNAs constitute a large portion of the transcriptome, and their genetic variance was found to be strongly correlated with the risk stratification of patients with prostate cancer.

PCGEM1 (prostate cancer gene expression marker 1), a long noncoding RNA, has a significantly higher expression level in prostate cancer cells in African-American men [39]. A study by Xue *et al.* indicated that polymorphisms in *PCGEM1*, specifically the two tSNPs (tagged single nucleotide polymorphisms) rs6434568 and rs16834898, are associated with the risk of prostate cancer in Chinese men [40]. Additionally, polymorphisms of another long noncoding RNA, *PCA3*, were associated with the risk of prostate cancer. Zhou *et al.* found that individuals with a short tandem TAAA repeat polymorphism in the PCA3 promoter have a higher risk of prostate cancer than individuals with fewer TAAA repeats [41]. Moreover, Chinese researchers [42] revealed the complex landscape of genomic alterations in Chinese patients with prostate cancer by analyzing the transcriptomes of 14 pairs of prostate cancer and adjacent normal tissues. Two novel gene fusions, *CTAGE5-KHDRBS3* and *USP9Y-TTTY15*, were identified that occur repeatedly in Chinese patients, with frequencies of 37% and 35.2%, respectively. However, the *TMPRSS2-ERG* fusion appeared at a much lower frequency (21.4%) than it does in Caucasian patients. Taken together, these results suggest a new role for long noncoding RNAs in prostate cancer beyond transcriptional regulation, as they additionally contribute to new methods for risk prediction in patients with prostate cancer based on genetic polymorphisms.

3. Long Noncoding RNAs as Potential Therapeutic Targets in Prostate Cancer

Long noncoding RNAs constitute a large cluster of transcripts; besides their promising role in clinical prostate cancer screening, these RNAs play an essential role in prostate cancer biology. These RNAs may (1) mediate prostate carcinogenesis through the androgen receptor (AR); (2) act as an oncogene or a tumor suppressor gene; and (3) participate in the process of DNA repair and tumor metabolism during prostate carcinogenesis. The studies discussed below have revealed that prostate cancer cell fates can be significantly influenced by interfering with the malignant network in which long noncoding RNAs participate. Hence, it will be interesting to develop new clinical therapeutic interventions based on the mechanisms of action of long noncoding RNAs in prostate cancer.

3.1. Long Noncoding RNAs Mediate Prostate Carcinogenesis through the Androgen Receptor

Hyperactive AR remains a key determinant in prostate cancer carcinogenesis and resistance to current therapies. Prostate cancer cells rely uniquely on androgens for proliferation [43], and blocking the AR pathway with androgen deprivation therapy invariably induces tumor regression [44,45]. However, in later stages, almost all prostate cancer cases inevitably progress to recurrent castration-resistant prostate cancer (CRPC), becoming androgen-independent and acquiring the ability to metastasize [46]. Although the mechanisms involved in regulating AR activity are poorly understood, it is essential to define this molecular event to better comprehend prostate cancer progression. To clarify this process, Takayama *et al.* demonstrated that AR-regulated transcripts of unknown functions are transcribed from the intergenic or AS (anti-sense) region of genes in prostate cancer by employing an AR transcriptional network analysis. This evidence indicates that the AR-regulated transcripts of unknown function may include a series of noncoding RNAs [47,48]. As mentioned above, long noncoding RNAs make up a large proportion of noncoding RNAs, and their presence affects prostate cancer viability and susceptibility. Hence, it is of great interest to elucidate the regulatory mechanisms involving AR and long noncoding RNAs in prostate cancer.

PlncRNA-1, prostate cancer up-regulated long noncoding RNA 1, has been reported to be up-regulated in prostate cancer and to be involved in reciprocal communication with AR, which contributes to prostate carcinogenesis [49]. Silencing *PlncRNA-1* expression inhibits the proliferation but promotes the apoptosis of prostate cancer cells as well as reduces the expression of AR mRNA, AR protein and its downstream target *NKX3.1*, a highly expressed prostate tissue-specific gene that is rapidly activated in response to AR signaling [50]. Notably, blocking AR signaling also suppresses *PlncRNA-1* expression. Taken together, these results demonstrate a mutual feedback loop between *PlncRNA-1* and AR that may contribute to prostate carcinogenesis.

CTBP1-AS, a long noncoding RNA, is transcribed from the AS region of the C-terminal binding protein 1 (*CTBP1*) gene. It is predominantly localized in the nucleus and is up-regulated in prostate cancer to promote the growth of both hormone-dependent and castration-resistant cancer [51,52]. Mechanistically, *CTBP1-AS* directly represses *CTBP1* expression by recruiting the RNA-binding transcriptional repressor PSF and histone deacetylases. *CTBP1-AS* also exhibits global androgen-dependent functions by inhibiting tumor suppressor genes via the PSF-dependent mechanism, thereby promoting cell cycle progression [51].

Of the long noncoding RNAs involved in prostate carcinogenesis, *PCGEM1* and *PRNCR1* (prostate cancer noncoding RNA1) have been identified as playing critical roles via coordination with AR [53]. *PCGEM1* is a prostate tissue-specific gene encoded on chromosome 2q32 that serves as a prostate cancer gene expression marker [54]. Evidence has revealed that this gene is expressed in prostate cancer, particularly in AR-positive cell lines. *PCGEM1* over-expression promotes proliferation and colony formation [39] and inhibits doxorubicin-induced apoptosis in prostate cancer cells [55]. However, whether the resistance to cell death that is associated with this gene in prostate cancer is mediated by AR must be further elucidated. *PRNCR1*, a 13-kb long noncoding RNA that is transcribed from chromosome 8q24, is involved in maintaining prostate cancer susceptibility [56]. Its inhibition attenuates the viability of prostate cancer cells and decreases the transactivation activity of AR, which indicates that *PRNCR1* could be involved in prostate carcinogenesis through an AR-mediated pathway. However, in a large cohort of more than 230 individuals, Prensner *et al.* observed that neither *PCGEM1* nor *PRNCR1* interacted with AR, and neither are components of AR signaling [57]. These findings refute the argument that these two long noncoding RNAs interact with AR signaling.

As we mentioned before, almost all prostate cancer cells inevitably progress in later stages to recurrent CRPC, which is androgen-independent and has the ability to metastasize. This begs the question of what mechanisms regulate this transition from AR-dependence to AR-independence. Wang *et al.* found that *Linc00963* (long intergenic non-protein coding RNA 00963) may participate in this transition by affecting EGFR (epidermal growth factor receptor) activity [58]. In their study, Linc00963 was over-expressed twofold in a hormone-insensitive prostate cancer cell line (C4-2) compared with the hormone-sensitive LNCaP cell line. Inhibiting Linc00963 expression attenuated the apoptosis, migration and invasion of C4-2 cells and down-regulated EGFR and its downstream gene p-AKT (phosphorylated protein kinase B). Specifically, these results suggest that studying long noncoding RNAs and AR-mediated signaling pathways may provide a better understanding of prostate carcinogenesis.

3.2. Long Noncoding RNAs Mediate Prostate Carcinogenesis by Acting as Oncogenes and Tumor Suppressor Genes

In normal cells, the cooperation between oncogenes and tumor suppressor genes maintains intracellular homeostasis. However, this delicate balance is usually disrupted in cancer. In cancer, most long noncoding RNAs are over-expressed and act as oncogenes (onco-lncRNA), whereas some long noncoding RNAs are underexpressed and act as tumor suppressors (TS lncRNA). Concentrating on the roles of these onco-lncRNAs and TS lncRNAs in prostate cancer to develop effective interventions to interrupt their behavior is a potential promising way to target prostate cancer.

3.2.1. Long Noncoding RNAs as Oncogenes

Inducing cell cycle arrest and activating apoptosis are common features of DNA damage response pathways that remove aberrant cells from the body. Certain long noncoding RNAs function in opposition to these mechanisms by acting as oncogenes. *PCAT-1* (prostate cancer-associated intergenic non-coding RNA transcript 1) is transcribed from chromosome 8q24, a locus that is associated with prostate cancer risk and susceptibility. *PCAT-1* is particularly up-regulated in a subset of high-grade localized and metastatic prostate cancers. This gene was found to promote prostate cancer progression [59]. Over-expression of *PCAT-1* increased cell proliferation, whereas its inhibition by siRNA (small interfering RNA) knockdown led to a reduced proliferation rate of 25%–50%. After knocking down *PCAT-1* in prostate cancer cells, gene expression profiling identified 255 up-regulated genes and 115 down-regulated genes. These up-regulated genes were strongly associated with mitosis and cell cycle control, whereas the down-regulated genes aided in stratifying patients into molecular subtypes, such as BRCA2 (breast cancer 2), CENPE (centromere associated protein E) and CENPF (centromere associated protein F). Therefore, these data indicate that *PCAT-1* acts as an oncogene and is an emerging molecular tool in the field of molecular research and therapy.

The long noncoding RNA *MALAT1* was recently reported to maintain prostate cancer tumorigenicity and progression. It is involved in pre-mRNA processing and regulates the alternative splicing of pre-mRNA by modulating the levels of serine/arginine splicing factors [60,61]. The aberrant expression of *MALAT1* affects the normal splicing of a subset of mRNAs. *MALAT1* is up-regulated in prostate cancer, and down-regulating it via siRNA attenuated prostate cancer cell growth, invasion and migration and induced CRPC cell cycle arrest in G0/G1 followed by concomitant prolongation of survival of tumor-bearing mice [32]. However, it remains unknown whether *MALAT1* affects normal mRNA splicing in prostate cancer.

SChLAP1, second chromosome locus associated with prostate-1, is a long noncoding RNA that is frequently over-expressed in aggressive prostate cancers. Prensner *et al.* found that this gene can drive malignancy by antagonizing the tumor-suppressive functions of the SWI/SNF (SWItch/Sucrose NonFermentable) complex [62]. *SChLAP1* can directly bind to SNF5 (Sucrose NonFermentable 5), a core component of the SWI/SNF complex, and prevent the SWI/SNF complex from binding to its target promoters, resulting in decreased target gene expression.

Another long noncoding RNA, *ANRIL* (antisense noncoding RNA in the INK4 locus), was also found to be critical for prostate cancer pathogenesis. This long noncoding RNA is encoded in the

INK4b-ARF-INK4a gene cluster on chromosome 9p21.3. Elevated expression of *ANRIL* contributes to the development of prostate cancer by inhibiting a tumor suppressor gene. *ANRIL* (1) silences INK4b/ARF/INK4a (a tumor suppressor locus in normal and cancerous cells) by binding to CBX7 (chromobox homolog 7), thereby impacting the ability of CBX7 to repress the function of INK4b/ARF/INK4a and control cell senescence [63] and (2) inactivates p15(INK4B) (a tumor suppressor) by binding to SUZ12 (suppressor of zeste 12 homolog), a subunit of polycomb repressive complex 2, promotes SUZ12 binding to the p15(INK4B) locus, and represses the expression of the p15(INK4B) locus [64]. Taken together, these findings support an important role for long noncoding RNAs as oncogenes in prostate cancer and suggest that the cancer-specific functions of these long noncoding RNAs may be harnessed to "control" tumorigenesis.

3.2.2. Long Noncoding RNAs as Tumor Suppressors

Similar to most tumor suppressor genes, TS lncRNAs are expressed to protect the cell from becoming cancerous. H19 is a long noncoding RNA that is transcribed from the H19/Igf2 gene cluster on chromosome 11p11.5. Evidence suggests that this long noncoding RNA plays a critical role in tumor progression by exhibiting oncogenic activity in choriocarcinoma [65] and bladder cancer [66]. However, Zhu *et al.* found that *H19* plays a tumor-suppressive role in metastatic prostate cancer by repressing the effects of TGFβ1, which is involved in metastasis [67]. *H19* and its derivative *miR-675* were both significantly down-regulated in metastatic prostate cancer cells but not in non-metastatic prostate cancer cells. Up-regulating *H19* increased *miR-675* levels and repressed cell migration, but the functions of both *H19* and *miR-675* were attenuated by TGFβ1. Moreover, *miR-675* repressed the translation of TGFβ1 by directly binding to the 3′UTR of TGFβ1. Altogether, these results indicate a suppressor role for the *H19/miR-675* axis in prostate cancer metastasis.

GAS5, growth arrest-specific 5, was demonstrated to promote the apoptosis of prostate cancer cells [68]. This gene is encoded at the prostate cancer-associated locus on chromosome 1q25, and its expression is decreased in CRPC cells. The over-expression of *GAS5* in prostate cancer cells reduces drug/UV resistance and promotes apoptosis. Based on the evidence stated above, long noncoding RNAs can function as transcriptional regulators, tumor suppressor genes or oncogenes in prostate carcinogenesis. Hence, the reintroduction/reactivation of TS lncRNAs and the suppression of onco-lncRNAs could provide new approaches for targeting prostate cancer. However, few long noncoding RNAs and their mechanisms of action have been elucidated. Therefore, further studies are needed to identify additional long noncoding RNAs and their mechanisms of action related to carcinogenesis so that we can better understand their regulatory networks and develop novel approaches for prostate cancer intervention.

3.3. Long Noncoding RNAs Mediate Prostate Carcinogenesis through Other Processes

3.3.1. Long Noncoding RNAs and DNA Repair

Double-strand break (DSB) repair is a method of DNA repair, and mutations in genes involved in this process are common in many cancers. Prensner *et al.* first described the involvement of long noncoding RNAs in the mechanisms by which DSB repair is impaired [69]. These authors found that the prostate

cancer outlier lncRNA *PCAT-1* can regulate the cellular response to genotoxins by repressing the expression of BRCA2 to create a deficiency in homologous recombination (HR). This evidence suggests a new mechanism for HR impairment in prostate cancer.

3.3.2. Long Noncoding RNAs and Tumor Metabolism

As mentioned above, the tumorigenic activity of *PCGEM1* is not correlated with AR. Hung *et al.* reported a novel function in which *PCGEM1* promotes prostate cancer growth predominantly by regulating tumor metabolism, regardless of hormone or AR status [70]. In their study, *PCGEM1* regulated metabolism at the transcriptional level. *PCGEM1* can directly bind to c-Myc, promote the recruitment of c-Myc to chromatin, enhance the transactivation of c-Myc and ultimately affect multiple metabolic pathways, including the pentose phosphate pathway, tricarboxylic acid cycle, glucose and glutamine metabolism, and nucleotide and fatty acid biosynthesis. This study indicated that long noncoding RNAs could transcriptionally regulate tumor metabolism in prostate carcinogenesis, making them promising targets for therapeutic intervention.

4. Perspectives and Conclusions

Recent studies have revealed that long noncoding RNAs play a role in prostate cancer, serving as promising biomarkers for prostate cancer screening and risk stratification. And the well-studied prostate cancer-associated long noncoding RNAs are summarized in Table 1. Although the long noncoding RNAs we reviewed herein have demonstrated high specificity and sensitivity in detecting prostate cancer, their accuracy is not better than that of biopsy, even when multiple biomarkers are used. Moreover, polymorphisms in certain long noncoding RNAs are strongly correlated with risk prediction and stratification within or among various populations; nonetheless, relatively few individuals were examined in these previous studies. Therefore, performing such studies in a large cohort of individuals is necessary to further strengthen the promising evidence for long noncoding RNAs as biomarkers in prostate cancer risk prediction and stratification. Appreciating the critical role of long noncoding RNAs in prostate carcinogenesis and elucidating their mechanisms of action will help us to develop more specific drugs to interfere with malignant signaling and to specifically eradicate prostate cancer cells. Long noncoding RNAs (1) participate in prostate carcinogenesis through AR-mediated signaling pathways; (2) act as oncogenes and tumor suppressor genes in prostate carcinogenesis; and (3) mediate prostate carcinogenesis by interfering with DNA repair and tumor metabolism. Hence, based on the roles of long noncoding RNAs in prostate cancer, it will be interesting to develop intracellular interventions to interfere with malignant signaling networks. Furthermore, based on the mechanisms of action of long noncoding RNAs in prostate carcinogenesis and development, there are two main strategies, down-regulating long noncoding RNAs and inducing anaplerosis. The goal of down-regulating long noncoding RNAs involves re-activating or silencing the expression of long noncoding RNAs that are critical for prostate carcinogenesis and development, whereas replenishing long noncoding RNAs involves re-activating the function of TS lncRNAs and activating repressed endogenous tumor suppressor pathways. However, many challenges remain in the development of long noncoding RNAs as therapeutic targets for prostate cancer, including the poor stability of RNA molecules outside the cell and the lack of specific, secure and effective vectors for intracellular delivery.

Certain solutions may be developed; enveloping RNA molecules in nanoparticles or conjugating them to cholesterol moieties improves RNA stability, and targeting these molecules specifically to cancer cells by linking tumor-specific ligands to the surfaces of nanoparticles has also been investigated. Although there is a promising future for long noncoding RNA as a potential target in prostate cancer, the malignant signaling network is complicated, and there is insufficient data to explain the function and regulation of the discovered long noncoding RNAs. Thus, it will be necessary to identify additional long noncoding RNAs that are involved in prostate carcinogenesis, to develop new effective methods for predicting their target genes and to investigate their functional motifs and molecular structures to fully elucidate their regulatory mechanisms. Together, these long noncoding RNAs provide new insights into the complicated malignant signaling networks and novel strategies for prostate cancer diagnosis and therapy.

Table 1. Summary of the well-studied prostate cancer-related long noncoding RNAs.

Long Noncoding RNA	Locus	Expression Level	Role	Description	Reference
DD3^{PCA3}	Chr9q21.2	high	Urine/Plasma-based biomarker	(1) Biomarker for prostate cancer detection; (2) Polymorphism in its promoter region is related to the risk of prostate cancer in Chinese men.	[23,41]
MALAT1	Chr11q13.1	high		Biomarker for prostate cancer detection and progression.	[31,32]
PCAT-1	Chr8q24.21	high		Associated with the risk of and susceptibility to prostate cancer.	[69]
PCAT-18	Chr18q11.2	high		Biomarker for prostate cancer metastasis.	[33]
SChLAP1	Chr2q31.3	high	Tissue-based biomarker	Biomarker for clinical outcome of prostate cancer.	[35]
PlncRNA-1	Chr21	high	AR-related modulator	Promotes prostate carcinogenesis through reciprocal communication with AR.	[49]
CTBP1-AS	Chr4p16.3	high		Promotes prostate cancer growth by (1) repressing CTBP1 via the recruitment of PSF and HDAC and (2) promoting cell cycle progression by inhibiting tumor suppressor genes via AR.	[51,52]
Linc00963	Chr9	high (especially in hormone-insensitive prostate cancer)		Participates in the transition from androgen-dependence to androgen-independence in the progression of prostate cancer via interaction with EGFP.	[58]
PCAT-1	Chr8q24.21	high	Oncogene	(1) Promotes prostate cancer proliferation and progression; (2) Regulates the cellular response to genotoxins by repressing the expression of BRCA2, causing a deficiency in homologous recombination.	[59]
MALAT1	Chr11q13.1	high		Maintains the tumorigenicity and progression of prostate cancer.	[60,61]
SChLAP1	Chr2q31.3	high (especially in aggressive prostate cancer)		Drives malignancy by antagonizing the SWI/SNF complex.	[62]
ANRIL	Chr9p21.3	high		An inhibitor of a tumor suppressor gene. (1) Impacts the ability of CBX7 to repress the function of INK4b/ARF/INK4a and cell senescence control; (2) Inactivates p15(INK4B) by binding to SUZ12.	[63,64]
H19	Chr11p11.5	low	Tumor suppressor gene	Represses prostate cancer metastasis through TGFβ1 via H19/miR-675.	[65–67]
GAS5	Chr1q25	low		Over-expression can reduce drug/UV resistance and promote apoptosis.	[68]
PRNCR1	Chr8q24.21	high		Maintains prostate cancer susceptibility.	[53,56,57]
PCGEM1	Chr2q32	high		(1) Promotes proliferation and colony formation and inhibits the apoptosis of prostate cancer cells; (2) Promotes prostate cancer growth predominantly by regulating tumor metabolism via c-myc; (3) Polymorphisms are associated with the risk of prostate cancer in Chinese men.	[38,40,53,54, 57,70]

Acknowledgments

The study was supported by grants from the Key Program of the National Natural Science Foundation of China (81272822 and 81402102) and the Key Program of the Postgraduate Education Reform Research of Chongqing, China (yJg142014).

Author Contributions

Jin Yang conceptualized this review; Ya-Qin Huang prepared the table; Jin Yu professionally edited the manuscript; and Yin-Jie Su wrote the manuscript.

Conflicts of Interest

The authors declare no conflict of interest.

References

1. Jemal, A.; Bray, F.; Center, M.M.; Ferlay, J.; Ward, E.; Forman, D. Global cancer statistics. *CA Cancer J. Clin.* **2011**, *61*, 69–90.
2. Ferlay, J.; Shin, H.R.; Bray, F.; Forman, D.; Mathers, C.; Parkin, D.M. Estimates of worldwide burden of cancer in 2008: GLOBOCAN 2008. *Int. J. Cancer* **2010**, *127*, 2893–2917.
3. Siegel, R.; Ma, J.; Zou, Z.; Jemal, A. Cancer statistics, 2014. *CA Cancer J. Clin.* **2014**, *64*, 9–29.
4. Coleman, M.P.; Quaresma, M.; Berrino, F.; Lutz, J.M.; de Angelis, R.; Capocaccia, R.; Baili, P.; Rachet, B.; Gatta, G.; Hakulinen, T.; *et al.* Cancer survival in five continents: A worldwide population-based study (CONCORD). *Lancet Oncol.* **2008**, *9*, 730–756.
5. Gutschner, T.; Diederichs, S. The hallmarks of cancer: A long non-coding RNA point of view. *RNA Biol.* **2012**, *9*, 703–719.
6. Carter, H.B.; Pearson, J.D. PSA velocity for the diagnosis of early prostate cancer. A new concept. *Urol. Clin. N. Am.* **1993**, *20*, 665–670.
7. Gandellini, P.; Folini, M.; Longoni, N.; Pennati, M.; Binda, M.; Colecchia, M.; Salvioni, R.; Supino, R.; Moretti, R.; Limonta, P.; *et al.* miR-205 Exerts tumor-suppressive functions in human prostate through down-regulation of protein kinase Cepsilon. *Cancer Res.* **2009**, *69*, 2287–2295.
8. Tucci, P.; Agostini, M.; Grespi, F.; Markert, E.K.; Terrinoni, A.; Vousden, K.H.; Muller, P.A.; Dotsch, V.; Kehrloesser, S.; Sayan, B.S.; *et al.* Loss of p63 and its microRNA-205 target results in enhanced cell migration and metastasis in prostate cancer. *Proc. Natl. Acad. Sci. USA* **2012**, *109*, 15312–15317.
9. Gandellini, P.; Profumo, V.; Casamichele, A.; Fenderico, N.; Borrelli, S.; Petrovich, G.; Santilli, G.; Callari, M.; Colecchia, M.; Pozzi, S.; *et al.* miR-205 regulates basement membrane deposition in human prostate: Implications for cancer development. *Cell Death Differ.* **2012**, *19*, 1750–1760.
10. Bonci, D.; Coppola, V.; Musumeci, M.; Addario, A.; Giuffrida, R.; Memeo, L.; D'Urso, L.; Pagliuca, A.; Biffoni, M.; Labbaye, C.; *et al.* The miR-15a-miR-16-1 cluster controls prostate cancer by targeting multiple oncogenic activities. *Nat. Med.* **2008**, *14*, 1271–1277.
11. Sun, T.; Wang, Q.; Balk, S.; Brown, M.; Lee, G.S.; Kantoff, P. The role of microRNA-221 and microRNA-222 in androgen-independent prostate cancer cell lines. *Cancer Res.* **2009**, *69*, 3356–3363.

12. Park, T.Y.; Chae, J.Y.; Kim, J.W.; Oh, M.M.; Yoon, C.Y.; Moon du, G. Prostate-specific antigen mass and free prostate-specific antigen mass for predicting the prostate volume of Korean men with biopsy-proven benign prostatic hyperplasia. *Korean J. Urol.* **2013**, *54*, 609–614.
13. Wang, Y.; Hu, H.L.; Liu, Z.F.; Sun, W.Z.; Chen, X.X.; Wu, C.L. Diagnosis and treatment of xanthogranulomatous prostatitis: A case report and review of the literature. *Zhonghua Nan Ke Xue* **2013**, *19*, 149–152.
14. Sanda, M.G.; Dunn, R.L.; Michalski, J.; Sandler, H.M.; Northouse, L.; Hembroff, L.; Lin, X.; Greenfield, T.K.; Litwin, M.S.; Saigal, C.S.; *et al.* Quality of life and satisfaction with outcome among prostate-cancer survivors. *N. Engl. J. Med.* **2008**, *358*, 1250–1261.
15. Wilt, T.J.; Brawer, M.K.; Jones, K.M.; Barry, M.J.; Aronson, W.J.; Fox, S.; Gingrich, J.R.; Wei, J.T.; Gilhooly, P.; Grob, B.M.; *et al.* Radical prostatectomy *versus* observation for localized prostate cancer. *N. Engl. J. Med.* **2012**, *367*, 203–213.
16. Novara, G.; Ficarra, V.; Rosen, R.C.; Artibani, W.; Costello, A.; Eastham, J.A.; Graefen, M.; Guazzoni, G.; Shariat, S.F.; Stolzenburg, J.U.; *et al.* Systematic review and meta-analysis of perioperative outcomes and complications after robot-assisted radical prostatectomy. *Eur. Urol.* **2012**, *62*, 431–452.
17. Brawley, O.W.; Knopf, K.; Merrill, R. The epidemiology of prostate cancer part I: Descriptive epidemiology. *Semin. Urol. Oncol.* **1998**, *16*, 187–192.
18. Greene, K.L.; Meng, M.V.; Elkin, E.P.; Cooperberg, M.R.; Pasta, D.J.; Kattan, M.W.; Wallace, K.; Carroll, P.R. Validation of the Kattan preoperative nomogram for prostate cancer recurrence using a community based cohort: Results from cancer of the prostate strategic urological research endeavor (capsure). *J. Urol.* **2004**, *171 6 Pt 1*, 2255–2259.
19. Perkel, J.M. Visiting "noncodarnia". *BioTechniques* **2013**, *54*, 301–304.
20. Zhang, H.; Chen, Z.; Wang, X.; Huang, Z.; He, Z.; Chen, Y. Long non-coding RNA: A new player in cancer. *J. Hematol. Oncol.* **2013**, *6*, 37.
21. Qiu, M.T.; Hu, J.W.; Yin, R.; Xu, L. Long noncoding RNA: An emerging paradigm of cancer research. *Tumour Biol.* **2013**, *34*, 613–620.
22. Yang, G.; Lu, X.; Yuan, L. LncRNA: A link between RNA and cancer. *Biochim. Biophys. Acta* **2014**, *1839*, 1097–1109.
23. Bussemakers, M.J.; van Bokhoven, A.; Verhaegh, G.W.; Smit, F.P.; Karthaus, H.F.; Schalken, J.A.; Debruyne, F.M.; Ru, N.; Isaacs, W.B. *DD3*: A new prostate-specific gene, highly overexpressed in prostate cancer. *Cancer Res.* **1999**, *59*, 5975–5979.
24. Tinzl, M.; Marberger, M.; Horvath, S.; Chypre, C. DD3^{PCA3} RNA analysis in urine—A new perspective for detecting prostate cancer. *Eur. Urol.* **2004**, *46*, 182–186; discussion 187.
25. Hessels, D.; Klein Gunnewiek, J.M.; van Oort, I.; Karthaus, H.F.; van Leenders, G.J.; van Balken, B.; Kiemeney, L.A.; Witjes, J.A.; Schalken, J.A. DD3^{PCA3}-based molecular urine analysis for the diagnosis of prostate cancer. *Eur. Urol.* **2003**, *44*, 8–15; discussion 15–16.
26. Schalken, J.A.; Hessels, D.; Verhaegh, G. New targets for therapy in prostate cancer: Differential display code 3 (*DD3^{PCA3}*), a highly prostate cancer-specific gene. *Urology* **2003**, *62* (5 Suppl. 1), 34–43.

27. Jung, M.; Xu, C.; Spethmann, J.; Johannsen, M.; Deger, S.; Stephan, C.; Loening, S.A.; Jung, K. Re: Hessels, D.; Klein Gunnewiek, J.M.T.; van Oort, I.; Karthaus, H.F.M.; van Leenders, G.J.L.; van Balken, B.; Kiemeney, L.A.; Witjes, J.A.; Schalken, J.A. $DD3^{PCA3}$-based molecular urine analysis for the diagnosis of prostate cancer. *Eur. Urol.* **2003**, *44*, 8–16. *Eur. Urol.* **2004**, *46*, 271–272.
28. Ploussard, G.; Durand, X.; Xylinas, E.; Moutereau, S.; Radulescu, C.; Forgue, A.; Nicolaiew, N.; Terry, S.; Allory, Y.; Loric, S.; *et al.* Prostate cancer antigen 3 score accurately predicts tumour volume and might help in selecting prostate cancer patients for active surveillance. *Eur. Urol.* **2011**, *59*, 422–429.
29. Ji, P.; Diederichs, S.; Wang, W.; Boing, S.; Metzger, R.; Schneider, P.M.; Tidow, N.; Brandt, B.; Buerger, H.; Bulk, E.; *et al.* MALAT-1, a novel noncoding RNA, and thymosin β4 predict metastasis and survival in early-stage non-small cell lung cancer. *Oncogene* **2003**, *22*, 8031–8041.
30. Ren, S.; Wang, F.; Shen, J.; Sun, Y.; Xu, W.; Lu, J.; Wei, M.; Xu, C.; Wu, C.; Zhang, Z.; *et al.* Long non-coding RNA metastasis associated in lung adenocarcinoma transcript 1 derived miniRNA as a novel plasma-based biomarker for diagnosing prostate cancer. *Eur. J. Cancer* **2013**, *49*, 2949–2959.
31. Wang, F.; Ren, S.; Chen, R.; Lu, J.; Shi, X.; Zhu, Y.; Zhang, W.; Jing, T.; Zhang, C.; Shen, J.; *et al.* Development and prospective multicenter evaluation of the long noncoding RNA MALAT-1 as a diagnostic urinary biomarker for prostate cancer. *Oncotarget* **2014**, *5*, 11091–11102.
32. Ren, S.; Liu, Y.; Xu, W.; Sun, Y.; Lu, J.; Wang, F.; Wei, M.; Shen, J.; Hou, J.; Gao, X.; *et al.* Long noncoding RNA MALAT-1 is a new potential therapeutic target for castration resistant prostate cancer. *J. Urol.* **2013**, *190*, 2278–2287.
33. Crea, F.; Watahiki, A.; Quagliata, L.; Xue, H.; Pikor, L.; Parolia, A.; Wang, Y.; Lin, D.; Lam, W.L.; Farrar, W.L.; *et al.* Identification of a long non-coding RNA as a novel biomarker and potential therapeutic target for metastatic prostate cancer. *Oncotarget* **2014**, *5*, 764–774.
34. Sun, Y.; Lin, J.; Katz, A.E.; Fisher, P.B. Human prostatic carcinoma oncogene *PTI-1* is expressed in human tumor cell lines and prostate carcinoma patient blood samples. *Cancer Res.* **1997**, *57*, 18–23.
35. Mehra, R.; Shi, Y.; Udager, A.M.; Prensner, J.R.; Sahu, A.; Iyer, M.K.; Siddiqui, J.; Cao, X.; Wei, J.; Jiang, H.; *et al.* A novel RNA *in situ* hybridization assay for the long noncoding RNA SChLAP1 predicts poor clinical outcome after radical prostatectomy in clinically localized prostate cancer. *Neoplasia* **2014**, *16*, 1121–1127.
36. Lee, B.; Mazar, J.; Aftab, M.N.; Qi, F.; Shelley, J.; Li, J.L.; Govindarajan, S.; Valerio, F.; Rivera, I.; Thurn, T.; *et al.* Long noncoding RNAs as putative biomarkers for prostate cancer detection. *J. Mol. Diagn.* **2014**, *16*, 615–626.
37. Tomlins, S.A.; Rhodes, D.R.; Perner, S.; Dhanasekaran, S.M.; Mehra, R.; Sun, X.W.; Varambally, S.; Cao, X.; Tchinda, J.; Kuefer, R.; *et al.* Recurrent fusion of *TMPRSS2* and ETS transcription factor genes in prostate cancer. *Science* **2005**, *310*, 644–648.
38. Schmidt, U.; Fuessel, S.; Koch, R.; Baretton, G.B.; Lohse, A.; Tomasetti, S.; Unversucht, S.; Froehner, M.; Wirth, M.P.; Meye, A. Quantitative multi-gene expression profiling of primary prostate cancer. *Prostate* **2006**, *66*, 1521–1534.

39. Petrovics, G.; Zhang, W.; Makarem, M.; Street, J.P.; Connelly, R.; Sun, L.; Sesterhenn, I.A.; Srikantan, V.; Moul, J.W.; Srivastava, S. Elevated expression of *PCGEM1*, a prostate-specific gene with cell growth-promoting function, is associated with high-risk prostate cancer patients. *Oncogene* **2004**, *23*, 605–611.
40. Xue, Y.; Wang, M.; Kang, M.; Wang, Q.; Wu, B.; Chu, H.; Zhong, D.; Qin, C.; Yin, C.; Zhang, Z.; *et al.* Association between lncRNA *PCGEM1* polymorphisms and prostate cancer risk. *Prostate Cancer Prostatic Dis.* **2013**, *16*, 139–144, S1.
41. Zhou, W.; Tao, Z.; Wang, Z.; Hu, W.; Shen, M.; Zhou, L.; Wen, Z.; Yu, Z.; Wu, X.; Huang, K.; *et al.* Long noncoding RNA *PCA3* gene promoter region is related to the risk of prostate cancer on Chinese males. *Exp. Mol. Pathol.* **2014**, *97*, 550–553.
42. Ren, S.; Peng, Z.; Mao, J.H.; Yu, Y.; Yin, C.; Gao, X.; Cui, Z.; Zhang, J.; Yi, K.; Xu, W.; *et al.* RNA-seq analysis of prostate cancer in the Chinese population identifies recurrent gene fusions, cancer-associated long noncoding RNAs and aberrant alternative splicings. *Cell Res.* **2012**, *22*, 806–821.
43. Visakorpi, T.; Hyytinen, E.; Koivisto, P.; Tanner, M.; Keinanen, R.; Palmberg, C.; Palotie, A.; Tammela, T.; Isola, J.; Kallioniemi, O.P. *In vivo* amplification of the androgen receptor gene and progression of human prostate cancer. *Nat. Genet.* **1995**, *9*, 401–406.
44. Thomsen, F.B.; Brasso, K.; Christensen, I.J.; Johansson, J.E.; Angelsen, A.; Tammela, T.L.; Iversen, P.; Scandinavian Prostate Cancer Group. Survival benefit of early androgen receptor inhibitor therapy in locally advanced prostate cancer: Long-term follow-up of the SPCG-6 study. *Eur. J. Cancer* **2015**, *51*, 1283–1292.
45. Ahmadi, H.; Daneshmand, S. Androgen deprivation therapy for prostate cancer: Long-term safety and patient outcomes. *Patient Relat. Outcome Meas.* **2014**, *5*, 63–70.
46. Molina, A.; Belldegrun, A. Novel therapeutic strategies for castration resistant prostate cancer: Inhibition of persistent androgen production and androgen receptor mediated signaling. *J. Urol.* **2011**, *185*, 787–794.
47. Takayama, K.; Kaneshiro, K.; Tsutsumi, S.; Horie-Inoue, K.; Ikeda, K.; Urano, T.; Ijichi, N.; Ouchi, Y.; Shirahige, K.; Aburatani, H.; *et al.* Identification of novel androgen response genes in prostate cancer cells by coupling chromatin immunoprecipitation and genomic microarray analysis. *Oncogene* **2007**, *26*, 4453–4463.
48. Takayama, K.; Tsutsumi, S.; Katayama, S.; Okayama, T.; Horie-Inoue, K.; Ikeda, K.; Urano, T.; Kawazu, C.; Hasegawa, A.; Ikeo, K.; *et al.* Integration of cap analysis of gene expression and chromatin immunoprecipitation analysis on array reveals genome-wide androgen receptor signaling in prostate cancer cells. *Oncogene* **2011**, *30*, 619–630.
49. Cui, Z.; Ren, S.; Lu, J.; Wang, F.; Xu, W.; Sun, Y.; Wei, M.; Chen, J.; Gao, X.; Xu, C.; *et al.* The prostate cancer-up-regulated long noncoding RNA PlncRNA-1 modulates apoptosis and proliferation through reciprocal regulation of androgen receptor. *Urol. Oncol.* **2013**, *31*, 1117–1123.
50. Xu, L.L.; Srikantan, V.; Sesterhenn, I.A.; Augustus, M.; Dean, R.; Moul, J.W.; Carter, K.C.; Srivastava, S. Expression profile of an androgen regulated prostate specific homeobox gene *NKX3.1* in primary prostate cancer. *J. Urol.* **2000**, *163*, 972–979.

51. Takayama, K.; Horie-Inoue, K.; Katayama, S.; Suzuki, T.; Tsutsumi, S.; Ikeda, K.; Urano, T.; Fujimura, T.; Takagi, K.; Takahashi, S.; *et al.* Androgen-responsive long noncoding RNA *CTBP1-AS* promotes prostate cancer. *EMBO J.* **2013**, *32*, 1665–1680.
52. Sung, Y.Y.; Cheung, E. Antisense now makes sense: Dual modulation of androgen-dependent transcription by *CTBP1-AS*. *EMBO J.* **2013**, *32*, 1653–1654.
53. Yang, L.; Lin, C.; Jin, C.; Yang, J.C.; Tanasa, B.; Li, W.; Merkurjev, D.; Ohgi, K.A.; Meng, D.; Zhang, J.; *et al.* lncRNA-dependent mechanisms of androgen-receptor-regulated gene activation programs. *Nature* **2013**, *500*, 598–602.
54. Srikantan, V.; Zou, Z.; Petrovics, G.; Xu, L.; Augustus, M.; Davis, L.; Livezey, J.R.; Connell, T.; Sesterhenn, I.A.; Yoshino, K.; *et al. PCGEM1*, a prostate-specific gene, is overexpressed in prostate cancer. *Proc. Natl. Acad. Sci. USA* **2000**, *97*, 12216–12221.
55. Fu, X.; Ravindranath, L.; Tran, N.; Petrovics, G.; Srivastava, S. Regulation of apoptosis by a prostate-specific and prostate cancer-associated noncoding gene, *PCGEM1*. *DNA Cell Biol.* **2006**, *25*, 135–141.
56. Chung, S.; Nakagawa, H.; Uemura, M.; Piao, L.; Ashikawa, K.; Hosono, N.; Takata, R.; Akamatsu, S.; Kawaguchi, T.; Morizono, T.; *et al.* Association of a novel long non-coding RNA in 8q24 with prostate cancer susceptibility. *Cancer Sci.* **2011**, *102*, 245–252.
57. Prensner, J.R.; Sahu, A.; Iyer, M.K.; Malik, R.; Chandler, B.; Asangani, I.A.; Poliakov, A.; Vergara, I.A.; Alshalalfa, M.; Jenkins, R.B.; *et al.* The lncRNAs *PCGEM1* and *PRNCR1* are not implicated in castration resistant prostate cancer. *Oncotarget* **2014**, *5*, 1434–1438.
58. Wang, L.; Han, S.; Jin, G.; Zhou, X.; Li, M.; Ying, X.; Wang, L.; Wu, H.; Zhu, Q. Linc00963: A novel, long non-coding RNA involved in the transition of prostate cancer from androgen-dependence to androgen-independence. *Int. J. Oncol.* **2014**, *44*, 2041–2049.
59. Prensner, J.R.; Iyer, M.K.; Balbin, O.A.; Dhanasekaran, S.M.; Cao, Q.; Brenner, J.C.; Laxman, B.; Asangani, I.A.; Grasso, C.S.; Kominsky, H.D.; *et al.* Transcriptome sequencing across a prostate cancer cohort identifies *PCAT-1*, an unannotated lincRNA implicated in disease progression. *Nat. Biotechnol.* **2011**, *29*, 742–749.
60. Tripathi, V.; Ellis, J.D.; Shen, Z.; Song, D.Y.; Pan, Q.; Watt, A.T.; Freier, S.M.; Bennett, C.F.; Sharma, A.; Bubulya, P.A.; *et al.* The nuclear-retained noncoding RNA MALAT1 regulates alternative splicing by modulating SR splicing factor phosphorylation. *Mol. Cell* **2010**, *39*, 925–938.
61. Hutchinson, J.N.; Ensminger, A.W.; Clemson, C.M.; Lynch, C.R.; Lawrence, J.B.; Chess, A. A screen for nuclear transcripts identifies two linked noncoding RNAs associated with SC35 splicing domains. *BMC Genomics* **2007**, *8*, 39.
62. Prensner, J.R.; Iyer, M.K.; Sahu, A.; Asangani, I.A.; Cao, Q.; Patel, L.; Vergara, I.A.; Davicioni, E.; Erho, N.; Ghadessi, M.; *et al.* The long noncoding RNA *SChLAP1* promotes aggressive prostate cancer and antagonizes the SWI/SNF complex. *Nat. Genet.* **2013**, *45*, 1392–1398.
63. Yap, K.L.; Li, S.; Munoz-Cabello, A.M.; Raguz, S.; Zeng, L.; Mujtaba, S.; Gil, J.; Walsh, M.J.; Zhou, M.M. Molecular interplay of the noncoding RNA *ANRIL* and methylated histone H3 lysine 27 by polycomb CBX7 in transcriptional silencing of *INK4a*. *Mol. Cell* **2010**, *38*, 662–674.
64. Kotake, Y.; Nakagawa, T.; Kitagawa, K.; Suzuki, S.; Liu, N.; Kitagawa, M.; Xiong, Y. Long non-coding RNA *ANRIL* is required for the PRC2 recruitment to and silencing of $p15^{INK4B}$ tumor suppressor gene. *Oncogene* **2011**, *30*, 1956–1962.

65. Lustig-Yariv, O.; Schulze, E.; Komitowski, D.; Erdmann, V.; Schneider, T.; de Groot, N.; Hochberg, A. The expression of the imprinted genes H19 and IGF-2 in choriocarcinoma cell lines. Is H19 a tumor suppressor gene? *Oncogene* **1997**, *15*, 169–177.
66. Ariel, I.; Sughayer, M.; Fellig, Y.; Pizov, G.; Ayesh, S.; Podeh, D.; Libdeh, B.A.; Levy, C.; Birman, T.; Tykocinski, M.L.; *et al.* The imprinted H19 gene is a marker of early recurrence in human bladder carcinoma. *Mol. Pathol.* **2000**, *53*, 320–323.
67. Zhu, M.; Chen, Q.; Liu, X.; Sun, Q.; Zhao, X.; Deng, R.; Wang, Y.; Huang, J.; Xu, M.; Yan, J.; *et al.* lncRNA H19/miR-675 axis represses prostate cancer metastasis by targeting TGFBI. *FEBS J.* **2014**, *281*, 3766–3775.
68. Pickard, M.R.; Mourtada-Maarabouni, M.; Williams, G.T. Long non-coding RNA GAS5 regulates apoptosis in prostate cancer cell lines. *Biochim. Biophys. Acta* **2013**, *1832*, 1613–1623.
69. Prensner, J.R.; Chen, W.; Iyer, M.K.; Cao, Q.; Ma, T.; Han, S.; Sahu, A.; Malik, R.; Wilder-Romans, K.; Navone, N.; *et al. PCAT-1*, a long noncoding RNA, regulates BRCA2 and controls homologous recombination in cancer. *Cancer Res.* **2014**, *74*, 1651–1660.
70. Hung, C.L.; Wang, L.Y.; Yu, Y.L.; Chen, H.W.; Srivastava, S.; Petrovics, G.; Kung, H.J. A long noncoding RNA connects c-Myc to tumor metabolism. *Proc. Natl. Acad. Sci. USA* **2014**, *111*, 18697–18702.

© 2015 by the authors; licensee MDPI, Basel, Switzerland. This article is an open access article distributed under the terms and conditions of the Creative Commons Attribution license (http://creativecommons.org/licenses/by/4.0/).

Int. J. Mol. Sci. **2015**, *16*, 14554-14570; doi:10.3390/ijms160714554

OPEN ACCESS
International Journal of
Molecular Sciences
ISSN 1422-0067
www.mdpi.com/journal/ijms

Review

Advances in the *in Vivo* Raman Spectroscopy of Malignant Skin Tumors Using Portable Instrumentation

Nikolaos Kourkoumelis [1,*], Ioannis Balatsoukas [1], Violetta Moulia [1], Aspasia Elka [1], Georgios Gaitanis [2] and Ioannis D. Bassukas [2]

[1] Department of Medical Physics, School of Health Sciences, University of Ioannina, 45110 Ioannina, Greece; E-Mails: ibalats@cc.uoi.gr (I.B.); biomoulia@yahoo.gr (V.M.); e.aspa@yahoo.com (A.E.)

[2] Department of Skin and Venereal Diseases, School of Health Sciences, University of Ioannina, 45110 Ioannina, Greece; E-Mails: ggaitan@uoi.gr (G.G.); ibassuka@cc.uoi.gr (I.D.B.)

* Author to whom correspondence should be addressed; E-Mail: nkourkou@cc.uoi.gr; Tel.: +30-2651-00-7594; Fax: +30-2651-00-7854.

Academic Editor: William Chi-shing Cho

Received: 11 June 2015 / Accepted: 24 June 2015 / Published: 26 June 2015

Abstract: Raman spectroscopy has emerged as a promising tool for real-time clinical diagnosis of malignant skin tumors offering a number of potential advantages: it is non-intrusive, it requires no sample preparation, and it features high chemical specificity with minimal water interference. However, *in vivo* tissue evaluation and accurate histopathological classification remain a challenging task for the successful transition from laboratory prototypes to clinical devices. In the literature, there are numerous reports on the applications of Raman spectroscopy to biomedical research and cancer diagnostics. Nevertheless, cases where real-time, portable instrumentations have been employed for the *in vivo* evaluation of skin lesions are scarce, despite their advantages in use as medical devices in the clinical setting. This paper reviews the advances in real-time Raman spectroscopy for the *in vivo* characterization of common skin lesions. The translational momentum of Raman spectroscopy towards the clinical practice is revealed by (i) assembling the technical specifications of portable systems and (ii) analyzing the spectral characteristics of *in vivo* measurements.

Keywords: Raman spectroscopy; *in vivo* spectroscopy; skin cancer

1. Introduction

The spectrum of skin cancers in humans currently encompasses the most frequent neoplasm types by tissue of origin and the most costly cancer categories to treat [1]. From the different types of skin neoplasms, cancers of keratinocytic origin (epithelial skin cancer, formerly designated preferentially as non-melanoma skin cancer (NMSC)) form the most frequent category. The two most common skin cancer types of this group, basal cell carcinoma (BCC) and squamous cell carcinoma (SCC) comprise ~95% of all skin cancers and together with the third most frequent, malignant melanoma (MM), constitute 99% of the incidence of all skin neoplasms. Several studies have documented the increasing trends in skin cancer occurrence all over the world [2–7]. Furthermore, distinct subpopulations exist with significantly increased risk for developing tumors in this organ like patients with multiple nevi [8] and those that are on long-term iatrogenic immunosuppresion [9]. However, the aforementioned three most frequent skin cancer types, *i.e.*, BCC, SCC and MM, differ substantially in their biological aggressiveness and relevant prognosis. Keratinocytic skin cancers are typically curable, especially if diagnosed early enough [10] and despite the increasing incidence, their mortality rates remain low [11,12]. Notably for BCC, there are reports of rapidly declining mortality rates despite the marked incidence increase during the same period [13]. On the other hand, MM is a biologically aggressive neoplasm. The diagnosis is often ambiguous and the course of the disease strongly depends on the tumor stage [14]. In general, it is highly unpredictable at the individual patient's level; the prognosis is markedly worse in advanced stages with the five-year survival rate as low as 16%. However, when melanoma is detected and excised in the initial *in situ* stage, survival reaches 99% and the disease can be considered practically curable [15].

Early diagnosis is critical for the successful treatment of skin neoplasms. The initial step of clinical evaluation in which suspicious lesions are selected for targeted invasive assessment with biopsies is crucial because the selection process is challenging even for the experienced clinician. Few lesions have to be picked up for biopsy between a multitude of benign and malignant and look-alike skin alterations coexist side by side in skin areas severely damaged by excessive life-long sunlight exposure. The specificity and the sensitivity of the above clinical procedure vary from 40% to 80%, imposing substantial uncertainty on this diagnostic process [16]. Moreover, it is very important to limit the use of skin biopsies since this invasive and time-consuming process is often associated with substantial patient discomfort. At this point, unbiased clinical decisions based on non-invasive, real-time and time-saving diagnostic techniques are preferable to facilitate the management of the increasing number of patients with skin cancer [17,18]. From the many optical spectroscopy techniques under evaluation for the early, non-invasive detection of skin lesions, two vibrational spectroscopy modalities seem to be the most promising: Fourier Transform Infrared (FTIR) and Raman Spectroscopy [16,19,20]. The strong absorption of mid-infrared radiation by water molecules limits the clinical *in vivo* applicability of the FTIR technique [21], although a lot of progress has been achieved towards this issue [22]. On the other hand, Raman spectroscopy is able to detect spectroscopic fingerprints of tissues in their native state within clinically acceptable measurement time (seconds) without the need for tissue pre-processing, like staining or fixation.

Raman spectroscopy is based on the inelastic scattering of photons exchanging energy via molecular vibrational modes. Due to the fact that molecular energy levels are quantized and unique for

each molecule, Raman spectra feature discrete and chemical bonds-specific bands, providing a "molecular fingerprint" of the samples under study [23]. Thus, Raman active molecules (*i.e.*, with anisotropic polarizability) can give spectroscopic signals with significant information about the chemical composition of the sample. The technique has been applied in a variety of biological and medical research branches as a reliable modality for the *in situ* diagnosis of malignancy at tissue level or for the analysis of subcellular molecular composition of tissues [24]. Moreover, it can be employed to determine steps in tumor progression or to evaluate response to radiation therapy [25].

This paper reviews the advances in the use of portable Raman systems for the clinical, *in vivo* spectroscopic characterization of skin lesions in real-time with emphasis in the diagnosis and management of the three most common skin cancers (BCC, SCC and MM). Where possible, we compare the experimental outcomes in an effort to identify the best practices for the clinical environment.

2. Instrumentation and Experimental Considerations

2.1. Portable Raman Acquisition Systems

Raman spectroscopy is an optical spectroscopic technique based on the inelastic scattering of monochromatic light. Raman scattering involves inelastic collisions between the photons of an irradiating laser beam and the sample (or tissue) molecules. The absorption of photons, results in energy exchange between photons and tissue molecules generating vibrations within the material that are molecule specific. A nonlinear polyatomic molecule with N atoms has 3*N*-6 modes of vibration, known as "normal modes" which are related to a fundamental frequency of vibration and symmetry. When photons are reemitted, their energy, and hence frequency, is shifted in comparison to the excitation frequency, yielding the so-called "Raman shift". The Raman shift is independent of the excitation (incident) wavelength, which means that it is constant and unique for the different molecules. Thus, the evaluation of the scattered light is transformed to the vibrational Raman spectrum of the sample, which contains substantial qualitative and quantitative information about the chemical composition of the examined probes. Since the detection of certain Raman bands correlates with the presence of specific molecules in a probe, Raman spectra can be used to differentiate between tissues of different pathological conditions. Raman cross section is wavelength dependent and varies according to $1/\lambda^4$, where λ is the excitation wavelength [26]. Thus, the intensity of the Raman peaks is proportional to f^4 (where f is the laser frequency) and, for example, a 488 nm laser gives an almost seven times more intense Raman signal than a 785 nm laser. Moreover, the transmission efficiency of the optics and detector sensitivity is also wavelength dependent [27]. The excitation wavelength is a significant parameter for the analysis of skin lesions because it has a major impact on the scattered intensity, the auto-fluorescence and the signal attenuation. Skin research can be conducted in a wide range of excitation frequencies from visible to near infrared (NIR) wavelengths and this has been an obstacle to compare methodologies and results. NIR generate lower auto-fluorescence intensities compared to the excitation with visible light but at the same time poorer scattering intensity too, resulting into lower sensitivity and thus to a lower signal to noise ratio. Laser sources at 785 or 830 nm are preferred for clinical Raman applications because the operation at these wavelengths combines reduced auto-fluorescence and adequate tissue penetration depth [28]. Sources at 1064 nm also have

a favorable profile of signal to noise ratio for skin applications but they usually require increased irradiation doses and annoying prolonged spectra acquisition times [29,30]. Nevertheless, optimally employed FT-Raman spectrometers at this excitation wavelength demonstrate relatively high signal to noise ratio [31]. The light attenuation in the skin tissue was evaluated on excised human skin by confocal Raman microspectroscopy [32–35] and confirmed that Raman signals are suitable for skin measurements at various depths (up to a few hundred micrometers) depending on the spectrometer setup. The safety issues of tissue irradiation and exposure times are regulated by consensus directives released by international organizations (ANSI Z136, ICNIRP, and IEC 60825-1).

Table 1 summarizes the major operation parameters (wavelength, power, focal spot size, and signal integration time) employed in *in vivo* studies of a variety of skin lesions with the use of portable Raman spectroscopy devices for the acquisition of spectra in real-time (the blue line separates *in vivo* studies which did not aim to the classification of common skin lesions but solely to biochemical characterization). In the clinical setting with the appropriate equipment, Raman spectroscopy does not require any specific tissue pre-treatment except from possible superficial cleaning of excess sebum with ethanol [16]. *Ex vivo* studies of skin tissue material samples and biopsy probes are not included in Table 1, even if they have been carried out with portable setups.

The diverse Raman implementations presented in Table 1 imply that there is neither any optimal experimental design nor any standardization among setups. The data clearly indicate that it is difficult to quantify the tradeoff between excitation wavelength and lower scattering cross section with auto-fluorescence intensity since the detection of a specific Raman band depends on both the experimental parameters and the (heterogeneous) composition of skin tissue. Tfayli *et al.* [28] have studied the wavelength effect on pig skin epidermis by recording spectra at 532, 633, and 785 nm and analyzing the variability and the repeatability of the experiments along with the effect of exposure time and in-depth signal attenuation. They suggested that the excitation wavelength at 785 nm is advantageous (compared to 532 and 633 nm) for the fingerprint skin region, having lower signal attenuation. Yet, in principle, it is rather difficult to extrapolate outcomes and directly compare results by different research groups using different wavelengths and instrumentation. Varying sampling rates and different statistical classification schemes add another level of complexity for the preparation of an accepted clinical protocol. Calibration of portable Raman systems with standard samples of exact composition, resembling human skin, is possibly a requirement for the future.

Table 1. Technical details of clinical applications of portable Raman spectroscopy in skin cancer diagnosis.

Cancer Type	Technique	Raman Excitation Wavelength (nm)	Spot Size (mm)	Power (mW)	Signal Integration Time (s)	Number of Skin Lesions Studied and/or Patients	Reference
MM, BCC, SCC, actinic keratosis (AK), atypical nevi, melanocytic nevi, blue nevi, and seborrheic keratoses	Raman	785	3.5	300	1	518 (453 patients)	[36]
BCC, inflammatory scar tissues	Raman + OCT [a]	785	0.044	40	30	1 patient	[15]
MM, BCC, SCC, pigmented nevi	Raman	785	1	150	30	50	[37]
MM, BCC, SCC, pigmented nevi	Raman + OCT	785	1	150	30	23, 50	[38,39]
MM, BCC, SCC, pigmented nevi	Raman	785	0.1	17	10	137	[40,41]
BCC, SCC, inflammatory scar tissues	Raman	825	0.005 [b]	40	30	21 (19 patients)	[42]
BCC	Raman	830	1.6	110	30	10 patients	[43]
BCC, SCC	Raman	830	-	200	20 (2 s × 10 spectra)	31 (17 patients)	[44]
BCC, SCC, AK	Raman	830	0.17	200	20 (2 s × 10 spectra)	49 (25 patients)	[45]
MM, BCC, SCC, AK, and non-melanoma pigmented lesions	Raman	830	0.2	100	1	137 (76 patients)	[46,47]
BCC	Multi modal [c]	830	0.2	56	4	1 (healthy) [d]	[48]
MM, eczema, psoriatic skin, malignant Kaposi sarcomas	Raman	1064	10	-	-	1 (healthy) [d]	[31]
MM, BCC, pigmented nevi	Raman	1064	0.1	120	480	81 (72 patients)	[49]
Carotenoid concentration in BCC and actinic keratoses	Raman	488	2	10	20	14 patients	[50]
MM	Multi modal [e]	1064	0.08	-	35	Mice injected with human MM cells	[51]

[a] OCT = Optical Coherence Tomography; [b] Value from identical instrumentation in [52]; [c] Raman, fluorescence, and reflectance spectroscopy; [d] compared with skin lesions from *in vitro* studies; [e] acoustic microscopy, infrared reflectance and Raman spectroscopy (proof-of-concept study); BCC: basal cell carcinoma; SCC: squamous cell carcinoma; MM: malignant melanoma.

2.2. Comparison between Portable and Benchtop Systems

As a rule of the thumb, the spectral quality of portable spectrometers is lower than benchtop ones due to the poorer sensitivity and scanning range [53]. However, the superior characteristics of the benchtop spectrometers (numerical aperture, lens, and focal length) and of the laser beam (intensity profile) are compensated by mass and size restrictions in the clinical environment along with the convenient accessibility of the skin lesions on the patients' bodies via optical fibers. In most cases, bands assignment and qualitative characterization was aided by measurements performed in biopsies and no significant alterations in bands shape and positions has been detected between *in vivo* and *in vitro* experiments. Even so, the overall spectra precision was characterized as low [54] due to the low signal to noise ratio. Thus, portable Raman setups should be able to address the question whether or not a band having 2–3 times greater intensity than the noise (which is typically defined as the square root of the raw intensity of measurement) can be detected at a certain position [27]. Raman signal is effectively the sum of two parts: the raw signal attributed to the sample's concentration of Raman active compounds and the overall noise due to (i) fluorescence (background) and (ii) the contribution from the optical components. In addition, the resulted spectra are affected by ambient light, beam powder density, measurement time and matrix effects. Biomolecules in skin tissues are by default weak Raman scatterers imposing an additional difficulty to the challenging task of skin tumors classification. In the majority of the relevant literature, the application of chemometrics was necessary to detect the subtle changes attributed to the pathological skin lesions.

3. Results and Discussion

3.1. Bands Assignment

The positions (typically reported in wavenumbers) and relative intensities of Raman bands are the major spectral characteristics for delineating the molecular background of skin diseases. Nonetheless, for optimizing the extraction of diagnostic information, three interwoven but distinct levels of spectral analysis must be combined [55]: (i) chemical analysis which pertains to the qualitative and quantitative biochemical composition of the tissue; (ii) statistical processing of the spectral variations; and (iii) integration of core spectroscopic findings with relevant clinical information. The most common Raman bands associated with pathological skin lesions together with their chemical assignment are shown in Table 2.

Table 2. Tentative assignment of the most prominent Raman bands showing differentiation in spectra between normal and skin cancer tissues (MM, BCC, and SCC specific).

Cancer Type	Peak Position (cm^{-1}) [a]	Assignment	Reference
BCC	500–600	S-S disulfide stretching	[56]
BCC	727	ν(CN)Adenine, Lipids	[56]
BCC	746	Thymine	[56]
BCC	786–788	Nucleic acid backbone (PO_2 symmetric stretching)	[56,57]
BCC, SCC, MM	832	Proline, hydroxyproline, tyrosine, stretch of nucleic acids, DNA (PO_2 symmetric stretching)	[44,46,56]
BCC, SCC	920–943	ν(CC) skeletal of collagen backbone Proline, hydroxyproline	[31,42,44,58]
BCC, SCC	1000–1010	Phenylalanine (ring breathing); keratin	[42,44,56]
BCC, SCC	1085–1098	ν(CC) lipids Nucleic acid backbone ν(PO_2) symmetric stretching	[15,31,56,57,59]
BCC, SCC	1127–1130	Lipids ν(CC) symmetric stretching of acyl-backbone, trans conformation	[44,56]
BCC, SCC	1207–1209	Tyrosine, phenylalanine	[44,56]
MM, BCC	1220–1280	Amide III (δ(NH) bending and ν(CN) stretching vibrations) (protein band), tropocollagen (proline-rich), ν(CH) ethylene (triolein and phospholipids)	[15,31,42,43,45,46,49,56,58–61]
MM, BCC	1300	δ(CH_2) twist, lipids	[46,60,62]
BCC	1336	CH deformations, adenine, phenylalanine	[37,38,56]
MM, BCC	1440–1460	δ(CH_2) scissoring in lipids and δ(CH_2) scissoring vibration in proteins	[15,42,46,56,59,62]
MM, BCC	1520–1570	Nucleic acids	[37]
MM, BCC	1640–1685	Amide I (C=O stretching), collagen, elastin	[37,38,42,43,46,59,60]
BCC	1651	Lipids (C=C stretching), phenylalanine	[56]
MM, BCC	3250	H_2O	[49]

[a] Approximate values.

Data in Table 2 indicate that quantitative modulations of amide moieties bands III and I are characteristic for tumor cell proliferation, probably as a result of Raman active modifications in the molecular composition of the proteins in malignant skin tissues. In particular, the majority of the studies report a significant decrease of the amide III band intensity, which is regarded to reflect important alterations in the secondary structure of the tissue proteins. It is important to note that this band gives quite strong signal with Raman but rather weak with IR spectroscopy [63]. Apart from reduced intensity, this band seems to also be shifted to higher frequencies in the case of BCC and MM [59]. Raman spectra from malignant skin lesions show lower amide I band intensities although the corresponding results are possibly tumor type specific. Significant changes are also observed in the lipids concentration. Moreover, it is expected that the concentration of nucleic acids increases in malignant tissues due to the unrestrained cell proliferation that leads to spatial overcrowding of nucleated cells [31,64] and to intensity increase of the corresponding Raman bands. Water is another major tissue constituent. Highly significant alterations in the respective water content were observed for MM and BCC [49]. Spectral fingerprints of stabilizing disulfide bridges between cysteine residues in macromolecules are localized in the lower spectra section; detection of decreased intensity of the respective bands in tissues has been attributed to protein oxidation [56]. Carotenoids play a significant role as major anti-oxidants in the skin and they possibly contribute to the mechanisms of skin cancer prevention. Hata *et al.* [50] studied the concentration of carotenoids in the skin by analyzing the intensity of the 1524 cm^{-1} peak (v(C=C) stretch vibration of the backbone). They suggested that BCC can be differentiated from healthy skin areas as a result of their significantly lower carotenoid concentration but at the same time they concluded that further analysis on the possible correlation of the dermal carotenoids with cutaneous pathology is needed. Indeed, recent studies using resonance Raman spectroscopy [65] and reflection spectroscopy [66] showed that carotenoids concentration mostly reflects nutritional habits and stress conditions. Poor nutrition, illness, and smoking are generally related to low carotenoid concentration while stress factors (solar irradiation, environmental hazards, fatigue, illness, *etc.*) contribute to the fast degradation of dermal carotenoids. Therefore, the low carotenoids concentration is undoubtedly a significant finding but probably not a biomarker.

It is evident that certain biochemical changes associated with skin malignancies can be successfully identified by Raman spectroscopy. To reduce the high number of parameters needed to characterize the variance in the acquired spectral datasets, researchers typically utilize multivariate statistical methods to generate linear discriminant models of classification [67]. In the subsequent section we also refer to the sensitivity and specificity of these models for BCC, SCC and MM.

3.2. Studies of NMSC and MM with Portable Raman Instrumentation

Liu *et al.* [36] performed the most comprehensive *in vivo* study to date presenting data from Raman spectroscopic analysis of 453 patients with benign and malignant skin lesions (MM, BCC, SCC, and actinic keratoses). They concluded that distinctive Raman spectral peaks or bands cannot be uniquely assigned to any of the different skin cancer types. Moreover, they showed that the chemical fingerprints of different skin lesions are not site-dependent unlike previous findings with healthy human skin [68]. Raman spectral bands with diagnostic impact were recognized at 855, 936, 1002, 1271, 1302, 1445, 1655, and 1745 cm^{-1}. It was suggested that bands in the region of 1055–1800 cm^{-1}

are critical for evaluating MM. Multivariate statistical methods were necessary to evaluate information from multiple band positions determinations in order to optimize the clinical classification of skin lesions. Although the sensitivity of the above approach for the discrimination between malignant and benign skin conditions is 99%, the specificity is limited to only 15% for the differentiation between MM and benign lesions and to 17% for that of keratinocytic skin neoplasms (BCC, SCC and actinic keratoses) *vs.* benign lesions. Lim *et al.* [46] have noticed a noteworthy low intensity of the amide band I region coupled with an increase in the intensity of the lipid bands at 1310–1340 cm^{-1} in the case of MM. The decrease in the amide I band was linked to collagen degradation or to the increased melanin concentration and pigmentation of the neoplasms. Moreover, only the MM spectra exhibited peaks between 800 and 900 cm^{-1} while both BCC and MM showed peaks with lower intensity in the 1450 cm^{-1} region. The integration of spectral information in the fingerprint region (900–1800 cm^{-1}) was suggested for the discrimination of skin cancers from benign lesions (Figure 1).

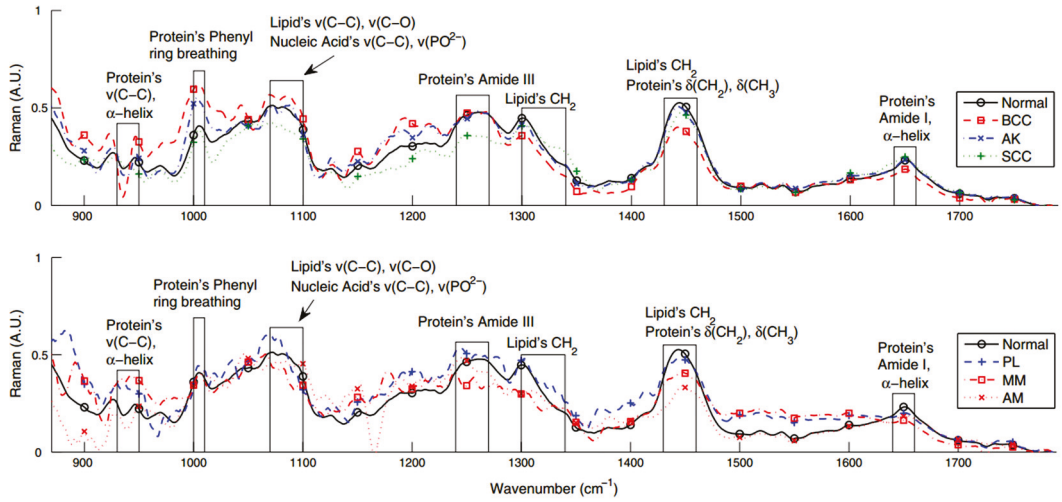

Figure 1. Mean Raman spectra acquired *in vivo* for basal cell carcinoma (BCC), squamous cell carcinoma (SCC), actinic keratosis (AK), nonmelanoma pigmented lesions (PL), amelanotic melanoma (AM) and normal skin. Adapted and reproduced with permission from [46].

The overall lower spectral intensity of malignant skin conditions was also confirmed by other studies [69], which consistently found that BCC and SCC exhibit weaker scattering than healthy skin, probably as a result of enhanced collagen breakdown. Principal component analysis (PCA) was employed for the classification of the different lesions. With this approach the authors demonstrated a 100% sensitivity and specificity in the discrimination of MM from non-melanoma pigmented skin lesions. With the same approach SCC, BCC and actinic keratoses could also be differentiated from normal skin with sensitivity and specificity of 90% and 85%, respectively. Patil *et al.* [15] identified distinct differences between the healthy skin and BCC in the Raman bands at 1090, 1300, and 1440 cm^{-1} while Tfayli *et al.* [43] for the same kind of comparison (normal skin *vs.* BCC) performed hierarchical cluster analysis concentrating on the amide III and the CH deformation band (1410 cm^{-1}) as the most promising bands; they noticed frequency shifting of the 1410 cm^{-1} peak, a weak shoulder at 1685 cm^{-1} in the BCC spectra (amide I region), differences in the amide III band and in the phospholipid content. Zakharov *et al.* [37] investigated major spectral differences between normal skin

and malignant tumors (MM and BCC) using a two-step method of tumor diagnosis to optimize the sensitivity and specificity of the discrimination. The method utilized characteristic spectral intensities in the 1300–1340, 1440–1460, and 1640–1680 cm^{-1} ranges. Plots of intensities' relative difference were constructed for healthy and malignant tissues; discriminant analysis and support vector machines assigned tissue classes with 88.9% sensitivity and 87.8% specificity for the *in vivo* Raman measurements. The authors reported a significant improvement in MM identification using this two-step classification. The same research group enhanced their technique by combining Raman spectroscopy with OCT [38] and in a recent publication, combined OCT, backscattering (BS) and Raman spectroscopy [39]. OCT is a highly accurate method for BCC diagnosis while BS was utilized for the qualification of tumor boundaries. This combined device coupled with the two-step analysis showed an increase accuracy of diagnosis by 9% for sensitivity and 8% for specificity compared to the values obtained by each method separately. Comparative results for BCC *vs.* normal tissues are depicted in Figure 2. Common significant spectral features are concentrated in the amide III and lipids bands while the band at 1410 cm^{-1} was not reported in studies other than [43]. The weak shoulder at 1685 cm^{-1} is present in two of the studies [15,43] while it was not evident in the third one [37]; this possibly shows that amide I alterations are tumor specific and readily expressed in MM but not in BCC.

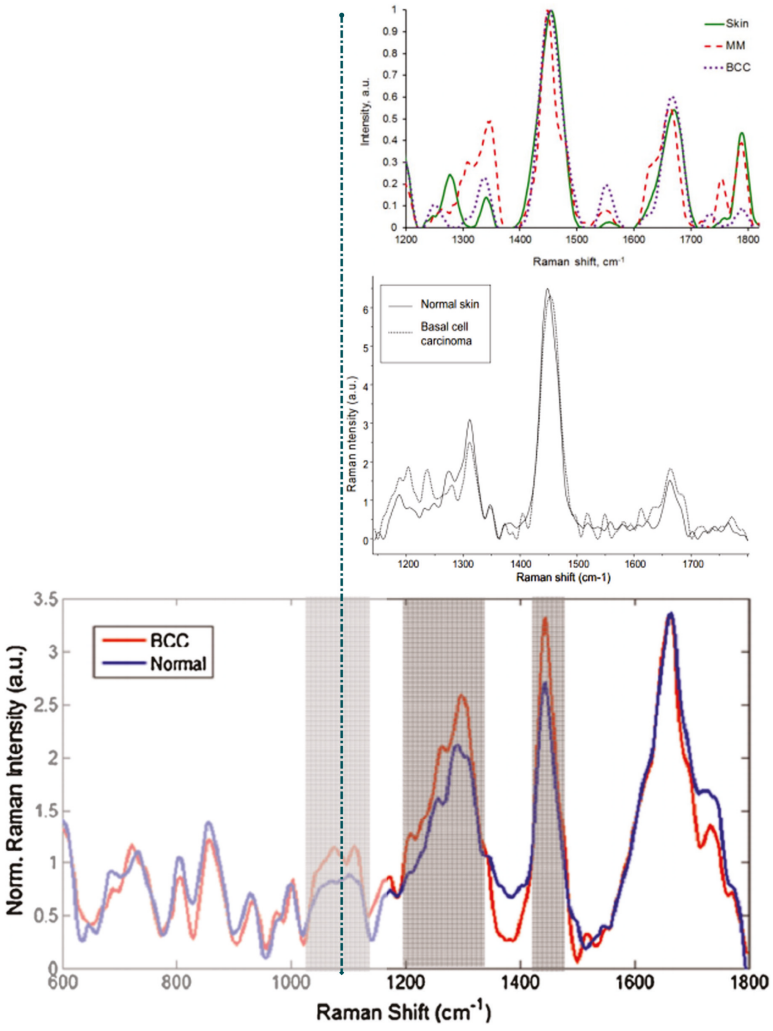

Figure 2. Comparative results (from three research groups) of *in vivo* Raman spectra for BCC and normal skin. Adapted and reproduced with permission from [15,37,43].

Amide III band also exhibited blue-shift and intensity decrease in *in vitro* studies [59], consistent with secondary protein structure changes in BCC. Moreover, it was shown that the CH_2 bending mode (lipids and protein) was shifted to higher frequencies and the $\nu(PO_2)$ symmetric stretching at 1085 cm^{-1} to lower frequency. The bands assigned to proteins, lipids, nucleic acids, and hemoglobin (832, 925, 943, 1006, 1034, 1130, 1209, 1343 and 1607 cm^{-1}) were used by Silveira *et al.* [44] for constructing an algorithm for skin cancer diagnosis. Based on Raman spectroscopy determinations of the relative concentrations of core biochemical tissue constituents (melanin, nucleic acid, elastin, ceramide, actin and phenylalanine), they demonstrated an efficient discrimination between healthy skin and pathological skin lesions (BCC and SCC). Statistically significant differences (ANOVA, $p < 0.05$) between normal skin and BCC and normal skin and SCC were found for the relative concentration of melanin, DNA, actin and phenylalanine. Discriminant analysis with the Mahalanobis distance method (identification of outliers) of the melanin *vs.* phenylalanine yielded an overall accuracy of 72.3% when BCC and SCC were considered as a unique disease group by a sensitivity and specificity of 80.9% and 65.0% respectively. In a recent paper [45], the same research group, found that the spectra of the lesions exhibited higher Raman bands intensities compared with normal skin; BCC in the 1300–1700 cm^{-1} range, while SCC and AK in almost the whole spectral range. The difference spectra showed that BCC feature higher lipids concentration while the spectra of SCC suggest higher contribution from both lipids and proteins. Using partial least squares discriminant analysis (PLS-DA) they achieved 89.1% sensitivity and 94.3% specificity for the discrimination of BCC, SCC and AK from normal tissue and benign lesions. The PCA-DA analysis yielded 82.2% accuracy. Spectral vectors showed differences in the Amide III region attributed to pathologic expression of collagen and triolein. The amide III band was also considered as the most significant Raman spectral feature by Philipsen *et al.* [49] for the discrimination of BCC from MM. MM showed the highest intensity increase of the amide III band while BCC the lowest. Other studies however, showed that MM, unlike BCC, exhibit decrease in the intensity of the amide III band [37,60]. Moreover, the amide III ratio which is defined as the protein to lipid ratio for the bands near 1250 and 1300 cm^{-1} ($I_{amide\text{-}III}/I_{1290–1330}$) [70] was significantly different ($p = 0.0075$) between MM and BCC. No consistent spectral alterations were noticed in the amide I band region between tumor and normal skin. The authors presented two particularly interesting results from the analysis of skin lesions *in vivo*: (i) the clinical diagnostic efficacy of the Raman spectroscopy does not depend on the skin pigmentation and (ii) there is statistically significant ($p < 0.05$) higher intensity in the water band region in BCC and MM compared to normal skin. Based on their classification scheme (Mann–Whitney test), the diagnostic accuracy was MM 93.3% *vs.* normal skin 96.4% and BCC 88.0% *vs.* normal skin 85.5%. On the other hand, Schleusener *et al.* [41] did not notice any increase in the amide III band nor in the phenylalanine band (~1000 cm^{-1}), contrary to [44,46]. They also reported increased melanin content and decrease of the amide I band. Contrary to [46], their results supported a significant increase in the lipids content for MM in accordance to [31,64]. Using partial least squares discriminant analysis (PLS-DA), BCC and SCC were discriminated from normal skin with a balanced accuracy of 73% and 85%, respectively. MM and pigmented nevi (PN) discrimination resulted in a balanced accuracy of 91%. Lieber *et al.* [42] reported a 100% sensitivity and 91% specificity in the differentiation between healthy and malignant tissues (BCC and SCC) with a 95% overall classification accuracy using a fiber-coupled portable Raman microscope. They suggested that the core differences in the Raman spectra between normal and

malignant lesions mainly rely on divergent protein and lipid compositions of these tissues. Finally, Karagiannis *et al.* [51] developed a novel method where human MM cells were injected in mice. Tumor growth in this animal model was *in vivo* visualized by acoustic microscopy and analyzed by IR and Raman spectroscopy. Significant changes were observed in the 350–2000 cm^{-1} region of the Raman spectra.

4. Conclusions

In vivo Raman spectroscopy demonstrates significant potential as an emerging clinical diagnostic technique of high sensitivity and specificity for skin cancer screening. Raman spectroscopy requires no sample preparation and features minimal water interference; thus it can be successfully applied to non-invasive *in vivo* evaluation of skin lesions. Results show that real time Raman spectroscopy is able to provide high diagnostic accuracy with acceptable sensitivity and specificity for the effective detection of subtle biochemical alterations in skin tumors with adequate safety and without the need for any tissue pre-treatment. Nevertheless, experimental data show that there are no characteristic Raman peaks that can be uniquely assigned to a particular skin cancer type and significant variations can only be exposed by the application of statistical methods. The problem that multivariate analyses try to solve is two-fold: (i) to expose certain biochemical moieties that mainly contribute to the Raman signals of underline pathologies and (ii) to provide skin cancer screening tests with high sensitivity and specificity for the discrimination between normal and malignant tissues and between different skin lesions. This review showed that the complex environment of the skin tissue provides limited information on the former and complementary techniques may be beneficial. On the contrary, high discrimination accuracy is evident in most cases. The transition from laboratory bench to clinical bed-side setting still remains a challenging task that will take some time to mature. Several prerequisites have to be fulfilled, including optimizing diagnostic accuracy with minimal classification errors, adequate solutions for ethical prerequisites for the *in vivo* use, and fulfillment of all issues that guarantee complete compliance of the portable Raman spectrophotometers with the directives for medical devices. Finally, biopsy with histopathologic assessment, to date the reference procedure for the diagnosis of malignant skin lesions, cannot be replaced by any spectroscopic non-invasive approaches before large-scale comparative clinical trials have established their clinical confidence. Until then, real time, clinical acquisition of Raman spectra can play a supplementary but significant role towards optimizing skin tumor management.

Acknowledgments

This research project has been co-financed by the European Union (European Regional Development Fund-ERDF) and Greek national funds through the Operational Program "THESSALY-MAINLAND GREECE AND EPIRUS-2007–2013" of the National Strategic Reference Framework (NSRF 2007–2013).

Author Contributions

Nikolaos Kourkoumelis conceived the study; Nikolaos Kourkoumelis, Ioannis Balatsoukas, Violetta Moulia and Aspasia Elka analyzed the data; Nikolaos Kourkoumelis, Georgios Gaitanis and Ioannis D. Bassukas wrote the manuscript.

Conflicts of Interest

The authors declare no conflict of interest.

References

1. Housman, T.S.; Feldman, S.R.; Williford, P.M.; Fleischer, A.B.; Goldman, N.D.; Acostamadiedo, J.M.; Chen, G.J. Skin cancer is among the most costly of all cancers to treat for the medicare population. *J. Am. Acad. Dermatol.* **2003**, *48*, 425–429.
2. Staples, M.P.; Elwood, M.; Burton, R.C.; Williams, J.L.; Marks, R.; Giles, G.G. Non-melanoma skin cancer in Australia: The 2002 national survey and trends since 1985. *Med. J. Aust.* **2006**, *184*, 6–10.
3. Rogers, H.W.; Weinstock, M.A.; Harris, A.R.; Hinckley, M.R.; Feldman, S.R.; Fleischer, A.B.; Coldiron, B.M. Incidence estimate of nonmelanoma skin cancer in the united states, 2006. *Arch. Dermatol.* **2010**, *146*, 283–287.
4. Brewster, D.H.; Bhatti, L.A.; Inglis, J.H.C.; Nairn, E.R.; Doherty, V.R. Recent trends in incidence of nonmelanoma skin cancers in the east of Scotland, 1992–2003. *Brit. J. Dermatol.* **2007**, *156*, 1295–1300.
5. Hoey, S.E.H.; Devereux, C.E.J.; Murray, L.; Catney, D.; Gavin, A.; Kumar, S.; Donnelly, D.; Dolan, O.M. Skin cancer trends in northern Ireland and consequences for provision of dermatology services. *Br. J. Dermatol.* **2007**, *156*, 1301–1307.
6. Donaldson, M.R.; Coldiron, B.M. No end in sight: The skin cancer epidemic continues. *Semin. Cutan. Med. Surg.* **2011**, *30*, 3–5.
7. Sng, J.; Koh, D.; Siong, W.C.; Choo, T.B. Skin cancer trends among Asians living in Singapore from 1968 to 2006. *J. Am. Acad. Dermatol.* **2009**, *61*, 426–432.
8. Gandini, S.; Sera, F.; Cattaruzza, M.S.; Pasquini, P.; Abeni, D.; Boyle, P.; Melchi, C.F. Meta-analysis of risk factors for cutaneous melanoma: I. Common and atypical naevi. *Eur. J. Cancer* **2005**, *41*, 28–44.
9. Forchetti, G.; Suppa, M.; del Marmol, V. Overview on non-melanoma skin cancers in solid organ transplant recipients. *G. Ital. Dermatol. V* **2014**, *149*, 383–387.
10. Simoes, M.C.F.; Sousa, J.J.S.; Pais, A.A.C.C. Skin cancer and new treatment perspectives: A review. *Cancer Lett.* **2015**, *357*, 8–42.
11. Jensen, A.O.; Bautz, A.; Olesen, A.B.; Karagas, M.R.; Sorensen, H.T.; Friis, S. Mortality in Danish patients with nonmelanoma skin cancer, 1978–2001. *Br. J. Dermatol.* **2008**, *159*, 419–425.
12. Lewis, K.G.; Weinstock, M.A. Nonmelanoma skin cancer mortality (1988–2000): The Rhode Island follow-back study. *Arch. Dermatol.* **2004**, *140*, 837–842.
13. Hannuksela-Svahn, A.; Pukkala, E.; Karvonen, J. Basal cell skin carcinoma and other nonmelanoma skin cancers in Finland from 1956 through 1995. *Arch. Dermatol.* **1999**, *135*, 781–786.

14. Bassukas, I.D.; Lippold, A.; Hundeiker M. Parametric estimation of the "risk of melanoma-related death" with the recursion formula of the gompertz survival function. In *Skin Cancer and UV Radiation*; Altmeyer, P., Hoffmann, K., Stücker, M., Eds.; Springer: Berlin, Germany; Heidelberg, Germany, 1997; pp. 527–533.
15. Patil, C.A.; Kirshnamoorthi, H.; Ellis, D.L.; van Leeuwen, T.G.; Mahadevan-Jansen, A. A clinical instrument for combined Raman spectroscopy-optical coherence tomography of skin cancers. *Laser Surg. Med.* **2011**, *43*, 143–151.
16. Mordechai, S.; Sahu, R.K.; Hammody, Z.; Mark, S.; Kantarovich, K.; Guterman, H.; Podshyvalov, A.; Goldstein, J.; Argov, S. Possible common biomarkers from FTIR microspectroscopy of cervical cancer and melanoma. *J. Microsc.* **2004**, *215*, 86–91.
17. Baranska, M.; Byrne, H.J. Optical diagnostics-spectropathology for the next generation. *Analyst* **2015**, *140*, 2064–2065.
18. Kourkoumelis, N. Spectroscopy for biosciences. *Contemp. Phys.* **2015**, doi:10.1080/00107514.2015.1006254.
19. Bigio, I.J.; Mourant, J.R. Ultraviolet and visible spectroscopies for tissue diagnostics: Fluorescence spectroscopy and elastic-scattering spectroscopy. *Phys. Med. Biol.* **1997**, *42*, 803–814.
20. Seddon, A.B. Mid-infrared (IR)—A hot topic: The potential for using mid-IR light for non-invasive early detection of skin cancer *in vivo*. *Phys. Status Solidi* **2013**, *250*, 1020–1027.
21. Kendall, C.; Isabelle, M.; Bazant-Hegemark, F.; Hutchings, J.; Orr, L.; Babrah, J.; Baker, R.; Stone, N. Vibrational spectroscopy: A clinical tool for cancer diagnostics. *Analyst* **2009**, *134*, 1029–1045.
22. Chan, J.W.; Lieu, D.K. Label-free biochemical characterization of stem cells using vibrational spectroscopy. *J. Biophotonics* **2009**, *2*, 656–668.
23. Kong, K.; Kendall, C.; Stone, N.; Notingher, I. Raman spectroscopy for medical diagnostics—From *in-vitro* biofluid assays to *in-vivo* cancer detection. *Adv. Drug Deliv. Rev.* **2015**, in press.
24. Kourkoumelis, N.; Polymeros, A.; Tzaphlidou, M. Background estimation of biomedical Raman spectra using a geometric approach. *J. Spectrosc.* **2012**, *27*, 441–447.
25. Devpura, S.; Barton, K.N.; Brown, S.L.; Palyvoda, O.; Kalkanis, S.; Naik, V.M.; Siddiqui, F.; Naik, R.; Chetty, I.J. Vision 20/20: The role of Raman spectroscopy in early stage cancer detection and feasibility for application in radiation therapy response assessment. *Med. Phys.* **2014**, *41*, doi:10.1118/1.4870981.
26. Wang, W.; Zhao, J.; Short, M.; Zeng, H. Real-time *in vivo* cancer diagnosis using Raman spectroscopy. *J. Biophotonics* **2014**, doi:10.1002/jbio.201400026.
27. Vandenabeele, P.; Jehlicka, J.; Vitek, P.; Edwards, H.G.M. On the definition of Raman spectroscopic detection limits for the analysis of biomarkers in solid matrices. *Planet. Space Sci.* **2012**, *62*, 48–54.
28. Tfaili, S.; Josse, G.; Gobinet, C.; Angiboust, J.F.; Manfait, M.; Piot, O. Shedding light on the laser wavelength effect in Raman analysis of skin epidermises. *Analyst* **2012**, *137*, 4241–4246.
29. Naito, S.; Min, Y.K.; Sugata, K.; Osanai, O.; Kitahara, T.; Hiruma, H.; Hamaguchi, H. *In vivo* measurement of human dermis by 1064 nm-excited fiber Raman spectroscopy. *Skin Res. Technol.* **2008**, *14*, 18–25.
30. Patil, C.A.; Pence, I.J.; Lieber, C.A.; Mahadevan-Jansen, A. 1064 nm dispersive Raman spectroscopy of tissues with strong near-infrared autofluorescence. *Opt. Lett.* **2014**, *39*, 303–306.

31. Fendel, S.; Schrader, B. Investigation of skin and skin lesions by NIR-FT-Raman spectroscopy. *Fresenius J. Anal. Chem.* **1998**, *360*, 609–613.
32. Franzen, L.; Selzer, D.; Fluhr, J.W.; Schaefer, U.F.; Windbergs, M. Towards drug quantification in human skin with confocal Raman microscopy. *Eur. J. Pharm. Biopharm.* **2013**, *84*, 437–444.
33. Tfaili, S.; Gobinet, C.; Josse, G.; Angiboust, J.F.; Baillet, A.; Manfait, M.; Piot, O. Vibrational spectroscopies for the analysis of cutaneous permeation: Experimental limiting factors identified in the case of caffeine penetration. *Anal. Bioanal. Chem.* **2013**, *405*, 1325–1332.
34. Tfayli, A.; Piot, O.; Pitre, F.; Manfait, M. Follow-up of drug permeation through excised human skin with confocal Raman microspectroscopy. *Eur. Biophys. J. Biophys.* **2007**, *36*, 1049–1058.
35. Franzen, L.; Anderski, J.; Planz, V.; Kostka, K.H.; Windbergs, M. Combining confocal Raman microscopy and freeze-drying for quantification of substance penetration into human skin. *Exp. Dermatol.* **2014**, *23*, 942–944.
36. Lui, H.; Zhao, J.H.; McLean, D.; Zeng, H.S. Real-time Raman spectroscopy for *in vivo* skin cancer diagnosis. *Cancer Res.* **2012**, *72*, 2491–2500.
37. Zakharov, V.P.; Bratchenko, I.A.; Kozlov, S.V.; Moryatov, A.A.; Myakinin, O.O.; Artemyev, D.N. Two-step Raman spectroscopy method for tumor diagnosis. In Proceedings of the SPIE 9129, Biophotonics: Photonic Solutions for Better Health Care IV, Brussels, Belgium, 14–17 April 2014; doi:10.1117/12.2052121.
38. Zakharov, V.P.; Bratchenko, I.A.; Kozlov, S.V.; Moryatov, A.A.; Kornilin, D.V.; Myakinin, O.O.; Artemyev, D.N. Advances in tumor diagnosis using OCT and Raman spectroscopy. In Proceedings of the SPIE 9129, Biophotonics: Photonic Solutions for Better Health Care IV, Brussels, Belgium, 14–17 April 2014; doi:10.1117/12.2052145.
39. Zakharov, V.P.; Bratchenko, I.A.; Artemyev, D.N.; Myakinin, O.O.; Kornilin, D.V.; Kozlov, S.V.; Moryatov, A.A. Comparative analysis of combined spectral and optical tomography methods for detection of skin and lung cancers. *J. Biomed. Opt.* **2015**, *20*, doi:10.1117/1.JBO.20.2.025003.
40. Schleusener, J.; Reble, C.; Helfmann, J.; Gersonde, I.; Cappius, H.J.; Glanert, M.; Fluhr, J.W.; Meinke, M.C. Design and technical evaluation of fibre-coupled Raman probes for the image-guided discrimination of cancerous skin. *Meas. Sci. Technol.* **2014**, *25*, doi:10.1088/0957-0233/25/3/035701.
41. Schleusener, J.; Gluszczynska, P.; Reble, C.; Gersonde, I.; Helfmann, J.; Fluhr, J.W.; Lademann, J.; Röwert-Huber, J.; Meinke, M.C. *In vivo* study for the discrimination of cancerous and normal skin using fiber probe based Raman spectroscopy. *Exp. Dermatol.* **2015**, in press.
42. Lieber, C.A.; Majumder, S.K.; Ellis, D.L.; Billheimer, D.D.; Mahadevan-Jansen, A. *In vivo* nonmelanoma skin cancer diagnosis using Raman microspectroscopy. *Laser Surg. Med.* **2008**, *40*, 461–467.
43. Tfayli, A.; Piot, O.; Derancourt, S.; Cadiot, G.; Diebold, M.D.; Bernard, P.; Manfait, M. *In vivo* analysis of tissue by Raman microprobe: Examination of human skin lesions and esophagus Barrett's mucosa on an animal model. In Proceedings of the SPIE 6093, Biomedical Vibrational Spectroscopy III: Advances in Research and Industry, San Jose, CA, USA, 27 February 2006; doi:10.1117/12.645874.
44. Silveira, F.L.; Pacheco, M.T.T.; Bodanese, B.; Zângaro, R.A.; Silveira, L. Discriminating model for skin cancer diagnosis *in vivo* through Raman spectroscopy. In Proceedings of the SPIE 8565, Photonic Therapeutics and Diagnostics IX, San Francisco, CA, USA, 2 February 2013; doi:10.1117/12.2007293.

45. Silveira, F.L.; Pacheco, M.T.; Bodanese, B.; Pasqualucci, C.A.; Zangaro, R.A.; Silveira, L., Jr. Discrimination of non-melanoma skin lesions from non-tumor human skin tissues *in vivo* using Raman spectroscopy and multivariate statistics. *Lasers Surg. Med.* **2015**, *47*, 6–16.
46. Lim, L.; Nichols, B.; Migden, M.R.; Rajaram, N.; Reichenberg, J.S.; Markey, M.K.; Ross, M.I.; Tunnell, J.W. Clinical study of noninvasive *in vivo* melanoma and nonmelanoma skin cancers using multimodal spectral diagnosis. *J. Biomed. Opt.* **2014**, *19*, doi:10.1117/1.JBO.19.11.117003.
47. Motz, J.T.; Gandhi, S.J.; Scepanovic, O.R.; Haka, A.S.; Kramer, J.R.; Dasari, R.R.; Feld, M.S. Real-time raman system for *in vivo* disease diagnosis. *J. Biomed. Opt.* **2005**, *10*, doi:10.1117/1.1920247.
48. Sharma, M.; Marple, E.; Reichenberg, J.; Tunnell, J.W. Design and characterization of a novel multimodal fiber-optic probe and spectroscopy system for skin cancer applications. *Rev. Sci. Instrum.* **2014**, *85*, doi:10.1063/1.4890199.
49. Philipsen, P.A.; Knudsen, L.; Gniadecka, M.; Ravnbak, M.H.; Wulf, H.C. Diagnosis of malignant melanoma and basal cell carcinoma by *in vivo* NIR-FT Raman spectroscopy is independent of skin pigmentation. *Photoch. Photobiol. Sci.* **2013**, *12*, 770–776.
50. Hata, T.R.; Scholz, T.A.; Ermakov, I.V.; McClane, R.W.; Khachik, F.; Gellermann, W.; Pershing, L.K. Non-invasive Raman spectroscopic detection of carotenoids in human skin. *J. Investig. Dermatol.* **2000**, *115*, 441–448.
51. Karagiannis, G.T.; Grivas, I.; Tsingotjidou, A.; Apostolidis, G.K.; Grigoriadou, I.; Dori, I.; Poulatsidou, K.-N.; Doumas, A.; Wesarg, S.; Georgoulias, P. Early detection of melanoma with the combined use of acoustic microscopy, infrared reflectance and Raman spectroscopy. In Proceedings of the SPIE 9323, Photons Plus Ultrasound: Imaging and Sensing, San Francisco, CA, USA, 13–18 February 2015; doi:10.1117/12.2079690.
52. Lieber, C.A.; Majumder, S.K.; Billheimer, D.; Ellis, D.L.; Mahadevan-Jansen, A. Raman microspectroscopy for skin cancer detection *in vitro*. *J. Biomed. Opt.* **2008**, *13*, doi:10.1117/1.2899155.
53. Zheng, J.K.; Pang, S.; Labuza, T.P.; He, L.L. Evaluation of surface-enhanced raman scattering detection using a handheld and a bench-top Raman spectrometer: A comparative study. *Talanta* **2014**, *129*, 79–85.
54. Mogensen, M.; Jemec, G.B.E. Diagnosis of nonmelanoma skin cancer/keratinocyte carcinoma: A review of diagnostic accuracy of nonmelanoma skin cancer diagnostic tests and technologies. *Dermatol. Surg.* **2007**, *33*, 1158–1174.
55. Hanlon, E.B.; Manoharan, R.; Koo, T.W.; Shafer, K.E.; Motz, J.T.; Fitzmaurice, M.; Kramer, J.R.; Itzkan, I.; Dasari, R.R.; Feld, M.S. Prospects for *in vivo* Raman spectroscopy. *Phys. Med. Biol.* **2000**, *45*, R1–R59.
56. Nijssen, A.; Schut, T.C.B.; Heule, F.; Caspers, P.J.; Hayes, D.P.; Neumann, M.H.A.; Puppels, G.J. Discriminating basal cell carcinoma from its surrounding tissue by Raman spectroscopy. *J. Investig. Dermatol.* **2002**, *119*, 64–69.
57. Kong, K.; Rowlands, C.J.; Varma, S.; Perkins, W.; Leach, I.H.; Koloydenko, A.A.; Pitiot, A.; Williams, H.C.; Notingher, I. Increasing the speed of tumour diagnosis during surgery with selective scanning Raman microscopy. *J. Mol. Struct.* **2014**, *1073*, 58–65.
58. Ly, E.; Piot, O.; Durlach, A.; Bernard, P.; Manfait, M. Polarized Raman microspectroscopy can reveal structural changes of peritumoral dermis in basal cell carcinoma. *Appl. Spectrosc.* **2008**, *62*, 1088–1094.

59. Choi, J.; Choo, J.; Chung, H.; Gweon, D.G.; Park, J.; Kim, H.J.; Park, S.; Oh, C.H. Direct observation of spectral differences between normal and basal cell carcinoma (BCC) tissues using confocal Raman microscopy. *Biopolymers* **2005**, *77*, 264–272.
60. Gniadecka, M.; Philipsen, P.A.; Sigurdsson, S.; Wessel, S.; Nielsen, O.F.; Christensen, D.H.; Hercogova, J.; Rossen, K.; Thomsen, H.K.; Gniadecki, R.; *et al*. Melanoma diagnosis by Raman spectroscopy and neural networks: Structure alterations in proteins and lipids in intact cancer tissue. *J. Investig. Dermatol.* **2004**, *122*, 443–449.
61. Larraona-Puy, M.; Ghita, A.; Zoladek, A.; Perkins, W.; Varma, S.; Leach, I.H.; Koloydenko, A.A.; Williams, H.; Notingher, I. Development of Raman microspectroscopy for automated detection and imaging of basal cell carcinoma. *J. Biomed. Opt.* **2009**, *14*, doi:10.1117/1.3251053.
62. Gniadecka, M.; Wulf, H.C.; Mortensen, N.N.; Nielsen, O.F.; Christensen, D.H. Diagnosis of basal cell carcinoma by Raman spectroscopy. *J. Raman Spectrosc.* **1997**, *28*, 125–129.
63. Dukor, R.K. Vibrational spectroscopy in the detection of cancer. In *Handbook of Vibrational Spectroscopy*; Chalmers, J., Griffiths, P.R., Eds; John Wiley and Sons Ltd.: Hoboken, NJ, USA, 2002; Volume 5, pp. 3335–3361.
64. Cartaxo, S.B.; Santos, I.D.D.O.; Bitar, R.; Oliveira, A.F.; Ferreira, L.M.; Martinho, H.S.; Martin, A.A. FT-Raman spectroscopy for the differentiation between cutaneous melanoma and pigmented nevus. *Acta Cir. Bras.* **2010**, *25*, 351–356.
65. Darvin, M.E.; Sterry, W.; Lademann, J.; Vergou, T. The role of carotenoids in human skin. *Molecules* **2011**, *16*, 10491–10506.
66. Lademann, J.; Kocher, W.; Yu, R.; Meinke, M.C.; Na Lee, B.; Jung, S.; Sterry, W.; Darvin, M.E. Cutaneous carotenoids: The mirror of lifestyle? *Skin Pharmacol. Physiol.* **2014**, *27*, doi:10.1159/000357222.
67. Chen, L.; Wang, Y.; Liu, N.; Lin, D.; Weng, C.; Zhang, J.; Zhu, L.; Chen, W.; Chen, R.; Feng, S. Near-infrared confocal micro-Raman spectroscopy combined with PCA-LDA multivariate analysis for detection of esophageal cancer. *Laser Phys.* **2013**, *23*, doi:10.1088/1054-660X/23/6/065601.
68. Zhao, J.; Huang, Z.; Zeng, H.; McLean, D.I.; Lui, H. Quantitative analysis of skin chemicals using rapid near-infrared Raman spectroscopy. In Proceedings of the SPIE 6842, Photonic Therapeutics and Diagnostics IV, San Jose, CA, USA, 19 January 2008; doi:10.1117/12.769373.
69. Salomatina, E.; Jiang, B.; Novak, J.; Yaroslavsky, A.N. Optical properties of normal and cancerous human skin in the visible and near-infrared spectral range. *J. Biomed. Opt.* **2006**, *11*, doi:10.1117/1.2398928.
70. Bodanese, B.; Silveira, L.; Albertini, R.; Zangaro, R.A.; Pacheco, M.T.T. Differentiating normal and basal cell carcinoma human skin tissues *in vitro* using dispersive Raman spectroscopy: A comparison between principal components analysis and simplified biochemical models. *Photomed. Laser Surg.* **2010**, *28*, S119–S127.

© 2015 by the authors; licensee MDPI, Basel, Switzerland. This article is an open access article distributed under the terms and conditions of the Creative Commons Attribution license (http://creativecommons.org/licenses/by/4.0/).

Int. J. Mol. Sci. **2015**, *16*, 15578-15591; doi:10.3390/ijms160715578

OPEN ACCESS
International Journal of
Molecular Sciences
ISSN 1422-0067
www.mdpi.com/journal/ijms

Article

DDX3X Biomarker Correlates with Poor Survival in Human Gliomas

Dueng-Yuan Hueng [1,2,*], Wen-Chiuan Tsai [3], Hsin-Ying Clair Chiou [1], Shao-Wei Feng [1], Chin Lin [4], Yao-Feng Li [3], Li-Chun Huang [2] and Ming-Hong Lin [5]

1 Department of Neurological Surgery, Tri-Service General Hospital, National Defense Medical Center, No. 325, Section 2, Taipei 11490, Taiwan; E-Mails: phoenixchiou@gmail.com (H.-Y.C.C.); heisenber0930@gmail.com (S.-W.F.)

2 Department of Biochemistry, National Defense Medical Center, No. 325, Section 2, Taipei 11490, Taiwan; E-Mail: emily7781@hotmail.com

3 Department of Pathology, Tri-Service General Hospital, National Defense Medical Center, Taipei 11490, Taiwan; E-Mails: drtsaiwenchuan@mail2000.com.tw (W.-C.T.); liyaofeng1109@gmail.com (Y.-F.L.)

4 Graduate Institute of Life Science, National Defense Medical Center, Taipei 11490, Taiwan; E-Mail: xup6fup@hotmail.com

5 Department and Graduate Institute of Microbiology and Immunology, National Defense Medical Center, Taipei 11490, Taiwan; E-Mail: blimp1@hotmail.com.tw

* Author to whom correspondence should be addressed; E-Mail: hondy2195@yahoo.com.tw; Tel.: +886-2-8792-7177; Fax: +886-2-8792-7178.

Academic Editor: William Chi-shing Cho

Received: 4 May 2015 / Accepted: 24 June 2015 / Published: 9 July 2015

Abstract: Primary high-grade gliomas possess invasive growth and lead to unfavorable survival outcome. The investigation of biomarkers for prediction of survival outcome in patients with gliomas is important for clinical assessment. The DEAD (Asp-Glu-Ala-Asp) box helicase 3, X-linked (DDX3X) controls tumor migration, proliferation, and progression. However, the role of DDX3X in defining the pathological grading and survival outcome in patients with human gliomas is not yet clarified. We analyzed the *DDX3X* gene expression, WHO pathological grading, and overall survival from de-linked data. Further validation was done using quantitative RT-PCR of cDNA from normal brain and glioma, and immunohistochemical (IHC) staining of tissue microarray. Statistical analysis of GEO datasets showed that DDX3X mRNA expression demonstrated statistically higher in WHO

grade IV (n = 81) than in non-tumor controls (n = 23, $p = 1.13 \times 10^{-10}$). Moreover, DDX3X level was also higher in WHO grade III (n = 19) than in non-tumor controls ($p = 2.43 \times 10^{-5}$). Kaplan–Meier survival analysis showed poor survival in patients with high DDX3X mRNA levels (n = 24) than in those with low DDX3X expression (n = 53) (median survival, 115 *vs.* 58 weeks, p = 0.0009, by log-rank test, hazard ratio: 0.3507, 95% CI: 0.1893–0.6496). Furthermore, DDX3X mRNA expression and protein production significantly increased in glioma cells compared with normal brain tissue examined by quantitative RT-PCR, and Western blot. IHC staining showed highly staining of high-grade glioma in comparison with normal brain tissue. Taken together, DDX3X expression level positively correlates with WHO pathologic grading and poor survival outcome, indicating that DDX3X is a valuable biomarker in human gliomas.

Keywords: glioma; WHO grades; GEO profile; tissue microarray; DDX3X; RNA Helicase DDX3X

1. Introduction

Glioblastomas are the most frequent primary brain cancers with poor outcome due to their invasive characteristics despite maximal surgical resection and current chemo-radiotherapy [1,2]. Currently, the standard treatment includes maximal surgical resection and concurrent chemo-radiotherapy. However, the overall survival in patients with glioblastomas undergoing radiotherapy and temozolomide is 14.6 months on average [3]. The pathologic grading of gliomas classified by World Health Organization (WHO) grade I to IV [4]. Higher grade gliomas carry worse prognosis and increased fatality [5]. Therefore a genetic biomarker to differentiate the genetic expression in brain gliomas is crucial for prediction of clinical outcome [6].

The DEAD (Asp-Glu-Ala-Asp) box helicase 3, X-linked (DDX3X) or DEAD box polypeptide 3, X-linked, or DDX3X, belongs to ATP-dependent RNA helicase, which acts as a cofactor for exportin-1 (XPO1)-mediated nuclear export of partly spliced HIV-1 Rev RNAs [7]. DDX3X is known to participate in HIV-1 replication [8]. DDX3X related particularly with hepatitis C virus core protein lead to an alteration in intracellular location [9], and nucleic acid metabolism [10].

Activation of DDX3X enhances proliferation and malignancy [11]. DDX3X is expressed in many human malignancies, including cancers of the breast [12], lung [13], colon [14], liver [15], gallbladder [16], cervical cancer [17], and brain [17]. However, the role of DDX3X in determining the survival outcome and WHO pathologic grading of human gliomas is not yet clarified.

This study hypothesized that high-grade glioma overexpressed DDX3X. Based on this hypothesis, we intended to investigate if DDX3X expression is associated with the survival outcome and WHO pathologic grading in human gliomas. Analyses of the dataset from the Gene Expression Omnibus (GEO) profiles, a database that provides extensive genetic analyses of human gene expression and specific disease associations [5,18,19], show that DDX3X expression level closely correlates with WHO grading and poor survival outcome in patients with primary gliomas. The quantitative RT-PCR showed DDX3X mRNA expression is significantly higher in glioma cells compared to normal brain

tissue. Western blot reveals DDX3X protein is highly produced in human glioma cell lines. Immunohistochemical (IHC) staining also demonstrates high affinity for high-grade glioma than normal brain tissue. Thus DDX3X can be a candidate biomarker in human gliomas.

2. Result

2.1. DDX3X Expression Positively Correlates with WHO Grading of Human Gliomas

As shown in Figure 1, the DDX3X expression level was higher in WHO grade IV (n = 81) than in non-tumor controls (n = 23) (p = 1.13 × 10^{-10}). It is also higher in WHO grade III (n = 19) than in non-tumor controls (p = 2.43 × 10^{-5}, p adjusted by Bonferroni method). These results show that high-grade gliomas overexpressed DDX3X.

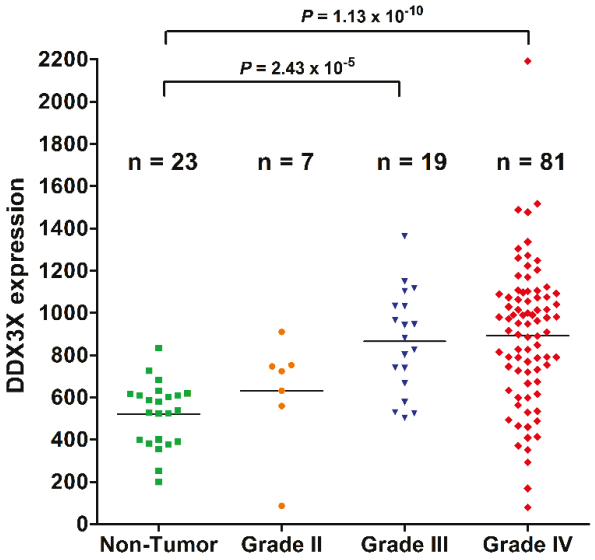

Figure 1. DDX3X expression positively correlates with WHO grading of human gliomas. The distributed plots show the *DDX3X* gene expression in low-grade glioma and non-tumor controls in comparison to those in high-grade gliomas. Increased DDX3X mRNA levels statistically correlates with WHO grades of human gliomas. The adjusted p value was calibrated between each group.

2.2. DDX3X Expression Correlates with Poor Survival in High-Grade Gliomas

The demographic data including WHO pathologic grades, gender, age, and survival times were mentioned previously [18]. There were 21 patients (13 male, 8 female) in grade III population, and 56 patients (38 male, 18 female) in grade IV population. The age of grade III, and IV patients were 37.4 ± 9.9, and 48.5 ± 12.8 years old, respectively. The overall survival time in grade III, and IV was 227.0 ± 161.1, and 106.7 ± 82.0 weeks, respectively. As shown in Figure 2, the Kaplan–Meier survival curve of 77 patients with grade III and grade IV gliomas showed that patients with low DDX3X mRNA expression levels (n = 53) had better overall survival than those with high DDX3X mRNA expression levels (n = 24) (p = 0.0009, by log-rank test; 95% CI: 0.1893–0.6496, Ratio 0.3507). The cut-off value was set at 3234.5. The median survival interval in the high- and low-DDX3X

expressions level was 58 and 115 weeks, respectively. In multivariate analysis, two variables showed significant correlation. These were DDX3X expression, and WHO pathologic grade. Survival rate was poor in the high DDX3X expression group (p = 0.02365, 1.879-fold hazard, 95% confidence interval: 1.088 to 3.246) than in the low DDX3X expression group after adjustments for WHO grade and age. Moreover, WHO grade IV showed a poorer survival rate than in the WHO grade III group (p = 0.00255, 2.767-fold hazard, 95% confidence interval: 1.429 to 5.361). In contrast, gender was excluded in multivariate analysis because it was not significant in univariate analysis (p = 0.269). The variable age did not reach statistical significance (p = 0.61747, 1.005-fold hazard, 95% confidence interval: 0.985 to 1.026).

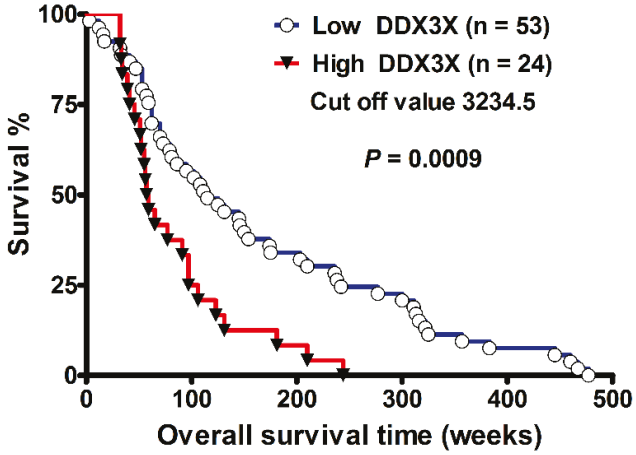

Figure 2. DDX3X expression correlates with poor survival in high-grade gliomas. The Kaplan–Meier survival curve demonstrated poor survival in those with high DDX3X (>3234.5) (n = 24) compared to those with low DDX3X (<3234.5) (n = 53) expression levels (median survival, 115 *vs.* 58 weeks, p = 0.0009, by log-rank test, hazard ratio: 0.3507, 95% CI: 0.1893–0.6496).

2.3. DDX3X mRNA Expression Is Increased in Human Glioma Cells

The DDX3X mRNA expressions were examined in glioma cells by q-RT PCR. The low-grade glioma cell line, LN229, and WHO grade IV glioma cell lines including U87MG, GBM8401, and U118MG were applied to compare DDX3X expression with normal brain. As shown in Figure 3, the expression of DDX3X was significantly increased in glioma cells in comparison with normal brain tissue.

2.4. DDX3X Protein Overexpresses in Human Glioma Cells

DDX3X protein production in human glioma cell lines and normal brain tissue was quantitated by Western blot analysis. As shown in Figure 4, DDX3X protein significantly overexpressed in human glioma cell lines, including LN229, U87MG, GBM8401 and U118MG, compared to normal brain tissue. HeLa cell was a positive control for DDX3X protein production [17].

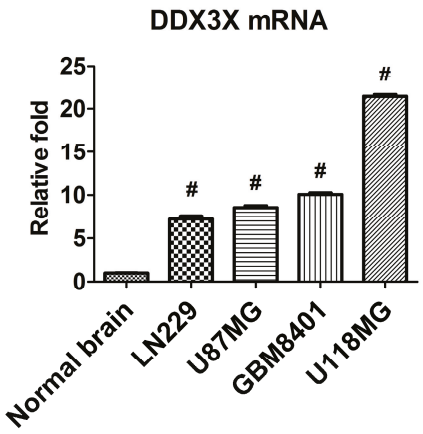

Figure 3. Expression of DDX3X mRNA in glioma cell lines and normal brain tissue. qRT-PCR was performed to examine DDX3X mRNA expression and the quantitative results are shown. The relative expressions were normalized with normal brain. Bars, mean ± SEM; # $p < 0.001$ showed significant differences. Data are representative of three independent experiments.

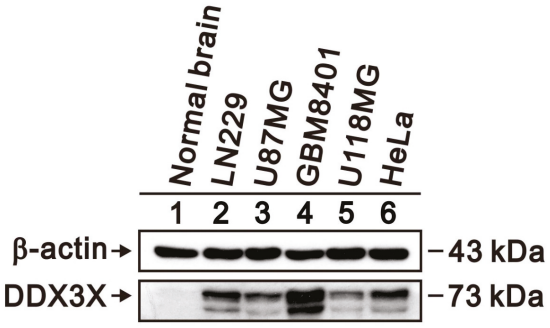

Figure 4. Expression of DDX3X protein in human glioma cell lines and normal brain tissue. Protein lysates of glioma cell lines, including LN229, U87MG, GBM8401 and U118MG, were applied to SDS-PAGE and Western blot analysis to quantitate DDX3X protein expression. HeLa cell was a positive control of DDX3X protein. β-actin served as a loading control.

2.5. DDX3X Protein Production Overexpressed in Human High-Grade Gliomas

DDX3X protein production in human gliomas tissues and normal brain tissues was checked by IHC staining of tissue microarray. As shown in Figure 5, DDX3X protein overexpressed in high-grade gliomas (WHO grade IV, and III) compared with low-grade gliomas, or non-tumor brain tissue control. Moreover, the correlation of DDX3X immunostain score in non-tumor brain tissue and gliomas revealed positive correlation ($p = 0.017$), which was analyzed by Pearson Product Method Correlation test (the correlation coefficient (γ) of this analysis is 0.466). Furthermore, as shown in Figure 5K, DDX3X immunostain scores were significantly higher in high-grade gliomas than in normal brain controls (average score, 99.29 *vs.* 25, $p = 0.007$). Finally, DDX3X immunostain scores were also statistically higher in low-grade gliomas (average score, 52.65) than in normal brain control ($p = 0.012$, p adjusted by Bonferroni method).

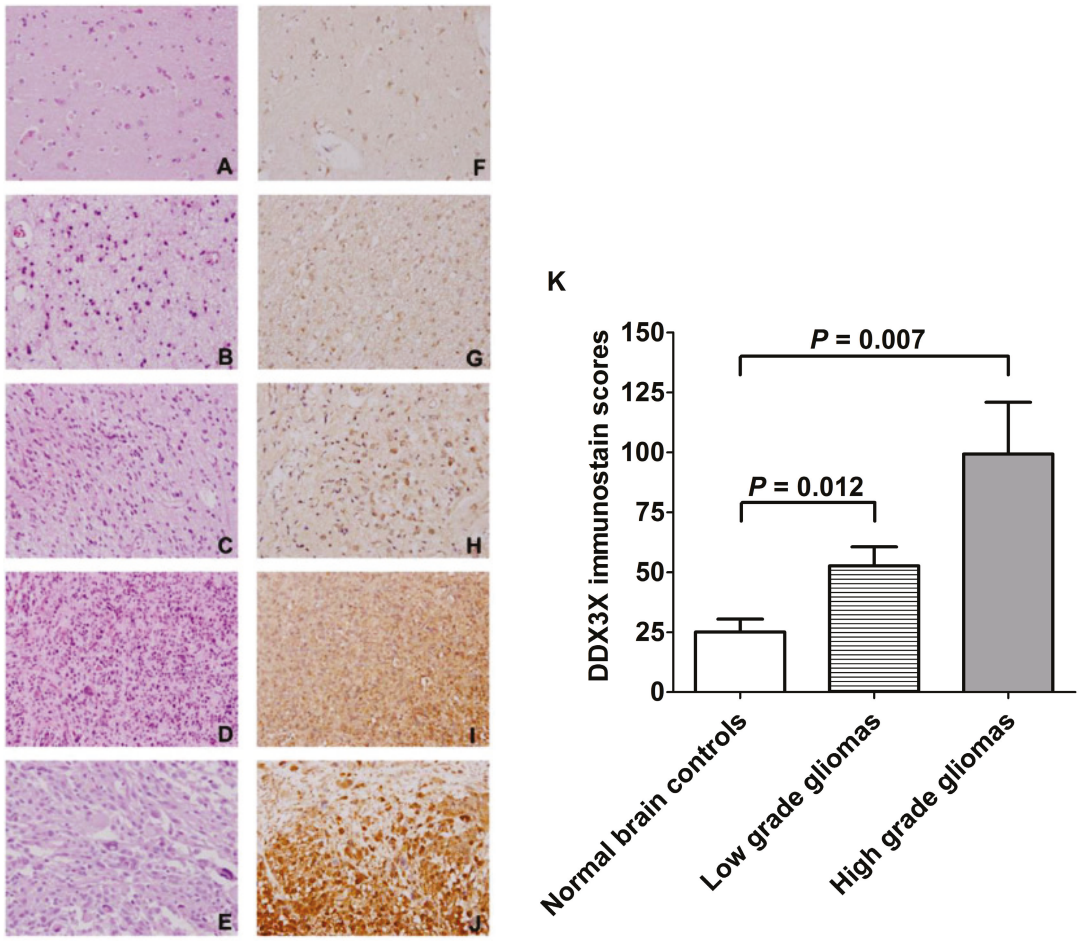

Figure 5. Hematoxylin and eosin staining of non-tumor brain tissue (**A**); pilocytic astrocytoma (**B**); diffuse astrocytoma (**C**); WHO grade III anaplastic astrocytoma (**D**); WHO grade IV glioblastoma multiforme (**E**); and IHC staining of DDX3X in non-tumor brain tissue (**F**); pilocytic astrocytoma (**G**); diffuse astrocytoma (**H**); anaplastic astrocytoma (**I**); and glioblastoma multiforme (**J**). Original magnification ×400; and (**K**) The DDX3X immunostain scores in normal brain tissue, low-grade glioma and high-grade glioma were statistically analyzed. The adjusted *p* value was calibrated between each group.

2.6. DDX3X Hub Protein and the Protein–Protein Interactions

The protein–protein interaction (PPI) network of DDX3X-regulated oncogenesis was generated using Search Tool for the Retrieval of Interacting Genes/Proteins (STRING) database [20]. The network revealed three PPI clusters linked by DDX3X as a potential hub protein (Figure 6A). Moreover, the Ingenuity pathway analysis (IPA) predicts that DDX3X plays the transcriptional regulation role for ESR1, SP1, XPO1, and serine/threonine-protein kinase TANK-binding kinase 1 (TBK1) to translocate into nucleus in signaling pathways (Figure 6B). Furthermore, the DDX3X-regulated proteins in human gliomas were validated by Western blot analysis. The DDX3X protein highly expresses in human glioma cells also correlates with the protein level of SP1, and ESR1 in human glioma cell lines including LN229, U87MG, GBM8401 and U118MG as compared with normal brain tissue (Figure 6C).

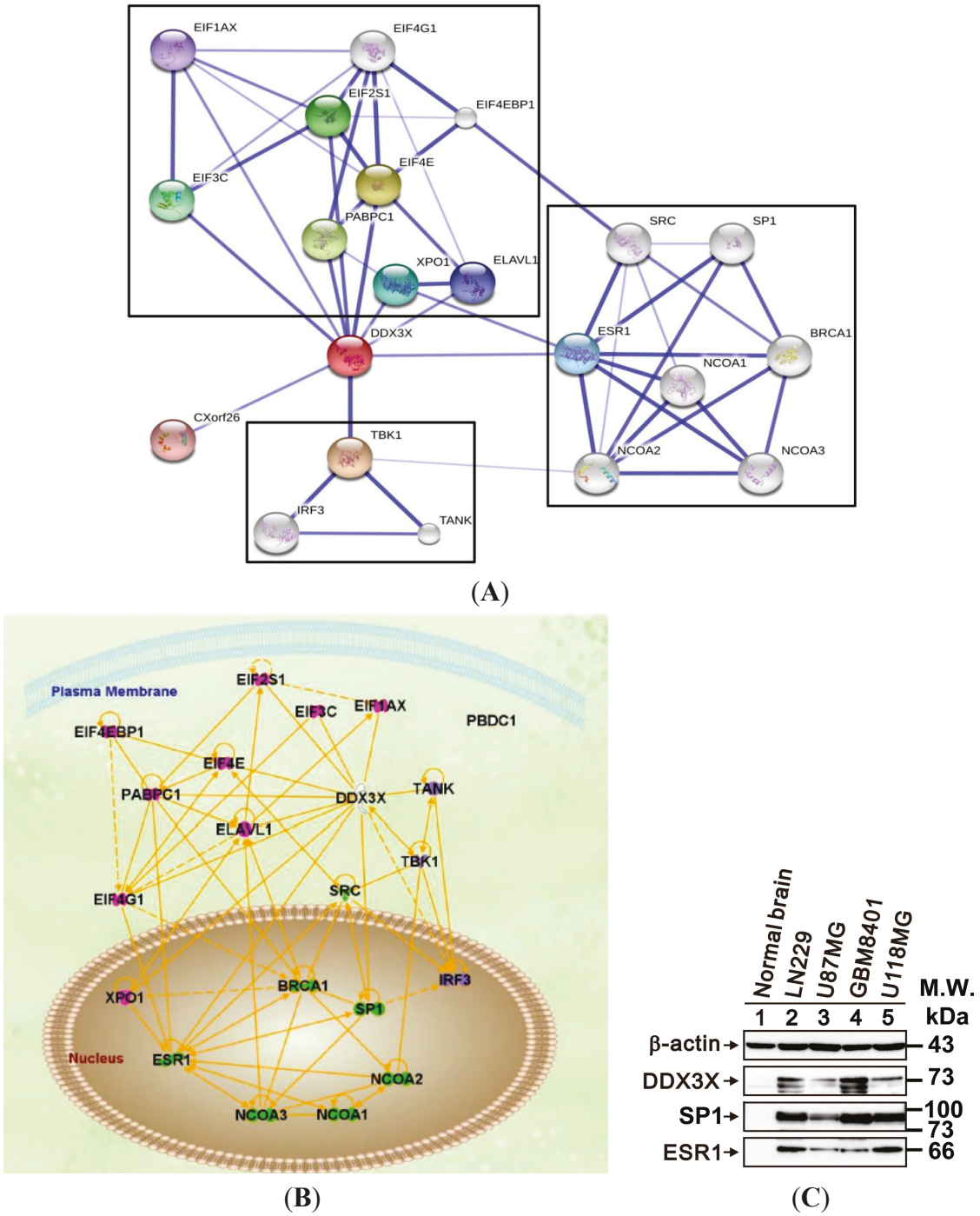

Figure 6. The protein–protein interaction (PPI) network and ingenuity pathway analysis (IPA). (**A**) The PPI network, as shown in the confidence view, created by the STRING database. DDX3X is controlling hub, and black squares show the protein clusters; (**B**) The IPA predicted signaling pathways transcriptionally regulated through DDX3X; and (**C**) The DDX3X-regulated genes including ESR1, and transcription factor SP1 were validated in normal brain tissue and human glioma cell lines. Protein lysates of glioma cell lines including LN229, U87MG, GBM8401 and U118MG were applied to SDS-PAGE and Western blot analysis to quantitate DDX3X, ESR1, and SP1 protein expression. These results are representative of two independent experiments. β-actin served as a loading control.

3. Discussion

The present studies suggest that DDX3X expression is significantly higher in patients with high-grade gliomas than in those with non-tumor brain controls and low-grade gliomas. High DDX3X expression is also associated with poor survival outcome. Molecular studies including qRT-PCR, Western blotting, and IHC staining further confirmed that DDX3X is over expressed in high-grade gliomas. This is the first study to establish the correlation between DDX3X biomarker with clinical outcome, and WHO pathological grading in human gliomas. Since the therapeutic outcome of GBM is not satisfactory, DDX3X provides one of the candidates for clinicians to choose biomarker to evaluate the survival outcome of patients with GBM stratified by the DDX3X expression in high-grade gliomas.

Western blot analysis of 31 patients with GBM showed high level expression of DDX3 in sixteen patients [17]. There is a statistically significant positive correlation between the levels of DDX3 and transcription factor Snail, which requires DDX3X to express. The fact that HDAC inhibitors also increased Snail expression hints that the action of DDX3X may contribute to the promotion of the progression in human GBM [17]. Inactivation of DDX3X suppressed Snail expression and alternate cell morphology as well as reduced migration and proliferation of HeLa and MCF-7 cell lines. The inactivation of DDX3X gene leads to suppression of Snail through the mechanism of epithelial mesenchymal transition reversal and increased E-cadherin. [17]. DDX3X also regulates DNA damage-induced apoptosis and p53 stabilization in MCF-7, suggesting suppression of DDX3X might leads to apoptosis and increased radiosensitization, which suggests suppression of DDX3X might enhance radiotherapy of human gliomas effectively.

The CD133 expressing glioma cell population plays a crucial role in radioresistance and recurrence of human gliomas [21]. The immunogenic protein DDX3X is shown in high quantity in CD133-expressing tumor cells. The DDX3X primed specific T cells vaccination contributed to defensive and beneficial antitumor immunity [14]. Overexpression of DDX3X in MCF 10A breast cancer cells prompts an epithelial-mesenchymal-like transformation, increased migration, invasion, and anchorage-independent colony formation [11]. However, currently the role of DDX3X in angiogenesis and autophagy is not yet clarified. Further investigations are needed.

The DDX3X has tissue specific differential protein production profiles and plays an oncogenic role in human brain glioma, breast cancer, and cervical cancer. In contrast, DDX3X is downregulated in hepatocellular carcinoma tissue compared to paired adjacent non-tumor tissues [22].

From the protein–protein interactions (PPI) database, STRING, three PPI clusters linked by hub protein DDX3X was found. PPI predicts the protein DDX3X is involved in regulation of the transcriptional signal ESR1, SP1, XPO1, and TBK1 that translocate into nucleus in signaling pathways. Validation of DDX3X-regulated genes found that DDX3X protein highly expresses in human glioma cells and correlates the protein level of SP1, and ESR1. Consistently, DDX3X also statistically associates with ESR1 in breast cancer [12]. ESR1, a known SP1 co-activator, is a nuclear hormone receptor, which is involved in regulation of cellular proliferation and binding to estrogen response element association with DNA-binding transcription factor SP1 with functional synergy [23,24]. Thus DDX3X is a crucial element of the TBK1-dependent innate immune response [25]. Further wet lab approach to validate downstream targets of DDX3X would be another one interesting study.

The limitations of this study include scarcity of human brain gliomas, rare incidence of grade I and low-grade glioma samples, and to pare with non-tumor control for validation of protein level or mRNA expression. For this reason, large-scale analyses of data from two GEO profiles were conducted to determine the role of DDX3X as a pathological grade and survival outcome markers as shown in the results. Using wet lab approaches such as qRT-PCR, Western blotting, and IHC staining consolidate the validation of the data from GEO profile. Moreover, the clinical validity of DDX3X as a true biomarker for unfavorable survival would be tested prospectively, and the underlying mechanism to explain the phenomenon will be conducted in future study. Theoretically, the examination of DDX3X protein expression in several pairs of glioma with different grades is important. However, to get normal brain pairs of glioma from human patients is not always accepted by human study ethics. It is not legal to cut the normal brain from patients for study purposes because it may lead to neurological deficits in patients. Brain surgery is not the same as with other cancers, such as breast, stomach, or colon, which can be resected with safe margin of non-tumor parts to be non-tumor part of pairs of cancer samples. Alternatively, we have examined DDX3X protein expression in four glioma cell lines and commercially available normal brain lysate to confirm the DDX3X protein expression is really higher in glioma than in non-tumor brain control.

4. Materials and Methods

4.1. Study Ethics and DDX3X Gene Expression in Human Brain Tumor

The institutional review board of Tri-Service General Hospital in Taipei, Taiwan, ROC approved the study (TSGHIRB No: B-102-10). The methodology for analyses of functional genomic databases was as described previously [5,18,19,26,27]. Briefly, 100 sheets of de-linked data (GDS1815/201210_at/DDX3X) on DDX3X mRNA expression, sex, age, pathologic grading, and survival of primary high-grade glioma were obtained from NCBI (Available online: http://www.ncbi.nlm.nih.gov/geo/tools/profileGraph.cgi?ID=GDS1815:201210_at). Twenty-three sheets of data without detailed information on age and survival times were excluded so that 77 sheet were included in the statistical analyses.

An additional database (GDS1962/201211_s_at/DDX3X) containing 180 sheets from 81 patients with grade IV glioma, 19 with grade III glioma, seven with grade II glioma, 23 without tumor (non-tumor control), 38 with grade II oligodendroglioma, and 12 with grade III oligodendroglioma with value on *DDX3X* gene expression obtained from NCBI (Available online: http://www.ncbi.nlm.nih.gov/geo/tools/profileGraph.cgi? ID=GDS1962:201211_s_at) was also included.

4.2. RNA Isolation and Quantitative RT-PCR (qRT-PCR)

LN229, U87MG, GBM8401, U118MG, and HeLa cells were maintained in Dulbecco's modified Eagle's medium (DMEM) containing 10% fetal bovine serum (FBS), penicillin, and streptomycin. Total RNA was extracted using the EasyPure Total RNA reagent (Bioman, Taipei, Taiwan) according to the manufacturer's protocol. For cDNA synthesis, 1.0 μg RNA was reverse transcribed (RT) into cDNA using Oligo dT primer with MMLV Reverse Transcriptase (Epicentre Biotechnologies,

Madison, WI, USA). The normal brain cDNA was purchased from Origene Technologies (Rockville, MD, USA).

Gene expression was quantified by qRT-PCR and performed in illumina ECO™ Real-Time PCR system. The amplifications were done using IQ^2 fast qPCR system with ROX (Bio-genesis Technology Inc., Taipei, Taiwan). The relative quantitative gene expression against an internal control, GAPDH was performed using the $2^{-\Delta\Delta Ct}$ method. The primer pairs used were: DDX3X forward, 5′-ATGGCTTGTGCCCAAACAG-3′ and reverse, 5′-CGCCTGGACCATCTGAATAAA-3′ [28] and GAPDH forward, 5′-CTTCATTGACCTCAACTAC-3′and reverse, 5′-GCCATCCACAGTCTTCTG-3′.

4.3. Cell Lysate Preparation and Western Blots

Cells were lysed by RIPA buffer (100 mM Tris-HCl, 150 mM NaCl, 0.1% SDS, and 1% Triton-X-100) at 4 °C for 10 min, and the cell lysates were harvested by centrifugation at 15,000 rpm for 10 min to obtain the supernatants. The normal brain lysate were purchased from Origene Technologies. Thirty-microgram cell lysates from each group were applied to 10% sodium dodecyl sulfate polyacrylamide gels electrophoresis. Proteins were transferred onto polyvinyldifluoride membranes (Millipore, MA, USA) and blocked with 5% skim milk in TBST for 1 h at room temperature. The antibodies used are anti-DDX3X (GeneTex, San Antonio, TX, USA), anti-estrogen receptor alpha (ERα) antibody (H-184) (cat. No. Sc-7207; Santa Cruz Biotechnology, Santa Cruz, CA, USA), anti-SP1 antibody (Millipore, Upstate, MA, USA) and β-actin (Santa Cruz Biotechnology, Inc.). Band detection was conducted by enhanced chemi-luminescence and X-ray film (GE Healthcare, Piscataway, NJ, USA).

4.4. Immunohistochemical (IHC) Staining

IHC staining of tissue microarray (BS17016; Biomax, Rochester, NY, USA) was conducted according to previous protocol [26,29], incubated with a polyclonal rabbit anti-human DDX3X antibody (N3C2) (1:250 diluted in phosphate buffered saline (PBS); GeneTex) for 1 h at room temperature, washed 3 times (each for 5 min in PBS), incubated with biotin-labeled secondary immunoglobulin (1:100, DAKO, Glostrup, Denmark) for 1 h at room temperature, washed 3 times, and treated with 3-amino-9-ethylcarbazole substrate chromogen (DAKO) at room temperature to visualize peroxidase activity [19]. Sections of breast cancer tissue (known to stain positive for DDX3X) were used as positive control [12].

4.5. Evaluation of DDX3X Immunostain Scores

The evaluation of DDX3X immunostain scores has been mentioned by previous study with minor modification [19]. To assess immuno-reactivity in histologic sections, all tissue microarray experiments were repeated twice and the histologic slides were checked and scored by two pathologists concurrently. To evaluate DDX3X immuno-staining scores, the intensity of membranous and cytoplasmic staining was scored as 3 (strong staining), 2 (moderate staining), 1 (weak staining), or 0 (absence of staining). Strong, moderate, and weak cytoplasmic stains were recognized by microscopy with magnification of 10×, 20×, and 40×, respectively. The cut-off value of DDX3X

intensity scores was deposit by the magnification of microscope objective lens. The percentage score of tissue staining was calculated. The DDX3X immunostain scores of human gliomas were defined by multiplying the percentage score and the corresponding intensity score.

4.6. PPI Network and Signaling Pathways Analysis

Known and predicted protein-protein interactions were analyzed by using Search Tool for the Retrieval of Interacting Genes/Proteins (STRING) database version 10.0 (http://string-db.org) [20]. The prediction of signaling pathway analysis was applied using Ingenuity Pathways Analysis (IPA) software (http://www.ingenuity.com) [30].

4.7. Statistical Analysis

The methodology for statistical analysis has been described previously [5]. Combined strategies were used to analyze the two datasets (GDS1815/201210_at/DDX3X and GDS1962/201211_s_at/DDX3X) gained from the GEO profiles. The values of *DDX3X* gene expression in the four WHO pathologic grades and the DDX3X immunostain scores were calculated by single tail test. The Bonferroni method was applied to adjust the p value to rule out the possibility of type I error in multi-groups analyses. The Kaplan–Meier method was applied for the overall survival analysis and cohorts of low- *vs.* high-DDX3X expressions were analyzed in high-grade gliomas. Chi-square test was used to analyze survival parameters in patients from WHO grade IV combined with grade III human glioma groups. The cut-off value of DDX3X expression was determined by statistical analysis to get the adequate value. Statistical analyses were performed using the R 3.1.2 software (Available online: http://cran.r-project.org). The figures were drawn using GraphPad Prism 5 software (San Diego, CA, USA). A p value less than 0.05 was considered as having statistical significance [5,18].

5. Conclusions

RNA Helicase DDX3 expression level positively correlates with WHO pathologic grades of gliomas. Overexpression of DDX3 associates with poor clinical survival outcome. Therefore, DDX3 is a valuable biomarker for poor prognosis in human gliomas.

Acknowledgments

This study was supported in part by grants from Health and Welfare surcharge of tobacco to the Ministry of Health and Welfare (MOHW104-TDU-B-211-124-005), Ministry of Science and Technology (MOST102-2628-B-016-002-MY2, MOST103-2314-B-016-027-MY3), and Tri-Service General Hospital (TSGH-C103-005-007-009-S05, TSGH-C104-008-S04), Taipei, Taiwan.

Author Contributions

Dueng-Yuan Hueng made substantial contributions to conception and design; Dueng-Yuan Hueng, Wen-Chiuan Tsai, Shao-Wei Feng, Chin Lin, and Ming-Hong Lin participated in acquisition, and interpretation of data; Wen-Chiuan Tsai and Yao-Feng Li conducted the IHC staining and analysis of pathological results; Li-Chun Huang and Hsin-Ying Clair Chiou performed the qRT-PCR, and Western

blot; Chin Lin and Dueng-Yuan Hueng participated in statistical analysis; Dueng-Yuan Hueng, Wen-Chiuan Tsai, and Hsin-Ying Clair Chiou participated in drawing the figures; Dueng-Yuan Hueng, Ming-Hong Lin, and Shao-Wei Feng prepared and drafted the manuscript. All authors read and approved the final manuscript.

Conflicts of Interest

The authors declare no conflict of interest.

References

1. Jan, H.J.; Lee, C.C.; Shih, Y.L.; Hueng, D.Y.; Ma, H.I.; Lai, J.H.; Wei, H.W.; Lee, H.M. Osteopontin regulates human glioma cell invasiveness and tumor growth in mice. *Neuro Oncol.* **2010**, *12*, 58–70.
2. Ma, H.I.; Hueng, D.Y.; Shui, H.A.; Han, J.M.; Wang, C.H.; Lai, Y.H.; Cheng, S.Y.; Xiao, X.; Chen, M.T.; Yang, Y.P. Intratumoral decorin gene delivery by AAV vector inhibits brain glioblastomas and prolongs survival of animals by inducing cell differentiation. *Int. J. Mol. Sci.* **2014**, *15*, 4393–4414.
3. Stupp, R.; Mason, W.P.; van den Bent, M.J.; Weller, M.; Fisher, B.; Taphoorn, M.J.; Belanger, K.; Brandes, A.A.; Marosi, C.; Bogdahn, U.; *et al.* Radiotherapy plus concomitant and adjuvant temozolomide for glioblastoma. *N. Engl. J Med.* **2005**, *352*, 987–996.
4. Louis, D.N.; Ohgaki, H.; Wiestler, O.D.; Cavenee, W.K.; Burger, P.C.; Jouvet, A.; Scheithauer, B.W.; Kleihues, P. The 2007 WHO classification of tumours of the central nervous system. *Acta Neuropathol.* **2007**, *114*, 97–109.
5. Cheng, Y.S.; Lin, C.; Cheng, Y.P.; Yu, Y.L.; Tang, C.T.; Hueng, D.Y. Epithelial cell transformation sequence 2 is a potential biomarker of unfavorable survival in human gliomas. *Neurol. India* **2014**, *62*, 406–409.
6. Roversi, G.; Pfundt, R.; Moroni, R.F.; Magnani, I.; van Reijmersdal, S.; Pollo, B.; Straatman, H.; Larizza, L.; Schoenmakers, E.F. Identification of novel genomic markers related to progression to glioblastoma through genomic profiling of 25 primary glioma cell lines. *Oncogene* **2006**, *25*, 1571–1583.
7. Yedavalli, V.S.; Neuveut, C.; Chi, Y.H.; Kleiman, L.; Jeang, K.T. Requirement of DDX3 DEAD box RNA helicase for HIV-1 Rev-RRE export function. *Cell* **2004**, *119*, 381–392.
8. Garbelli, A.; Beermann, S.; di Cicco, G.; Dietrich, U.; Maga, G. A motif unique to the human DEAD-box protein DDX3 is important for nucleic acid binding, ATP hydrolysis, RNA/DNA unwinding and HIV-1 replication. *PLoS ONE* **2011**, *6*, e19810.
9. Dolan, P.T.; Roth, A.P.; Xue, B.; Sun, R.; Dunker, A.K.; Uversky, V.N.; LaCount, D.J. Intrinsic disorder mediates hepatitis C virus core-host cell protein interactions. *Protein Sci.* **2015**, *24*, 221–235.
10. Zheng, Y.; Cheng, X.R.; Zhou, W.X.; Zhang, Y.X. Gene expression patterns of hippocampus and cerebral cortex of senescence-accelerated mouse treated with Huang-Lian-Jie-Du decoction. *Neurosci. Lett.* **2008**, *439*, 119–124.

11. Botlagunta, M.; Vesuna, F.; Mironchik, Y.; Raman, A.; Lisok, A.; Winnard, P., Jr.; Winnard, P.; Mukadam, S.; van Diest, P.; Chen, J.H.; *et al.* Oncogenic role of DDX3 in breast cancer biogenesis. *Oncogene* **2008**, *27*, 3912–3922.
12. Bol, G.M.; Raman, V.; van der Groep, P.; Vermeulen, J.F.; Patel, A.H.; van der Wall, E.; van Diest, P.J. Expression of the RNA helicase DDX3 and the hypoxia response in breast cancer. *PLoS ONE* **2013**, *8*, e63548.
13. Wu, D.W.; Lee, M.C.; Wang, J.; Chen, C.Y.; Cheng, Y.W.; Lee, H. DDX3 loss by p53 inactivation promotes tumor malignancy via the MDM2/Slug/E-cadherin pathway and poor patient outcome in non-small-cell lung cancer. *Oncogene* **2014**, *33*, 1515–1526.
14. Koshio, J.; Kagamu, H.; Nozaki, K.; Saida, Y.; Tanaka, T.; Shoji, S.; Igarashi, N.; Miura, S.; Okajima, M.; Watanabe, S.; *et al.* DEAD/H (Asp-Glu-Ala-Asp/His) box polypeptide 3, X-linked is an immunogenic target of cancer stem cells. *Cancer Immunol. Immunother.* **2013**, *62*, 1619–1628.
15. Schroder, P.C.; Fernandez-Irigoyen, J.; Bigaud, E.; Serna, A.; Renandez-Alcoceba, R.; Lu, S.C.; Mato, J.M.; Prieto, J.; Corrales, F.J. Proteomic analysis of human hepatoma cells expressing methionine adenosyltransferase I/III: Characterization of DDX3X as a target of *S*-adenosylmethionine. *J. Proteomics* **2012**, *75*, 2855–2868.
16. Miao, X.; Yang, Z.L.; Xiong, L.; Zou, Q.; Yuan, Y.; Li, J.; Liang, L.; Chen, M.; Chen, S. Nectin-2 and DDX3 are biomarkers for metastasis and poor prognosis of squamous cell/adenosquamous carcinomas and adenocarcinoma of gallbladder. *Int. J. Clin. Exp. Pathol.* **2013**, *6*, 179–190.
17. Sun, M.; Song, L.; Zhou, T.; Gillespie, G.Y.; Jope, R.S. The role of DDX3 in regulating Snail. *Biochim. Biophys. Acta* **2011**, *1813*, 438–447.
18. Cheng, Y.P.; Lin, C.; Lin, P.Y.; Cheng, C.Y.; Ma, H.I.; Chen, C.M.; Hueng, D.Y. Midkine expression in high grade gliomas: Correlation of this novel marker with proliferation and survival in human gliomas. *Surg. Neurol. Int.* **2014**, *5*, doi:10.4103/2152-7806.133205.
19. Tsai, W.C.; Chen, Y.; Huang, L.C.; Lee, H.S.; Ma, H.I.; Huang, S.M.; Sytwu, H.K.; Hueng, D.Y. EMMPRIN expression positively correlates with WHO grades of astrocytomas and meningiomas. *J. Neurooncol.* **2013**, *114*, 281–290.
20. Szklarczyk, D.; Franceschini, A.; Wyder, S.; Forslund, K.; Heller, D.; Huerta-Cepas, J.; Simonovic, M.; Roth, A.; Santos, A.; Tsafou, K.P.; *et al*. STRING v10: Protein–protein interaction networks, integrated over the tree of life. *Nucleic Acids Res.* **2015**, *43*, D447–D452.
21. Ma, H.I.; Chiou, S.H.; Hueng, D.Y.; Tai, L.K.; Huang, P.I.; Kao, C.L.; Chen, Y.W.; Sytwu, H.K. Celecoxib and radioresistant glioblastoma-derived CD133+ cells: improvement in radiotherapeutic effects. Laboratory investigation. *J. Neurosurg.* **2011**, *114*, 651–662.
22. Chang, P.C.; Chi, C.W.; Chau, G.Y.; Li, F.Y.; Tsai, Y.H.; Wu, J.C.; Wu Lee, Y.H. DDX3, a DEAD box RNA helicase, is deregulated in hepatitis virus-associated hepatocellular carcinoma and is involved in cell growth control. *Oncogene* **2006**, *25*, 1991–2003.
23. Porter, W.; Wang, F.; Wang, W.; Duan, R.; Safe, S. Role of estrogen receptor/Sp1 complexes in estrogen-induced heat shock protein 27 gene expression. *Mol. Endocrinol.* **1996**, *10*, 1371–1378.
24. Wu, F.; Ivanov, I.; Xu, R.; Safe, S. Role of SP transcription factors in hormone-dependent modulation of genes in MCF-7 breast cancer cells: Microarray and RNA interference studies. *J. Mol. Endocrinol.* **2009**, *42*, 19–33.

25. Soulat, D.; Burckstummer, T.; Westermayer, S.; Goncalves, A.; Bauch, A.; Stefanovic, A.; Hantschel, O.; Bennett, K.L.; Decker, T.; Superti-Furga, G. The DEAD-box helicase DDX3X is a critical component of the TANK-binding kinase 1-dependent innate immune response. *EMBO J.* **2008**, *27*, 2135–2146.
26. Hueng, D.Y.; Lin, G.J.; Huang, S.H.; Liu, L.W.; Ju, D.T.; Chen, Y.W.; Sytwu, H.K.; Chang, C.; Huang, S.M.; Yeh, Y.S.; *et al.* Inhibition of Nodal suppresses angiogenesis and growth of human gliomas. *J. Neurooncol.* **2011**, *104*, 21–31.
27. Lee, C.C.; Jan, H.J.; Lai, J.H.; Ma, H.I.; Hueng, D.Y.; Lee, Y.C.; Cheng, Y.Y.; Liu, L.W.; Wei, H.W.; Lee, H.M. Nodal promotes growth and invasion in human gliomas. *Oncogene* **2010**, *29*, 3110–3123.
28. Chen, Q.; Liu, Q.; Liu, D.; Wang, D.; Chen, H.; Xiao, S.; Fang, L. Molecular cloning, functional characterization and antiviral activity of porcine DDX3X. *Biochem. Biophys. Res. Commun.* **2014**, *443*, 1169–1175.
29. Tsai, W.C.; Hueng, D.Y.; Lin, C.K. Nuclear overexpression of urocortin discriminates primary brain tumors from reactive gliosis. *APMIS* **2015**, *123*, 465–472.
30. Kramer, A.; Green, J.; Pollard, J., Jr.; Tugendreich, S. Causal analysis approaches in ingenuity pathway analysis. *Bioinformatics* **2014**, *30*, 523–530.

© 2015 by the authors; licensee MDPI, Basel, Switzerland. This article is an open access article distributed under the terms and conditions of the Creative Commons Attribution license (http://creativecommons.org/licenses/by/4.0/).

Int. J. Mol. Sci. **2015**, *16*, 16144-16157; doi:10.3390/ijms160716144

OPEN ACCESS
International Journal of
Molecular Sciences
ISSN 1422-0067
www.mdpi.com/journal/ijms

Article

Deregulated SLC2A1 Promotes Tumor Cell Proliferation and Metastasis in Gastric Cancer

Shiyan Yan †, Yuqin Wang †, Meimei Chen, Guangming Li and Jiangao Fan *

Department of Gastroenterology, Xinhua Hospital, Shanghai Jiaotong University School of Medicine, Shanghai 200092, China; E-Mails: shiyan871111@gmail.com (S.Y.); yuqingwang02@gmail.com (Y.W.); chenmeimei27@gmail.com (M.C.); liguangming@gmail.com (G.L.)

† These authors contributed equally to this work.

* Author to whom correspondence should be addressed; E-Mail: fanjiangao@gmail.com; Tel./Fax: +86-21-2507-8999.

Academic Editor: William Chi-shing Cho

Received: 30 May 2015 / Accepted: 9 July 2015 / Published: 16 July 2015

Abstract: Gastric cancer (GC) is one of the common reasons of cancer-related death with few biomarkers for diagnosis and prognosis. Solute carrier family 2 (facilitated glucose transporter) member 1 protein SLC2A1, also known as glucose transporter type 1 (GLUT1), has been associated with tumor progression, metastasis, and poor prognosis in many human solid tumors. However, little is reported about its clinical significance and biological functions in GC. Here we observed a strong up-regulation of SLC2A1 in patients with GC and found that SLC2A1 was significantly correlated with depth of invasion and clinical stage. Additionally, over-expression of SLC2A1 in GC cells promotes cellular proliferation and metastasis *in vitro* and enhances tumor growth *in vivo* as well as enhancement of glucose utilization. Meanwhile, elevated SLC2A1 also contributes to tumor metastasis *in vitro*. Our results indicate SLC2A1 exhibits a pivotal role in tumor growth, metastasis and glucose metabolism, and also suggest SLC2A1 as a promising target for gastric cancer therapy.

Keywords: SLC2A1; GLUT1; gastric cancer; proliferation; metastasis

1. Introduction

Gastric cancer (GC) is one of the most common malignancies worldwide, with considerable incidence variation across various countries and contributes significantly to cancer mortality [1,2]. Although the traditional therapeutic strategies are used in patients with GC treatment, they are not effective enough to destroy GC cell thoroughly [3]. Recently, it has been reported that several regulators of the glycolysis pathway are detected in various premalignant lesions and tumors, which suggests that these proteins participate in early carcinogenesis and progression of cancer [4,5]. Aerobic glycolysis, also known as Warburg effect, not only favors tumor cell proliferation by providing cellular building blocks, but also contributes to tumor cell metastasis by acidified microenvironment through increased production of lactate [6]. Therefore, glycolysis pathway might be a potential targetable pathway for cancer therapy because of the glucose addiction of tumor cells.

Solute carrier family 2 facilitated glucose transporter member 1 (SLC2A1), also known as glucose transporter 1 (GLUT1), is a crucial protein in the cellular energy metabolism pathway [7–9]. SLC2A1 is over-expressed in several different types of carcinomas, including liver, lung, endometrial, oral and breast cancers, as well as gastric cancer [10–14]. These observations suggest that SLC2A1 could be one of the driver genes in tumors. However, the expression pattern and cellular functions of SLC2A1 in GC remain largely unexplored.

In our study, we observed that SLC2A1 was over-expressed in GC tumors by immunochemical staining (IHC) and found the significant correlation between SLC2A1 expression and depths of invasion and clinical stage. We further explored the functional significance of SLC2A1 in GC tumorigenesis and demonstrated that SLC2A1 promoted GC cells growth *in vitro* and *in vivo* and enhanced GC cells migration *in vitro* via enhancement of glucose utilization.

2. Results

2.1. Solute Carrier Family 2 Facilitated Glucose Transporter Member 1 (SLC2A1) Is Over-Expressed in Gastric Cancer (GC) Tissues

To determine the role of SLC2A1 in GC cells, immunohistochemical staining was performed to confirm the presence of this enzyme. In 57.8% (115/199) of the GC tumors, a predominantly cytoplasmatic staining with strong positive tumor cells for SLC2A1 was detected (Figure 1A), whereas 12.5% (1/8) normal gastric specimens showed only weak irregular cytoplasmatic staining (Figure 1B). To validate the up-regulation of SLC2A1 at the transcriptional level in GC, we further compared SLC2A1 expression patterns in 20 GC tumor tissues to their normal counterparts using real-time PCR. Our data revealed that the mean expression level for SLC2A1 in GC tumor tissues was roughly 3-fold higher than that in the normal gastric mucosa ($p < 0.001$, Figure 1C,D). Furthermore, we analyzed the correlation of SLC2A1 expression with the clinicopathological features. SLC2A1 expression was significantly correlated with depths of invasion ($p = 0.011$) and clinical stage ($p = 0.001$) (Table 1). Collectively, these findings suggest that SLC2A1 is over-expressed in GC tissues and might contribute to the progression of GC.

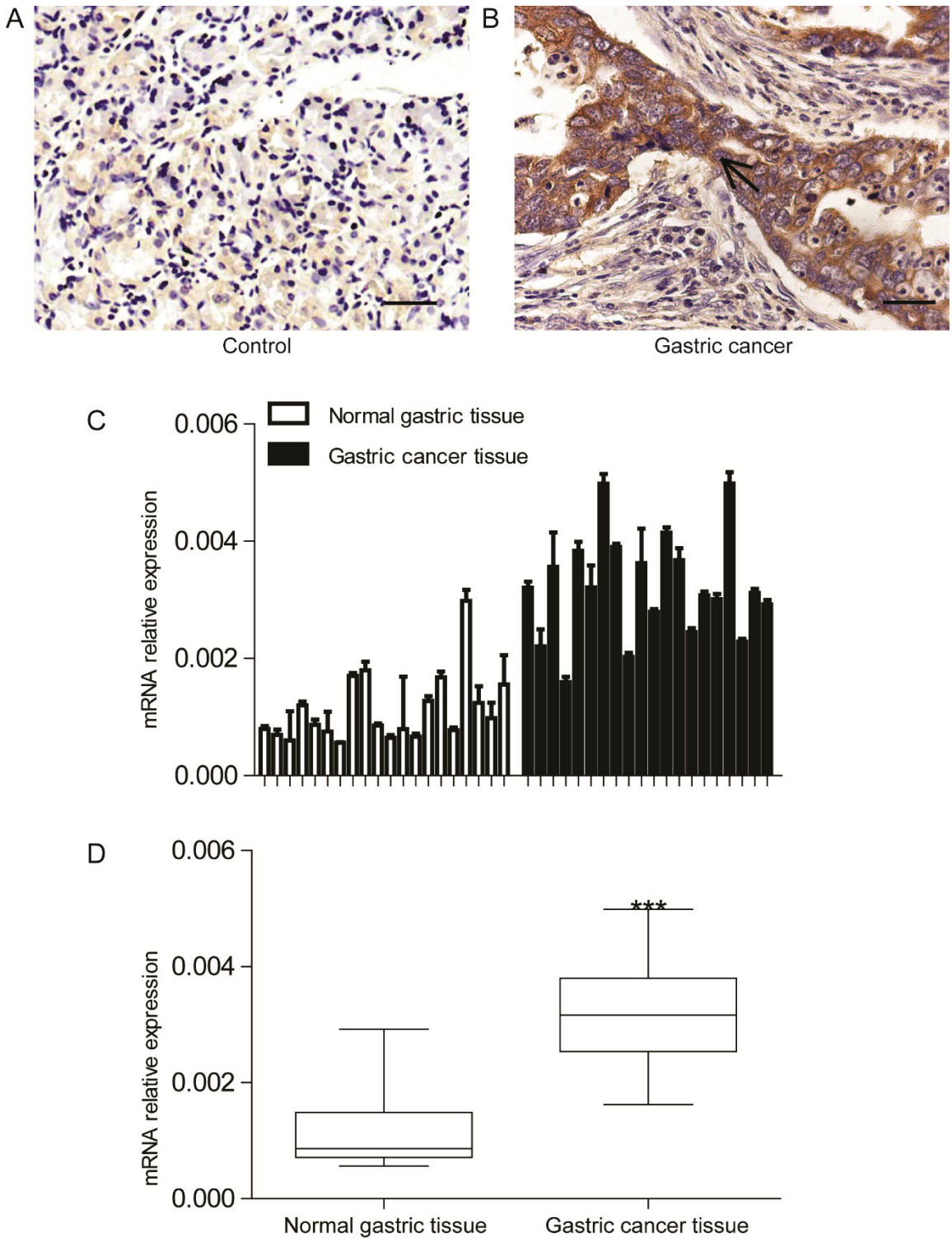

Figure 1. Solute carrier family 2 facilitated glucose transporter member 1 (SLC2A1) was over-expressed in GC tissues. Representative photographs of SLC2A1 immunoreactivity in gastric cancer (GC) tissues (**A**) and normal gastric mucosa (**B**) (scale bar: 50 μm). The arrow represents cytoplasmatic staining of SLC2A1 in tumor cells; (**C**,**D**) SLC2A1 expression in 20 pairs of GC tissues and their normal counterparts was demonstrated by real-time PCR. Normal gastric tissue *vs.* GC tissues, *** $p < 0.001$.

Table 1. Analysis of SLC2A1 expression with corresponding clinical parameters.

Characteristics		Cases	SLC2A1 Expression		*p* Value
			Low	High	
Normal gastric tissue		8	7	1	0.023
Gastric cancer tissue		199	84	115	
T classification	T1	14	10	4	0.011
	T2	130	59	71	
	T3	48	14	34	
	T4	7	1	6	
Clinical stage (AJCC)	I	134	69	65	0.001
	II	50	11	39	
	III	12	3	9	
	IV	3	1	2	

2.2. SLC2A1 Promotes GC Cells Growth in Vitro and in Vivo

We first examined the mRNA (Figure 2A) and protein (Figure 2B) level of ectopic SLC2A1 expression in several GC cells and found that MGC-803 and MKN28 cells expressed relatively lower endogenous levels of SLC2A1. To further characterize the functions of SLC2A1, we established stable cell lines over-expressing SLC2A1 in MGC-803 and MKN28 cells, and the transfection efficiency of SLC2A1 in the stable cell lines was verified by western blot (Figure 2C,D). Cell counting kit-8 (CCK-8) assay showed significant increases in MGC-803cellular proliferation after transfecting the SLC2A1 plasmid (Figure 3A). Similarly, the MKN28 cells transfected with the SLC2A1 plasmid grew faster than that transfected with empty vector (Figure 3B). Next, we subcutaneously injected the SLC2A1- or vector-expressing MGC-803 into nude mice (Figure 3C). After four weeks, mice were sacrificed. The mice injected with the SLC2A1-expressing MGC-803 cells demonstrated a significantly larger in tumor size than those injected with the vector-expressing MGC-803 cells ($p < 0.001$, Figure 3D). The mice injected with the SLC2A1-expressing MGC-803 cells also demonstrated a significant increase in tumor weight than those injected with the vector-expressing MGC-803 cells ($p < 0.001$, Figure 3E). Similarly, the mice injected with the SLC2A1-expressing MKN28 cells demonstrated a significant larger in tumor size and tumor weight than those injected with the vector-expressing MKN28 cells ($p < 0.01$, Figure 3F–H). Taken together, these results support the role of SLC2A1 in promoting growth of GC cells *in vitro* and *in vivo*.

2.3. SLC2A1 Enhances GC Cells Invasion in Vitro

As elevated SLC2A1 is closely associated with depth of invasion and clinical stage, we hypothesized that over-expression of SLC2A1 may facilitate tumor cell invasion and further contribute to distant metastasis. Thus, we investigated the effect SLC2A1 on GC cells invasion. By Transwell model, we observed that more numbers of invaded cells in SLC2A1-expressing group compared with the control group in both MGC-803 ($p < 0.01$, Figure 4A) and MKN28 ($p < 0.01$, Figure 4B) cells. These data suggest that over-expression of SLC2A1 provides an advantage for gastric cancer metastasis *in vitro*.

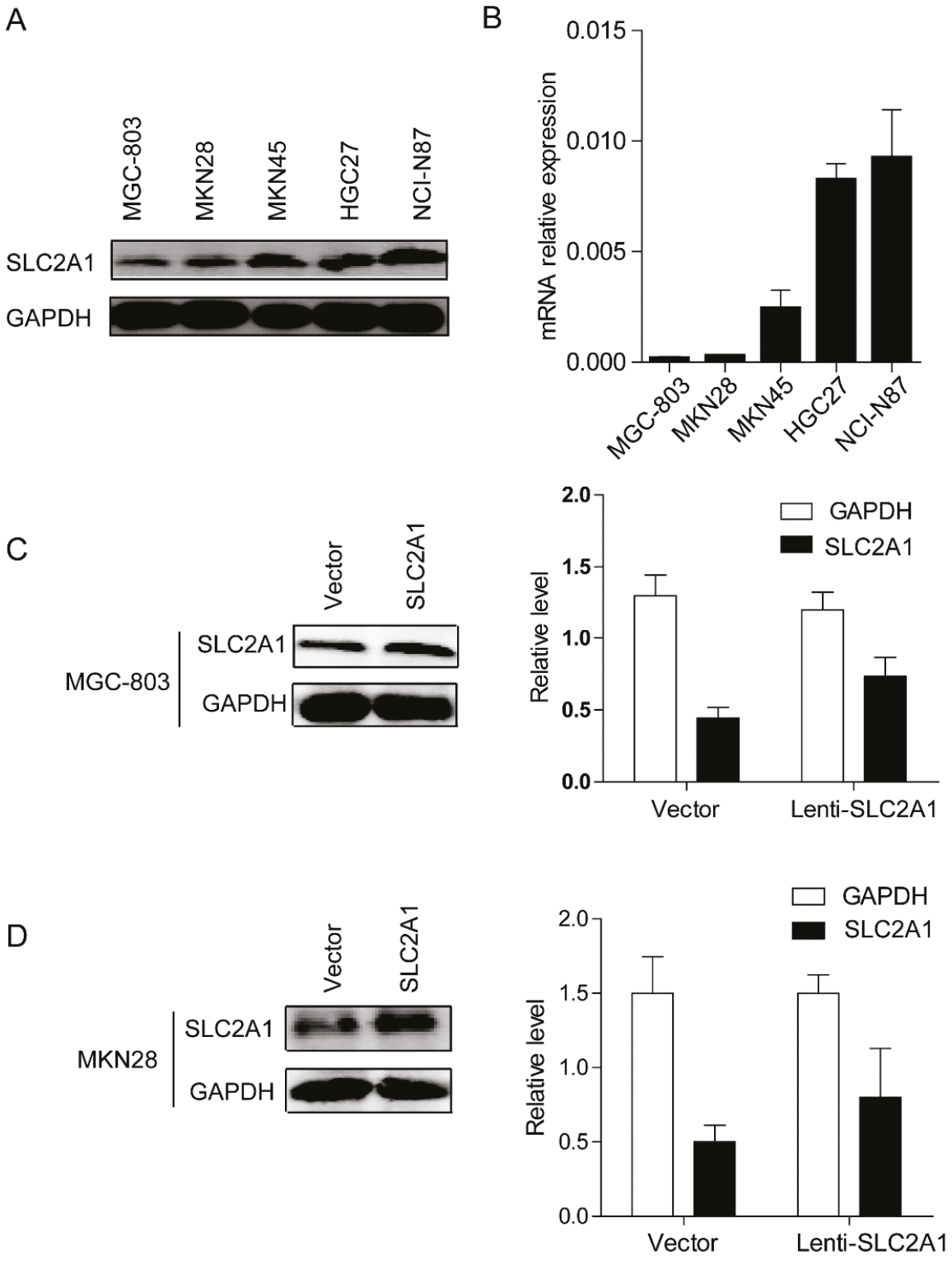

Figure 2. SLC2A1 expression in GC cell lines. The protein (**A**) and mRNA (**B**) levels of SLC2A1 in different gastric cancer cell lines; (**C**) The mRNA and protein levels of SLC2A1 in SLC2A1-expressing MGC-803 cells; (**D**) The mRNA and protein levels of SLC2A1 in SLC2A1-expressing MKN28 cells.

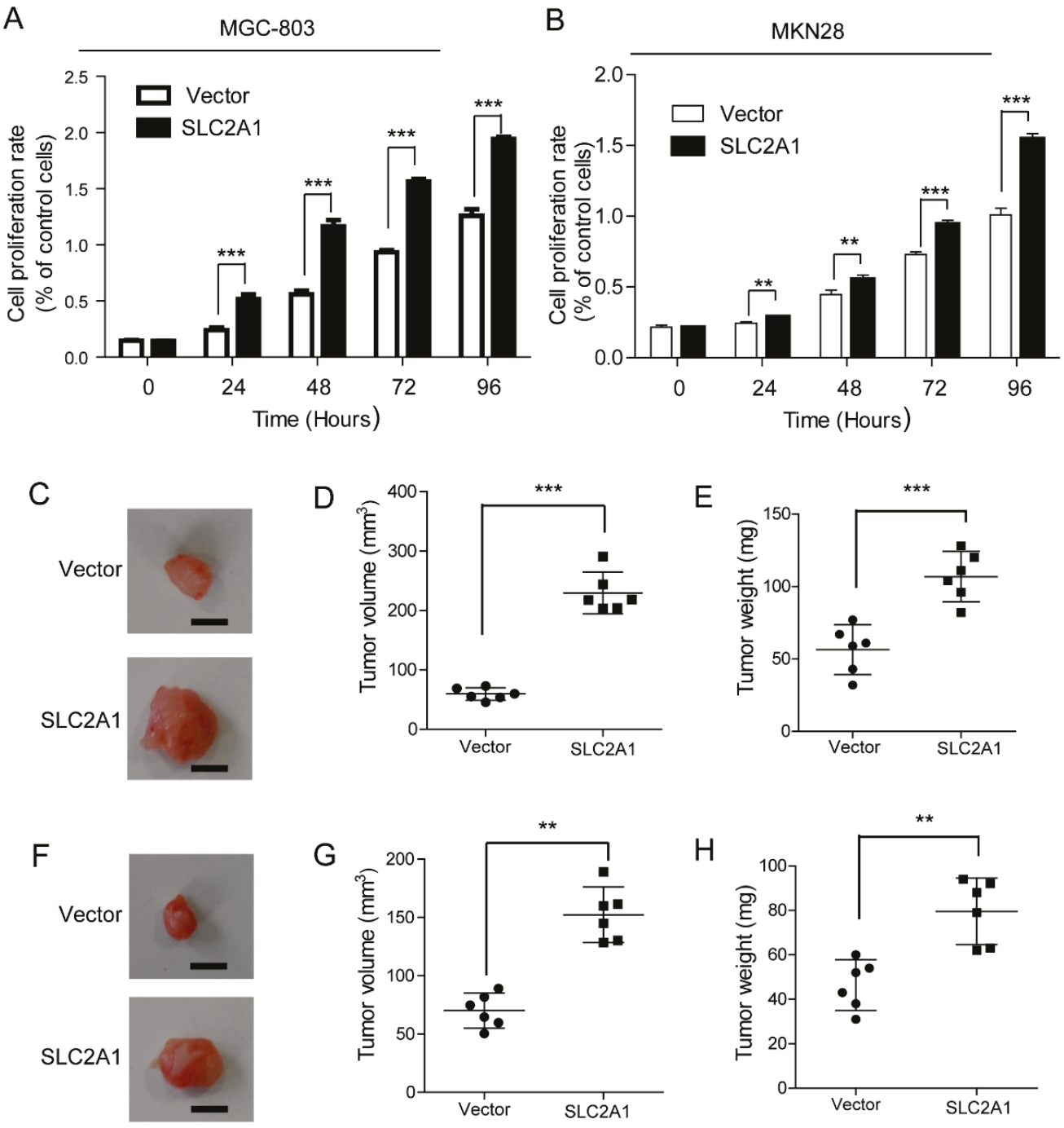

Figure 3. SLC2A1 promoted GC cell growth *in vitro* and *in vivo*. Cell counting kit-8 (CCK-8) assay showed over-expression of SLC2A1 promoted cell growth in MGC-803 (**A**) and MKN28 cells (**B**); (**C**–**E**) The mean tumor volume and weight in the mice inoculated with SLC2A1- and vector-expressing MGC-803 cells (n = 6); (**F**–**H**) The mean tumor volume and weight in the mice inoculated with SLC2A1- and vector-expressing MKN28 cells (n = 6). Vector *vs.* SLC2A1, ** $p < 0.01$, *** $p < 0.001$; Scale bar in (**C**,**F**): 5 mm.

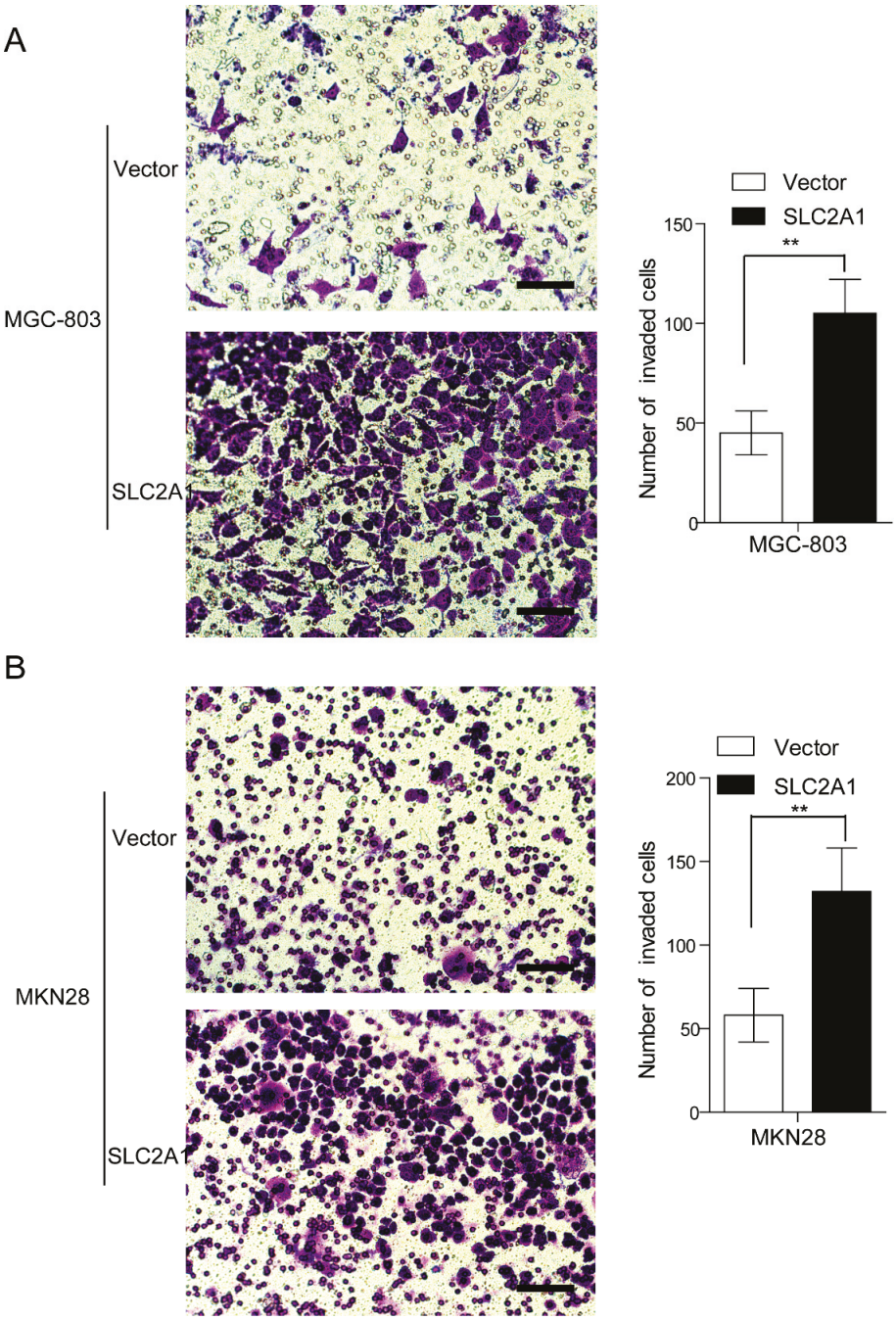

Figure 4. SLC2A1 enhanced GC cells invasion *in vitro*. The invasive potential of SLC2A1- and vector-expressing MGC-803 (**A**) and MKN28 cells (**B**) was assessed by Transwell model. Vector *vs.* SLC2A1, ** $p < 0.01$; Scale bar: 50 μm.

2.4. SLC2A1 Promotes GC Cells Glucose Utilization in Vitro

Next, we sought to determine whether the GC cells with increased SLC2A1 protein had altered glucose utilization. As shown in Figure 5A, SLC2A1-expressing MGC-803 cells took more 3H-2-deoxyglucose (3H-2-DOG) compared to the control cells ($p < 0.05$). Similarly, MGC-803 cells expressing SLC2A1 consumed more glucose than the negative control ($p < 0.05$, Figure 5B). Meanwhile, we found an increase in fructose-6-phosphate ($p < 0.01$, Figure 5C) and glyceraldehydes-3-phosphate production (G3P) ($p < 0.001$, Figure 5D) in SLC2A1-expressing MGC-803 cells compared with

vehicle-expressing cells. Furthermore, we found significantly increased pyruvate production in SLC2A1-expressing MGC-803 cells compared with vehicle-expressing cells ($p < 0.001$, Figure 5E). Similarly, there's an increase in lactate production in SLC2A1-expressing MGC-803 cells compared with vehicle-expressing cells ($p < 0.01$, Figure 5F). These data demonstrate that increase in SLC2A1 expression leads to an enhancement of glucose transport, glucose consumption and lactate secretion, indicating the critical roles of SLC2A1 in glycolysis and glucose metabolism. Overall, these data supported that GC cells with increased SLC2A1 protein had enhanced glucose utilization.

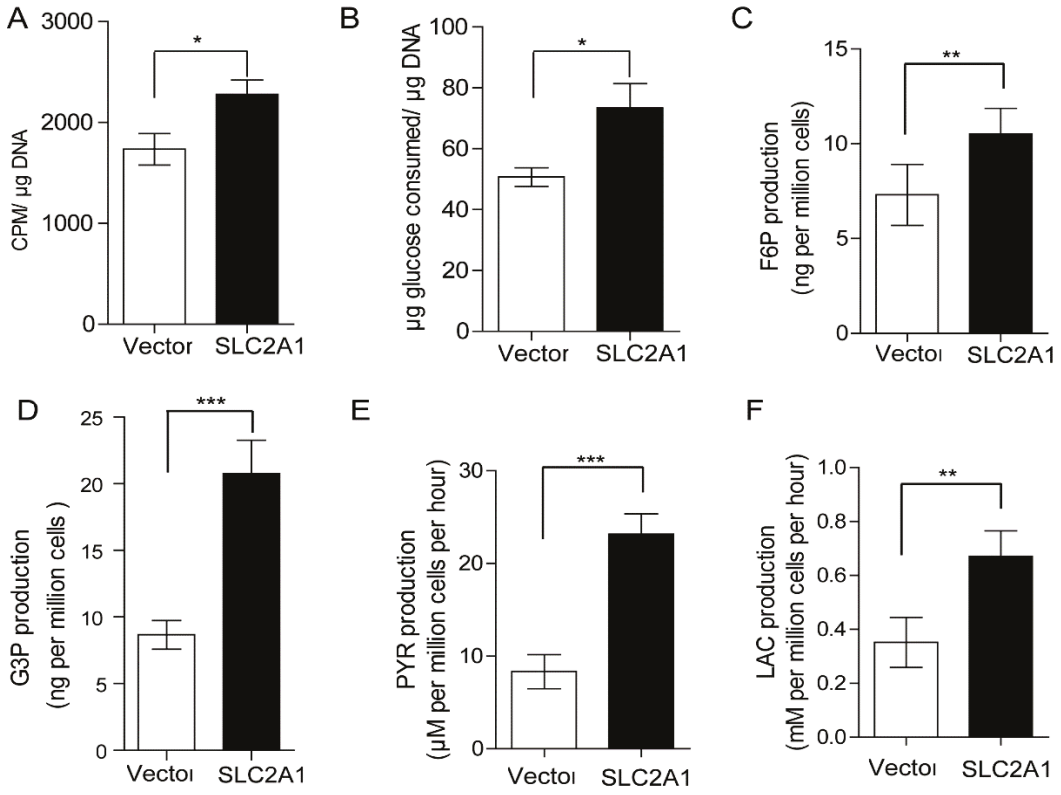

Figure 5. SLC2A1 promoted glucose utilization of GC cells. (**A**) SLC2A1-expressing MGC-803 cells took more 3H-2-deoxyglucose (3H-2-DOG) compared with the control cells; (**B**) MGC-803 cells expressing SLC2A1 consumed more glucose than controls; (**C**) The quantitative changes of fructose-6-phosphate (F6P) in SLC2A1-expressing MGC-803 cells compared with that in vector expressing cells; (**D**) The quantitative changes of G3P in SLC2A1-expressing MGC-803 cells compared with that in vector expressing cells; (**E**) The production level of pyruvate in the culture buffer of SLC2A1- and vector-expressing MGC-803 cells; (**F**) The production level of lactate in the culture buffer in SLC2A1- and vector-expressing MGC-803 cells. Vector *vs.* SLC2A1, * $p < 0.05$, ** $p < 0.01$, *** $p < 0.001$.

3. Discussion

Gastric cancer (GC) patients are diagnosed at a late stage with a poor prognosis, because of lack of reliable markers for early detection [15–17] and the mechanisms of GC is still unclear. *SLC2A1* gene encodes GLUT1 protein and is one of the isoforms of the protein family of facilitative glucose transporters, which is highly concentrated in tissue endothelium and epithelium [18,19]. Recently,

accumulated evidences demonstrated that high expression of SLC2A1 involves in the development of various carcinomas [20–22].

Previous immunohistochemical studies showed that SLC2A1 was highly expressed in about 25% of detected samples [23,24]. In breast cancer, SLC2A1 expression was closely correlated with higher tumor grade [25]. In our study, we observed that SLC2A1 was over-expressed in GC tissues, in relative to that in normal gastric tissues, and the high rate of GC tissues is 57.8%. It was also demonstrated that SLC2A1 over-expression was associated with several clinicopathologic parameters of endometrium and endometrial adenocarcinoma [26]. Consistent with this, our results indicated that SLC2A1 expression significantly correlated with depth of invasion and clinical stage. However, two researches in GC focused on SLC2A1 study demonstrated that none of normal gastric epithelium expressed SLC2A1 and nearly 30% carcinoma samples were positive staining of SLC2A1 [27,28]. These minor data differences might due to different scoring criteria in each study.

Up-regulated SLC2A1 expression contributes to carcinogenesis and tumor progression [29]. Next, we analyzed the oncogenic activity of SLC2A1 in GC cell lines. We established stable cell lines over-expressing SLC2A1 in MGC-803 and MKN28 cells to further explore the function of SLC2A1. Firstly, we observed that MGC-803 and MKN28 cells with exogenous SLC2A1 over-expression grew faster than control cells. Besides, we showed that SLC2A1-over-expressing MGC-803 and MKN28 cells grew faster and larger tumor xenografts than control cells. Secondly, we found over-expression of SLC2A1 provided an advantage for GC cells to invasion. Finally, SLC2A1-expressing MGC-803 cells took more 3H-2-DOG, consumed more glucose and produced more fructose-6-phosphate, glyceraldehydes-3-phosphate, pyruvate and lactate compared with vector-expressing MGC-803 cells. And consistent with this observation, it was reported that glyceraldehydes-3-phosphate was increased in disease progression from benign tissue to prostate cancer [30]. Given the roles of SLC2A1 in enhancing glucose utilization, thus supporting energy requirements, providing enormous biosynthetic needs and promoting the secretion of lactate and further contributing to the acidification of tumor microenvironment, which ultimately favors tumor growth and progression, it is reasonable to expect the oncogenic functions in gastric cancer.

In summary, our study provides evidence that elevated SLC2A1 expression is significantly correlated with depth of invasion and clinical stage. Meanwhile, over-expressed SLC2A1 promotes the proliferation, invasion and glucose utilization of GC cells. These results suggest that SLC2A1 might acts as a candidate target for developing treatment of GC.

4. Experimental Section

4.1. Cell Culture

The human gastric cancer cell lines (MGC-803, MKN28, MKN-45, HGC-27 and NCI-N87) were purchased from American Type Culture Collection (ATCC) and maintained in Dulbecco's modified Eagle's medium or RPMI 1640 medium (Gibco, Grand Island, NY, USA) supplemented with 10% fetal bovine serum (FBS) and penicillin-streptomycin (50 U/mL) at 37 °C in a atmosphere containing 5% CO_2.

4.2. Immunohistochemistry

Tissue microarray (TMA) contained 199 cases of GC tissues and eight cases of normal gastric tissues were purchased from Xi'an AlenabioInc (Xi'an, China). The clinical stages were classified according the definition by the American Joint Committee on Cancer (AJCC). After deparaffinized with dimethylbenzene and rehydrated through grade ethanol, the gastric carcinomas tissue arrays were treated with 10% BSA in phosphate-buffered saline (PBS) for 15 min and incubated with primary antibody (anti-SLC2A1, dilution at 1:50; Abcam, Shanghai, China) at 37 °C for 45 min. The sections were then washed with Tween and incubated with a universal biotinylated secondary antibody at 37 °C for 30 min. Scoring was conducted by two pathologists, according to the ratio and intensity of positive-staining cells.

4.3. Quantitative Reverse Transcriptase-PCR

The collection of human specimens for quantitative reverse transcriptase-PCR study is approved by the ethics committee of Xinhua Hospital, Shanghai Jiaotong University School of Medicine. Total RNA from frozen tissues or cell lines was purified using the TRIzol reagent (Invitrogen, Carlsbad, CA, USA) according to manufacturer's instructions. Complementary DNA synthesis (RT) was carried out starting with total RNA with Prime Script RT reagent kit (Takara, Dalian, China). The primers used for real-time PCR are as follows. GAPDH forward: 5′-TGACTTCAACAGCGACACCCA-3′, GAPDH reverse: 5′-CACCCTGTTGCTGTAGCCAAA-3′; SLC2A1 forward: 5′-AAGGTGATCGAGGAG TTCTACA-3′, SLC2A1 reverse: 5′-ATGCCCCCAACAGAAAAGATG-3′. The amplifications were performed in 10 μL reaction volumes with a denaturation at 94 °C for 2 min, 40 thermal cycles of 95 °C for 10 s, 60 °C for 34 s and 72 °C for 30 s. Relative expression was determined by normalizing expression of each *C*t value to glyceraldehyde-3-phosphate dehydrogenase (GAPDH) *C*t value and data were analyzed according to the $2^{-\Delta\Delta Ct}$ formula.

4.4. Western Blot Analysis

Cells were isolate by adding lysis buffer and an equal amount of protein lysates was separated by 8%–12% SDS-PAGE gel. After that, protein was transferred onto a nitrocellulose membrane. Membranes were blocked for 30 min and washed with Tris buffered saline (TBS) for three times and probed overnight at 4 °C with the antibody against SLC2A1 (Abcam, Shanghai, China) and β-actin (Sigma, Shanghai, China). The membranes were incubated for 1 h at room temperature with a 1:1000 dilution of secondary antibody (Invitrogen, Carlsbad, CA, USA). After that, the membranes were washed with TBS for three times. Finally, the signals were detected by Odyssey Infrared Imaging system (LI-COR Biosciences, Lincoln, NE, USA).

4.5. Lentirival Transduction

Lentivirus-containing supernatant was collected at 48 h after transfection in HEK-293T cells with the pLKO.1-TRC (FulenGen, Guangzhou, China) vector and CD510B-GLUT1 and packaging plasmids (Ppack) including VSV, REV and GAG, 0.2 μm filtered, and snap frozen at −80 °C. MGC-803 and MKN28 cells were infected with 2 mL of lentivirus for 8 h. Cells were selected in puromycin (Sigma) for one week.

4.6. Cell Proliferation Assay

Cell growth rate was measured by cell counting kit-8 (CCK-8, Dojindo, Shanghai, China). Briefly, 3000 cells per well were seeded into a 96-well plate and cultured overnight. At 24, 48, 72, and 96 h, cell viability was obtained at 450 nm wavelength and each sample was measured in triplicate to ensure quantitative accuracy.

4.7. Tumor Xenograft

For *in vivo* tumorigenicity assays, nude mice (6-week-old) were injected subcutaneously with 5×10^6 SLC2A1-expressing or vector-expressing MGC-803 or MKN28 cells in 0.1 mL volume of PBS. Each week after injection, Tumor size was monitored using micrometer calipers, and tumor volume was calculated as follows: Volume = length × $(\text{width})^2/2$. After 4 weeks, the mice were sacrificed and the tumors were dissected. Animal experiments were performed in full accordance with the Medicine Institutional Guidelines of Shanghai Jiaotong University.

4.8. Cell Invasion Assay

The invasive ability of gastric cancer cells was measured by Transwell model (Coster, Cambridge, MA, USA) according to the manufacturer's instructions. Briefly, 2×10^4 cells in 100 μL Roswell Park Memorial Institute-1640 (PRMI-1640) medium were seeded into the upper compartment coated with 100 μL matrigel (BD Bioscience, San Diego, CA, USA). The lower chambers were filled with 700 μL of RPMI-1640 medium containing 5% FBS. After the cells were incubated for 48 h, the non-invading cells that remained on the upper surface were removed and fixed with methanol and stained with hematoxylin. Each plate was measured five predetermined fields to ensure quantitative accuracy.

4.9. 3H-2-Deoxyglucose Transport Assay

Cells were incubated in glucose-free Dulbecco's modified eagle's medium (DMEM) and then pulsed with 2 μCi of 3H-2-deoxyglucose (~60 pmol) (PerkinElmer, Nanjing, China) for 10 min. The monolayers were quantitated by liquid scintillation counting. The data is presented as counts per minute (CPM) per μg DNA.

4.10. Measurement of Pyruvate, Lactate and Glucose

Cells were cultured in 24 well plates for 24 h. Pyruvate and lactate production was measured by the enzymetic method using a commercially available fluorescence-based assay kit (Invitrogen). The glucose in the conditioned media was quantified using the Glucose Assay kit (Sigma). Quantities of glucose consumed were normalized to the DNA content of each well and triplicate samples were analyzed.

4.11. Statistical Analysis

The SPSS software program (version 17.0; IBM Corporation, Armonk, NY, USA) was used for statistical analysis and Graphical representations were performed with GraphPad Prism 5 (GraphPad Software Inc., San Diego, CA, USA) software. The chi-square test and student's *t*-test were used for

comparison between groups. All data are presented as the means ± SD and p values less than 0.05 were considered statistically significant.

Acknowledgments

This work was supported by National Natural Science Foundation of China (No. 81071888, 81070344, 81070322 and 81270491), the National Key Basic Research Project (No. 2012CB517501), the 100-Talents Program of the Shanghai Municipal Health Bureau, (No. XBR2011007), Cross Research Fund of Shanghai Jiaotong University Biomedical Engineering (No. YG2012MS37) and Shanghai Natural Science Foundation (No. 13ZR1426700).

Author Contributions

Jiangao Fan conceived and designed the experiments; Shiyan Yan and Yuqin Wang performed the experiments; Meimei Chen analyzed the data; Guangming Li contributed reagents/materials/analysis tools; Jiangao Fan wrote the paper.

Conflicts of Interest

The authors declare no conflict of interest.

References

1. Torre, L.A.; Bray, F.; Siegel, R.L.; Ferlay, J.; Lortet-Tieulent, J.; Jemal, A. Global cancer statistics, 2012. *CA Cancer J. Clin.* **2015**, *65*, 87–108.
2. Terry, M.B.; Gaudet, M.M.; Gammon, M.D. The epidemiology of gastric cancer. *Semin. Radiat. Oncol.* **2002**, *12*, 111–127.
3. Brenner, H.; Rothenbacher, D.; Arndt, V. Epidemiology of stomach cancer. *Methods Mol. Biol.* **2009**, *472*, 467–477.
4. Hanahan, D.; Weinberg, R.A. Hallmarks of cancer: The next generation. *Cell* **2011**, *144*, 646–674.
5. Warburg, O. On the origin of cancer cells. *Science* **1956**, *123*, 309–314.
6. Asgari, Y.; Zabihinpour, Z.; Salehzadeh-Yazdi, A.; Schreiber, F.; Masoudi-Nejad, A. Alterations in cancer cell metabolism: The Warburg effect and metabolic adaptation. *Genomics* **2015**, *105*, 275–281.
7. Kunkel, M.; Reichert, T.E.; Benz, P.; Lehr, H.A.; Jeong, J.H.; Wieand, S.; Bartenstein, P.; Wagner, W.; Whiteside, T.L. Overexpression of Glut-1 and increased glucose metabolism in tumors are associated with a poor prognosis in patients with oral squamous cell carcinoma. *Cancer* **2003**, *97*, 1015–1024.
8. Sun, L.; Zeng, X.; Yan, C.; Sun, X.; Gong, X.; Rao, Y.; Yan, N. Crystal structure of a bacterial homologue of glucose transporters GLUT1–4. *Nature* **2012**, *490*, 361–366.
9. Sasaki, H.; Shitara, M.; Yokota, K.; Hikosaka, Y.; Moriyama, S.; Yano, M.; Fujii, Y. Overexpression of GLUT1 correlates with Kras mutations in lung carcinomas. *Mol. Med. Rep.* **2012**, *5*, 599–602.

10. Amann, T.; Maegdefrau, U.; Hartmann, A.; Agaimy, A.; Marienhagen, J.; Weiss, T.S.; Stoeltzing, O.; Warnecke, C.; Scholmerich, J.; Oefner, P.J.; *et al*. GLUT1 expression is increased in hepatocellular carcinoma and promotes tumorigenesis. *Am. J. Pathol.* **2009**, *174*, 1544–1552.
11. Wachi, S.; Yoneda, K.; Wu, R. Interactome-transcriptome analysis reveals the high centrality of genes differentially expressed in lung cancer tissues. *Bioinformatics* **2005**, *21*, 4205–4208.
12. Krzeslak, A.; Wojcik-Krowiranda, K.; Forma, E.; Jozwiak, P.; Romanowicz, H.; Bienkiewicz, A.; Brys, M. Expression of GLUT1 and GLUT3 glucose transporters in endometrial and breast cancers. *Pathol. Oncol. Res.* **2012**, *18*, 721–728.
13. Noguchi, Y.; Saito, A.; Miyagi, Y.; Yamanaka, S.; Marat, D.; Doi, C.; Yoshikawa, T.; Tsuburaya, A.; Ito, T.; Satoh, S. Suppression of facilitative glucose transporter 1 mRNA can suppress tumor growth. *Cancer Lett.* **2000**, *154*, 175–182.
14. Kawamura, T.; Kusakabe, T.; Sugino, T.; Watanabe, K.; Fukuda, T.; Nashimoto, A.; Honma, K.; Suzuki, T. Expression of glucose transporter-1 in human gastric carcinoma: Association with tumor aggressiveness, metastasis, and patient survival. *Cancer* **2001**, *92*, 634–641.
15. De Martel, C.; Forman, D.; Plummer, M. Gastric cancer: Epidemiology and risk factors. *Gastroenterol. Clin. N. Am.* **2013**, *42*, 219–240.
16. Patru, C.L.; Surlin, V.; Georgescu, I.; Patru, E. Current issues in gastric cancer epidemiology. *Rev. Med. Chir. Soc. Med. Nat. Iasi* **2013**, *117*, 199–204.
17. Kawaguchi, T.; Komatsu, S.; Ichikawa, D.; Kubota, T.; Okamoto, K.; Konishi, H.; Shiozaki, A.; Fujiwara, H.; Otsuji, E. Clinical significance of chemotherapy for geriatric patients with advanced or recurrent gastric cancer. *Mol. Clin. Oncol.* **2015**, *3*, 83–88.
18. Manel, N.; Kim, F.J.; Kinet, S.; Taylor, N.; Sitbon, M.; Battini, J.L. The ubiquitous glucose transporter GLUT-1 is a receptor for HTLV. *Cell* **2003**, *115*, 449–459.
19. Augustin, R. The protein family of glucose transport facilitators: It's not only about glucose after all. *IUBMB Life* **2010**, *62*, 315–333.
20. Jansson, T.; Wennergren, M.; Illsley, N.P. Glucose transporter protein expression in human placenta throughout gestation and in intrauterine growth retardation. *J. Clin. Endocrinol. Metab.* **1993**, *77*, 1554–1562.
21. Vardhana, P.A.; Illsley, N.P. Transepithelial glucose transport and metabolism in BeWo choriocarcinoma cells. *Placenta* **2002**, *23*, 653–660.
22. Barta, E.; Drugan, A. Glucose transport from mother to fetus—A theoretical study. *J. Theor. Biol.* **2010**, *263*, 295–302.
23. Kang, S.S.; Chun, Y.K.; Hur, M.H.; Lee, H.K.; Kim, Y.J.; Hong, S.R.; Lee, J.H.; Lee, S.G.; Park, Y.K. Clinical significance of glucose transporter 1 (GLUT1) expression in human breast carcinoma. *Jpn. J. Cancer Res.* **2002**, *93*, 1123–1128.
24. Schmidt, M.; Voelker, H.U.; Kapp, M.; Krockenberger, M.; Dietl, J.; Kammerer, U. Glycolytic phenotype in breast cancer: Activation of Akt, up-regulation of GLUT1, TKTL1 and down-regulation of M2PK. *J. Cancer Res. Clin. Oncol.* **2010**, *136*, 219–225.
25. Younes, M.; Brown, R.W.; Mody, D.R.; Fernandez, L.; Laucirica, R. GLUT1 expression in human breast carcinoma: Correlation with known prognostic markers. *Anticancer Res.* **1995**, *15*, 2895–2898.

26. Goldman, N.A.; Katz, E.B.; Glenn, A.S.; Weldon, R.H.; Jones, J.G.; Lynch, U.; Fezzari, M.J.; Runowicz, C.D.; Goldberg, G.L.; Charron, M.J. GLUT1 and GLUT8 in endometrium and endometrial adenocarcinoma. *Mod. Pathol.* **2006**, *19*, 1429–1436.
27. Kim, W.S.; Kim, Y.Y.; Jang, S.J.; Kimm, K.; Jung, M.H. Glucose transporter 1 (GLUT1) expression is associated with intestinal type of gastric carcinoma. *J. Korean Med. Sci.* **2000**, *15*, 420–424.
28. Wei, B.; Chen, L.; Li, J. Expression of glucose transporter 1 in gastric carcinoma and metastatic lymph nodes and its association with prognosis. *Zhonghua Wei Chang Wai Ke Za Zhi* **2009**, *12*, 277–280.
29. Ooi, A.T.; Gower, A.C.; Zhang, K.X.; Vick, J.L.; Hong, L.; Nagao, B.; Wallace, W.D.; Elashoff, D.A.; Walser, T.C.; Dubinett, S.M.; *et al*. Molecular profiling of premalignant lesions in lung squamous cell carcinomas identifies mechanisms involved in stepwise carcinogenesis. *Cancer Prev. Res. (Phila)* **2014**, *7*, 487–495.
30. Sreekumar, A.; Poisson, L.M.; Rajendiran, T.M.; Khan, A.P.; Cao, Q.; Yu, J.; Laxman, B.; Mehra, R.; Lonigro, R.J.; Li, Y.; *et al*. Metabolomic profiles delineate potential role for sarcosine in prostate cancer progression. *Nature* **2009**, *457*, 910–914.

© 2015 by the authors; licensee MDPI, Basel, Switzerland. This article is an open access article distributed under the terms and conditions of the Creative Commons Attribution license (http://creativecommons.org/licenses/by/4.0/).

Int. J. Mol. Sci. **2015**, *16*, 16469-16482; doi:10.3390/ijms160716469

OPEN ACCESS
International Journal of
Molecular Sciences
ISSN 1422-0067
www.mdpi.com/journal/ijms

Article

Sinulariolide Suppresses Human Hepatocellular Carcinoma Cell Migration and Invasion by Inhibiting Matrix Metalloproteinase-2/-9 through MAPKs and PI3K/Akt Signaling Pathways

Yu-Jen Wu [1,†], Choo-Aun Neoh [2,†], Chia-Yu Tsao [3], Jui-Hsin Su [3,4] and Hsing-Hui Li [3,4,*]

[1] Department of Beauty Science, Meiho University, Pingtung 91202, Taiwan; E-Mail: x00002180@meiho.edu.tw

[2] Department of Research, Pingtung Christian Hospital, Pingtung 90059, Taiwan; E-Mail: neohca@gmail.com

[3] Graduate Institute of Marine Biotechnology, National Dong Hwa University, Pingtung 94450, Taiwan; E-Mails: tsao-chiayu@umail.hinet.net (C.-Y.T.); x2219@nmmba.gov.tw (J.-H.S.)

[4] Industry Academia Collaboration Center, National Museum of Marine Biology and Aquarium, Pingtung 94450, Taiwan

† These authors contributed equally to this work.

* Author to whom correspondence should be addressed; E-Mail: hhli@nmmba.gov.tw; Tel.: +886-8-882-4632; Fax: +886-8-882-5087.

Academic Editor: William Chi-shing Cho

Received: 2 June 2015 / Accepted: 13 July 2015 / Published: 20 July 2015

Abstract: Sinulariolide is an active compound isolated from the cultured soft coral *Sinularia flexibilis*. In this study, we investigate the migration and invasion effects of sinulariolide in hepatocellular carcinoma cell HA22T. Sinulariolide inhibited the migration and invasion effects of hepatocellular carcinoma cells in a concentration-dependent manner. The results of zymography assay showed that sinulariolide suppressed the activities of matrix metalloproteinase (MMP)-2 and MMP-9. Moreover, protein levels of MMP-2, MMP-9, and urokinase-type plasminogen activator (uPA) were reduced by sinulariolide in a concentration-dependent manner. Sinulariolide also exerted an inhibitory effect on phosphorylation of c-Jun N-terminal kinase (JNK), extracellular signal-regulated kinases (ERK), phosphatidylinositol 3-kinase (PI3K), Akt, Focal adhesion kinase (FAK),

growth factor receptor-bound protein 2 (GRB2). Taken together, these results demonstrated that sinulariolide could inhibit hepatocellular carcinoma cell migration and invasion and alter HA22T cell metastasis by reduction of MMP-2, MMP-9, and uPA expression through the suppression of MAPKs, PI3K/Akt, and the FAK/GRB2 signaling pathway. These findings suggest that sinulariolide merits further evaluation as a chemotherapeutic agent for human hepatocellular carcinoma.

Keywords: hepatocellular carcinoma (HCC); *Sinularia flexibilis*; sinulariolide; matrix metalloproteinase-2/-9; migration; invasion

1. Introduction

Hepatocellular carcinoma (HCC) is a highly lethal cancer, ranks as the fifth leading cause of cancer death worldwide, which receives much public health attention [1]. HCC presents as an aggressive tumor type and the median survival after diagnosis is only 6 to 20 months [2,3]. More than half a million new cases are discovered each year, and the incidence in patients with cirrhosis ranges from 2.5%–7% [4]. Standard treatment options of HCC include surgical resection, liver transplantation, transarterial chemoembolization (TACE), percutaneous ethanol injection (PEI), radiofrequency ablation (RF), and target therapy, depending on cancer stage and suitable candidates [5]. The side effects of chemotherapy agents remain a major concern of these aggressive treatment options. Therefore, the potential agents for the treatment of hepatocellular carcinoma agents with fewer side effects are urgently needed in clinicals. Accordingly, therapy strategies focus on inhibiting growth of existing tumors, and blocking cancer cell invasion and metastasis.

Malignant tumor progression depends upon the ability of invasion and metastasis. Invasion and metastasis are principal characteristics of malignancy with poor clinical outcomes. Matrix metalloproteinase (MMP)-2 and -9 are proteolytic enzymes that are highly expressed in hepatocellular carcinoma [6]. These enzymes function to degrade the environmental extracellular matrix (ECM) and the basement membrane. The activity of MMPs is inhibited by endogenous tissue inhibitor of metalloproteinases (TIMPs), which are specific inhibitors of MMPs, and the imbalance between MMPs and TIMPs contribute to the degradation or deposition of the ECM. MMPs and TIMPs play an important role in hepatocellular carcinoma invasion by degrading extracellular matrix proteins [7]. Mitogen-activated protein kinases (MAPKs) play an important regulatory role in cell growth, differentiation, apoptosis, and metastasis [8]. In addition, the phosphatidylinositol-3-kinase (PI3K)/Akt signal transduction pathway is involved in the development, progression, and metastasis of various tumors [9–12].

The therapeutic applications of natural products isolated from marine soft corals have been widely investigated [13–16]. Several compounds such as diterpenes, diterpenoids, and prostanoids have been isolated from soft corals. Despite their unknown mechanisms, these compounds have been reported to exhibit the anti-cancer effects through the induction of apoptosis and cytotoxic against different cancer cell lines, such as prostate, breast, colon, melanoma, liver, oral cancer and cervical cell lines [17–28]. Sinulariolide, an active compound isolated from the cultured soft coral *Sinularia flexibilis* [15] has

various biological properties, including anti-microbial and anti-cancer activities, particularly in bladder cancer, hepatocellular carcinoma, and melanoma [22,29,30]. In the current research, we will evaluate the molecular mechanism inhibiting human HCC by sinulariolide. Overall, these results could provide valuable information for drug development or potential strategies against human HCC.

2. Results

2.1. Sinulariolide Inhibited Migration and Invasion of HA22T Cells

Cell matrix interaction and cell motility are important for cancer cell metastasis. To examine the potential anti-metastasis effects of sinulariolide, migration and invasion assays were performed in HA22T cells. The results indicated that HA22T cells were inhibited by sinulariolide in a concentration-dependent manner. Moreover, HA22T cells treated with 8 μg/mL sinulariolide for 24 and 48 h, the migratory abilities were reduced by 50% and 78% (Figure 1a,b), and invasive abilities were reduced by 80% and 84%, respectively (Figure 2). Monolayer scratch assays also supported that sinulariolide inhibited the migratory potential of HA22T cells (Figure 1c). These results suggest that sinulariolide is an inhibitor of hepatoma cells in migration and invasion.

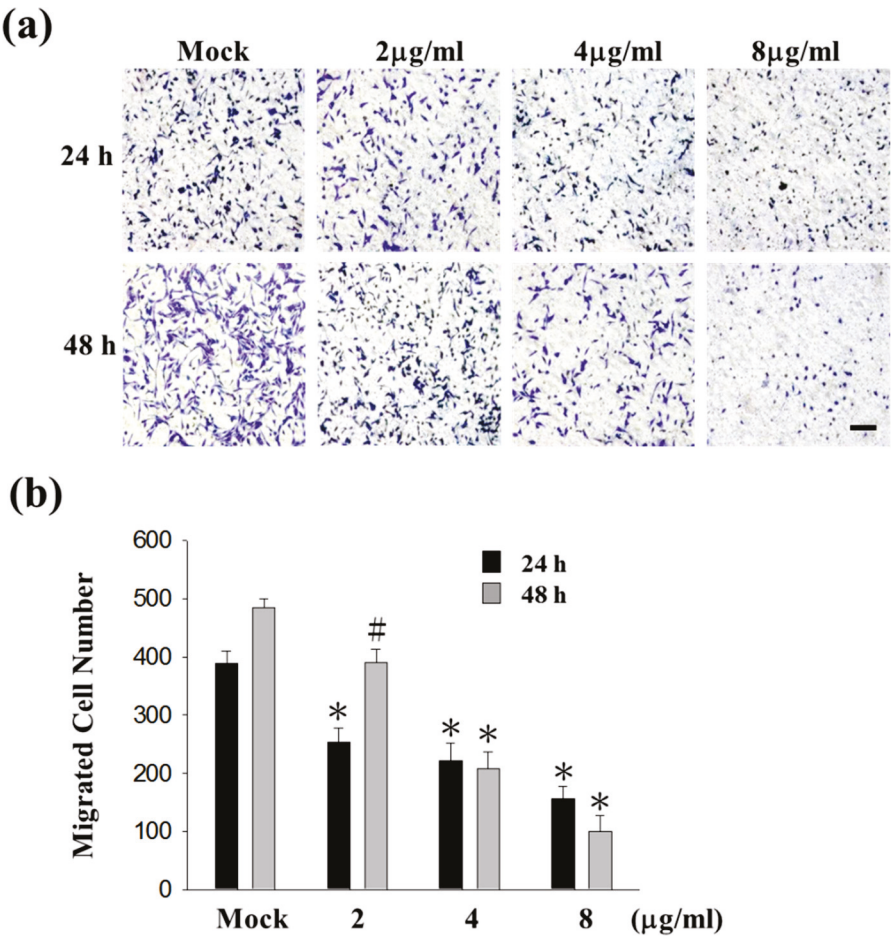

Figure 1. *Cont.*

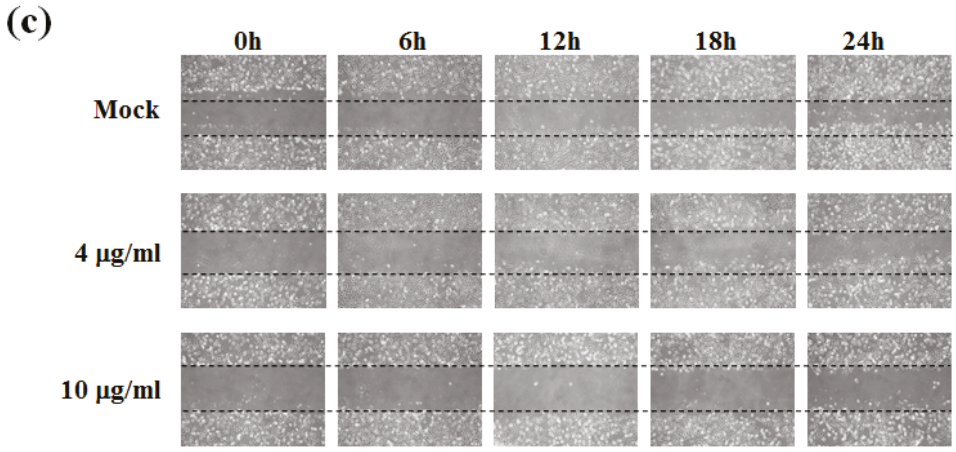

Figure 1. The anti-migratory effects of sinulariolide in HA22T cells. (**a**) After 24 and 48 h treating with sinulariolide, migrated HA22T cells were clearly reduced compared to control cells at the 100× magnification vision. The results shown are representative of three independent experiments. Scale bars = 20 μm. Mock: control, the DMSO-treated cell; (**b**) Quantitative analysis of figure (**a**) showed that sinulariolide dose-dependently suppresses HA22T cell migration (# $p < 0.05$, * $p < 0.001$ compared with the control); (**c**) Representative images of monolayer scratch assays supported that sinulariolide inhibited the migratory potential of HA22T cells.

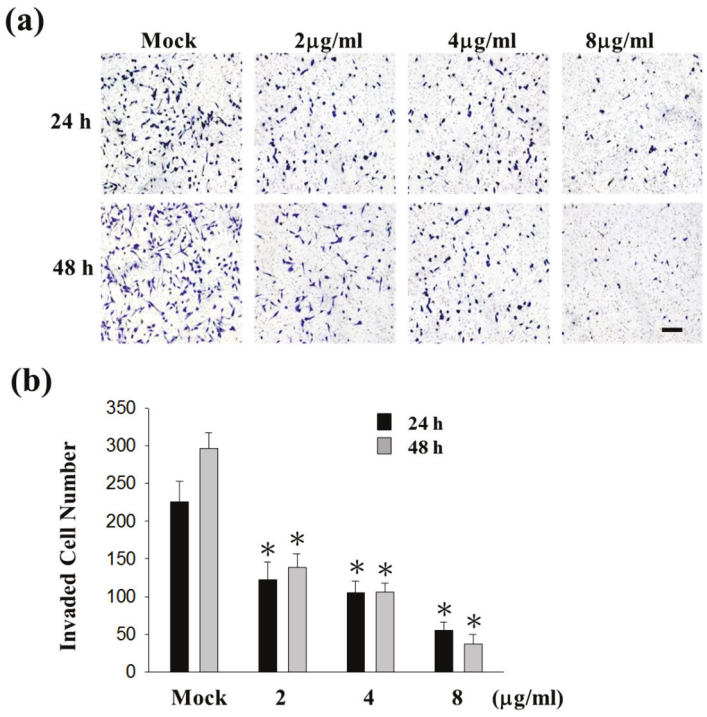

Figure 2. The anti-invasive effects of sinulariolide in HA22T cells. (**a**) After 24 and 48 h treating with sinulariolide, invaded HA22T cells were clearly reduced compared to control cells at the 100× magnification vision. The results shown are representative of three independent experiments. Scale bars = 20 μm. Mock: control, the DMSO-treated cell; (**b**) Quantitative analysis of figure (**a**) showed that sinulariolide dose-dependently suppresses HA22T cell invasion (* $p < 0.001$ compared with the control).

2.2. Sinulariolide Reduced the Matrix Metalloproteinase (MMP)-2/-9 Activities of HA22T Cells

To clarify whether the activity of MMP-2 and MMP-9 are involved in the invasion of HA22T cells, gelatin zymography assay was performed. The HA22T cells were incubated in serum-free media with sinulariolide (0, 2, 4, 6, 8 μg/mL) for 24 h, and the conditioned media were collected to analyze activities of MMP-2 and MMP-9. The result showed that sinulariolide reduced the activities of MMP-2 and MMP-9 in a conentration-dependent manner (Figure 3a).

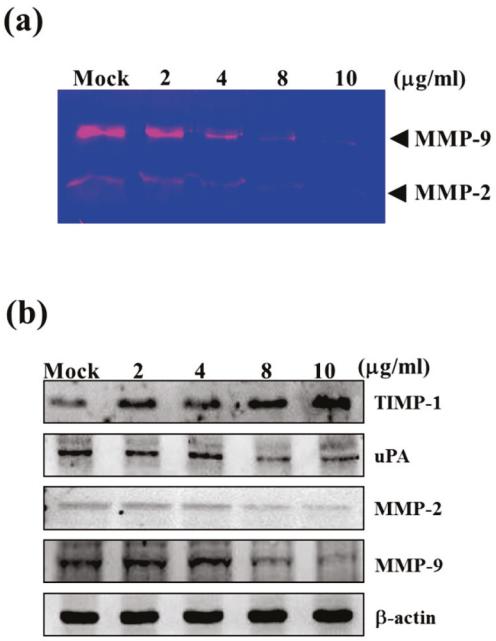

Figure 3. Effects of the MMP-2/-9 activities and protein levels in HA22T cells by sinulariolide. The HA22T cells were treated with different concentration of sinulariolide (0, 2, 4, 6, 8 μg/mL) for 24 h, and conditioned media and cell lysates were collected respectively for gelatin zymography assay and western blotting. (**a**) The gelatin zymography assay showed MMP-2/-9 activities were inhibited by sinulariolide in HA22T cells; (**b**) The MMP-2/-9 related proteins were validated, including TIMP-1, uPA, MMP-2, and MMP-9. The protein levels of MMP-2/-9 and uPA were decreased, but TIMP-1 was increased in HA22T cells. β-Actin was used as the internal control. Mock: control, the DMSO-treated cell.

2.3. Sinulariolide Down-Regulated Protein Levels of MMP-2, MMP-9, and uPA, but Increased Protein Levels of TIMP-1

The physiological activities of MMP-2 and MMP-9 are significantly related to TIMP and the urokinase-type plasminogen activator (uPA), which was involved in the invasiveness, metastasis, and prognosis of HCC [31]. The regulation of sinulariolide on the protein levels of MMP-2, MMP-9, TIMP-1 and uPA were determined by western blotting assay. The protein levels of MMP-2, MMP-9 and uPA were decreased in HA22T cells after treating with sinulariolide for 24 h, but TIMP-1 was increased (Figure 3b). The up-regulation of TIMP-1 protein levels and down-regulation of uPA may be a possible alternative strategy for the inhibition of MMP activity, with the added benefit of

anti-invasion activity. We conclude that the inhibitory effect of MMP-2 and MMP-9 in HA22T cells by sinulariolide may be through the regulating of uPA and TIMP-1.

2.4. Sinulariolide Inhibited MAPKs and PI3K/Akt Signaling Pathway Related Molecules

To elucidate the signaling pathways of sinulariolide in HA22T cells, the proteins involved in the MAPKs and PI3K/Akt signaling pathways were investigated by Western blotting assay, including p38, p-p38, ERK, p-ERK, JNK, p-JNK, c-jun, p-c-jun, PI3K, p-PI3K, Akt, p-Akt, mTOR and p-mTOR proteins. All the phosphorylation protein levels were decreased in HA22T cells after treating with sinulariolide, but others had no change (Figure 4). These results show that the inhibitory effect of sinulariolide may be through the MAPKs and PI3K/Akt signaling pathways.

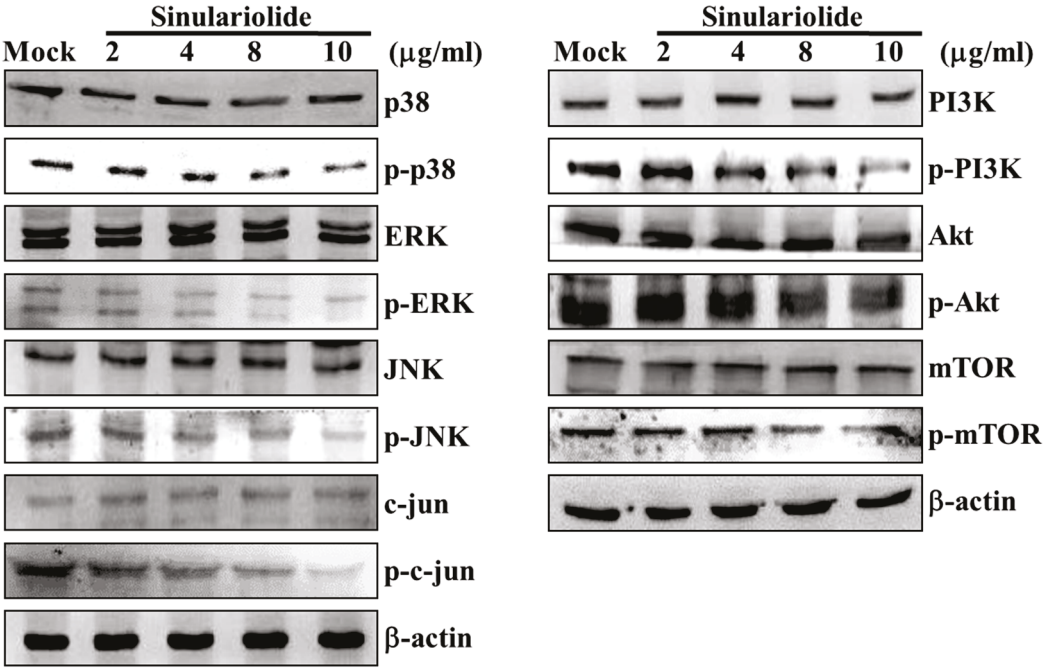

Figure 4. The effects of sinulariolide on MAPKs and PI3K/Akt signaling pathways. The HA22T cells were treated with different concentration of sinulariolide (0, 2, 4, 8, 10 μg/mL), and cell lysates were collected for western blotting assay. The MAPKs and PI3K/Akt related proteins were validated, including p38, p-p38, ERK, p-ERK, JNK, p-JNK, c-jun, p-c-jun, PI3K, p-PI3K, Akt, p-Akt, mTOR and p-mTOR. Sinulariolide inhibited seven phosphorylation protein levels in HA22T cells. β-Actin was used as the internal control. Mock: control, the DMSO-treated cell.

2.5. Sinulariolide Inhibited GRB2 and FAK Signaling Pathways

Focal adhesion kinase (FAK) is a key mediator of signaling by integrins, a major family of cell surface receptors for extracellular matrix. FAK also plays a prominent role in tumor progression and metastasis through its regulation of both cancer cells and their microenvironments including cancer cell migration, invasion, epithelial to mesenchymal transition, and angiogenesis [32]. Growth factor receptor-bound protein 2 (GRB2) is a key molecule in intracellular signal transduction, and its signaling is critical for cell cycle progression, actin-based cell motility, epithelial morphogenesis,

angiogenesis and vasculogenesis. These functions make GRB2 become a key molecules involved in spreading of solid tumors through invasion and metastasis [33].

To elucidate if the sinulariolide inhibit cell migration through GRB2 and FAK signaling pathway in HA22T cells, we examined the molecules that were involved in the GRB2 and FAK signaling pathway, including MEKK3, MEKK7, FAK, GRB2, Ras, and RhoA by Western blotting assay. All the protein levels were decreased in HA22T cells after treating with sinulariolide (Figure 5). These results suggest that sinulariolide suppress cell migration might through inhibiting GRB2 and FAK signaling pathways.

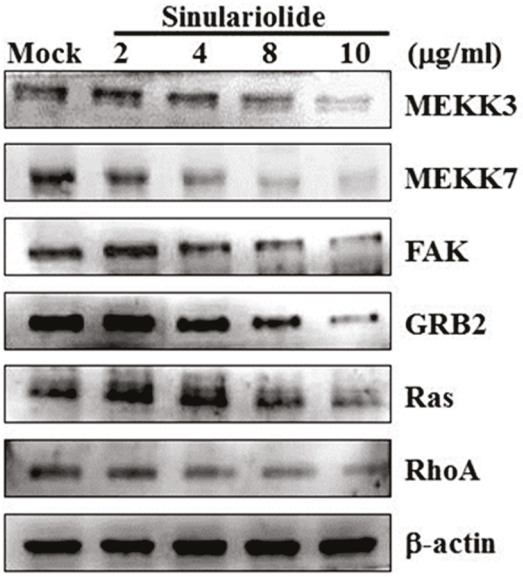

Figure 5. The effects of sinulariolide on GRB2 and FAK signaling pathways. The HA22T cells were treated with different concentration of sinulariolide (0, 2, 4, 8, 10 μg/mL), and cell lysates were collected for Western blotting assay. The GRB2 and FAK related proteins were validated, including MEKK3, MEKK7, FAK, GRB2, Ras, and RhoA. All the protein levels were all decreased after being treated by sinulariolide in HA22T cells. β-Actin was used as the internal control. Mock: control, the DMSO-treated cell.

3. Discussion

3.1. Sinulariolide Inhibits Hepatocarcinoma Cell Metastasis and Induces Apoptosis

Metastasis is responsible for more than 90% of cancer-related mortality [34]. A critical step in tumor metastasis is the degradation of basement membrane, which is catalyzed by proteolytic enzymes, such as MMPs and TIMPs [35,36]. We found that down-regulation of MMP-2 and MMP-9 via MAPKs and PI3K/Akt signaling pathways were required in the sinulariolide-mediated invasion of hepatocarcinoma cells. In our previous report, sinulariolide exerted the cell cytotoxic on four hepatocarcinoma cell lines (Huh7, HepG2, Hep3B, and HA22T) and apoptosis-induced effects through a mitochondria-related pathway on HA22T cells [29]. In another word, sinulariolide can induced hepatocarcinoma cell apoptosis and inhibit hepatocarcinoma cell metastasis at the same time.

Comprehensively, the marine compound sinulariolide has strong potential to be a pharmaceutical of human hepatocarcinoma cancer through inhibiting metastasis and induced apoptosis.

3.2. Sinulariolide Inhibits Multiple Signaling Pathways in HCC

FAK is overexpressed in many HCC specimens and is required for c-Met/β-catenin-driven hepatocarcinogenesis. Inhibition of FAK provides a potential strategy to treat HCC [37]. The clinical validation showed that the expression levels of both GRB2 and GAB1 proteins were significantly higher in HCC tissues than those in their adjacent non-neoplastic tissues. Moreover, the combined GRB2 and GAB1 protein expression was significantly associated with aggressive tumor progression and poor prognosis in patients with HCC. These results showed that GRB2 is a key molecule in HCC and GRB2 may be strongly related to tumor progression and prognosis in patients with HCC [38]. The uPA plays important roles with regard to HCC progression and metastasis [39]. The uPA is capable of degrading cancer tissue and the surrounding ECM and also modulate several biological processes including: cell adhesion, migration, proliferation, and gene expression under various physiological and pathological conditions. Previous studies have also demonstrated that uPA is up-regulated in human tumoral liver tissue. High level of uPA expression is related to reduce patient survival and can be considered a poor prognosis marker for HCC patients [40,41].

The three molecules (FAK, GRB2, and uPA) and related singling pathways play important role in regulating metastasis of HCC. Sinulariolide, an active compound isolated from the cultured soft coral *Sinularia flexibilis* had strong potential to be a therapeutic drug for HCC through regulating the three molecules and related singling pathways.

3.3. Sinulariolide Inhibits Hepatocarcinoma Cell Metastasis through Multiple Signaling Pathways

Figures 1 and 2 show that 2 and 4 μg/mL of sinulariolide inhibit approximately 50% cell migration and invasion of HA22T cells, but the metastasis pathway related molecules such as p-p38, p-ERK, p-JNK, p-c-jun, p-PI3K, MMP-2, MMP-9, MEKK3, MEKK7, FAK, and GRB2 (Figures 3–5) show obvious inhibition by sinulariolide at the dose of 8 and 10 μg/mL. It suggested that sinulariolide inhibits hepatocarcinoma cell migration and invasion through multiple signaling pathways, not only MAPKs and PI3K/Akt signaling pathways. The overall results infer that sinulariolide inhibits cell metastasis and induces cell apoptosis, and the signaling pathways are complicated and need more work to resolve them.

3.4. Both Sinulariolide and 11-epi-Sinulariolide Acetate Inhibits Hepatocellular Carcinoma

Our previous paper showed that 11-epi-sinulariolide acetate reduced cell migration and invasion in human hepatocellular carcinoma [42]. Eleven-epi-sinulariolide acetate and sinulariolide both isolated from soft coral *Sinularia flexibilis*, and they have a similar backbone. The substitute group in C-11 is hydroxyl group in sinulariolide, but 11-epi-sinulariolide acetate was determined to be 11-epi-acetyl derivative of sinulariolide. In addition, 5.32 μM 11-epi-sinulariolide acetate inhibits about 40% cell migration in HA22T [42], and 4 μg/mL (11.97 μM) sinulariolide have a similar effect (Figure 1b). It means that 11-epi-sinulariolide acetate had stronger inhibitory effects in HA22T. However, the yield

of sinulariolide is much higher than 11-epi-sinulariolide acetate. One kilogram (wet weight) of *Sinularia flexibilis* can extract 3–5 g sinulariolide, but only 30–50 mg of 11-epi-sinulariolide acetate. Considering the commercial drug exploration, sinulariolide has a higher economic value than 11-epi-sinulariolide acetate. Sinulariolide has a higher potential as a therapeutic drug for human hepatocellular carcinoma.

4. Experimental Section

4.1. Materials and Chemical Reagents

Rabbit anti-human mitogen-activated focal adhesion kinase (FAK), protein kinase kinase3 (MKK3), MAPK kinase kinasekinase4 (MEKK4), Rho A, growth factor receptor-bound protein 2 (GRB2), mTOR and p-mTOR antibodies were obtained from Epitomics (Burlingame, CA, USA). Rabbit anti-human TIMP-1, Akt and p-Akt antibodies were obtained from ProteinTech Group (Chicago, IL, USA). Rabbit anti-human uPA, matrix metalloproteinase-2 (MMP-2), matrix metalloproteinase-9 (MMP-9), extracellular signal regulated kinases (ERK), phosphorylated extracellular signal regulated kinases (p-ERK), c-jun N-terminal kinase (JNK), p-JNK, c-jun, p-c-jun, p38, p-p38, phosphoinositide 3-kinases (PI3K) and phosphorylated-phosphoinositide 3-kinases (p-PI3K) antibodies were obtained from cell signaling technology (Danvers, MA, USA). Dimethyl sulfoxide (DMSO), protease inhibitor cocktail, and rabbit anti-human β-actin antibodies were obtained from Sigma (St. Louis, MO, USA). PVDF (polyvinylidene difluoride) membranes and goat anti-rabbit and horseradish peroxidase conjugated IgG were obtained from Millipore (Bellerica, MA, USA). Chemiliminescent HRP substrate was purchased from Pierce (Rockford, IL, USA). Sinulariolide was isolated from the cultured soft coral *Sinularia flexibilis*, following the protocol by Hsieh *et al.* [15], and dissolved in DMSO.

4.2. Cell Culture

HA22T cells were purchased from Food Industry Research and Development Institute (Hsinchu, Taiwan) and were cultured in (Dulbecco's Modified Eagle's medium) DMEM (Biowest, Nuaillé, France) containing 4 mM L-glutamine, 1 mM sodium pyruvate, 100 μg/mL streptomycin, 100 U/mL penicillin and 10% (*v*/*v*) fetal bovine serum, in a 37 °C humidified atmosphere with 5% CO_2.

4.3. Cell Migration Assay

Cell migration assay was assayed according to the methods described by Su *et al.* [21]. HA22T cells were seeded onto a Boyden chamber (Neuro Probe, Cabin John, MD, USA) at 10^4 cells/well in serum-free media for 24 h. HA22T cells were than incubated with different concentration of sinulariolide (0, 2, 4, and 8 μg/mL) and were allowed to migrate for 24 h. The migrated cells on the lower site were fixed by 100% methanol and then stained with 5% Giemsa (Merck, Darmstadt, Germany). Cell numbers were observed and counted at 100× light microscope.

4.4. Wound Healing Assay

To determine cell motility, HA22T cells were seeded in a 12-well tissue culture plate. After one day, the center of the cell monolayers was scraped with a sterile micropipette tip to create a straight zone (gap) of constant width. Then, each well was washed with Phosphate-buffered saline (PBS), and HA22T cells were exposed to various concentrations of sinulariolide (0, 4, and 10 μg/mL). Wound closure was monitored and photographed at 0, 6, 12 and 18 h with a Nikon inverted microscope.

4.5. Gelatin Zymography Assay

HA22T cells (1×10^5 cells/well) cultured in 12-well plates were incubated in serum-free DMEM with different concentration of sinulariolide (0, 2, 4, 8, 10 μg/mL). After 24 h, MMPs released from HA22T cells and the conditioned medium was assayed using gelatin zymography (8% zymogram gelatin gels) according to the methods reported by Huang *et al.*, with some modification [37,38]. Briefly, the culture medium was electrophoresed in a sodium dodecyl sulfate polyacrylamide gel electrophoresis (SDS-PAGE) gel containing 0.2% gelatin. The gel was then washed twice in a wash buffer (100 mM NaCl and 2.5% Triton X-100 in 50 mM Tris-HCl, pH 7.5) and subsequently transferred to a reaction buffer (200 mM NaCl, 0.02% NaN_3, 1 μM $ZnCl_2$, 1 mM $CaCl_2$, 2% Triton-X 100, in 50 mM Tris-HCl, pH 7.5) for enzymatic reaction at 37 °C with shaking overnight. Finally, the gel was stained with Coomassie blue, and destained in 10% acetic acid (*v*/*v*) and 20% methanol (*v*/*v*) and quantified using Image J software (http://imagej.nih.gov/ij/).

4.6. Cell Invasion Assay

HA22T cells were suspended in serum-free DMEM, and added to the upper chamber of the transwell chamber coating with Matrigel. The DMEM with different concentration of sinulariolide (0, 2, 4, and 8 μg/mL) was added to the lower chamber. Cells were then incubated for 24 and 48 h and fixed in neutral formalin. The Matrigel and cells in upper chamber were removed, followed by Giemsa staining. Several fields were randomly selected under a light microscope followed by cell counting to determine the extent of invasion.

4.7. Western Blot Analysis

The treated samples and the control samples (25 μg) were separated by 12.5% SDS-PAGE, and then transferred onto PVDF membrane for 1.5 h at 400 mA using Transphor TE 62 (Hoeffer) and then proteins transfer checked by staining with Ponceau S solution. The membranes were incubated with 5% dehydrated skim milk to block nonspecific protein bindings, and then incubated with primary antibodies at 4 °C overnight. The primary anti-human TIMP-1, uPA, MMP-2, MMP-9, p38, p-p38, ERK, p-ERK, JNK, p-JNK, c-jun, p-c-jun, PI3K, p-PI3K, Akt, p-Akt, mTOR, p-mTOR, MEKK3, MEKK7, FAK, GRB2, Ras, RhoA, and β-actin antibodies were used. The second antibodies (horseradish peroxidase conjugate goat anti-rabbit, 1:5000 in blocking solution) were added and incubated for 2 h at 4 °C and then visualized using chemiluminesence (Pierce Biotechnology, Rockford, IL, USA).

4.8. Statistical Analysis

Data of cell migration assay and invasion assay were pooled from three independent experiments. The results were expressed as mean ± standard error of mean (SEM). Data acquisition and analysis of variance (ANOVA) was carried out by the Tukey-Kramer test, using GraphPad InStat 3 software (GraphPad Software, San Diego, CA, USA) to determine significant differences ($p \leq 0.05$) compare to experimental groups.

5. Conclusions

In conclusion, our results have established that natural marine compound sinulariolide possesses anti-cancer activity through the suppression of cell invasion and migration in HA22T cells. Gelatin zymography and Western blotting assay indicates MMP-2/-9 and related signal pathways were regulated through the cell metastasis progress. Overall, this study indicated that sinulariolide-inhibited cell metastasis can be summarized as shown in Figure 6. Sinulariolide-inhibited cell metastasis might be related to the suppression of the MAPKs and PI3K/Akt signaling pathways. Further, *in vivo* evaluation of the anti-metastasis activity of sinulariolide in an animal model is needed. Our study provides a potential therapeutic drug in hepatocellular carcinoma.

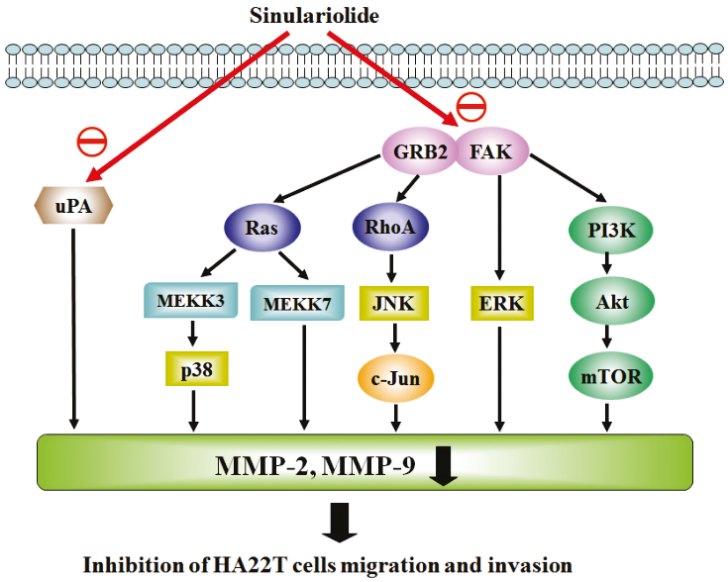

Figure 6. Proposed signaling pathways for sinulariolide-mediated inhibition of HA22T cell migration. The effect of sinulariolide is most likely achieved through the inhibition of FAK and GRB2, which regulates MMP-2/-9 expression through the MAPK and PI3K/Akt signaling pathways. Red arrows means sinulariolide inhibit the pathways. Black arrows means the upper molecules induced the following molecules.

Acknowledgments

This research was supported by grants from the National Museum of Marine Biology & Aquarium and the Ministry of Science and Technology (MOST 103-2320-B-291-001-MY3), Taiwan, awarded to Hsing-Hui Li and Jui-Hsin Su.

Author Contributions

Choo-Aun Neoh, and Chia-Yu Tsao performed the literature search and collected the data. Yu-Jen Wu, and Jui-Hsin Su performed the analysis and the interpretation of the results. Yu-Jen Wu, and Hsing-Hui Li conceived the project and supervised the work.

Conflicts of Interest

The authors declare no conflict of interest.

References

1. Siegel, R.; Ma, J.; Zou, Z.; Jemal, A. Cancer statistics, 2014. *CA Cancer J. Clin.* **2014**, *64*, 9–29.
2. Davar, D.; Tarhini, A.A.; Kirkwood, J.M. Adjuvant therapy for melanoma. *Cancer J.* **2012**, *18*, 192–202.
3. El-Serag, H.B.; Rudolph, K.L. Hepatocellular carcinoma: Epidemiology and molecular carcinogenesis. *Gastroenterology* **2007**, *132*, 2557–2576.
4. Montalto, G.; Cervello, M.; Giannitrapani, L.; Dantona, F.; Terranova, A.; Castagnetta, L.A. Epidemiology, risk factors, and natural history of hepatocellular carcinoma. *Ann. N. Y. Acad. Sci.* **2002**, *963*, 13–20.
5. Czaja, A.J. Current management strategies for hepatocellular carcinoma. *Minerva Gastroenterol. Dietol.* **2013**, *59*, 143–159.
6. Arii, S.; Mise, M.; Harada, T.; Furutani, M.; Ishigami, S.; Niwano, M.; Mizumoto, M.; Fukumoto, M.; Imamura, M. Overexpression of matrix metalloproteinase 9 gene in hepatocellular carcinoma with invasive potential. *Hepatology* **1996**, *24*, 316–322.
7. Terada, T.; Okada, Y.; Nakanuma, Y. Expression of immunoreactive matrix metalloproteinases and tissue inhibitors of matrix metalloproteinases in human normal livers and primary liver tumors. *Hepatology* **1996**, *23*, 1341–1344.
8. Reddy, K.B.; Nabha, S.M.; Atanaskova, N. Role of MAP kinase in tumor progression and invasion. *Cancer Metastasis Rev.* **2003**, *22*, 395–403.
9. Vivanco, I.; Sawyers, C.L. The phosphatidylinositol 3-kinase Akt pathway in human cancer. *Nat. Rev. Cancer* **2002**, *2*, 489–501.
10. Osaki, M.; Oshimura, M.; Ito, H. Pi3k-Akt pathway: Its functions and alterations in human cancer. *Apoptosis* **2004**, *9*, 667–676.
11. Gupta, A.K.; Soto, D.E.; Feldman, M.D.; Goldsmith, J.D.; Mick, R.; Hahn, S.M.; Machtay, M.; Muschel, R.J.; McKenna, W.G. Signaling pathways in NSCLC as a predictor of outcome and response to therapy. *Lung* **2004**, *182*, 151–162.
12. Shih, Y.W.; Chen, P.S.; Wu, C.H.; Jeng, F.Y.; Wang, C.J. α-Chaconine-reduced metastasis involves a PI3K/Akt signaling pathway with downregulation of NF-κB in human lung adenocarcinoma A549 cells. *J. Agric. Food Chem.* **2007**, *55*, 11035–11043.
13. Faulkner, D.J. Marine natural products. *Nat. Prod. Rep.* **2001**, *18*, 1–49.
14. Faulkner, D.J. Marine natural products. *Nat. Prod. Rep.* **2002**, *19*, 1–48.
15. Hsieh, P.W.; Chang, F.R.; McPhail, A.T.; Lee, K.H.; Wu, Y.C. New cembranolide analogues from the formosan soft coral *Sinularia flexibilis* and their cytotoxicity. *Nat. Prod. Res.* **2003**, *17*, 409–418.

16. Ojika, M.; Islam, M.K.; Shintani, T.; Zhang, Y.; Okamoto, T.; Sakagami, Y. Three new cytotoxic acylspermidines from the soft coral, *Sinularia* sp. *Biosci. Biotechnol. Biochem.* **2003**, *67*, 1410–1412.
17. Aceret, T.L.; Coll, J.C.; Uchio, Y.; Sammarco, P.W. Antimicrobial activity of the diterpenes flexibilide and sinulariolide derived from *Sinularia flexibilis* quoy and gaimard 1833 (coelenterata: alcyonacea, octocorallia). *Comp. Biochem. Physiol. C* **1998**, *120*, 121–126.
18. Hassan, H.M.; Khanfar, M.A.; Elnagar, A.Y.; Mohammed, R.; Shaala, L.A.; Youssef, D.T.; Hifnawy, M.S.; el Sayed, K.A. Pachycladins A–E, prostate cancer invasion and migration inhibitory eunicellin-based diterpenoids from the red sea soft coral cladiella pachyclados. *J. Nat. Prod.* **2010**, *73*, 848–853.
19. Su, C.C.; Su, J.H.; Lin, J.J.; Chen, C.C.; Hwang, W.I.; Huang, H.H.; Wu, Y.J. An investigation into the cytotoxic effects of 13-acetoxysarcocrassolide from the soft coral sarcophyton crassocaule on bladder cancer cells. *Mar. Drugs* **2011**, *9*, 2622–2642.
20. Liu, C.I.; Chen, C.C.; Chen, J.C.; Su, J.H.; Huang, H.H.; Chen, J.Y.; Wu, Y.J. Proteomic analysis of anti-tumor effects of 11-dehydrosinulariolide on Cal-27 cells. *Mar. Drugs* **2011**, *9*, 1254–1272.
21. Su, T.R.; Lin, J.J.; Chiu, C.C.; Chen, J.Y.; Su, J.H.; Cheng, Z.J.; Hwang, W.I.; Huang, H.H.; Wu, Y.J. Proteomic investigation of anti-tumor activities exerted by sinularin against A2058 melanoma cells. *Electrophoresis* **2012**, *33*, 1139–1152.
22. Neoh, C.A.; Wang, R.Y.; Din, Z.H.; Su, J.H.; Chen, Y.K.; Tsai, F.J.; Weng, S.H.; Wu, Y.J. Induction of apoptosis by sinulariolide from soft coral through mitochondrial-related and p38MAPK pathways on human bladder carcinoma cells. *Mar. Drugs* **2012**, *10*, 2893–2911.
23. Rabelo, L.; Monteiro, N.; Serquiz, R.; Santos, P.; Oliveira, R.; Oliveira, A.; Rocha, H.; Morais, A.H.; Uchoa, A.; Santos, E. A lactose-binding lectin from the marine sponge *Cinachyrella apion* (Cal) induces cell death in human cervical adenocarcinoma cells. *Mar. Drugs* **2012**, *10*, 727–743.
24. Maoka, T.; Tokuda, H.; Suzuki, N.; Kato, H.; Etoh, H. Anti-oxidative, anti-tumor-promoting, and anti-carcinogensis activities of nitroastaxanthin and nitrolutein, the reaction products of astaxanthin and lutein with peroxynitrite. *Mar. Drugs* **2012**, *10*, 1391–1399.
25. Liu, C.I.; Wang, R.Y.; Lin, J.J.; Su, J.H.; Chiu, C.C.; Chen, J.C.; Chen, J.Y.; Wu, Y.J. Proteomic profiling of the 11-dehydrosinulariolide-treated oral carcinoma cells Ca9–22: Effects on the cell apoptosis through mitochondrial-related and ER stress pathway. *J. Proteomics* **2012**, *75*, 5578–5589.
26. Kondratyuk, T.P.; Park, E.J.; Yu, R.; van Breemen, R.B.; Asolkar, R.N.; Murphy, B.T.; Fenical, W.; Pezzuto, J.M. Novel marine phenazines as potential cancer chemopreventive and anti-inflammatory agents. *Mar. Drugs* **2012**, *10*, 451–464.
27. Huang, K.J.; Chen, Y.C.; el-Shazly, M.; Du, Y.C.; Su, J.H.; Tsao, C.W.; Yen, W.H.; Chang, W.B.; Su, Y.D.; Yeh, Y.T.; *et al.* 5-episinuleptolide acetate, a norcembranoidal diterpene from the formosan soft coral *Sinularia* sp., induces leukemia cell apoptosis through Hsp90 inhibition. *Molecules* **2013**, *18*, 2924–2933.
28. Su, J.H.; Lin, Y.F.; Lu, Y.; Yeh, H.C.; Wang, W.H.; Fan, T.Y.; Sheu, J.H. Oxygenated cembranoids from the cultured and wild-type soft corals *Sinularia flexibilis*. *Chem. Pharm. Bull.* **2009**, *57*, 1189–1192.
29. Chen, Y.J.; Su, J.H.; Tsao, C.Y.; Hung, C.T.; Chao, H.H.; Lin, J.J.; Liao, M.H.; Yang, Z.Y.; Huang, H.H.; Tsai, F.J.; *et al.* Sinulariolide induced hepatocellular carcinoma apoptosis through activation of mitochondrial-related apoptotic and PERK/eIF2α/ATF4/CHOP pathway. *Molecules* **2013**, *18*, 10146–10161.

30. Li, H.H.; Su, J.H.; Chiu, C.C.; Lin, J.J.; Yang, Z.Y.; Hwang, W.I.; Chen, Y.K.; Lo, Y.H.; Wu, Y.J. Proteomic investigation of the sinulariolide-treated melanoma cells A375: Effects on the cell apoptosis through mitochondrial-related pathway and activation of caspase cascade. *Mar. Drugs* **2013**, *11*, 2625–2642.
31. Zheng, Q.; Tang, Z.Y.; Xue, Q.; Shi, D.R.; Song, H.Y.; Tang, H.B. Invasion and metastasis of hepatocellular carcinoma in relation to urokinase-type plasminogen activator, its receptor and inhibitor. *J. Cancer Res. Clin. Oncol.* **2000**, *126*, 641–646.
32. Zhao, J.; Guan, J.L. Signal transduction by focal adhesion kinase in cancer. *Cancer Metastasis Rev.* **2009**, *28*, 35–49.
33. Giubellino, A.; Burke, T.R., Jr.; Bottaro, D.P. GRB2 signaling in cell motility and cancer. *Expert Opin. Ther. Targets* **2008**, *12*, 1021–1033.
34. Ma, L.; Young, J.; Prabhala, H.; Pan, E.; Mestdagh, P.; Muth, D.; Teruya-Feldstein, J.; Reinhardt, F.; Onder, T.T.; Valastyan, S.; *et al.* miR-9, a MYC/MYCN-activated microRNA, regulates E-cadherin and cancer metastasis. *Nat. Cell Biol.* **2010**, *12*, 247–256.
35. Egeblad, M.; Werb, Z. New functions for the matrix metalloproteinases in cancer progression. *Nat. Rev. Cancer* **2002**, *2*, 161–174.
36. Chung, T.W.; Moon, S.K.; Chang, Y.C.; Ko, J.H.; Lee, Y.C.; Cho, G.; Kim, S.H.; Kim, J.G.; Kim, C.H. Novel and therapeutic effect of caffeic acid and caffeic acid phenyl ester on hepatocarcinoma cells: Complete regression of hepatoma growth and metastasis by dual mechanism. *FASEB J.* **2004**, *18*, 1670–1681.
37. Shang, N.; Arteaga, M.; Zaidi, A.; Stauffer, J.; Cotler, S.J.; Zeleznik-Le, N.; Zhang, J.; Qiu, W. FAK is required for c-Met/β-catenin-driven hepatocarcinogenesis. *Hepatology* **2014**, *61*, 214.
38. Zhang, Y.; Li, Z.; Yang, M.; Wang, D.; Yu, L.; Guo, C.; Guo, X.; Lin, N. Identification of GRB2 and GAB1 coexpression as an unfavorable prognostic factor for hepatocellular carcinoma by a combination of expression profile and network analysis. *PLoS ONE* **2013**, *8*, e85170.
39. Hsu, W.H.; Chen, C.N.; Huang, H.I.; Lai, Y.L.; Teng, C.Y.; Kuo, W.H. Urokinase induces stromal cell-derived factor-1 expression in human hepatocellular carcinoma cells. *J. Cell. Physiol.* **2012**, *227*, 697–704.
40. Itoh, T.; Hayashi, Y.; Kanamaru, T.; Morita, Y.; Suzuki, S.; Wang, W.; Zhou, L.; Rui, J.A.; Yamamoto, M.; Kuroda, Y.; *et al.* Clinical significance of urokinase-type plasminogen activator activity in hepatocellular carcinoma. *J. Gastroenterol. Hepatol.* **2000**, *15*, 422–430.
41. Mann, C.D.; Neal, C.P.; Garcea, G.; Manson, M.M.; Dennison, A.R.; Berry, D.P. Prognostic molecular markers in hepatocellular carcinoma: A systematic review. *Eur. J. Cancer* **2007**, *43*, 979–992.
42. Lin, J.J.; Su, J.H.; Tsai, C.C.; Chen, Y.J.; Liao, M.H.; Wu, Y.J. 11-epi-Sinulariolide scetate reduces cell migration andiInvasion of human hepatocellular carcinoma by reducing the activation of ERK1/2, p38MAPK and FAK/PI3K/Akt/mTOR signaling pathways. *Mar. Drugs* **2014**, *12*, 4783–4798.

© 2015 by the authors; licensee MDPI, Basel, Switzerland. This article is an open access article distributed under the terms and conditions of the Creative Commons Attribution license (http://creativecommons.org/licenses/by/4.0/).

Int. J. Mol. Sci. **2015**, *16*, 17181-17192; doi:10.3390/ijms160817181

OPEN ACCESS
International Journal of
Molecular Sciences
ISSN 1422-0067
www.mdpi.com/journal/ijms

Article

Prognostic Value of Preoperative Serum Levels of Periostin (PN) in Early Breast Cancer (BCa)

Pier Vitale Nuzzo [1,2], Alessandra Rubagotti [1,2], Francesca Argellati [1], Antonio Di Meglio [1,2], Elisa Zanardi [1,2], Linda Zinoli [1], Paola Comite [3], Michele Mussap [3] and Francesco Boccardo [1,2,*]

[1] Academic Unit of Medical Oncology, IRCCS San Martino University Hospital—IST National Cancer Research Institute, Largo Rosanna Benzi 10, 16132 Genoa, Italy;
E-Mails: piervitale.nuzzo@libero.it (P.V.N.); alessandra.rubagotti@unige.it (A.R.); francesca.argellati@libero.it (F.A.); antonio.dimeglio@rocketmail.com (A.D.M.); elisa.zanardi@unige.it (E.Z.); linda.zinoli@libero.it (L.Z.)

[2] Department of Medicine, School of Medicine, University of Genoa, Largo Rosanna Benzi 10, 16132 Genoa, Italy

[3] Department of Laboratory Medicine, IRCCS San Martino University Hospital—IST National Cancer Research Institute Largo Rosanna Benzi 10, 16132 Genoa, Italy;
E-Mails: paola.comite@libero.it (P.C.); michele.mussap@hsanmartino.it (M.M.)

* Author to whom correspondence should be addressed; E-Mail: f.boccardo@unige.it;
Tel.: +39-010-5600-560; Fax: +39-010-352753.

Academic Editor: William Chi-shing Cho

Received: 17 June 2015 / Accepted: 17 July 2015/ Published: 28 July 2015

Abstract: PN is a secreted cell adhesion protein critical for carcinogenesis. Elevated serum levels of PN have been implicated as playing an important role in different types of cancer, and a few reports suggest a potential role as a prognostic marker. We evaluated the prognostic significance of preoperative serum PN concentration in patients with BCa receiving curative surgery. Enzyme-Linked Immunosorbent Assay (ELISA) was performed to determine the preoperative serum PN level in 182 patients. The correlations between serum PN concentration with clinical pathological features and PN expression in primary tumor samples were analyzed. The prognostic impact of serum PN levels with all-cause and BCa-specific mortality was also investigated. Appropriate statistics were used. Elevated serum PN levels were significantly associated with patient age (p = 0.005), adjuvant systemic therapy (p = 0.04) and progesterone receptor (PgR) status (p = 0.02). No correlation between PN preoperative serum levels and other clinical-pathological parameters, including either the epithelial or the stromal PN expression of primary tumor

or the combination of the two, was found. Similarly, no association between serum PN levels and either all-cause or BCa-specific mortality was found. However, subgroup analysis revealed a correlation between higher PN serum levels and all-cause mortality in patients with node-negative disease (p = 0.05) and in those with a low PgR expression (p = 0.03). Higher levels of serum PN were also found to correlate with BCa-specific mortality in the subgroup of patients who did not receive any adjuvant systemic therapy (p = 0.04). Our findings suggest that PN was detectable in the serum of early BCa patients before surgery and increased base-line serum levels predicted worse long-term survival outcomes in specific subgroups of patients.

Keywords: periostin protein; breast neoplasms; extracellular matrix proteins; prognosis; biomarkers; enzyme-linked immunosorbent assay

1. Introduction

While the incidence of breast cancer (BCa) is still growing up, since the early 1990s there has been a slow but progressive decrease in BCa-specific mortality [1], probably as the result of both mammographic screening and a multimodal therapeutic approach [2]. Nevertheless, BCa remains the first leading cause of cancer-related death in the female population. Identifying women who might derive the most benefit from multimodal treatments is still an open task. In fact, the use of the prognostic information provided by clinical pathological features or, more recently, by gene signatures is not fully satisfactory for this purpose [3] and the great majority of patients still receive unhelpful treatments and are exposed to undue toxicities. For several decades it has been debated whether and how circulating tumor markers might improve the prognostic information provided by the phenotypic characteristics of the primary tumor. Unfortunately neither carcinoembryonic antigen (CEA) nor carbohydrate antigen 15.3 (CA 15.3), the most commonly used circulating biomarkers to monitor BCa, have been found to be adequately affordable in predicting a patient's prognosis following local treatment [4,5]. Therefore, researchers' attention has been focused on several alternative markers; none of them, however, has been proven so far to be effective in this regard [6,7]. Recently increasing attention has been paid to the extracellular matrix (ECM) proteins, which have been demonstrated to play a crucial role in driving carcinogenesis [8]. The crosstalk between cancer cells and ECM proteins, secreted by the neighboring stromal cells, does in fact create a supportive microenvironment that contributes to sustaining tumor growth and spreading [8].

Periostin (PN) is a protein produced and secreted by the fibroblasts as a major component of ECM, where it is involved in the regulation of intercellular adhesion [9]. This protein is thought to play a critical role in carcinogenesis and metastasization by interacting with integrins as well as with other signals mainly via the PI3-K/AKT pathway [10]. Moreover, PN was shown to be a marker and an inducer of epithelial-mesenchimal transition (EMT), a process responsible for the dissemination of primary tumor cells to the sites of metastasis and for the differentiation program leading to the increase in malignant behavior of tumors [11]. It has been reported that PN is frequently overexpressed in various types of human cancer tissues, including breast, prostate, colon, lung, ovarian, head and neck

cancer, melanoma, and neuroblastoma [10]. PN is also detectable in biologic fluids, either in healthy people or in cancer patients [12–16]. The role of circulating PN in sustaining tumor progression in cancer patients has been neither fully established nor investigated for the possible clinical implications.

A few studies have evaluated the prognostic significance of PN serum levels in patients affected by solid tumors [12–16] and, at least at our best knowledge, only one study has investigated this aspect in a small group of patients affected by BCa at different disease stages [17]. Lack of adequate information in this regard prompted us to take advantage of a previous study on the prognostic value of the tissue expression of PN in a selected cohort of BCa patients for whom at least one serum aliquot was collected at the time of surgery and cryopreserved [18]. This provided us with the opportunity to assess the prognostic role of serum PN concentration in the cohort patients, focusing on the correlation of preoperative serum PN levels with clinical pathologic variables and tissue expression of PN in primary tumor samples. The association between serum PN levels and patient mortality was also investigated.

2. Results

The serum levels of PN in the 182 patients forming the cohort in this study ranged from 43.7 pg/mL to 1034.0 pg/mL, with a median value of 219 pg/mL; this value was arbitrarily selected as the cut-off for statistical comparisons (see statistical analysis section). Patient demography is summarized in Table 1.

Table 1. Main characteristics of study patients (N = 182).

Variables	No. of Patients (%)
Age at surgery, years	
Median (range)	58 (31–84)
Menopausal status	
Pre-menopausal	58 (31.9)
Post-menopausal	124 (68.1)
Tumor size: cm in diameter	
≤2	89 (48.9)
>2	93 (51.1)
Stage	
I	69 (37.9)
II	76 (41.8)
III	37 (20.3)
ER status	
Poor (<10% of stained cells)	40 (22.0)
Rich (≥10% of stained cells)	142 (78.0)
PgR status	
Poor (<10% of stained cells)	80 (44.0)
Rich (≥10% of stained cells)	102 (56.0)
Ki-67	
Low (<14% stained cells)	85 (46.7)
High (≥14% stained cells)	97 (53.3)

Table 1. *Cont.*

Variables	No. of Patients (%)
HER2 status	
Negative	166 (91.2)
Positive	16 (8.8)
Phenotype *	
Luminal A	60 (33.1)
Luminal B (HER2-neg)	73 (40.1)
Luminal B (HER2-pos)	9 (4.9)
HER2 positive (non-luminal)	7 (3.8)
Triple negative	33 (18.1)
Adjuvant systemic therapy **	
Delivered	104 (57.1)
Undelivered	78 (42.9)
PN epithelial (E) expression	
0% immunostained cells	111 (61.0)
≥1% immunostained cells	71 (39.0)
PN stromal (S) expression	
<90% immunostained cells	94 (51.6)
≥90% immunostained cells	88 (48.4)
E/S PN expression	
E ≥ 1% S < 90%	31 (17.0)
E = 0 S < 90%	63 (34.6)
E = 0 S ≥ 90%	48 (26.4)
E ≥ 1% S ≥ 90%	40 (22.0)

* definition of intrinsic subtypes of breast cancer according to [3]; ** either chemotherapy or endocrine therapy, or both.

2.1. Correlation of Serum PN Level with Clinical Pathological Features and Tissue PN Expression

PN serum levels were not correlated with the clinical pathological parameters selected for the present analysis, except for tumor PgR status (p = 0.02), patient age at surgery (p = 0.005), and adjuvant systemic therapy (p = 0.04). No relationship was found between the serum PN levels and either the corresponding epithelial or stromal PN expression or the PN phenotype obtained by combining the expression of PN in both compartments (Table 2).

Table 2. Correlation of preoperative serum PN median level with clinical pathological features and tissue PN expression.

Variables	≤219 pg/mL (%)	>219 pg/mL (%)	*p*
Median age at surgery, years			
≤58	57 (62.6)	38 (41.8)	
>58	34 (37.4)	53 (58.2)	0.005
Menopausal status			
Pre-menopausal	32 (35.2)	26 (28.6)	
Post-menopausal	59 (64.8)	65 (71.4)	0.3

Table 2. *Cont.*

Variables	≤219 pg/mL (%)	>219 pg/mL (%)	*p*
Tumor size: cm in diameter			
≤2	45 (49.5)	44 (48.4)	
>2	46 (50.5)	47 (51.6)	0.8
Stage			
I	33 (36.3)	36 (39.6)	
II	40 (44.0)	36 (39.6)	
III	18 (19.7)	19 (20.8)	0.8
Nodal status			
Node-negative	44 (48.4)	49 (53.8)	
Node-positive	47 (51.6)	42 (46.2)	0.4
ER status			
Poor (<10% of stained cells)	24 (26.4)	16 (17.6)	
Rich (≥10% of stained cells)	67 (73.6)	75 (82.4)	0.1
PgR status			
Poor (<10% of stained cells)	48 (52.7)	32 (35.2)	
Rich (≥10% of stained cells)	43 (47.3)	59 (64.8)	0.02
Ki-67			
Low (<14% stained cells)	42 (46.2)	43 (47.3)	
High (≥14% stained cells)	49 (53.8)	48 (52.7)	0.8
HER2 status			
Negative	81 (89.0)	85 (93.4)	
Positive	10 (11.0)	6 (6.6)	0.3
Phenotype *			
Luminal A + Luminal B (HER2-neg)	25 (27.5)	35 (38.5)	
Others **	66 (72.5)	56 (61.5)	0.1
Adjuvant systemic therapy ***			
Undelivered	32 (35.2)	46 (50.5)	0.04
Delivered	59 (64.8)	45 (49.5)	
PN epithelial (E) expression			
0% immunostained cells	57 (62.6)	54 (59.3)	
≥1% immunostained cells	34 (37.4)	37 (40.7)	0.6
PN stromal (S) expression			
<90% immunostained cells	46 (50.5)	48 (52.7)	
≥90% immunostained cells	45 (49.5)	43 (47.3)	0.7
E/S PN expression			
E ≥ 1% S < 90%	15 (16.5)	16 (17.6)	
E = 0 S < 90%	31 (34.1)	32 (35.2)	
E = 0 S ≥ 90%	26 (28.6)	22 (24.1)	
E ≥ 1% S ≥ 90%	19 (20.8)	21 (23.1)	0.9

* definition of intrinsic subtypes of breast cancer according to [3]; ** Luminal B (HER2-pos) + HER2 positive (non-luminal) + triple negative; *** either chemotherapy or endocrine therapy, or both.

2.2. Correlation of Serum PN Levels with All-Cause Mortality and BCa-Specific Mortality

At a median follow-up time of 225 months (range: 5–353 months), 114 deaths were recorded, of which 67 were BCa-related. As is shown in Figure 1A,B, no association between PN serum levels and either all-cause or BCa-specific mortality was found. However, subgroup analysis showed that there was a statistically significant association between higher serum PN levels (*i.e.*, ≥the median level) and all-cause mortality in patients with node-negative disease (p = 0.05) and in those with poor (*i.e.*, <10% stained cells) PgR tumors (p = 0.03) (Figure 2A,C). No statistically significant correlation of serum PN levels with any of the other variables was evident relative to BCa-specific mortality, except for a correlation with adjuvant systemic therapy (p = 0.04 in favor of the patients who did not receive adjuvant systemic treatments, Figure 3B).

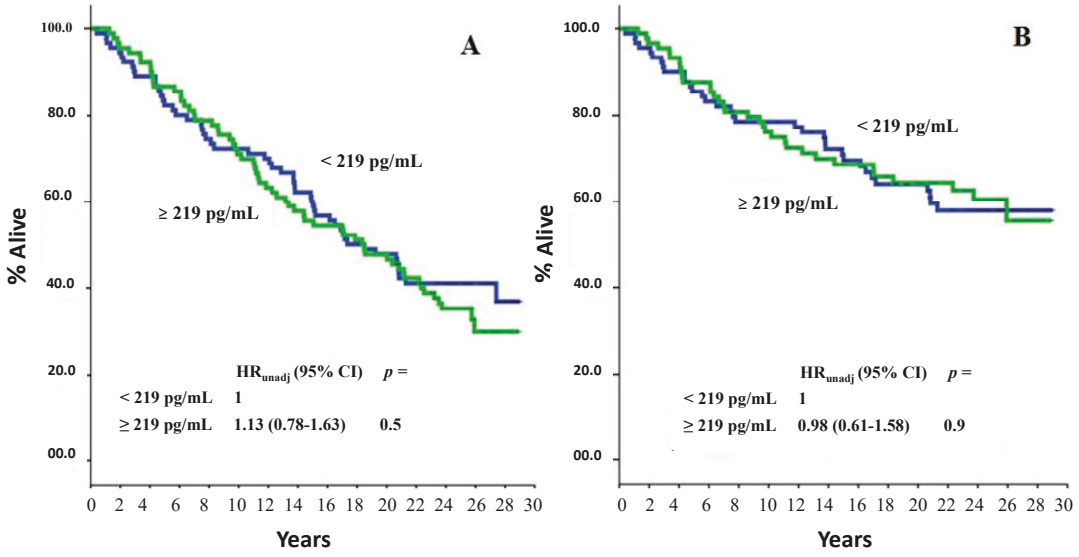

Figure 1. All-cause (**A**) and BCa-specific mortality (**B**) of study patients as a function of serum PN values. The median value, corresponding to 219 pg/mL, was used as an arbitrary cutoff. *HR*: hazard ratio; 95% *CI*: 95% confidence interval.

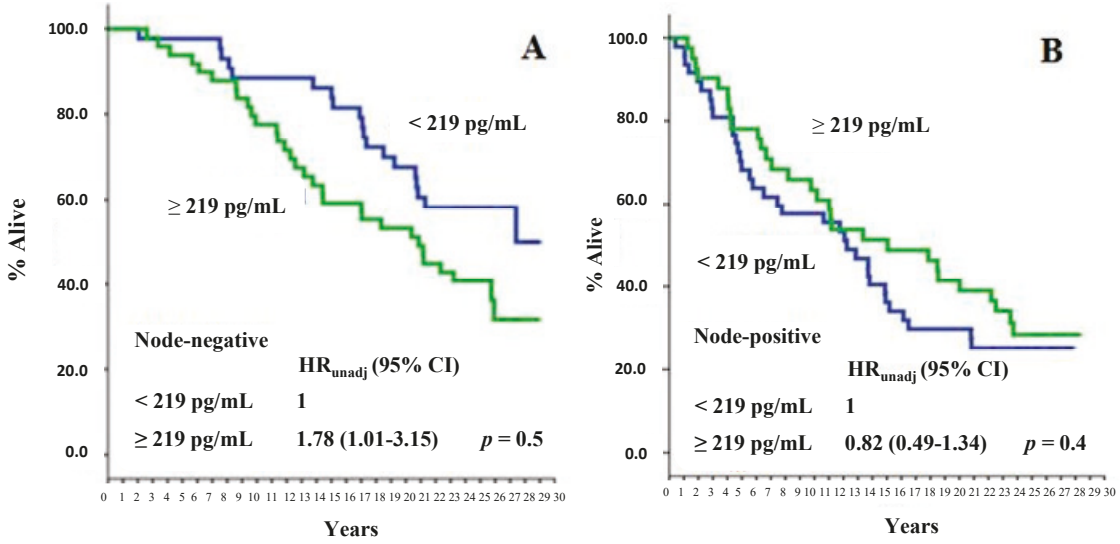

Figure 2. *Cont.*

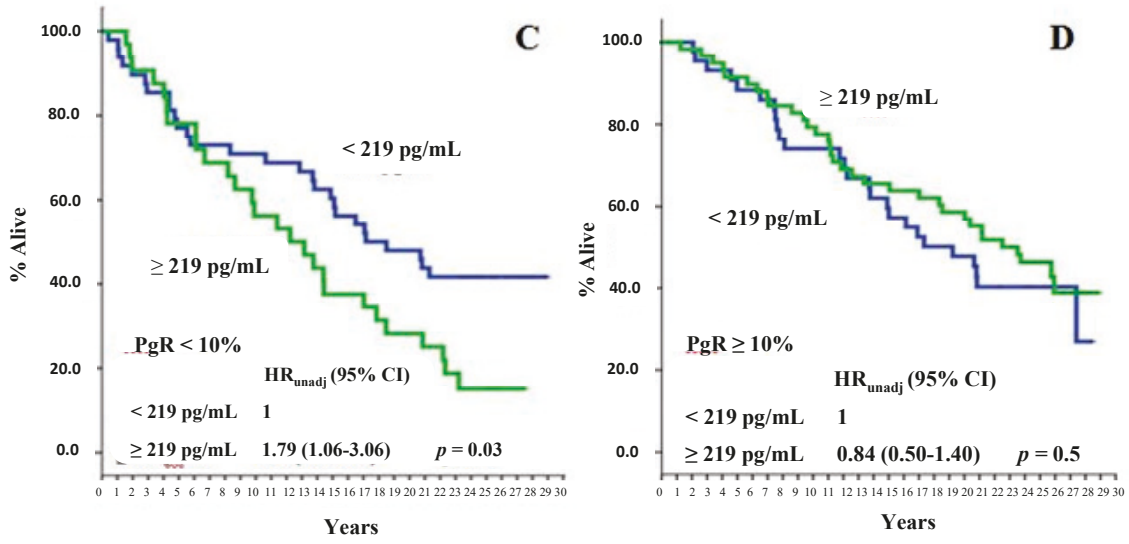

Figure 2. All-cause mortality of study patients as a function of serum PN values, according to nodal status (**A**,**B**) and PgR status (**C**,**D**). The median PN value, corresponding to 219 pg/mL, was used as an arbitrary cutoff. *HR*: hazard ratio; 95% *CI*: 95% confidence interval.

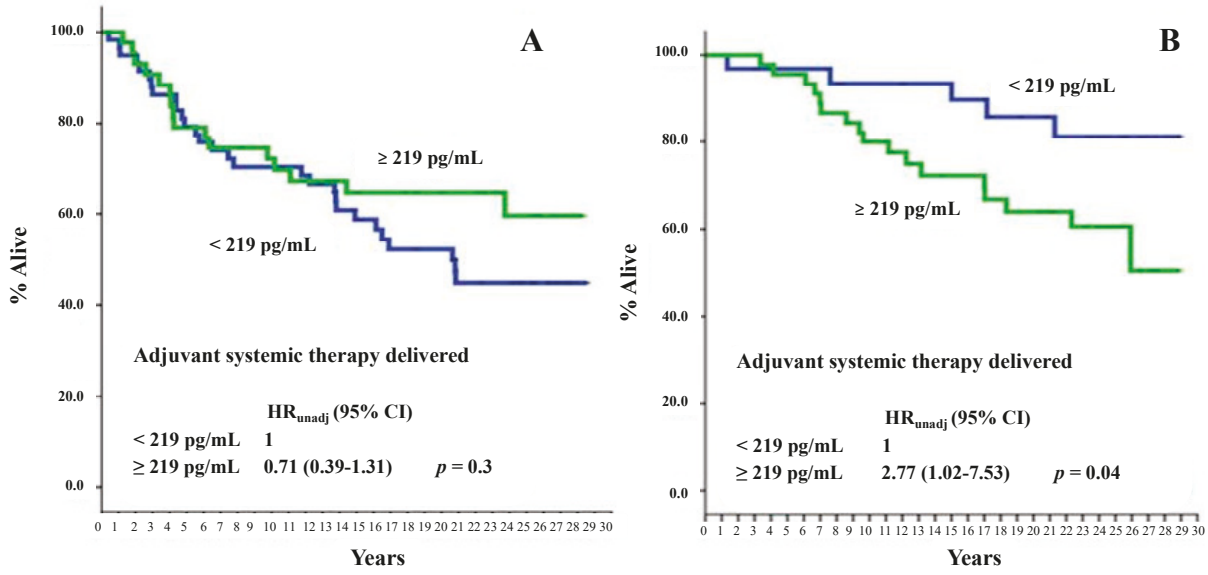

Figure 3. BCa-specific mortality of study patients as a function of serum PN values according to adjuvant systemic treatment (**A**,**B**). The median value, corresponding to 219 pg/mL, was used as an arbitrary cutoff. *HR*: hazard ratio; 95% *CI*: 95% confidence interval.

3. Discussion

3.1. General Remarks

Our study has some intrinsic limitations, and for this reason our data should be managed carefully.

Major limitations are represented by the relatively small size of the cohort and by the retrospective nature of the study. Both conditions can affect the statistical power of the study. Nevertheless, this is by far the largest cohort of patients among those studies that evaluated the serum concentration of PN

in cancer patients. The median value of serum levels of PN, measured by the ELISA technique, corresponded to 219 pg/mL, a value highly comparable with PN median values found by Hong *et al.* [16] in non-small cell lung cancer (24,284 pg/mL). However, various discrepancies related to the serum concentration of PN detectable in cancer patients exist among previous available studies [12–17]. These differences can be explained not only by the different tumor type or tumor stage affecting the patients included in the different studies [12–16], but also by the poor comparability of results due to the lack of commercial assays standardization. In fact, a number of critical issues may affect results: the lack of an international standard calibrator for PN, the heterogeneity of antibodies among commercial kits, including the affinity and the avidity, differences in analytical methods (ELISA *vs.* chemiluminescence), and, finally, variability due to manual procedures in such analytical protocols (e.g., ELISA).

3.2. Correlation of Serum PN Level with Clinical Pathological Features and Tissue PN Expression

In our study serum PN levels showed no relationship with established clinical pathological parameters (except for a weak correlation with tumor PgR status) as well as with PN tissue expression, while a significant correlation with patient age and adjuvant systemic therapy was found.

The significant relationship between serum levels of PN and age in our cohort could derive from multiple causes. Elevation in serum levels of PN could be attributable to normal or abnormal bone turnover or to other factors (including myocardial, vascular, and skeletal muscle injuries) [10,11], unrelated to the presence of the neoplasm. Unfortunately, information about these factors and other putative confounding factors such as smoking, infections, or other aging-related diseases is missing and cannot be obtained after such a long follow-up time (median follow-up time: 225 months) and the majority of the cohort patients died (114 out of 182).

Available literature data show that serum PN levels do not correlate with clinical-pathologic parameters in lung cancer, colorectal cancer, thymoma, and hepatocellular carcinoma [12,14–16]. However, a significant difference in serum PN levels was shown in patients with advanced stage III/IV colorectal cancer, stage IV thymoma, and metastatic hepatocellular carcinoma, as compared to earlier stages [12,14,15]. Comparably, Sasaki *et al.* [17] reported on the presence of elevated levels of serum PN in BCa patients affected by bone metastases, suggesting that serum PN might represent a marker of bone metastases in these patients [17]. We were not able to evaluate differences in terms of serum PN levels between early BCa patients and stage IV patients, as our samples were obtained pre-operatively only from non-metastatic BCa patients. The presence of elevated levels of serum PN in metastatic cancer patients could support the hypothesis that the greatest amount of circulating PN might be released into the blood stream from the metastatic sites rather than from the primary tumor. This assumption appears to be supported by the lack of any relationship between PN primary tumor levels and serum PN levels in our study and by the results of a previous experimental study on a BCa mouse model showing that the PN stromal response to the attachment of cancer stem cells at the metastatic niche level might contribute to the circulating levels of PN in the blood [19].

3.3. Correlation of Serum PN Level with All-Cause Mortality and BCa-Specific Mortality

No association between PN serum levels and either all-cause or BCa-specific mortality was found in our study.

However, subgroup analysis showed that there was a statistically significant association between higher serum PN levels and all-cause mortality in specific subgroups. For instance, we found that higher serum levels of PN were significantly associated with a higher all-cause mortality risk in node-negative but not in node-positive patients. This was not expected. However, the putative confounding role of adjuvant systemic therapies should be taken into account in interpreting these findings. In fact, at the time cohort patients were operated on, only those showing nodal involvement were usually treated prophylactically with either endocrine therapy or chemotherapy, or both. The effect of systemic therapies on micro-metastatic residual disease might well blunt the prognostic value of PN serum levels in this patient subgroup. This putative bias is lacking in node-negative patients, who were not candidates for either form of adjuvant systemic treatment. This assumption appears to be supported by the fact that a positive association of higher PN serum levels with a worse outcome in terms of BCa-specific survival was also found in our study. The association found between serum PN levels and tumor PgR expression (higher serum PN levels were associated with a poorer survival outcome in patients with PgR-poor tumors but not in those with PgR-rich tumors) could again be explained by the putative confounding effect of systemic therapy, since adjuvant endocrine therapies were commonly given to patients with PgR-positive tumors.

4. Experimental Section

4.1. Patient Selection and Sample Collection

Tissue PN expression had been previously evaluated in the archival material relative to 200 patients diagnosed with BCa and operated at our Institute between 1985 and 1990. Preliminary results were presented at the ESMO Impakt 2015 conference [18]. We found that of these 200 patients for whom it had been possible to update follow-up data, particularly in respect to mortality, serum samples had been obtained from 182 of them just before surgery and stored at −80 °C.

All patients consented to provide blood and to the cryopreservation of relative serum aliquots, and all of them were informed about the experimental nature of the studies that would be performed in the future and had been made aware of the fact that no beneficial effect would be obtained by their participation to the program. The use of archival and cryo-preserved material for the purpose of the present study was approved by the Ethics Committee of Regione Liguria–Section 1. Patient data were managed according to the Italian Data Protection Authority prescriptions [http://www.garanteprivacy.it].

4.2. Enzyme-Linked Immunosorbent Assay (ELISA) Evaluations

Patient serum PN levels were measured by ELISA technique using the commercial kit “Periostin Matched Pair Detection Set” (Adipogen International, San Diego, CA, USA), consisting of a 96-well microplate (Nunc MaxiSorp Plate, ThermoFisher Scientific, Waltham, MA, USA). The test was optimized and automated on the multiparameter analyzer (TRITURUS®, Pantec, Torino, Italy). Briefly, microplates

were coated with the specific antibody anti-PN (2 μg/mL, 100 μL), diluted in phosphate-buffered saline (PBS), and incubated overnight at 4 °C. The remaining protein-binding sites were blocked by keeping them in a buffer (2% bovine serum albumin in PBS) for 2 h at 25 °C, and then washed five times with 300 μL/well PBS containing 0.1% Tween-20. Subsequently, standard dilutions and serum samples were added and incubated for 2 h at room temperature.

After washing, plates were then incubated for 1h at room temperature with detection antibody (0.1 μg/mL, 100 μL/well) and, after washing, the detection antibody was labeled with horseradish peroxidase-labeled streptavidin (100 μL/well) for 30 min at room temperature. The enzyme reaction was activated by adding reaction solution (3,3',5,5'-tetramethylbenzidine) for 20 min at room temperature. The chromogenic reaction was stopped by the addition of 2 M H_2SO_4 and the absorbance was measured at 450 nm (primary wavelength) and 550 nm (secondary wavelength). The absorbance at 550 nm was subtracted from the absorbance at 450 nm. PN concentrations were calculated from the standard curve generated by a curve-fitting program (4PL). PN concentrations were expressed as pg/mL and the detection limit was 78 pg/mL. All samples were assayed in duplicate.

4.3. Statistical Analysis

Median serum PN values have been arbitrarily chosen for statistical analysis. In fact the discriminant power of tertile or quartile values was not better nor did ROC analysis allow us to discriminate values more strictly associated with individual mortality risk.

The chi-square test was used to study the relationship between median preoperative PN level in the serum and the following clinical-pathological parameters: patient age at surgery (≤58 *vs.* >58 years, *i.e.*, median age), menopausal status (pre- *vs.* post-), T size (≤2 cm *vs.* >2 cm), nodal status (negative *vs.* positive), tumor stage (I *vs.* II *vs.* III), estrogen-receptor (ER) status (<10% *vs.* ≥10%), PgR status (<10% *vs.* ≥10%), Ki-67 proliferation index value (<14% *vs.* ≥14%), HER2 status (negative *vs.* positive), tumor phenotype (luminal A + luminal B HER2-neg *vs.* the other immune-phenotypes), and adjuvant systemic therapy (delivered *vs.* undelivered).

The chi-square test was also used to correlate preoperative PN serum levels with either the epithelial or the stromal PN tissue expression, or with any of the four phenotypes arbitrarily obtained on the basis of both epithelial and stromal expression and showing different mortality probabilities as described in the previously mentioned study [18]. Concerning the correlation with all-cause and BCa-specific mortality, curves were constructed through the cumulative incidence function estimated by the Kaplan–Meier method and compared by way of the log-rank test [20]. All p values were two-tailed. The IBM software Statistical Package for Social Sciences (SPSS) version 21.0 forWindows (SPSS Inc., Chicago, IL, USA) and STATASE11 were used for data analysis.

5. Conclusions

In spite of the limitations already mentioned in the general remarks, our findings show that PN is present at detectable levels in the serum of early BCa patients. The production of circulating PN does not seem to occur at primary tumor sites or to be in any way correlated with PN tissue expression. Though PN serum levels do not appear to correlate with mortality in the whole cohort, higher serum levels of PN predicted worse survival outcomes in specific subgroups of patients, namely in those who,

by virtue of their nodal and PgR status, did not receive any form of adjuvant systemic treatment. Further investigations on the biological role of serum PN in early BCa patients and on its putative clinical significance are warranted.

Acknowledgments

This work was supported by grants from the Italian Ministry of Education, University, and Research [contract 2006063220_002] and from Compagnia di San Paolo, Italy [Grant number: 2012.1588].

Author Contributions

Pier Vitale Nuzzo participated in the design of the study, in data interpretation, and in drafting the manuscript. Alessandra Rubagotti participated in the design of the study and performed the statistical analysis. Linda Zinoli made substantial contributions in updating patient histories and helped in statistical analysis. Francesca Argellati and Paola Comite selected patients' sera and performed ELISA analysis. Antonio Di Meglio and Elisa Zanardi contributed in data interpretation and drafting the manuscript. Michele Mussap gave his professional technical support through laboratory ELISA analysis and interpretation of data. Francesco Boccardo made substantial contributions to the conception, design, analysis, and interpretation of data. He has been involved in drafting the manuscript and revising it critically for important intellectual content. He gave final approval of the version to be published.

Conflicts of Interest

The authors declare no conflicts of interest.

References

1. Siegel, R.L.; Miller, K.D.; Jemal, A. Cancer statistics, 2015. *CA Cancer J. Clin.* **2015**, *65*, 5–29.
2. Jin, J. JAMA patient page. Breast cancer screening: Benefits and harms. *JAMA* **2014**, *312*, 2585, doi:10.1001/jama.2014.13195.
3. Goldhirsch, A.; Winer, E.P.; Coates, A.S.; Gelber, R.D.; Piccart-Gebhart, M.; Thürlimann, B.; Senn, H.J. Panel members. Personalizing the treatment of women with early breast cancer: Highlights of the St Gallen International Expert Consensus on the Primary Therapy of Early Breast Cancer 2013. *Ann. Oncol.* **2013**, *24*, 2206–2223.
4. Jäger, W.; Krämer, S.; Palapelas, V.; Norbert, L. Breast cancer and clinical utility of CA 15-3 and CEA. *Scand. J. Clin. Lab. Investig. Suppl.* **1995**, *221*, 87–92.
5. Colomer, R.; Ruibal, A.; Genollá, J.; Rubio, D.; del Campo, J.M.; Bodi, R.; Salvador, L. Circulating CA 15-3 levels in the postsurgical follow-up of breast cancer patients and in non-malignant diseases. *Breast Cancer Res. Treat.* **1989**, *13*, 123–133.
6. Donepudi, M.S.; Kondapalli, K.; Amos, S.J.; Venkanteshan, P. Breast cancer statistics and markers. *J. Cancer Res. Ther.* **2014**, *10*, 506–511.
7. Witwer, K.W. Circulating microRNA biomarker studies: Pitfalls and potential solutions. *Clin. Chem.* **2015**, *61*, 56–63.

8. Oskarsson, T. Extracellular matrix components in breast cancer progression and metastasis. *Breast* **2013**, *22*, S66–S72.
9. Horiuchi, K.; Amizuka, N.; Takeshita, S.; Takamatsu, H.; Katsuura, M.; Ozawa, H.; Toyama, Y.; Bonewald, L.F.; Kudo, A. Identification and characterization of a novel protein, Periostin, with restricted expression to periosteum and periodontal ligament and increased expression by transforming growth factor beta. *J. Bone Miner. Res.* **1999**, *14*, 1239–1249.
10. Ruan, K.; Bao, S.; Ouyang, G. The multifaceted role of periostin in tumorigenesis. *Cell. Mol. Life Sci.* **2009**, *66*, 2219–2230.
11. Morra, L.; Moch, H. Periostin expression and epithelial-mesenchymal transition in cancer: A review and an update. *Virchows Arch.* **2011**, *459*, 465–475.
12. Sasaki, H.; Dai, M.; Auclair, D.; Kaji, M.; Fukai, I.; Kiriyama, M.; Yamakawa, Y.; Fujii, Y.; Chen, L.B. Serum level of the periostin, a homologue of an insect cell adhesion molecule, in thymoma patients. *Cancer Lett.* **2001**, *172*, 37–42.
13. Fujimoto, K.; Kawaguchi, T.; Nakashima, O.; Ono, J.; Ohta, S.; Kawaguchi, A.; Tonan, T.; Ohshima, K.; Yano, H.; Hayabuchi, N.; *et al*. Periostin, a matrix protein, has potential as a novel serodiagnostic marker for cholangiocarcinoma. *Oncol. Rep.* **2011**, *25*, 1211–1216.
14. Ben, Q.W.; Zhao, Z.; Ge, S.F.; Zhou, J.; Yuan, F.; Yuan, Y.Z. Circulating levels of periostin may help identify patients with more aggressive colorectal cancer. *Int. J. Oncol.* **2009**, *34*, 821–828.
15. Lv, Y.; Wang, W.; Jia, W.D.; Sun, Q.K.; Huang, M.; Zhou, H.C.; Xia, H.H.; Liu, W.B.; Chen, H.; Sun, S.N.; *et al*. High preoparative levels of serum periostin are associated with poor prognosis in patients with hepatocellular carcinoma after hepatectomy. *Eur. J. Surg. Oncol.* **2013**, *39*, 1129–1135.
16. Hong, L.; Sun, H.; Lv, X.; Yang, D.; Zhang, J.; Shi, Y. Expression of periostin in the serum of NSCLC and its function on proliferation and migration of human lung adenocarcinoma cell line (A549) *in vitro*. *Mol. Biol. Rep.* **2010**, *37*, 2285–2293.
17. Sasaki, H.; Yu, C.Y.; Dai, M.; Tam, C.; Loda, M.; Auclair, D.; Chen, L.B.; Elias, A. Elevated serum periostin levels in patients with bone metastases from breast but not lung cancer. *Breast Cancer Res. Treat.* **2003**, *77*, 245–252.
18. Nuzzo, P.V.; Rubagotti, A.; Zinoli, L.; Salvi, S.; Boccardo, S.; Boccardo, F. Prognostic value of stromal and epithelial periostin (PN) expression in human breast cancer (BCa): Correlation with clinical pathological features and mortality outcome. *Ann. Oncol.* **2015**, *26*, Abstract 68P.
19. Malanchi, I.; Santamaria-Martínez, A.; Susanto, E.; Peng, H.; Lehr, H.A.; Delaloye, J.F.; Huelsken, J. Interactions between cancer stem cells and their niche govern metastatic colonization. *Nature* **2011**, *481*, 85–89.
20. Kaplan, E.L.; Meier, P. Non parametric estimation from incomplete observation. *J. Am. Stat. Assoc.* **1958**, *53*, 457–481.

© 2015 by the authors; licensee MDPI, Basel, Switzerland. This article is an open access article distributed under the terms and conditions of the Creative Commons Attribution license (http://creativecommons.org/licenses/by/4.0/).

Int. J. Mol. Sci. **2015**, *16*, 18564-18579; doi:10.3390/ijms160818564

OPEN ACCESS
International Journal of
Molecular Sciences
ISSN 1422-0067
www.mdpi.com/journal/ijms

Article

Wnt3a Promotes the Vasculogenic Mimicry Formation of Colon Cancer via Wnt/β-Catenin Signaling

Lisha Qi [1,2,3,†], Wangzhao Song [1,2,3,†], Zhiyong Liu [1,2,3], Xiulan Zhao [4], Wenfeng Cao [1,2,3,*] and Baocun Sun [1,2,3,4,*]

1 Department of Pathology, Tianjin Medical University Cancer Institute and Hospital, Tianjin 300060, China; E-Mails: qilisha2005@163.com (L.Q.); baoer778@139.com (W.S.); liuzhiyong@tjmuch.com (Z.L.)
2 The Key Laboratory of Tianjin Cancer Prevention and Treatment, Tianjin 300060, China
3 National Clinical Research Center for Cancer, Tianjin 300060, China
4 Department of Pathology, Tianjin Medical University, Tianjin 300070, China; E-Mail: zhaoxiulan2014@163.com

† These authors contributed equally to this work.

* Authors to whom correspondence should be addressed; E-Mails: caowenfeng@tjmuch.com (W.C.); sunbaocun@tjmuch.com (B.S.); Tel./Fax: +86-22-2334-0123 (ext. 6007) (W.C. & B.S.).

Academic Editor: William Chi-shing Cho

Received: 12 July 2015 / Accepted: 4 August 2015 / Published: 10 August 2015

Abstract: Our previous study provided evidence that non-canonical Wnt signaling is involved in regulating vasculogenic mimicry (VM) formation. However, the functions of canonical Wnt signaling in VM formation have not yet been explored. In this study, we found the presence of VM was related to colon cancer histological differentiation ($p < 0.001$), the clinical stage ($p < 0.001$), and presence of metastasis and recurrence ($p < 0.001$). VM-positive colon cancer samples showed increased Wnt3a expression ($p < 0.001$) and β-catenin nuclear expression ($p < 0.001$) compared with the VM-negative samples. *In vitro*, over-regulated Wnt3a expression in HT29 colon cancer cells promoted the capacity to form tube-like structures in the three-dimensional (3-D) culture together with increased expression of endothelial phenotype-associated proteins such as VEGFR2 and VE-cadherin. The mouse xenograft model showed that Wnt3a-overexpressing cells grew into larger tumor masses and formed more VM than the control cells. In addition, the Wnt/β-catenin signaling antagonist Dickkopf-1(Dkk1) can reverse the capacity to form tube-like structures and can

decrease the expressions of VEGFR2 and VE-cadherin in Wnt3a-overexpressing cells. Taken together, our results suggest that Wnt/β-catenin signaling is involved in VM formation in colon cancer and might contribute to the development of more accurate treatment modalities aimed at VM.

Keywords: Wnt/β-catenin signaling; vasculogenic mimicry; Wnt3a; Dkk1; colon cancer

1. Introduction

Solid tumor formation is highly dependent on a continuous supply of oxygen and nutrition. Angiogenesis has a vital function in tumor development because tumors are supplied with oxygen and nutrients and tumor cells are provided with an entry route into circulation. For years, much attention has been focused on the function of sprouting angiogenesis or the recruitment of endothelial cells into tumors from surrounding, pre-existing blood vessels. However, over the last few years, several other tumor microcirculation patterns have been identified, including vessel co-option, recruitment of endothelial precursor cells, intussusception, and vasculogenic mimicry (VM) [1–3]. VM was first described in 1999 by Maniotis *et al.* [4], who found that uveal melanoma cells resembled the endothelial phenotype and form vascular networks in the absence of endothelial cells. Although the functionality and contribution of VM have been established, many studies involving the use of intravenously injected tracers, laser-scanning confocal angiography, or doppler ultrasonography have indicated that VM can provide blood and nutrition to tumor masses even in the absence of conventional endothelial vessels [5–7]. In the last 10 years, VM has been observed in many different tumor types, and its occurrence is strongly associated with unfavorable clinical outcomes [8–13]. Furthermore, the conventional anti-angiogenesis treatment aimed at endothelial cells cannot inhibit VM formation. Several recent studies have indicated that anti-angiogenesis modalities may even elicit a more aggressive tumor phenotype [14,15]. Therefore, such conventional treatment strategies need to be reconsidered, and studies on the molecular mechanisms underlying VM are needed to develop more effective treatment modalities.

Wnt signaling is involved in a wide range of physiological processes, including embryonic development, cell proliferation, and homeostasis. Activating the mutations of the Wnt-signaling pathway is crucial in tumorigenesis, especially in colorectal cancer. Wnt signaling also has an important function in vascular development and angiogenesis. Previous reports have shown that Wnt signaling contributes to endothelial cell differentiation and vascular remodeling [16]. Both the loss and gain of function of Wnt pathway may influence endothelial cell functions and result in abnormal vascular development and angiogenesis [17,18]. Signaling through the Wnt pathway starts with Wnt ligands, which consist of more than 19 cysteine-rich glycoproteins. Constitutive activation of Wnt signalling through mutation of APC, β-catenin or Axin appears to be a necessary initiating step for more than 85% colorectal cancers. However, emerging evidence demonstrates that the upstream components (*i.e.*, some Wnt ligands and Frizzled) are overexpressed in colon cancer and are involved in tumor progression [19,20]. Additionally, some recent studies demonstrate that inhibitors of Wnt-Frizzled interaction could suppress tumor growth and development [21,22]. All these indicate the additional modulation of Wnt signalling via the upstream components, despite mutations in the downstream components of the pathway. Particular Wnt ligands,

such as Wnt1, Wnt3a, and Wnt7a, stimulate the β-catenin dependent pathway; this stimulation is called Wnt/β-catenin or canonical Wnt signaling. Other ligands, such as Wnt4, Wnt5a, and Wnt11, may activate the Ca^{2+}-calmodulin kinase or the planar cell polarity pathway; this activation is called non-canonical Wnt signaling. Our previous reports have shown that overexpression of Wnt5a, a representative non-canonical Wnt ligand, may mediate VM formation in ovarian cancer and non-small cell lung cancer [23,24]. By contrast, data on canonical Wnt signaling in VM formation are still scarce.

Wnt3a is a representative Wnt protein that signals via Wnt/β-catenin signaling. Previous studies, including our own, have reported that by activating Wnt/β-catenin signaling, Wnt3a can promote epithelial-mesenchymal transition and enhance stemness of cancer cells [20], both of which are reported as important mechanisms underlying VM. Thus, we speculate that Wnt3a may be involved in regulating VM formation. In this study, the expression patterns of Wnt3a, β-catenin, and VM were examined on a large array of 217 human colon cancer cases. The relationships between Wnt3a, β-catenin, and VM were explored. The effects of ectopic expression of Wnt3a in colon cancer cell line HT29 on the tube-structure forming ability and VM-associated proteins *in vitro* as well as on the VM forming ability in animal xenograft model were studied. In addition, we treated Wnt3a-overexpressing cells with Dkk1, a Wnt/β-catenin pathway antagonist, and determined the tube-structure forming ability and expression of VM-related proteins to further verify the VM- promoting effect of the Wnt/β-catenin signaling pathway.

2. Results

2.1. Association of VM Frequency with Clinicopathological Features of Colon Cancer Cases

Using H&E staining (Figure 1A,B) and CD34/PAS double-staining (Figure 1C), VM was distinguished by channels lined with colon cancer cells instead of shuttle-like endothelial cells. The VM channel showed a positive expression for PAS but a negative expression for CD34, confirming that cells around the channels were not composed of endothelium. Red blood cells were found inside the VM channels. No necrotic and infiltrating inflammatory cells were observed around the channels. The endothelial-dependent vessels were positive for CD34.

VM was detected in 39 (19.2%) out of 217 colon cancer cases. The clinical and pathological features of VM in all 217 colon cancer cases are summarized in Table 1. The presence of VM was strongly correlated with histological differentiation ($p < 0.001$), TNM stages ($p < 0.001$), and metastasis/recurrence ($p < 0.001$). The frequency of VM was significantly higher in poorly differentiated colon cancer (30/53, 56.6%) than in well (1/14, 7.1%) and moderately (8/109, 7.3%) differentiated ones. VM was observed in 33 of 69 patients (47.8%) with advanced stage carcinomas (TNM stages III and IV), in 16 of 148 patients (10.8%) with early-stage carcinomas (TNM stages I and II). A total of 77 (35.5%) colon cancer patients experienced metastasis or recurrence. The patients with VM had a higher rate of metastasis or recurrence (24/77, 31.2%) than those ones without VM (15/77, 19.5%). No significant correlations were found between VM and patient age or gender, tumor location or size.

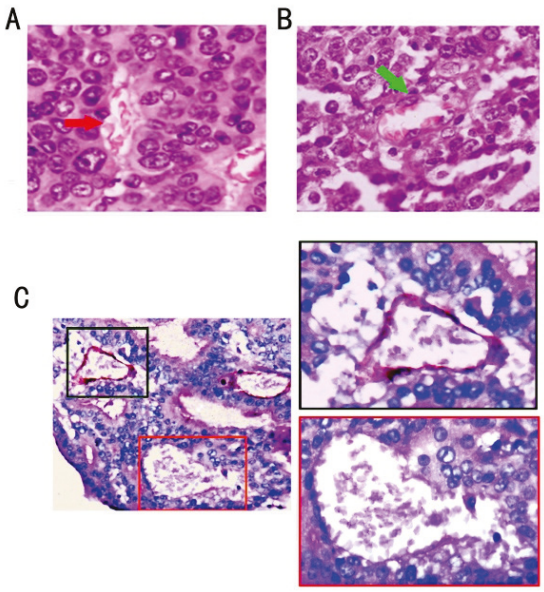

Figure 1. VM structure and endothelial-dependent vessels in colon cancer. (**A**) VM channel (red arrow) lined with tumor cells and containing red blood cells (H&E staining, ×400); (**B**) Endothelial-dependent vessel lined with flat endothelium cells (green arrow) (H&E staining, ×400); (**C**) VM channel formed by tumor cells was negative for CD34; the one lined with a base membrane-like structure was positive for PAS (red square frame); and the endothelial-dependent vessel was both positive for CD34 and PAS (black square frame) (CD34/PAS double staining, ×200).

Table 1. Correlation between VM and clinicopathologic characteristics of colon cancer and expression of Wnt3a and β-catenin.

Variable	Total (%)	Tissue Samples		χ^2	*p* Value
		VM (%)	nonVM (%)		
Age					
<45	28 (12.9)	7 (25.0)	21 (75.0)	1.077	0.298
⩾45	189 (87.1)	32 (16.9)	157 (83.1)		
Sex					
Male	101 (46.5)	19 (18.8)	82 (81.2)	0.09	0.86
Female	116 (53.5)	20 (17.2)	96 (82.8)		
Location					
Left hemicolon	125 (57.6)	25 (20.0)	100 (80.0)	0.475	0.822
Right hemicolon	92 (42.4)	14 (15.2)	78 (84.8)		
Tumor size(cm)					
⩾10	25 (11.5)	6 (24)	19 (76)	0.70	0.278
<10	192 (88.5)	33 (17.2)	159 (82.8)		
Histological differentiation					
Well differentiated	14 (6.4)	1 (7.1)	13 (92.9)	72.11	<0.001 *
Moderately differentiated	109 (50.2)	8 (7.3)	101 (92.7)		
Poorly differentiated	53 (24.4)	30 (56.6)	23 (43.4)		
Mucinous carcinoma	41 (18.9)	0 (0.0)	41 (100.0)		

Table 1. *Cont.*

Variable	Total (%)	Tissue Samples		χ^2	*p* Value
		VM (%)	nonVM (%)		
TNM stage					
TNM Ⅰ	10 (4.6)	0 (0.0)	10 (100.0)		
TNM Ⅱ	138 (63.6)	16 (11.6)	122 (88.4)	23.20	<0.001 *
TNMⅢ	57 (26.3)	16 (28.1)	41 (71.9)		
TNMⅣ	12 (5.5)	7 (58.3)	5 (41.7)		
Metastasis/recurrence					
Present	77 (35.5)	24 (31.2)	53 (68.8)	14.099	<0.001 *
Abscent	140 (64.5)	15 (10.7)	125 (89.3)		
Wnt3a expression					
Negative	22(10.1)	0(0.0)	22(12.4)		
Weak expression	97(44.7)	10(34.5)	87(48.9)	17.7	<0.001 *
Strong expression	98(45.2)	29(65.5)	69(38.7)		
β-catenin expression					
Nuclear negative	175 (80.6)	18 (46.2)	157 (88.2)	36.2	<0.001 *
Nuclear positive	42 (19.4)	21 (53.8)	21 (11.8)		

* Significantly different.

2.2. VM Was Associated with Wnt3a Expression and reCatenin Nuclear Expression

To assess the relationship between VM and Wnt/β-catenin signaling in colon cancer, we determined the expression of Wnt/β-catenin signaling-associated markers, including Wnt3a and β-catenin. The former is a representative canonical Wnt signaling ligand, and the latter is the key regulator of canonical Wnt signaling. As shown in Figure 2, the VM group showed higher Wnt3a expression and lower nuclear β-catenin expression than the non-VM group. In addition, in the non-VM group, β-catenin was expressed mainly in cytoplasm and membrane, whereas it was distributed in the nucleus in the VM group. Statistical analysis results (Table 1) revealed that the strong expression of Wnt3a was more frequently detected in the VM group than in the non-VM group (65.5% *vs.* 38.7%, $p < 0.05$). Meanwhile, the nuclear expression of β-catenin was more frequently found in the VM group than in the non-VM group (53.8% *vs.* 11.8%, $p < 0.05$). The results indicate that VM is associated with Wnt/β-catenin signaling activation in colon cancer.

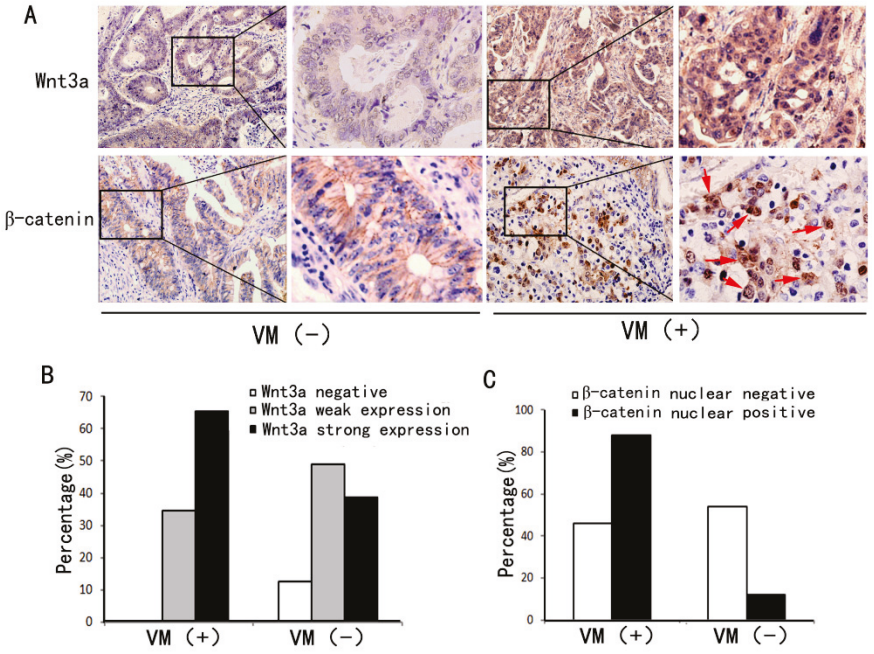

Figure 2. Expressions of Wnt3a and β-catenin in the VM-positive and VM-negative groups. (**A**) Wnt3a expression was higher in VM-positive colon cancer tissue sections (**right**) than in VM-negative samples (**left**). In VM-positive sections, the tumor cells displayed nuclear β-catenin accumulation (red arrows), whereas those in the VM-negative section showed only membranous localization of β-catenin (immunohistochemical staining, ×200); (**B**) Percentages of Wnt3a negative, weak, and strong expression in the VM-positive and VM-negative groups; (**C**) Percentages of β-catenin nuclear positive and negative expression in the VM-positive and VM-negative groups.

2.3. Wnt3a Overexpression Induced the Activation of Canonical Wnt Signaling in HT29 Cells

Our previous study showed that HT29 cells, a better differentiated and less invasive cell line, cannot form vascular networks *in vitro* at 3-D culture conditions [25]. Thus, we used HT29 cells to investigate the effect of canonical Wnt signaling activation and VM formation. We established stable Wnt3a-overexpressed HT29 cells to further study the VM-promoting effect of canonical Wnt signaling on colorectal cancer cells. To rule out clone-to-clone variations, we selected two clones (clone9 and clone20, Figure 3A). Immunofluorescence results showed that more β-catenin was accumulated in the nucleus of cells overexpressing Wnt3a than in control cells (Figure 3B), thereby suggesting that HT29 cells overexpressing Wnt3a activated canonical Wnt signaling.

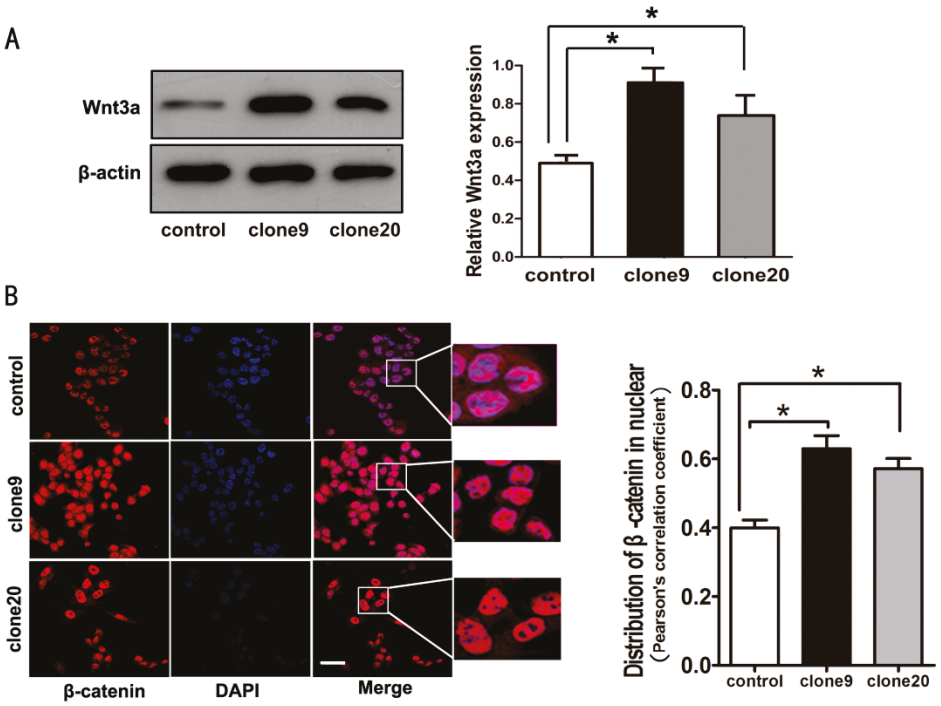

Figure 3. Wnt3a overexpression-induced activation of Wnt/β-catenin signaling in HT29 cells. (**A**) Wnt3a protein expression levels were significantly increased in clone9 and clone20, and HT29 cell pools transfected with Wnt3a plasmid (**left**). Relative amount of protein expression of Wnt3a/β-actin (**right**) (* $p < 0.05$); (**B**) Increased β-catenin accumulation in the nucleus was observed in cells overexpressing Wnt3a compared to control cells (immunofluorescent staining) (**left**). Scale bar: 50 μm. Red signal represents staining for β-catenin, and blue signal represents nuclear DNA staining by DAPI. Microscopic analysis of β-catenin with DAPI showed increased nuclear β-catenin distribution in cells overexpressing Wnt3a (**right**) (* $p < 0.05$).

2.4. Wnt3a Overexpression Promoted the Tube-Like Structure Formation of HT29 Cells in Vitro and Promoted in Vivo Tumor Growth and VM Formation in Animal Models

Three-dimensional culture is used to effectively test not only the vascular behavior of endothelial cells but also the ability of a number of tumor cells to form VM structures. We showed that HT29 cells cannot form tubular structures, whereas Wnt3a-overexpression HT29 cells (clone9 and clone20) formed few tubular structures, thereby indicating that Wnt3a may be an activator for VM formation in HT29 cells (Figure 4A).

Moreover, compared with the controls, the Wnt3a-overexpression cells showed increased expression of VE-cadherin and VEGFR2, which are the most representative VM-associated endothelial phenotype proteins. However, we did not observe a significant change in the VEGFR1 expression in the same cells (Figure 4B).

Wnt3a overexpressing cells grew into larger tumor masses compared with the control cells ($p < 0.05$) (Figure 4C). The VM counts of the xenograft mouse models were determined via CD34/PAS double staining. Similar to the *in vitro* findings, 3 of 10 tumor tissues from Wnt3a-overexpression HT29 cells

(clone9) exhibited a VM structure, whereas all those from control cells showed no VM structures (Figure 4D), thereby further indicating the VM-promoting effect of Wnt3a on colorectal tumors.

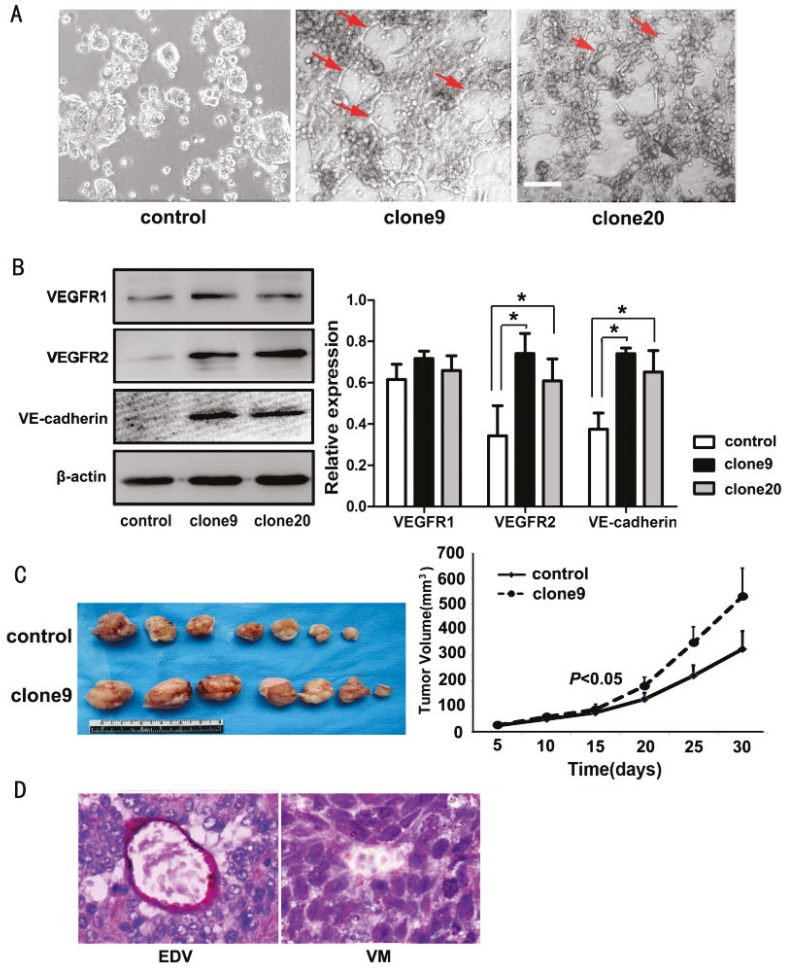

Figure 4. Wnt3a promoted the VM-forming ability in HT29 cells. (**A**) HT29 cells cannot form typical tube-like structures in the 3D culture, whereas Wnt3a-overexpressing clone9 and clone20 cells formed few tubular structures (red arrows). Scale bar: 100 μm; (**B**) Upregulated Wnt3a expression in HT29 cells results in increased VEGFR2 and VE-cadherin expressions. No significant change in VEGFR1 expression was observed (**left**) (* $p < 0.05$). Relative amount of protein expression of VEGFR1, VEGFR2, and VE-cadherin compared with β-actin (**right**); (**C**) Representative xenograft tumors of the control or Wnt3a-overexpressing HT29 cells (clone9) on the 30th day post injection (**left**). Tumor volumes are monitored over time (**right**); (**D**) VM structure and endothelial-dependent vessels in xenograft tumors (CD34/PAS double staining, ×400).

2.5. Dkk1 Inhibited the Tube-Structure Formation in Vitro and Restored the VEGFR2 and VE-Cadherin Expression in Wnt3a-Upregulation HT29 Cells

Dkk1 functions as an antagonist of the Wnt/β-catenin pathway by binding to lipoprotein receptor-related protein 5 or 6 (LRP5/6) and preventing the formation of Wnt-Fz-LRP ternary complexes and downstream signaling transduction. After Dkk1 treatment, Wnt3a-overexpressing cells failed to form vessel-like tube formation (Figure 5A). Furthermore, Dkk1 treatment decreased the VEGFR2 and

VE-cadherin expressions in Wnt3a-upregulation cells (Figure 5B). These findings further verified that Wnt/β-catenin pathway activation had an important function in the VM-inducing effect of Wnt3a.

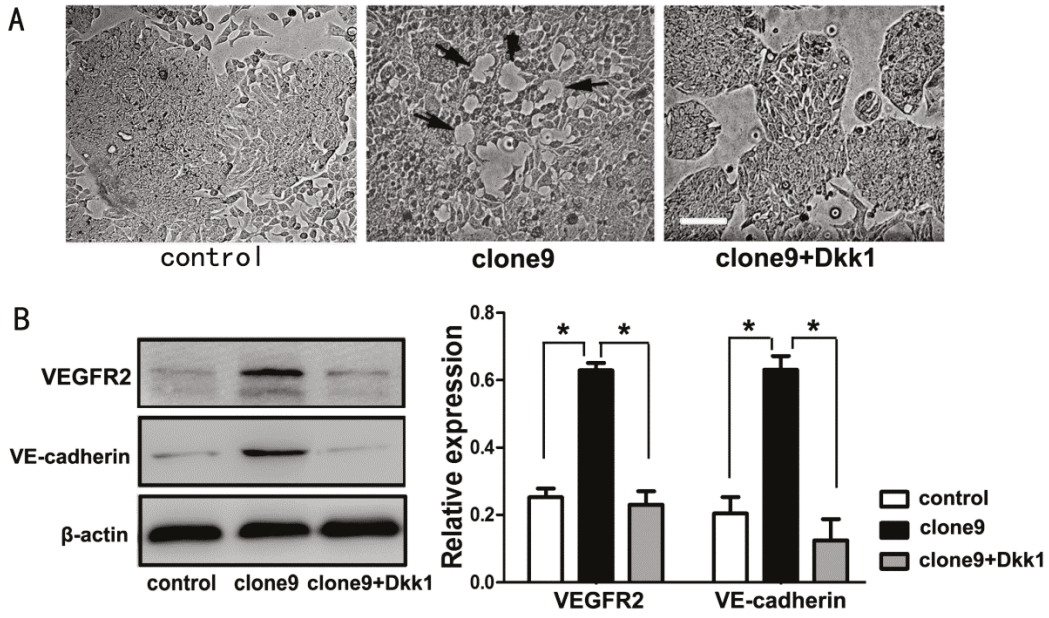

Figure 5. Dkk1 reversed the VM-forming ability in Wnt3a-overexpressing HT29 cells. (**A**) Dkk1 inhibited the *in vitro* tube-like structure formation (black arrows) of Wnt3a-overexpressing HT29 cells (clone9). Scale bar: 100 μm; (**B**) Dkk1 restored the expressions of VEGFR2 and VE-cadherin in clone9 cells (**left**). Relative amount of protein expressions of VEGFR2 and VE-cadherin compared with β-actin (**right**) (* $p < 0.05$).

3. Discussion

VM was first described in melanoma in 1999 [4], and this special tumor microcirculation pattern was observed in many different tumor types, including breast cancer, lung cancer, prostate cancer, ovarian cancer, synovial sarcoma, gastrointestinal stromal tumor, and glioblastoma [8–13]. VM describes the formation of a fluid-conducting vasculogenic-like network by tumor cells, particularly poorly differentiated ones. VM structures are composed of basement membranes that are stained positive with PAS and lined by tumor cells; no endothelial cells can be found on their inner wall. On one hand, VM may function as a complementary means to provide oxygen and nutrition to tumor masses independent of conventional endothelial vessels. On the other hand, the irregularly arranged tumor cells lining the lumen are directly exposed to the bloodstream. Thus, these cells can easily enter the microcirculation, which leads to distant dissemination. Except for its potential function in facilitating tumor cell metastasis to the blood stream and, subsequently, to distant organs, the tubular networks formed by highly aggressive tumor cells can contribute to tumor circulation because they appear to be capable of blood flow. Thus, the presence of VM in many tumors is strongly associated with poor clinical outcomes. In the present study, the presence of VM in colon cancer was characterized by histological differentiation and TNM stages. This result is consistent with the results of our previous study on colorectal carcinoma [25], in which we also indicated that VM is a prognostic marker for shorter survival.

A growing body of evidence has revealed the importance of Wnt/β-catenin signaling pathways in endothelial cell differentiation and vascular remodeling. During embryonic development, gain-of-function mutation of β-catenin in endothelial leads to vascular remodeling [26]. The activation of β-catenin can induce embryonic stem cells to differentiate into arterial endothelial cell [27]. Gherghe reported that the overexpression of Wnt1 in endothelial cells can elicit cellular responses that are critical for angiogenesis [28]. Blankesteijn observed that Wnt/β-catenin signaling is activated during pathological neovascularization but not in healthy, resting vasculatures [29]. Wnt/β-catenin signaling regulates the expression of angiogenic factors, including VEGF and IL-8 [30]. Although previous observations have shown the capacity of canonical Wnt signaling in regulating endothelial-dependent vessel formation, the present study provides the first clinical and experimental evidence that confirms the intimate link between Wnt/β-catenin signaling and VM formation. In human colon cancer tissue samples, higher levels of Wnt3a expression and β-catenin nuclear distribution were observed in the VM positive group than in the negative group. We further isolated stable Wnt3a-overexpressing HT29 cell clones and found that Wnt3a increased the intracellular distribution of β-catenin, which is an indicator of activated canonical Wnt signaling. More importantly, the ectopic expression of Wnt3a resulted in increased capacity to form tube-like structures on Matrigel *in vitro* and increased VM incidence in mouse-transplanted tumors. All these results indicated the VM-inducing effect of Wnt/β-catenin pathway in colon cancer.

VM repeats the pattern of embryonic vasculogenic networks. Molecular profiling of cells capable of VM showed that a number of highly upregulated genes are involved in angiogenesis and vasculogenesis [31]. When VEGF-A binds in an autocrine or paracrine manner, VEGFR2 primarily regulates endothelial cell differentiation, survival, proliferation, and migration. Moreover, the expression of VEGFR2 has been described as associated with VM formation [32]. VE-cadherin, a member of the cadherin family specifically expressed in endothelial cells, has a pivotal function in vascular integrity and regulates endothelial cell assembly into tubular structures. VE-cadherin was also identified as an important factor in VM formation because tumor cells lacking VE-cadherin are incapable of forming VM [33]. In this study, the activation of Wnt/β-catenin signaling by ectopic Wnt3a expression promoted VM formation and also enhanced the expressions of VEGFR2 and VE-cadherin, thereby suggesting that Wnt/β-catenin signaling may help colon cancer cells acquire a differentiation potential for endothelial cells.

Wnt3a not only activates Wnt/β-catenin signaling but also functions simultaneously with signaling pathways such as FAK or TGFβ [34,35]. Dkk1 is a potent antagonist of the Wnt/β-catenin signaling pathway. Dkk1 functions by binding to LRP5/6, thereby interfering the formation of frizzled-LRP6 complexes and inhibiting TCF/LEF transcription. Our results showed that Dkk1 treatment significantly inhibited the formation of tube-like structures of Wnt3a-overexpressing HT29 cells *in vitro* and induced decreased expressions of VEGFR2 and VE-cadherin, thereby indicating that the VM-inducing effect caused by Wnt3a was due to the stimulative effect of Wnt3a on the Wnt/β-catenin pathway.

In conclusion, this study is the first to report on a previously unrecognized function of Wnt/β-catenin signaling as an important regulatory pathway for VM formation. The results might have a number of implications for clinically useful therapy targets aimed at VM in the future.

4. Materials and Methods

4.1. Tissue Samples

In the current study, 217 formalin-fixed, paraffin-embedded human colon cancer tissue samples were from Tianjin Medical University Cancer Institute and Hospital from July 2002 to June 2004. All the patients did not receive chemotherapy or radiotherapy before operation. Data of clinical parameters were obtained from patients' clinical records. The pathological diagnosis of all cases were independently verified by two senior pathologists by observing the H&E sections conserved in Pathology Department of Tianjin Medical University Cancer Institute and Hospital.

4.2. Cells and Reagents

Human colon cancer cell line HT29 was obtained from Cell Resource Center, Institute of Basic Medical Sciences, Chinese Academy of Medical Sciences, Peking Union Medical College (Beijing, China). HT29 cells were cultured in DMEM/F12 medium supplemented with 5% fetal calf serum (FCS) at 37 °C and 5% CO_2. Antibodies for Dkk1, CD34, VEGFR1, VEGFR2 and β-actin were from Santa Cruz (CA, USA). Antibodies for Wnt3a, VE-cadherin and β-catenin were from Abcam (Cambridge, UK). The secondary HRP-conjugated antibodies were from Zhongshan Chemical Co. (Beijing, China). Goat anti-mouse IgG-FITC were from Santa Cruz. The eukaryotic expression vector GV230 containing whole coding sequence of Wnt3a was original obtained from Genechem Technology (Shanghai, China) (The plasmid contains a GFP tag and is neomycin resistant). In this study, the coding sequence of Wnt3a was amplified via PCR using the following primers: forward primer 5′-GAG GAA TTC ATG GCC CCA CTC GGA TAC-3′ which contains an EcoR I recognition site, reverse primer 5′-GAC AGC TCG AGCTA CT TGC AGG TGT GCA CGT CGT AG-3′, which contains an Xho I recognition site, and then subcloned into vector pcDNA3.1 (+) eukaryotic expression vector. The recombinant plasmid was verified by DNA sequencing and double enzyme digestion (EcoR I and Xho I). Matrigel was from BD Biosciences (San Jose, CA, USA). BALB/C nude mice (4 to 6 weeks old) were obtained from Wei Tong Li Hua Experimental Animal Co., Ltd. (Beijing, China). Dkk1 recombinant protein was from R&D Systems (South Logan, UT, USA). For Dkk1 administration *in vitro*, Dkk1 (1 μg/mL) was added to culture medium. Fifty percent of the medium was replaced with fresh conditioned medium containing Dkk1 every 24 h. After 48 h Dkk1 treatment, cells were harvested and the total cell lysates were collected for measurement by Western blot.

4.3. Tissue Immunohistochemical Analysis

The streptavidin-biotin-peroxidase immunohistochemical staining method was used in this study. Briefly, after antigen retrieval for 20 min in citrate buffer (0.01 M citric acid, pH 6.0) at room temperature, sections were incubated overnight at 4 °C with the primary specific antibody (Wnt3a 1:100, and β-catenin 1:50). Then secondary HRP-conjugated antibody was used for 1h at room temperature to immunostained the sections and 3,3′-diaminobenzidine buffer was used as substrate to reveal the signals. The sections were scored blindly by two pathologist using a microscope at 200× magnification. Wnt3a immunohistochemical staining was evaluated by assessing staining intensity and density established by

Qi *et al.* [20]. It was considered nuclear β-catenin-positive expression if more than 10% percentage of tumor cells showed brown granules in nuclei.

4.4. CD34/Periodic Acid Schiff Double Staining

After immunohistochemical staining for CD34 (1:100), the sections were washed with running distilled water for 5 min and incubated with periodic acid for 15 min and Schiff reagent. Finally, all of the sections were counterstained with hematoxylin, dehydrated with ascending grade ethanol and mounted.

4.5. Plasmid Transfection

Transfection with plasmid carrying Wnt3a and controlled scrambled plasmid was performed with Lipofectamine according to the manufacturer's instructions. HT29 cells were seeded in a 6-well plate (3×10^5 cells/well). After 16 h at approximately 60% confluence, the cells were transfected with Wnt3a plasmid (4 μg/well) in 10 μL of transfection reagent in a final volume of 2 mL of transfection medium. Four hours after transfection, full culture medium without antibiotics was added to the mixture. Twenty-four hours after transfection, neomycin-resistant cells were screened to establish stable HT29 cells that overexpressed Wnt3a.

4.6. Western Blot Analysis

Total protein (35 μg) was resolved by 10% SDS-PAGE and transferred by electroblotting onto PVDF membrane (Millipore, Temecula, CA, USA). Blots were blocked for 1 h and incubated with primary antibodies (Wnt3a 1:500, VEGFR1 1:200, VEGFR2 1:200, VE-cadherin 1:500 and β-actin 1:2000) overnight at 4 °C. Subsequently, blots were washed in TBS containing 0.1% Tween20 and labeled with goat anti-mouse or goat anti-rabbit IgG-HRP (1:5000; Santa Cruz Biotechnology). Immunoreactive bands were visualized on an autoradiography film (Blue X-Ray Film, Phoenix Research, Candler, NC, USA), and the relative density of bands was analyzed using an Odyssey infrared scanner (LI-COR Bioscience, Lincoln, NE, USA).

4.7. Immunofluorescence

Cells were plated on sterile glass cover slips 1 day prior to staining. Cells were fixed with 10% formalin in PBS for 10 min, quenched with 50 mM NH_4Cl for 10 min and 0.2% triton for 10 min. Then, after blocking with 3% BSA for 1 h, the slips were incubated overnight with anti-β-catenin (1:50) at 4 °C. Slides were washed in PBS and labeled with secondary antibodie for 1 h in the dark at room temperature. After immunolabeling, slides were washed, counterstained with DAPI and viewed with fluorescent microscopy (Olympus, Tokyo, Japan). Colocalization efficiency of DAPI and β-catenin was calculated through Image J software (NIH, Bethesda, MD, USA). The nuclear regions dyed with DAPI were selected as the region of interest to quantify the nuclear distribution efficiency of β-catenin. Eighteen images were analyzed.

4.8. In Vitro Three-Dimensional (3-D) Coculture

VM-forming ability was tested by using 3-D culture *in vitro*. Matrigel (0.1 mL/well) was applied on the twenty-four-well culture plate and incubated at 37 °C for half an hour. The cells were trypsinized and suspended in the complete medium at 2.5×10^5 cells/mL, plated onto the surface of Matrigel at 1 mL/well, and incubated at 37 °C for 48 h.

4.9. Xenograft Mouse Model

Twenty mice were randomly divided into two groups and received either 3×10^6 control cells or clone9 cells by subcutaneous injection in the right groin. Tumor volumes were measured every 5 days. All mice were killed on the 30th day post injection. Tumor masses were excised, fixed in formalin, embedded in paraffin, and then were subjected to H&E staining and CD34/PAS double staining.

4.10. Statistical Analysis

SPSS 16.0 software (SPSS Inc., Chicago, IL, USA) was used for data statistical analysis. $p < 0.05$ were considered statistically significant. The associations between VM and clinicopathologic parameters and the differential expression of Wnt3a and β-catenin between groups were compared using Chi-squared or Fisher's exact tests in human samples. Differences between groups were assessed by the Mann-Whitney U-test and Student's *t*-test.

5. Conclusions

Wnt/β-catenin signaling is involved in VM formation in colon cancer and might contribute to the development of more accurate treatment modalities aimed at VM.

Ackonwledgments

This study was supported by the Key Project of the National Natural Science Foundation of China (No. 81230050), the National Natural Science Foundation of China (No. 81402420 and No. 81201648), the Key Project of Tianjin Natural Science Foundation (No. 12JCZDJC23600), the Project of Tianjin Natural Science Foundation (No. 15JCQNJC12400).

Author Contributions

Lisha Qi, Baocun Sun and Wenfeng Cao designed the study and wrote the manuscript; Lisha Qi, Wangzhao Song, Zhiyong Liu and Xiulan Zhao performed the experiments.

Conflicts of Interest

The authors declare no conflict of interest.

References

1. Moschetta, M.; Mishima, Y.; Sahin, I.; Manier, S.; Glavey, S.; Vacca, A.; Roccaro, A.M.; Ghobrial, I.M. Role of endothelial progenitor cells in cancer progression. *Biochim. Biophys. Acta* **2014**, *1846*, 26–39.
2. Pezzella, F.; Gatter, K. Non-angiogenic tumours unveil a new chapter in cancer biology. *J. Pathol.* **2015**, *235*, 381–383.
3. Qian, C.N. Hijacking the vasculature in ccrcc-co-option, remodelling and angiogenesis. *Nat. Rev. Urol.* **2013**, *10*, 300–304.
4. Maniotis, A.J.; Folberg, R.; Hess, A.; Seftor, E.A.; Gardner, L.M.; Pe'er, J.; Trent, J.M.; Meltzer, P.S.; Hendrix, M.J. Vascular channel formation by human melanoma cells *in vivo* and *in vitro*: Vasculogenic mimicry. *Am. J. Pathol.* **1999**, *155*, 739–752.
5. Zhang, S.; Zhang, D.; Wang, Y.; Zhao, W.; Guo, H.; Zhao, X.; Sun, B. Morphologic research of microcirculation patterns in human and animal melanoma. *Med. Oncol.* **2006**, *23*, 403–409.
6. Frenkel, S.; Barzel, I.; Levy, J.; Lin, A.Y.; Bartsch, D.U.; Majumdar, D.; Folberg, R.; Pe'er, J. Demonstrating circulation in vasculogenic mimicry patterns of uveal melanoma by confocal indocyanine green angiography. *Eye* **2008**, *22*, 948–952.
7. Ruf, W.; Seftor, E.A.; Petrovan, R.J.; Weiss, R.M.; Gruman, L.M.; Margaryan, N.V.; Seftor, R.E.; Miyagi, Y.; Hendrix, M.J. Differential role of tissue factor pathway inhibitors 1 and 2 in melanoma vasculogenic mimicry. *Cancer Res.* **2003**, *63*, 5381–5389.
8. Zhang, S.; Fu, Z.; Wei, J.; Guo, J.; Liu, M.; Du, K. Peroxiredoxin 2 is involved in vasculogenic mimicry formation by targeting vegfr2 activation in colorectal cancer. *Med. Oncol.* **2015**, *32*, 414.
9. Zhang, D.; Sun, B.; Zhao, X.; Ma, Y.; Ji, R.; Gu, Q.; Dong, X.; Li, J.; Liu, F.; Jia, X.; *et al.* Twist1 expression induced by sunitinib accelerates tumor cell vasculogenic mimicry by increasing the population of cd133+ cells in triple-negative breast cancer. *Mol. Cancer* **2014**, *13*, 207.
10. Kaessmeyer, S.; Bhoola, K.; Baltic, S.; Thompson, P.; Plendl, J. Lung cancer neovascularisation: Cellular and molecular interaction between endothelial and lung cancer cells. *Immunobiology* **2014**, *219*, 308–314.
11. Du, J.; Sun, B.; Zhao, X.; Gu, Q.; Dong, X.; Mo, J.; Sun, T.; Wang, J.; Sun, R.; Liu, Y. Hypoxia promotes vasculogenic mimicry formation by inducing epithelial-mesenchymal transition in ovarian carcinoma. *Gynecol. Oncol.* **2014**, *133*, 575–583.
12. Liu, X.; Wang, X.; Du, W.; Chen, L.; Wang, G.; Cui, Y.; Liu, Y.; Dou, Z.; Wang, H.; Zhang, P.; *et al.* Suppressor of fused (sufu) represses gli1 transcription and nuclear accumulation, inhibits glioma cell proliferation, invasion and vasculogenic mimicry, improving glioma chemo-sensitivity and prognosis. *Oncotarget* **2014**, *5*, 11681–11694.
13. Liu, T.; Sun, B.; Zhao, X.; Li, Y.; Gu, Q.; Dong, X.; Liu, F. Oct4 expression and vasculogenic mimicry formation positively correlate with poor prognosis in human breast cancer. *Int. J. Mol. Sci.* **2014**, *15*, 19634–19649.
14. Soda, Y.; Myskiw, C.; Rommel, A.; Verma, I.M. Mechanisms of neovascularization and resistance to anti-angiogenic therapies in glioblastoma multiforme. *J. Mol. Med.* **2013**, *91*, 439–448.

15. Xu, Y.; Li, Q.; Li, X.Y.; Yang, Q.Y.; Xu, W.W.; Liu, G.L. Short-term anti-vascular endothelial growth factor treatment elicits vasculogenic mimicry formation of tumors to accelerate metastasis. *J. Exp. Clin. Cancer Res.* **2012**, *31*, 16.
16. Reis, M.; Liebner, S. Wnt signaling in the vasculature. *Exp. Cell Res.* **2013**, *319*, 1317–1323.
17. Choi, H.J.; Park, H.; Lee, H.W.; Kwon, Y.G. The wnt pathway and the roles for its antagonists, dkks, in angiogenesis. *IUBMB Life* **2012**, *64*, 724–731.
18. Dejana, E. The role of wnt signaling in physiological and pathological angiogenesis. *Circ. Res.* **2010**, *107*, 943–952.
19. Vincan, E.; Darcy, P.K.; Farrelly, C.A.; Faux, M.C.; Brabletz, T.; Ramsay, R.G. Frizzled-7 dictates three-dimensional organization of colorectal cancer cell carcinoids. *Oncogene* **2007**, *26*, 2340–2352.
20. Qi, L.; Sun, B.; Liu, Z.; Cheng, R.; Li, Y.; Zhao, X. Wnt3a expression is associated with epithelial-mesenchymal transition and promotes colon cancer progression. *J. Exp. Clin. Cancer Res.* **2014**, *33*, 107.
21. Qi, L.; Sun, B.; Liu, Z.; Li, H.; Gao, J.; Leng, X. Dickkopf-1 inhibits epithelial-mesenchymal transition of colon cancer cells and contributes to colon cancer suppression. *Cancer Sci.* **2012**, *103*, 828–835.
22. Lavergne, E.; Hendaoui, I.; Coulouarn, C.; Ribault, C.; Leseur, J.; Eliat, P.A.; Mebarki, S.; Corlu, A.; Clement, B.; Musso, O. Blocking wnt signaling by sfrp-like molecules inhibits *in vivo* cell proliferation and tumor growth in cells carrying active beta-catenin. *Oncogene* **2011**, *30*, 423–433.
23. Qi, H.; Sun, B.; Zhao, X.; Du, J.; Gu, Q.; Liu, Y.; Cheng, R.; Dong, X. Wnt5a promotes vasculogenic mimicry and epithelial-mesenchymal transition via protein kinase calpha in epithelial ovarian cancer. *Oncol. Rep.* **2014**, *32*, 771–779.
24. Yao, L.; Sun, B.; Zhao, X.; Zhao, X.; Gu, Q.; Dong, X.; Zheng, Y.; Sun, J.; Cheng, R.; Qi, H.; *et al.* Overexpression of wnt5a promotes angiogenesis in nsclc. *BioMed Res. Int.* **2014**, *2014*, 832562.
25. Liu, Z.; Sun, B.; Qi, L.; Li, H.; Gao, J.; Leng, X. Zinc finger e-box binding homeobox 1 promotes vasculogenic mimicry in colorectal cancer through induction of epithelial-to-mesenchymal transition. *Cancer Sci.* **2012**, *103*, 813–820.
26. Corada, M.; Nyqvist, D.; Orsenigo, F.; Caprini, A.; Giampietro, C.; Taketo, M.M.; Iruela-Arispe, M.L.; Adams, R.H.; Dejana, E. The wnt/beta-catenin pathway modulates vascular remodeling and specification by upregulating dll4/notch signaling. *Dev. Cell* **2010**, *18*, 938–949.
27. Wang, X.; Xiao, Y.; Mou, Y.; Zhao, Y.; Blankesteijn, W.M.; Hall, J.L. A role for the beta-catenin/t-cell factor signaling cascade in vascular remodeling. *Circ. Res.* **2002**, *90*, 340–347.
28. Goodwin, A.M.; Kitajewski, J.; D'Amore, P.A. Wnt1 and wnt5a affect endothelial proliferation and capillary length; wnt2 does not. *Growth Factors* **2007**, *25*, 25–32.
29. Blankesteijn, W.M.; van Gijn, M.E.; Essers-Janssen, Y.P.; Daemen, M.J.; Smits, J.F. Beta-catenin, an inducer of uncontrolled cell proliferation and migration in malignancies, is localized in the cytoplasm of vascular endothelium during neovascularization after myocardial infarction. *Am. J. Pathol.* **2000**, *157*, 877–883.
30. Masckauchan, T.N.; Shawber, C.J.; Funahashi, Y.; Li, C.M.; Kitajewski, J. Wnt/beta-catenin signaling induces proliferation, survival and interleukin-8 in human endothelial cells. *Angiogenesis* **2005**, *8*, 43–51.

31. Seftor, E.A.; Meltzer, P.S.; Schatteman, G.C.; Gruman, L.M.; Hess, A.R.; Kirschmann, D.A.; Seftor, R.E.; Hendrix, M.J. Expression of multiple molecular phenotypes by aggressive melanoma tumor cells: Role in vasculogenic mimicry. *Crit. Rev. Oncol./Hematol.* **2002**, *44*, 17–27.
32. Francescone, R.; Scully, S.; Bentley, B.; Yan, W.; Taylor, S.L.; Oh, D.; Moral, L.; Shao, R. Glioblastoma-derived tumor cells induce vasculogenic mimicry through flk-1 protein activation. *J. Biol. Chem.* **2012**, *287*, 24821–24831.
33. Hendrix, M.J.; Seftor, E.A.; Meltzer, P.S.; Gardner, L.M.; Hess, A.R.; Kirschmann, D.A.; Schatteman, G.C.; Seftor, R.E. Expression and functional significance of ve-cadherin in aggressive human melanoma cells: Role in vasculogenic mimicry. *Proc. Natl. Acad. Sci. USA* **2001**, *98*, 8018–8023.
34. Fonar, Y.; Frank, D. Fak and wnt signaling: The meeting of two pathways in cancer and development. *Anti-Cancer Agents Med. Chem.* **2011**, *11*, 600–606.
35. Van den Bosch, M.H.; Blom, A.B.; van Lent, P.L.; van Beuningen, H.M.; Davidson, E.N.B.; van der Kraan, P.M.; van den Berg, W.B. Canonical wnt signaling skews tgf-beta signaling in chondrocytes towards signaling via alk1 and smad 1/5/8. *Cell. Signal.* **2014**, *26*, 951–958.

© 2015 by the authors; licensee MDPI, Basel, Switzerland. This article is an open access article distributed under the terms and conditions of the Creative Commons Attribution license (http://creativecommons.org/licenses/by/4.0/).

Int. J. Mol. Sci. **2015**, *16*, 19612-19630; doi:10.3390/ijms160819612

OPEN ACCESS
International Journal of
Molecular Sciences
ISSN 1422-0067
www.mdpi.com/journal/ijms

Article

Preliminary Evidence on the Diagnostic and Molecular Role of Circulating Soluble EGFR in Non-Small Cell Lung Cancer

Filippo Lococo [1], Massimiliano Paci [1], Cristian Rapicetta [1], Teresa Rossi [2], Valentina Sancisi [2], Luca Braglia [3], Silvio Cavuto [3], Alessandra Bisagni [4], Italia Bongarzone [5], Douglas M. Noonan [6,7], Adriana Albini [2,*] and Sally Maramotti [2]

1 Thoracic Surgery Unit, Department of Cardiology, Thoracic and Vascular Surgery, IRCCS Arcispedale Santa Maria Nuova, Reggio Emilia 42123, Italy; E-Mails: filippo.lococo@asmn.re.it (F.L.); massimiliano.paci@asmn.re.it (M.P.); cristian.rapicetta@asmn.re.it (C.R.)

2 Laboratory of Translational Research, Research and Statistic Infrastructure, IRCCS Arcispedale Santa Maria Nuova, Reggio Emilia 42123, Italy; E-Mails: teresa.rossi@asmn.re.it (T.R.); valentina.sancisi@asmn.re.it (V.S.); sally.maramotti@asmn.re.it (S.M.)

3 Clinical Trials and Statistics Unit, Department of Infrastructure Research and Statistics, IRCCS Arcispedale Santa Maria Nuova, Reggio Emilia 42123, Italy; E-Mails: luca.braglia@asmn.re.it (L.B.); silvio.cavuto@asmn.re.it (S.C.)

4 Pathology Unit, Department of Oncology and Advanced Technologies, IRCCS Arcispedale Santa Maria Nuova, Reggio Emilia 42123, Italy; E-Mail: alessandra.bisagni@asmn.re.it

5 Proteomics Laboratory, Department of Experimental Oncology and Molecular Medicine, Fondazione IRCCS Istituto Nazionale Tumori, Milan 20133, Italy; E-Mail: italia.bongarzone@istitutotumori.mi.it

6 Department of Biotechnology and Life Sciences, University of Insubria, Varese 21100, Italy; E-Mail: douglas.noonan@uninsubria.it

7 Scientific and Technology Park, IRCCS MultiMedica, Milan 20138, Italy

* Author to whom correspondence should be addressed; E-Mail: adriana.albini@asmn.re.it or albini.adriana@gmail.com; Tel.: +39-0522-2956-45; Fax: +39-0522-2955-61.

Academic Editor: William Chi-shing Cho

Int. J. Mol. Sci. **2015**, *16*

Received: 16 June 2015 / Accepted: 5 August 2015 / Published: 19 August 2015

Abstract: Assessment of biological diagnostic factors providing clinically-relevant information to guide physician decision-making are still needed for diseases with poor outcomes, such as non-small cell lung cancer (NSCLC). Epidermal growth factor receptor (EGFR) is a promising molecule in the clinical management of NSCLC. While the EGFR transmembrane form has been extensively investigated in large clinical trials, the soluble, circulating EGFR isoform (sEGFR), which may have a potential clinical use, has rarely been considered. This study investigates the use of sEGFR as a potential diagnostic biomarker for NSCLC and also characterizes the biological function of sEGFR to clarify the molecular mechanisms involved in the course of action of this protein. Plasma sEGFR levels from a heterogeneous cohort of 37 non-advanced NSCLC patients and 54 healthy subjects were analyzed by using an enzyme-linked immunosorbent assay. The biological function of sEGFR was analyzed *in vitro* using NSCLC cell lines, investigating effects on cell proliferation and migration. We found that plasma sEGFR was significantly decreased in the NSCLC patient group as compared to the control group (median value: 48.6 *vs.* 55.6 ng/mL respectively; $p = 0.0002$). Moreover, we demonstrated that sEGFR inhibits growth and migration of NSCLC cells *in vitro* through molecular mechanisms that included perturbation of EGF/EGFR cell signaling and holoreceptor internalization. These data show that sEGFR is a potential circulating biomarker with a physiological protective role, providing a first approach to the functional role of the soluble isoform of EGFR. However, the impact of these data on daily clinical practice needs to be further investigated in larger prospective studies.

Keywords: Epidermal growth factor receptor (EGFR); EGFR isoform (sEGFR); non-small cell lung cancer (NSCLC); biomarker; diagnosis

1. Introduction

Primary lung cancer is the most common malignancy and the leading cause of human cancer deaths worldwide [1]. Even though many efforts to improve lung cancer outcomes have been accomplished, long-term survival has not improved significantly over the last 20 years, with a five-year cumulative survival rate that remains at only 15%. The role of early diagnosis using low-dose computed tomography (LDCT) in lung cancer mortality reduction is questioned by many researchers [2], despite the results of National Lung Screening Trial Research Team (NLST), which provided important information regarding the use of CT to reduce lung cancer mortality [3]. On the other hand, to date, there is no consensus on the proven clinical value for use of biomarkers for diagnosis, staging, prognosis, and monitoring for disease relapse or treatment response in lung cancer. The development of biomarkers for lung cancer is a public health imperative since accurate diagnosis and treatment are associated with up to a 92% five-year survival [4]. Epidermal Growth Factor Receptor (EGFR) is a membrane-bound tyrosine kinase glycoprotein, expressed on the surface of epithelial cells [5]. It has

been implicated in the molecular pathogenesis of several cancers, including non-small cell lung cancer (NSCLC) [6]. EGFR is composed of an extracellular domain (ECD), a transmembrane lipophilic segment, and an intracellular domain (ICD) containing a tyrosine kinase domain. EGFR is best known for its classical function as a receptor tyrosine kinase localized on the plasma membrane and activated upon ligand binding. Activated EGFR recruits a number of downstream signaling molecules, leading to the activation of several pathways involved in tumor growth, progression, and survival [7]. In addition to the full-length transmembrane form (p170) of EGFR (Figure S1, Isoform A), normal and malignant cells synthesize soluble EGFR isoforms (sEGFRs) that embody extensive portions of the ECD. These isoforms are produced either by proteolytic cleavage of the full-length receptor or by alternative splicing of mRNA transcripts, but their biological functions remain unclear [8,9]. The existence of two highly-glycosylated EGFR soluble isoforms of about 110 kDa each, composed of the ECD of the receptor, has been reported [8,10]. The isoform B (Figure S1) arises by proteolytic cleavage of EGFR at the plasma membrane between the amino acid residues gly 625 and met 626. This isoform is called PI-sEGFR and was detected in the conditioned medium of malignant cell lines that express 7×10^5 or higher receptors/cell [8]. The isoform C (Figure S1), also called p110 sEGFR, is derived from a 3-kb alternate mRNA transcript of the human EGFR protoncogene [10]. This protein corresponds to the extracellular domain of EGFR to amino acid residue 603, followed by 78 unique COOH-terminal amino acids. The p110 EGFR is associated with the cell membrane [11] and can be released, allowing detection in human serum and plasma [9,12]. The existence of this circulating sEGFR isoform stimulated investigation of its role as a potential circulating biomarker. Several studies suggest that alterations in sEGFR levels may be useful in cancer diagnosis and in monitoring disease recurrence and outcome, especially in patients with ovarian or breast cancer [9,13–15]. In the context of lung cancer, the debate about the use of sEGFR for NSCLC diagnosis is ongoing, although sEGFR has been studied in predicting prognosis and therapeutic responsiveness [16,17]. A few preliminary studies were conducted and the data obtained remain unclear; these publications report the puzzling observation that circulating sEGFR levels were higher in healthy subjects and tended to decrease in patients with neoplastic lesions [18–20]. Moreover, the biological role of sEGFR and the course of action of this protein in the context of NSCLC still needs to be defined. Here we investigated whether sEGFR may be a potential biomarker able to predict diagnosis in NSCLC patients, showing a significant negative correlation between NSCLC and sEGFR levels. We further characterized the biological function of sEGFR using *in vitro* models, demonstrating the antitumor activity of sEGFR and providing a first approach towards characterizing the functional role of the soluble isoform of EGFR.

2. Results

Patients (n = 37) and controls (n = 54) exhibit baseline differences regarding age (mean ± SD are 69.9 ± 8.3 for patients, 58.6 ± 6.0 for controls, $p < 0.0001$) and smoking habits (smokers are 81% of patients, 20.4% of controls, $p < 0.0001$). Gender distribution is not statistically different (females are 29.7% of patients, 18.5% for controls, $p = 0.320$). Focusing on cases, surgical procedures consisted of (bi)lobectomy in 32 cases (86.5%) and anatomic segmentectomy in the remaining five cases (13.5%), while no patients underwent pneumonectomy. Radical lymphnodal dissection was performed in all but

two patients (who underwent mediastinal nodal sampling). Complete resection was achieved in all cases. Histological examination revealed 27 adenocarcinomas and 10 squamous cell carcinomas.

2.1. Plasma Levels of sEGFR Are Lower in NSCLC Patients than Healthy Controls

Levels of sEGFR were examined by ELISA in a total of 91 plasma samples, 37 from patients with NSCLC and 54 healthy subjects. The levels of plasma sEGFR were significantly lower in patients with NSCLC as compared with healthy controls (median values: 48.6 *vs.* 55.6 ng/mL respectively; $p = 0.0002$; Table 1, Figure 1a). We estimated and plotted a ROC curve to assess the potential usefulness of plasma sEGFR as a non-invasive biomarker for the diagnosis of NSCLC. The ROC analyses revealed that plasma sEGFR levels were reasonably robust in discriminating patients with NSCLC from control subjects, with an AUC value of 0.727 (95% CI: 0.621 to 0.834) (Figure 1b). Using a cut-off value of 53.058 ng/mL, and considering a sEGFR value under this limit as predictive of disease (positive test), the sensitivity and specificity were 70.4% and 70.3%, respectively. The odds ratio according to the same cut-off value was 5.613 (95% CI: 2.247 to 14.023). However, the marker contribution to a diagnostic model that included age (in continuous), gender and smoking habits, was no longer statistically significant (OR for 1 unit increase of sEGFR to "case diagnosis" is 0.978, 95% CI: 0.909 to 1.046, $p = 0.519$). Furthermore, examining the associations between the sEGFR expression levels with the clinical-pathological characteristics of the NSCLC patients, we found no significant association for age, gender, smoking habit, and histological type (Table 2), suggesting that these factors did not influence sEGFR levels. There was a positive trend when we analyzed the correlation between grading and sEGFR levels; patients who presented with a G3-NSCLC had lower values of sEGFR (47.5 ng/mL) as compared to patients with G1/G2-NSCLC (56.2 and 54.2 ng/mL), although this difference did not reach statistical significance ($p = 0.082$). We also examined whether copy number changes (polysomy) involving the EGFR locus impacted on diagnosis when analyzed in the context of the sEGFR levels. EGFR copy numbers were tested in all patients by FISH analysis. When we compared sEGFR levels of patients with EGFR amplification ($n = 7$) to patients having wild type EGFR-copy numbers ($n = 30$), no significant association between the groups (median values: 51.35 *vs.* 47.65 ng/mL respectively; $p = 0.293$; Figure S2a) was found. Representative FISH images from NSCLC patients harboring EGFR copy number amplification (Figure S2b) and having EGFR-copy number wild type (Figure S2c) are shown in Figure S2.

Table 1. Comparison between soluble epidermal growth factor receptor (sEGFR) concentration in non-small cell lung cancer (NSCLC) patients and healthy subjects.

	Groups	*n*	M ± SD	Me	Range	M-WU Text
sEGFR (ng/mL)	P-group	37	49.9 ± 9.3	48.6	24.7–69.7	$p = 0.0002$
	C-group	54	58.2 ± 10.5	55.6	41.5–92.3	

sEGFR, soluble epidermal growth factor receptor; P-Group, C-Group, healthy subjects; M ± SD (standard deviation); Me, median; *n*, number of samples; M-WU test, Mann-Whitney *U* test.

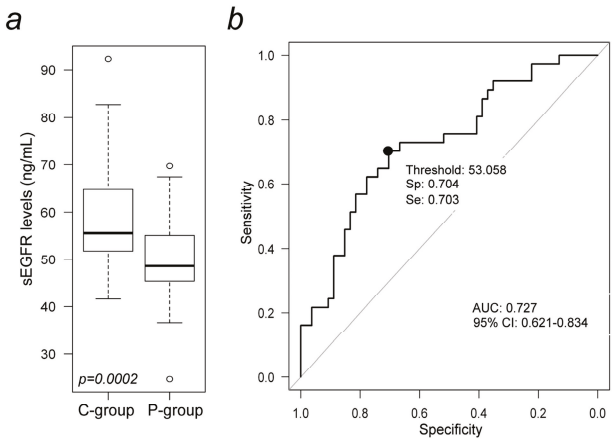

Figure 1. Quantification and diagnostic accuracy analysis of sEGFR levels in plasma of NSCLC patients and healthy controls. (**a**) Box plot illustrate the distributions of sEGFR (ng/mL) levels in plasma from 37 NSCLC patients (P-group) and 54 healthy controls (C-group). Horizontal bold line, median value; the interquartile range is indicated above and below each bar; circles, outliers; (**b**) The receiver operating characteristic (ROC) curves of plasma sEGFR in discriminating NSCLC patients from healthy subjects. The area under the ROC curves (AUC) was 0.727 (95% CI: 0.621 to 0.834). The point on the curve indicates the cut-off value (53.058 ng/mL), for which sensitivity and specificity were 70.4% and 70.3%, respectively. The odds ratio according to the cut-off value was 5.613 (95% CI: 2.247 to 14.023).

Table 2. sEGFR concentration according with demographic, clinical, and/or pathological characteristics.

Clinical-Pathological Variables	sEGFR (ng/mL)	*p* Value
Age		
Age ≤ 65 (*n* = 10)	52.5 ± 13.3	0.306
Age > 65 (*n* = 27)	48.9 ± 7.4	
Gender		
Male (*n* = 26)	49.2 ± 7.5	0.512
Female (*n* = 11)	51.4 ± 12.9	
Smoking Habits		
Smokers (*n* = 30)	49.5 ± 8.1	0.639
Non-Smokers (*n* = 7)	51.4 ± 14.0	
Tumor Stage(TNM)		
pI (*n* = 21)	49.4 ± 7.3	0.588
pII (*n* = 5)	53.9 ± 9.8	
pIII (*n* = 11)	49.0 ± 12.4	
Histologic cell type		
ADK (*n* = 27)	49.7 ± 10.0	0.907
SCC (*n* = 10)	50.2 ± 7.4	
Grading		
G1 (*n* = 3)	56.2 ± 9.7	0.082
G2 (*n* = 9)	54.2 ± 10.7	
G3 (*n* = 25)	47.5 ± 8.1	

sEGFR, soluble epidermal growth factor receptor; ADK, adenocarcinomas; SCC, squamous cell carcinomas.

2.2. Plasma Levels of sEGFR and Prognosis in NSCLC Patients

The study population was followed-up for a long-term clinical-radiological surveillance (median time 41.83 months, IQR: 25.99–46.86) through record linkages to death certificate databases and oncological registries. The median progression-free survival (PFS) was 42.2 months (95% CI: 31.5–NA). The mean sEGFR value recorded in the entire population was 49.9 ± 9.3 ng/mL, ranging from 24.7 ng/mL to 69.7 ng/mL. After Cox modeling of the PFS, we found that sEGFR, processed as a continuous variable, did not show a statistically significant role as a prognostic factor; HR = 0.987 (95% CI: 0.943–1.033) and $p = 0.572$ (the results were similar when we adjusted for sex, age, and smoking habits, HR = 0.988, 95% CI: 0.940–1.038, p-value = 0.618). However, considering its trend towards significance, we attempted to dichotomize the sEGFR distribution to locate a cut-off value useful for prognostic aims in clinical practice. Unfortunately, the Martingale residuals against the sEGFR plot (graph not shown) suggest that such a cut-off does not exist at all. Furthermore, adopting the Contal-O'Quigley approach, the best candidate as a possible cut-off (sEGFR = 45.8) reached only 0.964 as the p-value adjusted for multiplicity (based on a univariate Cox model having the dichotomized sEGFR as a predictive variable for PFS), while p-value without adjustment was 0.218.

2.3. sEGFR Has Growth and Migration Inhibitory Effects in EGFR-Wild Type NSCLC Cell Lines

Since the plasma sEGFR levels were decreased in patients with NSCLC, we hypothesized that sEGFR may have a suppressive effect on NSCLC. To test this hypothesis, we investigated the molecular effect of sEGFRon NSCLC cells. Exposure to recombinant sEGFR of four NSCLC cell lines (A549, H1299, H1650, H1975) with different EGFR-mutation status characteristics were compared with untreated cells. In order to determine the best treatment-dose, we tested recombinant sEGFR on A549 cells at different doses ranging from 0.01 to 1 μg/mL. We chose 1 μg/mL as a test dose as it induced significant inhibition of cell proliferation without causing cellular toxicity (data not shown). Cell proliferation was evaluated after 24, 48, and 72 h by a cell counting assay. A different effect of sEGFR treatment was observed depending on the EGFR mutation status. The H1650 and H1975 cell lines, that contain activating mutations in EGFR, were not affected by the sEGFR treatment. In contrast, sEGFR treatment resulted in a significant inhibition of cell proliferation in the EGFR-wild type A549 and H1299 cell lines (Figure 2a). We excluded a contribution of endogenous sEGFR in the different cell response rates by performing ELISA assay on conditioned medium obtained from all cell lines (data not shown). To assess the effects of sEGFR on cell migration, A549 and H1299 cell lines treated or untreated with sEGFR for 24, 48, and 72 h were seeded into Boyden chambers and migrating cells were counted after six hours. sEGFR treatment resulted in a strong inhibition of cell migration in both wild type cell lines (Figure 2b). While 24 h of sEGFR treatment was sufficient to induce repression of migration in H1299 cells, in A549 cell line a longer exposure to this factor was needed in order to observe the inhibitory effect. Taken together, these observations suggest that sEGFR protein is capable of inhibiting tumor cell proliferation and cell migration in NSCLC cell lines devoid of EGFR mutations in their TK domain.

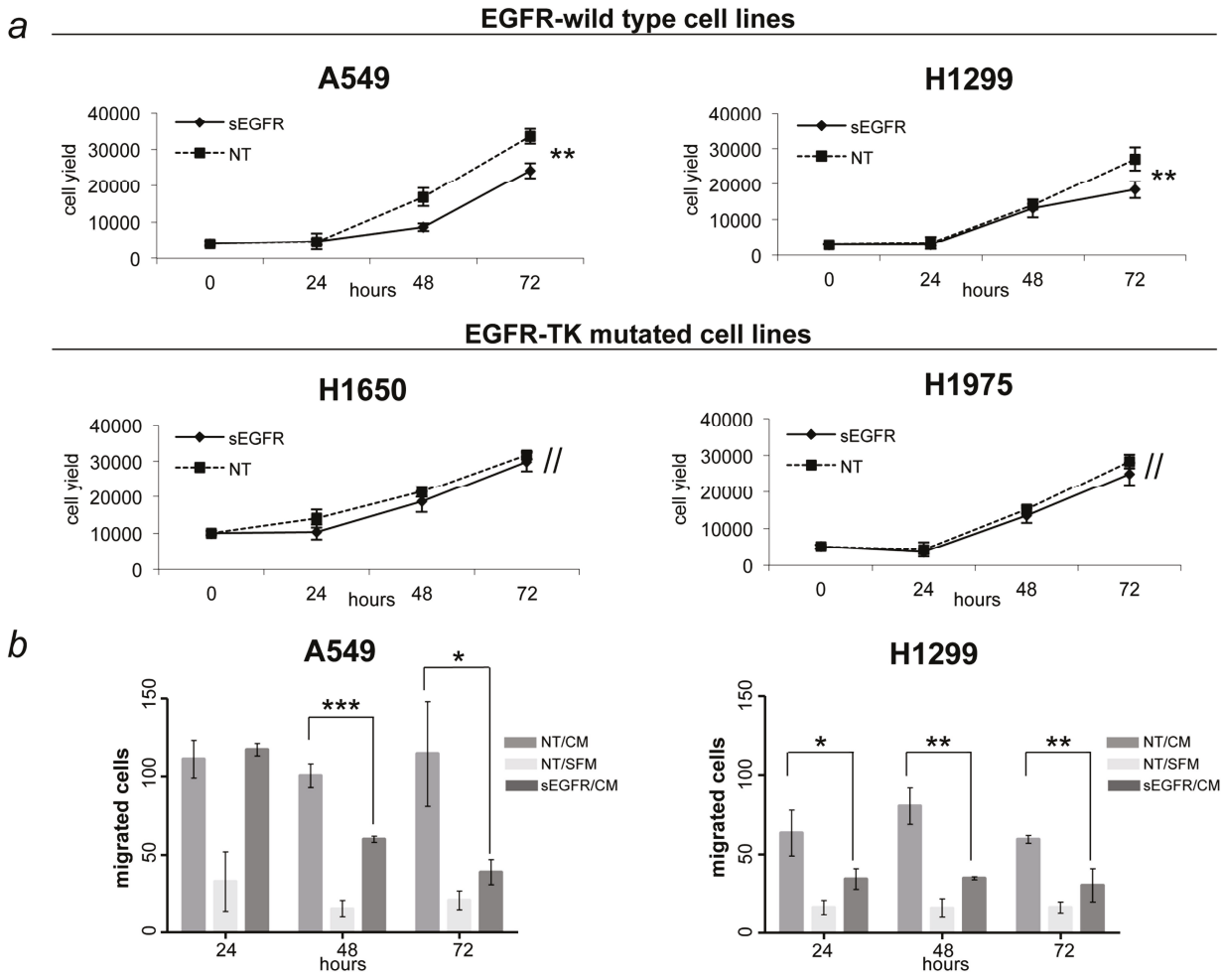

Figure 2. Effects of sEGFR on tumor cell growth and migration. (**a**) A549, H1299, H1650, and H1975 cell lines were exposed to sEGFR (1 μg/mL) or to the vehicle alone and cell counted over time; (**b**) A549 and H1299 cell lines were seeded into the upper compartment of Boyden chambers after 24, 48, and 72 h of pretreatment with sEGFR (1 μg/mL). Complete medium containing FBS 10% (CM) were placed in the lower compartment as a chemoattractant. After six hours of incubation, cells on the upper side of the filter were removed, and cells that migrated to the lower surface were fixed, stained, and counted. Serum-free medium (SFM) was used as negative control. Asterisks indicate significant differences (* $p < 0.05$, ** $p < 0.01$, *** $p < 0.001$, // p not significant) when comparing cells treated with sEGFR to those untreated (NT). Data are means ± SD from experiments with three replicates.

2.4. sEGFR Interferes with the EGF Signaling

Soluble receptors exert their biological effects through different mechanisms of action [21]. They may play specific roles in modifying the biological response to ligands, interfering with the ligand-induced transduction signaling. Most commonly, soluble receptors compete with membrane-bound receptors for ligands in the extracellular milieu. This led us to hypothesize that the sEGFR protein may exert its activity by inhibiting the pro-oncogenic pathway induced by EGF. To characterize the sEGFR mechanism of action in NSCLC behavior, we investigated whether sEGFR could interfere with the

EGF signaling. A549 and H1299 cell lines were treated with EGF recombinant protein in presence or absence of sEGFR. As expected, EGF treatment increased the cell proliferation in both cell lines (Figure 3a). Intriguingly, in A549 cells, the EGF proliferative effect was completely counteracted by the treatment with sEGFR. In contrast, in the presence of EGF, no significant effect of sEGFR was found in the H1299 cell line. The expression analysis of cyclin D1, a cell cycle marker whose down-regulation is consistent with cell cycle arrest, supported the proliferation data. We observed that cyclin D1 expression was up-regulated after EGF treatment and down-regulated after sEGFR treatment in both cell lines (Figure 3b). Consistent with the proliferation data, in A549 cells, sEGFR treatment restores basal levels of cyclin D1 expression in presence of EGF, while in H1299 cells the sEGFR treatment did not affect cyclin D1 expression in the presence of EGF. These data confirm that sEGFR protein inhibits NSCLC cell proliferation, likely by interfering with EGF signaling.

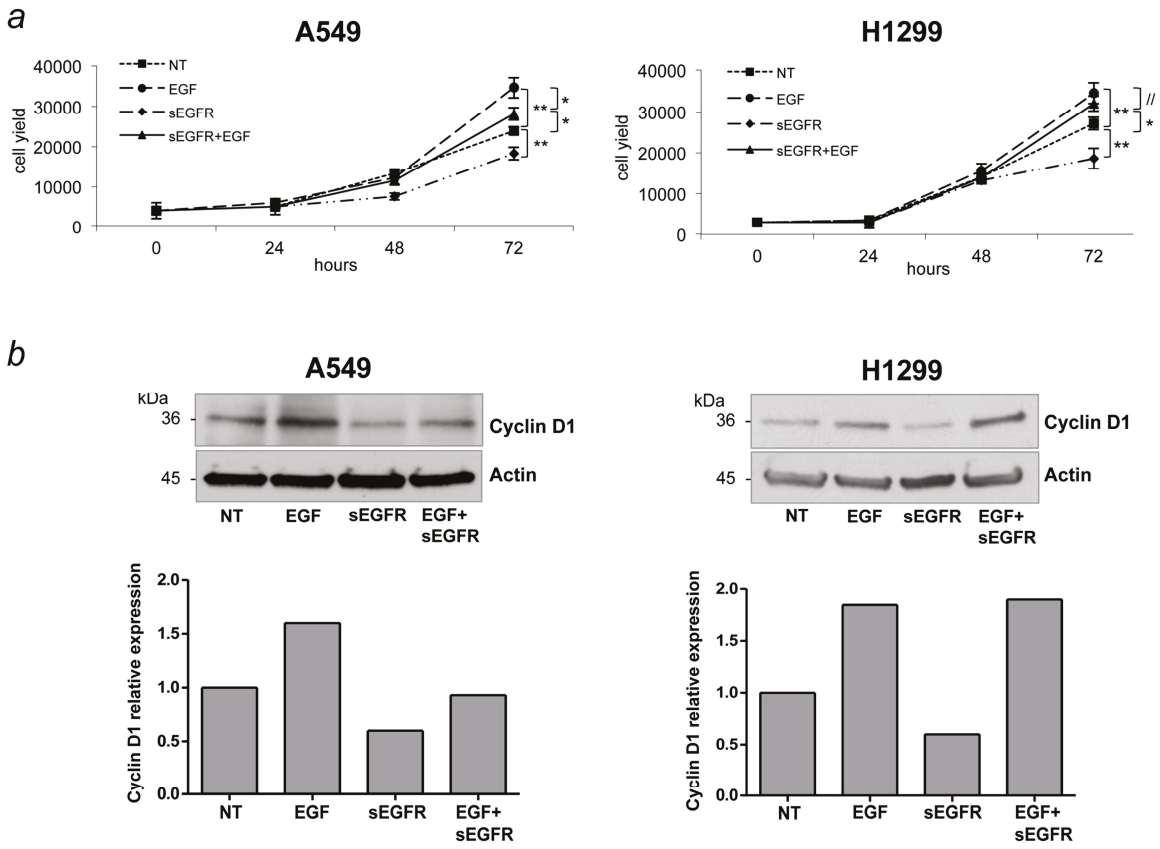

Figure 3. Effects of combined treatment with sEGFR and EGF on cell proliferation. EGFR-wild type cell lines (A549 and H1299) were treated with sEGFR (1 μg/mL) and EGF (100 ng/mL) alone and in combination (EGF + sEGFR). (**a**) Graph shows cell numbers at the indicated times after treatments. Untreated (NT) cells were used as a negative control. Asterisks indicate significant differences (* $p < 0.05$, ** $p < 0.01$, // p not significant) when comparing NT cells with: sEGFR, EGF, and sEGFR + EGF treatments. p value was also calculated for EGF-treated cells and those treated with EGF + sEGFR. Data are means ± SD from experiments with three replicates; (**b**) Western blot analysis of cyclin D1 expression levels in A549 and H1299 cell lysates obtained 24 h after treatment with sEGFR (1 ug/mL). β-actin was used as a loading control. The lower panels show cyclin D1 expression levels normalized to β-actin.

2.5. sEGFR Prevents the Plasma Membrane-EGFR Holoreceptor Internalization

To further understand the molecular mechanism of sEGFR on NSCLC cells, we analyzed the effect of the sEGFR treatment and its interaction with EGF protein on EGFR holoreceptor localization. A549 and H1299 cell lines were treated or not with sEGFR and EGF recombinant proteins, alone and in combination, and the EGFR localization was determined using an immunofluorescent (IF) assay. EGFR was mainly localized to the plasma membrane in both the cell lines before stimulation (Figure 4). After treatment with EGF, NSCLC cells showed a higher rate of receptor internalization, exhibiting perinuclear localization. A decrease in the EGFR levels was also observed. Treatment with sEGFR caused a clear EGFR localization and a homogeneous distribution at the membrane levels, preventing EGFR holoreceptor internalization. When the cells were treated with both EGF and sEGFR in combination, we observed a decrease in receptor internalization rate, with EGFR holoreceptor localized both at the membrane and cytoplasmic levels. We also observed a slight difference between A549 and H1299, in the H1299 cell line; the ratio between the internalized EGFR and plasma membrane EGFR levels was shifted toward the EGFR perinuclear localization. These data showed that the sEGFR affects EGFR holoreceptor extracellular domain internalization, thus interfering with EGF protein signaling.

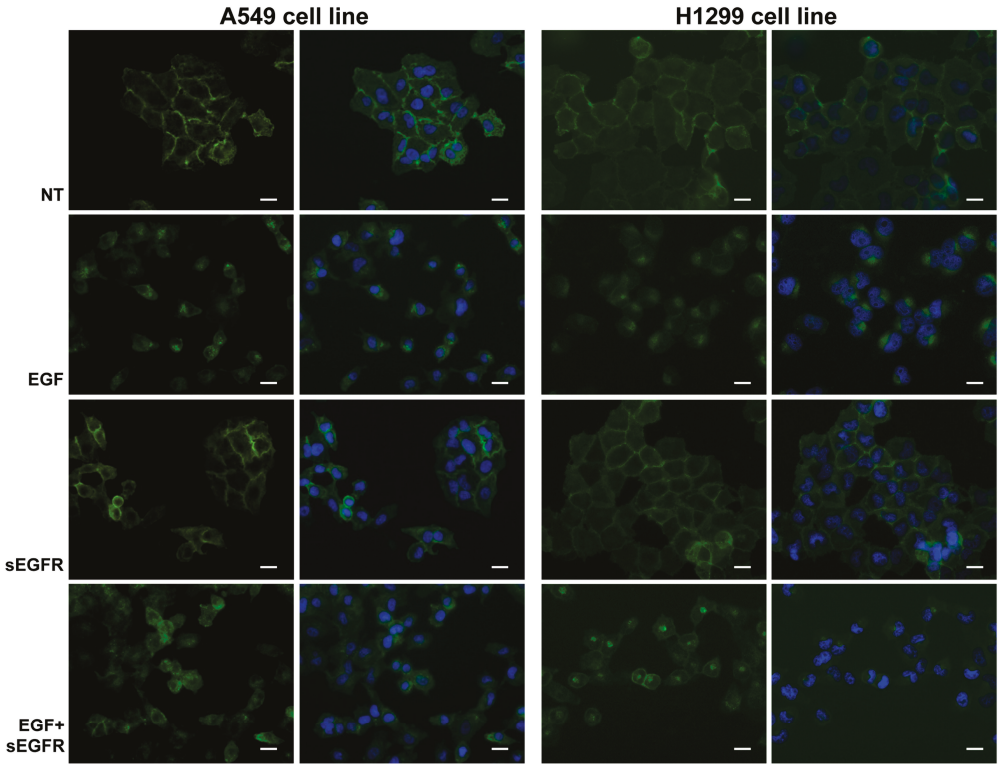

Figure 4. EGFR holoreceptor localization in lung tumor cells treated with sEGFR/EGF proteins. A549 and H1299 cell lines were untreated (NT) or treated with sEGFR (1 µg/mL) and EGF (100 ng/mL), alone and in combination (EGF + sEGFR), and EGFR holoreceptor localization was detected by using an immunofluorescent (IF) assay 24 h after treatment. Cells were treated with a polyclonal antibody against EGFR-ECD (Ab1_EGFR) and stained with FITC-conjugated anti-mouse secondary antibody (green). Cell nuclei were stained with DAPI (blue). Magnification: 40×. Scale bar: 20 µm.

2.6. EGF Treatment Inhibits sEGFR Synthesis in A549 Cells

Although sEGFR exhibited a strong inhibitory effect on the A549 and H1299 cell lines, some differences in the molecular response to sEGFR in the presence of EGF were observed. To test whether this discrepancy was due to intrinsic differences between the two cell types, A549 and H1299 cells were treated with recombinant EGF and compared with untreated cells. Cell lysate and conditioned medium were collected after 24 h of EGF treatment, and the sEGFR levels was detected by Western blot analysis. We previously showed that A549 cell line was able to produce a 110 kDa soluble isoform of EGFR. This isoform was detected in A549 cell line conditioned medium, had the same molecular weight of the plasma sEGFR, yet harbors different biochemical characteristics [20]. We observed that untreated cells from both lines were able to produce the sEGFR isoform (110 kDa), A549 and H1299 showed different levels of EGFR holoreceptor (170 kDa) (Figure 5a). The A549 cell line produced more sEGFR than the H1299 cell line, and this isoform was efficiently secreted into the medium (Figure 5b). Treatment with EGF caused a decrease in synthesis and secretion of sEGFR in the A549 cells, this effect was not observed in the H1299 cell line. These results indicate that sEGFR is a secreted protein produced by NSCLC cell lines whose production seems to be repressed by EGF stimulus in the A549 cell line.

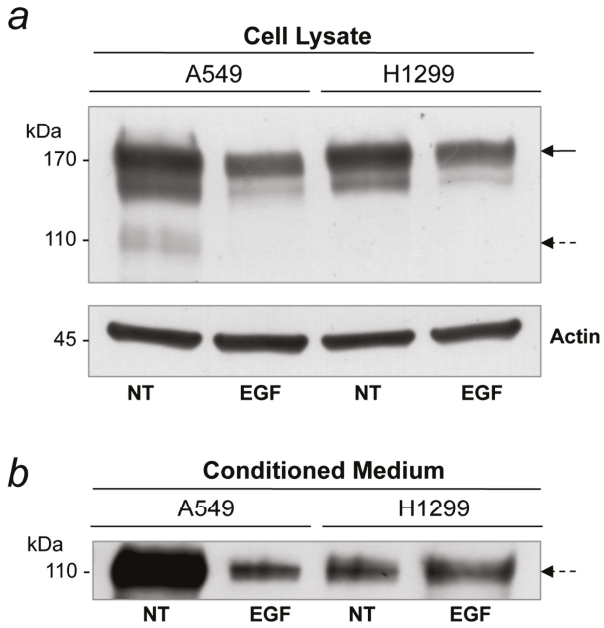

Figure 5. EGFR/sEGFR expression in tumor cells treated with EGF protein. A549 and H1299 cell lines were untreated or treated with EGF (100 ng/mL). (**a**) Western blot analysis of EGFR (170 kDa) and sEGFR (110 kDa) expression in A549 and H1299 cell lysates (50 µg) using the anti-EGFR ECD (Ab2_EGFR) antibody; (**b**) Western blot analysis of sEGFR (110 kDa) expression in A549 and H1299 conditioned medium (20 µg) using the anti-EGFR ECD (Ab2_EGFR) antibody. Solid arrows indicate the membrane p170 EGFR, and dashed arrows indicate the 110-kDa soluble EGFR.

3. Discussion

Assessment of biological diagnostic factors providing clinically-relevant information to guide physician decision-making are still needed for diseases with poor outcomes, such as NSCLC. The achievement of early diagnosis in NSCLC has been widely recognized to be crucial in the overall strategy of care and, accordingly, several screening program protocols adopting low-dose spiral computed tomography (LDCT) have been proposed to reduce overall mortality related with NSCLC. Nevertheless, the introduction of primary screening programs with LDCT has not been proposed on a large-scale population, to date; as stated by the NLST Research Team [22] "…recommendations on the basis of the findings of the NLST alone are insufficient to fully inform such important decisions". Indeed, although the rate of death from any cause was reduced in the low-dose CT group, as compared with the radiography group, by 6.7% (95% CI, 1.2 to 13.6; p = 0.02) [3], before public policy recommendations are crafted, the cost-effectiveness of low-dose CT screening must be rigorously analyzed. The same NLST Research Team in the conclusion of the manuscript stated [22] that "…Other strategies for early detection of lung cancer, in particular, molecular markers in blood, sputum, and urine…- may one day help select persons who are best suited for low-dose CT screening or identify persons with positive low-dose CT screening tests who should undergo more rigorous diagnostic evaluation". In this general scenario, it clearly emerged that the development of complementary strategies in the diagnostic process adopting bio-molecular markers stays as the main topic to be explored by the scientific community in the near future. EGFR is among the most promising molecules in the clinical management of this kind of tumor, considering its role in the carcinogenesis process and progression of NSCLC [6]. EGFR overexpression is observed in about 40%–80% of NSCLC patients and is related to a low grade of differentiation, increased tumor growth, and high metastatic rate [23,24]. Approved therapies targeting EGFR are now widely used for advanced NSCLC patients [25]. While the transmembrane EGFR form is well investigated in large clinical trials, the multiple isoforms of EGFR, that may have potential clinical use, are rarely considered. The isoforms containing only the ECD of the EGFR can be considered as "soluble receptors" since they can be detected in biological fluids such as serum and plasma. The biological function of these isoforms is not completely known. Baron *et al.* [9] were the first to identify a 110 kDa soluble isoform of EGFR (p110 sEGFR) in the bloodstream and to investigate the clinical utility of this circulating protein. Few studies have evaluated the role of sEGFR in NSCLC patients, with a dual aim of detecting its potential as a circulating tumor biomarker and its biological function. We previously characterized a 110 kDa sEGFR isoform with an extremely acidic isoelectric point (pI) (3.87–4.74) in plasma of NSCLC patients and healthy subjects. We demonstrated that this protein could discriminate between the presence or absence of lung cancer, despite the small number of subjects analyzed [20]. Here we extended these preliminary data, exploring potential of sEGFR as a diagnostic and/or prognostic biomarker in a larger and more heterogeneous cohort of non-advanced NSCLC patients. Regarding the diagnostic potential of sEGFR, we demonstrated that this protein could discern NSCLC patients from healthy subjects, showing a decrease in the patient group. Although the diagnostic value lost significance in multivariate analysis, univariate results are nonetheless meaningful considering the limited number of cases and the early phase of the study [26]. Further investigations including more homogeneous patient population should be designed to evaluate diagnostic performance. Decreased serum/plasma sEGFR has

been reported both in lung cancer as compared to other neoplasms [9,18–20,27]. This observation is extremely puzzling and intriguing. If we consider that the term "circulating biomarker" means a molecule produced by the tumor and released in the bloodstream, the sEGFR may be defined as a "negative-biomarker", that is, a physiological circulating molecule, probably produced by tissues that normally express the full-length EGFR and which levels decrease according with the tumor presence. When we analyzed the correlation between sEGFR and the pathological features of NSCLC patients, we found a positive trend between grading and sEGFR levels, indicating that lower values of sEGFR are detectable in patients with a high tumor grade, usually associated with clinical tumor progression and worse prognosis [28]. However, larger clinical cohorts are needed to consolidate this observation.

On the other hand, the data regarding the potential of sEGFR as a prognostic biomarker in patients with solid tumors from various sites are still conflicting. When considering NSCLC, only a few studies have been performed to evaluate if plasma sEGFR effectively influences the long-term survival [16,19]. Jantus-Lewintre and co-workers [16] reported, in a large cohort of advanced NSCLC patients, (308 patients with Stage IIIB/IV disease) a significant association between sEGFR value and prognosis, with lower baseline sEGFR values associated with reduced survival. Taking into proper consideration that our study was not sized to this aim, our findings showed just a non-statistical significant trend in line with the results obtained from Jantus-Lewintre *et al*. [16] (in terms of a protective effect of sEGFR), while we were not able to find a significant prognostic cut-off value in our cohort. The reasons may be that in our settings, the best candidate as possible cut-off (sEGFR = 45.8) is near the 32th percentile, while Jantus-Lewintre *et al*. [16] arbitrarily chose the third tercile.

The observation that plasma sEGFR levels decrease in NSCLC patients prompted us to investigate the biological function of this circulating protein *in vitro*. NSCLC cells frequently have activating mutations within the EGFR tyrosine kinase domain, which cause the constitutive activation of the EGFR-mediated signaling. Patients harboring these mutations are more sensitive to targeted therapies, such as gefitinib and erlotinib [29]. We, therefore, tested the effects of sEGFR in both TK-mutated and non-mutated NSCLC cell lines and we demonstrated that sEGFR showed anti-proliferative effects only in wild-type EGFR cell lines. We suggest a potential use of sEGFR in the clinical management of NSCLC patients not expressing EGFR TK mutations who are usually not responsive to EGFR target therapies. Restoring the physiological levels of circulating sEGFR in this group of patients might be an interesting therapeutic approach. The natural occurrence of circulating sEGFR produces yet another level of complexity on the regulation of EGFR receptor signal transduction.

To understand the biological role of sEGFR is of fundamental importance to clarify the course of action of this protein in the context of NSCLC, we therefore investigated the molecular mechanisms of sEGFR in NSCLC cells. The most known EGFR ligand is EGF, activating EGFR tyrosine kinase activity and downstream signaling pathways controlling cell proliferation, differentiation, survival, and motility [30]. Here we noted two major effects induced by sEGFR treatment in EGFR wild type NSCLC cell lines: the first was the decrease in cell proliferation and cyclin D1 expression, the second was the blocking of the EGFR holoreceptor internalization. Cyclin D1 plays a central role in the regulation of proliferation, linking the extracellular signaling environment to cell cycle progression, initiating transition from late G1 to the S phase of the cell cycle [31]. These data suggest that sEGFR inhibits the G1/S cell cycle transition. Moreover, there is emerging evidence that, when the EGFR holoreceptor is internalized, it translocates into the nucleus and acts as transcriptional factor, regulating

the transactivation of the cyclin D1, iNOS, and Aurora-A together with the transcriptional factor STAT3 and STAT5 [32,33]. We observed that sEGFR treatment retained the EGFR holoreceptor at the plasma membrane, avoiding internalization, suggesting that EGFR interferes with EGF ligands and inhibits EGFR-nuclear translocation. Our data, obtained in wild type NSCLC cell lines treated with EGF, showed a perinuclear EGFR localization, further studies are warranted to investigate the presence of EGFR in the NSCLC cell nuclei. Interestingly, we noted slight differences in the responses to a combination of EGF and sEGFR. Treatment with EGF also induced a remarkable decrease in sEGFR production only in the A549 cell line. Moreover, the sEGFR basal levels produced by A549 and H1299 were notably different. We conclude that a relationship between sEGFR and EGF exists, and that the cellular response to sEGFR may be influenced by the basal levels of EGF produced.

In conclusion, these results suggest that sEGFR molecule harbors potential diagnostic value and provide an initial approach toward defining the functional role of sEGFR in NSCLC, demonstrating that sEGFR inhibits proliferation, migration, and perturbs the EGF/EGFR axis in NSCLC cell lines. Our data suggest that sEGFR may not only represent a novel potential biomarker for the NSCLC diagnosis but could potentially be a bio-therapeutic molecule.

4. Experimental Section

4.1. Patients and Control Subjects

Plasma samples from 37 patients with histopathologically-demonstrated NSCLC, and 54 healthy subjects, were prospectively collected at IRCCS-Santa Maria Nuova Hospital in Reggio Emilia (Italy), from August 2008 to March 2009. The study was conducted after the Ethical Committee approval and has therefore been performed in accordance with the ethical standards laid down in the 1964 Declaration of Helsinki and its later amendments. Written informed consent was obtained from all subjects before entering the study. Inclusion criteria were the presence of NSCLC ascertained with a cytohistological diagnosis and surgery with diagnostic and therapeutic aims. Controls come from healthy donors of a blood transfusion center. Patients and control subjects were not matched in this early phase investigation. Blood samples from both groups were obtained and stored under the same conditions. They were collected in test tubes containing K3-EDTA, and the plasma fraction was separated by two rounds of centrifugation at 2500 rpm for 10 min at 4 °C and then stored at −80 °C until analysis. Tumor specimens were routinely fixed in 4% buffered formalin and embedded in paraffin. Blood samples from patients were collected before surgery and none received neoadjuvant chemo and/or radiotherapy.

4.2. Clinical Data Collection and Statistical Analysis

Patients' characteristics including age, gender, smoking habits, tumor stage, histologic cell type, and grading were recorded in a dedicated prospective database. Associations between the observation group (patients and controls) and common baseline variables (gender, smoking habits, and age) were assessed with two-tailed Chi-square and *t* tests. The sEGFR concentrations within patient and control groups were compared by two-tailed Mann-Whitney *U* test, while sEGFR concentration in patient groups according to demographic, clinical, and/or pathological characteristics were compared by ANOVA.

Two-tailed Mann-Whitney *U* test was also used to compare sEGFR levels between patients harboring EGFR copy number amplification and those having EGFR-copy number wild type. Receiver operating characteristic (ROC) curve analysis was performed to assess the sEGFR diagnostic accuracy. The area under the ROC curve (AUC) was estimated with a 95% confidence interval (CI). Diagnostic cut-off was located by Youden-Index maximization; then sensitivity, specificity, and odds ratio were calculated. 95% CI for the odds ratio was calculated using the Wald method. To assess the relevance of sEGFR as a prognostic factor, it was processed as a continuous variable using the Cox approach in a model having the progression-free survival as the dependent variable. In order to explore whether sEGFR could be dichotomized, to provide an easily applicable cutoff for prognosis discrimination in clinical practice, Martingale residuals of a null model on PFS were plotted against sEGFR values (graph not shown). To the same aim, a possible cut-off was sought using the Contal-O'Quigley approach, with the accompanying multiplicity-adjusted *p*-value (based on a univariate Cox model having the dichotomized sEGFR as a predictive variable for PFS); the unadjusted *p*-value was provided as well. Proportional hazards assumptions for each Cox regression was tested assessing Schoenfeld residuals' (null) slope against time (PH assumption was not refused in each one of the three Cox models, results not shown). Tests results were reported as *p*-values, and differences were considered statistically significant if $p < 0.05$. All statistical analyses were performed using SAS System release 9.2 (SAS Institute Inc., Cary, NC, USA) (descriptive statistics, ANOVA calculations, correlations), R release 3.1.1 (R Foundation for Statistical Computing, Vienna, Austria) (ROC and prognostic analysis) and GraphPad Prism release 5.0 (GraphPad Software, Inc., La Jolla, CA, USA) (remaining graphs).

4.3. Enzyme-Linked Immunosorbent Assay (ELISA)

Plasma sEGFR levels were assessed using a commercial Human EGFR Quantikine ELISA Kit (R&D Systems; Milan, Italy) and following the manufacturer's procedures. The R&D ELISA kit utilizes a polyclonal antibody directed against the N-terminal portion of EGFR. A recombinant human EGFR (R&D Systems; Milan, Italy) was used as a positive control. Evaluation of intra- and inter-assay precision showed a coefficient of variation that was less than 5%.

4.4. Fluorescent in Situ Hybridization (FISH)

Formalin-fixed, paraffin-embedded tissue sections were stained with hematoxylin and eosin, and a quality control assessment of the tumor tissue was performed to ensure that sufficient material was available. FISH analysis was performed as previously described by Varella-Garcia and colleagues [34] by using the Vysis EGFR probe and a semi-automated procedure (Abbott Laboratories; Des Plaines, IL, USA). Tumors with four or more copies of the EGFR gene in ≥40% of the cells or tumors with EGFR gene amplification (gene-to-chromosome ratio ≥2 or presence of gene cluster or ≥15 gene copies in ≥10% of the cells) were considered to be FISH-positive, whereas all other tumors were considered to be FISH-negative. The same observer scored 50 tumor cells each in at least four tumor areas. All FISH analyses were performed in a blinded fashion without access to the patient clinical characteristics or treatment outcome.

4.5. Cell Culture Conditions, Cell Lysates and Conditioned Medium

The human NSCLC cell lines A549, H1299, H1975, and H1650 were obtained from the American type Culture Collection. A549 and H1299 cells are EGFR wild type, while H1650 and H1975 harbor mutations in the EGFR tyrosine kinase-domain. H1650 cells contain a deletion in exon 19 (DelE746A750) and the H1975 cell line carries two missense mutations (L858R, T790M) in the EGFR gene [35]. Cells were grown in RPMI 1640 supplemented with 10% fetal bovine serum (FBS) (Euroclone; Milan, Italy) at 37 °C in 5% CO_2/95% air. Cells were counted under a microscope (10× objective) using a Bright Line hemocytometer (Sigma-Aldrich; Milan, Italy) and cell viability was estimated using trypan blue staining. RIPA buffer (50 mM HEPES (pH 7.6), 150 mM NaCl, 10% glycerol, 1% Triton X-100, 1.5 mM $MgCl_2$, 1 mM EGTA, 10 mM $Na_4P_2O_7$, 100 mM NaF, 1 mM Na_3VO_4) plus protease inhibitors (Roche; Milan, Italy) were used to obtain cell lysates and protein concentration was determined using the Bradford assay (Bio-Rad; Milan, Italy). Conditioned medium was obtained as previously described [20].

4.6. Treatments

sEGFR and EGF recombinant proteins were purchased by PeproTech (Rocky Hill, NJ, USA) and were dissolved in sterile water as a stock solutions of 100 μg/mL. Both molecules were stored at −20 °C in tightly sealed sterile tubes and diluted, to the concentrations of 1 μg/mL for sEGFR and 100 ng/mL for EGF, in RPMI 1640 during each experiment.

4.7. Cell Migration Assay

Cell migration was evaluated using modified Boyden chambers as previously described [36]. Briefly, cells were treated with sEGFR (1 μg/mL) for 24, 48, and 72 h, followed by washing of 5×10^4 cells with PBS, resuspended in serum-free medium and placed in the upper compartment. RPMI 1640 containing 0% or 10% FBS was added to the lower compartment. The chambers were separated by a polycarbonate filter (8 μm pore-size) that was pre-coated with collagen (50 μg/mL). After 6 h of incubation, the filters were recovered, cells on the upper surface mechanically removed, and cells migrated in the lower filter surface fixed with absolute ethanol and stained with DAPI. Cells were counted in a double-blind manner in five consecutive fields each with a fluorescent microscope. All experiments were performed three times.

4.8. Western Blot Analysis

Cell lysates were separated by SDS-PAGE (4%–20% Mini-Protean TGX precast gels; BioRad; Milan, Italy) and transferred to a nitrocellulose membrane. Membranes were probed with the specific antibody for 3 h at RT. Immunoblot analysis for sEGFR/EGFR status were performed by using two different antibodies against the N-terminal EGFR ECD: a mouse monoclonal antibody (Ab1_EGFR) kindly provided by Dr. Tagliabue (Fondazione IRCCS–Istituto Nazionale Tumori, Milan, Italy), and a goat polyclonal antibody (Ab2_EGFR) from R&D Systems (Milan, Italy). Cyclin D1 levels were determined by using a mouse monoclonal antibody (Santa Cruz Biotechnology; Santa Cruz, CA,

USA). As a loading control, blots were stained using a mouse monoclonal antibody against β-Actin (Sigma-Aldrich; Milan, Italy).

4.9. Immunofluorescence and Microscopy Analysis

To identify the EGFR holoreceptor localization we used an immunostaining procedure. Briefly, cells were fixed using 8% paraformaldehyde diluted 1:2 in PBS for 10 min and permeabilized with 0.2% Triton X-100 in PBS for two minutes. Following a blocking step with 2% bovine serum albumin (BSA) (Sigma-Aldrich; Milan, Italy) and 20% fetal bovine serum (Euroclone; Milan, Italy) in PBS for 30 min, the antibody Ab1_EGFR, diluted 1:750 in PBS with BSA 2%, was applied for one hour. After washing with PBS, samples were incubated with FITC-conjugated anti-mouse secondary antibody (Invitrogen, Milan, Italy) for 40 min. DAPI (Sigma-Aldrich; Milan, Italy) was used to counterstain the cell nuclei. Coverslips were mounted with Vectashield (Vector, Burlingame, CA, USA) and immunofluorescence visualized in fluorescence microscope (Nikon, Melville, NY, USA).

5. Conclusions

In the present study, we observed a significant decrease of plasmatic sEGFR values in NSCLC patients when compared with control group (healthy population). Moreover, we investigated the effect of recombinant sEGFR on lung cancer cell lines, observing an anti-proliferative effect of this protein.

These data suggest that sEGFR is a circulating EGFR isoform with a protective role, representing a potential biomarker in NSCLC early-detection. However, the real impact of these data on daily clinical practice needs to be further investigated in larger prospective clinical trials.

Supplementary Materials

Supplementary materials can be found at http://www.mdpi.com/1422-0067/16/08/19612/s1.

Acknowledgments

Teresa Rossi is a student of the PhD program in Biotechnology, Biosciences and Surgical Technologies, School in Biological and Medical Sciences, University of Insubria. Alessandra Bisagni is student of the PhD program in Biochemical and Molecular Biology, University of Parma.

We thank Serenella Pupa and Elda Tagliabue for Ab1_EGFR Antibody. We thank Alessia Ciarrocchi for her helpful suggestions.

This study was supported by: AIRC (Italian Association for Cancer), Pietro Manodori Foundation (Reggio Emilia, Italy) and the Vittorio Lodini Association (Reggio Emilia, Italy).

Author Contributions

Filippo Lococo, Massimiliano Paci and Cristian Rapicetta enrolled patients and collected clinical data. Sally Maramotti, Teresa Rossi, Valentina Sancisi and Alessandra Bisagni performed experiments and analyzed the molecular data. Sally Maramotti, Massimiliano Paci and Adriana Albini designed the study. Filippo Lococo and Sally Maramotti wrote the manuscript. Luca Braglia and Silvio Cavuto analyzed the data. Italia Bongarzone, Douglas M. Noonan and Adriana Albini supervised the study.

Conflicts of Interest

The authors declare no conflict of interest.

References

1. Jemal, A.; Bray, F.; Center, M.M.; Ferlay, J.; Ward, E.; Forman, D. Global cancer statistics. *CA Cancer J. Clin*. **2011**, *61*, 69–90.
2. Infante, M.; Cavuto, S.; Lutman, F.R.; Passera, E.; Chiarenza, M.; Chiesa, G.; Brambilla, G.; Angeli, E.; Aranzulla, G.; Chiti, A. Long-term follow-up results of the DANTE trial, a randomized study of lung cancer screening with spiral computed tomography. *Am. J. Respir. Crit. Care Med.* **2015**, *191*, 1166–1175.
3. National Lung Screening Trial Research Team. Reduced lung-cancer mortality with low-dose computed tomographic screening. *N. Engl. J. Med*. **2011**, *365*, 395–409.
4. The International Early Lung Cancer Action Program Investigators. Survival of patients with stage I lung cancer detected on CT screening. *N. Engl. J. Med.* **2006**, *355*, 1763–1771.
5. Schlessinger, J. Cell signaling by receptor tyrosine kinases. *Cell* **2000**, *103*, 211–225.
6. Peter, B.-J.; Tony, H. Oncogenic kinase signaling. *Nature* **2001**, *411*, 355–365.
7. Yarden, Y.; Shilo, B.Z. SnapShot: EGFR signaling pathway. *Cell* **2007**, *131*, doi:10.1016/j.cell.2007.11.013.
8. Marianela, P.-T.; Valle, B.L.; Maihle, N.J.; Maihle, N.J.; Lisandra, N.-V.; Rene, N.-A.; Elsa, M.C. Shedding of epidermal growth factor receptor is a regulated process that occurs with overexpression in malignant cells. *Exp. Cell Res.* **2008**, *314*, 2907–2918.
9. Baron, A.T.; Cora, E.M.; Lafky, J.M.; Boardman, C.H.; Buenafe, M.C.; Rademaker, A.; Liu, D.; Fishman, D.A.; Podratz, K.C.; Maihle N.J. Soluble epidermal growth factor receptor (sEGFR/sErbB1) as a potential risk, screening, and diagnostic serum biomarker of epithelial ovarian cancer. *Cancer Epidemiol. Biomark. Prev.* **2003**, *12*, 103–113.
10. Reiter, J.L.; Threadgill, D.W.; Eley, G.D.; Strunk, K.E.; Danielsen, A.J.; Sinclair, C.S.; Pearsall, R.S.; Green, P.J.; Yee, D.; Lampland, A.L.; *et al*. Comparative genomic sequence analysis and isolation of human and mouse alternative EGFR transcripts encoding truncated receptor isoforms. *Genomics* **2001**, *71*, 1–20.
11. Reiter, J.L.; Maihle, N.J. Characterization and expression of novel 60 kDa and 110 kDa EGFR isoforms in human placenta. *Ann. N. Y. Acad. Sci.* **2003**, *995*, 39–47.
12. Lafky, J.M.; Wilken, J.A.; Baron, A.T.; Maihle, N.J. Clinical implications of the ErbB/epidermal growth factor (EGF) receptor family and its ligands in ovarian cancer. *Biochim. Biophys. Acta* **2008**, *1785*, 232–265.
13. Baron, A.T.; Boardman, C.H.; Lafky, J.M.; Rademaker, A.; Liu, D.; Fishman, D.A.; Podratz, K.C.; Maihle, N.J. Soluble epidermal growth factor receptor (sEGFR) and cancer antigen 125 (CA125) as screening and diagnostic tests for epithelial ovarian cancer. *Cancer Epidemiol. Biomark. Prev.* **2005**, *14*, 306–318.

14. Müller, V.; Witzel, I.; Pantel, K.; Krenkel, S.; Lück, H.J.; Neumann, R.; Keller, T.; Dittmer, J.; Jänicke, F.; Thomssen, C. Prognostic and predictive impact of soluble epidermal growth factor receptor (sEGFR) protein in the serum of patients treated with chemotherapy for metastatic breast cancer. *Anticancer Res.* **2006**, *26*, 1479–1487.
15. Asgeirsson, K.S.; Agrawal, A.; Allen, C.; Hitch, A.; Ellis, I.O.; Chapman, C.; Cheung, K.L.; Robertson, J.F. Serum epidermal growth factor receptor and HER2 expression in primary and metastatic breast cancer patients. *Breast Cancer Res.* **2007**, *9*, doi:10.1186/bcr1788.
16. Jantus-Lewintre, E.; Sirera, R.; Cabrera, A.; Blasco, A.; Caballero, C.; Iranzo, V.; Rosell, R.; Camps, C. Analysis of the prognostic value of soluble epidermal growth factor receptor plasma concentration in advanced non-small-cell lung cancer patients. *Clin. Lung Cancer* **2011**, *12*, 320–327.
17. Gregorc, V.; Ceresoli, G.L.; Floriani, I.; Spreafico, A.; Bencardino, K.B.; Ludovini, V.; Pistola, L.; Mihaylova, Z.; Tofanetti, F.R.; Ferraldeschi, M. *et al*. Effects of Gefitinib on serum epidermal growth factor receptor and HER2 in patients with advanced non-small cell lung cancer. *Clin. Cancer Res.* **2004**, *10*, 6006–6012.
18. Carney, W.P. Circulating oncoproteins HER2/neu, EGFR and CAIX (MN) as novel cancer biomarkers. *Expert Rev. Mol. Diagn.* **2007**, *7*, 309–319.
19. Lemos-González, Y.; Rodríguez-Berrocal, F.J.; Cordero, O.J.; Gómez, C.; Páez de la Cadena, M. Alteration of the serum levels of the epidermal growth factor receptor and its ligands in patients with non-small cell lung cancer and head and neck carcinoma. *Br. J. Cancer* **2007**, *96*, 1569–1578.
20. Maramotti, S.; Paci, M.; Micciché, F.; Ciarrocchi, A.; Cavazza, A.; de Bortoli, M.; Vaghi, E.; Formisano, D.; Canovi, L.; Sgarbi, G.; *et al*. Soluble epidermal growth factor receptor isoforms in non-small cell lung cancer tissue and in blood. *Lung Cancer* **2012**, *76*, 332–338.
21. Heaney, M.L.; Golde, D.W. Soluble receptors in human disease. *J. Leukoc. Biol.* **1998**, *64*, 135–146.
22. Aberle, D.R.; Adams, A.M.; Berg, C.D.; Black, W.C.; Clapp, J.D.; Fagerstrom, R.M.; Gareen, I.F.; Gatsonis, C.; Marcus, P.M.; Sicks, J.D. Reduced lung-cancer mortality with low-dose computed tomographic screening. *N. Engl. J. Med*. **2011** *365*, 395–409.
23. Pavelic, K.; Banjac, Z.; Pavelic, J.; Spaventi, S. Evidence for a role of EGF receptor in the progression of human lung-carcinoma. *Anticancer Res.* **1993**, *13*, 1133–1138.
24. Hirsch, F.R.; Varella-Garcia, M.; Bunn, P.A.; di Maria, M.V.; Veve, R.; Bremmes, R.M.; Barón, A.E.; Zeng, C.; Franklin, W.A. Epidermal growth factor receptor in non-small-cell lung carcinomas: Correlation between gene copy number and protein expression and impact on prognosis. *J. Clin. Oncol.* **2003**, *21*, 3798–3807.
25. Domingo, G.; Perez, C.A.; Velez, M.; Cudris, J.; Raez, L.E.; Santos, E.S. EGF receptor in lung cancer: A successful story of targeted therapy. *Expert Rev. Anticancer Ther.* **2010**. *10*, 1577–1587.
26. Zhou, X.H.; Obuchowski, N.; McClish, D. *Statistical Methods in Diagnostic Medicine*, 2nd ed.; John Wiley & Sons, Inc.: Hoboken, NJ, USA, 2011.
27. Carney, W.P.; Burrell, M.; Morris, L.D.; Hamer, P.J. Normal levels of serum EGFr and decreases in several cancers. *Proc. AACR* **2002**, *43*, 47.
28. Riquet, M.; Manac'h, D.; Le Pimpec Barthes, F.; Dujon, A.; Debrosse, D.; Debesse, B. Prognostic value of T and N in non-small cell lung cancer three centimeters or less in diameter. *Eur. J. Cardiothorac. Surg.* **1997**, *11*, 440–443.

29. Siegelin, M.D.; Borczuk, A.C. Epidermal growth factor receptor mutations in lung adenocarcinoma. *Lab. Investig.* **2014**. *94*, 129–137.
30. Citri, A.; Yarden, Y. EGF–ERBB signalling: Towards the systems level. *Nat. Rev. Mol. Cell Biol.* **2006**, *7*, 505–516.
31. Sherr, C.J. D-Type Cyclins. *Trends Biochem. Sci.* **1995**, *20*, 187–190.
32. Lin, S.Y.; Makino, K.; Xia, W.; Matin, A.; Wen, Y.; Kwong, K.Y.; Bourguignon, L.; Hung, M.C. Nuclear localization of EGF receptor and its potential new role as a transcription factor. *Nat. Cell Biol.* **2001**, *3*, 802–808.
33. Wang, S.C.; Hung, M.C. Nuclear translocation of the epidermal growth factor receptor family membrane tyrosine kinase receptors. *Clin. Cancer Res.* **2009**, *15*, 6484–6489.
34. Varella-Garcia, M.; Diebold, J.; Eberhard, D.A.; Geenen, K.; Hirschmann, A.; Kockx, M.; Nagelmeier, I.; Rüschoff, J.; Schmitt, M.; Arbogast, S.; *et al*. EGFR fluorescence *in situ* hybridisation assay: Guidelines for application to non-small-cell lung cancer. *J. Clin. Pathol.* **2009**, *62*, 970–977.
35. Lynch, T.J.; Bell, D.W.; Sordella, R.; Gurubhagavatula, S.; Okimoto, R.A.; Brannigan, B.W.; Harris, P.L.; Haserlat, S.M.; Supko, J.G.; Haluska, F.G.; *et al*. Activating mutations in the epidermal growth factor receptor underlying responsiveness of non-small cell lung cancer to gefitinib. *N. Engl. J. Med.* **2004**, *350*, 2129–2139.
36. Albini, A.; Benelli, R. The chemoinvasion assay: A method to assess tumor and endothelial cell invasion and its modulation. *Nat. Protoc.* **2007**, *2*, 504–511.

© 2015 by the authors; licensee MDPI, Basel, Switzerland. This article is an open access article distributed under the terms and conditions of the Creative Commons Attribution license (http://creativecommons.org/licenses/by/4.0/).

Int. J. Mol. Sci. **2015**, *16*, 22662-22675; doi:10.3390/ijms160922662

OPEN ACCESS
International Journal of
Molecular Sciences
ISSN 1422-0067
www.mdpi.com/journal/ijms

Article

SOCS3 Methylation Predicts a Poor Prognosis in HBV Infection-Related Hepatocellular Carcinoma

Xin Zhang [1], Qingshan You [1,*], Xiaolei Zhang [2,†] and Xiangmei Chen [2,†]

[1] Department of Radiotherapy, Harbin Medical University Cancer Hospital, Harbin 150081, China; E-Mail: zhangxin1262008@126.com

[2] Department of Microbiology and Infectious Disease Center, School of Basic Medical Sciences, Peking University Health Science Center, Beijing 100191, China; E-Mails: xiaoleizhang8802@163.com (X.Z.); xm_chen6176@163.com (X.C.)

† These authors contributed equally to this work.

* Author to whom correspondence should be addressed; E-Mail: zxsdyx@163.com; Tel./Fax: +86-451-8629-8517.

Academic Editor: William Cho

Received: 18 August 2015 / Accepted: 11 September 2015 / Published: 18 September 2015

Abstract: Suppressor of cytokine signaling 3 (*SOCS3*) plays crucial roles in JAK/STAT signaling pathway inhibition in hepatocellular carcinoma (HCC). However, the methylation status of *SOCS3* in HBV infection-related HCC and the relationship between *SOCS3* methylation and the clinical outcome remain unknown. Here, we reported that in HCC tumor tissues, two regions of the CpG island (CGI) in the *SOCS3* promoter were subjected to methylation analysis and only the region close to the translational start site of *SOCS3* was hypermethylated. In HCC tumor tissues, *SOCS3* showed an increased methylation frequency and intensity compared with that in the adjacent non-tumor tissues. Moreover, *SOCS3* expression was significantly down-regulated in HCC cell lines and tumor tissues, and this was inversely correlated with methylation. Kaplan–Meier curve analysis revealed that in patients with an hepatitis B virus (HBV) infection background, *SOCS3* hypermethylation was significantly correlated with a poor clinical outcome of HCC patients. Our findings indicated that *SOCS3* hypermethylation has already happened in non-tumor tissues and increased in both frequency and intensity in tumor tissues. This suggests that the methylation of *SOCS3* could predict a poor prognosis in HBV infection-related HCC patients.

Keywords: hepatitis B virus; hepatitis C virus hepatocellular carcinoma; methylation; prognosis; *SOCS3*; translational start site

1. Introduction

Hepatocellular carcinoma (HCC) is a common malignancy worldwide with rapid progress and high short-term mortality. The initiation of HCC is intimately associated with chronically diseased liver tissue, induced by etiological factors such as hepatitis HBV or hepatitis C virus (HCV) infection, toxin exposure, excessive alcohol consumption, and/or other environmental or genetic factors [1]. Over 80% of HCC cases in China are attributed to chronic HBV infection [2,3]. Although surgical excision is still the most effective treatment so far, a large proportion of HCC patients show symptoms of intrahepatic metastases or post-surgical recurrence [1]. Therefore, the identification of more sensitive and specific biomarkers associated with HCC prognosis is essential to improve HCC management in China [4].

In the liver, the sequential progression to carcinoma is a multistep process with an accumulation of genetic and epigenetic alterations leading to the activation of oncogenes and the inactivation of tumor suppressor genes (TSG) [5,6]. DNA methylation, which is the first epigenetic regulation, has been suggested as one of the most important molecular mechanisms in hepatocarcinogenesis [5,7]. Mounting studies have revealed that HCC tumors exhibit specific DNA methylation signatures that are associated with major risk factors and tumor progression [8]. However, the methylation status of TSGs in HCC with different virus infection, especially HBV infection, is not fully understood.

The suppressor of cytokine signaling (*SOCS*) gene family has been found to play essential roles in suppressing tumor progression by inhibiting JAK/STAT, NFκB signaling, and promoting p53 signaling [9–12]. Among the *SOCS* family, *SOCS3* has been reported to be hypermethylated in various kinds of cancers, including head and neck cancer, lung cancer, prostate cancer, Barrett esophagus carcinoma, and ulcerative colitis-related colorectal cancer [13–19]. In HCC, Niwa *et al.* revealed that *SOCS3* was hypermethylated in 33.3% (6/18) of HCC tissues [20]. However, in our previous report, we did not observe *SOCS3* hypermethylation in HBV-related HCC tissues [21]. These conflicting results may be due to the complicated etiological mechanism of HCC and the different detected loci in the *SOCS3* promoter region. Therefore, it is imperative to explore the detailed methylation status of *SOCS3* in HCC with different virus infection backgrounds and the relationship between its methylation and clinicopathology.

In this study, the methylation status of two loci of the CpG island (CGI) in the *SOCS3* promoter was quantitatively investigated, with particular attention to the change in methylation intensities in primary HCC tissues with different virus infection backgrounds. Also, the clinicopathological significance of *SOCS3* methylation status was statistically analyzed.

2. Results and Discussion

2.1. Results

2.1.1. Suppressor of Cytokine Signaling 3 (*SOCS3*) CpG Island (CGI) Is Hypermethylated in the Region Close to the Translational Start Site

Using the online University of California Santa Cruz (UCSC) database, we searched for CGI at the *SOCS3* promoter region and one CGI surrounding the *SOCS3* gene promoter was predicted. This CGI region starts from −880 nt and ends at +1339 nt, covering the translation initiation site of the *SOCS3* gene. In our previous study, we detected the methylation status in the CGI region from +173 to +296 nt (region 1) in HCC tissues and did not find any methylation in this region. However, Niwaet *et al.* observed obvious methylation in the CGI region in HCC tissues, which was close to the translational start site (Figure 1A). To investigate whether the above conflicting results were due to the different detected regions in the *SOCS3* promoter, we designed another pair of primers to amplify the CGI region from +797 to +885 nt (region 2), which was close to the translational start site and near the locus reported in the Niwaet *et al.* report [20].

Firstly, we detected the methylation statuses of both region 1 and region 2 in 20 pairs of the HCC tumor and non-tumor tissues. With the cut-off value setting at 10%, any tissue that had a hypermethylation intensity ≥10% would be judged as the hypermethylation status, and the higher value implicated a higher CGI hypermethylation status in intensity [15]. As shown in Figure 1B, at target region 2, 12 of the 20 tumor tissues and six of the non-tumor tissues showed hypermethylation. The methylation intensity in HCC tumor tissues was also found to be significantly higher than that in the adjacent non-tumor tissues ($p = 0.0028$). However, the methylation status at region 1 showed no hypermethylation in both tumor and non-tumor tissues. Next, we detected the methylation statuses of both regions in eight HCC cell lines. We found that region 2 of the *SOCS3* CGI was hypermethylated in cell lines Huh-7, Hep3B, PLC/PRF/5, and SMMC7721, while it was unmethylated in SNU449, SNU182, SK-Hep1, and Huh-1 cells (Figure 1C). Similar to that in HCC tissues, no methylation was detected in region 1 in all these cell lines (data not shown). These results indicated that it was the locus close to the translational start site that showed increased methylation, rather than that near the transcription start site.

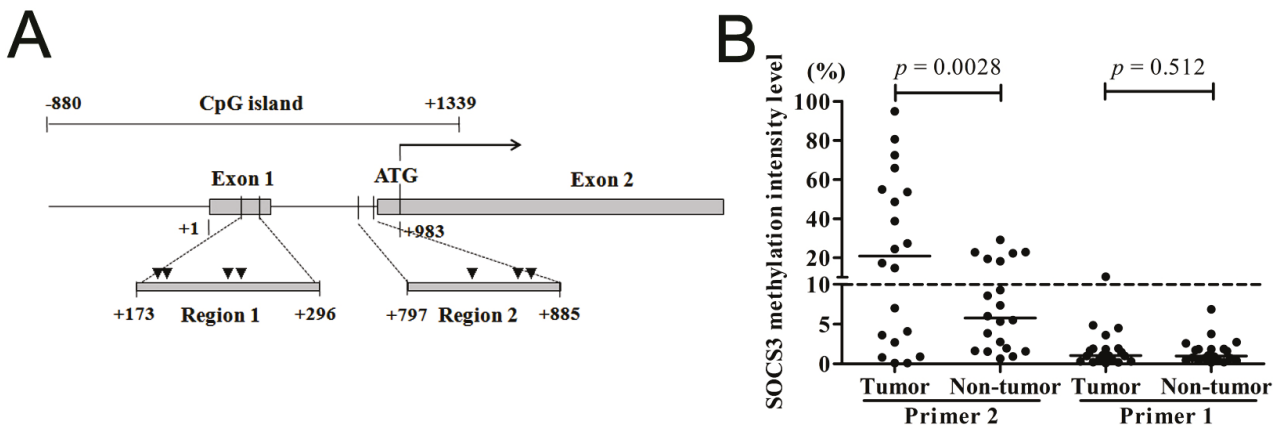

Figure 1. *Cont.*

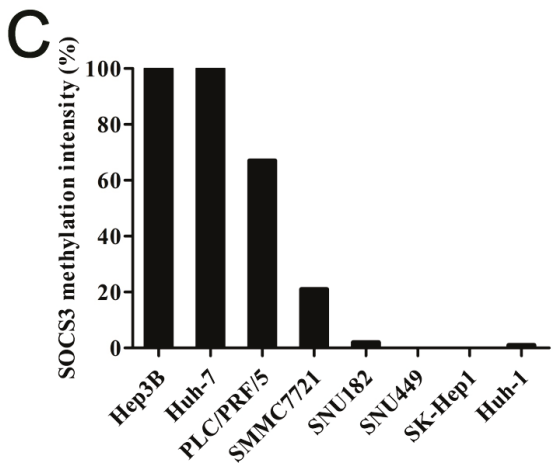

Figure 1. The methylation statuses of two loci of the *SOCS3* promoter in HCC tissues and cell lines. (**A**) Schematic representation of the two detected CGI loci of the *SOCS3* gene. The transcriptional start site for *SOCS3* gene is defined as +1. Shaded boxes are exons of *SOCS3*. "▼" represents the restriction enzyme cutting site; (**B**) The methylation statuses in the located regions of Primer 1 and Primer 2 in 20 pairs of tumors tissues and the adjacent non-tumor tissues; and (**C**) The methylation status of *SOCS3* at region 2 in eight HCC cell lines.

2.1.2. *SOCS3* Methylation Is Associated with Altered *mRNA* Expression in Hepatocellular Carcinoma (HCC) Cell Lines

To further investigate whether the hypermethylation of region 2 in the *SOCS3* CGI could suppress *SOCS3* gene expression, the expression levels of *SOCS3* in these eight HCC cell lines were quantitatively measured by real-time qPCR. As shown in Figure 2A, the *SOCS3 mRNA* expression level was relatively lower in cell lines with high *SOCS3* CGI methylation such as Huh-7, Hep3B, PLC/PRF/5, and SMMC7721. In contrast, in cell lines with *SOCS3* CGI non-methylation, such as SNU449, SNU182, and SK-Hep1 cells, the *mRNA* expression of *SOCS3* was relatively higher. Next, we processed Huh-7, Hep3B, and SK-Hep1 cells with the treatment of *DNA* demethylation reagent 5-aza-2′-deoxycytidine. We found that after 5-aza treatment, the mRNA levels of *SOCS3* significantly increased in Huh-7 and Hep3B cells with hypermethylation, but not in the SK-Hep1 cells with non-methylation (Figure 2B). These data suggest that the methylation in CGI region 2 is associated with the down-regulation of *SOCS3* expression in HCC cell lines. In addition, we noticed that the *mRNA* expression level of *SOCS3* was also very low in Huh-1 cells with non-methylation, suggesting that besides methylation modulation, there might be other regulation mechanisms of *SOCS3* expression, such as acetylation [22].

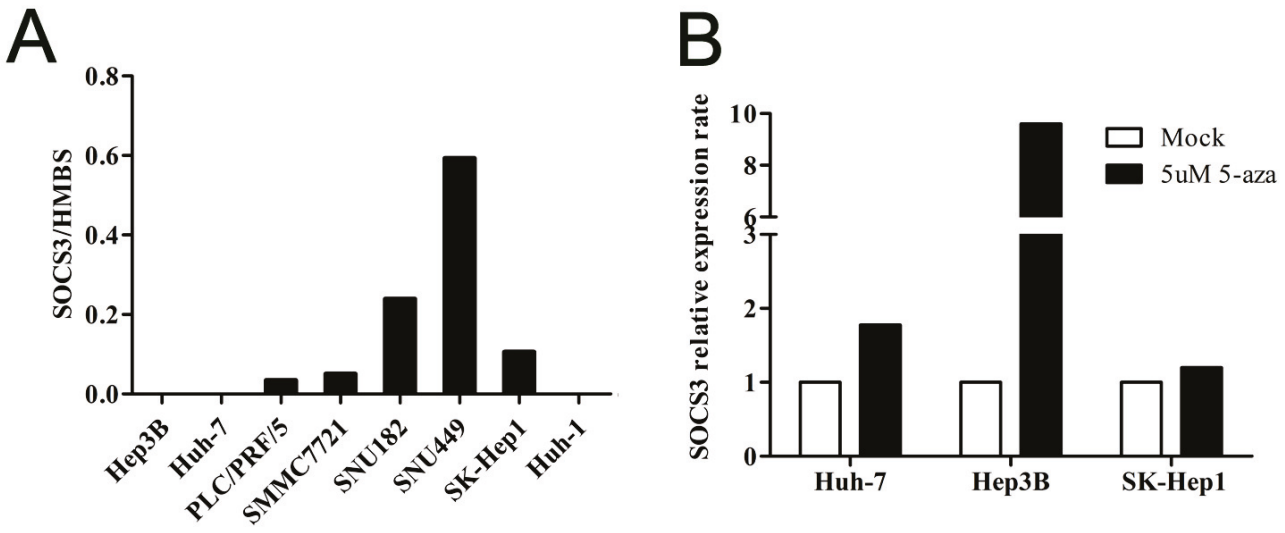

Figure 2. The *mRNA* expression of *SOCS3* in HCC cell lines. (**A**) The *mRNA* expression levels of *SOCS3* in eight cell lines; and (**B**) the normalized *mRNA* expression levels of *SOCS3* in cell lines Huh-7, Hep3B, and SK-Hep1 after treatment with 5-Aza-2′-deoxycytidine for three days.

2.1.3. *SOCS3* CGI Is Hypermethylated in Primary HCC Tumor Tissues

Next, we detected the methylation status of region 2 in *SOCS3* CGI in an enlarged HCC sample. In the paired 127 HCC specimens, 61 (48.03%) of the tumor tissues and 32 (25.21%) of the adjacent non-tumor tissues showed methylation ($p = 0.0002$), which meant that in non-tumor tissues, the *SOCS3* methylation had already happened. Meanwhile, the hypermethylation intensity in tumor tissues was significantly higher than that in the adjacent non-tumor tissues (26.63% *vs.* 8.31%, $p < 0.0001$, Figure 3A). In addition, in tumor tissues, there were 26.77% (34/127) specimens in which he *SOCS3* methylation intensity was over 40%, while there were only 2.36% (3/127) in non-tumor tissues.

To test whether the *SOCS3* CGI methylation in HCC tissues was associated with different virus infections, we analyzed the methylation frequency and intensity among 92 pairs of HCC tissues with HBV infection, 13 pairs with HCV infection, and 22 pairs with neither HBV nor HCV infection. In these three groups of HCC, the methylation frequencies in tumor tissues were 44.57% (41/92), 46.15% (6/13), and 63.63% (14/22), respectively; and in the adjacent non-tumor tissues, 25% (23/92), 0 (0/13), and 45.45% (10/22). Additionally, the methylation intensity of tumor tissues in each group was significantly higher than that in their corresponding non-tumor tissues ($p < 0.0001$, $p = 0.048$, and $p = 0.0013$). However, no marked difference was found among the tumor tissues with different virus infection backgrounds (Figure 3B). Taken together, these results suggested that the frequency of *SOCS3* CGI hypermethylation in HCC tissues was not related to the different virus infection backgrounds of HCC.

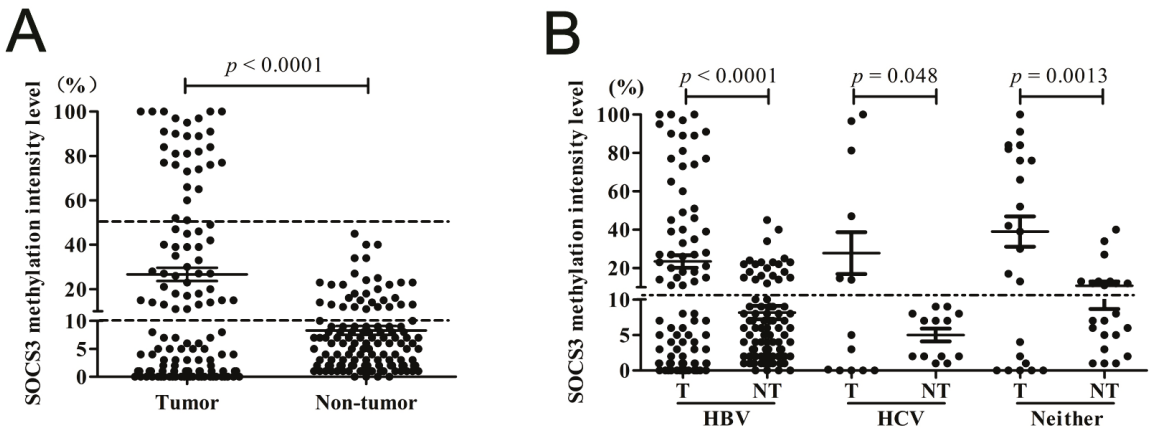

Figure 3. The methylation statuses of *SOCS3* at region 2 in HCC tumor and adjacent non-tumor tissues. (**A**) The methylation status in 127 enlarged paired tumor tissues and non-tumor tissues; and (**B**) the methylation status in tumor tissues and adjacent non-tumor tissues with different virus infection backgrounds.

2.1.4. *SOCS3* Is down-Regulated in Primary HCC Tumor Tissues

We also detected *SOCS3 mRNA* expression levels in 32 pairs of HBV-related HCC tumor tissues and non-tumor tissues (Figure 4A). As expected, the level of *SOCS3 mRNA* in tumor tissues was statistically lower than that in non-tumor tissues (p = 0.0115). Among these 32 tumor tissues, the *SOCS3* methylation intensity in five tumor tissues was extremely high (≥40%) and 10 specimens unmethylated (<3%). We found that the expression level of *SOCS3* in tumor tissues with extremely high *SOCS3* methylation was significantly lower than that in the tumor tissues without methylation (Figure 4B). Comparing the *SOCS3* expression levels of these two groups, they was inversely correlated with the CGI hypermethylation status. These data further demonstrated that the down-regulation of *SOCS3* expression in HCC tissues was associated with *SOCS3* methylation.

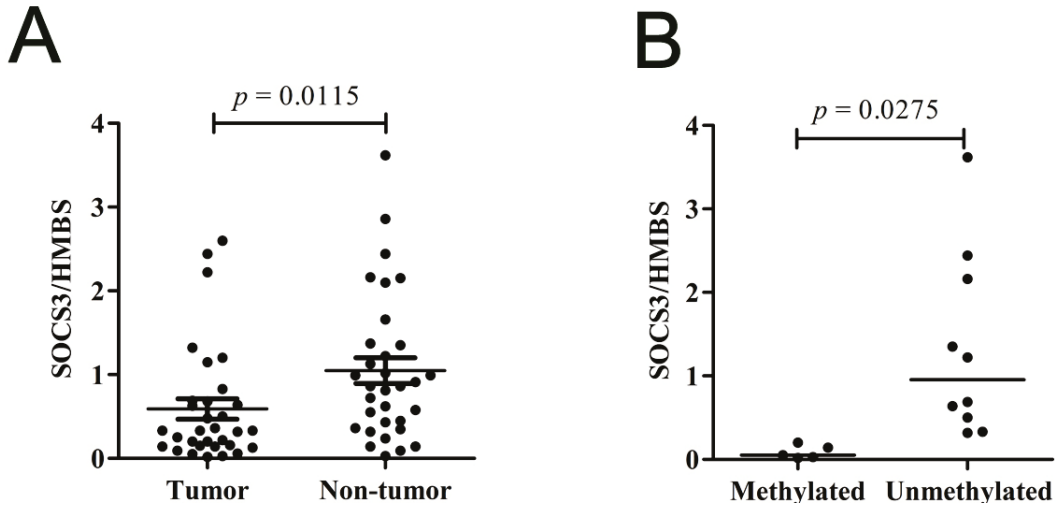

Figure 4. *SOCS3 mRNA* expression levels in tumor and non-tumor tissues. (**A**) *SOCS3 mRNA* expression level in 32 pairs of HCC tumor and non-tumor tissues; and (**B**) *SOCS3* expression level in hypermethylated HCC tissues (intensity ≥ 40%) and unmethylated tissues (intensity < 3%).

2.1.5. Methylation of *SOCS3* Is Associated with the Poor Prognosis of HCC with Hepatitis B Virus (HBV) Infection

We then statistically analyzed the association between *SOCS3* hypermethylation and patient clinicopathological features in HCC cases. As shown in Table 1, *SOCS3* methylation was not correlated with the tumor size, tumor-node-metastasis (TNM) stage, cirrhosis background, portal vein tumor thrombosis, and tumor encapsulation of the HCC patients. It was worth noting that in the older group of HCC patients (≥55 years), the methylation frequency of *SOCS3* in HCC tissues was higher than that in the younger group (<55 years). However, the difference of *SOCS3* methylation between younger and older HCC groups was not statistically significant.

We then evaluated the prognostic value of the *SOCS3* methylation status in HCC patients. The Kaplan–Meier curve analysis indicated that, for all the patients, there was no difference in clinical outcome between the methylated and unmethylated patients (p = 0.633, Figure 5A). However, in patients with an HBV infection background, *SOCS3* hypermethylation was significantly correlated with the poor prognosis of HCC patients (p = 0.0457, Figure 5B), which meant that HCC patients with *SOCS3* hypermethylation exhibited shortened overall survival compared with those with *SOCS3* unmethylation, while no correlation was found in the rest of the patients with HCV or no virus infection background (data not shown).

Table 1. *SOCS3* CGI hypermethylation and clinicopathological correlations in HCC.

Feature	Hypermethylation (n = 61)	Unmethylation (n = 66)	p-Value
Gender			
Male	46 (52.87%)	41 (47.13%)	0.107
Female	15 (37.5%)	25 (62.5%)	
Age			
≥55	42 (54.5%)	35 (45.5%)	0.068
<55	19 (38%)	31 (62%)	
Cirrhosis			
Yes	47 (47.47%)	52 (52.53%)	0.813
No	14 (50%)	14 (50%)	
TNM stage			
I–II	22 (48.89%)	23 (51.11%)	0.886
III–IV	39 (47.56%)	43 (52.44%)	
Portal vein tumor thrombosis			
Present	9 (40.91%)	13 (59.09%)	0.267
Absent	52 (50.98%)	50 (49.02%)	
Tumor size			
≥5 cm	46 (47.92%)	50 (52.08%)	0.964
<5 cm	15 (48.39%)	16 (51.61%)	
Tumor encapsulation			
Complete	52 (50%)	52 (50%)	0.800
Incomplete	6 (37.5%)	10 (62.5%)	

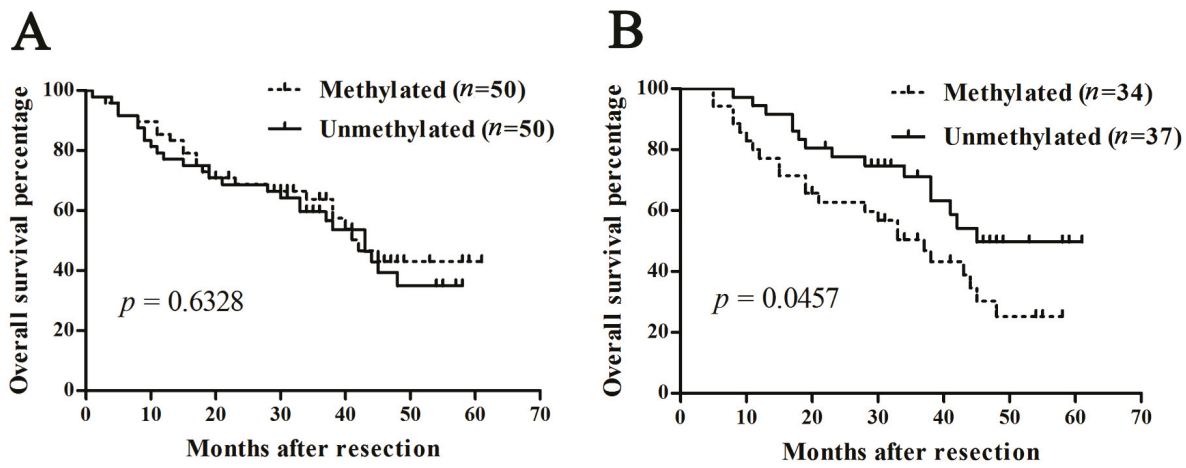

Figure 5. Kaplan–Meier survival plots for *SOCS3* methylation in HCC patients. Overall survival after surgery according to *SOCS3* methylation status in (**A**) general HCC patients and (**B**) HBV infection-related HCC patients.

2.2. Discussion

The aberration of *SOCS3* in human malignancy has been noted in recent years, but the detailed methylation status of *SOCS3* in HCC with different virus infection backgrounds has not been well understood. Here, we confirmed that *SOCS3* was hypermethylated in HCC tissues and *SOCS3* hypermethylation was significantly correlated with the poor prognosis of HCC patients with HBV infection.

Using Methylation-sensitive restriction enzyme-based quantitative PCR (MSRE-qPCR) assay, we found that it was the CGI region close to the translational start site of the *SOCS3* gene that was frequently hypermethylated in HCC tumor tissues and cell lines. *SOCS3* hypermethylation in HCC tissues was not related to the etiological mechanism of HCC. However, *SOCS3* CGI methylation was associated with poor prognosis in HCC with an HBV infection background, while it was not associated with poor prognosis in HCC with HCV or no virus infection background, which indicated that *SOCS3* might play a more powerful role in HBV infection-related HCC; the detection of the methylation of the *SOCS3* gene was of value for the prognosis of HCC with HBV infection. Additionally, we also found that *SOCS3* CGI hypermethylation occurred partially in non-tumor tissues, although its intensity and frequency were far lower than those in tumor tissues. Since most of these HCC patients had a cirrhosis background, it was reasonable to suppose a potential oncogenic role for *SOCS3* hypermethylation during hepatocarcinogenesis from as early as the precancerous cirrhotic stage. Furthermore, no methylation was found in non-tumor tissues in HCC patients with HCV infection, suggesting that different hepatitis viruses might have different effects on the methylation status of *SOCS3*.

Aberrant methylation of gene promoter regions is one of the mechanisms for TSG inactivation in cancers. The decreased expression of *SOCS3* has been reported to be correlated with poor patient survival in HCC tissues [23]. We also observed the frequent down-regulation of *SOCS3 mRNA* levels in HCC cell lines and tumor tissues, which was inversely associated with the *SOCS3* methylation status. In addition, treatment by the demethylation agent could restore *SOCS3* expression in the methylated cell lines. These findings confirmed that methylation modulation was an important

inhibiting factor for *SOCS3* expression. However, in Huh-1 cell lines and some HCC tissues with low expression of *SOCS3*, no methylation was detected, which indicated that other mechanisms could also lead to the down-regulation of *SOCS3*, including mutation, acetylation, and *microRNA* regulation, *etc.*

It has been reported that through inhibiting the JAK/STAT signaling pathway, the *SOCS* gene family plays an important role in suppressing tumor initiation and development [14]. As an essential member of this gene family, *SOCS3* may function as a tumor suppressor gene. In previous reports, *SOCS3* down-regulation was associated with vascular invasion and overall survival [24,25]. The silence of *SOCS3* expression facilitated tumor formation and growth in lung and liver [26], while the loss of *SOCS3* could promote aggressiveness in hepatocellular carcinoma [27]. However, the underlying mechanism of *SOCS3* in the pathogenesis of HCC remains elusive. Further study should be conducted to determine the precise intracellular signaling and explore potential mechanisms of *SOCS3* in the initiation and development of HCC.

In conclusion, our findings suggest that it is the CGI region close to the translational start site that is methylated in HCC, which might contribute to the aberrant expression of *SOCS3*. The hypermethylation of *SOCS3* has already happened in non-tumor tissues and increased in tumors in both frequency and intensity. *SOCS3* CGI methylation was associated with poor prognosis in HCC with a HBV infection background. However, it still needs a larger cohort to confirm this result.

3. Experimental Section

3.1. Tissue Samples

Primary HCC and the adjacent non-tumor tissues were obtained from 127 patients who underwent routine curative surgical treatment at Henan Cancer Hospital in Zhengzhou, Henan Province, China, from 2008 to 2014. Among the 127 patients, 92 patients were infected with HBV, 13 patients with HCV, and 22 patients with no virus infection background. All patients were diagnosed by ultrasonography and computed tomography, and confirmed by liver biopsy. No patients had received radiotherapy or chemotherapy prior to surgery. The 127 patients were histologically diagnosed with HCC. The clinicopathological characteristics were shown in Table 2. The follow-up data were described in detail previously [28]. The study protocol was approved by the institute ethics committee, and informed consent was acquired from all patients and donors before the study commenced.

Table 2. Clinicopathological parameters of 127 patients with HCC.

Clinicopathological Parameter Variables	Cases *n* (%) *n* = 127
Age	
Median (Range)	57 (11–80)
Gender	
Male	87 (68.50)
Female	40 (31.50)
Liver cirrhosis	
Yes	99 (77.95)
No	28 (22.05)

Table 2. *Cont.*

Clinicopathological Parameter Variables	Cases *n* (%) *n* = 127
TNM stage	
I–II	45 (35.43)
III–IV	82 (64.57)
Portal vein tumor thrombosis	
Present	22 (17.32)
Absent	102 (80.32)
N/A	3 (2.36)
Tumor size	
≥5 cm	96 (75.59)
<5 cm	31 (24.41)
Tumor encapsulation	
Complete	104 (81.89)
Incomplete	16 (12.60)
N/A	7 (5.51)

All patients were from the local ethnic Chinese Han population. TNM: Tumor, Lymph Node; Metastasis; and N/A: Not available.

3.2. Cell Culture and 5-Aza-2'-Deoxycytidine Treatment

Human HCC cell lines SMMC7721, Huh-1, Huh-7, Hep3B, SNU449, SK-Hep1, SNU182, and PLC/PRF/5 were kept in our laboratory and maintained in either Dulbecco's Modified Eagle Medium (DMEM) or Roswell Park Memorial Institute (RPMI) 1640 supplemented with 10% fetal bovine serum (GIBCO, Carlsbad, CA, USA). For 5-aza-2′-deoxycytidine treatment, cells were seeded in six-well plates at a concentration of 2–2.5 × 10^5 cells per well and treated with 2 μM of 5-aza-2′-deoxycytidine for three days.

3.3. DNA Extraction and Methylation Assay

Genomic *DNA* was isolated using DNeasy Blood & Tissue Kit (Qiagen, Germantown, MD, USA) and was quantified using NanoDrop 2000 spectrophotometer (Thermo Scientific, Waltham, MA, USA). MSRE-qPCR was performed to detect the methylation status of *SOCS3* as previously described [29]. The methylation primers of *SOCS3* were as follows: Primer 1, forward: AGCTCGAGGGACGCGCGC GCGAA, reverse: CTGAGCCCCCTCGGGTC-CCCAAG; Primer 2, forward: GGTGCCCCAGTCGC TCGGCGAAG, reverse: GGAAGGCG-CGAGCGCGTTGAGTGC. The cut-off value was set at 10%, as previously report [21].

3.4. RNA Extraction and Real-Time RT-qPCR

Total *RNA* was prepared using total RNA isolation (TRIZOL) reagents (Invitrogen, Carlsbad, CA, USA) in accordance with the manufacturer's instructions. The expression level of *SOCS3* was measured through the real-time RT-qPCR assay using the Roche lightcycler 480 (Roche, Mannheim, Germany) according to the manufacturer's instructions. The house-keeping gene *HMBS* was included

in the assay as control reference to normalize the expression levels, and primers of *HMBS* have been described previously [30]. The *SOCS3* qPCR primers were as follows: forward: GGAGACTTCGATTCGGGACC; reverse: GGTACTCGCTCTTGGAGCTG. Each experiment was conducted in duplicate or triplicate, and the comparative C_t method ($2^{-\Delta C_t}$) was adopted to determine the relative expression levels of *SOCS3*.

3.5. Statistical Analyses

The differences between groups were analyzed by two-tailed paired or unpaired *t*-test. The $\chi 2$ test or Fisher's exact test were adopted to determine the association between the *SOCS3* methylation status and the clinicopathological features. The Kaplan–Meier analysis with log-rank test was used to analyze the primary liver cancer (PLC) prognosis and survival time. All of the statistical analyses were performed by GRAPHPAD PRISM software (GraphPad Software, Inc., San Diego, CA, USA). In all cases, a *p*-value of less than 0.05 was considered significant.

4. Conclusions

Our findings suggested that *SOCS3* hypermethylation has already happened in non-tumor tissues, while its frequency and intensity were increased in tumors. The methylation of *SOCS3* predicted a poor prognosis in HBV infection-related HCC patients.

Acknowledgments

This work was supported by the Doctoral Fund of Ministry of Education of China (20110001120017), the National S & T Major Project for Infectious Diseases (2012ZX10004-904) and the National Natural Science Foundation of China (Grant Nos. 81101539 and 81372603).

Author Contributions

Xin Zhang performed the whole experiment, analyzed the data and wrote the manuscript; Xiaolei Zhang conceived and designed the study, and also prepared the entire manuscript; Xiangmei Chen helped the analysis with constructive discussions and revised the article critically for important intellectual content; Qingshan You generally supervised the research, reviewed and amended the manuscript. All authors read and approved the manuscript.

Conflicts of Interest

The authors declare no conflict of interest.

References

1. Portolani, N.; Coniglio, A.; Ghidoni, S.; Giovanelli, M.; Benetti, A.; Tiberio, G.A.; Giulini, S.M. Early and late recurrence after liver resection for hepatocellular carcinoma: Prognostic and therapeutic implications. *Ann. Surg.* **2006**, *243*, 229–235.

2. Wang, H.Q.; Yang, J.; Yan, L.N.; Zhang, X.W.; Yang, J.Y. Liver resection in hepatitis B related-hepatocellular carcinoma: Clinical outcomes and safety in elderly patients. *World J. Gastroenterol.* **2014**, *20*, 6620–6625.
3. Yeo, W.; Mo, F.K.; Chan, S.L.; Leung, N.W.; Hui, P.; Lam, W.Y.; Mok, T.S.; Lam, K.C.; Ho, W.M.; Koh, J.; *et al*. Hepatitis B viral load predicts survival of HCC patients undergoing systemic chemotherapy. *Hepatology* **2007**, *45*, 1382–1389.
4. Mikeska, T.; Bock, C.; Do, H.; Dobrovic, A. DNA methylation biomarkers in cancer: Progress towards clinical implementation. *Expert Rev. Mol. Diagn.* **2012**, *12*, 473–487.
5. Pogribny, I.P.; Rusyn, I. Role of epigenetic aberrations in the development and progression of human hepatocellular carcinoma. *Cancer Lett.* **2014**, *342*, 223–230.
6. Sproul, D.; Meehan, R.R. Genomic insights into cancer-associated aberrant CpG island hypermethylation. *Brief. Funct. Genom.* **2013**, *12*, 174–190.
7. Paziewska, A.; Dabrowska, M.; Goryca, K.; Antoniewicz, A.; Dobruch, J.; Mikula, M.; Jarosz, D.; Zapala, L.; Borowka, A.; Ostrowski, J. DNA methylation status is more reliable than gene expression at detecting cancer in prostate biopsy. *Br. J. Cancer* **2014**, *111*, 781–789.
8. Calvisi, D.F.; Ladu, S.; Gorden, A.; Farina, M.; Lee, J.S.; Conner, E.A.; Schroeder, I.; Factor, V.M.; Thorgeirsson, S.S. Mechanistic and prognostic significance of aberrant methylation in the molecular pathogenesis of human hepatocellular carcinoma. *J. Clin. Investig.* **2007**, *117*, 2713–2722.
9. Dhar, K.; Rakesh, K.; Pankajakshan, D.; Agrawal, D.K. *SOCS3* promotor hypermethylation and STAT3-NF-κB interaction downregulate *SOCS3* expression in human coronary artery smooth muscle cells. *Am. J. Physiol. Heart Circ. Physiol.* **2013**, *304*, H776–H785.
10. Iwahori, K.; Serada, S.; Fujimoto, M.; Nomura, S.; Osaki, T.; Lee, C.M.; Mizuguchi, H.; Takahashi, T.; Ripley, B.; Okumura, M.; *et al*. Overexpression of *SOCS3* exhibits preclinical antitumor activity against malignant pleural mesothelioma. *Int. J. Cancer* **2011**, *129*, 1005–1017.
11. Ogata, H.; Chinen, T.; Yoshida, T.; Kinjyo, I.; Takaesu, G.; Shiraishi, H.; Iida, M.; Kobayashi, T.; Yoshimura, A. Loss of *SOCS3* in the liver promotes fibrosis by enhancing STAT3-mediated TGF-β1 production. *Oncogene* **2006**, *25*, 2520–2530.
12. Zhang, L.; Badgwell, D.B.; Bevers, J.J., 3rd.; Schlessinger, K.; Murray, P.J.; Levy, D.E.; Watowich, S.S. IL-6 signaling via the STAT3/*SOCS3* pathway: Functional analysis of the conserved STAT3 N-domain. *Mol. Cell. Biochem.* **2006**, *288*, 179–189.
13. He, B.; You, L.; Uematsu, K.; Zang, K.; Xu, Z.; Lee, A.Y.; Costello, J.F.; McCormick, F.; Jablons, D.M. *SOCS*-3 is frequently silenced by hypermethylation and suppresses cell growth in human lung cancer. *Proc. Natl. Acad. Sci. USA* **2003**, *100*, 14133–14138.
14. Inagaki-Ohara, K.; Kondo, T.; Ito, M.; Yoshimura, A. *SOCS*, inflammation, and cancer. *JAKSTAT* **2013**, *2*, e24053.
15. Li, Y.; de Haar, C.; Chen, M.; Deuring, J.; Gerrits, M.M.; Smits, R.; Xia, B.; Kuipers, E.J.; van der Woude, C.J. Disease-related expression of the IL6/STAT3/*SOCS3* signalling pathway in ulcerative colitis and ulcerative colitis-related carcinogenesis. *Gut* **2010**, *59*, 227–235.

16. Liu, W.B.; Ao, L.; Zhou, Z.Y.; Cui, Z.H.; Zhou, Y.H.; Yuan, X.Y.; Xiang, Y.L.; Cao, J.; Liu, J.Y. CpG island hypermethylation of multiple tumor suppressor genes associated with loss of their protein expression during rat lung carcinogenesis induced by 3-methylcholanthrene and diethylnitrosamine. *Biochem. Biophys. Res. Commun.* **2010**, *402*, 507–514.
17. Pierconti, F.; Martini, M.; Pinto, F.; Cenci, T.; Capodimonti, S.; Calarco, A.; Bassi, P.F.; Larocca, L.M. Epigenetic silencing of *SOCS3* identifies a subset of prostate cancer with an aggressive behavior. *Prostate* **2011**, *71*, 318–325.
18. Tischoff, I.; Hengge, U.R.; Vieth, M.; Ell, C.; Stolte, M.; Weber, A.; Schmidt, W.E.; Tannapfel, A. Methylation of *SOCS*-3 and *SOCS*-1 in the carcinogenesis of Barrett's adenocarcinoma. *Gut* **2007**, *56*, 1047–1053.
19. Weber, A.; Hengge, U.R.; Bardenheuer, W.; Tischoff, I.; Sommerer, F.; Markwarth, A.; Dietz, A.; Wittekind, C.; Tannapfel, A. *SOCS*-3 is frequently methylated in head and neck squamous cell carcinoma and its precursor lesions and causes growth inhibition. *Oncogene* **2005**, *24*, 6699–6708.
20. Niwa, Y.; Kanda, H.; Shikauchi, Y.; Saiura, A.; Matsubara, K.; Kitagawa, T.; Yamamoto, J.; Kubo, T.; Yoshikawa, H. Methylation silencing of *SOCS*-3 promotes cell growth and migration by enhancing JAK/STAT and FAK signalings in human hepatocellular carcinoma. *Oncogene* **2005**, *24*, 6406–6417.
21. Zhang, X.; Wang, J.; Cheng, J.; Ding, S.; Li, M.; Sun, S.; Zhang, L.; Liu, S.; Chen, X.; Zhuang, H.; *et al*. An integrated analysis of *SOCS*1 down-regulation in HBV infection-related hepatocellular carcinoma. *J. Viral Hepat.* **2013**, doi:10.1111/jvh.12137.
22. Shire, A.; Lomberk, G.; Lai, J.P.; Zou, H.; Tsuchiya, N.; Aderca, I.; Moser, C.D.; Gulaid, K.H.; Oseini, A.; Hu, C.; *et al*. Restoration of epigenetically silenced SULF1 expression by 5-aza-2-deoxycytidine sensitizes hepatocellular carcinoma cells to chemotherapy-induced apoptosis. *Med. Epigenet.* **2015**, *3*, 1–18.
23. Wu, W.Y.; Li, J.; Wu, Z.S.; Zhang, C.L.; Meng, X.L.; Lobie, P.E. Prognostic significance of phosphorylated signal transducer and activator of transcription 3 and suppressor of cytokine signaling 3 expression in hepatocellular carcinoma. *Exp. Ther. Med.* **2011**, *2*, 647–653.
24. Deng, J.; Jiao, X.; Liu, H.; Wu, L.; Zhang, R.; Wang, B.; Pan, Y.; Hao, X.; Liang, H. Lymph node metastasis is mediated by suppressor of cytokine signaling-3 in gastric cancer. *Tumour Biol.* **2013**, *34*, 3627–3636.
25. Stofas, A.; Levidou, G.; Piperi, C.; Adamopoulos, C.; Dalagiorgou, G.; Bamias, A.; Karadimou, A.; Lainakis, G.A.; Papadoukakis, S.; Stravodimos, K.; *et al*. The role of CXC-chemokine receptor CXCR2 and suppressor of cytokine signaling-3 (*SOCS*-3) in renal cell carcinoma. *BMC Cancer* **2014**, *14*, 149.
26. Baltayiannis, G.; Baltayiannis, N.; Tsianos, E.V. Suppressors of cytokine signaling as tumor repressors. Silencing of *SOCS3* facilitates tumor formation and growth in lung and liver. *J. BUON* **2008**, *13*, 263–265.
27. Wu, W.Y.; Kim, H.; Zhang, C.L.; Meng, X.L.; Wu, Z.S. Loss of suppressors of cytokine signaling 3 promotes aggressiveness in hepatocellular carcinoma. *J. Investig. Surg.* **2014**, *27*, 197–204.
28. Xie, X.; Yao, M.; Chen, X.; Lu, W.; Lv, Q.; Wang, K.; Zhang, L.; Lu, F. Reduced red blood cell count predicts poor survival after surgery in patients with primary liver cancer. *Medicine* **2015**, *94*, e577.

29. Wang, Y.; Cheng, J.; Xu, C.; Liu, S.; Jiang, S.; Xu, Q.; Chen, X.; Zhuang, H.; Lu, F. Quantitative methylation analysis reveals gender and age differences in p16INK4a hypermethylation in hepatitis B virus-related hepatocellular carcinoma. *Liver Int.* **2012**, *32*, 420–428.
30. Liu, S.; Zhu, P.; Zhang, L.; Ding, S.; Zheng, S.; Wang, Y.; Lu, F. Selection of reference genes for RT-qPCR analysis in tumor tissues from male hepatocellular carcinoma patients with hepatitis B infection and cirrhosis. *Cancer Biomark.* **2013**, *13*, 345–349.

© 2015 by the authors; licensee MDPI, Basel, Switzerland. This article is an open access article distributed under the terms and conditions of the Creative Commons Attribution license (http://creativecommons.org/licenses/by/4.0/).

Int. J. Mol. Sci. **2015**, *16*, 22976-22988; doi:10.3390/ijms160922976

OPEN ACCESS
International Journal of
Molecular Sciences
ISSN 1422-0067
www.mdpi.com/journal/ijms

Review

Dual Inhibition of MEK and PI3K Pathway in KRAS and BRAF Mutated Colorectal Cancers

Sally Temraz *, Deborah Mukherji and Ali Shamseddine

Department of Internal Medicine, Hematology/Oncology Division, American University of Beirut Medical Center, Beirut 110 72020, Lebanon; E-Mails: dm25@aub.edu.lb (D.M.); as04@aub.edu.lb (A.S.)

* Author to whom correspondence should be addressed; E-Mail: st29@aub.edu.lb; Tel.: +9-611-374-374; Fax: +9-611-370-814.

Academic Editor: William Chi-shing Cho

Received: 31 August 2015 / Accepted: 17 September 2015 / Published: 23 September 2015

Abstract: Colorectal cancer (CRC) is a heterogeneous disease with multiple underlying causative genetic mutations. Genetic mutations in the phosphatidylinositol-3 kinase (PI3K) and the mitogen activated protein kinase (MAPK) pathways are frequently implicated in CRC. Targeting the downstream substrate MEK in these mutated tumors stands out as a potential target in CRC. Several selective inhibitors of MEK have entered clinical trial evaluation; however, clinical activity with single MEK inhibitors has been rarely observed and acquired resistance seems to be inevitable. Amplification of the driving oncogene KRAS(13D), which increases signaling through the ERK1/2 pathway, upregulation of the noncanonical wingless/calcium signaling pathway (Wnt), and coexisting PIK3CA mutations have all been implicated with resistance against MEK inhibitor therapy in KRAS mutated CRC. The Wnt pathway and amplification of the oncogene have also been associated with resistance to MEK inhibitors in CRCs harboring BRAF mutations. Thus, dual targeted inhibition of MEK and PI3K pathway effectors (mTOR, PI3K, AKT, IGF-1R or PI3K/mTOR inhibitors) presents a potential strategy to overcome resistance to MEK inhibitor therapy. Many clinical trials are underway to evaluate multiple combinations of these pathway inhibitors in solid tumors.

Keywords: colorectal cancer; drug resistance; phosphatidylinositol 3-kinase; mitogen-activated protein kinase; MEK

1. Introduction

Colorectal cancer (CRC) is a heterogeneous disease with multiple underlying causative genetic mutations. Activating genetic mutations in the phosphatidylinositol-3 kinase (PI3K) and the mitogen activated protein kinase (MAPK) pathways have been implicated in CRC. Insulin-like growth factor-1 receptor (IGF-1R) is a key activator of these two pro-survival signaling pathways [1]. In the PI3K pathway, activated receptor tyrosine kinases (RTK) cause phosphorylation of PI3K. Class 1 PI3K family members that convert phosphatidylinositol 4,5-bisphosphate (PIP2) to phosphatidylinositol 3,4,5-trisphosphate (PIP3) thereby activating AKT via two crucial phosphorylation events at threonine 308 catalyzed by phosphoinositide-dependent kinase-1 (PDK1) and at serine 473 catalyzed by mammalian target of rapamycin complex 2 (mTORC2) [2]. Phosphatase and tensin homolog (PTEN) reverses this process by dephosphorylating PIP3 to PIP2. Genetic anomalies of PI3K pathway components, such as PTEN loss, PI3K amplification/mutation, AKT mutation or RTK activation, result in activation of this pathway leading to tumorigensis [3]. Mutations in the PIK3CA gene, encoding the p110a catalytic subunit of class I PI3Ks are found in around 15% of CRCs [4].

The MAPK intracellular signaling cascade comprises RAS, RAF, MAPK extracellular signal-regulated kinase (MEK) and extracellular signal-regulated kinase (ERK1/2). The pathway is commonly activated through activating mutations of RAF or RAS. Activated MEK phosphorylates its only substrate ERK1/2 leading to dimerization, nuclear translocation and induction of target genes [5,6]. Mutations in the KRAS gene are the most common in CRCs comprising approximately 35%–45% [4]. Other mutations in this pathway, including NRAS and BRAF constitute approximately 4% and 8% of CRCs, respectively [4]. Thus, targeting the downstream substrate MEK in KRAS, BRAF or NRAS mutated tumors stands out as a potential target in CRC. Several selective inhibitors of MEK have entered clinical trial evaluation [7]; however, clinical activity with single MEK inhibitors has been rarely observed [8–10]. The first generation MEK inhibitor, CI-1040, was assessed in a phase II trial involving four tumor types. Generally, CI-1040 was well tolerated but failed to show sufficient antitumor activity to warrant further development [10]. In addition, the second-generation MEK1/2 inhibitor, Selumetinib (AZD6244), has not performed well in unselected patients with metastatic CRC. Selumetinib showed similar efficacy to capecitabine in terms of the number of patients with a disease progression event and progression-free survival [11]. Resistance to MEK inhibitors is largely due to compensatory up-regulation and crosstalk within the MAPK and PI3K pathways [12–15]. Identification of potential biomarkers for sensitivity or resistance to these agents is urgently needed. Moreover, with both of these pathways active in CRCs, targeting both pathways with small inhibitor molecules has shown greater clinical efficacy than single agents alone. With the increasing use of tumor sequencing for the purposes of treatment selection and identifying patients who may be eligible for clinical trials of agents targeting specific pathways, the molecular stratification of colorectal cancer is becoming a reality. Patients with KRAS/BRAF or NRAS mutated tumors are known to be resistant to monoclonal antibodies targeting the epidermal growth factor (EGFR), therefore options for palliative treatment are limited to cytotoxic chemotherapy, antti-angiogenic agents and most recently the multi-targeted tyrosine kinase inhibitor regorafenib that has been approved for use in patients refractory to these therapies in the third-line [16]. There is an urgent clinical need for the development of novel therapeutics that may be able to prolong survival in patients with RAS/BRAF mutated tumors.

2. Cross-Talk between MEK and PI3K Pathway

The frequent perturbation of the MAPK and PI3K signaling pathways in CRC make them promising candidates for the development of molecularly targeted agents. RAS and RAF gene mutations have been considered potential markers of sensitivity to MEK inhibition largely due to the constitutive activation of MEK seen in BRAF mutant cancer cells and to a lesser extent in KRAS mutant cells [17,18]. Thus, MEK has become a potential target for therapy given that mutation in these kinases has been identified as a negative predictor of benefit from EGFR inhibitor therapy [19–21]. However, acquired resistance after MEK inhibition seems inevitable. In KRAS mutated CRC cells, multiple mechanisms to resistance against MEK inhibition have been reported "Figure 1". Amplification of the driving oncogene KRAS(13D) has been shown to drive acquired resistance to MEK1/2 inhibitors by increasing signaling through the ERK1/2 pathway [22,23]. Increased abundance of the oncogenic driver in response to prolonged drug treatment results in increased flux through the ERK pathway and restoration of ERK activity above the threshold required for cell growth [13]. The up-regulation of KRAS(13D) leads to activation of multiple KRAS effector pathways, thus highlighting the therapeutic challenge posed by KRAS mutations [22]. Upregulation of the noncanonical wingless/calcium signaling pathway (Wnt) signaling pathway is another mechanism by which KRAS mutated CRC cell lines showed resistance to selumetinib [24]. Coexisting mutations of the PIK3CA, which occur in about 8%–9% of CRC cases [25,26], have also been implicated in the resistance of KRAS mutated CRC cells to MEK inhibition [27,28]. In KRAS mutant tumors, PIK3CA mutation restores cyclin D1 expression and G(1)-S cell cycle progression so that they are no longer dependent on KRAS and MEK/ERK signaling [27]. Among RAF/RAS mutant lines, co-occurring PIK3CA/PTEN mutations conferred a cytostatic response instead of a cytotoxic response for colon cancer cells [28]. In another report, activating mutations in PIK3CA reduced the sensitivity to MEK inhibition, whereas PTEN mutations seemed to cause complete resistance. In addition, dual inhibition of the PI3K/AKT and RAF/MEK/ERK pathways also seems to be required for complete inhibition of the downstream mTOR effector pathway [29]. CRC cell lines that were resistant to selumetinib exhibited low or no ERK1/2 activation or exhibited coincident activation of ERK1/2 and protein kinase B (PKB), the latter indicative of activation of the PI3K pathway. Cells that were sensitive arrested in G(1) and/or underwent apoptosis and the presence of BRAF or KRAS mutation was not sufficient to predict either fate; however, CRC cells that did not harbor any mutation tended to be resistant [30]. Another study found that MEK inhibition resulted in activation of PI3K/AKT from the hyperactivation of ERBB3 as a result of the loss of an inhibitory threonine phosphorylation in the conserved juxtamembrane domains of EGFR and HER2. Mutation of this amino acid led to increased ERBB receptor activation and upregulation of the ERBB3/PI3K/AKT signaling pathway, which was no longer responsive to MEK inhibition [14]. Consecutive patients with diverse tumor types and PIK3CA mutation were treated whenever possible with agents targeting the PI3K/AKT/mTOR pathway. Of the 17 patients with PIK3CA mutations, 6 (35%) had simultaneous KRAS or BRAF mutations (colorectal, $n = 4$; ovarian, $n = 2$). Colorectal cancer patients with PIK3CA and KRAS mutations did not respond to therapy [31]. These data suggest that tumors with both KRAS and phosphoinositide 3-kinase mutations are unlikely to respond to the inhibition of the MEK pathway alone or the PI3K pathway alone but will require effective inhibition of both MEK and PI3K/AKT pathway signaling.

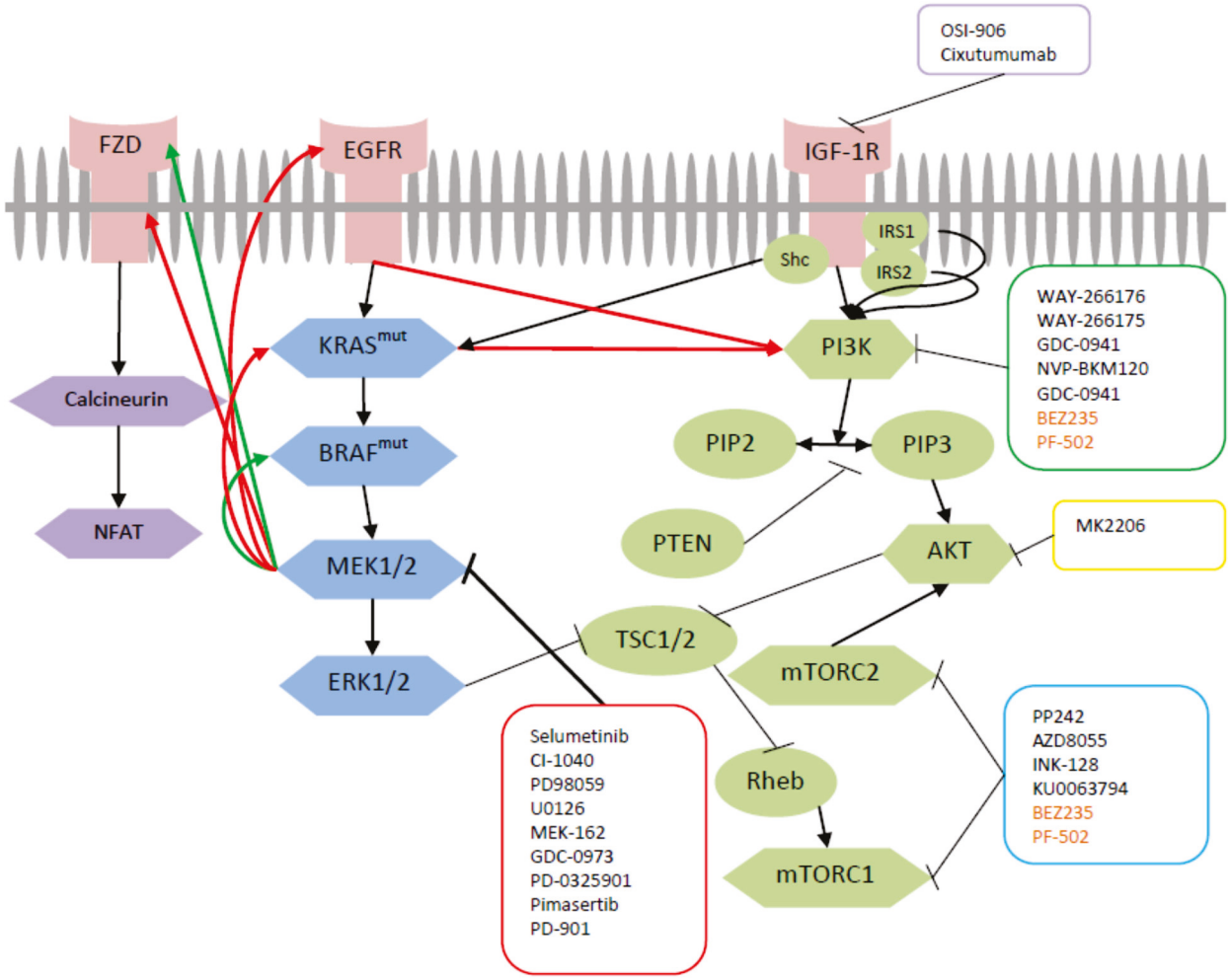

Figure 1. Cross talk between MAPK, PI3K and Wnt pathway in CRC. Upon MEK inhibition with one of the MEK inhibitors (shown in red box), KRAS mutated (Red lines) and BRAF mutated (Green lines) CRCs activate parallel pathways that incur resistance to MEK inhibition. Dual targeted inhibition of MEK with mTOR (shown in blue box), PI3K (shown in green box), AKT (shown in yellow box), IGF-1R (shown in purple box) or PI3K/mTOR (shown in orange) inhibitors has been studied to overcome this resistance. Regular arrow: activates; Arrow ending with a straight line: inhibits.

Tumor cells harboring the BRAF600E mutation have shown similar resistance to MEK1/2 inhibitors "Figure 1" by increasing signaling through the ERK1/2 pathway due to amplification of the oncogene [13,22]. For patients with BRAF mutant tumors, the results suggest that the addition of a RAF inhibitor to a MEK inhibitor may delay or overcome drug resistance [13]. Recently, the Wnt pathway was identified as a potential mediator of resistance to the MEK1/2 inhibitor selumetinib in tumors harboring BRAF mutation [32]. Concomitant use of selumetinib and cyclosporine, inhibited tumor growth and caused tumor regression in patient derived tumor xenografts [32].

3. Pre-Clinical Data on Dual Targeted Inhibition with MEK

3.1. Combined Inhibition of MEK and mTOR

Zhang *et al.* [33] assessed the combination effect of the MEK inhibitor PD98059 and mTOR inhibitor rapamycin on CRC cell lines. They found that combination treatment with PD98059 and rapamycin suppressed the proliferation of CRC cells, induced apoptosis, arrested cell cycle and reduced the incidence and volume of CRC in mice. They also demonstrated that combined administration of these two drugs was able to inhibit the phophorylation of mTOR and MEK signaling pathways and were significantly more effective than single agent treatment [33]. mTOR consists of two functionally distinct complexes, mTORC1 and mTORC2. mTORC1 has been shown to regulate cell growth by controlling mRNA translation initiation and to regulate ribosome biogenesis, autophagy and lipid biosynthesis [34]. mTORC2 on the other hand is involved in cell survival and proliferation through phosphorylation of AKT and protein kinase C [35]. mTORC1 has been shown to be sensitive to acute exposure to rapamycin while mTORC2 was not. Thus, ATP competitive inhibitors that target both mTOR complexes have been developed. Blaser *et al.* demonstrated that PP242, an ATP competitive inhibitor of mTORC1 and mTORC2, reduced the growth, proliferation and survival of colon cells more efficiently than rapamycin [36]. Moreover, the efficacy of ATP-competitive inhibitors of mTOR was enhanced by U0126, a MEK inhibitor. The authors also observed that ATP-competitive inhibitors of mTOR exhibited anticancer effects on both PIK3CA mutated as well as on PIK3CA wild type colon cancer cells [36]. Holt *et al.* also investigated the efficacy of AZD8055, a potent specific inhibitor of mTORC1 and mTORC2, in combination with selumetinib in human tumor non-small cell lung cancer (NSCLC) and CRC cell-derived xenograft and primary patient explants models [37]. Their results showed that combined use of AZD8055 and selumetinib enhanced antitumor activity, inhibited PI3K and MAPK pathways and induced apoptosis. Recently, Li *et al.* reported on the preclinical efficacy of INK-128, a novel ATP-competitive inhibitor of mTORC1 and mTORC2 [38]. INK-128 was capable of inhibiting CRC cell growth and survival and induced both apoptotic and non-apoptotic cancer cell death. INK-128 did not activate ERK and the use of the MEK inhibitor MEK-162 enhanced INK-128 cytotoxicity and inhibited Ht-29 xenograft growth in mice. Thus, combined use of MEK and mTOR inhibitors poses as a potential strategy in targeting not only tumors harboring KRAS mutation but also in those harboring PI3KCA mutation.

3.2. Combined MEK and PI3K Inhibition

Preclinical data suggest that combined MEK and PI3K inhibition will be required to enhance and prolong the anti-tumor activity of MEK inhibitors in KRAS-mutant colon cancers with alterations in the PI3K pathway. Yu *et al.* found that the HCT116 cell line, which harbors mutations in both KRAS and PIK3CA, was resistant to the PI3K inhibitors WAY-266176 and WAY-266175; however, combined therapy with the MEK inhibitors CI-1040 or UO126 led to growth suppression and apoptosis [39]. Data revealed that the down-regulation of PI3K re-sensitizes cell harboring mutations in KRAS and PIK3CA to MEK inhibition while re-expression of mutant PI3KCA allele in MEK inhibitor-resistant cells restores MEK pathway sensitivity [27,29]. Thus, the dual inhibition of both pathways seems to be required for complete inhibition and the induction of cell death. Hoeflich *et al.* further demonstrated that combined treatment with the MEK inhibitor GDC-0973 and PI3K inhibitor GDC-0941 results in apoptosis and

growth inhibition of BRAF and KRAS mutated cell lines and human xenograft tumor models [40]. Recently, Roper *et al.* have also demonstrated that combined PI3K and MEK inhibition with NVP-BKM120 and PD-0325901 induced tumor regression in a mouse model of PIK3CA wild-type and KRAS mutant colorectal cancer [41]. These data indicate that dual MEK and PI3K inhibition is a valid strategy in both PIK3CA wild-type and PIK3CA mutated CRCs with KRAS and/or BRAF mutations and that dual pathway inhibition may be more effective than inhibiting either single pathway alone.

3.3. Combined MEK and P13K/mTOR Inhibition

mTOR inhibition has been correlated with activation of MAPK pathway through PI3K's activation of RAS [42]. Thus, multiple preclinical studies have evaluated the efficacy of MEK inhibition combined with both PI3K and mTOR inhibitors. Martinelli *et al*. revealed that the selective MEK1/2 inhibitor pimasertib combined with the dual PI3K/mTOR inhibitor BEZ235 or with sorafenib caused significant tumor growth delays and increased survival in mice as compared to single agent treatment thereby suggesting that dual blockade of MAPK and PI3K pathways could overcome intrinsic resistance to MEK inhibition [43]. Migliardi *et al.* reported on an analysis of forty different patient-derived murine xenografts of metastatic CRC [44]. They found that the combination of selumetinib and BEZ235 achieved greater rates of disease stabilization than monotherapy (70% *vs.* 27.5% for selumetinib alone and 42.5% for BEZ235 alone). However, no substantial tumor regression was observed for combined therapy suggesting that this combination could be useful only in retarding disease progression. Similarly, Pitt *et al.* demonstrated synergistic anti-proliferative activity with the combination of PI3K/mTOR inhibitor PF-502 and the MEK1/2 inhibitor PD-901 [45]. Combination treatment demonstrated enhanced reduction in tumor growth against CRC cell line and patient-derived tumor xenograft models as compared to either single agent regardless of KRAS or PI3K mutational status. Recently, E *et al.* [46] also reported their results on the use of BEZ235 with selumetinib in HCT116 CRC cells harboring both KRAS and PIk3CA mutations. The combination treatment markedly enhanced their antitumor effects than either single agent alone. The authors also reported a reduction in the phosphorylation level of ERK1/2 and AKT and in the expression of VEGF and matrix metallopeptidase-9 in tumor tissue [46].

When comparing dual PI3K/mTOR inhibition with MEK inhibition against PI3K and MEK inhibition, Haagensen *et al.* found that the pan-PI3K inhibitor GDC-0941 demonstrated greater synergy than the dual PI3K/mTOR inhibitor BEZ235 when combined with the MEK inhibitors selumetinib and PD0325901 in BRAF/PIK3CA-double-mutant HT29 and KRAS/PIK3CA-double-mutant HCT116 CRC cell lines [47]. BEZ235 resulted in marked inhibition of 4EBP1 phosphorylation alone and in combination, whereas there was minimal inhibition with GDC-0941, suggesting that the dual mTOR/PI3K inhibitory activity of BEZ235 may underlie its ability to inhibit 4EBP1 phosphorylation. The addition of the mTORC1/2 inhibitor KU0063794 to GDC-0941 and selumetinib also compromised the synergy achieved between GDC-0941 and selumetinib and was likely due to mTOR inhibition with the addition of KU0063794. The results suggest that the combination of specific PI3K inhibitors, rather than dual mTOR/PI3K inhibitors, with MEK inhibitors results in greater synergy. Thus, these preclinical data suggest that MEK and PI3K/mTOR inhibition may delay tumor growth but may not affect tumor size regression and is likely to be inferior to MEK and PI3K inhibition.

3.4. Combined MEK and AKT Inhibition

AKT upregulation occurs in approximately 60% of CRC cases which renders AKT a potential target for inhibition [48]. Halilovic *et al.* [27] observed increased antitumor activity with combined MEK and AKT inhibition in KRAS/PIK3CA-double-mutant HCT15. Mutant HCT15 tumor xenografts were treated with the MEK inhibitor PD0325901 and AKTi-1/2 alone or in combination. Treatment with either agent alone had no significant effect on tumor growth; however, combined treatment abrogated the growth of tumor xenografts [27].

3.5. Combined Inhibition of MEK and IGFR

IGF-1R is a key regulator of both PI3K and MAPK pathways; however, trials of single agent inhibitors of IGF-1R have shown only modest clinical responses [49]. Previous experimentation with OSI-906, an (IGF1R)/insulin receptor (IR) tyrosine kinase inhibitor (TKI), revealed resistance to OSI-906 that was coupled with simultaneous activation of the MAPK pathway in CRC cell lines [50]. Thus, Flanigan *et al.* [51] tested the efficacy of OSI-906 in combination with selumetinib and U0126. The combination of OSI-906 and U0126 revealed synergistic effects in 11 out of 13 CRC cell lines. In addition, *in vivo* xenograft studies with OSI-906 and selumetinib showed synergistic effects that resulted in apoptosis or cell cycle arrest [51].

4. Clinical Trials on Dual Targeted Inhibition with MEK

Data from patients treated with phase I study drugs targeting the PI3K and/or MAPK pathways revealed that CRC patients harboring mutations in both pathways had tumor regression ranging between 2% and 64% when treated with PI3K and MAPK inhibitors. Dual pathway inhibition may potentially exhibit greater efficacy than single targeted therapy at the expense of greater toxicity. In this study, the most frequent drug-related grade >III adverse events were liver transaminase elevations, mucositis and skin rash [52]. Other clinical trials targeting MEK and one or more effectors of the PI3K pathway are underway and whose results are eagerly awaited particularly concerning patients with KRAS or concomitant KRAS and PIK3CA mutations “Table 1”.

Cixutumumab is a recombinant human IgG1/monoclonal antibody that blocks interaction of IGF-1R and ligands IGF-1 and IGF-2 and thus leads to degradation of IGF-1R. Combination of cixutumumab and selumetinib were evaluated recently in an open label, phase I dose-escalation clinical trial in patients with advanced solid tumors. Wilky *et al*. reported the combination to be well tolerated at maximum doses of 50 mg twice daily for selumetinib and 12 mg/kg every two weeks for cixutumumab. Six patients out of 30 achieved time to progression of >6 months, including patients with thyroid carcinoma, colorectal carcinoma and basal cell carcinoma and two patients achieved partial responses [53]. The results revealed preliminary evidence of clinical benefit and pharmacodynamic evidence of targeted inhibition with IGF-1R and MEK inhibition and which deserve further evaluation in clinical trials.

In a recent biomarker phase 2 trial, Do *et al*. [54] reported the results of combined inhibition with selumetinib and MK-2206, an allosteric inhibitor of the three human isoforms of AKT. Of the 21 patients with advanced CRC enrolled, none reported an objective response regardless of KRAS mutational status. The desired level of target inhibition of pERK and pAKT levels in paired tumor biopsies was not

achieved. Common toxicities were gastrointestinal, hepatic, dermatologic, and hematologic. These toxicities hindered the possibility of dose escalation to achieve levels needed for clinical activity [54]. Based on these results, the authors did not recommend the further evaluation of this combination until appropriate dosing is established in these tumors. One phase I clinical trial in advanced solid tumors targeting both AKT and MEK with GDC-0068 and GDC-0973 "Table 1" is underway and which will aim to evaluate the safety and tolerability of this combination. Until those results are available, current evidence does not support the use of this combination in metastatic CRC patients.

Table 1. Ongoing clinical trials on MEK and PI3K pathway inhibitors in colorectal cancer.

Trial	MEK Inhibitor	PI3K Inhibitor	Phase	Population
NCT01363232	MEK162	BKM120	Phase I	Patients with advanced solid cancers (colorectal cancer, triple-negative breast cancer, pancreatic cancer, and other cancers harboring KRAS, BRAF and NRAS mutations)
NCT01392521	BAY86-9766	BAY80-6946	Phase Ib	Patients with advanced solid cancers
NCT01449058	MEK162	BYL719	Phase II	Patients with advanced solid cancers (colorectal cancer, esophageal cancer, pancreatic cancer, non-small cell lung cancer, and other advanced solid tumors harboring RAS or BRAF mutations)
Trial	**MEK Inhibitor**	**PI3K/mTOR Inhibitor**	**Phase**	**Population**
NCT00996892	GDC-0973	Pictilisb (GDC-0941)	Phase I	Patients with advanced solid cancers
NCT01337765	MEK162	BEZ235	Phase 1	Patients with advanced solid cancers (colorectal cancer, triple-negative breast cancer, pancreatic cancer, malignant melanoma, non-small cell lung cancer, and other cancers harboring KRAS, BRAF and NRAS mutation)
NCT01390818	Pimasertib (MSC1936369B)	SAR245409	Phase 1	Patients with advanced solid cancers (colorectal cancer, pancreatic cancer, thyroid cancer, non-small cell lung cancer, renal cancer, breast cancer, melanoma, ovarian cancer) and any cancer diagnosed with aberrations in one or more the following genes: PTEN, BRAF, KRAS, NRAS, PI3KCA, ErbB1, ErbB2)
NCT01347866	PD0325901	PF-05212384	Phase 1	Patients with advanced solid cancers harboring KRAS or BRAF mutation and patients with KRAS mutation with no more than one prior systemic therapy regimen
Trial	**MEK Inhibitor**	**AKT Inhibitor**	**Phase**	**Population**
NCT01562275	GDC-0973	GDC-0068	Phase 1	Patients with locally advanced or metastatic solid tumors

5. Conclusions

Currently, no targeted KRAS inhibitors exist for KRAS mutated CRC patients. Thus, MEK inhibitors have been studied in this patient population and to a lesser extent in patients harboring BRAF mutated tumors. Regardless of initial response to MEK inhibition, tumors eminently become resistant as a result of various alternative signaling pathways that induce cell proliferation and survival. Thus multiple pathway inhibition has become the focus of treatment to overcome this resistance seen with MEK inhibition "Figure 1".

Preclinical data thus far support dual targeted inhibition of MEK and one or more of the PI3K pathway effectors in metastatic CRC, which was superior to single agent alone. Many clinical trials are underway to evaluate multiple combinations of these pathway inhibitors in solid tumors. But until the results of these are available and the safety and tolerability levels of these targeted inhibitors are established, KRAS and BRAF mutated CRCs remain to have limited treatment options. Preclinical data also suggest that combined MEK and PI3K inhibition is more effective than MEK and PI3K/mTOR inhibition, which needs to be further evaluated. Co-targeted inhibition of IGF-1R and MEK has also shown potential in a recent phase I trial and will require further clinical evaluation in the future. Preclinical data have also identified the Wnt pathway as being activated in KRAS and BRAF mutated tumors treated with MEK inhibitors. The combination of a Wnt pathway inhibitor such as cyclosporine and a MEK1/2 inhibitor needs to be clinically evaluated. Future clinical trials with appropriate molecular stratification and biomarker development have the potential to improve outcomes for patients suffering from advanced colorectal cancer for whom current palliative treatment options are limited.

Author Contributions

Sally Temraz and Ali Shamseddine conceived the topic of the review. Sally Temraz wrote the paper. Ali Shamseddine, Deborah Mukherji and Sally Temraz collected the data. Deborah Mukherji proofread and corrected the final version.

Conflicts of Interest

Sally Temraz has received honoraria and travel support from Roche and Novartis. Deborah Mukherji received travel support from Roche and Merck. Ali Shamseddine has received research grants from Roche, Sanofi, Novartis and GSK. Ali Shamseddine is on the advisory board of Roche, Sanofi, Pharmamed, Pfizer, Astella and Bayer. Ali Shamseddine has received honoraria from Roche, Sanofi, Amgen and Lilly.

References

1. LeRoith, D.; Roberts, C.T., Jr. The insulin-like growth factor system and cancer. *Cancer Lett.* **2003**, *195*, 127–137.
2. Sarbassov, D.D.; Guertin, D.A.; Ali, S.M.; Sabatini, D.M. Phosphorylation and regulation of Akt/PKB by the rictor-mTOR complex. *Science* **2005**, *307*, 1098–1101.
3. Yuan, T.L.; Cantley, L.C. PI3K pathway alterations in cancer: Variations on a theme. *Oncogene* **2008**, *27*, 5497–5510.

4. De Roock, W.; de Vriendt, V.; Normanno, N.; Ciardiello, F.; Tejpar, S. KRAS, BRAF, PIK3CA, and PTEN mutations: Implications for targeted therapies in metastatic colorectal cancer. *Lancet Oncol.* **2011**, *12*, 594–603.
5. Chang, L.; Karin, M. Mammalian map kinase signalling cascades. *Nature* **2001**, *410*, 37–40.
6. Khokhlatchev, A.V.; Canagarajah, B.; Wilsbacher, J.; Robinson, M.; Atkinson, M.; Goldsmith, E.; Cobb, M.H. Phosphorylation of the MAP kinase ERK2 promotes its homodimerization and nuclear translocation. *Cell* **1998**, *93*, 605–615.
7. Fremin, C.; Meloche, S. From basic research to clinical development of MEK1/2 inhibitors for cancer therapy. *J. Hematol. Oncol.* **2010**, *3*, 8, doi:10.1186/1756-8722-3-8.
8. Banerji, U.; Camidge, D.R.; Verheul, H.M.; Agarwal, R.; Sarker, D.; Kaye, S.B.; Desar, I.M.; Timmer-Bonte, J.N.; Eckhardt, S.G.; Lewis, K.D.; *et al.* The first-in-human study of the hydrogen sulfate (Hyd-sulfate) capsule of the MEK1/2 inhibitor AZD6244 (ARRY-142886): A phase I open-label multicenter trial in patients with advanced cancer. *Clin. Cancer Res.* **2010**, *16*, 1613–1623.
9. Lorusso, P.M.; Adjei, A.A.; Varterasian, M.; Gadgeel, S.; Reid, J.; Mitchell, D.Y.; Hanson, L.; DeLuca, P.; Bruzek, L.; Piens, J.; *et al.* Phase I and pharmacodynamic study of the oral MEK inhibitor CI-1040 in patients with advanced malignancies. *J. Clin. Oncol.* **2005**, *23*, 5281–5293.
10. Rinehart, J.; Adjei, A.A.; Lorusso, P.M.; Waterhouse, D.; Hecht, J.R.; Natale, R.B.; Hamid, O.; Varterasian, M.; Asbury, P.; Kaldjian, E.P.; *et al.* Multicenter phase II study of the oral MEK inhibitor, CI-1040, in patients with advanced non-small-cell lung, breast, colon, and pancreatic cancer. *J. Clin. Oncol.***2004**, *22*, 4456–4462.
11. Bennouna, J.; Lang, I.; Valladares-Ayerbes, M.; Boer, K.; Adenis, A.; Escudero, P.; Kim, T.Y.; Pover, G.M.; Morris, C.D.; Douillard, J.Y. A phase II, open-label, randomised study to assess the efficacy and safety of the MEK1/2 inhibitor AZD6244 (ARRY-142886) *versus* capecitabine monotherapy in patients with colorectal cancer who have failed one or two prior chemotherapeutic regimens. *Investig. New Drug.* **2011**, *29*, 1021–1028.
12. O'Reilly, K.E.; Rojo, F.; She, Q.B.; Solit, D.; Mills, G.B.; Smith, D.; Lane, H.; Hofmann, F.; Hicklin, D.J.; Ludwig, D.L.; *et al.* mTOR inhibition induces upstream receptor tyrosine kinase signaling and activates Akt. *Cancer Res.* **2006**, *66*, 1500–1508.
13. Poulikakos, P.I.; Solit, D.B. Resistance to MEK inhibitors: Should we co-target upstream? *Sci. Signal.* **2011**, *4*, pe16, doi:10.1126/scisignal.2001948.
14. Turke, A.B.; Song, Y.; Costa, C.; Cook, R.; Arteaga, C.L.; Asara, J.M.; Engelman, J.A. MEK inhibition leads to PI3K/Akt activation by relieving a negative feedback on ERBB receptors. *Cancer Res.* **2012**, *72*, 3228–3237.
15. Britten, C.D. PI3K and MEK inhibitor combinations: Examining the evidence in selected tumor types. *Cancer Chemother. Pharm.* **2013**, *71*, 1395–1409.
16. Temraz, S.; Mukherji, D.; Shamseddine, A. Sequencing of treatment in metastatic colorectal cancer: Where to fit the target. *World J. Gastroenterol.* **2014**, *20*, 1993–2004.
17. Solit, D.B.; Garraway, L.A.; Pratilas, C.A.; Sawai, A.; Getz, G.; Basso, A.; Ye, Q.; Lobo, J.M.; She, Y.; Osman, I.; *et al.* Braf mutation predicts sensitivity to MEK inhibition. *Nature* **2006**, *439*, 358–362.

18. Davies, B.R.; Logie, A.; McKay, J.S.; Martin, P.; Steele, S.; Jenkins, R.; Cockerill, M.; Cartlidge, S.; Smith, P.D. AZD6244 (ARRY-142886), a potent inhibitor of mitogen-activated protein kinase/extracellular signal-regulated kinase kinase 1/2 kinases: Mechanism of action *in vivo*, pharmacokinetic/pharmacodynamic relationship, and potential for combination in preclinical models. *Mol. Cancer Ther.* **2007**, *6*, 2209–2219.
19. Cui, D.; Cao, D.; Yang, Y.; Qiu, M.; Huang, Y.; Yi, C. Effect of BRAF V600E mutation on tumor response of anti-EGFR monoclonal antibodies for first-line metastatic colorectal cancer treatment: A meta-analysis of randomized studies. *Mol. Biol. Rep.* **2014**, *41*, 1291–1298.
20. Sorich, M.J.; Wiese, M.D.; Rowland, A.; Kichenadasse, G.; McKinnon, R.A.; Karapetis, C.S. Extended RAS mutations and anti-EGFR monoclonal antibody survival benefit in metastatic colorectal cancer: A meta-analysis of randomized, controlled trials. *Ann. Oncol.* **2014**, doi:10.1093/annonc/mdu378.
21. Li, W.; Shi, Q.; Wang, W.; Liu, J.; Ren, J.; Li, Q.; Hou, F. KRAS status and resistance to epidermal growth factor receptor tyrosine-kinase inhibitor treatment in patients with metastatic colorectal cancer: A meta-analysis. *Colorectal Dis.* **2014**, *16*, 370–378.
22. Little, A.S.; Balmanno, K.; Sale, M.J.; Newman, S.; Dry, J.R.; Hampson, M.; Edwards, P.A.; Smith, P.D.; Cook, S.J. Amplification of the driving oncogene, KRAS or BRAF, underpins acquired resistance to MEK1/2 inhibitors in colorectal cancer cells. *Sci. Signal.* **2011**, *4*, ra17, doi:10.1126/scisignal.2001752.
23. Wang, Y.; van Becelaere, K.; Jiang, P.; Przybranowski, S.; Omer, C.; Sebolt-Leopold, J. A role for K-ras in conferring resistance to the MEK inhibitor, CI-1040. *Neoplasia* **2005**, *7*, 336–347.
24. Tentler, J.J.; Nallapareddy, S.; Tan, A.C.; Spreafico, A.; Pitts, T.M.; Morelli, M.P.; Selby, H.M.; Kachaeva, M.I.; Flanigan, S.A.; Kulikowski, G.N.; *et al.* Identification of predictive markers of response to the MEK1/2 inhibitor selumetinib (AZD6244) in K-ras-mutated colorectal cancer. *Mol. Cancer Ther.* **2010**, *9*, 3351–3362.
25. Nosho, K.; Kawasaki, T.; Ohnishi, M.; Suemoto, Y.; Kirkner, G.J.; Zepf, D.; Yan, L.; Longtine, J.A.; Fuchs, C.S.; Ogino, S. PIK3CA mutation in colorectal cancer: Relationship with genetic and epigenetic alterations. *Neoplasia* **2008**, *10*, 534–541.
26. De Roock, W.; Claes, B.; Bernasconi, D.; de Schutter, J.; Biesmans, B.; Fountzilas, G.; Kalogeras, K.T.; Kotoula, V.; Papamichael, D.; Laurent-Puig, P.; *et al.* Effects of KRAS, BRAF, NRAS, and PIK3CA mutations on the efficacy of cetuximab plus chemotherapy in chemotherapy-refractory metastatic colorectal cancer: A retrospective consortium analysis. *Lancet Oncol.* **2010**, *11*, 753–762.
27. Halilovic, E.; She, Q.B.; Ye, Q.; Pagliarini, R.; Sellers, W.R.; Solit, D.B.; Rosen, N. PIK3CA mutation uncouples tumor growth and cyclin D1 regulation from MEK/ERK and mutant KRAS signaling. *Cancer Res.* **2010**, *70*, 6804–6814.
28. Jing, J.; Greshock, J.; Holbrook, J.D.; Gilmartin, A.; Zhang, X.; McNeil, E.; Conway, T.; Moy, C.; Laquerre, S.; Bachman, K.; *et al.* Comprehensive predictive biomarker analysis for MEK inhibitor GSK1120212. *Mol. Cancer Ther.* **2012**, *11*, 720–729.
29. Wee, S.; Jagani, Z.; Xiang, K.X.; Loo, A.; Dorsch, M.; Yao, Y.M.; Sellers, W.R.; Lengauer, C.; Stegmeier, F. PI3K pathway activation mediates resistance to MEK inhibitors in KRAS mutant cancers. *Cancer Res.* **2009**, *69*, 4286–4293.
30. Balmanno, K.; Chell, S.D.; Gillings, A.S.; Hayat, S.; Cook, S.J. Intrinsic resistance to the MEK1/2 inhibitor AZD6244 (ARRY-142886) is associated with weak ERK1/2 signalling and/or strong PI3K signalling in colorectal cancer cell lines. *Int. J. Cancer* **2009**, *125*, 2332–2341.

31. Janku, F.; Tsimberidou, A.M.; Garrido-Laguna, I.; Wang, X.; Luthra, R.; Hong, D.S.; Naing, A.; Falchook, G.S.; Moroney, J.W.; Piha-Paul, S.A.; *et al.* PIK3CA mutations in patients with advanced cancers treated with PI3K/AKT/mTOR axis inhibitors. *Mol. Cancer Ther.* **2011**, *10*, 558–565.
32. Spreafico, A.; Tentler, J.J.; Pitts, T.M.; Tan, A.C.; Gregory, M.A.; Arcaroli, J.J.; Klauck, P.J.; McManus, M.C.; Hansen, R.J.; Kim, J.; *et al.* Rational combination of a MEK inhibitor, selumetinib, and the Wnt/calcium pathway modulator, cyclosporin A, in preclinical models of colorectal cancer. *Clin. Cancer Res.* **2013**, *19*, 4149–4162.
33. Zhang, Y.J.; Tian, X.Q.; Sun, D.F.; Zhao, S.L.; Xiong, H.; Fang, J.Y. Combined inhibition of MEK and mTOR signaling inhibits initiation and progression of colorectal cancer. *Cancer Investig.* **2009**, *27*, 273–285.
34. Ma, X.M.; Blenis, J. Molecular mechanisms of mTOR-mediated translational control. *Nat. Rev. Mol. Cell Biol.* **2009**, *10*, 307–318.
35. Ikenoue, T.; Inoki, K.; Yang, Q.; Zhou, X.; Guan, K.L. Essential function of TORC2 in PKC and Akt turn motif phosphorylation, maturation and signalling. *EMBO J.* **2008**, *27*, 1919–1931.
36. Blaser, B.; Waselle, L.; Dormond-Meuwly, A.; Dufour, M.; Roulin, D.; Demartines, N.; Dormond, O. Antitumor activities of ATP-competitive inhibitors of mTOR in colon cancer cells. *BMC Cancer* **2012**, *12*, 86, doi:10.1186/1471-2407-12-86.
37. Holt, S.V.; Logie, A.; Davies, B.R.; Alferez, D.; Runswick, S.; Fenton, S.; Chresta, C.M.; Gu, Y.; Zhang, J.; Wu, Y.L.; *et al.* Enhanced apoptosis and tumor growth suppression elicited by combination of MEK (selumetinib) and mTOR kinase inhibitors (AZD8055). *Cancer Res.* **2012**, *72*, 1804–1813.
38. Li, C.; Cui, J.F.; Chen, M.B.; Liu, C.Y.; Liu, F.; Zhang, Q.D.; Zou, J.; Lu, P.H. The preclinical evaluation of the dual mTORC1/2 inhibitor INK-128 as a potential anti-colorectal cancer agent. *Cancer Biol. Ther.* **2015**, *16*, 34–42.
39. Yu, K.; Toral-Barza, L.; Shi, C.; Zhang, W.G.; Zask, A. Response and determinants of cancer cell susceptibility to PI3K inhibitors: Combined targeting of PI3K and MEK1 as an effective anticancer strategy. *Cancer Biol. Ther.* **2008**, *7*, 307–315.
40. Hoeflich, K.P.; Merchant, M.; Orr, C.; Chan, J.; Den Otter, D.; Berry, L.; Kasman, I.; Koeppen, H.; Rice, K.; Yang, N.Y.; *et al.* Intermittent administration of MEK inhibitor GDC-0973 plus PI3K inhibitor GDC-0941 triggers robust apoptosis and tumor growth inhibition. *Cancer Res.* **2012**, *72*, 210–219.
41. Roper, J.; Sinnamon, M.J.; Coffee, E.M.; Belmont, P.; Keung, L.; Georgeon-Richard, L.; Wang, W.V.; Faber, A.C.; Yun, J.; Yilmaz, O.H.; *et al.* Combination PI3K/MEK inhibition promotes tumor apoptosis and regression in PIK3CA wild-type, KRAS mutant colorectal cancer. *Cancer Lett.* **2014**, *347*, 204–211.
42. Carracedo, A.; Pandolfi, P.P. The PTEN-PI3K pathway: Of feedbacks and cross-talks. *Oncogene* **2008**, *27*, 5527–5541.
43. Martinelli, E.; Troiani, T.; D'Aiuto, E.; Morgillo, F.; Vitagliano, D.; Capasso, A.; Costantino, S.; Ciuffreda, L.P.; Merolla, F.; Vecchione, L.; *et al.* Antitumor activity of pimasertib, a selective MEK 1/2 inhibitor, in combination with PI3K/mTOR inhibitors or with multi-targeted kinase inhibitors in pimasertib-resistant human lung and colorectal cancer cells. *Int. J. Cancer.* **2013**, *133*, 2089–2101.

44. Migliardi, G.; Sassi, F.; Torti, D.; Galimi, F.; Zanella, E.R.; Buscarino, M.; Ribero, D.; Muratore, A.; Massucco, P.; Pisacane, A.; *et al.* Inhibition of MEK and PI3K/mTOR suppresses tumor growth but does not cause tumor regression in patient-derived xenografts of RAS-mutant colorectal carcinomas. *Clin. Cancer Res.* **2012**, *18*, 2515–2525.
45. Pitts, T.M.; Newton, T.P.; Bradshaw-Pierce, E.L.; Addison, R.; Arcaroli, J.J.; Klauck, P.J.; Bagby, S.M.; Hyatt, S.L.; Purkey, A.; Tentler, J.J.; *et al.* Dual pharmacological targeting of the map kinase and PI3K/mTOR pathway in preclinical models of colorectal cancer. *PLoS ONE* **2014**, *9*, e113037, doi:10.1371/journal.pone.0113037.
46. E, J.; Xing, J.; Gong, H.; He, J.; Zhang, W. Combine MEK inhibition with PI3K/mTOR inhibition exert inhibitory tumor growth effect on KRAS and PIK3CA mutation CRC xenografts due to reduced expression of vegf and matrix metallopeptidase-9. *Tumor Biol.* **2015**, *36*, 1091–1097.
47. Haagensen, E.J.; Kyle, S.; Beale, G.S.; Maxwell, R.J.; Newell, D.R. The synergistic interaction of MEK and PI3K inhibitors is modulated by mTOR inhibition. *Br. J. Cancer* **2012**, *106*, 1386–1394.
48. Roy, H.K.; Olusola, B.F.; Clemens, D.L.; Karolski, W.J.; Ratashak, A.; Lynch, H.T.; Smyrk, T.C. AKT proto-oncogene overexpression is an early event during sporadic colon carcinogenesis. *Carcinogenesis* **2002**, *23*, 201–205.
49. Jin, M.; Petronella, B.A.; Cooke, A.; Kadalbajoo, M.; Siu, K.W.; Kleinberg, A.; May, E.W.; Gokhale, P.C.; Schulz, R.; Kahler, J.; *et al.* Discovery of novel insulin-like growth factor-1 receptor inhibitors with unique time-dependent binding kinetics. *ACS Med. Chem. Lett.* **2013**, *4*, 627–631.
50. Pitts, T.M.; Tan, A.C.; Kulikowski, G.N.; Tentler, J.J.; Brown, A.M.; Flanigan, S.A.; Leong, S.; Coldren, C.D.; Hirsch, F.R.; Varella-Garcia, M.; *et al.* Development of an integrated genomic classifier for a novel agent in colorectal cancer: Approach to individualized therapy in early development. *Clin. Cancer Res.* **2010**, *16*, 3193–3204.
51. Flanigan, S.A.; Pitts, T.M.; Newton, T.P.; Kulikowski, G.N.; Tan, A.C.; McManus, M.C.; Spreafico, A.; Kachaeva, M.I.; Selby, H.M.; Tentler, J.J.; *et al.* Overcoming IGF1R/IR resistance through inhibition of MEK signaling in colorectal cancer models. *Clin. Cancer Res.* **2013**, *19*, 6219–6229.
52. Shimizu, T.; Tolcher, A.W.; Papadopoulos, K.P.; Beeram, M.; Rasco, D.W.; Smith, L.S.; Gunn, S.; Smetzer, L.; Mays, T.A.; Kaiser, B.; *et al.* The clinical effect of the dual-targeting strategy involving PI3K/AKT/mTOR and RAS/MEK/ERK pathways in patients with advanced cancer. *Clin. Cancer Res.* **2012**, *18*, 2316–2325.
53. Wilky, B.A.; Rudek, M.A.; Ahmed, S.; Laheru, D.A.; Cosgrove, D.; Donehower, R.C.; Nelkin, B.; Ball, D.; Doyle, L.A.; Chen, H.; *et al.* A phase I trial of vertical inhibition of IGF signalling using cixutumumab, an anti-IGF-1R antibody, and selumetinib, an MEK 1/2 inhibitor, in advanced solid tumours. *Br. J. Cancer* **2015**, *112*, 24–31.
54. Do, K.; Speranza, G.; Bishop, R.; Khin, S.; Rubinstein, L.; Kinders, R.J.; Datiles, M.; Eugeni, M.; Lam, M.H.; Doyle, L.A.; *et al.* Biomarker-driven phase 2 study of MK-2206 and selumetinib (AZD6244, ARRY-142886) in patients with colorectal cancer. *Investig. New Drug* **2015**, *33*, 720–728.

© 2015 by the authors; licensee MDPI, Basel, Switzerland. This article is an open access article distributed under the terms and conditions of the Creative Commons Attribution license (http://creativecommons.org/licenses/by/4.0/).

Int. J. Mol. Sci. **2015**, *16*, 24772-24790; doi:10.3390/ijms161024772

OPEN ACCESS
International Journal of
Molecular Sciences
ISSN 1422-0067
www.mdpi.com/journal/ijms

Article

Elevated STAT3 Signaling-Mediated Upregulation of MMP-2/9 Confers Enhanced Invasion Ability in Multidrug-Resistant Breast Cancer Cells

Fei Zhang [1,2,3], Zhiyong Wang [1,2,3], Yanling Fan [1,2,3], Qiao Xu [1,2,3], Wei Ji [1,2,3], Ran Tian [1,2,3] and Ruifang Niu [1,2,3,*]

1 Public Laboratory, Tianjin Medical University Cancer Institute and Hospital, National Clinical Research Center for Cancer, Tianjin 300060, China; E-Mails: feizhang03@tmu.edu.cn (F.Z.); wzy7848354@hotmail.com (Z.W.); fanyanling402@163.com (Y.F.); xq691589132@hotmail.com (Q.X.); jiwei217@126.com (W.J.); tianrants1985@163.com (R.T.)

2 Key Laboratory of Breast Cancer Prevention and Therapy, Tianjin Medical University, Ministry of Education, Tianjin 300060, China

3 Key Laboratory of Cancer Prevention and Therapy, Tianjin 300060, China

* Author to whom correspondence should be addressed; E-Mail: rniu@tmu.edu.cn; Tel./Fax: +86-22-2334-0123 (ext. 6018).

Academic Editor: William Chi-shing Cho

Received: 4 September 2015 / Accepted: 9 October 2015 / Published: 16 October 2015

Abstract: The development of multidrug resistance greatly impedes effective cancer therapy. Recent advances in cancer research have demonstrated that acquisition of multidrug resistance by cancer cells is usually accompanied by enhanced cell invasiveness. Several lines of evidence indicated that cross activation of other signaling pathways during development of drug resistance may increase invasive potential of multidrug-resistant (MDR) cancer cells. However, the accurate mechanism of this process is largely undefined. In this study, to better understand the associated molecular pathways responsible for cancer progression induced by drug resistance, a MDR human breast cancer cell line SK-BR-3/EPR with P-glycoprotein overexpression was established using stepwise long-term exposure to increasing concentration of epirubicin. The SK-BR-3/EPR cell line exhibited decreased cell proliferative activity, but enhanced cell invasive capacity. We showed that the expression of metastasis-related matrix metalloproteinase (MMP)-2/9 was elevated in SK-BR-3/EPR cells. Moreover, SK-BR-3/EPR cells showed elevated activation of STAT3. Activation of STAT3

signaling is responsible for enhanced invasiveness of SK-BR-3/EPR cells through upregulation of MMP-2/9. STAT3 is a well-known oncogene and is frequently implicated in tumorigenesis and chemotherapeutic resistance. Our findings augment insight into the mechanism underlying the functional association between MDR and cancer invasiveness.

Keywords: STAT3; MMP-2; MMP-9; multidrug-resistant (MDR); invasion; breast cancer

1. Introduction

Breast cancer remains the major cause of cancer death among females in spite of advances in breast cancer therapy in the past three decades [1]. Chemotherapy is one of the major strategies for treating this fatal disease, especially for advanced stage of breast cancer [2–4]. However, development of drug resistance greatly impedes effective cancer therapy [2,5–7]. More intractably, resistance to single chemotherapeutic drug by cancer cells are always associated with the emergence of cross-resistance to multiple structurally, functionally, and mechanistically unrelated anticancer drugs [2,5–7]. This phenomenon is known as multidrug resistance. Numerous studies have revealed several mechanisms that contribute to multi-drug resistance [2,5–7]. Overexpression of multidrug-efflux transporters, such as P-glycoprotein, MRP1, and BCRP, contributes to multidrug resistance [2,5–8]. These membrane transporters function as pumps that efflux cytotoxic reagents out of the cell, thereby resulting in drug resistance. Several studies have demonstrated that activation of cellular signaling contributes to upregulated expression of these drug transporters [9–11]. However, detailed mechanisms on how cancer cells upregulate these drug pumps and evolve the ability to resist apoptotic stimuli by anticancer drugs remain poorly understood.

Acquisition of drug resistance by cancer cells *in vitro* is usually accompanied by other changes of cellular activities, such as alterations in cell proliferative rate, resistance to apoptosis stimuli, and enhanced cell invasiveness [12–19]. Moreover, expression of metastasis-related genes is upregulated in many multidrug-resistant (MDR) cancer cells as compared to drug-sensitive cells [20–23]. In addition, MDR cancer cells even exhibit epithelial to mesenchymal transition signatures, which are associated with cancer invasion and metastasis [13,14,24–27]. Consistently, several *in vivo* studies found that MDR cancer cells displayed enhanced metastatic potential than parental cells in animal models [14,28]. Moreover, multidrug resistance also promotes tumor relapse and cancer metastasis clinically [21,22,29–32]. These results suggest a functional relationship between drug resistance and cancer cell invasion and metastasis. Thus, overcoming cancer progression caused by chemotherapy failure is urgently needed for cancer treatment. However, the accurate mechanism involved in this process is still largely unknown.

Several lines of evidence indicate that cross-activation of other signaling pathways during acquisition of drug resistance may increase the invasiveness potential of MDR cancer cells [9,10,23,33–36]. Establishing MDR cancer cell lines is highly important to improve the understanding of associated molecular pathways responsible for cancer progression induced by drug resistance. In the present study, a human breast cancer cell line SK-BR-3/EPR with MDR phenotype and overexpressing P-glycoprotein was established. In addition, we showed that SK-BR-3/EPR cells exhibited enhanced cell invasiveness along with upregulated expression of metastasis-related matrix metalloproteinase (MMP)-2/9.

Moreover, SK-BR-3/EPR cells showed elevated activation of STAT3. We further provide evidence that activation of STAT3 signaling was responsible for enhanced invasiveness of SK-BR-3/EPR cells through upregulation of MMP-2/9. STAT3 is a well-known oncogene and frequently implicated in tumorigenesis and chemotherapeutic resistance. Therefore, our findings suggest a novel plausible mechanism employed by MDR cancer cells to promote their invasiveness.

2. Results

2.1. Establishment of Multidrug-Resistant (MDR) SK-BR-3/EPR Cells

SK-BR-3 is frequently used for studies on breast cancer cell biology and anticancer therapy, but induction of drug resistance in this well-known cell line has not been explored. An epirubicin-resistant cancer cell line was induced from parental SK-BR-3 cell lines by stepwise long-term exposure to increasing concentration of epirubicin over eight months. Epirubicin concentration was increased from 0.05 to 4.0 μM. The established resistant cells were designated as SK-BR-3/EPR (epirubicin resistant). As shown in Figure 1A and Table 1, the SK-BR-3/EPR cells were approximately 200-fold resistant to epirubicin than the parent cells. In addition, we also examined the sensitivity of these two cells to paclitaxel and 5-Fluorouracil (5-FU). As shown in Figure 1A,B, the SK-BR-3/EPR cells also exhibited a cross-resistant phenotype to these two chemotherapeutics drugs (Table 1), which they were not exposed to, suggesting it was a potential MDR cell line.

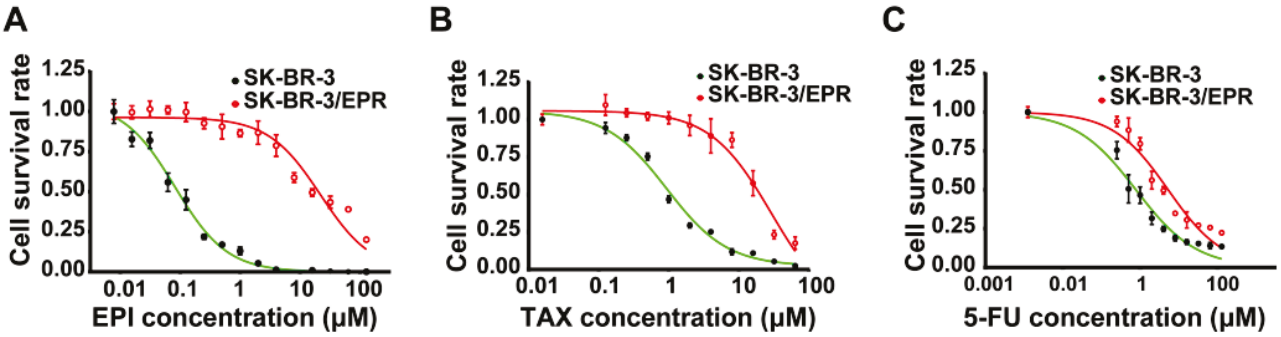

Figure 1. Establishment of a multi-drug resistant human breast cancer cell line SK-BR-3/EPR. (**A**–**C**) Drug sensitivity assay of SK-BR-3 and SK-BR-3/EPR cells to epirubicin, paclitaxel and 5-Fluorouracil (5-FU). Cell viability assay was determined using a Cell Counting Kit-8 (CCK-8) according to the manufacturer's protocol. In brief, cells were seeded in 96 well plate at a density of 5×10^3 cells per well and cultured for 24 h, then different concentration of indicated drugs were added into each well and further cultured for 72 h. After removal of culture medium, 10 μL of CCK-8 reagent in 200 μL medium were added into each well and incubated for 3 h, then the cell viability were calculated by measuring the absorbance at 450 nm on a micro-ELISA reader. The assays were performed using five replicates for each concentration and repeated three times. IC_{50} is defined as the concentration of drug causing half inhibition of cell growth compared with the cell growth of the control group. The IC_{50} was calculated by the Graphpad Prism 6.00 software.

Table 1. IC_{50} (the concentration of drug causing half inhibition of cell growth compared with the cell growth of the control group) values in parental SK-BR-3 and SK-BR-3/EPR to various chemotherapeutic drugs.

Drugs	IC_{50} (μM)		*RI*	*p*-Value
	SK-BR-3	SK-BR-3/EPR		
Epirubicin	0.113 ± 0.0123	22.61 ± 1.258	199.4	<0.0001
Paclitaxel	1.372 ± 0.1050	23.50 ± 1.154	17.1	<0.0001
5-fluorouracil	1.080 ± 0.1661	5.81 ± 0.697	5.4	<0.0001

2.2. Elevated Expression of P-Glycoprotein Is Responsible for Acquisition of MDR Phenotype in SK-BR-3/EPR Cells

Upregulation of drug transporters, namely, MDR1/P-glycoprotein, MRP1, and BCRP is well-known to confer to multidrug resistance [6]. We investigated the expression patterns of MDR1, MRP1 and BCRP mRNA in SK-BR-3, as well as SK-BR-3/EPR, by quantitative PCR. As shown in Figure 2A, the expression of MDR1 mRNA in SK-BR-3/EPR cells was markedly upregulated approximately 150-fold than that in the parent cells, whereas the mRNA expression of MRP1 and BCRP was not detected in both cells. Further analysis of PCR products by agarose gel electrophoresis confirmed the upregulated expression of MDR1 mRNA in SK-BR-3/EPR cells (Figure 2B). Consistently, data from Western blotting showed strong positive expression of P-glycoprotein in SK-BR-3/EPR cells, while, P-glycoprotein was undetected in parent SK-BR-3 cells (Figure 2C). In addition, confocal immunofluorescence microscopy analysis also confirmed the apparent expression of P-glycoprotein in the cell membrane of SK-BR-3/EPR cells, but not in drug sensitive cells (Figure 2D). Moreover, SK-BR-3/EPR cells exhibited markedly reduced retention of intracellular rhodamine 123 dye compared with SK-BR-3 cells as measured by rhodamine efflux assay (Figure 2E). This phenomenon is also correlated with P-glycoprotein expression and function

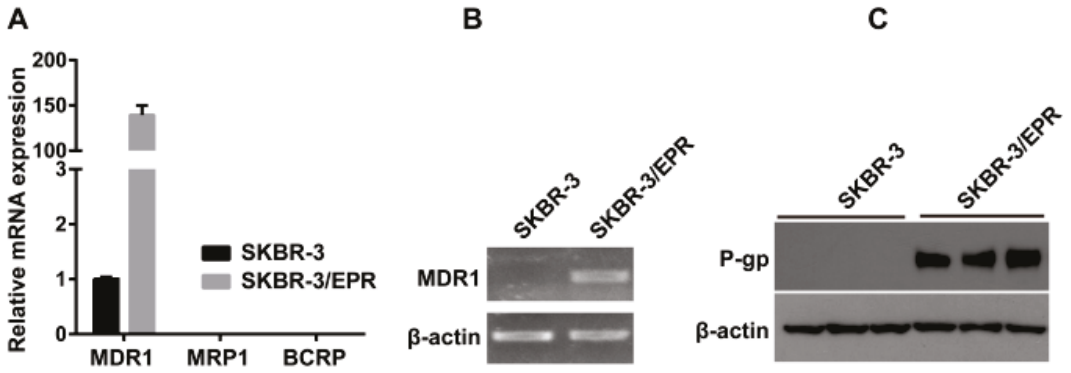

Figure 2. *Cont.*

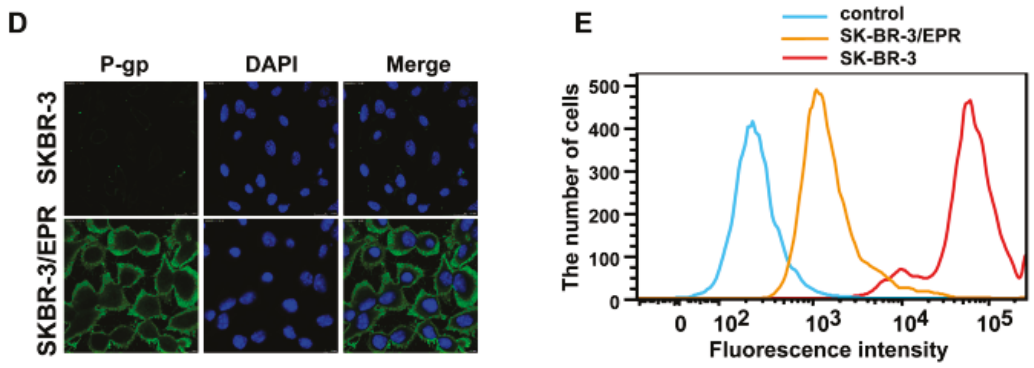

Figure 2. P-glycoprotein is upregulated in SK-BR-3/EPR cells. (**A**) Quantitative PCR analysis of expression of MDR1, MRP1, BCRP mRNA in SK-BR-3 and SK-BR-3 cells. The experiments were performed using three replicates for each group and repeated three times; (**B**) Further analysis of PCR products by agarose gel electrophoresis confirmed the upregulated expression of MDR1 mRNA in SK-BR-3/EPR cells; (**C**) Western blotting analysis of P-glycoprotein expression in SK-BR-3 and SK-BR-3/EPR cells; (**D**) Confocal immunofluorescence microscopy analysis showed positive expression of P-glycoprotein in SK-BR-3/EPR cells, but not in drug sensitive SK-BR-3 cells (×600 magnification); (**E**) SK-BR-3/EPR cells showed markedly reduced retention of intracellular Rh123 compared with SK-BR-3 cells as measured by rhodamine efflux assay.

2.3. SK-BR-3/EPR Cells Maintained the MDR Phenotype after Sequential Passages in Epirubicin-Free Medium for Six Weeks

Long-term persistence of the MDR phenotype in SK-BR-3/EPR cells under drug-free conditions was investigated. The SK-BR-3/EPR cells were cultured in epirubicin-free condition for six consecutive weeks. Then, the cells resistant to epirubicin and paclitaxel were examined. As shown in Figure 3A,B and Table 2, the SK-BR-3/EPR cells displayed evident resistance to the two tested drugs after sequential passages in epirubicin-free medium for six weeks. Western blot and immunofluorescence results showed positive expression of P-glycoprotein in SK-BR-3/EPR cells compared with that in the parent SK-BR-3 cells (Figure 3B,C). Thus, these data suggest that the SK-BR-3/EPR cells could sustain the MDR phenotype in a drug-free condition.

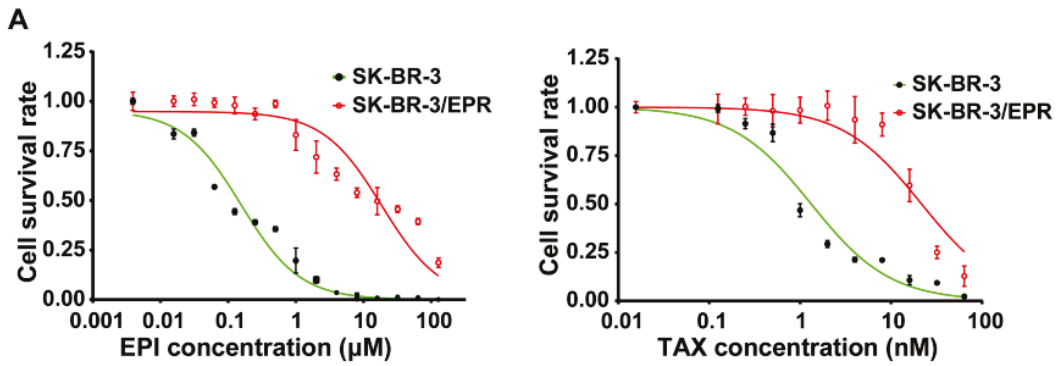

Figure 3. *Cont.*

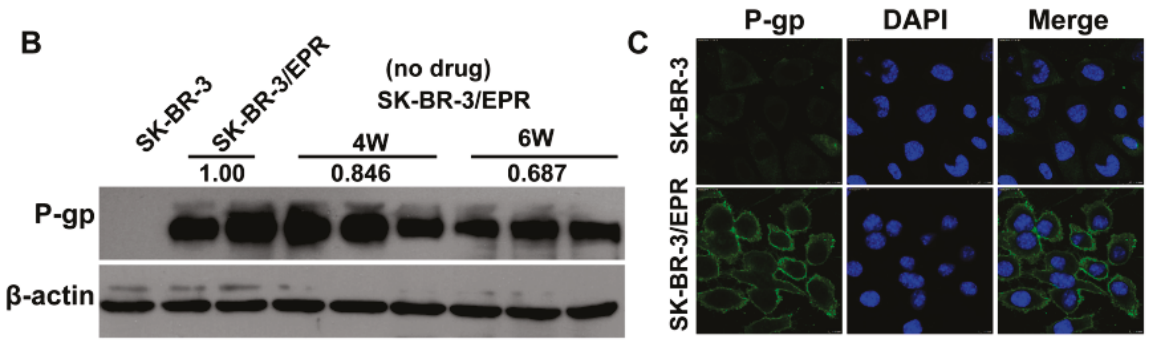

Figure 3. The SK-BR-3/EPR cells maintained MDR phenotype after sequential passages in epirubicin-free medium for six weeks. (**A**) Drug sensitivity assay of SK-BR-3 and SK-BR-3/EPR cells to epirubicin and paclitaxel. The SK-BR-3/EPR cells were cultured in epirubicin-free medium and sequential passages for six-consecutive weeks, then IC_{50} assay was performed by using the CCK-8 based method; (**B**) Western blotting analysis of P-glycoprotein expression (P-gp) in SK-BR-3, SK-BR-3/EPR, and SK-BR-3/EPR cells cultured in drug-free condition for indicated times. The numbers above the blots show the relative values from the densitometric analysis. The levels of P-gp was normalized to β-actin, values are expressed as fold changes compared to SK-BR-3/EPR cells; (**C**) Confocal immunofluorescence microscopy analysis of P-glycoprotein expression in SK-BR-3 and SK-BR-3/EPR cells cultured in epirubicin-free medium for six-consecutive weeks (×600 magnification).

Table 2. IC_{50} values in SK-BR-3 and SK-BR-3/EPR cells after sequential passages in epirubicin-free medium for six weeks.

Drugs	IC_{50} (μM)		*RI*	*p*-Value
	SK-BR-3	SK-BR-3/EPR		
Epirubicin	0.139 ± 0.0151	21.28 ± 2.899	153.1	<0.0001
Paclitaxel	1.416 ± 0.1542	20.87 ± 0.560	14.7	<0.0001

2.4. The SK-BR-3/EPR Cells Displayed a Marked Reduction in Cell Proliferation Rate, and Enhancement in Cell Invasion Ability

The cell proliferative potential of SK-BR-3/EPR and its parent cells was also examined using the CCK-8 based assay. As shown in Figure 4A, SK-BR-3/EPR cells displayed a significantly reduced in cell proliferation ability in the absence or presence of epirubicin. Similarly, SK-BR-3/EPR cells also showed remarkably reduced formation of cell colonies compared with that of drug sensitive SK-BR-3 cells, as measured by colony formation assay (Figure 4B). We then compared the invasive potential between SK-BR-3/EPR and its parental cells using Transwell-based assay. Interestingly, the number of SK-BR-3/EPR cells that invade through the Matrigel-coated membrane was two-fold greater than that of SK-BR-3 cells, thereby indicating the enhanced invasiveness of SK-BR-3/EPR cells (Figure 4C).

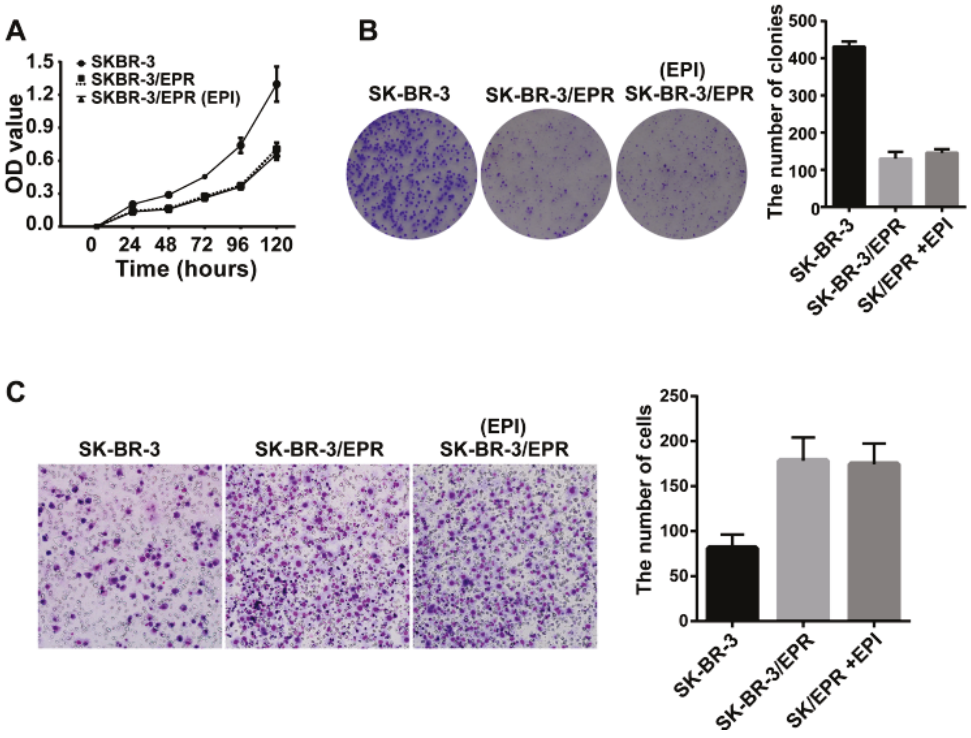

Figure 4. The SK-BR-3/EPR cells exhibited a marked reduction in cell proliferation rate, and enhancement in cell invasion ability. (**A**) The SK-BR-3/EPR cells showed decreased cell proliferation rate in the presence or absence of epirubicin in comparison with that of drug sensitive SK-BR-3 cells; (**B**) The SK-BR-3/EPR cells showed a remarkably reduction in the formation of cell colonies compared with that of in drug sensitive SK-BR-3 cells. Cells were seeded in 35-mm dishes at a density of 500 cells per dish and then cultured for 10–14 days, the number of colonies was counted under an inverted microscope, and only colonies of more than 50 individual cells were counted (×20 magnification). The assays were performed in triplicate for each group and repeated three times; (**C**) The SK-BR-3/EPR cells exhibited enhanced invasive ability compared with that of drug sensitive SK-BR-3 cells. The cells were cultured to 80% confluence, and harvested by trypsinization, then the cell suspension at a density of 4 × 105 cells/mL were added into the matrigel pre-coated transwell insert. The lower insert was filled with 10% FBS-containing medium. After incubation for 24 h at 37 °C, the invaded cells were fixed, stained, and counted. The assay was performed in triplicate and repeated three times (×200 magnification).

2.5. Expression of MMP-2/9 Was Upregulated in SK-BR-3/EPR Cells

Invasion processes require upregulation of proteolytic enzymes, such as MMP-2/9, to degrade extracellular matrix, thereby facilitating the invasion of cancer cells to surrounding tissues [29,37–39]. We then determined the expression levels of MMP-2/9 in these two cells using quantitative PCR and Western blotting methods. As shown in Figure 5A, the expression levels of MMP-2/9 mRNA were significantly upregulated in SK-BR-3/EPR cells than SK-BR-3 cells. Consistently, the protein levels of MMP-2/9 was significantly upregulated in MDR SK-BR-3/EPR cells (Figure 5B).

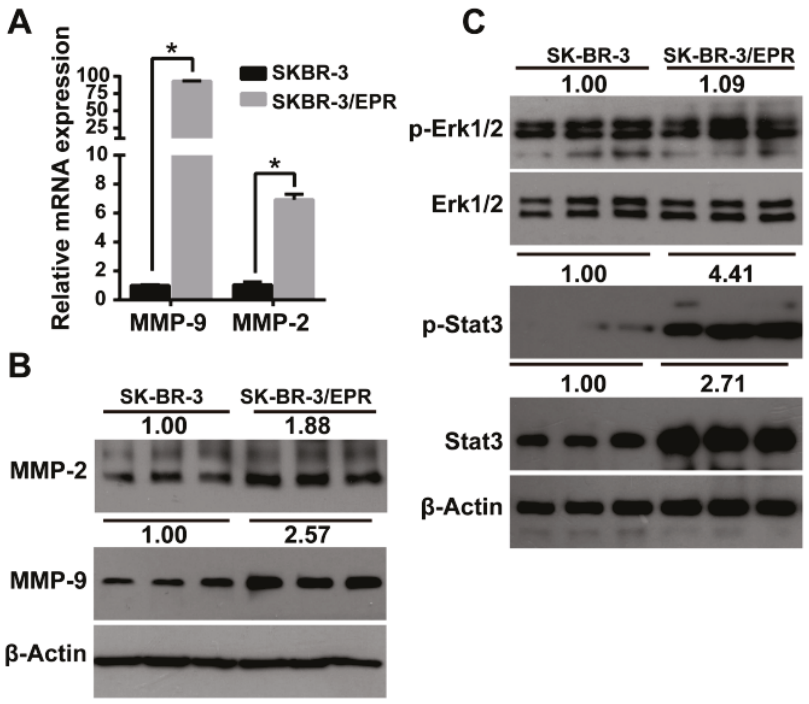

Figure 5. Expression of MMP-2 and -9 as well as phosphorylation of STAT3 was elevated in SK-BR-3/EPR cells. (**A**) Quantitative PCR analysis of expression of MMP-2 and -9 mRNA in SK-BR-3 and SK-BR-3/EPR cells. The experiments were performed using three replicates for each group and repeated three times; (**B**) Western blotting analysis of expression of MMP-2 and -9 protein in SK-BR-3 and SK-BR-3/EPR cells. The numbers above the blots show the relative values from the densitometric analysis. The levels of MMP-2 and -9 were normalized to β-actin, values are expressed as fold changes compared to SK-BR-3 cells; (**C**) Phosphorylation and activation of STAT3 was increased in MDR SK-BR-3/EPR cells. Western blotting analysis of expression of phosphorylation of Erk1/2 and STAT3 in SK-BR-3 and SK-BR-3/EPR cells. SK-BR-3 and SK-BR-3/EPR cells were grown to 90% confluence, then total cellular proteins were extracted and subjected to Western blotting analysis. The numbers above the blots show the relative values from the densitometric analysis. The level of Stat3 was normalized to β-actin, p-Erk1/2 and p-Stat3 were normalized to the corresponding total Erk1/2 and Stat3, values are expressed as fold changes compared to SK-BR-3 cells. * $p < 0.05$.

2.6. Phosphorylation and Activation of STAT3 Was Increased in MDR SK-BR-3/EPR Cells

Previous studies have demonstrated that activation of Erk1/2 and STAT3 signaling is involved in the upregulation of the expression of MMP-2/9 [20,38–40]. Therefore, the expression and phosphorylation of STAT3 and Erk1/2 in the parental and SK-BR-3/EPR cell lines were examined by Western blot analysis. Figure 5C showed that no significant difference of Erk1/2 and its phosphorylation was observed between these two cells. However, phosphorylation of STAT3 was remarkably increased in SK-BR-3/EPR cells compared with its parental SK-BR-3 cells (Figure 5C), which indicated that the activation of STAT3 was increased in SK-BR-3/EPR cells compared with that in the parental cells.

2.7. Knockdown of STAT3 Inhibited Cell Invasion and Downregulated the Expression of MMP-2/9 in SK-BR-3/EPR Cells

To further investigate whether the elevated activation of STAT3 contributes to the enhancement in cell invasiveness of SK-BR-3/EPR cells, STAT3 expression was downregulated using STAT3 specific siRNA. Figure 6A showed that the expression levels of MMP-2/9 was significantly downregulated in STAT3 knockdown cells compared with control cells and non-transfectedSK-BR-3/EPR cells. Then, the effect of STAT3 knockdown on cell invasion ability was analyzed using Transwell-based assay. As shown in Figure 6C, the amount of cells that invaded through the membrane to the lower chamber in STAT3-silenced group was significantly reduced compared with that in the control group. Moreover, the sensitivity to epirubicin in STAT3 silenced cells was also investigated, as shown in Figure 6B and Table 3, the IC_{50} value of epirubicin in STAT3 silenced cells was slightly reduced compared with that of control cells. This phenomenon indicated that activation of STAT3 is partially responsible for elevated drug resistance in SK-BR-3/EPR cells.

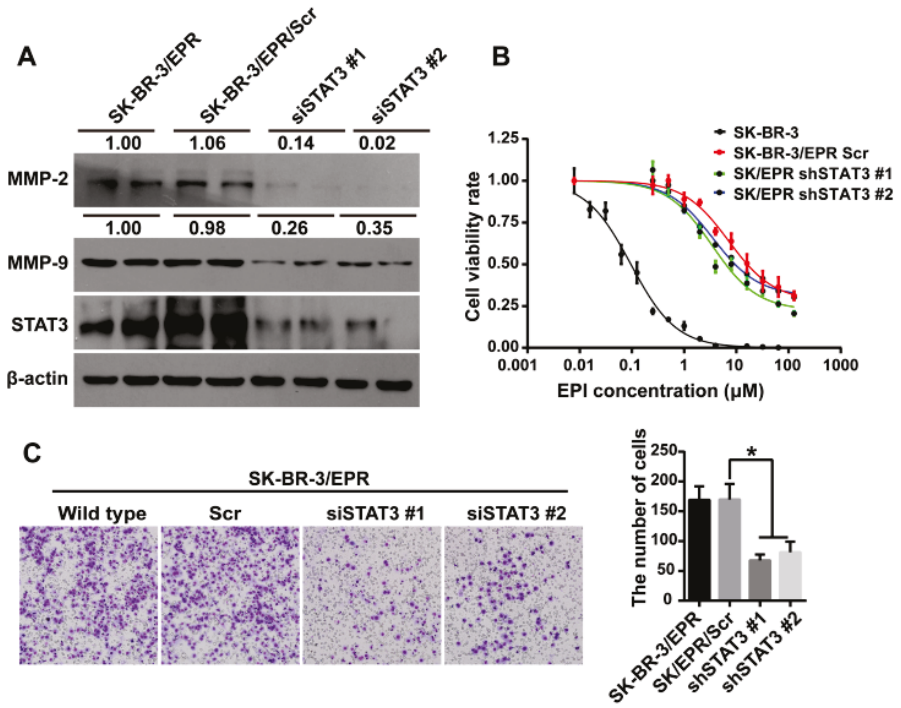

Figure 6. Knockdown of STAT3 inhibited cell invasion and downregulated expression of MMP-2 and -9 in SK-BR-3/EPR cells. (**A**) Knockdown of STAT3 significantly reduced the expression levels of MMP-2 and -9 protein in SK-BR-3/EPR cells. Western blotting analysis of STAT3, MMP-2, and -9 expression in SK-BR-3/EPR cells and SK-BR-3/EPR cells transfected with control or STAT3 specific siRNAs. The numbers above the blots show the relative values from the densitometric analysis. The levels of MMP-2 and -9 were normalized to β-actin, values are expressed as fold changes compared to SK-BR-3/EPR cells; (**B**) Knockdown of STAT3 in SK-BR-3/EPR cells slightly increased the sensitivity to epirubicin in comparison with control cells; (**C**) Knockdown of STAT3 remarkably inhibited the invasive ability of SK-BR-3/EPR cells as measured by transwell based assay (×200 magnification). * $p < 0.05$.

Table 3. IC_{50} of epirubicin in SK-BR-3 and SK-BR-3/EPR cells transfected with control or STAT3 specific siRNAs.

Cell Type	IC_{50} (μM)	*RI*	*p*-Value
SK-BR-3	0.127 ± 0.0289	-	-
SK-BR-3/EPR Scr	19.42 ± 0.0483	152.9	<0.0001
SK-BR-3/EPR shSTAT3 #1	7.913 ± 0.0574	62.3	<0.0001
SK-BR-3/EPR shSTAT3 #2	12.87 ± 0.0605	101.3	<0.0001

3. Discussion

Chemotherapy is the major treatment of most metastatic solid tumors, especially for advanced breast cancer [2–4]. However, resistance to chemotherapeutic drugs greatly impedes effective treatment of this fatal disease [5–8]. Recent advances in anticancer research revealed that acquisition of drug resistance by cancer cells not only leads to treatment failure, but also promotes cancer progression, such as more rapid tumor relapse and enhancement in cancer cell invasion and metastasis [32]. Thus, defining the accurate mechanism involved in the development of drug resistance and associated molecular pathways responsible for cancer progression induced by drug resistance is urgent for anticancer therapy. In the present study, a novel MDR breast cancer cell line was successfully established. Cellular function analysis demonstrated that SK-BR-3/EPR cell line exhibited reduced proliferative activity, but enhanced cell invasiveness. Therefore, this work provides a novel model for studying enhanced invasiveness of MDR cancer cells. Moreover, the expression of MMP-2 and -9 was upregulated in the established SK-BR-3/EPR cell line. The elevated phosphorylation and activation of STAT3 is responsible for the enhanced invasive properties and upregulated expression of MMP-2 and -9 in SK-BR-3/EPR breast cancer cells. Thus, our findings suggest a novel mechanism employed by drug-resistant breast cancer cells to promote cell invasion capacity.

Anthracyclines, such as epirubicin and adriamycin, are major chemotherapeutic agents for breast cancer chemotherapy [8]. However, resistance to these drugs often develops cross resistance of cells to other drugs that the cells have not been exposed to, leads to MDR phenotype [5–8]. Overcoming multidrug resistance is certainly beneficial for cancer treatment to improve the prognosis of cancer patients. However, acquisition of MDR is a very complex process, such that cancer cells can evolve several mechanisms to against different cytotoxic drugs [5–8]. Therefore, further elucidating the molecular process during the acquirement of MDR phenotype is essential. The establishment of drug-resistant cell lines is critical for investigating the mechanisms of MDR and exploring approaches for reversal of resistance. In this study, a stable epirubicin-resistant SK-BR-3 cell line with P-glycoprotein overexpression was successfully established. In addition to epirubicin resistance, the SK-BR-3/EPR cells also exhibited cross resistance to paclitaxel and 5-FU, indicating that this cell line was an MDR cell line. P-glycoprotein is important in mediating drug efflux. Thus, our study provides a new cell line for further exploration of the mechanism of drug resistance induced by P-glycoprotein overexpression. To our knowledge, this paper is the first report of the establishment of epirubicin-resistant SK-BR-3 cell line with MDR phenotype and P-glycoprotein overexpression.

Evolution of chemotherapy resistance of cancer cells has been associated with elevated cell invasiveness *in vitro* [17]. MDR cancer cells also displayed enhanced metastatic potential in animal

models [14,28]. In the clinic, MDR in cancer patients is always correlated with more rapid tumor recurrence and metastasis [21,22,29–32]. However, the mechanism by which drug-resistant cancer cells acquire enhanced invasiveness, in addition to their acquired MDR phenotype, remains poorly understood. Thus, clarifying the mechanism for cancer cell invasiveness induced by drug resistance is urgent for improving cancer treatment. In this study, we found that the mRNA and protein levels of MMP-2/9 was significantly upregulated in SK-BR-3/EPR cells compared with that in the parental SK-BR-3 cells. This result is consistent with findings of previous reports in which MDR cancer cells displayed increased production of MMP-2 or MMP-9 [23,41,42]. MMPs are key proteolytic enzymes for degradation of the extracellular matrix by cancer cells. These results indicated that upregulation of MMP-2/9 may be a mechanism for enhanced cell invasion of SK-BR-3/EPR cells.

The mechanism by which MDR cancer cells upregulate MMPs and promote their invasiveness is very worthy of investigation. The expression of MMP-2/9 is reported to be regulated by Erk1/2 signaling [20,38,39,41,43]. Previous studies have demonstrated that several MDR cancer cells exhibited increased phosphorylation of Erk1/2 compared with drug-sensitive cells [20,41,44,45]. However, in our study, the phosphorylation of Erk1/2 was not significantly altered in SK-BR-3/EPR cells compared with that in drug-sensitive SK-BR-3 cells. Thus, the upregulated expression of MMP-2/9 may not be regulated by Erk1/2 signaling in this cell model. In addition to Erk1/2 signaling, other studies have shown that the expression of MMP-2/9 is also regulated by the STAT3 pathway [38,39,46,47], and activation of STAT3 is also associated with drug resistance of cancer cells [48–50]. Here, we showed that the phosphorylation of STAT3 as well as its nuclear translocation, which indicating the activation of STAT3, was remarkably increased in SK-BR-3/EPR cells. Moreover, we further showed that silencing of STAT3 through siRNA significantly downregulated the protein levels of MMP-2/9. This phenomenon suggested that elevated activation of STAT3 is responsible for the upregulation of MMP-2 and -9 in SK-BR-3/EPR cells. Depletion of STAT3 also inhibited invasiveness of MDR SK-BR-3/EPR cells. Hence, activation of STAT3 signaling is responsible for the enhanced cell invasiveness via upregulation of MMP-2/9 expression.

In summary, an epirubicin-resistant cell line SK-BR-3/EPR with P-glycoprotein overexpression was established in this study. The cell line showed MDR phenotype and decreased cell proliferative activity, but enhanced cell invasiveness. We also showed that the expression of MMP-2/9 was upregulated in SK-BR-3/EPR cells. Moreover, we provided evidence that elevated STAT3 signaling mediates upregulation of MMP-2/9 and confers increased invasiveness in SK-BR-3/EPR breast cancer cells. Thus, our findings augment insight into the mechanism underlying the functional association between MDR and cancer invasiveness.

4. Experimental Section

4.1. Reagents and Drugs

RPMI 1640 medium and Trypsin were obtained from Hyclone (Logan, UT, USA). Fetal bovine serum (FBS) was obtained from Gibco (Carlsbad, CA, USA). Epirubicin was obtained from Hisunpharm Co. (Taizhou, Zhejiang, China). Cell Counting Kit-8 (CCK-8) was purchased from Dojindo Laboratories (Kumamoto, Japan). M-MLV reverse transcriptase and SYBR real-time PCR kit were obtained from Takara (Dalian, China). Trizol reagent and Lipofectamine 2000 was purchased from Invitrogen

(Carlsbad, CA, USA). Transwell inserts were obtained from Millipore (Darmstadt, Germany). Protease inhibitor (EDTA-free) were obtained from Roche Diagnostics (Mannheim, Germany).Rabbit polyclonal antibodies against P-glycoprotein, MRP1 and mouse monoclonal antibodies against β-actin was obtained from Santa Cruz Inc. (Santa Cruz, CA, USA). Rabbit monoclonal antibodies against STAT3, MMP-2, and MMP-9 were purchased from Epitomics (Burlingame, CA, USA). Rabbit monoclonal antibodies against Erk1/2, p-Erk1/2 (Thr202/Tyr204), and p-STAT3 (Tyr 705) were purchased from Cell Signaling Technology (Danvers, MA, USA). Mouse monoclonal antibody against BCRP was purchased from Abcam (Cambridge, UK). Enhanced chemiluminescence reagents (ECL) were purchased from Millipore (Darmstadt, Germany).

4.2. Cell Culture and Induction of Drug Resistance

Human breast cancer cell lines SK-BR-3 were obtained from the American Type Culture Collection (Manassas, Virginia, USA). Cells were cultured in RPMI-1640 culture medium containing 10% FBS in an incubator humidified at 37 °C with 5% CO_2. For induction of drug resistance cell line, SK-BR-3 cells were cultured in 6 cm dishes at a density of approximately 20% confluence. The cells were initially exposed to approximately 25% of IC_{50} doses of epirubicin (0.025 μM). The medium was changed every two days. Survival cells were continuously exposed to 0.025 μM epirubicin until the cells could grow steadily at this drug concentration. Then, the cells were exposed to epirubicin at 1.5- to 2-fold increase from the previous concentration. After 8 months induction, the cells grew stably in the presence of 4.0 μM of epirubicin. Subsequently, the cells were continuously exposed to 4.0 μM of epirubicin for 2 months. The generated resistant cell line was designated as SK-BR-3/EPR (epirubicin resistant). Before experimentation, he SK-BR-3/EPR cells were cultured in drug-free medium for at least 2 weeks.

4.3. IC_{50} Assay

IC_{50} assay was evaluated using CCK-8-based method (according to the manufacturer's instruction). SK-BR-3/EPR cells were cultured in drug-free condition for 2 weeks. Then SK-BR-3/EPR and parental cells were cultured in 96-well plate at a density of 5×10^3 cells per well. After 24 h of incubation, different concentrations of drugs were added into cells and further incubated for 72 h. Cell viability was evaluated at 450 nm on a micro-ELISA reader. IC_{50} is defined as the concentration of drug causing half inhibition of cell growth compared with the cell growth of the control group. Assays were carried out using five replicates for each concentration and repeated thrice. IC_{50} was calculated by the Graphpad Prism 6.00 software (Graphpad Software, La Jolla, CA, USA). The ratio between IC_{50} values of the MDR cancer cells and the sensitive cells was defined as the resistance index (*RI*). *RI* values ≥ 3 indicated chemoresistant cancer cell line.

4.4. Reverse Transcription and Quantitative PCR

Reverse Transcription and Quantitative PCR was carried out as described previously [17]. Briefly, total cellular RNA was extracted using the Trizol reagent, and 1 μg of total RNA was reverse-transcribed to complementary DNA (cDNA) using the M-MLV RT kit. Then the cDNA was used for quantitative real-time PCR analysis using the SYBR Premix Ex Taq according to the manufacturer's protocol. The

PCR Primers are as follows: MDR1 (upper: 5′-TCCTGGAGCGGTTCTACGAC-3′, lower: 5′-ATGGG CTCCTGGGACACGAT-3′), MRP1 (upper: 5′-GGAACTACTGCCTGCGCTAC-3′, lower: 5′-TC TCCTTCGGCAGACTCGTT-3′), BCRP (upper: 5′-AGTACTTCAGCATTCCACGAT-3′, lower: 5′-TCGATGCCCTGCTTTACCAA-3′), β-Actin (upper: 5′-CAGAGCAAGAGAGGCATCC-3′, lower: 5′-CTGGGGTGTTGAAGGTCTC-3′). The assays were conducted using three replicates for each cell line and repeated thrice.

4.5. Western Blotting

Western blotting assay was carried out as described previously [51]. In brief, cells were cultured to 90% confluence in 6 cm dishes, then cells were washed with PBS and total cellular protein was extracted using 400 μL of 1× SDS cell lysis buffer (50 mM Tris, 150 mM NaCl, 2% SDS, 10% glycerol, 5% 2-mercaptoethanol, and 1× protease inhibitor cocktail at pH 6.8). The lysates were quantified, and 20 μg of cell lysates was resolved on SDS-PAGE and transferred onto PVDF membranes. The membrane was blocked with 5% non-fat milk in TBST buffer at room temperature for 1 h, and then probed with corresponding primary antibodies overnight at 4 °C. Followed by incubation with corresponding horseradish peroxidase (HRP)-linked secondary antibody, and then detected using an ECL reagents according to the manufacturer's instructions. β-actin was used as a loading control.

4.6. Immunofluorescence Assay

Immunofluorescence assay was carried out as described previously [52]. Briefly, cells were seeded on glass coverslips at a density of 5×10^4 cells/mL in 12 well plates and incubation for 24 h. Then the cells were washed with PBS, fixed with freshly prepared 4% PFA/PBS at RT for 10 min. After permeabilization in 0.2% triton X-100 for 10 min, the cells were blocked in 3% BSA at RT for 1 h, and probed with the indicated primary antibodies at 4 °C overnight. The cells were then stained with corresponding Alexa Fluor 488 and 594-conjugated secondary antibodies at RT for 1 h, followed by staining nucleus by using 1 ng/mL of DAPI. The coverslips were finally mounted with Mowiol-based anti-fading medium and visualized under a laser scanning confocal microscope (Leica TCS SP5, Leica Microsystems, Wetzlar, Hesse-Darmstadt, Germany).

4.7. Rhodamine 123 (R123) Dye Efflux Assay

R123 efflux assay was carried out as described previously [17]. Briefly, cells were cultured to 90% confluence in 6-cm dishes. The cells were harvested with trypsin, washed twice with PBS, and adjusted to a density of 5×10^5 cells/mL. Then, Rh123 dye was added into the cell suspension to reach final concentration of 2 μg/mL. After incubation for 30 min at 37 °C, cells were washed twice with PBS, resuspended with 500 μL PBS and further incubated in Rh123-free medium for 10 min at 37 °C. After another twice washes with PBS, the mean fluorescence intensity (MFI) was immediately analyzed using flow cytometric analysis. The excitation and emission wavelength is 488 and 530 nm respectively. The assay was carried out in triplicate and repeated thrice.

4.8. Cell Proliferation Assay/Colony Formation Assay

Cell proliferative activity was evaluated using CCK-8 and colony formation assay. For CCK-8 assay, cells were cultured in 96-well plate at a concentration of 2×10^3 cells per well and incubated for 24, 48, 72, 96, and 120 h. At each time point, each well was added with 10 μL of CCK-8 reagent, and further incubated for 3 h at 37 °C. The cell proliferative activity was calculated by a micro-ELISA reader using a filter for 450 nm. The assays were carried out using five replicates for each time group and repeated thrice. Colony formation assay was carried out as described previously [53]. In brief, 500 cells were seeded in 35-mm dishes and cultured for 10–14 days. After washing thrice with PBS, the cells were fixed with ice-cold methanol at 4 °C, and stained using a three-Step Stain Set kit (Thermo Scientific, Kalamazoo, MI, USA). The colonies containing more than 50 individual cells was counted. The assay was carried out in triplicate.

4.9. Cell Invasion Assay

Cell invasion ability was evaluated using a transwell-based assay as described previously [17]. Briefly, exponentially growing cells were harvested by trypsin digestion, washed thrice with PBS, resuspended in FBS-free medium and adjusted to a density of 4×10^5 cells/mL. Then, 200 μL of cells (8×10^4 cells) were added into the transwell insert (8 μm pore), which were pre-coated with matrigel. The lower insert was filled with 10% FBS-containing medium. After subsequent incubation for 24 h at 37 °C, the invaded cells were fixed with ice-cold ethanol, and stained using a three-Step Stain Set kit. The numbers of invaded cells were calculated under a light microscope. The experiment was carried out in triplicate and repeated thrice.

4.10. Statistical Analysis

All quantitative data were expressed as mean ± SD. Statistical analysis was conducted by one-way ANOVA using the Graphpad Prim 6.00 software. A p value less than 0.05 (two-tailed) was considered as significant. The asterisk indicates a p value <0.05.

5. Conclusions

An MDR breast cancer cell line SK-BR-3/EPR with P-glycoprotein overexpression was established in this study. SK-BR-3/EPR cells exhibited enhanced cell invasiveness and upregulation of MMP-2/9. Moreover, we showed that elevated STAT3 signaling-mediated upregulation of MMP-2/9 is responsible for the enhanced invasive properties in SK-BR-3/EPR breast cancer cells.

Acknowledgments

This research was supported by grants from the National Natural Science Foundation of China (Nos. 81372844 and 81472474), Tianjin Municipal Science and Technology Commission (Nos. 12JCZDJC24500 and 12JCQNJC07000), Changjiang Scholars and Innovative Research Team (IRT_14R40), 863 Project (2012AA020206-5), Specialized Research Fund for the Doctoral Program of Higher Education (20131202110002).

Author Contributions

Fei Zhang and Ruifang Niu designed the study and wrote the manuscript; Fei Zhang, Zhiyong Wang, Yanling Fan, Qiao Xu, Wei Ji and Ran Tian performed the experiments.

Conflicts of Interest

The authors declare no conflict of interest.

References

1. Jemal, A.; Bray, F.; Center, M.M.; Ferlay, J.; Ward, E.; Forman, D. Global cancer statistics. *CA Cancer J. Clin.* **2011**, *61*, 69–90.
2. Chabner, B.A.; Roberts, T.G. Timeline: Chemotherapy and the war on cancer. *Nat. Rev. Cancer* **2005**, *5*, 65–72.
3. Munzone, E.; Colleoni, M. Clinical overview of metronomic chemotherapy in breast cancer. *Nat. Rev. Clin. Oncol.* **2015**, *131*, doi:10.1038/nrclinonc.2015.131.
4. Hart, C.D.; Migliaccio, I.; Malorni, L.; Guarducci, C.; Biganzoli, L.; di Leo, A. Challenges in the management of advanced, ER-positive, HER2-negative breast cancer. *Nat. Rev. Clin. Oncol.* **2015**, *12*, 541–552.
5. Wu, Q.; Yang, Z.; Nie, Y.; Shi, Y.; Fan, D. Multi-drug resistance in cancer chemotherapeutics: Mechanisms and lab approaches. *Cancer Lett.* **2014**, *347*, 159–166.
6. Wu, C.P.; Hsieh, C.H.; Wu, Y.S. The emergence of drug transporter-mediated multidrug resistance to cancer chemotherapy. *Mol. Pharm.* **2011**, *8*, 1996–2011.
7. Housman, G.; Byler, S.; Heerboth, S.; Lapinska, K.; Longacre, M.; Snyder, N.; Sarkar, S. Drug resistance in cancer: An overview. *Cancers* **2014**, *6*, 1769–1792.
8. Choi, Y.H.; Yu, A.M. ABC transporters in multidrug resistance and pharmacokinetics, and strategies for drug development. *Curr. Pharm. Des.* **2014**, *20*, 793–807.
9. Abedini, M.R.; Muller, E.J.; Bergeron, R.; Gray, D.A.; Tsang, B.K. Akt promotes chemoresistance in human ovarian cancer cells by modulating cisplatin-induced, p53-dependent ubiquitination of FLICE-like inhibitory protein. *Oncogene* **2010**, *29*, 11–25.
10. Li, Q.Q.; Xu, J.D.; Wang, W.J.; Cao, X.X.; Chen, Q.; Tang, F.; Chen, Z.Q.; Liu, X.P.; Xu, Z.D. Twist1-mediated adriamycin-induced epithelial-mesenchymal transition relates to multidrug resistance and invasive potential in breast cancer cells. *Clin. Cancer Res.* **2009**, *15*, 2657–2665.
11. Hui, R.C.; Francis, R.E.; Guest, S.K.; Costa, J.R.; Gomes, A.R.; Myatt, S.S.; Brosens, J.J.; Lam, E.W. Doxorubicin activates FOXO3a to induce the expression of multidrug resistance gene *ABCB1* (*MDR1*) in K562 leukemic cells. *Mol. Cancer Ther.* **2008**, *7*, 670–678.
12. Wattanawongdon, W.; Hahnvajanawong, C.; Namwat, N.; Kanchanawat, S.; Boonmars, T.; Jearanaikoon, P.; Leelayuwat, C.; Techasen, A.; Seubwai, W. Establishment and characterization of gemcitabine-resistant human cholangiocarcinoma cell lines with multidrug resistance and enhanced invasiveness. *Int. J. Oncol.* **2015**, *47*, 398–410.

13. Iseri, O.D.; Kars, M.D.; Arpaci, F.; Atalay, C.; Pak, I.; Gunduz, U. Drug resistant MCF-7 cells exhibit epithelial-mesenchymal transition gene expression pattern. *Biomed. Pharmacother.* **2011**, *65*, 40–45.
14. Kajiyama, H.; Shibata, K.; Terauchi, M.; Yamashita, M.; Ino, K.; Nawa, A.; Kikkawa, F. Chemoresistance to paclitaxel induces epithelial-mesenchymal transition and enhances metastatic potential for epithelial ovarian carcinoma cells. *Int. J. Oncol.* **2007**, *31*, 277–283.
15. Kotchetkov, R.; Cinatl, J.; Blaheta, R.; Vogel, J.U.; Karaskova, J.; Squire, J.; Hernaiz Driever, P.; Klingebiel, T.; Cinatl, J., Jr. Development of resistance to vincristine and doxorubicin in neuroblastoma alters malignant properties and induces additional karyotype changes: A preclinical model. *Int. J. Cancer* **2003**, *104*, 36–43.
16. Liang, Y.; Meleady, P.; Cleary, I.; McDonnell, S.; Connolly, L.; Clynes, M. Selection with melphalan or paclitaxel (taxol) yields variants with different patterns of multidrug resistance, integrin expression and *in vitro* invasiveness. *Eur. J. Cancer* **2001**, *37*, 1041–1052.
17. Zhang, F.; Zhang, H.; Wang, Z.; Yu, M.; Tian, R.; Ji, W.; Yang, Y.; Niu, R. P-glycoprotein associates with Anxa2 and promotes invasion in multidrug resistant breast cancer cells. *Biochem. Pharmacol.* **2014**, *87*, 292–302.
18. Galski, H.; Oved-Gelber, T.; Simanovsky, M.; Lazarovici, P.; Gottesman, M.M.; Nagler, A. P-glycoprotein-dependent resistance of cancer cells toward the extrinsic trail apoptosis signaling pathway. *Biochem. Pharmacol.* **2013**, *86*, 584–596.
19. Rocco, A.; Compare, D.; Liguori, E.; Cianflone, A.; Pirozzi, G.; Tirino, V.; Bertoni, A.; Santoriello, M.; Garbi, C.; D'Armiento, M.; *et al.* MDR1-P-glycoprotein behaves as an oncofetal protein that promotes cell survival in gastric cancer cells. *Lab. Investig.* **2012**, *92*, 1407–1418.
20. Karroum, A.; Mirshahi, P.; Benabbou, N.; Faussat, A.M.; Soria, J.; Therwath, A.; Mirshahi, M.; Hatmi, M. Matrix metalloproteinase-9 is required for tubular network formation and migration of resistant breast cancer cells MCF-7 through PKC and ERK1/2 signalling pathways. *Cancer Lett.* **2010**, *295*, 242–251.
21. Hao, J.; Chen, H.; Madigan, M.C.; Cozzi, P.J.; Beretov, J.; Xiao, W.; Delprado, W.J.; Russell, P.J.; Li, Y. Co-expression of CD147 (emmprin), CD44v3–10, MDR1 and monocarboxylate transporters is associated with prostate cancer drug resistance and progression. *Br. J. Cancer* **2010**, *103*, 1008–1018.
22. Chen, H.; Hao, J.; Wang, L.; Li, Y. Coexpression of invasive markers (UPA, CD44) and multiple drug-resistance proteins (MDR1, MRP2) is correlated with epithelial ovarian cancer progression. *Br. J. Cancer* **2009**, *101*, 432–440.
23. Li, Q.Q.; Wang, W.J.; Xu, J.D.; Cao, X.X.; Chen, Q.; Yang, J.M.; Xu, Z.D. Up-regulation of CD147 and matrix metalloproteinase-2, -9 induced by P-glycoprotein substrates in multidrug resistant breast cancer cells. *Cancer Sci.* **2007**, *98*, 1767–1774.
24. Mallini, P.; Lennard, T.; Kirby, J.; Meeson, A. Epithelial-to-mesenchymal transition: What is the impact on breast cancer stem cells and drug resistance. *Cancer Treat. Rev.* **2014**, *40*, 341–348.
25. Byers, L.A.; Diao, L.; Wang, J.; Saintigny, P.; Girard, L.; Peyton, M.; Shen, L.; Fan, Y.; Giri, U.; Tumula, P.K.; *et al.* An epithelial-mesenchymal transition gene signature predicts resistance to EGFR and PI3k inhibitors and identifies Axl as a therapeutic target for overcoming EGFR inhibitor resistance. *Clin. Cancer Res.* **2013**, *19*, 279–290.

26. Su, Y.C.; Lin, Y.H.; Zeng, Z.M.; Shao, K.N.; Chueh, P.J. Chemotherapeutic agents enhance cell migration and epithelial-to-mesenchymal transition through transient up-regulation of tNOX (ENOX2) protein. *Biochim. Biophys. Acta* **2012**, *1820*, 1744–1752.
27. Yang, A.D.; Fan, F.; Camp, E.R.; van Buren, G.; Liu, W.; Somcio, R.; Gray, M.J.; Cheng, H.; Hoff, P.M.; Ellis, L.M. Chronic oxaliplatin resistance induces epithelial-to-mesenchymal transition in colorectal cancer cell lines. *Clin. Cancer Res.* **2006**, *12*, 4147–4153.
28. Lopes, E.C.; Ernst, G.; Aulicino, P.; Vanzulli, S.; Garcia, M.; Alvarez, E.; Hajos, S.E. Dissimilar invasive and metastatic behavior of vincristine and doxorubicin-resistant cell lines derived from a murine T cell lymphoid leukemia. *Clin. Exp. Metastasis* **2002**, *19*, 283–290.
29. Lu, L.S.; Chen, L.; Ding, W.X.; Li, K.; Wu, J.J. Elevated expression of both *MDR1* and *MMP-2* genes in metastasized lymph node of invasive ductal breast cancer. *Eur. Rev. Med. Pharmacol. Sci.* **2012**, *16*, 2037–2043.
30. Matsuo, K.; Eno, M.L.; Ahn, E.H.; Shahzad, M.M.; Im, D.D.; Rosenshein, N.B.; Sood, A.K. Multidrug resistance gene (MDR-1) and risk of brain metastasis in epithelial ovarian, fallopian tube, and peritoneal cancer. *Am. J. Clin. Oncol.* **2011**, *34*, 488–493.
31. Hoffmann, A.C.; Wild, P.; Leicht, C.; Bertz, S.; Danenberg, K.D.; Danenberg, P.V.; Stohr, R.; Stockle, M.; Lehmann, J.; Schuler, M.; *et al.* MDR1 and ERCC1 expression predict outcome of patients with locally advanced bladder cancer receiving adjuvant chemotherapy. *Neoplasia* **2010**, *12*, 628–636.
32. Fletcher, J.I.; Haber, M.; Henderson, M.J.; Norris, M.D. ABC transporters in cancer: More than just drug efflux pumps. *Nat. Rev. Cancer* **2010**, *10*, 147–156.
33. Xu, J.W.; Li, Q.Q.; Tao, L.L.; Cheng, Y.Y.; Yu, J.; Chen, Q.; Liu, X.P.; Xu, Z.D. Involvement of EGFR in the promotion of malignant properties in multidrug resistant breast cancer cells. *Int. J. Oncol.* **2011**, *39*, 1501–1509.
34. Li, L.; Jiang, A.C.; Dong, P.; Wang, H.; Xu, W.; Xu, C. MDR1/*P*-gp and VEGF synergistically enhance the invasion of HEP-2 cells with multidrug resistance induced by taxol. *Ann. Surg. Oncol.* **2009**, *16*, 1421–1428.
35. Cheng, G.Z.; Chan, J.; Wang, Q.; Zhang, W.; Sun, C.D.; Wang, L.H. Twist transcriptionally up-regulates Akt2 in breast cancer cells leading to increased migration, invasion, and resistance to paclitaxel. *Cancer Res.* **2007**, *67*, 1979–1987.
36. Miletti-Gonzalez, K.E.; Chen, S.; Muthukumaran, N.; Saglimbeni, G.N.; Wu, X.; Yang, J.; Apolito, K.; Shih, W.J.; Hait, W.N.; Rodriguez-Rodriguez, L. The CD44 receptor interacts with *P*-glycoprotein to promote cell migration and invasion in cancer. *Cancer Res.* **2005**, *65*, 6660–6667.
37. Chakraborti, S.; Mandal, M.; Das, S.; Mandal, A.; Chakraborti, T. Regulation of matrix metalloproteinases: An overview. *Mol. Cell. Biochem.* **2003**, *253*, 269–285.
38. Xie, T.X.; Wei, D.; Liu, M.; Gao, A.C.; Ali-Osman, F.; Sawaya, R.; Huang, S. STAT3 activation regulates the expression of matrix metalloproteinase-2 and tumor invasion and metastasis. *Oncogene* **2004**, *23*, 3550–3560.
39. Dechow, T.N.; Pedranzini, L.; Leitch, A.; Leslie, K.; Gerald, W.L.; Linkov, I.; Bromberg, J.F. Requirement of matrix metalloproteinase-9 for the transformation of human mammary epithelial cells by Stat3-C. *Proc. Natl. Acad. Sci. USA* **2004**, *101*, 10602–10607.

40. Litherland, G.J.; Elias, M.S.; Hui, W.; Macdonald, C.D.; Catterall, J.B.; Barter, M.J.; Farren, M.J.; Jefferson, M.; Rowan, A.D. Protein kinase C isoforms zeta and iota mediate collagenase expression and cartilage destruction via STAT3- and ERK-dependent c-*fos* induction. *J. Biol. Chem.* **2010**, *285*, 22414–22425.
41. Colone, M.; Calcabrini, A.; Toccacieli, L.; Bozzuto, G.; Stringaro, A.; Gentile, M.; Cianfriglia, M.; Ciervo, A.; Caraglia, M.; Budillon, A.; *et al.* The multidrug transporter P-glycoprotein: A mediator of melanoma invasion? *J. Investig. Dermatol.* **2008**, *128*, 957–971.
42. Liang, Y.; O'Driscoll, L.; McDonnell, S.; Doolan, P.; Oglesby, I.; Duffy, K.; O'Connor, R.; Clynes, M. Enhanced *in vitro* invasiveness and drug resistance with altered gene expression patterns in a human lung carcinoma cell line after pulse selection with anticancer drugs. *Int. J. Cancer* **2004**, *111*, 484–493.
43. Kim, S.; Choi, J.H.; Lim, H.I.; Lee, S.K.; Kim, W.W.; Cho, S.; Kim, J.S.; Kim, J.H.; Choe, J.H.; Nam, S.J.; *et al.* EGF-induced MMP-9 expression is mediated by the JAK3/ERK pathway, but not by the JAK3/STAT-3 pathway in a SKBR3 breast cancer cell line. *Cell Signal.* **2009**, *21*, 892–898.
44. Chung, L.Y.; Tang, S.J.; Sun, G.H.; Chou, T.Y.; Yeh, T.S.; Yu, S.L.; Sun, K.H. Galectin-1 promotes lung cancer progression and chemoresistance by upregulating p38 MAPK, ERK, and cyclooxygenase-2. *Clin. Cancer Res.* **2012**, *18*, 4037–4047.
45. Li, Q.Q.; Wang, W.J.; Xu, J.D.; Cao, X.X.; Chen, Q.; Yang, J.M.; Xu, Z.D. Involvement of CD147 in regulation of multidrug resistance to P-gp substrate drugs and *in vitro* invasion in breast cancer cells. *Cancer Sci.* **2007**, *98*, 1064–1069.
46. Yu, H.; Lee, H.; Herrmann, A.; Buettner, R.; Jove, R. Revisiting STAT3 signalling in cancer: New and unexpected biological functions. *Nat. Rev. Cancer* **2014**, *14*, 736–746.
47. Xie, T.X.; Huang, F.J.; Aldape, K.D.; Kang, S.H.; Liu, M.; Gershenwald, J.E.; Xie, K.; Sawaya, R.; Huang, S. Activation of STAT3 in human melanoma promotes brain metastasis. *Cancer Res.* **2006**, *66*, 3188–3196.
48. Ara, T.; Nakata, R.; Sheard, M.A.; Shimada, H.; Buettner, R.; Groshen, S.G.; Ji, L.; Yu, H.; Jove, R.; Seeger, R.C.; *et al.* Critical role of STAT3 in IL-6-mediated drug resistance in human neuroblastoma. *Cancer Res.* **2013**, *73*, 3852–3864.
49. Zhu, H.; Chen, X.; Chen, B.; Chen, B.; Fan, J.; Song, W.; Xie, Z.; Jiang, D.; Li, Q.; Zhou, M.; *et al.* Activating transcription factor 4 mediates a multidrug resistance phenotype of esophageal squamous cell carcinoma cells through transactivation of STAT3 expression. *Cancer Lett.* **2014**, *354*, 142–152.
50. Huang, S.; Chen, M.; Shen, Y.; Shen, W.; Guo, H.; Gao, Q.; Zou, X. Inhibition of activated STAT3 reverses drug resistance to chemotherapeutic agents in gastric cancer cells. *Cancer Lett.* **2012**, *315*, 198–205.
51. Zhang, F.; Liu, Y.; Wang, Z.; Sun, X.; Yuan, J.; Wang, T.; Tian, R.; Ji, W.; Yu, M.; Zhao, Y.; *et al.* A novel Anxa2-interacting protein Ebp1 inhibits cancer proliferation and invasion by suppressing Anxa2 protein level. *Mol. Cell. Endocrinol.* **2015**, *411*, 75–85.

52. Wang, T.; Yuan, J.; Zhang, J.; Tian, R.; Ji, W.; Zhou, Y.; Yang, Y.; Song, W.; Zhang, F.; Niu, R. Anxa2 binds to STAT3 and promotes epithelial to mesenchymal transition in breast cancer cells. *Oncotarget* **2015**, *6*, 30975–30992.
53. Zhang, F.; Wang, Z.; Yuan, J.; Wei, X.; Tian, R.; Niu, R. RNAi-mediated silencing of Anxa2 inhibits breast cancer cell proliferation by downregulating cyclin D1 in STAT3-dependent pathway. *Breast Cancer Res. Treat.* **2015**, *153*, 263–275.

© 2015 by the authors; licensee MDPI, Basel, Switzerland. This article is an open access article distributed under the terms and conditions of the Creative Commons Attribution license (http://creativecommons.org/licenses/by/4.0/).

International Journal of
Molecular Sciences

MDPI

Review

The Role of Autophagy in Hepatocellular Carcinoma

Yoo Jin Lee and Byoung Kuk Jang *

Received: 21 September 2015 ; Accepted: 30 October 2015 ; Published: 6 November 2015
Academic Editor: William Chi-shing Cho

Division of Gastroenterology and Hepatology, Department of Internal Medicine,
Keimyung University School of Medicine, Daegu 700-712, Korea; doctorlyj@naver.com
* Correspondence: jangha106@dsmc.or.kr; Tel.: +82-53-250-7088; Fax: +82-53-250-7442

Abstract: Autophagy is a catabolic process involved in cellular homeostasis under basal and stressed conditions. Autophagy is crucial for normal liver physiology and the pathogenesis of liver diseases. During the last decade, the function of autophagy in hepatocellular carcinoma (HCC) has been evaluated extensively. Currently, autophagy is thought to play a dual role in HCC, *i.e.*, autophagy is involved in tumorigenesis and tumor suppression. Recent investigations of autophagy have suggested that autophagy biomarkers can facilitate HCC prognosis and the establishment of therapeutic approaches. In this review, we briefly summarize the current understanding of autophagy and discuss recent evidence for its role in HCC.

Keywords: hepatocellular carcinoma; autophagy; tumorigenesis; tumor suppression; prognosis; therapy

1. Introduction

Autophagy is a catabolic process with crucial roles in development, differentiation, homeostasis, and the survival of cells in nutrient-deprived conditions [1,2]. There have been three major modes of autophagy: macroautophagy, microautophagy, and chaperone-mediated autophagy [3,4]. Macroautophagy is usually referred to as "autophagy" owing to the limited data for the other forms [4]. Upon induction, the isolated membrane or phagophore wraps around portions of the cytoplasm to form a double-membraned vesicle known as an autophagosome [1]. Autophagosomes which subsequently fuse with lysosomes are degraded by lysosomal proteases during maturation [5]. In addition to preserve intracellular metabolic homeostasis, autophagy is induced in response to starvation, protein aggregation, and other forms of stress such as oxidative and endoplasmic reticulum (ER) stress [6,7].

Abundant evidence has revealed that autophagy is involved in the pathogenesis of various diseases, such as neurodegenerative diseases, infectious diseases, metabolic diseases, and cancers [4,8–11]. Increasing studies have indicated the crucial role of autophagy in liver diseases. The dysregulation of autophagy is associated with viral hepatitis, non-alcoholic fatty liver disease, alcoholic liver disease, fibrosis, cirrhosis, and hepatocellular carcinoma (HCC) [1,12]. Recently, many investigators have suggested that tumor cells rely on autophagy for survival in HCC, although it is still controversial whether autophagy serves as an anti-cancer or pro-cancer mechanism [13,14].

Although there are several treatment options for HCC, the effectiveness of most curative treatments is limited to the early stage of HCC [15]. Currently, there is no effective treatment for patients showing advanced- or intermediate-stage HCC [16]. Furthermore, dysregulation of apoptosis has been observed, which is associated with resistance to HCC treatment [17,18]. Thus, autophagy-related markers, including microtubule-associated protein 1 light chain 3 (LC3) and beclin-1, are potential prognostic factors for HCC [19,20]. In recent studies, autophagy-based therapies, such as hydroxychloroquine (HCQ) or chloroquine (CQ), have also been examined in mice

xenograft models [21,22]. These autophagy-modulating compounds have potential applications in the treatment of HCC in the near future. In this review, we provide a brief overview of autophagy and HCC, with focusing on: (1) the current understanding of autophagy pathways; (2) autophagy function in HCC; and (3) prognostic and therapeutic clinical applications in HCC.

2. Autophagy

Autophagy is a highly conserved process consisting of sequential stages: initiation, elongation, autophagosome formation, and autophagosome fusion with lysosomes then degradation [23]. These steps are regulated by autophagy-related genes (Atgs). To date, more than 30 Atgs have been identified and their functions have been evaluated extensively. In particular, experiments using specific Atg-deletion models in the liver provide evidence of the critical roles of autophagy in adaptive responses to starvation and various forms of stress, homeostasis, and cellular differentiation and development [24–28]. The details of the autophagy process are presented below. (i) The initiation stage is regulated by the adenosine monophosphate-activated protein kinase (AMPK), UNC51-like kinase 1 (ULK1) and mammalian target of rapamycin complex 1 (mTORC1) complexes. mTORC1 is the main inhibitor of autophagosome formation by ULK1. Under nutrient starvation such as glucose, the activated AMPK inhibits mTORC1, then directly phosphorylates ULK1, and leads to autophagy initiation [29,30]; (ii) Nucleation of the phagophore is mediated by the Beclin-1-class III phosphatidylinositol 3-kinase (PI3K) complex that includes Beclin-1, Vps34 (class II PI3K), p150 (homolog of Vps15), Atg14L/Barkor, and Ambra-1 [4]; (iii) Elongation of the phagophore into a complete autophagosome is regulated by two ubiquitin-like protein conjugated complexes: Atg5-Atg12-Atg16L1 and LC3-II. Several Atgs, such as E1-like protein, Atg7, E2-like protein, and Atg 10, are necessary mediators of these processes [31–33]. LC3 is the major mammalian ortholog of Atg8. LC3-1 is converted to LC3-II and degraded after autophagosomes fuse with lysosomes [34]. Thus, LC3-II is considered an autophagosome marker [10]. Microautophagy can engulf cargo nonselectively (through random sequenstation) or selectively (by individual targeting of each cargo molecule) [35]; (iv) The final stage is autophagic degradation. As there are many excellent reviews regarding the autophagy process, reading those reviews will be helpful for further understanding of the autophagic pathway [36,37].

3. The Role of Autophagy in the Liver

Several selective modes of autophagy, mitophagy [38,39] and lipophagy [25], were first suggested based on experiments with cultured hepatocytes and whole livers. Since then, considerable data related to the role of autophagy in the liver has accumulated. Autophagy is involved in diverse liver physiology and pathophysiology, e.g., clearing misfolded proteins, nutrient and energy metabolism in hepatocytes, regulating selective organelle degradation, lipid and alcohol metabolism, and hepatitis virus infection [40].

The liver highly relies on the autophagy for its physiology and pathology. In particular, lysosome-mediated degradation is crucial in both normal physiological conditions and in stress responses, such as in proteotoxicity, metabolic dysregulation, infection, and carcinogenesis [35]. Therefore, the dysfunction of autophagy is associated with various liver diseases, suggesting that the regulation of this process is a potential therapeutic approach [40].

Viral infections, such as chronic hepatitis B or C infections, and alcohol abuse are frequent etiologic factors of HCC [16]. In these conditions, multiple steps are involved in the development of HCC: liver cell death, inflammation, liver cell proliferation, liver fibrosis, and finally HCC development [41]. Non-alcoholic fatty liver disease, diabetes, ingestion of aflatoxin B1, chronic alcohol abuse, obesity, and genetic disorders also can be risk factors of HCC [42]. Autophagy is deeply involved in both the above mentioned etiologic factors and HCC itself. In mice models of obesity, the suppressed hepatic autophagy such as Atg is causal to impaired hepatic sensitivity and

glucose homeostasis [43]. The details regarding the mechanisms of autophagy in the liver are well reviewed elsewhere [1,37,40,44].

4. Dual Role of Autophagy in Hepatocellular Carcinoma

Although the mechanism of autophagy has been extensively investigated, the actual functions of autophagy in HCC are still largely unknown. The dual role of autophagy in the development and promotion of HCC has been suggested as a model for the autophagy in HCC, *i.e.*, it is involved in tumorigenesis and tumor suppression (Figure 1).

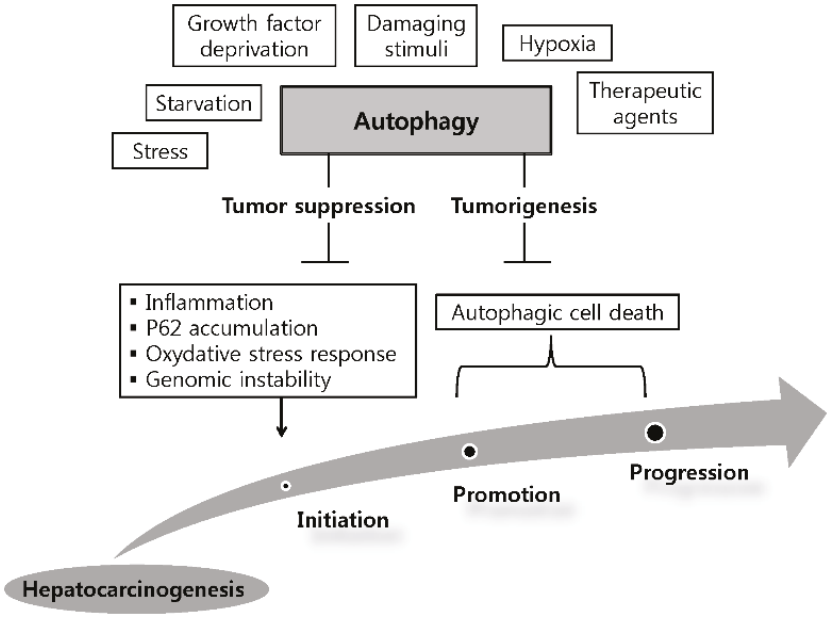

Figure 1. Dual role of autophagy in the initiation and development of hepatocellular carcinoma. Hepatic autophagy is activated by various factors. By limiting inflammation, P62 accumulation, oxidative stress response and consequently inhibiting genomic instability, autophagy can serve as a tumor suppressor in the initiation stage of hepatoneogenesis. On the other hand, autophagy can facilitates tumorigenesis via autophagic cell death in other stages of hepatoneogenesis.

Early studies have demonstrated a tumor suppressive function of autophagy, while more recent studies have revealed a tumorigenesis function [35]. In normal cells, autophagy inhibits tumorigenesis by removing damaged organelles and aggregated proteins. By contrast, in tumor cells, autophagy serves the survival of tumor cells via the following mechanisms: (1) promotion of metabolite turnover and absorption in tumor cells; (2) inhibition of apoptosis and reactive oxygen species production; and (3) increasing drug resistance [45]. Abundant evidence supports these two functions of autophagy in HCC carcinogenesis. Understanding the involvement of autophagy in HCC is crucial because it may facilitate the development of future therapeutic approaches to HCC.

4.1. Tumor Suppressive Function of Autophagy

One of the earliest and representative results supporting the tumor suppressive role of autophagy was related to Beclin-1-knockout mice. Mice with homozygous knockout of Becliln-1 have markedly reduced autophagic activity and a highly prevalent cancer such as HCC [46]. Similarly, other study has shown that the mice model of Beclin-1 heterozygous disruption leads to increased frequency of malignancies and promotes the development of premalignant lesions. Additionally, heterozygous disruption of Beclin-1 leads to increased cellular proliferation and reduced autophagy [47].

Particularly convincing evidence for the tumor-suppressive role of autophagy is the development of multiple liver adenomas in mice with a deletion of Atg5 and Atg7 [28]. Notably, Atg5 mosaic knockouts develop tumors only in the liver, but not in other tissues, suggesting that hepatocytes have a dependence on the tumor-suppressive role of autophagy [28]. Atg5 and Atg7 constitute two ubiquitin-like conjugation systems, which are required for the formation of autophagosome [26]. It is noteworthy that Beclin-1- and Atg5/7-knockout mice have different phenotypes. For example, Atg5- and Atg7-knockout mice survive until birth [26,48]; however, Beclin-1-knockout mice die during early embryonic development [46]. These data indicate that Beclin-1 might have other complex functions in addition to autophagy.

The stress-inducible intracellular protein p62 targets the autophagosome formation site on ER [49]. It directly interacts with LC3, and is merged to the autophagosome and degraded by autophagy [50]. It is involved in multiple cellular functions, including tumorigenesis [51]. Some studies have shown that accumulated p62 via an autophagy deficiency results in tumor development and progression. Autophagy-defective tumor cells accumulate p62 in response to stress, contributing to hepatocarcinogenesis via NF-kB regulation and gene expression. Suppressing p62 accumulation prevents defective autophagy-related damage, suggesting that a failure to regulate p62 causes oxidative stress [52]. In mice with liver-specific knockouts of Atg7, the growth of liver adenomas is strongly suppressed in combination with p62 knockouts [28]. Together, these results establish a crucial role for autophagy as a tumor suppressor in HCC.

4.2. Autophagy as a Tumorigenesis Mechanism

To sustain their rapid proliferation, cancer cells need abundant nutrients and oxygen during progression and invasion. As a key regulator for cellular homeostasis, autophagy is related to the maintenance and survival of tumor cells [53]. Since autophagy is activated in tumor cells in response to various types of stress, it plays a pro-survival function of cancer cells [11,54]. Cancer cells are thought to increase autophagic activity to survive in hostile microenvironments [55].

For example, mRNA of LC3 is markedly higher in HCC tissues than in non-tumor parenchymal cells, and is significantly correlated with tumor size [56]. Additionally, LC3-II increased in human HCC tissues showing decreased glucose uptake and increased K-Ras expression [57]. The tumorigenesis mechanism is also partly supported by a study that growth factor-deprived animal cells maintained cell survival via autophagy [58]. Furthermore, increased autophagic activity has been observed in hypoxic tumor regions [59].

The tumorigenesis function of autophagy is a promising target of future research focused on cancer management. Several agents that block the autophagy process, such as CQ and HCQ, have been actively studied in pre-clinical studies and clinical trials. The details of these studies are presented in the subsequent section.

5. Autophagy as a Prognostic Factor for HCC

HCC is one of the most aggressive and lethal tumors worldwide. It shows a very low 5-year survival rate (<15%) owing to its late diagnosis and compromised underlying liver function [60]. Patients who are eligible for current curative therapies are limited, and alternative therapies do not improve patient survival [15]. Thus, prognostic factors and promising therapies for HCC need to be established. Investigations have identified that the dysregulation of autophagy is associated with tumorigenesis in diverse types of cancer [10,61–63]. The role of autophagy in HCC is relatively well established [14]. However, few studies have identified autophagic proteins that are prognostic parameters in HCC, and these should be further elucidated considering the crucial role of autophagy during carcinogenesis. Here, we summarize the existing autophagy-related markers, which have prognostic potential in HCC. Autophagy-related markers that are predictive for the prognosis of HCC are presented in Table 1.

Table 1. Autophagy-related markers predictive for prognosis of hepatocellular carcinoma.

Markers	Target Mechanism	Expression Level in Human HCC Tissue	Expression Assessed	Implication	References
Beclin-1	Autophagosome formation	↓	protein	↑: Good prognosis	[20]
		↓	protein	↓: Aggressive behavior	[64]
		↓	mRNA, protein	↑: Good prognosis	[65]
		↓	mRNA, protein	↓: Progression of tumor	[66]
Microtubule-associated protein 1 light chain 3 (LC3)	Autophagosome formation	↓	protein	↑: Good prognosis	[19]
		↑	protein	↑: Poor prognosis	[67]
		↑	protein	↑: Poor prognosis	[68]
		↑	protein	↑: Poor prognosis	[69]
		↓	protein	↑: Poor prognosis	[70]
		↓	protein	↑: Good prognosis	[71]
Stearoyl-CoA desaturases (SCD1)	Adenosine monophosphate-activated protein kinase (AMPK) signaling	↑	mRNA, protein	↑: Poor prognosis	[71]
CCAAT-enhancer-binding protein α (C/EBPa)	Transmembrane protein 166 (TMEM166)	↑	protein	↑: Poor prognosis	[72]
GABA receptor-associated protein like 1 (GABARAPL1)	Autophagosome formation	↓	mRNA, protein	↓: Poor prognosis	[73]
UNC51-like kinase 1 (ULK1)	Autophagosome formation	↑	protein	↑: Poor prognosis	[74]
Gankyrin	Upregulate Atg7	↑	mRNA, protein	↑: Poor prognosis	[75]

↑, increase; ↓, decrease.

5.1. Beclin-1

Beclin-1, the mammalian ortholog of yeast Atg6, is required for double-membrane autophagosome formation [76,77]. It promotes the initial stages of autophagy via binding with other autophagic proteins, including Bcl-2, p150, Vps34, Atg14L, ultraviolet irradiation resistance-associated gene (UVRAG), Rubicon, and Bif1, to form a huge protein complex [78–82]. In fact, the identifying Beclin-1 as a tumor suppressor gene in human cancer provided early evidence for the tumor suppressive role of autophagy [83]. In a microarray analysis of HCC tissues obtained at the time of hepatectomy, investigators found lower expression of Beclin-1 in HCC than in adjacent nontumorous tissue, indicating that defective autophagy can contribute to carcinogenesis [64,65]. Studies have demonstrated that aberrant expression of Beclin-1 in diverse kinds of cancer is linked with poor prognosis [84–86]. Consistent with these findings, increased Beclin-1 expression is correlated with better prognosis, such as longer disease-free survival and overall survival (OS), in HCC [65]. The association between higher expression of Beclin-1 and longer OS supports the use of Beclin-1 as a prognostic marker for HCC. Additionally, Beclin-1 was proposed as a marker of HCC progression as co-expression of related genes was linked to HCC tumor progression [20]. A more recent study has confirmed the role of Beclin-1 in the progression of HCC by revealing a significant association between reduced Beclin-1 and high HIF-1α expression [64]. Combined, Beclin-1 is expected to be a valuable prognostic marker of HCC.

5.2. LC3

LC3, the mammalian homolog of yeast Atg8, plays an important role in human autophagy. It is activated by an ubiquitination-like reaction that is regulated by Atg7 and Atg3 [87]. The LC3 proform is cleaved into soluble LC3-I and lipidated LC3-II. LC3-I is converted to LC3-II, which is recruited for autophagosome formation [32]. Thus, LC3-II is an indicator of autophagosome formation [34]. However, LC3-II can reflect either autophagy induction or suppression [2]. The link between aberrant expression of LC3 and cancer prognosis has been reported for several tumor types [88–91]. A recent study suggested that high expression of a stone-like pattern of LC3A is an independent predictor of HCC prognosis [68]. Similarly, we identified LC3 expression as an independent prognostic factor of OS and time to recurrence. Interestingly, LC3 expression at an advanced stage is correlated with a longer OS, but this correlation is not observed in the early stage of HCC. These results imply that LC3

plays different roles depending on tumor stage [19]. The prognostic role of LC3 in HCC has been supported by several studies [67,69,70]. Collectively, these results indicate that LC3 is a potential prognostic factor in patients with HCC; however, its application as a potential therapeutic target for HCC requires additional research.

5.3. ULK1

ULK1, a mammalian serine/threonine protein kinase, contributes to the initial stages of autophagy [74]. There are conflicting data regarding the association between ULK1 and cancer prognosis. For instance, increased expression of ULK1 is associated with poor prognosis in esophageal squamous cell carcinoma [92]; however, in breast cancer, decreased ULK1 expression is associated with poor prognosis [93]. For HCC, one study showed that increased ULK1 expression is associated with poor OS, indicating that it is a possible prognostic marker for HCC [74]. Taken together, autophagy acts differently for different cancer types.

5.4. GABARAPL1

GABA receptor-associated protein like 1 (GABARAPL1) is one of six human Atg8 family proteins that shares high sequence identity with GABARAP, GATE-pro15, and LC3 [94]. Studies have revealed that GABARAPL1 is involved in autophagosome formation [94,95]. Some evidence suggests that GABARAPL1 expression is lower in HCC tissues than in adjacent non-tumor tissues and that there is an association between low GABARAPL1 expression and poor prognosis in HCC patients [73]. GABARAPL1 has previously been associated with the risk of metastasis in breast adenocarcinoma [96]. Further studies are required to understand the detailed mechanism of GABARAPL1 in HCC carcinogenesis and progression.

5.5. Other Loci Associated with Autophagy

Several additional autophagy-associated markers have been proposed for HCC prognosis. Stearoyl-CoA desaturases (SCDs) are ER-bound enzymes involved in *de novo* fatty acid synthesis of cellular lipids [97]. It regulates autophagy via lipogenesis [98]. Huang *et al*. [71], showed that SCD1 expression is significantly increased in mRNA and protein of HCC tissues and both LC3 and SCD1 were identified as independent predictors of OS in HCC. They also suggested that the tumor suppressive roles of SCD1 negatively modulate autophagy-induced apoptosis through the activation of AMPK signaling in human HCC.

CCAAT-enhancer-binding protein α (C/EBPα) is a transcription factor which belongs to the CCAAT/enhancer-binding protein family that inhibits cell proliferation and promotes terminal differentiation in various cell types [99]. It is involved in glucose and lipid metabolism [100]. Lu *et al.* [101] reported that C/EBPα is upregulated in protein of human HCC and promotes cell growth in HCC cell lines. They also demonstrated that C/EBPα overexpression is an independent prognosticator of poor OS in HCC patients [72]. It is noteworthy that C/EBPα is related to autophagy-mediated lipid metabolism and resistance to energy starvation, which lead to HCC carcinogenesis [72]. These results provide important molecular evidence for future therapeutic targets of HCC.

Gankyrin (also known as PSMD10 or p28) is a small protein that was identified as a regulatory subunit of the 26S proteasome complex [102,103]. Although the detailed mechanism is poorly understood, Gankyrin is overexpressed in mRNA and protein of HCC and acts as an oncoprotein [103,104]. A study reported that Gankyrin promotes autophagy in response to starvation or stress in HCC. Moreover, the significant correlation between Gankyrin and Atg7 indicates that the combination of these two molecules might be used in the prognosis of HCC [75]. The precise impact of Gankyrin on the prognosis of patients with HCC requires further investigation.

6. Autophagy Modulation for HCC Therapy

As autophagy acts a dual role in the initiation and development of HCC, many researches have evaluated its mechanisms and applications to HCC treatment. Increasing evidence supports the fact that autophagy also contributes to tumor cell responses to therapies and changing environmental stimuli. In this section, we discuss important autophagy inhibitors and inducers in HCC.

6.1. Autophagy Inhibitors in Anti-HCC Therapy

Since autophagy maintains cellular homeostasis, cancer cells also use autophagy for survival against cellular stress, including anti-HCC therapies. Autophagy inhibition prohibits the pro-survival effect of autophagy and enhances cytotoxicity in combination with anti-HCC therapies [105]. CQ and HCQ, which are used in the treatment of malaria, inhibit autophagy by increasing pH of lysosome via sinking protons. Eventually, CQ and HCQ are able to block the final stage of autophagy that demands acidic lysosomes for degradation [106]. It has been reported that autophagy inhibitors can potentiate the efficacy of oxaliplatin, cisplatin, 5-FU, and sorafenib in HCC [22,107–109]. The combination of oxaliplatin with CQ induces marked tumor suppression compared with either agent alone in HCC xenografts [22]. Similarly, the co-administration of CQ and sorafenib leads to marked tumor suppression in an HCC cell line [109]. MicroRNAs, which are small non-coding RNAs, have been proposed as key players in cancer cell proliferation, tumorigenesis, and apoptosis in HCC [110,111]. A recent study showed that miR-375 is downregulated in HCC tissues and inhibits hypoxia-induced autophagosome formation and autophagic flux in HCC cells [112]. Additionally, small interfering RNAs inhibit specific autophagy functions by silencing Atgs, and promote chemotherapeutic agent-induced cell death in a HCC cell line [113,114]. Zoe *et al*. [115], reported that oroxylin A which is a natural mono-flavonoid extracted from *Scutellariae radix*, leads to Beclin-1-mediated autophagy in human HCC cells. An *in vivo* study demonstrated that oroxylin A impedes the growth of xenograft tumors and causes apparent autophagy in tumors. The clinical application of these autophagy inhibitors remains unclear, but they are a promising therapeutic strategy to overcome therapeutic resistance in HCC treatment. Although there are over thirty ongoing clinical trials targeting autophagy for cancer treatment, none focus on HCC. Accordingly, clinical trials targeting autophagy for HCC therapy are required.

6.2. Autophagy Inducers in Anti-HCC Therapy

Based on the protective function of autophagy against hepatocarginogenesis, many researchers have focused on tumor cell death by autophagy. Autophagic cell death has been identified in many cancer cells [116–118]. The PI3K/Akt/mTOR pathway is a main regulator of cell proliferation, growth, survival, protein synthesis, and glucose metabolism in cancer cells [119]. In this pathway, mTOR inhibitors show anti-tumor activity in HCC [120]. The mTOR pathway is upregulated in a significant number of HCCs, suggesting that targeting this pathway may be particularly beneficial in the treatment of HCC [121]. Rapamycin and its derivatives act as mTOR inhibitors and are common autophagy inducers. For instance, rapamycin showed an anti-tumoral effect in a phase II study with 25 patients with advanced HCC [122]. Other study showed that rapamycin-based immunosuppression is relate to improved patient OS after liver transplantation for HCC [123]. However, it is premature to generalize about the utility of rapamycin and its derivatives in HCC therapy owing to insufficient or conflicting data for each agent. For example, everolimus (RAD001) shows anti-tumor activity in xenograft models of human HCC [124]; however, a recent large study (EVOLVE-1 trial) revealed that it had no benefit for survival and disease progression in a phase III trial [125]. By contrast, more fully targeting mTOR with RAD001 and a PI3K/mTOR dual inhibitor showed greater efficacy by increasing autophagy/mitophagy in tumors and decreasing tumor size in a mouse model of HCC [126]. Interestingly, a more recent study suggested that compound SBI-0206965 which is a highly selective ULK1 inhibitor may have promise as a more specific inhibitor

of autophagy in the treatment of HCC, potentially in combination with mTOR inhibitor [127]. Further studies supporting clinical implication of rapamycin are necessary.

Sorafenib is a multi-kinase inhibitor that is used a first-line systemic therapy for advanced HCC. It promotes autophagic cell death via the Mcl-1 signaling pathway [122]. Currently, representative phase III trials have shown that sorafenib significantly improves overall survival in patients with advanced HCC [128,129]. The co-administration of sorafenib and autophagy inhibitors also shows improved efficacy via autophagic cell death. However, sorafenib-induced autophagic cell death can result in drug resistance in patients with HCC [130]. Further, conventional chemotherapeutics, such as doxorubicin, are suppressed by sorafenib, resulting in cell progression, increased survival, and decreased autophagy in tumor cells [131]. Future research regarding the application of autophagy inducers to ameliorate the current limits of HCC therapy should facilitate better treatment outcomes in HCC.

7. Conclusions

The liver plays a crucial role in metabolism; therefore, dysregulation of liver autophagy has great clinical implications. Extensive studies have revealed the involvement of autophagy in HCC. According to current knowledge, autophagy plays a dual role in HCC. Most studies support the tumor suppressive role of autophagy. However, recently, abundant evidence suggests that autophagy is involved in tumorigenesis. We presume that the heterogeneousity of HCC tumors partly contributes to the different role of autophagy in various populations of HCC cells. Thus, the complexity of autophagy in HCC requires individualized approaches for the management of HCC.

Although abundant evidence suggests the high potential for autophagy modulation as a therapeutic method for HCC, the clinical application of these autophagy modulators remains unclear. Much has yet to be determined about the diverse and complex process of autophagy. A promising challenge is to identify the specific molecular mechanisms of autophagy for the development of therapeutic targets and to overcome resistance to current therapies. Another challenge is to identify biomarkers that can differentiate patients who need early intensive treatment and meticulous surveillance. Additional research on the various functions of autophagy according to tumor stage, differentiation, and environmental and genetic factors may lead to the establishment of an effective strategy against HCC.

Author Contributions: Yoo Jin Lee reviewed the literature and prepared the initial manuscript; Byoung Kuk Jang conceived the topic and produced the final manuscript.

Conflicts of Interest: The authors declare no conflict of interest.

References

1. Rautou, P.E.; Mansouri, A.; Lebrec, D.; Durand, F.; Valla, D.; Moreau, R. Autophagy in liver diseases. *J. Hepatol.* **2010**, *53*, 1123–1134. [CrossRef] [PubMed]
2. Czaja, M.J. Functions of autophagy in hepatic and pancreatic physiology and disease. *Gastroenterology* **2011**, *140*, 1895–1908. [CrossRef] [PubMed]
3. Kroemer, G.; Marino, G.; Levine, B. Autophagy and the integrated stress response. *Mol. Cell* **2010**, *40*, 280–293. [CrossRef] [PubMed]
4. Mizushima, N.; Komatsu, M. Autophagy: Renovation of cells and tissues. *Cell* **2011**, *147*, 728–741. [CrossRef] [PubMed]
5. Klionsky, D.J. Autophagy: From phenomenology to molecular understanding in less than a decade. *Nat. Rev. Mol. Cell Biol.* **2007**, *8*, 931–937. [CrossRef] [PubMed]
6. Ding, W.X.; Ni, H.M.; Gao, W.; Yoshimori, T.; Stolz, D.B.; Ron, D.; Yin, X.M. Linking of autophagy to ubiquitin-proteasome system is important for the regulation of endoplasmic reticulum stress and cell viability. *Am. J. Pathol.* **2007**, *171*, 513–524. [CrossRef] [PubMed]

7. Singh, R.; Cuervo, A.M. Autophagy in the cellular energetic balance. *Cell Metab.* **2011**, *13*, 495–504. [CrossRef] [PubMed]
8. Nixon, R.A. The role of autophagy in neurodegenerative disease. *Nat. Med.* **2013**, *19*, 983–997. [CrossRef] [PubMed]
9. Levine, B.; Mizushima, N.; Virgin, H.W. Autophagy in immunity and inflammation. *Nature* **2011**, *469*, 323–335. [CrossRef] [PubMed]
10. Choi, A.M.; Ryter, S.W.; Levine, B. Autophagy in human health and disease. *N. Engl. J. Med.* **2013**, *368*, 651–662. [CrossRef] [PubMed]
11. White, E. Deconvoluting the context-dependent role for autophagy in cancer. *Nat. Rev. Cancer* **2012**, *12*, 401–410. [CrossRef] [PubMed]
12. Kwanten, W.J.; Martinet, W.; Michielsen, P.P.; Francque, S.M. Role of autophagy in the pathophysiology of nonalcoholic fatty liver disease: A controversial issue. *World J. Gastroenterol.* **2014**, *20*, 7325–7338. [CrossRef] [PubMed]
13. Lozy, F.; Karantza, V. Autophagy and cancer cell metabolism. *Semin. Cell Dev. Biol.* **2012**, *23*, 395–401. [CrossRef] [PubMed]
14. Cui, J.; Gong, Z.; Shen, H.M. The role of autophagy in liver cancer: Molecular mechanisms and potential therapeutic targets. *Biochim. Biophys. Acta* **2013**, *1836*, 15–26. [CrossRef] [PubMed]
15. Bruix, J.; Sherman, M. Management of hepatocellular carcinoma: An update. *Hepatology* **2011**, *53*, 1020–1022. [CrossRef] [PubMed]
16. Forner, A.; Llovet, J.M.; Bruix, J. Hepatocellular carcinoma. *Lancet* **2012**, *379*, 1245–1255. [CrossRef]
17. Yan, J.; Zhou, Y.; Chen, D.; Li, L.; Yang, X.; You, Y.; Ling, X. Effects of mitochondrial translocation of telomerase on drug resistance in hepatocellular carcinoma cells. *J. Cancer* **2015**, *6*, 151–159. [CrossRef] [PubMed]
18. Huo, X.; Zhang, Q.; Liu, A.M.; Tang, C.; Gong, Y.; Bian, J.; Luk, J.M.; Xu, Z.; Chen, J. Overexpression of Yes-associated protein confers doxorubicin resistance in hepatocellullar carcinoma. *Oncol. Rep.* **2013**, *29*, 840–846. [PubMed]
19. Lee, Y.J.; Hah, Y.J.; Kang, Y.N.; Kang, K.J.; Hwang, J.S.; Chung, W.J.; Cho, K.B.; Park, K.S.; Kim, E.S.; Seo, H.Y.; *et al*. The autophagy-related marker LC3 can predict prognosis in human hepatocellular carcinoma. *PLoS ONE* **2013**, *8*, e81540. [CrossRef] [PubMed]
20. Qiu, D.M.; Wang, G.L.; Chen, L.; Xu, Y.Y.; He, S.; Cao, X.L.; Qin, J.; Zhou, J.M.; Zhang, Y.X.; Qun, E. The expression of beclin-1, an autophagic gene, in hepatocellular carcinoma associated with clinical pathological and prognostic significance. *BMC Cancer* **2014**, *14*. [CrossRef] [PubMed]
21. Pan, H.; Wang, Z.; Jiang, L.; Sui, X.; You, L.; Shou, J.; Jing, Z.; Xie, J.; Ge, W.; Cai, X.; *et al*. Autophagy inhibition sensitizes hepatocellular carcinoma to the multikinase inhibitor linifanib. *Sci. Rep.* **2014**, *4*. [CrossRef] [PubMed]
22. Ding, Z.B.; Hui, B.; Shi, Y.H.; Zhou, J.; Peng, Y.F.; Gu, C.Y.; Yang, H.; Shi, G.M.; Ke, A.W.; Wang, X.Y.; *et al*. Autophagy activation in hepatocellular carcinoma contributes to the tolerance of oxaliplatin via reactive oxygen species modulation. *Clin. Cancer Res.* **2011**, *17*, 6229–6238. [CrossRef] [PubMed]
23. Yang, Z.; Klionsky, D.J. An overview of the molecular mechanism of autophagy. *Curr. Top. Microbiol. Immunol.* **2009**, *335*, 1–32. [PubMed]
24. Ezaki, J.; Matsumoto, N.; Takeda-Ezaki, M.; Komatsu, M.; Takahashi, K.; Hiraoka, Y.; Taka, H.; Fujimura, T.; Takehana, K.; Yoshida, M.; *et al*. Liver autophagy contributes to the maintenance of blood glucose and amino acid levels. *Autophagy* **2011**, *7*, 727–736. [CrossRef] [PubMed]
25. Singh, R.; Kaushik, S.; Wang, Y.; Xiang, Y.; Novak, I.; Komatsu, M.; Tanaka, K.; Cuervo, A.M.; Czaja, M.J. Autophagy regulates lipid metabolism. *Nature* **2009**, *458*, 1131–1135. [CrossRef] [PubMed]
26. Komatsu, M.; Waguri, S.; Ueno, T.; Iwata, J.; Murata, S.; Tanida, I.; Ezaki, J.; Mizushima, N.; Ohsumi, Y.; Uchiyama, Y.; *et al*. Impairment of starvation-induced and constitutive autophagy in Atg7-deficient mice. *J. Cell Biol.* **2005**, *169*, 425–434. [CrossRef] [PubMed]
27. Inami, Y.; Waguri, S.; Sakamoto, A.; Kouno, T.; Nakada, K.; Hino, O.; Watanabe, S.; Ando, J.; Iwadate, M.; Yamamoto, M.; *et al*. Persistent activation of Nrf2 through p62 in hepatocellular carcinoma cells. *J. Cell Biol.* **2011**, *193*, 275–284. [CrossRef] [PubMed]

28. Takamura, A.; Komatsu, M.; Hara, T.; Sakamoto, A.; Kishi, C.; Waguri, S.; Eishi, Y.; Hino, O.; Tanaka, K.; Mizushima, N. Autophagy-deficient mice develop multiple liver tumors. *Genes Dev.* **2011**, *25*, 795–800. [CrossRef] [PubMed]
29. Kim, J.; Kundu, M.; Viollet, B.; Guan, K.L. AMPK and mTOR regulate autophagy through direct phosphorylation of Ulk1. *Nat. Cell Biol.* **2011**, *13*, 132–141. [CrossRef] [PubMed]
30. Egan, D.F.; Shackelford, D.B.; Mihaylova, M.M.; Gelino, S.; Kohnz, R.A.; Mair, W.; Vasquez, D.S.; Joshi, A.; Gwinn, D.M.; Taylor, R.; *et al*. Phosphorylation of ULK1 (hATG1) by AMP-activated protein kinase connects energy sensing to mitophagy. *Science* **2011**, *331*, 456–461. [CrossRef] [PubMed]
31. Ichimura, Y.; Kirisako, T.; Takao, T.; Satomi, Y.; Shimonishi, Y.; Ishihara, N.; Mizushima, N.; Tanida, I.; Kominami, E.; Ohsumi, M.; *et al*. A ubiquitin-like system mediates protein lipidation. *Nature* **2000**, *408*, 488–492. [PubMed]
32. Kabeya, Y.; Mizushima, N.; Ueno, T.; Yamamoto, A.; Kirisako, T.; Noda, T.; Kominami, E.; Ohsumi, Y.; Yoshimori, T. LC3, a mammalian homologue of yeast Apg8p, is localized in autophagosome membranes after processing. *EMBO J.* **2000**, *19*, 5720–5728. [CrossRef] [PubMed]
33. Behrends, C.; Sowa, M.E.; Gygi, S.P.; Harper, J.W. Network organization of the human autophagy system. *Nature* **2010**, *466*, 68–76. [CrossRef] [PubMed]
34. Ogata, M.; Hino, S.; Saito, A.; Morikawa, K.; Kondo, S.; Kanemoto, S.; Murakami, T.; Taniguchi, M.; Tanii, I.; Yoshinaga, K.; *et al*. Autophagy is activated for cell survival after endoplasmic reticulum stress. *Mol. Cell. Biol.* **2006**, *26*, 9220–9231. [CrossRef] [PubMed]
35. Schneider, J.L.; Cuervo, A.M. Liver autophagy: Much more than just taking out the trash. *Nat. Rev. Gastroenterol. Hepatol.* **2014**, *11*, 187–200. [CrossRef] [PubMed]
36. Mizushima, N. Autophagy: Process and function. *Genes Dev.* **2007**, *21*, 2861–2873. [CrossRef] [PubMed]
37. Yin, X.M.; Ding, W.X.; Gao, W. Autophagy in the liver. *Hepatology* **2008**, *47*, 1773–1785. [CrossRef] [PubMed]
38. Kim, I.; Rodriguez-Enriquez, S.; Lemasters, J.J. Selective degradation of mitochondria by mitophagy. *Arch. Biochem. Biophys.* **2007**, *462*, 245–253. [CrossRef] [PubMed]
39. Rodriguez-Enriquez, S.; Kim, I.; Currin, R.T.; Lemasters, J.J. Tracker dyes to probe mitochondrial autophagy (mitophagy) in rat hepatocytes. *Autophagy* **2006**, *2*, 39–46. [CrossRef] [PubMed]
40. Ding, W.X. Role of autophagy in liver physiology and pathophysiology. *World J. Biol. Chem.* **2010**, *1*, 3–12. [CrossRef] [PubMed]
41. Wang, Z.; Han, W.; Sui, X.; Fang, Y.; Pan, H. Autophagy: A novel therapeutic target for hepatocarcinoma (Review). *Oncol. Lett.* **2014**, *7*, 1345–1351. [CrossRef] [PubMed]
42. Farazi, P.A.; DePinho, R.A. Hepatocellular carcinoma pathogenesis: From genes to environment. *Nat. Rev. Cancer* **2006**, *6*, 674–687. [CrossRef] [PubMed]
43. Yang, L.; Li, P.; Fu, S.; Calay, E.S.; Hotamisligil, G.S. Defective hepatic autophagy in obesity promotes ER stress and causes insulin resistance. *Cell Metab.* **2010**, *11*, 467–478. [CrossRef] [PubMed]
44. Czaja, M.J.; Ding, W.X.; Donohue, T.M., Jr.; Friedman, S.L.; Kim, J.S.; Komatsu, M.; Lemasters, J.J.; Lemoine, A.; Lin, J.D.; Ou, J.H.; *et al*. Functions of autophagy in normal and diseased liver. *Autophagy* **2013**, *9*, 1131–1158. [CrossRef] [PubMed]
45. Yang, S.; Wang, X.; Contino, G.; Liesa, M.; Sahin, E.; Ying, H.; Bause, A.; Li, Y.; Stommel, J.M.; Dell'antonio, G.; *et al*. Pancreatic cancers require autophagy for tumor growth. *Genes Dev.* **2011**, *25*, 717–729. [CrossRef] [PubMed]
46. Yue, Z.; Jin, S.; Yang, C.; Levine, A.J.; Heintz, N. Beclin 1, an autophagy gene essential for early embryonic development, is a haploinsufficient tumor suppressor. *Proc. Natl. Acad. Sci. USA* **2003**, *100*, 15077–15082. [CrossRef] [PubMed]
47. Qu, X.; Yu, J.; Bhagat, G.; Furuya, N.; Hibshoosh, H.; Troxel, A.; Rosen, J.; Eskelinen, E.L.; Mizushima, N.; Ohsumi, Y.; *et al*. Promotion of tumorigenesis by heterozygous disruption of the beclin 1 autophagy gene. *J. Clin. Investig.* **2003**, *112*, 1809–1820. [CrossRef] [PubMed]
48. Kuma, A.; Hatano, M.; Matsui, M.; Yamamoto, A.; Nakaya, H.; Yoshimori, T.; Ohsumi, Y.; Tokuhisa, T.; Mizushima, N. The role of autophagy during the early neonatal starvation period. *Nature* **2004**, *432*, 1032–1036. [CrossRef] [PubMed]
49. Itakura, E.; Mizushima, N. p62 Targeting to the autophagosome formation site requires self-oligomerization but not LC3 binding. *J. Cell Biol.* **2011**, *192*, 17–27. [CrossRef] [PubMed]

50. Johansen, T.; Lamark, T. Selective autophagy mediated by autophagic adapter proteins. *Autophagy* **2011**, *7*, 279–296. [CrossRef] [PubMed]
51. Gan, N.; Sun, X.; Song, L. Activation of Nrf2 by microcystin-LR provides advantages for liver cancer cell growth. *Chem. Res. Toxicol.* **2010**, *23*, 1477–1484. [CrossRef] [PubMed]
52. Mathew, R.; Karp, C.M.; Beaudoin, B.; Vuong, N.; Chen, G.; Chen, H.Y.; Bray, K.; Reddy, A.; Bhanot, G.; Gelinas, C.; *et al*. Autophagy suppresses tumorigenesis through elimination of p62. *Cell* **2009**, *137*, 1062–1075. [CrossRef] [PubMed]
53. Chen, S.; Rehman, S.K.; Zhang, W.; Wen, A.; Yao, L.; Zhang, J. Autophagy is a therapeutic target in anticancer drug resistance. *Biochim. Biophys. Acta* **2010**, *1806*, 220–229. [CrossRef] [PubMed]
54. Eskelinen, E.L. The dual role of autophagy in cancer. *Curr. Opin. Pharmacol.* **2011**, *11*, 294–300. [CrossRef] [PubMed]
55. Morselli, E.; Galluzzi, L.; Kepp, O.; Vicencio, J.M.; Criollo, A.; Maiuri, M.C.; Kroemer, G. Anti- and pro-tumor functions of autophagy. *Biochim. Biophys. Acta* **2009**, *1793*, 1524–1532. [CrossRef] [PubMed]
56. Yang, J.D.; Seol, S.Y.; Leem, S.H.; Kim, Y.H.; Sun, Z.; Lee, J.S.; Thorgeirsson, S.S.; Chu, I.S.; Roberts, L.R.; Kang, K.J. Genes associated with recurrence of hepatocellular carcinoma: Integrated analysis by gene expression and methylation profiling. *J. Korean Med. Sci.* **2011**, *26*, 1428–1438. [CrossRef] [PubMed]
57. Kim, J.H.; Kim, H.Y.; Lee, Y.K.; Yoon, Y.S.; Xu, W.G.; Yoon, J.K.; Choi, S.E.; Ko, Y.G.; Kim, M.J.; Lee, S.J.; *et al*. Involvement of mitophagy in oncogenic K-Ras-induced transformation: Overcoming a cellular energy deficit from glucose deficiency. *Autophagy* **2011**, *7*, 1187–1198. [CrossRef] [PubMed]
58. Lum, J.J.; Bauer, D.E.; Kong, M.; Harris, M.H.; Li, C.; Lindsten, T.; Thompson, C.B. Growth factor regulation of autophagy and cell survival in the absence of apoptosis. *Cell* **2005**, *120*, 237–248. [CrossRef] [PubMed]
59. Degenhardt, K.; Mathew, R.; Beaudoin, B.; Bray, K.; Anderson, D.; Chen, G.; Mukherjee, C.; Shi, Y.; Gelinas, C.; Fan, Y.; *et al*. Autophagy promotes tumor cell survival and restricts necrosis, inflammation, and tumorigenesis. *Cancer Cell* **2006**, *10*, 51–64. [CrossRef] [PubMed]
60. Villanueva, A.; Hernandez-Gea, V.; Llovet, J.M. Medical therapies for hepatocellular carcinoma: A critical view of the evidence. *Nat. Rev. Gastroenterol. Hepatol.* **2013**, *10*, 34–42. [CrossRef] [PubMed]
61. Cook, K.L.; Shajahan, A.N.; Clarke, R. Autophagy and endocrine resistance in breast cancer. *Expert Rev. Anticancer Ther.* **2011**, *11*, 1283–1294. [CrossRef] [PubMed]
62. Kaza, N.; Kohli, L.; Roth, K.A. Autophagy in brain tumors: A new target for therapeutic intervention. *Brain Pathol.* **2012**, *22*, 89–98. [CrossRef] [PubMed]
63. Pandey, S.; Chandravati. Autophagy in cervical cancer: An emerging therapeutic target. *Asian Pac. J. Cancer Prev. APJCP* **2012**, *13*, 4867–4871. [CrossRef] [PubMed]
64. Osman, N.A.; Abd El-Rehim, D.M.; Kamal, I.M. Defective Beclin-1 and elevated hypoxia-inducible factor (HIF)-1α expression are closely linked to tumorigenesis, differentiation, and progression of hepatocellular carcinoma. *Tumour Biol.* **2015**. [CrossRef] [PubMed]
65. Ding, Z.B.; Shi, Y.H.; Zhou, J.; Qiu, S.J.; Xu, Y.; Dai, Z.; Shi, G.M.; Wang, X.Y.; Ke, A.W.; Wu, B.; *et al*. Association of autophagy defect with a malignant phenotype and poor prognosis of hepatocellular carcinoma. *Cancer Res.* **2008**, *68*, 9167–9175. [CrossRef] [PubMed]
66. Kotsafti, A.; Farinati, F.; Cardin, R.; Cillo, U.; Nitti, D.; Bortolami, M. Autophagy and apoptosis-related genes in chronic liver disease and hepatocellular carcinoma. *BMC Gastroenterol.* **2012**, *12*, 118. [CrossRef] [PubMed]
67. Wu, W.Y.; Kim, H.; Zhang, C.L.; Meng, X.L.; Wu, Z.S. Clinical significance of autophagic protein LC3 levels and its correlation with XIAP expression in hepatocellular carcinoma. *Med. Oncol.* **2014**, *31*, 108. [CrossRef] [PubMed]
68. Xi, S.Y.; Lu, J.B.; Chen, J.W.; Cao, Y.; Luo, R.Z.; Wu, Q.L.; Cai, M.Y. The "stone-like" pattern of LC3A expression and its clinicopathologic significance in hepatocellular carcinoma. *Biochem. Biophys. Res. Commun.* **2013**, *431*, 760–766. [CrossRef] [PubMed]
69. Toshima, T.; Shirabe, K.; Matsumoto, Y.; Yoshiya, S.; Ikegami, T.; Yoshizumi, T.; Soejima, Y.; Ikeda, T.; Maehara, Y. Autophagy enhances hepatocellular carcinoma progression by activation of mitochondrial β-oxidation. *J. Gastroenterol.* **2014**, *49*, 907–916. [CrossRef] [PubMed]
70. Wu, D.H.; Jia, C.C.; Chen, J.; Lin, Z.X.; Ruan, D.Y.; Li, X.; Lin, Q.; Min, D.; Ma, X.K.; Wan, X.B.; *et al*. Autophagic LC3B overexpression correlates with malignant progression and predicts a poor prognosis in hepatocellular carcinoma. *Tumour Biol.* **2014**, *35*, 12225–12233. [CrossRef] [PubMed]

71. Huang, G.M.; Jiang, Q.H.; Cai, C.; Qu, M.; Shen, W. SCD1 negatively regulates autophagy-induced cell death in human hepatocellular carcinoma through inactivation of the AMPK signaling pathway. *Cancer Lett.* **2015**, *358*, 180–190. [CrossRef] [PubMed]
72. Lu, G.D.; Ang, Y.H.; Zhou, J.; Tamilarasi, J.; Yan, B.; Lim, Y.C.; Srivastava, S.; Salto-Tellez, M.; Hui, K.M.; Shen, H.M.; *et al*. CCAAT/enhancer binding protein α predicts poorer prognosis and prevents energy starvation-induced cell death in hepatocellular carcinoma. *Hepatology* **2015**, *61*, 965–978. [CrossRef] [PubMed]
73. Liu, C.; Xia, Y.; Jiang, W.; Liu, Y.; Yu, L. Low expression of GABARAPL1 is associated with a poor outcome for patients with hepatocellular carcinoma. *Oncol. Rep.* **2014**, *31*, 2043–2048. [CrossRef] [PubMed]
74. Xu, H.; Yu, H.; Zhang, X.; Shen, X.; Zhang, K.; Sheng, H.; Dai, S.; Gao, H. UNC51-like kinase 1 as a potential prognostic biomarker for hepatocellular carcinoma. *Int. J. Clin. Exp. Pathol.* **2013**, *6*, 711–717. [PubMed]
75. Luo, T.; Fu, J.; Xu, A.; Su, B.; Ren, Y.; Li, N.; Zhu, J.; Zhao, X.; Dai, R.; Cao, J.; *et al*. PSMD10/Gankyrin Induces Autophagy to Promote Tumor Progression through Cytoplasmic Interaction with ATG7 and Nuclear Transactivation of ATG7 Expression. *Autophagy* **2015**. [CrossRef] [PubMed]
76. Cao, Y.; Klionsky, D.J. Physiological functions of Atg6/Beclin 1: A unique autophagy-related protein. *Cell Res.* **2007**, *17*, 839–849. [CrossRef] [PubMed]
77. Sun, Q.; Fan, W.; Zhong, Q. Regulation of Beclin 1 in autophagy. *Autophagy* **2009**, *5*, 713–716. [CrossRef] [PubMed]
78. Itakura, E.; Mizushima, N. Atg14 and UVRAG: Mutually exclusive subunits of mammalian Beclin 1-PI3K complexes. *Autophagy* **2009**, *5*, 534–536. [CrossRef] [PubMed]
79. Itakura, E.; Kishi, C.; Inoue, K.; Mizushima, N. Beclin 1 forms two distinct phosphatidylinositol 3-kinase complexes with mammalian Atg14 and UVRAG. *Mol. Biol. Cell* **2008**, *19*, 5360–5372. [CrossRef] [PubMed]
80. Takahashi, Y.; Coppola, D.; Matsushita, N.; Cualing, H.D.; Sun, M.; Sato, Y.; Liang, C.; Jung, J.U.; Cheng, J.Q.; Mule, J.J.; *et al*. Bif-1 interacts with Beclin 1 through UVRAG and regulates autophagy and tumorigenesis. *Nat. Cell Biol.* **2007**, *9*, 1142–1151. [CrossRef] [PubMed]
81. Matsunaga, K.; Saitoh, T.; Tabata, K.; Omori, H.; Satoh, T.; Kurotori, N.; Maejima, I.; Shirahama-Noda, K.; Ichimura, T.; Isobe, T.; *et al*. Two Beclin 1-binding proteins, Atg14L and Rubicon, reciprocally regulate autophagy at different stages. *Nat. Cell Biol.* **2009**, *11*, 385–396. [CrossRef] [PubMed]
82. Pattingre, S.; Tassa, A.; Qu, X.; Garuti, R.; Liang, X.H.; Mizushima, N.; Packer, M.; Schneider, M.D.; Levine, B. Bcl-2 antiapoptotic proteins inhibit Beclin 1-dependent autophagy. *Cell* **2005**, *122*, 927–939. [CrossRef] [PubMed]
83. Liang, X.H.; Jackson, S.; Seaman, M.; Brown, K.; Kempkes, B.; Hibshoosh, H.; Levine, B. Induction of autophagy and inhibition of tumorigenesis by beclin 1. *Nature* **1999**, *402*, 672–676. [PubMed]
84. Wan, X.B.; Fan, X.J.; Chen, M.Y.; Xiang, J.; Huang, P.Y.; Guo, L.; Wu, X.Y.; Xu, J.; Long, Z.J.; Zhao, Y.; *et al*. Elevated Beclin 1 expression is correlated with HIF-1α in predicting poor prognosis of nasopharyngeal carcinoma. *Autophagy* **2010**, *6*, 395–404. [CrossRef] [PubMed]
85. Yu, M.; Gou, W.F.; Zhao, S.; Xiao, L.J.; Mao, X.Y.; Xing, Y.N.; Takahashi, H.; Takano, Y.; Zheng, H.C. Beclin 1 expression is an independent prognostic factor for gastric carcinomas. *Tumour Biol.* **2013**, *34*, 1071–1083. [CrossRef] [PubMed]
86. Giatromanolaki, A.; Koukourakis, M.I.; Koutsopoulos, A.; Chloropoulou, P.; Liberis, V.; Sivridis, E. High Beclin 1 expression defines a poor prognosis in endometrial adenocarcinomas. *Gynecol. Oncol.* **2011**, *123*, 147–151. [CrossRef] [PubMed]
87. Tanida, I.; Tanida-Miyake, E.; Ueno, T.; Kominami, E. The human homolog of Saccharomyces cerevisiae Apg7p is a Protein-activating enzyme for multiple substrates including human Apg12p, GATE-16, GABARAP, and MAP-LC3. *J. Biol. Chem.* **2001**, *276*, 1701–1706. [CrossRef] [PubMed]
88. Giatromanolaki, A.; Koukourakis, M.I.; Harris, A.L.; Polychronidis, A.; Gatter, K.C.; Sivridis, E. Prognostic relevance of light chain 3 (LC3A) autophagy patterns in colorectal adenocarcinomas. *J. Clin. Pathol.* **2010**, *63*, 867–872. [CrossRef] [PubMed]
89. Fujii, S.; Mitsunaga, S.; Yamazaki, M.; Hasebe, T.; Ishii, G.; Kojima, M.; Kinoshita, T.; Ueno, T.; Esumi, H.; Ochiai, A. Autophagy is activated in pancreatic cancer cells and correlates with poor patient outcome. *Cancer Sci.* **2008**, *99*, 1813–1819. [CrossRef] [PubMed]

90. Zhu, W.; Pan, X.; Li, F.; Zhang, Y.; Lu, X. Expression of Beclin 1 and LC3 in FIGO stage I-II cervical squamous cell carcinoma and relationship to survival. *Tumor Biol.* **2012**, *33*, 1653–1659. [CrossRef] [PubMed]
91. Huang, X.; Bai, H.M.; Chen, L.; Li, B.; Lu, Y.C. Reduced expression of LC3B-II and Beclin 1 in glioblastoma multiforme indicates a down-regulated autophagic capacity that relates to the progression of astrocytic tumors. *J. Clin. Neurosci.* **2010**, *17*, 1515–1519. [CrossRef] [PubMed]
92. Jiang, S.; Li, Y.; Zhu, Y.H.; Wu, X.Q.; Tang, J.; Li, Z.; Feng, G.K.; Deng, R.; Li, D.D.; Luo, R.Z.; *et al*. Intensive expression of UNC-51-like kinase 1 is a novel biomarker of poor prognosis in patients with esophageal squamous cell carcinoma. *Cancer Sci.* **2011**, *102*, 1568–1575. [CrossRef] [PubMed]
93. Tang, J.; Deng, R.; Luo, R.Z.; Shen, G.P.; Cai, M.Y.; Du, Z.M.; Jiang, S.; Yang, M.T.; Fu, J.H.; Zhu, X.F. Low expression of ULK1 is associated with operable breast cancer progression and is an adverse prognostic marker of survival for patients. *Breast Cancer Res. Treat.* **2012**, *134*, 549–560. [CrossRef] [PubMed]
94. Le Grand, J.N.; Chakrama, F.Z.; Seguin-Py, S.; Fraichard, A.; Delage-Mourroux, R.; Jouvenot, M.; Boyer-Guittaut, M. GABARAPL1 (GEC1): Original or copycat? *Autophagy* **2011**, *7*, 1098–1107. [PubMed]
95. Chakrama, F.Z.; Seguin-Py, S.; Le Grand, J.N.; Fraichard, A.; Delage-Mourroux, R.; Despouy, G.; Perez, V.; Jouvenot, M.; Boyer-Guittaut, M. GABARAPL1 (GEC1) associates with autophagic vesicles. *Autophagy* **2010**, *6*, 495–505. [CrossRef] [PubMed]
96. Berthier, A.; Seguin, S.; Sasco, A.J.; Bobin, J.Y.; de Laroche, G.; Datchary, J.; Saez, S.; Rodriguez-Lafrasse, C.; Tolle, F.; Fraichard, A.; *et al*. High expression of gabarapl1 is associated with a better outcome for patients with lymph node-positive breast cancer. *Br. J. Cancer* **2010**, *102*, 1024–1031. [CrossRef] [PubMed]
97. Ntambi, J.M.; Miyazaki, M. Recent insights into stearoyl-CoA desaturase-1. *Curr. Opin. Lipidol.* **2003**, *14*, 255–261. [CrossRef] [PubMed]
98. Tan, S.H.; Shui, G.; Zhou, J.; Shi, Y.; Huang, J.; Xia, D.; Wenk, M.R.; Shen, H.M. Critical role of SCD1 in autophagy regulation via lipogenesis and lipid rafts-coupled AKT-FOXO1 signaling pathway. *Autophagy* **2014**, *10*, 226–242. [CrossRef] [PubMed]
99. Schuster, M.B.; Porse, B.T. C/EBPα: A tumour suppressor in multiple tissues? *Biochim. Biophys. Acta* **2006**, *1766*, 88–103. [CrossRef] [PubMed]
100. Matsusue, K.; Gavrilova, O.; Lambert, G.; Brewer, H.B., Jr.; Ward, J.M.; Inoue, Y.; LeRoith, D.; Gonzalez, F.J. Hepatic CCAAT/enhancer binding protein α mediates induction of lipogenesis and regulation of glucose homeostasis in leptin-deficient mice. *Mol. Endocrinol.* **2004**, *18*, 2751–2764. [CrossRef] [PubMed]
101. Lu, G.D.; Leung, C.H.; Yan, B.; Tan, C.M.; Low, S.Y.; Aung, M.O.; Salto-Tellez, M.; Lim, S.G.; Hooi, S.C. C/EBPα is up-regulated in a subset of hepatocellular carcinomas and plays a role in cell growth and proliferation. *Gastroenterology* **2010**, *139*, 632–643. [CrossRef] [PubMed]
102. Mayer, R.J.; Fujita, J. Gankyrin, the 26 S proteasome, the cell cycle and cancer. *Biochem. Soc. Trans.* **2006**, *34*, 746–748. [CrossRef] [PubMed]
103. Higashitsuji, H.; Itoh, K.; Nagao, T.; Dawson, S.; Nonoguchi, K.; Kido, T.; Mayer, R.J.; Arii, S.; Fujita, J. Reduced stability of retinoblastoma protein by gankyrin, an oncogenic ankyrin-repeat protein overexpressed in hepatomas. *Nat. Med.* **2000**, *6*, 96–99. [PubMed]
104. Fu, J.; Chen, Y.; Cao, J.; Luo, T.; Qian, Y.W.; Yang, W.; Ren, Y.B.; Su, B.; Cao, G.W.; Yang, Y.; *et al*. p28GANK overexpression accelerates hepatocellular carcinoma invasiveness and metastasis via phosphoinositol 3-kinase/AKT/hypoxia-inducible factor-1α pathways. *Hepatology* **2011**, *53*, 181–192. [CrossRef] [PubMed]
105. Ni, H.M.; Williams, J.A.; Yang, H.; Shi, Y.H.; Fan, J.; Ding, W.X. Targeting autophagy for the treatment of liver diseases. *Pharmacol. Res.* **2012**, *66*, 463–474. [CrossRef] [PubMed]
106. Zhi, X.; Zhong, Q. Autophagy in cancer. *F1000prime Rep.* **2015**, *7*, 18. [CrossRef] [PubMed]
107. Guo, X.L.; Li, D.; Hu, F.; Song, J.R.; Zhang, S.S.; Deng, W.J.; Sun, K.; Zhao, Q.D.; Xie, X.Q.; Song, Y.J.; *et al*. Targeting autophagy potentiates chemotherapy-induced apoptosis and proliferation inhibition in hepatocarcinoma cells. *Cancer Lett.* **2012**, *320*, 171–179. [CrossRef] [PubMed]
108. Shimizu, S.; Takehara, T.; Hikita, H.; Kodama, T.; Tsunematsu, H.; Miyagi, T.; Hosui, A.; Ishida, H.; Tatsumi, T.; Kanto, T.; *et al*. Inhibition of autophagy potentiates the antitumor effect of the multikinase inhibitor sorafenib in hepatocellular carcinoma. *Int. J. Cancer* **2012**, *131*, 548–557. [CrossRef] [PubMed]
109. Shi, Y.H.; Ding, Z.B.; Zhou, J.; Hui, B.; Shi, G.M.; Ke, A.W.; Wang, X.Y.; Dai, Z.; Peng, Y.F.; Gu, C.Y.; *et al*. Targeting autophagy enhances sorafenib lethality for hepatocellular carcinoma via ER stress-related apoptosis. *Autophagy* **2011**, *7*, 1159–1172. [CrossRef] [PubMed]

110. Kota, J.; Chivukula, R.R.; O'Donnell, K.A.; Wentzel, E.A.; Montgomery, C.L.; Hwang, H.W.; Chang, T.C.; Vivekanandan, P.; Torbenson, M.; Clark, K.R.; *et al*. Therapeutic microRNA delivery suppresses tumorigenesis in a murine liver cancer model. *Cell* **2009**, *137*, 1005–1017. [CrossRef] [PubMed]
111. Gailhouste, L.; Ochiya, T. Cancer-related microRNAs and their role as tumor suppressors and oncogenes in hepatocellular carcinoma. *Histol. Histopathol.* **2013**, *28*, 437–451. [PubMed]
112. Chang, Y.; Yan, W.; He, X.; Zhang, L.; Li, C.; Huang, H.; Nace, G.; Geller, D.A.; Lin, J.; Tsung, A. miR-375 inhibits autophagy and reduces viability of hepatocellular carcinoma cells under hypoxic conditions. *Gastroenterology* **2012**, *143*, 177–187. [CrossRef] [PubMed]
113. Luo, Z.; Yu, G.; Lee, H.W.; Li, L.; Wang, L.; Yang, D.; Pan, Y.; Ding, C.; Qian, J.; Wu, L.; *et al*. The Nedd8-activating enzyme inhibitor MLN4924 induces autophagy and apoptosis to suppress liver cancer cell growth. *Cancer Res.* **2012**, *72*, 3360–3371. [CrossRef] [PubMed]
114. Chen, L.H.; Loong, C.C.; Su, T.L.; Lee, Y.J.; Chu, P.M.; Tsai, M.L.; Tsai, P.H.; Tu, P.H.; Chi, C.W.; Lee, H.C.; *et al*. Autophagy inhibition enhances apoptosis triggered by BO-1051, an N-mustard derivative, and involves the ATM signaling pathway. *Biochem. Pharmacol.* **2011**, *81*, 594–605. [CrossRef] [PubMed]
115. Zou, M.; Lu, N.; Hu, C.; Liu, W.; Sun, Y.; Wang, X.; You, Q.; Gu, C.; Xi, T.; Guo, Q. Beclin 1-mediated autophagy in hepatocellular carcinoma cells: Implication in anticancer efficiency of oroxylin A via inhibition of mTOR signaling. *Cell Signal.* **2012**, *24*, 1722–1732. [CrossRef] [PubMed]
116. Kanzawa, T.; Kondo, Y.; Ito, H.; Kondo, S.; Germano, I. Induction of autophagic cell death in malignant glioma cells by arsenic trioxide. *Cancer Res.* **2003**, *63*, 2103–2108. [PubMed]
117. Kim, E.H.; Sohn, S.; Kwon, H.J.; Kim, S.U.; Kim, M.J.; Lee, S.J.; Choi, K.S. Sodium selenite induces superoxide-mediated mitochondrial damage and subsequent autophagic cell death in malignant glioma cells. *Cancer Res.* **2007**, *67*, 6314–6324. [CrossRef] [PubMed]
118. Dupere-Richer, D.; Kinal, M.; Menasche, V.; Nielsen, T.H.; Del Rincon, S.; Pettersson, F.; Miller, W.H., Jr. Vorinostat-induced autophagy switches from a death-promoting to a cytoprotective signal to drive acquired resistance. *Cell Death Dis.* **2013**, *4*, e486. [CrossRef] [PubMed]
119. Yap, T.A.; Garrett, M.D.; Walton, M.I.; Raynaud, F.; de Bono, J.S.; Workman, P. Targeting the PI3K–AKT–mTOR pathway: Progress, pitfalls, and promises. *Curr. Opin. Pharmacol.* **2008**, *8*, 393–412. [CrossRef] [PubMed]
120. Sieghart, W.; Fuereder, T.; Schmid, K.; Cejka, D.; Werzowa, J.; Wrba, F.; Wang, X.; Gruber, D.; Rasoul-Rockenschaub, S.; Peck-Radosavljevic, M.; *et al*. Mammalian target of rapamycin pathway activity in hepatocellular carcinomas of patients undergoing liver transplantation. *Transplantation* **2007**, *83*, 425–432. [CrossRef] [PubMed]
121. Villanueva, A.; Chiang, D.Y.; Newell, P.; Peix, J.; Thung, S.; Alsinet, C.; Tovar, V.; Roayaie, S.; Minguez, B.; Sole, M.; *et al*. Pivotal role of mTOR signaling in hepatocellular carcinoma. *Gastroenterology* **2008**, *135*, 1972–1983. [CrossRef] [PubMed]
122. Decaens, T.; Luciani, A.; Itti, E.; Hulin, A.; Roudot-Thoraval, F.; Laurent, A.; Zafrani, E.S.; Mallat, A.; Duvoux, C. Phase II study of sirolimus in treatment-naive patients with advanced hepatocellular carcinoma. *Dig. Liver Dis.* **2012**, *44*, 610–616. [CrossRef] [PubMed]
123. Toso, C.; Merani, S.; Bigam, D.L.; Shapiro, A.M.; Kneteman, N.M. Sirolimus-based immunosuppression is associated with increased survival after liver transplantation for hepatocellular carcinoma. *Hepatology* **2010**, *51*, 1237–1243. [CrossRef] [PubMed]
124. Huynh, H.; Chow, K.H.; Soo, K.C.; Toh, H.C.; Choo, S.P.; Foo, K.F.; Poon, D.; Ngo, V.C.; Tran, E. RAD001 (everolimus) inhibits tumour growth in xenograft models of human hepatocellular carcinoma. *J. Cell. Mol. Med.* **2009**, *13*, 1371–1380. [CrossRef] [PubMed]
125. Zhu, A.X.; Kudo, M.; Assenat, E.; Cattan, S.; Kang, Y.K.; Lim, H.Y.; Poon, R.T.; Blanc, J.F.; Vogel, A.; Chen, C.L.; *et al*. Effect of everolimus on survival in advanced hepatocellular carcinoma after failure of sorafenib: The EVOLVE-1 randomized clinical trial. *JAMA* **2014**, *312*, 57–67. [CrossRef] [PubMed]
126. Thomas, H.E.; Mercer, C.A.; Carnevalli, L.S.; Park, J.; Andersen, J.B.; Conner, E.A.; Tanaka, K.; Matsutani, T.; Iwanami, A.; Aronow, B.J.; *et al*. mTOR inhibitors synergize on regression, reversal of gene expression, and autophagy in hepatocellular carcinoma. *Sci. Transl. Med.* **2012**, *4*, 139ra184. [CrossRef]
127. Egan, D.F.; Chun, M.G.; Vamos, M.; Zou, H.; Rong, J.; Miller, C.J.; Lou, H.J.; Raveendra-Panickar, D.; Yang, C.C.; Sheffler, D.J.; *et al*. Small Molecule Inhibition of the Autophagy Kinase ULK1 and Identification of ULK1 Substrates. *Mol. Cell* **2015**, *59*, 285–297. [PubMed]

128. Llovet, J.M.; Ricci, S.; Mazzaferro, V.; Hilgard, P.; Gane, E.; Blanc, J.F.; de Oliveira, A.C.; Santoro, A.; Raoul, J.L.; Forner, A.; *et al*. Sorafenib in advanced hepatocellular carcinoma. *N. Engl. J. Med.* **2008**, *359*, 378–390. [PubMed]
129. Cheng, A.L.; Kang, Y.K.; Chen, Z.; Tsao, C.J.; Qin, S.; Kim, J.S.; Luo, R.; Feng, J.; Ye, S.; Yang, T.S.; *et al*. Efficacy and safety of sorafenib in patients in the Asia-Pacific region with advanced hepatocellular carcinoma: A phase III randomised, double-blind, placebo-controlled trial. *Lancet Oncol.* **2009**, *10*, 25–34. [CrossRef]
130. Gauthier, A.; Ho, M. Role of sorafenib in the treatment of advanced hepatocellular carcinoma: An update. *Hepatol. Res.* **2013**, *43*, 147–154. [CrossRef] [PubMed]
131. Manov, I.; Pollak, Y.; Broneshter, R.; Iancu, T.C. Inhibition of doxorubicin-induced autophagy in hepatocellular carcinoma Hep3B cells by sorafenib—The role of extracellular signal-regulated kinase counteraction. *FEBS J.* **2011**, *278*, 3494–3507. [CrossRef] [PubMed]



© 2015 by the authors; licensee MDPI, Basel, Switzerland. This article is an open access article distributed under the terms and conditions of the Creative Commons by Attribution (CC-BY) license (http://creativecommons.org/licenses/by/4.0/).

International Journal of
Molecular Sciences

MDPI

Review

Therapeutic Implications for Overcoming Radiation Resistance in Cancer Therapy

Byeong Mo Kim [1], Yunkyung Hong [2,3,4], Seunghoon Lee [2,3,4], Pengda Liu [5], Ji Hong Lim [6], Yong Heon Lee [7], Tae Ho Lee [8], Kyu Tae Chang [9,*] and Yonggeun Hong [2,3,4,10,*]

Received: 31 August 2015 ; Accepted: 29 October 2015 ; Published: 10 November 2015
Academic Editor: William Chi-shing Cho

1 Severance Integrative Research Institute for Cerebral & Cardiovascular Diseases (SIRIC), Yonsei University College of Medicine, Seoul 03722, Korea; bkimtwo@gmail.com
2 Department of Physical Therapy, College of Biomedical Science & Engineering, Inje University, Gimhae 50834, Korea; dangmoo777@naver.com (Y.H.); stormyboy@nate.com (S.L.)
3 Biohealth Products Research Center (BPRC), Inje University, Gimhae 50834, Korea
4 Ubiquitous Healthcare & Anti-aging Research Center (u-HARC), Inje University, Gimhae 50834, Korea
5 Department of Pathology, Beth Israel Deaconess Medical Center, Harvard Medical School, Boston, MA 02215, USA; pengdaliu@gmail.com
6 Department of Biomedical Chemistry, College of Biomedical and Health Science, Konkuk University, Chungju 380-701, Korea; jhlim@kku.ac.kr
7 Department of Biomedical Laboratory Science, Dongseo University, Busan 617-716, Korea; yhlee@gdsu.dongseo.ac.kr
8 Division of Gerontology, Department of Medicine, Beth Israel Deaconess Medical Center, Harvard Medical School, Boston, MA 02215, USA; tlee3@bidmc.harvard.edu
9 National Primate Research Center (NPRC), Korea Research Institute of Bioscience and Biotechnology (KRIBB), Ochang 28116, Korea
10 Department of Rehabilitation Science, Graduate School of Inje University, Gimhae 50834, Korea
* Correspondence: changkt@kribb.re.kr (K.T.C.); yonghong@inje.ac.kr (Y.H.); Tel.: +82-43-240-6300 (K.T.C.); +82-55-320-3681 (Y.H.); Fax: +82-43-240-6309 (K.T.C.); +82-55-329-1678 (Y.H.)

Abstract: Ionizing radiation (IR), such as X-rays and gamma (γ)-rays, mediates various forms of cancer cell death such as apoptosis, necrosis, autophagy, mitotic catastrophe, and senescence. Among them, apoptosis and mitotic catastrophe are the main mechanisms of IR action. DNA damage and genomic instability contribute to IR-induced cancer cell death. Although IR therapy may be curative in a number of cancer types, the resistance of cancer cells to radiation remains a major therapeutic problem. In this review, we describe the morphological and molecular aspects of various IR-induced types of cell death. We also discuss cytogenetic variations representative of IR-induced DNA damage and genomic instability. Most importantly, we focus on several pathways and their associated marker proteins responsible for cancer resistance and its therapeutic implications in terms of cancer cell death of various types and characteristics. Finally, we propose radiation-sensitization strategies, such as the modification of fractionation, inflammation, and hypoxia and the combined treatment, that can counteract the resistance of tumors to IR.

Keywords: cancer therapy; ionizing radiation (IR); resistance; cell death; DNA damage; prognostic markers; therapeutic targets

1. Introduction

Radiation therapy is a useful cancer treatment strategy and is a highly cost-effective single-modality treatment. Radiation therapy uses high doses of radiation to destroy or slow tumor growth. Ionizing radiation (IR), such as X-rays and gamma (γ)-rays, is usually used for cancer treatment because it can pass through tissue, break chemical bonds, and remove electrons from atoms

to become ionized. The resulting ions can kill or cause serious damage to cancer cells. IR does not kill cancer cells immediately; a significant period of treatment time is required before a large number of cancer cells start to be killed. IR can also lessen or ease problems and symptoms caused by a growing tumor. IR may be given before, during, or after surgery or chemotherapies to enhance the effectiveness of these therapies. IR exposure may be external or internal. External beam radiation therapies, such as X-rays and γ-rays, involve the targeting of radiation at the cancer in a specific part of the body. Internal radiation therapies based on the use of electrons, protons, neutrons, carbon ions, α particles, or β particles are treatments in which a source of radiation, either solid or liquid, is placed inside the body.

The biological effectiveness of IR in killing cancer cells depends on the type of radiation, total dose, fractionation rate, and the targeted organs [1]. Although radiotherapy is an effective cancer treatment, a large portion of patients subsequently experience radioresistance and recurrence of their cancers. Whereas IR alone can be somewhat effective for the treatment of some cancers such as larynx cancer, non-small-cell lung cancer, skin cancer, prostate cancer, cervical cancer, head and neck carcinomas, and lymphomas, it is not effective against other cancers such as breast cancer, bladder cancer, glioblastoma, soft tissue carcinoma, and advanced non-small-cell lung cancer possibly due to the intrinsic radioresistance of cancer cells [2]. IR therapy in combination with other modalities shows promise in the treatment of these radio-resistant cancers. In this review, we will discuss cellular and molecular mechanisms (signaling pathways) of radioresistance in terms of various types of cell death and cytogenetic variations. We will also evaluate strategies to overcome radioresistance during cancer treatment.

2. IR-Induced Cell Death Outcomes

IR therapy, like other types of anticancer treatments, may induce multiple forms of cancer cell death through a variety of molecular mechanisms. Several modes of cell killing, such as apoptosis, necrosis, autophagy, mitotic catastrophe, and senescence, occur after exposure to IR (Figure 1).

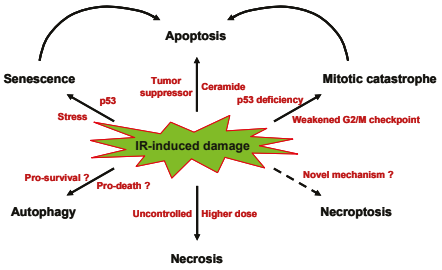

Figure 1. Various modes of cancer cell death induced by IR. Apoptosis and mitotic catastrophe are major forms of cell death induced by IR. Tumor suppressor proteins such as p53 and tumor suppressor lipids such as ceramide promote IR-induced apoptosis. Mitotic catastrophe occurs from premature or inappropriate entry of cells into mitosis caused by irradiation. A p53 mutation can make the cancer cells susceptible to premature mitosis. Furthermore, the loss of the p53-mediated arm of the G2/M checkpoint leads to mitotic catastrophe in cancer cells following exposure to IR. Mitotic catastrophe results from aberrant mitosis and eventually causes cell death through apoptosis or necrosis. Necrosis is an uncontrolled mode of cell death caused by rapid and severe impairment. Even though necrosis is seen less frequently following IR treatment, it does occur after receiving higher doses of IR. Autophagy has a dual role in response to cancer cells to IR; it causes cancer cell survival or death depending on the specific context (pro-survival or pro-death?). Senescence occurs in cancer cells following IR-caused DNA damage and involves p53-mediated cell cycle arrest. Senescent cells later die, typically through apoptosis. Stress-induced premature senescence usually occurs in p53-proficient cells. Necroptosis is a programmed form of necrosis. Although there is evidence that necroptosis is involved in IR-induced cancer cell death, the role of this type of death is a very inchoate area of research (novel mechanism of IR-induced cell death?).

2.1. Apoptosis

Apoptosis, type I programmed cell death, is a prevalent form of cell death underlying radiation therapy. Apoptosis is characterized by a series of distinctive morphological features including cell shrinkage, membrane blebbing, chromatin condensation, DNA fragmentation, and the resultant formation of apoptotic bodies in which the cellular membrane remains intact. Among a spectrum of cellular components, DNA is the main target of IR. Damaged DNA triggers signal transduction pathways involved in cell cycle arrest and apoptosis. DNA damage monitoring and signaling systems are responsible for cell cycle arrest and checkpoint, and failure of these controls leads to cell death. Second messengers such as ceramide and free radicals can also mediate IR-induced apoptosis [3].

Various factors are involved in IR-induced apoptosis. Poly(ADP-ribose) polymerase (PARP), DNA-dependent protein kinase (DNA-PK), p53, and ataxia-telangiectasia-mutated (ATM) play a role in DNA damage signaling. First, in response to IR-induced DNA damage, especially DNA strand breaks, PARP detects and binds to DNA strand breaks, resulting in quantitative synthesis of a poly(ADP-ribose) chain as a signal for the other DNA-repairing enzymes [4]. A transient and extensive poly(ADP-ribosyl)ation of nuclear proteins occurs early during apoptosis, prior to the commitment of cell death [5]. Several animal studies indicate that PARP is involved in survival responses against IR [6–10]. DNA–PK, a nuclear serine–threonine protein kinase, is a member of the phosphatidylinositol-3 kinase (PI3K) family. The DNA–PK catalytic subunit (DNA–PKcs) forms foci in response to IR and is upregulated in radiation-resistant tumors or in tumors with poor survival rates [11,12]. The deficiency of DNA–PKcs increases IR-induced genomic instability [13]. p53 plays a major role in the cellular response to IR by regulating the transcriptional activation of a number of downstream target genes, such as p21, GADD45, 14-3-3, bax, and Mdm2. ATM functions upstream of p53 by phosphorylating Ser15 and stabilizing p53 [14,15]. ATM is involved in the G1/S cell cycle checkpoint arrest following DNA damage through p53 accumulation and the p53-mediated induction of p21 and, at the G2 checkpoint, through the phosphorylation of the Chk2 protein [14–18]. ATM/ataxia-telangiectasia-related (ATR)-Chk1/2-CDC25 also participates in the G2 checkpoint.

If cellular damage is too severe to be repaired, the cell undergoes apoptosis. Caspase promotes the degradation of key cellular components during apoptosis. Interestingly, caspases also cleave many of the DNA damage repair enzymes to prevent unpromising cellular DNA repair and force apoptosis. A role for the Rb protein in decision-making at the interface between cell cycle and apoptosis has been identified [19,20]. The loss of Rb function leads to increased apoptosis largely by the liberation of the free E2F cell cycle regulator. Hypophosphorylated Rb also triggers apoptosis and then is cleaved by caspases [21,22]. p53-Dependent apoptosis is an important mechanism by which tumor growth and progression is inhibited. The transcriptional induction of Bax appears to be a key feature of this p53-mediated apoptosis [23]. p53 also has a transcription-independent role in apoptosis through its interaction with Bax, which promotes its activation as well as its insertion into the mitochondrial membrane [24,25]. The Bax-independent pathway, which involves protein kinase A, is another mechanism of p53-dependent apoptosis [26]. The roles of p53-independent pathways in IR-induced apoptosis have also been well documented [27,28]. p53-independent apoptosis is generally detected late relative to p53-dependent apoptosis [29]. Interestingly, both p53-dependent and p53-independent apoptotic responses to IR are functionally active in an ATM-independent fashion [30], indicating that apoptosis does not require increased p53 levels. Mdm2, a p53-specific E3 ubiquitin ligase, has been shown to be dispensable for IR-induced apoptosis [31].

Ceramide is a potent mediator of the initiation of IR-induced apoptosis. Several tumor cells resistant to IR-induced apoptosis show defective ceramide signaling [32,33]. A number of downstream targets for ceramide action against IR, such as ceramide-activated protein kinase (CAPK), ceramide-activated protein phosphatase (CAPP), PKC, Bad, Akt, and JNK, have been identified. Pro-apoptotic ceramide signaling has been shown to be mediated by Bad in COS cells [34]. In contrast, PKC activation attenuates ceramide-induced apoptosis in some cancer cell types [35]. Ceramide also suppresses the kinase activity of Akt [36]. Nonetheless, the most important target for

ceramide action in IR-induced apoptosis seems to be stress-activated protein kinase (SAPK)/c-Jun N-terminal kinase (JNK). IR utilizes JNK for the amplification of mitochondrial apoptotic death in cancer cells, and JNK activation is PI3K- or reactive oxygen species (ROS)-dependent. Ceramide also induces Fas ligand (FasL) expression, and the soluble FasL-activated sphingomyelin pathway has been demonstrated in IR-induced apoptosis [37].

2.2. Necrosis

Necrotic cells are swollen with nuclear vacuolization, protein denaturation/coagulation, and random DNA degradation followed by rupture of cellular membranes. Necrosis has historically been regarded as an uncontrolled, *i.e.*, not genetically regulated, form of cell death. Necrosis is much less common after IR treatment but does occur. The decision as to whether they will undergo apoptosis or necrosis after IR exposure seems to be dose-dependent in some cancer cell types. For example, MG-63 osteosarcoma spheroids die by apoptosis after exposure to 5 Gy IR, while they die by necrosis after exposure to 30 Gy IR [38], suggesting that a much higher dose of IR triggers necrotic cell death.

2.3. Autophagy

Cells undergoing autophagy, a form of type II programmed cell death, utilize the autophagic/lysosomal compartment to auto-digest proteins and damaged organelles and to recycle amino and fatty acids. Autophagy is characterized by sequestration of targeted cytoplasmic components and organelles from the rest of the cell within a double-membrane vesicle called the autophagosome. The autophagy pathway is known to be negatively regulated by the PI3K/Akt/mTOR pathway [39]. Hyperactivation of the autophagy pathway contributes to cell death but controlled expression has a pro-survival effect.

Autophagy is a genetically regulated stress response seen in some human cancer cell lines exposed to IR. Compared to apoptosis, autophagic cellular changes are observed after IR in any cell line. Similar to the continuing debate as to whether the induction of autophagy results in cancer suppression or progression, the autophagic response of cancer cells to IR reveals somewhat different effects in terms of radiotherapy. IR treatment induces autophagy in both normal and cancer cells. IR-induced autophagic cell death has been reported in malignant glioma, breast, and prostate cancer cells [40]. Some studies suggest that the induction of autophagy might be an advantageous strategy to increase the anticancer effects of radiotherapy and that chemoagent-induced autophagy provokes sensitization of cells to irradiation and increases the anticancer effects of radiotherapy [41,42]. In particular, the considerable susceptibility of glioblastoma cells to IR-induced cell death is due to autophagy rather than to apoptosis. The inhibition of autophagy also tunes the radiosensitization parameters of malignant glioma cells [43]. On the other hand, autophagy has been found to contribute to the IR resistance of some cancer cell types [44,45]. These conflicting effects might be due to the critical role of autophagy for the removal of misfolded/damaged proteins and organelles. Therefore, autophagy seems to play a double-edged role in the balance between survival and death processes depending on the tissue type and the expression profiles of genes and proteins that regulate the apoptosis machinery.

2.4. Mitotic Catastrophe

Mitotic catastrophe or mitotic cell death occurs during aberrant mitosis as a result of aberrant chromosome segregation, leading to formation of giant cells with an aberrant spindle, de-condensed chromatin, and multiple micronuclei. This type of cell death is accompanied by the presence of one or more micronuclei and centrosome overduplication. Together with apoptosis, mitotic catastrophe accounts for the majority of IR-induced cancer cell death. Mitotic catastrophe occurs due to faulty mitosis and causes delayed mitotic-linked cell death that takes place via apoptosis or necrosis. For example, irradiated breast cancer cells die by apoptosis due to delayed cell death associated with mitotic catastrophe after growth arrest [46]. The FasL, TRAIL (TNF-related apoptosis-inducing

ligand), and TNF-α death-inducing signaling pathways mediate mitotic catastrophe in these cancer cells through interactions of their ligands and receptors [47]. In this regard, mitotic catastrophe seems to be an absolute requirement for late-type cell death and accounts for the late apoptosis observed after IR exposure.

Interestingly, mitotic catastrophe can be enhanced by p53 deficiency and a weakened G2/M checkpoint [48,49]. The induction of mitotic catastrophe induced by IR is associated with the increased expression of cyclin B1 and the kinase activity of Cdc2 [50]. G2/M checkpoint disruptors, such as caffeine, okadaic acid, or staurosporine, have been shown to promote IR-induced mitotic catastrophe [51]. Mitotic cell death is also enhanced by inactivating mutations in G2/M checkpoint genes, such as p21 and 14-3-3-σ [49,52]. These findings suggest that IR-induced cellular damage may induce the premature entry of cells into mitosis and that mitotic cell death may be a key contributor to the loss of clonogenic potential in tumor cells and solid tumors exposed to IR, especially those with p53 deficiency.

2.5. Programmed Necrosis

Recently, a programmed/genetically regulated type of necrosis, necroptosis, was identified. Necroptosis, also called programmed necrosis or type III programmed cell death, is caspase-independent and controlled by the receptor-interacting protein 1 and 3 (RIP1/3) kinases [53]. This type of death is a key process in chronic inflammatory diseases, but its role in cancer is largely unclear. Interestingly, recent studies indicate necroptosis to be a novel mechanism of IR-induced death of some endocrine cancer cell types, such as thyroid and adrenocortical carcinoma cells [54].

2.6. Senescence

Senescent cells are viable but non-dividing and undergo irreversible cell cycle arrest, stop DNA synthesis, and become enlarged and flattened with increased granularity. Cellular senescence is a process that results from multiple mechanisms, including telomere shortening, tumor suppressor signals such as p53 and p16INK4A/pRb, and DNA damage. These mechanisms prevent uncontrolled proliferation, and so the cellular senescence can protect cells from developing cancer. Cellular senescence is triggered by a variety of intrinsic and extrinsic stresses, including IR. Senescence can occur in cancer cells following IR-induced DNA damage, eventually leading to cell death mainly by apoptosis. Although p53-independent mechanisms have also been described in IR-induced senescence [55,56], a genetically regulated response to IR-induced DNA damage is usually seen in solid tumor-derived cell lines, especially those with wild-type p53 [57]. IR-induced senescence is a beneficial mechanism through which IR suppresses tumor cell growth. Indeed, the IR-induced retardation of tumor growth is attributable largely to the induction of senescence, not apoptosis, in some lung cancer cell types [58]. Given that IR-induced senescence can usually be achieved at much lower doses of IR than those required to induce apoptosis and that the reduced dose of IR can help prevent adverse side effects of cancer therapy, other strategies using low-dose IR for cancer therapy deserve much consideration.

Stress-induced premature senescence (SIPS) may greatly affect the efficacy of radiotherapy, and the radiation doses achievable using clinical therapeutic regimens can induce SIPS in specific human tumor cell lines. Irradiated cells undergoing SIPS share many cellular and molecular phenomena with cells undergoing replicative senescence. Although replicative senescence is programmed at times when telomeric DNA ends are exposed, SIPS is not programmed but is instead a response to a given stress [59]. Due to the constitutive activation of telomerase, telomeres are typically stable and replicative senescence is not usually induced in cancer cells. However, many anticancer agents, including IR, can induce SIPS in cancer cells while not affecting telomere lengths. These agents produce double-strand breaks (DSBs), and a common cause of SIPS induction in cancer cells appears to be irreparable DNA breaks.

IR-induced DNA damage can occur both directly and indirectly. Actually, the radiation-induced bystander effect in which irradiated cells transfer damage signals to neighboring unirradiated cancer cells is a big part of IR-mediated damage. There is emerging evidence that the bystander effect has a role in the genomic instability and carcinogenesis. [60]. ROS are important factors in the IR-induced bystander effect [61,62]. Additionally, activated macrophages, nitric oxide (NO), and various cytokines have been implicated in this phenomenon [63].

Although cellular senescence can exert a strong tumor-suppressive effect by arresting the growth of cells permanently at risk of malignant transformation, it can also be harmful to the surrounding microenvironment. The senescence-associated secretory phenotype (SASP) is responsible for these deleterious effects, promoting the senescence-associated pro-inflammatory response and resulting tumor progression [64]. Actually, a senescent cell is not a quiescent cell and adopts an immunogenic phenotype, ultimately leading to the SASP. Senescent cells can exert potential effects on their microenvironment by triggering SASP factors such as soluble signaling factors and proteases. Soluble signaling factors, such as interleukins, inflammatory cytokines, and growth and angiogenic factors, are major components of SASP and can affect neighboring cells. In addition, senescent cells also secrete some proteases such as matrix metalloproteinases (MMPs), contributing to tissue remodeling [65]. Moreover, cells undergoing senescence increase the expression of extracellular insoluble molecules such as fibronectin [66]. Fibronectin exerts multiple effects on biological processes, including cell adhesion, survival, growth, differentiation, and migration. Additionally, senescent cells may also exert effects on the tissue microenvironment through the secretion of molecules other than proteins. Together, these SASP components secreted from senescent cells can modify neighboring cells and microenvironment by altering cell-surface receptor signal transduction.

However, SASP is also known to contribute senescence reinforcement in damaged cells. In fact, even a low dose of IR induces SIPS, and these premature cells overexpress several SASP proteins. Some studies suggest that the IR-induced increase in secretory inflammatory signals might contribute to the development of IR-induced damage and premature senescence [67]. Therefore, the secretory program triggered by IR-induced DNA damage can be a critical determinant of the response of tumors to radiotherapy (the sensitivity or resistance to IR) by modifying the tumor microenvironment and its interaction with tumor cells.

3. Genomic Instability and Cytogenetic Alterations Induced by IR

One of the potent ways in which IR works is through damaging the DNA of exposed tumor tissue, leading to cell death. IR triggers DNA damage in cells both directly and indirectly. The direct effect occurs when the radiation interacts with the DNA molecule itself, while indirect DNA damage is caused by radiolytic products like free radicals that are highly reactive due to the presence of unpaired electrons. IR simultaneously produces various types of lesions, such as base modifications, alkali-labile sites, DNA–DNA intra- and inter-strand crosslinks, DNA–protein crosslinks, single-strand breaks (SSBs), and double-strand breaks (DSBs). These lesions are efficiently detected and repaired by different mechanisms (Figure 2).

3.1. Base Damage

IR irradiates and exerts damaging action on free bases, nucleosides, and nucleotides in DNA. IR-induced modifications of bases affect the DNA structure by distorting the DNA double helix. In general, the damaged bases have a minor role in IR-induced cytotoxicity and can be repaired easily through base excision repair (BER) or nucleotide excision repair (NER), with the help of an undamaged template strand and repair enzymes. DNA glycosylases excise the damaged base to generate abasic (AP) sites which are further processed by an AP endonuclease. Although polymerase β is important in the repair of oxidized bases in *in vitro* studies, IR-induced base damage is repaired primarily by the DNA polymerase β-independent long-patch subpathway [68].

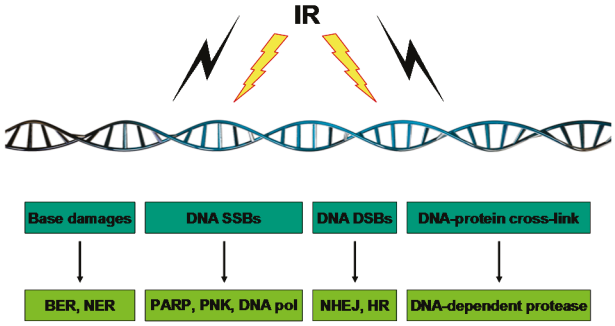

Figure 2. Different types of repairs fix different types of DNA damage caused by IR. Through direct effects involving the deposition of ionizing energy in the DNA itself or indirect effects involving the absorption of ionizing energy by water, leading to the production of water radicals and their subsequent reaction with DNA, IR induces several types of damage to DNA. While IR induces a variety of DNA damages, the DNA DSB is a main lesion responsible for the aimed cancer-cell killing in radiotherapy. DNA repair machineries in response to different types of IR-triggered DNA damage are illustrated.

3.2. DNA SSBs

High-energy IR can disrupt the sugar phosphate backbone, causing either SSBs or DSBs. SSBs are discontinuities or nicks in the deoxyribose backbone of one of the DNA double helixes and are usually accompanied by the loss of a single nucleotide at the site of the break. SSBs arise either directly from damage on the deoxyribose or indirectly as normal intermediates of DNA BER. SSB repair is performed by the serial actions of PARP, polynucleotide kinase (PNK), DNA polymerase, and DNA ligase. XRCC1 also plays an important role in SSB repair by stimulating the activity of PNK at damaged DNA termini [69]. DNA polymerase fills the gap and the remaining nick is then sealed by DNA ligase. Both PARP and XRCC1 mutant cells exhibit an enhanced sensitivity to IR [70,71]. Although DNA polymerase β does not seem to affect radioresistance, it has been shown to contribute to SSB repair through its interaction with XRCC1 [72].

3.3. DNA DSBs

DSBs are breaks in the phosphodiester backbone of both strands of the DNA separated by ~10 base pairs or fewer. Unlike SSBs, DSBs are highly toxic, irreparable, and more responsible for a great part of the killing of cancer cells as well as surrounding normal cells because they lead to the large-scale loss or rearrangement of genetic materials during replication and mitosis. Hence, DSBs are the most deleterious lesion produced by IR.

In mammalian cells, DSBs are repaired primarily by the following two mechanisms: non-homologous end-joining (NHEJ) and homologous recombination (HR). The balance between NHEJ and HR is highly regulated, and the choice between these two mechanisms is affected by the chemical complexity of the breaks, chromatin conformation, and the cell cycle.

Simple and primary DSBs are likely repaired by NHEJ. NHEJ starts with the binding of the Ku70/Ku80 heterodimer to the DSB termini, followed by the recruitment and activation of DNA–PK. Incompatible ends are trimmed by nucleases. The ligation complex, which consists of DNA ligase IV, X-ray cross-complementation group 4 (XRCC4), and Xrcc4 like factor (XLF), seals the break. NHEJ is the primary method of repairing breaks due to IR because DSBs produced in euchromatin are repaired mainly by NHEJ throughout the cell cycle [73,74]. HR provides greater repair fidelity than NHEJ [75].

DSBs in heterochromatin are processed mainly by HR mechanisms [76]. In the HR pathway, the MRN (Mre11/RAD50/Nbs1) complex recognizes and binds to DSB ends and subsequently recruits and activates ATM to initiate HR. CtIP (CtBP-interacting protein) is also critical for HR-mediated DSB repair. MRN–CtIP–complex is important for facilitating the DNA resection at the DSB to

generate 3′-single-stranded DNA (ssDNA). The ssDNA tail is first coated by replication protein A (RPA), which is subsequently replaced by Rad51 to form a RAD51–ssDNA nucleofilament. This nucleofilament searches for the homologous sequence elsewhere in the genome and mediates DNA strand invasion. RAD51-mediated DNA strand invasion forming a displacement loop (D-loop) can establish a replication fork with a Holiday junction. HR is mostly involved in the repair of clustered and secondary DSBs that occur later after IR during S and G2 phases when the replication fork collapses at unresolved single-strand DNA lesions and the sister chromatids are available to allow recombination processing.

In addition to the formation of radiation-induced prompt DSBs, replication-mediated DSBs are also formed after ionizing radiation [77]. Replication-mediated DSBs, which are chemically distinct from prompt DSBs, are formed when unrepaired non-DSB clustered damage sites meet replication forks to produce replication-mediated DSBs, which require HR for their repair.

3.4. DNA–Protein Crosslinks

DNA–protein crosslinks are covalent bonds and biologically active nucleoprotein complexes formed between one strand of DNA and proteins. The crosslinking of DNA to nuclear proteins can impair many cellular processes such as DNA replication, transcription, and repair. DNA–protein crosslinks are induced linearly with γ-rays doses at a frequency of ~150 Gy [78]. At high doses of more than 200 Gy, the number of crosslinks approaches a plateau value corresponding to the number of sites at which DNA attaches to the nuclear matrix [79]. Free-radical formation is believed to be primarily responsible for the production of DNA–protein crosslinks. The role of this crosslinking in response to IR is generally not well defined, although some evidence suggests that it does not play a major role in IR-induced cell killing [80].

4. Resistance Pathway

IR is effective for the treatment of many cancer types; however, in some patients a few tumors become resistant to radiation, making radiotherapy less effective. Resistance to radiation therapy remains a major clinical problem, leading to a poor outcome for cancer patients. Several specific signaling pathways contribute to cellular resistance against IR (Figure 3). Below we review the molecular signaling pathways associated with resistance to IR.

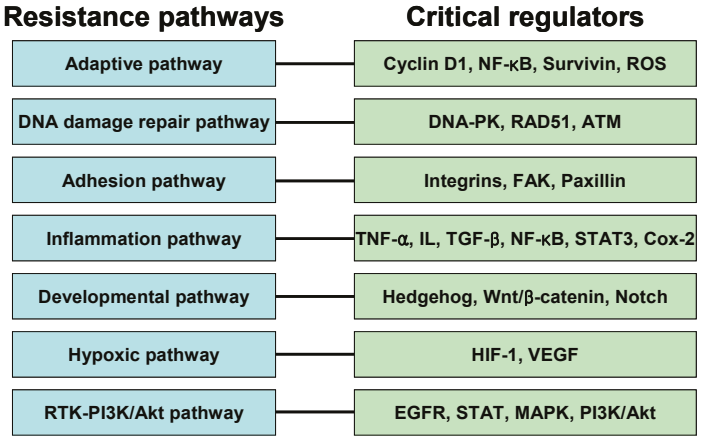

Figure 3. Mechanisms of resistance against radiotherapy. Various signaling pathways may contribute to radiation resistance mechanisms in cancer cells. Resistance against IR may be intrinsic or acquired. The roles of some important regulators in each resistance mechanism have been described.

4.1. Adaptive Pathway

The recent development of precise radiation delivery techniques increases the efficacy of radiotherapy for cancer treatment. However, when malignant tumor cells recur after radiation treatment, they may acquire a resistance to additional radiotherapy. The use of low-dose IR for radioadaptive protection is known to be efficacious because cells exposed earlier to a lower inducing radiation dose have reduced sensitivity to a higher challenge dose. The exposure of mammalian cells to low-dose IR results in beneficial effects in terms of maintenance of genomic integrity and ability to repair damaged DNA [81,82]. Mitochondria are key sources of ROS as by-products of aerobic metabolism, and induced ROS production is counteracted by mitochondrial enzymatic antioxidant systems. Given that IR treatment significantly upregulates the most powerful antioxidant, manganese-containing superoxide dismutase (Mn–SOD) [83], and that the low-dose IR-induced adaptive response is linked to alterations in the mitochondrial protein import [84], mitochondrial signaling (particularly during apoptosis) seems to be implicated in the adaptive response to IR. As described below, several pro-survival signaling pathways are involved in radioadaptive resistance.

Cyclins bind and activate cyclin-dependent kinases (CDKs), important regulators of the cell cycle. A fluctuation in cyclin expression and the resultant oscillation in CDK activity drives the mitosis. Induced cyclin D1 interacts with CDK4 or CDK6 and activates its kinase activity, which is required for G1/S cell cycle progression [85]. Cyclin D1–CDK4/6 complex has also been shown to phosphorylates and it inactivates tumor suppressor protein Rb whose inhibition induces the expression of several genes involved in S phase progression [86]. This protein is frequently overexpressed in a variety of tumors and contributes to tumor therapy resistance and a poor prognosis in cancer patients [87–89]. The enforced translocation of cyclin D1–CDK4/6 from cytosol to nucleus triggers apoptosis [90]. Cyclin D1 also has a function in low-dose IR-induced adaptive radioresistance [91]. Contrary to high-dose IR (e.g., 5-Gy ã-ray) triggering 14-3-3ζ-mediated cyclin D1 nuclear import, low-dose IR (e.g., 10-cGy X-ray) causes a dissociation of the cyclin D1/14-3-3ζ complex and cytosolic accumulation of cyclin D1, indicating that increased cytosolic cyclin D1 expression is required for the low-dose IR-induced adaptive response. Free and increased cyclin D1 protects cells from high-dose IR-induced apoptosis by binding to and inhibiting the action of Bax, suggesting that low-dose IR-induced accumulation of cytosolic cyclin D1 protein plays an important role in suppressing mitochondrial apoptosis in the IR-induced adaptive resistance.

The Rel/NF-kappaB (NF-κB) protein comprises a family of highly regulated dimeric transcription factors that are implicated in the control of diverse cellular functions, such as the stress response, inflammation, cellular growth, and programmed cell death. The high basal NF-κB activity confers the resistance of certain cancers to chemotherapy and radiotherapy [92,93]. Several studies show that the fractional IR triggers NF-κB activation and clonogenic survival [94], indicating that the activation of NF-κB is required for the induction of radioadaptive resistance following exposure to a radiation dose equivalent to that used medically for diagnostic purposes. The IR-mediated induction of cytokines (e.g., TNF-α), MEK/ERK pathways, and ATM is involved in NF-κB activation. IR treatment also induces a variety of NF-κB target proteins that may be responsible for tumor radioresistance. For example, cyclin B1 is responsible for radioadaptive resistance induced by chronic exposure to fractionated IR [95]. A recent study also indicates that the non-canonical NF-κB pathway component RelB regulates Mn-SOD and the resistance to IR of prostate cancer cells [96], suggesting that, as well as the canonical pathway, the non-canonical pathway is important for radiation resistance.

Survivin, a member of the inhibitor of apoptosis (IAP) family, functions to prevent caspase activation and inhibit apoptosis. Survivin has also been implicated in many adaptive responses to cellular stress, acting as an important factor in tumor cell resistance [97]. The low-dose IR induces the elevation of survivin levels and the reduction of apoptosis [97]. The knockdown of survivin induces the loss of the adaptive response, and the survivin-mediated adaptive response

has the potential to affect outcomes if induced regularly throughout a course of radiation therapy. A small increase in survival, each day of treatment, induced through exposure to a very low dose of radiation can lead to persistent induction and maintenance of the survivin-mediated adaptive response. Because survivin is overexpressed in malignant cells and can be elevated by both high and very low doses of IR, it is recognized as an important risk factor associated with adverse outcomes in radiotherapy. The survivin-mediated radioadaptive response is dependent upon the ability of cells to activate NF-κB [98].

ROS, which seem to be transiently produced in response to IR, contribute importantly to the cytotoxic effect of IR. Free radicals produced upon IR treatment are the primary source of ROS and reactive nitrogen species (RNS). However, ROS also participate in the cellular signaling processes that lead to an adaptive response that reduces the effectiveness of radiation therapy [99]. ROS generated by IR not only serve to trigger oxidative stress but also contribute to TRAF-mediated NF-κB activation. The NF-κB-mediated anti-apoptotic gene transcription provides enhanced cell survival upon re-exposure of irradiated cells to IR. Antioxidant defense mechanisms, including various antioxidant enzymes, are regulated by NF-κB and prevent tissue damage and ROS-related complications. These antioxidant enzymes, including SOD, catalase, and glutathione peroxidase, have enzymatic ROS-scavenging systems. Peroxiredoxins (Prxs), members of a family of peroxidases, play crucial roles in maintaining redox balance, thereby reducing peroxide-induced redox damage. Peroxiredoxin II (PrxII) is induced by oxidative stress and plays an important role in antioxidant defense by modulating ROS/RNS regulating networks [100,101]. PrxII is significantly upregulated in radioresistant cancer cells, and this upregulation is related to the radioresistant phenotype [102], suggesting that Prx confers radioresistance by eliminating the IR-induced ROS. Therefore, PrxII is likely one of the key players in the protection against oxidative stimuli and in the increased resistance of cancer cells to IR.

4.2. DNA Damage Repair Pathway

Although IR is by far the most common therapy for glioblastoma, the most aggressive brain cancer, standard radiotherapy has only limited effectiveness due to its radioresistance. Glioma stem cells confer radioresistance by eliciting DNA damage checkpoint signal transduction and a highly efficient DNA repair system. Deficiency in DNA repair pathways may alter the IR resistance of glioblastomas.

DNA-dependent protein kinase (DNA–PK) plays a central role in the repair of IR-induced DSBs [103], and its deficiency has been implicated in IR sensitivity in glioblastoma cells [104]. DNA-PK, a nuclear serine/threonine protein kinase, phosphorylates several transcription factors and is responsible for DNA repair, cell cycle arrest, apoptosis, and so on. It is a trimeric enzyme consisting of a large catalytic subunit (DNA–PKcs) and heterodimer DNA-binding complex, which comprises 70 (Ku70) and 80 (Ku80) kDa subunits. When a DSB is introduced, the Ku heterodimer binds to the DSB ends, and it then recruits DNA–PKcs. Although the exact mechanism by which the Ku/DNA complex activates the kinase activity of DNA–PKcs is unclear, the conformational change in DNA–PKcs that occurs upon association with the Ku/DNA complex may account for the activation of kinase activity. Because the expression of a kinase-dead mutant of DNA-PKcs fails to confer the radioresistant phenotype in a DNA–PKcs-deficient mammalian cell line [103], the kinase activity of DNA–PK is believed to be needed for DNA repair. In particular, DNA–PK plays a key role in NHEJ and has the structural and regulatory functions of being activated by DSBs and mediating DSB end-joining [105].

In humans, RAD51 acts as a key facilitator of the HR DSB repair pathway [106,107]. Its overexpression is observed in many tumors and is linked to increased radioresistance and poor outcomes [108]. RAD51-related radioresistance is likely to be affected by p53 status because p53 negatively regulates RAD51 expression [108] and is the most frequently mutated gene in human

cancers. Several reports suggest that HR and high levels of RAD51 are positively correlated and that RAD51 overexpression increases HR [106–108].

PARP is intimately involved in the early stages of DNA damage responses, together with other DNA damage sensors, such as DNA–PK, ATM, and ATR. It recognizes and binds to DNA strand breaks [109] and transfers ADP ribose groups from NAD^+ to target nuclear proteins, mainly itself [110]. Upon the PAR polymer formations, the poly(ADP-ribose) glycohydrolase (PARG) enzyme catalyzes the hydrolysis of PAR, permitting access of the DNA repair machinery to the lesion [4,111]. PARP has been shown to play a role in both SSB and DSB repair pathways. PARP is a central regulator in BER and participates in SSB repair. Although the mechanisms by which PARP contributes to NHEJ and HR are not as well defined as in BER and SSB repair, PARP has been shown to interact with DSB repair proteins such as NBS1, Mre11, Ku80, DNA–PKcs, and ATM [112–115]. Given that IR significantly induces PARP and levels of PARP are higher in tumors [116,117], PARP might be useful therapeutic target in radiotherapy. The BRCA1 tumor suppressor protein repairs damaged DNA and, therefore, ensures the stability of the cell's genetic materials. BRCA1 relocates to DNA damage sites, colocalizes with RAD51, and forms nuclear RAD51 foci in response to IR-induced DNA DSBs [118]. BRCA1 participates in both NHEJ and HR repair process. BRCA1 binds to the MRN complex [119] and suppresses the exonuclease activity of MRE11 [120]. It is also involved in ATM-mediated phosphorylation of NBS1 after DNA damage [121]. The formation of BRCA1-PALB2-BRCA2 complex is essential for RAD51-dependent HR repair [122,123]. Interestingly, potent PARP inhibitors have cytotoxic effects on BRCA1- and BRCA2-deficient cells, including tumor cells [124,125], suggesting that PARP inhibitors can be promising therapeutic agents for cancer with disruption of BRCA genes.

One of the apical activators of DNA damage response is the ATM kinase. Mutation in this gene is associated with ataxia telangiectasia, an autosomal recessive disorder. ATM may regulate radiosensitivity in that ataxia telangiectasia patients are hypersensitive to radiotherapy. The radiosensitizing effects of nonspecific inhibitors, such as caffeine, and highly selective ATM inhibitors, such as KU55933 and CP466722, have also been documented [126].

While IR induces a variety of DNA lesions, including base damage and SSBs, DSBs are widely considered to be the main contributors to IR-induced cell killing through the induction of chromosomal aberrations. Therefore, the pathways for the processing of DSB represent a major mechanism of radiation resistance in tumor cells. The two different cellular pathways contribute to DSB repair and genome integrity in higher eukaryotes: NHEJ, which can be subdivided into DNA–PK-dependent NHEJ, alternative/backup NHEJ, and HR. Normal and cancer cells utilize the DNA–PK-dependent NHEJ pathway extensively to remove DSBs from their genome. Alternative/backup NHEJs, like DNA–PK-dependent NHEJ, are active in all four stages of the cell cycle, but their activity is significantly enhanced during S and G2, probably because the DNA end-resection step occurs primarily in these cell cycle phases [127]. The HR pathway requires sequence information present on intact DNA strands to remove DSBs and to faithfully restore genomic integrity. One form of HR utilizes the sister chromatid as the information donor and is therefore restricted to the late S and G2 phases. Therefore, HR, like alternative NHEJ, regulates DNA damage repair in a cell cycle-dependent manner. The HR pathway is aberrantly expressed in many tumors, and tumor radioresistance, poor prognosis, and increased HR activity are correlated [127], indicating that this pathway is an ideal target for therapeutic intervention in radiotherapy. Therefore, targeting the DNA damage checkpoint response and repair pathways in cancer cells (or cancer stem cells) may offer potential therapeutic advantages to overcome radioresistance.

4.3. Adhesion Pathway

Cell adhesion influences cell survival, preventing cell death through multiple mechanisms. The adhesion of cells to the extracellular matrix (ECM) as well as to other cells can regulate various cellular processes, and has been implicated in the development of radioresistance. Especially, cell

adhesion to ECM protein fibronectin modulates radiation-induced G2/M arrest and increases resistance to IR. Adhesion, migration, and invasion of the surrounding ECM by cancer cells are mediated predominantly by cell surface receptors, including integrins and other associated adhesion molecules.

Integrins are transmembrane receptors that are the bridges for the interactions between cell and cell or cell and ECM, and are involved in cell adhesion in many cellular processes, including immune defense, embryogenesis, wound healing, and metastasis. Resistance to radiotherapy is modulated by the interaction between the ECM and integrins. Integrins modulate the cellular response to IR and decrease IR-induced cancer cell death [128,129]. Some studies indicate that integrins and type 1 insulin-like growth factor receptor (IGF-1R) may play a concerted role in the radioresistance of cancer cells [130–133]. Integrins are heterodimeric proteins comprising á and β subunits, and at least 18 á and 8 β subunits have been described in mammals. Among the various integrin units, β_1 integrins are associated with very late antigen receptors and conjoin with the $á_3$ subunit to create the á3β1 complex, which reacts to netrin-1 and reelin. β_1 integrins, whose expression is tightly regulated by IGF-1R, are believed to mediate resistance to IR through inhibition of JNK activation [133]. Likewise, β_1 downregulation or inhibition plays an important role in increasing cancer cell sensitivity to radiotherapy [133], implying a therapeutic strategy. However, the role of JNK activation in radioresistance is somewhat controversial given that β_1-mediated signaling through the FAK/cortactin/JNK pathway was recently reported to be associated with radioresistance in head and neck squamous cell carcinoma [134]. Integrin cleavage can also be a sensitizing factor to IR in prostate cancer [135].

Integrins regulate cellular functions through the signaling molecules colocalized in the focal adhesion complex. Focal adhesions and large macromolecular assemblies form structural links between the ECM and the actin cytoskeleton and are important sites for regulatory signal transduction. Focal adhesion kinase (FAK) is a cytoplasmic focal complex-associated tyrosine kinase that is elevated in a variety of human cancers [136]. It triggers the expression of various antiapoptotic proteins. Compared to HL-60 cells, HL-60/FAK cells are highly resistant to IR-induced apoptosis through the activation of the PI3K-Akt pathway and the induction of IAP proteins such as c-IAP-2 and XIAP [137]. FAK overexpression usually prevents IR-induced mitochondria-dependent apoptosis. Paxillin, one of the main focal adhesion proteins of integrin signaling, is a multi-domain adaptor protein that is localized in the focal adhesion complex [138]. To facilitate adhesion, paxillin is phosphorylated and activated by FAK [139]. Mechanistically, interactions of the β_1 integrin with Akt, p130Cas, and paxillin contribute to radiation resistance [140]. Furthermore, the interconnected cytoskeletal network involving ECM, integrins, cytoskeleton, nuclear matrix, and chromatin organization may affect the cancer cell responses to various anticancer agents, including IR.

4.4. Inflammation Pathway

The immune system plays a pivotal role in controlling tumor development, suppression, or progression. Radiotherapy can modulate antitumor immune responses, modifying the tumor and its microenvironment through the activation of cytokine cascades. Cytokines, such as TNF-α, IL-1α, IL-1β, IL-6, and TGF-β, are produced by tumor cells and tumor-infiltrating lymphocytes and can greatly influence cellular radiosensitivity and the onset of tissue complications. For example, IL-6 upregulation is positively linked to radiation resistance while its inhibition enhances the radiation sensitivity of prostate cancer cells [141]. The balance between proinflammatory and anti-inflammatory cytokines is critical in determining the outcome of, and adverse reactions and resistance to, radiation treatment. Cytokines can influence the dose-dependent IR response by their pleiotropic effects, modulating inflammation, invasiveness, and fibrosis. Many factors, including radiation dose, tissue type, and the intrinsic characteristics of tumor cells, can cause the local response to be a pro- or anti-tumor effect after radiation exposure. Total dose and number of fraction applied are likely to be key determinants in the immune response after radiation exposure. A large single dose

of irradiation may produce a more potent immune response than low-dose fractionated radiation. An inflammatory IR response can also favor the invasion of cancer cells, providing a favorable environment for tumor promotion and metastasis. The ability of radiation to increase invasiveness has been reported for pancreatic, rectal, and colon cancer cells [142]. Both IL-8 and IL-6 are involved in the IR inflammatory response and enhance cancer cell invasiveness [142,143]. In addition, IR-induced IL-1β expression can also favor cancer cell invasion [142]. Moreover, some preclinical models suggest that radiation-activated TGF-β can contribute to metastasis, inducing the appearance of mesenchymal characteristics [144].

Radiation-induced transcription factors, such as the NF-κB family and signal transducer and activator of transcription-3 (STAT3), are linked to radioresistance due to the production of a variety of proteins including cyclin D1, VEGF, MMP, and proinflammatory cytokines [145]. Whereas the induced expression of these target genes in response to radiotherapy is responsible for the inducible and/or adaptive radioresistance, constitutively activated NF-κB or STAT3 contributes to intrinsic radioresistance [145]. Upregulation of NF-κB by TNF exposure confers increased radiation resistance to cancer cells. The STAT3-mediated radioresistant phenotype is the result of multiple mechanisms in combination with radiation-induced activation of the Janus-activated kinase (JAK)-STAT pathway [145–147]. Erythropoietin, which plays an important role in the neoplastic transformation and malignant phenotype progression observed in malignancy, induces resistance to IR in human cancer cells in a JAK2-dependent manner [148].

Radiation is also known to induce inflammation through cyclooxygenase-2 (Cox-2) [142]. Cox is necessary for the conversion of arachidonic acid to the family of prostaglandins and its activity in cancer can be directly stimulated by NF-κB after radiation exposure or indirectly by the activity of several cytokines. Cox-2 is overexpressed in various types of cancer [142]. In particular, Cox-2 upregulation is associated with a higher tumor grade and distant metastases in breast cancers [149]. This protein has assumed an important role as a therapeutic target for anticancer and anti-inflammatory therapies. In particular, Cox-2-derived prostaglandins are thought to protect cells from radiation-induced damage, contributing to tumor growth and resistance to radiation therapy. Cox-2 activation via the PI3K/AKt pathway can also induce resistance to radiation in human cancer cells [150]. Collectively, the use of specific inhibitors or drugs that manipulate cytokine pathways should be encouraged to improve radiation therapy because TNF-α, IL-1β, IL-8, IL-6, or TGF-β can influence the response to IR by inducing inflammation, cancer cell invasiveness, and fibrosis in irradiated tissues.

4.5. Developmental Pathway

Although IR represents the optimum non-invasive therapy for many cancers with benefits in terms of overall survival, it may also cause therapy failure due to the presence of cancer stem cells. Cancer stem cells account for only a small part of the bulk tumor, but are the cardinal reason for therapeutic resistance. Developmental pathways, including the Hedgehog, Wnt/β-catenin, and Notch pathways, have long been postulated to play an important role in maintaining cancer stem cells and thereby the cancer itself. Self-renewal pathways are known to contribute to cancer stem cell resistance to IR. IR treatment commonly induces stemness in cancer cells.

The Hedgehog signaling pathway plays a crucial role in development and patterning during mammalian embryogenesis [151–153]. The binding of the Hedgehog ligand to the Patched receptor regulates target genes that are involved in many cellular functions including survival, proliferation, and metastasis. This pathway also affects the maintenance of the cancer stem cell population by exerting pro-proliferative effects in cancer stem cell/stem cell-like populations in many types of cancer [154–156]. Moreover, Hedgehog pathway signaling is upregulated in various cancers [157–159] and is associated with the epithelial-to-mesenchymal transition (EMT) [160,161]. Given that stem cells confer resistance to chemotherapy and radiotherapy, the Hedgehog pathway may have a role in radiotherapy. For example, this pathway modulates radiation therapy resistance in head and neck

cancer [162]. The combination of IR and the Hedgehog pathway inhibitor cyclopamine demonstrates improved tumor cell control both *in vitro* and *in vivo* [162], suggesting an additive benefit over either therapy alone.

In fractionated IR treatment, a small amount of radiation is delivered to the patient at regular intervals over a prolonged period. However, the first fraction of radiation can stimulate the migratory and invasive capacities of the tumor cells, resulting in tumor relapse and metastasis [163,164]. IR treatment can activate multiple signaling pathways in tumor cells, which modulate cellular functions and induce the secretion of cytokines and growth factors, promoting the migration and invasion of various types of cancer cells, including glioblastoma, the most common and lethal brain cancer [163]. The Wnt/β-catenin pathway, especially the canonical pathway, is believed to be important in maintaining the stemness of cancer stem cells and in promoting cellular invasiveness through the regulation of the EMT in many cancers [165]. The Wnt/β-catenin pathway mediates the radioresistance of glioblastoma by promoting invasion [166,167], raising the interesting possibility that invasiveness and radioresistance are phenotypes associated with Wnt/β-catenin signaling. Therefore, targeting radiation-induced invasion can be a promising therapeutic modality for the treatment of cancer.

The Notch signaling pathway plays crucial roles in the control of cell–cell communication, cell fate, and pattern formation [168,169]. The Notch pathway is also involved in stem cell proliferation, differentiation, and apoptosis [170]. The role of the Notch pathway can be either oncogenic or tumor-suppressive in that it functions as an oncoprotein in most human cancers, including lung, colon, cervical, prostate, pancreatic, and head and neck cancer, but acts as a tumor suppressor in skin cancer, hepatoma, and small-cell lung cancer (SCLC) [171–173]. This pathway is often overactivated in a variety of cancers [174], and is believed to be a candidate target for therapies designed to eliminate cancer stem cells. Notch activity in established breast cancer cells is increased in response to radiotherapy [175]. High Notch activity is correlated with radioresistance and poor prognosis in non-small-cell lung cancer (NSCLC) patients [176]. Moreover, cancer stem cells lose their ability to repopulate the tumor after IR treatment when Notch activity is suppressed.

4.6. Hypoxia Pathway

The variety and severity of DNA damage from IR is influenced by the tumor microenvironment. In particular, the molecular oxygen status of a tumor is known to influence the biological effect of IR; cells become radioresistant under hypoxic conditions [177,178]. Many tumors comprise poorly oxygenated hypoxic regions that are radioresistant and this depletion of oxygen results in inefficient formation of DNA strand breaks by IR. Moreover, patients displaying highly hypoxic tumors have a much poorer outcome than those with well-oxygenated tumors.

Hypoxia inducible factor 1 (HIF-1), the critical regulator of cellular responses to hypoxia, has been shown to be involved in hypoxia-related tumor radioresistance [179–181]. HIF-1 modulates the expression of over 100 genes involved in the regulation of proliferation, apoptosis, and angiogenesis. HIF-1 expression levels increase under IR treatment as early as 24 h, and this effect persists for up to one week. After irradiation, when radiosensitive cells are killed and they free up oxygen to be delivered to the previously hypoxic regions, the hypoxic cells undergo reoxygenation. The oxidative stress generated during reoxygenation causes activation of the HIF-1 pathway. Therefore, paradoxically, reoxygenation causes activation of the HIF-1 pathway, which usually responds to low oxygen levels. Due to its critical role in tumor radioresistance, HIF-1 may constitute a therapeutic target for hypoxic tumors.

The interactions among hypoxia, angiogenesis, and radioresistance are well known. Activation of the PI3K/Akt pathway, an important pathway involved in radioresistance, contributes to the increased transcription and expression of HIF-1 [182]. VEGF, a major transcription target of HIF-1 in hypoxic conditions, regulates various endothelial cell functions and induces tumor neovascularization [183,184]. One of the important mechanisms by which inhibition of the

epidermal growth factor receptor (EGFR) enhances tumor oxygenation is the regulation of VEGF. Cooperation between the PTEN mutation and EGFR activation upregulates VEGF even under normoxic conditions through the PI3K/Akt pathway. Tumor cell proliferation and angiogenesis, which may be implicated in radioresistance, require the interaction between EGFR and VEGF and downstream signaling of the PI3K/Akt pathway.

4.7. RTK-PI3K-Akt Pathway

In cancer cells, radiation-induced or constitutive signaling pathways that act through receptor tyrosine kinases (RTKs) are implicated in modulating radioresistance. EGFR, an ErbB family member, is a membrane-spanning tyrosine kinase receptor that plays an important role in regulating tumor cell proliferation, survival, invasion, and angiogenesis. High-level EGFR expression is correlated with radioresistance and poor outcome after radiotherapy in preclinical and clinical studies [185,186]. EGFR exerts prosurvival and pro-proliferation activities through the activation of downstream signaling pathways, including the PI3K/Akt, STAT, and Ras–Raf–MAPK [187–189]. Among them, the PI3K/Akt pathway is a key downstream survival pathway activated in cancer cells. The Akt serine/threonine protein kinase, a central kinase downstream of PI3K, is involved in different aspects of cellular regulation, such as cell growth, proliferation, survival, migration/invasion, metastasis, angiogenesis, and metabolism.

Similar to ligand stimulation, IR stimulates EGFR signaling into its downstream PI3K/Akt [190–192]. Hyperactive PI3K/Akt signaling is one of the factors responsible for the development of cancer cells with increased resistance to radiotherapy. The role of PI3K/Akt activity in radioresistance has been reported in various cancers, including those of the brain, lung, colon, cervix, and head and neck. For example, constitutive phosphorylations of Akt, presumably at Ser473 and Thr308, mediate radiotherapy resistance in NSCLC cells [193], and activation of the PI3K/Akt/Cox-2 pathway enhances resistance to radiation in human cervical cancer [150]. RLIP76 can regulate PI3K/Akt signaling and induce radioresistance in pancreatic cancer, which is an aggressive malignancy with characteristic resistance to conventional chemo-radiotherapy. The function of the PI3K/Akt pathway in response to radiation is believed to be independent of p53 status. Moreover, although PI3K activates other prosurvival effectors, such as SGK, Akt plays a central role in PI3K-mediated radioresistance. Given that inhibition of Akt activity leads to impaired DNA DSB repair following radiation and enhanced radiosensitivity, activation of Akt improves post-irradiation cell survival by promoting the repair of IR-induced DNA DSBs, and might be of particular importance in terms of radiotherapy outcome. Akt seems also to be involved in the radioresistance of cancer stem cells through an as-yet-unknown mechanism.

Like apoptosis, autophagy has also been recognized as an important factor in determining the response of tumor cells to radiotherapy. The PI3K/Akt signaling pathway is a major regulator of autophagy [194,195]. Autophagy exhibits a biphasic effect against exposure of tumor cells to IR, inducing a cytoprotective or cytotoxic effect [196,197]. The PI3K/Akt/mTOR pathway has been implicated in the cytotoxic effect of radiation-induced autophagy. Akt inhibition exerts a radiosensitizing effect in malignant glioma cells by inducing autophagy [198].

As mentioned above, two pathways are involved in DNA DSB repair: the NHEJ and HR pathways. In the NHEJ repair pathway, Akt forms a functional complex with DNA-PKcs at the DNA DSB site and stimulates DNA–PKcs kinase activity, all of which are necessary for the DNA DSB repair. Akt-dependent phosphorylation/activation of DNA-PKcs indicates that Akt is involved in the first initiating step of DNA DSB repair [199]. Akt can also be activated by the MRE11–RAD50–NBS1 (MRN)–ATM pathway as well as the PI3K pathway. The role of Akt in DSB repair is further substantiated by radiation-induced colocalization of γH2AX foci and phosphorylated Akt in the site of DSB [199–201]. BRCA1, BRCA2, and RAD51 are critical components of the HR repair pathway, to which Akt activity is also linked. Particularly, whereas Akt stimulates the NHEJ pathway, its aberrant activation suppresses the HR pathway and generates genetic instability in tumor cells [202].

Because NHEJ is the predominant pathway in mammals, activation of the EGFR/PI3K/Akt signaling pathway is crucial for tumor cell survival after radiation and the inhibition of Akt activity by targeting the RTK–PI3K–Akt axis suppresses faithful repair of IR-induced DNA DSBs and improves radiotherapy efficacy [203–206].

5. Strategies for Overcoming Resistance to IR

Radiation-induced apoptosis is a major cell death form in tumors derived from hematopoietic, lymphoid, and germ cells. However, epithelial solid tumors show extensive resistance to IR-induced apoptosis. Radioresistance is a serious concern, causing radiotherapy failure and subsequent tumor relapse. Therefore, novel therapeutic radiosensitizers are urgently needed for overcoming tumor radioresistance and thus improving the outcome of radiotherapy. A growing number of inhibitors that target specific components of radioresistance pathways are being developed for clinical use. Moreover, natural radiosensitizers have also been developed in an effort to compensate for the limitations of synthetic inhibitors. Several strategies have been suggested for overcoming resistance to IR in cancer treatment (Figure 4).

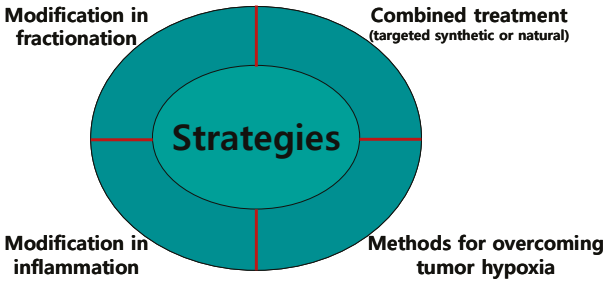

Figure 4. Strategies for overcoming radioresistance in cancer treatment. Several therapeutic strategies have been suggested to overcome the radioresistance of cancer cells.

5.1. Modifications in Fractionation

Fractionated radiation therapy for cancer has advantages over a single administration of radiation because it can increase the anticancer therapeutic effect and decrease the occurrence of severe side effects in normal tissues. In the most conventional fractionated radiation therapy, about 2.0 Gy of radiation is given per day, about 10 Gy per week, and up to about 60 Gy for six weeks in total. Unfortunately, however, this strategy cannot sufficiently control locally advanced cancers and is not satisfactory to patients due to its limited efficacy and the occurrence of side effects. New strategies such as hypofractionation have been proposed to compensate for the limitations of conventional fractionated radiation therapy. First, clinical trials are assessing the administration of larger doses of radiotherapy per fraction in fewer fractions. Therefore, in the future, conventional radiotherapy strategies will be replaced largely by hypofractionated radiation therapy, which delivers very potent, focused beams of radiation to tumors but gives fewer radiation treatments. Hypofractionation involves the delivery of daily doses larger than 2.0 Gy, shorter overall treatment times, and lower overall doses. In this hypofractionated radiotherapy, although the dose of the single fraction is higher, the total dose delivered is lower than in conventional radiotherapy. Hypofractionation regimens take advantage of greater cell killing per fraction of the cell survival curve and combat accelerated repopulation of tumor tissues. In particular, the use of hypofractionated radiation treatment to specifically target brain tumors will be beneficial in terms of saving normal brain tissue and preserving the brain's various sub-functions (such as memory) compared to irradiating the entire brain. Researchers are investigating various ways of giving standard external beam radiotherapy, such as hyperfractionation and accelerated fractionation as well as hypofractionation. In hyperfractionation, a smaller dose of radiation (e.g., ~1.2 Gy) is delivered twice per day with an

interval of about 6 h, allowing the total dose of radiation to be increased, which has therapeutic benefits and fewer side effects. In accelerated fractionation, a relatively high dose of radiation (e.g., ~1.6 Gy) is applied twice per day but the total dose is identical to that used in conventional radiotherapy. Because the total duration is shorter than that of conventional fractionation treatment, this treatment strategy is advantageous, especially in very rapidly growing tumors.

5.2. Combined Treatment

In an effort to overcome tumor radioresistance, much research has focused on developing tumor-specific radiosensitizers. Combined anticancer therapy has been emerging as an established clinical practice. In many solid tumors, simultaneous treatment with chemotherapeutic agents and radiation is far more effective than sequential single treatment. This is based on the principle that a single chemotherapeutic or radiotherapeutic agent has low therapeutic activity in many tumor types, whereas combining therapeutic agents with unrelated action mechanisms may result in synergistic, or at least additive, anti-neoplastic effects.

5.2.1. Selective Molecularly Targeted Synthetic Agents

Hence, a variety of radiosensitizing agents have been developed to target DNA DSB repair pathways, including small interfering RNAs, aptamers, antisense RNAs, and small-molecule inhibitors, which are being clinically developed by a number of corporations. Various inhibitors of Akt, mTOR, and Chk1/2 have been shown to act as potential radiosensitizers [198,203,207–212].

Because an intact or hyperactive HR is often correlated with radioresistance, exploring means of inhibiting the HR repair pathway in cancer cells may be beneficial. A number of radiosensitizers have been found to inhibit HR. Nucleoside and base analogs such as gemcitabine, TAS-106, gimeracil, pentoxifylline, and caffeine are examples [127]. Furthermore, the ATR inhibitor VE-821 and the Chk1/2 inhibitor AZD7762 have also been reported to inhibit HR [213,214]. The tyrosine kinase inhibitors imatinib and erlotinib, the HDAC inhibitor PCI-24781, the proteasome inhibitor MG132, and the HSP90 inhibitor 17-allylamino-17-demethoxygeldanamycin (17-AAG), all of which are less directly implicated in the DNA damage signaling, are also suggested to radiosensitize cancer cells by targeting the HR repair pathway [127].

Emerging evidence shows a novel role for radiotherapy as a therapeutic partner of cancer immunotherapy. IR can act as an immune adjuvant, contributing to systemic antitumor immunity. IR leads to the activation of several immunological proteins and transcription factors that modulate the expression of numerous immune mediators that may promote cancer development. Thus, the targeting of IR-induced inflammatory signaling pathways offers the opportunity to improve the clinical outcomes of radiation therapy by enhancing radiosensitivity. Several studies have reported the radiosensitizing effect of NF-κB inhibition in various models [215–217]. Clinical approaches for NF-κB inhibition to induce tumor radiosensitization include corticosteroids, phytochemicals, proteasome inhibitors, and synthetic peptides. The inhibition of Cox-2, one of the central enzymes in the inflammatory response, using pharmacological inhibitors such as ascoxibs, celecoxib, and SC-236, represents a radiosensitization strategy [142]. The combined treatment of radiation and cisplatin might complement the intrinsic inability of this drug to induce redistribution of calreticulin, a cisplatin-binding protein, thus affecting cell death. The combination of radiation and the poly(ADP-ribose) polymerase inhibitor veliparib exerts its effect by promoting tumor immunogenicity [218]. Preclinical studies have demonstrated that combining radiotherapy with immune stimulation can induce antitumor immunity, enhancing cell death.

5.2.2. Radiosensitizers Derived from Natural Products

The clinical benefits of synthetic inhibitors in terms of improving treatment outcomes are limited. In addition, the unintended and adverse side effects of these inhibitors are growing concerns. These limitations prompt the development of novel and more effective radiosensitizers

to address these unmet medical needs. Naturally occurring radiosensitizers are frequently believed to be relatively safe compared to synthetic compounds because they are normally found in foods. Moreover, natural products with antioxidant and immune-enhancing effects are believed to have better biological and radioprotective effects for normal cells. Several natural radiosensitizers have been reported (Table 1).

Curcumin

Curcumin, a polyphenol, is a natural compound derived from tumeric and curry powders. Curcumin has various anticancer activities. It suppresses cancer cell proliferation, downregulates NF-κB target genes, reduces the activity of growth factor receptors, and counteracts tumorigenesis [219]. Interestingly, curcumin suppresses all three stages of carcinogenesis: initiation, promotion, and progression. Resistance to radiation can be caused by increased expression of NF-κB-induced prosurvival genes such as antiapoptotic Bcl-2 family members. Curcumin has been shown to downregulate STAT3 phosphorylation as well as NF-κB expression induced by various inflammatory stimuli [220]. Some studies show that curcumin sensitizes cancer cells to IR through the inhibition of NF-κB activation [221,222]. Curcumin has also been reported to confer protective effects against radiation-induced toxicity in normal cells/tissues through the activation of Nrf2 antioxidant signaling pathways [222–224]. The fact that curcumin can achieve efficient radiosensitizing effects without any toxicity makes its development as an adjunct to standard radiotherapy an important goal.

Table 1. Effective natural radiosensitizers for the treatment of cancer. These compounds act as radiosensitizers for cancer cells and, at the same time, radioprotectors for normal cells.

Name	Types	Source	Radiosensitization	Target in Radiosensitization	Radioprotection	Target in Radioprotection
Curcumin	Polyphenol	Tumeric	Arrest, Apoptosis	NF-kB	Yes	NRF2, Antioxidant enzymes
Resveratrol	Polyphenol	Grapes	Apoptosis, Senescence	NF-kB, Cox-2, 5-LOX	Yes	Not determined
Genistein	Polyphenol	Soybean	Arrest, Apoptosis	Akt, Erk, Survivin, Cycline B, NF-kB	Yes	Not determined
Quercetin	Polyphenol	Ubiquitous	Arrest, Apoptosis	ATM	Yes	Not determined

Resveratrol

Resveratrol is a polyphenol compound found in various dietary sources, including grapes, wine, soy, berries, and peanuts. Resveratrol, a natural antioxidant, exerts an anticancer effect by suppressing the proliferation of a variety of cancer cells. Resveratrol has been shown to potentiate the apoptotic effects of IR as well as cytokines and chemotherapeutic agents [222,225,226]. Resveratrol induces radiosensitization through the inhibition of NF-κB, Cox-2, and 5-lipooxygenase (5-LOX) [222]. Resveratrol also potentiates the IR-induced accumulation of ceramide, a potential anticancer agent, by promoting its *de novo* biosynthesis [227]. Interestingly, resveratrol treatment enhances IR-induced premature senescence rather than apoptosis in NSCLC [228].

In addition, chromosome aberration analyses in an irradiated mouse model support the use of resveratrol as a radioprotector that has the potential for widespread application [229].

Genistein

Genistein is a naturally occurring soybean-derived isoflavone glycoside that inhibits protein tyrosine kinase. Genistein can inhibit cancer cell growth by inducing apoptosis and differentiation and/or by suppressing angiogenesis and metastasis. Anticancer effects of genistein are mediated by the inhibition of protein tyrosine kinases, topoisomerase I/II, protein histidine kinases, and the expression of cell cycle–related genes in multiple malignant tissues. Genistein in combination with IR may enhance the efficacy of radiotherapy in numerous cancer cells by inhibiting DNA

synthesis, cell division, and cell growth. For example, genistein greatly enhances the radiosensitivity of human esophageal cancer cells by suppressing radiation-induced activation of survival signals such as Akt and Erk [230]. Combination treatment with genistein and IR significantly induces G2/M arrest followed by apoptosis by reducing the expression of survivin and cyclin B in cervical cancer cells [231]. Genistein also increases radiation-induced apoptosis and promotes arrest at the G2 phase of the cell cycle in leukemia cells [232]. Because cells in the G2/M phase are more sensitive to radiation damage than those in other phases, G2/M arrest in response to genistein treatment can sensitize cancer cells to IR-induced death. Combined treatment-induced G2/M arrest has been also reported in other cancer cell types, such as prostate cancer cells [233]. In contrast, genistein can also protect from IR-induced injury in human normal lymphocytes [234]. Moreover, the administration of genistein alleviates the IR-induced injury in mice without adverse effects on motor activity, body weight, or histopathology [224]. NF-κB inhibition mediated by genistein is also suggested to be an underlying mechanism by which genistein exerts its anticancer and radiosensitizing effects. The increased cancer cell death induced by the combined treatment of genistein and IR is assumed to occur largely via the inhibition of NF-κB, leading to the decrease in cyclin B levels and/or the increase in the levels of the cdk inhibitor p21, thus promoting G2/M arrest and increasing radiosensitivity.

Quercetin

Quercetin, one of the main components of flavonoids, is distributed ubiquitously in vegetables and fruits such as apples, nuts, berries, onions, cauliflowers, and cabbages, and in red wine, tea, and the propolis of honeybee hives. It has multiple effects on the immune system and has been found to have antioxidant, antiviral, anti-inflammatory, and cardioprotective activities. Quercetin has anticancer activity against several types of cancer by promoting apoptotic cell death and inducing cell cycle arrest [235–237]. Quercetin also induces autophagy [236]. Its radiosensitizing activity has been demonstrated in various cancer cells and a human tumor xenograft model [238]. Mechanistically, quercetin enhances tumor radiosensitization through inhibition of the ATM-mediated pathway, one of the key DNA damage signaling pathways, in response to radiation [238]. Quercetin exerts radioprotective and immunoprotective effects against radiotherapy in normal tissue [239,240]. It also effectively protects lung tissue against radiation-induced pulmonary injuries [240].

5.3. Modification of Inflammation

Recently, radiation oncologists came to pay attention to tumor stroma to increase the efficacy of radiotherapy. Depletion of tumor-associated macrophages can increase the antitumor effects of IR. For example, VEGF-neutralizing antibodies can enhance the antitumor response to IR through downregulation of IR-induced VEGF in macrophages [241]. Immunestrategy exerts synergistic antitumor activity with local radiation in preclinical studies. Since radiotherapy elicits *in situ* vaccination, some novel approaches have tested radiotherapy in combination with cancer vaccines or adoptive T-cell transfer [242]. Antibodies targeting immune checkpoint receptors and/or inducible T-cell costimulatory receptors can also be successfully treated with radiotherapy [242].

5.4. Methods of Overcoming Tumor Hypoxia

Tumor hypoxia is considered one of major problems for radiation therapy because hypoxic tumor cells are more likely to survive IR. To overcome tumor hypoxia, several therapeutic strategies have been developed. The most common methods employed to overcome tumor hypoxia-related resistance include radiation fractionation, the use of high linear energy transfer (LET) particles in the management of hypoxic tumors, and the implementation of bioreductive drugs, such as adjuvant treatment. Several methods of overcoming tumor hypoxia are outlined below.

First, the direct delivery of sufficient oxygen to locally advanced solid tumors during IR treatment is one of the simplest and most effective options. Indeed, hyperbaric oxygenation, red

blood cell transfusions, and erythropoietin administration have been investigated as methods of increasing tumor oxygenation. Although these approaches showed therapeutic benefits in preclinical studies, they are not in widespread use because of the conflicting results of clinical trials.

In the 1970s, nitroimidazole derivatives, such as misonidazole, were found to mimic the effect of oxygen in the radiochemical process, raising the possibility of their use to enhance the cytotoxic effect of IR under hypoxic conditions [181,243]. However, dose-limiting toxicities, mainly due to its low solubility, led to a limited therapeutic benefit of misonidazole in clinical trials. Effective doses of this drug were found to cause peripheral neuropathy, which has prevented its routine clinical use. To solve this problem, other nitroimidazole derivatives with high solubility, such as etanidazole and doranidazole, have been developed as promising candidates [181].

Because of its active role in the radioresistance of hypoxic tumor cells, HIF-1 has been recognized as a prime molecular target for sensitization to the therapeutic effect of radiation. For example, targeting tumor metabolism through HIF-1 inhibition enhances the radiation response in cervical and head and neck xenograft tumors [244]. The well-known HIF-1 inhibitor YC-1 was found to downregulate HIF-1α and HIF-2α through post-translational modifications and to inactivate the carboxyl-terminal transactivation domain of HIF-1α [245]. It was also reported to decrease HIF-1 target gene expression under hypoxic conditions, thereby inhibiting the growth and spread of tumors [246,247]. Inhibition of the radiation-induced upregulation of HIF-1 activity by YC-1 dramatically suppresses tumor recurrence after radiotherapy [248]. Inhibition of the dimerization of HIF-1α with HIF-1β also likely exerts a radiosensitizing effect because dimerization is a prerequisite for DNA binding by, and transcriptional activity of, HIF-1 [249]. In this sense, acriflavine may also be a potent HIF-1 inhibitor because it binds directly to HIF-1α and inhibits HIF-1 dimerization and transcriptional activity [250]. However, the radiosensitizing activity of acriflavine has not been examined to date. The negative regulation of key factors that upregulate the expression or activity of HIF-1 represents another approach to HIF-1 inhibition. The PI3K-Akt-mTOR signaling pathway is known to upregulate the expression of HIF-1α protein. Therefore, inhibitors of these pathways, such as RAD-001, LY294002, wortmannin, and rapamycin, contribute to radiosensitization presumably by suppressing HIF-1. HSP90 can also enhance HIF-1 expression; it binds to HIF-1α in competition with RACK1 and inhibits the oxygen-independent degradation of HIF-1α [251]. Additionally, 17-AAG or deguelin, a novel naturally occurring inhibitor of HSP90, suppresses an increase in the interaction of HIF-1α with HSP90 in cancer cells [252]. Furthermore, combined treatment with IR and deguelin significantly overcomes radioresistance in lung cancer cells [252].

A gene therapy strategy targeting hypoxic cancer cells would be also a good option for enhancing radiosensitivity. A heterodimer with HIF-1α and HIF-1β binds directly to the hypoxia response element (HRE) present in the promoter regions of target genes. HIF-1/HRE-mediated transcriptional initiation has been suggested to facilitate induction of therapeutic gene expression in hypoxic regions of solid tumors [181]. In particular, the targeted expression of apoptosis-related genes using the HRE promoter in HIF-1-active malignant cancer cells will enable the resistance of hypoxic cells to IR to be overcome.

Novel drugs, such as antiangiogenic/vascular targeting agents, that target genetically stable vascular endothelial cells rather than unstable mutating tumor cells have been developed recently. Tumor angiogenesis enables division of the primary cancer cells by adequately delivering oxygen and nutrients, and targeting angiogenesis can enhance the efficacy of radiotherapy. Considerable preclinical evidence suggests the efficacy of tumor radiosensitization in combination with radiation and angiogenesis inhibition [253–255], and clinical trials of combinations of angiogenesis inhibitors with radiotherapy are underway. Novel drugs that cause vascular normalization or reduce tumor oxygen consumption will also be effective in terms of reducing tumor hypoxia. Additionally, direct evidence shows that downregulation of prostaglandins by Cox-2 inhibitors results in a reduction of angiogenesis increasing radiosensitivity [256], confirming the important role of angiogenesis in tumor radioresistance.

6. Perspectives and Conclusions

Cancer is the global leading cause of disease and injury, the incidence of which will increase due to the aging population. The number of patients receiving radiotherapy has been increasing steadily. Radiotherapy can benefit patients for whom surgery is not possible by significantly shrinking or destroying tumors. The exposure of tumors to IR triggers a variety of changes (either immediate or persistent), ranging from mild biochemical changes to several forms of death. The total dose and number of fractionation of IR can determine the degree and/or type of cellular damage. IR exerts anti-cancer activity by eliciting multiple DNA lesions, such as DSBs, SSBs, DNA crosslinks, and base modifications.

While radiation is effective against some types of tumors, other tumor types, such as pancreatic carcinoma and glioblastoma multiforme, are intrinsically resistant to conventional radiation therapy, making them more difficult to target. Several pathways determine the resistance of tumor cells to IR. These include DNA repair pathways, developmental pathways, the adaptive response pathway, adhesion pathways, the hypoxic pathway, and other survival pathways. Therefore, an urgent clinical need exists to develop radiosensitizers to overcome tumor radioresistance and thus enhance the effectiveness of radiotherapy. Combined chemotherapy and radiotherapy was clinically successful in the treatment of many tumor types. Clinical trials are investigating drugs that sensitize cancer cells to the effects of radiation, making them easier to destroy with radiation therapy. Meanwhile, protective drugs may facilitate the recovery of normal and healthy cells after exposure to radiation. Many current radiosensitization approaches target the DNA damage response. Overall, however, the clinical outcomes of these attempts using targeted drugs as radiosensitizers have generally remained disappointing. Therefore, novel radiosensitizing drugs should undergo more extensive and careful preclinical studies before being introduced in the clinic by increasing knowledge of their mechanisms of action.

To enhance the efficacy and cost-effectiveness of radiotherapy, the patient should also be treated with radiotherapy that is more fine-tuned. Advances in technology and biology have led to improvements in tumor delineation and targeting, resulting in improvement of tumor coverage and a reduction in normal tissue exposure. Good examples of progress in radiotherapy are technical advances such as image-guided radiotherapy (IGRT) and intensity-modulated radiation therapy (IMRT), which target the tumor more accurately, sparing healthy normal tissue. These allow physicians to shape radiotherapy very closely around a tumor from different directions, thereby reducing the impact of high radiation doses on nearby healthy cells such as the spinal cord or salivary glands, which, if damaged, would cause long-term problems. IMRT is a recently developed powerful therapeutic strategy that enables radiation oncologists to precisely control the distribution of radiation according to the overall shape of the tumor. Radiological imaging using computed tomography (CT) and magnetic resonance imaging (MRI) and multileaf collimators can enhance tumor specificity. With the help of these technologies, IMRT allows the delivery of precise radiation doses to tumors without increasing the adverse effects on surrounding normal tissue. In particular, simultaneous integrated boost IMRT (SIB-IMRT) enables the delivery of a booster dose of radiation to tumor cells with high efficiency and accuracy.

Acknowledgments: We thank members of the Hong's lab for critical reading and comments for this manuscript. This work was supported by grants from the National Research Foundation (NRF-2013R1A2A2A01067169 to Yonggeun Hong), and by the KRIBB Research Initiative Program (KGM4611512 to Yonggeun Hong), Korea. Yunkyung Hong, Seunghoon Lee in leading authors are supported by the Post-doctoral Research Program of Inje University during 2014 to 2016. This study was also supported by a grant of the Korea Healthcare technology R&D Project, Ministry for Health & Welfare Affairs, Korea (HI08C2149).

Author Contributions: This review article was conceptualized by Yonggeun Hong, Kyu Tae Chang and Byeong Mo Kim; Yunkyung Hong, Seunghoon Lee and Ji Hong Lim prepared figures and table; Pengda Liu, Yong Heon Lee and Tae Ho Lee professionally edited the manuscript; Byeong Mo Kim and Yonggeun Hong wrote the manuscript.

Conflicts of Interest: The authors declare no conflict of interest.

References

1. Hall, E.J. Cancer caused by X-rays—A random event? *Lancet Oncol.* **2007**, *8*, 369–370. [CrossRef]
2. Begg, A.C.; Stewart, F.A.; Vens, C. GENOMIC INSTABILITY IN CANCER Strategies to improve radiotherapy with targeted drugs. *Nat. Rev. Cancer* **2011**, *11*, 239–253. [CrossRef] [PubMed]
3. Kolesnick, R.; Fuks, Z. Radiation and ceramide-induced apoptosis. *Oncogene* **2003**, *22*, 5897–5906. [CrossRef] [PubMed]
4. D'Amours, D.; Desnoyers, S.; D'Silva, I.; Poirier, G.G. Poly(ADP-ribosyl)ation reactions in the regulation of nuclear functions. *Biochem. J.* **1999**, *342*, 249–268. [CrossRef] [PubMed]
5. Simbulan-Rosenthal, C.M.; Rosenthal, D.S.; Iyer, S.; Boulares, A.H.; Smulson, M.E. Transient poly(ADP-ribosyl)ation of nuclear proteins and role of poly(ADP-ribose) polymerase in the early stages of apoptosis. *J. Biol. Chem.* **1998**, *273*, 13703–13712. [CrossRef] [PubMed]
6. Kelland, L.R.; Tonkin, K.S. The effect of 3-aminobenzamide in the radiation response of 3 human cervix carcinoma xenografts. *Radiother. Oncol.* **1989**, *15*, 363–369. [CrossRef]
7. Calabrese, C.R.; Almassy, R.; Barton, S.; Batey, M.A.; Calvert, A.H.; Canan-Koch, S.; Durkacz, B.W.; Hostomsky, Z.; Kumpf, R.A.; Kyle, S.; *et al*. Anticancer chemosensitization and radiosensitization by the novel poly(ADP-ribose) polymerase-1 inhibitor AG14361. *J. Natl. Cancer Inst.* **2004**, *96*, 56–67. [CrossRef] [PubMed]
8. Donawho, C.K.; Luo, Y.; Luo, Y.; Penning, T.D.; Bauch, J.L.; Bouska, J.J.; Bontcheva-Diaz, V.D.; Cox, B.F.; DeWeese, T.L.; Dillehay, L.E.; *et al*. ABT-888, an orally active poly(ADP-ribose) polymerase inhibitor that potentiates DNA-damaging agents in preclinical tumor models. *Clin. Cancer Res.* **2007**, *13*, 2728–2737. [CrossRef] [PubMed]
9. Khan, K.; Araki, K.; Wang, D.Y.; Li, G.Y.; Li, X.; Zhang, J.; Xu, W.Z.; Hoover, R.K.; Lauter, S.; O'Malley, B.; *et al*. Head and neck cancer radiosensitization by the novel poly(ADP-ribose) polymerase inhibitor GPI-15427. *Head Neck* **2010**, *32*, 381–391. [CrossRef] [PubMed]
10. Senra, J.M.; Telfer, B.A.; Cherry, K.E.; McCrudden, C.M.; Hirst, D.G.; O'Connor, M.J.; Wedge, S.R.; Stratford, I.J. Inhibition of PARP-1 by olaparib (AZD2281) increases the radiosensitivity of a lung tumor xenograft. *Mol. Cancer Ther.* **2011**, *10*, 1949–1958. [CrossRef] [PubMed]
11. Chan, D.W.; Chen, B.P.C.; Prithivirajsingh, S.; Kurimasa, A.; Story, M.D.; Qin, J.; Chen, D.J. Autophosphorylation of the DNA-dependent protein kinase catalytic subunit is required for rejoining of DNA double-strand breaks. *Genes Dev.* **2002**, *16*, 2333–2338. [CrossRef] [PubMed]
12. Shrivastav, M.; Miller, C.A.; de Haro, L.P.; Durant, S.T.; Chen, B.P.C.; Chen, D.J.; Nickoloff, J.A. DNA-PKcs and ATM co-regulate DNA double-strand break repair. *DNA Repair* **2009**, *8*, 920–929. [CrossRef] [PubMed]
13. Zhang, Y.; Zhou, J.Q.; Cao, X.F.; Zhang, Q.M.; Lim, C.U.K.; Ullrich, R.L.; Bailey, S.M.; Liber, H.L. Partial deficiency of DNA-PKcs increases ionizing radiation-induced mutagenesis and telomere instability in human cells. *Cancer Lett.* **2007**, *250*, 63–73. [CrossRef] [PubMed]
14. Banin, S.; Moyal, L.; Shieh, S.; Taya, Y.; Anderson, C.W.; Chessa, L.; Smorodinsky, N.I.; Prives, C.; Reiss, Y.; Shiloh, Y.; *et al*. Enhanced phosphorylation of p53 by ATM in response to DNA damage. *Science* **1998**, *281*, 1674–1677. [CrossRef] [PubMed]
15. Canman, C.E.; Lim, D.S.; Cimprich, K.A.; Taya, Y.; Tamai, K.; Sakaguchi, K.; Appella, E.; Kastan, M.B.; Siliciano, J.D. Activation of the ATM kinase by ionizing radiation and phosphorylation of p53. *Science* **1998**, *281*, 1677–1679. [CrossRef] [PubMed]
16. Sherr, C.J.; Roberts, J.M. CDK inhibitors: Positive and negative regulators of G1-phase progression. *Genes Dev.* **1999**, *13*, 1501–1512. [CrossRef] [PubMed]
17. Bartek, J.; Lukas, J. Pathways governing G1/S transition and their response to DNA damage. *FEBS Lett.* **2001**, *490*, 117–122. [CrossRef]
18. Sancar, A.; Lindsey-Boltz, L.A.; Unsal-Kacmaz, K.; Linn, S. Molecular mechanisms of mammalian DNA repair and the DNA damage checkpoints. *Annu. Rev. Biochem.* **2004**, *73*, 39–85. [CrossRef] [PubMed]
19. Dou, Q.P. Putative roles of retinoblastoma protein in apoptosis. *Apoptosis* **1997**, *2*, 5–18. [CrossRef] [PubMed]
20. Delston, R.B.; Harbour, J.W. Rb at the interface between cell cycle and apoptotic decisions. *Curr. Mol. Med.* **2006**, *6*, 713–718. [PubMed]

21. An, B.; Dou, Q.P. Cleavage of retinoblastoma protein during apoptosis: An interleukin 1 beta-converting enzyme-like protease as candidate. *Cancer Res.* **1996**, *56*, 438–442. [PubMed]
22. Watters, D. Molecular mechanisms of ionizing radiation-induced apoptosis. *Immunol. Cell Biol.* **1999**, *77*, 263–271. [CrossRef] [PubMed]
23. Miyashita, T.; Reed, J.C. Tumor-suppressor P53 is a direct transcriptional activator of the human bax gene. *Cell* **1995**, *80*, 293–299. [PubMed]
24. Chipuk, J.E.; Kuwana, T.; Bouchier-Hayes, L.; Droin, N.M.; Newmeyer, D.; Schuler, M.; Green, D.R. Direct activation of Bax by p53 mediates mitochondrial membrane permeabilization and apoptosis. *Science* **2004**, *303*, 1010–1014. [CrossRef] [PubMed]
25. Geng, Y.; Walls, K.C.; Ghosh, A.P.; Akhtar, R.S.; Klocke, B.J.; Roth, K.A. Cytoplasmic p53 and activated bax regulate p53-dependent, transcription-independent neural precursor cell apoptosis. *J. Histochem. Cytochem.* **2010**, *58*, 265–275. [CrossRef] [PubMed]
26. Okoshi, R.; Ozaki, T.; Yamamoto, H.; Ando, K.; Koida, N.; Ono, S.; Koda, T.; Kamijo, T.; Nakagawara, A.; Kizaki, H. Activation of AMP-activated protein kinase induces p53-dependent apoptotic cell death in response to energetic stress. *J. Biol. Chem.* **2008**, *283*, 3979–3987. [CrossRef] [PubMed]
27. Haas-Kogan, D.A.; Dazin, P.; Hu, L.; Deen, D.F.; Israel, A. P53-independent apoptosis: A mechanism of radiation-induced cell death of glioblastoma cells. *Cancer J. Sci. Am.* **1996**, *2*, 114–121. [PubMed]
28. Kyprianou, N.; Rock, S. Radiation-induced apoptosis of human prostate cancer cells is independent of mutant p53 overexpression. *Anticancer Res.* **1998**, *18*, 897–905. [PubMed]
29. Bracey, T.S.; Miller, J.C.; Preece, A.; Paraskeva, C. Gamma-radiation-induced apoptosis in human colorectal adenoma and carcinoma cell lines can occur in the absence of wild type p53. *Oncogene* **1995**, *10*, 2391–2396. [PubMed]
30. Barlow, C.; Brown, K.D.; Deng, C.X.; Tagle, D.A.; Wynshaw-Boris, A. Atm selectively regulates distinct p53-dependent cell-cycle checkpoint and apoptotic pathways. *Nat. Genet.* **1997**, *17*, 453–456. [CrossRef] [PubMed]
31. Reinke, V.; Lozano, G. The p53 targets mdm2 and Fas are not required as mediators of apoptosis *in vivo*. *Oncogene* **1997**, *15*, 1527–1534. [CrossRef] [PubMed]
32. Chmura, S.J.; Nodzenski, E.; Beckett, M.A.; Kufe, D.W.; Quintans, J.; Weichselbaum, R.R. Loss of ceramide production confers resistance to radiation-induced apoptosis. *Cancer Res.* **1997**, *57*, 1270–1275. [PubMed]
33. Michael, J.M.; Lavin, M.F.; Watters, D.J. Resistance to radiation-induced apoptosis in Burkitt's lymphoma cells is associated with defective ceramide signaling. *Cancer Res.* **1997**, *57*, 3600–3605. [PubMed]
34. Basu, S.; Bayoumy, S.; Zhang, Y.; Lozano, J.; Kolesnick, R. BAD enables ceramide to signal apoptosis via Ras and Raf-1. *J. Biol. Chem.* **1998**, *273*, 30419–30426. [CrossRef] [PubMed]
35. Jarvis, W.D.; Fornari, F.A., Jr.; Browning, J.L.; Gewirtz, D.A.; Kolesnick, R.N.; Grant, S. Attenuation of ceramide-induced apoptosis by diglyceride in human myeloid leukemia cells. *J. Biol. Chem.* **1994**, *269*, 31685–31692. [PubMed]
36. Schubert, K.M.; Scheid, M.P.; Duronio, V. Ceramide inhibits protein kinase B/Akt by promoting dephosphorylation of serine 473. *J. Biol. Chem.* **2000**, *275*, 13330–13335. [CrossRef] [PubMed]
37. Herr, I.; Wilhelm, D.; Bohler, T.; Angel, P.; Debatin, K.M. Activation of CD95 (APO-1/Fas) signaling by ceramide mediates cancer therapy-induced apoptosis. *EMBO J.* **1997**, *16*, 6200–6208. [CrossRef] [PubMed]
38. Rainaldi, G.; Ferrante, A.; Indovina, P.L.; Santini, M.T. Induction of apoptosis or necrosis by ionizing radiation is dose-dependent in MG-63 osteosarcoma multicellular spheroids. *Anticancer Res.* **2003**, *23*, 2505–2518. [PubMed]
39. Takeuchi, H.; Kondo, Y.; Fujiwara, K.; Kanzawa, T.; Aoki, H.; Mills, G.B.; Kondo, S. Synergistic augmentation of rapamycin-induced autophagy in malignant glioma cells by phosphatidylinositol 3-kinase/protein kinase B inhibitors. *Cancer Res.* **2005**, *65*, 3336–3346. [PubMed]
40. Paglin, S.; Hollister, T.; Delohery, T.; Hackett, N.; McMahill, M.; Sphicas, E.; Domingo, D.; Yahalom, J. A novel response of cancer cells to radiation involves autophagy and formation of acidic vesicles. *Cancer Res.* **2001**, *61*, 439–444. [PubMed]
41. Zhuang, W.; Qin, Z.; Liang, Z. The role of autophagy in sensitizing malignant glioma cells to radiation therapy. *Acta Biochim. Biophys. Sin.* **2009**, *41*, 341–351. [CrossRef] [PubMed]
42. Wu, S.Y.; Liu, Y.W.; Wang, Y.K.; Lin, T.H.; Li, Y.Z.; Chen, S.H.; Lee, Y.R. Ionizing radiation induces autophagy in human oral squamous cell carcinoma. *J. Balk. Union Oncol.* **2014**, *19*, 137–144.

43. Jo, G.H.; Bogler, O.; Chwae, Y.J.; Yoo, H.; Lee, S.H.; Park, J.B.; Kim, Y.J.; Kim, J.H.; Gwak, H.S. Radiation-induced autophagy contributes to cell death and induces apoptosis partly in malignant glioma cells. *Cancer Res. Treat.* **2015**, *47*, 221–241. [CrossRef] [PubMed]
44. Ito, H.; Daido, S.; Kanzawa, T.; Kondo, S.; Kondo, Y. Radiation-induced autophagy is associated with LC3 and its inhibition sensitizes malignant glioma cells. *Int. J. Oncol.* **2005**, *26*, 1401–1410. [CrossRef] [PubMed]
45. Yuan, X.; Du, J.; Hua, S.; Zhang, H.; Gu, C.; Wang, J.; Yang, L.; Huang, J.; Yu, J.; Liu, F. Suppression of autophagy augments the radiosensitizing effects of STAT3 inhibition on human glioma cells. *Exp. Cell Res.* **2015**, *330*, 267–276. [CrossRef] [PubMed]
46. Vares, G.; Ory, K.; Lectard, B.; Levalois, C.; Altmeyer-Morel, S.; Chevillard, S.; Lebeau, J. Progesterone prevents radiation-induced apoptosis in breast cancer cells. *Oncogene* **2004**, *23*, 4603–4613. [CrossRef] [PubMed]
47. Luce, A.; Courtin, A.; Levalois, C.; Altmeyer-Morel, S.; Romeo, P.H.; Chevillard, S.; Lebeau, J. Death receptor pathways mediate targeted and non-targeted effects of ionizing radiations in breast cancer cells. *Carcinogenesis* **2009**, *30*, 432–439. [CrossRef] [PubMed]
48. Ianzini, F.; Bertoldo, A.; Kosmacek, E.A.; Phillips, S.L.; Mackey, M.A. Lack of p53 function promotes radiation-induced mitotic catastrophe in mouse embryonic fibroblast cells. *Cancer Cell Int.* **2006**, *6*, 11. [CrossRef] [PubMed]
49. Chan, T.A.; Hermeking, H.; Lengauer, C.; Kinzler, K.W.; Vogelstein, B. 14–3-3Sigma is required to prevent mitotic catastrophe after DNA damage. *Nature* **1999**, *401*, 616–620. [PubMed]
50. Ianzini, F.; Mackey, M.A. Spontaneous premature chromosome condensation and mitotic catastrophe following irradiation of HeLa S3 cells. *Int. J. Radiat. Biol.* **1997**, *72*, 409–421. [CrossRef] [PubMed]
51. Ree, A.H.; Stokke, T.; Bratland, A.; Patzke, S.; Nome, R.V.; Folkvord, S.; Meza-Zepeda, L.A.; Flatmark, K.; Fodstad, O.; Andersson, Y. DNA damage responses in cell cycle G2 phase and mitosis—Tracking and targeting. *Anticancer Res.* **2006**, *26*, 1909–1916. [PubMed]
52. Bunz, F.; Dutriaux, A.; Lengauer, C.; Waldman, T.; Zhou, S.; Brown, J.P.; Sedivy, J.M.; Kinzler, K.W.; Vogelstein, B. Requirement for p53 and p21 to sustain G2 arrest after DNA damage. *Science* **1998**, *282*, 1497–1501. [CrossRef] [PubMed]
53. Cho, Y.S.; Challa, S.; Moquin, D.; Genga, R.; Ray, T.D.; Guildford, M.; Chan, F.K. Phosphorylation-driven assembly of the RIP1–RIP3 complex regulates programmed necrosis and virus-induced inflammation. *Cell* **2009**, *137*, 1112–1123. [CrossRef] [PubMed]
54. Nehs, M.A.; Lin, C.I.; Kozono, D.E.; Whang, E.E.; Cho, N.L.; Zhu, K.; Moalem, J.; Moore, F.D., Jr.; Ruan, D.T. Necroptosis is a novel mechanism of radiation-induced cell death in anaplastic thyroid and adrenocortical cancers. *Surgery* **2011**, *150*, 1032–1039. [CrossRef] [PubMed]
55. Le, O.N.; Rodier, F.; Fontaine, F.; Coppe, J.P.; Campisi, J.; DeGregori, J.; Laverdiere, C.; Kokta, V.; Haddad, E.; Beausejour, C.M. Ionizing radiation-induced long-term expression of senescence markers in mice is independent of p53 and immune status. *Aging Cell* **2010**, *9*, 398–409. [CrossRef] [PubMed]
56. Chen, W.S.; Yu, Y.C.; Lee, Y.J.; Chen, J.H.; Hsu, H.Y.; Chiu, S.J. Depletion of securin induces senescence after irradiation and enhances radiosensitivity in human cancer cells regardless of functional p53 expression. *Int. J. Radiat. Oncol. Biol. Phys.* **2010**, *77*, 566–574. [CrossRef] [PubMed]
57. Mirzayans, R.; Scott, A.; Cameron, M.; Murray, D. Induction of accelerated senescence by gamma radiation in human solid tumor-derived cell lines expressing wild-type TP53. *Radiat. Res.* **2005**, *163*, 53–62. [CrossRef] [PubMed]
58. Luo, H.; Yount, C.; Lang, H.; Yang, A.; Riemer, E.C.; Lyons, K.; Vanek, K.N.; Silvestri, G.A.; Schulte, B.A.; Wang, G.Y. Activation of p53 with Nutlin-3a radiosensitizes lung cancer cells via enhancing radiation-induced premature senescence. *Lung Cancer* **2013**, *81*, 167–73. [CrossRef] [PubMed]
59. Suzuki, M.; Boothman, D.A. Stress-induced premature senescence (SIPS)—Influence of SIPS on radiotherapy. *J. Radiat. Res.* **2008**, *49*, 105–112. [CrossRef] [PubMed]
60. Baskar, R. Emerging role of radiation induced bystander effects: Cell communications and carcinogenesis. *Genome Integr.* **2010**, *1*, 13. [CrossRef] [PubMed]
61. Blyth, B.J.; Sykes, P.J. Radiation-induced bystander effects: What are they, and how relevant are they to human radiation exposures? *Radiat. Res.* **2011**, *176*, 139–157. [CrossRef] [PubMed]
62. Panganiban, R.A.; Snow, A.L.; Day, R.M. Mechanisms of radiation toxicity in transformed and non-transformed cells. *Int. J. Mol. Sci.* **2013**, *14*, 15931–15958. [CrossRef] [PubMed]

63. Najafi, M.; Fardid, R.; Hadadi, G.; Fardid, M. The mechanisms of radiation-induced bystander effect. *J. Biomed. Phys. Eng.* **2014**, *4*, 163–172. [PubMed]
64. Coppe, J.P.; Desprez, P.Y.; Krtolica, A.; Campisi, J. The senescence-associated secretory phenotype: The dark side of tumor suppression. *Annu. Rev. Pathol.* **2010**, *5*, 99–118. [CrossRef] [PubMed]
65. Davalos, A.R.; Coppe, J.P.; Campisi, J.; Desprez, P.Y. Senescent cells as a source of inflammatory factors for tumor progression. *Cancer Metastasis Rev.* **2010**, *29*, 273–283. [CrossRef] [PubMed]
66. Kumazaki, T.; Robetorye, R.S.; Robetorye, S.C.; Smith, J.R. Fibronectin expression increases during *in vitro* cellular senescence: Correlation with increased cell area. *Exp. Cell Res.* **1991**, *195*, 13–19. [CrossRef]
67. Sabin, R.J.; Anderson, R.M. Cellular Senescence—Its role in cancer and the response to ionizing radiation. *Genome Integr.* **2011**, *2*, 7. [CrossRef] [PubMed]
68. Vens, C.; Dahmen-Mooren, E.; Verwijs-Janssen, M.; Blyweert, W.; Graversen, L.; Bartelink, H.; Begg, A.C. The role of DNA polymerase beta in determining sensitivity to ionizing radiation in human tumor cells. *Nucleic Acids Res.* **2002**, *30*, 2995–3004. [CrossRef] [PubMed]
69. Hoeijmakers, J.H. Genome maintenance mechanisms for preventing cancer. *Nature* **2001**, *411*, 366–374. [CrossRef] [PubMed]
70. De Murcia, J.M.; Niedergang, C.; Trucco, C.; Ricoul, M.; Dutrillaux, B.; Mark, M.; Oliver, F.J.; Masson, M.; Dierich, A.; LeMeur, M.; *et al*. Requirement of poly(ADP-ribose) polymerase in recovery from DNA damage in mice and in cells. *Proc. Natl. Acad. Sci. USA* **1997**, *94*, 7303–7307. [CrossRef] [PubMed]
71. Thompson, L.H.; Brookman, K.W.; Jones, N.J.; Allen, S.A.; Carrano, A.V. Molecular cloning of the human XRCC1 gene, which corrects defective DNA strand break repair and sister chromatid exchange. *Mol. Cell. Biol.* **1990**, *10*, 6160–6171. [CrossRef] [PubMed]
72. Wong, H.K.; Wilson, D.M., 3rd. XRCC1 and DNA polymerase beta interaction contributes to cellular alkylating-agent resistance and single-strand break repair. *J. Cell Biochem.* **2005**, *95*, 794–804. [CrossRef] [PubMed]
73. Ferreira, M.G.; Cooper, J.P. Two modes of DNA double-strand break repair are reciprocally regulated through the fission yeast cell cycle. *Genes Dev.* **2004**, *18*, 2249–2254. [CrossRef] [PubMed]
74. Vignard, J.; Mirey, G.; Salles, B. Ionizing-radiation induced DNA double-strand breaks: A direct and indirect lighting up. *Radiother. Oncol.* **2013**, *108*, 362–369. [CrossRef] [PubMed]
75. Mao, Z.; Bozzella, M.; Seluanov, A.; Gorbunova, V. DNA repair by nonhomologous end joining and homologous recombination during cell cycle in human cells. *Cell Cycle* **2008**, *7*, 2902–2906. [CrossRef] [PubMed]
76. Chiolo, I.; Minoda, A.; Colmenares, S.U.; Polyzos, A.; Costes, S.V.; Karpen, G.H. Double-strand breaks in heterochromatin move outside of a dynamic HP1a domain to complete recombinational repair. *Cell* **2011**, *144*, 732–744. [CrossRef] [PubMed]
77. Lomax, M.E.; Folkes, L.K.; O'Neill, P. Biological consequences of radiation-induced DNA damage: relevance to radiotherapy. *Clin. Oncol.* **2013**, *25*, 578–585. [CrossRef] [PubMed]
78. Chiu, S.M.; Xue, L.Y.; Friedman, L.R.; Oleinick, N.L. Comparison of DNA–protein cross-links induced by 4'-(9-acridinylamino)-methanesulfon-m-anisidide and by gamma-radiation. *Cancer Res.* **1989**, *49*, 910–914. [PubMed]
79. Ramakrishnan, N.; Chiu, S.M.; Oteinick, N.L. Yield of DNA–protein cross-links in gamma-irradiated Chinese hamster cells. *Cancer Res.* **1987**, *47*, 2032–2035. [PubMed]
80. Frankenberg-Schwager, M. Induction, repair and biological relevance of radiation-induced DNA lesions in eukaryotic cells. *Radiat. Environ. Biophys.* **1990**, *29*, 273–292. [CrossRef] [PubMed]
81. Kelsey, K.T.; Memisoglu, A.; Frenkel, D.; Liber, H.L. Human lymphocytes exposed to low doses of X-rays are less susceptible to radiation-induced mutagenesis. *Mutat. Res.* **1991**, *263*, 197–201. [CrossRef]
82. Feinendegen, L.E.; Bond, V.P.; Sondhaus, C.A.; Muehlensiepen, H. Radiation effects induced by low doses in complex tissue and their relation to cellular adaptive responses. *Mutat. Res.* **1996**, *358*, 199–205. [CrossRef]
83. Guo, G.; Yan-Sanders, Y.; Lyn-Cook, B.D.; Wang, T.; Tamae, D.; Ogi, J.; Khaletskiy, A.; Li, Z.; Weydert, C.; Longmate, J.A.; *et al*. Manganese superoxide dismutase-mediated gene expression in radiation-induced adaptive responses. *Mol. Cell. Biol.* **2003**, *23*, 2362–2378. [CrossRef] [PubMed]
84. Pandey, B.N.; Gordon, D.M.; de Toledo, S.M.; Pain, D.; Azzam, E.I. Normal human fibroblasts exposed to high- or low-dose ionizing radiation: Differential effects on mitochondrial protein import and membrane potential. *Antioxid. Redox Signal.* **2006**, *8*, 1253–1261. [CrossRef] [PubMed]

85. Sherr, C.J. Mammalian G1 cyclins. *Cell* **1993**, *73*, 1059–1065. [CrossRef]
86. Giacinti, C.; Giordano, A. RB and cell cycle progression. *Oncogene* **2006**, *25*, 5220–5227. [CrossRef] [PubMed]
87. Diehl, J.A. Cycling to cancer with cyclin D1. *Cancer Biol. Ther.* **2002**, *1*, 226–231. [CrossRef] [PubMed]
88. Shintani, M.; Okazaki, A.; Masuda, T.; Kawada, M.; Ishizuka, M.; Doki, Y.; Weinstein, I.B.; Imoto, M. Overexpression of cyclin DI contributes to malignant properties of esophageal tumor cells by increasing VEGF production and decreasing Fas expression. *Anticancer Res.* **2002**, *22*, 639–647. [PubMed]
89. Thomas, G.R.; Nadiminti, H.; Regalado, J. Molecular predictors of clinical outcome in patients with head and neck squamous cell carcinoma. *Int. J. Exp. Pathol.* **2005**, *86*, 347–363. [CrossRef] [PubMed]
90. Alao, J.P.; Gamble, S.C.; Stavropoulou, A.V.; Pomeranz, K.M.; Lam, E.W.; Coombes, R.C.; Vigushin, D.M. The cyclin D1 proto-oncogene is sequestered in the cytoplasm of mammalian cancer cell lines. *Mol. Cancer* **2006**, *5*, 7. [CrossRef] [PubMed]
91. Ahmed, K.M.; Fan, M.; Nantajit, D.; Cao, N.; Li, J.J. Cyclin D1 in low-dose radiation-induced adaptive resistance. *Oncogene* **2008**, *27*, 6738–6748. [CrossRef] [PubMed]
92. Camp, E.R.; Li, J.; Minnich, D.J.; Brank, A.; Moldawer, L.L.; MacKay, S.L.; Hochwald, S.N. Inducible nuclear factor-kappaB activation contributes to chemotherapy resistance in gastric cancer. *J. Am. Coll. Surg.* **2004**, *199*, 249–258. [CrossRef] [PubMed]
93. Scartozzi, M.; Bearzi, I.; Pierantoni, C.; Mandolesi, A.; Loupakis, F.; Zaniboni, A.; Catalano, V.; Quadri, A.; Zorzi, F.; Berardi, R.; *et al*. Nuclear factor-kB tumor expression predicts response and survival in irinotecan-refractory metastatic colorectal cancer treated with cetuximab-irinotecan therapy. *J. Clin. Oncol.* **2007**, *25*, 3930–3935. [CrossRef] [PubMed]
94. Li, Z.; Xia, L.; Lee, L.M.; Khaletskiy, A.; Wang, J.; Wong, J.Y.; Li, J.J. Effector genes altered in MCF-7 human breast cancer cells after exposure to fractionated ionizing radiation. *Radiat. Res.* **2001**, *155*, 543–553. [CrossRef]
95. Ozeki, M.; Tamae, D.; Hou, D.X.; Wang, T.; Lebon, T.; Spitz, D.R.; Li, J.J. Response of cyclin B1 to ionizing radiation: Regulation by NF-kappaB and mitochondrial antioxidant enzyme MnSOD. *Anticancer Res.* **2004**, *24*, 2657–2663. [PubMed]
96. Holley, A.K.; Xu, Y.; St Clair, D.K.; St Clair, W.H. RelB regulates manganese superoxide dismutase gene and resistance to ionizing radiation of prostate cancer cells. *Ann. N. Y. Acad. Sci.* **2010**, *1201*, 129–136. [CrossRef] [PubMed]
97. Grdina, D.J.; Murley, J.S.; Miller, R.C.; Mauceri, H.J.; Sutton, H.G.; Li, J.J.; Woloschak, G.E.; Weichselbaum, R.R. A survivin-associated adaptive response in radiation therapy. *Cancer Res.* **2013**, *73*, 4418–4428. [CrossRef] [PubMed]
98. Grdina, D.J.; Murley, J.S.; Miller, R.C.; Woloschak, G.E.; Li, J.J. NFkappaB and Survivin-Mediated Radio-Adaptive Response. *Radiat. Res.* **2015**, *183*, 391–397. [CrossRef] [PubMed]
99. Cao, N.; Li, S.; Wang, Z.; Ahmed, K.M.; Degnan, M.E.; Fan, M.; Dynlacht, J.R.; Li, J.J. NF-kappaB-mediated HER2 overexpression in radiation-adaptive resistance. *Radiat. Res.* **2009**, *171*, 9–21. [CrossRef] [PubMed]
100. Rhee, S.G.; Kang, S.W.; Chang, T.S.; Jeong, W.; Kim, K. Peroxiredoxin, a novel family of peroxidases. *IUBMB Life* **2001**, *52*, 35–41. [CrossRef] [PubMed]
101. Smith-Pearson, P.S.; Kooshki, M.; Spitz, D.R.; Poole, L.B.; Zhao, W.; Robbins, M.E. Decreasing peroxiredoxin II expression decreases glutathione, alters cell cycle distribution, and sensitizes glioma cells to ionizing radiation and H_2O_2. *Free Radic. Biol. Med.* **2008**, *45*, 1178–1189. [CrossRef] [PubMed]
102. Wang, T.; Tamae, D.; LeBon, T.; Shively, J.E.; Yen, Y.; Li, J.J. The role of peroxiredoxin II in radiation-resistant MCF-7 breast cancer cells. *Cancer Res.* **2005**, *65*, 10338–10346. [CrossRef] [PubMed]
103. Kurimasa, A.; Kumano, S.; Boubnov, N.V.; Story, M.D.; Tung, C.S.; Peterson, S.R.; Chen, D.J. Requirement for the kinase activity of human DNA-dependent protein kinase catalytic subunit in DNA strand break rejoining. *Mol. Cell. Biol.* **1999**, *19*, 3877–3884. [CrossRef] [PubMed]
104. Liu, Y.; Zhang, L.; Liu, Y.; Sun, C.; Zhang, H.; Miao, G.; Di, C.X.; Zhou, X.; Zhou, R.; Wang, Z. DNA-PKcs deficiency inhibits glioblastoma cell-derived angiogenesis after ionizing radiation. *J. Cell. Physiol.* **2015**, *230*, 1094–1103. [CrossRef] [PubMed]
105. Smith, G.C.; Jackson, S.P. The DNA-dependent protein kinase. *Genes Dev.* **1999**, *13*, 916–934. [CrossRef] [PubMed]
106. Shinohara, A.; Ogawa, H.; Ogawa, T. Rad51 protein involved in repair and recombination in *S. cerevisiae* is a RecA-like protein. *Cell* **1992**, *69*, 457–470. [CrossRef]

107. Daboussi, F.; Dumay, A.; Delacote, F.; Lopez, B.S. DNA double-strand break repair signalling: The case of RAD51 post-translational regulation. *Cell Signal.* **2002**, *14*, 969–975. [CrossRef]
108. Klein, H.L. The consequences of Rad51 overexpression for normal and tumor cells. *DNA Repair* **2008**, *7*, 686–693. [CrossRef] [PubMed]
109. Althaus, F.R.; Richter, C. ADP-ribosylation of proteins. Enzymology and biological significance. *Mol. Biol. Biochem. Biophys.* **1987**, *37*, 1–237. [PubMed]
110. Lindahl, T.; Satoh, M.S.; Poirier, G.G.; Klungland, A. Posttranslational modification of poly(ADP-ribose) polymerase induced by DNA strand breaks. *Trends Biochem. Sci.* **1995**, *20*, 405–411. [CrossRef]
111. Bernardi, R.; Rossi, L.; Poirier, G.G.; Scovassi, A.I. Analysis of poly(ADP-ribose) glycohydrolase activity in nuclear extracts from mammalian cells. *Biochim. Biophys. Acta* **1997**, *1338*, 60–68. [CrossRef]
112. Haince, J.F.; McDonald, D.; Rodrigue, A.; Dery, U.; Masson, J.Y.; Hendzel, M.J.; Poirier, G.G. PARP1-dependent kinetics of recruitment of MRE11 and NBS1 proteins to multiple DNA damage sites. *J. Biol. Chem.* **2008**, *283*, 1197–1208. [CrossRef] [PubMed]
113. Galande, S.; Kohwi-Shigematso, T. Poly(ADP-ribose) polymerase and Ku autoantigen form a complex and synergistically bind to matrix attachment sequences. *J. Biol. Chem.* **1999**, *274*, 20521–20528. [CrossRef] [PubMed]
114. Ariumi, Y.; Masutani, M.; Copeland, T.D.; Mimori, T.; Sugimura, T.; Shimotohno, K.; Ueda, K.; Hatanaka, M.; Noda, M. Suppression of the poly(ADP-ribose) polymerase activity by DNA-dependent protein kinase *in vitro*. *Oncogene* **1999**, *18*, 4616–4625. [CrossRef] [PubMed]
115. Haince, J.F.; Kozlov, S.; Dawson, V.L.; Dawson, T.M.; Hendzel, M.J.; Lavin, M.F.; Poirier, G.G. Ataxia telangiectasia mutated (ATM) signaling network is modulated by a novel poly(ADP-ribose)-dependent pathway in the early response to DNA-damaging agents. *J. Biol. Chem.* **2007**, *282*, 16441–16453. [CrossRef] [PubMed]
116. Schiewer, M.J.; Goodwin, J.F.; Han, S.M.; Brenner, J.C.; Augello, M.A.; Dean, J.L.; Liu, F.Z.; Planck, J.L.; Ravindranathan, P.; Chinnaiyan, A.M.; *et al*. Dual roles of PARP-1 promote cancer growth and progression. *Cancer Discov.* **2012**, *2*, 1134–1149. [CrossRef] [PubMed]
117. Zaremba, T.; Thomas, H.D.; Cole, M.; Coulthard, S.A.; Plummer, E.R.; Curtin, N.J. Poly(ADP-ribose) polymerase-1 (PARP-1) pharmacogenetics, activity and expression analysis in cancer patients and healthy volunteers. *Biochem. J.* **2011**, *436*, 671–679. [CrossRef] [PubMed]
118. Scully, R.; Chen, J.J.; Ochs, R.L.; Keegan, K.; Hoekstra, M.; Feunteun, J.; Livingston, D.M. Dynamic changes of BRCA1 subnuclear location and phosphorylation state are initiated by DNA damage. *Cell* **1997**, *90*, 425–435. [CrossRef]
119. Zhong, Q.; Chen, C.F.; Li, S.; Chen, Y.M.; Wang, C.C.; Xiao, J.; Chen, P.L.; Sharp, Z.D.; Lee, W.H. Association of BRCA1 with the hRad50-hMre11-p95 complex and the DNA damage response. *Science* **1999**, *285*, 747–750. [CrossRef] [PubMed]
120. Paull, T.T.; Cortez, D.; Bowers, B.; Elledge, S.J.; Gellert, M. Direct DNA binding by Brca1. *Proc. Natl. Acad. Sci. USA* **2001**, *98*, 6086–6091. [CrossRef] [PubMed]
121. Foray, N.; Marot, D.; Gabriel, A.; Randrianarison, V.; Carr, A.M.; Perricaudet, M.; Ashworth, A.; Jeggo, P. A subset of ATM- and ATR-dependent phosphorylation events requires the BRCA1 protein. *EMBO J.* **2003**, *22*, 2860–2871. [CrossRef] [PubMed]
122. Zhang, F.; Fan, Q.; Ren, K.Q.; Andreassen, P.R. PALB2 Functionally connects the breast cancer susceptibility proteins BRCA1 and BRCA2. *Mol. Cancer Res.* **2009**, *7*, 1110–1118. [CrossRef] [PubMed]
123. Zhang, F.; Ma, J.L.; Wu, J.X.; Ye, L.; Cai, H.; Xia, B.; Yu, X.C. PALB2 Links BRCA1 and BRCA2 in the DNA-damage response. *Curr. Biol.* **2009**, *19*, 524–529. [CrossRef] [PubMed]
124. Bryant, H.E.; Schultz, N.; Thomas, H.D.; Parker, K.M.; Flower, D.; Lopez, E.; Kyle, S.; Meuth, M.; Curtin, N.J.; Helleday, T. Specific killing of BRCA2-deficient tumours with inhibitors of poly(ADP-ribose) polymerase. *Nature* **2005**, *434*, 913–917. [CrossRef] [PubMed]
125. Farmer, H.; McCabe, N.; Lord, C.J.; Tutt, A.N.J.; Johnson, D.A.; Richardson, T.B.; Santarosa, M.; Dillon, K.J.; Hickson, I.; Knights, C.; *et al*. Targeting the DNA repair defect in BRCA mutant cells as a therapeutic strategy. *Nature* **2005**, *434*, 917–921. [CrossRef] [PubMed]
126. Rainey, M.D.; Charlton, M.E.; Stanton, R.V.; Kastan, M.B. Transient inhibition of ATM kinase is sufficient to enhance cellular sensitivity to ionizing radiation. *Cancer Res.* **2008**, *68*, 7466–7474. [CrossRef] [PubMed]

127. Mladenov, E.; Magin, S.; Soni, A.; Iliakis, G. DNA double-strand break repair as determinant of cellular radiosensitivity to killing and target in radiation therapy. *Front. Oncol.* **2013**, *3*, 113. [CrossRef] [PubMed]
128. Fitzgerald, T.J.; Wang, T.; Goel, H.L.; Huang, J.; Stein, G.; Lian, J.; Davis, R.J.; Doxsey, S.; Balaji, K.C.; Aronowitz, J.; *et al*. Prostate carcinoma and radiation therapy: Therapeutic treatment resistance and strategies for targeted therapeutic intervention. *Expert Rev. Anticancer Ther.* **2008**, *8*, 967–974. [CrossRef] [PubMed]
129. Wang, T.; Languino, L.R.; Lian, J.; Stein, G.; Blute, M.; Fitzgerald, T.J. Molecular targets for radiation oncology in prostate cancer. *Front. Oncol.* **2011**, *1*, 17. [CrossRef] [PubMed]
130. Goel, H.L.; Fornaro, M.; Moro, L.; Teider, N.; Rhim, J.S.; King, M.; Languino, L.R. Selective modulation of type 1 insulin-like growth factor receptor signaling and functions by beta1 integrins. *J. Cell Biol.* **2004**, *166*, 407–418. [CrossRef] [PubMed]
131. Goel, H.L.; Breen, M.; Zhang, J.; Das, I.; Aznavoorian-Cheshire, S.; Greenberg, N.M.; Elgavish, A.; Languino, L.R. beta1A integrin expression is required for type 1 insulin-like growth factor receptor mitogenic and transforming activities and localization to focal contacts. *Cancer Res.* **2005**, *65*, 6692–6700. [CrossRef] [PubMed]
132. Sayeed, A.; Alam, N.; Trerotola, M.; Languino, L.R. Insulin-like growth factor 1 stimulation of androgen receptor activity requires beta(1A) integrins. *J. Cell. Physiol.* **2012**, *227*, 751–758. [CrossRef] [PubMed]
133. Goel, H.L.; Sayeed, A.; Breen, M.; Zarif, M.J.; Garlick, D.S.; Leav, I.; Davis, R.J.; Fitzgerald, T.J.; Morrione, A.; Hsieh, C.C.; *et al*. beta1 integrins mediate resistance to ionizing radiation *in vivo* by inhibiting c-Jun amino terminal kinase 1. *J. Cell. Physiol.* **2013**, *228*, 1601–1609. [CrossRef] [PubMed]
134. Eke, I.; Deuse, Y.; Hehlgans, S.; Gurtner, K.; Krause, M.; Baumann, M.; Shevchenko, A.; Sandfort, V.; Cordes, N. beta(1)Integrin/FAK/cortactin signaling is essential for human head and neck cancer resistance to radiotherapy. *J. Clin. Investig.* **2012**, *122*, 1529–1540. [CrossRef] [PubMed]
135. Pawar, S.C.; Dougherty, S.; Pennington, M.E.; Demetriou, M.C.; Stea, B.D.; Dorr, R.T.; Cress, A.E. alpha6 integrin cleavage: Sensitizing human prostate cancer to ionizing radiation. *Int. J. Radiat. Biol.* **2007**, *83*, 761–767. [CrossRef] [PubMed]
136. Han, E.K.; McGonigal, T. Role of focal adhesion kinase in human cancer: A potential target for drug discovery. *Anticancer Agents Med. Chem.* **2007**, *7*, 681–684. [CrossRef] [PubMed]
137. Kasahara, T.; Koguchi, E.; Funakoshi, M.; Aizu-Yokota, E.; Sonoda, Y. Antiapoptotic action of focal adhesion kinase (FAK) against ionizing radiation. *Antioxid. Redox Signal.* **2002**, *4*, 491–499. [CrossRef] [PubMed]
138. Turner, C.E.; Glenney, J.R., Jr.; Burridge, K. Paxillin: A new vinculin-binding protein present in focal adhesions. *J. Cell Biol.* **1990**, *111*, 1059–1068. [CrossRef] [PubMed]
139. Bellis, S.L.; Miller, J.T.; Turner, C.E. Characterization of tyrosine phosphorylation of paxillin *in vitro* by focal adhesion kinase. *J. Biol. Chem.* **1995**, *270*, 17437–17441. [CrossRef] [PubMed]
140. Seidler, J.; Durzok, R.; Brakebusch, C.; Cordes, N. Interactions of the integrin subunit beta1A with protein kinase B/Akt, p130Cas and paxillin contribute to regulation of radiation survival. *Radiother. Oncol.* **2005**, *76*, 129–134. [CrossRef] [PubMed]
141. Wu, C.T.; Chen, M.F.; Chen, W.C.; Hsieh, C.C. The role of IL-6 in the radiation response of prostate cancer. *Radiat. Oncol.* **2013**, *8*, 159. [CrossRef] [PubMed]
142. Di Maggio, F.M.; Minafra, L.; Forte, G.I.; Cammarata, F.P.; Lio, D.; Messa, C.; Gilardi, M.C.; Bravata, V. Portrait of inflammatory response to ionizing radiation treatment. *J. Inflamm. Lond.* **2015**, *12*. [CrossRef] [PubMed]
143. Pasi, F.; Facoetti, A.; Nano, R. IL-8 and IL-6 bystander signalling in human glioblastoma cells exposed to gamma radiation. *Anticancer Res.* **2010**, *30*, 2769–2772. [PubMed]
144. Biswas, S.; Guix, M.; Rinehart, C.; Dugger, T.C.; Chytil, A.; Moses, H.L.; Freeman, M.L.; Arteaga, C.L. Inhibition of TGF-beta with neutralizing antibodies prevents radiation-induced acceleration of metastatic cancer progression. *J. Clin. Investig.* **2007**, *117*, 1305–1313. [CrossRef] [PubMed]
145. Laine, A.; Iyengar, P.; Pandita, T.K. The role of inflammatory pathways in cancer-associated cachexia and radiation resistance. *Mol. Cancer Res.* **2013**, *11*, 967–972. [CrossRef] [PubMed]
146. Kim, K.W.; Mutter, R.W.; Cao, C.; Albert, J.M.; Shinohara, E.T.; Sekhar, K.R.; Lu, B. Inhibition of signal transducer and activator of transcription 3 activity results in down-regulation of Survivin following irradiation. *Mol. Cancer Ther.* **2006**, *5*, 2659–2665. [CrossRef] [PubMed]

147. Skvortsova, I.; Skvortsov, S.; Stasyk, T.; Raju, U.; Popper, B.A.; Schiestl, B.; von Guggenberg, E.; Neher, A.; Bonn, G.K.; Huber, L.A.; *et al*. Intracellular signaling pathways regulating radioresistance of human prostate carcinoma cells. *Proteomics* **2008**, *8*, 4521–4533. [CrossRef] [PubMed]
148. Belenkov, A.I.; Shenouda, G.; Rizhevskaya, E.; Cournoyer, D.; Belzile, J.P.; Souhami, L.; Devic, S.; Chow, T.Y.K. Erythropoietin induces cancer cell resistance to ionizing radiation and to cisplatin. *Mol. Cancer Ther.* **2004**, *3*, 1525–1532. [PubMed]
149. Reader, J.; Holt, D.; Fulton, A. Prostaglandin E-2 EP receptors as therapeutic targets in breast cancer. *Cancer Metastasis Rev.* **2011**, *30*, 449–463. [CrossRef] [PubMed]
150. Xia, S.; Zhao, Y.; Yu, S.Y.; Zhang, M.X. Activated PI3K/Akt/COX-2 pathway induces resistance to radiation in human cervical cancer hela cells. *Cancer Biother. Radiopharm.* **2010**, *25*, 317–323. [CrossRef] [PubMed]
151. Ingham, P.W.; McMahon, A.P. Hedgehog signaling in animal development: Paradigms and principles. *Genes Dev.* **2001**, *15*, 3059–3087. [CrossRef] [PubMed]
152. McMahon, A.P.; Ingham, P.W.; Tabin, C.J. Developmental roles and clinical significance of hedgehog signaling. *Curr. Top. Dev. Biol.* **2003**, *53*, 1–114. [PubMed]
153. Varjosalo, M.; Taipale, J. Hedgehog: Functions and mechanisms. *Genes Dev.* **2008**, *22*, 2454–2472. [CrossRef] [PubMed]
154. Medina, V.; Calvo, M.B.; Diaz-Prado, S.; Espada, J. Hedgehog signalling as a target in cancer stem cells. *Clin. Transl. Oncol.* **2009**, *11*, 199–207. [CrossRef] [PubMed]
155. Gulino, A.; Ferretti, E.; De Smaele, E. Hedgehog signalling in colon cancer and stem cells. *EMBO Mol. Med.* **2009**, *1*, 300–302. [CrossRef] [PubMed]
156. Varnat, F.; Duquet, A.; Malerba, M.; Zbinden, M.; Mas, C.; Gervaz, P.; Altaba, A.R.I. Human colon cancer epithelial cells harbour active HEDGEHOG-GLI signalling that is essential for tumour growth, recurrence, metastasis and stem cell survival and expansion. *EMBO Mol. Med.* **2009**, *1*, 338–351. [CrossRef] [PubMed]
157. Thayer, S.P.; di Magliano, M.P.; Heiser, P.W.; Nielsen, C.M.; Roberts, D.J.; Lauwers, G.Y.; Qi, Y.P.; Gysin, S.; Fernandez-del Castillo, C.F.; Yajnik, V.; *et al*. Hedgehog is an early and late mediator of pancreatic cancer tumorigenesis. *Nature* **2003**, *425*, 851–856. [CrossRef] [PubMed]
158. Kubo, M.; Nakamura, M.; Tasaki, A.; Yamanaka, N.; Nakashima, H.; Nomura, M.; Kuroki, S.; Katano, M. Hedgehog signaling pathway is a new therapeutic target for patients with breast cancer. *Cancer Res.* **2004**, *64*, 6071–6074. [CrossRef] [PubMed]
159. Ma, X.L.; Chen, K.; Huang, S.H.; Zhang, X.L.; Adegboyega, P.A.; Evers, B.M.; Zhang, H.W.; Xie, J.W. Frequent activation of the hedgehog pathway in advanced gastric adenocarcinomas. *Carcinogenesis* **2005**, *26*, 1698–1705. [CrossRef] [PubMed]
160. Katoh, Y.; Katoh, M. Hedgehog signaling, epithelial-to-mesenchymal transition and miRNA (Review). *Int. J. Mol. Med.* **2008**, *22*, 271–275. [CrossRef] [PubMed]
161. Lei, J.J.; Ma, J.G.; Ma, Q.Y.; Li, X.Q.; Liu, H.; Xu, Q.H.; Duan, W.X.; Sun, Q.; Xu, J.; Wu, Z.; *et al*. Hedgehog signaling regulates hypoxia induced epithelial to mesenchymal transition and invasion in pancreatic cancer cells via a ligand-independent manner. *Mol. Cancer* **2013**, *12*. [CrossRef] [PubMed]
162. Gan, G.N.; Eagles, J.; Keysar, S.B.; Wang, G.L.; Glogowska, M.J.; Altunbas, C.; Anderson, R.T.; Le, P.N.; Morton, J.J.; Frederick, B.; *et al*. Hedgehog signaling drives radioresistance and stroma-driven tumor repopulation in head and neck squamous cancers. *Cancer Res.* **2014**, *74*, 7024–7036. [CrossRef] [PubMed]
163. Wild-Bode, C.; Weller, M.; Rimner, A.; Dichgans, J.; Wick, W. Sublethal irradiation promotes migration and invasiveness of glioma cells: Implications for radiotherapy of human glioblastoma. *Cancer Res.* **2001**, *61*, 2744–2750. [PubMed]
164. Qian, L.W.; Mizumoto, K.; Urashima, T.; Nagai, E.; Maehara, N.; Sato, N.; Nakajima, M.; Tanaka, M. Radiation-induced increase in invasive potential of human pancreatic cancer cells and its blockade by a matrix metalloproteinase inhibitor, CGS27023. *Clin. Cancer Res.* **2002**, *8*, 1223–1227. [PubMed]
165. Fodde, R.; Brabletz, T. Wnt/beta-catenin signaling in cancer stemness and malignant behavior. *Curr. Opin. Cell Biol.* **2007**, *19*, 150–158. [CrossRef] [PubMed]
166. Nager, M.; Bhardwaj, D.; Canti, C.; Medina, L.; Nogues, P.; Herreros, J. beta-Catenin Signalling in Glioblastoma Multiforme and Glioma-Initiating Cells. *Chemother. Res. Pract.* **2012**, *2012*, 192362. [PubMed]
167. Kim, Y.; Kim, K.H.; Lee, J.; Lee, Y.A.; Kim, M.; Lee, S.J.; Park, K.; Yang, H.; Jin, J.; Joo, K.M.; *et al*. Wnt activation is implicated in glioblastoma radioresistance. *Lab. Investig.* **2012**, *92*, 466–473. [CrossRef] [PubMed]

168. Artavanis-Tsakonas, S.; Rand, M.D.; Lake, R.J. Notch signaling: Cell fate control and signal integration in development. *Science* **1999**, *284*, 770–776. [CrossRef] [PubMed]
169. Lai, E.C. Notch signaling: Control of cell communication and cell fate. *Development* **2004**, *131*, 965–973. [CrossRef] [PubMed]
170. VanDussen, K.L.; Carulli, A.J.; Keeley, T.M.; Patel, S.R.; Puthoff, B.J.; Magness, S.T.; Tran, I.T.; Maillard, I.; Siebel, C.; Kolterud, A.; *et al*. Notch signaling modulates proliferation and differentiation of intestinal crypt base columnar stem cells. *Development* **2012**, *139*, 488–497. [CrossRef] [PubMed]
171. Radtke, F.; Raj, K. The role of Notch in tumorigenesis: Oncogene or tumour suppressor? *Nat. Rev. Cancer* **2003**, *3*, 756–767. [CrossRef] [PubMed]
172. Lobry, C.; Oh, P.; Aifantis, I. Oncogenic and tumor suppressor functions of Notch in cancer: It's NOTCH what you think. *J. Exp. Med.* **2011**, *208*, 1931–1935. [CrossRef] [PubMed]
173. Avila, J.L.; Kissil, J.L. Notch signaling in pancreatic cancer: Oncogene or tumor suppressor? *Trends Mol. Med.* **2013**, *19*, 320–327. [CrossRef] [PubMed]
174. Capaccione, K.M.; Pine, S.R. The Notch signaling pathway as a mediator of tumor survival. *Carcinogenesis* **2013**, *34*, 1420–1430. [CrossRef] [PubMed]
175. Phillips, T.M.; McBride, W.H.; Pajonk, F. The response of CD24(−/low)/CD44(+) breast cancer-initiating cells to radiation. *J. Natl. Cancer Inst.* **2006**, *98*, 1777–1785. [CrossRef] [PubMed]
176. Theys, J.; Yahyanejad, S.; Habets, R.; Span, P.; Dubois, L.; Paesmans, K.; Kattenbeld, B.; Cleutjens, J.; Groot, A.J.; Schuurbiers, O.C.J.; *et al*. High NOTCH activity induces radiation resistance in non small cell lung cancer. *Radiother. Oncol.* **2013**, *108*, 440–445. [CrossRef] [PubMed]
177. Nordsmark, M.; Overgaard, M.; Overgaard, J. Pretreatment oxygenation predicts radiation response in advanced squamous cell carcinoma of the head and neck. *Radiother. Oncol.* **1996**, *41*, 31–39. [CrossRef]
178. Brizel, D.M.; Sibley, G.S.; Prosnitz, L.R.; Scher, R.L.; Dewhirst, M.W. Tumor hypoxia adversely affects the prognosis of carcinoma of the head and neck. *Int. J. Radiat. Oncol. Biol. Phys.* **1997**, *38*, 285–289. [CrossRef]
179. Harada, H.; Kizaka-Kondoh, S.; Li, G.; Itasaka, S.; Shibuya, K.; Inoue, M.; Hiraoka, M. Significance of HIF-1-active cells in angiogenesis and radioresistance. *Oncogene* **2007**, *26*, 7508–7516. [CrossRef] [PubMed]
180. Kessler, J.; Hahnel, A.; Wichmann, H.; Rot, S.; Kappler, M.; Bache, M.; Vordermark, D. HIF-1 alpha inhibition by siRNA or chetomin in human malignant glioma cells: Effects on hypoxic radioresistance and monitoring via CA9 expression. *BMC Cancer* **2010**, *10*. [CrossRef] [PubMed]
181. Harada, H. How Can We Overcome Tumor Hypoxia in Radiation Therapy? *J. Radiat. Res.* **2011**, *52*, 545–556. [CrossRef] [PubMed]
182. Zhong, H.; Chiles, K.; Feldser, D.; Laughner, E.; Hanrahan, C.; Georgescu, M.M.; Simons, J.W.; Semenza, G.L. Modulation of hypoxia-inducible factor 1 alpha expression by the epidermal growth factor/phosphatidylinositol 3-kinase/PTEN/AKT/FRAP pathway in human prostate cancer cells: Implications for tumor angiogenesis and therapeutics. *Cancer Res.* **2000**, *60*, 1541–1545. [PubMed]
183. Neufeld, G.; Cohen, T.; Gengrinovitch, S.; Poltorak, Z. Vascular endothelial growth factor (VEGF) and its receptors. *FASEB J.* **1999**, *13*, 9–22. [PubMed]
184. McMahon, G. VEGF receptor signaling in tumor angiogenesis. *Oncologist* **2000**, *5*, 3–10. [CrossRef] [PubMed]
185. Noordhuis, M.G.; Eijsink, J.J.H.; ten Hoor, K.A.; Roossink, F.; Hollema, H.; Arts, H.J.G.; Pras, E.; Maduro, J.H.; Reyners, A.K.L.; de Bock, G.H.; *et al*. Expression of epidermal growth factor receptor (EGFR) and activated EGFR predict poor response to (chemo)radiation and survival in cervical cancer. *Clin. Cancer Res.* **2009**, *15*, 7389–7397. [CrossRef] [PubMed]
186. Hayashi, H.; Okamoto, I.; Kimura, H.; Sakai, K.; Nishimura, Y.; Nishio, K.; Nakagawa, K. Clinical outcomes of thoracic radiotherapy for locally advanced NSCLC with EGFR mutations or EML4-ALK rearrangement. *Anticancer Res.* **2012**, *32*, 4533–4537. [PubMed]
187. Rodemann, H.P.; Blaese, M.A. Responses of normal cells to ionizing radiation. *Semin. Radiat. Oncol.* **2007**, *17*, 81–88. [CrossRef] [PubMed]
188. Rodemann, H.P.; Dittmann, K.; Toulany, M. Radiation-induced EGFR-signaling and control of DNA-damage repair. *Int. J. Radiat. Biol.* **2007**, *83*, 781–791. [CrossRef] [PubMed]
189. Toulany, M.; Rodemann, H.P. Membrane receptor signaling and control of DNA repair after exposure to ionizing radiation. *Nuklearmedizin* **2010**, *49*, S26–S30. [PubMed]

190. Valerie, K.; Yacoub, A.; Hagan, M.P.; Curiel, D.T.; Fisher, P.B.; Grant, S.; Dent, P. Radiation-induced cell signaling: Inside-out and outside-in. *Mol. Cancer Ther.* **2007**, *6*, 789–801. [CrossRef] [PubMed]
191. Li, H.F.; Kim, J.S.; Waldman, T. Radiation-induced Akt activation modulates radioresistance in human glioblastoma cells. *Radiat. Oncol.* **2009**, *4*. [CrossRef] [PubMed]
192. Toulany, M.; Minjgee, M.; Kehlbach, R.; Chen, J.Y.; Baumann, M.; Rodemann, H.P. ErbB2 expression through heterodimerization with erbB1 is necessary for ionizing radiation—But not EGF-induced activation of Akt survival pathway. *Radiother. Oncol.* **2010**, *97*, 338–345. [CrossRef] [PubMed]
193. Brognard, J.; Clark, A.S.; Ni, Y.C.; Dennis, P.A. Akt/protein kinase B is constitutively active in non-small cell lung cancer cells and promotes cellular survival and resistance to chemotherapy and radiation. *Cancer Res.* **2001**, *61*, 3986–3997. [PubMed]
194. Noguchi, M.; Hirata, N.; Suizu, F. The links between AKT and two intracellular proteolytic cascades: Ubiquitination and autophagy. *Biochim. Biophys. Acta* **2014**, *1846*, 342–352. [CrossRef] [PubMed]
195. Heras-Sandoval, D.; Perez-Rojas, J.M.; Hernandez-Damian, J.; Pedraza-Chaverri, J. The role of PI3K/AKT/mTOR pathway in the modulation of autophagy and the clearance of protein aggregates in neurodegeneration. *Cell Signal.* **2014**, *26*, 2694–2701. [CrossRef] [PubMed]
196. Wilson, E.N.; Bristol, M.L.; Di, X.; Maltese, W.A.; Koterba, K.; Beckman, M.J.; Gewirtz, D.A. A switch between cytoprotective and cytotoxic autophagy in the radiosensitization of breast tumor cells by chloroquine and vitamin D. *Horm. Cancer* **2011**, *2*, 272–285. [CrossRef] [PubMed]
197. Bristol, M.L.; Di, X.; Beckman, M.J.; Wilson, E.N.; Henderson, S.C.; Maiti, A.; Fan, Z.; Gewirtz, D.A. Dual functions of autophagy in the response of breast tumor cells to radiation Cytoprotective autophagy with radiation alone and cytotoxic autophagy in radiosensitization by vitamin D-3. *Autophagy* **2012**, *8*, 739–753. [CrossRef] [PubMed]
198. Fujiwara, K.; Iwado, E.; Mills, G.B.; Sawaya, R.; Kondo, S.; Kondo, Y. Akt inhibitor shows anticancer and radiosensitizing effects in malignant glioma cells by inducing autophagy. *Int. J. Oncol.* **2007**, *31*, 753–760. [CrossRef] [PubMed]
199. Toulany, M.; Lee, K.J.; Fattah, K.R.; Lin, Y.F.; Fehrenbacher, B.; Schaller, M.; Chen, B.P.; Chen, D.J.; Rodemann, H.P. Akt Promotes Post-irradiation survival of human tumor cells through initiation, progression, and termination of DNA-PKcs-dependent DNA double-strand break repair. *Mol. Cancer Res.* **2012**, *10*, 945–957. [CrossRef] [PubMed]
200. Bozulic, L.; Surucu, B.; Hynx, D.; Hemmings, B.A. PKB alpha/Akt1 acts downstream of DNA-PK in the DNA double-strand break response and promotes survival. *Mol. Cell* **2008**, *30*, 203–213. [CrossRef] [PubMed]
201. Fraser, M.; Harding, S.M.; Zhao, H.; Coackley, C.; Durocher, D.; Bristow, R.G. MRE11 promotes AKT phosphorylation in direct response to DNA double-strand breaks. *Cell Cycle* **2011**, *10*, 2218–2232. [CrossRef] [PubMed]
202. Plo, I.; Laulier, C.; Gauthier, L.; Lebrun, F.; Calvo, F.; Lopez, B.S. AKT1 inhibits homologous recombination by inducing cytoplasmic retention of BRCA1 and RAD51. *Cancer Res.* **2008**, *68*, 9404–9412. [CrossRef] [PubMed]
203. Albert, J.M.; Kim, K.W.; Cao, C.; Lu, B. Targeting the Akt/mammalian target of rapamycin pathway for radiosensitization of breast cancer. *Mol. Cancer Ther.* **2006**, *5*, 1183–1189. [CrossRef] [PubMed]
204. Chang, L.; Graham, P.H.; Hao, J.; Ni, J.; Bucci, J.; Cozzi, P.J.; Kearsley, J.H.; Li, Y. PI3K/Akt/mTOR pathway inhibitors enhance radiosensitivity in radioresistant prostate cancer cells through inducing apoptosis, reducing autophagy, suppressing NHEJ and HR repair pathways. *Cell Death Dis.* **2014**, *5*, e1437. [CrossRef] [PubMed]
205. Kao, G.D.; Jiang, Z.; Fernandes, A.M.; Gupta, A.K.; Maity, A. Inhibition of phosphatidylinositol-3-OH kinase/Akt signaling impairs DNA repair in glioblastoma cells following ionizing radiation. *J. Biol. Chem.* **2007**, *282*, 21206–21212. [CrossRef] [PubMed]
206. Qiao, Q.; Jiang, Y.; Li, G. Inhibition of the PI3K/AKT-NF-kappaB pathway with curcumin enhanced radiation-induced apoptosis in human Burkitt's lymphoma. *J. Pharmacol. Sci.* **2013**, *121*, 247–256. [CrossRef] [PubMed]
207. Chautard, E.; Loubeau, G.; Tchirkov, A.; Chassagne, J.; Vermot-Desroches, C.; Morel, L.; Verrelle, P. Akt signaling pathway: A target for radiosensitizing human malignant glioma. *Neuro Oncol.* **2010**, *12*, 434–443. [PubMed]

208. Liu, W.L.; Gao, M.; Tzen, K.Y.; Tsai, C.L.; Hsu, F.M.; Cheng, A.L.; Cheng, J.C.H. Targeting Phosphatidylinositide3-Kinase/Akt pathway by BKM120 for radiosensitization in hepatocellular carcinoma. *Oncotarget* **2014**, *5*, 3662–3672. [CrossRef] [PubMed]
209. Ekshyyan, O.; Rong, Y.H.; Rong, X.H.; Pattani, K.M.; Abreo, F.; Caldito, G.; Chang, J.K.S.; Arnpil, F.; Glass, J.; Nathan, C.A.O. Comparison of radiosensitizing effects of the mammalian target of rapamycin inhibitor CCI-779 to cisplatin in experimental models of head and neck squamous cell carcinoma. *Mol. Cancer Ther.* **2009**, *8*, 2255–2265. [CrossRef] [PubMed]
210. Kim, K.W.; Myers, C.J.; Jung, D.K.; Lu, B. NVP-BEZ-235 enhances radiosensitization via blockade of the PI3K/mTOR pathway in cisplatin-resistant non-small cell lung carcinoma. *Genes Cancer* **2014**, *5*, 293–302. [PubMed]
211. Ma, Z.K.; Ya, G.L.; Zhou, B.; Fan, Y.G.; Gao, S.G.; Feng, X.S. The Chk1 inhibitor AZD7762 sensitises p53 mutant breast cancer cells to radiation *in vitro* and *in vivo*. *Mol. Med. Rep.* **2012**, *6*, 897–903. [PubMed]
212. Borst, G.R.; McLaughlin, M.; Kyula, J.N.; Neijenhuis, S.; Khan, A.; Good, J.; Zaidi, S.; Powell, N.G.; Meier, P.; Collins, I.; *et al*. Targeted radiosensitization by the Chk1 inhibitor SAR-020106. *Int. J. Radiat. Oncol. Biol. Phys.* **2013**, *85*, 1110–1118. [CrossRef] [PubMed]
213. Morgan, M.A.; Parsels, L.A.; Zhao, L.L.; Parsels, J.D.; Davis, M.A.; Hassan, M.C.; Arumugarajah, S.; Hylander-Gans, L.; Morosini, D.; Simeone, D.M.; *et al*. Mechanism of radiosensitization by the Chk1/2 inhibitor AZD7762 involves abrogation of the G(2) checkpoint and inhibition of homologous recombinational DNA repair. *Cancer Res.* **2010**, *70*, 4972–4981. [CrossRef] [PubMed]
214. Prevo, R.; Fokas, E.; Reaper, P.M.; Charlton, P.A.; Pollard, J.R.; McKenna, W.G.; Muschel, R.J.; Brunner, T.B. The novel ATR inhibitor VE-821 increases sensitivity of pancreatic cancer cells to radiation and chemotherapy. *Cancer Biol. Ther.* **2012**, *13*, 1072–1081. [CrossRef] [PubMed]
215. Munshi, A.; Kurland, J.F.; Nishikawa, T.; Chiao, P.J.; Andreeff, M.; Meyn, R.E. Inhibition of constitutively activated nuclear factor-kappa B radiosensitizes human melanoma cells. *Mol. Cancer Ther.* **2004**, *3*, 985–992. [PubMed]
216. Kim, B.Y.; Kim, K.A.; Kwon, O.; Kim, S.O.; Kim, M.S.; Kim, B.S.; Oh, W.K.; Kim, G.D.; Jung, M.; Ahn, J.S. NF-kappa B inhibition radiosensitizes Ki-Ras-transformed cells to ionizing radiation. *Carcinogenesis* **2005**, *26*, 1395–1403. [CrossRef] [PubMed]
217. Tsuboi, Y.; Kurimoto, M.; Nagai, S.; Hayakawa, Y.; Kamiyama, H.; Hayashi, N.; Kitajima, I.; Endo, S. Induction of autophagic cell death and radiosensitization by the pharmacological inhibition of nuclear factor-kappa B activation in human glioma cell lines. *J. Neurosurg.* **2009**, *110*, 594–604. [CrossRef] [PubMed]
218. Meng, Y.R.; Efimova, E.V.; Hamzeh, K.W.; Darga, T.E.; Mauceri, H.J.; Fu, Y.X.; Kron, S.J.; Weichselbaum, R.R. Radiation-inducible immunotherapy for cancer: senescent tumor cells as a cancer vaccine. *Mol. Ther.* **2012**, *20*, 1046–1055. [CrossRef] [PubMed]
219. Wilken, R.; Veena, M.S.; Wang, M.B.; Srivatsan, E.S. Curcumin: A review of anti-cancer properties and therapeutic activity in head and neck squamous cell carcinoma. *Mol. Cancer* **2011**, *10*. [CrossRef]
220. Glienke, W.; Maute, L.; Wicht, J.; Bergmann, L. Curcumin inhibits constitutive STAT3 phosphorylation in human pancreatic cancer cell lines and downregulation of survivin/BIRC5 gene expression. *Cancer Investig.* **2010**, *28*, 166–171. [CrossRef] [PubMed]
221. Chendil, D.; Ranga, R.S.; Meigooni, D.; Sathishkumar, S.; Ahmed, M.M. Curcumin confers radiosensitizing effect in prostate cancer cell line PC-3. *Oncogene* **2004**, *23*, 1599–1607. [CrossRef] [PubMed]
222. Garg, A.K.; Buchholz, T.A.; Aggarwal, B.B. Chemosensitization and radiosensitization of tumors by plant polyphenols. *Antioxid. Redox Signal.* **2005**, *7*, 1630–1647. [CrossRef] [PubMed]
223. Okunieff, P.; Xu, J.H.; Hu, D.P.; Liu, W.M.; Zhang, L.R.; Morrow, G.; Pentland, A.; Ryan, J.L.; Ding, I. Curcumin protects against radiation-induced acute and chronic cutaneous toxicity in mice and decreases mRNA expression of inflammatory and fibrogenic cytokines. *Int. J. Radiat. Oncol. Biol. Phys.* **2006**, *65*, 890–898. [CrossRef] [PubMed]
224. Kim, W.; Seong, K.M.; Youn, B. Phenylpropanoids in radioregulation: Double edged sword. *Exp. Mol. Med.* **2011**, *43*, 323–333. [CrossRef] [PubMed]
225. Rashid, A.; Liu, C.Q.; Sanli, T.; Tsiani, E.; Singh, G.; Bristow, R.G.; Dayes, I.; Lukka, H.; Wright, J.; Tsakiridis, T. Resveratrol enhances prostate cancer cell response to ionizing radiation. Modulation of the AMPK, Akt and mTOR pathways. *Radiat. Oncol.* **2011**, *6*, 144. [CrossRef] [PubMed]

226. Kma, L. Synergistic effect of resveratrol and radiotherapy in control of cancers. *Asian Pac. J. Cancer Prev.* **2013**, *14*, 6197–6208. [CrossRef] [PubMed]
227. Scarlatti, F.; Sala, G.; Ricci, C.; Maioli, C.; Milani, F.; Minella, M.; Botturi, M.; Ghidoni, R. Resveratrol sensitization of DU145 prostate cancer cells to ionizing radiation is associated to ceramide increase. *Cancer Lett.* **2007**, *253*, 124–130. [CrossRef] [PubMed]
228. Luo, H.M.; Wang, L.; Schulte, B.A.; Yang, A.M.; Tang, S.S.; Wang, G.Y. Resveratrol enhances ionizing radiation-induced premature senescence in lung cancer cells. *Int. J. Oncol.* **2013**, *43*, 1999–2006. [PubMed]
229. Carsten, R.E.; Bachand, A.M.; Bailey, S.M.; Ullrich, R.L. Resveratrol reduces radiation-induced chromosome aberration frequencies in mouse bone marrow cells. *Radiat. Res.* **2008**, *169*, 633–638. [CrossRef] [PubMed]
230. Akimoto, T.; Nonaka, T.; Ishikawa, H.; Sakurai, H.; Saitoh, J.; Takahashi, T.; Mitsuhashi, N. Genistein, a tyrosine kinase inhibitor, enhanced radiosensitivity in human esophageal cancer cell lines *in vitro*: Possible involvement of inhibition of survival signal transduction pathways. *Int. J. Radiat. Oncol. Biol. Phys.* **2001**, *50*, 195–201. [CrossRef]
231. Zhang, B.; Liu, J.Y.; Pan, J.S.; Han, S.P.; Yin, X.X.; Wang, B.; Hu, G. Combined treatment of ionizing radiation with genistein on cervical cancer HeLa cells. *J. Pharmacol. Sci.* **2006**, *102*, 129–135. [CrossRef] [PubMed]
232. Jeong, M.H.; Jin, Y.H.; Kang, E.Y.; Jo, W.S.; Park, H.T.; Lee, J.D.; Yoo, Y.J.; Jeong, S.J. The modulation of radiation-induced cell death by genistein in K562 cells: Activation of thymidine kinase 1. *Cell Res.* **2004**, *14*, 295–302. [CrossRef] [PubMed]
233. Raffoul, J.J.; Wang, Y.; Kucuk, O.; Forman, J.D.; Sarkar, F.H.; Hillman, G.G. Genistein inhibits radiation-induced activation of NF-kappa B in prostate cancer cells promoting apoptosis and G(2)/M cell cycle arrest. *BMC Cancer* **2006**, *6*, 107. [CrossRef] [PubMed]
234. Kim, I.G.; Kim, J.S.; Lee, J.H.; Cho, E.W. Genistein decreases cellular redox potential, partially suppresses cell growth in HL-60 leukemia cells and sensitizes cells to gamma-radiation-induced cell death. *Mol. Med. Rep.* **2014**, *10*, 2786–2792. [PubMed]
235. Priyadarsini, R.V.; Murugan, R.S.; Maitreyi, S.; Ramalingam, K.; Karunagaran, D.; Nagini, S. The flavonoid quercetin induces cell cycle arrest and mitochondria-mediated apoptosis in human cervical cancer (HeLa) cells through p53 induction and NF-kappa B inhibition. *Eur. J. Pharmacol.* **2010**, *649*, 84–91. [CrossRef] [PubMed]
236. Kim, H.; Moon, J.Y.; Ahn, K.S.; Cho, S.K. Quercetin induces mitochondrial mediated apoptosis and protective autophagy in human glioblastoma U373MG cells. *Oxidative Med. Cell. Longev.* **2013**. [CrossRef] [PubMed]
237. Sudan, S.; Rupasinghe, H.P.V. Quercetin-3-*O*-glucoside Induces Human DNA Topoisomerase II Inhibition, cell cycle arrest and apoptosis in hepatocellular carcinoma cells. *Anticancer Res.* **2014**, *34*, 1691–1699. [PubMed]
238. Lin, C.H.; Yu, Y.; Zhao, H.G.; Yang, A.M.; Yan, H.; Cui, Y.L. Combination of quercetin with radiotherapy enhances tumor radiosensitivity *in vitro* and *in vivo*. *Radiother. Oncol.* **2012**, *104*, 395–400. [CrossRef] [PubMed]
239. Benkovic, V.; Knezevic, A.H.; Dikic, D.; Lisicic, D.; Orsolic, N.; Basic, I.; Kopjar, N. Radioprotective effects of quercetin and ethanolic extract of propolis in gamma-irradiated mice. *Arch. Ind. Hyg. Toxicol.* **2009**, *60*, 129–138. [CrossRef] [PubMed]
240. Liu, H.; Xue, J.X.; Li, X.; Ao, R.; Lu, Y. Quercetin liposomes protect against radiation-induced pulmonary injury in a murine model. *Oncol. Lett.* **2013**, *6*, 453–459. [CrossRef] [PubMed]
241. Meng, Y.R.; Beckett, M.A.; Liang, H.; Mauceri, H.J.; van Rooijen, N.; Cohen, K.S.; Weichselbaum, R.R. Blockade of tumor necrosis factor alpha signaling in tumor-associated macrophages as a radiosensitizing strategy. *Cancer Res.* **2010**, *70*, 1534–1543. [CrossRef] [PubMed]
242. Formenti, S.C.; Demaria, S. Combining radiotherapy and cancer immunotherapy: A paradigm shift. *J. Natl. Cancer Inst.* **2013**, *105*, 256–265. [CrossRef] [PubMed]
243. Overgaard, J. Hypoxic radiosensitization: Adored and ignored. *J. Clin. Oncol.* **2007**, *25*, 4066–4074. [CrossRef] [PubMed]
244. Meijer, T.W.H.; Kaanders, J.H.A.M.; Span, P.N.; Bussink, J. Targeting hypoxia, HIF-1, and tumor glucose metabolism to improve radiotherapy efficacy. *Clin. Cancer Res.* **2012**, *18*, 5585–5594. [CrossRef] [PubMed]

245. Li, S.H.; Shin, D.H.; Chun, Y.S.; Lee, M.K.; Kim, M.S.; Park, J.W. A novel mode of action of YC-1 in HIF inhibition: Stimulation of FIH-dependent p300 dissociation from HIF-1 alpha. *Mol. Cancer Ther.* **2008**, *7*, 3729–3738. [CrossRef] [PubMed]
246. Yeo, E.J.; Chun, Y.S.; Cho, Y.S.; Kim, J.H.; Lee, J.C.; Kim, M.S.; Park, J.W. YGI: A potential anticancer drug targeting hypoxia-inducible factor 1. *J. Natl. Cancer Inst.* **2003**, *95*, 516–525. [CrossRef] [PubMed]
247. Shin, D.H.; Kim, J.H.; Jung, Y.J.; Kim, K.E.; Jeong, J.M.; Chun, Y.S.; Park, J.W. Preclinical evaluation of YG-1, a HIF inhibitor, for the prevention of tumor spreading. *Cancer Lett.* **2007**, *255*, 107–116. [CrossRef] [PubMed]
248. Harada, H.; Inoue, M.; Itasaka, S.; Hirota, K.; Morinibu, A.; Shinomiya, K.; Zeng, L.H.; Ou, G.F.; Zhu, Y.X.; Yoshimura, M.; *et al*. Cancer cells that survive radiation therapy acquire HIF-1 activity and translocate towards tumour blood vessels. *Nat. Commun.* **2012**, *3*. [CrossRef] [PubMed]
249. Kallio, P.J.; Pongratz, I.; Gradin, K.; McGuire, J.; Poellinger, L. Activation of hypoxia-inducible factor 1 alpha: Posttranscriptional regulation and conformational change by recruitment of the Arnt transcription factor. *Proc. Natl. Acad. Sci. USA* **1997**, *94*, 5667–5672. [CrossRef] [PubMed]
250. Lee, K.; Zhang, H.F.; Qian, D.Z.; Rey, S.; Liu, J.O.; Semenza, G.L. Acriflavine inhibits HIF-1 dimerization, tumor growth, and vascularization. *Proc. Natl. Acad. Sci. USA* **2009**, *106*, 17910–17915. [CrossRef] [PubMed]
251. Liu, Y.V.; Baek, J.H.; Zhang, H.; Diez, R.; Cole, R.N.; Semenza, G.L. RACK1 competes with HSP90 for binding to HIF-1 alpha and is required for O-2-independent and HSP90 inhibitor-induced degradation of HIF-1 alpha. *Mol. Cell* **2007**, *25*, 207–217. [CrossRef] [PubMed]
252. Kim, W.Y.; Oh, S.H.; Woo, J.K.; Hong, W.K.; Lee, H.Y. Targeting heat shock protein 90 overrides the resistance of lung cancer cells by blocking radiation-induced stabilization of hypoxia-inducible factor-1 alpha. *Cancer Res.* **2009**, *69*, 1624–1632. [CrossRef] [PubMed]
253. Nieder, C.; Wiedenmann, N.; Andratschke, N.; Molls, M. Current status of angiogenesis inhibitors combined with radiation therapy. *Cancer Treat. Rev.* **2006**, *32*, 348–364. [CrossRef] [PubMed]
254. Dings, R.P.M.; Loren, M.; Heun, H.; McNiel, E.; Griffioen, A.W.; Mayo, K.H.; Griffin, R.J. Scheduling of radiation with angiogenesis inhibitors anginex and avastin improves therapeutic outcome via vessel normalization. *Clin. Cancer Res.* **2007**, *13*, 3395–3402. [CrossRef] [PubMed]
255. Kleibeuker, E.A.; Griffioen, A.W.; Verheul, H.M.; Slotman, B.J.; Thijssen, V.L. Combining angiogenesis inhibition and radiotherapy: A double-edged sword. *Drug Resist. Updates* **2012**, *15*, 173–182. [CrossRef] [PubMed]
256. Choy, H.; Milas, L. Enhancing radiotherapy with cyclooxygenase-2 enzyme inhibitors: A rational advance? *J. Natl. Cancer Inst.* **2003**, *95*, 1440–1452. [CrossRef] [PubMed]



© 2015 by the authors; licensee MDPI, Basel, Switzerland. This article is an open access article distributed under the terms and conditions of the Creative Commons by Attribution (CC-BY) license (http://creativecommons.org/licenses/by/4.0/).

International Journal of
Molecular Sciences

MDPI

Article

Danusertib Induces Apoptosis, Cell Cycle Arrest, and Autophagy but Inhibits Epithelial to Mesenchymal Transition Involving PI3K/Akt/mTOR Signaling Pathway in Human Ovarian Cancer Cells

Dan Zi [1,2], Zhi-Wei Zhou [2], Ying-Jie Yang [1,3], Lin Huang [1], Zun-Lun Zhou [1], Shu-Ming He [4], Zhi-Xu He [5,*] and Shu-Feng Zhou [2,*]

Received: 20 August 2015 ; Accepted: 5 November 2015 ; Published: 13 November 2015 ;
Corrected: 14 April 2026
Academic Editor: William Chi-shing Cho

1 Department of Obstetrics and Gynecology, Affiliated Hospital of Guizhou Medical University, Guiyang 550004, China; zidangy08@163.com (D.Z.); yyjgmc@163.com (Y.-J.Y.); hllgmc@163.com (L.H.); zzlgmc@163.com (Z.-L.Z.)
2 Department of Pharmaceutical Sciences, College of Pharmacy, University of South Florida, Tampa, FL 33612, USA; zhouzw105@outlook.com
3 Department of Gynecologic Oncology Surgery, Affiliated Cancer Hospital of Guizhou Medical University, Guiyang 550002, China
4 Department of Obstetrics and Gynecology, Xiaolan Hospital, Southern Medical University, Zhongshan 528415, China; hsmgmc@163.com
5 Guizhou Provincial Key Laboratory for Regenerative Medicine, Stem Cell and Tissue Engineering Research Center & Sino-US Joint Laboratory for Medical Sciences, Guizhou Medical University, Guiyang 550004, China
* Correspondence: hzxgmc@163.com (Z.-X.H.); szhou@hqu.edu.cn (S.-F.Z.); Tel.: +86-851-8690-8118 (Z.-X.H.); +1-813-974-6276 (S.-F.Z.); Fax: +86-851-8841-6015 (Z.-X.H.); +1-813-905-9885 (S.-F.Z.)

Abstract: Ovarian carcinoma (OC) is one of the most common gynecological malignancies, with a poor prognosis for patients at advanced stage. Danusertib (Danu) is a pan-inhibitor of the Aurora kinases with unclear anticancer effect and underlying mechanisms in OC treatment. This study aimed to examine the cancer cell killing effect and explore the possible mechanisms with a focus on proliferation, cell cycle progression, apoptosis, autophagy, and epithelial to mesenchymal transition (EMT) in human OC cell lines C13 and A2780cp. The results showed that Danu remarkably inhibited cell proliferation, induced apoptosis and autophagy, and suppressed EMT in both cell lines. Danu arrested cells in G_2/M phase and led to an accumulation of polyploidy through the regulation of the expression key cell cycle modulators. Danu induced mitochondria-dependent apoptosis and autophagy in dose and time-dependent manners. Danu suppressed PI3K/Akt/mTOR signaling pathway, evident from the marked reduction in the phosphorylation of PI3K/Akt/mTOR, contributing to the autophagy inducing effect of Danu in both cell lines. In addition, Danu inhibited EMT. In aggregate, Danu exerts potent inducing effect on cell cycle arrest, apoptosis, and autophagy, but exhibits a marked inhibitory effect on EMT. PI3K/Akt/mTOR signaling pathway contributes, partially, to the cancer cell killing effect of Danu in C13 and A2780cp cells.

Keywords: danusertib; ovarian cancer; cell cycle; apoptosis; autophagy; epithelial to mesenchymal transition

1. Introduction

Ovarian cancer is the eighth most common type of cancer and the seventh most common cause of cancer-related death in women globally, with 239,000 new cases and around 152,000 deaths in 2012 [1]. In 2015, there has been an estimated 21,290 cases and 14,180 deaths related to ovarian cancer in the US [2], it is the eighth most common cancer and the fifth leading cause of cancer related death, after lung and bronchus, breast, colorectal, and pancreatic cancers in the US [3]. In China, there is an increasing estimated incidence of ovarian cancer [1,4]. The incidence has increased by 30% in the last decade and the mortality rate has increased by 18% with 15,000 deaths each year [1,4]. Clinically, most patients with epithelial ovarian cancer (EOC) are diagnosed at advanced stage with cancer cell metastasis, which substantially jeopardizes the therapeutic opportunity, compromises the therapeutic effect, and increases the risk of recurrence and early death [5]. It has been demonstrated that peritoneal dissemination and ascites are the major causes of patient morbidity and mortality; and currently, platinum- and taxane-based chemotherapy is standard of care for the first-line treatment of patients with advanced ovarian, fallopian tube, or peritoneal cancer [5]. Although responses are observed in up to ~80% of patients; 70%–80% of responding patients eventually will relapse and require further systemic chemotherapy and the five-year survival rate is about 30% to 60% [6]. Patients who relapse >6–12 months after completing platinum-based chemotherapy may respond again to platinum-based therapy, however, it considerably limits the repeated use of platinum agents due to acquired resistance or intolerance in clinical practice [6]. Therefore, there is an urgent need to develop new, safe, and effective therapeutics for the treatment of advanced EOC.

The Aurora kinases belong to the family of highly conserved serine/threonine protein kinases, with an essential role in controlling entry into mitosis, centrosome function, chromosome assembly and segregation [7]. There are three members of the family, including aurora kinase A, B, and C (AURKA/B/C). AURKA is essential for the timely entry into the M phase of the cell cycle, maintaining spindle bipolarity and chromosome segregation. AURKB is required for chromosome condensation, alignment on the spindle, spindle checkpoint function, and cytokinesis. Little is known about the role of AURKC. As the key regulators of mitosis, Aurora kinases are frequently overexpressed in cancer cells and accumulating evidence shows that the aberration in the activity and expression of Aurora kinases has been implicated in the pathogenesis of many types of cancer [8]. Therefore, Aurora kinases have emerged as attractive therapeutic targets for cancer therapies [9,10].

Recently, several small-molecule inhibitors of Aurora kinases have been developed and some of them have shown clinical efficacy in phase I and II clinical trials [11,12]. Among of those, one of the most advanced compounds is Danusertib (Danu, formerly PHA-739358) (Figure 1A), which exerts potent inhibitory activity against AURKA, B, and C with the IC_{50} value of 13, 79, and 61 nM, respectively [13–15]. Danu has been investigated in Phase I and II trials, showing a great therapeutic potential in the treatment of a wide range of cancers [14,16]. Moreover, Danu has also shown variable anticancer effect at different stages of preclinical experimental settings [17,18]. However, the effect and underlying mechanisms of Danu have not yet been fully unveiled in ovarian cancer, in particular, under the circumstance of drug resistance. In the present study, we aimed to investigate the effect of Danu on the proliferation, cell cycle distribution, apoptosis, autophagy, and epithelial-to-mesenchymal transition (EMT), and explored the possible mechanisms underlying the anticancer effect of Danu in ovarian cancer cell lines C13 and A2780cp. Notably, these two cell lines are resistant to cisplatin, which often causes therapeutic failure in clinical practice, which emphasizes the importance of the investigation on the effect of Danu in cisplatin resistant cells in the present study.

2. Results

2.1. Danu Inhibits the Viability of C13 and A2780cp Cells

First, we tested the effect of Danu on the viability of C13 and A2780cp cells using MTT assay. Danu treatment significantly decreased viability at concentrations from 0.01 to 50 μM for 24 and

48 h in both cell lines (Figure 1A,B). In comparison to the control cells, the percentage of the viability for C13 cells was 80.0%–31.0% and 82.9%–14.5% when treated with Danu from 0.01 to 50 μM for 24 and 48 h, respectively (Figure 1B); and the percentage of the viability for A2780cp cells was 94.0%–34.4% and 88.4%–23.4%, when exposed to Danu from 0.01 to 50 μM for 24 and 48 h, respectively (Figure 1C). The IC_{50} values were 10.40 and 1.83 μM for C13 cells after 24- and 48-h incubation with Danu, respectively (Figure 1B). For A2780cp cells, the IC_{50} values were 19.89 and 3.88 μM after 24- and 48-h treatment of Danu, respectively (Figure 1C). Taken together, the results show that Danu exerts a potent inhibitory effect on cell growth in C13 and A2780cp cells.

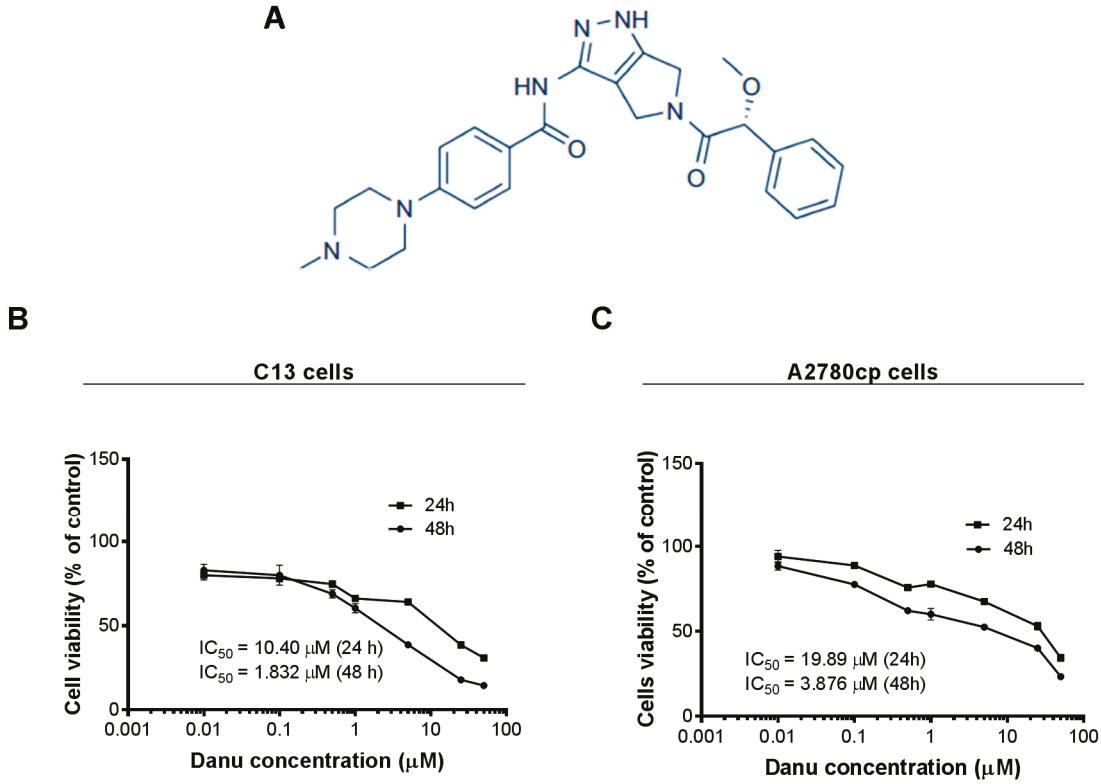

Figure 1. Chemical structure of Danu and cytotoxicity of Danu towards C13 and A2780cp cells. C13 and A2780cp cells were treated with Danu at concentrations ranging from 0.01 to 50 μM for 24 and 48 h. (**A**) Chemical structure of Danu; (**B**) Cell viability of C13 cells; and (**C**) Cell viability of A2780cp cells.

2.2. Danu Induces Cell Cycle Arrest in G_2/M Phase in C13 and A2780cp Cells

After the observation on the effect of Danu on the viability of C13 and A2780cp cells, we examined the effect of Danu on cell cycle distribution of these two cell lines using flow cytometry. Danu induced a remarkable cell cycle arrest in G_2/M phase and led to an accumulation of polyploidy in dose dependent manners in C13 and A2780cp cells (Figure 2). Compared to the basal level (13.3%), the percentage of C13 cells arrested in G_2/M phase ascended to 47.6% and 91.2% when treated with Danu at 0.1 and 0.5 μM for 24 h, respectively ($p < 0.001$, Figure 2A,B). Similarly, in comparison to the control cells (15.6%), the percentage of A2780cp cells arrested in G_2/M phase was 35.0% and 84.8% when treated with Danu at 0.1 and 0.5 μM, respectively ($p < 0.001$, Figure 2A,B). On the other hand, Danu treatment with increased concentration led to a marked reduction in the number of cells in both G_1 and S phases (Figure 2A,B). Intriguingly, we observed the accumulation of polyploidy when cells were treated with Danu at 0.1 and 0.5 μM for 24 h, with a 37.7% and 60.5% increase in C13 cells and 69.2% and 90.1% elevation in A2780cp cells, respectively (Figure 2A,B); whereas there was a marked decrease in the percentage of diploidy when treated with Danu at 0.1 and 0.5 μM. The percentage of

diploidy decreased from 62.4% to 39.5% in C13 cells and the percentage of diploid decreased from 30.8% to 9.9% in A2780cp cells (Figure 2A,B).

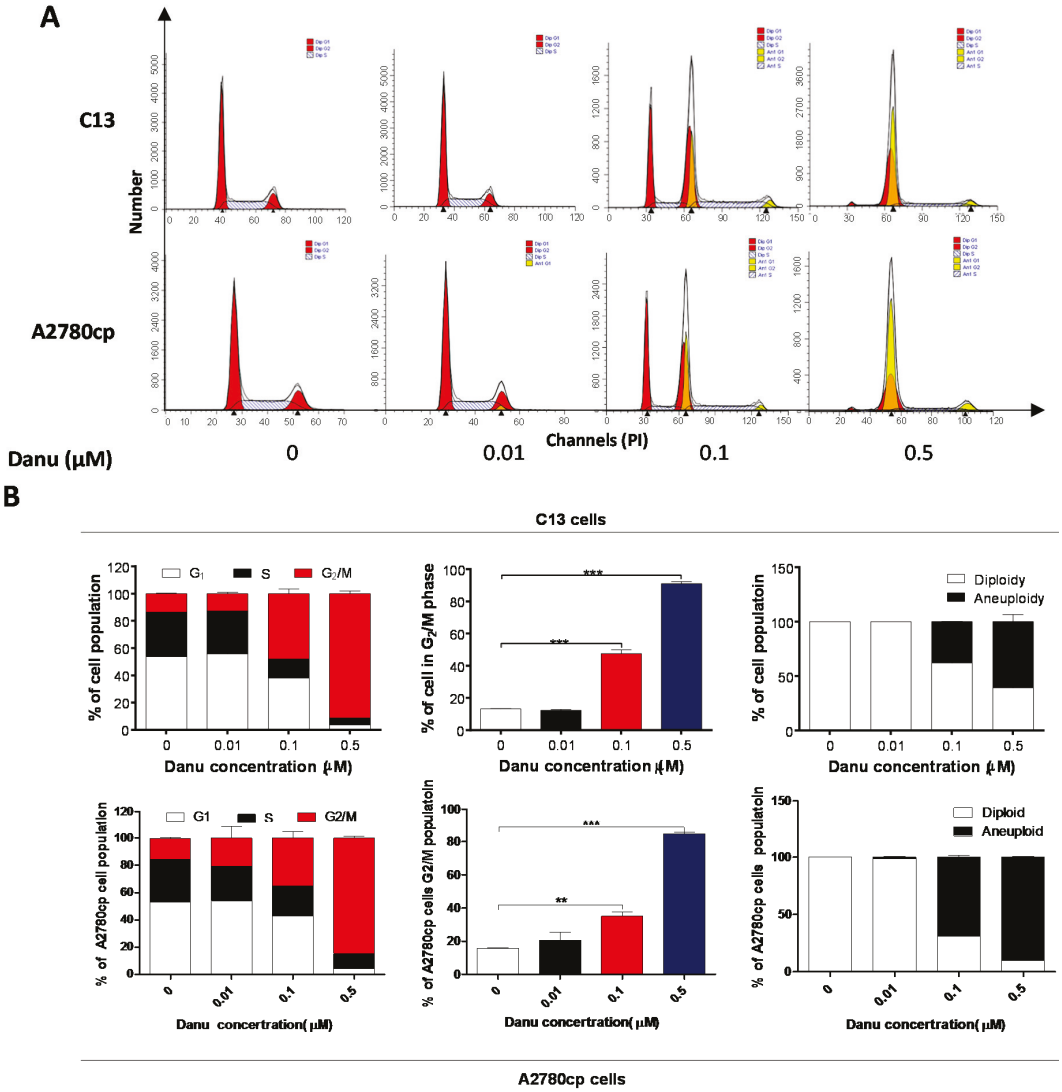

Figure 2. Danu induces cell cycle arrest in G_2/M phase in C13 and A2780cp cells. Cells were treated with Danu at 0.01, 0.1, and 0.5 μM for 24 h and then subject to flow cytometry. (**A**) Flow cytometric plots of cell cycle distribution of C13 and A2780cp cells and (**B**) bar graphs showing the percentage of C13 and A2780cp cells in G_1, S, and G_2/M phases and the percentage of diploidy and polyploidy in C13 and A2780cp cells. Data represent the mean ± SD of three independent experiments. ** $p < 0.01$ and *** $p < 0.001$ by one-way analysis of variance.

To further examine the cell cycle arresting effect of Danu on C13 and A2780cp cells, these two cell lines were treated with 0.5 μM Danu over 72 h. Danu treatment resulted in a marked increase in the percentage of cells arrested in G_2/M phase and an accumulation of polyploidy in C13 and A2780cp cells (Figure 3A,B). The percentage of C13 cells arrested in G_2/M phase was increased to 48.7%, 89.7%, and 86.0% from the basal level (15.8%) and the percentage of A2780cp cells arrested in G_2/M phase was increased to 72.8%, 89.8%, and 88.2% from the basal level (7.2%), when cells were exposed to Danu for 24, 48, and 72 h, respectively (Figure 3A,B). There was also a remarkable reduction in the percentage of cells in both G_1 and S phases in these two cell lines when treated with Danu treatment for 24, 48, and 72 h (Figure 3A,B). However, there was no alteration in the percentage of cells in G_2/M phase when C13 and A2780cp cells were incubated with Danu for 4, 8, and 12 h (Figure 3A,B).

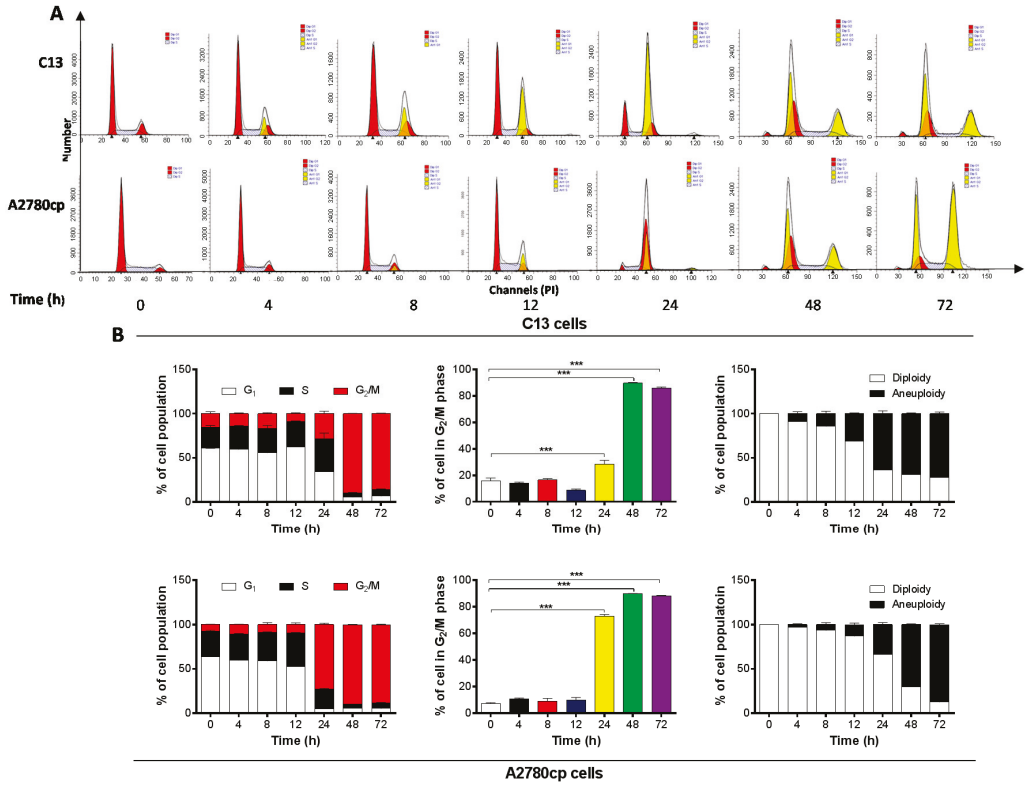

Figure 3. Danu arrests C13 and A2780cp cells in G_2/M phase over a 72-h treatment period. Cells were treated with 0.5 μM Danu for 4, 8, 12, 24, 48, and 72 h and then subject to flow cytometry. (**A**) Flow cytometric plots of cell cycle distribution of C13 and A2780cp cells and (**B**) bar graphs showing the percentage of C13 and A2780cp cells in G_1, S, and G_2/M phases and the percentage of diploidy and polyploidy in C13 and A2780cp cells. Data represent the mean ± SD of three independent experiments. *** $p < 0.001$ by one-way analysis of variance.

Notably, there was an evident occurrence of polyploidy in C13 and A2780cp cells when cells were treated with 0.5 μM Danu from 4 to 72 h. With 4-, 8-, 12-, 24-, 48- to 72-h treatment, the percentage of polyploidy of C13 cells was increased from 8.9%, 14.4%, 31.3%, 63.8%, 68.9% to 72.2%, correspondently, the percentage of diploidy was decreased from 91.1%, 85.6%, 68.7%, 36.2%, 31.1% to 27.8% (Figure 3B). Similarly, the percentage of polyploidy of A2780cp cells was increased from 2.8%, 6.6%, 13.1%, 33.7%, 70.0% to 87.4%, correspondently, the percentage of diploidy was decreased from 7.2%, 93.5%, 86.9%, 66.3%, 30.0% to 12.6% (Figure 3B). Collectively, these results demonstrate that Danu exerts a potent cell cycle arresting effect in C13 and A2780cp cells.

2.3. Danu Alters the Expression of Key Cell Cycle Regulators in C13 and A2780cp Cells

We next examined the effect of Danu on the expression of key cell cycle regulators to explain the cell cycle arresting effect, including CDK1/CDC2, cyclin B1, p21 Waf1/Cip1, p27 Kip1, and p53 in C13 and A2780cp cells. Incubation of C13 and A2780cp cells with Danu at 0.01, 0.1, and 0.5 μM resulted in varying alterations in the expression level of key cell cycle regulators (Figure 4). CDC2 and cyclin B1 are two key regulators for G_2-to-M phase transition [19]. The expression of CDC2 and cyclin B1 was markedly suppressed in both cell lines (Figure 4A,B). There was a 14.3%, 58.4%, and 63.8% reduction in the expression level of CDC2, and 12.8%, 47.4%, and 55.4% decline in the expression level of cyclin B1 in C13 cells, with the treatment of Danu at concentrations of 0.01, 0.1, and 0.5 μM for 24 h, respectively (Figure 4A,B). Similarly, in A2780 cells, there was a 4.1%, 36.9%, and 52.5% decrease in the expression level of CDC2 in A2780cp cells with the treatment of Danu at concentrations of 0.01,

0.1, and 0.5 μM for 24 h, and 43.7%, and 49.1% decrease in the expression level of cyclin B1 with the treatment of Danu at concentrations of 0.1 and 0.5 μM for 24 h, respectively (Figure 4A,B).

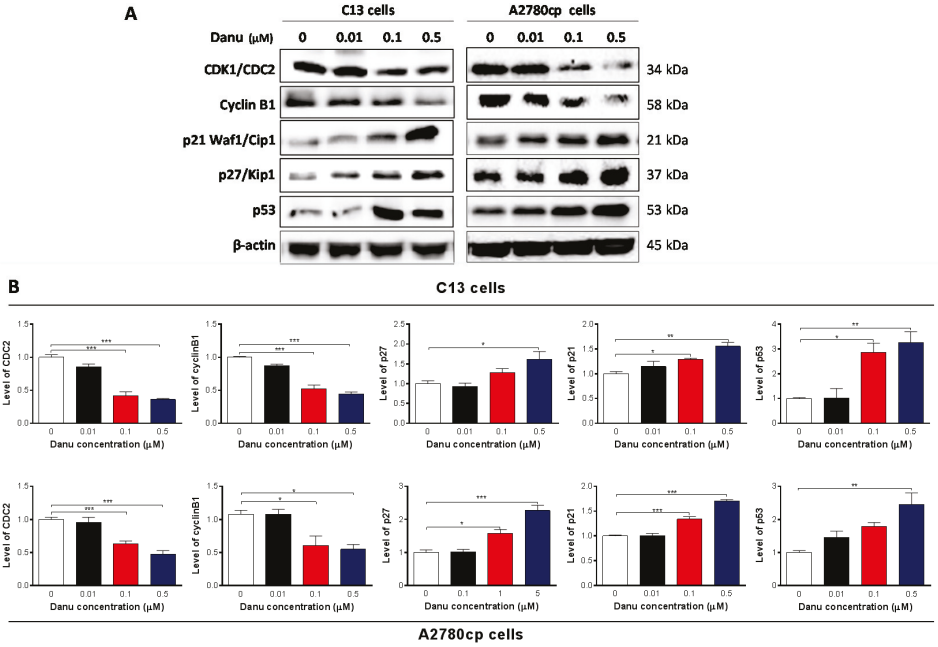

Figure 4. Danu demotes the expression of CDK1/CDC2 and cyclin B1 but promotes the expression of p21 Waf1/Cip1, p27 Kip1, and p53. C13 and A2780cp cells were incubated with Danu 0.01, 0.1, and 0.5 μM for 24 hours and protein samples were subject to Western blotting assays. (**A**) Representative blots of cyclin B1, p21 Waf1/Cip1, p27 Kip1, and p53 and (**B**) bar graphs showing the relative expression level of CDK1/CDC2, cyclin B1, p21 Waf1/Cip1, p27 Kip1, and p53. β-actin was used as the internal control. Data represent the mean ± SD of three independent experiments. * $p < 0.05$, ** $p < 0.01$, and *** $p < 0.001$ by one-way analysis of variance.

Furthermore, p21 Waf1/Cip1, p27 Kip1, and p53 play an important role in the regulation of cell cycle distribution. The tumor suppressor protein p21 Waf1/Cip1 acts as an inhibitor of cell cycle progression, and it serves to inhibit kinase activity and block progression through G_1/S in association with the CDC2/CDK1-Cyclin B1 complex [20]. Phosphorylated p53 upregulates p21 Waf1/Cip1 transcription via a p53-responsive element, and activation of p53 leads to either cell cycle arrest and DNA repair or apoptosis. The expression of p21 Waf1/Cip1, p27 Kip1, and p53 was significantly increased in both cell lines with the treatment of Danu at concentrations of 0.01, 0.1, and 0.5 μM for 24 h. In comparison to the control cells, incubation of C13 cells with Danu at 0.01, 0.1, and 0.5 μM led to a 1.1-, 1.3- and 1.6-fold increase in the expression level of p21 Waf1/Cip1, respectively (Figure 4A,B). There was a 1.3- and 1.6-fold rise in the expression level of p27 Kip1, and 1.9- and 2.7-fold elevation in the expression level of p53 with the treatment of Danu at 0.1 and 0.5 μM, respectively (Figure 4A,B). There was a similar regulatory effect of Danu on the expression levels of p21 Waf1/Cip1, p27 Kip1, and p53 in A2780cp cells. Treating cells with Danu at 0.1 and 0.5 μM increased the expression level of p21 Waf1/Cip1 1.3- and 1.7-fold, elevated the expression level of p27 Kip1 1.5- and 2.3-fold, and increased the expression level of p53 1.8- and 2.5-fold compared to the control cells, respectively (Figure 4A,B). These results indicate that Danu significantly down-regulates the expression level of CDC2, cyclin B1 but up-regulates the expression level of p21 Waf1/Cip1, p27 Kip1, and p53 in both C13 and A2780cp cells, contributing, at least in part, to the cell cycle arresting effect of Danu in both cell lines.

2.4. Danu Induces Apoptosis of C13 and A2780cp Cells via Activation of Mitochondria-Dependent Pathway

To further examine the cancer cell killing effect of Danu on C13 and A2780cp cells, the effect of Danu on apoptosis was tested by flow cytometry. Exposure of cells to Danu for 48 h resulted in a remarkable apoptosis of C13 and A2780cp cells (Figures 5 and 6). In C13 cells, the total percentage of apoptotic cells (early + late apoptosis) was 3.2%, 8.0%, and 37.4% when treated with Danu at 0.01, 0.1, and 0.5 μM for 48 h, respectively (Figure 5A,B). There was a 2.6- and 11.9-fold increase when treated with 0.1 and 0.5 μM Danu, compared to the control cells ($p < 0.001$; Figure 5A,B). Treating A2780cp cells with Danu 0.1 and 0.5 μM for 48 h increased the total percentage of apoptotic cells (early and late apoptosis) from 3.2% at the basal level to 32.4% and 49.2%, and there was a 10.1-, and 15.4-fold increase in apoptotic A2780cp cells, compared with the control, respectively ($p < 0.001$, Figure 5A,B). In addition, the effect of Danu on the apoptosis of C13 and A2780cp cells was examined when the cells were treated over 72 h. Incubation of C13 and A2780cp cells with 0.5 μM Danu time-dependently increased the number of apoptotic cells (Figure 6A,B). The percentage of apoptotic C13 cells was increased from 8.2% at basal level (zero time) to 11.6%, 11.4%, 11.0%, 14.5%, 19.9%, and 32.0% when treated with 0.5 μM Danu for 4, 8, 12, 24, 48, and 72 h, respectively; and there was a 2.4- and 3.9-fold rise in the apoptotic C13 cells after 48- and 72-h treatment, respectively ($p < 0.01$ or 0.001; Figure 6A,B). Similarly, the percentage of apoptotic A2780cp cells was increased from 2.2% at basal level to 3.1%, 3.3%, 5.4%, 17.3%, and 34.1% when treated with 0.5 μM Danu for 4, 12, 24, 48 and 72 h, respectively; and there was a 7.9- and 15.5-fold elevation in the apoptotic A2780cp cells after 48- and 72-h treatment, respectively ($p < 0.001$; Figure 6A,B). In aggregate, Danu remarkably induces apoptotic cell death in both C13 and A2780cp cells.

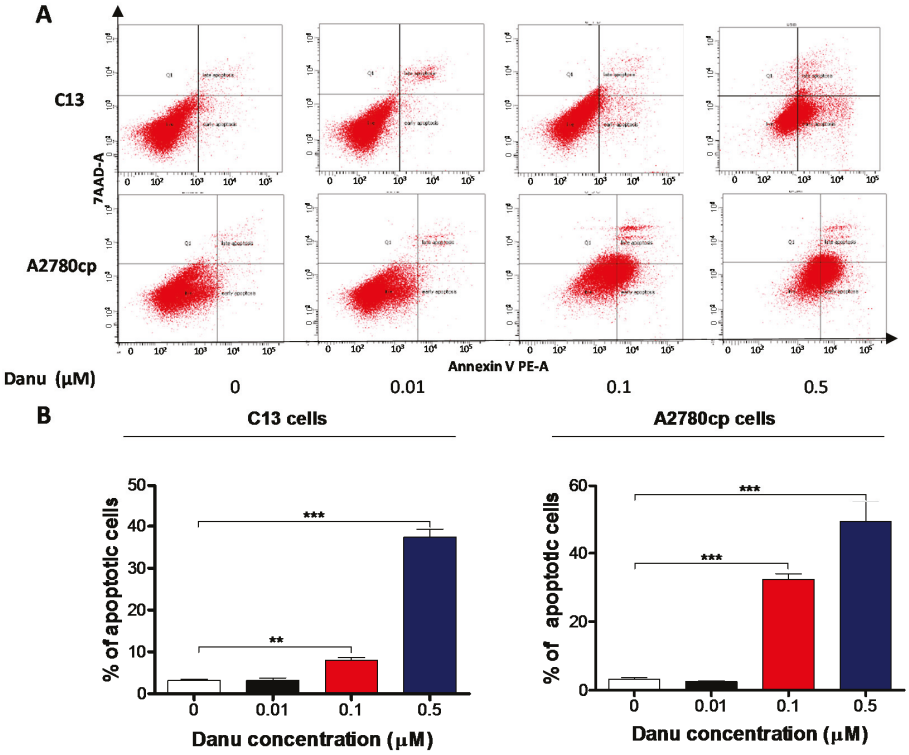

Figure 5. Danu induces apoptotic cell death in C13 and A2780cp cells. C13 and A2780cp cells were incubated with Danu 0.01, 0.1, and 0.5 μM for 48 h and then subject to flow cytometry. (**A**) Flow cytometric plots of specific cell population (live, early apoptosis, and late apoptosis) in C13 and A2780cp cells and (**B**) bar graphs showing the percentage of apoptosis of C13 and A2780cp cells. Data represent the mean ± SD of three independent experiments.** $p < 0.01$ and *** $p < 0.001$ by one-way analysis of variance.

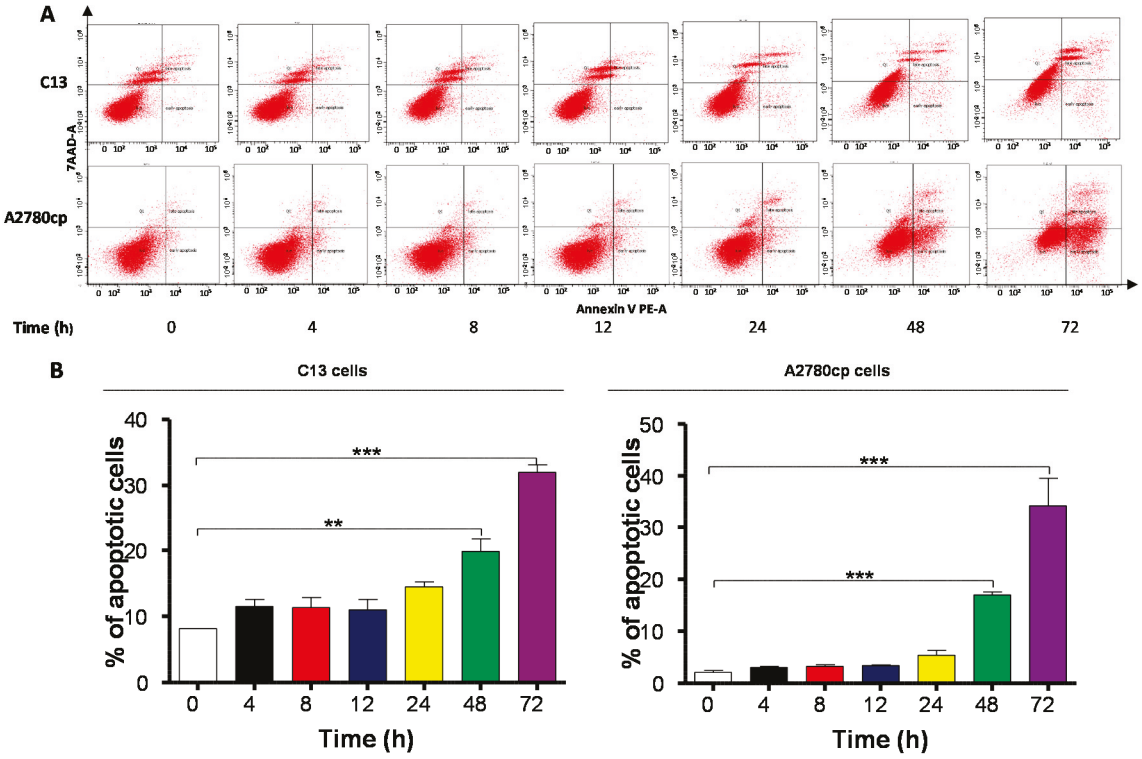

Figure 6. Danu induces apoptotic cell death in C13 and A2780cp cells over a 72-h treatment period. C13 and A2780cp cells were incubated with Danu 0.5 μM for 4, 8, 12, 24, 48, and 72 h and then subject to flow cytometry. (**A**) Flow cytometric plots of specific cell population (live, early apoptosis, and late apoptosis) in C13 and A2780cp cells and (**B**) bar graphs showing the percentage of apoptosis of C13 and A2780cp cells. Data represent the mean ± SD of three independent experiments. ** $p < 0.01$ and *** $p < 0.001$ by one-way analysis of variance.

Following the observation of apoptosis-inducing effect of Danu on C13 and A2780 cells, we further examined the effect of Danu on the expression of the key pro-apoptotic and anti-apoptotic proteins in C13 and A2780cp cells to explore the possible mechanisms for the apoptosis-inducing effect of Danu in these two cell lines. As shown in Figure 7A,B, Danu treatment markedly increased the expression level of Bax, while reducing the expression level of Bcl-xl and Bcl-2 in both cell lines. Incubating C13 cells with 0.1 and 0.5 μM Danu for 48 h resulted in a 2.2- and 2.2-fold increase in the expression level of Bax, respectively ($p < 0.05$ or 0.01, Figure 7A,B). In contrast, the expression level of Bcl-xl was decreased 50.9% and 34.3% and the expression level of Bcl-2 was reduced 40.5% and 51.9%, when treated with Danu at 0.1 and 0.5 μM for 48 h, respectively ($p < 0.05$, 0.01, or 0.001, Figure 7A,B). In A2780cp cells, 0.5 μM Danu increased the expression level of Bax 1.5-fold; whereas the expression level of Bcl-xl was decreased 53.4% and 47.5% and the expression level of Bcl-2 was reduced 23.9% and 41. 3% when treated with Danu at 0.1 and 0.5 μM, respectively ($p < 0.05$ or 0.01, Figure 7A,B). Due to the promoting effect of PUMA on apoptosis, the effect of Danu on the expression level of PUMA was also examined. Incubation of C13 cells with 0.1 and 0.5 μM Danu increased the expression level of PUMA 2.0- and 2.1-fold, respectively ($p < 0.05$, Figure 7A,B). In A2780cp cells, the expression level of PUMA was increased 1.6-fold when cells were treated with 0.1 μM Danu ($p < 0.05$, Figure 7A,B).

Disturbance of the balance of pro-apoptotic protein Bax and anti-apoptotic protein Bcl-2 initiates the release of cytochrome c from the mitochondria to the cytosol that is the early event and in turn triggers the activation of the caspase-dependent apoptotic cascade [21]. As such, we examined the effect of Danu treatment on the release of cytochrome c from mitochondria to cytosol in C13 and A2780cp cells. Treatment of these two cell lines with Danu for 48 h markedly increased the cytosolic content of cytochrome c and increased the level of c-caspase 9 and c-caspase 3 ($p < 0.05$, 0.01 or 0.001,

Figure 7A,B). Taken together, these results indicate that Danu induces mitochondria-dependent apoptosis in C13 and A2780cp cells.

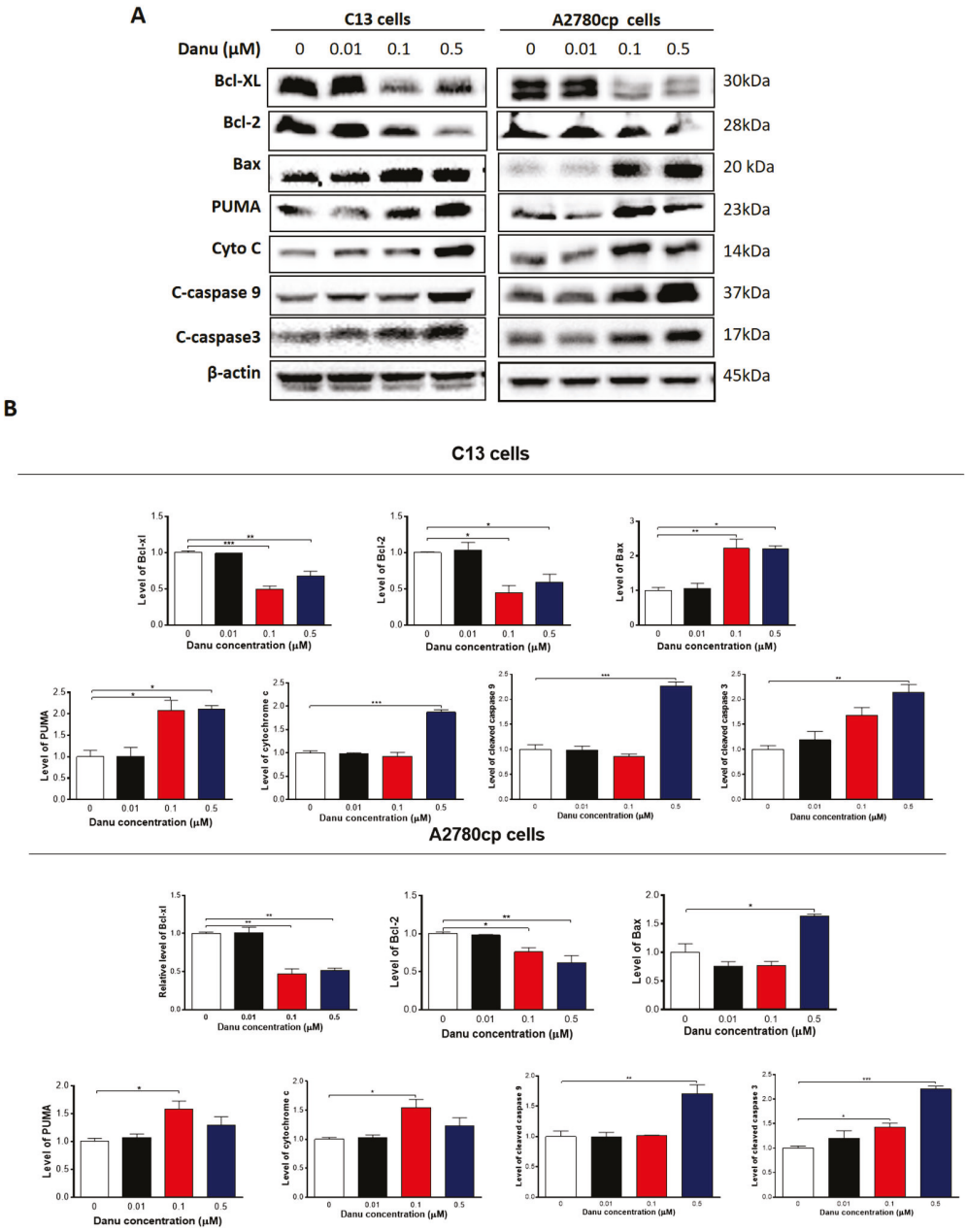

Figure 7. Danu alters the expression of pro-apoptotic and anti-apoptotic proteins in C13 and A2780cp cells. C13 and A2780cp cells were incubated with Danu 0.01, 0.1, and 0.5 μM for 48 h and the protein samples were subject to Western blotting assay. (**A**) Representative blots of B-cell lymphoma-extra-large (Bcl-xl), B-cell lymphoma 2 (Bcl-2), Bcl-2-like protein 4/Bcl-2-associated X protein (Bax), p53 up-regulated modulator of apoptosis (PUMA), cytochrome c, c-caspase 9, and c-caspase 3 in C13 and A2780cp cells. (**B**) Bar graphs showing relative expression level of Bcl-xl, Bcl-2, Bax, PUMA, cytochrome c, c-caspase 9, and c-caspase 3 in C13 and A2780cp cells. β-actin was used as the internal control. Data represent the mean ± SD of the three independent experiments. * $p < 0.05$, ** $p < 0.01$, and *** $p < 0.001$ by one-way analysis of variance. The raw data can be found in the Supplementary Material.

2.5. Danu Induces Autophagy in C13 and A2780cp Cells

Next, we also examined the effect of Danu on another dominant type of programmed cell death-autophagy in C13 and A2780cp cells using flow cytometric analysis, confocal fluorescence microscopic examination. As shown in Figure 8A,B, the percentage of autophagy at basal level was 8.0% and 8.9% for C13 and A2780cp cells, respectively. Incubation of C13 and A2780cp cells with Danu for 24 h remarkably increased the percentage of autophagy. In C13 cells, there was a 2.3- and 4.2-fold increase in the percentage of autophagy when treated with 0.1 and 0.5 μM Danu for 24 h compared to the control cells, respectively ($p < 0.01$ or 0.001, Figure 8A,B). Treatment of A2780cp cells with 0.1 and 0.5 μM Danu for 24 h resulted in a 1.6- and 1.8-fold increase in the percentage of autophagy, respectively ($p < 0.01$, Figure 8A,B). Low concentration of Danu (0.01 μM) did not significantly induce autophagy in both cell lines (Figure 8A,B).

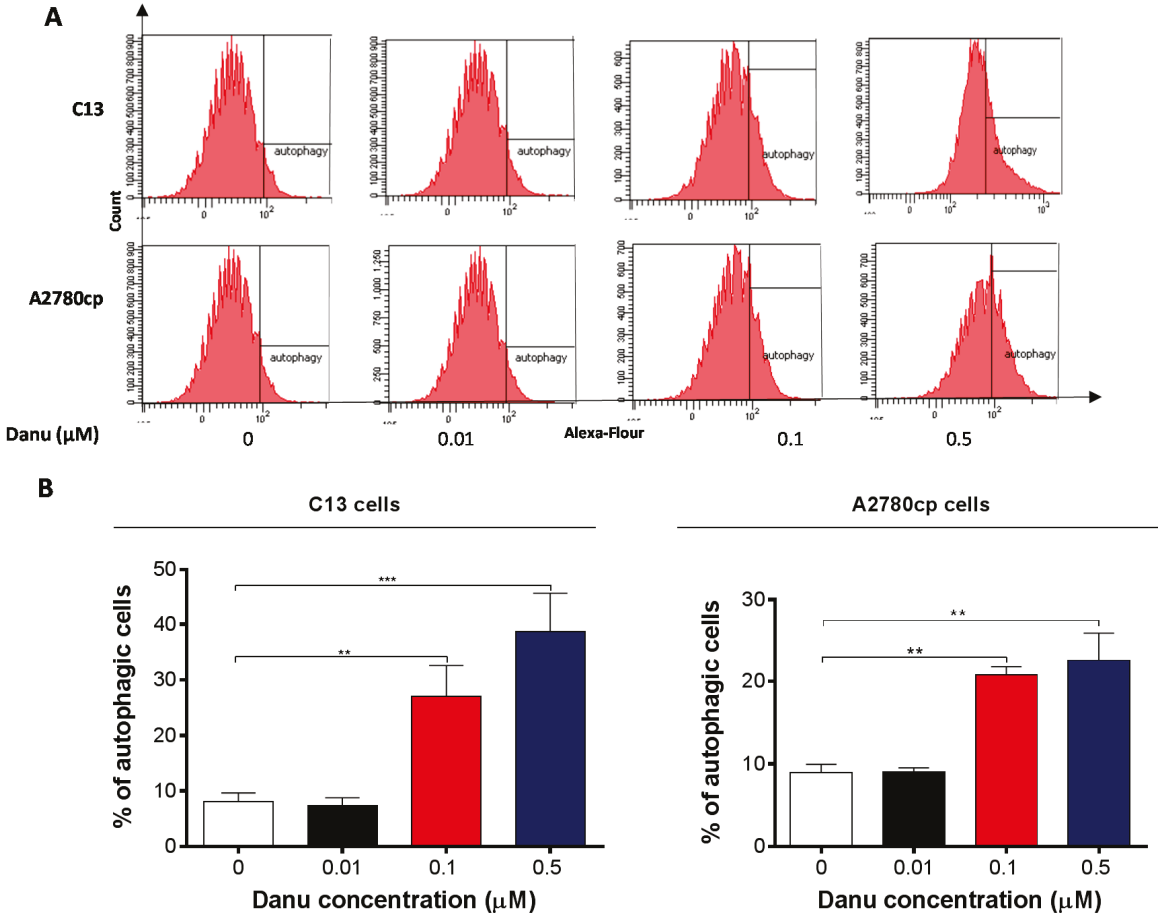

Figure 8. Danu induces autophagy in C13 and A2780cp cells determined by flow cytometry. C13 and A2780cp cells were incubated with Danu 0.01, 0.1, and 0.5 μM for 24 h and the samples were subject to flow cytometry. (**A**) Flow cytometric plots showing autophagy of C13 and A2780cp cells and (**B**) bar graphs showing the percentage of autophagic C13 and A2780cp cells. Data represent the mean ± SD of three independent experiments. ** $p < 0.01$ and *** $p < 0.001$ by one-way analysis of variance.

In separate experiments, the autophagic effect of Danu in C13 and A2780cp cells was examined when cells were treated over 72 h. Danu treatment induced a time-dependent increase in autophagy in both cell lines (Figure 9A,B). In C13 cells, the percentage of autophagy was increased from 9.0% at basal level (zero time) to 9.7%, 12.1%, 13.6%, 25.0%, 30.4%, and 64.7% when treated with Danu for 4, 8, 12, 24, 48, and 72 h, respectively (Figure 9A,B). Treatment of A2780cp cells with 0.5 μM Danu increased the percentage of autophagy from 7.5% at basal level (zero time) to 9.3%, 7.3%, 11.2%, 34.7%, 58.7%, and 85.4% when treated with Danu for 4, 8, 12, 24, 48, and 72 h, respectively (Figure 9A,B).

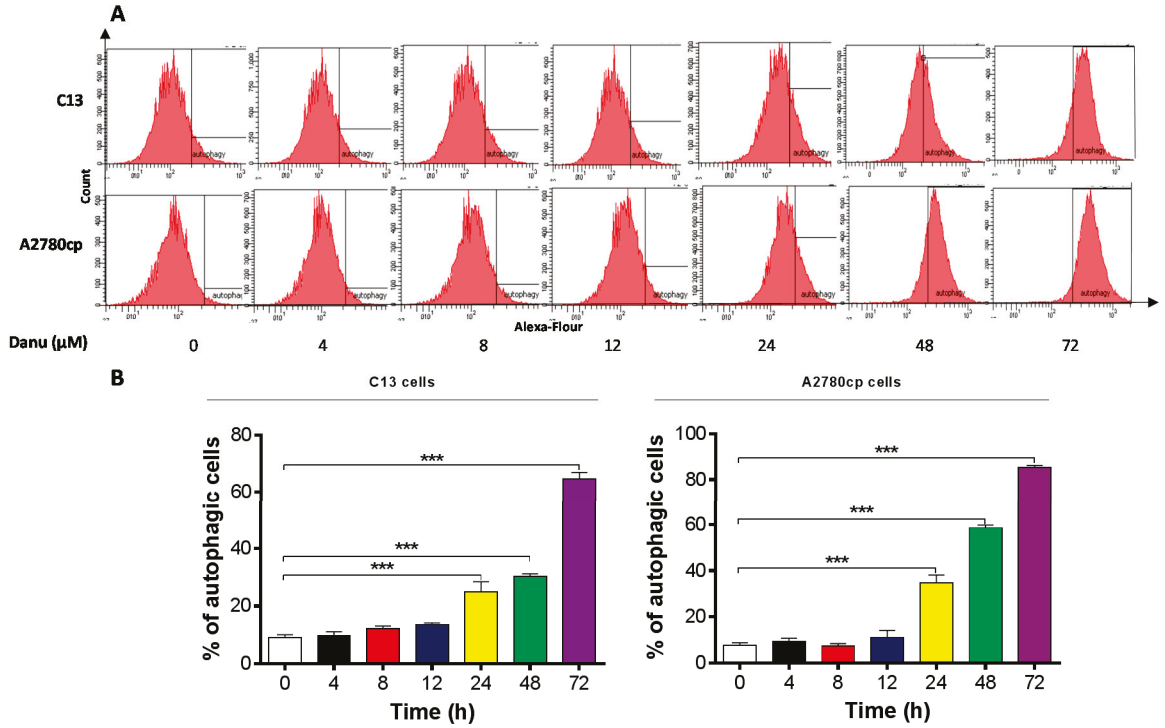

Figure 9. Danu induces autophagy in C13 and A2780cp cells over a 72-h treatment period determined by flow cytometry. C13 and A2780cp cells were incubated with Danu 0.5 μM for 4, 8, 12, 24, 48, and 72 h and the samples were subject to flow cytometry. (**A**) Flow cytometric plots showing autophagy of C13 and A2780cp cells and (**B**) bar graphs showing the percentage of autophagic C13 and A2780cp cells. Data represent the mean ± SD of three independent experiments. *** $p < 0.001$ by one-way analysis of variance.

Further, the autophagy-inducing effect of Danu in C13 and A2780cp cells was examined using confocal microscopy. In comparison to the control cells, Danu treatment concentration-dependently increased the autophagy in C13 and A2780cp cells (Figure 10A,B). There was a 1.8- and 2.7-fold increase in the autophagy of C13 cells when treated with Danu at 0.1 and 0.5μM for 24 h, respectively ($p < 0.001$, Figure 10A,B). In A2780cp cells, there was a 1.6- and 2.6-fold elevation in autophagy when treated with 0.1 and 0.5 μM Danu, respectively ($p < 0.001$, Figure 10A,B). Taken together, these results demonstrate that Danu exerts a potent autophagy-inducing effect in C13 and A2780cp cells.

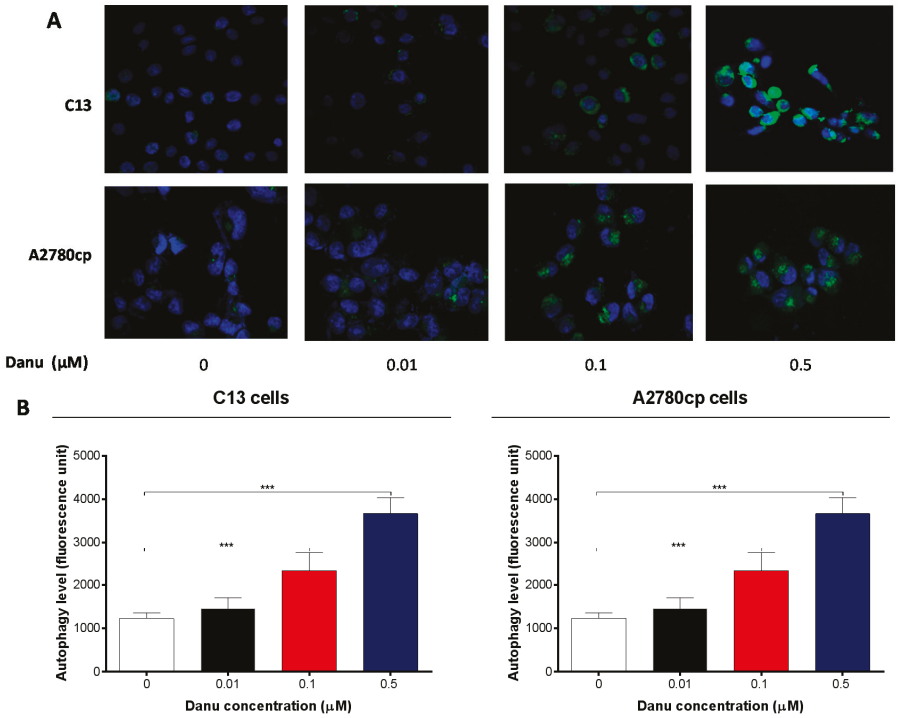

Figure 10. Danu induces autophagy in C13 and A2780cp cells determined by confocal microscopy. C13 and A2780cp cells were incubated with Danu 0.01, 0.1, and 0.5 μM for 24 h and then subject to confocal microscopy. (**A**) Representative images showing autophagy of C13 and A2780cp cells and (**B**) bar graphs showing the percentage of autophagic C13 and A2780cp cells. Data represent the mean ± SD of three independent experiments. Magnification: 60×; scale bar: 5 μm. *** $p < 0.001$ by one-way analysis of variance.

2.6. Danu Suppresses the PI3K/Akt/mTOR Signaling Pathway in C13 and A2780cp Cells

Next, we explored the possible mechanisms for the autophagy-inducing effect of Danu in C13 and A2780cp cells. PI3K/Akt/mTOR signaling is the major pathway involved in autophagy [22]. We initially examined the phosphorylation of PI3K at Tyr458. In comparison to the control cells, Danu treatment markedly inhibited the phosphorylation of PI3K at Tyr458 rather than the expression level of PI3K when these two cell lines were treated with Danu at 0.1 and 0.5 μM. Consequently, the p-PI3K/PI3K ratio was decreased in C13 and A2780cp cells in a concentration-dependent manner in response to Danu treatment (Figure 11A,B). There was a 30.0% and 52.6% decrease in p-PI3K/PI3K ratio when C13 cells were treated with Danu 0.1 and 0.5 μM for 24 h compared to the control, respectively ($p < 0.05$ or 0.01; Figure 11A,B). In A2780cp cells, the ratio of p-PI3K over PI3K was decreased by 36.6% and 58.1% in response to 0.1 and 0.5 μM Danu treatment, compared with the control, respectively ($p < 0.05$ or 0.001; Figure 11A,B). Having determined the regulatory effect of Danu on PI3K, we next evaluated the effect of Danu on phosphorylation of Akt at Ser473 and mTOR at Ser2448 and the expression of phosphatase and tensin homolog (PTEN) in C13 and A2780cp cells (Figure 11A,B). As a downstream effector of PI3K, Akt is involved in regulation of various signaling pathways involved in cell metabolism, proliferation, survival, growth, and angiogenesis [23]. Danu inhibited the activation of Akt at Ser473 without a significant change in the expression level of Akt in either cell line (Figure 11A,B). The ratio of p-Akt over Akt was decreased 37.2% when C13 cells were treated with 0.5 μM Danu for 24 h, compared with control cells ($p < 0.01$, Figure 11A,B). Similarly, the ratio of p-Akt over Akt was decreased by 57.4% and 51.3% in A2780cp cells when treated with 0.1 and 0.5 μM Danu, respectively ($p < 0.001$, Figure 11A,B). The expression level of PTEN that leads to the constitutive activation of downstream components of the PI3K pathway in cancer cells, was markedly

increased in C13 and A2780cp cells when treated with Danu (Figure 11A,B). In addition, exposure of these two cell lines to Danu resulted in a marked decrease in the phosphorylation of mTOR at Ser2448, whereas there was no significant change in expression of mTOR in these two cell lines. The ratio of p-mTOR over mTOR was decreased 34.9% and 38.1% when C13 cells were treated with Danu at 0.1 and 0.5 μM for 24 h, respectively ($p < 0.01$, Figure 11A,B). In A2780cp cells, the p-mTOR/mTOR ratio was decreased 43.0% and 52.5% in response to Danu treatment at 0.1 and 0.5 μM for 24 h, respectively ($p < 0.05$ or 0.01, Figure 11A,B).

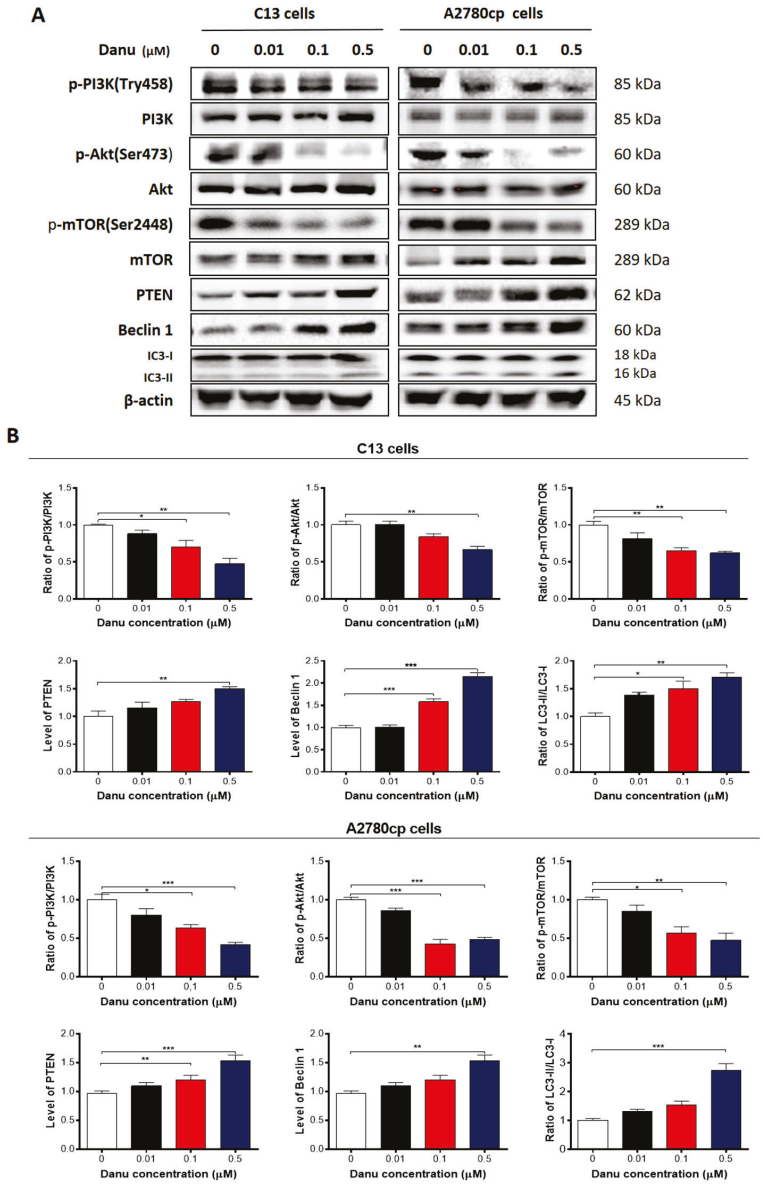

Figure 11. Danu alters the expression of pro-autophagic and anti-autophagic proteins in C13 and A2780cp cells. C13 and A2780cp cells were incubated with Danu 0.01, 0.1, and 0.5 μM for 24 h and the protein samples were subject to Western blotting assay. (**A**) Representative blots of phosphorylation level of PI3K, Akt, and mTOR, and the total level of PI3K, Akt, mTOR, PTEN, beclin 1, LC 3-I, and LC 3-II in C13 and A2780cp cells. (**B**) Bar graphs showing the ratio of p-PI3K/PI3K, p-Akt/Akt, and p-mTOR/mTOR, and expression of PTEN, beclin 1, LC 3-I, and LC 3-II in C13 and A2780cp cells. β-actin was used as the internal control. Data represent the mean ± SD of the three independent experiments. * $p < 0.05$, ** $p < 0.01$, and *** $p < 0.001$ by one-way analysis of variance. The raw data can be found in the Supplementary Material.

Next, we evaluated the effect of Danu on expression of beclin 1, LC3-I, and LC3-II in C13 and A2780cp cells which are important markers of vesicle expansion and formation during the autophagy process. Treating the cells with Danu significantly increased the expression level of beclin 1 and conversion of LC3-I to LC3-II in C13 and A2780cp cells (Figure 11A,B). There was a 1.6- and 2.2-fold increase in expression level of beclin 1 in C13 cells treated with 0.1 and 0.5 μM Danu for 24 h, respectively ($p < 0.001$, Figure 11A,B). In A2780cp cells, there was a 1.5-fold increase in expression level of beclin 1 in response to 0.5 μM Danu treatment for 24 h ($p < 0.01$, Figure 11A,B). In addition, there was a marked increase in the expression level of LC3-II in both C13 and A2780cp cells (Figure 11A,B). Compared with control cells, there was a 1.5- and 1.7-fold increase in the ratio of LC3-II/LC3-I when C13 cells were treated with 0.1 and 0.5 μM Danu for 24 h, respectively ($p < 0.05$ or 0.01, Figure 11A,B). In A2780cp cells, treatment with 0.1 and 0.5 μM Danu resulted in a 2.6-fold increase in the ratio of LC3-II/LC3-I ($p < 0.001$, Figure 11A,B). Collectively, these findings indicate that inactivation of PI3K/Akt/mTOR signaling pathway contributes to Danu-induced autophagy in C13 and A2780cp cells.

2.7. PI3K/Akt/mTOR Pathway Inhibitors Contribute to Danu-Induced Autophagy in C13 and A2780cp Cells

Since we have observed regulatory effect of Danu on PI3K/Akt/mTOR pathway in both C13 and A2780cp cells, we then employed specific chemical inhibitors (MK-2206, an inhibitor of Akt and rapamycin, an inhibitor of mTOR) to further validate the role of this signaling pathway in Danu-induced autophagy. As shown in Figure 12A,B, MK-2206 (1 μM) or rapamycin (10 μM) markedly induced autophagy in C13 and A2780cp cells; compared to the control, incubation of cells with MK2206 and rapamycin increased 2.8- and 8.2-fold in the autophagy of C13 cells and 3.6- and 5.1-fold in the autophagy of A2780cp cells, respectively ($p < 0.001$, Figure 12A,B). Notably, co-incubation of MK-2206 (1 μM) or rapamycin (10 μM) with Danu enhanced Danu-induced autophagy (Figure 12). Compared to Danu treated cells, co-treatment of C13 cells with Danu and MK2206 or rapamycin increased 1.2- and 3.3-fold in autophagy cells, respectively ($p < 0.001$, Figure 12A,B). In A2780cp cells, co-incubation cells with Danu and MK2206 or rapamycin led to a 1.9- and 2.8-fold increase in the autophagic cells compared to Danu treated cells ($p < 0.001$, Figure 12A,B). Taken together, the results suggest that Danu-induced autophagy may be, at least in part, ascribed to the regulation of PI3K/Akt/mTOR signaling pathway.

2.8. Danu Inhibits EMT Phenotype in C13 and A2780cp Cells

EMT is a critical process playing an important role in cancer invasion and metastasis [24]. Reduction in expression of epithelial markers drives EMT with the involvement of a number of key functional proteins, such as E-cadherin, while other mesenchymal markers and transcription factors, such as *N*-cadherin, snail, slug, and, vimentin, are upregulated in EMT [24]. Herein, we examined the effect of Danu on EMT-associated key functional proteins in C13 and A2780cp cells using Western blotting assays. As shown in Figure 13A,B, incubation of C13 cells with Danu resulted in a marked increase in expression level of E-cadherin and a decrease in expression level of *N*-cadherin. In comparison with the control cells, there was a 1.6- and 2.0-fold increase in the level of *E*-cadherin when C13 cells were treated with Danu at 0.1 and 0.5 μM, respectively ($p < 0.05$ or 0.01, Figure 13A,B); and there was a 39.7% decrease in level of *N*-cadherin when C13 cells were treated with 0.5 μM Danu ($p < 0.05$, Figure 13A,B). In A2780cp cells, there was a 1.6- and 1.6-fold increase in level of E-cadherin in response to 0.1 and 0.5 μM Danu treatment, respectively ($p < 0.05$, Figure 13A,B); and the level of *N*-cadherin was decreased 21.1% and 41.9% when treated with Danu at 0.1 and 0.5 μM, respectively ($p < 0.05$ or 0.01, Figure 13A,B). Consequently, Danu treatment enhanced the epithelial features in both cell lines, evident from the marked increase in the ratio of E-cadherin over *N*-cadherin.

We next examined the expression of snail and slug, which are suppressors of E-cadherin. As shown in Figure 13A,B, Danu concentration-dependently reduced the expression level of snail and slug in both cell lines. In C13 cells, Danu treatment at 0.1 and 0.5 μM resulted in a 47.4% and

63.5% reduction in the expression level of slug, respectively, compared with control cells ($p < 0.05$, Figure 13A,B), and 0.5 μM Danu caused a 39.0% decrease in the expression level of snail when compared with control cells ($p < 0.05$, Figure 13A,B). There was a similarly effect of Danu in A2780cp cells. In comparison with the control cells, there was a 25.5% and 32.9% decrease in the level of slug when treated with 0.1 and 0.5 μM Danu, respectively; and there was a 47.5% decrease in the level of snail when treated with 0.5 μM Danu ($p < 0.05$ or 0.01, Figure 13A,B). Moreover, there was a concentration-dependent reduction in the level of vimentin in C13 and A2780cp cells when exposed to Danu for 24 h (Figure 13A,B). Treatment of cells with Danu at 0.1 and 0.5 μM led to 41.0% and 53.1% decrease in the level of vimentin in C13 cells and 33.1% and 56.1% decline in A2780cp cells, respectively ($p < 0.05$ or 0.01, Figure 13A,B). Taken together, Danu possesses a potent inhibitory effect on EMT evident from the concentration-dependent regulatory effect on EMT-associated markers in C13 and A2780cp cells.

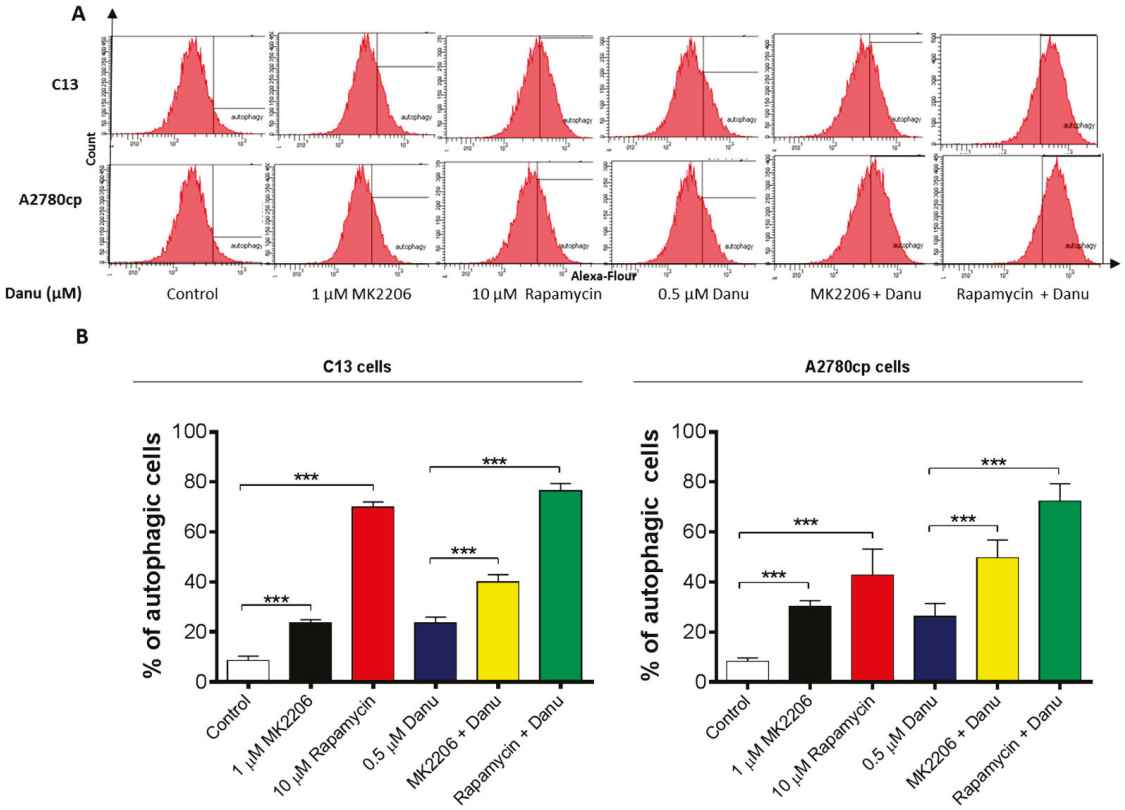

Figure 12. Danu induces autophagy with the involvement of PI3K/Akt/mTOR signaling pathway. C13 and A2780cp cells were pretreated with MK-2206 (1 μM) or rapamycin (10 μM) for 1 hour and then co-treated with 0.5 μM Danu for 24 h. The samples were subject to flow cytometric analysis. (**A**) Histograms show autophagy of C13 and A2780cp cells. (**B**) Bar graph showing the percentage of autophagic C13 and A2780cp cells. Data are the mean ± SD of three independent experiments. *** $p < 0.001$ by one-way analysis of variance.

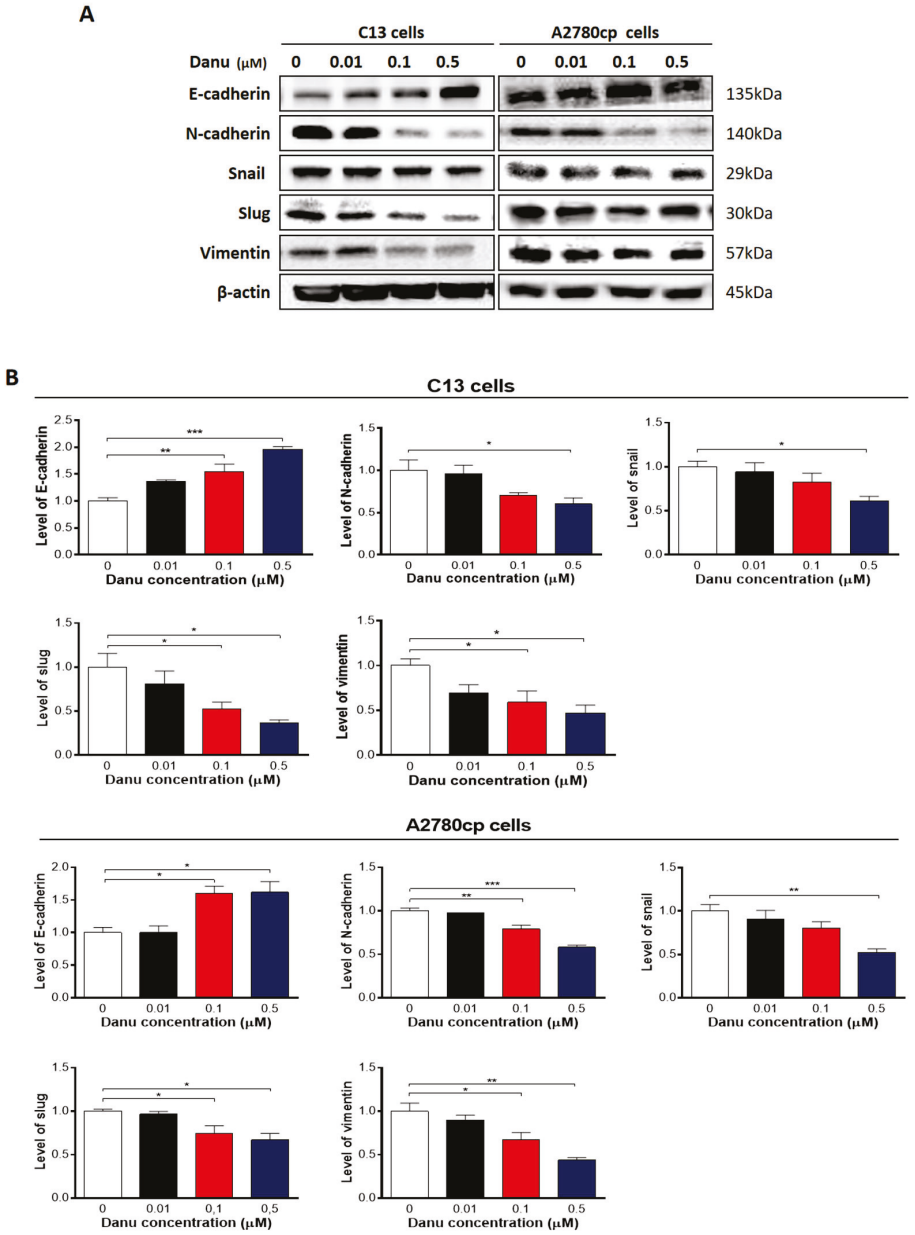

Figure 13. Danu inhibits EMT in C13 and A2780cp cells. C13 and A2780cp cells were incubated with Danu 0.01, 0.1, and 0.5 μM for 24 h and the protein samples were subject to Western blotting assay. (**A**) Representative blots showing E-cadherin, N-cadherin, snail, slug, and vimentin levels in C13 and A2780cp cells. (**B**) Bar graphs showing the relative expression of E-cadherin, N-cadherin, snail, slug, and vimentin in C13 and A2780cp cells. β-actin was used as the internal control. Data represent the mean ± SD of the three independent experiments. * $p < 0.05$, ** $p < 0.01$, and *** $p < 0.001$ by one-way analysis of variance. The raw data can be found in the Supplementary Material.

3. Discussion

Ovarian cancer has the highest fatality to case ratio of all gynecological cancers because the majority of cases are diagnosed at late stage. Despite of significant effort to improve the early detection and advances in chemotherapy, clinical management of ovarian cancer remains a major challenge to human health [25–27]. The standard treatment for advanced OC includes both cytoreductive surgery and platinum-based chemotherapy [28,29]. Initial response rates are high, within a 3-year period, although most (~70%) patients experience recurrence, ultimately,

the development of chemoresistance [30,31]. Improved understanding of the tumor biology led to the development of targeted anticancer medications that have the ability to improve tumor responses to chemotherapy, thereby alleviating some of the limitations of the chemotherapy [32,33]. The more advanced agent in this regard is Danu, a small adenosine triphosphate competitive molecule that inhibits AURKA/B/C, which has entered Phase II clinical trials for patients with solid tumors [14]. Danu exhibits potent inhibitory effect on AURKB activity, as determined by inhibition of its substrate histone H3 in position Ser10 and also on AURKA, as determined by inhibition of autophosphorylation in position Thr288 [34,35]. It has been shown that Danu inhibits the proliferation of gastric cancer and breast cancer cells via inducing cell cycle arrest and programmed cell death and inhibits EMT [17,18]. In the present study, our findings have shown a potent inhibitory effect of Danu on cell proliferation in two ovarian cancer cell lines C13 and A278cp cells. The findings indicate that Danu induces cell cycle arrest and promotes cell apoptosis and autophagy, with the involvement of PI3K/Akt/mTOR signaling pathway in both of cell lines. Additionally, the results suggest that Danu also inhibits EMT contributing to the anticancer effect in both cell lines.

AURKA, B, and C are a family of serine/threonine kinases with the highest degree of sequence homology in their catalytic domains [8,36]. Enhanced activity or expression of aurora kinases has been observed in different human malignancies [37,38]. Recently, a number of Aurora kinase inhibitors have been discovered and are under preclinical or clinical experimental settings. Danu, a pan-aurora kinases inhibitor, has the inhibitory effect on the proliferation of hepatocellular carcinoma, pancreatic cancer, gastric, and breast cancer cells via inducing cell division failure and resulting in polyploidy [17,18,39,40]; and Danu has been under Phase II clinical trials for patients with solid tumors [14].

Our study found that cell cycle transition from G_2 phase to M phase was inhibited by Danu in C13 and A278cp cell lines. It has been firstly reported that the Danu induced cell cycle arrest in G_2/M phase in cisplatin resistant C13 and A2780cp cells. G_2/M transition is controlled by CDC2, also known as CDK1, which partners with cyclin B1. CDC family proteins and cyclin complexes play a critical role in the regulation of G_2/M transitions [20]. We further found that the cell cycle checkpoints regulators including CDC2/CDK1 and cyclin B1 were involved. This is evident from a remarkable reduction in the expression level of CDC2/CDK1 and cyclin B1 after Danu treatment, which is associated with G_2/M cell cycle arrest. Moreover, the inhibition of cyclin–CDK complex might be amplified by simultaneous up-regulation of the p21Waf1/Cip1 protein that is a CDK inhibitor [41]. Activated p53 can inhibit cell cycle progression by regulation of p21Waf1/Cip1 [42]. Our findings showed that Danu treatment increased the level of p21Waf1/Cip1 and p53 in both cell lines, which probably contributes to the inhibitory effect of Danu on cell proliferation and inducing effect on cell cycle arrest in G_2/M phase in C13 and A2780cp cells.

Apoptosis, a tightly regulated signaling process that involves the coordination of both anti-apoptotic and pro-apoptotic proteins, is vital for anti-carcinogenesis [43]. Increasing evidence shows that manipulating apoptosis by modulation of the key regulators of apoptosis is a promising therapeutic strategy in the treatment of cancer [44,45]. The Bcl-2 family members, such as Bcl-xl, Bcl-2 and Bax, are essential for the initiation of mitochondrial dysfunction during apoptotic process. Bcl-2 can be inhibited by post-translational modification and/or by increased expression of PUMA, which is an essential regulator of p53-mediated cell apoptosis [45]. In the present study, we observed concentration- and time-dependent pro-apoptotic effect of Danu on C13 and A2780cp cells. The findings showed that the expression of pro-apoptotic factor Bax was markedly enhanced in Danu treatment group. However, the expression of anti-apoptotic factor Bcl-xl and Bcl-2 was inhibited significantly. Also, Danu treatment led to an increase in the level of cleaved caspase-3 and caspase-9. Danu could also induce release of cytochrome c from mitochondria to cytosol in C13 and A2780cp cells. These results indicate that Danu could induce apoptosis in C13 and A2780cp cells by activating the mitochondrial apoptosis pathway.

Autophagy is an evolutionarily conserved catabolic pathway where cells deliver their own cytoplasmic material and/or organelles to lysosomes for degradation [46]. It is an important type of programmed cell death involving the engulfment and degradation of nonessential or abnormal cellular organelles and proteins in living cells [47,48]. This autophagy cells via a lysosomal catabolic pathway for engulfment, degradation, and recycling of nonessential or abnormal cellular organelles and proteins in living cells. This complicated process is executed through multiple steps from intracellular membrane/vesicle reorganization to form double-membraned autophagosomes that fuse with lysosomes to form autophagolysomes, which degrade the contents via acidic lysosomal hydrolases [6,49]. Recently, the role of autophagy in the treatment of cancer has been debated. We observed that Danu-induced autophagy in dose- and time-dependent manners in the present study. This could be regarded as one of the anticancer effects, although more studies are needed to further test this autophagy-inducing effect in the treatment of ovarian cancer. The PI3K/Akt/mTOR signaling pathway is a central pathway involved in autophagy through the regulation of cell growth, motility, protein synthesis, cell metabolism, cell survival, and cell death in response to various stimuli [50]. The phosphorylation of Akt would be up-regulated following the activation of PI3K and mTOR can integrate upstream activating signals through PI3K/Akt pathway and become phosphorylated, and then inhibits autophagy [51]. In our study, Danu can down-regulate the phosphorylation level of PI3K, Akt, and mTOR, while promoting the expression of PTEN, as a regulator of the PI3K/Akt/mTOR pathway. Rapamycin is allosteric inhibitors of mTOR via their binding to FKBP12, and were among the first mTOR-targeted therapeutics to enter the clinic [52]. A number of studies have shown that rapamycin induce feedback activation of Akt and the combination of rapamycin and Akt inhibitors results in additive or synergistic antitumor effects [53–55]. MK2206, a potent, irreversible, and selective Akt inhibitor and a blocker of autophagosome formation, markedly increased the Danu-induced autophagic cell death in both C13 and A2780cp cells. We combined the treatment of Danu with MK-2206 and rapamycin respectively, which resulted an enhanced effect on Danu-induced autophagy. Thus, the findings suggest that Danu induces autophagy via suppressing the PI3K/Akt/mTOR pathway in both C13 and A2780cp cells. Taken together, Danu-induced apoptosis and autophagy contributes to the cancer cell killing effect on C13 and A2780cp cells. Notably, the present study showed a higher IC_{50} value of Danu towards the cisplatin resistant A2780cp cells than that in A2780 cells [13]. Moreover, Danu exhibited a more potent cancer cell killing effect evident from the lower IC_{50} values in previous studies in different cancer cell lines [17,18]. The findings suggest that drug resistance affect the effect of Danu in C13 and A2780cp cells.

The ability of epithelial cells to undergo mesenchymal transition during embryogenesis, wound healing and malignant tumor progression is now widely accepted as a core biological process termed the EMT [24,56]. Tumor cells shed their differentiated epithelial characteristics, in order to invade and metastasize, including cell–cell adhesion and polarity, and acquire mesenchymal traits, such as invasiveness, motility and, importantly, many of the attributes of stem cells [57,58]. In the metastasis of cancer, the increased motility and invasive behavior of cancer cells underwent EMT, due to the loss of adhesion molecules such as E-cadherin, and the gain of mesenchymal proteins such as *N*-cadherin and vimentin [59]. In this study, Danu significantly promoted the expression of E-cadherin; however, it demoted the expression of N-cadherin, leading to an EMT inhibition in ovarian cancer cell. Danu suppressed the expression of snail and slug, in C13 and A2780cp cells, which provides an explanation for the inhibitory effect of Danu on EMT. Snail and slug are master regulators of EMT, down-regulating *E*-cadherin by silencing gene expression. Furthermore, Danu decreased the expression level of vimentin. Vimentin is a marker expressed in mesenchymal cells [60,61]. Collectively, these results suggest that Danu could inhibit EMT in C13 and A2780cp cells.

In conclusion, Danu inhibits cell proliferation, induces cell-cycle arrest, mitochondria-dependent apoptosis and autophagy in C13 and A2780cp cells. Inhibition of PI3K/Akt/mTOR signaling pathway is involved in the autophagy-inducing effect of Danu in C13 and A2780cp cells. Suppression

of EMT may render Danu as a promising agent to curb cancer metastasis in patients at advanced stage. Danu may represent a new anticancer drug that can kill ovarian cancer cells and prevent metastasis. More functional and mechanistic studies are warranted to elucidate the role of Danu in the treatment of human ovarian carcinoma.

4. Materials and Methods

4.1. Chemicals and Reagents

4,6-Diamidino-2-phenylindole was obtained from Invitrogen Inc. (Carlsbad, CA, USA). MK-2206 (a selective inhibitor of protein Kinase B, (Akt)) and rapamycin (a specific inhibitor of mammalian target of rapamycin, (mTOR)) were purchased from Selleckchem Inc. (Houston, TX, USA). Dulbecco's Modified Eagle's Medium (DMEM) was sourced from Corning Cellgro Inc. (Herndon, VA, USA). Dulbecco's phosphate-buffered saline (D-PBS), fetal bovine serum (FBS), phosphatase and protease inhibitor cocktails, propidium iodide (PI), 4-(2-hydroxyethyl) piperazine-1-ethanesulfonic acid (HEPES), ethylenediaminetetraacetic acid, RNase A, and thiazolyl blue tetrazo-lium bromide (MTT) were purchased from Sigma-Aldrich (St. Louis, MO, USA). The Annexin V: phycoerythrin (PE) apoptosis detection kit was bought from BD Biosciences Inc. (San Jose, CA, USA) and the Cyto-ID® autophagy detection kit was obtained from Enzo Life Sciences Inc. (Farmingdale, NY, USA). The Pierce bicinchoninic acid (BCA) protein assay kit, skim milk, and Western blotting substrate were purchased from Thermo Scientific Inc. (Hudson, NH, USA). A polyvinylidene difluoride (PVDF) membrane was obtained from Bio-Rad Inc. (Hercules, CA, USA). Primary antibodies against human cyclin B1, cyclin-dependent kinase 1 (CDK1/CDC2/CDKN1), p21 Waf1/Cip1, p27 Kip1, p53, cytochrome c, Bcl-2-like protein 4/Bcl-2-associated X protein (Bax), B-cell lymphoma-extra large (Bcl-xl), B-cell lymphoma 2 (Bcl-2), cleaved (c-) caspase 9, c-caspase 3, p53 up-regulated modulator of apoptosis (PUMA), phosphatidylinositol 3-kinase (PI3K), phosphorylated (p-) PI3K/p85 at Tyr458, Akt, p-Akt at Ser473, mTOR, p-mTOR at Ser2448, PTEN, beclin 1, microtubule-associated protein 1A/1B-light chain 3 (LC3-I), LC3-II, *E*-cadherin, *N*-cadherin, vimentin, slug, and snail were all purchased from Cell Signaling Technology Inc. (Beverly, MA, USA). The antibody against human β-actin was sourced from Santa Cruz Biotechnology Inc. (Dallas, TX, USA).

4.2. Cell Lines and Cell Culture

C13 and A2780cp cells are human EOC cell lines that were obtained from Chengxiong Xu (Moffitt Cancer Center & Research Institute, Tampa, FL, USA) and were cultured in DMEM media. These two cell lines are epithelial ovarian cancer cell lines and belong to high-grade serous carcinoma. They exhibit similar biological behavior regarding the characteristics of aggressiveness, invasiveness, and metastasis. All media containing L-glutamine, phenol red, L-cysteine and L-methionine, sodium bicarbonate were supplemented with 10% heat-inactivated FBS. The cells were maintained at 37 °C in a 5% CO2/95% air humidified incubator. Danu was dissolved in DMSO with a stock concentration of 50 mM, and was freshly diluted to the desired concentrations with culture medium. The final concentration of DMSO was at 0.05% (v/v).

4.3. Cell Viability Assay

The MTT assay was performed to examine the effect of Danu on the viability of C13 and A2780cp cells. Briefly, cells were seeded in 96-well culture plates at a density of 8×10^3 cells/well. After cells were attached, the cells were treated with Danu at different concentrations (0.01–50 μM). The control cells received the vehicle only. After 24-h incubation, 10 μL MTT (5 g/L) was added to each well and cultured for another 4 h. Then, the media was carefully aspirated and 100 μL DMSO was added. The absorbance at the 450 nm wavelength was measured with a Synergy H4 Hybrid microplate reader (BioTek Inc., Winooski, VT, USA). The IC_{50} values were determined using the relative viability over Danu concentration curve using GraphPad Prism 6.0 (GraphPad Software, Inc., La Jolla, CA, USA).

4.4. Cell Cycle Analysis

The effect of Danu on cell cycle distribution was determined by flow cytometry. Briefly, C13 and A2780cp cells were treated with Danu at different concentrations of 0.01, 0.1, and 0.5 μM for 24 h. In separate experiments, C13 and A2780cp cells were treated with 0.5 μM Danu for 4, 8, 12, 24, 48, or 72 h. Cells were suspended, washed by PBS, centrifuged, and fixed in 70% ethanol at −20 °C overnight. Then, the cells were resuspended in 1 mL of PBS containing 1 mg/mL RNase A and 50 μg/mL PI. Cells were incubated in the dark for 30 min at room temperature. A total number of 2×10^4 cells was subject to cell cycle analysis using a flow cytometer (Becton Dickinson Immunocytometry Systems, San Jose, CA, USA).

4.5. Quantification of Cellular Apoptosis

The effect of Danu on apoptosis of C13 and A2780cp cells was quantitated using the Annexin V: PE apoptosis detection kit (San Jose, CA, USA) according to the manufacturer's instruction. Cells were treated with Danu at concentrations of 0.01, 0.1, and 0.5 μM for 48 h. The cells were resuspended at a concentration of 1×10^6 cells/mL in 1× binding buffer. A quota of cell suspension (100 μL) was transferred into a clean 5 mL tube and incubated with 5 μL of Annexin V: PE and 5 μL of 7-amino-actinomycin D (a vital nucleic acid dye) in the dark for 15 min at room temperature. A quota of 1× binding buffer (400 μL) was then added to each tube, and the number of apoptotic cells was quantified using a flow cytometer within one hour. Cells that stain positive for Annexin V: PE and negative for 7-amino-actinomycin D are undergoing apoptosis, cells that stain positive for both Annexin V: PE and 7-amino-actinomycin D are either in the final stage of apoptosis, are undergoing necrosis, or are already dead, and cells that stain negative for both Annexin V: PE and 7-amino-actinomycin D are alive and not undergoing measurable apoptosis.

4.6. Quantification of Cellular Autophagy

To examine the effect of Danu on autophagy in C13 and A2780cp cells, cellular autophagy was detected using flow cytometry. Briefly, C13 and A2780cp cells were seeded in 60 mm Petri dishes for 24 h and the cells reached ~75% confluence, then treated with fresh medium alone, control vehicle alone (0.05% DMSO, *v*/*v*), or Danu (0.01, 0.1, and 0.5 μM) for 24 h. In separate experiments, C13 and A2780cp cells were treated with 0.5 μM Danu for 4, 8, 12, 24, 48, or 72 h. Following the Danu treatment, cells were resuspended in 250 μL of phenol red-free culture medium containing 5% FBS and 250 μL of the diluted Cyto-ID® Green stain solution was added to each sample and mixed well. Cells were incubated for 30 min at 37 °C in the dark and then collected by centrifugation at 250× g for 3 min. The cell pellet was washed with 1× assay buffer in the Cyto-ID® autophagy detection kit and resuspended in 500 μL fresh 1× assay buffer. Cells were analyzed using the green (FL1) channel of the flow cytometer.

4.7. Confocal Fluorescence Microscopy

The effect of Danu on cellular autophagy was further examined using confocal microscopy with the application of Cyto-ID® autophagy detection kit according to the manufacture's instruction. The C13 and A2780cp cells were seeded into 8-well chamber slide at 30% confluence. After incubation overnight, the cells were treated with Danu at 0.01, 0.1, and 0.5 μM. After incubation for 24 h, the cells reached ~60% of confluence and were washed with 1×assay buffer, following by incubation with 100 μL of microscopy dual detection reagent for 30 min at 37 °C in the dark. After incubation, the cells were washed with 1× assay buffer to remove the detection reagent, and then examined using a TCS SP2 laser scanning confocal microscope (Leica, Wetzlar, Germany) using a standard fluorescein isothiocyanate filter set for imaging the autophagic signal at wavelengths of 405/488 nm.

4.8. Western Blotting Analysis

C13 and A2780cp cells were washed with pre-cold PBS after 24-h treatment with Danu at 0.01, 0.1, and 0.5 μM, lysed with the RIPA buffer (50 mmol HEPES at pH 7.5, 150 mmol NaCl, 10% glycerol, 1.5 mmol $MgCl_2$, 1% Triton-X 100, 1 mmol EDTA at pH 8.0, 10 mmol sodium pyrophosphate, 10 mmol sodium fluoride) containing the protease and phosphatase inhibitor cocktails, and centrifuged at 3000× *g* for 10 min at 4 °C. Protein concentrations were measured using Pierce BCA protein assay kit. Equal amount of protein sample (30 μg) was resolved by sodium dodecyl sulfate polyacrylamide gel electrophoresis (SDS-PAGE) sample loading buffer and electrophoresed on 7%–12% SDS-PAGE mini-gel after thermal denaturation at 95 °C for 5 min. Proteins were transferred onto PVDF membrane at 400 mA for 1–2 h at 4 °C. Membranes were probed with indicated primary antibody overnight at 4 °C and then blotted with respective secondary anti-mouse or anti-rabbit antibody. Visualization was performed using Bio-Rad ChemiDocTM XRS system (Hercules, CA, USA) with enhanced-chemiluminescence substrate and the blots were analyzed using Image Lab 3.0 (BioRad, Hercules, CA, USA). Protein level was normalized to the matching densitometry values of the internal control β-actin.

4.9. Statistical Analysis

Data are presented as the mean ± standard deviation (SD). Comparisons of multiple groups were evaluated by one-way analysis of variance (ANOVA) followed by Tukey's multiple comparison procedure. Values of $p < 0.05$ were considered statistically significant. Assays were performed at least three times independently.

Supplementary Materials: The following supporting information can be downloaded at: https://www.mdpi.com/article/10.3390/ijms161126018/s1.

Acknowledgments: The authors appreciate the financial support from the Startup Funds of the College of Pharmacy, University of South Florida, Tampa, FL, USA. Zhi-Wei Zhou holds a postdoctoral scholarship from the College of Pharmacy, University of South Florida, Tampa, FL, USA.

Author Contributions: Dan Zi, Zhi-Wei Zhou, and Shu-Feng Zhou conceived and designed the experiments; Dan Zi performed the experiments; Ying-Jie Yang, Lin Huang, Zun-Lun Zhou, and Shu-Ming He analyzed the data; Zhi-Xu He and Shu-Feng Zhou contributed reagents/materials/analysis tools; Zhi-Wei Zhou and Shu-Feng Zhou wrote the paper.

Conflicts of Interest: The authors declare no conflict of interest.

References

1. Ferlay, J.; Soerjomataram, I.; Ervik, M.; Dikshit, R.; Eser, S.; Mathers, C.; Rebelo, M.; Parkin, D.M.; Forman, D.; Bray, F. *GLOBOCAN 2012 v1.0, Cancer Incidence and Mortality Worldwide: IARC CancerBase No. 11*; GLOBOCAN: Lyon, France, 2013.
2. Howlader, N., Noone, A.M., Krapcho, M., Garshell, J., Miller, D., Altekruse, S.F., Kosary, C.L., Yu, M., Ruhl, J., Tatalovich, Z., *et al*, Eds.; *SEER Cancer Statistics Review, 1975–2012*; National Cancer Institute: Bethesda, MD, USA, 2015.
3. Group. *United States Cancer Statistics: 1999–2011 Incidence and Mortality Web-based Report*; Department of Health and Human Services, Centers for Disease Control and Prevention and National Cancer Institute: Atlanta, Georgia, 2014.
4. Lowe, K.A.; Chia, V.M.; Taylor, A.; O'Malley, C.; Kelsh, M.; Mohamed, M.; Mowat, F.S.; Goff, B. An international assessment of ovarian cancer incidence and mortality. *Gynecol. Oncol.* **2013**, *130*, 107–114. [CrossRef] [PubMed]
5. Jayson, G.C.; Kohn, E.C.; Kitchener, H.C.; Ledermann, J.A. Ovarian cancer. *Lancet* **2014**, *384*, 1376–1388. [CrossRef]
6. Davis, A.; Tinker, A.V.; Friedlander, M. "Platinum resistant" ovarian cancer: What is it, who to treat and how to measure benefit? *Gynecol. Oncol.* **2014**, *133*, 624–631. [CrossRef] [PubMed]

7. Nigg, E.A. Mitotic kinases as regulators of cell division and its checkpoints. *Nature reviews. Mol. Cell. Biol.* **2001**, *2*, 21–32. [CrossRef] [PubMed]
8. Fu, J.; Bian, M.; Jiang, Q.; Zhang, C. Roles of Aurora kinases in mitosis and tumorigenesis. *Mol. Cancer Res.* **2007**, *5*, 1–10. [CrossRef] [PubMed]
9. Keen, N.; Taylor, S. Aurora-kinase inhibitors as anticancer agents. *Nat. Rev. Cancer* **2004**, *4*, 927–936. [CrossRef] [PubMed]
10. Swanton, C. Cell-cycle targeted therapies. *Lancet. Oncol.* **2004**, *5*, 27–36. [CrossRef]
11. Kollareddy, M.; Zheleva, D.; Dzubak, P.; Brahmkshatriya, P.S.; Lepsik, M.; Hajduch, M. Aurora kinase inhibitors: Progress towards the clinic. *Investig. New Drugs* **2012**, *30*, 2411–2432. [CrossRef] [PubMed]
12. Lok, W.; Klein, R.Q.; Saif, M.W. Aurora kinase inhibitors as anti-cancer therapy. *Anti-Cancer Drugs* **2010**, *21*, 339–350. [CrossRef] [PubMed]
13. Carpinelli, P.; Ceruti, R.; Giorgini, M.L.; Cappella, P.; Gianellini, L.; Croci, V.; Degrassi, A.; Texido, G.; Rocchetti, M.; Vianello, P.; *et al*. PHA-739358, a potent inhibitor of Aurora kinases with a selective target inhibition profile relevant to cancer. *Mol. Cancer Ther.* **2007**, *6*, 3158–3168. [CrossRef] [PubMed]
14. Meulenbeld, H.J.; Mathijssen, R.H.; Verweij, J.; de Wit, R.; de Jonge, M.J. Danusertib, an aurora kinase inhibitor. *Expert Opin. Investig. Drugs* **2012**, *21*, 383–393. [CrossRef] [PubMed]
15. Gontarewicz, A.; Brummendorf, T.H. Danusertib (formerly PHA-739358)—A novel combined pan-aurora kinases and third generation Bcr-Abl tyrosine kinase inhibitor. *Small Mol. Oncol.* **2010**, *184*, 199–214.
16. Schoffski, P.; Besse, B.; Gauler, T.; de Jonge, M.J.; Scambia, G.; Santoro, A.; Davite, C.; Jannuzzo, M.G.; Petroccione, A.; Delord, J.P. Efficacy and safety of biweekly intravenous administrations of the Aurora kinase inhibitor danusertib hydrochloride in independent cohorts of patients with advanced or metastatic breast, ovarian, colorectal, pancreatic, small-cell and non-small-cell lung cancer: A multi-tumour, multi-institutional phase II study. *Ann. Oncol.* **2015**, *26*, 598–607. [PubMed]
17. Yuan, C.X.; Zhou, Z.W.; Yang, Y.X.; He, Z.X.; Zhang, X.; Wang, D.; Yang, T.; Pan, S.Y.; Chen, X.W.; Zhou, S.F. Danusertib, a potent pan-Aurora kinase and ABL kinase inhibitor, induces cell cycle arrest and programmed cell death and inhibits epithelial to mesenchymal transition involving the PI3K/Akt/mTOR-mediated signaling pathway in human gastric cancer AGS and NCI-N78 cells. *Drug Des. Dev. Ther.* **2015**, *9*, 1293–1318.
18. Li, J.P.; Yang, Y.X.; Liu, Q.L.; Zhou, Z.W.; Pan, S.T.; He, Z.X.; Zhang, X.; Yang, T.; Pan, S.Y.; Duan, W.; *et al*. The pan-inhibitor of Aurora kinases danusertib induces apoptosis and autophagy and suppresses epithelial-to-mesenchymal transition in human breast cancer cells. *Drug Des. Dev. Ther.* **2015**, *9*, 1027–1062.
19. Hu, X.; Moscinski, L.C. Cdc2: A monopotent or pluripotent CDK? *Cell Prolif.* **2011**, *44*, 205–211. [CrossRef] [PubMed]
20. Warfel, N.A.; El-Deiry, W.S. p21WAF1 and tumourigenesis: 20 years after. *Curr. Opin. Oncol.* **2013**, *25*, 52–58. [CrossRef] [PubMed]
21. Christensen, M.E.; Jansen, E.S.; Sanchez, W.; Waterhouse, N.J. Flow cytometry based assays for the measurement of apoptosis-associated mitochondrial membrane depolarisation and cytochrome c release. *Methods* **2013**, *61*, 138–145. [CrossRef] [PubMed]
22. Levine, B.; Kroemer, G. Autophagy in the pathogenesis of disease. *Cell* **2008**, *132*, 27–42. [CrossRef] [PubMed]
23. Manning, B.D.; Cantley, L.C. AKT/PKB signaling: Navigating downstream. *Cell* **2007**, *129*, 1261–1274. [CrossRef] [PubMed]
24. Lamouille, S.; Xu, J.; Derynck, R. Molecular mechanisms of epithelial-mesenchymal transition. *Nat. Rev. Mol. Cell Biol.* **2014**, *15*, 178–196. [CrossRef] [PubMed]
25. Agarwal, R.; Kaye, S.B. Ovarian cancer: Strategies for overcoming resistance to chemotherapy. *Nat. Rev. Cancer* **2003**, *3*, 502–516. [CrossRef] [PubMed]
26. Naora, H.; Montell, D.J. Ovarian cancer metastasis: Integrating insights from disparate model organisms. *Nat. Rev. Cancer* **2005**, *5*, 355–366. [CrossRef] [PubMed]
27. Hennessy, B.T.; Coleman, R.L.; Markman, M. Ovarian cancer. *Lancet* **2009**, *374*, 1371–1382. [CrossRef]
28. Ledermann, J.A.; Raja, F.A.; Fotopoulou, C.; Gonzalez-Martin, A.; Colombo, N.; Sessa, C.; Group, E.G.W. Newly diagnosed and relapsed epithelial ovarian carcinoma: ESMO clinical practice guidelines for diagnosis, treatment and follow-up. *Ann. Oncol.* **2013**, *24*, 24–32. [CrossRef] [PubMed]
29. Integrated genomic analyses of ovarian carcinoma. *Nature* **2011**, *474*, 609–615.

30. Wiedemeyer, W.R.; Beach, J.A.; Karlan, B.Y. Reversing platinum resistance in high-grade serous ovarian carcinoma: Targeting BRCA and the homologous recombination system. *Front. Oncol.* **2014**, *4*, 34. [CrossRef] [PubMed]
31. Ledermann, J.; Harter, P.; Gourley, C.; Friedlander, M.; Vergote, I.; Rustin, G.; Scott, C.L.; Meier, W.; Shapira-Frommer, R.; Safra, T.; *et al*. Olaparib maintenance therapy in patients with platinum-sensitive relapsed serous ovarian cancer: A preplanned retrospective analysis of outcomes by BRCA status in a randomised phase 2 trial. *Lancet Oncol.* **2014**, *15*, 852–861. [CrossRef]
32. Raja, F.A.; Chopra, N.; Ledermann, J.A. Optimal first-line treatment in ovarian cancer. *Ann. Oncol.* **2012**, *23*, 118–127. [CrossRef] [PubMed]
33. Markman, M. Maintenance chemotherapy in the management of epithelial ovarian cancer. *Cancer Metastasis Rev.* **2015**, *34*, 11–17. [CrossRef] [PubMed]
34. Bayliss, R.; Sardon, T.; Vernos, I.; Conti, E. Structural basis of Aurora-A activation by TPX2 at the mitotic spindle. *Mol. Cell* **2003**, *12*, 851–862. [CrossRef]
35. Crosio, C.; Fimia, G.M.; Loury, R.; Kimura, M.; Okano, Y.; Zhou, H.; Sen, S.; Allis, C.D.; Sassone-Corsi, P. Mitotic phosphorylation of histone H3: Spatio-temporal regulation by mammalian Aurora kinases. *Mol. Cell. Biol.* **2002**, *22*, 874–885. [CrossRef] [PubMed]
36. Ducat, D.; Zheng, Y. Aurora kinases in spindle assembly and chromosome segregation. *Exp. Cell Res.* **2004**, *301*, 60–67. [CrossRef] [PubMed]
37. Gautschi, O.; Heighway, J.; Mack, P.C.; Purnell, P.R.; Lara, P.N., Jr.; Gandara, D.R. Aurora kinases as anticancer drug targets. *Clin. Cancer Res.* **2008**, *14*, 1639–1648. [CrossRef] [PubMed]
38. Katayama, H.; Brinkley, W.R.; Sen, S. The Aurora kinases: Role in cell transformation and tumorigenesis. *Cancer Metastasis Rev.* **2003**, *22*, 451–464. [CrossRef] [PubMed]
39. Benten, D.; Keller, G.; Quaas, A.; Schrader, J.; Gontarewicz, A.; Balabanov, S.; Braig, M.; Wege, H.; Moll, J.; Lohse, A.W.; *et al*. Aurora kinase inhibitor PHA-739358 suppresses growth of hepatocellular carcinoma *in vitro* and in a xenograft mouse model. *Neoplasia* **2009**, *11*, 934–944. [CrossRef] [PubMed]
40. Xie, L.; Kassner, M.; Munoz, R.M.; Que, Q.Q.; Kiefer, J.; Zhao, Y.; Mousses, S.; Yin, H.H.; von Hoff, D.D.; Han, H. Kinome-wide siRNA screening identifies molecular targets mediating the sensitivity of pancreatic cancer cells to Aurora kinase inhibitors. *Biochem. Pharmacol.* **2012**, *83*, 452–461. [CrossRef] [PubMed]
41. Abbas, T.; Dutta, A. p21 in cancer: Intricate networks and multiple activities. *Nat. Rev. Cancer* **2009**, *9*, 400–414. [CrossRef] [PubMed]
42. Aylon, Y.; Oren, M. Living with p53, dying of p53. *Cell* **2007**, *130*, 597–600. [CrossRef] [PubMed]
43. Tang, D.; Lotze, M.T.; Kang, R.; Zeh, H.J. Apoptosis promotes early tumorigenesis. *Oncogene* **2011**, *30*, 1851–1854. [CrossRef] [PubMed]
44. Ashkenazi, A. Targeting the extrinsic apoptotic pathway in cancer: Lessons learned and future directions. *J. Clin. Investing.* **2015**, *125*, 487–489. [CrossRef] [PubMed]
45. Taylor, R.C.; Cullen, S.P.; Martin, S.J. Apoptosis: Controlled demolition at the cellular level. *Nat. Rev. Mol. Cell Biol.* **2008**, *9*, 231–241. [CrossRef] [PubMed]
46. Eskelinen, E.L. The dual role of autophagy in cancer. *Curr. Opin. Pharmacol.* **2011**, *11*, 294–300. [CrossRef] [PubMed]
47. Klionsky, D.J.; Emr, S.D. Autophagy as a regulated pathway of cellular degradation. *Science* **2000**, *290*, 1717–1721. [CrossRef] [PubMed]
48. Denton, D.; Nicolson, S.; Kumar, S. Cell death by autophagy: Facts and apparent artefacts. *Cell Death Differ.* **2012**, *19*, 87–95. [CrossRef] [PubMed]
49. Do, T.V.; Xiao, F.; Bickel, L.E.; Klein-Szanto, A.J.; Pathak, H.B.; Hua, X.; Howe, C.; O'Brien, S.W.; Maglaty, M.; Ecsedy, J.A.; *et al*. Aurora kinase A mediates epithelial ovarian cancer cell migration and adhesion. *Oncogene* **2014**, *33*, 539–549. [CrossRef] [PubMed]
50. Rodon, J.; Dienstmann, R.; Serra, V.; Tabernero, J. Development of PI3K inhibitors: lessons learned from early clinical trials. *Nat. Rev. Clin. Oncol.* **2013**, *10*, 143–153. [CrossRef] [PubMed]
51. Polivka, J., Jr.; Janku, F. Molecular targets for cancer therapy in the PI3K/AKT/mTOR pathway. *Pharmacol. Ther.* **2014**, *142*, 164–175. [CrossRef] [PubMed]
52. Benjamin, D.; Colombi, M.; Moroni, C.; Hall, M.N. Rapamycin passes the torch: A new generation of mTOR inhibitors. *Nat. Rev. Drug Discov.* **2011**, *10*, 868–880. [CrossRef] [PubMed]

53. Li, Z.; Yan, S.; Attayan, N.; Ramalingam, S.; Thiele, C.J. Combination of an allosteric Akt Inhibitor MK-2206 with etoposide or rapamycin enhances the antitumor growth effect in neuroblastoma. *Clin. Cancer Res.* **2012**, *18*, 3603–3615. [CrossRef] [PubMed]
54. Petrich, A.M.; Leshchenko, V.; Kuo, P.Y.; Xia, B.; Thirukonda, V.K.; Ulahannan, N.; Gordon, S.; Fazzari, M.J.; Ye, B.H.; Sparano, J.A.; *et al*. Akt inhibitors MK-2206 and nelfinavir overcome mTOR inhibitor resistance in diffuse large B-cell lymphoma. *Clin. Cancer Res.* **2012**, *18*, 2534–2544. [CrossRef] [PubMed]
55. Xu, S.; Li, S.; Guo, Z.; Luo, J.; Ellis, M.J.; Ma, C.X. Combined targeting of mTOR and AKT is an effective strategy for basal-like breast cancer in patient-derived xenograft models. *Mol. Cancer Ther.* **2013**, *12*, 1665–1675. [CrossRef] [PubMed]
56. Yang, J.; Weinberg, R.A. Epithelial-mesenchymal transition: At the crossroads of development and tumor metastasis. *Dev. Cell* **2008**, *14*, 818–829. [CrossRef] [PubMed]
57. Mani, S.A.; Guo, W.; Liao, M.J.; Eaton, E.N.; Ayyanan, A.; Zhou, A.Y.; Brooks, M.; Reinhard, F.; Zhang, C.C.; Shipitsin, M.; *et al*. The epithelial-mesenchymal transition generates cells with properties of stem cells. *Cell* **2008**, *133*, 704–715. [CrossRef] [PubMed]
58. Gupta, P.B.; Fillmore, C.M.; Jiang, G.; Shapira, S.D.; Tao, K.; Kuperwasser, C.; Lander, E.S. Stochastic state transitions give rise to phenotypic equilibrium in populations of cancer cells. *Cell* **2011**, *146*, 633–644. [CrossRef] [PubMed]
59. Beavon, I.R. The E-cadherin-catenin complex in tumour metastasis: Structure, function and regulation. *Eur. Cancer* **2000**, *36*, 1607–1620. [CrossRef]
60. Liu, C.Y.; Lin, H.H.; Tang, M.J.; Wang, Y.K. Vimentin contributes to epithelial-mesenchymal transition cancer cell mechanics by mediating cytoskeletal organization and focal adhesion maturation. *Oncotarget* **2015**, *6*, 15966–15983. [CrossRef] [PubMed]
61. Cannito, S.; Novo, E.; di Bonzo, L.V.; Busletta, C.; Colombatto, S.; Parola, M. Epithelial-mesenchymal transition: From molecular mechanisms, redox regulation to implications in human health and disease. *Antioxid. Redox Signal.* **2010**, *12*, 1383–1430. [CrossRef] [PubMed]



© 2015 by the authors; licensee MDPI, Basel, Switzerland. This article is an open access article distributed under the terms and conditions of the Creative Commons by Attribution (CC-BY) license (http://creativecommons.org/licenses/by/4.0/).

International Journal of
Molecular Sciences

MDPI

Review

Prostate Cancer Stem Cells: Research Advances

Dagmara Jaworska, Wojciech Król and Ewelina Szliszka *

Received: 5 September 2015 ; Accepted: 8 October 2015 ; Published: 17 November 2015
Academic Editor: William Chi-shing Cho

Department of Microbiology and Immunology, School of Medicine with the Division of Dentistry in Zabrze, Medical University of Silesia in Katowice, H. Jordana 19, 41-808 Zabrze, Poland; djaworska@sum.edu.pl (D.J.); wkrol@sum.edu.pl (W.K.)
* Correspondence: eszliszka@sum.edu.pl; Tel./Fax: +48-322-722-554

Abstract: Cancer stem cells have been defined as cells within a tumor that possesses the capacity to self-renew and to cause the heterogeneous lineages of cancer cells that comprise the tumor. Experimental evidence showed that these highly tumorigenic cells might be responsible for initiation and progression of cancer into invasive and metastatic disease. Eradicating prostate cancer stem cells, the root of the problem, has been considered as a promising target in prostate cancer treatment to improve the prognosis for patients with advanced stages of the disease.

Keywords: cancer stem cell; prostate cancer; metastasis; castration-resistant prostate cancer

1. Introduction

Prostate cancer continues to be the most common cancer diagnosed in male patients and the second leading malignancy of cancer-related deaths in Europe and the United States [1,2]. Most patients with advanced stages of the disease respond to the current treatment (hormonal therapy, radiotherapy, or chemotherapy) only in the beginning, mostly developing progression and subsequently widespread metastasis, resistant to prostate cancer therapeutic methods. Numerous basic research studies on the mechanisms of carcinogenesis did not significantly improve the prognosis and therapy outcome of patients with prostate cancer [3–5].

Early observations in the 1960s based on experiments conducted on blood neoplasms, proved cell heterogeneity within the tumor mass, suggesting the existence of immature cell population that may arise from the entire population of tumor cells [6,7]. The first evidence confirming the hypothesis of the existence of cancer stem cells derives from the 1990s and is based on the study of blood diseases such as acute myeloid leukemia (AML) [8]. The following years of research showed the presence of cancer stem cells also in other types of tumors, *inter alia*, prostate cancer [9–11].

Although still controversial, the cancer stem cell maybe the root cell of cancer and the most crucial target in the treatment of the disease. Therefore, the understanding of its biology might allow this cell type to be eliminated by targeted therapy, leading to improvement in therapeutic outcome [12].

Prostate cancer research is now focused on the cancer stem cells to get better understanding of the tumor initiation mechanisms, progression and metastasis formation, and it will eventually help to provide the patients with a better therapeutic effect [13–16].

This review is focused on the following aspects: the main differences between stem cells and cancer stem cells, prostate cancer stem cell identification and their molecular markers, current theories on the origin of prostate cancer stem cells, and finally the current research helping to understand biology of castration-resistant prostate cancer (CRPC) and develop new strategies to eliminate all cancer cells.

2. Stem Cells and Cancer Stem Cells (CSC)

Stem cells are immature cells characterized by significant proliferative properties, self-renewal, and the potential to differentiate into specialized cells in a tissue [17]. Stem cell division may be symmetric or asymmetric. A stem cell during asymmetric division gives rise to one mother cell that is identical to the cell of origin (has the same proliferative potential) and another daughter cell that will differentiate. Thus the population of stem cells remains constant. The other type of division results in two identical stem cells and it is defined as symmetric [18,19]. Fundamentally, there are two kinds of normal stem cells: embryonic which are pluripotent and can give rise to all cell types, and non-embryonic stem cells with a limited potential to differentiate into other cell types [17].

Cancer stem cells (CSCs) possess stem-like nature to a degree sufficient to compare them with normal stem cells. According to American Association for Cancer Research (a statement accepted in 2006) a cancer stem cell is "a cell within a tumor that possesses the capacity to self-renew and to cause the heterogeneous lineages of cancer cells that comprise the tumor" [20].

According to the definition, both normal and cancer stem cells share at least one feature—the ability to self-renew. The self-renewal is defined as the ability to produce posterity which retains stem-like characteristics. Therefore the division of cancer stem cell results in one or two daughter cells that have the same ability to proliferate and generate new cells—identical as the original, parental cell [19,20].

These cancer stem cells possess the capacity to extend the cancer stem cell population and moreover, after differentiation, become other cancer cell types which constitute the tumor bulk of cells [20,21]. The tumor is then organized in a cellular hierarchy, like it is arranged in the normal tissues. The non-stem cells in the tumor have high, but not unrestricted ability to proliferate. Therefore, the only cells within the tumor with unlimited potential are cancer stem cells, so they are capable of driving growth and metastasis [18,20]. Because the time between divisions in CSC is very long, it has been suggested that this phenomenon can be responsible for the resistance to treatment. For this reason, CSC which are relatively insensitive to therapies currently focused on eradication of dividing cells, may be a source of cancer relapse [22–24].

The main difference between CSCs and normal stem cells is their frequency of occurrence. Normal stem cells are present in the tissues in a very small amount. Contrariwise, CSCs can be a rather large population in the bulk of tumor cells [21]. The proportion of cancer stem cells in the whole tumor mass may be very different depending on the type of cancer, and it has been reported to have certain significance for predicting the prognosis [25–27].

CSCs are similar to normal stem cells in that they are long lived, slow cycling, self-renewing cells in undifferentiated state, which can generate a large number of differentiated progeny cells. CSCs frequently express many early developmental markers of normal stem cells. The difference lies in the regulation and control of their proliferation [20,28]. Normal stem cell functions are under strict control, while the divisions of cancer stem cells are out of control. There are also emerging evidences that cancer stem cells gain independence from factors suppressing their proliferation, including the role of their microenvironment (niche), and get the ability to occupy other niches [29–31]. These cells are programmed to maintain tumor growth and development by producing a large number of cancer cells [17–20].

3. The CSC Hypothesis

Two models of tumor development have been proposed; the stochastic model and the hierarchy model which assume the existence of CSCs. The stochastic model (which has only historical significance nowadays) predicts that any cell in the tumor has an identical probability to be the tumor-initiating cell, when it develops the ability to self-renew. This process is controlled stochastically. The second model, originally proposed in the mid-19th century by Rudolf Virchow is the model of cancer stem cells [32]. Although this concept is not new, because it has been discussed already decades ago, the identification and isolation of stem—like cells in human malignancies was

not successful until 1997. This was accomplished by Bonnet and Dick in acute myeloid leukemia (AML) who showed that small subset of leukemic cells ($CD34^+CD38^-$) was able to initiate the disease when transplanted into a NOD/SCID mouse (non-obese diabetic/ severe combined immunodeficient mouse) [8]. Since then, this method has become the gold standard in stem cell research [20]. For the solid tumors proving the presence of cancer stem cells was much more difficult for several reasons. These cells are an integral part of the tissue which makes them less accessible. Furthermore the markers for cancer stem cells from solid tumors have not been investigated enough yet. Only several years later it was observed that $CD44^+CD24^{-/low}$ cells isolated from human breast cancer can induce breast cancer in NOD/SCID mice, while the remainder of cells failed to induce tumors. These innovative experiments suggested existence of cancer stem cells also in solid tumors [33]. In the last decade, CSCs have been identified and isolated in other solid tumors, including colon cancer [34], prostate cancer [35], hepatocellular carcinomas [36], or brain tumors [37] (Table 1). These studies provide evidence that tumor tissue is organized hierarchically, and only a sub-population of cells possesses the ability to initiate the tumor growth and survival.

Table 1. Cancer stem cell (CSC) in solid tumors and their first isolation year.

Cancer Types	Markers of CSCs	Year of Identification	Reference
Brain tumor	$CD133^+$	2004	[37]
Breast cancer	$CD44^+/CD24^-$	2003	[33]
Colon cancer	$CD133^+$	2007	[34]
Hepatic carcinoma	$CD90^+/CD45^-/CD44^+$	2008	[38]
Lung cancer	$CD133^+$	2005	[39]
Melanoma	$ABCB5^+$	2008	[40]
Ovarian cancer	$CD44^+/CD117^+$	2008	[41]
Pancreatic cancer	$CD44^+/CD24^+/ESA^+$	2007	[42]
Prostate cancer	$CD44+/\alpha_2\beta_1{}^{(hi)}/CD133^+$	2005	[35]

Moreover, it was established for human AML stem cells which are capable of regenerating the tumor that these cells display $CD34^+CD38^-$ cell surface markers. This kind of phenotype is similar to one typical of normal human hematopoietic progenitors. It may suggest that AML stem cells arise from normal stem cells [20]. However this statement is not necessarily true for all types of cancer. Actually, three hypotheses for the origin of CSCs exist. One of them declares that CSCs come just from normal adult stem cells that have acquired many genetic mutations. Another hypothesis states that CSCs develop from tumor cells across cellular dedifferentiation through the EMT (epithelial-mesenchymal transition) pathway [43]. The third one is related to induced pluripotent stem cells (iPS) [44]. Nowadays, most studies support the hypothesis that stem cells existing in normal adult tissue are the targets of carcinogenesis and transformation. The accumulation of mutations is a long lasting process and can take even several years. In this context, the only cells that live long enough in adult organism are normal stem cells. This premise makes adult stem cells ideal candidates for the cells of origin for cancer stem cells. According to the theory of carcinogenesis, malignant transformation may occur as result of wide range of mutagenic agents acting on stem cells present in the adult tissue.

4. Prostate Cancer Stem Cells

4.1. Prostate Epithelial Stem Cells in the Adult Gland

Normal, mature prostatic epithelium consists of three basic cell types: basal, luminal (secretory), and neuroendocrine that are identified by distinct marker expression. Additionally, there is a small group of intermediate cells that express both basal and luminal cell markers. These cells are referred to as transient amplifying cells (Figure 1).

The luminal cells are the most differentiated cells in the prostatic epithelium, express high levels of androgen receptor (AR) and low molecular weight keratins, secrete prostatic specific antigen (PSA), and prostatic acid phosphatase (PAP). Luminal cells are the main cell type in the epithelium and depend on androgens for survival in contrast to basal cells which do not express AR and are androgen-independent and undifferentiated [9,10].

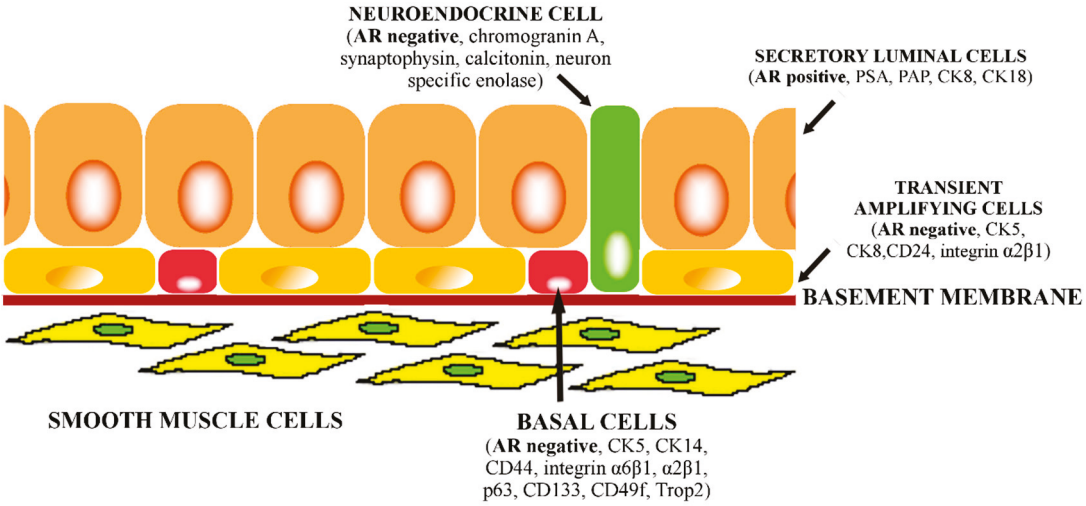

Figure 1. Schematic diagram of prostatic cellular compartments and their identity markers.

Neuroendocrine cells are very rare cells located in the luminal epithelial layer. These differentiated cells express chromogranin A, synaptophysin, calcitonin, and neuron specific enolase (NSE) but do not express AR or PSA. Neuroendocrine cells are distributed in prostatic glands in all anatomic areas and they constitute less than 1% of prostatic epithelium [45,46].

The basal cells are located on the basement membrane in prostate gland epithelium. These cells are characterized by the expression of high-molecular weight cytokeratins 5 and 14 (CK5 and CK14) [47,48], CD44 [49], integrin $\alpha_6\beta_1$ [50,51], and p63 (a member of p53 transcription factors family) [52].

Basal and luminal cells are hierarchically related. Basal cells are the progenitors of secretory cells, forasmuch as the existence of intermediate cells between these two types has been observed. These cells with an intermediate phenotype represent the transient amplifying cells [10,53–56]. One of the markers expressed on these cells is a CD24 surface molecule. CD24 distinguishes between low differentiated basal cells and transient amplifying cells and may play a significant role in the prostate gland cells differentiation [57].

A small number of cells among the population of basal cells have been recognized as the stem cells of the prostate both in mice and human. It is unclear how many subtypes of basal cells are present in the prostate and which subtype contains the main stem cell niche in the adult prostate [54,58].

Goldstein *et al.* [59] reported that specific marker, namely, tumor-associated calcium signal transducer 2 (TACSTD2/Trop2/M1S1/GA733-1) functionally discriminates between the two distinct basal cells subpopulations. Only the basal cells that express high levels of Trop 2 had the stem cell characteristics in the murine and human prostate [59]. Whereas, Lee *et al.* [58] identified seven basal cells subpopulations according to their p63, cytokeratin 14 and 5 expression. This group discovered that $p63^+/CK5^-/CK14^-$ subpopulation contain self-renewable stem cells with the greatest potential for differentiation [58].

In the adult human prostate CD133 (also known as Prominin-1) expression is thought to be characteristic of stem-like populations based on their expression of $\alpha_2\beta_1$ integrin and high clonogenic properties. Moreover, CD133 expression has been reported for prostate cancer stem cells [60,61].

CD133 expression is not restricted to the prostate gland; adult stem cells in other tissues also can often exhibit expression of this surface marker [62–64].

4.2. Origin of Prostate Cancer

The origin of prostate cancer remains controversial. The cell-of-origin of cancer—is the first cell which gains the mutations leading to cancer initiation. Whereas, cancer stem cells, defined by self-renewal and differentiation potential are the group of cells that maintain the tumor proliferation. The connection between both types is not completely understood yet. Their phenotypes may be different but they can also dynamically change. Two experimental approaches are used to characterize these two types of cells: transplantation assay and lineage-tracing assay [65]. Transplantation assay is a current "gold standard" for identifying cancer stem cells. This assay is based on xenografting isolated cells (with a specific phenotype) into immunodeficient mice. It has been used to prove the existence of cancer stem cells in several human cancers [20,33–35]. On the other hand, lineage-tracing assay is used to identify the potential cell-of-origin of cancer, however it can be also helpful in studying cancer stem cells. Lineage-tracing assay involves genetic labeling to determine individual cell fate. Then transformed, lineage-traced cells that formed a tumor can be analyzed to establish if they have cancer stem cells properties [65,66]. However, these classic types of experiments are not perfect in their design. Some authors impute that since they are performed in immune-deficient animals, they do not reflect the real state. If similar studies were done in immune-competent animals they would be more solid and reliable [67].

There are two possible cell-of-origin in prostate cancer, specifically—basal cell or luminal cell of origin. The prostate cancer cells usually have phenotype of the luminal cells, but they are not terminally differentiated as normal luminal cells. The cancer cells possess the unlimited proliferative capacity, unlike normal luminal cells, and they resemble more the basal cell characteristics. Firstly, it was assumed that the luminal cells were the source of all tumorigenicity, forasmuch as they constitute the bulk of the tumor mass. Nevertheless, several studies have brought evidence that prostate cancer stem cells are involved in the process of oncogenesis in the prostate gland. Basal cells in the prostate gland express surface molecules that regulate stem cell self-renewal such as p63, CD44, CD49f, CD133, therefore the prostate basal cells have been proposed to contain stem cells [7,35,68–70].

Cancer stem cells can arise from normal stem cells which are located in the basal layer of prostate gland. In the normal state, the stem cells can give rise to a second population—transient amplifying cells which subsequently differentiate into mature secretory cells [58,71,72]. It has been proposed that during carcinogenesis the normal stem cells accumulate mutations and are converted to highly tumorigenic and metastasis—initiating cancer stem cells. The main assumption was that cancer may arise as a result of genetic mutation in these cells, and this mutation concerns mainly oncogenes and tumor suppressor genes, in consequence resulting in uncontrolled cell growth [73–78]. It has been revealed that the tumorigenic prostate cancer stem cells can express specific markers such as telomerase, CD44, CD133, $\alpha_2\beta_1$-integrin, multidrug resistance proteins, aldehyde dehydrogenase, and low or undetectable levels of AR. Moreover, several studies in prostate regenerative systems and xenograft mouse models confirmed that prostate cancer stem cells could play critical role in carcinogenesis, metastasis, and resistance to currently used therapies [73,75–77,79–81].

However, there is some evidence that supports an existence of luminal cells with stem activity. Several groups have investigated if luminal progenitor cells are luminal-restricted or not. It has been described earlier, that PTEN protein is involved in the stem cell self-renewal [82,83]. Korsten *et al.* [84] demonstrated that, in the prostate specific *Pten*-knockout mouse model, this type of deletion results in prostatic hyperplasia. In this model, a shift in the balance of differentiation was showed. Complete *Pten* inactivation is also observed in primary prostate tumors in human. This study showed that hyperplastic cells in *Pten*-knockout mice overexpress CK8, CK19, and Sca-1 which is characteristic for luminal epithelial progenitor cells. The obtained data led researchers to conclusion that luminal

epithelial progenitor cells identified in the study are strong candidates for tumor initiating cells in the *Pten*-knockout prostate cancer model [84].

Moreover, Wang *et al.* [85] demonstrated that in the castrated mouse a rare luminal cell persists which expresses Nkx3.1 (regulator of prostate epithelial differentiation, marker of stem cell population). These cells are defined as CARNs (castration-resistant Nkx3.1-expressing cells). The lineage-tracing assay was used to identify CARNs as rare luminal epithelial population, possessing stem cell properties in prostate regeneration. CARNs cells were demonstrated to self-renew, and reconstitute prostate ducts in renal grafts after transplantation in immune-deficient mice. Eventually, a deletion of the *Pten* gene in CARNs resulted in rapid formation of carcinoma. These observations might indicate a novel luminal stem cell population as a cell-of-origin in prostate cancer [85].

Another group has recently performed a lineage-marking of basal and luminal cells to determine whether these cells contribute to tumors in a diverse range of mouse models. Their study showed that luminal cells are favored as the cell of origin for prostate cancer, however, explanted basal cells from these mice can generate tumors in grafts, after differentiation into luminal cells [86]. This results lead to the conclusion that both luminal and basal prostate cells can be a potential cellular origin for prostate cancer.

The hierarchy theory of the origin of prostate cancer suggests that rare tumor initiating cells can be identified in the population of whole tumor mass and they are distinct from the other cells. This model also predicts that the eradication of the stem cells will lead to complete eradication of the tumor [3,76,77,87–89].

The identification of these cells depends on the understanding of prostate cell differentiation lineage during development as well as adult prostate epithelium renewal. On the basis of this knowledge, the isolation and characterization of prostate cancer stem cells will become a true possibility and it should provide an explanation for the known clinical and molecular heterogeneity of human prostate cancer.

4.3. The Prostate Cancer Stem Cell Niche

The cancer stem cell hypothesis can partially explain the minimal residual disease occurrence. After radical prostatectomy, the persistence of one single cell in an appropriate environment could be the source of relapse. Several studies suggest the existence of functional microenvironments that support CSCs which is called the CSC niche. The signals that originate from this tumor niche regulate CSCs self-renewal, survival, and ability to invade tissues and the metastases development [18,20,74,90,91].

Microenvironment of the tumor might play the critical role in maintenance of stem-like features of prostate cancer cells. Cancer cell subpopulations can interact with other normal cells which are present in the tumor environment cooperating with them for benefits or even more often, taking advantage of them. Mateo *et al.* [92] recently described the co-operative interactions between the two clonal subpopulations of the PC-3 prostate cancer cell line. They found out that the invasiveness of a cancer stem cell enriched subpopulation is enhanced by a non-CSC subpopulation and can result in a significant increase of tumorigenic and metastatic potential of cancer stem cells. The knockdown and complementation experiments supported that SPARC protein (osteonectin, a matricellular glycoprotein, regulating tissue repair, and remodeling the extracellular matrix) is the main factor mediating the cooperation between CSCs and non-CSCs [92].

Furthermore, it has been observed that some changes in the tumor environment such as hypoxia, may induce, through HIF (hypoxia inducing factor) generation, the reprogramming of prostate cancer cells and increase the expression of stemness markers like CD44, Oct-3/4, Nanog, and drug resistance-associated molecules or anti-apoptotic proteins [93–96].

Eventually, CSC niches can also exist or be created in other, even distant from the primary tumor growth, locations. It is believed that a subpopulation of circulating tumor cells exists, which can settle

down in the new environment such as bone marrow. The cells which create this microenvironment are defined as disseminated tumor cells (DTCs) [97].

Some patients that appear cured of prostate cancer can develop bone metastases even years after radical prostatectomy. This phenomenon indicates that prostate cancer cells can metastasize very early, and are present in the bone marrow at the time of surgical resection. For many years, these cells remain dormant, until they develop clinically detectable metastases. DTCs are a heterogeneous population but some of them might have characteristics of cancer stem cells. It has been revealed that the microenvironment within the bone marrow plays a crucial role in the process of metastasis [29–31,98]. It has been recently discovered that DTCs take over the bone marrow hematopoietic stem cells niche, and even direct competition for the niche was demonstrated. Eventually, it was shown that disseminated tumor cells affect the function of bone marrow, while settled in the marrow niche [30].

Some cells in the tumor microenvironment such as macrophages, endothelial cells, and fibroblasts may support prostate cancer progression. It was demonstrated that the bone marrow-derived mesenchymal stem cells (BM-MSCs) also participate in this process. Luo *et al.* [99] found out that BM-MSCs could be recruited into prostate tumor and lead to the increase of metastatic ability by the augmentation of cancer stem cell population respectively. Prostate cancer cells when cocultured with BM-MSCs grew as floating spheres which is characteristic feature of stem cells. They also showed that BM-MSCs coculture led to increased expression of stem cell markers such as CD133, OCT4, and Sox2 in the prostate cancer cell population [99].

The results of these findings confirm the importance of the tumor microenvironment and cancer stem cell niche during carcinogenesis and metastasis formation.

4.4. Markers of Prostate Cancer Stem Cells

For the distinction of prostate cancer stem cells from the other cells in tumor, several candidate markers have been tested. The most important are CD24, CD44 [69], CD49f [59], CD133 [35,61], CD166 [71], and $\alpha_2\beta_1$ integrins [35]. Those markers have been tested alone and in several combinations but the ideal combination has not been found yet, which could clearly lead in the all cases to distinct cancer stem cells. The cause of this situation is the considerable diversity in the tumor histotypes and their genetic heterogeneity [35,71,100].

CD133 (Prominin-1 or AC133) is a cell surface glycoprotein whose biological function is poorly characterized, except that it interacts with cholesterol in cell membrane and is a marker of cholesterol-based "lipid raft" [101]. This membrane protein has been identified first as hematopoietic stem cell marker [102]. Richardson *et al.* [61] showed that approximately 1% of normal human prostate basal cells express the marker CD133, and these cells when restricted also to $\alpha_2\beta_1{}^{hi}$ population, possessed high *in vitro* proliferative potential. Moreover, this group demonstrated the ability of $\alpha_2\beta_1{}^{hi}$/CD133 normal prostate stem cells to form acini with prostatic—specific differentiation when grafted into athymic, nude mice [61]. CD133 has been proposed to be a putative surface marker in a number of tumors, however Collins *et al.* [35] used this marker to identify the prostate cancer stem cell population, and reported for the first time the identification and characterization of a cancer stem cell population from human prostate tumors. Cancer stem cells isolated by this group had a $CD44^+/\alpha_2\beta_1{}^{hi}/CD133^+$ phenotype, and possessed a significant capacity for self-renewal [35]. CD133 is often expressed in adult stem cells and it is believed that CD133—cholesterol microdomains might be implicated in the determination of cell fate and maintaining stem cell properties [103]. It has been investigated, using a series of anti-CD133 monoclonal antibodies, that attachment and growth of normal $CD133^+$ prostate epithelial cell cultures requires expression of full-length glycosylated CD133 protein. In contrast to normal adult stem cells, prostate cancer stem cells do not require functional CD133 [103,104].

$CD133^+$ prostate cancer stem cells have been also identified based on their integrin expression pattern. Rentala *et al.* [105] have recently identified the role of integrin profile in the prostate cancer

stem cells isolated from the tissue specimens of patients with prostate cancer. They showed that the levels of β_1 and $\alpha_2\beta_1$ integrins were significantly higher than those of other integrins. $CD133^+$ cells presented an increased degree of attachment to extracellular matrix protein. The study revealed for the first time the importance of the role of α_1 and β_1 integrins in the homing and differentiation of prostate cancer stem cells *in vitro* [105].

CD44 is a glycoprotein which exists as a standard isoform and a range of variant isoforms that are produced as a result of extensive alternative splicing. This alternative splicing mechanism and expression of variant isoforms contributes to uncontrolled tumor cell proliferation and transformation and induces metastasis formation [90,106,107]. CD44 antigen was first described as a lymphocyte homing receptor but it can be expressed by a wide range of cells. It belongs to the family of cartilage link proteins, while the ligands for this protein are collagen, laminin, fibronectin, E-selectin, L-selectin, and the extracellular matrix glycosaminoglycan hyaluronic acid (HA) [90,108–110]. In one of the studies performed *in vitro* and *in vivo* on cell lines and xenograft tumor models, Patrawala *et al.* [70] showed that $CD44^+$ prostate cancer stem cells have stem—like properties such as increased clonoge nic and metastatic potential. These cells can form colonies in soft agar and have the potential to form tumors in NOD/SCID mice. It was concluded that this population of $CD44^+$ stem cells is a heterogeneous population where primitive cells coexist with later progenitor cells [70]. These results provided convincing evidence that CD44 is associated with stem cells in prostate tumors.

In 2008, Hurt *et al.* [69] defined human prostate $CD44^+CD24^-$ subpopulation as prostate cancer stem cells with the ability to grow as nonadherent spheres in serum replacement medium. Only $CD44^+CD24^-$ population, but not $CD44^+CD24^-$ depleted population, had the potential to form tumors in NOD/SCID mice. This study defined an additional marker for prostate cancer stem cells and identified an almost homogenous population of stem cells with preserved colony—initiation ability [69]. Recent papers identified $CD44^+CD24^-$ cells in different prostate cancer cell lines [111,112]. These reports showed that both in primary and established prostate cancer cell lines, cancer stem cells can be more invasive. The data revealed that $CD44^+$ subpopulation of stem-like cells actively invaded Matrigel, while $CD44^-$ cells were characterized by a lack of invasiveness. Moreover, $CD44^+$ cells were more tumorigenic when transplanted in NOD/SCID mice compared with non-invasive $CD44^-$ cells [111].

Jiao *et al.* [71] identified subsequently CD166 as a surface molecule that can enrich sphere forming activity of $Lin^-Sca1^+CD49f^{hi}$ population of cells in murine model. The aforementioned phenotype cannot be used for isolation of human cancer stem cells, because Sca-1 is only expressed in the mouse. However, CD166 is expressed in human organs and can be upregulated in certain tumor types. Therefore, this group found out that CD166 expression is upregulated in human prostate cancer, particularly in castration-resistant prostate cancer subpopulations. Similar to previous findings with murine prostate cells, the sphere forming activity was identified in the cells expressing high levels of CD166 surface molecule [71].

Altogether, all these studies of cell markers suggest that cancer stem cells may be derived from normal stem cells, since the expression patterns in these two cell types are very similar.

5. Implications for Prostate Cancer Treatment

Prostate cancer is one of the most common malignancies in male patients. Despite the progress that has been made in understanding of the molecular basis of carcinogenesis, and the introduction of early diagnostics protocols or effective therapeutic intervention, the disease progression to invasive and metastatic castration-resistant prostate cancers (mCRPCs) is still observed. Moreover, it is almost always associated with poor prognosis. In the beginning, advanced prostate cancer is treated with androgen deprivation therapy (ADT). Although it is initially very effective, it will finally lead to the development of aggressive and usually incurable conditions [1,2,113,114]. The current anti-androgen therapy and chemotherapy against CRPCs show limited survival benefits, because these types of

treatment target primarily the bulk of neoplastic, fast-growing cancer cells but not cancer stem cells [115,116].

Prostate cancer stem cells are resistant to hormonotherapy, chemotherapy, and radiotherapy, so cancer relapse may be due to preferential killing of more differentiated cells while leaving undifferentiated stem cancer cells. Currently existing therapies often lead to an increase of resistant cancer stem cell subpopulation by selecting the most resistant clones within a heterogeneous population of cancer cells [116–118].

Several mechanisms for the development of CRPC have been described, most of which are based on the AR signaling regulation. Therefore, targeting the dysregulation of AR signaling in prostate cancer cells has been among the main interests in prostate cancer research [119–123].

Kregel *et al.* [124] have recently investigated the role of Sox2 (Sex determining region Y-box 2) transcription factor in normal and malignant prostate cancer cells. Sox2 is an oncogene and the fundamental regulator of the survival and pluripotency of stem cells, promoting more aggressive tumor phenotypes. Prostate tumors which are Sox2 positive have also high score in Gleason scale. They revealed that the expression of Sox2 was repressed by AR signaling in castration-resistant prostate cancer cells lines. However, AR—mediated repression of Sox2 expression can be reversed by the treatment with the anti-androgen factor. Moreover, in the castration-sensitive cell line which does not express Sox2 and does not normally form tumors in castrated nude mouse, lentiviral Sox2 expression was sufficient to significantly increase tumor formation in a castrated host [124]. This model points to the eventuality that the increased castration-resistant tumor formation may be due to the promotion of cancer stem cell proliferation and survival by Sox2 increased expression.

Past findings beg the question why the cells can survive androgen deprivation therapy which eventually leads to tumor relapse? Recent studies have revealed that AR splice variants without ligand-binding domain, can be found in androgen independent cell lines. These other forms of the receptor are usually constitutively expressed, therefore their activity is not regulated by androgens [125–128]. Tumor relapse and metastatic potential was shown to be connected to EMT phenotype (epithelial-to-mesenchymal transition). Moreover, EMT phenotype is linked with androgen deprivation therapy application [129]. Kong *et al.* [130] showed that overexpression of one of the AR variants—AR3 led to induction of EMT phenotype and is also involved in the regulation of the expression of stem cells marker genes. Besides, it was showed that androgen deprivation therapy enhanced AR and AR spliced variants expression leading authors to the conclusion that this upregulation is involved in progression to castration-resistant prostate cancer [130].

There is still a pressing need for the discovery of more effective therapy for advanced prostate cancer which would target the CSCs. Interestingly, metformin, a common oral biguanide used to treat type 2 diabetes, has been demonstrated to have anticancer effects as well. It was shown that metformin acts selectively on CSCs in several types of cancer among others: breast cancer, pancreatic cancer, colon cancer and finally prostate cancer. Metformin targets the mitochondria and reduces ATP production by oxidative phosphorylation which is the main energy source in CSCs [131–135]. Therefore metformin could be used to increase CSC sensitivity to existing therapies, enhance treatment efficacy and prevent relapses. Bilen *et al.* [136] has observed, in a case series, that metformin used alone or in combination with Zyflamend (herbal extract containing turmeric, holy basil, green tea, oregano, ginger, rosemary, Chinese goldthread, hu zhang, barberry, and basil skullcap) decreased level of PSA in prostate cancer patients in metastatic stage of disease. Authors proposed this treatment as a maintenance therapy for castration-resistant prostate cancer patients. Metformin and/or Zyflamend presumably target cancer stem cells and the tumor niche and keep the cancer in a dormant state [136].

Iliopoulos *et al.* [133] showed that metformin acts together with several chemotherapeutic agents to prevent relapse in xenografts generated with prostate and lung cancer cell lines. Consequently, it could be used as a part of combined therapy or to reduce the chemotherapy dose in patients treated for prostate cancer [133].

Furthermore, several articles have been published regarding phytochemicals and plant extracts which are able to target and selectively eliminate CSCs in many different types of cancer. It has been shown that sulforaphane, curcumin, piperine, β-carotene, and *Sasa quelpaertensis* extract exhibit not only anti-tumor properties but also are able to kill CSCs [137,138]. In relation to prostate cancer, anti-CSC effects were observed in the case of curcumin, the principal bright-yellow colored curcuminoid of turmeric (a plant of the ginger family). Curcumin was showed to cause effect on cell death and proliferation mediated by Wnt signaling in androgen-dependent and androgen-independent prostate cancer cell lines [139]. Recently Botchkina *et al.* [140] reported that structural analog of curcumin as a single agent or in combination with new-generation taxoid can exhibit significant activity against prostate $CD133^{hi}/CD44^{+/hi}$ cells. Moreover these drugs have been shown to inhibit expression of stem-related genes and even to induce expression of silent genes, which could potentially reverse drug resistance in these cells [140].

These recent findings support a better understanding of the prostate cancer stem cells' role in the process of tumorigenesis. However, it is still essential to investigate the signaling pathways that regulate the self-renewal and survival of CSCs. In the future, such research may help to introduce novel therapeutic strategies for eliminating aggressive tumor cells and possibly prolong survival in patients with CRPC.

6. Conclusions

The stem cell theory provides a new framework for viewing the molecular mechanisms that underlie cancer cell hierarchy and heterogeneity within tumor mass. Clear understanding of the lineage hierarchy in prostate cancer cells will provide insights into the properties and characteristics of the origin of prostate cancer cells. An increasing body of evidence has shown that cancer stem cells represent a significant effort to effective cancer treatment in view of resistance to currently used clinical therapy. However, there is still a pressing need for the discovery of unique cancer stem cell markers to distinguish the cancer stem cells from the normal stem cells. But the ultimate challenge in the next few years will be developing new stem cell—directed drugs and reducing risk of relapse.

Acknowledgments: This work was supported by a research grants: KNW-1-080/K/4/0 and KNW-2-016/D/4/N from the Medical University of Silesia in Katowice (Poland).

Author Contributions: Dagmara Jaworska wrote the manuscript and generated Figure 1. Wojciech Król and Ewelina Szliszka contributed to the manuscript conception, planning, and writing. Ewelina Szliszka reviewed and proofread of the manuscript.

Conflicts of Interest: The authors declare no conflict of interest.

References

1. Siegel, R.L.; Miller, K.D.; Jemal, A. Cancer statistics, 2015. *CA Cancer J. Clin.* **2015**, *65*, 5–29. [CrossRef] [PubMed]
2. Torre, L.A.; Bray, F.; Siegel, R.L.; Ferlay, J.; Lortet-Tieulent, J.; Jemal, A. Global cancer statistics, 2012. *CA Cancer J. Clin.* **2012**, *65*, 87–108. [CrossRef] [PubMed]
3. Merseburger, A.S.; Bellmunt, J.; Jenkins, C.; Parker, C.; Fitzpatrick, J.M. Perspectives on treatment of metastatic castration-resistant prostate cancer. *Oncologist* **2013**, *18*, 558–567. [CrossRef] [PubMed]
4. Hammerer, P.; Madersbacher, S. Landmarks in hormonal therapy for prostate cancer. *BJU Int.* **2012**, *110* (Suppl. 1), 23–29. [CrossRef] [PubMed]
5. Clarke, N.W. Landmarks in non-hormonal pharmacological therapies for castration-resistant prostate cancer. *BJU Int.* **2012**, *110* (Suppl. 1), 14–22. [CrossRef] [PubMed]
6. Sabbath, K.D.; Ball, E.D.; Larcom, P.; Davis, R.B.; Griffin, J.D. Heterogeneity of clonogenic cells in acute myeloblastic leukemia. *J. Clin. Investig.* **1985**, *75*, 746–753. [CrossRef] [PubMed]
7. Collins, A.T.; Maitland, N.J. Prostate cancer stem cells. *Eur. J. Cancer* **2006**, *42*, 1213–1218. [CrossRef] [PubMed]

8. Bonnet, D.; Dick, J.E. Human acute myeloid leukemia is organized as a hierarchy that originates from a primitive hematopoietic cell. *Nat. Med.* **1997**, *3*, 730–737. [CrossRef] [PubMed]
9. Sherwood, E.R.; Theyer, G.; Steiner, G.; Berg, L.A.; Kozlowski, J.M.; Lee, C. Differential expression of specific cytokeratin polypeptides in the basal and luminal epithelia of the human prostate. *Prostate* **1991**, *18*, 303–314. [CrossRef] [PubMed]
10. Verhagen, A.P.; Ramaekers, F.C.; Aalders, T.W.; Schaafsma, H.E.; Debruyne, F.M.; Schalken, J.A. Colocalization of basal and luminal cell-type cytokeratins in human prostate cancer. *Cancer Res.* **1992**, *52*, 6182–6187. [PubMed]
11. Bonkhoff, H. Role of the basal cells in premalignant changes of the human prostate: A stem cell concept for the development of prostate cancer. *Eur. Urol.* **1996**, *30*, 201–205. [PubMed]
12. Taylor, R.A.; Toivanen, R.; Risbridger, G.P. Stem cells in prostate cancer: Treating the root of the problem. *Endocr. Relat. Cancer* **2010**, *17*, R273–R285. [CrossRef] [PubMed]
13. Nouri, M.; Ratther, E.; Stylianou, N.; Nelson, C.C.; Hollier, B.G.; Williams, E.D. Androgen-targeted therapy-induced epithelial mesenchymal plasticity and neuroendocrine transdifferentiation in prostate cancer: An opportunity for intervention. *Front. Oncol.* **2014**, *4*, 1–19. [CrossRef] [PubMed]
14. Feitelson, M.A.; Arzumanyan, A.; Kulathinal, R.J.; Blain, S.W.; Holcombe, R.F.; Mahajna, J.; Marino, M.; Martinez-Chantar, M.L.; Nawroth, R.; Sanchez-Garcia, I.; *et al*. Sustained proliferation in cancer: Mechanisms and novel therapeutic targets. *Semin. Cancer Biol.* **2015**. [CrossRef] [PubMed]
15. Zhou, Y.; Yang, J.; Zhang, R.; Kopecek, J. Combination therapy of prostate cancer with HPMA copolymer conjugates containing PI3K/mTOR inhibitor and docetaxel. *Eur. J. Pharm. Biopharm.* **2015**, *89*, 107–115. [CrossRef] [PubMed]
16. Alberti, C. Prostate cancer: Radioresistance molecular target-related markers and foreseeable modalities of radiosensitization. *Eur. Rev. Med. Pharmacol. Sci.* **2014**, *18*, 2275–2282. [PubMed]
17. Tuch, B.E. Stem cells—A clinical update. *Aust. Fam. Physician* **2006**, *35*, 719–721. [PubMed]
18. D'Andrea, V.; Guarino, S.; di Matteo, F.M.; Maugeri Saccà, M.; de Maria, R. Cancer stem cells in surgery. *G. Chir.* **2014**, *35*, 257–259. [PubMed]
19. Fulawka, L.; Donizy, P.; Halon, A. Cancer stem cells—The current status of an old concept: Literature review and clinical approaches. *Biol. Res.* **2014**, *47*. [CrossRef] [PubMed]
20. Clarke, M.F.; Dick, J.E.; Dirks, P.B.; Eaves, C.J.; Jamieson, C.H.; Jones, D.L.; Visvader, J.; Weissman, I.L.; Wahl, G.M. Cancer stem cells—Perspectives on current status and future directions: AACR workshop on cancer stem cells. *Cancer Res.* **2006**, *66*, 9339–9344. [CrossRef] [PubMed]
21. Jiang, W.; Peng, J.; Zhang, Y.; Cho, W.C.; Jin, K. The implications of cancer stem cells for cancer therapy. *Int. J. Mol. Sci.* **2012**, *13*, 16636–16657. [CrossRef] [PubMed]
22. Chen, X.; Zhang, J.; Zhang, Z.; Li, H.; Cheng, W.; Liu, J. Cancer stem cells, epithelial-mesenchymal transition, and drug resistance in high-grade ovarian serous carcinoma. *Hum. Pathol.* **2013**, *44*, 2373–2384. [CrossRef] [PubMed]
23. Economopoulou, P.; Kaklamani, V.G.; Siziopikou, K. The role of cancer stem cells in breast cancer initiation and progression: Potential cancer stem cell-directed therapies. *Oncologist* **2012**, *17*, 1394–1401. [CrossRef] [PubMed]
24. Chen, J.; Li, Y.; Yu, T.S.; McKay, R.M.; Burns, D.K.; Kernie, S.G.; Parada, L.F. A restricted cell population propagates glioblastoma growth after chemotherapy. *Nature* **2012**, *488*, 522–526. [CrossRef] [PubMed]
25. Yang, G.; Xue, F.; Chen, X. Prognostic value of different amounts of cancer stem cells in different molecular subtypes of breast cancer. *Gland Surg.* **2012**, *1*, 20–24. [PubMed]
26. Gudadze, M.; Kankava, Q.; Mariamidze, A.; Burkadze, G. Features of CD44+/CD24-low phenotypic cell distribution in relation to predictive markers and molecular subtypes of invasive ductal carcinoma of the breast. *Georgian Med. News* **2014**, *228*, 81–87. [PubMed]
27. Korski, K.; Malicka-Durczak, A.; Breborowicz, J. Expression of stem cell marker CD44 in prostate cancer biopsies predicts cancer grade in radical prostatectomy specimens. *Pol. J. Pathol.* **2014**, *65*, 291–295. [CrossRef] [PubMed]
28. Clarke, M.F.; Fuller, M. Stem cells and cancer: Two faces of eve. *Cell* **2006**, *124*, 1111–1115. [CrossRef] [PubMed]
29. Pedersen, E.A.; Shiozawa, Y.; Pienta, K.J.; Taichman, R.S. The prostate cancer bone marrow niche: More than just 'fertile soil'. *Asian J. Androl.* **2012**, *14*, 423–427. [CrossRef] [PubMed]

30. Shiozawa, Y.; Pedersen, E.A.; Havens, A.M.; Jung, Y.; Mishra, A.; Joseph, J.; Kim, J.K.; Patel, L.R.; Ying, C.; Ziegler, A.M.; *et al*. Human prostate cancer metastases target the hematopoietic stem cell niche to establish footholds in mouse bone marrow. *J. Clin. Investig.* **2011**, *121*, 1298–1312. [CrossRef] [PubMed]
31. Shiozawa, Y.; Eber, M.R.; Berry, J.E.; Taichman, R.S. Bone marrow as a metastatic niche for disseminated tumor cells from solid tumors. *BoneKEy Rep.* **2015**, *4*. [CrossRef] [PubMed]
32. Soeda, A.; Shaffrey, M.E.; Park, D.M. Cancer stem cells and glioblastoma multiforme: Pathophysiological and clinical aspects. In *Advances in Cancer Stem Cells Biology*; Scatena, R., Mordente, A., Giardina, B., Eds.; Springer Science & Business Media: New York, NY, USA, 2011; pp. 123–140.
33. Al-Hajj, M.; Wicha, M.S.; Benito-Hernandez, A.; Morrison, S.J.; Clarke, M.F. Prospective identification of tumorigenic breast cancer cells. *Proc. Natl. Acad. Sci. USA* **2003**, *100*, 3983–3988. [CrossRef] [PubMed]
34. O'Brien, C.A.; Pollett, A.; Gallinger, S.; Dick, J.E. A human colon cancer cell capable of initiating tumour growth in immunodeficient mice. *Nature* **2007**, *445*, 106–110. [CrossRef] [PubMed]
35. Collins, A.T.; Berry, P.A.; Hyde, C.; Stower, M.J.; Maitland, N.J. Prospective identification of tumorigenic prostate cancer stem cells. *Cancer Res.* **2005**, *65*, 10946–10951. [CrossRef] [PubMed]
36. Sell, S.; Leffert, H.L. Liver cancer stem cells. *J. Clin. Oncol.* **2008**, *26*, 2800–2805. [CrossRef] [PubMed]
37. Singh, S.K.; Clarke, I.D.; Terasaki, M.; Bonn, V.E.; Hawkins, C.; Squire, J.; Dirks, P.B. Identification of a cancer stem cell in human brain tumors. *Cancer Res.* **2003**, *63*, 5821–5828. [PubMed]
38. Yang, Z.F.; Ho, D.W.; Ng, M.N.; Lau, C.K.; Yu, W.C.; Ngai, P.; Chu, P.W.; Lam, C.T.; Poon, R.T.; Fan, S.T. Significance of $CD90^{+}$ cancer stem cells in human liver cancer. *Cancer Cell* **2008**, *13*, 153–166. [CrossRef] [PubMed]
39. Eramo, A.; Lotti, F.; Sette, G.; Pilozzi, E.; Biffoni, M.; di Virgilio, A.; Conticello, C.; Ruco, L.; Peschle, C.; de Maria, R. Identification and expansion of the tumorigenic lung cancer stem cell population. *Cell Death Differ.* **2008**, *15*, 504–514. [CrossRef] [PubMed]
40. Schatton, T.; Murphy, G.F.; Frank, N.Y.; Yamaura, K.; Waaga-Gasser, A.M.; Gasser, M.; Zhan, Q.; Jordan, S.; Duncan, L.M.; Weishaupt, C.; *et al*. Identification of cells initiating human melanomas. *Nature* **2008**, *451*, 345–349. [CrossRef] [PubMed]
41. Zhang, S.; Balch, C.; Chan, M.W.; Lai, H.C.; Matei, D.; Schilder, J.M.; Yan, P.S.; Huang, T.H.; Nephew, K.P. Identification and characterization of ovarian cancer-initiating cells from primary human tumors. *Cancer Res.* **2008**, *68*, 4311–4320. [CrossRef] [PubMed]
42. Li, C.; Heidt, D.G.; Dalerba, P.; Burant, C.F.; Zhang, L.; Adsay, V.; Wicha, M.; Clarke, M.F.; Simeone, D.M. Identification of pancreatic cancer stem cells. *Cancer Res.* **2007**, *67*, 1030–1037. [CrossRef] [PubMed]
43. Mani, S.A.; Guo, W.; Liao, M.J.; Eaton, E.N.; Ayyanan, A.; Zhou, A.Y.; Brooks, M.; Reinhard, F.; Zhang, C.C.; Shipitsin, M.; *et al*. The epithelial-mesenchymal transition generates cells with properties of stem cells. *Cell* **2008**, *133*, 704–715. [CrossRef] [PubMed]
44. Corominas-Faja, B.; Cufí, S.; Oliveras-Ferraros, C.; Cuyàs, E.; López-Bonet, E.; Lupu, R.; Alarcón, T.; Vellon, L.; Iglesias, J.M.; Leis, O.; *et al*. Nuclear reprogramming of luminal-like breast cancer cells generates Sox2-overexpressing cancer stem-like cellular states harboring transcriptional activation of the mTOR pathway. *Cell Cycle* **2013**, *12*, 3109–3124. [CrossRef] [PubMed]
45. Parimi, V.; Goyal, R.; Poropatich, K.; Yang, X.J. Neuroendocrine differentiation of prostate cancer: A review. *Am. J. Clin. Exp. Urol.* **2014**, *2*, 273–285. [PubMed]
46. Amorino, G.P.; Parsons, S.J. Neuroendocrine cells in prostate cancer. *Crit. Rev. Eukaryot. Gene Expr.* **2004**, *14*, 287–300. [CrossRef] [PubMed]
47. De Marzo, A.M.; Meeker, A.K.; Epstein, J.I.; Coffey, D.S. Prostate stem cell compartments: Expression of the cell cycle inhibitor $p27^{Kip1}$ in normal, hyperplastic, and neoplastic cells. *Am. J. Pathol.* **1998**, *153*, 911–919. [CrossRef]
48. Brawer, M.K.; Peehl, D.M.; Stamey, T.A.; Bostwick, D.G. Keratin immunoreactivity in the benign and neoplastic human prostate. *Cancer Res.* **1985**, *45*, 3663–3667. [PubMed]
49. Alam, T.N.; O'Hare, M.J.; Laczkó, I.; Freeman, A.; Al-Beidh, F.; Masters, J.R.; Hudson, D.L. Differential expression of CD44 during human prostate epithelial cell differentiation. *J. Histochem. Cytochem.* **2004**, *52*, 1083–1090. [CrossRef] [PubMed]
50. Bello-DeOcampo, D.; Kleinman, H.K.; Deocampo, N.D.; Webber, M.M. Laminin-1 and alpha6beta1 integrin regulate acinar morphogenesis of normal and malignant human prostate epithelial cells. *Prostate* **2001**, *46*, 142–153. [CrossRef]

51. Knox, J.D.; Cress, A.E.; Clark, V.; Manriquez, L.; Affinito, K.S.; Dalkin, B.L.; Nagle, R.B. Differential expression of extracellular matrix molecules and the alpha 6-integrins in the normal and neoplastic prostate. *Am. J. Pathol.* **1994**, *145*, 167–174. [PubMed]
52. Signoretti, S.; Waltregny, D.; Dilks, J.; Isaac, B.; Lin, D.; Garraway, L.; Yang, A.; Montironi, R.; McKeon, F.; Loda, M. p63 is a prostate basal cell marker and is required for prostate development. *Am. J. Pathol.* **2000**, *157*, 1769–1775. [CrossRef]
53. Wang, Y.; Hayward, S.; Cao, M.; Thayer, K.; Cunha, G. Cell differentiation lineage in the prostate. *Differentiation* **2001**, *68*, 270–279. [CrossRef] [PubMed]
54. Hudson, D.L.; O'Hare, M.; Watt, F.M.; Masters, J.R. Proliferative heterogeneity in the human prostate: Evidence for epithelial stem cells. *Lab. Investig.* **2000**, *80*, 1243–1250. [CrossRef] [PubMed]
55. Xue, Y.; Smedts, F.; Debruyne, F.M.; de la Rosette, J.J.; Schalken, J.A. Identification of intermediate cell types by keratin expression in the developing human prostate. *Prostate* **1998**, *34*, 292–301. [CrossRef]
56. Liu, A.Y.; Peehl, D.M. Characterization of cultured human prostatic epithelial cells by cluster designation antigen expression. *Cell Tissue Res.* **2001**, *305*, 389–397. [CrossRef] [PubMed]
57. Petkova, N.; Hennenlotter, J.; Sobiesiak, M.; Todenhöfer, T.; Scharpf, M.; Stenzl, A.; Bühring, H.J.; Schwentner, C. Surface CD24 distinguishes between low differentiated and transit-amplifying cells in the basal layer of human prostate. *Prostate* **2013**, *73*, 1576–1590. [CrossRef] [PubMed]
58. Lee, D.K.; Liu, Y.; Liao, L.; Wang, F.; Xu, J. The prostate basal cell (BC) heterogeneity and the p63-positive BC differentiation spectrum in mice. *Int. J. Biol. Sci.* **2014**, *10*, 1007–1017. [CrossRef] [PubMed]
59. Goldstein, A.S.; Lawson, D.A.; Cheng, D.; Sun, W.; Garraway, I.P.; Witte, O.N. Trop2 identifies a subpopulation of murine and human prostate basal cells with stem cell characteristics. *Proc. Natl. Acad. Sci. USA* **2008**, *105*, 20882–20887. [CrossRef] [PubMed]
60. Trerotola, M.; Rathore, S.; Goel, H.L.; Li, J.; Alberti, S.; Piantelli, M.; Adams, D.; Jiang, Z.; Languino, L.R. CD133, Trop-2 and $\alpha 2\beta 1$ integrin surface receptors as markers of putative human prostate cancer stem cells. *Am. J. Transl. Res.* **2010**, *2*, 135–144. [PubMed]
61. Richardson, G.D.; Robson, C.N.; Lang, S.H.; Neal, D.E.; Maitland, N.J.; Collins, A.T. CD133, a novel marker for human prostatic epithelial stem cells. *J. Cell Sci.* **2004**, *117*, 3539–3545. [CrossRef] [PubMed]
62. Kania, G.; Corbeil, D.; Fuchs, J.; Tarasov, K.V.; Blyszczuk, P.; Huttner, W.B.; Boheler, K.R.; Wobus, A.M. Somatic stem cell marker prominin-1/CD133 is expressed in embryonic stem cell-derived progenitors. *Stem Cells* **2005**, *23*, 791–804. [CrossRef] [PubMed]
63. Sykes, A.M.; Huttner, W.B. Prominin-1 (CD133) and the cell biology of neural progenitors and their progeny. *Adv. Exp. Med. Biol.* **2013**, *777*, 89–98. [PubMed]
64. Missol-Kolka, E.; Karbanová, J.; Janich, P.; Haase, M.; Fargeas, C.A.; Huttner, W.B.; Corbeil, D. Prominin-1 (CD133) is not restricted to stem cells located in the basal compartment of murine and human prostate. *Prostate* **2011**, *71*, 254–267. [CrossRef] [PubMed]
65. Rycaj, K.; Tang, D.G. Cell-of-origin of cancer *versus* cancer stem cells: Assays and interpretations. *Cancer Res.* **2015**. [CrossRef] [PubMed]
66. Sharpe, B.; Beresford, M.; Bowen, R.; Mitchard, J.; Chalmers, A.D. Searching for prostate cancer stem cells: Markers and methods. *Stem Cell Rev.* **2013**, *9*, 721–730. [CrossRef] [PubMed]
67. Tu, S.M.; Bilen, M.A.; Tannir, N.M. The scientific method: Pillar and pitfall of cancer research. *Cancer Med.* **2014**, *3*, 1035–1037. [CrossRef] [PubMed]
68. Signoretti, S.; Loda, M. Prostate stem cells: From development to cancer. *Semin. Cancer Biol.* **2007**, *17*, 219–224. [CrossRef] [PubMed]
69. Hurt, E.M.; Kawasaki, B.T.; Klarmann, G.J.; Thomas, S.B.; Farrar, W.L. $CD44^{+}CD24^{-}$ prostate cells are early cancer progenitor/stem cells that provide a model for patients with poor prognosis. *Br. J. Cancer* **2008**, *98*, 756–765. [CrossRef] [PubMed]
70. Patrawala, L.; Calhoun, T.; Schneider-Broussard, R.; Li, H.; Bhatia, B.; Tang, S.; Reilly, J.G.; Chandra, D.; Zhou, J.; Claypool, K.; *et al*. Highly purified $CD44^{+}$ prostate cancer cells from xenograft human tumors are enriched in tumorigenic and metastatic progenitor cells. *Oncogene* **2006**, *25*, 1696–1708. [CrossRef] [PubMed]
71. Jiao, J.; Hindoyan, A.; Wang, S.; Tran, L.M.; Goldstein, A.S.; Lawson, D.; Chen, D.; Li, Y.; Guo, C.; Zhang, B.; *et al*. Identification of CD166 as a surface marker for enriching prostate stem/progenitor and cancer initiating cells. *PLoS ONE* **2012**, *7*, e42564. [CrossRef] [PubMed]

72. Lang, S.H.; Frame, F.M.; Collins, A.T. Prostate cancer stem cells. *J. Pathol.* **2009**, *217*, 299–306. [CrossRef] [PubMed]
73. Baccelli, I.; Trumpp, A. The evolving concept of cancer and metastasis stem cells. *J. Cell Biol.* **2012**, *198*, 281–293. [PubMed]
74. Zenzmaier, C.; Untergasser, G.; Berger, P. Aging of the prostate epithelial stem/progenitor cell. *Exp. Gerontol.* **2008**, *43*, 981–985. [CrossRef] [PubMed]
75. Gu, G.; Yuan, J.; Wills, M.; Kasper, S. Prostate cancer cells with stem cell characteristics reconstitute the original human tumor *in vivo*. *Cancer Res.* **2007**, *67*, 4807–4815. [CrossRef] [PubMed]
76. Maitland, N.J.; Bryce, S.D.; Stower, M.J.; Collins, A.T. Prostate cancer stem cells: A target for new therapies. *Ernst Schering Found. Symp. Proc.* **2006**, *5*, 155–179. [PubMed]
77. Maitland, N.J.; Collins, A.T. Prostate cancer stem cells: A new target for therapy. *J. Clin. Oncol.* **2008**, *26*, 2862–2870. [CrossRef] [PubMed]
78. Dunning, N.L.; Laversin, S.A.; Miles, A.K.; Rees, R.C. Immunotherapy of prostate cancer: Should we be targeting stem cells and EMT? *Cancer Immunol. Immunother.* **2011**, *60*, 1181–1193. [CrossRef] [PubMed]
79. Liu, T.; Xu, F.; Du, X.; Lai, D.; Zhao, Y.; Huang, Q.; Jiang, L.; Huang, W.; Cheng, W.; Liu, Z. Establishment and characterization of multi-drug resistant, prostate carcinoma-initiating stem-like cells from human prostate cancer cell lines 22RV1. *Mol. Cell. Biochem.* **2010**, *340*, 265–273. [CrossRef] [PubMed]
80. Mimeault, M.; Johansson, S.L.; Vankatraman, G.; Moore, E.; Henichart, J.P.; Depreux, P.; Lin, M.F.; Batra, S.K. Combined targeting of epidermal growth factor receptor and hedgehog signaling by gefitinib and cyclopamine cooperatively improves the cytotoxic effects of docetaxel on metastatic prostate cancer cells. *Mol. Cancer Ther.* **2007**, *6*, 967–978. [CrossRef] [PubMed]
81. Mimeault, M.; Johansson, S.L.; Henichart, J.P.; Depreux, P.; Batra, S.K. Cytotoxic effects induced by docetaxel, gefitinib, and cyclopamine on side population and nonside population cell fractions from human invasive prostate cancer cells. *Mol. Cancer Ther.* **2010**, *9*, 617–630. [CrossRef] [PubMed]
82. Rossi, D.J.; Weissman, I.L. *Pten*, tumorigenesis, and stem cell self-renewal. *Cell* **2006**, *125*, 229–231. [CrossRef] [PubMed]
83. Hill, R.; Wu, H. *Pten*, stem cells, and cancer stem cells. *J. Biol. Chem.* **2009**, *284*, 11755–11759. [CrossRef] [PubMed]
84. Korsten, H.; Ziel-van der Made, A.; Ma, X.; van der Kwast, T.; Trapman, J. Accumulating progenitor cells in the luminal epithelial cell layer are candidate tumor initiating cells in a *Pten* knockout mouse prostate cancer model. *PLoS ONE* **2009**, *4*, e5662. [CrossRef] [PubMed]
85. Wang, X.; Kruithof-de Julio, M.; Economides, K.D.; Walker, D.; Yu, H.; Halili, M.V.; Hu, Y.P.; Price, S.M.; Abate-Shen, C.; Shen, M.M. A luminal epithelial stem cell that is a cell of origin for prostate cancer. *Nature* **2009**, *461*, 495–500. [CrossRef] [PubMed]
86. Wang, Z.A.; Toivanen, R.; Bergren, S.K.; Chambon, P.; Shen, M.M. Luminal cells are favored as the cell of origin for prostate cancer. *Cell Rep.* **2014**, *8*, 1339–1346. [CrossRef] [PubMed]
87. Azmi, A.S.; Sarkar, F.H. Prostate cancer stem cells: Molecular characterization for targeted therapy. *Asian J. Androl.* **2012**, *14*, 659–660. [CrossRef] [PubMed]
88. Dawood, S.; Austin, L.; Cristofanilli, M. Cancer stem cells: Implications for cancer therapy. *Oncology (Williston Park)* **2014**, *28*, 1101–1107, 1110. [PubMed]
89. Sharifi, N.; Kawasaki, B.T.; Hurt, E.M.; Farrar, W.L. Stem cells in prostate cancer: Resolving the castrate-resistant conundrum and implications for hormonal therapy. *Cancer Biol. Ther.* **2006**, *5*, 901–906. [CrossRef] [PubMed]
90. Williams, K.; Motiani, K.; Giridhar, P.V.; Kasper, S. CD44 integrates signaling in normal stem cell, cancer stem cell and (pre)metastatic niches. *Exp. Biol. Med. (Maywood)* **2013**, *238*, 324–338. [CrossRef] [PubMed]
91. Yu, C.; Shiozawa, Y.; Taichman, R.S.; McCauley, L.K.; Pienta, K.; Keller, E. Prostate cancer and parasitism of the bone hematopoietic stem cell niche. *Crit. Rev. Eukaryot. Gene Expr.* **2012**, *22*, 131–148. [CrossRef] [PubMed]
92. Mateo, F.; Meca-Cortés, O.; Celià-Terrassa, T.; Fernández, Y.; Abasolo, I.; Sánchez-Cid, L.; Bermudo, R.; Sagasta, A.; Rodríguez-Carunchio, L.; Pons, M.; *et al*. SPARC mediates metastatic cooperation between CSC and non-CSC prostate cancer cell subpopulations. *Mol. Cancer* **2014**, *13*. [CrossRef] [PubMed]

93. Mathieu, J.; Zhang, Z.; Zhou, W.; Wang, A.J.; Heddleston, J.M.; Pinna, C.M.; Hubaud, A.; Stadler, B.; Choi, M.; Bar, M.; *et al*. HIF induces human embryonic stem cell markers in cancer cells. *Cancer Res.* **2011**, *71*, 4640–4652. [CrossRef] [PubMed]
94. Ravenna, L.; Principessa, L.; Verdina, A.; Salvatori, L.; Russo, M.A.; Petrangeli, E. Distinct phenotypes of human prostate cancer cells associate with different adaptation to hypoxia and pro-inflammatory gene expression. *PLoS ONE* **2014**, *9*, e96250. [CrossRef] [PubMed]
95. Dai, Y.; Bae, K.; Siemann, D.W. Impact of hypoxia on the metastatic potential of human prostate cancer cells. *Int. J. Radiat. Oncol. Biol. Phys.* **2011**, *81*, 521–528. [CrossRef] [PubMed]
96. Ma, Y.; Liang, D.; Liu, J.; Axcrona, K.; Kvalheim, G.; Stokke, T.; Nesland, J.M.; Suo, Z. Prostate cancer cell lines under hypoxia exhibit greater stem-like properties. *PLoS ONE* **2011**, *6*, e29170. [CrossRef] [PubMed]
97. Weckermann, D.; Müller, P.; Wawroschek, F.; Harzmann, R.; Riethmüller, G.; Schlimok, G. Disseminated cytokeratin positive tumor cells in the bone marrow of patients with prostate cancer: Detection and prognostic value. *J. Urol.* **2001**, *166*, 699–703. [CrossRef]
98. Rahim, F.; Hajizamani, S.; Mortaz, E.; Ahmadzadeh, A.; Shahjahani, M.; Shahrabi, S.; Saki, N. Molecular regulation of bone marrow metastasis in prostate and breast cancer. *Bone Marrow Res.* **2014**, *2014*. [CrossRef] [PubMed]
99. Luo, J.; Ok Lee, S.; Liang, L.; Huang, C.K.; Li, L.; Wen, S.; Chang, C. Infiltrating bone marrow mesenchymal stem cells increase prostate cancer stem cell population and metastatic ability via secreting cytokines to suppress androgen receptor signaling. *Oncogene* **2014**, *33*, 2768–2778. [CrossRef] [PubMed]
100. Mulholland, D.J.; Xin, L.; Morim, A.; Lawson, D.; Witte, O.; Wu, H. $Lin^{-}Sca\text{-}1^{+}CD49f^{high}$ stem/progenitors are tumor-initiating cells in the *Pten*-null prostate cancer model. *Cancer Res.* **2009**, *69*, 8555–8562. [CrossRef] [PubMed]
101. Corbeil, D.; Röper, K.; Fargeas, C.A.; Joester, A.; Huttner, W.B. Prominin: A story of cholesterol, plasma membrane protrusions and human pathology. *Traffic* **2001**, *2*, 82–91. [CrossRef] [PubMed]
102. Yin, A.H.; Miraglia, S.; Zanjani, E.D.; Almeida-Porada, G.; Ogawa, M.; Leary, A.G.; Olweus, J.; Kearney, J.; Buck, D.W. AC133, a novel marker for human hematopoietic stem and progenitor cells. *Blood* **1997**, *90*, 5002–5012. [PubMed]
103. Bauer, N.; Fonseca, A.V.; Florek, M.; Freund, D.; Jászai, J.; Bornhäuser, M.; Fargeas, C.A.; Corbeil, D. New insights into the cell biology of hematopoietic progenitors by studying prominin-1 (CD133). *Cells Tissues Organs* **2008**, *188*, 127–138. [CrossRef] [PubMed]
104. Vander Griend, D.J.; Karthaus, W.L.; Dalrymple, S.; Meeker, A.; DeMarzo, A.M.; Isaacs, J.T. The role of CD133 in normal human prostate stem cells and malignant cancer-initiating cells. *Cancer Res.* **2008**, *68*, 9703–9711. [CrossRef] [PubMed]
105. Rentala, S.; Yalavarthy, P.D.; Mangamoori, L.N. $\alpha 1$ and $\beta 1$ integrins enhance the homing and differentiation of cultured prostate cancer stem cells. *Asian J. Androl.* **2010**, *12*, 548–555. [CrossRef] [PubMed]
106. Liu, S.; Cheng, C. Alternative RNA splicing and cancer. *Wiley Interdiscip. Rev. RNA* **2013**, *4*, 547–566. [CrossRef] [PubMed]
107. Iborra, S.; Hirschfeld, M.; Jaeger, M.; Zur Hausen, A.; Braicu, I.; Sehouli, J.; Gitsch, G.; Stickeler, E. Alterations in expression pattern of splicing factors in epithelial ovarian cancer and its clinical impact. *Int. J. Gynecol. Cancer* **2013**, *23*, 990–996. [CrossRef] [PubMed]
108. Jordan, A.R.; Racine, R.R.; Hennig, M.J.; Lokeshwar, V.B. The role of CD44 in disease pathophysiology and targeted treatment. *Front. Immunol.* **2015**, *6*. [CrossRef] [PubMed]
109. Shirure, V.S.; Liu, T.; Delgadillo, L.F.; Cuckler, C.M.; Tees, D.F.; Benencia, F.; Goetz, D.J.; Burdick, M.M. CD44 variant isoforms expressed by breast cancer cells are functional E-selectin ligands under flow conditions. *Am. J. Physiol. Cell Physiol.* **2015**, *308*, C68–C78. [CrossRef] [PubMed]
110. Salmi, M.; Karikoski, M.; Elima, K.; Rantakari, P.; Jalkanen, S. CD44 binds to macrophage mannose receptor on lymphatic endothelium and supports lymphocyte migration via afferent lymphatics. *Circ. Res.* **2013**, *112*, 1577–1582. [CrossRef] [PubMed]
111. Klarmann, G.J.; Hurt, E.M.; Mathews, L.A.; Zhang, X.; Duhagon, M.A.; Mistree, T.; Thomas, S.B.; Farrar, W.L. Invasive prostate cancer cells are tumor initiating cells that have a stem cell-like genomic signature. *Clin. Exp. Metastasis* **2009**, *26*, 433–446. [CrossRef] [PubMed]

112. Rybak, A.P.; He, L.; Kapoor, A.; Cutz, J.C.; Tang, D. Characterization of sphere-propagating cells with stem-like properties from DU145 prostate cancer cells. *Biochim. Biophys. Acta* **2011**, *1813*, 683–694. [CrossRef] [PubMed]
113. Grasso, C.S.; Wu, Y.M.; Robinson, D.R.; Cao, X.; Dhanasekaran, S.M.; Khan, A.P.; Quist, M.J.; Jing, X.; Lonigro, R.J.; Brenner, J.C.; *et al*. The mutational landscape of lethal castration-resistant prostate cancer. *Nature* **2012**, *487*, 239–243. [CrossRef] [PubMed]
114. Vis, A.N.; Schröder, F.H. Key targets of hormonal treatment of prostate cancer. Part 1: The androgen receptor and steroidogenic pathways. *BJU Int.* **2009**, *104*, 438–448. [CrossRef] [PubMed]
115. Semenas, J.; Allegrucci, C.; Boorjian, S.A.; Mongan, N.P.; Persson, J.L. Overcoming drug resistance and treating advanced prostate cancer. *Curr. Drug Targets* **2012**, *13*, 1308–1323. [CrossRef] [PubMed]
116. Ni, J.; Cozzi, P.; Hao, J.; Duan, W.; Graham, P.; Kearsley, J.; Li, Y. Cancer stem cells in prostate cancer chemoresistance. *Curr. Cancer Drug Targets* **2014**, *14*, 225–240. [CrossRef] [PubMed]
117. Bishop, J.L.; Davies, A.; Ketola, K.; Zoubeidi, A. Regulation of tumor cell plasticity by the androgen receptor in prostate cancer. *Endocr. Relat. Cancer* **2015**, *22*, R165–R182. [CrossRef] [PubMed]
118. Zhang, L.; Jiao, M.; Li, L.; Wu, D.; Wu, K.; Li, X.; Zhu, G.; Dang, Q.; Wang, X.; Hsieh, J.T.; *et al*. Tumorspheres derived from prostate cancer cells possess chemoresistant and cancer stem cell properties. *J. Cancer Res. Clin. Oncol.* **2012**, *138*, 675–686. [CrossRef] [PubMed]
119. Singh, P.; Uzgare, A.; Litvinov, I.; Denmeade, S.R.; Isaacs, J.T. Combinatorial androgen receptor targeted therapy for prostate cancer. *Endocr. Relat. Cancer* **2006**, *13*, 653–666. [CrossRef] [PubMed]
120. Njar, V.C.; Brodie, A.M. Discovery and development of galeterone (TOK-001 or VN/124-1) for the treatment of all stages of prostate cancer. *J. Med. Chem.* **2015**, *58*, 2077–2087. [CrossRef] [PubMed]
121. Adeniji, A.O.; Chen, M.; Penning, T.M. AKR1C3 as a target in castrate resistant prostate cancer. *J. Steroid Biochem. Mol. Biol.* **2013**, *137*, 136–149. [CrossRef] [PubMed]
122. Shiota, M.; Yokomizo, A.; Fujimoto, N.; Naito, S. Androgen receptor cofactors in prostate cancer: Potential therapeutic targets of castration-resistant prostate cancer. *Curr. Cancer Drug Targets* **2011**, *11*, 870–881. [CrossRef] [PubMed]
123. De Leon, J.T.; Iwai, A.; Feau, C.; Garcia, Y.; Balsiger, H.A.; Storer, C.L.; Suro, R.M.; Garza, K.M.; Lee, S.; Kim, Y.S.; *et al*. Targeting the regulation of androgen receptor signaling by the heat shock protein 90 cochaperone FKBP52 in prostate cancer cells. *Proc. Natl. Acad. Sci. USA* **2011**, *108*, 11878–11883. [CrossRef] [PubMed]
124. Kregel, S.; Kiriluk, K.J.; Rosen, A.M.; Cai, Y.; Reyes, E.E.; Otto, K.B.; Tom, W.; Paner, G.P.; Szmulewitz, R.Z.; Vander Griend, D.J. Sox2 is an androgen receptor-repressed gene that promotes castration-resistant prostate cancer. *PLoS ONE* **2013**, *8*, e53701. [CrossRef] [PubMed]
125. Li, Y.; Hwang, T.H.; Oseth, L.A.; Hauge, A.; Vessella, R.L.; Schmechel, S.C.; Hirsch, B.; Beckman, K.B.; Silverstein, K.A.; Dehm, S.M. AR intragenic deletions linked to androgen receptor splice variant expression and activity in models of prostate cancer progression. *Oncogene* **2012**, *31*, 4759–4767. [CrossRef] [PubMed]
126. Zhang, X.; Morrissey, C.; Sun, S.; Ketchandji, M.; Nelson, P.S.; True, L.D.; Vakar-Lopez, F.; Vessella, R.L.; Plymate, S.R. Androgen receptor variants occur frequently in castration resistant prostate cancer metastases. *PLoS ONE* **2011**, *6*, e27970. [CrossRef] [PubMed]
127. Lu, J.; Van der Steen, T.; Tindall, D.J. Are androgen receptor variants a substitute for the full-length receptor? *Nat. Rev. Urol.* **2015**, *12*, 137–144. [CrossRef] [PubMed]
128. Lu, C.; Luo, J. Decoding the androgen receptor splice variants. *Transl. Androl. Urol.* **2013**, *2*, 178–186. [PubMed]
129. Sun, Y.; Wang, B.E.; Leong, K.G.; Yue, P.; Li, L.; Jhunjhunwala, S.; Chen, D.; Seo, K.; Modrusan, Z.; Gao, W.Q.; *et al*. Androgen deprivation causes epithelial-mesenchymal transition in the prostate: Implications for androgen-deprivation therapy. *Cancer Res.* **2012**, *72*, 527–536. [CrossRef] [PubMed]
130. Kong, D.; Sethi, S.; Li, Y.; Chen, W.; Sakr, W.A.; Heath, E.; Sarkar, F.H. Androgen receptor splice variants contribute to prostate cancer aggressiveness through induction of EMT and expression of stem cell marker genes. *Prostate* **2015**, *75*, 161–174. [CrossRef] [PubMed]
131. Hirsch, H.A.; Iliopoulos, D.; Struhl, K. Metformin inhibits the inflammatory response associated with cellular transformation and cancer stem cell growth. *Proc. Natl. Acad. Sci. USA* **2013**, *110*, 972–977. [CrossRef] [PubMed]

132. Iliopoulos, D.; Hirsch, H.A.; Wang, G.; Struhl, K. Inducible formation of breast cancer stem cells and their dynamic equilibrium with non-stem cancer cells via IL6 secretion. *Proc. Natl. Acad. Sci. USA* **2011**, *108*, 1397–1402. [CrossRef] [PubMed]
133. Iliopoulos, D.; Hirsch, H.A.; Struhl, K. Metformin decreases the dose of chemotherapy for prolonging tumor remission in mouse xenografts involving multiple cancer cell types. *Cancer Res.* **2011**, *71*, 3196–3201. [CrossRef] [PubMed]
134. Mayer, M.J.; Klotz, L.H.; Venkateswaran, V. Metformin and prostate cancer stem cells: A novel therapeutic target. *Prostate Cancer Prostatic Dis.* **2015**. [CrossRef] [PubMed]
135. Vallianou, N.G.; Evangelopoulos, A.; Kazazis, C. Metformin and cancer. *Rev. Diabet. Stud.* **2013**, *10*, 228–235. [CrossRef] [PubMed]
136. Bilen, M.A.; Lin, S.H.; Tang, D.G.; Parikh, K.; Lee, M.H.; Yeung, S.C.; Tu, S.M. Maintenance therapy containing Metformin and/or Zyflamend for advanced prostate cancer: A case series. *Case Rep. Oncol. Med.* **2015**. [CrossRef] [PubMed]
137. Li, Y.; Wicha, M.S.; Schwartz, S.J.; Sun, D. Implications of cancer stem cell theory for cancer chemoprevention by natural dietary compounds. *J. Nutr. Biochem.* **2011**, *22*, 799–806. [CrossRef] [PubMed]
138. Scarpa, E.S.; Ninfali, P. Phytochemicals as innovative therapeutic tools against cancer stem cells. *Int. J. Mol. Sci.* **2015**, *16*, 15727–15742. [CrossRef] [PubMed]
139. Teiten, M.H.; Gaigneaux, A.; Chateauvieux, S.; Billing, A.M.; Planchon, S.; Fack, F.; Renaut, J.; Mack, F.; Muller, C.P.; Dicato, M.; *et al*. Identification of differentially expressed proteins in curcumin-treated prostate cancer cell lines. *OMICS* **2012**, *16*, 289–300. [CrossRef] [PubMed]
140. Botchkina, G.I.; Zuniga, E.S.; Rowehl, R.H.; Park, R.; Bhalla, R.; Bialkowska, A.B.; Johnson, F.; Golub, L.M.; Zhang, Y.; Ojima, I.; *et al*. Prostate cancer stem cell-targeted efficacy of a new-generation taxoid, SBT-1214 and novel polyenolic zinc-binding curcuminoid, CMC2.24. *PLoS ONE* **2013**, *8*, e69884. [CrossRef] [PubMed]



© 2015 by the authors; licensee MDPI, Basel, Switzerland. This article is an open access article distributed under the terms and conditions of the Creative Commons by Attribution (CC-BY) license (http://creativecommons.org/licenses/by/4.0/).

International Journal of
Molecular Sciences

MDPI

Article

High SPARC Expression Starting from Dysplasia, Associated with Breast Carcinoma, Is Predictive for Bone Metastasis without Enhancement of Plasma Levels

Paola Maroni [1], Paola Bendinelli [2], Daniele Morelli [3], Lorenzo Drago [1,2], Alessandro Luzzati [1], Giuseppe Perrucchini [1], Chiara Bonini [3], Emanuela Matteucci [2] and Maria Alfonsina Desiderio [2,*]

Received: 24 June 2015; Accepted: 3 August 2015; Published: 26 November 2015
Academic Editor: William Chi-shing Cho

1 Istituto Ortopedico Galeazzi, Scientific Institute for Research, Hospitalization and Helth Care (IRCCS), 20161 Milano, Italy; paola.maroni@grupposandonato.it (P.M.); lorenzo.drago@unimi.it (L.D.); sandroluzzati@tiscali.it (A.L.); pergiudoc@yahoo.com (G.P.)

2 Dipartimento di Scienze Biomediche per la Salute, Molecular Pathology Laboratory, Università degli Studi di Milano, 20133 Milano, Italy; paola.bendinelli@unimi.it (P.B.); emanuela.matteucci@unimi.it (E.M.)

3 Department of Pathology and Laboratory Medicine, Fondazione IRCCS Istituto Nazionale dei Tumori, 20133 Milano, Italy; daniele.morelli@istitutotumori.mi.it (D.M.); chiara.bonini@istitutotumori.mi.it (C.B.)

* Correspondence: a.desiderio@unimi.it; Tel.: +39-02-503-15334; Fax: +39-02-503-15338

Abstract: In order to become established in the skeleton, metastatic cells disseminating from the breast carcinoma need to acquire organ-specific traits. There are no effective predictors for who will develop bone metastasis to guide long-term predictive therapy. Our purpose was to individuate events critical for bone colonization to make a molecular classification of breast carcinoma useful for bone-metastasis outcome. In dysplasia adjacent to carcinoma and in pair-matched specimens of bone metastasis we examined SPARC expression and localization as well as Endothelin 1/ET_AR signals by immunohistochemistry, and the evaluation of plasma levels of SPARC by ELISA was also performed. In patients with breast carcinoma metastasizing to bone, SPARC and Endothelin 1/ET_AR axis were highly expressed from dysplasia until bone metastasis, but the SPARC plasma level was as low as that of normal women, in contrast to patients that never develop bone metastasis, suggesting that circulating SPARC was counter adhesive. Altogether, the early identification of SPARC/Endothelin 1/ET_AR in dysplastic lesions would be important to devise therapies preventing metastasis engraftment, since often carcinoma cells spread to distant organs at the time or even before patients present with cancer.

Keywords: bone metastasis; dysplasia; SPARC; Endothelin 1; ET_AR; breast carcinoma

1. Introduction

Secreted protein acidic and rich in cysteine (SPARC) belongs to the matricellular group of proteins, that are transiently secreted to the Extracellular matrix (ECM) without becoming part of the ECM mesh. Acting at the interface between the cell surface and the ECM, matricellular proteins regulate cellular processes such as adhesion, migration, proliferation and differentiation [1–3]. SPARC, also known as basement membrane-40 (BM-40) tumour protein or osteonectin, is a 32–35 kDa multifunctional ECM protein, with affinity for collagens and calcium ions; a high molecular weight form in the bone (43 kDa) is due to glycosylation [4].

The role of SPARC in tumorigenesis is controversial, and some investigations report a positive relationship between elevated levels of SPARC and more aggressive cancers, with poorer clinical outcome, even if this largely depends on the tumour type [5,6]. While normal mammary tissue has undetectable or lightly detectable amounts of SPARC, and benign breast lesions are weakly positive, 75% of both *in situ* and invasive breast carcinomas are strongly positive for SPARC in stromal cells (CD-34-negative, α-SMA-positive) [7,8]. Moreover, SPARC is associated with clinicopathological parameters such as histological differentiation, tumour size, depth of invasion, lymph node metastasis, distant metastasis, and Tumor-Node-Metastasis (TNM) stage [6].

Metastatic occurrence in the skeleton, one of the preferential secondary sites, is the leading cause of death for breast carcinoma, and bone metastases develop also ten years after surgical removal of the primary tumour, since osteotropic malignant cells may have a long period of quiescence before secondary outgrowth [9]. Complications of bone metastases include pain, increased risk of fracture, hypercalcemia and decreased levels of blood cell count. Having reached the bone, malignant cells disrupt the remodelling process that normally occurs. Osteoclast number increases, stimulating bone resorption and the release of factors important for metastasis outgrowth, and osteoblast number might decrease in case of osteolytic bone metastasis while increasing in the osteoblastic or mixed type [3,9].

Improved knowledge of the biochemical processes underlying bone metastasis, has prompted investigation whether skeletal events in patients may correlate with levels of serum or urine markers of bone turnover, thus facilitating early detection and screening for such events. The prevention and the development of therapeutic strategies against bone metastasis implicate the understanding of the carcinoma cell preference to metastasize in the bone tissue. The bone microenvironment may provide growth stimulating factors or other proteins that induce preferential adhesion and proliferation. Based on transgenic models of breast cancer, SPARC expression could be used as a potential prognostic biomarker of tumour severity and/or aggressiveness [10].

As already mentioned, the survival rate in the case of patients with bone metastasis from breast carcinoma is very low. The understanding of molecular mechanisms of organotropism would help the prevention of metastasis, and the establishment of a valid therapy in order to improve the patient's quality of life and to increase survival. Until now there are only few studies regarding breast carcinoma that tried to disclose the roles of SPARC in bone metastasis.

We have demonstrated a favouring function of endogenous SPARC for bone metastasis from breast cancer using a xenograft model, prepared with clone 1833 derived from MDA-MB231 human breast carcinoma cells. SPARC was induced by Endothelin 1 in 1833 cells with bone tropism, but not in parental cells, and the expression of the two biological stimuli is orchestrated by DNA methyltransferases. Of note, SPARC and Endothelin 1 are expressed in the bone marrow of the bone metastasis xenograft model [11].

The bone marrow is a common homing organ, and reservoir for disseminated tumour cells from breast cancer. Although only a small fraction of patients present overt bone marrow metastasis, 70% of advanced breast cancer patients develop metastasis in the bone [12]. Bone marrow is a source of mesenchymal stem cells that can give rise to cells of mesodermal lineages, such as osteocytes [13]. These mesenchymal stem cells play an important pro-tumorigenic role in the microenvironment of bone metastasis [14], and are also known as bone marrow stromal fibroblasts expressing SPARC/osteonectin [15], that home to sites of tumorigenesis and integrate in primary tumour stroma [13].

Recent research is devoted to understand critical events in breast cancer progression to make a molecular classification. Until now the breast carcinomas are classified as Basal and Luminal, and the latter in A and B principally on Ki67 value [16]. Ki67 is a molecular marker expressed in all cell-cycle phases except G0; the optimal Ki67 level discriminating Luminal A from B is 13.2% [17].

Our hypothesis was that SPARC might be a key molecular signal released from primary breast carcinoma and/or locally produced in bone metastasis to influence the bone niche formation in the

secondary site. It has been proposed that bone colonization is initiated in a microenvironment niche exhibiting active osteogenesis, and heterotypic adherens junctions take place between metastatic and osteogenic cells [18]. In this context, the present paper deals with the evaluation of SPARC expression during ductal breast carcinoma progression, from the dysplastic lesion until bone metastasis establishment: SPARC distribution in neoplastic cells *versus* stroma, and the plasma levels were examined. Concomitantly, the expression of Endothelin 1 and of its receptor ET_AR were assayed to clarify whether the Endothelin 1/ET_AR pattern completed SPARC findings as predictive value for bone metastasis. Activation of autocrine and paracrine signalling by Endothelin 1 binding to its receptors elicits pleiotropic effects on tumour cells and on the host microenvironment for immunomodulation and intravasation [19]. Also, Endothelin 1 and ET_AR are expressed in breast carcinoma metastasizing to bone [20], even if the predictive value of this axis has not been clarified until now.

The aim of the present paper was to individuate molecular events to extend the classification of invasive ductal carcinoma, adding predictive markers for the outcome of breast cancer patients related to the development of bone metastasis.

The results indicate that the biological function of SPARC depended on the phase of breast cancer progression, the tissue compartment in which it was expressed, and its body distribution, with plasma release of SPARC being opposite to metastasis engraftment. SPARC was highly expressed in the stroma of bone metastasis, suggesting a positive effect on the outgrowth also due to a cross talk with metastatic cells expressing SPARC. The association of SPARC with Endothelin 1 and ET_AR—starting from dysplasia until the end of the metastatic process—appears to be of fundamental importance as a predictive index of bone metastasis formation.

2. Results

2.1. SPARC Expression, Distribution and Intracellular Localization during Breast Carcinoma Progression

To clarify whether SPARC had a differential involvement in the various phases of breast carcinoma progression, we evaluated SPARC expression in dysplastic lesions, primary ductal carcinoma and bone metastasis using human specimens pair-matched (n = 5). We took into consideration the distribution in tissue compartments, the intracellular localization and the cell types expressing SPARC.

Representative images for Patients 1, 2 and 3 are shown in Figures 1–3. The Patients 1 and 3 had invasive ductal carcinoma, and Patient 2 had an invasive ductal/lobular (mixed) carcinoma: all the three Patients developed metastasis within 7–16 years. As shown in Supplementary Table S1, the percentage of positive cells for SPARC signal was estimated by analyzing 100 cells per field in 10 fields, and the immunoreactivity score was indicated [21]. We examined the localization and degree of SPARC expression in cytosol and nuclei of carcinoma and metastatic cells, and in primary tumour and metastasis stroma compartments, *i.e.*, ECM and supportive cells, and the semiquantitative evaluation was made and used for the histograms of Figures 1–3.

All the three Patients showed extraordinary similarities in SPARC expression: a strong immunostaining occurred in epithelial-dysplastic cells and in breast carcinoma cells. In the latter, SPARC almost equally localized in the cytosol and the nuclei. As regards primary tumour stroma, the ECM had lower levels of the matricellular protein than the supportive cells; this was particularly evident in Patient 1. Thus, in primary carcinoma SPARC distributed principally in tumour cells, compared to the stroma. For Patient 2 (Figure 2), the expression of SPARC occurred both in infiltrated-invasive carcinoma (left panel) and in the infiltrating-lobular component (right panel).

In bone metastases of Patients 1, 2 and 3, SPARC was highly expressed in stromal cells, while being variously expressed in metastatic cells within the cytosol. For Patient 3, we showed SPARC immunostaining for bone metastases established in the vertebra (C6) and in the mandible.

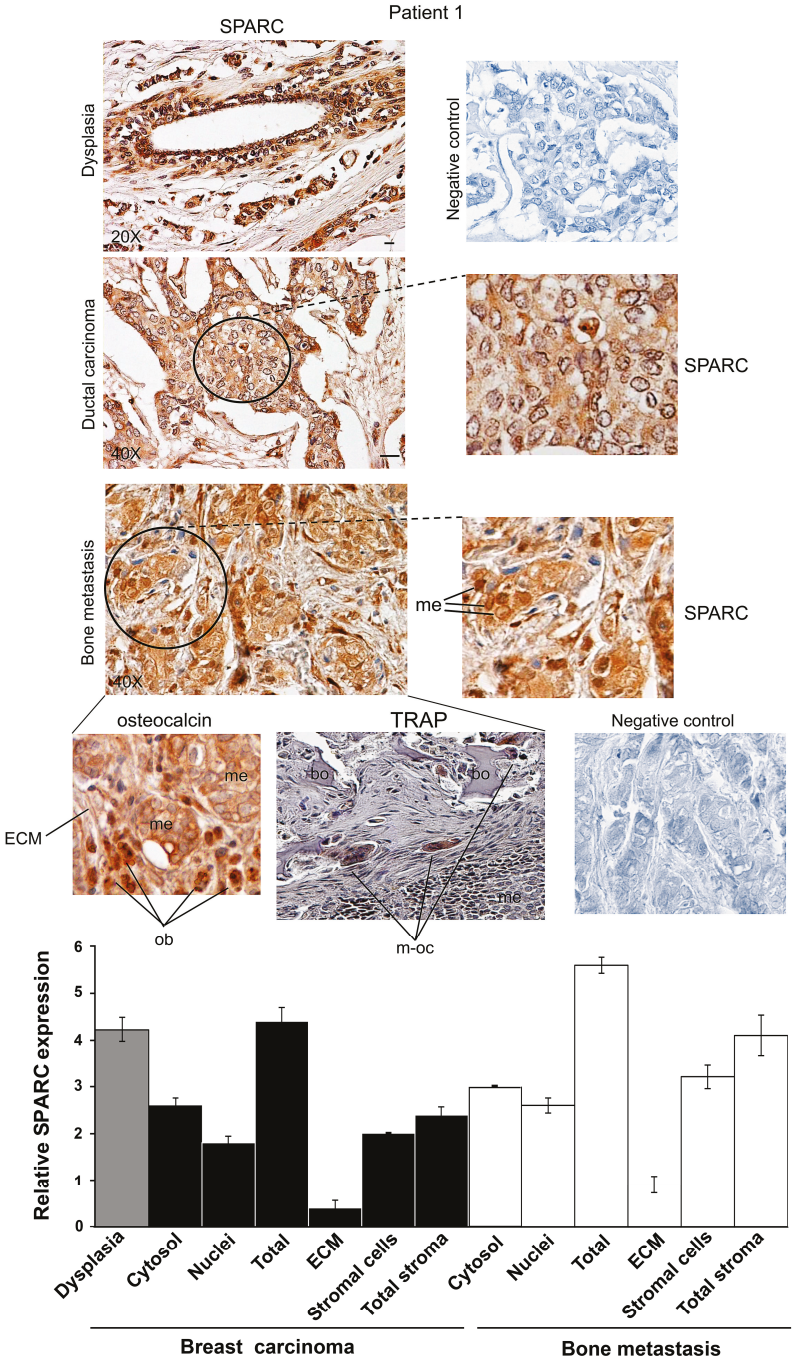

Figure 1. SPARC expression during ductal breast carcinoma progression from dysplasia until bone metastasis for Patient 1. Representative images of immunohistochemical staining for SPARC and osteocalcin were shown. In bone metastasis, TRAP assay was also performed. Magnifications of details are shown. Bar = 100 μm. ECM, Extracellular matrix; me, metastatic cells; bo, bone; ob, osteoblasts; m-oc, mature osteoclasts. Negative controls were assayed without the specific antibody. The histograms, showing the relative values for SPARC expression, were prepared by using the score values reported in Supplementary Table S1. The data are the means ± S.E. of experiments performed in triplicate.

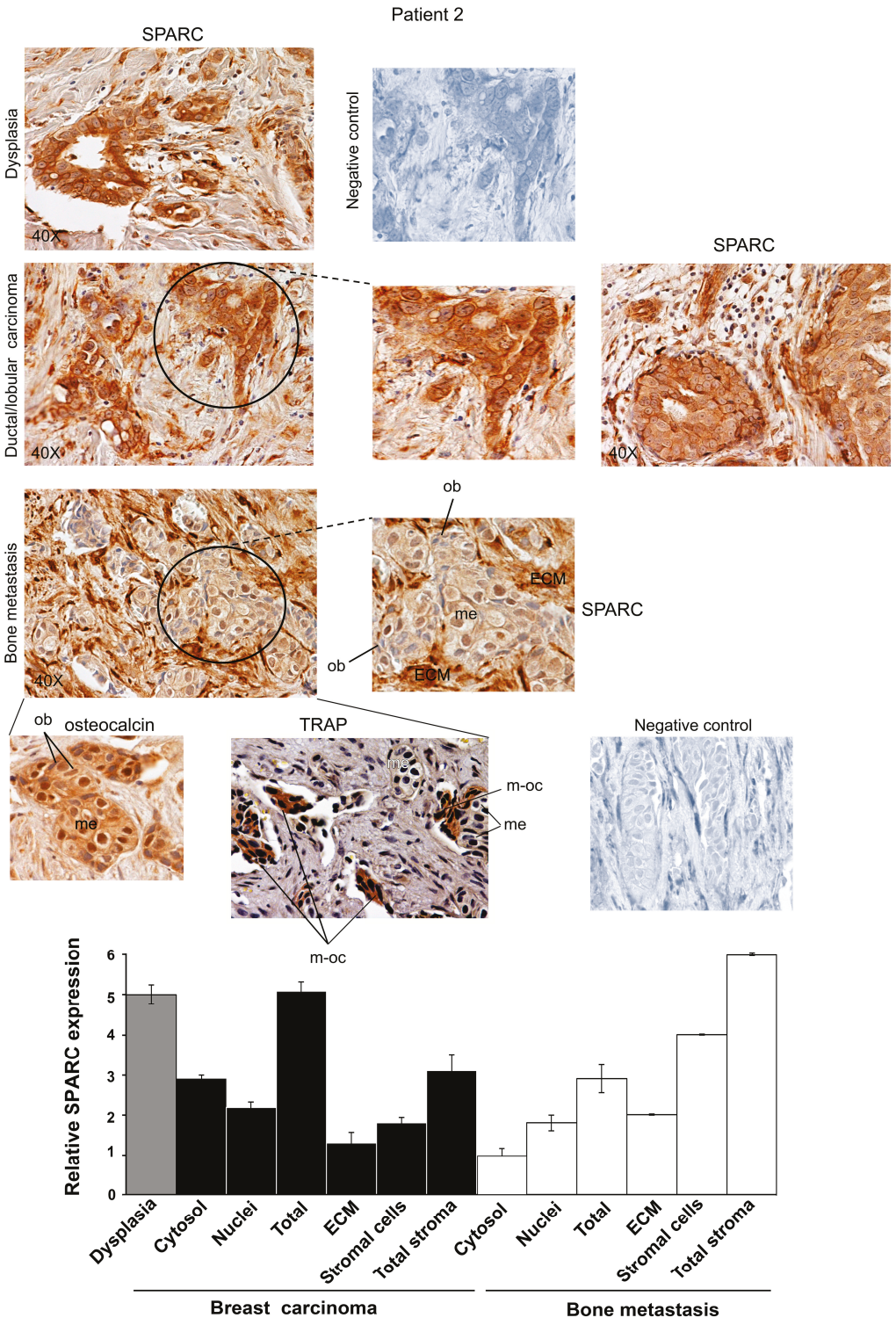

Figure 2. SPARC expression during ductal/lobular breast carcinoma progression from dysplasia until bone metastasis for Patient 2. Representative images of immunohistochemical staining for SPARC and osteocalcin were shown. In bone metastasis, TRAP assay was also performed. Magnifications of details are shown. ECM, Extracellular matrix; me, metastatic cells; ob, osteoblasts; m-oc, mature osteoclasts. Negative controls were assayed without the specific antibody. The histograms, showing the relative values for SPARC expression, were prepared by using the score values reported in Supplementary Table S1. The data are the means ± S.E. of experiments performed in triplicate.

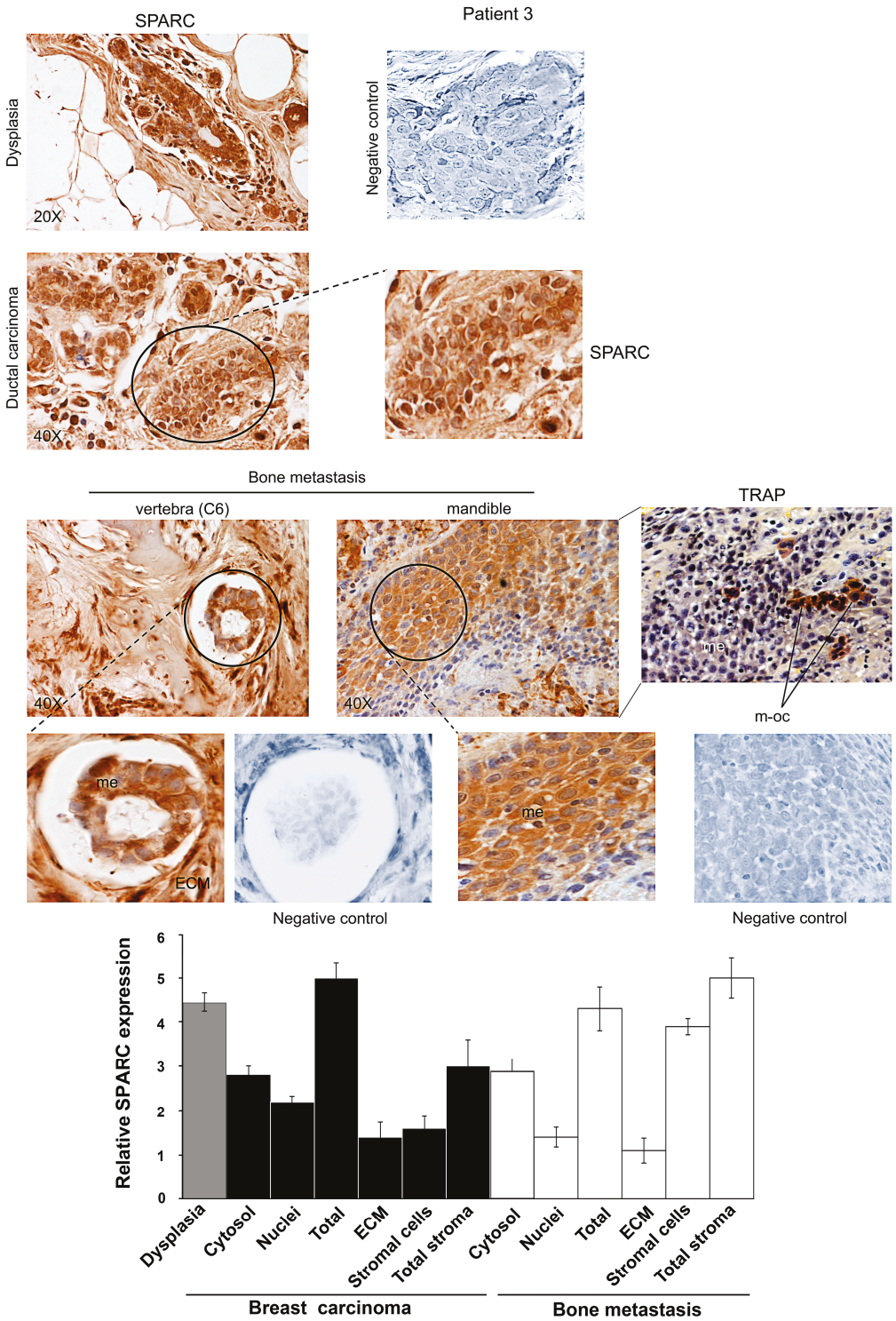

Figure 3. SPARC expression during ductal breast carcinoma progression from dysplasia until bone metastasis for Patient 3. Representative images of immunohistochemical staining for SPARC were shown. In bone metastasis established in the mandible, TRAP assay was also performed. Magnifications of details are shown. ECM, Extracellular matrix; me, metastatic cells; m-oc, mature osteoclasts. Negative controls were assayed without the specific antibody. The histograms, showing the relative values for SPARC expression, were prepared by using the score values reported in Supplementary Table S1. The data are the means ± S.E. of experiments performed in triplicate.

In addition, cells morphologically different from metastatic cells were also positive for SPARC in all the samples of bone metastasis tissues for Patients 1, 2 and 3; SPARC negative cells (blue) were evident after SPARC immunostaining (Figures 1–3). We tried to identify these SPARC negative cells by immunohistochemistry analysis of osteocalcin, an osteoblast marker [22], and by tartrate-resistant acid phosphatase (TRAP), index of osteoclasts [23]. As shown in Figures 1 and 2 the bone metastasis contained osteocalcin-positive cells, *i.e.*, osteoblasts (index of osteogenesis). In addition, osteocalcin was expressed by metastatic cells (index of osteomimicry). Concomitantly, in serial sections we showed mature osteoclasts (m-oc) on the basis of the number of nuclei (more than three) and TRAP activity: m-oc were shown in the areas of osteolysis, with presence of bone (bo) residues (Figure 1 and Supplementary Figure S1). In Figure 3, the invasive leading edge of bone metastasis also contained TRAP-positive mature osteoclasts, which seemed to correspond in part to the cells that remained blue (unstained) after SPARC immunostaining.

The statistical evaluation of the mean values for the Patients 1–3 has been reported in Figure 4A. The parameters under investigation for SPARC expression showed remarkable differences, indicating that SPARC might have different functions in the various phases of breast carcinoma progression with metastasis outcome.

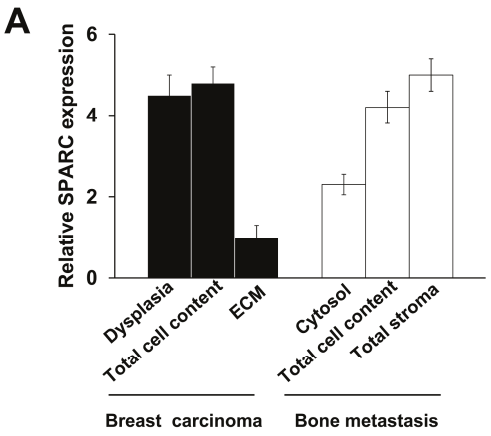

B

	Ki67	ER	PR	Her2/neu	subtype
Patient 1	32%	90%	30%	(-)	Luminal B
Patient 2	3%	80%	70%	70%	Luminal A
Patient 3	47%	70%	15%	(-)	Luminal B

(-) negative

Figure 4. SPARC values and Classification of Patients 1, 2 and 3. (**A**) For Patients 1–3, the mean values for SPARC (n = 3) were shown, and the statistical evaluation with the analysis of variance (one way ANOVA) has been performed. F = 9.92; $p < 0.001$; and (**B**) The Classification for Patients 1, 2 and 3 has been reported. The Patient 2 had a ductal/lobular carcinoma: The ductal and the lobular components were Her2/neu positive and negative, respectively.

The three Patients positively correlated for SPARC signal in dysplasia, total cell content and stroma of metastasis. The SPARC signal in the ECM of carcinoma tissue had the lowest value in respect to that of all the other parameters.

Figure 4B shows breast carcinoma subtypes for Patients 1, 2 and 3, based on Ades *et al.* [17]. Patients 1 and 3 were classified as Luminal B, without Her2/neu, with lower expression of progesterone receptor (PR) and a higher value of Ki67 (proliferation gene) in respect to Patient 2 (ductal component). Patient 2 was characterized as having the highest combined expression of

oestrogen receptor (ER) plus PR, with positive expression of Her2/neu in the ductal component of the breast carcinoma, that was classified as Luminal A.

Altogether, this classical molecular classification did not seem suitable enough to predict the formation of bone metastasis. The analysed patients without bone metastases, belonged to Luminal A more than B subtype (Supplementary Table S2).

Therefore, further studies were undertaken to make a molecular classification that considered molecular events critical for invasive breast carcinoma to develop bone metastasis.

2.2. SPARC as Predictive Marker of Bone Metastasis: Association with Plasma Levels of SPARC and Tissue Endothelin 1/ET_AR

We evaluated plasma levels of SPARC (Figure 5A), and tissue Endothelin 1/ET_AR (Figures 6 and 7), to determine whether there was a correlation with bone metastasis formation.

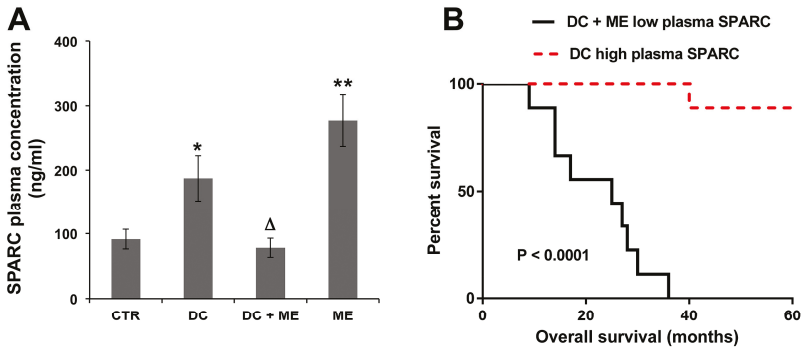

C

Patients (% of SPARC positivity)	Degree of immunoreactivity	Plasma	Bone metastasis
70	+++ Dysplasia +++ Breast Carcinoma	++	yes
25	- Dysplasia +/++ Breast Carcinoma	++++	no
5	- Dysplasia - Breast Carcinoma	+	no

Figure 5. Plasma levels of SPARC and predictivity of bone metastasis. (**A**) ELISA assay was performed using the plasma samples from control (CTR), ductal carcinoma-bearing patients (DC), with or without bone metastasis (ME). The data are the means ± S.E. of nine samples, assayed in triplicate; * $p < 0.05$ and ** $p < 0.005$ versus CTR; Δ $p < 0.05$ versus DC; (**B**) Survival curve on Kaplan-Meier plots of the data from breast carcinoma patients with or without bone metastasis development; and (**C**) The Table shows the percentage of positivity for SPARC at the degree indicated (second column); the plasma value score was also shown (third column), and the relationship with bone metastasis formation is indicated (fourth column). − (negative signal); + (weak signal); ++ (moderate signal); +++ (strong signal); ++++ (very strong signal).

As shown in Figure 5A, SPARC plasma levels in ductal carcinoma (DC) and in bone metastasis (ME)-bearing patients doubled and tripled, respectively, compared to that of normal women (CTR). Notably, in the breast carcinoma-bearing patients who developed metastasis (DC + ME), the plasma level was similar to that of CTR; the blood was collected at the moment of removal of the primary carcinoma from patients not receiving therapy. In Figure 5B, we show the Overall survival curve referred to low and high SPARC expression in the blood of patients with primary breast carcinoma, developing or not bone metastasis, respectively. According to the available information at the time,

the patients without bone metastasis survived free of diseases for 60 months, except for one patient who died at 40 months after the surgery, due to ovary/Fallopian tubes carcinoma disseminated to the peritoneum. Bone metastasis bearing-patients, however, died within 36 months after surgical removal of the primary carcinoma.

In Figure 5C, we considered the data obtained until now. A high degree of immunoreactivity for SPARC, as shown in the Table, was present in 70% of breast carcinoma patients examined (3/5), and pair-matched for developing bone metastasis; the plasma level was not elevated.

Certainly, the highest plasma levels of SPARC were those of the patients who did not develop metastasis, and who showed variable positivity for SPARC (from + to ++, n = 3) in the breast carcinoma tissue (see representative images of fields for Patient 5, Figure 6). The lowest plasma levels of SPARC were those of SPARC negative primary tumours (n = 3), that showed 5% of cases with faint SPARC staining (representative images for Patient 4, Figure 6).

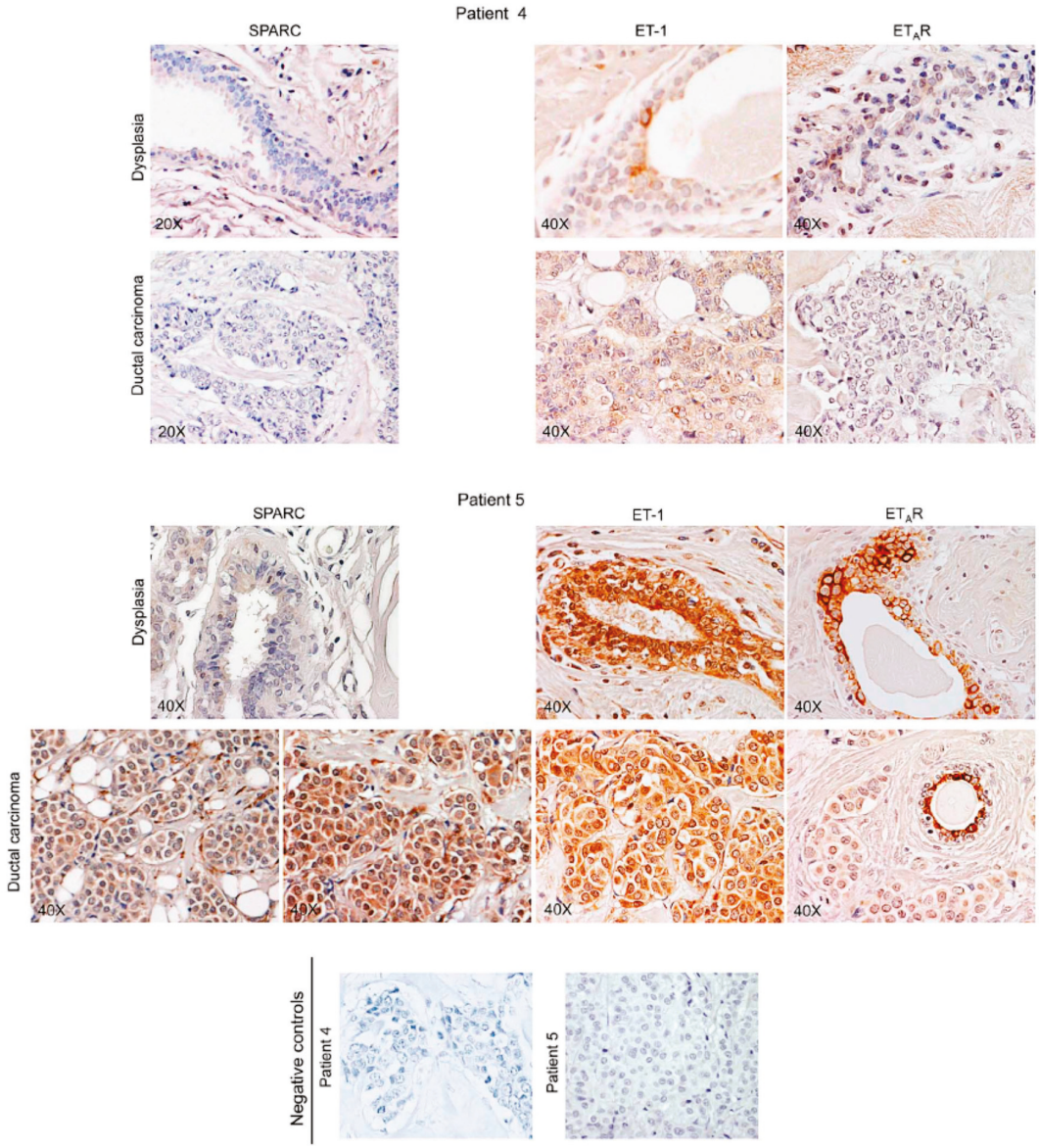

Figure 6. SPARC and Endothelin 1 (ET-1)/ET$_A$R in tissue specimens from patients without bone metastasis development. For Patients 4 and 5, representative images of immunohistochemical staining for SPARC and ET-1/ET$_A$R in dysplastic lesions, associated with ductal breast carcinoma, are shown. Negative controls were assayed without the specific antibody.

Figures 6 and 7 also report Endothelin 1 and ET_AR expression. For dysplasia and breast carcinoma of Patients 5 and 4, Endothelin 1/ET_AR axis showed intermediate (+/++) and negative values, respectively, while Patient 1 showed strong signals (+++/++++) in specimens of dysplastic tissue and bone metastasis, with breast carcinoma staining positively (++). In particular, ET_AR distribution at plasma membrane level characterizes the dysplastic-epithelial and bone metastatic cells [20].

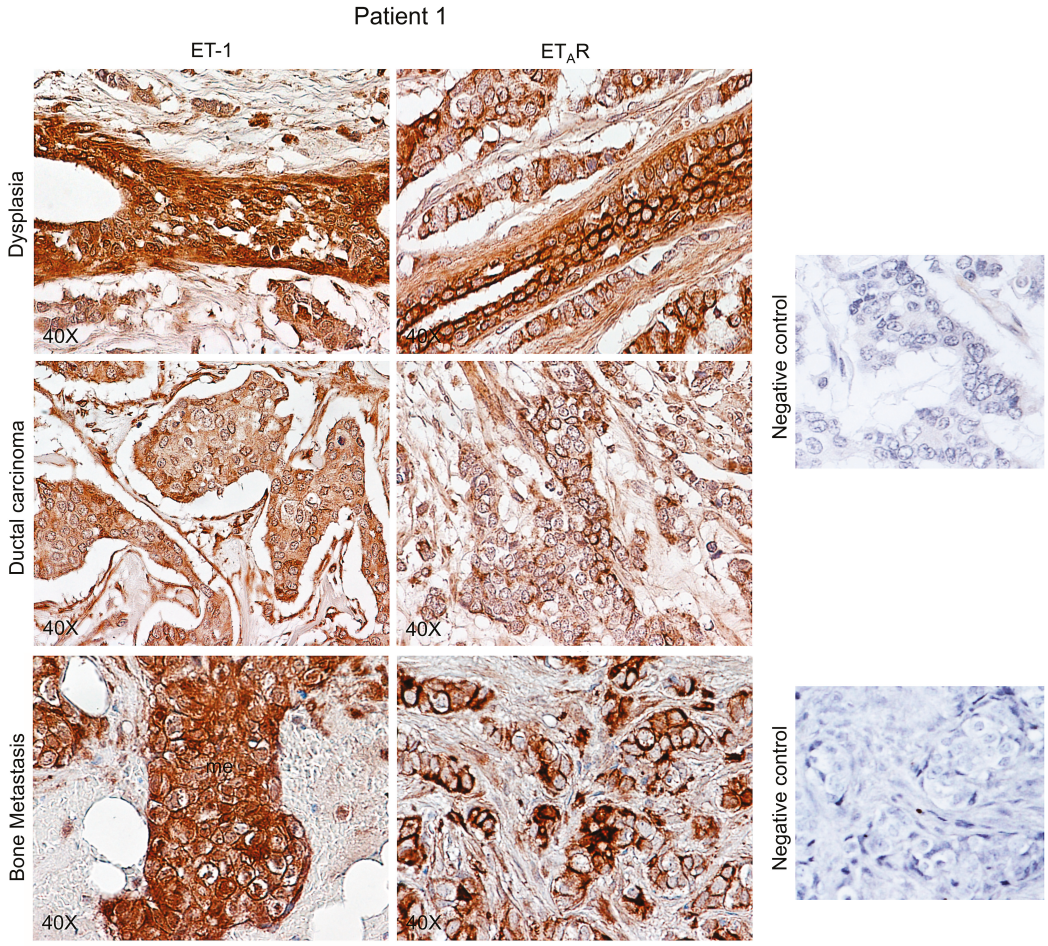

Dysplasia

SPARC	Endothelin 1	ET_AR	Bone metastasis
+ + +	+ + +	+ + +	yes
-	-	-	no
-	+ +	+	no

Figure 7. Endothelin 1 (ET-1)/ET_AR in tissue specimens from Patient 1 during breast carcinoma progression until bone metastasis. Representative images of immunohistochemical staining for ET-1 and ET_AR in dysplastic lesions, associated with ductal breast carcinoma, and in bone metastasis are shown. Negative controls were assayed without the specific antibody. The Table reports the indicative predictability of SPARC combined with ET-1/ET_AR for metastasis formation in the skeleton. − (negative signal); + (weak signal); ++ (moderate signal); +++ (strong signal).

In conclusion, without associated strong SPARC expression, the Endothelin 1/ET_AR positivity in dysplastic lesions did not appear to be sufficient as predictive index of bone metastasis (Figure 7, Table). All the five pair-matched patients had SPARC/Endothelin 1/ET_AR (+++) in dysplastic lesions; as shown in Patients 1–3, the strong signal of SPARC remained persistently elevated in breast carcinoma cells as well as in bone metastasis cells and stroma, while the other two pair-matched patients had a lower staining of SPARC (+) in the carcinoma cells (data not shown).

3. Discussion

Here we show that elucidating the molecular basis of ductal breast carcinoma progression might lead to effective ways to predict the bone colonization of metastasis, and to make a valid molecular classification important to devise a preventive therapy.

The ectopic secretion of proteins, known to be microenvironmental stimuli like SPARC and Endothelin 1, appeared to confer osteogenic traits to disseminated breast carcinoma cells, important for the attachment to bone matrix [7,22]. We demonstrated for the first time in bone metastasis of humans that at the site of colonization, SPARC was expressed by metastatic cells as well as by osteoblasts, which were identified on the basis of osteocalcin immunostaining. We suggest that osteoblasts were involved not only in osteogenesis, but also in the recruitment of osteoclasts [22], maintaining an elevated bone turnover with a consequent release of Endothelin 1 in the microenvironment. Thus, the induction of SPARC by Endothelin 1 was likely to occur also in metastatic cells of patients, as reported before for 1833 clone [11]. In addition, SPARC is a marker of differentiation of osteogenic bone cells [22]. Altogether, the events reported here might be critical for microscopic bone metastasis to progress into clinically significant lesions.

Our data are consistent with those obtained by Wang *et al.* with an experimental model [18], in which he demonstrates that bone colonization is initiated by a microenvironment niche exhibiting active osteogenesis. We hypothesize that bone niche evolution requires SPARC. Since human bone metastasis from ductal breast carcinoma shows E-cadherin expression [24], an heterotypic interaction with osteogenic cells would occur, as reported in a human/mouse experimental system, giving a proliferative advantage [18]. We cannot exclude that the observed high SPARC signal in supportive cells of bone metastasis conferred a proliferative advantage to metastatic cells [25], and that the latter producing SPARC competed with stem cell fibroblasts for the niche becoming hospitable [26].

The strength of our study in patients is the analysis of pair-matched invasive ductal breast carcinoma from the early preneoplastic stages until bone metastasis formation. The function of SPARC seems to depend on the microenvironment, in terms of local composition of matrix molecules, cytokines and protease profile, and on whether it is expressed by the malignant cells themselves or by neighboring stromal cells [3].

Our principal finding useful for a molecular classification was the very high expression of SPARC (70% incidence, as bone metastasis) in dysplastic epithelium, associated with ductal breast carcinoma, and in bone metastatic cells and stroma (ECM and supportive cells). Since SPARC is able to organize collagen and other ECM proteins, we suggest that in patients it would be involved in creating a fibrotic environment favorable for colonization, similar to lysyl oxidase (LOX) [27,28]. However, for bone metastasis predictive value, the association of SPARC signal with those of Endothelin 1/ET_AR seemed essential, starting from their presence in the dysplastic lesions. It is known that cancer cells may disseminate very early, even before patients present with cancer, and might form micrometastasis in a permissive environment of the secondary site such as that of bone. Our hypothesis is that a local production of SPARC in the hospitable bone, possibly regulated by Endothelin 1/ET_AR axis, would be important for bone niche formation and evolution. Notably, the plasma level of SPARC was not elevated in breast cancer patients with bone metastasis outcome.

Moreover, stem cell fibroblasts seem to migrate to primary carcinoma [13], and we suggest that they were responsible for the release of SPARC to tumor cells. In human specimens, breast carcinoma cells and stroma presented SPARC signals, in agreement with the literature [29]. A recycling of

SPARC would occur in the primary breast carcinoma, and a role of exosomes cannot be excluded since these microvescicles can modulate nearby or distant target cells by direct contact of their surface molecules, to activate intracellular pathways. Alternatively, on internalization by membrane fusion or endocytosis, exosomes deliver their protein content [30]. Studies are in progress to evaluate this mechanism, since the study with MDA-MB231 cells indicates that *in vitro* breast carcinoma scarcely produces the matricellular protein SPARC [11]. Consistently, primary breast carcinoma that did not give bone metastasis abundantly release SPARC in the plasma, likely preventing, therefore, the engraftment of disseminated cells in the secondary bone site. In primary tumor, SPARC was likely to exert counter-adhesive roles important for the intermediate state of adhesiveness, and responsible for motility and invasiveness. Except for one, all of these breast carcinoma bearing patients are still alive 60 months after surgery. Circulating tumor cells shed from breast carcinoma, are a heterogeneous population including EpCAM-positive cells and cells with mesenchymal phenotype (EMT), which are studied for the analysis of the therapeutic response to different chemotherapeutic regimens [31].

In the future personalized medicine, the molecular classification based on SPARC associated with Endothelin 1/ET_AR would be of great importance to devise therapies against bone metastasis with nanoparticles, that target drugs with a SPARC-dependent endosomal mechanism [32].

4. Experimental Section

4.1. Patient Recruitment

We studied by immunohistochemistry 11 patients bearing invasive ductal breast carcinoma (Patient 2 had a ductal/lobular form): 5 were pair-matched with bone metastasis; 6 did not have bone metastasis. ELISA assay in the plasma of the following groups of women was performed (each with n = 9): normal women (control, CTR), ductal carcinoma without bone metastasis (DC), ductal carcinoma with bone metastasis (DC + ME), bone metastasis (ME). DC were examined for clinical classification (Supplementary Table S2).

4.2. Immunohistochemistry Assay

We analysed 5 serial sections prepared from human specimens of primary-invasive ductal or mixed breast carcinoma and associated dysplastic lesions, and from pair matched bone metastasis (collected during surgical interventions at Istituto Ortopedico Galeazzi, Milano, Italy). All patients provided informed consent, in accordance with the Declaration of Helsinki. The tissue sections were fixed and decalcified before immunostaining [24]. The following antibodies were used: anti-SPARC (1:50, H-90 from Santa Cruz Biotechnology, Santa Cruz, CA, USA), anti-Endothelin 1 (1:50, H-38 from Santa Cruz Biotechnology), anti-ET_AR (4 μg/mL, from Abcam, Cambridge, UK), anti-osteocalcin (5 μg/mL, from Abcam). Negative controls were assayed without the specific antibodies. We made a semiquantitative evaluation of the sample after immunostaining, and the scores were: no staining = 0, very weak staining = 1, weak staining = 2, moderate staining = 3, strong staining = 4, very strong staining = 5.

4.3. Tartrate-Resistant Acid Phosphatase (TRAP) Staining

The detection of osteoclasts was performed on TRAP-stained paraffin-embedded sections with the use of a commercial kit (Sigma-Aldrich, St. Louis, MO, USA), following manufacturer's instructions. After incubation for 1 h at 37 °C, the sections were counterstained with hematoxylin, and the osteoclasts were monitored under a microscope (Eclipse 80i; Nikon, Milano, Italy).

4.4. ELISA Assay of Plasma SPARC

The plasma levels of SPARC were evaluated on samples prepared at the moment of the removal of the breast carcinoma (Istituto Nazionale dei Tumori, Milano, Italy), and on plasma samples from bone metastasis bearing-patients before surgical removal of the metastatic tissue (Istituto Ortopedico

Galeazzi, that also furnished plasma samples of control healthy women). We used the commercial kit Quantikine, human SPARC (R&D System, Abingdon, UK). The O.D. values were measured with Glomax Discover System (Promega, Madison, WI, USA), using the standard curve of the kit.

4.5. Statistical Analysis

The semiquantitative data of SPARC expression in tissue samples of breast carcinoma and associated dysplasia, and of bone metastasis were evaluated by the analysis of variance of the means, with $p < 0.05$ considered significant. The survival data were analyzed by Kaplan-Meier method, and the log-Rank (Mantel-Cox) test. $p < 0.05$ was considered significant.

Supplementary Materials: Supplementary materials can be found at http://www.mdpi.com/1422-0067/16/12/25997/s1.

Acknowledgments: This work was supported by the following Grants: UNIMI, Piano di Sostegno alla Ricerca 2015, Linea 2, Azione B, and Ministero della Salute, Ricerca Corrente (L4069, L4071 and L4077) Italy. We thank Dr. Alessandro Fulgenzi for the graphical display of the file.

Author Contributions: Maria Alfonsina Desiderio and Paola Maroni, conceived and designed the experiments; Paola Maroni, prepared the tissue specimens and performed the immunohistochemistry; Paola Maroni and Paola Bendinelli, carried out ELISA assay; Emanuela Matteucci and Paola Bendinelli, performed the statistical analysis of the data; Daniele Morelli and Lorenzo Drago, contributed the plasma of patients; Chiara Bonini, analyzed the clinical data; Alessandro Luzzati and Giuseppe Perrucchini, made the surgical interventions; Maria Alfonsina Desiderio, wrote the paper.

Conflicts of Interest: The authors declare no conflict of interest.

References

1. Brekken, R.A.; Sage, E.H. SPARC, a matricellular protein: At the crossroads of cell-matrix communication. *Matrix Biol.* **2001**, *19*, 816–827. [CrossRef]
2. Bornstein, P.; Sage, E.H. Matricellular proteins: Extracellular modulators of cell function. *Curr. Opin. Cell Biol.* **2002**, *14*, 608–616. [CrossRef]
3. Ribeiro, N.; Sousa, S.R.; Brekken, R.A.; Monteiro, F.J. Role of SPARC in bone remodeling and cancer-related bone metastasis. *J. Cell. Biochem.* **2014**, *115*, 17–26. [CrossRef] [PubMed]
4. Kaufmann, B.; Müller, S.; Hanisch, F.G.; Hartmann, U.; Paulsson, M.; Maurer, P.; Zaucke, F. Structural variability of BM-40/SPARC/osteonectin glycosylation: Implications for collagen affinity. *Glycobiology* **2004**, *14*, 609–619. [CrossRef] [PubMed]
5. Nagaraju, G.P.; Dontula, R.; El-Rayes, B.F.; Lakka, S.S. Molecular mechanisms underlying the divergent roles of SPARC in human carcinogenesis. *Carcinogenesis* **2014**, *35*, 967–973. [CrossRef] [PubMed]
6. Sato, T.; Oshima, T.; Yamamoto, N.; Yamada, T.; Hasegawa, S.; Yukawa, N.; Numata, K.; Kunisaki, C.; Tanaka, K.; Shiozawa, M.; *et al*. Clinical significance of *SPARC* gene expression in patients with gastric cancer. *J. Surg. Oncol.* **2013**, *108*, 364–368. [CrossRef] [PubMed]
7. Bellahcène, A.; Castronovo, V. Increased expression of osteonectin and osteopontin, two bone matrix proteins, in human breast cancer. *Am. J. Pathol.* **1995**, *146*, 95–100. [PubMed]
8. Barth, P.J.; Moll, R.; Ramaswamy, A. Stromal remodeling and SPARC (secreted protein acid rich in cysteine) expression in invasive ductal carcinomas of the breast. *Wirchows Arch.* **2005**, *446*, 532–536. [CrossRef] [PubMed]
9. Rucci, N.; Sanità, P.; Delle Monache, S.; Alesse, E.; Angelucci, A. Molecular pathogenesis of bone metastases in breast cancer: Proven and emerging therapeutic targets. *World J. Clin. Oncol.* **2014**, *5*, 335–347. [CrossRef] [PubMed]
10. Wong, S.Y.; Crowley, D.; Bronson, R.T.; Hynes, R.O. Analyses of the role of endogenous SPARC in mouse models of prostate and breast cancer. *Clin. Exp. Metastasis* **2008**, *25*, 109–118. [CrossRef] [PubMed]
11. Matteucci, E.; Maroni, P.; Disanza, A.; Bendinelli, P.; Desiderio, M.A. Coordinate regulation of microenvironmental stimuli and role of methylation in bone metastasis from breast carcinoma. *Biochim. Biophys. Acta* **2015**. [CrossRef] [PubMed]

12. Del Valle, P.R.; Milani, C.; Brentani, M.M.; Katayama, M.L.; de Lyra, E.C.; Carraro, D.M.; Brentani, H.; Puga, R.; Lima, L.A.; Rozenchan, P.B.; *et al*. Transcriptional profile of fibroblasts obtained from the primary site, lymph node, and bone marrow of breast cancer patients. *Genet. Mol. Biol.* **2014**, *37*, 480–489. [CrossRef] [PubMed]
13. El-Haibi, C.P.; Karnoub, A.E. Mesenchymal stem cells in the pathogenesis and therapy of breast cancer. *J. Mammary Gland Biol. Neoplasia* **2010**, *15*, 399–409. [CrossRef] [PubMed]
14. Martinez, L.M.; Vallone, V.B.; Labovsky, V.; Choi, H.; Hofer, E.L.; Feldman, L.; Bordenave, R.H.; Batagelj, E.; Dimase, F.; Villafañe, A.R.; *et al*. Changes in the peripheral blood and bone marrow from untreated advanced breast cancer patients that are associated with the establishment of bone metastases. *Clin. Exp. Metastasis* **2014**, *31*, 213–232. [CrossRef] [PubMed]
15. Dieudonné, S.C.; Xu, T.; Chou, J.Y.; Kutznetsov, S.A.; Satomura, K.; Mankani, M.; Fedarko, N.S.; Smith, E.P.; Robey, P.G.; Young, M.F. Immortalization and characterization of bone marrow stromal fibroblasts from a patient with a loss of function mutation in the estrogen receptor-alpha gene. *J. Bone Miner. Res.* **1998**, *13*, 598–608. [CrossRef] [PubMed]
16. García Fernández, A.; Chabrera, C.; García Font, M.; Fraile, M.; Lain, J.M.; Gónzalez, S.; Braco, I.; González, C.; Torres, J.; Piqueras, M.; *et al*. Differential patterns of recurrence and specific survival between luminal A and luminal B breast cancer according to recent changes in the 2013 St Gallen immunhistochemical classification. *Clin. Transl. Oncol.* **2015**, *17*, 238–246. [CrossRef] [PubMed]
17. Ades, F.; Zarvadas, D.; Bozovic-Spasojevic, I.; Pugliano, L.; Fumagalli, D.; de Azambuja, E.; Viale, G.; Sotiriou, C.; Piccart, M. Luminal B breast cancer: Molecular characterization, clinical management, and future perspectives. *J. Clin. Oncol.* **2014**, *32*, 2794–2803. [CrossRef] [PubMed]
18. Wang, H.; Yu, C.; Gao, X.; Welte, T.; Muscarella, A.M.; Tian, L.; Zhao, H.; Zhao, Z.; Du, S.; Tao, J.; *et al*. The osteogenic niche promotes early-stage bone colonization of disseminated breast cancer cells. *Cancer Cell* **2015**, *27*, 193–210. [CrossRef] [PubMed]
19. Rosanò, L.; Spinella, F.; Bagnato, A. Endothelin 1 in cancer: Biological implications and therapeutic opportunities. *Nat. Rev. Cancer* **2013**, *13*, 637–651. [CrossRef] [PubMed]
20. Bendinelli, P.; Maroni, P.; Matteucci, E.; Luzzati, A.; Perrucchini, G.; Desiderio, M.A. Microenvironmental stimuli affect Endothelin-1 signaling responsible for invasiveness and osteomimicry of bone metastasis from breast cancer. *Biochim. Biophys. Acta* **2014**, *1843*, 815–826. [CrossRef] [PubMed]
21. Alevizos, L.; Kataki, A.; Derventzi, A.; Gomatos, I.; Loutraris, C.; Gloustianou, G.; Manouras, A.; Konstadoulakis, M.M.; Zografos, G. Breast cancer nodal metastasis correlates with tumor and lymph node methylation profiles of Caveolin-1 and CXCR4. *Clin. Exp. Metastasis* **2014**, *31*, 511–520. [CrossRef] [PubMed]
22. Ram, V.S.; Parthiban; Sudhakar, U.; Mithradas, N.; Prabhakar, R. Bone biomarkers in periodontal disease: A review article. *J. Clin. Diagn. Res.* **2015**, *9*, ZE07–ZE10. [PubMed]
23. Croset, M.; Goehrig, D.; Frackowiak, A.; Bonnelye, E.; Ansieau, S.; Puisieux, A.; Clézardin, P. TWIST1 expression in breast cancer cells facilitates bone metastasis formation. *J. Bone Miner. Res.* **2014**, *29*, 1886–1899. [CrossRef] [PubMed]
24. Matteucci, E.; Maroni, P.; Luzzati, A.; Perrucchini, G.; Bendinelli, P.; Desiderio, M.A. Bone metastatic process of breast cancer involves methylation state affecting E-cadherin expression through TAZ and WWOX nuclear effectors. *Eur. J. Cancer* **2013**, *49*, 231–244. [CrossRef] [PubMed]
25. Haber, C.L.; Gottifredi, V.; Llera, A.S.; Salvatierra, E.; Prada, F.; Alonso, L.; Sage, E.H.; Podhajcer, O.L. SPARC modulates the proliferation of stromal but not of melanoma cells unless endogenous SPARC expression is downregulated. *Int. J. Cancer* **2008**, *122*, 1465–1475. [CrossRef] [PubMed]
26. Esposito, M.; Kang, Y. Targeting tumor-stromal interactions in bone metastasis. *Pharmacol. Ther.* **2014**, *141*, 222–233. [CrossRef] [PubMed]
27. Cox, T.R.; Bird, D.; Baker, A.M.; Barker, H.E.; Ho, M.W.; Lang, G.; Erler, J.T. LOX-mediated collagen crosslinking is responsible for fibrosis-enhanced metastasis. *Cancer Res.* **2013**, *73*, 1721–1732. [CrossRef] [PubMed]
28. Cox, T.R.; Rumnei, R.M.H.; Schoof, E.M.; Perryman, L.; Høye, A.M.; Agrawal, A.; Bird, D.; Ab Latif, N.; Forrest, H.; Evens, H.R.; *et al*. The hypoxic cancer secretome induces pre-metastatic bone lesions through lysyl oxidase. *Nature* **2015**, *522*, 106–110. [CrossRef] [PubMed]

29. Lindner, J.L.; Loibl, S.; Denkert, C.; Ataseven, B.; Fasching, P.A.; Pfitzner, B.M.; Gerber, B.; Gade, S.; Darb-Esfahani, S.; Sinn, B.V.; *et al*. Expression of secreted protein acidic and rich in cysteine (SPARC) in breast cancer and response to neoadjuvant chemotherapy. *Ann. Oncol.* **2015**, *26*, 95–100. [CrossRef] [PubMed]
30. De Toro, J.; Herschlik, L.; Waldner, C.; Mongini, C. Emerging roles of exosomes in normal and pathological conditions: New insights for diagnosis and therapeutic applications. *Front. Immunol.* **2015**, *6*, 203. [CrossRef] [PubMed]
31. Satelli, A.; Brownlee, Z.; Mitra, A.; Meng, Q.H.; Li, S. Circulating tumor cell enumeration with a combination of epithelial cell adhesion molecule- and cell-surface vimentin-based methods for monitoring breast cancer therapeutic response. *Clin. Chem.* **2015**, *61*, 259–266. [CrossRef] [PubMed]
32. Hoang, B.; Ernsting, M.J.; Roy, A.; Murakami, M.; Undzys, E.; Li, S.-D. Docetaxel-carboxymethylcellulose nanoparticles target cells via a SPARC and albumin dependent mechanism. *Biomaterials* **2015**, *59*, 66–76. [CrossRef] [PubMed]



© 2015 by the authors; licensee MDPI, Basel, Switzerland. This article is an open access article distributed under the terms and conditions of the Creative Commons by Attribution (CC-BY) license (http://creativecommons.org/licenses/by/4.0/).

International Journal of
Molecular Sciences

MDPI

Article

DAG/PKCδ and IP3/Ca^{2+}/CaMK IIβ Operate in Parallel to Each Other in PLCγ1-Driven Cell Proliferation and Migration of Human Gastric Adenocarcinoma Cells, through Akt/mTOR/S6 Pathway

Lianzhi Dai [1], Luhua Zhuang [1], Bingchang Zhang [1], Fen Wang [1], Xiaolei Chen [2], Chun Xia [2,*] and Bing Zhang [1,*]

Received: 27 October 2015; Accepted: 20 November 2015; Published: 1 December 2015
Academic Editor: William Chi-shing Cho

[1] Medical School, Xiamen University, Fujian 361102, China; 24520131153431@stu.xmu.edu.cn (L.D.); zhuangluhua@gmail.com (L.Z.); bczhang@foxmail.com (B.Z.); 24520141153450@stu.xmu.edu.cn (F.W.)
[2] Zhongshan Hospital, Xiamen University, Fujian 361004, China; cxl910904@gmail.com
* Correspondence: chunxia@xmu.edu.cn (C.X.); cristal66@xmu.edu.cn (B.Z.); Tel./Fax: +86-592-299-3080 (C.X.); Tel./Fax: +86-592-218-8421 (B.Z.)

Abstract: Phosphoinositide specific phospholipase Cγ (PLCγ) activates diacylglycerol (DAG)/protein kinase C (PKC) and inositol 1,4,5-trisphosphate (IP3)/Ca^{2+}/calmodulin-dependent protein kinase II (CaMK II) axes to regulate import events in some cancer cells, including gastric adenocarcinoma cells. However, whether DAG/PKCδ and IP3/Ca^{2+}/CaMK IIβ axes are simultaneously involved in PLCγ1-driven cell proliferation and migration of human gastric adenocarcinoma cells and the underlying mechanism are not elucidated. Here, we investigated the role of DAG/PKCδ or CaMK IIβ in PLCγ1-driven cell proliferation and migration of human gastric adenocarcinoma cells, using the BGC-823 cell line. The results indicated that the inhibition of PKCδ and CaMK IIβ could block cell proliferation and migration of BGC-823 cells as well as the effect of inhibiting PLCγ1, including the decrease of cell viability, the increase of apoptotic index, the down-regulation of matrix metalloproteinase (MMP) 9 expression level, and the decrease of cell migration rate. Both DAG/PKCδ and CaMK IIβ triggered protein kinase B (Akt)/mammalian target of rapamycin (mTOR)/S6 pathway to regulate protein synthesis. The data indicate that DAG/PKCδ and IP3/Ca^{2+}/CaMK IIβ operate in parallel to each other in PLCγ1-driven cell proliferation and migration of human gastric adenocarcinoma cells through Akt/mTOR/S6 pathway, with important implication for validating PLCγ1 as a molecular biomarker in early gastric cancer diagnosis and disease surveillance.

Keywords: PLCγ1; DAG/PKCδ; IP3/Ca^{2+}/CaMK IIβ; Akt/mTOR/S6; cell proliferation; migration; human gastric adenocarcinoma cells

1. Introduction

Human gastric cancer is the second leading cause of cancer death and the fourth most prevalent malignancy worldwide [1]. Many factors including the pathogenesis of gastric cancer, diagnosis, and treatment approaches result in the high incidence and mortality rates of gastric cancer [2,3]. Recent literature has shown the involvement of important signal molecules in the pathogenesis of gastric cancers, which is beneficial to developing efficacious molecular biomarkers for early gastric cancer diagnosis and

disease surveillance. As an example, the expression of cyclin D1, p21 and p27, alone or in combination, are early events in gastric tumorigenesis and may serve as a candidate molecular marker for the early gastric carcinoma [4]. Mitogen-activated protein kinase (MAPK) kinase 4 (MKK4) kinase expression could serve as a significant prognostic factor for disease-free survival and for overall survival in human gastric cancer [5]. However, the expressions of these molecules are not always in accordance with the pathological progression of gastric cancers. For example, the expression of cyclin D1, p21 and p27 inversely correlated with the lymph node metastasis [4], to the extent that the application of molecular biomarkers could be decreased, due to their complex regulatory mechanism. Hence, studying the expressions of important signal molecules in the pathogenesis of gastric cancer and understanding the underlying transduction mechanism are required to validate the molecular biomarkers.

Phosphoinositide specific phospholipase Cγ (PLCγ), one of PLCs family, has two isoforms, PLCγ1 and PLCγ2. PLCγ1 is ubiquitously expressed in mammalian cells, and has been reported to be highly expressed in some tumor tissues, including colorectal cancer, squamous cell carcinoma, and breast cancer, regulating cancer cell metabolism [6–8]. As an example, elevated content of PLCγ1 in colorectal cancer tissues is observed [6]. PLCγ1 is required for the epidermal growth factor receptor (EGFR)-induced squamous cell carcinoma cell mitogenesis [7]. PLCγ mediates high levels of glucose and insulin-induced cell proliferation and migration in MDA-MB-468 breast cancer and SW480 colon cancer cells *in vitro* [8]. Our previous study also showed the higher expression of PLCγ1 in human gastric adenocarcinoma tissue and that the metastasis of human gastric adenocarcinoma cells partly depends on PLCγ1 expression [9]. Moreover, it has been shown that the depletion of PLCγ expression or inhibition of its activity not only significantly increases cisplatin-induced apoptosis but also suppresses the invasive ability of RhoGDI2-overexpressing SNU-484 gastric cancer cells [10]. Therefore, PLCγ may be a potential molecular biomarker in human gastric cancer, and understanding its regulatory mechanism is beneficial to confirm its implication in early cancer diagnosis and monitoring.

PLCγ is activated by many growth factor receptors, including epidermal growth factor (EGF), platelet derived growth factor (PDGF), nerve growth factor (NGF), and type I insulin-like growth factor (IGF-1), and induces hydrolysis of phosphatidylinositol 4,5-bisphosphate (PtdIns(4,5)P2) to form the second messengers diacylglycerol (DAG) and inositol 1,4,5-trisphosphate (IP3), which in turn activate protein kinase C (PKC) and intracellular calcium mobilization, respectively [11–16]. Activated DAG/PKC and IP3/Ca^{2+}/CaMK II axes, the two classical axes of PLCγ, regulate important events of cancer cell metabolism [17,18]. As an example, activated PLCγ by interleukin-8 generates DAG and IP3, which in turn trigger PKC and the release of calcium from the endoplasmatic reticulum, respectively, and participates in human T24 bladder carcinoma cell migration [17]. In estrogen receptor α (ERα)-positive (ERα(+)) cancer cells, 3,3-*bis*(4-hydroxyphenyl)-7-methyl-1,3-dihydro-2*H*-indol-2-one (BHPI) rapidly hyperactivates plasma membrane PLCγ, generating IP3, which opens EnR IP3R calcium channels, rapidly depleting EnR Ca^{2+} stores [18]. However, the underlying mechanism of DAG/PKCδ and IP3/Ca^{2+}/CaMK IIβ axes in PLCγ-driven cell proliferation and migration of human gastric adenocarcinoma cells has not been elucidated.

In this study, we examined the role of PKCδ and CaMK IIβ signal molecules in cell proliferation and migration of human gastric adenocarcinoma cells, using the BGC-823 cell line. Furthermore, the regulatory mechanism related to Akt, mTOR, and S6 signal molecules was investigated. Consequently, both DAG/PKCδ and IP3/Ca^{2+}/CaMK IIβ operate in parallel to each other in PLCγ1-driven cell proliferation and migration of human gastric adenocarcinoma cells.

2. Results

The effect of inhibiting PKCδ and CaMK IIβ on PLCγ1-driven cell proliferation and apoptosis in human gastric adenocarcinoma cells.

To investigate whether DAG/PKCδ and IP3/Ca^{2+}/CaMK IIβ were simultaneously involved in regulating cell proliferation and apoptosis in human gastric adenocarcinoma cells, BGC-823 cells

were treated with those inhibitors, U73122 (PLCγ inhibitor), KN93 (CaMK II inhibitor) and R59949 (DAG-kinase inhibitor), or were transfected with lentiviral-shRNA of PKCδ or CaMK IIβ vectors for different time points, followed by the detection of cell viability using an MTT assay and apoptotic index using DAPI or PI staining. Figure 1A indicated that both CaMK II inhibitor (KN93) and DAG-kinase inhibitor (R59949) led to the decrease of cell viability significantly as well as the effect of PLCγ inhibitor (U73122) (* $p < 0.05$, ** $p < 0.01$, *** $p < 0.001$, **** $p < 0.0001$, *versus* Dimethylsulphoxide (DMSO) group). The cell viability of BGC-823 cells transfected with sh-PKCδ or sh-CaMK IIβ vectors also decreased, compared with sh-Control group (Figure 1B, * $p < 0.05$, ** $p < 0.01$, *** $p < 0.001$, **** $p < 0.0001$). Meanwhile, the apoptotic index (%) increased in BGC-823 cells transfected with sh-PKCδ or sh-CaMK IIβ vectors (Figure 1C,D, * $p < 0.05$, ** $p < 0.01$, *** $p < 0.001$, *versus* sh-Control group). Together, the inhibition of DAG/PKCδ or CaMK IIβ could block cell proliferation or promote cell apoptosis as well as the inhibitory effect of PLCγ1.

The effect of inhibiting DAG/PKCδ and CaMK IIβ on cell migration in human gastric adenocarcinoma cells.

Our previous study indicated that the migration of gastric adenocarcinoma cells partly depended on PLCγ1 activation. To investigate the role of IP3/Ca^{2+}/CaMK IIβ and DAG/PKCδ axes in cell migration of human gastric adenocarcinoma cells, cells were treated with U73122, KN93, and R59949, respectively, or were transfected with sh-PKCδ or sh-CaMK IIβ vectors, followed the detection of cell migration rate using a Transwell assay and MMP9 expression level with Western blotting analysis. Figure 2A showed that the numbers of migrate cells decreased in response to the treatment by those inhibitors including U73122, KN93, and R59949 (** $p < 0.01$, *** $p < 0.001$, *versus* DMSO group). Similar results were observed in BGC-823 cells with the transfection of sh-PKCδ or sh-CaMK IIβ vectors (Figure 2B, * $p < 0.05$, *versus* sh-Control group). Meanwhile, the expression level of MMP9 protein was down-regulated in BGC-823 cells transfected with sh-PKCδ or sh-CaMK IIβ vectors (Figure 2C). Additionally, the mRNA level of MMP9 was reduced in BGC-823 cells transfected with sh-PKCδ or sh-CaMK IIβ vectors or treated with KN93 or R59949, as well as the effect of sh-PLCγ1 or U73312 (Figure 2D,E, * $p < 0.05$, ** $p < 0.01$, *** $p < 0.001$, *versus* DMSO or sh-Control group). Collectively, the data indicated that the blockade of DAG/PKCδ and CaMK IIβ down-regulated cell migration of gastric adenocarcinoma cells, as well as the effect of PLCγ1 inhibition.

The involvement of Akt, mTOR, S6, and NF-κB signal molecules in regulatory mechanism of IP3/Ca^{2+}/CaMK II and DAG/PKCδ axes in human gastric adenocarcinoma cells.

To investigate the regulatory mechanism of the two classical signal axes of PLCγ1, IP3/Ca^{2+}/CaMK IIβ and DAG/PKCδ, in cell proliferation and migration of human gastric adenocarcinoma cells, the expression levels of some important signal molecules, including Akt, extracellular signal-regulated kinase (ERK), mTOR, NF-κB, and S6, were detected in BGC-823 cells transfected with sh-PKCδ or sh-CaMK IIβ vectors using Western blotting analysis. The results showed that the transfection of either shRNA-PKCδ or shRNA-CaMK IIβ vectors led to a potent decrease in the phosphorylation level of AKT, mTOR, and S6, without the alteration of total Akt and mTOR (Figure 3A,B). Interestingly, the expression level of NF-κB only was reduced in BGC-823 cells transfected with sh-CaMK IIβ vectors (Figure 3B), whereas, the depletion of PKCδ by shRNA did not affect the expression of NF-κB protein (Figure 3A). Meanwhile, the depletion of PKCδ by shRNA down-regulated the phosphorylation level of ERK, while the transfection with sh-CaMK IIβ vectors did not change the level of p-ERK. As a result, the data indicated that the regulatory mechanism of IP3/Ca^{2+}/CaMK IIβ and DAG/PKCδ axes, the two classical axes of PLCγ1, could be associated with the phosphorylation of Akt, mTOR, and S6, while NF-κB or ERK was only involved in the regulation of IP3/Ca^{2+}/CaMK II axis or DAG/PKCδ axis, respectively.

The expression of PKCδ and CaMK IIβ in mice tumor xenograft model derived from gastric adenocarcinoma cells with the transfection of sh-PLCγ1.

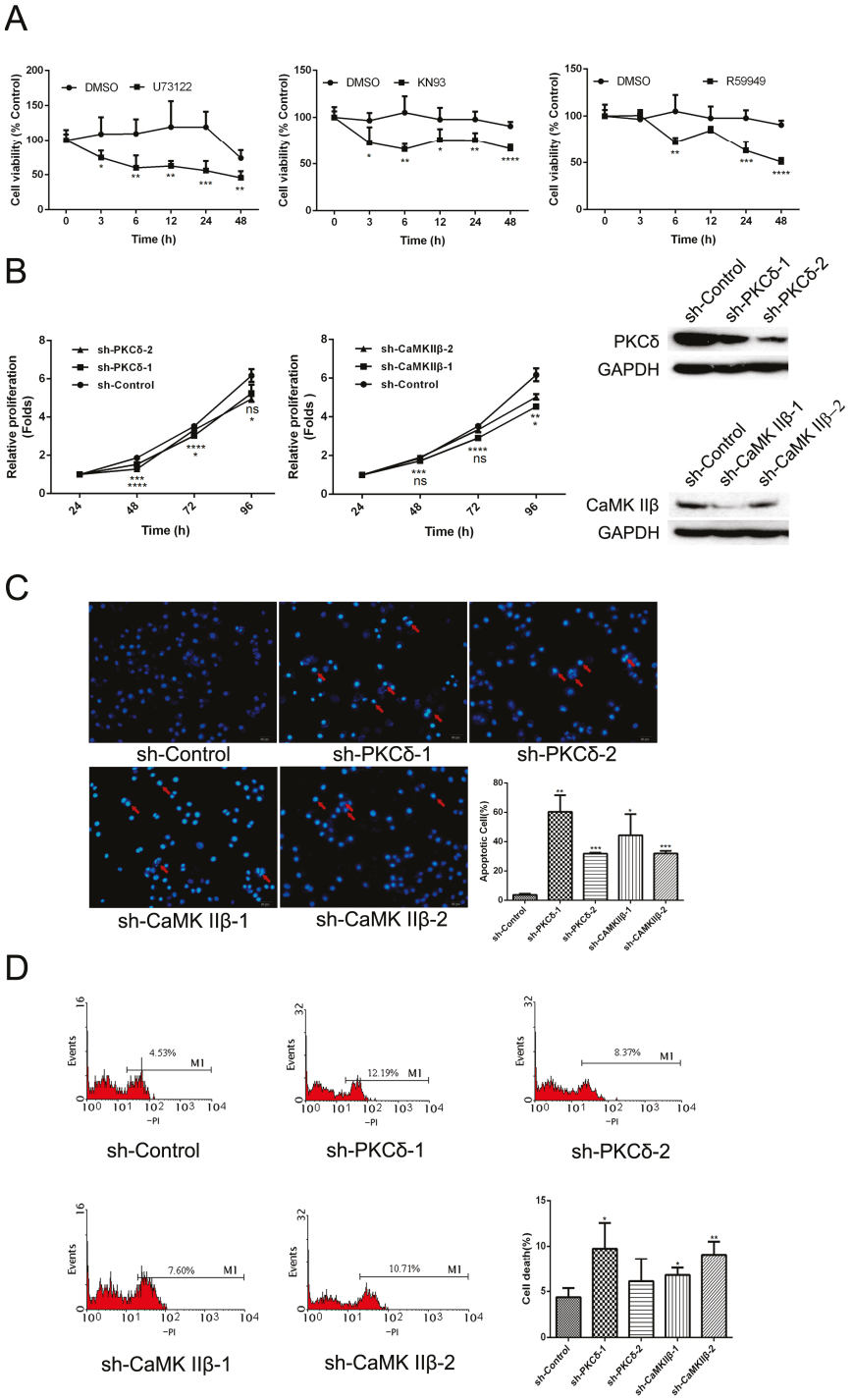

Figure 1. The effect of inhibiting CaMK IIβ and DAG/PKCδ on cell proliferation and apoptosis in human gastric adenocarcinoma. (**A**) Cells were exposed to DMSO (2 μL), U73122 (10 μM), KN93 (16 μM), or R59949 (10 μM) for different time points, respectively. Cell viability was then measured by an MTT assay as described in Materials and Methods; (**B**) Cells were transfected with sh-PKCδ or sh-CaMK IIβ vectors for different time points. Cell viability was measured using an MTT assay as described in Materials and Methods; (**C**) Cells were transfected with sh-PKCδ or sh-CaMK IIβ vectors for 48 h, followed by DAPI staining and counting under OLYMPUS 41 microscope as described in Materials and Methods. The cell nuclei were stained by DAPI staining (blue), and the apoptotic bodies were indicated by red arrows (magnification 200×); (**D**) Cells were transfected with sh-PKCδ or sh-CaMK IIβ vectors for 48 h, followed by PI staining. The cell apoptosis index was analyzed by flow cytometry as described in Materials and Methods. Data are expressed as mean ± S.D. of three independent experiments, each yielding similar results (* $p < 0.05$, ** $p < 0.01$, *** $p < 0.001$, **** $p < 0.0001$, *versus* control).

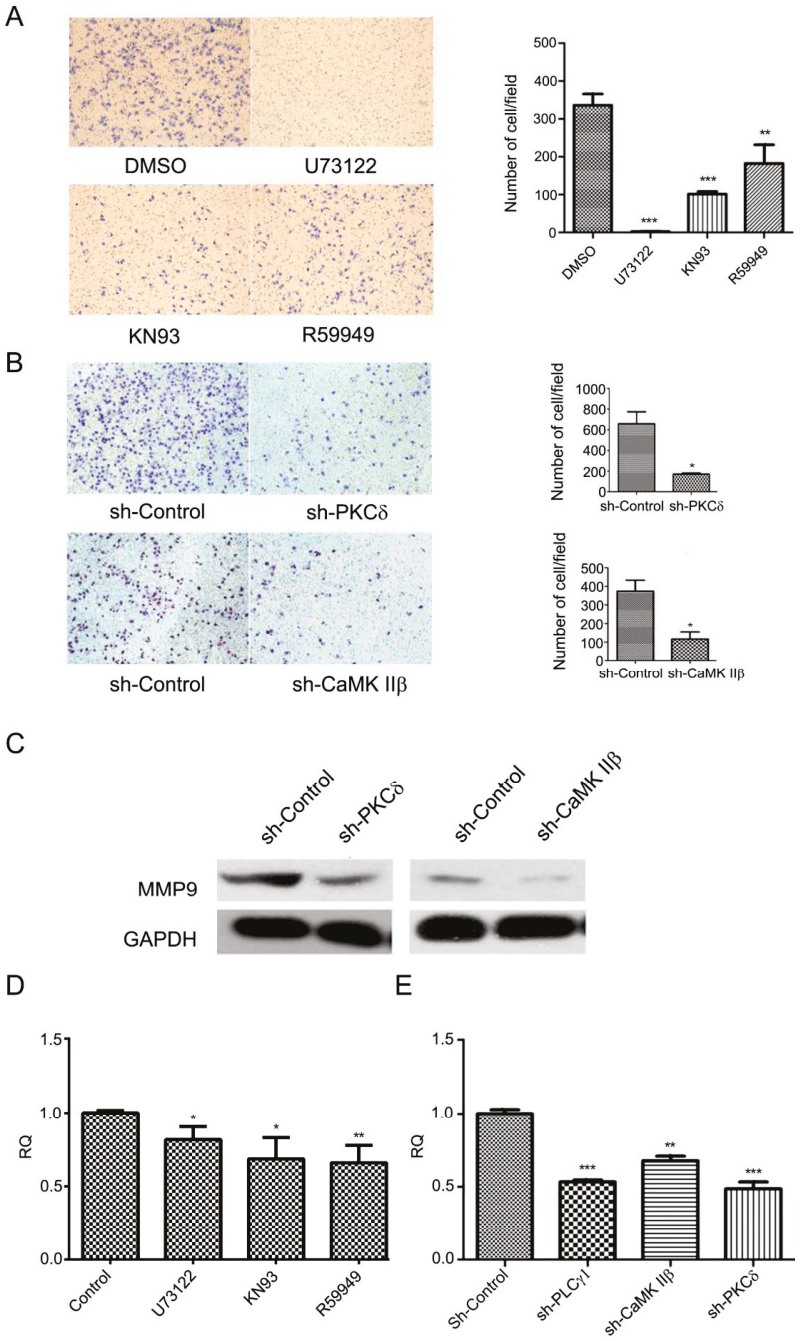

Figure 2. The effect of inhibiting CaMK IIβ and DAG/PKCδ on cell migration in human gastric adenocarcinoma cells. (**A**) Cells were treated with DMSO (2 μL), U73122 (10 μM), KN93 (16 μM), and R59949 (20 μM) for 3 h, respectively. The migration ability were measured by a transwell assay as described in Materials and Methods (magnification 200×); (**B**) Cells were transfected with sh-PKCδ-2 or sh-CaMK IIβ-1 vectors for 48 h, and the migration ability were measured by a transwell assay as described in Materials and Methods (magnification 200×); (**C**) Cells were transfected with sh-PKCδ-2 and sh-CaMK IIβ-1 vectors for 48 h. The expression level of MMP9 was determined by Western blotting analysis as described in Materials and Methods. Glyceraldehyde-3-phosphate dehydrogenase (GAPDH) was used as an internal control; (**D**) Cells were treated with DMSO (2 μL), U73122 (10 μM), KN93 (16 μM), or R59949 (10 μM), respectively. The mRNA levels of MMP9 were measured by RT-PCR analysis as described in Materials and Methods; (**E**) Cells were transfected with sh-PLCγ1, sh-PKCδ-2, or sh-CaMK IIβ-1 vectors for 48 h. The mRNA levels of MMP9 were measured by RT-PCR analysis as described in section Materials and Methods. Data are expressed as mean ± S.D. of three independent experiments, each yielding similar results (* $p < 0.05$, ** $p < 0.01$, *** $p < 0.001$, *versus* control).

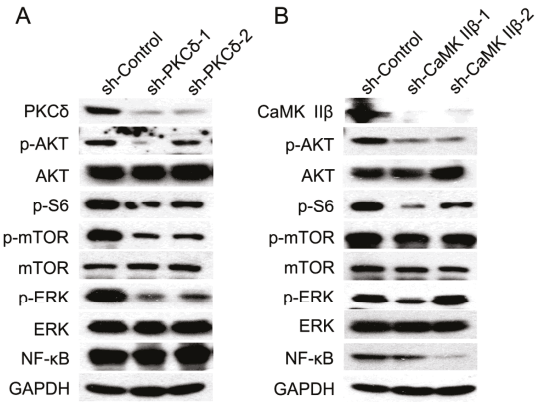

Figure 3. The expression level of Akt, mTOR, S6, and NF-κB in human gastric adenocarcinoma cells with the transfection of sh-PKCδ or sh-CaMK IIβ vectors. (**A**) Cells were transfected with sh-PKCδ-2 vector for 48 h. The expression levels of PKCδ, CaMK IIβ, Akt, p-Akt, mTOR, p-mTOR, p-S6, ERK, p-ERK, and NF-κB were detected by Western blotting analysis as described in Materials and Methods. GAPDH was used as an internal control; (**B**) Cells were transfected with sh-CaMK IIβ vector for 48 h. The expression levels of PKCδ, CaMK IIβ, Akt, p-Akt, mTOR, p-mTOR, p-S6, ERK, p-ERK, and NF-κB were detected by Western blotting analysis as described in Materials and Methods. GAPDH was used as an internal control. Data are representative of three independent experiments, each yielding similar results.

Our other study's results showed that the depletion of PLCγ1 by shRNA could suppress tumor growth and metastasis in mice tumor xenograft model derived from BGC-823 cells with the transfection of sh-PLCγ1 vector (under review) [19]. Here, we investigated the expression levels of PKCδ and CaMK IIβ protein in the subcutaneous tumor tissue of mice tumor xenograft model using Western blotting analysis. Figure 4 showed that the expression levels of PKCδ and CaMK IIβ protein were down-regulated in tumor tissues as well as the depletion of PLCγ1 by shRNA, while the expression level of MMP9 protein and cleaved-PARP were reduced (** $p < 0.01$). Thus, the data indicated that the levels of PKCδ and CaMK IIβ were down-regulated in the depletion of PLCγ1 by shRNA-mediated tumor growth and metastasis suppression.

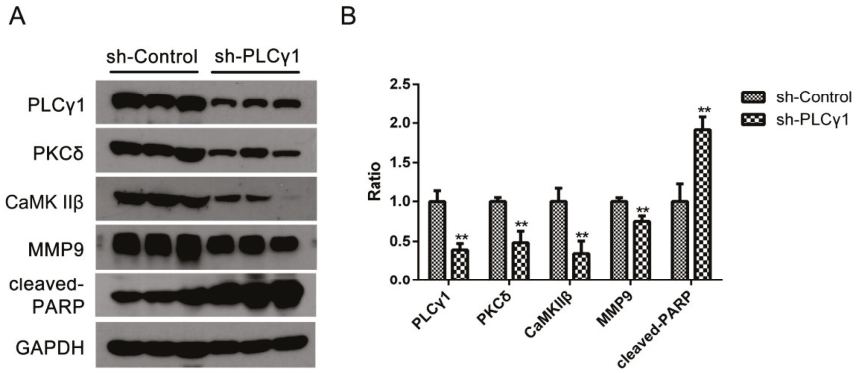

Figure 4. The expression level of PKCδ and CaMK IIβ in mice tumor xenograft model derived from gastric adenocarcinoma cells with the transfection of sh-PLCγ1. Mice were injected human gastric adenocarcinoma cells, BGC-823, for 40 days, and finally sacrified. Tissue protein in subcutaneous tumor tissue was then extracted. (**A**) The expression level of PLCγ1,PKCδ, CaMK IIβ, cleaved-PARP, and MMP9 in the tumor samples were detected by Western blotting analysis as described in Materials and Methods; (**B**) The histogram represents the means ± S.D. of the expression level of PLCγ1,PKCδ, CaMK IIβ, cleaved-PARP, and MMP9 in the tumor samples. (** $p < 0.01$, *versus* control group).

3. Discussion

In this study, we demonstrated that the inhibition of DAG/PKCδ and CaMK IIβ could block cell proliferation and migration of human gastric adenocarcinoma cells as well as the inhibition of PLCγ1. The expression levels of PKCδ and CaMK IIβ protein were down-regulated in mice tumor xenograft model derived from human gastric adenocarcinoma cells, BGC-823, with the transfection of sh-PLCγ1 vector. Furthermore, both DAG/PKCδ and IP3/Ca^{2+}/CaMK IIβ triggered Akt/mTOR/S6 pathway to regulate protein synthesis. Therefore, DAG/PKCδ and IP3/Ca^{2+}/CaMK IIβ operate in parallel to each other in PLCγ1-driven cell proliferation and migration of human gastric adenocarcinoma cells.

PLCγ isozymes catalyzes the hydrolysis of PIP2 to generate two intracellular messengers, DAG and IP3, and then triggers DAG/PKC and IP3/Ca^{2+}/CaMK II cascade classically. PKCδ, a member of the novel family isoforms, has been a marker of aggressive breast cancers [20,21]. It is described that increased PKCδ in mammary tumor cells relates to transformation and metastatic progression [21]. Furthermore, PKCδ is required for ErbB2 (HER2)-driven mammary gland tumorigenesis and negatively correlates with prognosis in human breast cancer [22]. Increasing concentrations of PKCδ mRNA were associated with reduced overall patient survival ($p = 0.004$) [23]. A very recent study indicates that the pharmacological inhibition of PKCδ impairs LM38-LP cells (derived from a murine mammary papillary adenocarcinoma with tumorigenic and metastatic capacity in BALB/c mice) proliferation through cell cycle arrest [24]. The above studies indicate that PKCδ plays a role in cancer cell proliferation and metastasis. Meanwhile, the involvement of IP3/Ca^{2+}/CaMK II axis in cell metabolism has been stated in some studies. IP3/Ca^{2+}/CaMK II axis is involved in regulating cholangiocyte growth [25]. CaMK II suppresses the expression of CaMK IV to promote leukemia cell proliferation [26]. TNF-α induced CD44 expression is regulated by AP-1 through the activation of the CaMK-II pathway to mediate cell migration in human monocytic cells [27]. Therefore, both DAG/PKCδ and IP3/Ca^{2+}/CaMK II axes play important role in cell proliferation and migration. However, their regulatory effects on cell metabolism are not always identical in the same cell line. In human astroglioma cells, epigallocatechin gallate regulates phosphatidylcholine-specific phospholipase D (PLD) activity via a signaling pathway involving changes in the redox state that stimulates a PLCγ1/IP3/CaMK II/PLD and a PLCγ1/DAG/PKC/PLD axes [28]. The CaMK axis, not the PKC axis, is responsible for the earliest protein phosphorylation event following activation of PLCγ in living *Drosophila* photoreceptors [29,30]. Here, we demonstrated that the inhibitory effect of the depletion of PKCδ or CaMK IIβ by shRNA or the pharmacological inhibiting on cell proliferation and migration was the same as the effect of PLCγ1 inhibition, consistent with other authors' and our previous studies [9,19,31]. Therefore, it is suggested that the two classical axes of PLCγ1, DAG/PKCδ and IP3/Ca^{2+}/CaMK IIβ, are involved simultaneously in PLCγ1-driven cell proliferation and metastasis of human gastric adenocarcinoma cells.

Akt/mTOR pathway is crucial for cell metabolism including cell survival and apoptosis [32], in which mTOR could regulate translation in response to nutrients and growth factors by phosphorylating key components of the protein synthesis machinery, including S6 protein (which is phosphorylated by the S6 kinase) and eIF4G [33]. It is determined that Akt/mTOR/S6 pathway is involved in cell proliferation and apoptosis of cancer cells [34,35]. As an example, the inactivation of Akt/mTOR/S6 pathway is required for an increase in pancreatic cancer cells apoptosis and tumor growth inhibition by thymoquinone pretreatment following gemcitabine treatment synergistically [34].A very recent study also shows that resveratrol synergistically enhanced the antitumor effects of erlotinib in non-small-cell lung cancer cells by inhibiting the Akt/mTOR/S6 pathway [35]. Furthermore, the associations of Akt/mTOR/S6 with PKCδ and CaMK II have been studied. PKCδ is required for ET-1-stimulated or insulin-stimulated mTOR/S6 pathway in adult cardiac muscle cells [36]. The inhibition of PKCδ by rottlerin is supposed to attenuate non-specific airway sensitivity and inflammation through suppressing the PI3K/Akt/mTOR pathway in an asthma model [37]. Meanwhile, our previous study indicated that PLCγ1/IP3/Ca^{2+}/CaMK IIβ axis regulated the ECM synthesis of human chondrocytes

through triggering mTOR/P70S6K/S6 pathway [38]. Consequently, it is confirmed that the inhibition of PKCδ or CaMK IIβ could suppress the Akt/mTOR/S6 pathway in human gastric adenocarcinoma cells.

Additionally, our data that inhibiting CaMK IIβ led to the down-regulation of NF-κB (one of Akt downstreams) indicate that CaMK IIβ could trigger Akt/NF-κB pathway to resist cell apoptosis, in accordance with previous study that the inhibition of CaMK II prevents PAF-induced priming events including NF-κB activation [39]. Our data is consistent with previous study that DAG/PKC/ERK pathway is involved in the development of glomerular dysfunction in diabetes [40], our finding of the reduced p-ERK by the depletion of PKCδ suggests the existence of DAG/PKCδ/ERK pathway in PLCγ1-driven cell proliferation and migration of human gastric adenocarcinoma cells. The non-alteration of NF-κB or p-ERK level in sh-PKCδ or sh-CaMK IIβ-transduced cells imply that the regulatory effect of PKCδ or CaMK IIβ on NF-κB expression or ERK phosphorylation may be blocked by other signal molecules. We need to further study the complex regulatory mechanism related to PKCδ or CaMK IIβ on NF-κB expression or ERK phosphorylation and validate PKCδ and CaMK IIβ as a molecular biomarker in early diagnosis and disease surveillance.

4. Materials and Methods

4.1. Reagents and Antibodies

Antibodies against PLCγ1, p-PLCγ1 (Tyr783), PKCδ, CaMK IIβ, Akt, p-Akt (S473), ERK, p-ERK (Thr202/Tyr204), mTOR, p-mTOR (Ser2481), p-S6 (Ser235/236), and NF-κB were purchased from Cell Signaling Technology Inc. (Beverly, MA, USA). Cleaved-PARP, Matrix metalloproteinase-9 (MMP9), and GAPDH were purchased from Abcam (Cambridge, MA, USA). Inhibitors (U73122, KN93, and R59949) were obtained from Sigma-Aldrich in China (Shanghai, China). Other reagents were of the highest grade commercially available.

4.2. Cell Culture

The human gastric cancer cell line, BGC-823 cell, was obtained from the Shanghai Institute of Cell Biology, Chinese Academy of Sciences (Shanghai, China), and was maintained in RPMI1640 medium (Thermo Fisher Scienctific, Waltham, MA, USA) supplemented with 10% fetal bovine serum (FBS), 100 U/mL penicillin, and 100 μg/mL streptomycin, at 37 °C in a water-saturated atmosphere of 5% CO_2.

4.3. Plasmid Construction and Transfection

Lentiviral-mediated shorthairpin RNA (shRNA) targeting PLCγ1 (sh-PLCγ1), (5′-CCGGCCTGTGAACCACGAATGGTATCTCGAGATACCATTCGTGGTTCACAGGTTTTTG-3′), sh-PKCδ (Sh1: 5′-CCGGGCAAGACAACAGTGGGACCTACTCGAGTAGGTCCCACTGTTGTCTTGC TTTTTG3′, Sh2: 5′-CCGGGGCCGCTTTGAACTCTACCGTCTCGAGACGGTAGAGTTCAAAGC GGCCTTTTTG-3′), and sh-CaMK IIβ (Sh1: 5′-CCGGGATCATTAAGACCACGGAGCACTCGAGTG CTCCGTGGTCTTAATGATCTTTTTG-3′.Sh2: 5′-CCGGACAAGAAAGCAGATGGAGTCACTCGAG TGACTCCATCTGCTTTCTTGTTTTTTG-3′) were purchased from Gene Chem (Gene Chem, Shanghai, China). The different sh-PLCγ1, sh-PKCδ, and sh-CaMK IIβ vectors were transfected into BGC-823 cells using a lentiviral transfection strategy, respectively. Sh-PLCγ1, sh-PKCδ, and sh-CaMK IIβ stable cell lines were obtained under the pressure of puromycin (2 μg/mL, BioVision, Inc., Milpitas, CA, USA).The expression levels of PLCγ1,PKCδ, and CaMK IIβ protein were detected with Western blotting analysis prior to the other experiments.

4.4. MTT Assay

Cells were plated in 96-well plates (1×10^4 cells/well) and cultured for the indicated time. As described as previous studies [41,42], the number of viable cells was detected using 3-(4,5-dimethylthiazol-2-y)-2,5-diphenyl-tetrazolium bromide (MTT) assay.

4.5. Apoptosis Assay

Cells were seeded on glass coverslips in 6-well plates for 24 h, rinsed with PBS once, fixed in 4% paraformaldehyde for 10 min, washed three times with PBS, and stained by 50 μg/mL 4,6-diamidino-2-phenylindole (DAPI) stain [43]. The apoptotic cells were observed under Olympus BX41 microscope equipped with a digital camera (Olympus, Tokyo, Japan). Additionally, cells were cultured and stained with Propidium Iodide (PI) stain, followed by flow cytometry (FACScan, Becton Dickinson, Franklin Lakes, NJ, USA) analysis according to previous study [44].

4.6. Transwell Assay

According to the previous studies [9,45], 2×10^4 cells in serum-free dulbecco's modified eagle medium (DMEM) were placed into the upper chambers of Transwell inserts set within wells with 8 μm pore filters, and incubated at 37 °C for 12 h. Cells on the upper surface of the chambers were then removed with cotton swabs. The migrated cells on the lower membrane surface were fixed in methanol and stained with 0.1% Giemsa stain. Eight microscope fields (200×) from each Transwell chamber were randomly selected, and cells adhering to the undersurface of the filter were imaged and counted using an Olympus BX41 microscope equipped with a digital camera (Olympus, Tokyo, Japan).

4.7. Western Blot Analysis

Protein extracts were subjected to sodium dodecyl sulfate (SDS)-polyacrylamide gel electrophoresis (PAGE) (8%–10%) and transferred to nitrocellulose membrane for Western blotting analysis [9,42,46]. The membrane was incubated at 4 °C for different time with various antibodies as required, and followed by the addition of the corresponding secondary antibody at room temperature for 1 to 2 h. An enhanced chemiluminescence detection (ECL) kit was used to detect antibody reactivity (Pierce, Rockford, IL, USA).

4.8. Real-Time PCR Analysis

Total RNA in cells was extracted using Trizol (Invitrogen, Carlsbad, CA, USA). The amount and quality of the extracted RNA was assessed by spectrophotometry using NanoDrop 2000 (Thermo scientific, Wilmington, DE, USA). cDNA synthesis was performed with 1 μg of total RNA at 37 °C for 15min using the Primescript RT Master Mix Kit (Takara, Dalian, China), and subsequently diluted 10-fold. Real-time PCR was performed using the ABI StepOnePlus Sequence Detection System v2.1 (Applied Biosystems, Foster City, CA, USA) with SYBR Premix Ex Taq II Kit (Takala, Dalian, China). Results were normalized to GAPDH and analyzed using SDS software v2.1 according to previous study [47] .The following primers were used in quantitative PCR for measuring gene expression relative to GAPDH (MMP9: Forward 5′-TGACAGCGACAAGAAGTG-3′, Reverse 5′-CAGTGAAGCGGTACATAGG-3′; GAPDH: Forward 5′-GGAAGGTGAAGGTCGGAGTCA-3′, Reverse 5′-GTCATTGATGGCAACAATATCCACT-3′).

4.9. Xenograft Assay in Nude Mice

Thirty-two 6-week-old female BALB/c nu/nu mice were purchased from Shanghai Slac Laboratory Animal Co., Ltd. (Shanghai, China). All animal studies were conducted according to the regulations of the Institutional Animal Care and Use Committee protocol. This study was approved by the Committee on the Ethics of Animal Experiments of the University of Xiamen (ID No. 20110916). Animals bearing tumors were randomly assigned to 4 groups, 200 μL relevant stable cells (sh-Control, sh-PLCγ1, 2×10^6/mouse) in PBS were subcutaneously injected into the right hind leg of mouse, with 8 mice per group [42]. Tumor volume and animal weight were measured every 3–4 days. All animals were killed since injected for 40 days. The protein expression levels of relative signal molecules in these subcutaneous tumors were detected with Western blotting analysis.

4.10. Statistical Analysis

The differences between the groups were examined for statistical significance using the Student's *t*-test with GraphPad Prism 5 software (GraphPad Software, Inc., LaJolla, CA, USA). A value of $p < 0.05$ was considered significant.

5. Conclusions

In conclusion, the blockade of both the DAG/PKCδ and IP3/Ca^{2+}/CaMK IIβ axes could inhibit cell proliferation and migration, as well as the effect of the inhibition of PLCγ1. Furthermore, their regulatory mechanism is associated with the activation of Akt/mTOR/S6 pathway. Therefore, it is suggested that both DAG/PKCδ and IP3/Ca^{2+}/CaMK IIβ operate in parallel to each other in PLCγ1-driven cell proliferation and migration of human gastric adenocarcinoma cells through Akt/mTOR/S6 pathway (Scheme 1).

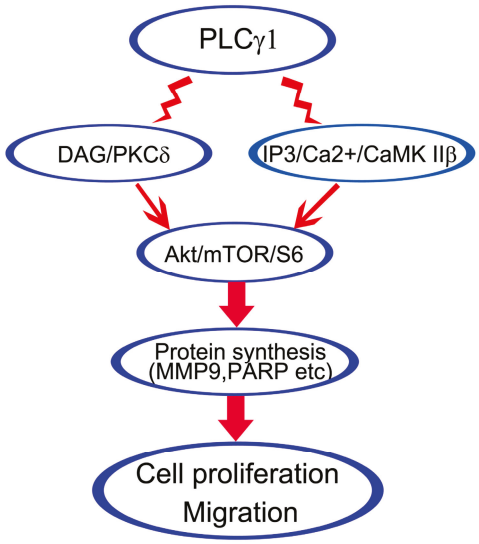

Scheme 1. Schematic representation of DAG/PKCδ and IP3/Ca^{2+}/CaMK IIβ operate in PLCγ1-driven cell proliferation and migration of human gastric adenocarcinoma cells.

Acknowledgments: This study was supported by the National Natural Science Foundation of China (No. 81572189, 81371952, and 81072015).

Author Contributions: Lianzhi Dai, Luhua Zhuang, and Bingchang Zhang performed the experiments. Bing Zhang and Chun Xia designed the study, wrote the manuscript and took the responsibility for the correctness of the study results. Xiaolei Chen helped to perform the complementary experiments. All authors read and approved the final manuscript.

Conflicts of Interest: The authors declare no conflict of interest.

References

1. Jemal, A.; Bray, F.; Center, M.M.; Ferlay, J.; Ward, E.; Forman, D. Global cancer statistics. *CA Cancer J. Clin.* **2011**, *61*, 69–90. [CrossRef] [PubMed]
2. Lin, X.; Zhao, Y.; Song, W.; Zhang, B. Molecular classification and prediction in gastric cancer. *Comput. Struct. Biotechnol. J.* **2015**, *13*, 448–458. [CrossRef] [PubMed]
3. Shen, L.; Shan, Y.S.; Hu, H.M.; Price, T.J.; Sirohi, B.; Yeh, K.H.; Yang, Y.H.; Sano, T.; Yang, H.K.; Zhang, X.; *et al*. Management of gastric cancer in Asia: Resource stratified guidelines. *Lancet Oncol.* **2013**, *14*, e535–e547. [CrossRef]

4. Lee, K.H.; Lee, H.E.; Cho, S.J.; Cho, Y.J.; Lee, H.S.; Kim, J.H.; Nam, S.Y.; Chang, M.S.; Kim, W.H.; Lee, B.L. Immunohistochemical analysis of cell cycle-related molecules in gastric carcinoma: Prognostic significance, correlation with clinicopathological parameters, proliferation and apoptosis. *Pathobiology* **2008**, *75*, 364–372. [CrossRef] [PubMed]
5. Wu, C.W.; Li, A.F.; Chi, C.W.; Huang, C.L.; Shen, K.H.; Liu, W.Y.; Lin, W. Human gastric cancer kinase profile and prognostic significance of MKK4 kinase. *Am. J. Pathol.* **2000**, *156*, 2007–2015. [CrossRef]
6. Noh, D.Y.; Lee, Y.H.; Kim, S.S.; Kim, Y.I.; Ryu, S.H.; Suh, P.G.; Park, J.G. Elevated content of phospholipase C-γ1 in colorectal cancer tissues. *Cancer* **1994**, *73*, 36–41. [CrossRef]
7. Xie, Z.; Chen, Y.; Liao, E.Y.; Jiang, Y.; Liu, F.Y.; Pennypacker, S.D. Phospholipase C-γ1 is required for the epidermal growth factor receptor-induced squamous cell carcinoma cell mitogenesis. *Biochem. Biophys. Res. Commun.* **2010**, *397*, 296–300. [CrossRef] [PubMed]
8. Tomas, N.M.; Masur, K.; Piecha, J.C.; Niggemann, B.; Zänker, K.S. Akt and phospholipase Cγ are involved in the regulation of growth and migration of MDA-MB-468 breast cancer and SW480 colon cancer cells when cultured with diabetogenic levels of glucose and insulin. *BMC Res. Notes* **2012**, *5*, 214. [CrossRef] [PubMed]
9. Zhuang, L.; Zhang, B.; Zeng, G.; Dai, L.; Qian, H.; Hu, T.; Song, G.; Zhang, B.; Xia, C. Metastasis of human gastric adenocarcinoma partly depends on phosphoinositide-specific phospholipase γ1 expression. *Folia Histochem. Cytobiol.* **2014**, *52*, 178–186. [CrossRef] [PubMed]
10. Cho, H.J.; Baek, K.E.; Nam, I.K.; Park, S.M.; Kim, I.K.; Park, S.H.; Im, M.J.; Ryu, K.J.; Yoo, J.M.; Hong, S.C.; *et al*. PLCγ is required for RhoGDI2-mediated cisplatin resistance in gastric cancer. *Biochem. Biophys. Res. Commun.* **2011**, *414*, 575–580. [CrossRef] [PubMed]
11. Rhee, S.G. Regulation of phosphoinositide-specific phospholipase C. *Annu. Rev. Biochem.* **2001**, *70*, 281–312. [CrossRef] [PubMed]
12. Wells, A.; Grandis, J.R. Phospholipase C-γ1 in tumor progression. *Clin. Exp. Metastasis* **2003**, *20*, 285–290. [CrossRef] [PubMed]
13. Yamaguchi, H.; Condeelis, J. Regulation of the actin cytoskeleton in cancer cell migration and invasion. *Biochim. Biophys. Acta* **2007**, *1773*, 642–652. [CrossRef] [PubMed]
14. Shepard, C.R.; Kassis, J.; Whaley, D.L.; Kim, H.G.; Wells, A. PLC γ contributes to metastasis of *in situ*-occurring mammary and prostate tumors. *Oncogene* **2007**, *26*, 3020–3026. [CrossRef] [PubMed]
15. Kim, M.J.; Chang, J.S.; Park, S.K.; Hwang, J.I.; Ryu, S.H.; Suh, P.G. Direct interaction of SOS1 Ras exchange protein with the SH3 domain of phospholipase C-γ1. *Biochemistry* **2000**, *39*, 8674–8682. [CrossRef] [PubMed]
16. Rebecchi, M.J.; Pentyala, S.N. Structure, function, and control of phosphoinositide-specific phospholipase C. *Physiol. Rev.* **2000**, *80*, 1291–1335. [PubMed]
17. Lang, K.; Niggemann, B.; Zanker, K.S.; Entschladen, F. Signal processing in migrating T24 human bladder carcinoma cells: Role of the autocrine interleukin-8 loop. *Int. J. Cancer* **2002**, *99*, 673–680. [CrossRef] [PubMed]
18. Andruska, N.D.; Zheng, X.; Yang, X.; Mao, C.; Cherian, M.M.; Mahapatra, L.; Helferich, W.G.; Shapiro, D.J. Estrogen receptor α inhibitor activates the unfolded protein response, blocks protein synthesis, and induces tumor regression. *Proc. Natl. Acad. Sci. USA* **2015**, *112*, 4737–4742. [CrossRef] [PubMed]
19. Bingchang, Z.; Fen, W.; Lianzhi, D.; Yanyan, Z.; Song, G.; Tianhui, H.C.; Bing, Z. Lentivirus-mediated *PLCγ1* gene short-hairpin RNA suppresses tumor growth and metastasis of human gastric adenocarcinoma. *Oncotarget* **2015**. submitted for publication.
20. Chang, Y.; Zuka, M.; Perez-Pinera, P.; Astudillo, A.; Mortimer, J.; Berenson, J.R.; Deuel, T.F. Secretion of pleiotrophin stimulates breast cancer progression through remodeling of the tumor microenvironment. *Proc. Natl. Acad. Sci. USA* **2007**, *104*, 10888–10893. [CrossRef] [PubMed]
21. Kiley, S.C.; Clark, K.J.; Duddy, S.K.; Welch, D.R.; Jaken, S. Increased protein kinase Cδ in mammary tumor cells: Relationship to transformtion and metastatic progression. *Oncogene* **1999**, *18*, 6748–6757. [CrossRef] [PubMed]
22. Allen-Petersen, B.L.; Carter, C.J.; Ohm, A.M.; Reyland, M.E. Protein kinase Cδ is required for ErbB2-driven mammary gland tumorigenesis and negatively correlates with prognosis in human breast cancer. *Oncogene* **2014**, *33*, 1306–1315. [CrossRef] [PubMed]
23. McKiernan, E.; O'Brien, K.; Grebenchtchikov, N.; Geurts-Moespot, A.; Sieuwerts, A.M.; Martens, J.W.; Magdolen, V.; Evoy, D.; McDermott, E.; Crown, J.; *et al*. Protein kinase Cδ expression in breast cancer as

measured by real-time PCR, Western blotting and ELISA. *Br. J. Cancer* **2008**, *99*, 1644–1650. [CrossRef] [PubMed]

24. Berardi, D.E.; Flumian, C.; Rodriguez, C.E.; Díaz Bessone, M.I.; Cirigliano, S.M.; Bal de Kier Joffé, E.D.; Fiszman, G.L.; Urtreger, A.J.; Todaro, L.B. PKCδ inhibition impairs mammary cancer proliferative capacity but selects cancer stem cells, involving autophagy. *J. Cell. Biochem.* **2015**. [CrossRef] [PubMed]
25. Marzioni, M.; Alpini, G.; Saccomanno, S.; de Minicis, S.; Glaser, S.; Francis, H.; Trozzi, L.; Venter, J.; Orlando, F.; Fava, G.; *et al*. Endogenous opioids modulate the growth of the biliary tree in the course of cholestasis. *Gastroenterology* **2006**, *130*, 1831–1847. [CrossRef] [PubMed]
26. Monaco, S.; Rusciano, M.R.; Maione, A.S.; Soprano, M.; Gomathinayagam, R.; Todd, L.R.; Campiglia, P.; Salzano, S.; Pastore, L.; Leggiero, E.; *et al*. A novel crosstalk between calcium/calmodulin kinases II and IV regulates cell proliferation in myeloid leukemia cells. *Cell Signal.* **2015**, *27*, 204–214. [CrossRef] [PubMed]
27. Mishra, J.P.; Mishra, S.; Gee, K.; Kumar, A. Differential involvement of calmodulin-dependent protein kinase II-activated AP-1 and c-Jun N-terminal kinase-activated EGR-1 signaling pathways in tumor necrosis factor-α and lipopolysaccharide-induced CD44 expression in human monocytic cells. *J. Biol. Chem.* **2005**, *280*, 26825–26837. [CrossRef] [PubMed]
28. Kim, S.Y.; Ahn, B.H.; Kim, J.; Bae, Y.S.; Kwak, J.Y.; Min, G.; Kwon, T.K.; Chang, J.S.; Lee, Y.H.; Yoon, S.H.; *et al*. Phospholipase C, protein kinase C, Ca^{2+}/calmodulin-dependent protein kinase II, and redox state are involved in epigallocatechin gallate-induced phospholipase D activation in human astroglioma cells. *Eur. J. Biochem.* **2004**, *271*, 3470–3480. [CrossRef] [PubMed]
29. Kahn, E.S.; Kinumi, T.; Tobin, S.L.; Matsumoto, H. Phosrestide-1, a peptide derived from the Drosophila photoreceptor protein phosrestin I, is a potent substrate for Ca^{2+}/calmodulin-dependent protein kinase II from rat brain. *Comp. Biochem. Physiol. B Biochem. Mol. Biol.* **1998**, *119*, 739–746. [CrossRef]
30. Matsumoto, H.; Kurien, B.T.; Takagi, Y.; Kahn, E.S.; Kinumi, T.; Komori, N.; Yamada, T.; Hayashi, F.; Isono, K.; Pak, W.L.; *et al*. Phosrestin I undergoes the earliest light-induced phosphorylation by a calcium/calmodulin-dependent protein kinase in *Drosophila* photoreceptors. *Neuron* **1994**, *12*, 997–1010. [CrossRef]
31. Banerjee, C.; Khatri, P.; Raman, R.; Bhatia, H.; Datta, M.; Mazumder, S. Role of calmodulin-calmodulin kinase II, cAMP/protein kinase A and ERK 1/2 on Aeromonas hydrophila-induced apoptosis of head kidney macrophages. *PLoS Pathog.* **2014**, *10*, e1004018. [CrossRef] [PubMed]
32. Laplante, M.; Sabatini, D.M. mTOR signaling at a glance. *J. Cell Sci.* **2009**, *122*, 3589–3594. [CrossRef] [PubMed]
33. Wendel, H.G.; de Stanchina, E.; Fridman, J.S.; Malina, A.; Ray, S.; Kogan, S.; Cordon-Cardo, C.; Pelletier, J.; Lowe, S.W. Survival signalling by Akt and eIF4E in oncogenesis and cancer therapy. *Nature* **2004**, *428*, 332–337. [CrossRef] [PubMed]
34. Mu, G.G.; Zhang, L.L.; Li, H.Y.; Liao, Y.; Yu, H.G. Thymoquinone pretreatment overcomes the insensitivity and potentiates the antitumor effect of gemcitabine through abrogation of Notch1, PI3K/Akt/mTOR regulated signaling pathways in pancreatic cancer. *Dig. Dis. Sci.* **2015**, *60*, 1067–1080. [CrossRef] [PubMed]
35. Nie, P.; Hu, W.; Zhang, T.; Yang, Y.; Hou, B.; Zou, Z. Synergistic induction of Erlotinib-mediated apoptosis by resveratrol in human non-small-cell lung cancer cells by down-regulating survivin and up-regulating PUMA. *Cell. Physiol. Biochem.* **2015**, *35*, 2255–2271. [CrossRef] [PubMed]
36. Moschella, P.C.; Rao, V.U.; McDermott, P.J.; Kuppuswamy, D. Regulation of mTOR and S6K1 activation by the nPKC isoforms, PKCepsilon and PKCδ, in adult cardiac muscle cells. *J. Mol. Cell. Cardiol.* **2007**, *43*, 754–766. [CrossRef] [PubMed]
37. Choi, Y.H.; Jin, G.Y.; Li, L.C.; Yan, G.H. Inhibition of protein kinase Cδ attenuates allergic airway inflammation through suppression of PI3K/Akt/mTOR/HIF-1 α/VEGF pathway. *PLoS ONE* **2013**, *8*, e81773. [CrossRef] [PubMed]
38. Zeng, G.; Cui, X.; Liu, Z.; Zhao, H.; Zheng, X.; Zhang, B.; Xia, C. Disruption of phosphoinositide-specific phospholipases Cγ1 contributes to extracellular matrix synthesis of human osteoarthritis chondrocytes. *Int. J. Mol. Sci.* **2014**, *15*, 13236–13246. [CrossRef] [PubMed]
39. Cuschieri, J.; Bulger, E.; Garcia, I.; Jelacic, S.; Maier, R.V. Calcium/calmodulin-dependent kinase II is required for platelet-activating factor priming. *Shock* **2005**, *23*, 99–106. [CrossRef] [PubMed]

40. Haneda, M.; Koya, D.; Kikkawa, R. Cellular mechanisms in the development and progression of diabetic nephropathy: Activation of the DAG-PKC-ERK pathway. *Am. J. Kidney Dis.* **2001**, *38*, S178–S181. [CrossRef] [PubMed]
41. Mosmann, T. Rapid colorimetric assay for cellular growth and survival: Application to proliferation and cytotoxicity assays. *J. Immunol. Methods* **1983**, *65*, 55–63. [CrossRef]
42. Yi, T.; Zhuang, L.; Song, G.; Zhang, B.; Li, G.; Hu, T. Akt signaling is associated with the berberine-induced apoptosis of human gastric cancer cells. *Nutr. Cancer* **2015**, *67*, 523–531. [CrossRef] [PubMed]
43. Zheng, X.; Xia, C.; Chen, Z.; Huang, J.; Gao, F.; Li, G.; Zhang, B. Requirement of the phosphatidylinositol 3-kinase/Akt signaling pathway for the effect of nicotine on interleukin-1β-induced chondrocyte apoptosis in a rat model of osteoarthritis. *Biochem. Biophys. Res. Commun.* **2012**, *423*, 606–612. [CrossRef] [PubMed]
44. Ottonello, L.; Bertolotto, M.; Montecucco, F.; Bianchi, G.; Dallegri, F. Delayed apoptosis of human monocytes exposed to immune complexes is reversed by oxaprozin: Role of the Akt/IκB kinase/nuclear factor κB pathway. *Br. J. Pharmacol.* **2009**, *157*, 294–306. [CrossRef] [PubMed]
45. Beloueche-Babari, M.; Peak, J.C.; Jackson, L.E.; Tiet, M.Y.; Leach, M.O.; Eccles, S.A. Changes in choline metabolism as potential biomarkers of phospholipase Cγ1 inhibition in human prostate cancer cells. *Mol. Cancer Ther.* **2009**, *8*, 1305–1311. [CrossRef] [PubMed]
46. Zhang, B.; Xia, C. 12-*O*-Tetradecanoylphorbol-1,3-acetate-induced degradation of protein kinase B via ubiquitin proteasomal pathway depends on its Ser473 phosphorylation in gastric cancer cells. *Folia Histochem. Cytobiol.* **2013**, *51*, 11–17. [CrossRef] [PubMed]
47. Tam, W.L.; Lu, H.; Buikhuisen, J.; Soh, B.S.; Lim, E.; Reinhardt, F.; Wu, Z.J.; Krall, J.A.; Bierie, B.; Guo, W.; *et al*. Protein kinase C α is a central signaling node and therapeutic target for breast cancer stem cells. *Cancer Cell* **2013**, *24*, 347–364. [CrossRef] [PubMed]



© 2015 by the authors; licensee MDPI, Basel, Switzerland. This article is an open access article distributed under the terms and conditions of the Creative Commons by Attribution (CC-BY) license (http://creativecommons.org/licenses/by/4.0/).

International Journal of
Molecular Sciences

MDPI

Article

Overexpression of X-Box Binding Protein 1 (XBP1) Correlates to Poor Prognosis and Up-Regulation of PI3K/mTOR in Human Osteosarcoma

Jielai Yang [1,†], Dongdong Cheng [1,†], Shumin Zhou [2], Bin Zhu [1], Tu Hu [1] and Qingcheng Yang [1,*]

Received: 3 November 2015; Accepted: 26 November 2015; Published: 2 December 2015
Academic Editor: William Chi-shing Cho

1 Department of Orthopedics, Shanghai Jiao Tong University Affiliated Sixth People's Hospital, No. 600, Yishan Road, Shanghai 200233, China; jielai1990@163.com (J.Y.); 18817314717@163.com (D.C.); zhubin.0526@163.com (B.Z.); zzuhutu@163.com (T.H.)
2 Institute of Orthopaedics, Shanghai Jiao Tong University Affiliated Sixth People's Hospital, No. 600, Yishan Road, Shanghai 200233, China; zhoushumin168@hotmail.com
* Correspondence: tjyqc@163.com; Tel.: +86-21-6436-9181
† These authors contributed equally to this work.

Abstract: Increasing evidence demonstrates that dysregulation of XBP1 function contributes to tumorigenesis in some cancers. However, little is known about the role of XBP1 in the progression of osteosarcoma (OS). The expression of XBP1 in OS samples was measured by quantitative RT-PCR and Western blotting assays. Cell cycle analysis and cell counting kit 8 (CCK8) assays were performed to determine the effects of XBP1 expression on cells growth capacity. Cell apoptosis coassay was applied to determine cell survival. The expression of genes affected by XBP1 was examined by quantitative RT-RCR and validated by Western blotting assays. XBP1 was overexpressed in OS clinical samples compared with corresponding non-cancerous tissues. Overexpression of XBP1 was significantly associated with advanced clinical stages, high degree of malignancy and low tumor necrosis rate. Furthermore, hypoxia activated XBP1, and silencing XBP1 significantly enhanced OS cell apoptosis. Knock-down of XBP1 resulted in inhibition of OS growth. Most importantly, knockdown of XBP1 led to down-regulation of PIK3R3 and mTOR. Taken together, XBP1 is up-regulated and has a pro-tumor effect in OS with activation of PI3K/mTOR signaling. Thus, targeting XBP1 may provide a new potential therapeutic method for OS.

Keywords: X-box binding protein 1; growth; survival; PI3K/mTOR signaling; osteosarcoma

1. Introduction

Osteosarcoma (OS) is the most frequent primary bone malignant neoplasm in children and young adults, which is of high propensity of local invasion and distant metastases [1,2]. Despite current advances in treatments, comprising chemotherapy and wide excision of tumors, the recurrence rate of patients with localized or metastasis disease at diagnosis is high [3,4]. Though the survival rate has increased approximately fourfold from 1960s to 1980s, it remains almost unchanged during the recent three decades [5]. Thus, new treatment is eagerly needed.

Tumor cells can induce a series of adaptive response signaling pathways to survival in the condition of deprivation of oxygen, ATP, or other essential nutrients [6]. One such adaptive pathway is the endoplasmic reticulum (ER) stress response. Inositol-requiring enzyme-1α (IRE1α)/X-box binding protein 1 (XBP1) axis, a vital branch of ER stress response, exists in both invertebrate and vertebrate cells [7,8]. Human X-box binding protein 1 exists in two different forms, spliced (XBP1s) and un-spliced (XBP1u) isoforms [9], which is involved in a variety of human physiological and pathologic processes such as lipogenesis [10,11], adipogenesis [12], atherosclerosis [13], and ischemia [14].

Previous studies reported that XBP1 was activated in various human cancers, including both mesenchymal and epithelial cancers [15–18]. In multiple myeloma (MM), XBP1s overexpression in bone marrow stromal cells is critical for myeloma cell growth and osteoclast formation, and the increased ratio of XBP1s to XBP1u predicts poor outcome of myeloma patients [19,20]. In breast cancer, XBP1 was activated and correlated with poor prognosis in triple-negative breast cancer patients [18]. As for the biological mechanisms, the hypoxia-inducible factor 1 (HIF-1)/Vascular endothelial growth factor A (VEGF-A) signaling was most investigated. However, recent researches in human endothelial cells suggest a new mechanism that XBP1 is involved. Martin *et al.* observed that XBP1 protected endothelial cells from oxidative stress through interaction with histone deacetylase 3, which form a complex with Akt1 and mTOR [21]. Zeng *et al.* indicated that VEGF-induced XBP1s regulated endothelial cell growth in a PI3K/Akt/GSK3β/β-catenin/E2F2–dependent manner [22]. Though these findings were not reported in tumor cells, it provided us new perspectives to investigate cancers.

The role of XBP1 in OS progression is unknown. In this study, we found that the overexpression of XBP1 in human OS. Moreover, we find that the expression levels of XBP1 correlated with clinical stages in a cohort of OS patients. We also discovered that knockdown of XBP1 resulted in growth inhibition but promoted apoptosis of OS cell lines. Most importantly, we found that PI3K/mTOR signaling was involved in the process of XBP1-regulated OS progression, which suggests a novel mechanism of XBP1's role in OS. Therefore, XBP1 may be a novel target for OS treatment.

2. Result

2.1. XBP1 Expression Was Up-Regulated in OS Clinical Samples and Associated with the Progress of OS

Previous studies showed that XBP1 was overexpressed and correlated with clinical progress in multiple cancers, including the myeloma and breast cancer [18,19]. To investigate whether XBP1 was overexpressed and involved in the progression of OS, we detected the mRNA expression of XBP1 (both un-spliced and spliced) in 20 pairs of human OS and their corresponding normal tissues. The correlation between XBP1 expression and the data of OS patients was shown in Table 1. The XBP1 mRNA expression was not correlated to age, gender, anatomic location, or tumor size statistically significant. However, there was a significant correlation of XBP1 expression with clinical stage ($p < 0.01$), degree of malignancy ($p < 0.05$), and tumor necrosis rate ($p < 0.05$). In addition, XBP1u and XBP1s were overexpressed, respectively, in 65% and 70% of OS tissues (Figure 1a), both isoforms unregulated almost twofold (Figure 1c) in OS compared with non-cancerous tissues. However, the ratios of XBP1s to XBP1u of the two groups were similar (Figure 1e). We also observed a significant increase of XBP1 mRNA in advanced clinical stages compared with early clinical stage (Figure 1d). More importantly, we extracted proteins from eight fresh OS specimens and their corresponding non-cancerous tissues, and observed that XBP1 protein was up-regulated in all of the eight OS tissues compared with their corresponding non-cancerous tissues (Figure 1b). Taken together, these results indicate that XBP1 is up-regulated and potentially had a pivotal role in the growth and survival of OS.

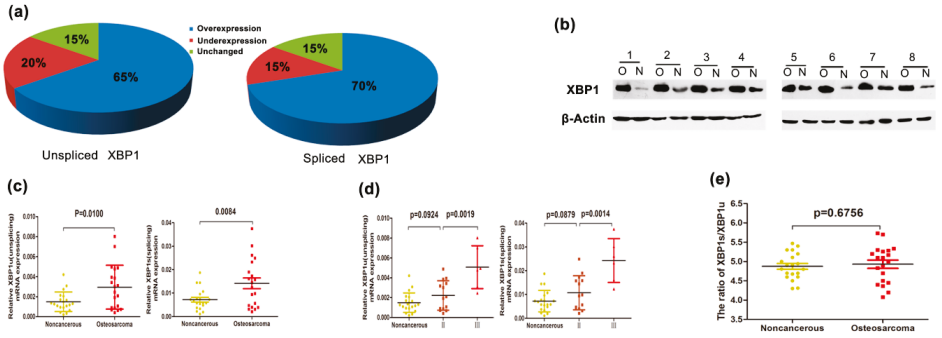

Figure 1. XBP1 is up-regulated in OS and correlated with the advanced clinical stage. (**a**) Relative expression of XBP1u and XBP1s were detected by RT-PCR in 20 pairs of OS clinical samples and their matched noncancerous tissues. The up-regulated XBP1u and XBP1s were, respectively, observed in 65% and 70% OS samples compared with the corresponding non-cancerous tissues; (**b**) XBP1 was overexpressed in OS clinical samples; Western blot tests showed XBP1 protein was higher in eight OS samples than their corresponding non-cancerous tissues. O: osteosarcoma; N: noncancerous; (**c**) Up-regulation of XBP1u and XBP1s was observed in 20 pairs OS comparing to their corresponding noncancerous tissue; (**d**) XBP1u and XBP1s mRNA expression in different clinical stages of OS; (**e**) The ratio of XBP1u to XBP1s. The dots in different color and sharp were used to differentiate different clinical stage. (Yellow for noncancerous tissue, Gray for stage II, Red for stage III). The patients were staged in accordance with the Ennecking musculoskeletal tumor staging system. Error bars represent mean ± s.d. of triplicate experiments. The statistical analysis was performed using paired *t*-test (**c**,**e**) and Student's *t*-test (**d**).

Table 1. Relationship between XBP1 mRNA expression and their clinicopathologic parameters in 20 of osteosarcoma.

Parameters	*N* (%)	Median Expression of XBP1u		Median Expression of XBP1s	
		Mean ± s.d.	*p*-Value	Mean ± s.d.	*p*-Value
Age (years)					
<20	12 (60%)	0.0027 ± 0.0019	0.5053	0.0126 ± 0.0085	0.4340
≥20	8 (40%)	0.0034 ± 0.0026		0.0164 ± 0.0127	
Gender					
Male	14 (70%)	0.0032 ± 0.0020	0.1031	0.0166 ± 0.0100	0.0993
Female	6 (30%)	0.0016 ± 0.0016		0.0084 ± 0.0091	
Anatomic location					
Tibia/Femur	14 (70%)	0.0027 ± 0.0021	0.5421	0.0132 ± 0.0099	0.5277
Elsewhere	6 (30%)	0.0034 ± 0.0025		0.0164 ± 0.0114	
Clinical stage					
II	14 (70%)	0.0020 ± 0.0015	0.0019 **	0.0098 ± 0.0073	0.0014 **
III	6 (30%)	0.0051 ± 0.0022		0.0243 ± 0.0092	
Tumor size (cm^3)					
<50	10 (50%)	0.0033 ± 0.0025	0.4580	0.0117 ± 0.0086	0.3094
≥50	10 (50%)	0.0025 ± 0.0018		0.0165 ± 0.0115	
Degree of malignancy					
Low	9 (45%)	0.0018 ± 0.0015	0.0109 *	0.0091 ± 0.0076	0.0099 **
High	11 (55%)	0.0042 ± 0.0022		0.0203 ± 0.0098	
Tumor necrosis rate (%)					
<90	11 (55%)	0.0035 ± 0.0025	0.0450 *	0.0192 ± 0.0103	0.0103 *
≥90	9 (45%)	0.0015 ± 0.0012		0.0079 ± 0.0060	

Clinical stage is classified by Ennecking-Musculoskeletal Tumor Staging System. *p*-value represents the probability from a Student's *t*-test for XBP1 mRNA expression between variable subgroups. * $p < 0.05$, ** $p < 0.01$, which was considered to have a significant difference.

2.2. Knockdown of XBP1-Inhibited OS Cell Proliferation Following Hypoxic Treatment

To explore the potential role of XBP1 in OS tumorigenesis, we knocked down XBP1 by siRNA that targets both isoforms of XBP1. We performed CCK-8 assays, and observed that after knockdown of XBP1, the viabilities of MG63 and U2OS cells decreased (Figure 2a,b). In addition, knockdown of XBP1 delayed the cell cycle progression, both MG63 (Figure 2c,e) and U2OS cell (Figure 2d,f) showing G2/M phase arrest. To summarize, these results indicate that XBP1 is required for OS cell growth.

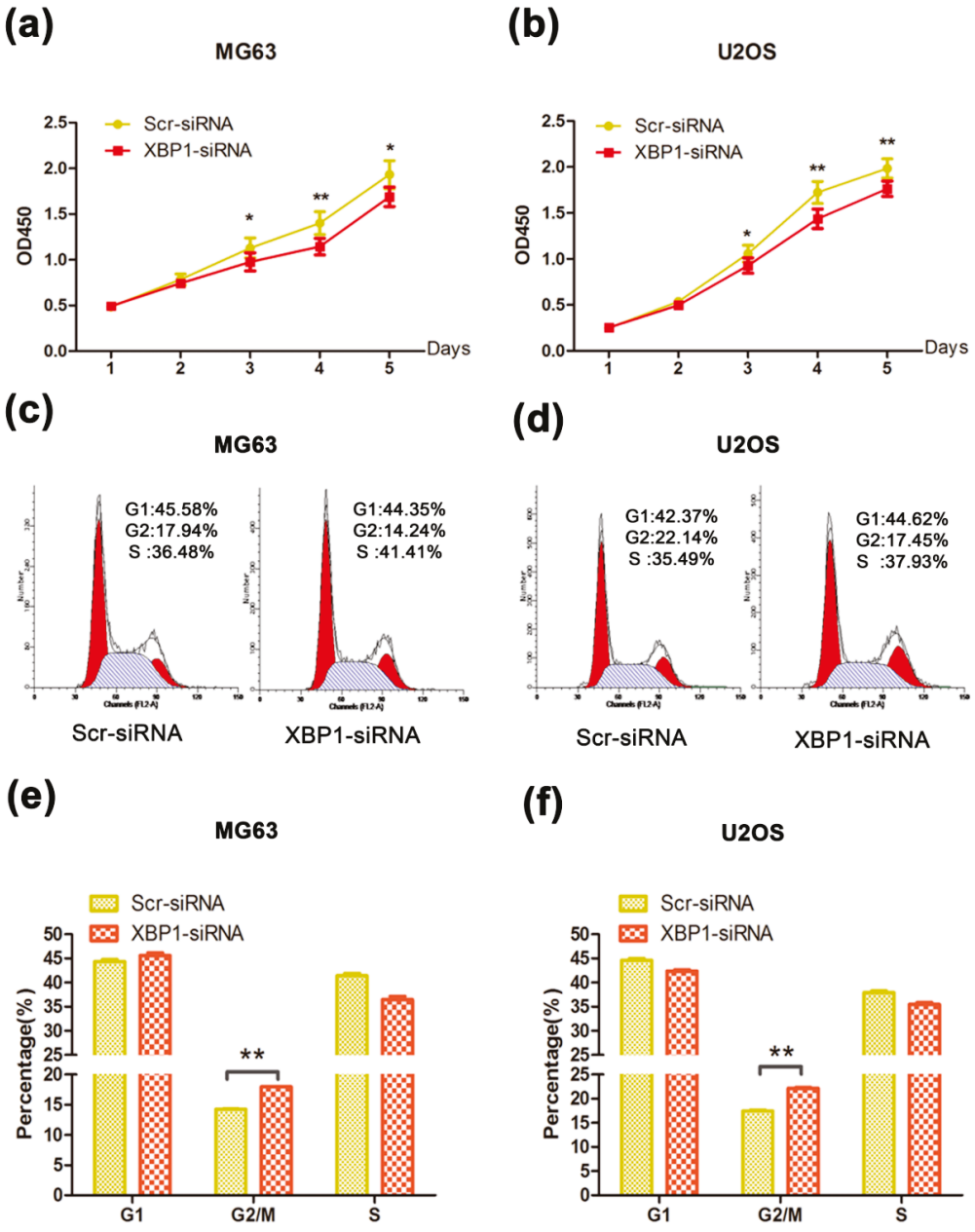

Figure 2. (**a**,**b**) Knockdown of XBP1 inhibited the growth and proliferation in OS cells. The viability of MG63 and U2OS was examined by CCK8 assay at different time points as indicated; (**c**,**d**) Flow cytometry of cell distribution after transfection; (**e**,**f**) Histograms of each phase in cell cycle of MG63 and U2OS. Silencing XBP1 increased cell proportion of G2/M phrase in MG63 and U2OS cells. Data represent mean ± s.d. Each performed in triplicate. * $p < 0.05$, ** $p < 0.01$, by Student's *t*-test. Transfected cells was treated in the hypoxia (24 h) chamber before the assays.

2.3. Silencing XBP1-Attenuated OS Cells' Survival under Both Normoxic and Hypoxic Condition

To identify whether XBP1 was activated in OS cells under hypoxic condition, we treated MG63 and U2OS cells with hypoxia (1% O_2) condition. The XBP1 mRNA expression increased significantly in MG63 and U20S cells after 24 h hypoxia (Figure 3a,c). We next examined the protein levels of XBP1 after hypoxia (1% O_2) treatment for 24 h and 48 h. In consistent with the mRNA levels, protein levels of XBP1 elevated significantly by hypoxia 24 h, but subsequently decreased in 48 h (Figure 3b,d), which indicated that the activation of XBP1 reach to a peak for about 24 h hypoxic treatment.

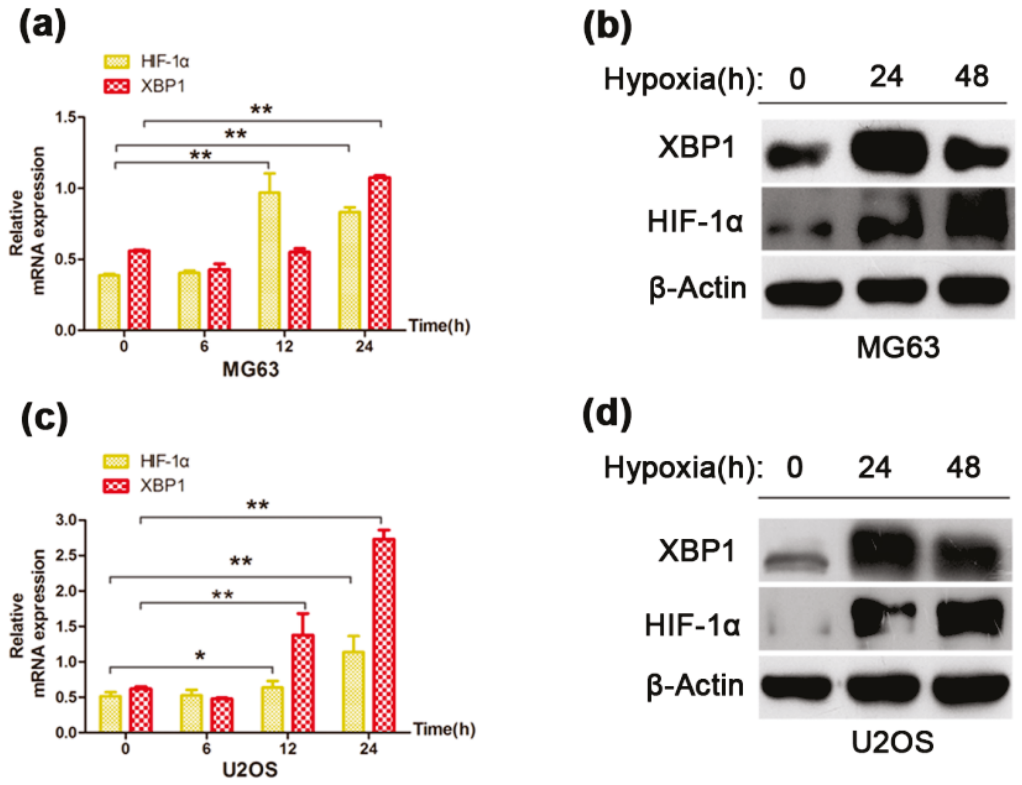

Figure 3. The up-regulation of XBP1 under hypoxia condition in OS cells. (**a**,**c**) The mRNA expression of XBP1 and HIF-1α in MG63 and U2OS cells for indicated h of hypoxia (1% O_2) treatment; (**b**,**d**) The protein expression of XBP1 and HIF-1α in MG63 and U2OS cells for indicated h of hypoxia treatment. HIF-1α expression demonstrated specificity of treatment to hypoxia. β-Actin was used as an internal control. Error bars represent mean ± s.d. of triplicate experiments.* $p < 0.05$, ** $p < 0.01$ by Student's *t*-test.

Next, to determine the role of XBP1 in cell survival under normoxic and hypoxic conditions, we compared the apoptotic rates between the control group and XBP1-knockdown group. Under normoxic condition, silencing XBP1 promoted cell apoptosis in OS cells, but the effect was mild (Figure 4a,c). After 24 h of hypoxia, the apoptotic rate increased significantly in two OS cells and the pro-apoptosis effect was more obvious in the XBP1-knockdown group (Figure 4b,d). In general, these data suggest that XBP1 is activated under hypoxic conditions, and this activation is essential for OS cell survival in hypoxic conditions.

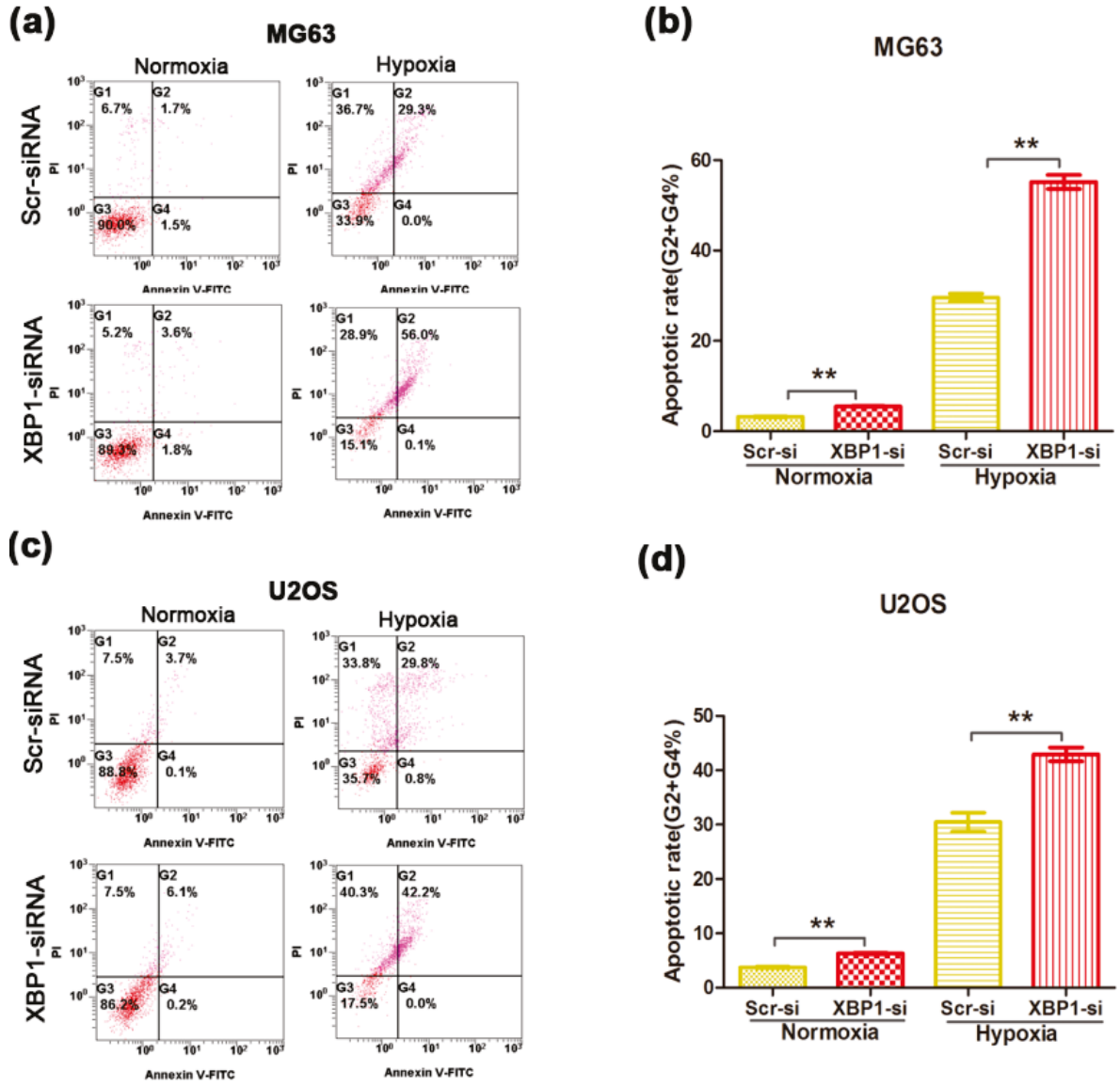

Figure 4. Knockdown of XBP1 increased the apoptosis rate of OS cells under both normoxic and hypoxic condition. (**a**,**b**) Comparison of apoptosis between Scramble and XBP1-knockdown group in MG63 under normoxic and hypoxic condition; (**c**,**d**) Comparison of apoptosis between Scramble and XBP1-knockdown group in U2OS under normoxic and hypoxic condition. The data represent mean ± s.d. of triplicate (**b**,**d**). ** $p < 0.01$ by Student's *t*-test. The cells were transfected with XBP1 siRNA (50 nM) for 48 h, and treated with or without hypoxia (1% O_2) for 24 h. All the apoptotic rates were measured by using the fluorescein isothiocyanate Annexin V apoptosis assay. PI, propidium iodide.

2.4. Knockdown of XBP1 Down-Regulated the Expression of PIK3R3/mTOR in OS Cells

To investigate a potential mechanism by which XBP1 affects the proliferation and apoptosis of OS cells, a series of pathways functioning in the stressful condition were detected. After some initial screening work, we found that knockdown of XBP1 decreased the mRNA levels of PIK3R3 and mTOR in MG63 (Figure 5a) and U2OS cells (Figure 5b) under both normoxic and hypoxic conditions. In addition, we detected the protein expression of PIK3R3 and mTOR after knockdown of XBP1. The result was consistent with those of mRNA expression (Figure 5c,d). Taken together, these data show that the expression of PIK3R3 and mTOR was affected by XBP1 in OS cells, which indicated that XBP1 might play a crucial role in the growth and apoptosis by influencing PI3K/mTOR signaling.

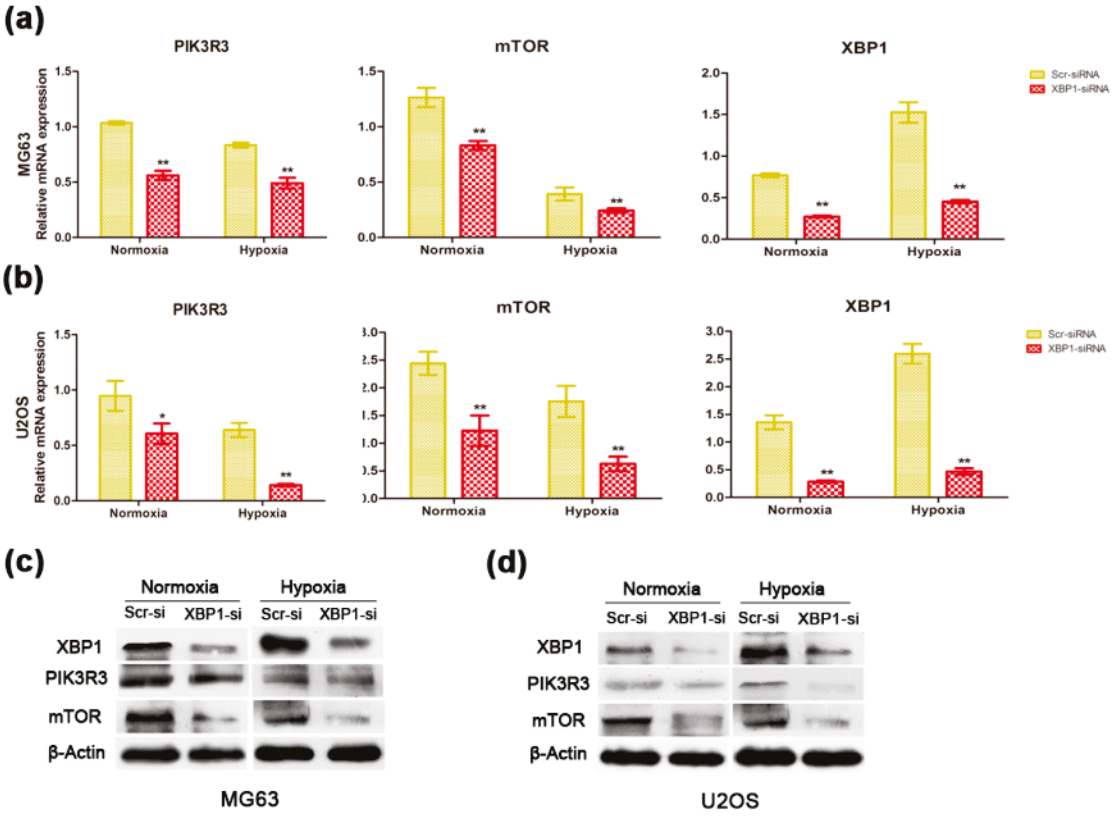

Figure 5. Down-regulation of PIK3R3 and mTOR after inhibiting the expression of XBP1. (**a**,**b**) The mRNA expression of PIK3R3, mTOR, and XBP1 between the scrambled and XBP1-knockdown group under both normoxic and hypoxic condition in MG63 and U2OS cells; (**c**,**d**) The protein expression of PIK3R3, mTOR, and XBP1 between the scrambled and XBP1-knockdown group under both normoxic and hypoxic condition in MG63 and U2OS cells. Transfection efficacy of XBP1-siRNA was confirmed by qRT-PCR and Western blot assays. The data are representative of three independent experiments. Error bars represent mean ± s.d. * $p < 0.05$, ** $p < 0.01$ by Student's *t*-test.

3. Discussion

Accumulating evidence has demonstrated that ER-stress plays an indispensable role for tumor cells growth and survival under various stressors [23,24]. The IRE1α-XBP1 pathway is one of the most important ER-stress response pathways that are implicated in tumor growth, metastatic progression, and chemo-resistance [25]. In previous studies, activation of XBP1 was reported and correlated with clinical outcome in breast cancer [18,26]. Tumor growth and survival was severely compromised by blocking the expression of XBP1 in human pancreatic adenocarcinomas under hypoxic condition [27]. Multiple studies had demonstrated that IRE1α-XBP1 pathway is implicated in the pathogenesis of MM and XBP1 is a promising therapeutic target in treating MM [28–30]. Furthermore, XBP1 was involved in the progression of chemotherapy resistance in MM [31], and a recent study got the opposite result [32], suggesting the complexity of its role in regulating this function.

In the present study, we showed that XBP1 was significantly elevated in OS clinical samples at both mRNA and protein levels. The mRNA level of XBP1 correlated with advanced clinical stages, high degree of malignancy, and low tumor necrosis rate in OS patients. However, the ratio of XBP1s to XBP1u was similar between OS tissues and their matched non-cancerous ones (Figure 1e), which was different from previous results from MM [19] and breast cancer [18]. There are several possible reasons explaining the result: firstly, XBP1u and XBP1s might function in a synchronous effect in OS, which indicating a new mechanism for ER activity. For most studies, XBP1s or XBP1u was solely investigated regarding the activation of the IRE1 pathway and the XBP1s/XBP1u ratio was

not regarded as an essential index. Secondly, the sample size may be a factor resulting in the different result. Previous studies of MM and breast cancer analyzed the ratio in a huge population sample, thus, more comprehensive clinical studies were required to get a more convincing outcome in OS. Taken together, the clinical results suggested that XBP1 might be involved in the growth of OS.

XBP1 was known to be activated under stressful conditions in various cancer cells [33,34]. Our *in vitro* data showed that knockdown of XBP1 resulted in a moderate inhibition of cellular growth and a mild apoptotic effect in OS cells under normoxic condition. However, when exposed to hypoxic conditions, XBP1 knockdown significantly promoted the apoptotic rate, which was inconsistent with elevated expression of XBP1 for hypoxia treatment. Though the transfection efficacy of siRNA varied in two OS cells, 70% in MG63 cells and 80% in U2OS cells, the effect of XBP1 on the growth and survival of OS was similar and was enhanced by hypoxia condition. These findings suggest that XBP1 is required for OS growth and survival under hypoxia, which was similar with previous studies in fibrosarcoma [16]. Further *in vivo* study is needed to validate the role of XBP1 in OS on a mouse model.

Though the importance of XBP1 has been indicated by studies with various cancer cells, the detailed mechanism underlying the importance remains largely unknown. The most widely accepted target of XBP1 was CHOP, which plays a crucial role in the apoptosis pathway [35]. For the study of MM, knockdown of XBP1 greatly compromised the expression of VCAM-1, IL-6, and RANKL in BM stromal cells [17], which were key players in supporting MM cell growth and destroying the bone. For breast cancer, XBP1 promoted triple-negative breast cancer by regulating HIF-1α pathway [18]. For human glioma, inhibition of IRE1α resulted in down-regulating of VEGF-A, IL-1β, IL-6, and IL-8 [36]. Other cancers, like liver and colon cancers [37,38], were also reported to be with activation of XBP1, however, the specific mechanisms were seldom explored.

Increasing evidence indicates that XBP1 has critical roles in the tumorigenesis and progression of various cancer cells [39,40]. Romero-Ramirez *et al.* observed that XBP1 was crucial for tumor cell survival under severe hypoxic condition, but it was activated in a HIF-1α-independent manner [16]. To understand the mechanism underlying the promoting effect of XBP1 in OS, we focused on pathways that are activated by stressful conditions. Thus, the HIF-1 signaling pathway, which has been reported to be activated in fibrosarcoma [16] and breast cancer [18], and has been proposed to be a general stress responsive pathway [41,42], was investigated. However, knockdown of XBP1 result in slightly down-regulation of HIF targets, like VEGF-A (Figure S1). We then considered PI3K/mTOR signaling pathways, which played an important role in cell growth and survival [43,44]. Furthermore, recent studies in endothelial cells showed that XBP1s may regulate cell proliferation and growth in a PI3K/Akt/GSK3β/β-catenin/E2F2-dependent manner [22]. Martin *et al.* [21] showed that XBP1, interacting with HDAC3, exert a protective effect on oxidative stress by up-regulating mTORC2-dependent Akt1 phosphorylation and Nrf2-mediated HO-1 expression. In this report, we observed that the expression of PIK3R3 and mTOR was down-regulated when inhibiting XBP1 expression, which was consistent with previous studies in endothelial cells [21,22]. Our results suggest that XBP1 exerts its effect on OS probably by influencing PI3K/mTOR signaling, which could be a novel mechanism by which XBP1 promotes cancer progression. However, the exact mechanism that XBP1 is required for the activation of PI3K/mTOR blurs, and further investigation is warranted.

4. Materials and Methods

4.1. Cell Culture and Hypoxia Treatment

Two OS cell lines (U2OS and MG63) were maintained at 37 °C in a humidified air atmosphere containing 5% CO_2 in RPMI-1640 and DMEM media respectively. 10% fetal bovine serum (Biowest, Kansas, MO, USA), 100 U/mL penicillin, and 100 mg/mL streptomycin (Sigma-Aldrich, St. Louis, MO, USA) were added in the media. For hypoxia experiments, cells were treated at 60% to 70% confluence and maintained in a hypoxic chamber with 1% O_2.

4.2. Human OS Samples

From 2014 to 2015, the 20 paired human OS clinical samples, including 20 OS samples and 20 non-cancerous tissues, were collected at the time of surgery at the department of bone oncology. Once the tumor was resected, specimens were selected, and put into tiny tubes. The tubes were then frozen in liquid nitrogen and stored at −80 °C in the refrigerator for a long period. All procedures involving human specimens were performed with written informed consent according to the Declaration of Helsinki and the research was approved by the Ethics Committee of the Sixth Peoples' Hospital of Shanghai Jiao Tong University.

4.3. RNA Isolation and qRT-PCR Assays

Total RNA of human tissue samples and cultured cells was extracted and quantified with Trizol Kit (Invitrogen, Carlsbad, CA, USA) and Nanodrop 2000 (Thermo Fisher Scientific, Waltham, MA, USA), respectively, according to the manufacturer's protocol. The PrimeScript RT Reagent kit (TaKaRa, Shiga, Japan) was used to synthesize the first-strand cDNA. RT-PCR was performed with SYBR Green premix Ex Taq (TaKaRa). Sequences of used primers were detailed in Table S1. β-Actin was used as internal control.

4.4. siRNA Transfection

The siRNAs were synthesized by BioMics. The cells were transfected with siRNA using Lipofectamine 2000 Reagent (invitrogen) following the manufacturer's protocol. The sequence of siRNA targeting XBP1 was 5′-CAACCCUGAAUUCAUUGUCUdTdT-3′. Transfection with the final concentration of 50 nM siRNA was conducted when the cell density was approximately 40% in six-well plates.

4.5. Cell Proliferation and Cell Cycle Analysis

Cell Counting Kit-8 (CCK-8) Dojindo Molecular Technologies, Inc, Kumamoto, Japan) was used to measure the cell viability. In short, transfected cells previously treated in the hypoxia (24 h) chamber were seeded at the density of 3000 or 2500 per well in 96-well microplates. 10 μL of CCK8 solution and 100 μL DMEM was added to each well and incubated for 2 h. The optical density was detected at a wavelength of 450 nm by microplate reader (Model 680, Bio-Rad Laboratories, Hercules, CA, USA). This procedure was repeated once a day for five days. For cell cycle assay, transfected cells in the hypoxia chamber (24 h) were fixed in 70% ethanol at −20 °C in the refrigerator for 12–24 h. After that, cells were treated with staining solution, which containing 50 μg/mL propidium iodide (PI) (Biolegend, San Diego, CA, USA) and 50 μg/mL RNase A (BD LSRII, San Jose, CA, USA). Each experiment was repeated three times.

4.6. Cell Apoptosis Analysis

For the apoptosis analysis, 48 h post transfection, hypoxia-treated cells were placed into a hypoxia chamber for 24 h, normoxic cells were plated at the same density and maintained in 37 °C incubator. The fluorescein isothiocyanate Annexin V Apoptosis Detection kit I (BD Pharmingen, San Diego, CA, USA) was used. Briefly, the cells were collected and centrifuged at 2000× g for 5 min. The cells were then suspended in 500 μL binding buffer, supplemented with 5 μL Annexin V and 5 μL propidium iodide (PI), for 15 min of dark treatment at the room temperature. The flow cytometry (FC500 MPL, Beckman Coulter, Brea, CA, USA) was used to analyze the samples.

4.7. Western Blotting Analysis

The procedures were performed as described previously [18]. Briefly, total protein of cells and fresh tissues were isolated and separated by 6%–8% SDS-PAGE gels. Following the standard procedure, the blocking proteins in the nitrocellulose filter membranes were incubated

with primary antibodies against the following antigens: XBP1 (Santa Cruz Biotechnology, Dallas, TX, USA), HIF1α (Santa Cruz Biotechnology), PIK3R3 (Abgent, San Diego, CA, USA), mTOR (Abgent), β-Actin (Sigma-Aldrich, New York, NY, USA). The secondary antibody was horseradish peroxidase-conjugated anti-rabbit IgG (Sigma-Aldrich). SuperSignal West Femto Maximun Sensitivity Substrate (Thermo Fisher Scientific, Waltham, MA, USA) was used in the subsequent visualization.

4.8. Statistical Analysis

Data was imaged with GraphPad Prism 5 software (Graphpad Software, Inc., La Jolla, CA, USA). Quantitative variables were presented as means ± standard deviation. A two-tailed Student's *t*-test was used to compare the differences between two groups. The SPSS version 16.0 (SPSS, Inc., Chicago, IL, USA) software was used to analyze the data. $p < 0.05$ was considered statistically significant different.

5. Conclusions

We demonstrated for the first time that XBP1 was overexpressed in human OS tissues. High levels of XBP1 correlated with advanced clinical stages, high degree of malignancy, and low tumor necrosis rate in OS. In culture OS cells, knockdown of XBP1 inhibited cell growth and survival. More importantly, XBP1 expression correlates to up-regulation of PI3K/mTOR, a signaling pathway critical for cell growth and proliferation. These data indicate that XBP1 may be a prognostic biomarker and therapeutic target for OS.

Supplementary Materials: Supplementary materials can be found at http://www.mdpi.com/1422-0067/16/12/26123/s1.

Acknowledgments: We thank Jingjun Li for providing writing and language help in this article and thank Mingxia Yan for providing technical assistance during the research.

Author Contributions: Jielai Yang and Qingcheng Yang conceived and designed the experiments; Jielai Yang and Dongdong Cheng performed the experiments; Jielai Yang, Shumin Zhou and Dongdong Cheng analyzed the data; Bin Zhu and Tu Hu contributed reagents/materials/analysis tools; Jielai Yang and Qingcheng Yang wrote the paper. Authorship must be limited to those who have contributed substantially to the work reported.

Conflicts of Interest: The authors declare no conflict of interest.

References

1. Ando, K.; Heymann, M.F.; Stresing, V.; Mori, K.; Rédini, F.; Heymann, D. Current therapeutic strategies and novel approaches in osteosarcoma. *Cancers* **2013**, *5*, 591–616. [CrossRef] [PubMed]
2. Raymond, A.K.; Jaffe, N. Osteosarcoma multidisciplinary approach to the management from the pathologist's perspective. *Pediatr. Adolesc. Osteosarcoma* **2009**, *152*, 63–84.
3. Luetke, A.; Meyers, P.A.; Lewis, I.; Juergens, H. Osteosarcoma treatment–where do we stand? A state of the art review. *Cancer Treat. Rev.* **2014**, *40*, 523–532. [CrossRef] [PubMed]
4. O'Day, K.; Gorlick, R. Novel therapeutic agents for osteosarcoma. *Expert Rev. Anticancer Ther.* **2009**, *9*, 511–523. [CrossRef] [PubMed]
5. Allison, D.C.; Carney, S.C.; Ahlmann, E.R.; Hendifar, A.; Chawla, S.; Fedenko, A.; Angeles, C.; Menendez, L.R. A meta-analysis of osteosarcoma outcomes in the modern medical era. *Sarcoma* **2012**, *2012*, 704872. [CrossRef] [PubMed]
6. Hanahan, D.; Weinberg, R.A. Hallmarks of cancer: The next generation. *Cell* **2011**, *144*, 646–674. [CrossRef] [PubMed]
7. Uemura, A.; Oku, M.; Mori, K.; Yoshida, H. Unconventional splicing of XBP1 mRNA occurs in the cytoplasm during the mammalian unfolded protein response. *J. Cell Sci.* **2009**, *122*, 2877–2886. [CrossRef] [PubMed]

8. Lee, K.; Tirasophon, W.; Shen, X.; Michalak, M.; Prywes, R.; Okada, T.; Yoshida, H.; Mori, K.; Kaufman, R.J. IRE1-mediated unconventional mRNA splicing and S2P-mediated ATF6 cleavage merge to regulate XBP1 in signaling the unfolded protein response. *Genes Dev.* **2002**, *16*, 452–466. [CrossRef] [PubMed]
9. Yoshida, H. ER stress and diseases. *FEBS J.* **2007**, *274*, 630–658. [CrossRef] [PubMed]
10. Fang, D.L.; Wan, Y.; Shen, W.; Cao, J.; Sun, Z.X.; Yu, H.H.; Zhang, Q.; Cheng, W.H.; Chen, J.; Ning, B. Endoplasmic reticulum stress leads to lipid accumulation through upregulation of SREBP-1c in normal hepatic and hepatoma cells. *Mol. Cell. Biochem.* **2013**, *381*, 127–137. [CrossRef] [PubMed]
11. Ning, J.; Hong, T.; Ward, A.; Pi, J.; Liu, Z.; Liu, H.-Y.; Cao, W. Constitutive role for IRE1α-XBP1 signaling pathway in the insulin-mediated hepatic lipogenic program. *Endocrinology* **2011**, *152*, 2247–2255. [CrossRef] [PubMed]
12. Sha, H.; He, Y.; Chen, H.; Wang, C.; Zenno, A.; Shi, H.; Yang, X.; Zhang, X.; Qi, L. The IRE1α-XBP1 pathway of the unfolded protein response is required for adipogenesis. *Cell Metab.* **2009**, *9*, 556–564. [CrossRef] [PubMed]
13. Martinet, W.; Croons, V.; Timmermans, J.P.; de Meyer, G. Nitric oxide selectively depletes macrophages in atherosclerotic plaques via induction of endoplasmic reticulum stress. *Br. J. Pharmacol.* **2007**, *152*, 493–500. [CrossRef] [PubMed]
14. Zeng, L.; Zampetaki, A.; Margariti, A.; Pepe, A.E.; Alam, S.; Martin, D.; Xiao, Q.; Wang, W.; Jin, Z.-G.; Cockerill, G.; *et al*. Sustained activation of XBP1 splicing leads to endothelial apoptosis and atherosclerosis development in response to disturbed flow. *Proc. Natl. Acad. Sci. USA* **2009**, *106*, 8326–8331. [CrossRef] [PubMed]
15. Breckenridge, D.G.; Germain, M.; Mathai, J.P.; Nguyen, M.; Shore, G.C. Regulation of apoptosis by endoplasmic reticulum pathways. *Oncogene* **2003**, *22*, 8608–8618. [CrossRef] [PubMed]
16. Romero-Ramirez, L.; Cao, H.; Nelson, D.; Hammond, E.; Lee, A.-H.; Yoshida, H.; Mori, K.; Glimcher, L.H.; Denko, N.C.; Giaccia, A.J.; *et al*. XBP1 is essential for survival under hypoxic conditions and is required for tumor growth. *Cancer Res.* **2004**, *64*, 5943–5947.
17. Xu, G.; Liu, K.; Anderson, J.; Patrene, K.; Lentzsch, S.; Roodman, G.D.; Ouyang, H. Expression of XBP1s in bone marrow stromal cells is critical for myeloma cell growth and osteoclast formation. *Blood* **2012**, *119*, 4205–4214. [CrossRef] [PubMed]
18. Chen, X.; Iliopoulos, D.; Zhang, Q.; Tang, Q.; Greenblatt, M.B.; Hatziapostolou, M.; Lim, E.; Tam, W.L.; Ni, M.; Chen, Y.; *et al*. XBP1 promotes triple-negative breast cancer by controlling the HIF1alpha pathway. *Nature* **2014**, *508*, 103–107. [CrossRef] [PubMed]
19. Gambella, M.; Rocci, A.; Passera, R.; Gay, F.; Omedè, P.; Crippa, C.; Corradini, P.; Romano, A.; Rossi, D.; Ladetto, M.; *et al*. High XBP1 expression is a marker of better outcome in multiple myeloma patients treated with bortezomib. *Haematologica* **2014**, *99*, 14–16. [CrossRef] [PubMed]
20. Vincenz, L.; Jager, R.; O'Dwyer, M.; Samali, A. Endoplasmic reticulum stress and the unfolded protein response: targeting the Achilles heel of multiple myeloma. *Mol. Cancer Ther.* **2013**, *12*, 831–843. [CrossRef] [PubMed]
21. Martin, D.; Li, Y.; Yang, J.; Wang, G.; Margariti, A.; Jiang, Z.; Yu, H.; Zampetaki, A.; Hu, Y.; Xu, Q.; *et al*. Unspliced X-box-binding protein 1 (XBP1) protects endothelial cells from oxidative stress through interaction with histone deacetylase 3. *J. Biol. Chem.* **2014**, *289*, 30625–30634. [CrossRef] [PubMed]
22. Zeng, L.; Xiao, Q.; Chen, M.; Margariti, A.; Martin, D.; Ivetic, A.; Xu, H.; Mason, J.; Wang, W.; Cockerill, G.; *et al*. Vascular endothelial cell growth-activated XBP1 splicing in endothelial cells is crucial for angiogenesis. *Circulation* **2013**, *127*, 1712–1722. [CrossRef] [PubMed]
23. Clarke, H.J.; Chambers, J.E.; Liniker, E.; Marciniak, S.J. Endoplasmic reticulum stress in malignancy. *Cancer Cell* **2014**, *25*, 563–573. [CrossRef] [PubMed]
24. Koumenis, C. ER stress, hypoxia tolerance and tumor progression. *Curr. Mol. Med.* **2006**, *6*, 55–69. [CrossRef] [PubMed]
25. Shajahan, A.N.; Riggins, R.B.; Clarke, R. The role of X-box binding protein-1 in tumorigenicity. *Drug News Perspect.* **2009**, *22*, 241–246. [CrossRef] [PubMed]
26. Davies, M.P.; Barraclough, D.L.; Stewart, C.; Joyce, K.A.; Eccles, R.M.; Barraclough, R.; Rudland, P.S.; Sibson, D.R. Expression and splicing of the unfolded protein response gene XBP-1 are significantly associated with clinical outcome of endocrine-treated breast cancer. *Int. J. Cancer* **2008**, *123*, 85–88. [CrossRef] [PubMed]

27. Romero-Ramirez, L.; Cao, H.; Regalado, M.P.; Kambham, N.; Siemann, D.; Kim, J.J.; Le, Q.T.; Koong, A.C. X box-binding protein 1 regulates angiogenesis in human pancreatic adenocarcinomas. *Transl. Oncol.* **2009**, *2*, 31–38. [CrossRef] [PubMed]
28. Nakamura, M.; Gotoh, T.; Okuno, Y.; Tatetsua, H.; Sonokia, T.; Unedaa, S.; Morib, M.; Mitsuyaa, H.; Hata, H. Activation of the endoplasmic reticulum stress pathway is associated with survival of myeloma cells. *Leuk. Lymphoma* **2006**, *47*, 531–539. [CrossRef] [PubMed]
29. Papandreou, I.; Denko, N.C.; Olson, M.; van Melckebeke, H.; Lust, S.; Tam, A.; Solow-Cordero, D.E.; Bouley, D.M.; Offner, F.; Niwa, M.; *et al*. Identification of an Ire1alpha endonuclease specific inhibitor with cytotoxic activity against human multiple myeloma. *Blood* **2011**, *117*, 1311–1314. [CrossRef] [PubMed]
30. Mimura, N.; Fulciniti, M.; Gorgun, G.; Tai, Y.-T.; Cirstea, D.; Santo, L.; Hu, Y.; Fabre, C.; Minami, J.; Ohguchi, H.; *et al*. Blockade of XBP1 splicing by inhibition of IRE1alpha is a promising therapeutic option in multiple myeloma. *Blood* **2012**, *119*, 5772–5781. [CrossRef] [PubMed]
31. Carrasco, D.R.; Sukhdeo, K.; Protopopova, M.; Sinha, R.; Enos, M.; Carrasco, D.E.; Zheng, M.; Mani, M.; Henderson, J.; Pinkus, G.S.; *et al*. The differentiation and stress response factor XBP-1 drives multiple myeloma pathogenesis. *Cancer Cell* **2007**, *11*, 349–360. [CrossRef] [PubMed]
32. Leung-Hagesteijn, C.; Erdmann, N.; Cheung, G.; Keats, J.J.; Stewart, A.K.; Reece, D.E.; Chung, K.C.; Tiedemann, R.E. Xbp1s-negative tumor B cells and pre-plasmablasts mediate therapeutic proteasome inhibitor resistance in multiple myeloma. *Cancer Cell* **2013**, *24*, 289–304. [CrossRef] [PubMed]
33. Hetz, C.; Martinon, F.; Rodriguez, D.; Glimcher, L.H. The unfolded protein response: Integrating stress signals through the stress sensor IRE1α. *Physiol. Rev.* **2011**, *91*, 1219–1243. [CrossRef] [PubMed]
34. Kim, R.; Emi, M.; Tanabe, K.; Murakami, S. Role of the unfolded protein response in cell death. *Apoptosis* **2006**, *11*, 5–13. [CrossRef] [PubMed]
35. Oyadomari, S.; Mori, M. Roles of CHOP/GADD153 in endoplasmic reticulum stress. *Cell Death Differ.* **2004**, *11*, 381–389. [CrossRef] [PubMed]
36. Auf, G.; Jabouille, A.; Guerit, S.; Pineau, R.; Delugin, M.; Bouchecareilh, M.; Magnin, N.; Favereaux, A.; Maitref, M.; Gaiser, T.; *et al*. Inositol-requiring enzyme 1alpha is a key regulator of angiogenesis and invasion in malignant glioma. *Proc. Natl. Acad. Sci. USA* **2010**, *107*, 15553–15558. [CrossRef] [PubMed]
37. Fujimoto, T.; Yoshimatsu, K.; Watanabe, K.; Yokomizo, H.; Otani, T.; Matsumoto, A.; Osawa, G.; Onda, M.; Ogawa, K. Overexpression of human X-box binding protein 1 (XBP-1) in colorectal adenomas and adenocarcinomas. *Anticancer Res.* **2007**, *27*, 127–131. [PubMed]
38. Niederreiter, L.; Fritz, T.M.; Adolph, T.E.; Krismer, A.M.; Offner, F.A.; Tschurtschenthaler, M.; Flak, M.B.; Hosomi, S.; Tomczak, M.F.; Kaneider, N.C.; *et al*. ER stress transcription factor Xbp1 suppresses intestinal tumorigenesis and directs intestinal stem cells. *J. Exp. Med.* **2013**, *210*, 2041–2056. [CrossRef] [PubMed]
39. Koong, A.C.; Chauhan, V.; Romero-Ramirez, L. Targeting XBP-1 as a novel anti-cancer strategy. *Cancer Biol. Ther.* **2006**, *5*, 756–759. [CrossRef] [PubMed]
40. Jiang, D.; Niwa, M.; Koong, A.C. Targeting the IRE1α-XBP1 branch of the unfolded protein response in human diseases. *Semin. Cancer Biol.* **2015**, *33*, 48–56. [CrossRef] [PubMed]
41. Chen, S.; Sang, N. Hypoxia-Inducible Factor-1: A Critical Player in the Survival Strategy of Stressed Cells. *J. Cell. Biochem.* **2015**. [CrossRef] [PubMed]
42. Chen, S.; Yin, C.; Lao, T.; Lianga, D.; Hea, D.; Wang, C.; Sanga, N. AMPK-HDAC5 pathway facilitates nuclear accumulation of HIF-1alpha and functional activation of HIF-1 by deacetylating Hsp70 in the cytosol. *Cell Cycle* **2015**, *14*, 2520–2536. [CrossRef] [PubMed]
43. Mizukami, Y.; Kohgo, Y.; Chung, D.C. Hypoxia inducible factor-1 independent pathways in tumor angiogenesis. *Clin. Cancer Res.* **2007**, *13*, 5670–5674. [CrossRef] [PubMed]
44. Porta, C.; Paglino, C.; Mosca, A. Targeting PI3K/Akt/mTOR Signaling in Cancer. *Front. Oncol.* **2014**, *4*, 64. [CrossRef] [PubMed]



© 2015 by the authors; licensee MDPI, Basel, Switzerland. This article is an open access article distributed under the terms and conditions of the Creative Commons by Attribution (CC-BY) license (http://creativecommons.org/licenses/by/4.0/).

International Journal of
Molecular Sciences

MDPI

Article

Next-Generation Sequencing Workflow for NSCLC Critical Samples Using a Targeted Sequencing Approach by Ion Torrent PGM™ Platform

Irene Vanni [1,*,†], Simona Coco [1,†], Anna Truini [1,2], Marta Rusmini [3], Maria Giovanna Dal Bello [1], Angela Alama [1], Barbara Banelli [4], Marco Mora [5], Erika Rijavec [1], Giulia Barletta [1], Carlo Genova [1], Federica Biello [1], Claudia Maggioni [1] and Francesco Grossi [1]

Received: 7 July 2015; Accepted: 24 November 2015; Published: 3 December 2015
Academic Editor: William Chi-shing Cho

[1] Lung Cancer Unit, IRCCS AOU San Martino-IST National Cancer Research Institute, L. go R. Benzi 10, 16132 Genoa, Italy; simona.coco@hsanmartino.it (S.C.); anna.truini@hsanmartino.it (A.T.); mariagiovanna.dalbello@hsanmartino.it (M.G.D.B.); angela.alama@hsanmartino.it (A.A.); ery80x@yahoo.it (E.R.); giulia.barletta@yahoo.it (G.B.); carlo.genova1985@gmail.com (C.G.); febiello@gmail.com (F.B.); claudia_87m@yahoo.it (C.M.); francesco.grossi@hsanmartino.it (F.G.)
[2] Department of Internal Medicine and Medical Specialties (DIMI), University of Genoa, IRCCS AOU San Martino-IST National Cancer Research Institute, L. go R. Benzi 10, 16132 Genoa, Italy
[3] Laboratory of Molecular Genetics, IRCCS, Giannina Gaslini Institute, L. go G. Gaslini 5, 16148 Genoa, Italy; marta.rusmini@gmail.com
[4] Laboratory of Tumor Epigenetics, IRCCS AOU San Martino-IST National Cancer Research Institute, L. go R. Benzi 10, 16132 Genoa, Italy; barbara.banelli@hsanmartino.it
[5] Department of Pathology, IRCCS AOU San Martino-IST National Cancer Research Institute, L. go R. Benzi 10, 16132 Genoa, Italy; marco.mora@hsanmartino.it
* Correspondence: irene.vanni@hsanmartino.it; Tel.: +39-010-555-8463; Fax: +39-010-555-8335
† These authors contributed equally to this work.

Abstract: Next-generation sequencing (NGS) is a cost-effective technology capable of screening several genes simultaneously; however, its application in a clinical context requires an established workflow to acquire reliable sequencing results. Here, we report an optimized NGS workflow analyzing 22 lung cancer-related genes to sequence critical samples such as DNA from formalin-fixed paraffin-embedded (FFPE) blocks and circulating free DNA (cfDNA). Snap frozen and matched FFPE gDNA from 12 non-small cell lung cancer (NSCLC) patients, whose gDNA fragmentation status was previously evaluated using a multiplex PCR-based quality control, were successfully sequenced with Ion Torrent PGM™. The robust bioinformatic pipeline allowed us to correctly call both Single Nucleotide Variants (SNVs) and indels with a detection limit of 5%, achieving 100% specificity and 96% sensitivity. This workflow was also validated in 13 FFPE NSCLC biopsies. Furthermore, a specific protocol for low input gDNA capable of producing good sequencing data with high coverage, high uniformity, and a low error rate was also optimized. In conclusion, we demonstrate the feasibility of obtaining gDNA from FFPE samples suitable for NGS by performing appropriate quality controls. The optimized workflow, capable of screening low input gDNA, highlights NGS as a potential tool in the detection, disease monitoring, and treatment of NSCLC.

Keywords: next-generation sequencing; NGS workflow; NSCLC; Ion Torrent PGM; FFPE; cfDNA

1. Introduction

Non-small cell lung cancer (NSCLC) is the leading cause of cancer-related death worldwide, and the majority of patients are diagnosed at advanced stages of NSCLC, with a dramatically poor five-year overall survival rate of 15% [1].

Recently, the identification of the molecular pathology of individual patient tumors has emerged as a promising opportunity for treatment of patients affected by advanced disease. Indeed, specific genetic alterations that drive cancer development can be targeted by selected inhibitors. In particular, the signaling pathway downstream of the Epidermal Growth factor Receptor (EGFR) has been investigated in advanced NSCLC patients harboring activating EGFR mutations (approximately 15% of Caucasian and 50% of Asian patients) treated with first-line tyrosine kinase inhibitors (TKIs), such as gefitinib, erlotinib, and afatinib. These patients report significant improvement in response and progression-free survival compared with patients treated with traditional chemotherapy [2].

Additionally, the application of molecular-based targeted approaches directed to other driver mutations, such as *KRAS*, *BRAF*, and the PI3K/AKT/mTOR pathway, is currently under evaluation, and several trials have been designed to assess the pharmacological efficacies of these compounds, reporting encouraging results [3].

Currently, traditional tools such as Sanger Sequencing (SS), real-time PCR, and pyosequencing (PS) can screen mutations on few genes per run with a sensitivity of approximately 20%, 10%, and 1%–2%, respectively [4–7]. However, the increasing number of novel potential targets results in more time-consuming and expensive diagnostic tests [8]. The advent of NGS has revolutionized the approach to detect gene mutations but requires high-quality DNA. The majority of advanced NSCLC tumor samples are usually represented by FFPE biopsies that result in limited quantity and low-quality DNA, affecting NGS feasibility. Recently, the evaluation of mutations in circulating free DNA (cfDNA) in the plasma of patients affected by advanced NSCLC has emerged as a hypothetical alternative approach to detect gene mutations from a liquid biopsy [9]. However, the feasibility of performing NGS on critical samples remains challenging, and increased efforts should be made in this direction to offer the best individual therapeutic option.

Here we present an optimized workflow to perform deep sequencing using the Ion AmpliSeq Colon and Lung Cancer Panel *v.*1 (Life Technologies, Carlsbad, CA, USA), which analyzes hotspot and targeted regions of 22 genes frequently mutated in colon and lung cancer. Analyses were performed on DNA resulting from critical samples, such as FFPE biopsy blocks and cfDNA, including a quality control step to assess the DNA quality from these samples.

2. Results

2.1. Assessment of NGS (Next-Generation Sequencing) Detection Limit, Specificity, Sensitivity, and Positive Predictive Value

gDNAs obtained from FFPE sections of engineered cell lines with clinical relevant mutations in tyrosine kinase domain of *EGFR*, such as p.T790M and the p.Glu746_Ala750del, were used to assess the limit of detection (LOD) of our NGS workflow. Firstly, dilution series of p.Thr790Met *EGFR* mutated gDNA with wild-type EGFR gDNA were used to obtain mutant allele frequencies of 50%, 10%, 5%, and 1%, respectively. All dilutions underwent to library preparation and sequenced by Ion PGM, achieving an average coverage per amplicon >1200× and uniformity >96% across the samples. Notably, the p.Thr790Met *EGFR* mutation was detected up to the third dilution (5%) with allele frequencies of 49.6%, 10.7%, and 5.6%, respectively, whereas the call of p.Thr790Met mutation was missed in the lowest dilution (1%). Similarly, we also assessed the LOD of our assay to correctly call the indel, applying a serial dilution of the p.Glu746_Ala750del gDNA with EGFR wild type, confirming the previous LOD of 5% also for indel detection. To evaluate the specificity, sensitivity, and Positive Predictive Value (PPV), we also sequenced two NSCLC cell lines (NCI-H1650 and NCI-H1975) and the two reference standards with EGFR mutation at 50% of frequency. NGS

data analysis revealed a specificity of 100% for the detection of SNVs and INDELs compared to the genotypes of NCI-H1650 and NCI-H1975 cell lines (genotype data assessed by Coco *et al.*, using NGS platform) and the two FFPE reference standards (genotype data assessed by Horizon using Droplet Digital PCR), whereas the sensitivity for detecting variants at the LOD of 5% was 96% (Confidence Interval (CI) 95% = 80.5, 99.3) with PPV of 100% (95% CI = 86.7, 100.0).

2.2. FFPE (Formalin-Fixed Paraffin-Embedded) Quality Control

gDNA from FFPE tissues reported very high purity (both 260/280 and 260/230 ratios > 1.7) and underwent multiplex PCR-based quality control assay, with degradation status ranging from 0.3 to 0.8 Average Yield Ratio (AYR). To identify an AYR cut-off suitable for library preparation, we chose three FFPE DNA samples with different AYR values (0.3, 0.6, and 0.8) and prepared the libraries starting from 10 and 20 ng of gDNA. As expected, all samples were successfully amplified when starting from 20 ng, whereas only two out of three were amplified when starting from 10 ng; indeed, the sample that did not show any amplification products was the most fragmented (0.3 AYR, corresponding to 70% degradation). Additionally, to set the gDNA degradation status cutoff, as a prerequisite for proceeding to a downstream workflow, we increased the fragmentation status of gDNA with the lowest AYR (0.3) by heat. In more detail, by adjusting the fragmentation time we obtained a gDNA test with AYR of 0.2 that was amplified starting from 20 ng as input DNA for the library construction. However, this sample did not display any amplification products, suggesting that 0.3 AYR was a reliable decision criterion to predict the NGS suitability of FFPE samples.

Then, to evaluate the degradation effect on sequencing output, all positive libraries were sequenced. Notably, the sample with 0.6 AYR, although successfully amplified starting from 10 and 20 ng of gDNA, displayed much higher coverage (2/90 amplicons < 500×) using 20 ng compared with 10 ng (6/90 amplicons < 500×). Therefore, we decided to use a DNA input of 20 ng for the library construction of all FFPE DNA samples.

2.3. FFPE and Snap Frozen (SF) NGS

Twelve FFPE (AYR range 0.3–0.8) and matched SF gDNAs were sequenced. The coverage and uniformity of each sample run are reported in Supplementary Table S1. The total number of reads was 6,993,993 and 6,538,054 for SF and FFPE samples, respectively. NGS analysis disclosed an average number of reads per amplicon of 6475.9 in SF samples compared with 6050.5 in FFPE samples. Despite this high coverage, seven of 12 FFPE samples revealed at least one amplicon (range: 1–5) with coverage less than 500×, whereas only one SF sample showed one amplicon with unsatisfactory coverage. More specifically, the FFPE sample ID12 with an AYR = 0.3, showed 19 amplicons with a coverage <500×, suggesting that low quality of gDNA could affect sequencing results. Notably, the aforementioned seven FFPE DNAs reported recurrent amplicons not fully covered: AKT1_1 (chr14: 105246446-105246583), FGFR3_2 (chr4: 1806082-1806187), NOTCH1_1 (content; chr9: 139399338-139399447), STK11_3 (chr19: 1220481-1220603), and TP53_2 (chr17: 7579351-7579485). Interestingly, these amplicons displayed high GC content (greater than 61%). Notably, the coverage uniformity also correlated with gDNA fragmentation status; more specifically, all SF samples displayed 100% coverage uniformity, except for one with 98.9%, whereas FFPE samples ranged from 73.3% to 100%, referring to 0.4 and 0.8 AYR samples, respectively.

The Variant Caller (VC) plugin reported a total of 102 genetic variants (100 SNVs and two indels) (Supplementary Table S2). Notably, all the *EGFR* and *KRAS* mutations previously detected by SS were confirmed in all NSCLC samples reporting identical results starting from SF and matched FFPE tissue, although with different allele frequencies due to intra-tumor heterogeneity (Table 1), whereas the other seven genes present in the colon-lung panel showed discordant results between FFPE and matched SF samples. In particular, 11 discordant nucleotide substitutions were identified: six genetic variants at a frequency less than 5% (1 in SF; 5 in FFPE), and five ranging from 5% to 20% (three in SF; two in FFPE) (Supplementary Table S3).

Table 1. *EGFR* and *KRAS* mutational status comparison between Sanger Sequencing and NGS (Next-Generation Sequencing) Variant Caller software. This table reports the *EGFR* or *KRAS* mutational status, previously defined by Sanger Sequencing from the 12 patients compared to the Variant Caller NGS results. The *EGFR* or *KRAS* mutation nomenclature is based on the convention recommended by the Human Genome Variation Society [10,11].

Patient	Tumor Type	*EGFR* and *KRAS* Status by Sanger Sequencing	*EGFR* and *KRAS* Status Confirmed by VC Software	Allele Name
1	SF	NM_033360.3 (KRAS): c.34G>C (p.Gly12Arg)	Confirmed *KRAS* mutation AF: 29.8%	COSM518
1	FFPE	NM_033360.3 (KRAS): c.34G>C (p.Gly12Arg)	Confirmed *KRAS* mutation AF: 58.6%	COSM518
2	SF	NM_033360.3 (KRAS): c.34G>T (p.Gly12Cys)	Confirmed *KRAS* mutation AF: 24.1%	COSM516
2	FFPE	NM_033360.3 (KRAS): c.34G>T (p.Gly12Cys)	Confirmed *KRAS* mutation AF: 6.4%	COSM516
3	SF	NM_005228.3 (EGFR): c.2239_2240TT>CC (p.Lys747Pro)	Confirmed *EGFR* mutation AF: 37.8%	COSM24267
3	FFPE	NM_005228.3 (EGFR): c.2239_2240TT>CC (p.Lys747Pro)	Confirmed *EGFR* mutation AF: 45.6%	COSM24267
4	SF	NM_033360.3 (KRAS): c.35G>T (p.Gly12Val)	Confirmed *KRAS* mutation AF: 24.0%	COSM520
4	FFPE	NM_033360.3 (KRAS): c.35G>T (p.Gly12Val)	Confirmed *KRAS* mutation AF: 23.2%	COSM520
5	SF	NM_005228.3 (EGFR): c.2237_2255delinsT (p.Glu746_Ser752delinsVal)	Confirmed *EGFR* mutation AF: 5.6%	COSM12384
5	FFPE	NM_005228.3 (EGFR): c.2237_2255delinsT (p.Glu746_Ser752delinsVal)	Confirmed *EGFR* mutation AF: 10.5%	COSM12384
6	SF	NM_005228.3 (EGFR): c.2236_2250del (p.Glu746_Ala750del)	Confirmed *EGFR* mutation AF: 7.8%	COSM6225

Table 1. *Cont.*

Patient	Tumor Type	*EGFR* and *KRAS* Status by Sanger Sequencing	*EGFR* and *KRAS* Status Confirmed by VC Software	Allele Name
6	FFPE	NM_005228.3 (EGFR): c.2236_2250del (p.Glu746_Ala750del)	Confirmed *EGFR* mutation AF: 45.8%	COSM6225
7	SF	NM_033360.3 (KRAS): c.35G>A (p.Gly12Asp)	Confirmed *KRAS* mutation AF: 38.6%	COSM521
7	FFPE	NM_033360.3 (KRAS): c.35G>A (p.Gly12Asp)	Confirmed *KRAS* mutation AF: 26.3%	COSM521
8	SF	NM_033360.3 (KRAS): c.34G>T (p.Gly12Cys)	Confirmed *KRAS* mutation AF: 50.5%	COSM516
8	FFPE	NM_033360.3 (KRAS): c.34G>T (p.Gly12Cys)	Confirmed *KRAS* mutation AF: 24.5%	COSM516
9	SF	NM_033360.3 (KRAS): c.34G>T (p.Gly12Cys)	Confirmed *KRAS* mutation AF: 42.0%	COSM516
9	FFPE	NM_033360.3 (KRAS): c.34G>T (p.Gly12Cys)	Confirmed *KRAS* mutation AF: 41.7%	COSM516
10	SF	NM_005228.3 (EGFR): c.2573T>G (p.Leu858Arg)	Confirmed *EGFR* mutation AF: 45.3%	COSM6224
10	FFPE	NM_005228.3 (EGFR): c.2573T>G (p.Leu858Arg)	Confirmed *EGFR* mutation AF: 40.2%	COSM6224
11	SF	NM_033360.3 (KRAS): c.37G>T (p.Gly13Cys)	Confirmed *KRAS* mutation AF: 32.0%	COSM527
11	FFPE	NM_033360.3 (KRAS): c.37G>T (p.Gly13Cys)	Confirmed *KRAS* mutation AF: 24.2%	COSM527
12	SF	NM_033360.3 (KRAS): c.34G>T (p.Gly12Cys)	Confirmed *KRAS* mutation AF: 31.0%	COSM516
12	FFPE	NM_033360.3 (KRAS): c.34G>T (p.Gly12Cys)	Confirmed *KRAS* mutation AF: 42.6%	COSM516

Abbreviations: SF: Snap Frozen; FFPE: Formalin-Fixed Paraffin-Embedded; VC: Variant Caller; AF: Allele Frequency.

To confirm the Single Nucleotide Variants (SNVs) (excluding indels) identified by the VC software, we performed a second round of analysis using the GATK software, which identified 103 nucleotide substitutions. Notably, GATK validated 93 SNVs identified by VC: 89 FFPE-SF matching SNVs and four of five VC-SNVs (5%–20% frequency) FFPE-SF non-matching, reported as pathogenic mutations (COSM516; COSM1579024; COSM710; COSM11496). Conversely, this pipeline did not confirm the six VC-SNVs (<5% frequency) and one VC-SNV (5%–20% frequency). Moreover, the GATK software identified an additional 10 non-matching novel SNVs (six with a frequency <20% and four with a frequency higher than 20%; range: 20%–35%). However, since none of those four (>20%) was confirmed by SS, we consider them as false positives (data not shown).

We also applied the PS to further validate the five genetic variants (5%–20% frequency) discordant between the FF and matching FFPE samples, confirming all VC-SNVs as true positives (Supplementary Table S3). Overall these data suggest the superiority of the VC pipeline to the call genetic variants generated by Ion PGM. Therefore, we considered 94 SNVs and two indels called by VC to define the tumor samples' mutational profile, excluding six genetic variants at a frequency lower than 5%, according to our assay LOD.

Data reported an average of 7.4 genetic variants (range 5–12) per patient, including Single Nucleotide Polymorphisms (SNPs) and pathogenic mutations. More specifically, only two SNPs involving the *DDR2* intron region (rs200983597 and rs143729297) reported a Minor Allele Frequency (MAF) smaller than 0.01 defined as "rare" variants [12]. Among the pathogenic variants (Figure 1A), tumor protein p53 (*TP53*) was the most altered gene: five out of 12 patients harbored pathogenic mutations (COSM44571; COSM43814; COSM45413; COSM40942; COSM10769) and all reported a SNP (rs1042522). Additionally, five patients harbored *MET* proto-oncogene receptor tyrosine kinase (*MET*) gene mutations (COSM706; COSM710; COSM1579024). Notably, COSM710 and COSM1579024 coexisted with *KRAS* mutations (COSM518; COSM520; COSM516). Further somatic mutations involved the serine/threonine kinase 11 (COSM49004), catenin (cadherin-associated protein) beta 1 (COSM5670), and SMAD family member 4 (COSM14151).

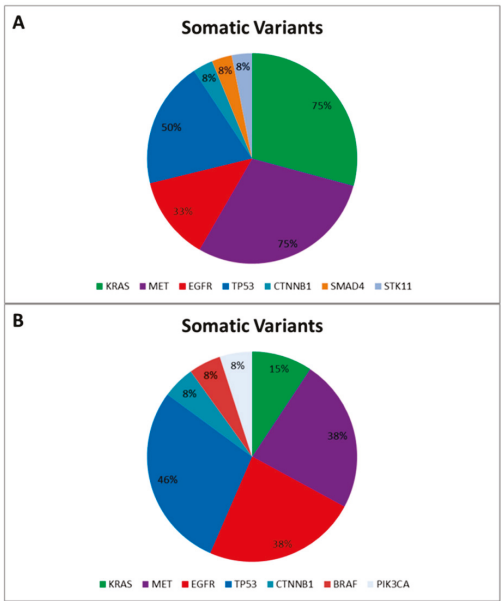

Figure 1. Somatic Variants identified in the "Training Set" (**A**) and in the "Validation Set" (**B**), respectively. The pie charts report the frequency of mutated genes in the "Training Set" (**A**) and in the "Validation Set" (**B**) based on the Catalogue of Somatic Mutation in Cancer (COSMIC) [13].

Finally, to correctly call genetic variants also including indel, we sequenced a further cohort of 13 NSCLC patients, previously tested for *EGFR* mutational status by SS in order to validate our optimized

workflow and test the ability of the bioinformatic pipeline. All gDNA underwent to a multiplex-PCR quality control step, reporting AYR values greater than 0.3, predictive of NGS suitability. Then all FFPE gDNAs were subjected to the Ion PGM workflow and successfully sequenced. In particular, the data analysis properly called four *EGFR* variants detected by SS. Similarly to the training set, the data analysis identified a mean of 7.0 genetic variants (ranging from five to 10) per patient, and, besides the *EGFR* activating mutations, we identified further pathogenic variants involving *BRAF*, *CTNNB1*, *KRAS*, *MET*, *PI3KCA*, and *TP53* genes (Figure 1B).

2.4. cfDNA NGS

Plasma samples, collected at diagnosis, were available for nine out of 12 patients for cfDNA extraction. Quantification of cfDNA was evaluated by qPCR using the *hTERT* assay, showing total concentrations ranging from 0.08 to 10 ng. Because the gDNA input recommended for library construction is 10 ng, we used a Whole Genome Amplification (WGA) technique to increase the starting cfDNA amount. First, we evaluated the WGA technique performance by a scalar dilution of NCI-H1650 human cell line gDNA (10, 1, and 0.1 ng), reporting final gDNA yields of approximately 20 μg regardless of the starting gDNA input. Then, 10 ng of each WGA NCI-H1650 was sequenced to evaluate the specificity and sensitivity of the WGA technique. The sequencing outputs reported a coverage of WGA gDNA greater than 500× and uniformity of 95.2%, except for the WGA 0.1 ng input gDNA sample that displayed four unsatisfactory covered amplicons and a uniformity of 81.1%. The NGS data analysis showed an optimum variant call concordance and identical results in terms of frequencies of variant calls starting from 10, 1, and 0.1 ng of NCI-H1650 gDNA (data not shown). However, the comparison between WGA and the original unamplified NCI-H1650 gDNA displayed five novel insertions in common among all WGA samples. Because these insertions occurred in homopolymeric regions (five or more nucleotide repeats), we hypothesized them to be amplification artefacts due to the WGA technique. Additionally, four out of five novel insertions displayed an AF lower than our LOD (5%); therefore, these insertions were excluded from the performance analysis of NGS workflow on WGA samples resulting in specificity, sensitivity, and PPV of 87.5% (CI 95% = 52.9, 97.7), 100.0% (CI 95% = 67.5, 100), and 100.0% (CI 95% = 67.5, 100), respectively. Therefore, due to the introduction of amplification artefacts in WGA cell lines, we decided to limit the use of the WGA approach to the three samples characterized by low input cfDNA (<1 ng). The remaining six samples were then enriched starting from a lower amount of recommended input cfDNA (2–10 ng) by increasing the cycle number of library PCRs. This modified protocol allowed us to obtain suitable no-WGA libraries; the coverage and uniformity of each run are displayed in Supplementary Table S1.

Although the average reads per amplicon for WGA cfDNA was higher compared with no-WGA cfDNA samples (6719.7 *vs.* 4858.5), the coverage uniformity was better in the no-WGA cfDNA; more specifically, WGA cfDNA showed an average of 83.7% (81.1%–85.6%) *vs.* 99.4% of the no-WGA (98.9%–100%). Indeed, no-WGA cfDNA sample exhibited coverage greater than 500× for all amplicons, except for one sample with 64 amplicons<500×, likely because of a low input of cfDNA (2.1 ng). Conversely, WGA cfDNAs always displayed five amplicons with coverage less than 500×. Notably, as previously observed in the seven FFPE samples, the recurrent uncovered amplicons (AKT1_1, FGFR3_2, NOTCH1_1, STK11_3, and STK11_5) contained high GC-content. Data obtained from VC were compared to the matched tumor mutational profile. As expected, the WGA cfDNA displayed additional insertions; notably, these insertions, likely due to non-specific amplification artefacts of WGA, were the same observed in the NGS analysis of WGA NCI-H1650 and therefore filtered out. Moreover, the comparison analysis identified two additional SNVs with frequencies of 4.4% and 20.6%. However, the second variant call by GATK (Supplementary Table S4) validated all SNVs identified by VC, excluding the nucleotide variant below 5%. Although the remaining discordant variant (20.6%) was confirmed by GATK, it occurred in a WGA-cfDNA sample, suggesting a possible PCR artefact. Unexpectedly, eight out of nine cfDNAs did not disclose any somatic mutations either in the gatekeeper gene *TP53* or in the other genes mutated in their

matched tumors; by contrast, one cfDNA from a patient with metastatic disease presented the identical mutational profile reported in the corresponding tumor.

3. Discussion

Recently, targeted therapy has emerged as a promising therapeutic option for the subgroup of advanced NSCLC patients carrying activating mutations in druggable genes [2]. Currently, the screening of clinically-actionable mutations is performed on FFPE tumor biopsies, but the amount of tumor tissue is often limited, and the gDNA quality may not be always optimal. Moreover, the increasing number of candidate targets requires the validation of highly sensitive throughput technologies, such as NGS, into clinical settings. To date, several studies have investigated targeted deep sequencing on FFPE samples from different cancer types [14–16], including NSCLC [17]; here, we propose an optimized workflow using a specific 22-gene enrichment lung cancer panel to successfully sequence critical samples, such as FFPE biopsies and cfDNA, assuring good quality of NGS data. The workflow includes correct quantification and quality control of input gDNA, a WGA approach to linearly increase the gDNA for low input of starting gDNA (<1 ng), library protocols tailored for specific gDNA type (FFPE and cfDNA), and a robust bioinformatic pipeline to correctly call both SNVs and indels (Figure 2). Similarly to other NGS workflows [18], our assay was able to detect up to 5% of AF either SNV and indel, achieving an optimal assay performance for FFPE samples (100% of specificity and PPV; 96% of sensitivity). The NGS workflow was retrospectively evaluated on DNA extracted from SF and matching FFPE and cfDNA belonging to 12 resected NSCLC patients previously tested for *EGFR* and *KRAS* mutations by SS.

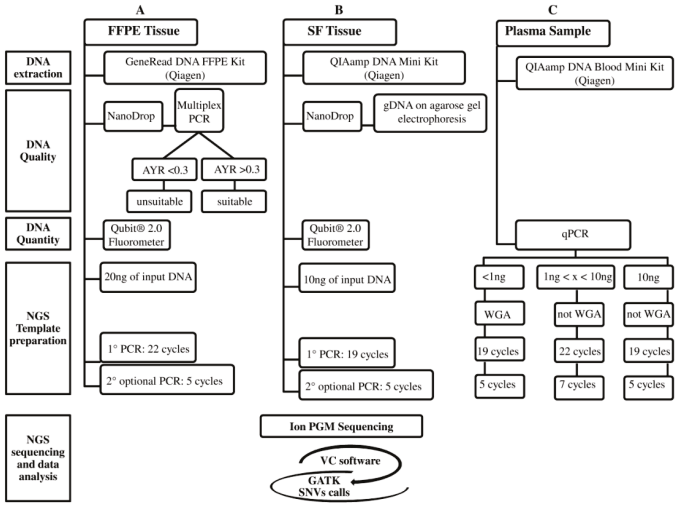

Figure 2. The three analytical NGS (Next-Generation Sequencing) workflows are: (**A**) FFPE (Formalin-Fixed Paraffin-Embedded); (**B**) SF (Snap Frozen); and (**C**) Plasma. These workflows, currently designed for the Ion PGM platform, are divided into five steps: DNA extraction, gDNA Quality, gDNA Quantity, NGS Template preparation, and NGS sequencing and data analysis. The latter, in common among three workflows, includes: Ion PGM sequencing and variant identification using VC software and then GATK for SNVs call. The NGS cost (from DNA extraction to NGS data analysis), excluding personnel, is approximately 250€ for each FFPE, SF, and plasma sample (**A**–**C**). The NGS turnaround time for processing SF (**B**) and no-WGA cfDNA (**C**) samples is approximately five days, whereas for FFPE (**A**) and WGA cfDNA (**C**) samples one more day is required for the multiplex PCR DNA quality control (**A**) and WGA technique (**C**).

Pre-analytic quality control to define suitable DNA for NGS application is crucial, particularly when it is applied to highly degraded DNA, such as FFPE DNA. The majority of studies, aimed to define FFPE deep sequencing guidelines, focused on the correct DNA quantification method [19,20], whereas

our workflow, which involves a multiplex-PCR approach, defined an AYR parameter, indicative of gDNA degradation status, that highly correlates with sequencing quality metrics, such as uniformity and coverage. Notably, we identified an integrity threshold for the processing of FFPE gDNAs estimated at 0.3 AYR, which corresponds to 70% of gDNA fragmentation. Moreover, although the library protocol requires 10 ng of input FFPE gDNA, we demonstrated that when doubling the input FFPE DNA amount (20 ng), highly fragmented DNAs up to 0.3 AYR were successfully sequenced. Notably, this improvement increased the number of amplicons covered to at least 500×, a parameter required for any clinically-oriented cancer panel [18]. However, we identified five recurrent amplicons that were insufficiently covered in highly-degraded FFPE gDNAs because of high GC content (>60%), as previously reported [21].

One critical point of the NGS analysis is generating a list of trustworthy variants; therefore, we tested whether the integration of two different bioinformatic pipelines could improve the SNVs call with higher sensitivity and accuracy compared with single software performance. Specifically, we compared the VC, the Ion PGM plugin with optimized pre-set parameters, with GATK, one of the most used free NGS tools. Each pipeline showed different results in the detection of SNVs (100 SNVs by VC *vs.* 103 by GATK (95 in common between the two pipelines). Differences between the pipelines could be due to the different alignment and calling algorithms [22]. Furthermore, the GATK software exhibited a very high error rate in indel calling (approximately 20 indels per sample; data not shown), leading us to exclude it in the indel calling. A possible explanation is that the GATK pipeline was developed for Illumina data analysis, in contrast to the VC pipeline that has been set up for the analysis of FastQ data generated from Ion-platforms [23]. In this context, some evidence has been previously reported regarding the high rate of false positive variants detected by GATK with non Illumina-FastQ data. These false positives particularly refer to small insertions and deletions (indels) in homopolymeric regions where the difficulty in detecting and determining the genotype of short indels remains a challenge because of the propensity for polymerase slipping during PCR, resulting in sequence artifacts that GATK cannot distinguish [24]. The validation with the PS confirmed all VC discordant genetic variants between SF and matching FFPE samples (>5% frequency), demonstrating that the VC pipeline is optimized for Ion PGM data. Indeed, these discordant variants among SF and matching FFPE samples may be explained by intra-tumor heterogeneity, as previously observed in NSCLC [25–29]. Although the integration of GATK did not exclude any false positive SNVsby VC, it removed all the SF/FFPE discordant SNVs detected by the VC pipeline with frequencies less than 5%, confirming our LOD assay.

EGFR and *KRAS* somatic mutations, previously detected by SS, were confirmed by both pipelines either in SF and matched FFPE, validating the high specificity of the Ion AmpliSeq Colon and Lung Cancer panel for the identification of these mutations. Our data revealed that *TP53* was the most frequent pathogenically-mutated gene [30,31], and all patients harbored the SNP rs1042522 in *TP53*. Interestingly, this SNP, responsible for a substitution of a proline residue with an arginine residue in codon 72 of *TP53*, has been associated with lung cancer susceptibility [32] and a risk of toxicity during platinum-based chemotherapy treatment in advanced NSCLC patients [33]. Notably, we also observed a recurrent association between *MET* genetic variants and *KRAS* activating mutations, as already described in NSCLC by Govindan *et al.* [34]. Due to its high sensitivity, NGS represents an optimal approach to investigate the mutational profile of cfDNA as a non-invasive diagnostic approach to monitor disease progression during treatment. Indeed, a fraction of cfDNA derives from tumor cells and is referred to as ctDNA in cancer patients [35]. To date, several studies have demonstrated the feasibility of using ctDNA as a potential tumor marker in a limited number of patients with various solid cancers; however, few studies focused on NSCLC have been performed [9]. Therefore, we developed an optimized workflow for cfDNA mutational screening, combining a WGA approach for low input samples (<1 ng) and a specific protocol for sequencing library construction, resulting in high numbers of good-quality reads. Currently, several WGA approaches, differing in assay chemistry and complexity, have been developed [36–40]. Here, we used a WGA based on the MDA technology that employs the phi29 DNA polymerase and

random primers to amplify gDNA without thermocycling [40,41]. Several studies revealed that MDA can amplify the genome with higher uniformity, longer length, and less bias compared with PCR-based WGA methods [41–45]. Therefore, MDA-based WGA has been shown to be the best method to obtain high quality cfDNA for different applications, such as the NGS [44,46,47]. Another important concern of the WGA approach is the correct quantification of the amplified DNA. Indeed, WGA techniques report non-specific side products and residual WGA reagents that may influence DNA quantification by fluorometric methods [43,48]. Therefore, we suggested performing WGA-DNA quantification using real-time PCR, which has been demonstrated to be the most reliable method [49]. The sequencing output obtained from the WGA NCI-H1650 displayed a similar performance to the standard no-WGA cell line, irrespective of input gDNA. Similar SNV frequencies were reported across the WGA NCI-H1650 samples, suggesting that this technology may be applied to the colon and lung assay when the starting gDNA amount is limited. However, it should be taken into account that the MDA-based WGA introduces some amplification biases that mainly occur in DNA homopolymeric regions, as previously observed, resulting in a lower specificity of the assay [41,50,51]. Because the WGA application might be necessary to yield sufficient DNA for the subsequent sequencing workflow [52], we tried to limit all critical points. Our optimized workflow and NGS analysis on cfDNAs allowed for detection of the same mutational profile of the corresponding tumor in one cfDNA sample. However, among nine NSCLC patients with available plasma, only two were at stage IV of disease. Because several studies revealed that the presence of ctDNA was mainly detected in aggressive disease [9,53], this observation could explain why we detected ctDNA in only one of two patients with advanced NSCLC. The unidentified somatic mutations in localized (stage I–III) cfDNA samples could also be explained by the detection limit of mutation allele frequencies of our NGS assay, estimated at 5% [54].

However, since the Ion PGM technology utilizes scalable semiconductor chips, a lower number of samples in the same run could increase the amplicon coverage; this might allow for the detection of variants with lower frequency (<5%) in the hypothesis to also apply the NGS workflow to the ctDNA screening. Such higher throughput, might also permit us to detect tumor heterogeneity e.g., in the profiling of ctDNA and to call variants at very low frequencies. Furthermore, since the correct amplicon size is critical to the success of sequencing experiments, designing custom panels with a shorter length of amplicons could improve the sequencing performances, especially for highly fragmented DNA such as FFPE and cfDNA. Finally, it should be kept in mind that customizing panels for a subset of druggable genes of a specific cancer type may offer testing at a lower cost, thereby yielding a higher coverage.

4. Experimental Section

4.1. Sample Collection

Twelve patients who underwent surgery for NSCLC at different stage of the disease were enrolled in our study as the "Training Set", based on their previously known *EGFR* and *KRAS* mutational statuses. The clinical characteristics of the patients are reported in Table 2. SF tumors from all patients were available in the tissue biobank of our Institute. Additionally, matched FFPE tissues were obtained from the pathology archive. All samples were evaluated by a pathologist for malignant cell content to macrodissect and enrich the tumor component up to 50%, when necessary. Nine of the 12 plasma samples from patients were also collected at time of diagnosis.

We also enrolled a further 13 NSCLC patients as the "Validation Set" (Table 3), and for each case the FFPE tissue block was revised by the pathologist to verify the tumor cell content. Moreover, three Horizon FFPE standards (*EGFR* p.Thr790Met, *EGFR* p.Glu746_Ala750del, and *EGFR* wild-type reference standards; Horizon, Cambridge, UK) and two human NSCLC cell lines (NCI-H1650 p.Glu746_Ala750del and NCI-H1975 p.Thr790Met/p.Leu858Arg; American Type Culture Collection, Manassas, VA, USA) were used to assess the parameter performances of our assay. The present study was approved by the local ethics committee (TP-01-2014; 255REG2014) and written informed consent was obtained from every patient.

Table 2. Clinical characteristics of NSCLC (Non-small cell lung cancer) in the "Training Set".

Patient	Block Age	% TC	SF	FFPE	cfDNA	Histology	TNM	Stage	Age at Diagnosis	G	Smoking Habits	PS	OS	Status
1	2012	>50	x	x	x	SCC	T1b, N0, M0	IA	77	M	S	1	30	A
2	2010	>50	x	x	x	ADK	T1a,N2,M0	IIIA	67	M	NS	1	18	DOD
3	2013	>50	x	x	x	ADK	T2, N2, M1a	IV	76	F	NS	1	14	DOD
4	2010	>50	x	x	x	ADK	T2b,N0,MX	IIA	76	M	FS	1	11	DOD
5	2013	>50	x	x	NA	ADK	T2a,N2,M1b	IV	75	F	NS	1	13	A
6	2011	>50	x	x	NA	ADK	T2a, N0, MX	IB	78	F	NS	1	29	DOD
7	2013	>50	x	x	x	ADK	T2a, N2, M1b	IV	65	M	S	1	3	DOD
8	2013	>50	x	x	x	ADK	T2b, N1, M0	IIB	59	F	S	1	23	A
9	2012	>50	x	x	x	ADK	T2a, N0, MX	IB	72	M	FS	0	28	A
10	2011	>50	x	x	NA	ADK	T2b, N0, M0	IIB	66	F	FS	1	42	A
11	2010	>50	x	x	x	ADK	T1a, N0, M0	IA	77	M	FS	0	49	DOD
12	2010	>50	x	x	x	ADK	T1a, N0, M0	IA	60	F	S	1	32	DOD

Table 3. Clinical characteristics of NSCLC patients in the "Validation Set".

Patient	Block Age	% TC	SF	FFPE	cfDNA	Histology	TNM	Stage	Age at Diagnosis	G	Smoking Habits	PS	OS	Status
13	2015	>50	NA	x	NA	ADK	T2, N2, M0	IIIB	59	M	S	0	5	A
14	2014	>50	NA	x	NA	ADK	Tx, Nx, M1a	IV	42	M	NS	0	14	A
15	2015	>50	NA	x	NA	ADK	T3, N3, M1a	IV	64	M	FS	1	4	A
16	2014	>50	NA	x	NA	ADK	T4, N2, M1b	IV	77	F	NS	0	12	A
17	2014	>50	NA	x	NA	ADK	T3, N2, M0	IIIA	70	F	NS	1	8	A
18	2012	>50	NA	x	NA	ADK	T3, N2, M1b	IV	63	M	S	1	37	A
19	2014	>50	NA	x	NA	ADK	T4, N2, M1b	IV	70	M	FS	1	2	DOD
20	2014	>50	NA	x	NA	ADK	T4, N0, M0	IIIA	68	M	FS	0	16	A
21	2011	>50	NA	x	NA	ADK	T1a, N0, M0	IA	71	F	NS	1	42	DOD
22	2014	>50	NA	x	NA	ADK	T2, N2, M1b	IV	81	F	NS	1	10	DOD
23	2013	>50	NA	x	NA	ADK	T1b, N2, M0	IIIA	72	M	FS	1	22	A
24	2014	>50	NA	x	NA	ADK	T3, N3, M1b	IV	61	M	NS	1	11	DOD
25	2015	>50	NA	x	NA	ADK	Tx, Nx, M1b	IV	55	F	FS	0	7	A

Abbreviations: TC: Tumor Content; ADK: Adenocarcinoma; SCC: squamous cell carcinoma; TNM: Tumor-Nodes-Metastasis; G: Gender; F: Female; M: Male; S: Smoker; NS: never smoker; FS: Former smoker; PS: Performance Status; OS: Overall Survival (Month); A: Alive; DOD: Dead of disease; x: present; NA: not available.

4.2. DNA Extraction and Quality Control

gDNA from SF samples and the NCI-H1650 cell line was isolated using a QIAamp® DNA Mini Kit (Qiagen, Hilden, Germany), whereas gDNA from FFPE tissues was extracted using the GeneRead DNA FFPE Kit (Qiagen), according to the manufacturer's recommendations. All gDNA samples were then quantified by a Qubit® 2.0 Fluorometer (Invitrogen, Carlsbad, CA, USA) using a Qubit® dsDNA HS Assay Kit. cfDNA was extracted from 400 µL of plasma with a QIAamp DNA Blood Mini Kit (Qiagen) and quantified by quantitative PCR (qPCR) using the human telomerase reverse transcriptase (*hTERT*) TaqMan® Copy Number Reference Assay (Catalog: 4403316; Life Technologies). The calibration curve was defined based on a dilution series (10–1 × 10^6 pg) of a control human genomic DNA standard (Promega, Madison, WI, USA). The qPCR reaction was performed in a final reaction volume of 10 µL using 5 µL of TaqMan Universal Mastermix (Life Technologies, Carlsbad, CA, USA), 1 µL of the TaqMan® Copy Number Reference Assay *hTERT* (Life Technologies), and 4 µL of cfDNA on a RealPlex (Eppendorf, Hamburg, Germany) device. Each sample was run in duplicate, and the final concentration calculated by interpolation of the CT value with the aforementioned calibration curve. Both SF and FFPE gDNA underwent a quality control assay. DNA quality was first assessed using a NanoDrop ND-1000 (Thermo Scientific, Wilmington, DE, USA) to measure the whole absorption spectrum (220–750 nm) and calculating absorbance ratios at both 260/280 and 260/230. SF gDNA was analyzed on 0.8% agarose gel electrophoresis to visualize the DNA size distribution, whereas we performed a multiplex PCR-based quality control assay using a slight modification of the van Beers *et al.* [55] protocol to assess FFPE gDNA fragmentation status. Briefly, 30 ng of FFPE gDNA, as measured by Qubit, was analyzed by a multiplex PCR reaction performed using three independent sets of *GAPDH* primers that amplify 200, 300, and 400 bp fragments. The amplification was performed in a reaction volume of 30 µL with final concentrations of 0.133 µM of each primer, 1.5 U AmpliTaq Gold® DNA Polymerase (Life Technologies, Carlsbad, CA, USA), GeneAmp® 10× PCR Gold Buffer, 1.5 mmol/L $MgCl_2$, and 0.2 mmol/L dNTPs. PCR was conducted in a Mastercycler® nexus Thermal Cycler (Eppendorf) as follows: 95 °C for 7 min, 35 cycles of 1 min at 94 °C, 1 min at 56 °C, and 3 min at 72 °C, followed by a hold at 72 °C for 7 min. PCR products were then analyzed with an Agilent 2100 Bioanalyzer using the Agilent High Sensitivity DNA Kit (Agilent Technologies, Santa Clara, CA, USA). The yield of the resulting three amplicons was evaluated by comparison with the yield of amplicons from a reference DNA template (Promega). The Average Yield Ratio (AYR), calculated for each amplicon, was used as a quantitative indicator of FFPE DNA integrity.

4.3. Whole Genome Amplification (WGA)

cfDNA less than 1 ng, estimated by qPCR, underwent WGA using the REPLI-g Single Cell Kit (Qiagen). The REPLI-g Single Cell Kit is based on a Multiple Displacement Amplification (MDA) technology that achieves highly uniform amplification across the entire genome with minimal locus bias and reduced nonspecific amplification artefacts [41]. To evaluate the performance of this assay for subsequent NGS application, we previously amplified a scalar dilution of NCI-H1650 cell line gDNA (10, 1, and 0.1 ng). The amplified gDNAs were diluted 1:100 and evaluated by qPCR using the *hTERT* assay, as previously described.

4.4. Next Generation Sequencing (NGS)

Libraries were amplified using the Ion AmpliSeq Colon and Lung Cancer Panel *v.*1 (Life Technologies), which analyzes 90 amplicons in hotspots and target regions of 22 genes (*AKT1*, *ALK*, *BRAF*, *CTNNB1*, *DDR2*, *EGFR*, *ERBB2*, *ERBB4*, *FBXW7*, *FGFR1*, *FGFR2*, *FGFR3*, *KRAS*, *MAP2K1*, *MET*, *NOTCH1*, *NRAS*, *PIK3CA*, *PTEN*, *SMAD4*, *STK11*, and *TP53*) with a coverage of over 500 mutations involved in colon and lung cancers. Overall, 20 ng for FFPE, 10 ng for SF gDNA and WGA cfDNA, and a range from 1 to 10 ng for no-WGA cfDNA were amplified using the Ion AmpliSeq™ Library Kit 2.0

(Life Technologies), barcoding each sample. Different cycling conditions were performed according to the DNA type: 22 cycles for FFPE gDNA and no-WGA cfDNA and 19 cycles for SF gDNA and WGA cfDNA in the first multiplex PCR, whereas in the second, optional PCR, the SF, FFPE and WGA cfDNA were subjected to five cycles, and the no-WGA cfDNA underwent seven cycles.

The library size was checked using the Agilent High Sensitivity DNA Kit by the Bioanalyzer 2100 instrument (Agilent Technologies), and library concentration was evaluated with a Qubit® 2.0 Fluorometer using the Agilent High Sensitivity DNA Kit (Life Technologies). Each diluted library (100 pM) was amplified through emulsion PCR using the OneTouch™ Instrument (Life Technologies) and enriched by the OneTouch™ ES Instrument (Life Technologies) using the Ion PGM Template OT2 200 KIT, following the manufacturer's instructions. Finally, sequencing was performed on the Ion PGM (Life Technologies) with the Ion PGM 200 Sequencing Kit (Life Technologies), loading barcoded samples into a 314*v.*2 or 316*v.*2 chip.

4.5. NGS Data Analysis

The PGM sequencing data were analyzed by the Ion Torrent Software Suite *v.*4.2 (Life Technologies) using the plugin Variant Caller (VC) *v.*4.2-r88446. Hotspot and targeted regions, together with the json parameters files associated with the Ion AmpliSeq Colon and Lung Cancer Panel *v.*1 (Life Technologies), were then loaded into the VC plugin. All identified variants were visually confirmed by the Integrative Genomics viewer (IGV) [56]. To validate data, a second round of analysis was performed as follows: FastQ data, generated by the Ion PGM™ semiconductor, were aligned to the Hg19 genome reference using BWA (Burrows-Wheeler Alignment)-MEM tool optimized for 70 bp–1 Mb long reads. Then, the resulting SAM (Sequence Alignment Map) files were converted and sorted to the BAM (binary version of SAM) format by SAMtools. Post-alignment steps included local realignment in the proximity of known indels and recalibration of the quality score, both performed by the Genome Analysis Toolkit (GATK) 2.5 Unified Genotyper (Realigner Target Creator, Indel Realigner and Base Recalibrator options) starting from sorted BAM files. Finally, GATK called variants in the target regions included in the BED file with Phred scores greater than 5 (those with a Phred score between 5 and 30 were marked as low-quality variants). Only Single Nucleotide Variants (SNVs) were considered, annotated by SNPEff, and compared to those called with the Ion Reporter™ tool [57]. All the samples belonging to the same patients were analyzed in multi-sample mode. Variants were annotated using the PolyPhen-2) [58], SIFT [59], and Genomic Evolutionary Rate Profiling (GERP) tools to predict the effect of missense mutations on the protein and calculate their conservation scores. Additionally, variants were named according to the Catalogue of Somatic Mutation in Cancer (COSMIC) [13] and Single Nucleotide Polymorphism Database (dbSNP). To distinguish common polymorphisms from rare variants, Global Minor Allele Frequency (GMAF) was calculated using the allele frequencies across all 1000 Genomes Phase I populations [60].

4.6. NGS Parameter Performance

To assess the performance parameters of our assay, two NSCLC cell lines and two DNA FFPE reference standards were sequenced according to our workflow. NGS data from the cell lines (NCI-H1650 and NCI-1975) were compared to genotypes obtained from published NGS data using Ion AmpliSeq™ Cancer Panel on Ion PGM sequencer (Life Technologies) [61]. Similarly, the data from the two FFPE reference standards were compared to genotype assessed by Horizon using droplet digital PCR. We also evaluated the performance parameters of our assay on WGA samples by comparing the mutation profiles of WGA amplified of NCI-H1650 scalar dilutions (10, 1, and 0.1 ng) with the corresponding unamplified cell line. The sensitivity, specificity, and PPV of the tests were calculated as described [62] and confidence intervals were calculated using the Confidence Interval Calculator (accessed on 1 February 2015).

4.7. Sanger Sequencing (SS) and Pyrosequencing (PS)

NGS variants with frequencies higher than 20% were validated by SS, using the specific gene primer of the panel as described by Coco (2012) [63]. Genetic variants with a frequency range from 5% to 20% were validated by PS. The primer sets for the PS assays (which include a PCR primer pair and a sequencing primer) were designed with the Pyrosequencing Assay Design software (Biotage, Uppsala, Sweden). All the primer sequences, the PCR amplification conditions, and the sequence to analyze are reported in Supplementary Table S5. The PCR reactions were performed by amplifying 100 ng of gDNA in a final volume of 50 µL containing 200 mol/L dNTPs, 1× Taq buffer, 1.5 mM $MgCl_2$, 0.2 µM of each PCR primer, 1.5 U of AmpliTaq Gold® DNA Polymerase (Life Technologies). The PCR program consists of 10 min at 95 °C and 45 cycles with 30 s at 95 °C, 30 s at specific annealing temperature of primer, and 30 s at 72 °C, followed by 5 min at 72 °C. The PS assays were performed with a PSQ 96MA instrument (Qiagen); the sequencing reactions were performed with the Pyro Gold reagent kit PSQ 96MA, according to the manufacturer's instructions, and the sequencing analysis conducted with the PSQTM 96MA software *v*.2.02 (Biotage AB, Uppsala, Sweden).

5. Conclusions

In conclusion, here we demonstrate the feasibility of obtaining DNA suitable for NGS from FFPE tissues by performing an appropriate DNA quality control assay based on a multiplex PCR. Indeed, adequate quality control of extracted DNA represents the most critical step of the entire procedure and in particular gDNA from an FFPE biopsy, which is highly fragmented and limited. The assessment of the suitability of the starting DNA for subsequent sequencing is mandatory for reducing the time and costs of the downstream processes due to a possible sequencing failure.

In particular, our NGS-based workflow was successfully able to screen critical samples, such as FFPE tissues, demonstrating the possibility of transferring this novel technology into routine clinical context. Our criterion for considering a variant as true positive was a variant allele frequency greater than 5% with coverage higher than 500×.

We also report that VC is a reliable software program for identifying SNVs and indels using Ion PGM NGS data, that streamline and simplify the data analysis, annotation, and reporting of data, reducing the time to results. However, a second round of variant calling by GATK software is suggested, particularly in a starting setup. The inclusion of a reference standard, harboring mutation with AF at 5%, to sequence in each run as well as a validation step with an independent test to confirm clinically actionable mutations, are recommended to confidently call mutations in a clinical contest.

We also report a feasible sequencing workflow by starting from low-input gDNA to be applicable in the detection of ctDNA mutational profiles. However, to translate this technology into the disease monitoring and treatment of NSCLC, further validation studies on a greater number of samples, specifically on cfDNA from metastatic NSCLC patients, are required.

Supplementary Materials: Supplementary materials can be found at http://www.mdpi.com/1422-0067/16/12/26129/s1.

Acknowledgments: We kindly thank Cristina Bruzzo and Zita Cavalieri for technical support. We are grateful to the Biological Resource Center (CRB) of IRCCS AOU San Martino-IST National Cancer Research Institute for providing the samples. The present study was supported by Italian Ministry of Health (GR 2011-12; 02350922) and Banca Carige Italia (2013.0277-12).

Author Contributions: Irene Vanni, Simona Coco, and Francesco Grossi conceived and planned the study. Marco Mora revised the cell content of all tumors; Maria Giovanna Dal Bello performed the gDNA quality control. Irene Vanni, Simona Coco, and Anna Truini performed sequencing analysis by Next generation Sequencing and Sanger, and data interpretation. Barbara Banelli performed the validation analysis and data interpretation by PS. Marta Rusmini set up the bioinformatics pipeline for NGS data analysis. Irene Vanni, Simona Coco, Anna Truini, and Angela Alama contributed to the interpretation of the data and wrote the manuscript. Francesco Grossi, Erika Rijavec, Carlo Genova, Federica Biello, and Claudia Maggioni contributed to the interpretation of the data and revised the manuscript. All authors discussed the results and reviewed and approved the manuscript.

Conflicts of Interest: The authors declare no conflict of interest.

References

1. Siegel, R.; Ma, J.; Zou, Z.; Jemal, A. Cancer statistics, 2014. *CA Cancer J. Clin.* **2014**, *64*, 9–29. [CrossRef] [PubMed]
2. Pao, W.; Miller, V.; Zakowski, M.; Doherty, J.; Politi, K.; Sarkaria, I.; Singh, B.; Heelan, R.; Rusch, V.; Fulton, L.; *et al*. EGF receptor gene mutations are common in lung cancers from "never smokers" and are associated with sensitivity of tumors to gefitinib and erlotinib. *Proc. Natl. Acad. Sci. USA* **2004**, *101*, 13306–13311. [CrossRef] [PubMed]
3. Coco, S.; Truini, A.; Vanni, I.; dal Bello, M.G.; Alama, A.; Rijavec, E.; Genova, C.; Barletta, G.; Sini, C.; Burrafato, G.; *et al*. Next generation sequencing in non-small cell lung cancer: New avenues toward the personalized medicine. *Curr. Drug Targets* **2015**, *16*, 47–59. [CrossRef] [PubMed]
4. Sanger, F.; Nicklen, S.; Coulson, A.R. DNA sequencing with chain terminating inhibitors. *Proc. Natl. Acad. Sci. USA* **1977**, *74*, 5463–5467. [CrossRef] [PubMed]
5. Higuchi, R.; Fockler, C.; Dollinger, G.; Watson, R. Kinetic PCR analysis: Real-time monitoring of DNA amplification reactions. *Biotechnology* **1993**, *11*, 1026–1030. [CrossRef] [PubMed]
6. Ronaghi, M.; Uhlén, M.; Nyrén, P. A sequencing method based on real-time pyrophosphate. *Science* **1998**, *281*, 363–365. [CrossRef] [PubMed]
7. Hantson, I.; Dooms, C.; Verbeken, E.; Vandenberghe, P.; Vliegen, L.; Roskams, T.; Borght, S.V.; Nackaerts, K.; Wauters, I.; Vansteenkiste, J. Performance of standard procedures in detection of *EGFR* mutations in daily practice in advanced NSCLC patients selected according to the ESMO guideline: A large Caucasian cohort study. *Transl. Respir. Med.* **2014**, *2*. [CrossRef] [PubMed]
8. Cronin, M.; Ross, J.S. Comprehensive next-generation cancer genome sequencing in the era of targeted therapy and personalized oncology. *Biomark. Med.* **2011**, *5*, 293–305. [CrossRef] [PubMed]
9. Couraud, S.; Vaca-Paniagua, F.; Villar, S.; Oliver, J.; Schuster, T.; Blanché, H.; Girard, N.; Trédaniel, J.; Guilleminault, L.; Gervais, R.; *et al*. BioCAST/IFCT-1002 investigators: Noninvasive diagnosis of actionable mutations by deep sequencing of circulating free DNA in lung cancer from never-smokers: A proof-of-concept study from BioCAST/IFCT-1002. *Clin. Cancer Res.* **2014**, *20*, 4613–4624. [CrossRef] [PubMed]
10. Nomenclature for the description of sequence variants. Available online: http://www.hgvs.org/mutnomen/ (accessed on 10 April 2015).
11. Den Dunnen, J.T.; Antonarakis, S.E. Mutation nomenclature extensions and suggestions to describe complex mutations: A discussion. *Hum. Mutat.* **2000**, *15*, 7–12. [CrossRef]
12. Richards, S.; Aziz, N.; Bale, S.; Bick, D.; Das, S.; Gastier-Foster, J.; Grody, W.W.; Hegde, M.; Lyon, E.; Spector, E.; *et al*. Standards and guidelines for the interpretation of sequence variants: A joint consensus recommendation of the American College of Medical Genetics and Genomics and the Association for Molecular Pathology. *Genet. Med.* **2015**, *17*, 405–424. [CrossRef] [PubMed]
13. COSMIC (Catalogue of Somatic Mutations in Cancer). Available online: http://cancer.sanger.ac.uk/cosmic (accessed on 28 February 2015).
14. Choudhary, A.; Mambo, E.; Sanford, T.; Boedigheimer, M.; Twomey, B.; Califano, J.; Hadd, A.; Oliner, K.S.; Beaudenon, S.; Latham, G.J.; *et al*. Evaluation of an integrated clinical workflow for targeted next-generation sequencing of low-quality tumor DNA using a 51-gene enrichment panel. *BMC Med. Genom.* **2014**, *7*. [CrossRef] [PubMed]
15. Zhang, L.; Chen, L.; Sah, S.; Latham, G.J.; Patel, R.; Song, Q.; Koeppen, H.; Tam, R.; Schleifman, E.; Mashhedi, H.; *et al*. Profiling cancer gene mutations in clinical formalin-fixed, paraffin-embedded colorectal tumor specimens using targeted next-generation sequencing. *Oncologist* **2014**, *19*, 336–343. [CrossRef] [PubMed]
16. Hadd, A.G.; Houghton, J.; Choudhary, A.; Sah, S.; Chen, L.; Marko, A.C.; Sanford, T.; Buddavarapu, K.; Krosting, J.; Garmirek, L.; *et al*. Targeted, high-depth, next-generation sequencing of cancer genes in formalin-fixed, paraffin-embedded and fine-needle aspiration tumor specimens. *J. Mol. Diagn.* **2013**, *15*, 234–247. [CrossRef] [PubMed]

17. Hagemann, I.S.; Devarakonda, S.; Lockwood, C.M.; Spencer, D.H.; Guebert, K.; Bredemeyer, A.J.; al-Kateb, H.; Nguyen, T.T.; Duncavage, E.J.; Cottrell, C.E.; *et al*. Clinical next-generation sequencing in patients with non-small cell lung cancer. *Cancer* **2015**, *121*, 631–639. [CrossRef] [PubMed]
18. D'Haene, N.; le Mercier, M.; de Nève, N.; Blanchard, O.; Delaunoy, M.; el Housni, H.; Dessars, B.; Heimann, P.; Remmelink, M.; Demetter, P.; *et al*. Clinical Validation of Targeted Next Generation Sequencing for Colon and Lung Cancers. *PLoS ONE* **2015**, *10*, e0138245. [CrossRef] [PubMed]
19. Sah, S.; Chen, L.; Houghton, J.; Kemppainen, J.; Marko, A.C.; Zeigler, R.; Latham, G.J. Functional DNA quantification guides accurate next-generation sequencing mutation detection in formalin-fixed, paraffin-embedded tumor biopsies. *Genome Med.* **2013**, *5*, 77. [CrossRef] [PubMed]
20. Simbolo, M.; Gottardi, M.; Corbo, V.; Fassan, M.; Mafficini, A.; Malpeli, G.; Lawlor, R.T.; Scarpa, A. DNA qualification workflow for next generation sequencing of histopathological samples. *PLoS ONE* **2013**, *8*, e62692. [CrossRef] [PubMed]
21. Ross, M.G.; Russ, C.; Costello, M.; Hollinger, A.; Lennon, N.J.; Hegarty, R.; Nusbaum, C.; Jaffe, D.B. Characterizing and measuring bias in sequence data. *Genome Biol.* **2013**, *14*. [CrossRef] [PubMed]
22. Wilm, A.; Aw, P.P.; Bertrand, D.; Yeo, G.H.; Ong, S.H.; Wong, C.H.; Khor, C.C.; Petric, R.; Hibberd, M.L.; Nagarajan, N. LoFreq: A sequence quality aware, ultra-sensitive variant caller for uncovering cell population heterogeneity from high-throughput sequencing datasets. *Nucleic Acids Res.* **2012**, *40*, 11189–11201. [CrossRef] [PubMed]
23. Genome Analysis Toolkit (GATK). Available online: https://www.broadinstitute.org/gatk/index.php (accessed on 3 February 2015).
24. Boland, J.F.; Chung, C.C.; Roberson, D.; Mitchell, J.; Zhang, X.; Im, K.M.; He, J.; Chanock, S.J.; Yeager, M.; Dean, M. The new sequencer on the block: Comparison of Life Technology's Proton sequencer to an Illumina HiSeq for whole-exome sequencing. *Hum. Genet.* **2013**, *132*, 1153–1163. [CrossRef] [PubMed]
25. Gerlinger, M.; Rowan, A.J.; Horswell, S.; Larkin, J.; Endesfelder, D.; Gronroos, E.; Martinez, P.; Matthews, N.; Stewart, A.; Tarpey, P.; *et al*. Intratumor heterogeneity and branched evolution revealed by multiregion sequencing. *N. Engl. J. Med.* **2012**, *366*, 883–892. [CrossRef] [PubMed]
26. Vogelstein, B.; Papadopoulos, N.; Velculescu, V.E.; Zhou, S.; Diaz, L.A., Jr.; Kinzler, K.W. Cancer genome landscapes. *Science* **2013**, *339*, 1546–1558. [CrossRef] [PubMed]
27. Sakurada, A.; Lara-Guerra, H.; Liu, N.; Shepherd, F.A.; Tsao, M.S. Tissue heterogeneity of EGFR mutation in lung adenocarcinoma. *J. Thorac. Oncol.* **2008**, *3*, 527–529. [CrossRef] [PubMed]
28. Zhang, J.; Fujimoto, J.; Zhang, J.; Wedge, D.C.; Song, X.; Zhang, J.; Seth, S.; Chow, C.W.; Cao, Y.; Gumbs, C.; *et al*. Intratumor heterogeneity in localized lung adenocarcinomas delineated by multiregion sequencing. *Science* **2014**, *346*, 256–259. [CrossRef] [PubMed]
29. De Bruin, E.C.; McGranahan, N.; Mitter, R.; Salm, M.; Wedge, D.C.; Yates, L.; Jamal-Hanjani, M.; Shafi, S.; Murugaesu, N.; Rowan, A.J.; *et al*. Spatial and temporal diversity in genomic instability processes defines lung cancer evolution. *Science* **2014**, *346*, 251–256. [CrossRef] [PubMed]
30. Imielinski, M.; Berger, A.H.; Hammerman, P.S.; Hernandez, B.; Pugh, T.J.; Hodis, E.; Cho, J.; Suh, J.; Capelletti, M.; Sivachenko, A.; *et al*. Mapping the hallmarks of lung adenocarcinoma with massively parallel sequencing. *Cell* **2012**, *150*, 1107–1120. [CrossRef] [PubMed]
31. Cancer Genome Atlas Research Network. Comprehensive genomic characterization of squamous cell lung cancers. *Nature* **2012**, *489*, 519–525.
32. Zhang, X.; Miao, X.; Guo, Y.; Tan, W.; Zhou, Y.; Sun, T.; Wang, Y.; Lin, D. Genetic polymorphisms in cell cycle regulatory genes MDM2 and TP53 are associated with susceptibility to lung cancer. *Hum. Mutat.* **2006**, *27*, 110–117. [CrossRef] [PubMed]
33. Zheng, D.; Chen, Y.; Gao, C.; Wei, Y.; Cao, G.; Lu, N.; Hou, Y.; Jiang, X.; Wang, J. Polymorphisms of *p53* and *MDM2* genes are associated with severe toxicities in patients with non-small cell lung cancer. *Cancer Biol. Ther.* **2014**, *15*, 1542–1551. [CrossRef] [PubMed]
34. Govindan, R.; Ding, L.; Griffith, M.; Subramanian, J.; Dees, N.D.; Kanchi, K.L.; Maher, C.A.; Fulton, R.; Fulton, L.; Wallis, J.; *et al*. Genomic landscape of non-small cell lung cancer in smokers and never-smokers. *Cell* **2012**, *50*, 1121–1134. [CrossRef] [PubMed]
35. Diaz, L.A., Jr.; Bardelli, A. Liquid biopsies: Genotyping circulating tumor DNA. *J. Clin. Oncol.* **2014**, *32*, 579–586. [CrossRef] [PubMed]

36. Zhang, L.; Cui, X.; Schmitt, K.; Hubert, R.; Navidi, W.; Arnheim, N. Whole genome amplification from a single cell: Implications for genetic analysis. *Proc. Natl. Acad. Sci. USA* **1992**, *89*, 5847–5851. [CrossRef] [PubMed]
37. Telenius, H.; Carter, N.P.; Bebb, C.E.; Nordenskjold, M.; Ponder, B.A.; Tunnacliffe, A. Degenerate oligonucleotide-primed PCR: General amplification of target DNA by a single degenerate primer. *Genomics* **1992**, *13*, 718–725. [CrossRef]
38. Kamberov, E.; Sleptsova, I.; Suchyta, S.; Bruening, E.; Zeihler, W.; Nagel, J.S.; Langmore, J.; Makarov, V. Use of *in vitro* OmniPlex Libraries for high-throughput comparative genomics and molecular haplotyping. *Proc. SPIE* **2002**, *4626*, 340–351.
39. Langmore, J.P. Rubicon Genomics, Inc. *Pharmacogenomics* **2002**, *3*, 557–560. [CrossRef] [PubMed]
40. Lizardi, P.M.; Huang, X.; Zhu, Z.; Bray-Ward, P.; Thomas, D.C.; Ward, D.C. Mutation detection and single-molecule counting using isothermal rolling-circle amplification. *Nat. Genet.* **1998**, *19*, 225–232. [CrossRef] [PubMed]
41. Dean, F.B.; Hosono, S.; Fang, L.; Wu, X.; Faruqi, A.F.; Bray-Ward, P.; Sun, Z.; Zong, Q.; Du, Y.; Du, J.; *et al*. Comprehensive human genome amplification using multiple displacement amplification. *Proc. Natl. Acad. Sci. USA* **2002**, *99*, 5261–5266. [CrossRef] [PubMed]
42. Barker, D.L.; Hansen, M.S.; Faruqi, A.F.; Giannola, D.; Irsula, O.R.; Lasken, R.S.; Latterich, M.; Makarov, V.; Oliphant, A.; Pinter, J.H.; *et al*. Two methods of whole-genome amplification enable accurate genotyping across a 2320-SNP linkage panel. *Genome Res.* **2004**, *14*, 901–907. [CrossRef] [PubMed]
43. Bergen, A.W.; Haque, K.A.; Qi, Y.; Beerman, M.B.; Garcia-Closas, M.; Rothman, N.; Chanock, S.J. Comparison of yield and genotyping performance of multiple displacement amplification and OmniPlex whole genome amplified DNA generated from multiple DNA sources. *Hum. Mutat.* **2005**, *26*, 262–270. [CrossRef] [PubMed]
44. Park, J.W.; Beaty, T.H.; Boyce, P.; Scott, A.F.; McIntosh, I. Comparing whole-genome amplification methods and sources of biological samples for single-nucleotide polymorphism genotyping. *Clin. Chem.* **2005**, *51*, 1520–1523. [CrossRef] [PubMed]
45. Pask, R.; Rance, H.E.; Barratt, B.J.; Nutland, S.; Smyth, D.J.; Sebastian, M.; Twells, R.C.; Smith, A.; Lam, A.C.; Smink, L.J.; *et al*. Investigating the utility of combining Phi29 whole genome amplification and highly multiplexed single nucleotide polymorphism BeadArray genotyping. *BMC Biotechnol.* **2004**, *4*. [CrossRef] [PubMed]
46. Pinard, R.; de Winter, A.; Sarkis, G.J.; Gerstein, M.B.; Tartaro, K.R.; Plant, R.N.; Egholm, M.; Rothberg, J.M.; Leamon, J.H. Assessment of whole genome amplification-induced bias through high-throughput, massively parallel whole genome sequencing. *BMC Genom.* **2006**, *7*. [CrossRef] [PubMed]
47. Yilmaz, S.; Singh, A.K. Single cell genome sequencing. *Curr. Opin. Biotechnol.* **2011**, *23*, 1–7. [CrossRef] [PubMed]
48. Bergen, A.W.; Qi, Y.; Haque, K.A.; Welch, R.A.; Chanock, S.J. Effects of DNA mass on multiple displacement whole genome amplification and genotyping performance. *BMC Biotechnol.* **2005**, *5*. [CrossRef] [PubMed]
49. Hansen, H.M.; Wiemels, J.L.; Wrensch, M.; Wiencke, J.K. DNA quantification of whole genome amplified samples for genotyping on a multiplexed bead array platform. *Cancer Epidemiol. Biomark. Prev.* **2007**, *16*, 1686–1690. [CrossRef] [PubMed]
50. Paez, J.G.; Lin, M.; Beroukhim, R.; Lee, J.C.; Zhao, X.; Richter, D.J.; Gabriel, S.; Herman, P.; Sasaki, H.; Altshuler, D.; *et al*. Genome coverage and sequence fidelity of Phi29 polymerase-based multiple strand displacement whole genome amplification. *Nucleic Acids Res.* **2004**, *32*. [CrossRef] [PubMed]
51. Hosono, S.; Faruqi, A.F.; Dean, F.B.; Du, Y.; Sun, Z.; Wu, X.; Du, J.; Kingsmore, S.F.; Egholm, M.; Lasken, R.S. Unbiased whole-genome amplification directly from clinical samples. *Genome Res.* **2003**, *13*, 954–964. [CrossRef] [PubMed]
52. Lim, E.H.; Zhang, S.L.; Li, J.L.; Yap, W.S.; Howe, T.C.; Tan, B.P.; Lee, Y.S.; Wong, D.; Khoo, K.L.; Seto, K.Y.; *et al*. Using whole genome amplification (WGA) of low-volume biopsies to assess the prognostic role of EGFR, KRAS, p53, and CMET mutations in advanced-stage non-small cell lung cancer (NSCLC). *J. Thorac. Oncol.* **2009**, *4*, 12–21. [CrossRef] [PubMed]
53. Bettegowda, C.; Sausen, M.; Leary, R.J.; Kinde, I.; Wang, Y.; Agrawal, N.; Bartlett, B.R.; Wang, H.; Luber, B.; Alani, R.M.; *et al*. Detection of circulating tumor DNA in early- and late-stage human malignancies. *Sci. Transl. Med.* **2014**, *6*. [CrossRef] [PubMed]

54. Diehl, F.; Schmidt, K.; Choti, M.A.; Romans, K.; Goodman, S.; Li, M.; Thornton, K.; Agrawal, N.; Sokoll, L.; Szabo, S.A.; *et al*. Circulating mutant DNA to assess tumor dynamics. *Nat. Med.* **2008**, *14*, 985–990. [CrossRef] [PubMed]
55. Van Beers, E.H.; Joosse, S.A.; Ligtenberg, M.J.; Fles, R.; Hogervorst, F.B.; Verhoef, S.; Nederlof, P.M. A multiplex PCR predictor for aCGH success of FFPE samples. *Br. J. Cancer* **2006**, *94*, 333–337. [CrossRef] [PubMed]
56. Thorvaldsdóttir, H.; Robinson, J.T.; Mesirov, J.P. Integrative Genomics Viewer (IGV): High-performance genomics data visualization and exploration. *Brief. Bioinform.* **2013**, *14*, 178–192. [CrossRef] [PubMed]
57. Cingolani, P.; Platts, A.; Wang, L.L.; Coon, M.; Nguyen, T.; Wang, L.; Land, S.J.; Lu, X.; Ruden, D.M. A program for annotating and predicting the effects of single nucleotide polymorphisms, SnpEff: SNPs in the genome of Drosophila melanogaster strain w1118; iso-2; iso-3. *Fly* **2012**, *6*, 80–92. [CrossRef] [PubMed]
58. PolyPhen-2 prediction of functional effects of human nsSNPs. Available online: http://genetics.bwh.harvard.edu/pph2/ (accessed on 28 February 2015).
59. SIFT Blink. Available online: http://sift.jcvi.org/ (accessed on 28 February 2015).
60. 1000Genomes. Available online: http://www.1000genomes.org/ (accessed on 28 February 2015).
61. Coco, S.; Truini, A.; Alama, A.; dal-Bello, M.G.; Venè, R.; Garuti, A.; Carminati, E.; Rijavec, E.; Genova, C.; Barletta, G.; *et al*. Afatinib resistance in non-small cell lung cancer involves the PI3K/AKT and MAPK/ERK signalling pathways and epithelial-to-mesenchymal transition. *Target Oncol.* **2015**, *10*, 393–404. [CrossRef] [PubMed]
62. Rehm, H.L.; Bale, S.J.; Bayrak-Toydemir, P.; Berg, J.S.; Brown, K.K.; Deignan, J.L.; Friez, J.; Funke, B.H.; Hegde, M.R.; Lyon, E.; *et al*. ACMG clinical laboratory standards for next-generation sequencing. *Genet. Med.* **2013**, *15*, 733–747. [CrossRef] [PubMed]
63. Coco, S.; de Mariano, M.; Valdora, F.; Servidei, T.; Ridola, V.; Andolfo, I.; Oberthuer, A.; Tonini, G.P.; Longo, L. Identification of ALK germline mutation (3605delG) in pediatric anaplastic medulloblastoma. *J. Hum. Genet.* **2012**, *57*, 682–684. [CrossRef] [PubMed]



© 2015 by the authors; licensee MDPI, Basel, Switzerland. This article is an open access article distributed under the terms and conditions of the Creative Commons by Attribution (CC-BY) license (http://creativecommons.org/licenses/by/4.0/).

International Journal of
Molecular Sciences

MDPI

Article

Fulvic Acid Attenuates Resistin-Induced Adhesion of HCT-116 Colorectal Cancer Cells to Endothelial Cells

Wen-Shih Huang [1,2], Jen-Tsung Yang [3], Chien-Chang Lu [1,4], Shun-Fu Chang [5], Cheng-Nan Chen [6], Yu-Ping Su [7] and Ko-Chao Lee [4,*]

Received: 1 September 2015; Accepted: 30 November 2015; Published: 9 December 2015
Academic Editor: William Chi-shing Cho

1 Graduate Institute of Clinical Medical Sciences, College of Medicine, Chang Gung University, Taoyuan 333, Taiwan; wen1204@adm.cgmh.org.tw (W.-S.H.); cclu999@gmail.com (C.-C.L.)
2 Division of Colon and Rectal Surgery, Department of Surgery, Chang Gung Memorial Hospital, Chiayi 613, Taiwan
3 Department of Neurosurgery, Chang Gung Memorial Hospital at Chiayi, Chang-Gung University College of Medicine, Chiayi 613, Taiwan; jents716@ms32.hinet.net
4 Division of Colorectal Surgery, Department of Surgery, Chang Gung Memorial Hospital-Kaohsiung Medical Center, Chang Gung University College of Medicine, Kaohsiung 833, Taiwan
5 Department of Medical Research and Development, Chang Gung Memorial Hospital Chiayi Branch, Chiayi 613, Taiwan; sfchang@cgmh.org.tw
6 Department of Biochemical Science and Technology, National Chiayi University, Chiayi 600, Taiwan; cnchen@mail.ncyu.edu.tw
7 Department of Orthopaedics and Traumatology, Taipei Veterans General Hospital & School of Medicine, National Yang-Ming University, Taipei 112, Taiwan; ypsu@vghtpe.gov.tw
* Correspondence: kmch4329@gmail.com; Tel.: +886-7-731-7123; Fax: +886-7-731-8762

Abstract: A high level of serum resistin has recently been found in patients with a number of cancers, including colorectal cancer (CRC). Hence, resistin may play a role in CRC development. Fulvic acid (FA), a class of humic substances, possesses pharmacological properties. However, the effect of FA on cancer pathophysiology remains unclear. The aim of this study was to investigate the effect of resistin on the endothelial adhesion of CRC and to determine whether FA elicits an antagonistic mechanism to neutralize this resistin effect. Human HCT-116 (p53-negative) and SW-48 (p53-positive) CRC cells and human umbilical vein endothelial cells (HUVECs) were used in the experiments. Treatment of both HCT-116 and SW-48 cells with resistin increases the adhesion of both cells to HUVECs. This result indicated that p53 may not regulate this resistin effect. A mechanistic study in HCT-116 cells further showed that this resistin effect occurs via the activation of NF-κB and the expression of intercellular adhesion molecule-1 (ICAM-1) and vascular cell adhesion molecule-1 (VCAM-1). Co-treating cells with both FA and resistin revealed that FA significantly attenuated the resistin-increased NF-κB activation and ICAM-1/VCAM-1 expression and the consequent adhesion of HCT-116 cells to HUVECs. These results demonstrate the role of resistin in promoting HCT-116 cell adhesion to HUVECs and indicate that FA might be a potential candidate for the inhibition of the endothelial adhesion of CRC in response to resistin.

Keywords: colorectal carcinoma; fulvic acid; intercellular adhesion molecule-1; resistin; vascular cell adhesion molecule-1

1. Introduction

Fulvic acid (FA) is a natural, acidic organic polymer extracted from humus found in soil, sediment, or aquatic environments [1,2]. It is composed of a mixture of closely related complex aromatic polymers, and spectroscopic and chemical analysis have demonstrated the presence of multiple active functional groups, including aromatic rings and phenolic hydroxyl, ketone carbonyl, quinone carbonyl, carboxyl and alkoxyl groups [3]. Traditionally, FA is used as a supplement, as these active functional groups help the absorption of other essential nutrients into the body [1]. Recently, it was reported that FA has antioxidant properties and apparent neuro-protective effects [4]. Additional antimicrobial and anti-inflammatory properties of FA have also been reported [5,6]. These results from pharmacological studies of FA imply that FA may modulate and control the pathophysiology of multiple diseases. However, the detailed roles and mechanisms underlying these regulatory effects of FA remain unclear.

Colorectal cancer (CRC) is one of the leading causes of malignancy deaths worldwide [7]. Its incidence rate has accelerated in developing countries over the past few decades [8]. Recently, accumulating studies have shown that central obesity may be the most important risk factor for CRC development [9]. Moreover, obesity (body mass index, BMI > 25 kg/m^2) increases CRC risk 7%–60% compared to an individual with BMI < 25 kg/m^2 [10,11]. Adipose tissue has been revealed as an endocrine organ, releasing various adipokines with multiple regulatory activities for the pathogenesis of disease [12,13]. Resistin is a newly discovered adipokine. Recent studies have indicated that the plasma levels of resistin are increased in many inflammation-related disorders such as atherosclerosis and arthritis [14]. Increasing evidence has also revealed that serum resistin positively correlates with the development and metastasis of malignancies [15]. Although the studies have some discrepancies, the circulating levels of serum resistin may serve as biomarkers for the pathogenesis and progression of many cancers, in particular CRC. However, information is lacking about the detailed regulatory mechanisms of resistin in CRC development.

Cancer metastasis is the most life-threatening clinical issue associated with human cancer. It results in poor prognosis and is responsible for approximately 90% of patient mortality [16–18]. Metastasis is facilitated by the adhesion of cancer cells to the endothelium in the second tissue site. Moreover, cell adhesion molecules (CAMs) including selectins, integrins, and immunoglobulin superfamily proteins play critical and necessary roles in metastasis [19]. The intercellular adhesion molecule-1 (ICAM-1) and vascular cell adhesion molecule-1 (VCAM-1) are two immunoglobulin superfamily adhesion molecules. Both contribute to the endothelium adhesion of cancer cells and the immune responses of cancers [16,20]. The expression of ICAM-1 and VCAM-1, which are regulated by the transcription factor NF-κB, in endothelial cells initiates the adhesion of cancer cells and monocytes to the endothelium [16,21,22]. Moreover, our previous study showed that ICAM-1 and VCAM-1 were also expressed in hepatocellular carcinoma (HCC) and promoted HCC cell adhesion to the endothelium [15]. Hence, ICAM-1 and VCAM-1 in both cancer and endothelial cells may play synergistic roles in metastasis progressions.

In this study, we determined the effects of resistin and FA on the endothelium adhesion of human CRC cells and the underlying mechanism. We found that resistin activates NF-κB to induce ICAM-1 and VCAM-1 expression in HCT-116 cells, promoting CRC cell adhesion to endothelial cells. However, FA attenuated these resistin effects on HCT-116 cells. Our data reveal the resistin regulatory effects on CRC adhesion to the endothelium and suggest that FA may serve as a potential therapeutic candidate to inhibit the endothelium adhesion of CRC under resistin stimulation.

2. Results

2.1. Resistin Induces Adhesion of HCT-116 and SW-48 Cells to HUVECs (Human Umbilical Vein Endothelial Cells)

To determine the level of CRC cell adhesion to the endothelium, HCT-116 (p53-negative) and SW-48 (p53-positive) cells were maintained as controls or stimulated with resistin at 5, 10, 25 and 50 ng/mL for 4 h. After co-culturing both cell lines with HUVECs for 1 h and then removing non-adherent cells, the remaining adherent cells were stained with crystal violet solution and measured using a spectrophotometer. Treating cells with resistin increased the adhesion of both HCT-116 and SW-48 cells to HUVECs in a dose-dependent manner compared with untreated control (Figure 1). This effect was specific to resistin, as resistin-neutralizing antibodies completely inhibited the resistin-increased HCT-116 and SW-48 cell adhesion to HUVECs. We further investigated the molecular mechanism of this resistin effect by treating HCT-116 cells with 50 ng/mL of resistin.

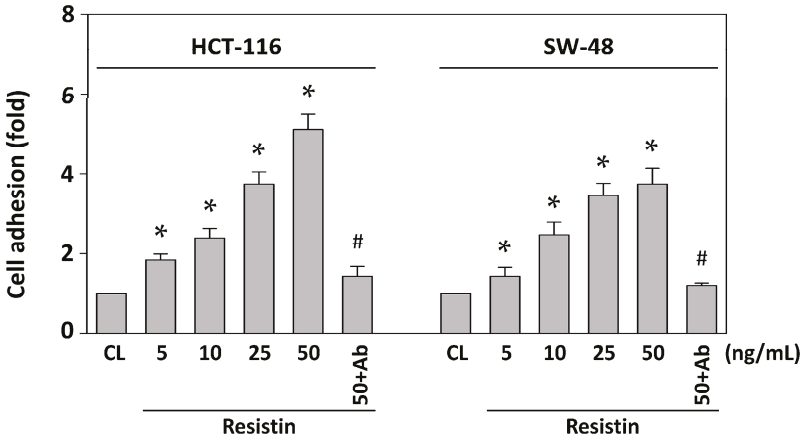

Figure 1. Resistin induces HCT-116 and SW-48 cell adhesion to HUVECs. HCT-116 and SW-48 cells were maintained as controls or stimulated with resistin and then stained with a crystal violet solution. The adhesion of HCT-116 and SW-48 cells to HUVECs was assessed. HCT-116 and SW-48 cells incubated with resistin (50 ng/mL) plus resistin-neutralizing antibodies (Ab) exhibited no increase in HUVEC adhesion. Data represent the mean ± standard error of the mean (SEM) from four independent experiments. * $p < 0.05$ *vs.* control cells; # $p < 0.05$ *vs.* cells treated with resistin only.

2.2. Resistin Increases the Expressions of ICAM-1 and VCAM-1 in HCT-116 Cells

Both ICAM-1 and VCAM-1 play a crucial role in cancer metastasis [15,16]. Hence, we determined whether resistin induces ICAM-1 and VCAM-1 expression in HCT-116 cells. HCT-116 cells were maintained as control or stimulated with resistin for 1, 2, 4 and 8 h, and the mRNA and protein expression of ICAM-1 and VCAM-1 were analyzed. Treating cells with resistin significantly increased ICAM-1 and VCAM-1 mRNA (Figure 2A,B) and protein (Figure 2C,D) expression within 1 h compared with the untreated control. The increased levels reached a maximum within 4 h and then declined but remained elevated after 8 h of treatment.

2.3. Blocking ICAM-1 and VCAM-1 in HCT-116 Cells Inhibits Adhesion to HUVECs

To determine whether the induction of both ICAM-1 and VCAM-1 expression under resistin stimulation in HCT-116 cells regulates the HUVEC adhesion of HCT-116 cells, HCT-116 cells were pretreated with ICAM-1 and VCAM-1 specific blocking antibodies or siRNAs and then were maintained as control or stimulated with resistin for 4 h. The resistin-increased HUVEC adhesion of HCT-116 cells was inhibited by ICAM-1 or VCAM-1 antibody pretreatment. Co-pretreatment with both antibodies resulted in greater inhibitory effects compared to IgG and single-antibody

pretreated cells (Figure 3A). Moreover, these inhibitory effects on the resistin-increased HUVEC adhesion of HCT-116 cells were further verified by transfecting HCT-116 cells with ICAM-1- and/or VCAM-1-specific siRNAs, which showed similar results to the blocking antibody pretreatment (Figure 3B).

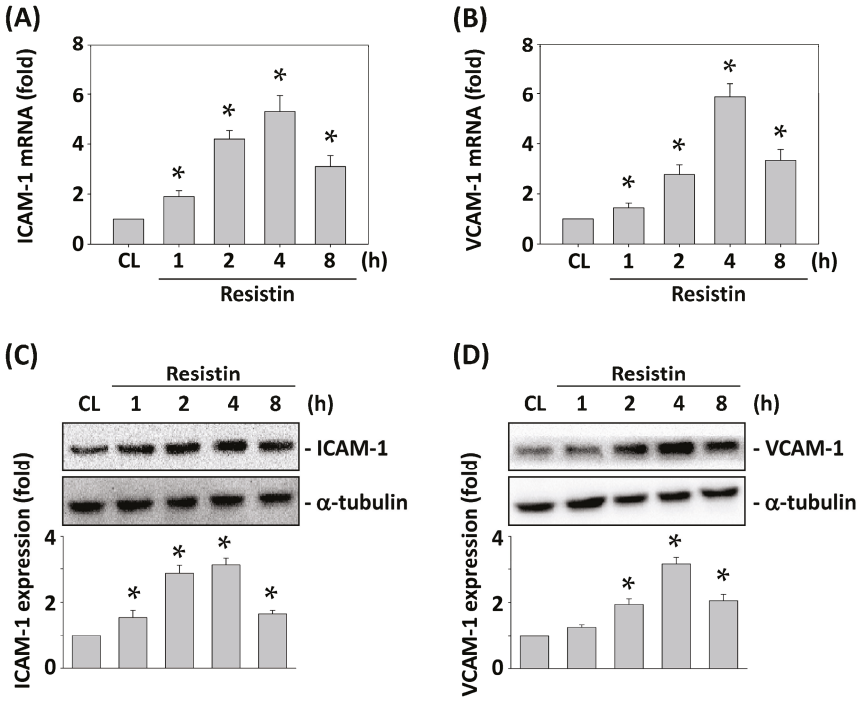

Figure 2. Resistin increases the expressions of ICAM-1 and VCAM-1 in HCT-116 cells. HCT-116 cells were maintained as control or stimulated with resistin. ICAM-1 and VCAM-1 mRNA (**A**,**B**) and protein (**C**,**D**) expression was analyzed. Data in (**A**,**B**) represent the mean ± SEM from three independent experiments. The results in (**C**,**D**) are representative of three independent experiments with similar results. * $p < 0.05$ *vs.* control cells.

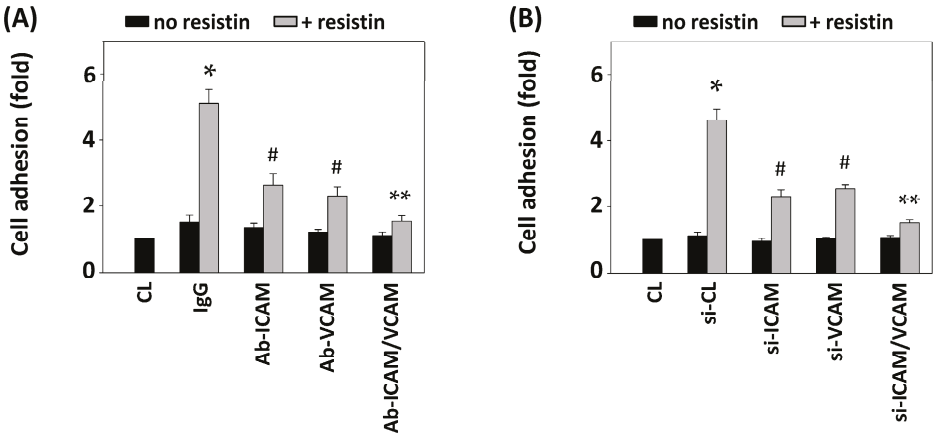

Figure 3. Blocking ICAM-1 and VCAM-1 in HCT-116 cells inhibits their adhesion to HUVECs. HCT-116 cells were pretreated with specific neutralizing antibodies (**A**) or siRNAs (**B**) for control (IgG/si-CL), ICAM-1, VCAM-1, or both and then were maintained as control or stimulated with resistin. HCT-116 cell adhesion was determined. Data represent the mean ± SEM from four independent experiments. * $p < 0.05$ *vs.* control cells (CL); # $p < 0.05$ *vs.* cells pretreated with IgG or si-CL and then treated with resistin only; ** $p < 0.05$ *vs.* cells pretreated with ICAM-1 or VCAM-1 neutralizing antibody and then treated with resistin.

2.4. Resistin-Initiated HCT-116 Adhesion to HUVECs Is Mediated by the NF-κB Activation

ICAM-1 and VCAM-1 expression are mainly regulated by the transcription factor NF-κB [15,16]. Therefore, we further determined whether NF-κB activation in HCT-116 cells regulates resistin-initiated HCT-116 cell adhesion to HUVECs. HCT-116 cells were maintained as control or stimulated with resistin for 1, 2, and 4 h, and the NF-κB activity was analyzed using the NF-κB activation ELISA kit. Treatment with resistin for 1, 2, and 4 h induced NF-κB activation within 1 h, which reached a maximum level within 2 h and then declined after 4 h (Figure 4A). Pretreating HCT-116 cells with DMSO or the NF-κB inhibitors pyrrolidine dithiocarbamate (PDTC) (20 μM) or SN50 (50 μg/mL) for 1 h and then stimulating cells with resistin for 4 h revealed that pretreating cells with PDTC or SN50 significantly inhibited the resistin effects on the expression of ICAM-1 and VCAM-1 in HCT-116 cells (Figure 4B). We further demonstrated that resistin induced NF-κB p65 phosphorylation in HCT-116 cells (Figure 4C). Moreover, Pretreating HCT-116 cells with DMSO or different doses of NF-κB inhibitors, PDTC: 20 (1×) and 40 (2×) μM or SN50: 50 (1×) and 100 (2×) μg/mL, revealed the dose-dependent inhibitory effect of inhibitors on the adhesion of HCT-116 cells to HUVECs in response to resistin stimulation (Figure 4D). Gene knockdown of p65 by different doses of p65 specific siRNA (20 and 30 nM), which caused 70% and over 90% reduction separately in the expression of the corresponding proteins, significantly inhibited the adhesion of HCT-116 cells to HUVECs in a dose-dependent manner under resistin stimulation (Figure 4E).

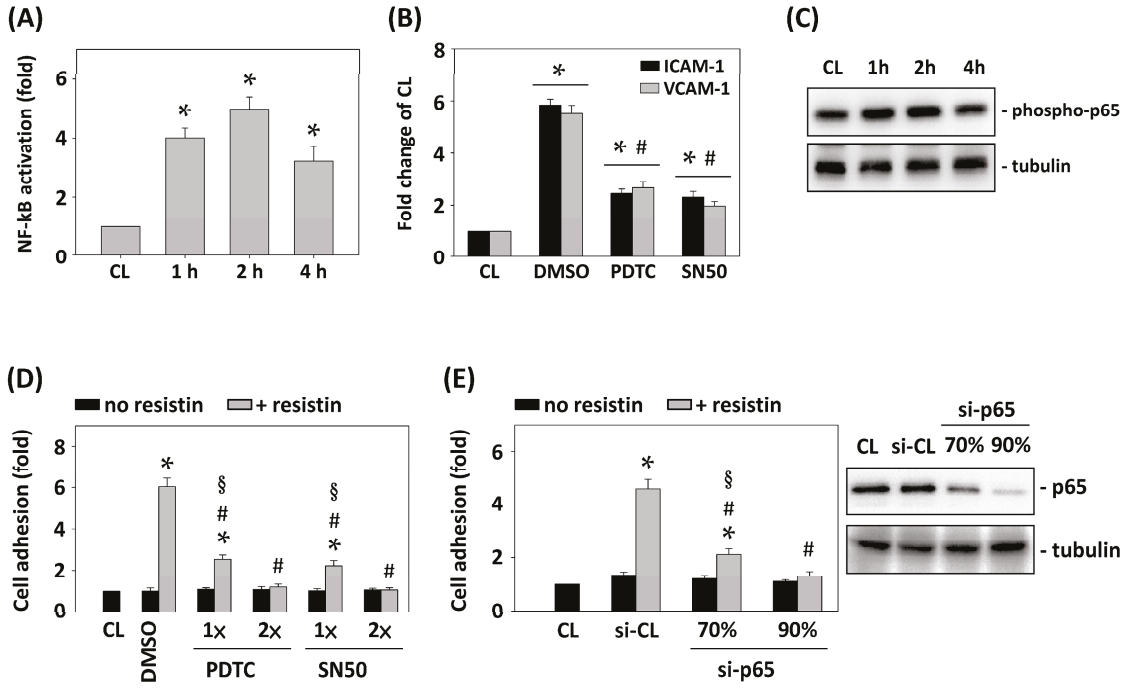

Figure 4. Resistin-initiated HCT-116 adhesion to HUVECs is mediated by NF-κB activation. (**A**) and (**C**) HCT-116 cells were maintained as control or stimulated with resistin for 1, 2, and 4 h and then NF-κB activation (**A**) and p65 phosphorylation (**C**) were determined by ELISA kit and Western blot, respectively; (**B**,**D**,**E**) HCT-116 cells were pretreated with (**B**,**D**) DMSO or NF-κB inhibitors (PDTC or SN50) and (**E**) control or p65 specific siRNA and then stimulated with resistin. HCT-116 cell adhesion and ICAM-1/VCAM-1 mRNA expression were analyzed. Data represent the mean ± SEM from three independent experiments. * $p < 0.05$ *vs.* control cells; # $p < 0.05$ *vs.* DMSO or si-CL cells with resistin treatment; § $p < 0.05$ *vs.* PDTC, SN50, or si-p65 cells without resistin treatment.

2.5. FA (Fulvic Acid) Inhibits Resistin-Initiated HCT-116 Cell Adhesion to HUVECs

FA is a potential therapeutic candidate for many diseases [1,4]. Hence, we determined whether the effects of resistin on the HUVEC adhesion of HCT-116 cells are modulated by FA. HCT-116 cells were pretreated with FA at 0, 1, 5 and 10 μg/mL for 1 h and then were maintained as control or stimulated with resistin for 4 h, and HCT-116 cell adhesion to HUVECs was examined. Treating cells with only resistin increased HCT-116 cell adhesion to HUVECs compared with the untreated control. However, pretreating cells with FA significantly inhibited the resistin effects on the HUVEC adhesion of HCT-116 cells in a dose-dependent manner (Figure 5A). Treating cells with FA (10 μg/mL) alone did not induce the adhesion of HCT-116 cells to HUVECs (Figure 5A). Moreover, pretreating HCT-116 cells with 0 or 10 μg/mL of FA for 1 h and then maintaining them as control or stimulating with resistin at 10, 25 and 50 ng/mL for 4 h showed that FA significantly inhibited the effects of all three concentrations of resistin on the HUVEC adhesion of HCT-116 cells compared with the resistin-only treated cells (Figure 5B).

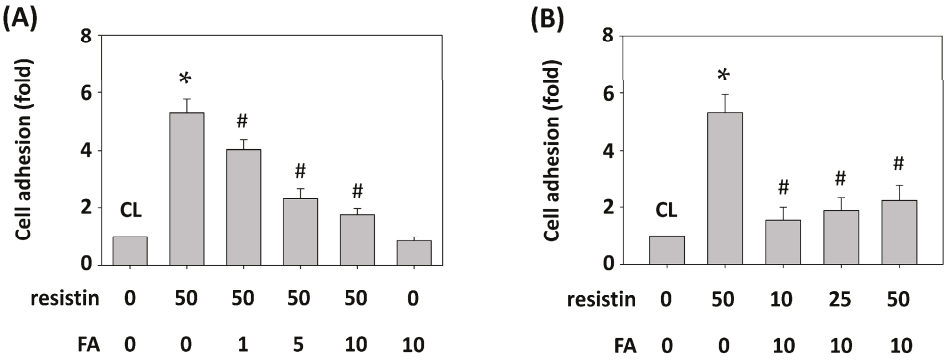

Figure 5. FA inhibits resistin-initiated HCT-116 cell adhesion to HUVECs. (**A**) HCT-116 cells were pretreated with FA at 0, 1, 5 and 10 μg/mL and then were maintained as control or stimulated with resistin; (**B**) HCT-116 cells were pretreated with FA at 0 or 10 μg/mL and then were maintained as control or stimulated with resistin at 10, 25 and 50 ng/mL. HCT-116 cell adhesion was determined. Data represent the mean ± SEM from three independent experiments. * $p < 0.05$ *vs.* control cells; # $p < 0.05$ *vs.* cells treated with resistin only.

2.6. FA Inhibits Resistin-Induced ICAM-1 and VCAM-1 Expression in HCT-116 Cells

Next, we investigated whether FA mediates the resistin-increased ICAM-1 and VCAM-1 expression in HCT-116 cells. HCT-116 cells were pretreated with FA at 0, 1, 5 and 10 μg/mL for 1 h and then were maintained as control or stimulated with resistin for 4 h. The ICAM-1 and VCAM-1 mRNA and protein expression in HCT-116 cells was determined. Treating cells with only resistin induced ICAM-1 and VCAM-1 mRNA (Figure 6A,B) and protein (Figure 6C,D) expression compared with the untreated control. However, pretreating cells with FA at 1, 5 and 10 μg/mL significantly decreased ICAM-1 and VCAM-1 mRNA and protein expression in HCT-116 cells compared with the resistin-only treated cells.

2.7. FA Inhibits the Resistin Effect on HCT-116 Cell Adhesion to HUVECs by Down-Regulating NF-κB Activity

HCT-116 cells were pretreated with FA at 0, 1, 5 and 10 μg/mL for 1 h and then were maintained as control or stimulated with resistin for 4 h, and NF-κB activity was determined. Treatment with resistin alone activated NF-κB in HCT-116 cells (Figure 7, compared with the untreated control). However, pretreatment with FA at 1, 5 and 10 μg/mL significantly decreased NF-κB activity in HCT-116 cells.

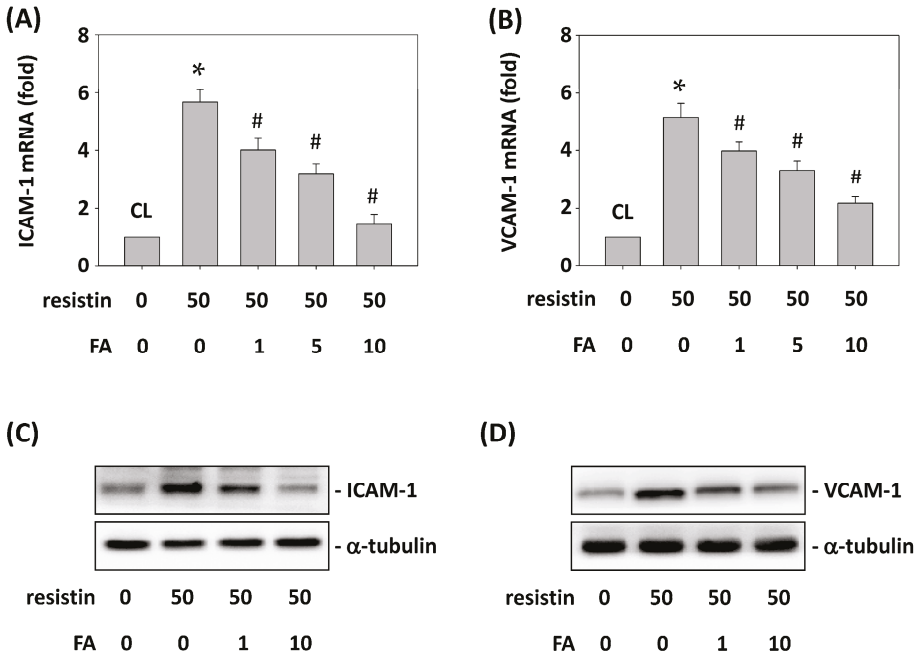

Figure 6. FA inhibits resistin-induced ICAM-1 and VCAM-1 expression in HCT-116 cells. HCT-116 cells were pretreated with FA at 0, 1, 5 and 10 μg/mL and then were maintained as control or stimulated with resistin. ICAM-1 and VCAM-1 mRNA (**A**,**B**) and protein (**C**,**D**) expression was determined. Data in (**A**,**B**) represent the mean ± SEM from three independent experiments. The results in (**C**,**D**) are representative of three independent experiments with similar results. * $p < 0.05$ *vs.* control cells; # $p < 0.05$ *vs.* cells treated with resistin only.

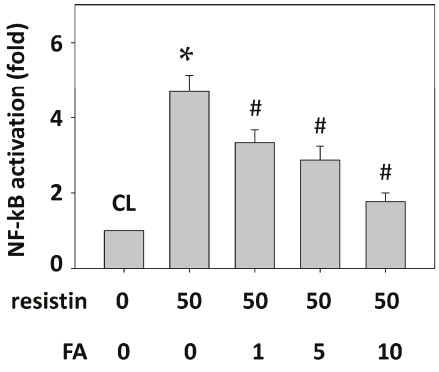

Figure 7. FA inhibits the resistin effect on HCT-116 cell adhesion to HUVECs by down-regulating NF-κB activity. HCT-116 cells were pretreated with FA at 0, 1, 5 and 10 μg/mL and then were maintained as control or stimulated with resistin. The activation of NF-κB was determined. Data represent the mean ± SEM from three independent experiments. * $p < 0.05$ *vs.* control cells; # $p < 0.05$ *vs.* cells treated with resistin only.

3. Discussion

This study has made the unique discovery that resistin can initiate the endothelial adhesion of CRC cells through increasing NF-κB activity and the consequent ICAM-1 and VCAM-1 expression in HCT-116 cells. FA may play an antagonistic role to suppress this resistin effect. Our study has generated the following findings. First, this work shows that resistin increases both HCT-116 (p53-negative) and SW-48 (p53-positive) cell adhesion to HUVECs and demonstrated that this resistin effect is p53 tumor suppressor-independent. Second, the resistin-increased HCT-116 cell adhesion to HUVECs occurs through the induction of ICAM-1 and VCAM-1 mRNA and protein expression by

the canonical NF-κB pathway, p65 subunit phosphorylation, in HCT-116 cells. Finally, FA attenuates the resistin effect on HCT-116 cell adhesion to HUVECs by inhibiting NF-κB activity and ICAM-1 and VCAM-1 expression. Thus, these results elucidate the molecular basis of resistin in promoting the adhesion of CRC cells to endothelium and the antagonistic role of FA in this effect.

Natural organic substrates are important and interesting sources in developing healthy foods and drugs. Recently, FA, derived from the humification of natural organic substrates, has been widely considered an attractive pharmacological research candidate because of its structure and composition of multiple active groups [3]. For example, the anti-oxidative activity [4] and anti-microbial [5], anti-allergy [23], anti-inflammation [6], and ultraviolet (UV)-protective properties [24] of FA have been elucidated and demonstrated. Moreover, the latest report indicated that FA interacts with human serum transferring, and this interaction might be applied to drug delivery design and tumor treatment [1]. Our present study investigates the effect of FA on the endothelial adhesion of cancer cells and demonstrates for the first time that FA exerts inhibitory effects on resistin-induced HCT-116 CRC cell adhesion to HUVECs, thereby possibly serving as potent inhibitory candidate in the endothelium adhesion of cancer cells during metastasis. Our results also prove that one mechanism of this FA effect is through inhibiting resistin-activated NF-κB in HCT-116 cells. This mechanism is similar to the reported anti-inflammatory activity of FA, which decreases TNF-α release in U937 monocyte-like cells and NF-κB activation in HUVECs [24]. Recently, cancer has also been identified as a chronic inflammatory disease [16,25]. Therefore, we suggest that FA may be applied in studying cancer treatment through blocking the inflammatory reactions in the cancer microenvironment, including monocyte, cancer, and endothelial cells.

Increasing epidemiological evidence since 2012 has demonstrated that the serum resistin level positively correlates to CRC carcinogenesis [26]. However, to our knowledge, the present study is the first to elucidate that part of the mechanism whereby resistin positively enhances CRC cell adhesion to the endothelium is p53 tumor suppressor-independent and occurs through inducing canonical NF-κB activity to up-regulate the genes encoding the ICAM-1 and VCAM-1 adhesion proteins in HCT-116 cells. Previously studies have demonstrated that NF-κB p65 subunit and p53 regulate each other's activity to affect target gene transcription and cell function [27]. However, we excluded this possibility in our model, as resistin could induce the adhesion of p53-negative HCT-116 and p53-positive SW-48 cells to HUVECs. Resistin has been reported to exert its biological effects by binding to Toll-like receptor 4 (TLR4) on the surface of target cells [28]. NF-κB is an important transcription factor that can be activated by TLR4 which leads to potentiate expression of various genes involved in inflammation [29]. Prior published work has indicated that the canonical NF-κB is an important positive regulator of ICAM-1 and VCAM-1 gene transcription [15,30], and also enhanced monocyte adhesion to HUVECs [21]. Here, by employing several NF-κB-specific inhibitors, we evaluated the functional role of the canonical NF-κB pathway in the mechanism whereby resistin enhances CRC cell adhesion. Treatment of CRC cells with high doses of PDTC, SN50, or p65 siRNA efficiently blocked resistin-mediated CRC cell adhesion to HUVECs. Thus, our results demonstrate that resistin-induced NF-κB activation promotes CRC cell adhesion, in conjunction with inducing their ICAM-1 and VCAM-1 expression. Moreover, our results suggest that high serum resistin levels are related to cancer-associated chronic inflammation and support the previous study in which resistin exhibited pro-inflammatory properties by up-regulating the expression of TNF-α and IL-6 and the activation of monocytes [25–27,31–33]. Although resistin is an adipose tissue-secreted cytokines, recent studies have found that resistin could also be expressed in peripheral blood mononuclear cells, macrophages, and bone marrow cells [25,34,35]. Some reports have also indicated that the resistin releases the modulatory activities in inflammatory related diseases, including CRC [36–40]. Moreover, S. Ghaemmaghami *et al.* [25], indicated that resistin is not expressed in CRC cells and may act in a paracrine manner for CRC carcinogenesis. Inflammatory cells, including monocytes, but not CRC cells could play a major role in the high resistin expression in tissue and plasma levels due to the chronic low-grade inflammatory status in CRC. Although there

is still some controversy over the precise role of high serum resistin and CRC cancer development, our study provides evidence that resistin modulates CRC cell adhesion to the endothelium.

Cancer metastasis, a major clinical problem of human cancer, is responsible for most cancer patient mortality [16]. The endothelial adhesion of cancer cells plays a crucial role in cancer metastasis. This is an important step for executing the subsequent steps of invasion and survival of cancer cells [41,42]. In the present study, we demonstrated that the resistin-initiated HCT-116 cell adhesion to the endothelium is achieved through inducing the expression of ICAM-1 and VCAM-1 in HCT-116 cells. ICAM-1 and VCAM-1 are two important cell surface adhesion molecules that are mainly expressed in endothelial cells to modulate the immune process and cancer cell adhesion to the endothelium [16,42]. Resistin increases ICAM-1 and VCAM-1 expression in endothelial cells to induce monocyte-endothelial cell adhesion [21]. However, the present study shows that resistin not only induces ICAM-1 and VCAM-1 expression in CRC cells but also mediates cancer cell adhesion to the endothelium. Recently, soluble forms of adhesion molecules, including ICAM-1 and VCAM-1, have been found in the serum of cancer patients, in the supernatant of cytokine-activated endothelial cells and in the culture medium of CRC cell lines [43,44]. Moreover, an elevated serum-soluble adhesion molecule level correlates significantly with cancer progression and can serve as clinical diagnostic and prognostic markers [15]. Therefore, although we have not yet determined the precise role of ICAM-1 and VCAM-1 expression in CRC cells, ICAM-1 and VCAM-1 in the resistin-treated cancer and endothelial cells may be secreted into the cancer microenvironment and mediate the interactions of cancer, immune, and endothelial cells. On the other hand, recent studies have indicated that cancer metastasis could be initiated by cancer cell-leukocyte interactions [45]. The specific receptors of ICAM-1 and VCAM-1, *i.e.*, lymphocyte function-associated antigen (LFA)-1 and very-late antigen (VLA)-4 integrins, respectively, are expressed in immune cells [46]. Thus, the issue of whether the resistin-initiated endothelial adhesion of CRC cells through ICAM-1 and VCAM-1 in CRC cells is controlled by cancer cell-leukocyte interactions warrants further investigation.

This study has indicated that resistin can initiate the endothelial adhesion of CRC cells, with concomitant increases in NF-κB activity and ICAM-1 and VCAM-1 expression in CRC cells. However, FA antagonizes this resistin-induced response. As a result, this study proposes novel roles for resistin and FA in modulating CRC adhesion to the endothelium. Moreover, a new perspective on the antagonistic effects of FA on the endothelial adhesion of cancer cells warrants further exploration.

4. Experimental Section

4.1. Materials

Recombinant human resistin was purchased from R & D Systems (Minneapolis, MN, USA). FA was supplied from the Esther Material Technology Co., Ltd., Kaohsiung, Taiwan. Human polyclonal antibodies against p65, ICAM-1 and VCAM-1 were purchased from R & D Systems (Minneapolis, MN, USA). Mouse monoclonal anti-resistin neutralizing antibody was purchased from Biocompare. The specific siRNAs for control, ICAM-1, VCAM-1, and p65 were purchased from Invitrogen (Carlsbad, CA, USA). NF-κB inhibitors (PDTC and SN50) and all other chemicals of reagent grade were purchased from Sigma (St. Louis, MO, USA) unless otherwise noted.

4.2. Cell Cultures

Human HCT-116 and SW-48 cells were obtained from the cell bank in the Food Industry Research and Development Institute (Hsinchu, Taiwan) and were grown in DMEM (Life Technologies, Inc., Gaithersburg, MD, USA) supplemented with 10% fetal bovine serum (FBS; Life Technologies, Inc., Gaithersburg, MD, USA) and 1% penicillin/streptomycin in a 37 °C incubator. Human umbilical vein endothelial cells (HUVECs) were obtained from Cambrex Bio Science (Walkersville, MD, USA) and were grown in endothelial cell growth medium-2 (EGM-2) and maintained in a 37 °C incubator. HUVECs of passage 3–5 were used for the experiments.

4.3. Cell Adhesion Assay

The binding of HCT-116 cells to HUVECs was determined using a colorimetric method [47]. Briefly, HCT-116 cells were grown in 0.5% FBS medium overnight and then were stimulated with resistin. For inhibition experiments, HCT-116 cells were pretreated with specific inhibitors or neutralizing antibodies or were transfected with specific siRNAs before stimulating with resistin. The HCT-116 cells (2×10^5 cells/mL) were co-cultured with HUVECs, and non-adherent cells were removed by washing with PBS. The cells were fixed with 1.0% glutaraldehyde for 20 min and then stained with 0.1% crystal violet for 15 min. After washing with sterile water, the stained cells were solubilized in 0.1% Triton X-100 overnight. The adhesion level of HCT-116 cells were determined at 595 nm wavelength by using a spectrophotometer. The data were normalized by the background determined from the staining of HUVECs alone.

4.4. Western Blot Analysis

The cells were collected and lysed with RIPA buffer (1% nonylphenoxypolyethoxyethanol (NP)-40, 0.5% sodium deoxycholate, 0.1% SDS, and protease/phosphatase inhibitor cocktail (phenylmethylsulfonyl fluoride, aprotinin, and sodium orthovanadate)). The concentration of total cell lysate was determined using the protein assay kit (Bio-Rad, Hercules, CA, USA), separated by sodium dodecyl sulfate-polyacrylamide gel electrophoresis (SDS-PAGE) (10% running and 4% stacking), transferred onto a nitrocellulose membrane, and analyzed using the designated antibodies. Immunodetection was performed using the Western-Light chemiluminescent detection system (Applied Biosystems, Forster City, CA, USA).

4.5. Quantitative Real-Time PCR

RNA was extracted and converted to cDNA. The cDNA was amplified using the ABI Prism 7900HT with the FastStart DNA SYBR Green I kit (Invitrogen, Carlsbad, CA, USA) with primers for ICAM-1 (forward: 5′-GTGACATGCAGCACCTCCTG-3′; reverse: 5′-TCCATGGTGATCTCTCCTCA-3′), VCAM-1 (forward: 5′-CCGGATTGCTGCTCAGATTGGA-3′; reverse: 5′-AGCGTGGAATTGGTCCCCTCA-3′), and 18S rRNA (forward: 5′-CGGCGACGACCCATTCGAAC-3′; reverse: 5′-GAAT CGAACCCTGAT TCCCCGTC-3′). The quantification of gene expression levels was performed using the $2^{-\Delta\Delta Ct}$ method. The PCR for all genes was performed in duplicate.

4.6. siRNA Transfection

HCT-116 cells at 70% confluence were transfected with the specific siRNA, which caused ~60%–90% reductions in the expressions of the corresponding proteins, for 48 h using the RNAiMAX transfection kit (Invitrogen, Carlsbad, CA, USA).

4.7. NF-κB Activation Enzyme-Linked Immunosorbent Assay (ELISA)

The cell nuclear extracts were purified using a nuclear protein extract kit (EK1121) (Panomics, Redwood City, CA, USA), and the activation of NF-κB p65 in equal amounts of nuclear proteins was measured using commercially available ELISA kits (EK1121) (Panomics, Redwood City, CA, USA). Briefly, an oligonucleotide containing a NF-κB 65 consensus binding site (supplied by the ELISA kit) was immobilized on the 96-well plate. Nuclear proteins were added to the plate to bind to this oligonucleotide. The p65/DNA complex was identified by a NF-κB p65 specific antibody and a secondary horseradish peroxidase (HRP)-conjugated antibody and was determined by using spectrophotometry.

4.8. Statistical Analysis

The experiment was performed at least three times. Results are represented as the mean ± standard error of mean (SEM). Statistical significance was calculated by using an independent Student's paired

t test for comparisons of two groups of data and an ANOVA followed by Scheffe's test for multiple comparisons. *p* value less than 0.05 was considered to be significant.

Acknowledgments: This work was supported by grant MOST 103-2320-B-182A-021-MY3 from Ministry of Science and Technology and by grants CMRPG8C0241, CMRPG8C1262, CMRPG6C0013 and CMRPG8E0491 from Chang Gung Memorial Hospital-Kaohsiung Medical Center, and Chang Gung Memorial Hospital, Chia-Yi, Taiwan.

Author Contributions: All authors were involved in conception and design of the study. Wen-Shih Huang, Jen-Tsung Yang, Chien-Chang Lu, Shun-Fu Chang, Cheng-Nan Chen, and Yu-Ping Su were involved in the acquisition of data. Wen-Shih Huang, Chien-Chang Lu, and Ko-Chao Lee were involved in the statistical analysis and the interpretation of the data. Wen-Shih Huang and Ko-Chao Lee wrote the manuscript. All authors commented and approved the final version. All authors had full access to all data.

Conflicts of Interest: The authors declare no conflict of interest.

References

1. Zhang, X.F.; Yang, G.; Dong, Y.; Zhao, Y.Q.; Sun, X.R.; Chen, L.; Chen, H.B. Studies on the binding of fulvic acid with transferrin by spectroscopic analysis. *Spectrochim. Acta A Mol. Biomol. Spectrosc.* **2015**, *137*, 1280–1285. [CrossRef] [PubMed]
2. Alvarez-Puebla, R.A.; Valenzuela-Calahorro, C.; Garrido, J.J. Theoretical study on fulvic acid structure, conformation and aggregation. A molecular modelling approach. *Sci. Total Environ.* **2006**, *358*, 243–254. [CrossRef] [PubMed]
3. Wang, C.; Wang, Z.; Peng, A.; Hou, J.; Xin, W. Interaction between fulvic acids of different origins and active oxygen radicals. *Sci. China C Life Sci.* **1996**, *39*, 267–275. [PubMed]
4. Motojima, H.; Yamada, P.; Han, J.; Ozaki, M.; Shigemori, H.; Isoda, H. Properties of fulvic acid extracted from excess sludge and its inhibiting effect on beta-hexosaminidase release. *Biosci. Biotechnol. Biochem.* **2009**, *73*, 2210–2216. [CrossRef] [PubMed]
5. Van Rensburg, C.E.; van Straten, A.; Dekker, J. An *in vitro* investigation of the antimicrobial activity of oxifulvic acid. *J. Antimicrob. Chemother.* **2000**, *46*, 853–854. [CrossRef] [PubMed]
6. Van Rensburg, C.E.; Malfeld, S.C.K.; Dekker, J. Topical application of oxifulvic acid suppresses the cutaneous immune response in mice. *Drug Dev. Res.* **2001**, *53*, 29–32. [CrossRef]
7. Joshi, R.K.; Kim, W.J.; Lee, S.A. Association between obesity-related adipokines and colorectal cancer: A case-control study and meta-analysis. *World J. Gastroenterol.* **2014**, *20*, 7941–7949. [CrossRef] [PubMed]
8. Gunter, M.J.; Hoover, D.R.; Yu, H.; Wassertheil-Smoller, S.; Rohan, T.E.; Manson, J.E.; Howard, B.V.; Wylie-Rosett, J.; Anderson, G.L.; Ho, G.Y.; *et al*. Insulin, insulin-like growth factor-I, endogenous estradiol, and risk of colorectal cancer in postmenopausal women. *Cancer Res.* **2008**, *68*, 329–337. [CrossRef] [PubMed]
9. Ma, Y.; Yang, Y.; Wang, F.; Zhang, P.; Shi, C.; Zou, Y.; Qin, H. Obesity and risk of colorectal cancer: A systematic review of prospective studies. *PLoS ONE* **2013**, *8*, e53916. [CrossRef] [PubMed]
10. Dai, Z.; Xu, Y.C.; Niu, L. Obesity and colorectal cancer risk: A meta-analysis of cohort studies. *World J. Gastroenterol.* **2007**, *13*, 4199–4206. [CrossRef] [PubMed]
11. Larsson, S.C.; Wolk, A. Obesity and colon and rectal cancer risk: A meta-analysis of prospective studies. *Am. J. Clin. Nutr.* **2007**, *86*, 556–565. [PubMed]
12. Wang, S.N.; Lee, K.T.; Ker, C.G. Leptin in hepatocellular carcinoma. *World J. Gastroenterol.* **2010**, *16*, 5801–5809. [CrossRef] [PubMed]
13. Vázquez-Vela, M.E.; Torres, N.; Tovar, A.R. White adipose tissue as endocrine organ and its role in obesity. *Arch. Med. Res.* **2008**, *39*, 715–728. [CrossRef] [PubMed]
14. Dalamaga, M.; Sotiropoulos, G.; Karmaniolas, K.; Pelekanos, N.; Papadavid, E.; Lekka, A. Serum resistin: A biomarker of breast cancer in postmenopausal women? Association with clinicopathological characteristics, tumor markers, inflammatory and metabolic parameters. *Clin. Biochem.* **2013**, *46*, 584–590. [CrossRef] [PubMed]
15. Yang, C.C.; Chang, S.F.; Chao, J.K.; Lai, Y.L.; Chang, W.E.; Hsu, W.H.; Kuo, W.H. Activation of AMP-activated protein kinase attenuates hepatocellular carcinoma cell adhesion stimulated by adipokine resistin. *BMC Cancer* **2014**, *14*. [CrossRef] [PubMed]

16. Reymond, N.; d'Água, B.B.; Ridley, A.J. Crossing the endothelial barrier during metastasis. *Nat. Rev. Cancer* **2013**, *13*, 858–870. [CrossRef] [PubMed]
17. Hanahan, D.; Weinberg, R.A. Hallmarks of cancer: The next generation. *Cell* **2011**, *144*, 646–674. [CrossRef] [PubMed]
18. Reddy, B.Y.; Lim, P.K.; Silverio, K.; Patel, S.A.; Won, B.W.; Rameshwar, P. The Microenvironmental effect in the progression, metastasis, and dormancy of breast cancer: A model system within bone marrow. *Int. J. Breast Cancer* **2012**, *2012*. [CrossRef] [PubMed]
19. Alexiou, D.; Karayiannakis, A.J.; Syrigos, K.N.; Zbar, A.; Kremmyda, A.; Bramis, I.; Tsigris, C. Serum levels of E-selectin, ICAM-1 and VCAM-1 in colorectal cancer patients: Correlations with clinicopathological features, patient survival and tumour surgery. *Eur. J. Cancer* **2001**, *37*, 2392–2397. [CrossRef]
20. Yoong, K.F.; McNab, G.; Hübscher, S.G.; Adams, D.H. Vascular adhesion protein-1 and ICAM-1 support the adhesion of tumor-infiltrating lymphocytes to tumor endothelium in human hepatocellular carcinoma. *J. Immunol.* **1998**, *160*, 3978–3988. [PubMed]
21. Hsu, W.Y.; Chao, Y.W.; Tsai, Y.L.; Lien, C.C.; Chang, C.F.; Deng, M.C.; Ho, L.T.; Kwok, C.F.; Juan, C.C. Resistin induces monocyte-endothelial cell adhesion by increasing ICAM-1 and VCAM-1 expression in endothelial cells via p38MAPK-dependent pathway. *J. Cell. Physiol.* **2011**, *226*, 2181–2188. [CrossRef] [PubMed]
22. Kawanami, D.; Maemura, K.; Takeda, N.; Harada, T.; Nojiri, T.; Imai, Y.; Manabe, I.; Utsunomiya, K.; Nagai, R. Direct reciprocal effects of resistin and adiponectin on vascular endothelial cells: A new insight into adipocytokine-endothelial cell interactions. *Biochem. Biophys. Res. Commun.* **2004**, *314*, 415–419. [CrossRef] [PubMed]
23. Yamada, P.; Isoda, H.; Han, J.K.; Talorete, T.P.; Abe, Y. Inhibitory effect of fulvic acid extracted from Canadian sphagnum peat on chemical mediator release by RBL-2H3 and KU812 cells. *Biosci. Biotechnol. Biochem.* **2007**, *71*, 1294–1305. [CrossRef] [PubMed]
24. Junek, R.; Morrow, R.; Schoenherr, J.I.; Schubert, R.; Kallmeyer, R.; Phull, S.; Klöcking, R. Bimodal effect of humic acids on the LPS-induced TNF-α release from differentiated U937 cells. *Phytomedicine* **2009**, *16*, 470–476. [CrossRef] [PubMed]
25. Ghaemmaghami, S.; Mohaddes, S.M.; Hedayati, M.; Gorgian Mohammadi, M.; Dehbashi, G. Resistin and visfatin expression in HCT-116 colorectal cancer cell line. *Int. J. Mol. Cell Med.* **2013**, *2*, 143–150. [PubMed]
26. Danese, E.; Montagnana, M.; Minicozzi, A.M.; Bonafini, S.; Ruzzenente, O.; Gelati, M.; de Manzoni, G.; Lippi, G.; Guidi, G.C. The role of resistin in colorectal cancer. *Clin. Chim. Acta* **2012**, *413*, 760–764. [CrossRef] [PubMed]
27. Tergaonkar, V.; Perkins, N.D. p53 and NF-κB crosstalk: IKKα tips the balance. *Mol. Cell* **2007**, *26*, 158–159. [CrossRef] [PubMed]
28. Benomar, Y.; Gertler, A.; de Lacy, P.; Crépin, D.; Ould Hamouda, H.; Riffault, L.; Taouis, M. Central resistin overexposure induces insulin resistance through Toll-like receptor 4. *Diabetes* **2013**, *62*, 102–114. [CrossRef] [PubMed]
29. Chen, R.; Alvero, A.B.; Silasi, D.A.; Steffensen, K.D.; Mor, G. Cancers take their Toll—The function and regulation of Toll-like receptors in cancer cells. *Oncogene* **2008**, *27*, 225–233. [CrossRef] [PubMed]
30. Kim, S.R.; Bae, Y.H.; Bae, S.K.; Choi, K.S.; Yoon, K.H.; Koo, T.H.; Jang, H.O.; Yun, I.; Kim, K.W.; Kwon, Y.G.; *et al*. Visfatin enhances ICAM-1 and VCAM-1 expression through ROS-dependent NF-κB activation in endothelial cells. *Biochim. Biophys. Acta* **2008**, *1783*, 886–895. [CrossRef] [PubMed]
31. Sălăgeanu, A.; Tucureanu, C.; Lerescu, L.; Caraş, I.; Pitica, R.; Gangurà, G.; Costea, R.; Neagu, S. Serum levels of adipokines resistin and leptin in patients with colon cancer. *J. Med. Life* **2010**, *3*, 416–420. [PubMed]
32. Sun, C.A.; Wu, M.H.; Chu, C.H.; Chou, Y.C.; Hsu, G.C.; Yang, T.; Chou, W.Y.; Yu, C.P.; Yu, J.C. Adipocytokine resistin and breast cancer risk. *Breast Cancer Res. Treat.* **2010**, *123*, 869–876. [CrossRef] [PubMed]
33. Bokarewa, M.; Nagaev, I.; Dahlberg, L.; Smith, U.; Tarkowski, A. Resistin, an adipokine with potent proinflammatory properties. *J. Immunol.* **2005**, *174*, 5789–5795. [CrossRef] [PubMed]
34. Kaser, S.; Kaser, A.; Sandhofer, A.; Ebenbichler, C.F.; Tilg, H.; Patsch, J.R. Resistin messenger-RNA expression is increased by proinflammatory cytokines *in vitro*. *Biochem. Biophys. Res. Commun.* **2003**, *309*, 286–290. [CrossRef] [PubMed]

35. Qatanani, M.; Szwergold, N.R.; Greaves, D.R.; Ahima, R.S.; Lazar, M.A. Macrophage-derived human resistin exacerbates adipose tissue inflammation and insulin resistance in mice. *J. Clin. Investig.* **2009**, *119*, 531–539. [CrossRef] [PubMed]
36. Stofkova, A. Resistin and visfatin: Regulators of insulin sensitivity, inflammation and immunity. *Endocr. Regul.* **2010**, *44*, 25–36. [CrossRef] [PubMed]
37. Axelsson, J.; Bergsten, A.; Qureshi, A.R.; Heimbürger, O.; Bárány, P.; Lönnqvist, F.; Lindholm, B.; Nordfors, L.; Alvestrands, A.; Stenvinkel, P. Elevated resistin levels in chronic kidney disease are associated with decreased glomerular filtration rate and inflammation, but not with insulin resistance. *Kidney Int.* **2006**, *69*, 596–604. [CrossRef] [PubMed]
38. Pang, S.S.; Le, Y.Y. Role of resistin in inflammation and inflammation-related diseases. *Cell. Mol. Immunol.* **2006**, *3*, 29–34. [PubMed]
39. Konrad, A.; Lehrke, M.; Schachinger, V.; Seibold, F.; Stark, R.; Ochsenkühn, T.; Parhofer, K.G.; Göke, B.; Broedl, U.C. Resistin is an inflammatory marker of inflammatory bowel disease in humans. *Eur. J. Gastroenterol. Hepatol.* **2007**, *19*, 1070–1074. [CrossRef] [PubMed]
40. Almehed, K.; d'Elia, H.F.; Bokarewa, M.; Carlsten, H. Role of resistin as a marker of inflammation in systemic lupus erythematosus. *Arthritis Res. Ther.* **2008**, *10*. [CrossRef] [PubMed]
41. Tung, S.Y.; Chang, S.F.; Chou, M.H.; Huang, W.S.; Hsieh, Y.Y.; Shen, C.H.; Kuo, H.C.; Chen, C.N. CXC chemokine ligand 12/stromal cell-derived factor-1 regulates cell adhesion in human colon cancer cells by induction of intercellular adhesion molecule-1. *J. Biomed. Sci.* **2012**, *19*. [CrossRef] [PubMed]
42. Kobayashi, H.; Boelte, K.C.; Lin, P.C. Endothelial cell adhesion molecules and cancer progression. *Curr. Med. Chem.* **2007**, *14*, 377–386. [CrossRef] [PubMed]
43. Pigott, R.; Dillon, L.P.; Hemingway, I.H.; Gearing, A.J. Soluble forms of E-selectin, ICAM-1 and VCAM-1 are present in the supernatants of cytokine activated cultured endothelial cells. *Biochem. Biophys. Res. Commun.* **1992**, *187*, 584–589. [CrossRef]
44. Dippold, W.; Wittig, B.; Schwaeble, W.; Mayet, W.; Meyer zum Büschenfelde, K.H. Expression of intercellular adhesion molecule 1 (ICAM-1, CD54) in colonic epithelial cells. *Gut* **1993**, *34*, 1593–1597. [CrossRef] [PubMed]
45. Pawelek, J.M.; Chakraborty, A.K. Fusion of tumour cells with bone marrow-derived cells: A unifying explanation for metastasis. *Nat. Rev. Cancer* **2008**, *8*, 377–386. [CrossRef] [PubMed]
46. Yusuf-Makagiansar, H.; Anderson, M.E.; Yakovleva, T.V.; Murray, J.S.; Siahaan, T.J. Inhibition of LFA-1/ICAM-1 and VLA-4/VCAM-1 as a therapeutic approach to inflammation and autoimmune diseases. *Med. Res. Rev.* **2002**, *22*, 146–167. [CrossRef] [PubMed]
47. Chana, R.S.; Wheeler, D.C. Fibronectin augments monocyte adhesion to low-density lipoprotein-stimulated mesangial cells. *Kidney Int.* **1999**, *55*, 179–188. [CrossRef] [PubMed]



© 2015 by the authors; licensee MDPI, Basel, Switzerland. This article is an open access article distributed under the terms and conditions of the Creative Commons by Attribution (CC-BY) license (http://creativecommons.org/licenses/by/4.0/).

International Journal of
Molecular Sciences

MDPI

Article

CHMP4C Disruption Sensitizes the Human Lung Cancer Cells to Irradiation

Kang Li, Jianxiang Liu, Mei Tian, Gang Gao, Xuesong Qi, Yan Pan, Jianlei Ruan, Chunxu Liu and Xu Su *

Received: 17 November 2015; Accepted: 18 December 2015; Published: 24 December 2015
Academic Editor: William Chi-shing Cho

Key Laboratory of Radiological Protection and Nuclear Emergency, China CDC,
National Institute for Radiological Protection, Chinese Center for Disease Control and Prevention,
2 Xinkang Street, Dewai, Beijing 10088, China; likangtianyi@163.com (K.L.); jxliu@163.com (J.L.);
tianmei1203@aliyun.com (M.T.); gaogang@nirp.cn (G.G.); cedar121@sina.com (X.Q.);
ruanjl2013@sohu.com (Y.P.); ananpy@163.com (J.R.); liuchunxu0214@126.com (C.L.)
* Correspondence: suxu@nirp.cn; Tel.: +86-10-6238-9720

Abstract: Human lung cancer is highly invasive and the most malignant among human tumors. Adenocarcinoma as a specific type of non-small cell lung cancer occurs with high frequency and is also highly resistant to radiation therapy. Thus, how to avoid radiation resistance and improve radiotherapy effectiveness is a crucial question. In the present study, human lung cancer A549 and H1299 cells were irradiated using γ-rays from a Co60 irradiator. Protein expression was detected by Western blotting. Cell cycle and apoptosis were measured by flow cytometry. Surviving fraction was determined by colony formation assay. γH2AX and 53BP1 foci formation were examined by fluorescence microscopy. In the results, we show that CHMP4C, a subunit of Endosomal sorting complex-III (ESCRT-III), is involved in radiation-induced cellular response. Radiation-induced Aurora B expression enhances CHMP4C phosphorylation in non-small cell lung cancer (NSCLC) cells, maintaining cell cycle check-point and cellular viability as well as resisting apoptosis. CHMP4C depletion enhances cellular sensitivity to radiation, delays S-phase of cell cycle and reduces ionizing radiation (IR)-induced γH2AX foci formation. We found that Aurora B targets CHMP4C and inhibition of Aurora B exhibits similar effects with silencing of CHMP4C in radioresistance. We also confirm that CHMP4C phosphorylation is elevated after IR both in p53-positive and-negative cells, indicating that the close correlation between CHMP4C and Aurora B signaling pathway in mediating radiation resistance is not p53 dependent. Together, our work establishes a new function of CHMP4C in radiation resistance, which will offer a potential strategy for non-small cell lung cancer by disrupting CHMP4C.

Keywords: CHMP4C; Aurora B; human non-small lung cancer cells; radiation

1. Introduction

Human lung cancer is highly invasive and most malignant among human tumors, which is classified into non-small cell lung cancer and small cell lung cancer. Non-small cell lung cancer accounts for about 85% of lung cancers and the current therapeutic strategy includes surgical resection together with radiation and/or chemo-treatment. Radiation resistance is the severe outcome of lung cancer radiotherapy and therefore poses a critical barrier for the radio-therapeutic effect. Hence, how to avoid the radiation resistance and to improve its treatment efficiency is a major challenge [1,2].

Ionizing radiation initiates DNA damage and arrests cell cycle progression, leading to cellular genomic instability and loss of genetic information. In response to the damage stress, the ataxia telangiectasia mutated kinase (ATM) and ataxia telangiectasia and Rad3-related protein (ATR) are

activated. ATM and ATR can also engage in cell division control via activating cyclins and cyclin-dependent kinases (Cdks) [3,4]. A recent study found that in the cell division, there is a very important cytokinetic abscission checkpoint regulated by CHMP4C, which controls abscission time to coordinate mid-body resolution and prevents accumulation of DNA damage. CHMP4C can check the abscission timing through Aurora B-directed phosphorylation [5].

Aurora B kinase is the key kinase of CPC (Chromosomal Passenger Complex) essential for the mitotic processes. Aurora B expression and activity are altered during the cell cycle and peaks at the G2-M transition. Aurora B is elevated in a variety of human tumors and its over-expression is susceptible to tumor formation and poor outcomes of non-small cell lung cancer radiotherapy, therefore indicating that Aurora B might be a drug target for lung cancer [6–8]. However, whether Aurora B directly participates in lung cancer development is still unknown.

That ESCRT (Endosomal sorting complex) is required for the CPC (Chromosomal passenger complex)-mediated cytokinetic abscission, during which CPC monitors the right abscission time of two daughter cells. ESCRT has six distinct complexes (containing ESCRT-0, -I, -II, -III, ALIX and Vps4) engaging in multi-vesicular body formation, cytokinesis and HBV (Hepatitis B virus) budding [9–11]. ESCRT-III (Endosome sorting complex-III) mediates membrane fission at the end of cytokinesis. A recent study reported that CHMP4C, a subunit of ESCRT-III, retards abscission and inhibits DNA damage accumulation in abscission checkpoint [12–15]. Meanwhile, CHMP4C enhances autophagy and endosome production, during which p53 transcriptionally regulates CHMP4C via binding the CHMP4C promoter from −512~−450 DNA sequence in response to stress [16,17]. As the common target of Aurora B and p53, CHMP4C has lower expression in normal tissues and high expression in cancers [18]. Overall, despite CHMP4C is involved in abscission checkpoint and autophagy, how it serves its function in DNA damage response as well as in lung cancer formation still remains unclear.

In the study, we first demonstrate that the subunit of ESCRT-III CHMP4C is involved in cellular radiation reactions. Radiation enhances Aurora B expression and CHMP4C phosphorylation in NSCLC cells, collectively directing cell cycle check-point and promoting cell survival. CHMP4C silencing increases cellular sensitivity to radiation, hinders S-phase progression in cell cycle and diminishes ionizing radiation (IR)-triggered γH2AX foci formation. We show that CHMP4C is the major target of Aurora B and has a similar effect with Aurora B upon radiation. We further reveal that the phosphorylation level of CHMP4C is rising both in p53-positive and-negative cells, showing that the close correlation between CHMP4C and Aurora B signaling pathway in mediating radiation resistance is not p53 dependent. Overall, our work discovers a novel action of CHMP4C in radiation resistance, suggesting CHMP4C as a new drug target for non-small cell lung cancer treatments.

2. Results

2.1. Radiation Induces CHMP4C Expression and Phosphorylation

To test if CHMP4C is involved in DNA damage response, cells were γ-irradiated with 2, 4, and 6 Gy and CHMP4C expression as well as phosphorylation was checked. We found that CHMP4C protein increases after irradiation (IR) and peaks at 24 h in A549 but not in H1299 cells (Figure 1A,B). However, the level of CHMP4C phosphorylation and Aurora B expression both increase with IR in both A549 and H1299 (Figure 1C–E). Further, we detected p53 and CHMP4C expression after p53 silencing with or without IR (2 Gy). We found that CHMP4C protein did not increase after irradiation in p53-cleaned A549 cells (Figure 1F). These data maybe indicate increased CHMP4C protein level relies on p53 whereas its phosphorylation is just dependent of Aurora B.

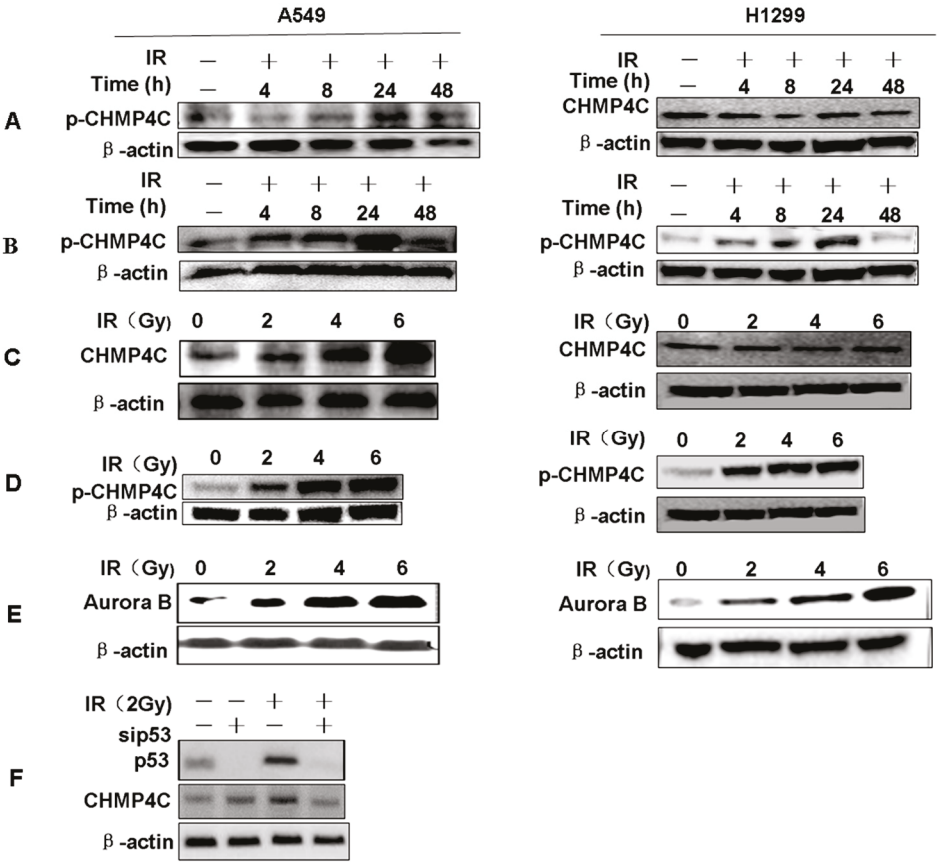

Figure 1. Radiation induces CHMP4C expression and phosphorylation. (**A**,**B**) The A549 or H1299 cells were irradiated with 2 Gy, and harvested at 4, 8, 24 and 48 h. CHMP4C expression or phosphorylation level was tested by Western blot using indicated antibodies; (**C**,**D**) Western blot analysis of CHMP4C expression or phosphorylation level at 24 h after treated with 2, 4, and 6 Gy IR in A549 or H1299 cells; (**E**) Aurora B expression level was tested by Western blot at 24 h after cells exposure to 2, 4, and 6 Gy IR; (**F**) Western blot analysis of expression of CHMP4C and P53 after p53 silencing with or without IR (2 Gy) in A549 cells.

2.2. CHMP4C Silencing Delayed S-Phase of the Cell Cycle

Next, we wondered if CHMP4C exerts its regulatory role in cell cycle progression. A549 and H1299 cells were depleted of CHMP4C for 24 h and the S phase delay was checked, indicating that CHMP4C could impact S phase exit (Figure 2A–D,G–J). Further, to identify whether CHMP4C depletion could enhance the radio-sensitivity to A549 and H1299 cells, we analyzed the cell cycle of A549 and H1299 cells cleared of CHMP4C after IR. When A549 and H1299 cells were treated with 2 Gy of radiation, G2/M transition was severely blocked and S-phase was retarded, whereas combined radiation and CHMP4C knockdown only results in S-phase delay. In the meantime, similar results were found in p21-cleaned A549 cells (Figure 2A–D), implying that CHMP4C might overlay or replenish the p21 function in cell cycle checkpoint during DNA damage response in A549 cells.

In addition, CHMP4C knockdown has no influence on p21 expression (Figure 2E), and p21 depletion cannot effect CHMP4C expression (Figure 2F), which reveals that although CHMP4C and P21 are both p53 target genes, they may be in the different signaling pathway. The double siRNA experiments show that both CHMP4C and p21 depletion exerts an additive effect in the S phase exit (Figure 3), suggesting that CHMP4C might overlay or replenish the p21 function in cell cycle checkpoint during DNA damage response in A549 cells, by participating in different signaling pathways.

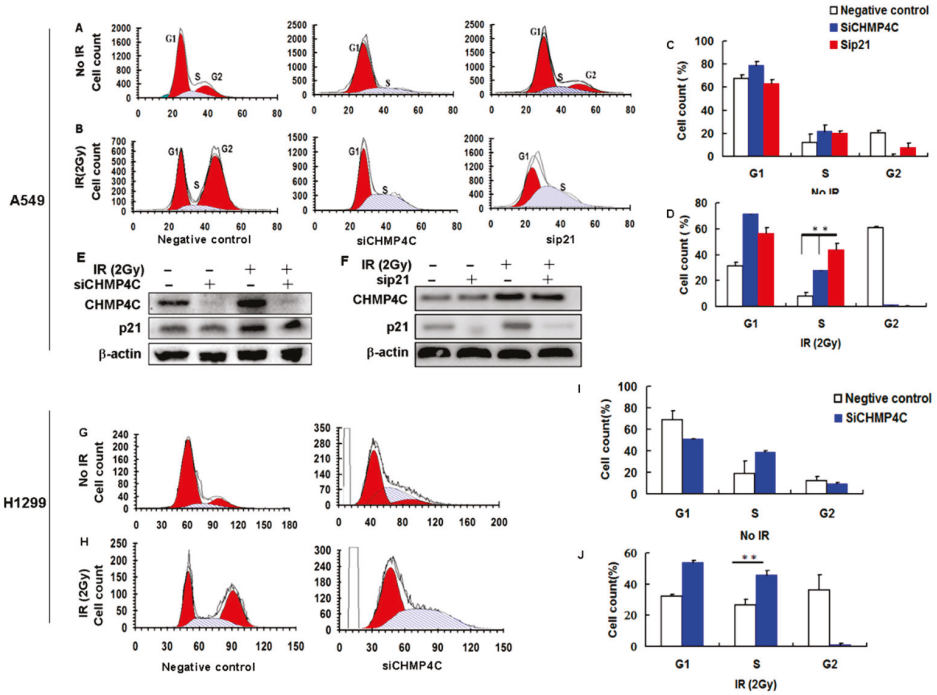

Figure 2. CHMP4C silencing delayed S-phase of the cell cycle. (**A**,**B**) A549 cells were transfected with negative control, siCHMP4C or sip21 for 24 h and/or exposed to 2 Gy IR. After 24 h, the cells were stained with Vibrant Dyecycle green stain and tested on a flow cytometer; (**C**,**D**) Cell cycle analyses of A549 cells. The data are presented as the mean ± S.E. of three independent experiments, ** $p < 0.01$; (**E**,**F**) Western blot analysis of Expression of CHMP4C and P21 after CHMP4C or p21 silencing with or without IR (2 Gy); (**G**,**H**) H1299 cells were transfected with negative control or siCHMP4C for 24 h and/or exposed to 2 Gy IR; After 24 h, the cells were stained with Vibrant Dyecycle green stain and analyzed on a flow cytometer; (**I**,**J**) Cell cycle analyses of H1299 cells. The data are presented as the mean ± S.E. of three independent experiments, ** $p < 0.01$.

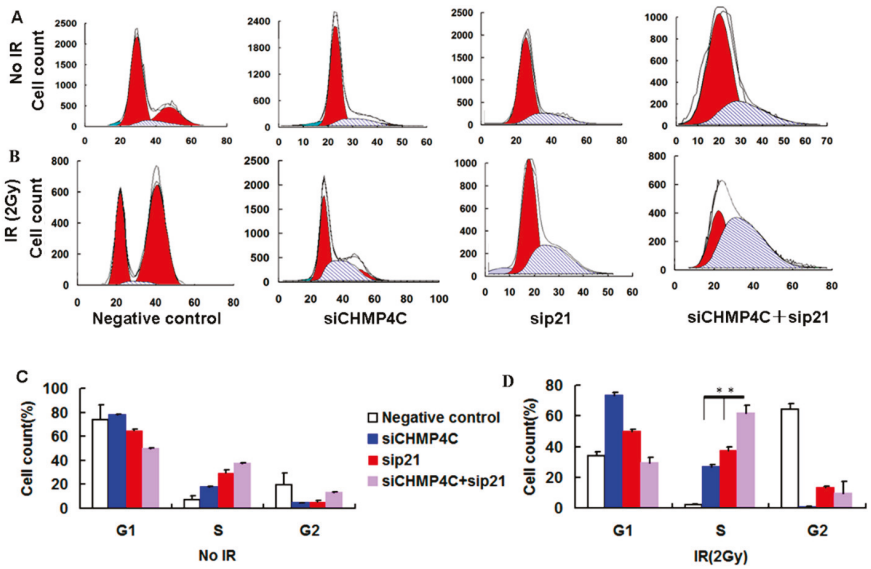

Figure 3. CHMP4C and p21 double silencing exerts an additive effect in S-phase delay of the cell cycle in A549 cells. (**A**,**B**) A549 cells were transfected with negative control, siCHMP4C, sip21, or double siCHMP4C and sip21 for 24 h and/or exposed to 2 Gy IR. After 24 h, the cells were stained with Vibrant Dyecycle green stain and tested on a flow cytometer; (**C**,**D**) Cell cycle analyses of A549 cells. The data are presented as the mean ± S.E. of three independent experiments, ** $p < 0.05$.

2.3. CHMP4C and Aurora B Increase Radioresistance

The above data indicate that CHMP4C inhibition can arrest S-phase of cell cycle. Colony formation assays were next employed to detect if CHMP4C acts in cell radioresistance. These assays showed that CHMP4C knockdown decreases cell survival compared to control with IR. Similarly, the result was also found in Aurora B clearing. Inversely, CHMP4C or Aurora B expression can increase cell growth upon irradiation (Figure 4A,B).

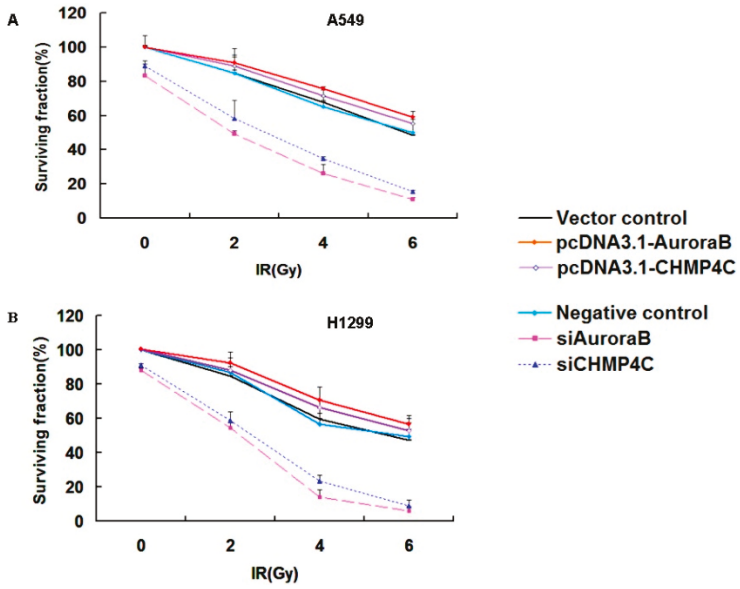

Figure 4. CHMP4C and Aurora B increase radioresistance. (**A**) A549 or (**B**) H1299 cells were transfected with siRNAs or plasmids for 24 h before exposed to 2, 4, and 6 Gy-irradiation. One thousand cells per plate were seeded immediately after IR and incubated for 14 days. Colonies were stained with 1% crystal violet. The number of colonies was counted and surviving fraction was calculated as the mean number of colonies/(cells seeded × plating efficiency). The data are expressed as the mean ± S.E. of three independent experiments.

2.4. CHMP4C Acts Downstream of Aurora B

To verify whether Aurora B regulates CHMP4C, we silenced or overexpressed the Aurora B with siRNA or Aurora B expression plasmids in A549 or H1299. CHMP4C knockdown has no effect on Aurora B protein level, whereas Aurora B silencing inhibits CHMP4C protein level indicating that Aurora B acts upstream of CHMP4C (Figure 5A). Moreover, Aurora B overexpression leads to increased CHMP4C phosphorylation and inhibiting Aurora B kinase activity using phosphorylation inhibitor AZD1152-HQPA reduces CHMP4C phosphorylation (Figure 5B–D). We then found the CHMP4C mRNA level was unchanged following Aurora B downregulation (Figure 5E), further making sure that Aurora B regulates the CHMP4C at the protein level. Collectively, these data suggest that Aurora B modulates CHMP4C expression at the protein level.

2.5. CHMP4C Silencing Increases Cell Apoptosis with Irradiation

The results of colony formation assay indicate that the surviving fraction of NSCLC cells was significantly attenuated after IR treatment of 4, 6 Gy. We next want to ascertain whether CHMP4C knockdown can enhance IR-induced apoptosis under three conditions in A549 cells: radiation only (6 Gy), CHMP4C knockdown, combined CHMP4C knockdown and IR (6 Gy). We found that combined CHMP4C silencing and irradiation produce more evident apoptosis than single treatment (Figure 6). Hence, these assays reveal that CHMP4C can facilitate cellular proliferation and radiation resistance, further confirming the colony formation assays.

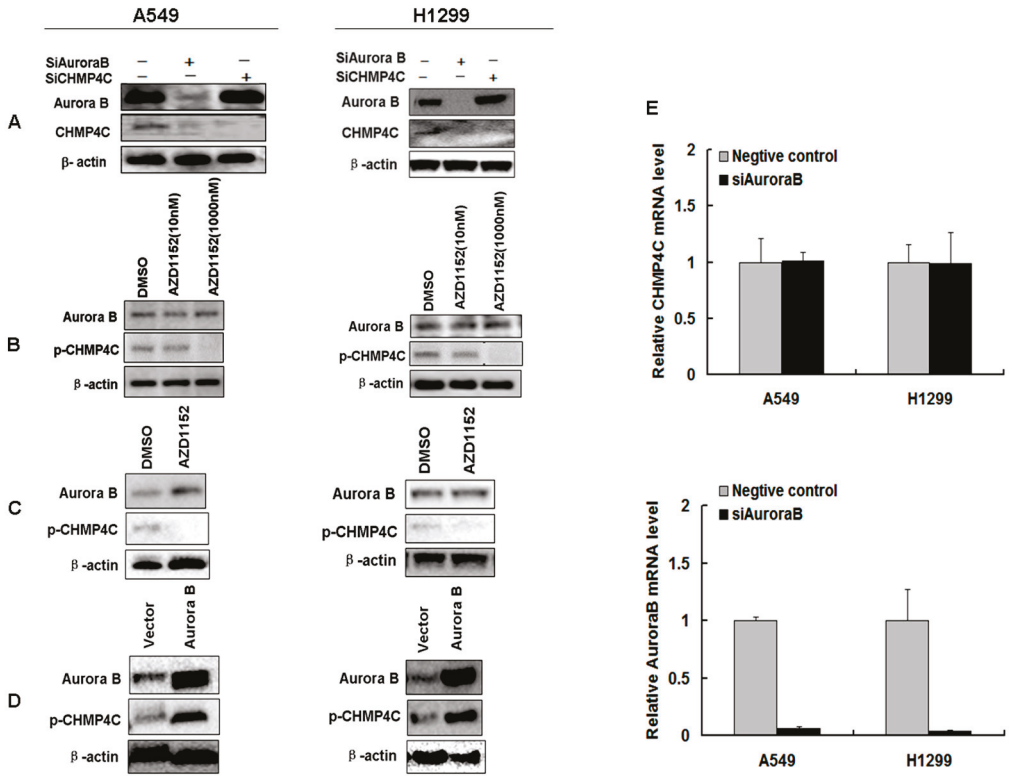

Figure 5. CHMP4C acts downstream of Aurora B. (**A**) Expression of Aurora B and CHMP4C after Aurora B or CHMP4C knockdown in A549 and H1299 cells; (**B**) The phosphorylation level of CHMP4C in untreated and AZD1152 treated (10 and 1000 nM) A549 and H1299 cells; (**C**) The phosphorylation level of CHMP4C in untreated and AZD1152 treated (100 nM) A549 and H1299 cells; (**D**) Western blot analysis of CHMP4C phosphorylation level in A549 and H1299 cells transfected with pCDNA3.1-Aurora B; (**E**) The mRNA expression level of CHMP4C or Aurora B was quantitated with real-time PCR (mean ± S.E., n = 3) after the A549 and H1299 cells undergone transfection of negative control or siAurora B.

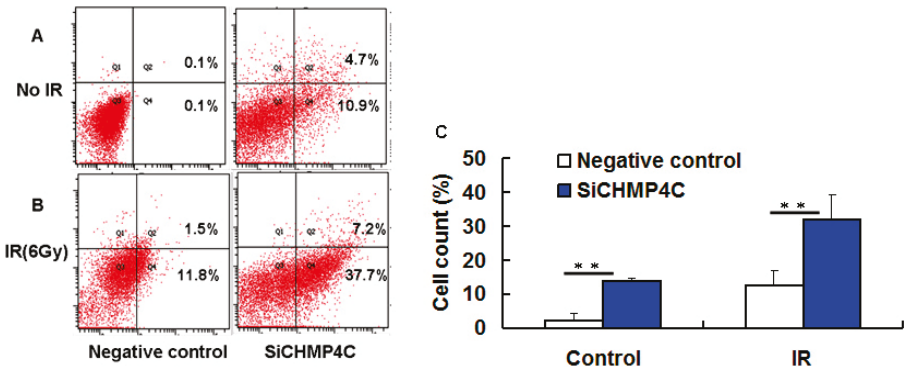

Figure 6. CHMP4C silencing increases cell apoptosis with irradiation. (**A**) CHMP4C-defective cells without IR; (**B**) siRNA transfected cells were exposed to 6 Gy of irradiation. (**C**) Quantification of cell apoptosis assays. The data are presented as the mean ± S.E. of three independent experiments. ** $p < 0.01$

2.6. CHMP4C Reduction Suppresses IR-Induced γH2AX and 53BP1foci Formation

Next, to analyze if CHMP4C is immediately involved in DNA damage signaling, we examined the γH2AX and 53BP1 foci assembly in A549 cells with or without CHMP4C silencing. The IR dose

of 4 Gy was selected in this analysis according to the results of colony formation and apoptosis assay. As shown in Figure 6, the indicated dose (4 Gy) of γ-irradiation is sufficient to induce γH2AX and 53BP1foci formation in nuclear (Figures 7C,D and 8C,D). The results demonstrated that during 4 Gy of irradiation, CHMP4C reduction decreased the intensity and number of γH2AX and 53BP1foci compared with the normal CHMP4C, proving that CHMP4C repression indeed represses recruitment of γH2AX, 53BP1 and other related proteins to the DNA lesions (Figures 7 and 8).

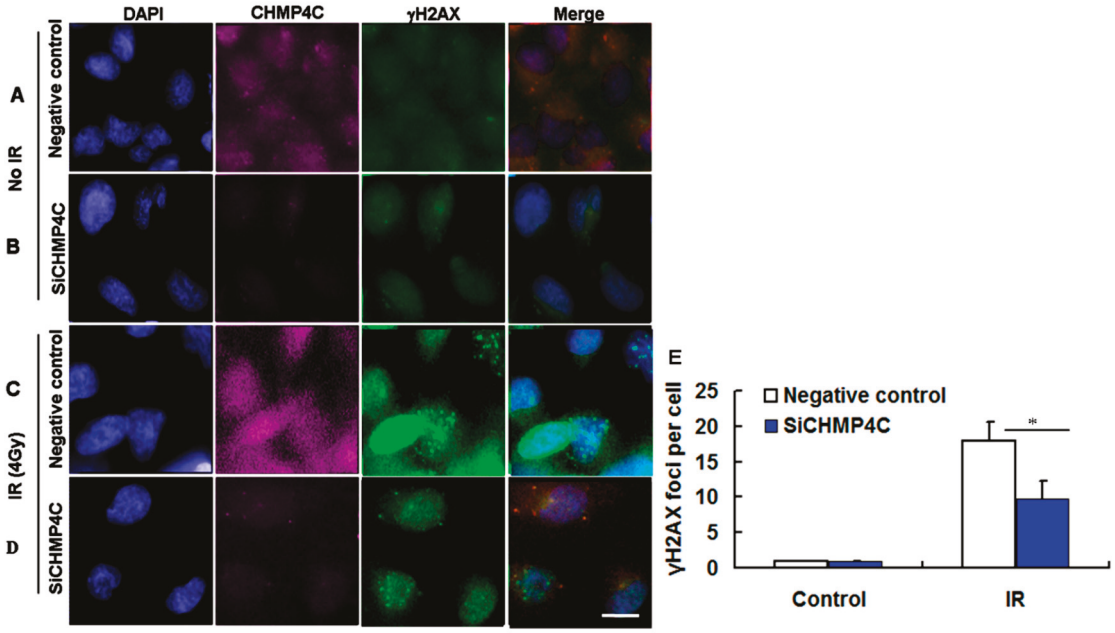

Figure 7. CHMP4C reduction suppresses IR-induced γH2AX foci formation. (**A**,**B**) Negative control and siCHMP4C transfected cells without IR; (**C**,**D**) A549 cells with or without CHMP4C knockdown were exposed to 4 Gy radiation; and (**E**) image of γH2AX foci formation. The number of foci per nucleus was quantitated. The data are presented as the mean ± S.E. of three independent experiments, * $p < 0.05$. Scale bar, 10 μm.

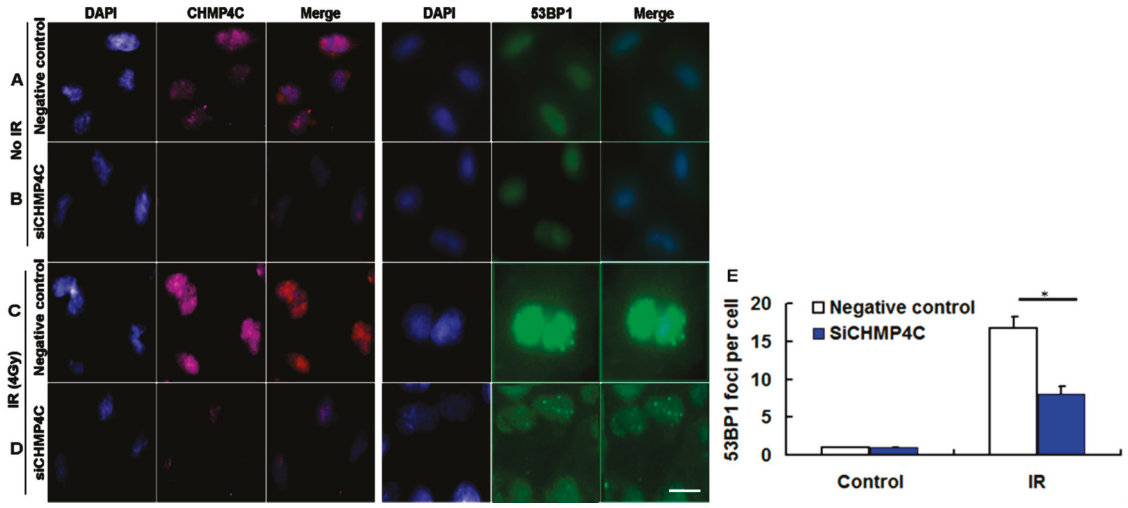

Figure 8. CHMP4C abrogation represses IR-induced 53BP1 foci formation. (**A**,**B**) Negative control or siCHMP4C transfected cells without IR; (**C**,**D**) A549 infected with negative control or siCHMP4C were then treated with 4 Gy radiation; and (**E**) image of 53BP1 foci formation. The number of foci per nucleus was quantitated. The data are presented as the mean ± S.E. of three independent experiments, * $p < 0.05$. Scale bar, 10 μm.

3. Discussion

Current investigations on CHMP4C mainly focus its function on endosome generation. However, whether and how it serves its part in cell cycle, viability and apoptosis under irradiation is not clear. It has been reported that p53 regulates transcription of CHMP4C in the autophagy and endosome production [16]. p53 plays a critical role in regulating DNA-damage-associated cell cycle progression, DNA repair, or apoptosis in the p53/p21 pathway. As the classic target gene of p53, p21 regulates the cyclin-Cdk and PCNA complexes required for the G_1 to S transition [19–21]. We then supposed that they might have similar function in p53-directed cell cycle switch. In support of this hypothesis, our results indicated that CHMP4C knockdown was engaged in cellular S-phase delay, showing the similar regulation with p21 in cell cycle progression in A549. Moreover, double knockdown of CHMP4C and p21 produced an additive effect in S-phase delay of the cell cycle. However, CHMP4C knockdown has no influence on p21 expression and p21 depletion cannot effect CHMP4C expression, which reveals that the novel role of CHMP4C in cell cycle shows an alternative pathway paralleling the p21 signal pathway (Figure 9).

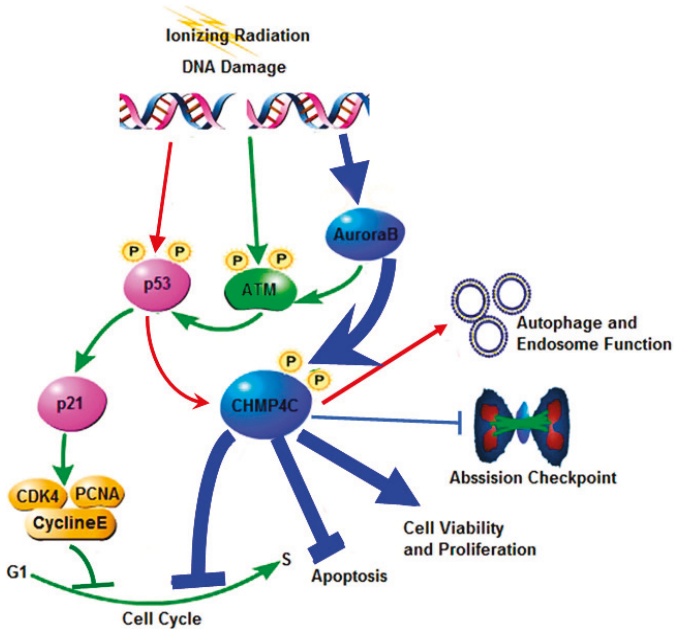

Figure 9. The summary of CHMP4C signaling in response to stress. CHMP4C is phosphorylated by Aurora B to regulate the abscission timing checkpoint and cell cycle progression, promote cell survival and cell viability and resist apoptosis (Blue arrows). The ataxia telangiectasia mutated kinase (ATM) is activated in mitosis in Aurora B-dependent manner (Green arrows). p53 transcriptionally regulates CHMP4C to enhance autophagy and endosome production (Red arrows). p21 is the target gene of p53 and functions in the G1 to S checkpoint (Green arrows).

Further, our results also showed that CHMP4C can promote cell survival and cell viability upon IR, indicating that CHMP4C offer the radioresistance to the irradiated cells. We next studied if CHMP4C was connected with DNA repair, and found that CHMP4C inhibition repressed DNA repair by decreasing γH2AX and 53BP1 foci reacting to radiation stress. Hence, the novel functions of CHMP4C in cell cycle control and DNA repair not only enriches the content of the DNA damage pathway but also extends its specific role in cell regulation.

p53 is often mutated in NSCLC and its mutation increases sensitivity to ionizing radiation in tumor cells [22]. CHMP4C transcription is controlled by p53 in endosome function [16]. CHMP4C functions in the Aurora B-dependent abscission checkpoint and inhibits abscission upon phosphorylation by Aurora B, eventually preventing premature resolution of intercellular

chromosome bridges and DNA damage accumulation. Our results reveal that increased Aurora B kinase enhances the CHMP4C phosphorylation after IR, which is independent of p53. This is also supported by the facts that the cell lines displayed higher sensitivities to IR after CHMP4C inhibition compared to IR alone, and CHMP4C can increase cell survival both in A549 and H1299 cells.

Several Aurora kinase inhibitors are tested in clinical trials [23]. Studies have shown that inhibition of Aurora B radiosensitizes tumor cells [6,7]. In the study, we observed the reduction of CHMP4C protein level but its mRNA expression remains unchanged following silencing of Aurora B, revealing that Aurora B might regulate the CHMP4C protein stability. Inhibited Aurora kinase B activity by AZD1152 suppresses CHMP4C phosphorylation. However, overexpression of Aurora kinase B upregulates CHMP4C phosphorylation because of the large amount of Aurora B proteins. Furthermore, CHMP4C suppression also radiosensitizes NSCLC cells similar to that during Aurora B inhibition. We demonstrate that Aurora B kinase is essential to phosphorylate CHMP4C and the role of CHMP4C in radioresistance is dependent on Aurora B, which proves that CHMP4C is the major downstream target of Aurora B. Therefore, we identify the close relation between CHMP4C and Aurora B signaling pathway in mediating radiation resistance in NSCLC cells, which is independent on p53.

CHMP4C can check the cytokinetic abscission to prevent premature and accumulated DNA damage as an abscission timer. CHMP4C deficiency generates the defective abscission check, which makes injured cells quickly pass through M to S phase, leading to DNA repair disability and genomic instability. These data suggests that CHMP4C deficiency disorganizes the cell cycle and enhances cell sensitivity to radiation, thus providing a new combined strategy to diagnosis and treatment of the lung cancer.

We propose that ATM is activated by Aurora B, followed by p53-mediated activation of CHMP4C. In turn, CHMP4C promotes cell viability and proliferation. However, there is another major tumor suppressor factor, the alternative reading frame (ARF), which is negatively regulated by ATM in a transcription-independent manner. Contrary to the function of CHMP4C on cell fate, inhibition of ATM enhances ARF levels and stimulates the tumor-suppressive effects of ARF in human oncogene-transformed and cancer cells [24]. These findings provide insights into our study and broaden the aspects of our further research.

4. Materials and Methods

4.1. Cell Culture and Irradiation

The human NSCLC cell lines A549 (p53 wild type) and H1299 (p53 deficient) (Cell resource center, Peking union medical college, Beijing, China) were cultured in RPMI-1640 containing 10% fetal bovine serum (Invitrogen, Carlsbad, CA, USA), incubated in 37 °C humidified incubator with 5% CO_2 and treated with different radiation of 2, 4, and 6 Gy using Co_{60} γ-rays with a dose rate of 1 Gy/min in the Irradiation (IR) Center (Beijing Radiation Center, Beijing Academy of Science and Technology, Beijing, China).

4.2. siRNAs and Plasmids Transfection

A549 and H1299 cells were grown at 80% confluence and then introduced with siRNAs against CHMP4C (Ambion, Austin, TX, USA), Aurora B (Ambion), p53 and p21 (GenePharma, Beijing, China) as well as control siRNA (Ambion). CHMP4C, Aurora B, p53 and p21 siRNA sequence is respectively: 5′-CCUGCGUCUCUACAACUAU-3′, 5′-CAUGGAUCUGAACAAAAUATT-3′, 5′-CUACUUCCUGAAAACAACG-3′ and 5′-CCUCUGGCAUUAGAAUUAUTT-3′. siRNA tansfections were performed using Lipofectamine RNAi MAX reagent (Invitrogen). Twenty-four hours after transfection, the cells were irradiated and harvested.

pcDNA3.1-CHMP4C or -Aurora B was contrasted and transfected into A549 or H1299 cells using Lipofectamine 3000 reagent (Invitrogen). Twenty-four hours later, cells were collected and performed for subsequent experiments as siRNAs treatment.

4.3. Kinase Inhibition Assays

Aurora B kinase inhibitor AZD1152-HQPA was dissolved in dimethyl sulphoxide (DMSO). The A549 and H1299 cells were treated with AZD1152-HQPA at the concentration of 10, 100 and 1000 nM. After 24 h of treatment, CHMP4C phosphorylation was examined by Western blot.

4.4. Western Blot

The cells were harvested and lysed in RIPA lysis buffer (Thermo Scientific Pierce, Waltham, MA, USA). The protein was collected at 12,000× *g* for 15 min at 4 °C and measured by BCA protein assay kit (Thermo Scientific Pierce). Equal amounts of protein were separated on 10% sodium dodecyl sulfate (SDS)-polyacrylamide gels and blotted on nitrocellulose membranes for Western blot analysis. The membranes were blocked in 5% nonfat milk and then incubated with the following primary antibodies: CHMP4C (Abcam, Cambridge, UK), phosphorylated (p)—CHMP4C (Abmart, Arlington, MA, USA), Aurora B (Abcam), p53 (Cell Signaling Technology, Boston, MA, USA), p21 (Cell Signaling Technology) and β-actin (Cell Signaling Technology). The CHMP4C antibody is diluted in 1:500, and the rest were used in 1:1000 dilutions. Membranes were washed in tris-buffered saline containing 0.5% tween-20 and then incubated with goat anti-rabbit lgG (Abcam, 1:2000) or goat anti-mouse lgG (Abcam, 1:3000) conjugated to horseradish peroxidase for 1 h at room temperature. The membranes were detected using Chemiluminescence liquid (Thermo Scientific Pierce) according to the manufacturer's protocol and analyzed by the Image J software (Bio-Rad, Hercules, CA, USA).

4.5. Real-Time PCR

Total RNA was extracted using SV total RNA isolation system kit (Promega, Madison, WI, USA) followed by reverse transcription using the GoScript reverse transcription system kit (Promega). The subsequent cDNA products were used as templates to perform the real-time PCR assays. The primers for the amplification of Aurora B or CHMP4C are as follows; Aurora B forward: TTTGAGATTGGGCGTCCTCT and reverse: CGCCCTCCTTCTCTATCTGG; CHMP4C forward: AGAAGCCCTGGAGAACTCAC and reverse: CTTGGGCAGTATCCTGTTGC. The β-actin was used as the internal control using primers forward: TGCCAGAAAACAAGATGAG and reverse: CACCTTCACCGTTCCAGTTT. PCR amplifications were performed in triplicate wells and each experiment was repeated for three times. The relative expression levels of genes were analyzed through the use of the $2^{-\Delta\Delta Ct}$ method.

4.6. Cell Cycle Assay

Cells were harvested and treated with Vibrant Dyecycle green stain (Invitrogen) at 37 °C for 30 min in a dark place. Then, cell cycle was analyzed on a flow cytometer using 488-nm excitation and green emission.

4.7. Colony Formation Assay

To analyze colony formation, Single cell was plated in the 6 cm dish at a density of 1000 cells/mL for 10 to 14 days to form spheres. Colonies were fixed with 4% paraformaldehyde for 20 min and then stained with 1% crystal violet for 15 min. Colonies were counted and surviving fraction was calculated as the mean number of colonies/(cells seeded × plating efficiency).

4.8. Cell Apoptosis Assay

Cells were harvested and washed twice with cold PBS. Cells were resuspended in 1× binding buffer (BD) at a concentration of 1×10^6 cells/mL and stained with PE AnnexinV and 7-AAD (BD) for 15 min at room temperature in the dark. Samples were analyzed by flow cytometry.

4.9. γH2AX and 53BP1 Foci Formation

Cells were seeded on the glass sheets into 6-well plates. Cells were transfected with siRNAs and then exposed to 4 Gy of irradiation. 30 min later, cells were washed twice in PBS, and then incubated with anti-γH2AX (Millipore, FITC conjugate, Billerica, MA, USA), anti-53BP1 (Abcam) or anti-CHMP4C antibody at a dilution of 1:200 overnight at 4 °C. After washing twice in washing buffer (0.05% Tween-20 in PBS), the cells were incubated with goat anti-rabbit lgG (Abcam, Alexa fluor conjugate) at 37 °C for 1 h. Cells were washed twice with washing buffer and once with PBS. The coverslips were then mounted with mounting medium for fluorescence with DAPI (Vectashield). The image of γH2AX and 53BP1 foci was detected using a Leica DMRXA fluorescent microscope (Leica, Wetzlar, Germany). γH2AX and 53BP1 foci were counted in cells with more than five foci.

4.10. Statistical Analysis

Data are presented as the mean ± S.E. of three independent experiments, and the statistics were analyzed by students' *t* test using Microsoft Excel (Microsoft Campus, Redmond, WA, USA). *p*-value <0.05 indicates statistical significance.

5. Conclusions

In conclusion, we identify that CHMP4C is a new radiation-inducible protein engaged in cell cycle and cell survival. We first confirm CHMP4C offers lung cancer cells radioresistance, which will provide a potential radio-therapeutic strategy for non-small cell lung cancer by disrupting CHMP4C expression. In future research, the role of CHMP4C combined with radiation *in vivo*, for example the function of CHMP4C in xenografts [24], will be investigated, which would provide *in vivo* evidence for the new action of CHMP4C.

Author Contributions: Xu Su, Jianxiang Liu, Mei Tian and Kang Li conceived and designed the experiments; Kang Li performed the experiments; Xu Su, Jianxiang Liu, Mei Tian and Kang Li analyzed the data; Gang Gao, Yan Pan and Xuesong Qi contributed analysis tools; Jianlei Ruan and Chunxu Liu contributed reagents and materials; and Xu Su and Kang Li wrote the paper.

Conflicts of Interest: The authors declare no conflict of interest.

References

1. Nguyen, K.S.; Neal, J.W.; Wakelee, H. Review of the current targeted therapies for non-small-cell lung cancer. *World J. Clin. Oncol.* **2014**, *5*, 576–587. [CrossRef] [PubMed]
2. Gower, A.; Wang, Y.; Giaccone, G. Oncogenic drivers, targeted therapies, and acquired resistance in non-small-cell lung cancer. *J. Mol. Med.* **2014**, *92*, 697–707. [CrossRef] [PubMed]
3. Caiozzo, V.J.; Giedzinski, E.; Baker, M.; Suarez, T.; Izadi, A.; Lan, M.; Cho-Lim, J.; Tseng, B.P.; Limoli, C.L. The radiosensitivity of satellite cells: Cell cycle regulation, apoptosis and oxidative stress. *Radiat. Res.* **2010**, *174*, 582–589. [CrossRef] [PubMed]
4. Jazayeri, A.; Falck, J.; Lukas, C.; Bartek, J.; Smith, G.C.; Lukas, J.; Jackson, S.P. ATM- and cell cycle-dependent regulation of ATR in response to DNA double-strand breaks. *Nat. Cell Biol.* **2006**, *8*, 37–45. [CrossRef] [PubMed]
5. Carlton, J.G.; Caballe, A.; Agromayor, M.; Kloc, M.; Martin-Serrano, J. ESCRT-III governs the Aurora B-mediated abscission checkpoint through CHMP4C. *Science* **2012**, *336*, 220–225. [CrossRef] [PubMed]
6. Wu, X.; Liu, W.; Cao, Q.; Chen, C.; Chen, Z.; Xu, Z.; Li, W.; Liu, F.; Yao, X. Inhibition of Aurora B by CCT137690 sensitizes colorectal cells to radiotherapy. *J. Exp. Clin. Cancer Res.* **2014**, *33*, 13. [PubMed]

7. Niermann, K.J.; Moretti, L.; Giacalone, N.J.; Sun, Y.; Schleicher, S.M.; Kopsombut, P.; Mitchell, L.R.; Kim, K.W.; Lu, B. Enhanced radiosensitivity of androgen-resistant prostate cancer: AZD1152-mediated Aurora kinase B inhibition. *Radiat. Res.* **2011**, *175*, 444–451. [CrossRef] [PubMed]
8. Yang, C.; Tang, X.; Guo, X.; Niikura, Y.; Kitagawa, K.; Cui, K.; Wong, S.T.; Fu, L.; Xu, B. Aurora-B mediated ATM serine 1403 phosphorylation is required for mitotic ATM activation and the spindle checkpoint. *Mol. Cell* **2011**, *44*, 597–608. [CrossRef] [PubMed]
9. Caballe, A.; Martin-Serrano, J. ESCRT machinery and cytokinesis: The road to daughter cell separation. *Traffic* **2011**, *12*, 1318–1326. [CrossRef] [PubMed]
10. Van der Waal, M.S.; Hengeveld, R.C.C.; van der Horst, A.; Lens, S.M. Cell division control by the chromosomal passenger complex. *Exp. Cell Res.* **2012**, *318*, 1407–1420. [CrossRef] [PubMed]
11. Jimenez, A.J.; Maiuri, P.; Lafaurie-Janvore, J.; Divoux, S.; Piel, M.; Perez, F. ESCRT machinery is required for plasma membrane repair. *Science* **2014**, *343*, 1247136. [CrossRef] [PubMed]
12. Lata, S.; Schoehn, G.; Solomons, J.; Pires, R.; Göttlinger, H.G.; Weissenhorn, W. Structure and function of ESCRT-III. *Biochem. Soc. Trans.* **2009**, *37*, 156–160. [CrossRef] [PubMed]
13. Lafaurie-Janvore, J.; Maiuri, P.; Wang, I.; Pinot, M.; Manneville, J.B.; Betz, T.; Balland, M.; Piel, M. ESCRT-III assembly and cytokinetic abscission are induced by tension release in the intercellular bridge. *Science* **2013**, *339*, 1625–1629. [CrossRef] [PubMed]
14. Wollert, T.; Wunder, C.; Lippincott-Schwartz, J.; Hurley, J.H. Membrane scission by the ESCRT-III complex. *Nature* **2009**, *458*, 172–177. [CrossRef] [PubMed]
15. Thoresen, S.B.; Campsteijn, C.; Vietri, M.; Schink, K.O.; Liestøl, K.; Andersen, J.S.; Raiborg, C.; Stenmark, H. ANCHR mediates Aurora-B-dependent abscission checkpoint control through retention of VPS4. *Nat. Cell Biol.* **2014**, *16*, 547–557. [CrossRef] [PubMed]
16. Feng, Z. p53 Regulation of the IGF-1/AKT/mTOR pathways and the endosomal compartment. *Cold Spring Harb. Perspect. Biol.* **2010**, *2*, a001057. [CrossRef] [PubMed]
17. Yu, X.; Riley, T.; Levine, A.J. The regulation of the endosomal compartment by p53 the tumor suppressor gene. *FEBS J.* **2009**, *276*, 2201–2212. [CrossRef] [PubMed]
18. Pharoah, P.D.P.; Tsai, Y.Y.; Ramus, S.J.; Phelan, C.M.; Goode, E.L.; Lawrenson, K.; Buckley, M.; Fridley, B.L.; Tyrer, J.P.; Shen, H.; *et al*. GWAS meta-analysis and replication identifies three new susceptibility loci for ovarian cancer. *Nat. Genet.* **2013**, *45*, 362–370. [CrossRef] [PubMed]
19. Satyanarayana, A.; Hilton, M.B.; Kaldis, P. p21 Inhibits Cdk1 in the absence of Cdk2 to maintain the G1/S phase DNA damage checkpoint. *Mol. Biol. Cell* **2008**, *19*, 65–77. [CrossRef] [PubMed]
20. Gillis, L.D.; Leidal, A.M.; Hill, R.; Lee, P.W. p21Cip1/WAF1mediates cyclin B1 degradation in response to DNA damage. *Cell Cycle* **2014**, *8*, 253–256. [CrossRef]
21. Mirzayans, R.; Andrais, B.; Scott, A.; Murray, D. New insights into p53 signaling and cancer cell response to DNA damage: Implications for cancer therapy. *J. Biomed. Biotechnol.* **2012**, *2012*, 170325. [CrossRef] [PubMed]
22. Gudkov, A.V.; Komarova, E.A. The role of p53 in determining sensitivity to radiotherapy. *Cancer* **2003**, *3*, 117–129. [CrossRef] [PubMed]
23. Lapenna, S.; Giordano, A. Cell cycle kinases as therapeutic targets for cancer. *Nat. Rev. Drug Discov.* **2009**, *8*, 547–566. [CrossRef] [PubMed]
24. Velimezi, G.; Michalis, L.; Konstantinos, V.; Roumeliotis, T.; Bartkova, J.; Sideridou, M.; Dereli-Oz, A.; Kocylowski, M.; Pateras, I.S.; Evangelou, K.; *et al*. Functional interplay between the DNA-damage-response kinase ATM and ARF tumour suppressor protein in human cancer. *Nat. Cell Biol.* **2013**, *15*, 967–977. [CrossRef] [PubMed]



© 2015 by the authors; licensee MDPI, Basel, Switzerland. This article is an open access article distributed under the terms and conditions of the Creative Commons by Attribution (CC-BY) license (http://creativecommons.org/licenses/by/4.0/).

International Journal of
Molecular Sciences

MDPI

Review

Targeted Radionuclide Therapy of Human Tumors

Sergey V. Gudkov [1,2,3,*], Natalya Yu. Shilyagina [1], Vladimir A. Vodeneev [1] and Andrei V. Zvyagin [1,4]

Received: 26 September 2015; Accepted: 22 December 2015; Published: 28 December 2015
Academic Editors: William Chi-shing Cho and Anthony Lemarié

1 Laboratory of Optical Theranostics, Lobachevsky Nizhny Novgorod State University, Gagarin Ave. 23, Nizhny Novgorod 603950, Russia; nat-lekanova@yandex.ru (N.Y.S.); v.vodeneev@mail.ru (V.A.V.); andrei.zvyagin@mq.edu.au (A.V.Z.)
2 Institute of Theoretical and Experimental Biophysics, Russian Academy of Sciences, Institutskaya St, 3, Pushchino, Moscow 142290, Russia
3 Prokhorov Institute of General Physics, Russian Academy of Sciences, Vavilova St, 38, Moscow 119991, Russia
4 ARC Centre of Excellence for Nanoscale BioPhotonics (CNBP), Macquarie University, Sydney 2109, Australia
* Correspondance: S_makariy@rambler.ru; Tel.: +7-4967-739-497

Abstract: Targeted radionuclide therapy is one of the most intensively developing directions of nuclear medicine. Unlike conventional external beam therapy, the targeted radionuclide therapy causes less collateral damage to normal tissues and allows targeted drug delivery to a clinically diagnosed neoplastic malformations, as well as metastasized cells and cellular clusters, thus providing systemic therapy of cancer. The methods of targeted radionuclide therapy are based on the use of molecular carriers of radionuclides with high affinity to antigens on the surface of tumor cells. The potential of targeted radionuclide therapy has markedly grown nowadays due to the expanded knowledge base in cancer biology, bioengineering, and radiochemistry. In this review, progress in the radionuclide therapy of hematological malignancies and approaches for treatment of solid tumors is addressed.

Keywords: radio-immunotherapy; radionuclide; targeted therapy; α-emitter; β-emitter; Auger electron; antibody; peptide

1. Introduction

Throughout its entire history the human race desired to hit the target with high precision. In the beginning this aim was realized though the invention of a sling, then with the help of bow and arrows, firearms, high-precision rocket weapons, lasers, *etc.* The target moved farther and became smaller, but it just forced the human intelligence to invent more complicated and accurate systems. Another evolutionary approach was the invention of bombs. This strategy does not necessarily require precision, the power is more important; the target is hit anyway, despite the great collateral damage. The radiotherapy of malignancies also includes both of these approaches, and radiation therapy can be compared to bombs, affecting healthy tissues in one way or another. The weapon of high precision here is targeted radionuclide therapy (TRNT), which is the topic of the current review.

The targeted radionuclide therapy is based on the use of high-affinity molecules as carriers of radionuclides to tumor cells [1]. Pharmaceuticals for targeted radionuclide therapy are often injected intravenously or intracavitary. Following the injection, such drugs enter the blood stream and eventually reach their target—a target molecule on the surface of tumor cells. A radionuclide attached to the pharmaceutical directly interacts with the rumor cell [2]. Cursory analysis of the existing clinical practices shows that, presently, TRNT occupies several percents of the total number of the

clinically-used procedures, as presented in Figure 1, which is translated into the value of sub-million cases, considering more than 14 million oncology patients registered annually.

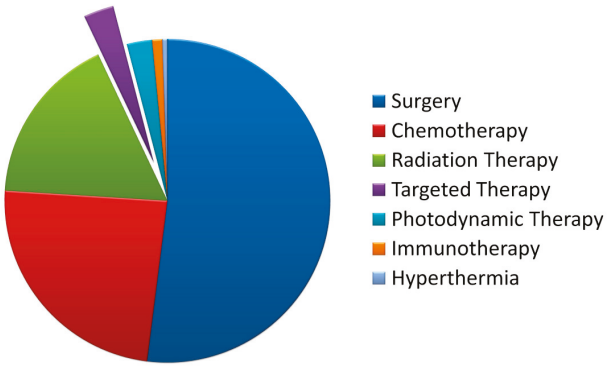

Figure 1. A pie chart of the prevalence of cancer treatments.

In clinical practice, TRNT is widely applied in the treatment of the most radiosensitive tumors, particularly to leukemias and lymphomas. Solid tumors are generally more radio-resistant and sometimes require an order-of-magnitude greater doses of ionizing radiation. The relative radiosensitivity of cancer cells normally correlates with that of normal tissue, from which the tumor is originated. Tissues with the higher radiosensitivity, for instance, red bone marrow, produce radiosensitive tumors, and conversely, radio-resistant tumors originate from radio-resistant tissues, such as the brain [3]. Regardless of the initial radiosensitivity, the main objective of the TRNT is the delivery of radionuclides to cancer cells without any risks for normal tissues, exposure of these cells to highly absorbed doses of ionizing radiation and their damage. At the present time, the development of novel spatial visualization methods for the assessment of absorbed dose both in tumors and normal tissues upon application of TRNT allows avoiding the side effects and toxicity from excessive irradiation, leading to personalization of the treatment regimen for every individual patient. This integration of therapy and diagnostics is a fundamental example of the possibilities of a theranostics approach, when a pharmaceutical is used for diagnostics (in trace amount), as well as for therapeutic purposes [4]. The clinical practice often involves the application of quantitative high-resolution positron emission tomography (PET) or computed tomography (CT) in order to realize the theranostic approach in targeted radionuclide therapy. Such a paradigm provides clinicians with a precise tumor topography and spatial dosimetry, making it possible to develop the most optimal personalized treatment regimen.

2. Features of Targeted Radionuclide Therapy

The method of TRNT is based on the selective accumulation of radionuclide-containing pharmaceuticals only in tumorous tissues. Ideally, TRNT should directly affect only cancer cells evading influence on normal cells. This requirement provides an opportunity to create a pharmaceutical with a high or—ideally—infinitely high therapeutic index, affording to acquire high efficiency with minimal health risks. In practice, this ideal case is virtually impossible, since slight damage to normal tissues occurs in the process of transportation to the target due to the bystander effect and catabolism of the pharmaceutical accompanied by a release of radionuclide [5]. Another advantage of the TRNT is patient convenience. Pharmaceuticals for targeted radionuclide therapy are injected within several minutes and subsequently affect the tumor, whereas the patient does not need to go through additional procedures and get more injections during this period of time [6]. The creation of such pharmaceuticals, possessing a prolonged effect and high therapeutic index, requires a careful selection of radionuclide along with a platform for its delivery into tumor.

3. Radionuclide Selection

It is obvious that radionuclides for targeted therapy must comply with several requirements.

(1) The radioactive decay of radionuclides is expected to cause significant damage to cancer cells. Particulate radiation from the decaying radionuclide has much lower probably to damage biomolecules. This damage is mediated by reactive oxygen species (ROS) generated as the result of the radiolysis of water. Potentially, α-emitters, β-emitters, and Auger electron emitters are assumed to exhibit the highest therapeutic efficiency, because these types of radiation have the greatest relative biological effectiveness, *i.e.*, provide stronger destruction to biological systems at a given dose, in comparison to ionizing electromagnetic types of radiation (X-rays and γ-radiation) (Figure 2) [7]. However, Auger electron emitters appeared to be less effective compared to α- or β-emitters in clinical trials [8].

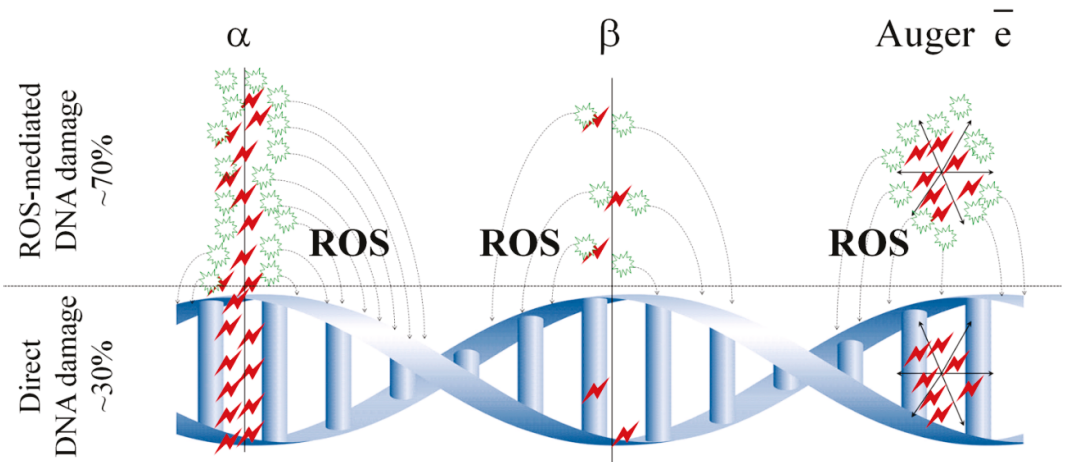

Figure 2. Schematic representation of ionization density along the path of α-, β-particles, and Auger electrons (α-particles are considered densely-ionizing radiation, β-particles are sparsely ionizing, and Auger electrons form clusters with a high density of ionization).

Linear energy transfer for α-particles is ~80 keV/μm; for β-particles, 0.2–2.0 keV/μm; for Auger electrons, 4–26 keV/μm. α-particles cause irreversible DNA damage and induce cell death if 2–3 tracks transit the cross-section of the DNA structure, while it requires 10^2–10^3 tracks for β-particles. The energy of β-particles has a more serious impact on the efficiency of therapy. This parameter should be tailored for treatment specific types of cancers via the choice of suitable radionuclides. For example, it is preferable to use the low-energy particles (less than 1 MeV) in case of treatment of leukemias, lymphomas, and metastases, whereas the use of β-particles with the high energy (>1 MeV) is beneficial for treatment of solid tumors [9].

(2) The choice of the irradiation type depends on tumor size and heterogeneity, as well as the inhomogeneity of the radionuclide distribution, pharmacokinetics, *etc.* [10]. The β-particle path length in biotissues can exceed ten millimeters, which underpin their rational use for relatively small tumors. The path length of α-particles in biotissues is in the range of 50–100 μm, making them most efficient against moderate-size neoplasms and micrometastases. Radionuclides emitting electrons due to the Auger effect are generally effective only when their carrier molecules can penetrate through the cell membrane and reach the nucleus (for example, using a compound ^{111}In-Octreotide).

(3) Radionuclide half-life should correspond to pharmacokinetics of the carrier *in vivo*. This means that the half-life must be longer (although not much longer) than the time required for the preparation of pharmaceutical, its delivery to clinic, injection, and localization in a tumor. An optimal half-life for isotopes used for radionuclide therapy ranges from six hours to seven days [11]. The only exception is the isotope ^{89}Sr having a half-life of 50 days [12]. More short-lived isotopes are inconvenient in terms of delivery to the site of therapy and storage, while radionuclides with longer life span promote an

increase of absorbed dose not only in the target tissues, but also in the surrounding areas. Upon that, patients who were injected with long-lived radionuclides, for instance, the already mentioned ^{89}Sr with the half-life period of 50 days, can themselves become a source of radiation hazard, underlying the necessity of their isolation, as well as organization of maximum security in clinical facilities, including isolated systems of water disposal and purification.

In clinical practice, the complete life span (T) is determined not only by the half-life of an isotope (T_i), but also by the half-clearance time of an agent from the organism or target organ (T_b). [13]. In general, the pattern is described by the formula: $1/T = 1/T_i + 1/T_b$. The half-life of an isotope (T_i) is a tabular value. The half-clearance time of a drug from the organism or target organ (T_b) is largely due to the delivery system of choice, assuming the necessity of experimental studying of clearance dynamics for each agent. Analysis of dynamics often involves the short-lived gamma-emitting radionuclides, which are attached to carrier molecules instead of beta- or alpha-emitting radionuclides used in TRNT [14].

(4) Isotopes used for TRNT ought to have a high grade of chemical purity and free from trace impurities of the concomitant elements and metals. In particular, metal impurities inhibit the process of "labeling" of carrier molecules with metal radionuclides.

(5) When therapy is accompanied by diagnostics, visualized dosimetry measurements and treatment response monitoring can be efficiently realized with the use of γ-emitting radionuclides. Ideally, γ-radiation is characterized by the low energy (between 70 and 300 keV, with an optimum around 140 keV), so as to ensure an effective activity of the γ-ray chamber and minimize the adverse effects on normal tissues [15].

(6) The ability of a radionuclide to bind to a wide variety of carrier molecules belonging to different chemical classes is an important property. The resulting pharmaceutical should be stable during short-term storage, as well as upon contact with biological liquids.

(7) Large-scale production of radionuclides for targeted therapy ought to be organized in a cost-effective manner. Extremely expensive radionuclides, even those having attractive characteristics, can hardly be widely applied.

This is due to the fact that to the cost of a radiopharmaceutical is to a large extent determined by the cost and availability of obtaining of its main component—radioactive isotope. The main sources of radionuclides are nuclear reactors, accelerators and radionuclide generators. In the global production of radionuclides a significant part is realized with the use of charged particle accelerators, most of which are cyclotrons of different types. Historically this fact is usually linked with a large number of research accelerators and their availability in the first years of the development of nuclear medicine at the turn of the 1940s and 1950s, as well as with a relatively low cost of production of most radionuclides. It should be noted that the production of some types of radionuclides requires a cyclotron with unique technical characteristics. For instance, ^{211}At can be obtained only in 30 cyclotrons in the world [16]. An alternative approach for obtaining radionuclides assumes generators of short-lived radionuclides. This technology is based on the use of relatively long-lived isotopes (half-lives of months and years, like ^{90}Sr with a half-life of 28 years), and their radioactive decay yield the formation of a daughter isotope, which has a therapeutic importance because of the short half-life (for example, ^{90}Y with a half-life of 64 h) and stability of the resulting fallout. Daughter isotopes are occasionally derived from the generator by chemical extraction [17]. Long-lived radionuclides used in generators are produced in nuclear reactors, and the deriving of some isotopes also requires nuclear reactors with unique technical characteristics. For instance, ^{188}W, whose daughter isotope is ^{188}Re, can be obtained only in 2–3 reactors in the world [18].

The major features, such a half-life, decay nature, power, and method of producing, of radionuclides most frequently used today for targeted radionuclide therapy are presented in Table 1. Beta-emitting radionuclides ^{131}I and ^{90}Y are used in the clinical practice in approximately 90% cases of TRNT.

Table 1. Radionuclides applied in targeted radionuclide therapy.

Radionuclide	$T_{1/2}$, h	E_{max}, MeV (*)	Method of Producing
^{124}I	100.1	β − 1.6 (~90%); 2.2 (~10%)	cyclotron
^{131}I	192.0	β − 0.7 (89%); γ − 0.4 (82%); β/γ ** = 1	nuclear reactor
^{86}Y	14.7	β − 1.2 (~90%); 1.6 (~10%)	cyclotron
^{90}Y	64.8	β − 2.2 (100%)	generator ^{90}Sr→^{90}Y
^{177}Lu	160.8	β − 0.5 (100%)	nuclear reactor
^{188}Re	17.0	β − 2.0 (100%)	generator ^{188}W→^{188}Re
^{64}Cu	12.7	β − 0.65 (61.5%), β − 0.58 (38.5%)	Cyclotron
^{67}Cu	61.9	β − 0.4 (100%)	cyclotron
^{89}Zr	78.0	B ± 0.9 (100%)	cyclotron
^{212}Pb	10.6	β − 0.6 (~80%); γ − 0.2 (44%); 0.08 (18%)	generator ^{228}Th→^{220}Rn→^{216}Po→^{212}Pb
^{212}Bi	1.0	α − 6.0 (100%); β − 2.0 (100%); α/β ** = 0.67	generator ^{228}Th→^{224}Ra→^{212}Bi
^{213}Bi	0.7	α − 5.8 (97%); β − 1.4 (100%); α/β ** = 0.02	generator ^{229}Th→^{225}Ac→^{213}Bi
^{211}At	7.21	α − 5.9 (42)	cyclotron
^{225}Ac	240.2	α − 5.7 (100%)	generator ^{229}Th→^{225}Ac
^{223}Ra	273.6	α − 5.7 (100%)	cyclotron
^{149}Tb	4.1	α − 4.0 (~80%)	cyclotron
^{226}Th	0.5	α − 6.3 (~50%)	generator ^{230}U→^{226}Th
^{227}Th	448.8	α − 6.0 (48%)	generator ^{227}Ac→^{227}Th
^{89}Sr	1212	β − 1.5 (100%)	nuclear reactor
^{153}Sm	46.3	β − 0.81 (100%)	cyclotron

* Percentage of quanta with the indicated energy value in the total amount of quanta of this type emitted by a given radionuclide; ** Ratio of the amount of quanta of different emission types.

These isotopes represent a standard being used for comparison with all other radionuclides [19]. The widespread use of ^{131}I and ^{90}Y in TRNT because of their suitable emission characteristics, facile and affordable production, and amenable chemical properties, which allow simple and stable attachment of radionuclides to carrier molecules. There are a number of published studies describing the efficiency of these radionuclides for clinical treatment of hematological and, more rarely, solid malignancies. Radionuclide ^{131}I is relatively inexpensive and can be used in both visualization and therapy, with many years of successful implementation in the therapy of a number of malignant tumors, including thyroid cancer. A disadvantage of the application of ^{131}I is stems from the ^{131}I-tyrosine and free ^{131}I in the blood flow of patients, and this event is especially sharply manifested upon fast biodegradation of molecules carrying ^{131}I via endocytosis by tumor cells [20]. Additionally, γ-rays emitted by ^{131}I can pose radiological hazard for patient family members and healthcare personnel. Injection of high doses of ^{131}I-containing pharmaceuticals in some cases requires hospitalization and isolation of the patient. A radionuclide ^{90}Y is a reasonable alternative to ^{131}I for therapeutic applications. Its advantage stems from that its ionizing radiation hardly leaves the patients' organism, and the healthcare personnel and family members bear much lower load of the radiation in comparison to that of ^{131}I. Moreover, ^{90}Y has a shorter half-life, nearly two-fold higher energy of β-particles and high retention in tumor cells. A higher price can be seen as a disadvantage [21]. Attempts for application of a number of radionuclides in targeted therapy are described in the literature [22,23].

It should be noted that some radionuclides do not require the use of carrier molecules due to their chemical properties. Such radionuclides exhibit tropism for certain tissues and thus effectively accumulate in them, allowing for targeted therapeutic effect. Such radionuclides include isotopes ^{223}Ra, ^{89}Sr, ^{153}Sm accumulating in the bone tissue, and ^{131}I in the thyroid gland.

The use of ^{131}I in clinical practice without any carrier molecules lasts for more than 70 years. In the beginning of the XX century a method for hyperthyroidism treatment with ^{131}I was proposed and implemented, and starting from 1942 this innovation has been successfully applied in different clinics around the world [24]. Since 1946 ^{131}I has been successfully applied as an effective means for diagnosis and treatment of bone metastases of differentiated thyroid carcinomas of papillary and follicular types [25]. Today it is known that iodine accumulation by thyroid cells though the action of Na-I-symporter (NIS), a protein actively capturing iodine in thyroid cells [26]. Following the discovery

of NIS, an idea of pharmacological correction of NIS expression appeared; the higher the level of NIS in the membrane, the more the efficiency of ^{131}I accumulation in cancer cells. It is currently known that NIS increase in the tissues can be achieved though the use of some agents, such as early growth response protein 1 from nonthyroid malignancies (Egr1, early growth response 1) [27], TSH-dependent transcription factor of NIS (NTF-1, NIS TSH-responsive factor-1) [28], redox factor-1 (Ref-1) [29] box-8 (Pax-8) [30] *etc.* Despite the achieved progress in this direction, these proteins are at present not used in clinical practice. In the last five years a novel approach was developed for NIS-dependent radioiodine therapy of non-thyroid malignancies. This method is based on a significant increase in the speed of radioactive iodine uptake by tumor cells after transfection of these cells with the NIS gene using viral and non-viral vectors [24,31].

Drugs that include ^{89}Sr, ^{153}Sm, and ^{223}Ra, also without any carrier molecules, can be used in palliative therapy of ostealgia in patients with multiple painful bone metastases in various forms of cancer, including prostate cancer, breast cancer, *etc.* Based on ^{223}Ra a pharmaceutical of radium dichloride was developed and clinically tested [32]; it is currently utilized for therapy of bone metastases in disseminated prostate cancer [33]. Notably, unlike ^{153}Sm and ^{89}Sr, the ^{223}Ra-containing drug is an alpha-emitter, and ^{219}Rn, ^{215}Po, ^{211}Bi in the series of its derivatives are also alpha-emitters with short half-lives, with total decay energy ^{223}Ra equaling 28.2 MeV. The ^{223}Ra-based drug possesses a high rate and selectivity of accumulation in target tissues, so that only 20% of the initial amount of ^{223}Ra persists in the blood within 15 minutes after intravenous injection, with about 60% of the isotope localized in the bones and 40% excreted without significant accumulation in non-target organs (heart, liver, spleen) [34].

As described previously, in TRNT in some cases alpha-emitting radionuclides are used, which are characteristic for high relative biological effectiveness, linear energy transfer and the energy of radioactive decay. For a number of isotopes long chains of daughter products of decay are known (^{225}Ac, ^{223}Ra, ^{227}Th, ^{226}Th), and their daughter isotopes are also alpha-emitters that can reduce the required amount of drug compared to beta-emitters. These advantages make alpha-emitting radionuclides particularly attractive for the therapy of non-solid tumors and micrometastases [35]. However, despite the obvious advantages, there are objective reasons hindering the use of alpha-emitting radionuclides in TRNT. The most critical of those are (1) the presence of beta-emitters among daughter products, which cause radiation injury to adjacent tissues (for example, ^{211}Pb and ^{207}Tl, which are products of decay of ^{223}Ra; ^{213}Bi and ^{209}Pb–^{225}Ac); (2) the presence of long-lived isotopes among daughter products, resulting in the necessity for patient isolation (for example, beta-emitting ^{207}Bi, with a half-life of 33 years, daughter product ^{211}At); (3) potential volatility of the chemical bond with the carrier molecule (in particular, similarity in the chemical properties of ^{211}At and iodine are often considered to be advantages of this nuclide; however, *in vivo* the stability of the majority of compounds labeled with astatine, is poor), resulting in a decrease in delivery orientation of the isotope to the target organs and tissues; and (4) potential tendency to self-radiolysis, partial drug destruction due to its radioactivity.

4. Choice of Carrier Molecule

It is clear that carrier molecules for targeted therapy ought to meet the following criteria.

(1) The carrier molecule must possess high affinity and specificity for the target.
(2) The carrier molecule should not be toxic or immunogenic, with a preferable LD_{50} value of greater than 1.5 g per kg of body weight.
(3) The carrier molecule has no resistance to self-radiolysis and well-preserved both under storage conditions and upon contact with biological liquids.
(4) Production of the carrier molecules with sufficient chemical purity ought to be simple and cost effective.

(5) The carrier molecule has binding affinity to a variety of radionuclides. Specific chemical modifications are preferred to involve a minimum number of reactions.

The main carriers of radionuclides in therapy are antibodies and peptides, though attempts have been made to exploit liposomes and bisphosphonate molecules, dextran, *etc.* as carrier agents [36]. Owing to the high specificity, monoclonal antibodies and their fragments are among the most suitable carrier molecules for TRNT [37]. Most malignancies are characterized by the overexpression of discriminative antigens predominant in tumors. Monoclonal antibodies with the affinity to the cancer-specific antigen is produced by means of well-established hybridoma technology. Antibodies can be bound to radionuclides by a direct bioconjugation or by using a bifunctional chelate. Although this technology has been proved very useful and efficient, its drawbacks include large size, as exemplified by the smallest immunoglobulin G (IgG) weighing 150 kDa, and slow kinetics in comparison to peptides [38]. Excessive expression of numerous peptide receptors on the surface of human tumor cells against that in normal tissue cells makes analogues of signal peptides effective for the role of carrier molecules for TRNT. The peptide carriers are most often used in the therapy of neuroendocrine tumors (predominantly somatostatin analogues [39]), as well as in the treatment of rectal cancer (peptides to antigens EphA2, RNF43-721, ABT-737) [40].

The other transport carriers have been also employed for target delivery of radionuclides. Among these, liposomes can transport radionuclides to highly vascularized tumors, harbored predominantly in the liver or spleen. The radionuclides can be encapsulated either in the cavity space of a liposome or between the layers [41]. Such polymers as dextran, chitosan, polylactide or polylactide glycolide, *etc.*, are also employed as the transport carriers in TRNT [41]. Dextran, being one of the representatives of the transport carriers, is a branched polysaccharide, with glucose molecules as monomers. Dextran is used for passive accumulation of radionuclides in vascularized tumors predominantly in the liver and spleen, where the accumulation mechanism is similar to that of liposomes [36]. The accumulation of these transport carriers in the tumor is primarily due to an increased permeability of the tumor blood vessels featuring abnormally variable and large mean-size fenestrations (100–200 nm). Biomolecular polymers and nanoparticles sized in excess of 10 nm extravasate into the tumor interstitial space and are retained in the tumor interstitium due to the dysfunctional lymphatic drainage. This effect was called the enhanced permeability and retention (EPR) effect in the literature [42]. Another carrier type, bisphosphonates, are natural biologically-stable analogues of pyrophosphates. They inhibit bone resorption by preventing activation of osteoclasts and contribute to the bone formation though the stimulation of osteoblast differentiation. Bisphosphonates are successfully used for radionuclide delivery because they effectively bind to hydroxyapatite in the regions of active osteogenesis, which favors their accumulation in the vicinity of bone tumors [43].

5. Selection of a Target Antigen of Tumor Cells

The choice of an optimal antigen exposed on the membrane of tumor cells is crucial for therapy and diagnostics. An ideal TRNT antigen must meet the following criteria:

(1) Even expression and distribution over the entire cells surface of malignant tumors;
(2) Low or negligible expression in normal cells to minimize the side effects;
(3) Detainment in the cancer site, with no leakage to the blood flow.

More detailed requirements for the selection of target antigens of tumor cells for clinical purposes are described in a recent review [38].

Target antigens are usually represented by macromolecules localized on the surface of cell membrane of tumor cells. They are easily accessible from the blood and extracellular fluid and often possess hematopoietic clusters of differentiation (CD), which are normally expressed during the maturation of various types of blood cells. Suitable target antigens commonly include cell surface glycoproteins (mucins, GPA33, NG2), enzymes (PSMA, CAIX), glycolipid (GD2), stromal components

(FAPα), blood vessel elements (integrins, VEGFR, fibronectin B), and signal transduction molecules (GFR, EGFR, HER2) [44]. None of the existing target antigen is ideal for TRNT, although several types of tumors present nearly ideal targets. For example, CD20 and CD22 represent target antigens for lymphoma treatment [45], CD33 and CD45—for acute myeloid leukemia [46], PSMA [47] and fibronectin B [48]—for solid tumors, and GPA33—for colorectal cancer [49].

6. Targeted Radionuclide Therapy of Hematological Malignancies

The application of targeted radionuclide therapy for the treatment of hematological malignancies is in many aspects an effective approach due to the following reasons: (1) First of all, many cancer cell lines express specific surface antigens, which are not present in the other tissues of the organism; (2) At present time, a rich choice of high-quality antibodies against these antigens are available; (3) Leukemias and lymphomas are extremely sensitive to ionizing radiation [50]. Moreover, the availability of transplantation technologies for bone marrow cells allows increasing the irradiation dose. This is particularly important on application of the autotransplantation stem cell rescue (SCR) approach, when the irradiation at high doses follows native stem cells picking from the patient, with their subsequent use after a therapy course to replenish the largely depleted pool of stem cells. In clinical practice, radionuclide therapy of hematological malignancies often utilizes anti-CD20 antibodies, and these are applied for the production of conjugates with radionuclides ^{131}I or ^{90}Y. The overall therapy efficiency of deployment these pharmaceuticals is high, reaching 60%–80%, with a complete remission rate of 15%–40%. The median of complete remission duration for this TRNT is about 1–2 years, and 15%–20% of cases demonstrate a sustained remission lasting up to 10 years and longer [19]. Similarly, TRNT of the hematopoietic system makes use of antibodies against antigens CD33, CD45, and CD66 [51]. Promising targeting agents for preclinical and clinical studies include antigens CD5 in the therapy of chronic lymphocytic leukemia [52], CD30 and ferritin—for Hodgkin's lymphoma treatment [53] and CD25—for the therapy of acute T-cell leukemias and lymphomas [54].

7. Targeted Radionuclide Therapy of Solid Tumors

The clinical efficiency of the existing TRNT of solid tumors remains low. The extreme resilience of solid tumor cells to the effects of ionizing radiation is at the heart of this problem and represents the major challenge of TRNT. This resilience is due to the uneven distribution of the radiopharmaceuticals in the tumor body, where the major portion is accumulated in the periphery. Cells located in the tumor parenchyma receive small ionizing radiation doze from the alpha- or beta-emitters localized at the periphery. In addition, a single cell is known to be more susceptible to the ionizing radiation that a monolayer of the same cells, and this is more susceptible that the cells in 3D matrix of scaffolds. It is also known that cancer cells located in tumor parenchyma are exposed to hypoxic conditions, which hampers generation of reactive oxygen species, which are characterized by the highest damaging potential.

Multi-step pre-targeted radionuclide therapy is presently utilized to solve this issue, which is capable of providing a significant increase of the therapeutic selectivity and enhance the tumor radiation exposure (Figure 3).

It is therefore worthwhile to present several cases of successful TRNT of solid tumors. For example, the clinical practice of targeted radionuclide therapy of metastases of hepatic colorectal carcinoma involved the use of anti-CEA antibodies, which were employed to produce a conjugate with ^{131}I isotopes. The median survival time in such TRNT was approximately 68 months, with the median of complete remission duration of 18 months [55]. The treatment of castration-resistant prostate cancer, where antibodies against PSMA antigen were utilized to produce a conjugate with ^{177}Lu radionuclides represent another successful approach, achieving the median survival time up to 10 months [56]. In stage IV melanoma treatment antibodies against NG2 were used with a radionuclide ^{213}Bi. In 50% of patients, a long-lasting stable course of the disease was registered, while 14% had a partial

remission [57]. Metastasizing melanoma therapy included anti-NG2 antibodies with radionuclide ^{213}Bi, and the median survival time in that targeted radionuclide therapy was increased by nine months [58].

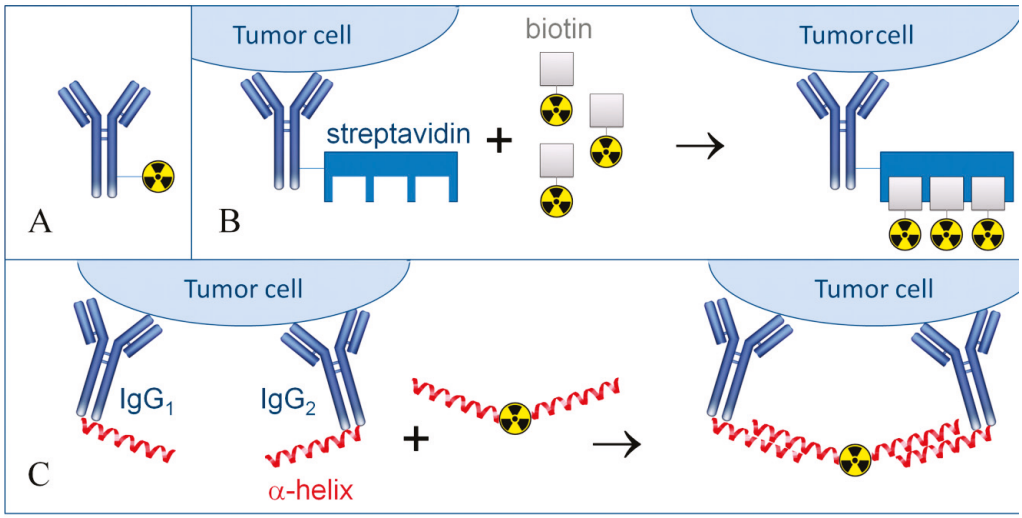

Figure 3. Schematic representation of conventional and pre-targeted radionuclide therapy. (**A**) Conventional targeted radionuclide therapy is realized only using monoclonal antibodies or other carrier molecules directly conjugated with a radionuclide; (**B**) Multi-step pre-targeted radionuclide therapy, "amplifier" mode. At first, antibodies conjugated with streptavidin are used and following antibody binding radiolabelled DOTA-biotin is introduced. It is presumed that each streptavidin molecule binds to four molecules of radionuclide-labeled biotin; (**C**) Multi-step pre-targeted radionuclide therapy, mode for specificity increase.

The first step assumes the use of antibodies against one or several antigens, conjugated with an α-helix, for example, from phosphorodiamidate morpholino oligomer. After antibody binding, radionuclides are introduced, which are conjugated with α-helices complementary to antibody-bound α-helices.The TRNT of solid neuroendocrine malignancies effectively takes advantage of applying selective peptides. For example, in clinical practice the targeted radionuclide therapy of pancreatic tumor is realized using peptide DOTATATE, a somatostatin analog, conjugated with a radionuclide ^{177}Lu. Over a period of 20 months, 12% of patients exhibited a complete remission, with a partial remission in 27% of patients and a stable disease course without complications in 46% cases [59]. When peptide DOTATOC and radionuclide ^{90}Y were utilized in pancreatic tumor treatment, 4% of patients demonstrated a complete remission, 23% had a partial remission, and a stable disease course without complications was registered in 62% of patients [60]. The application of an equivalent pharmaceutical in the treatment of gastroneuroendopancreatic tumors resulted in a complete remission in 5% of patients, a partial remission in 18% of patients and a stable disease course without complications in 69% cases [61]. The overall progress achieved in the application of peptide-mediated tumor radiotherapy is reviewed in the literature [62–64].

8. Determination of the Dose Load in TRNT

In documents regulating the radiation impact on human body, the concept of critical organ is applied as an organ or tissue, a body part, the irradiation of which can cause the highest damage to the health of a biological object or its progeny under certain conditions. In case of internal irradiation the concept of a critical organ seems to be more complicated than in external exposure. The values of threshold damaging doses for different organs/tissues and the distribution of radionuclides in organs/tissues (tropism of radionuclides) are of major importance. The most radiosensitive organs are lymphoid organs, red bone marrow, gonads, and the small intestine, which are damaged upon radiation at the lowest doses [65]. It should be noted that different subjects possess significant

individual levels of radiosensitivity in various organs, which can be nearly up to 20% of the values regarding the dose load [66]. The ability of preferential accumulation in certain organs allows defining osteotropic (radionuclides selectively deposited in the bones—radium, strontium, barium, calcium), hepatotropic (selectively accumulated in organs rich in reticuloendothelial elements—lanthanum, cerium, promethium, praseodymium, as well as actinium, thorium, some compounds of plutonium) and radionuclides evenly distributed throughout the body (isotopes of cesium, potassium, sodium, rubidium, hydrogen, carbon, nitrogen, and other elements, including polonium). Separate groups include radioactive isotopes of iodine, which are selectively accumulated in the thyroid gland, and poorly reabsorbed radionuclides, which cause local processes that are localized depending on their modes of intake.

TRNT is implemented with the assessment of radiation doses to healthy tissue and organs. One of the methods for determination of the predicted absorbed dose for organs and tissues is the modeling method used, for example, for assessing the exposure upon application of radium-223 chloride [67]. The most objective assessment is based on extensive statistical material and operates such indicators as the manifestation of long-term side effects and the overall survival of patients; however, a number of individual factors specific for each individual patient are necessary to be taken into account in determining the dose of a drug for TRNT [68]. The task of providing an individual approach to the dosing of a drug for TRNT is aided by the conduction of individualized dosimetry studies. Pre-treatment dosimetry is implemented to estimate the radiation load for tissues and organs of a patient, which uses the carrier molecule; however, the radionuclide used in the therapy is replaced with a short-lived gamma- or β-emitting isotope. In some cases an isotope of the same element that is used in therapy is used as a label—for example, ^{124}I, a source of positron emission is used as a label for the therapeutic isotope ^{131}I [69,70]. Another widely used therapeutic radionuclide ^{90}Y is used along with ^{87}Y [71], though this application is limited by the osteotropism of the daughter product of radioactive decay ^{87}Sr. The medications of ^{90}Y are often accompanied by the use of gamma-emitting ^{111}In having a stable decay product ^{111}Cd and a half-life of 2.8 days [14] The application of pre-treatment dosimetry allows the creation of a radiation dose record and determine the required dose of the drug individually [72].

9. Available Commercial Pharmaceuticals for Targeted Radionuclide Therapy

Currently, several pharmaceuticals for TRNT of tumors are being introduced into clinical practice (Table 2) [73]. The radionuclide component of the most known drugs is featured by ^{90}Y or ^{131}I. These pharmaceuticals are mostly effective against hematological malignancies. Most preparations are extremely costly, sometimes having noncompetitive prices, and some of them, like Bexxar (produced in 2003–2014), were taken out of production because of commercial reasons.

Zevalin® (Ibritumomab tiuxetan) is the first pharmaceutical for radio-immunotherapy commercially available worldwide. In February 2002, the U.S. Food and Drug Administration (FDA) approved it for the therapy of recurrent and resistant forms of low-grade follicular B-cell non-Hodgkin's lymphoma. CD20 and ^{90}Y were used as an antigen and a radionuclide, respectively [74]. The results of phase III of clinical trials for Zevalin (90Y-ibritumomab tiuxetan) undertaken in 2001–2005 are presented in the study [75], which is an update of a previous work of the same working group published in 2008 [76]. An international randomized study involved 414 patients with CD20-positive stage III or IV follicular Non-Hodgkin's lymphoma. Mandatory inclusion criteria were complete or unconfirmed complete remission after first-line therapy (complete response (CR), unconfirmed CR (CRu), or partial response (PR) after first-line induction treatment). Patients from the therapeutic group received ^{90}Y once at a dose of 14.8 MBq/kg (but not exceeding 1.184 GBq). On an eight-year interval progression-free survival (PFS) of 41% was demonstrated compared with 22% for patients in the control group. Long-term side effects were not reported.

Table 2. Drugs for radio-immunotherapy.

Commercial Name (Other Names)	Antigen/Radionuclide	Disease	Clinical Trial Status
Zevalin (^{90}Y–ibritumomab tiuxetan)	CD20/^{90}Y	non-Hodgkin's lymphoma	Approved by FDA
Bexxar (^{131}I–tositumomab)	CD20/^{131}I	non-Hodgkin's lymphoma	Approved by FDA
Oncolym (^{131}I–Lym 1)	HLA-DR10/^{131}I	non-Hodgkin's lymphoma, chronic lymphocytic leukaemia	Phase III
Lymphocide (Epratuzumab)	CD22/^{90}Y	non-Hodgkin's lymphoma, chronic lymphocytic leukaemia, immune diseases	Phase III
Cotara (^{131}I–chTNT–1/B)	DNA/^{131}I	glioblastoma, anaplastic astrocytoma	Phase III
Labetuzumab (CEA–Cide)	CEA/^{90}Y or ^{131}I	breast, lung, pancreatic, stomach, colorectal carcinoma	Phase III
Theragin (Pemtumomab)	PEM/^{90}Y	ovarian, gastric carcinoma	Phase III
Licartin (^{131}I–metuximab)	(Hab18G/CD147)/^{131}I	hepatocellular carcinoma	Phase II
Radretumab (^{131}I–L19)	Fibronectin/^{131}I	hepatological malignancy, refractory Hodgkin's lymphoma, non-small cell lung cancer, melanoma, head and neck carcinoma	Phase II
PAM4 (^{90}Y–clivatuzumab tetraxetan)	MUC1/^{90}Y	Pancreatic adenocarcinoma	Phase III
Xofigo (^{223}Ra dichloride)	–/^{223}Ra	metastatic castration-resistant prostate cancer	Approved by FDA
Lutathera (^{177}Lu–DOTA–Tyr^3–Octreotate)	SST/^{177}Lu	metastatic GastroEnteroPancreatic NeuroEndocrine Tumors	Phase III
^{131}I–MIBG	norepinephrine (NE)/^{131}I	neuroblastoma, Pheochromocytoma, Paraganglioma	Phase III

Lymphocide® (Epratuzumab) is a pharmaceutical, which is being tested in phase III of clinical trials. CD22 and ^{90}Y were used as an antigen and a radionuclide, respectively. The pharmaceutical was designed for the therapy of B-cell non-Hodgkin's lymphoma and chronic lymphocytic leukemia [77]. Theragyn® (Pemtumomab)—a pharmaceutical also known as Theragyn or HMFG1; it is being tested in phase III of clinical trials. Monoclonal mouse antibody against mucin MUC1 was combined with radionuclide ^{90}Y. Glycoproteid mucin is expressed on the surface of epithelial cancer cells, including ovarian, gastric, breast, and lung cancer types [78]. PAM4 (^{90}Y-clivatuzumab tetraxetan)—pharmaceutical characterized by a high efficiency against pancreatic cancer is currently in phase III of clinical trials. It does not accumulate in normal tissues and exhibits limited accumulation in the other types of tumors. ^{90}Y, and antigen CA19–9 associated with pancreatic adenocarcinoma were deployed in this case [79]. The results of phase I clinical trials of efficiency of a drug based on 90Y-clivatuzumab tetraxetan against pancreatic carcinoma were published in [14,72]. The studies involved 42 and 21 patients, respectively, aged 33–86 years, at stages III-IV of the disease. During the study the patients received the ^{90}Y-based drug three times at a dose of 6.5–15 mCi/m^2 [14] and 15–25 mCi/m^2 [72]. The survival median was 7.7 in the studies (six months for patients at stage IV and 19.6 months for patients at stage III) and 4.3 months, respectively.

CEA-Cide (Labetuzumab) is under preparation for phase III of clinical trials. The antibodies used possess affinity for carcinoembryonic antigen (CEA). CEA is expressed in 90% of colorectal cancer cases [55]. Labetuzumab can incorporate either ^{90}Y or ^{131}I as the radionuclide component. Bexxar® (Tositumomab) is a ^{131}I radionuclide containing drug, also known as ^{131}I-Tositumomabor, was approved by FDA in 2003.

Bexxar is trophic to the CD20 receptors on the surface of tumor cells. It was reported to have efficacy for the therapy of B-cell non-Hodgkin's lymphoma, diffuse B-cell lymphoma, and multiple myeloma [80]. Randomized phase III clinical trials (ClinicalTrials.gov Identifier NCT00006721), published in the Journal of Clinical Oncology [81] involved 532 patients with biopsy-proven, untreated,

bidimensionally-measurable bulky stage II or stage III–IV FL (grade 1, 2, or 3) expressing CD20. Every patient received six cycles of treatment with cyclophosphamide, doxorubicin, vincristine and prednisone (CHOP) chemotherapy at three-week intervals. After that patients from the control group received 6 doses of rituximab (CHOP-R), while the patients from the experimental group followed by consolidation with tositumomab/iodine I-131 tositumomab radioimmunotherapy (RIT). The results of the study on a two-year interval showed a progression-free survival (PFS) of 76% and 80% for CHOP-R and CHOP-RIT arms, correspondingly. The two-year estimate of the overall survival (OS) was 97% on the CHOP-R arm and 93% on the CHOP-RIT arm. In another randomized study (ClinicalTrials.gov Identifier NCT00329030), published the same year [82], the efficiency of radioimmunotherapeutic approach (dose of 5 mCi of ^{131}I-tositumomab resulting in the absorbed dose of 0.75 Gy in seven days) was compared with the effectiveness of rituximab (375 mg/m^2) for relapsed diffuse large B-cell lymphoma, conducted in both cases according to the same protocol. Both drugs were administered 14 days before the start of chemotherapy and rituximab was administered again seven days before chemotherapy. The study involved 224 patients, 111 of which received a course of radioimmune therapy. Two-year progression-free survival (PFS) rates, the primary end point, were 48.6% and 47.9% for rituximab and ^{131}I-tositumomab, respectively. The two-year overall survival (OS) rates were 65.6% and 61%. Thus, the results obtained for rituximab and ^{131}I-tositumomab are statistically indistinguishable [83], though an improvement of PFS was registered in patients with normal serum β2M, whereas in patients with high serum β2M, the PFS was similar by arm.

Oncolym® (^{131}I-Lym-1) is a pharmaceutical being evaluated in phase III of clinical trials. It binds to human leukocyte antigen (HLA) [84] DR10, which is exposed only on the surface of B-lymphocytes, such as cancer B-lymphocytes. Cotara® (^{131}I-chTNT-1/B)—pharmaceutical based on a chimeric monoclonal antibody is in phase III of clinical studies. Its molecules bind to the complex DNA-histone H1, wherein ^{131}I is used as the radionuclide component. This pharmaceutical is efficient against anaplastic astrocytoma, brain glioblastoma, hepatocellular carcinoma, colorectal cancer and glioma [85]. Licartin® (^{131}I-metuximab) is a pharmaceutical composed of a monoclonal mouse antibody Hab18 F(ab') trophic to an antigen Hab18G/CD147 of hepatocellular carcinoma and radionuclide ^{131}I. The monoclonal antibody itself possesses cytotoxic activity and is potentially capable to inhibit metastasis of hepatocellular carcinoma through blockade of matrix metalloproteinase synthesis. In a complex with ^{131}I, this pharmaceutical exhibits enhanced potency due to tis direct effect on tumor cells. The drug is in phase II of clinical trials, although it has already gained approval of the China Food and Drug Administration (CFDA) for patients with inoperable or recurrent hepatocellular carcinoma [86]. Radretumab® (^{131}I-L19) is a pharmaceutical being tested in phase II of clinical trials and represents monoclonal antibodies specific for isoforms originating upon alternative splicing of fibronectin and tenastin-C, combined with a radionuclide ^{131}I. The drug is effective against non-small cell types of lung cancer and hematological malignances [87]. Xofigo is a trade mark of radium-223 dichloride produced by Bayer HealthCare Pharmaceuticals Inc. The drug was approved by the FDA in May 2013 for use in the therapy of metastatic castration-resistant prostate cancer [88]. Due to osteotropism of radium Xofigo accumulates in the bone tissue [34]. Peculiarities of *Ra* localization in the bone matrix condition its low mobility, thus, despite the long decay chain the drug has low toxicity for the surrounding tissues. A review of main clinical and preclinical studies for drugs containing ^{223}Ra is presented in the works [34,89]. The most large-scale clinical trials using radiul-223 cloride Xofigo™ took place from 2008 to 2011 (ClinicalTrials.gov Identifier NCT00699751, A Phase III Study of Radium-223 Dichloride in Patients With Symptomatic Hormone Refractory Prostate Cancer With Skeletal Metastases (ALSYMPCA)) and were published in [90]. International, placebo-controlled, randomized studies included 921 patients with bone-metastatic, castrate-resistant prostate cancer. The patients were subjected to six-time injection of Xofigo™ at a dose of 50 kBq/kg with an interval between injections of four weeks. The overall survival was 14.9 months, compared to 11.3 months for placebo.

The drug Lutathera (^{177}Lu-DOTA-Tyr3-Octreotate) is available for clinical trials by Advanced Accelerator Applications. The specificity of Octreotate binding with SSTRs determines its effectiveness in the therapy of NET. Currently the drug is being successfully tested in phase III clinical trials (ClinicalTrials.gov Identifier NCT01578239), and the successful results of randomized studies in 230 patients were published in September 2015 [91]. The study involved 230 patients with Grade 1–2 metastatic midgut NETs. In the studies the patients were injected four times with Lutathera with 8-week intervals at an activity of 7.4 GBq. By the time of results presentation, the median progression-free survival (PFS) for Lutathera has not been achieved, while in the control group (drug Octreotide LAR 60 mg every 4 weeks) the median PFS was 8.4 months (mortality in the group of Lutathera and the control group by the date of announcement of the results was 23 and 67 cases, respectively. Starting from April 2015, the FDA allowed the application of Lutathera in the treatment of inoperable progressive midgut NETs. The pharmaceutical of ^{131}I-MIBG (metaiodobenzylguanidine) was originally tested for NET treatment, however, the highest interest was connected with the ability of MIBG to penetrate through cell membranes via norepinephrine(NE)-transporter, which is actively expressed in neuroblastoma cells [92]. One of the major obstacles for the wide application of the ^{131}I-MIBG-based drug in clinical practice is its toxicity for the tissues of the thyroid gland and liver, which, however, can be reduced by means of prophylactic intake of medications with potassium iodide and potassium perchlorate [93]. In 2011–2015 the drug ^{131}I-MIBG was tested for identification of the possible toxicity at high (15–18 mCi/kg) doses in combination with vincristine and inhibitor of topoisomerase irinotecan for resistant/relapsed neuroblastoma (ClinicalTrials.gov Identifier NCT01313936). The testing was performed with the participation of the University of California, supervised by Steven G. DuBois. A total of 32 people aged 2 to 30 years took park in the study. All patients received a five-day course of chemotherapy with irinotecan and a one-dose injection of ^{131}I-MIBG on the second day of chemotherapy. The therapeutic effect was achieved in nine cases, though two cases exhibited a marked side effect of dehydration. Similar studies, in which the use of beta-emitting ^{131}I-MIBG was combined with chemotherapy using histone deacetylase inhibitor vorinostat were described in the publication [94]. The studies were conducted in 27 patients aged up to 30 years, who were subjected to a two-week chemotherapy course including injection of ^{131}I-MIBG at a dose of 8–18 mCi/kg on the third day of therapy. The therapeutic effect was observed in 28% cases, and the combination of 180 mg/m^2/dose vorinostat and 18 mCi/kg ^{131}I-MIBG was recommended for transition to stage II clinical trials (therapeutic effect of 67% in 6 patients). The overall retrospective analysis of the efficiency of ^{131}I-MIBG therapy in the treatment of recurrent and chemotherapy-resistant neuroblastoma is provided in the study [95], testifying a partial or complete efficiency of the drug in 27% cases given the 24-month overall survival of 47% (65% and 39% in the case of recurrent and chemotherapy-resistant neuroblastoma, respectively). Currently the drug is in phase III of clinical trials conducted by the New Approaches to Neuroblastoma Therapy Consortium (ClinicalTrials.gov Identifier NCT02035137) and Tehran University of Medical Sciences (ClinicalTrials.gov Identifier NCT00798148).

10. Conclusions

Currently, significant progress has been made in targeted radionuclide therapy due to the development of molecular and cell biology, immunology, radiation and medical biophysics, nuclear physics, chemical technology, and other related disciplines. To date, a large number of tumor cell antigens suitable for application in targeted radionuclide therapy have been introduced and characterized. A wide variety of carrier molecules, mainly antibodies and some peptides, have been constructed and synthesized. A variety of α-, β-, and Auger electron-emitting radionuclides have been introduced, along with the technologies for their synthesis, isolation, and purification. These radionuclides can now be reliably attached to carrier molecules and target-delivered to practically all types of tumors in the human organism upon intravenous and intracisternal injections, owing to the developed techniques and protocols. Additionally, deposition and dosage of these radionuclides

can be measured and controlled. These advances lead to a novel theranostic approach towards personalized treatment regimens and provide an overall increase of the therapeutic efficiency. Overall, the key fundamental concepts and technology platform of the targeted radionuclide therapy have been established. At the same time, tangible therapeutic outcomes have been demonstrated only in the therapy of hematological malignancies. The efficiency of TRNT of solid tumors, especially large-sized tumors is notoriously low.

In order to achieve a high therapeutic index of TRNT of solid tumors, the key problem of accumulation of high doses of ionizing radiation in tumor tissue cells must be solved. Reliable destruction of radiosensitive tumors requires the absorbed doses to be in the range of approximately 3000–5000 cGy, while elimination of solid tumors with the highest radioresistance, such as thyroid tumors therapy needs up to 10,000 cGy. At the same time, the absorbed doses in organ tissues, including kidneys, lungs, colon mucosa bone marrow should not exceed 2000 cGy, 1500 cGy, 250 cGy and 100 cGy, respectively [19]. It should be noted that in TRNT the effect of ionizing radiation on normal tissues takes place not only during the "trip" of a pharmaceutical through the organism from the injection point to the tumor, but also in the result of metabolism of the complex pharmaceutical-antigen. The metabolism of this complex can either enhance the antitumor effect through radionuclide deposition, or inhibit it due to radionuclide elimination from the cell. Some antigens, including CD5 and PSMA are rapidly internalized in cancer cells, leading to catabolism of the carrier-target complex and, specifically, radionuclide separation from the carrier molecule followed by its efflux from the cell. On the other hand, the uptake rate of such antigens as GPA33 and CD20 is slow, leading to an increased effective period of radionuclide immobilization on cancer cells. The disintegration of the carrier molecule and concomitant radionuclide release from the cell leads not only to the reduction of the therapeutic efficiency, but also causes normal tissue overexposure to the ionizing radiation, especially the liver and kidneys. It is, therefore, reasonable to implement dosimetry and practice symptomatic application of radioprotective adaptogenic drugs ineffective in tumor tissues, which combine radioprotective and hepatoprotective properites [96]. Guanosine [97], inosine [98], IMP [98], and GMP [99] represent such drugs for the liver. By all means, the development and identification of novel more efficient multifunctional radioprotective drugs can offer an alternative solution to the problem of high absorbed doses in normal tissues.

To summarize, TRNT is an important area of medicine, with a great potential to be unveiled, where multidisciplinary approach is deemed essential. Thus, the age of inventing the "sling, bow and firearms" in targeted radionuclide therapy is finished, and it is time to work on "high-precision rocket weapons and lasers".

Acknowledgments: We wish to acknowledge the Targeted Federal Program of the Ministry of Education and Science of The Russian Federation, Grant No. 14.578.21.0030 (RFMEFI57814X0030).

Conflicts of Interest: The authors declare no conflict of interest.

References

1. Curcio, C.G.; Vasile, C.; Gianciotta, A.; Casali, A.; Gionfra, T.; Rinaldi, M.; Guadagni, A.; Le Pera, V.; Sega, E. Short-term results of combined radioimmunotherapy in inoperable lung cancer. *Tumori* **1976**, *62*, 587–598. [PubMed]
2. Sfakianakis, G.N.; DeLand, F.H. Radioimmunodiagnosis and radioimmunotherapy, 1982. *J. Nucl. Med.* **1982**, *23*, 840–850. [PubMed]
3. Reilly, R.M. Radioimmunotherapy of malignancies. *Clin. Pharm.* **1991**, *10*, 359–375. [PubMed]
4. Goldenberg, D.M.; Chang, C.H.; Rossi, E.A.; McBride, J.W.; Sharkey, R.M. Pretargeted molecular imaging and radioimmunotherapy. *Theranostics* **2012**, *2*, 523–540. [CrossRef] [PubMed]
5. Pouget, J.P.; Lozza, C.; Deshayes, E.; Boudousq, V.; Navarro-Teulon, I. Introduction to radiobiology of targeted radionuclide therapy. *Front. Med.* **2015**, *2*. [CrossRef] [PubMed]
6. Golden, E.B.; Apetoh, L. Radiotherapy and immunogenic cell death. *Semin. Radiat. Oncol.* **2015**, *25*, 11–17. [CrossRef] [PubMed]

7. Ward, J.F. DNA damage produced by ionizing radiation in mammalian cells: Identities, mechanisms of formation, and reparability. *Prog. Nucleic Acid Res. Mol. Biol.* **1988**, *35*, 95–125. [PubMed]
8. Jackson, M.R.; Falzone, N.; Vallis, K.A. Advances in anticancer radiopharmaceuticals. *Clin. Oncol.* **2013**, *25*, 604–609. [CrossRef] [PubMed]
9. Kassis, A.I.; Adelstein, S.J. Radiobiologic principles in radionuclide therapy. *J. Nucl. Med.* **2005**, *46*, 4S–12S. [PubMed]
10. Barendsen, G.W.; Beusker, T.L.; Vergroesen, A.J.; Budke, L. Effects of different radiations on human cells in tissue culture. Ii. Biological experiments. *Radiat. Res.* **1960**, *13*, 841–849. [CrossRef] [PubMed]
11. Qaim, S.M. Therapeutic radionuclides and nuclear data. *Radiochim. Acta* **2001**, *89*, 297–302. [CrossRef]
12. Kuroda, I. Effective use of strontium-89 in osseous metastases. *Ann. Nucl. Med.* **2012**, *26*, 197–206. [CrossRef] [PubMed]
13. Toohey, R.E.; Stabin, M.G.; Watson, E.E. The aapm/rsna physics tutorial for residents: Internal radiation dosimetry: Principles and applications. *Radiographics* **2000**, *20*, 533–546. [CrossRef] [PubMed]
14. Ocean, A.J.; Pennington, K.L.; Guarino, M.J.; Sheikh, A.; Bekaii-Saab, T.; Serafini, A.N.; Lee, D.; Sung, M.W.; Gulec, S.A.; Goldsmith, S.J.; *et al*. Fractionated radioimmunotherapy with (90) y-clivatuzumab tetraxetan and low-dose gemcitabine is active in advanced pancreatic cancer: A phase 1 trial. *Cancer* **2012**, *118*, 5497–5506. [CrossRef] [PubMed]
15. Kraeber-Bodere, F.; Rousseau, C.; Bodet-Milin, C.; Frampas, E.; Faivre-Chauvet, A.; Rauscher, A.; Sharkey, R.M.; Goldenberg, D.M.; Chatal, J.F.; Barbet, J. A pretargeting system for tumor pet imaging and radioimmunotherapy. *Front. Pharmacol.* **2015**, *6*. [CrossRef]
16. Zalutsky, M.R.; Pruszynski, M. Astatine-211: Production and availability. *Curr. Radiopharm.* **2011**, *4*, 177–185. [CrossRef] [PubMed]
17. Abmel, X.C.; Chinol, M.; Jin, X.-H.; Knapp, F.F., Jr.; Rostislav, K.; van So, L.; Renata, M.; Fabiola, M.; Osso, J.A., Jr.; Park, S.H.; *et al*. *Therapeutic Radionuclide Generators: 90sr/90y and 188w/188re Generators*; International Atomic Energy Agency: Vienna, Austria, 2009; p. 235.
18. Pillai, M.R.; Dash, A.; Knapp, F.F., Jr. Rhenium-188: Availability from the (188)w/(188)re generator and status of current applications. *Curr. Radiopharm.* **2012**, *5*, 228–243. [CrossRef] [PubMed]
19. Larson, S.M.; Carrasquillo, J.A.; Cheung, N.K.; Press, O.W. Radioimmunotherapy of human tumours. *Nat. Rev. Cancer* **2015**, *15*, 347–360. [CrossRef] [PubMed]
20. Press, O.W.; Shan, D.; Howell-Clark, J.; Eary, J.; Appelbaum, F.R.; Matthews, D.; King, D.J.; Haines, A.M.; Hamann, P.; Hinman, L.; *et al*. Comparative metabolism and retention of iodine-125, yttrium-90, and indium-111 radioimmunoconjugates by cancer cells. *Cancer Res.* **1996**, *56*, 2123–2129. [PubMed]
21. Govindan, S.V.; Goldenberg, D.M. New antibody conjugates in cancer therapy. *Sci. World J.* **2010**, *10*, 2070–2089. [CrossRef] [PubMed]
22. Seidl, C. Radioimmunotherapy with alpha-particle-emitting radionuclides. *Immunotherapy* **2014**, *6*, 431–458. [CrossRef] [PubMed]
23. Ogawa, K.; Aoki, M. Radiolabeled apoptosis imaging agents for early detection of response to therapy. *Sci. World J.* **2014**, *2014*, 732603. [CrossRef] [PubMed]
24. Chung, J.K.; Cheon, G.J. Radioiodine therapy in differentiated thyroid cancer: The first targeted therapy in oncology. *Endocrinol. Metab.* **2014**, *29*, 233–239. [CrossRef] [PubMed]
25. Seidlin, S.M.; Marinelli, L.D.; Oshry, E. Radioactive iodine therapy: Effect on functioning metastases of adenocarcinoma of the thyroid. *J. Am. Med. Assoc.* **1990**, *40*, 299–317. [CrossRef]
26. Dai, G.; Levy, O.; Carrasco, N. Cloning and characterization of the thyroid iodide transporter. *Nature* **1996**, *379*, 458–460. [CrossRef] [PubMed]
27. Guo, R.; Zhang, R.; Pan, Y.; Xu, H.; Zhang, M.; Liang, S.; Wang, L.; Zhang, Y.; Li, B. Feasibility of a novel positive feedback effect of 131i-promoted bac-egr1-hnis expression in malignant glioma through baculovirus: A comparative study with bac-cmv-hnis. *Nucl. Med. Commun.* **2011**, *32*, 402–409. [CrossRef] [PubMed]
28. Carvalho, D.P.; Ferreira, A.C. The importance of sodium/iodide symporter (nis) for thyroid cancer management. *Arq. Bras. Endocrinol. Metab.* **2007**, *51*, 672–682. [CrossRef]
29. Puppin, C.; Arturi, F.; Ferretti, E.; Russo, D.; Sacco, R.; Tell, G.; Damante, G.; Filetti, S. Transcriptional regulation of human sodium/iodide symporter gene: A role for redox factor-1. *Endocrinology* **2004**, *145*, 1290–1293. [CrossRef] [PubMed]

30. Nicola, J.P.; Nazar, M.; Mascanfroni, I.D.; Pellizas, C.G.; Masini-Repiso, A.M. Nf-kappab p65 subunit mediates lipopolysaccharide-induced Na(+)/I(−) symporter gene expression by involving functional interaction with the paired domain transcription factor pax8. *Mol. Endocrinol.* **2010**, *24*, 1846–1862. [CrossRef] [PubMed]
31. Chung, J.-K.; Youn, H.W.; Kang, J.H.; Lee, H.Y.; Kang, K.W. Sodium iodide symporter and the radioiodine treatment of thyroid carcinoma. *Nucl. Med. Mol. Imaging* **2010**, *44*, 4–14. [CrossRef] [PubMed]
32. Pandit-Taskar, N.; Larson, S.M.; Carrasquillo, J.A. Bone-seeking radiopharmaceuticals for treatment of osseous metastases, part 1: Alpha therapy with 223ra-dichloride. *J. Nucl. Med.* **2014**, *55*, 268–274. [CrossRef] [PubMed]
33. Tomblyn, M. The role of bone-seeking radionuclides in the palliative treatment of patients with painful osteoblastic skeletal metastases. *Cancer Control* **2012**, *19*, 137–144. [PubMed]
34. Maffioli, L.; Florimonte, L.; Costa, D.C.; Correia Castanheira, J.; Grana, C.; Luster, M.; Bodei, L.; Chinol, M. New radiopharmaceutical agents for the treatment of castration-resistant prostate cancer. *Q. J. Nucl. Med. Mol. Imaging* **2015**, *59*, 420–438. [PubMed]
35. Allen, B. Systemic targeted alpha radiotherapy for cancer. *J. Biomed. Phys. Eng.* **2013**, *3*, 67–80. [CrossRef] [PubMed]
36. Dash, A.; Knapp, F.F.; Pillai, M.R. Targeted radionuclide therapy—An overview. *Curr. Radiopharm.* **2013**, *6*, 152–180. [CrossRef] [PubMed]
37. Scott, A.M.; Wolchok, J.D.; Old, L.J. Antibody therapy of cancer. *Nat. Rev. Cancer* **2012**, *12*, 278–287. [CrossRef] [PubMed]
38. Weiner, G.J. Building better monoclonal antibody-based therapeutics. *Nat. Rev. Cancer* **2015**, *15*, 361–370. [CrossRef] [PubMed]
39. Bodei, L.; Cremonesi, M.; Kidd, M.; Grana, C.M.; Severi, S.; Modlin, I.M.; Paganelli, G. Peptide receptor radionuclide therapy for advanced neuroendocrine tumors. *Thorac. Surg. Clin.* **2014**, *24*, 333–349. [CrossRef] [PubMed]
40. Shapira, S.; Fokra, A.; Arber, N.; Kraus, S. Peptides for diagnosis and treatment of colorectal cancer. *Curr. Med. Chem.* **2014**, *21*, 2410–2416. [CrossRef] [PubMed]
41. Cole, J.T.; Holland, N.B. Multifunctional nanoparticles for use in theranostic applications. *Drug Deliv. Transl. Res.* **2015**, *5*, 295–309. [CrossRef] [PubMed]
42. Maeda, H. Toward a full understanding of the epr effect in primary and metastatic tumors as well as issues related to its heterogeneity. *Adv. Drug Deliv. Rev.* **2015**, *91*, 3–6. [CrossRef] [PubMed]
43. Anderson, P.M.; Subbiah, V.; Rohren, E. Bone-seeking radiopharmaceuticals as targeted agents of osteosarcoma: Samarium-153-edtmp and radium-223. *Adv. Exp. Med. Biol.* **2014**, *804*, 291–304. [PubMed]
44. Hofmeister, V.; Schrama, D.; Becker, J.C. Anti-cancer therapies targeting the tumor stroma. *Cancer Immunol. Immunother.* **2008**, *57*, 1–17. [CrossRef] [PubMed]
45. Jabbour, E.; O'Brien, S.; Ravandi, F.; Kantarjian, H. Monoclonal antibodies in acute lymphoblastic leukemia. *Blood* **2015**, *125*, 4010–4016. [CrossRef] [PubMed]
46. Seifert, R.P.; Bulkeley, W., 3rd; Zhang, L.; Menes, M.; Bui, M.M. A practical approach to diagnose soft tissue myeloid sarcoma preceding or coinciding with acute myeloid leukemia. *Ann. Diagn. Pathol.* **2014**, *18*, 253–260. [CrossRef] [PubMed]
47. Slovin, S. Biomarkers for immunotherapy in genitourinary malignancies. *Urol. Oncol.* **2015**, *18*, 253–260. [CrossRef] [PubMed]
48. Ronca, R.; Sozzani, S.; Presta, M.; Alessi, P. Delivering cytokines at tumor site: The immunocytokine-conjugated anti-edb-fibronectin antibody case. *Immunobiology* **2009**, *214*, 800–810. [CrossRef] [PubMed]
49. Garinchesa, P.; Sakamoto, J.; Welt, S.; Real, F.; Rettig, W.; Old, L. Organ-specific expression of the colon cancer antigen a33, a cell surface target for antibody-based therapy. *Int. J. Oncol.* **1996**, *9*, 465–471. [CrossRef] [PubMed]
50. Huang, C.Y.; Pourgholami, M.H.; Allen, B.J. Optimizing radioimmunoconjugate delivery in the treatment of solid tumor. *Cancer Treat. Rev.* **2012**, *38*, 854–860. [CrossRef] [PubMed]
51. Jurcic, J.G. Radioimmunotherapy for hematopoietic cell transplantation. *Immunotherapy* **2013**, *5*, 383–394. [CrossRef] [PubMed]
52. Tabata, R.; Iwama, H.; Tabata, C.; Yasumizu, R.; Kojima, M. Cd5- and cd23-positive splenic diffuse large b-cell lymphoma with very low cd20 expression. *J. Clin. Exp. Hematop.* **2014**, *54*, 155–161. [CrossRef] [PubMed]

53. Koon, H.B.; Junghans, R.P. Anti-cd30 antibody-based therapy. *Curr. Opin. Oncol.* **2000**, *12*, 588–593. [CrossRef] [PubMed]
54. Zhang, M.; Yao, Z.; Zhang, Z.; Garmestani, K.; Talanov, V.S.; Plascjak, P.S.; Yu, S.; Kim, H.S.; Goldman, C.K.; Paik, C.H.; *et al*. The anti-cd25 monoclonal antibody 7g7/b6, armed with the alpha-emitter 211at, provides effective radioimmunotherapy for a murine model of leukemia. *Cancer Res.* **2006**, *66*, 8227–8232. [CrossRef] [PubMed]
55. Liersch, T.; Meller, J.; Kulle, B.; Behr, T.M.; Markus, P.; Langer, C.; Ghadimi, B.M.; Wegener, W.A.; Kovacs, J.; Horak, I.D.; *et al*. Phase ii trial of carcinoembryonic antigen radioimmunotherapy with 131i-labetuzumab after salvage resection of colorectal metastases in the liver: Five-year safety and efficacy results. *J. Clin. Oncol.* **2005**, *23*, 6763–6770. [CrossRef] [PubMed]
56. Tagawa, S.T.; Milowsky, M.I.; Morris, M.; Vallabhajosula, S.; Christos, P.; Akhtar, N.H.; Osborne, J.; Goldsmith, S.J.; Larson, S.; Taskar, N.P.; *et al*. Phase ii study of lutetium-177-labeled anti-prostate-specific membrane antigen monoclonal antibody j591 for metastatic castration-resistant prostate cancer. *Clin. Cancer Res.* **2013**, *19*, 5182–5191. [CrossRef] [PubMed]
57. Raja, C.; Graham, P.; Abbas Rizvi, S.M.; Song, E.; Goldsmith, H.; Thompson, J.; Bosserhoff, A.; Morgenstern, A.; Apostolidis, C.; Kearsley, J.; *et al*. Interim analysis of toxicity and response in phase 1 trial of systemic targeted alpha therapy for metastatic melanoma. *Cancer Biol. Ther.* **2007**, *6*, 846–852. [CrossRef] [PubMed]
58. Allen, B.J.; Singla, A.A.; Rizvi, S.M.; Graham, P.; Bruchertseifer, F.; Apostolidis, C.; Morgenstern, A. Analysis of patient survival in a phase I trial of systemic targeted alpha-therapy for metastatic melanoma. *Immunotherapy* **2011**, *3*, 1041–1050. [CrossRef] [PubMed]
59. Sansovini, M.; Severi, S.; Ambrosetti, A.; Monti, M.; Nanni, O.; Sarnelli, A.; Bodei, L.; Garaboldi, L.; Bartolomei, M.; Paganelli, G. Treatment with the radiolabelled somatostatin analog lu-dotatate for advanced pancreatic neuroendocrine tumors. *Neuroendocrinology* **2013**, *97*, 347–354. [CrossRef] [PubMed]
60. Forrer, F.; Waldherr, C.; Maecke, H.R.; Mueller-Brand, J. Targeted radionuclide therapy with 90y-dotatoc in patients with neuroendocrine tumors. *Anticancer Res.* **2006**, *26*, 703–707. [PubMed]
61. Waldherr, C.; Pless, M.; Maecke, H.R.; Schumacher, T.; Crazzolara, A.; Nitzsche, E.U.; Haldemann, A.; Mueller-Brand, J. Tumor response and clinical benefit in neuroendocrine tumors after 7.4 gbq (90)y-dotatoc. *J. Nucl. Med.* **2002**, *43*, 610–616. [PubMed]
62. Nisa, L.; Savelli, G.; Giubbini, R. Yttrium-90 dotatoc therapy in gep-net and other sst2 expressing tumors: A selected review. *Ann. Nucl. Med.* **2011**, *25*, 75–85. [CrossRef] [PubMed]
63. Shah, M.; da Silva, R.; Gravekamp, C.; Libutti, S.K.; Abraham, T.; Dadachova, E. Targeted radionuclide therapies for pancreatic cancer. *Cancer Gene Ther.* **2015**, *22*, 375–379. [CrossRef] [PubMed]
64. Kraeber-Bodere, F.; Bodet-Milin, C.; Rousseau, C.; Eugene, T.; Pallardy, A.; Frampas, E.; Carlier, T.; Ferrer, L.; Gaschet, J.; Davodeau, F.; *et al*. Radioimmunoconjugates for the treatment of cancer. *Semin. Oncol.* **2014**, *41*, 613–622. [CrossRef] [PubMed]
65. Khaled, S.; Held, K.D. *Radiation Biology: A Handbook for Teachers and Students*; International Atomic Energy Agency: Vienna, Austria, 2010; p. 166.
66. Burnet, N.G.; Wurm, R.; Nyman, J.; Peacock, J.H. Normal tissue radiosensitivity–how important is it? *Clin. Oncol.* **1996**, *8*, 25–34. [CrossRef]
67. Bruland, O.S.; Nilsson, S.; Fisher, D.R.; Larsen, R.H. High-linear energy transfer irradiation targeted to skeletal metastases by the alpha-emitter 223ra: Adjuvant or alternative to conventional modalities? *Clin. Cancer Res.* **2006**, *12*, 6250s–6257s. [CrossRef] [PubMed]
68. Trieu, M.; DuBois, S.G.; Pon, E.; Nardo, L.; Hawkins, R.A.; Marachelian, A.; Twist, C.J.; Park, J.R.; Matthay, K.K. Impact of whole-body radiation dose on response and toxicity in patients with neuroblastoma after therapy with i-metaiodobenzylguanidine (mibg). *Pediatr. Blood Cancer* **2016**, *63*. [CrossRef]
69. Seo, Y.; Gustafson, W.C.; Dannoon, S.F.; Nekritz, E.A.; Lee, C.L.; Murphy, S.T.; VanBrocklin, H.F.; Hernandez-Pampaloni, M.; Haas-Kogan, D.A.; Weiss, W.A.; *et al*. Tumor dosimetry using [124i]m-iodobenzylguanidine micropet/ct for [131i]m-iodobenzylguanidine treatment of neuroblastoma in a murine xenograft model. *Mol. Imaging Biol.* **2012**, *14*, 735–742. [CrossRef] [PubMed]

70. Huang, S.Y.; Bolch, W.E.; Lee, C.; van Brocklin, H.F.; Pampaloni, M.H.; Hawkins, R.A.; Sznewajs, A.; DuBois, S.G.; Matthay, K.K.; Seo, Y. Patient-specific dosimetry using pretherapy [^{124}I]m-iodobenzylguanidine ([^{124}I]mibg) dynamic pet/ct imaging before [^{131}I]mibg targeted radionuclide therapy for neuroblastoma. *Mol. Imaging Biol.* **2015**, *17*, 284–294. [CrossRef] [PubMed]
71. Sgouros, G. Yttrium-90 biodistribution by yttrium-87 imaging: A theoretical feasibility analysis. *Med. Phys.* **1998**, *25*, 1487–1490. [CrossRef] [PubMed]
72. Gulec, S.A.; Cohen, S.J.; Pennington, K.L.; Zuckier, L.S.; Hauke, R.J.; Horne, H.; Wegener, W.A.; Teoh, N.; Gold, D.V.; Sharkey, R.M.; *et al*. Treatment of advanced pancreatic carcinoma with 90y-clivatuzumab tetraxetan: A phase I single-dose escalation trial. *Clin. Cancer Res.* **2011**, *17*, 4091–4100. [CrossRef] [PubMed]
73. Yeong, C.H.; Cheng, M.H.; Ng, K.H. Therapeutic radionuclides in nuclear medicine: Current and future prospects. *J. Zhejiang Univ. Sci. B* **2014**, *15*, 845–863. [CrossRef] [PubMed]
74. Sanchez Ruiz, A.C.; de la Cruz-Merino, L.; Provencio Pulla, M. Role of consolidation with yttrium-90 ibritumomab tiuxetan in patients with advanced-stage follicular lymphoma. *Ther. Adv. Hematol.* **2014**, *5*, 78–90. [CrossRef] [PubMed]
75. Morschhauser, F.; Radford, J.; van Hoof, A.; Botto, B.; Rohatiner, A.Z.; Salles, G.; Soubeyran, P.; Tilly, H.; Bischof-Delaloye, A.; van Putten, W.L.; *et al*. 90yttrium-ibritumomab tiuxetan consolidation of first remission in advanced-stage follicular non-hodgkin lymphoma: Updated results after a median follow-up of 7. 3 years from the international, randomized, phase iii first-lineindolent trial. *J. Clin. Oncol.* **2013**, *31*, 1977–1983. [CrossRef] [PubMed]
76. Morschhauser, F.; Radford, J.; van Hoof, A.; Vitolo, U.; Soubeyran, P.; Tilly, H.; Huijgens, P.C.; Kolstad, A.; d'Amore, F.; Gonzalez Diaz, M.; *et al*. Phase iii trial of consolidation therapy with yttrium-90-ibritumomab tiuxetan compared with no additional therapy after first remission in advanced follicular lymphoma. *J. Clin. Oncol.* **2008**, *26*, 5156–5164. [CrossRef] [PubMed]
77. Leonard, J.P.; Coleman, M.; Ketas, J.C.; Chadburn, A.; Furman, R.; Schuster, M.W.; Feldman, E.J.; Ashe, M.; Schuster, S.J.; Wegener, W.A.; *et al*. Epratuzumab, a humanized anti-cd22 antibody, in aggressive non-hodgkin's lymphoma: Phase i/ii clinical trial results. *Clin. Cancer Res.* **2004**, *10*, 5327–5334. [CrossRef] [PubMed]
78. Beatson, R.E.; Taylor-Papadimitriou, J.; Burchell, J.M. Muc1 immunotherapy. *Immunotherapy* **2010**, *2*, 305–327. [CrossRef] [PubMed]
79. Han, S.; Jin, G.; Wang, L.; Li, M.; He, C.; Guo, X.; Zhu, Q. The role of pam4 in the management of pancreatic cancer: Diagnosis, radioimmunodetection, and radioimmunotherapy. *J. Immunol. Res.* **2014**, *2014*, 268479. [CrossRef] [PubMed]
80. Goldsmith, S.J. Radioimmunotherapy of lymphoma: Bexxar and zevalin. *Semin. Nucl. Med.* **2010**, *40*, 122–135. [CrossRef] [PubMed]
81. Press, O.W.; Unger, J.M.; Rimsza, L.M.; Friedberg, J.W.; LeBlanc, M.; Czuczman, M.S.; Kaminski, M.; Braziel, R.M.; Spier, C.; Gopal, A.K.; *et al*. Phase iii randomized intergroup trial of chop plus rituximab compared with chop chemotherapy plus (131)iodine-tositumomab for previously untreated follicular non-hodgkin lymphoma: Swog s0016. *J. Clin. Oncol.* **2013**, *31*, 314–320. [CrossRef] [PubMed]
82. Vose, J.M.; Carter, S.; Burns, L.J.; Ayala, E.; Press, O.W.; Moskowitz, C.H.; Stadtmauer, E.A.; Mineshi, S.; Ambinder, R.; Fenske, T.; *et al*. Phase iii randomized study of rituximab/carmustine, etoposide, cytarabine, and melphalan (beam) compared with iodine-131 tositumomab/beam with autologous hematopoietic cell transplantation for relapsed diffuse large b-cell lymphoma: Results from the bmt ctn 0401 trial. *J. Clin. Oncol.* **2013**, *31*, 1662–1668. [PubMed]
83. Press, O.W.; Unger, J.M.; Rimsza, L.M.; Friedberg, J.W.; LeBlanc, M.; Czuczman, M.S.; Kaminski, M.; Braziel, R.M.; Spier, C.; Gopal, A.K.; *et al*. A comparative analysis of prognostic factor models for follicular lymphoma based on a phase iii trial of chop-rituximab *versus* chop + 131iodine—Tositumomab. *Clin. Cancer Res.* **2013**, *19*, 6624–6632. [CrossRef] [PubMed]
84. Dechant, M.; Bruenke, J.; Valerius, T. Hla class ii antibodies in the treatment of hematologic malignancies. *Semin. Oncol.* **2003**, *30*, 465–475. [CrossRef]
85. Hdeib, A.; Sloan, A. Targeted radioimmunotherapy: The role of ^{131}I-chtnt-1/b mab (cotara) for treatment of high-grade gliomas. *Future Oncol.* **2012**, *8*, 659–669. [CrossRef] [PubMed]
86. Fujiki, M.; Aucejo, F.; Kim, R. Adjuvant treatment of hepatocellular carcinoma after orthotopic liver transplantation: Do we really need this? *Clin. Transplant.* **2013**, *27*, 169–177. [CrossRef] [PubMed]

87. Erba, P.A.; Sollini, M.; Orciuolo, E.; Traino, C.; Petrini, M.; Paganelli, G.; Bombardieri, E.; Grana, C.; Giovannoni, L.; Neri, D.; *et al*. Radioimmunotherapy with radretumab in patients with relapsed hematologic malignancies. *J. Nucl. Med.* **2012**, *53*, 922–927. [CrossRef] [PubMed]
88. FDA_USA. Xofigo (radium ra 223 dichloride) injection: Prescribing information. Available online: http://www.accessdata.fda.gov/drugsatfda_docs/label/2013/203971lbl.pdf (accessed on 31 October 2015).
89. Humm, J.L.; Sartor, O.; Parker, C.; Bruland, O.S.; Macklis, R. Radium-223 in the treatment of osteoblastic metastases: A critical clinical review. *Int. J. Radiat. Oncol. Biol. Phys.* **2015**, *91*, 898–906. [CrossRef] [PubMed]
90. Parker, C.; Nilsson, S.; Heinrich, D.; Helle, S.I.; O'Sullivan, J.M.; Fossa, S.D.; Chodacki, A.; Wiechno, P.; Logue, J.; Seke, M.; *et al*. Alpha emitter radium-223 and survival in metastatic prostate cancer. *N. Engl. J. Med.* **2013**, *369*, 213–223. [CrossRef] [PubMed]
91. Strosberg, J.; Wolin, E.; Chasen, B.; Kulke, M.; Bushnell, D.; Caplin, M.; Baum, R.P.; Mittra, E.; Hobday, T.; Hendifar, A.; *et al*. 177-Lu-dotatate significantly improves progression-free survival in patients with midgut neuroendocrine tumours: Results of the Phase III NETTER-1 trial. In Proceedings of the 2015 European Cancer Congress, Vienna, Austria, 25–29 September 2015; p. 6LBA.
92. Kayano, D.; Kinuya, S. Iodine-131 metaiodobenzylguanidine therapy for neuroblastoma: Reports so far and future perspective. *Sci. World J.* **2015**, *2015*, 1–9. [CrossRef] [PubMed]
93. Quach, A.; Ji, L.; Mishra, V.; Sznewajs, A.; Veatch, J.; Huberty, J.; Franc, B.; Sposto, R.; Groshen, S.; Wei, D.; *et al*. Thyroid and hepatic function after high dose (131)i-metaiodobenzylguanidine ((131)i-mibg) therapy for neuroblastoma. *Pediatr. Blood Cancer* **2011**, *56*, 191–201. [CrossRef] [PubMed]
94. DuBois, S.G.; Groshen, S.; Park, J.R.; Haas-Kogan, D.A.; Yang, X.; Geier, E.; Chen, E.; Giacomini, K.; Weiss, B.; Cohn, S.L.; *et al*. Phase I study of vorinostat as a radiation sensitizer with 131i-metaiodobenzylguanidine (131i-mibg) for patients with relapsed or refractory neuroblastoma. *Clin. Cancer Res.* **2015**, *21*, 2715–2721. [CrossRef] [PubMed]
95. Zhou, M.J.; Doral, M.Y.; DuBois, S.G.; Villablanca, J.G.; Yanik, G.A.; Matthay, K.K. Different outcomes for relapsed *versus* refractory neuroblastoma after therapy with (131)i-metaiodobenzylguanidine ((131)i-mibg). *Eur. J. Cancer* **2015**, *51*, 2465–2472. [CrossRef] [PubMed]
96. Gudkov, S.V.; Popova, N.R.; Bruskov, V.I. Radioprotective substances: History, trends and prospects. *Biophysics* **2015**, *60*, 659–667. [CrossRef]
97. Gudkov, S.V.; Shtarkman, I.N.; Smirnova, V.S.; Chernikov, A.V.; Bruskov, V.I. Guanosine and inosine display antioxidant activity, protect DNA *in vitro* from oxidative damage induced by reactive oxygen species, and serve as radioprotectors in mice. *Radiat. Res.* **2006**, *165*, 538–545. [CrossRef] [PubMed]
98. Gudkov, S.V.; Gudkova, O.Y.; Chernikov, A.V.; Bruskov, V.I. Protection of mice against X-ray injuries by the post-irradiation administration of guanosine and inosine. *Int. J. Radiat. Biol.* **2009**, *85*, 116–125. [CrossRef] [PubMed]
99. Asadullina, N.R.; Usacheva, A.M.; Smirnova, V.S.; Gudkov, S.V. Antioxidative and radiation modulating properties of guanosine-5′-monophosphate. *Nucleosides Nucleotides Nucleic Acid* **2010**, *29*, 786–799. [CrossRef] [PubMed]



© 2015 by the authors; licensee MDPI, Basel, Switzerland. This article is an open access article distributed under the terms and conditions of the Creative Commons by Attribution (CC-BY) license (http://creativecommons.org/licenses/by/4.0/).

International Journal of
Molecular Sciences

MDPI

Article

Alisertib Induces Cell Cycle Arrest, Apoptosis, Autophagy and Suppresses EMT in HT29 and Caco-2 Cells

Bao-Jun Ren [1,2], Zhi-Wei Zhou [2], Da-Jian Zhu [1], Yong-Le Ju [1], Jin-Hao Wu [1], Man-Zhao Ouyang [1], Xiao-Wu Chen [1,*] and Shu-Feng Zhou [2,*]

Received: 2 November 2015; Accepted: 9 December 2015; Published: 29 December 2015
Academic Editor: William Chi-shing Cho

[1] Department of Gastrointestinal Surgery, Shunde First People's Hospital Affiliated to Southern Medical University, Guangdong 528300, China; rbjsdyy@outlook.com (B.-J.R.); zdjsdyy@outlook.com (D.-J.Z.); jylsdyy@outlook.com (Y.-L.J.); wjhsdyy@outlook.com (J.-H.W.); oymzsdyy@outlook.com (M.-Z.O.)
[2] Department of Pharmaceutical Sciences, College of Pharmacy, University of South Florida, 12901 Bruce B. Downs Blvd., MDC 30, Tampa, FL 33612, USA; zzhou1@health.usf.edu
* Correspondence: cxwsdyy@outlook.com (X.-W.C.); szhou@health.usf.edu (S.-F.Z.); Tel.: +86-757-2231-8555 (X.-W.C.); +1-813-974-6276 (S.-F.Z.); Fax: +86-757-2222-3899 (X.-W.C.); +1-813-905-9885 (S.-F.Z.)

Abstract: Colorectal cancer (CRC) is one of the most common malignancies worldwide with substantial mortality and morbidity. Alisertib (ALS) is a selective Aurora kinase A (AURKA) inhibitor with unclear effect and molecular interactome on CRC. This study aimed to evaluate the molecular interactome and anticancer effect of ALS and explore the underlying mechanisms in HT29 and Caco-2 cells. ALS markedly arrested cells in G_2/M phase in both cell lines, accompanied by remarkable alterations in the expression level of key cell cycle regulators. ALS induced apoptosis in HT29 and Caco-2 cells through mitochondrial and death receptor pathways. ALS also induced autophagy in HT29 and Caco-2 cells, with the suppression of phosphoinositide 3-kinase (PI3K)/protein kinase B (Akt)/mammalian target of rapamycin (mTOR), but activation of 5′ AMP-activated protein kinase (AMPK) signaling pathways. There was a differential modulating effect of ALS on p38 MAPK signaling pathway in both cell lines. Moreover, induction or inhibition of autophagy modulated basal and ALS-induced apoptosis in both cell lines. ALS potently suppressed epithelial to mesenchymal transition (EMT) in HT29 and Caco-2 cells. Collectively, it suggests that induction of cell cycle arrest, promotion of apoptosis and autophagy, and suppression of EMT involving mitochondrial, death receptor, PI3K/Akt/mTOR, p38 MAPK, and AMPK signaling pathways contribute to the cancer cell killing effect of ALS on CRC cells.

Keywords: alisertib; colorectal cancer; cell cycle; programmed cell death; EMT

1. Introduction

Colorectal cancer (CRC) is the third most common malignancy in male and the second most common one in female worldwide in 2012 [1]. It was estimated that about 136,830 new cases and 50,310 deaths occurred in US which renders CRC as the third leading cause of cancer related death in 2014 [2]. In China, CRC was the fifth most common cancer and the fifth leading cause of cancer death in 2011 [3]. There were 253,000 new CRC cases, 139,000 CRC deaths, and 583,000 people living with CRC (within 5 years of diagnosis) in 2012 in China [1]. The overall 5-year survival rate is up to 90% in patients with localized CRC [4]; however, it was only 5%–8% in patients with distant metastases in USA [5]. In clinic, there were about 20%–30% of patients who were newly diagnosed with unresectable metastatic disease and 50%–60% patients with CRC will develop metastatic disease,

mainly due to the epithelial to mesenchymal transition (EMT) [6]. Therefore, it is of great importance to develop new therapeutics for CRC treatment, in particular, the distant metastatic CRC.

In addition to the primary surgical resection, the current systemic chemotherapies for CRC, including FOLFIRI (5-fluorouracil, leucovorin and irinotecan) and FOLFOX (5-fluorouracil, leucovorin and oxaliplatin) are the cornerstone of treatment for metastatic CRC patients. The advent of targeted agents (e.g., the anti-vascular endothelial growth factor monoclonal antibody bevacizumab or the anti-epidermal growth factor receptor monoclonal antibodies cetuximab and panitumumab) were recognized as a landmark advance in the treatment of metastatic CRC. However, in many patients, all of the above schemes lead to a poor outcome due to the drug-related adverse events and drug resistance [7]. Thus, it is of clinical importance to identify more effective biological agents with specific therapeutic targets and reduced side effect.

There were three members of Aurora kinases (Aurora A, B, and C) that are affiliated to a family of serine/threonine kinases in mammals, and Aurora kinases have emerged as crucial mitotic regulators required for genome stability [8]. The Aurora kinases regulate multiple aspects of mitosis, including centrosome duplication, spindle assembly, chromosome alignment, chromosome segregation and the fidelity-monitoring spindle checkpoint [9]. Aurora kinase A (AURKA) localizes to duplicated centrosomes and spindle poles, with key functions of centrosomes maturation, timing of mitotic entry and construction and control of a bipolar spindle. Aberrant mRNA or protein expression of AURKA causes abnormalities in mitosis (e.g., aneuploidy, supernumerary centrosomes, and defective mitotic spindles) and induces resistance to apoptosis. In clinic, amplification or overexpression of AURKA was observed in many solid cancers, such as ovarian, gastric, pancreatic, and breast cancers [10]. Also, the abnormal condition of AURKA has been frequently investigated in CRC and is associated with poor prognosis and response to chemotherapy [11,12]. The expression of AURKA protein is higher in CRC liver metastasis than the corresponding primary tumor, which can be recognized as a molecular biomarker with prognostic value for patients with CRC liver metastasis, independent of established clinicopathological variables [13]. It was also suggested that AURKA was essential for CRC stem cells regeneration and resistance to cytotoxic stimuli in CRC [14].

Given the specific localization and function in cells and pathological activation of AURKA in many malignant diseases, AURKA have been an attractive target for the development of new therapeutic approaches for cancer treatment. Numerous compounds of AURKA inhibitor have undergone preclinical testing into Phase I or II trials, including AMG900, AT9283, MLN8237, AZD1152, and ENMD2076 [15]. MLN8237, also known as alisertib (ALS, Figure S1A), is one of secondary generation AURKA inhibitors. *In vitro*, ALS has displayed its effects on inhibition of proliferation and cell cycle progression in glioblastoma neurosphere tumor, malignant bladder cancer, pancreatic cancer, ovarian cancer, breast cancer, osteosarcoma, gastric cancer, and esophageal adenocarcinoma cell lines [16–22]. The anticancer effect of ALS was also examined *in vivo* in multiple myeloma and acute lymphoblastic leukemia xenograft models [23]. Implanted tumors shrunk considerably in multiple myeloma models and the overall survival or disease-free survival was significantly improved in animal models.

However, the role of AURKA in the tumorigenesis and development of CRC and the underlying mechanism have not been fully elucidated, which renders the anticancer effect and molecular mechanisms of ALS in the treatment of CRC remain unclear. In this study, we aimed to unveil the molecular targets, examine the cancer cell killing effect of ALS and elucidate the molecular mechanism for its anticancer effect, with a focus on the cell proliferation, cell cycle distribution, programmed cell death, and EMT in human CRC cell lines HT29 and Caco-2 cells.

2. Results

2.1. Alisertib (ALS) Inhibits the Proliferation of HT29 and Caco-2 Cells

We first examined the effect of ALS on the viability of HT29 and Caco-2 cells using 3-(4,5-dimethylthiazol-2-yl)-2,5-diphenyltetrazolium bromide (MTT) assay. Treatment of both cell lines with ALS at concentrations ranging from 0.1 to 100 μM for 24 or 48 h significantly decreased the viability (Figure S1B,C). Compared with the control cells, the viability of HT29 cells was decreased from 78.5% to 47.3% when exposed to ALS for 24 h and declined from 71.0% to 31.2% when treated with ALS for 48 h at concentrations from 0.1 to 100 μM, respectively (Figure S1B). The IC_{50} values were 49.31 and 17.86 μM for HT29 cells after 24 and 48 h incubation with ALS, respectively. As shown in Figure S1C, the percentage of the viability of Caco-2 cells was decreased from 89.7% to 45.7% when treated with ALS for 24 h and declined from 100.3% to 18.8% when incubated with ALS for 48 h at concentrations from 0.1 to 100 μM, respectively. The IC_{50} values were 88.8 and 52.1 μM for Caco-2 cells after 24 and 48 h incubation with ALS, respectively. These results suggest that ALS inhibits the cell proliferation in concentration- and time-dependent manners and displays a potent inhibitory effect on the growth of HT29 and Caco-2 cells.

2.2. Overview of Proteomic Response to ALS Treatment in HT29 and Caco-2 Cells

Following, we performed a stable isotope labeling by amino acids in cell culture (SILAC)-based proteomic study to quantitatively determine the molecular interactome in HT-29 and Caco-2 cells responding to ALS. There were 893 and 582 protein molecules identified as the potential targets of ALS in HT-29 (Table 1) and Caco-2 cells (Table 2), respectively. ALS increased the expression level of 459 protein molecules, while decreasing the expression level of 434 protein molecules in HT-29 cells. In Caco-2 cells, ALS increased the expression level of 207 protein molecules, but decreased the expression level of 375 protein molecules. Subsequently, these proteins were subject to IPA pathway and network analysis. There were 24 and 25 networks of signaling pathway and cellular function that were potentially regulated by ALS in HT-29 and Caco-2 cells, respectively. These included a number of molecules involved in cell proliferation, metabolism, migration, invasion, survival, and death (Tables 1 and 2). As such, the following experiments were performed to validate the effect of ALS in HT-29 and Caco-2 cells, with a focus on cell cycle distribution, programmed cell death, and EMT.

2.3. ALS Decreases the Phosphorylation Level of Aurora Kinase A (AURKA) in HT29 and Caco-2 Cells

To determine whether ALS effectively targeted AURKA and affected cellular mitosis, we first examined the phosphorylation level of AURKA and the total expression level of AURKA after HT29 and Caco-2 cells were treated with ALS at 0.1, 1, and 5 μM for 48 h. Intriguingly, there were variable alterations in the phosphorylation and expression level of AURKA in these two cell lines when exposed to ALS (Figure 1A,B). In HT29 cells, the phosphorylation level of AURKA was decreased 54.4% and 93.7% when treated with ALS at 1 and 5 μM for 48 h, respectively ($p < 0.001$; Figure 1A,B). However, there was no significant difference in the expression level of AURKA ($p > 0.05$). Consequently, it led to a 66.4% and 93% reduction in the ratio of p-AURKA/AURKA when HT29 cells were treated with ALS 1 and 5 μM for 48 h, respectively, ($p < 0.05$; Figure 1A,B).

Table 1. Molecules and networks were regulated by alisertib (ALS) in HT-29 cells.

ID	Molecules in Network	Score	Focus Molecules	Top Diseases and Functions
1	60S ribosomal ubunit, DDX1, DDX5, DDX17, DDX21, DDX3X, DHX9, EIF3E, HDGF, HNRNPU, ILF2, ILF3, KPNA6, LYAR, MTDH, NEDD8, RAD23B, RBM39, Rnr, RPL3, RPL5, RPL8, RPL9, RPL10, RPL14, RPL18, RPL24, RPL28, RPL30, RPL27A, RPLP0, RPS2, RPS15A, Vegf, XRCC5	52	32	Protein synthesis, infectious disease, gene expression
2	AHSA1, ALYREF, CAND1, ERK1/2, FUBP1, GIGYF2, HNRNPK, HNRNPL, LARS, LOC102724594/U2AF1, MARS, NOLC1, NOP56, NOP58, OLA1, PABPC1, PCBP1, PCBP2, PDE6H, Pki, PTBP1, PUF60, QARS, RALY, RNA polymerase I, SF3B1, SF3B2, Srp30, SRSF1, SRSF2, SRSF3, Tap, TOP1, U2af, U2AF2	44	29	RNA post-transcriptional modification, protein synthesis, cancer
3	CALU, CLIC4, creatine kinase, CUTA, EFTUD2, FUS, Histone H1, HNRNPC, HNRNPD, HNRNPF, HNRNPH1, HNRNPM, HNRNPUL1, Importin α, Importin β, IPO5, IPO7, P38 MAPK, PQBP1, PRMT1, PRMT5, PRPF19, PTMA, PYCR1, RAN, RANBP1, SF3B4, snRNP, SNRPD3, SYNC, TNPO1, Transportin, TRAP/Media, UBA2, WDR1	40	27	RNA post-transcriptional modification, amino acid metabolism, post-translational modification
4	AGR2, Akt, ANXA4, Calcineurin A, CALR, Collagen α1, Collagen type VI, COP I, COPA, COPB1, COPG1, Cytoplasmic Dynein, DSTN, DYNC1LI2, FKBP4, Mre11, PA2G4, PDIA3, PDIA4, PDIA6, peptidylprolyl isomerase, peroxidase (miscellaneous), PPIA, PPIB, PPT1, PRDX1, PRDX2, PRDX4, PRDX5, PRDX6, RRBP1, SAE1, TMED9, TXNDC5, ZYX	38	26	Cancer, endocrine system disorders, organismal injury and abnormalities
5	ACTN1, ACTN4, ANP32B, ASPH, ATP synthase, C1QBP, CAMK2D, CaMKII, COX5A, CSRP1, CTNNA1, Cytochrome bc1, cytochrome C, ERP44, Filamin, ITPR, KLK3, LONP1, MAP4, Mitochondrial complex 1, MRPL12, MT-CO1, MT-CO2, MT-CYB, NDUFA5, Pde, PDS5A, PDXDC1, PHB, PHB2, Pka, PPP2R1A, PRDX3, PYGB, STMN1	38	26	Drug metabolism, lipid metabolism, small molecule biochemistry
6	19S proteasome, 20s proteasome, ADRM1, BUB3, COTL1, CPNE1, DAD1, FLII, Immunoproteasome Pa28/20s, MHC CLASS I (family), NFkB (complex), OTUB1, Proteasome PA700/20s, PSMA, PSMA4, PSMA7, PSMB5, PSMC2, PSMD, PSMD2, PSMD6, PSMD8, PSMD14, PSME1, PSME2, RNF13, S100, S100A2, S100P, UBA1, UBE2, UBE2L3, UBE2N, USMG5, USP14	35	25	Cellular movement, protein degradation, protein synthesis

Table 1. *Cont.*

ID	Molecules in Network	Score	Focus Molecules	Top Diseases and Functions
7	adenosine-tetraphosphatase, α tubulin, ATP5H, ATP5J, ATP5J2, β Tubulin, BZW1, BZW2, CCT4, CCT5, CCT8, CCT6A, DCTN1, Dynein, Ephb, ERP29, F0 ATP synthase, FAM162A, H2AFV, KDELR, LGALS3BP, MAPK1, OGFR, PGAM1, SAR1A, Sec23, TBCA, TSPO, TUBA4A, TUBB6, tubulin (family), VBP1, Vdac, VDAC1, VDAC2	35	25	Cellular assembly and organization, cell-to-cell signaling and interaction, reproductive system development and function
8	CD9, chymotrypsin, CTSH, EIF1, EIF3, EIF3A, EIF3B, EIF3F, EIF3G, EIF3J, EIF3L, EIF4B, Eif4g, Erm, EZR, G6PD, GLRX3, GPIIB-IIIA, IPO9, Lamin b, LBR, Lh, PEBP1, Pkc(s), Pkg, PLCB3, PLIN3, PSIP1, RAB1A, RBM3, Rho gdi, SERPINB1, SLC12A2, TLN1, VAT1	35	25	Gene expression, protein synthesis, cellular growth and proliferation
9	ABCB8, Aconitase, Adaptor protein 1, Aldose Reductase, Angiotensin II receptor type 1, AP1B1, Arf, ARF1, ARF4, ARF5, ARL1, COPB2, CRIP2, cytochrome-c oxidase, DAB2IP, DHCR24, Gef, glutathione peroxidase, glutathione transferase, GST, GSTK1, GSTO1, GSTP1, Jnk, MGST1, PARK7, RAB1B, RPN2, SFXN1, SLC25A3, SLC25A11, SOD2, SRP54, SSR3, USO1	33	24	Drug metabolism, protein synthesis, DNA replication, recombination, and repair
10	ABCC1, AK2, ALDH2, ANXA3, ATPase, atypical protein kinase C, CAPG, Caveolin, CLTA, DBNL, DNPEP, Dynamin, ETFA, ETFB, GANAB, IL-2R, Integrin α 3 β 1, MTCH2, NSF, NUDC, OSBP, PAK2, PCMT1, PHGDH, PI3K (complex), Ptk, Raf, RAP1B, SEPT11, SHMT2, SLC3A2, TPP2, trypsin, VAPA, Vla-4	33	24	Developmental disorder, hereditary disorder, metabolic disease
11	ALDOA, AP2B1, C11orf54, CAD, CBX3, CYP, DHCR7, DPP3, Focal adhesion kinase, GGCT, Histone h4, HMGCS1, IDI1, Ldh (complex), LDHA, LDHB, MAT2A, NPC2, NQO1, PI3K (family), POR, Rar, RBBP4, RBP2, RPN1, Rxr, SLC16A1, Sod, Sos, STAT5a/b, TGM2, thymidine kinase, TPP1, TXNRD1, UGDH	33	24	DNA replication, recombination, and repair, energy production, nucleic acid metabolism
12	ACAA1, APEX1, BTF3, BTF3L4, Cbp/p300, CPSF6, Cyclin A, Cyclin D, Cyclin E, E2f, EDF1, EEF2, EPCAM, FEN1, Hat, HAT1, Holo RNA polymerase II, HSD17B4, Ku, Mcm, MCM3, MCM7, MTHFD1, NASP, NONO, PCNA, POLβ-POLepsilon-POLγ-XRCC1-LIGI-PARP1-PCNA-FEN1, POLR2H, PRKDC, RAD50, Ras, Rb, SSRP1, TIP60, XRCC6	29	22	DNA replication, recombination, and repair, cellular response to therapeutics, cell morphology
13	ANXA5, BCR (complex), CAPZA2, CAPZB, caspase, CDC37, DENR, EIF4G1, FAS, FLNA, FLNB, Hsp27, HSPB1, IFIH1, JINK1/2, Lamin, LMNB1, MAP2K1/2, MCTS1, Mlc, MTORC2, MTPN, Pak, PARP, PARP1, PDCD6, PLEC, PP2A, PYGL, RHOA, Rsk, RTN3, RTN4, Sapk, SRP72	29	22	Cellular compromise, cell morphology, cellular movement

Table 1. *Cont.*

ID	Molecules in Network	Score	Focus Molecules	Top Diseases and Functions
14	ACTG1, ATP5C1, Calmodulin, Caspase 3/7, CD3, CD44, CSTF2, DDX19A, ECH1, EEF1D, Eif2, HNRNPR, HSPA5, Ifn γ, LMNA, MYH9, PGK1, PPM1G, Proinsulin, RAB10, RAB8A, Ribosomal 40s subunit, RPS7, RPS24, RPS3A, RPSA, Secretase γ, SRPRB, TCF, TCR, Tgf β, TSTA3, TUBB, tubulin (complex), tyrosine kinase	29	22	Hematological disease, immunological disease, inflammatory disease
15	26s Proteasome, AMPK, CD59, CS, CTBP1, CTBP2, DDB1, GFPT1, HDL, hemoglobin, HISTONE, Hsp70, Hsp90, HUWE1, IDH3A, IL1, LMAN1, MIF, NADPH oxidase, Nos, NSUN2, PRKAA, Pro-inflammatory Cytokine, PTGES3, Ras homolog, SDHA, SGTA, SSBP1, succinate dehydrogenase, SURF4, TMED2, TRAP1, Ubiquitin, UBXN1, UCHL3	25	20	Cellular assembly and organization, cellular function and maintenance, cellular development
16	ABCE1, ACLY, Ap1, ATP1A1, Calcineurin protein(s), CK1, Ck2, Gsk3, HMBS, HMGA1, HMGB1, HMGB2, HMGB3, HNRNPAB, MEF2, Mek, MVP, NAP1L1, NFAT (complex), Nfat (family), NMDA Receptor, NUDT5, p70 S6k, PDAP1, Pdgf (complex), phosphatase, PICALM, PP1 protein complex group, PP1-C, PPP1R7, Ppp2c, STARD10, TECR, WARS, XPO1	24	19	DNA replication, recombination, and repair, gene expression, nucleic acid metabolism
17	ACTB, Actin, ACTR2, aldo, α actin, α Actinin, α catenin, API5, Arp2/3, ARPC2, ARPC3, Cadherin, CAP1, CLIC1, CNN2, Cofilin, DIAPH1, DPYSL2, ERK, F Actin, FCGR1A/2A/3A, G-Actin, GOT1, LASP1, LTA4H, MYH14, Profilin, Rock, Talin, TPM3, TPM4, Tropomyosin, Troponin t, TWF1, VASP	22	18	Cellular assembly and organization, cellular function and maintenance, cell morphology
18	Adaptor protein 2, AHR, AKR1A1, APP, ATIC, BIN3, BOLA2/BOLA2B, C11orf54, C14orf93, Clathrin, CORO1C, CPN2, CUL3, DDX55, DNAAF2, ERH, EWSR1, FAM98B, GCSH, HEATR5A, MYC, NLE1, NUDT21, OARD1, OLFML2A, PAICS, RAB7A, SLC25A1, SRSF10, TKT, TMEM183A, TPGS2, UBC, UBL4A, UGT1A9 (includes others)	22	19	Cell cycle, hepatic system development and function, cell morphology

Table 1. *Cont.*

ID	Molecules in Network	Score	Focus Molecules	Top Diseases and Functions
19	ACY1, APMAP, APRT, BBS7, BCKDK, C21orf33/LOC102724023, CARHSP1, CLN5, CMPK1, CNN3, CNPY2, CRYZ, CS, EFHD2, FAM98B, GLS, IARS2, KIF20A, MARCH8, MDH1, MTAP, MYLIP, NME3, NME4, NME7, PADI2, PGM3, RAB6B, RABGAP1, RASA4, REXO4, SCT, SLC25A22, TTC1, UBC	20	20	Nucleic acid metabolism, small molecule biochemistry, cell-to-cell signaling and interaction
20	ACSL3, ADCY, ADRB, Alp, ANP32E, ANXA2, Creb, CTNNB1, DPY30, estrogen receptor, G protein, G protein α, G protein β γ, GTPase, Hdac, Histone h3, HSPA9, Insulin, MATR3, Mmp, NOMO1 (includes others), p85 (pik3r), Pdgfr, PLC, PMM2, RCC2, RNA polymerase II, SFPQ, Shc, SRC (family), STIP1, SUMO2, TOP2A, WDR12, WDR36	18	16	Cell cycle, hair and skin development and function, cancer
21	APPBP2, ARIH2, ARL4D, CD70, CDV3, COQ6, EDNRA, ELF4, EML4, GALE, GMDS, H32, HKDC1, ISOC2, KIF6, LSM8, MAGEA11, NME4, NME1-NME2, NUP210L, OARD1, PCSK5, PODXL, RBM47, RRS1, SCFD1, SELL, SYT11, TBL3, TCIRG1, TNKS, TRMT1, UBC, YBX2, ZCCHC12	15	15	Cell-to-cell signaling and interaction, hematological system development and function, immune cell trafficking
22	AAMP, ANXA1, calpain, Casein, Collagen type I, Collagen type III, Collagen type IV, Collagen(s), COMT, Cpla2, DDAH1, Fc γ receptor, Fibrin, Fibrinogen, GADD45, Growth hormone, Integrin, Laminin, LAMP1, LDL, Mac1, Mapk, MCFD2, NAMPT, PDGF BB, PLCE1, Pld, Rap1, SEC13, SERPINH1, SLIRP, SYK, thyroid hormone receptor, TSH, VAV	12	12	Lipid metabolism, molecular transport, small molecule biochemistry
23	AChR, ALDOC, FABP5, Fcer1, Gm-csf, GOT, HINT1, HLA-DR, HSP, Ifn, IFN β, Ige, IgG, IgG1, IgG2a, Igm, Ikb, Ikk (family), IL12 (complex), IL12 (family), Immunoglobulin, Interferon α, mediator, MHC Class I (complex), MHC Class II (complex), NACA, NPEPPS, OGDH, PI3K p85, PLA2, PLC γ, PRKRA, Rac, Tlr, TXLNA	7	8	Cancer, hematological disease, immunological disease
24	ACPP, ACTR2, ARHGAP1, CBR1, CBR3, CDC42, CDC42EP4, Cg, chemokine, CLDN11, COL15A1, collagen, DHCR7, Endothelin, EPHA3, FCGR1A/2A/3A, FSH, GNRH, GNRH2, GNRHR, HSD3B1, Hsd3b4 (includes others), IKK (complex), LIMK2, Metalloprotease, MTORC1, MYO5B, NPC1L1, PAPPA, PEPD, PHKA2, RAB11A, Tnf (family), TNFRSF6B, UCN2	4	8	Endocrine system development and function, lipid metabolism, small molecule biochemistry

Table 2. Molecules and networks were regulated by ALS in Caco-2 cell.

ID	Molecules in Network	Score	Focus Molecules	Top Diseases and Functions
1	60S ribosomal subunit, AARS, AHSA1, AIMP1, C11orf58, DARS, EEF1A1, EEF1B2, EEF1D, EEF1G, EPRS, ERK1/2, GARS, HARS, KARS, MARS, OLA1, PDE6H, PDGF (family), Pki, QARS, RPL8, RPL10, RPL18, RPL21, RPL23, RPL27, RPL30, RPL32, RPL10A, RPL13A, RPLP0, RPLP1, RPS3A, VARS	48	31	Protein synthesis, gene expression, RNA post-transcriptional modification
2	ANXA3, APEX1, BTF3, Cbp/p300, CDH17, CTNNB1, CYB5R3, ESD, FEN1, GANAB, GOLPH3, GST, GSTO1, HDLBP, HIST2H2AC, Holo RNA polymerase II, LMNA, NACA, OAT, PCNA, PGAM1, PRKCSH, PRKDC, RUVBL1, SERBP1, SLC38A2, SSRP1, SUPT16H, TAGLN2, TCF/LEF, thymidine kinase, TMPO, XRCC5, XRCC6, YBX3	45	30	DNA replication, recombination, and repair, cellular response to therapeutics, cell morphology
3	DDOST, DDX17, FUBP1, FUS, hnRNP H, HNRNPA1, HNRNPDL, HNRNPF, HNRNPH1, HNRNPK, HNRNPL, HNRNPR, HNRNPU, IGF2BP3, Karyopherin β, KHSRP, Mapk, MATR3, NONO, PCBP1, PCBP2, PDGF-AA, PSPC1, PTBP1, PUF60, RAN, RAN-GTP, RANGAP1, RBM14, SF3A3, SFPQ, SYNCRIP, TNPO1, Transportin, YBX1	43	29	RNA post-transcriptional modification, protein synthesis, DNA replication, recombination, and repair
4	14-3-3 (β, ε, ζ), CALU, CAPZA1, CAPZB, caspase, CLTC, DLAT, FLNA, GNB2L1, HMBS, HNRNPM, Hsp27, Hsp90, HSP90AA1, HSP90AB1, HSPA8, NCL, NPM1, NUDT21, NUMA1, p85 (pik3r), PCMT1, PKM, PLEC, RPL12, RPL22, SFMBT2, SPTBN1, TRIM28, tubulin (complex), UBXN1, VPS35, YWHAB, YWHAE, YWHAH	43	29	Cancer, gastrointestinal disease, hepatic system disease
5	14-3-3(β, γ, θ, η, ζ), AChR, ACTR3, ALDOC, ALYREF, ATP5A1, Calmodulin, DDX39B, DYNC1H1, EPCAM, F1 ATPase, FABP5, GTPase, IARS2, IMMT, IQGAP1, KIF5B, LRPPRC, MARCKS, mediator, MYH9, Pde, RPL3, RPL4, RPL7, RPLP2, RTN4, SARNP, SLC25A3, TPD52L2, TPI1, TUFM, YWHAG, YWHAQ, ZFC3H1	40	28	Metabolic disease, molecular transport, RNA trafficking
6	14-3-3(η, θ, ζ), Cytokeratin, DSP, EIF3, EIF2S2, EIF3A, EIF3B, EIF3C, EIF3E, EIF3F, EIF3I, EIF3M, EIF4A, EIF4A1, EIF4A3, EIF4B, EIF4F, Eif4g, EIF4G1, EIF4G2, EIF4H, GPI, KRT1, KRT2, KRT8, KRT9, KRT14, KRT18, KRT19, p70 S6k, PABPC1, PI3K (complex), PKP2, PNN, YWHAZ	38	27	Gene expression, protein synthesis, cellular assembly and organization
7	3-hydroxyacyl-CoA dehydrogenase, ACAA1, ACAA2, ACAT1, ACAT2, acetyl-CoA C-acetyltransferase, acetyl-CoA C-acyltransferase, CD99, CNBP, DDX21, DHX9, EDC4, FBL, GLUD1, GSR, H2AFY, HADH, HADHA, HDGF, HNRNPA3, HSD17B10, LOC102724594/U2AF1, NFkB (complex), OTUB1, PDLIM1, peptidase, PPARα-RXRα, RBM39, RCC2, SRSF1, Tap, TOP1, U2af, U2AF2, UBE2	36	26	Renal damage, renal tubule injury, endocrine system development and function

Table 2. *Cont.*

ID	Molecules in Network	Score	Focus Molecules	Top Diseases and Functions
8	Adaptor protein 1, α tubulin, Ap1 γ, AP1B1, AP1G1, β Tubulin, CCT4, CCT5, CCT8, CCT6A, CNN3, CS, DPYSL2, Dynein, EHD1, ERP29, ETFB, FH, Integrin α 5 β 1, LCP1, malate dehydrogenase, MAPK1, MDH1, MDH2, TKT, TUBA1B, TUBB6, TUBB8, TUBB2B, TUBB4B, tubulin (family), Vdac, VDAC1, VDAC2, WARS	36	26	Cancer, hematological disease, immunological disease
9	adenosine-tetraphosphatase, ATP synthase, ATP5B, ATP5H, collagen, Collagen α1, Collagen type III, Cytoplasmic Dynein, DCTN2, DHX15, EFTUD2, FKBP4, HNMT, HNRNPA2B1, MAPRE1, P38 MAPK, PA2G4, peroxidase (miscellaneous), PGK1, PPIA, PRDX1, PRDX2, PRDX6, PRPF8, PRPF19, RRBP1, SERPINH1, SF3B1, SF3B2, SND1, snRNP, SNRPD1, STIP1, TARS, VIL1	36	26	RNA post-transcriptional modification, free radical scavenging, small molecule biochemistry
10	ACLY, ALDH1A1, ANXA5, CK1, CYB5B, DHCR7, DNAJA2, ECHS1, FASN, Focal adhesion kinase, HMGCS1, HSP, Hsp70, HSPA4, HSPA9, HSPB1, HSPE1, HSPH1, IDI1, JINK1/2, MHC Class II (complex), PGD, Pias, POR, PPA1, PSAP, SLC25A6, Srebp, ST13, TOMM22, TOMM40, UBA1, UBE2L3, Ubiquitin, UGDH	36	26	Cell cycle, endocrine system development and function, lipid metabolism
11	ADK, Akt, ARHGDIA, atypical protein kinase C, CADM1, CAPRIN1, CPNE1, EEF2, Fascin, GDI2, HN1, ILF2, ILF3, LRRC47, Mcm, MCM2, MCM3, MCM4, MCM6, N-Cadherin, Pak, PLIN3, PPP2R1B, Rab5, Rab11, RAB11A, RAB2A, RAB7A, RDX, Rho gdi, RNH1, RPA, SEC13, TWF2, VAT1	34	25	DNA replication, recombination, and repair, cell signaling, post-translational modification
12	ADH5, API5, Arp2/3, ARPC2, ARPC5, CLIC1, CNN2, DDX1, Eif2, ERK, GPIIB-IIIA, HNRNPH3, IGF2BP1, Ku, LAMB1, Laminin1, LAP3, Profilin, Ribosomal 40s subunit, Rnr, RPS2, RPS7, RPS8, RPS10, RPS12, RPS14, RPS15, RPS24, RPS27A, RPS4X, RPSA, RTCB, Talin, TLN1, VCL	34	25	Developmental disorder, hematological disease, hereditary disorder
13	Arf, ARF1, ARHGAP1, B2M, B2m-Mhc1a, CALR, CANX, CCAR2, CCDC47, Cd1, CD1D-CANX-CALR-ERp57, COP I, COPA, COPB1, COPE, COPG1, DNAJ, DNAJA1, DNAJC8, HLA-B27, Hsp22/Hsp40/Hsp90, HSP90B1, HSPA5, HYOU1, Jnk, LMAN1, MHC Class I (complex), P4HB, PDIA3, PDIA4, PDIA6, PRDX4, RAB1B, RPN1, TXNDC5	34	25	Post-translational modification, protein folding, developmental disorder

Table 2. *Cont.*

ID	Molecules in Network	Score	Focus Molecules	Top Diseases and Functions
14	ACO2, Aconitase, AHCY, AKR1C3, AKR1C1/AKR1C2, Aldose Reductase, CACYBP, chymotrypsin, COMT, ENO1, ERP44, ETF1, Filamin, FLNB, FLNC, G6PD, GADD45, GCN1L1, glutathione peroxidase, Lamin b, LONP1, LRRC59, ME1, N-cor, PARK7, PEBP1, PFKP, Pkc(s), PTGES3, Rar, RPL7A, SEPT2, T3-TR-RXR, TALDO1, thyroid hormone receptor	30	23	Nucleic acid metabolism, small molecule biochemistry, cellular movement
15	14-3-3, APC/APC2, ATIC, CBX3, CHD4, CLIC4, CSE1L, GART, H3F3A/H3F3B, HIST1H1C, Histone H1, Histone h3, Histone h4, IDH1, IL-2R, Importin α, Importin β, IPO5, IPO7, KPNA2, KPNA3, KPNB1, Mucin, NuRD, NUTF2, PAICS, PHGDH, PTMA, RANBP1, SAE1, SNRPD3, SSB, TIP60, Vegf, WDR1	30	23	Molecular transport, protein trafficking, amino acid metabolism
16	ACTA1, ACTG1, Actin, ACTN4, ACTR2, aldo, α actin, α Actinin, BASP1, Cadherin, CAP1, CFL1, CFL2, CKB, Cofilin, CORO1C, COTL1, DBN1, F Actin, G-Actin, LMO7, MYH10, MYL12A, Myosin2, NAPA, NWASP, PAFAH1B2, PDCD6IP, Pka, PLS3, TMOD3, TPM3, TPM4, Tropomyosin, TWF1	30	23	Cellular assembly and organization, cellular function and maintenance, developmental disorder
17	19S proteasome, 20s proteasome, 26s Proteasome, ATP5C1, ATPase, CCT3, CCT7, Cyclin E, Immunoproteasome Pa28/20s, LRP, MHC CLASS I (family), NSFL1C, Proteasome PA700/20s, PSMA, PSMA1, PSMA2, PSMA4, PSMA7, PSMB1, PSMC4, PSMD, PSMD1, PSMD2, PSMD3, PSME1, PSME2, Rac, SLC3A2, SOD1, SQSTM1, TUBB, UBE2N, USP5, VAPA, VCP	30	23	Developmental disorder, hereditary disorder, inflammatory disease
18	ACTN1, α catenin, ANXA2, ATP6V1A, C1QBP, CAPNS1, Caveolin, CDHE/CDHN, CSRP1, CTNNA1, CTNND1, CTNNα-CTNNβ-CTNNδ, CYC1, Cyclin B, Cytochrome bc1, cytochrome C, cytochrome-c oxidase, DNM1L, Dynamin, EPPK1, ETFA, HSPD1, Il8r, JUP, MDK, Mitochondrial complex 1, PARP, PHB, PHB2, PRDX3, Ras homolog, SPTAN1, STOML2, UQCRC1, ZYX	28	22	Cellular movement, cell morphology, cellular function and maintenance

Table 2. *Cont.*

ID	Molecules in Network	Score	Focus Molecules	Top Diseases and Functions
19	ALDOA, AP2B1, APOA1, ATP2A2, calpain, CAPN1, CAPN2, Casein, creatine kinase, DBI, DPP3, Fibrinogen, GC, Growth hormone, HBD, HDL, hemoglobin, HIST1H2BL, Ldh (complex), LDHA, LDHB, LDL, NAMPT, Nos, Nr1h, PF4, Pro-inflammatory Cytokine, QDPR, SAA, SERPINA1, Sod, SRC (family), TFRC, TGM2, VLDL-cholesterol	22	19	Cellular function and maintenance, carbohydrate metabolism, free radical scavenging
20	Alp, APLP2, BCAT1, CDH1, Collagen type I, Collagen type IV, Collagen(s), CTSB, CTTN, elastase, F11R, Fgf, Fgfr, Fibrin, FN1, GLG1, GOT, GOT1, GOT2, GPD2, Integrin, Laminin, LMNB1, MAT2A, Mmp, Notch, PDGF BB, Rap1, RPN2, Secretase γ, SERPINA3, SERPINB1, TAGLN, Tgf β, trypsin	19	17	Amino acid metabolism, small molecule biochemistry, dermatological diseases and conditions
21	ACTL8, AGPAT2, ANP32E, BROX, CDV3, CEP78, CHMP6, CHMP7, CHMP1B, CHMP2A, CHMP4A, CHMP4B, CMPK1, GMPS, HEBP1, HIST1H2AE, HSDL2, NAP1L2, NAP1L4, NARS, NME3, NME4, NME7, NME1-NME2, NPM3, PNPO, QPRT, RNPEP, TCEAL1, TSN, TTLL4, TUBAL3, UBC, USP54, ZBTB18	17	16	Infectious disease, cell morphology, cellular assembly and organization
22	ATP1A1, ATP6V1B2, Calcineurin A, CCT2, Ck2, Dishevelled, EIF2S1, EIF5A, Gsk3, ITPR, MAP2K1/2, MIR124, Mlc, Pdgf (complex), PFN1, phosphatase, PICALM, Pkg, PP1 protein complex group, PP1-C, PP1/PP2A, PP2A, PPP1CA, Ppp2c, PPP2R4, PPP2R1A, PRKAA, Rb, RCN1, Rock, SET, SHMT2, Spectrin, STARD10, XPO1	16	15	Molecular transport, RNA trafficking, hereditary disorder
23	ACKR1, ACSL3, AFP, ALDH18A1, AP4S1, APLNR, CCND1, CKAP4, DPY30, E2f, EMR2, EMR3, ENOPH1, FPR3, FSD1, γ tubulin, Gpcr, GPR15, GPR35, GPR137B, GPRC5C, Metalloprotease, MFSD1, miR-491-5p (and other miRNAs w/seed GUGGGGA), NAP1L1, NDC1, NUP155, PXN, RAB10, RXFP2, SSR4, STAT, STX2, TTLL4, UBC	9	10	Cell-to-cell signaling and interaction, cellular assembly and organization, cellular compromise
24	AHNAK, BCR (complex), Complement component 1, CXADR, DDX6, ENaC, EZR, Fcer1, GTF2I, HINT1, HLA-DR, Iga, Ige, IgG1, Igg3, Igm, Ikb, IMPDH2, JAK, KHDRBS1, MEF2, MIRLET7, NFAT (complex), Nfat (family), NFkB (family), PI3K (family), PI3K p85, PLC γ, Ptk, Raf, Ras, Rsk, Sapk, SYK/ZAP, TEC	7	9	Cancer, organismal injury and abnormalities, infectious disease
25	Adaptor protein 2, ADCY, ADRB, Ap1, BSG, Calcineurin protein(s), CaMKII, CDK1, Cg, Clathrin, Creb, DDX5, estrogen receptor, FSH, G protein, GFPT1, GML, GSTP1, IKK (complex), Insulin, Lh, MCTS1, MTORC1, NADPH oxidase, NMDA Receptor, Pdgfr, Pka catalytic subunit, PLC, Proinsulin, RNA polymerase II, Shc, SKP1, Sos, TCF, UCHL1	7	9	Neurological disease, psychological disorders, skeletal and muscular disorders

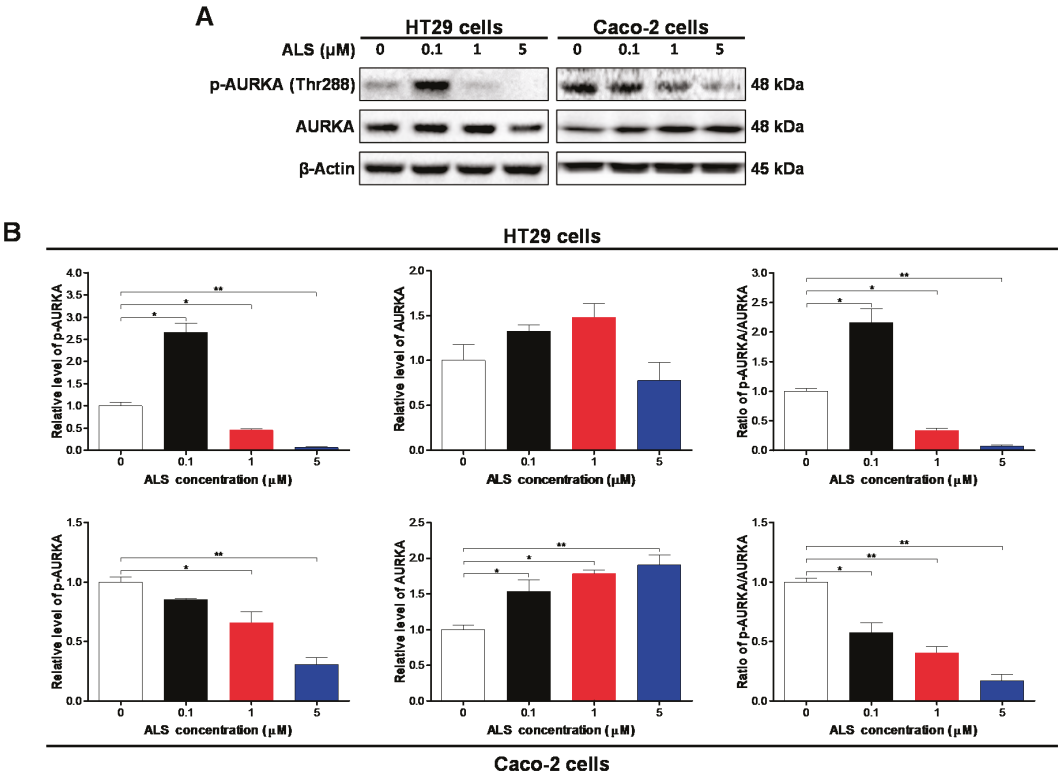

Figure 1. Alisertib (ALS) inhibits the phosphorylation of Aurora kinase A (AURKA) in HT29 and Caco-2 cells. HT29 and Caco-2 cells were exposed to ALS at 0.1, 1, and 5 μM for 48 h and protein samples were subject to Western blotting assay. (**A**) Representative blots of p-AURKA and total AURKA examined by Western blotting assay; (**B**) Bar graphs showing the level of p-AURKA and AURKA in HT29 and Caco-2 cells. β-Actin was used as the internal control. Data are shown as the mean ± SD of three independent experiments. * $p < 0.05$ and ** $p < 0.01$ by one-way analysis of variance (ANOVA).

Also, as shown in Figure 1, treatment of Caco-2 cells with ALS significantly inhibited the phosphorylation of AURKA at Thr288 in a concentration-dependent manner, whereas there was no significant change in the expression level of AURKA when treated with ALS at 0.1, 1, and 5 μM for 48 h. Moreover, in comparison to the control cells, incubation of Caco-2 cells with ALS at 0.1, 1, and 5 μM led to a 42.4%, 59.5%, and 82.9% reduction in the ratio of p-AURKA over AURKA, respectively ($p < 0.05$; Figure 1A,B). Collectively, treatment of HT29 and Caco-2 cells with ALS significantly inhibits the phosphorylation of AURKA at Thr288 in a concentration-dependent manner.

2.4. ALS Modulates the Cell Cycle Distribution of HT29 and Caco-2 Cells

As the inhibitory effect of ALS on cell proliferation and phosphorylation of AURKA has been observed, we next assessed the effect of ALS on the cell cycle distribution of HT29 and Caco-2 cells by flow cytometry. Treatment of HT29 cells with ALS at 0.1, 1, and 5 μM for 24 h resulted in a remarkable increase in the percentage of cells in G_2/M phase from 10.5% at basal level to 16.8%, 85.7%, and 87.7%, respectively ($p < 0.001$; Figure 4A and Figure S2A). Similarly, the percentage of Caco-2 cells in G_2/M phase was raised from 17.3% at basal level to 56.2%, 77.2%, and 77.5% when treated with ALS at 0.1, 1, and 5 μM for 24 h, respectively ($p < 0.001$; Figure 4A and Figure S2A). Meanwhile, the percentage of both cell lines in the G_1 and S phases was decreased correspondingly. The data show that ALS induces significant cell cycle arrest in the G_2/M phase in both cell lines in a concentration-dependent manner.

We also performed separate experiments to assess the effect of ALS at 1 μM on cell cycle distribution over 72 h in HT29 and Caco-2 cells. We found the appearance of aneuploid cells after

ALS treatment over 48 h in both cell lines. Compared with control cells, the percentage of diploid HT29 cells in G_2/M phase was increased from 7.0% at the basal level to 12.7%, 24.3%, 37.3%, and 71.4% after treatment with 1 μM ALS for 4, 8, 12, and 24 h and declined to 21.1% and 12% after 48 and 72 h, respectively ($p < 0.001$; Figure 4B and Figure S2B), while the percentage of aneuploid HT29 cells in G_2/M phase was increased from 23.9% to 69.3% after treatment with ALS from 48 to 72 h (Figure 4B and Figure S2B). Similarly, the percentage of diploid Caco-2 cells in G_2/M phase increased from 18.5% at the basal level to 19.9%, 20.8%, 34.1%, 80.8%, 64.7% and 57.7% when the cells were incubated with 1 μM ALS for 4, 8, 12, 24, 48 and 72 h, respectively ($p < 0.001$; Figure 4C and Figure S2C), while the percentage of aneuploid Caco-2 cells in G_2/M phase was increased from 16.5% to 34.2% after treatment with ALS from 48 to 72 h. On the contrary, the percentage of HT29 and Caco-2 diploid cells in G_1 phase was markedly reduced ($p < 0.001$; Figure 4 and Figure S2). Taken together, these results suggest that ALS induces a time-dependent cell cycle arrest in G_2/M phase in HT29 and Caco-2 cells.

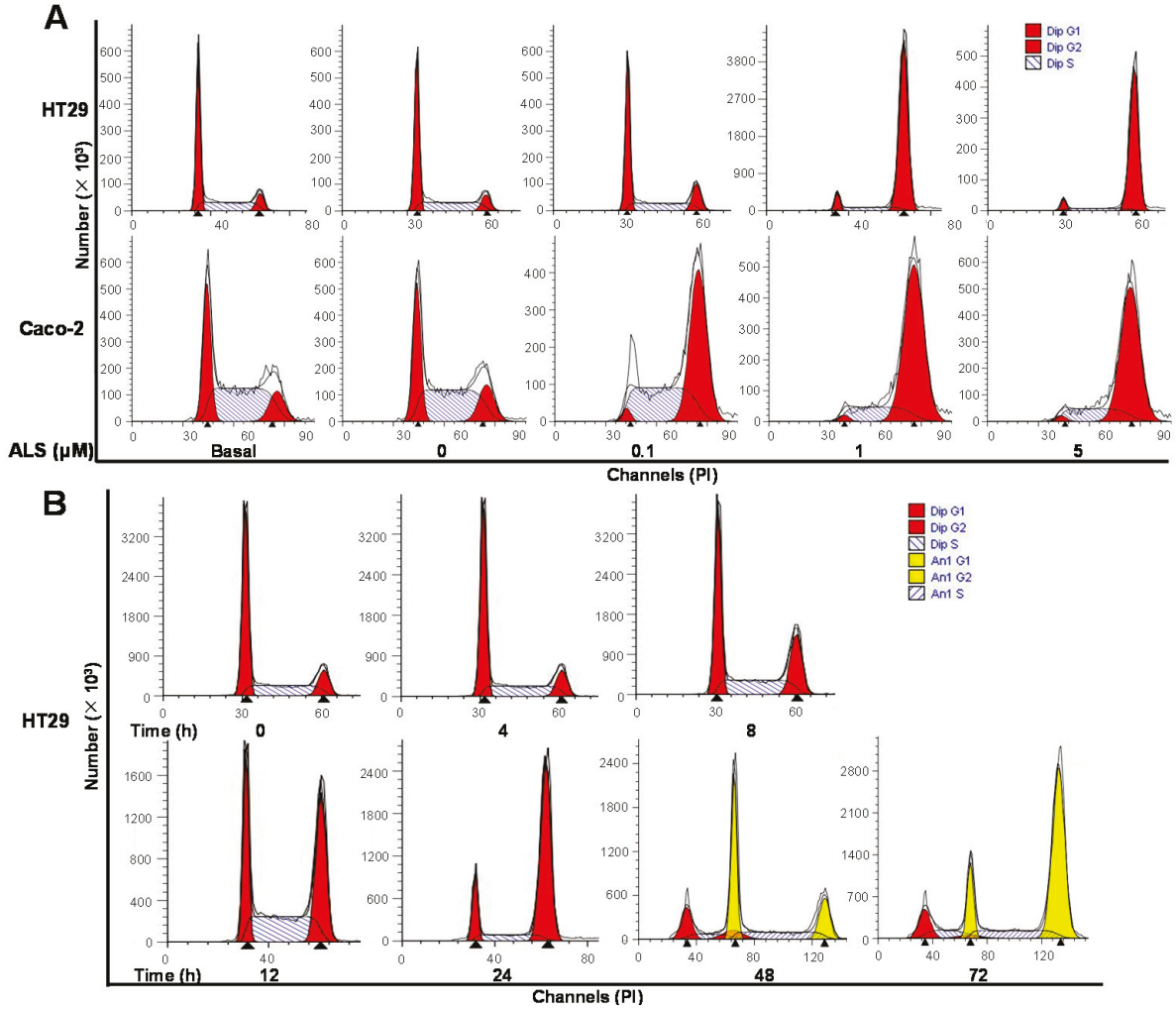

Figure 2. *Cont.*

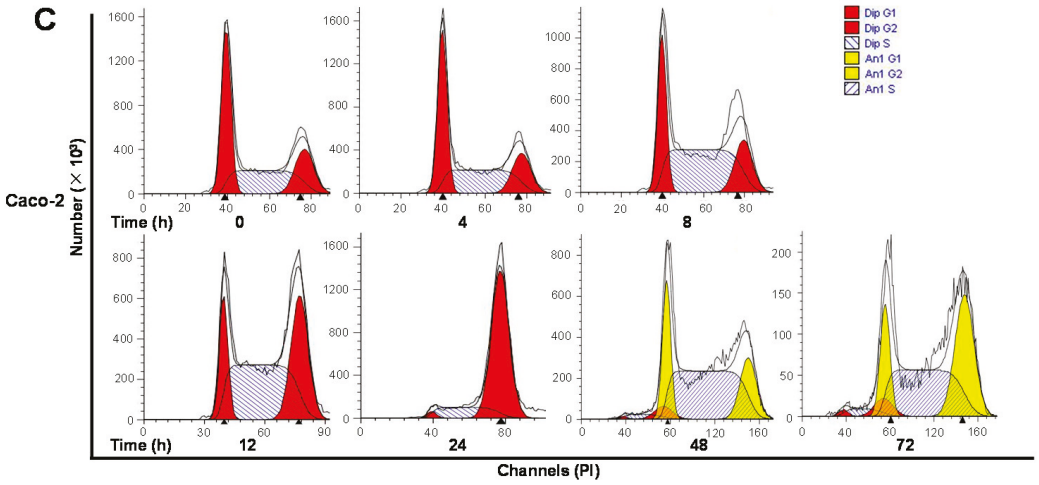

Figure 2. ALS induces cell cycle arrest in G2/M phase in HT29 and Caco-2 cells. (**A**) HT29 and Caco-2 cells were treated with ALS at 0.1, 1, and 5 μM for 24 h and then subjected to flow cytometric analysis. Representative DNA fluorescence histograms of propidium iodide (PI)-stained HT29 and Caco-2 cells showing the cell cycle distribution; (**B**) Time course of ALS-induced cell cycle change over 72 h in HT29 cells. Flow cytometric histograms showing the cell cycle distribution when HT29 cells were incubated with ALS at 1 μM for 4, 8, 12, 24, 48, and 72 h; (**C**) Time course of ALS-induced cell cycle change over 72 h in Caco-2 cells. Flow cytometric histograms show the cell cycle distribution when Caco-2 cells were incubated with ALS at 1 μM for 4, 8, 12, 24, 48, and 72 h. Cells were stained with PI and subjected to flow cytometric analysis that collected 15,000 events. Data represent the mean ± SD of three independent experiments. Dip: diploid; Ani: aneuploid.

2.5. ALS Differentially Alters Key Regulators of Cell Cycle in HT29 and Caco-2 Cells

To unveil the underlying mechanism for ALS-induced cell cycle arrest, we further dissected the expression of key cell cycle regulating proteins, including CDK1/CDC2, p-CDC2 (Tyr15), cyclin B1, p-cyclin B1 (Ser133), p-CDC25C (Ser216), PLK1, p53, and p21/Waf1 in HT29 and Caco-2 cells using Western blotting assay. As shown in Figure 3A and Figure S3A, incubation of HT29 cells with ALS significantly inhibited the expression of the positive regulators but enhanced the expression of negative regulators that are responsible for the G_2 to M phase transition. The expression level of cyclin B1 and CDC2 was declined in a concentration-dependent manner. There was 1.3-fold reduction and a 30.0% decrease in the expression level of cyclin B1 and CDC2 when treated with 1 μM ALS, respectively ($p > 0.05$), whereas there was a 69.8% and 45.2% reduction in the expression level of cyclin B1 and CDC2 when treated with 5 μM ALS, compared to the control cells, respectively ($p < 0.05$ or 0.01; Figure 3A and Figure S3A). In contrast, the expression level of the negative regulators of cell cycle progression were significantly increased in a concentration-dependent manner. As shown in Figure 3A and Figure S3A, the expression level of p53 was increased 1.5- and 1.4-fold when HT29 cells were incubated with ALS at 1 μM ($p < 0.05$) and 5 μM ($p > 0.05$), respectively, compared to the control cells. The expression level of p21 Waf1/Cip1 was increased 3.3- and 2.5-fold when HT29 cells were treated with 1 and 5 μM ALS, respectively, compared to the control cells ($p < 0.001$; Figure 3A and Figure S3A). Collectively, the decreased expression of cyclin B1 and CDC2 and the increased expression of p53 and p21 contribute to ALS-induced G_2/M phase arrest of HT29 cells.

For Caco-2 cells, the regulatory effect of ALS on the expression level of key cell cycle regulators was in a concentration-dependent manner (Figure 3B and Figure S3B). We found that the expression level of cyclin B1 and CDC2 were remarkably increased (Figure 3B and Figure S3B). Therefore, we further examined the level of PLK1, p-cyclin B1 (Ser133), p-CDC2 (Tyr15), and p-CDC25C (Ser216). In comparison to the control cells, the level of p-cyclin B1 (Ser133) was decreased 36.2% and 66.4% when

treated with 1 and 5 μM ALS for 48 h, respectively ($p < 0.01$; Figure 3B and Figure S3B). Similarly, the expression level of PLK1 was decreased 87.3% and 88.3% when treated with 1 and 5 μM ALS for 48 h, respectively ($p < 0.01$; Figure 3B and Figure S3B). In contrast, the level of p-CDC25C (Ser216) was increased 2.3- and 2.6-fold when cells were incubated with 1 and 5 μM ALS, respectively, compared to the control cells ($p < 0.01$; Figure 3B and Figure S3B). The level of p-CDC2 (Tyr15) was increased 2.8- and 2.7-fold when incubated with 1 and 5 μM ALS, respectively, compared to the control cells ($p < 0.01$; Figure 3B and Figure S3B). Taken together, the decreased level of p-cyclin B1 (Ser133) and PLK1 and the increased level of p-CDC2 (Tyr15), critical regulators for the G_2/M transition, contribute to ALS-induced G_2/M phase arrest of Caco-2 cells.

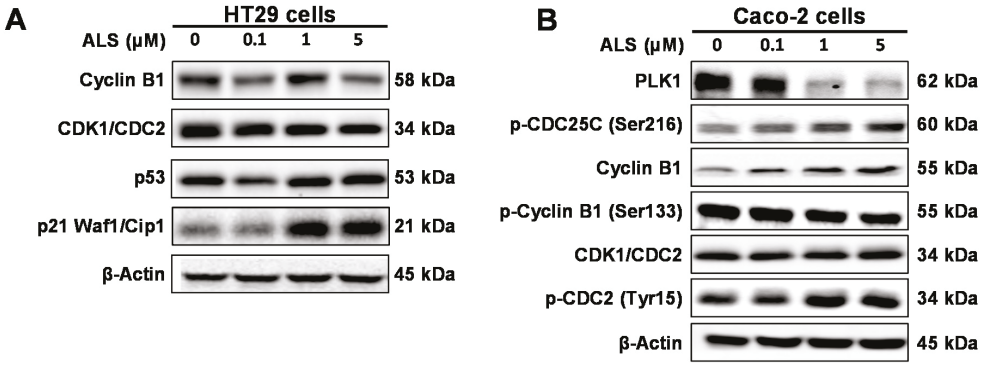

Figure 3. Effect of ALS on the expression level of key regulators of cell cycle in HT29 and Caco-2 cells. (**A**) Representative blots showing the expression of CDK1/CDC2, cyclin B1, p21 Waf1/Cip1, and p53 when HT29 cells were treated with ALS at 0.1, 1, and 5 μM for 48 h; (**B**) Representative blots showing the level of PLK1, CDK1/CDC2, p-CDC2 (Tyr15), cyclin B1, p-cyclin B1 (Ser133), and p-CDC25C (Ser216) in Caco-2 cells.

2.6. ALS Differentially Induces Cell Death in HT29 and Caco-2 Cells

To examine the cancer cell killing effect of ALS on HT29 and Caco-2 cells, the number of apoptotic cells was first quantified using flow cytometry. As shown in Figure 4A and Figure S4A, the total percentage of apoptotic cells (early + late apoptosis) was 6.2% in HT29 cells when incubated with the control vehicle only (0.05% dimethyl sulfoxide (DMSO), v/v). In comparison with the control cells, there was 2.4- and 2.6-fold increase in total apoptotic cells when HT29 cells were treated with 1 and 5 μM ALS, respectively ($p < 0.05$; Figure 4A and Figure S4A). In Caco-2 cells, there was a 2.0- and 1.8-fold increase in total apoptotic cells when exposed to 1 and 5 μM ALS, compared with the control cells (8.8%), respectively ($p < 0.05$; Figure 4A and Figure S4A).

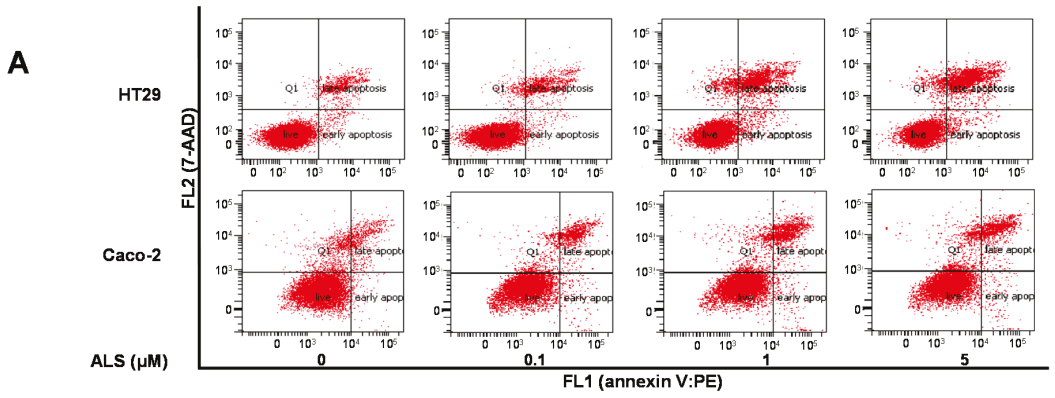

Figure 4. *Cont.*

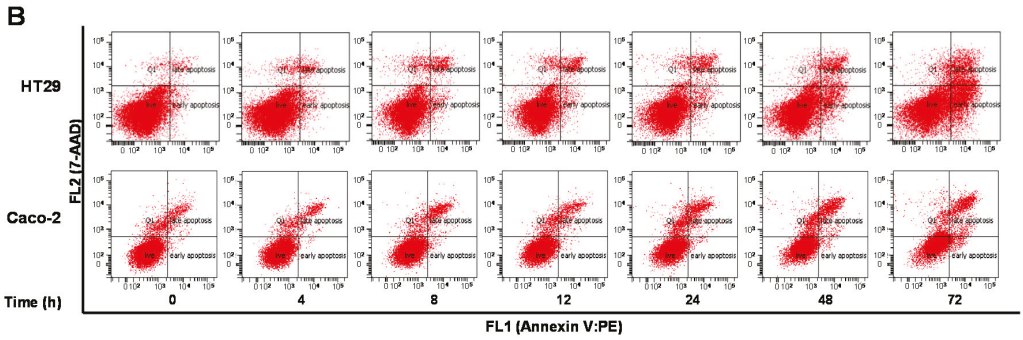

Figure 4. ALS induces apoptotic death in HT29 and Caco-2 cells. (**A**) HT29 and Caco-2 cells were exposed to ALS at 0.1, 1, and 5 μM for 24 h and then subject to flow cytometric analysis. Flow cytometric dot plots of specific cell populations (live, early apoptosis and late apoptosis) in HT29 and Caco-2 cells; (**B**) HT29 and Caco-2 cells were treated with ALS at 1 μM for 4, 8, 12, 24, 48, and 72 h and then subject to flow cytometric analysis. Flow cytometric dot plots showing specific cell populations (live, early apoptosis, and late apoptosis) in HT29 and Caco-2 cells. The apoptotic cells were detected by an annexin-V:PE (phycoerythrin) and 7-Aminoactinomycin D (7-AAD) double staining assay. The flow cytometer collected 15,000 events. Q1 indicated necrotic cells due to the machanical damage. Early apoptotic cells are located in the lower right corner (annexin V:PE positive only). Late apoptotic cells are located in the upper right corner (double positive with annexin V:PE and 7-AAD). The viable cells are located in the lower left corner (double negative with annexin V:PE and 7-AAD staining).

Next, we evaluated the effect of ALS on the apoptosis of HT29 and Caco-2 cells when cells were exposed to 1 μM ALS over 72 h (Figure 4B and Figure S4B). The percentage of apoptotic HT29 cells was increased from 3.8% at the basal level (time 0) to 4.6%, 4.6%, 5.3%, 6.8%, 12.1%, and 24.3% with the treatment of ALS for 4, 8, 12, 24, 48, and 72 h, respectively. Compared with the control cells, incubation with ALS for 24, 48, and 72 h caused a 1.8-, 3.2-, and 6.4-fold increase in total apoptotic cells ($p < 0.001$; Figure 4B and Figure S4B). For Caco-2 cells, the percentage of apoptotic cells was increased from 6.0% at the basal level (time 0) to 5.9%, 8.7%, 7.6%, 9.4%, 11.8%, and 12.9% with the treatment of ALS for 4, 8, 12, 24, 48, and 72 h, respectively. In comparison to the control cells, treatment of Caco-2 cells with ALS for 24, 48, and 72 h caused a 1.6-, 2.0-, and 2.2-fold increase in total apoptotic cells ($p < 0.001$; Figure 4B and Figure S4B). Taken together, the results clearly suggest that ALS induces apoptotic cell death in HT29 and Caco-2 cells in concentration- and time-dependent manners.

The mechanism for ALS-induced apoptosis was delineated in HT29 and Caco-2 cells by western blotting analysis. We evaluated the expression level of key molecules involved in apoptosis process, including Bcl-xl, Bcl-2, Bax, PUMA, cytochrome c, cleaved caspase 3, cleaved caspase 9, cleaved PARP, RIP, p-FADD, and FADD. HT29 and Caco-2 cells were treated with ALS at 0.1, 1, and 5 μM for 48 h. In comparison to the control cells, incubation of HT29 cells with 1 and 5 μM ALS increased Bax level 1.8- and 2.1-fold, respectively ($p < 0.05$; Figure 5A and Figure S5A); whereas incubation of HT29 cells with 5 μM ALS decreased Bcl-2 and Bcl-xl level 72.1% and 47.7%, respectively, compared to the control cells ($p < 0.01$ or 0.05; Figure 5A and Figure S5A). Given the marked increase in the expression level of Bax but a dramatic decrease in the expression level of Bcl-xl and Bcl-2, the disturbed balance of mitochondria-mediated apoptotic status may shift to pro-apoptotic state. We assessed the expression of other pro-apoptotic and anti-apoptotic proteins involved in mitochondria-mediated apoptotic pathway. Compared to the control cells, treatment of HT29 cells with 1 and 5 μM ALS for 48 h markedly increased 2.7- and 3.3-fold in the expression level of PUMA, respectively ($p < 0.01$; Figure 5A and Figure S5A). The cytosolic level of cytochrome c was increased 2.6-fold when treated with 5 μM ALS ($p < 0.05$; Figure 5A and Figure S5A). Furthermore, a significant increase in the level of cleaved caspases 9, cleaved caspase 3, and cleaved PARP was observed. Compared to the control cells, incubation of HT29 cells with ALS at 1 and 5 μM resulted in a 2.2- and 2.3-fold increase

in the level of cleaved caspase 3, a 2.0- and 1.7-fold rise in the level of cleaved caspase 9, and a 4.4- and 5.3-fold elevation in the level of cleaved PARP, respectively ($p < 0.01$; Figure 5A and Figure S5A). Taken together, these data demonstrate that ALS induces apoptotic death of HT29 cells via mitochondria-mediated apoptotic pathway.

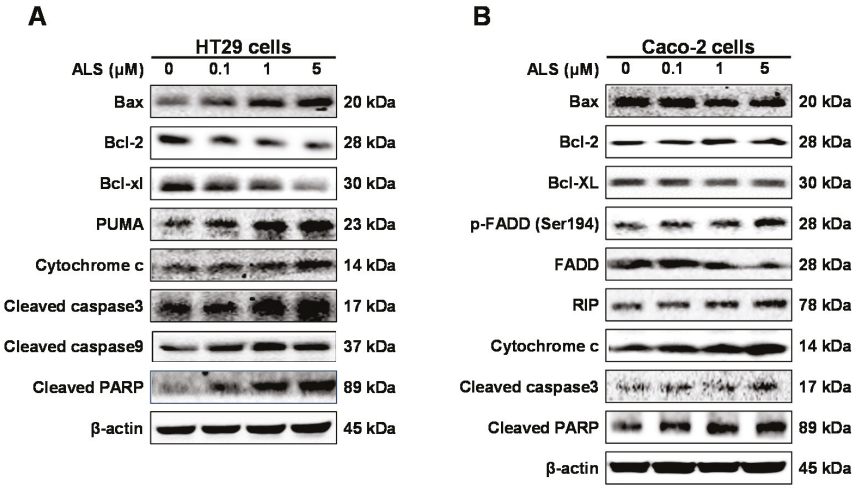

Figure 5. Effect of ALS on the expression level of key proapoptotic and antiapoptotic molecules in HT29 and Caco-2 cells. (**A**) Effect of ALS on the expression level of Bcl-xl, Bax, Bcl-2, PUMA, cytochrome c, cleaved caspase 3, cleaved caspase 9, and cleaved PARP in HT29 cells; (**B**) Effect of ALS on the expression level of Bcl-xl, Bax, Bcl-2, p-FADD (Ser194), FADD, RIP, cytochrome c, cleaved caspase 3, and cleaved PARP in Caco-2 cells.

For Caco-2 cells, we also first evaluated the expression levels of the pro-apoptotic protein Bax and the anti-apoptotic proteins Bcl-2 and Bcl-xl. Caco-2 cells were exposed to ALS at 0.1, 1, and 5 μM for 48 h. Surprisingly, the expression level of Bax was decreased 61% and 62.7% when treated with 1 and 5 μM ALS for 48 h, compared with the control cells, respectively ($p < 0.05$; Figure 5B and Figure S5B). In contrast, the level of Bcl-2 was increased 1.5- and 1.5-fold when treated with 1 and 5 μM ALS for 48 h, respectively, compared to the control cells (Figure 5B and Figure S5B). There was no significant alteration in expression level of Bcl-xl between the control cells and ALS-treated cells (Figure 5B and Figure S5B). These results suggest that mitochondrial pathway is not involved in the ALS-induced apoptosis in Caco-2 cells. Therefore, we next assessed the expression level of key proteins regulating death receptor signaling pathway. There was a 1.5- and 2.5-fold increase in the expression level of RIP when cells were treated with ALS at 1 and 5 μM for 48 h, respectively, compared to the control cells ($p < 0.01$; Figure 5B and Figure S5B). There was a 1.5-, 1.3-, and 1.8-fold increase in the level of p-FADD, although there was no statistical significance, while there was a 15.4%, 34.2%, and 36.9% decrease in the expression level of FADD, when cells were incubated in ALS at 0.1, 1, and 5 μM for 48 h, respectively, compared to the control cells (Figure 5B and Figure S5B). Consequently, the p-FADD/FADD ratio was remarkably increased 2.0- and 3.0-fold when cells were treated with 1 and 5 μM ALS for 48 h, respectively, compared to control cells ($p < 0.01$; Figure 5B and Figure S5B). Furthermore, the expression of downstream regulators was also tested. There was a 2.3- and 3.2-fold increase in the cytosolic level of cytochrome c when cells were treated with ALS at 1 and 5 μM for 48 h, respectively, compared to the control cells ($p < 0.05$; Figure 5B and Figure S5B). There was a 1.9- and 2.2-fold increase in the level of cleaved caspase 3 when treated with ALS at 1 and 5 μM for 48 h, respectively, compared to the control cells ($p < 0.01$; Figure 5B and Figure S5B). There was a 1.9- and 2.1-fold increase in the level of cleaved PARP when treated with ALS at 1 and 5 μM for 48 h, respectively, compared to the control cells ($p < 0.01$; Figure 5B and Figure S5B). Taken together, these results reveal that ALS induces apoptotic death of Caco-2 cells via death receptor signaling

pathway. The differential responses to ALS treatment may be ascribed to the different cell type, in particular, the difference in p53 in these cell lines.

2.7. ALS Induces Autophagy of HT29 and Caco-2 Cells

As there was a clear ALS-induced apoptosis in HT29 and Caco-2 cells, we next investigated the effect of ALS on the autophagy of HT29 and Caco-2 cells by flow cytometric analysis and confocal microscopic examination. As shown in Figure 6A and Figure S6A, treatment of HT29 and Caco-2 cells with ALS for 24 h induced autophagy in a concentration-dependent manner. The percentage of intracellular autophagic signal at the basal level was 6.9% and 9.6% for HT29 and Caco-2 cells, respectively. Incubation of HT29 cells with 1 and 5 μM ALS for 24 h resulted in a 5.3- and 6.1-fold increase in the percentage of autophagic signal, respectively, compared to the control cells ($p < 0.01$; Figure 6A and Figure S6A). For Caco-2 cells, incubation with 1 and 5 μM ALS for 24 h resulted in a 1.7- and 2.0-fold increase in the percentage of autophagic signal, respectively, compared to the control cells ($p < 0.01$; Figure 6A and Figure S6A).

Furthermore, the effect of ALS on intracellular autophagy of HT29 and Caco-2 cells over time-course was evaluated. Both cells were exposed to ALS at 1 μM for 4, 8, 12, 24, 48, and 72 h. The percentage of autophagic signal was increased 3.2-, 5.6-, and 7.0-fold when HT29 cells were treated for 24, 48, and 72 h, respectively, compared to control cells ($p < 0.001$; Figure 6B and Figure S6B). For Caco-2 cells, the percentage of autophagic signal was increased 2.0-, 3.0-, and 2.5-fold when cells were treated for 24, 48, and 72 h, respectively, compared to control cells ($p < 0.001$; Figure 6B and Figure S6B). These results indicate that ALS induces a remarkable autophagy of HT29 and Caco-2 cells in concentration- and time-dependent manners.

Next, we performed the confocal microscopy to determine the autophagy-inducing effect of ALS in HT29 and Caco-2 cells. As shown in Figure 6C and Figure S6C, in comparison to the control cells, there was a 2.2- and 3.1-fold increase in the autophagy level of HT29 cells when treated with ALS at 1 and 5 μM for 24 h, respectively ($p < 0.001$). For Caco-2 cells, treatment with ALS at 1 and 5 μM for 24 h caused a 1.9- and 2.2-fold increase in the autophagy level when compared with the control cells, respectively ($p < 0.001$; Figure 6C and Figure S6C). There was no significant change in the autophagy level when both cell lines were treated with ALS at low concentration (0.1 μM). These results show that ALS treatment induces a significant concentration-dependent increase in autophagy of HT29 and Caco-2 cells.

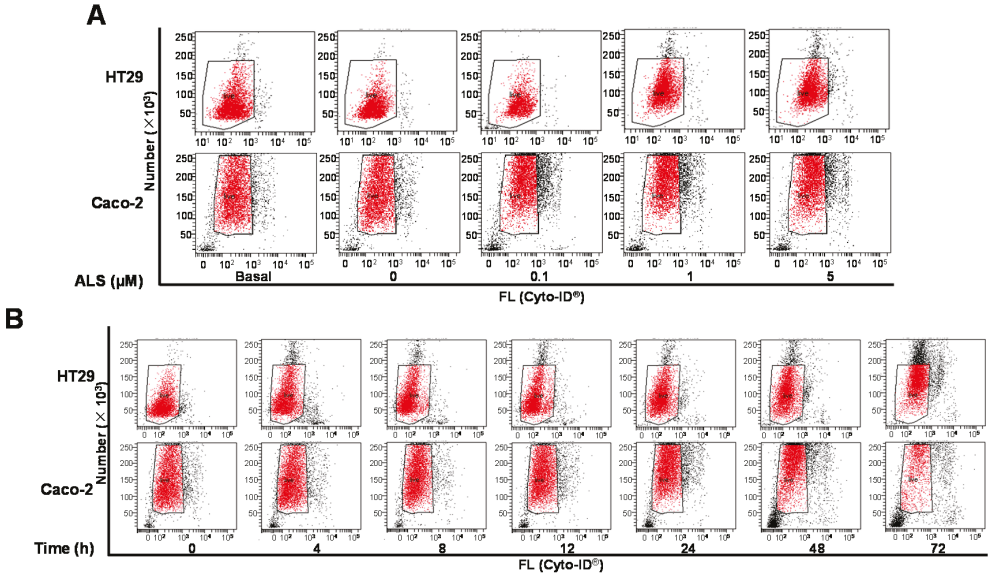

Figure 6. *Cont.*

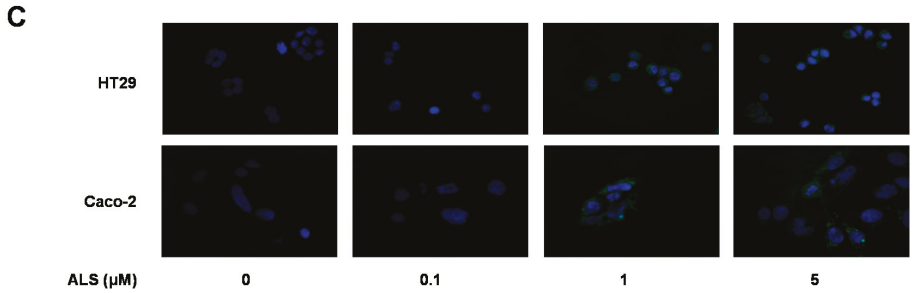

Figure 6. ALS induces autophagic cell death in HT29 and Caco-2 cells. (**A**) Cells were treated with ALS at concentrations of 0.1, 1, and 5 μM for 24 h and cell samples were subject to flow cytometry analysis. Flow cytometric dot plots showing autophagic HT29 and Caco-2 cells stained by Cyto-ID®; (**B**) HT29 and Caco-2 cells were treated with ALS at 1 μM for 4, 8, 12, 24, 48, and 72 h and then subject to flow cytometry analysis. Flow cytometric dot plots showing autophagic HT29 and Caco-2 cells stained by Cyto-ID®; (**C**) HT29 and Caco-2 Cells were treated with ALS at 0.1, 1, and 5 μM for 24 h. Cells were stained with green fluorescent Cyto-ID® and subjected to confocal microscopy to detect autophagy. Confocal microscopic images showing autophagy in HT29 and Caco-2 cells. The box indicates the events that were counted. FL: fluoresence. Maganification: 40×.

2.8. ALS Regulates PI3K/Akt/mTOR Axis, AMPK, and p38 MAPK Signaling Pathways in HT29 and Caco-2 Cells

After determining the autophagy-inducing effect of ALS in HT29 and Caco-2 cells, we further elucidated the latent mechanism for the ALS-induced autophagy. ALS treatment results in remarkable changes in the expression and phosphorylation levels of key functional molecules involved in autophagy signaling pathway. First, we assessed the phosphorylation level of PI3K at Tyr199, AMPK at Thr172, and p38 MAPK at Thr180/Tyr182. These proteins execute critical roles in the regulation of cell proliferation, cell survival, cell migration and cell death as the upstream signaling molecules of the protein kinase B (Akt)/mammalian target of rapamycin (mTOR) pathway [24–26]. Exposure of HT29 cells to ALS for 48 h declined the phosphorylation level of PI3K (Tyr199) and increased the expression level of total PI3K (Figure 7A,B). Consequently, the p-PI3K/PI3K ratio was decreased 4.4%, 29.1%, and 33.7% ($p < 0.001$; Figure 7A,B) when treated with ALS at 0.1, 1, and 5 μM, respectively, compared to control cells. The p-AMPK/AMPK ratio was increased 1.3-, 1.3-, and 1.2-fold when HT29 cells were treated with ALS at 0.1, 1, and 5 μM, respectively, compared to control cells (Figure 7A,B); while the p-p38/p38 ratio was increased 1.6-, 3.1-, and 3.0-fold when HT29 cells were treated with ALS at 0.1, 1, and 5 μM, respectively, compared to control cells ($p < 0.05$ or 0.01; Figure 7A,B).

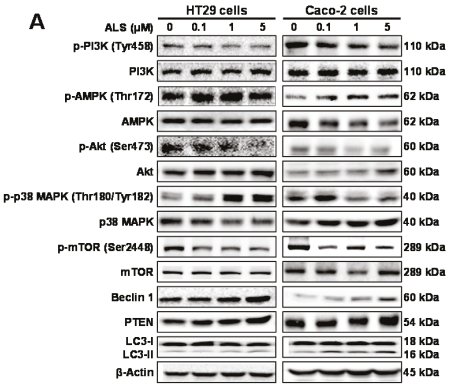

Figure 7. *Cont.*

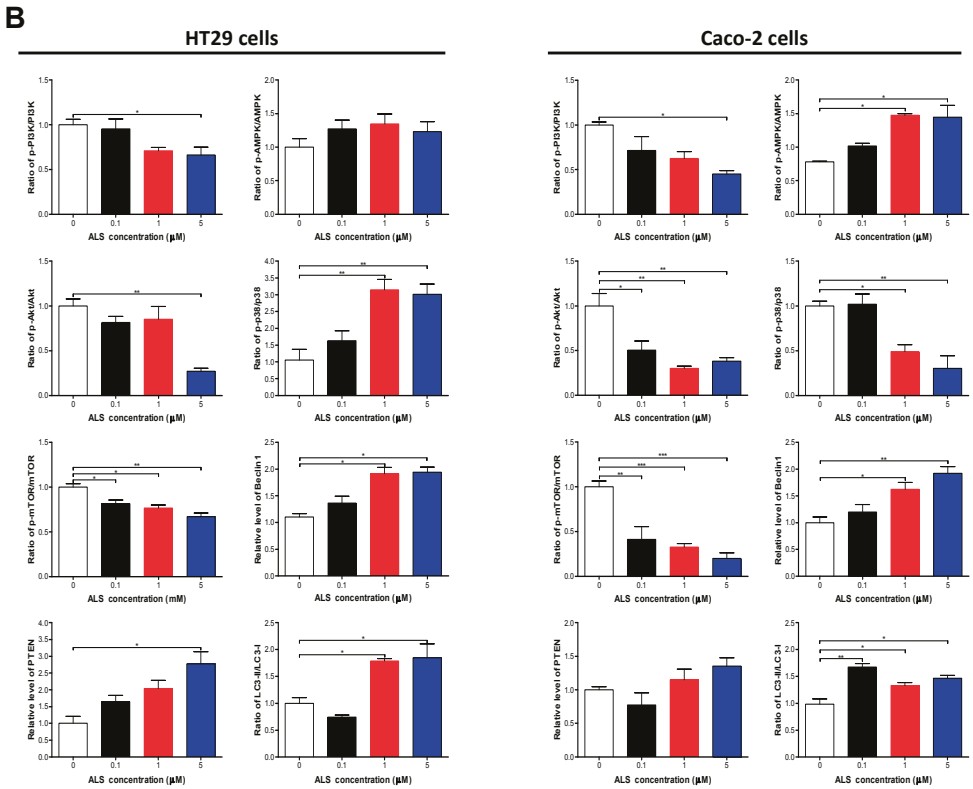

Figure 7. Effect of ALS on the expression or phospharylation levels of key autophagy-regulating molecules in HT29 and Caco-2 cells. Cells were treated with ALS at 0.1, 1, and 5 μM for 48 h. The phosphorylation level of PI3K, AMPK, Akt, p38 MAPK, and mTOR, and the total level of mTOR, beclin 1, PTEN, LC3-I, and LC3-II in HT29 and Caco-2 cells determined by Western blotting assay. (**A**) Representative blots of p-PI3K, PI3K, p-AMPK, AMPK, p-Akt, Akt, p-p38 MAPK, p38 MAPK, p-mTOR, mTOR, beclin 1, LC3-I, and LC3-II in HT29 and Caco-2 cells treated with ALS for 48 h; and (**B**) Bar graphs showing the ratio of p-PI3K/PI3K, p-AMPK/AMPK, p-Akt/Akt, p-p38 MAPK/p38 MAPK, p-mTOR/mTOR, LC3-II/LC3-I, and the expression levels of beclin 1 and PTEN in HT29 and Caco-2 cells treated with ALS for 48 h. β-Actin was used as the internal control. Data are expressed as the mean ± SD of three independent experiments. * $p < 0.05$, ** $p < 0.01$, and *** $p < 0.001$ by one-way ANOVA.

As a downstream effector of PI3K, Akt plays a key role in regulating diverse cellular functions including metabolism, cell proliferation, survival, growth, migration, invasion, and angiogenesis [27]. The mTOR kinase is a downstream target of Akt, which is phosphorylated and activated at Ser473 by mTORC2 and at Thr308 by 3-phosphoinositide-dependent protein kinase-1 [28]. mTOR is regulated by signaling pathway originating from starvation, growth factors, and cellular stressors, and plays a critical role in cell growth, autophagic cell death, and homeostasis [29]. We next evaluated the phosphorylation of Akt at Ser473 and mTOR at Ser2448 after ALS treatment of HT29 cells. There was a concentration-dependent decline in the phosphorylation level of Akt and mTOR with ALS treatment at 0.1, 1, and 5 μM (Figure 7A,B). However, the expression of total Akt and mTOR was not significantly altered after ALS incubation (Figure 7A,B). Thus, in comparison to the control cells, the ratio of p-Akt over Akt was markedly reduced 18.6%, 14.8%, and 72.8% and the ratio of p-mTOR over mTOR was declined 18.4%, 23.3%, and 33.1% when HT29 cells were treated with ALS at 0.1, 1, and 5 μM, respectively ($p < 0.01$; Figure 7A,B). PTEN is a dual-specificity phosphatase and tumor suppressor gene, acting as a negative regulator of Akt/mTOR and MAPK signaling, with a key function of cell death [30]. Therefore, we examined the expression level of PTEN when HT29 cells were treated with ALS for 48 h. Exposure of HT29 cells to ALS at 0.1, 1, and 5 μM resulted in a 1.6-,

2.0-, and 2.8-fold increase in the expression level of PTEN, respectively, compared to the control cells ($p < 0.01$; Figure 7A,B).

Beclin 1 and LC3 are two important markers of vesicle expansion and formation during the autophagy process. Thus, we examined the effect of ALS on expression of beclin 1, LC3-I, and LC3-II in HT29 cells. There was a significant increase in the expression of beclin 1 and ratio of LC3-II over LC3-I when cells were treated with ALS (Figure 7A,B). In comparison with the control cells, the expression level of beclin 1 was increased 1.6- and 1.9-fold with the treatment of ALS at 1 and 5 μM, respectively, and the level of LC3-II was increased after ALS treatment in HT29 cells. The ratio of LC3-II/LC3-I was increased 1.8- and 1.8-fold when cells were treated with ALS at 1 and 5 μM, respectively ($p < 0.01$; Figure 7A,B). These results indicate that inhibition of the PI3K/Akt/mTOR pathway and activation of AMPK and p38MAPK contribute to the autophagy-inducing effect of ALS on HT29 cells.

For Caco-2 cells, incubation with ALS for 24 h led to marked alteration in the phosphorylation level of PI3K, p38 MAPK, and AMPK, but did not affect the total expression level (Figure 7A,B). There was a 37.4% and 54.8% decline in the ratio of p-PI3K over PI3K, a 51.0% and 69.6% decrease in the ratio of p-p38 over p38, and a 1.9- and 1.9-fold increase in the ratio of p-AMPK over AMPK when treated with ALS at 1 and 5 μM, respectively (Figure 7A,B). We further assessed the change in the phosphorylation of Akt at Ser473 and mTOR at Ser2448. In comparison with the control cells, there was a concentration-dependent decrease in the phosphorylation level of Akt and mTOR, while there was no significant alteration in the total expression level of Akt and mTOR when treated with ALS at 0.1, 1, and 5 μM (Figure 7A,B). Consequently, compared to the control cells, there was a 49.6%, 69.9%, and 61.8% decrease in the ratio of p-Akt over Akt ($p < 0.01$; Figure 7A,B), and a 58.7%, 67.5%, and 79.9% reduction in the ratio of p-mTOR over mTOR in Caco-2 cells incubated with ALS at 0.1, 1, and 5 μM, respectively ($p < 0.001$; Figure 7A,B). We also observed the expression level of PTEN after ALS incubation. In comparison with the control cells, there was a 1.2- and 1.4-fold increase in the expression level of PTEN in Caco-2 cells exposed to ALS at 1 and 5 μM, respectively (Figure 7A,B). Finally, we evaluated the expression levels of beclin 1, LC3-I, and LC3-II in Caco-2 cells treated with ALS. ALS caused a prominent increase in the expression levels of beclin 1 and LC3-II, but did not caused alteration in the expression level of LC3-I (Figure 7A,B). In comparison to the control cells, there was a 1.6- and 1.9-fold increase in the expression level of beclin 1 when treated with ALS at 1 and 5 μM, respectively; and there was a 1.7-, 1.4-, and 1.5-fold increase in LC3-II/LC3-I ratio when treated with ALS at 0.1, 1, and 5 μM, respectively ($p < 0.01$; Figure 7A,B). These findings show that inhibition of PI3K/Akt/mTOR pathway, suppression of p38MAPK, and activation of AMPK contribute to the autophagy-inducing effect of ALS on Caco-2 cells.

2.9. There Is a Crosstalk between ALS-Induced Apoptosis and Autophagy in HT29 and Caco-2 Cells

To further dissect the crosstalk between autophagy and apoptosis in HT29 and Caco-2 cells responding to ALS treatment, the flow cytometry was used to simultaneously examine cellular autophagy and apoptosis. First, we assessed the effect of induction or inhibition of autophagy on basal and ALS-induced autophagy in both cell lines. In HT29 cells, incubation with 0.5 μM rapamycin (a mTOR inhibitor and autophagy inducer), 10 μM WM (a PI3K inhibitor and autophagy blocker), 1 μM MK2206 (a selective inhibitor of Akt and autophagy inducer), or 10 μM SB202190 (a selective p38 MAPK inhibitor and autophagy inducer) alone for 24 h led to a 5.4-, 4.3-, 2.0-, or 3.7-fold increase in basal autophagy compared to the control cells, respectively ($p < 0.001$; Figure 8A and Figure S7). Co-incubation with 0.5 μM rapamycin or 10 μM SB202190 increased ALS-induced autophagy 1.9- or 1.9-fold in HT29 cells, respectively ($p < 0.001$; Figure 8A and Figure S7), while co-incubation with 10 μM WM or 1 μM MK2206 only slightly enhanced ALS-induced autophagy. In Caco-2 cells, treatment with 0.5 μM rapamycin, 1 μM MK2206, or 10 μM SB202190 alone for 24 h induced a 2.7-, 6.5-, or 3.4-fold increase in basal autophagy compared to the control cells, respectively ($p < 0.001$; Figure 8A and Figure S7), while 10 μM WM diminished the basal autophagy. Pre-incubation with

0.5 μM rapamycin, 1 μM MK2206, or 10 μM SB202190 increased ALS-induced autophagy 1.5-, 3.1-, or 1.9-fold in Caco-2 cells ($p < 0.001$; Figure 8A and Figure S7). Of note, pre-treatment with 10 μM WM significantly decreased ALS-induced autophagy (Figure 8A and Figure S7).

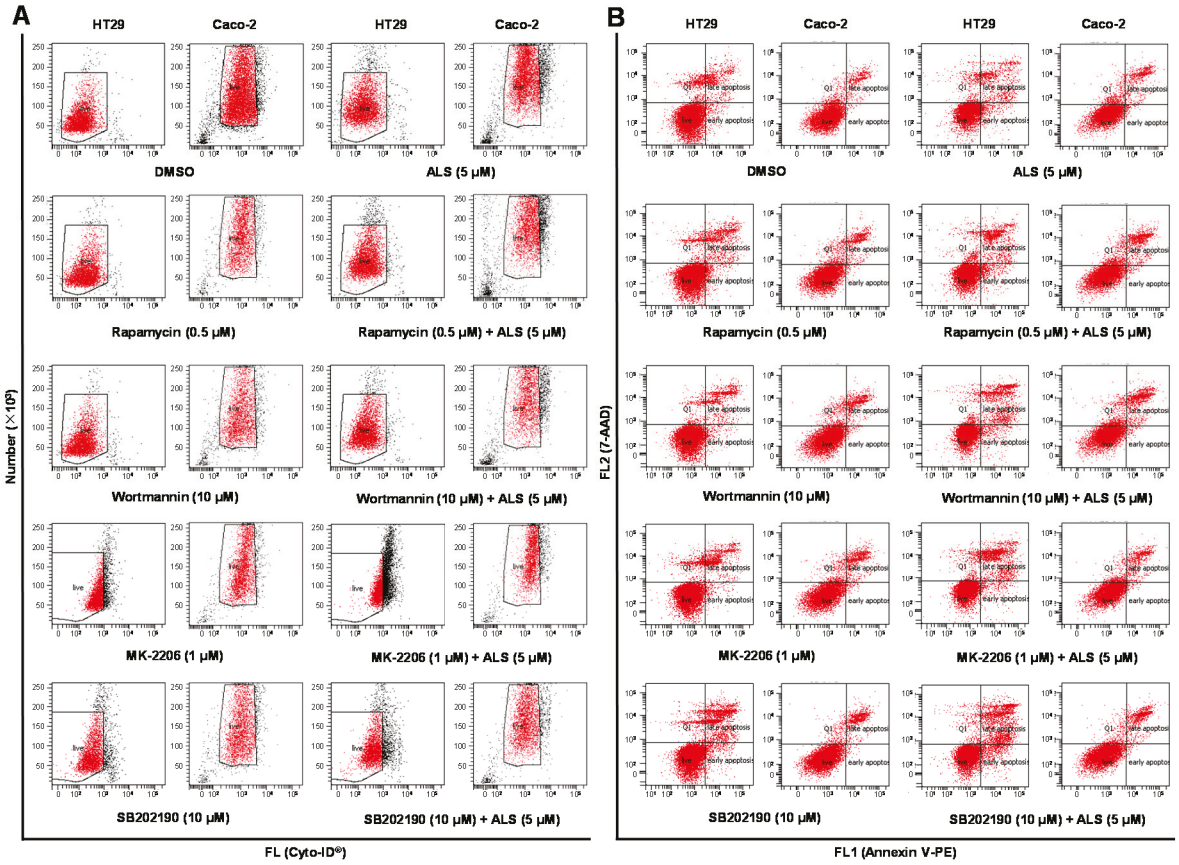

Figure 8. Effect of various inducers and inhibitors on the apoptosis and autophagy induced by ALS in HT29 and Caco-2 cells. The cells were pretreated with each of the compounds for 1 h before ALS was added and incubated for a further 24 h. Cells were double stained with Annexin V:PE (phycoerythrin) and 7-Aminoactinomycin D (7-AAD) to detect cellular apoptosis, after the cells were treated with ALS for 24 h. The autophagy was detected using the Cyto-ID® green fluorescent dye to stain autophagy-associated vacuoles. (**A**) Flow cytometric dot plots showing the effects of a series of compounds on basal and ALS-induced apoptosis in HT29 and Caco-2 cells; (**B**) Flow cytometric dot plots showing the effects of the compounds on basal and ALS-induced autophagy in HT29 and Caco-2 cells. The box indicates the events that were counted. DMSO: dimethyl sulfoxide.

Next, we evaluated the effect of induction or inhibition of autophagy on basal and ALS-induced apoptosis in HT29 and Caco-2 cells. Incubation of HT29 cells with 10 μM SB202190 alone for 24 h remarkably induced apoptosis (9.6% *vs.* 19.4%, $p < 0.05$ Figure 8B and Figure S7), while incubation of the cells with 0.5 μM rapamycin, 10 μM WM, or 1 μM MK2206 for 24 h had no significant effect on the basal apoptosis of HT29 cells (Figure 8B and Figure S7). In addition, co-incubation of HT29 cells with 10 μM SB202190 increased ALS-induced apoptosis (14.4% *vs.* 23.7%, $p < 0.001$; Figure 8B and Figure S7), whereas co-incubation with 0.5 μM rapamycin, 10 μM WM, or 1 μM MK2206 only slightly altered ALS-induced apoptosis. In Caco-2 cells, exposure to 0.5 μM rapamycin, 10 μM WM, 10 μM SB202190 or 1 μM MK2206 alone only slightly increased the basal apoptosis (Figure 8B and Figure S7). Pre-incubation with 10 μM WM enhanced ALS-induced apoptosis (9.7% *vs.* 14.0%, $p < 0.001$; Figure 8B and Figure S7), whereas co-incubation with 0.5 μM rapamycin, 1 μM MK2206, or 10 μM SB202190 only slightly altered ALS-induced apoptosis (Figure 8B and Figure S7). Taken together,

these data shows that regulation of p38 MAPK by SB202190 may alter ALS-induced autophagy and apoptosis in HT29 cells and modulation of PI3K by WM may alter ALS-induced autophagy and apoptosis in Caco-2 cells with differential effects depending on the cell type. The autophagy inducer SB202190 enhances the ALS-induced apoptosis in both HT29 and Caco-2 cells, whereas the autophagy blocker WM increases ALS-induced autophagy in HT29 cells but decreases it in Caco-2 cells.

2.10. ALS Suppresses EMT in HT29 and Caco-2 Cells

Epithelial-to-mesenchymal transition (EMT) is a critical event in which epithelial cells trans-differentiate into fibroblastic migratory cells through losing intracellular adhesion and cellular polarity and obtaining mesenchymal properties and increased motility. It has been suggested that EMT contributes to the cancer cells spreading and migrating to distant organs to form metastases [31,32]. E-cadherin is a hallmarker of the epithelial phenotype while N-cadherin is considered a key mesenchymal phenotype. Loss of E-cadherin and increasing N-cadherin expression facilitates the occurring of EMT and metastasis [33]. We speculated that ALS can inhibit EMT phenotype in HT29 and Caco-2 cells. So we examined the expression of EMT-associated regulators, including E-cadherin, N-cadherin, slug, TCF-8, and ZO-1. First, ALS incubation resulted in remarkable effect on the expression level of E-cadherin and N-cadherin (Figure 9A,B). Treatment of HT29 cells with ALS at 1 and 5 μM led to a 2.3- and 2.6-fold increase in the expression level of E-cadherin, respectively, compared to the control cells ($p < 0.01$; Figure 9A,B), but treatment of HT29 cells with ALS at 0.1, 1, and 5 μM resulted in a 3.4%, 5.3%, and 27.4% decrease in the expression level of N-cadherin, respectively (Figure 9A,B). Although there was no significant difference in the expression of N-cadherin, an increased ratio of E-cadherin over N-cadherin was observed. The ratio of E-cadherin/N-cadherin was increased 1.4-, 2.5-, and 3.7-fold when HT29 cells were exposed to ALS at 0.1, 1, and 5 μM for 48 h, respectively ($p < 0.01$; Figure 9A,B). In Caco-2 cells, in comparison to the control cells, the expression level of E-cadherin was increased by 2.7- and 2.7-fold when cells were treated with ALS at 1 and 5 μM, respectively, ($p < 0.01$; Figure 9A,B). Meanwhile, the expression level of N-cadherin was decreased by 46.4%, 72.8%, and 69.1% when cells were incubated with ALS at 0.1, 1, and 5 μM, respectively, ($p < 0.01$; Figure 9A,B). The ratio of E-cadherin/N-cadherin was increased 3.2-, 13.0-, and 9.8-fold when Caco-2 cells were incubated with ALS at 0.1, 1, and 5 μM for 48 h, respectively, ($p < 0.01$; Figure 9A,B).

Slug is a zinc finger transcriptional factor, together with TCF8/ZEB1 acting as suppressors of E-cadherin in EMT [34]. We further examined the effect of ALS incubation of HT29 and Caco-2 cells on the expression of slug and TCF-8/ZEB1. As shown in Figure 9A,B, there was a significant reduction in the expression levels of slug and TCF-8/ZEB1. In comparison with control cells, exposure of HT29 cells to ALS at 1 and 5 μM led to a 55.3% and 44.1% decline in the expression level of slug, respectively ($p < 0.05$; Figure 9A,B). Exposure of HT29 cells to ALS at 1 and 5 μM resulted in a 44.5% and 53.4% reduction in the expression level of TCF-8/ZEB1, respectively ($p < 0.001$; Figure 9A,B). Similarly, in Caco-2 cells, treatment of cells to ALS led to a concentration-dependent reduction in the expression level of slug and TCF-8/ZEB1 ($p < 0.05$ or 0.01; Figure 9A,B).

In the end, we assessed the effect of ALS on expression of ZO-1 in HT29 and Caco-2 cells. ZO-1 is a member of Zonula occludens proteins which are involved in the regulation of cytoskeletal organization, signal transduction, transcriptional modulation and cell polarity maintenance. ZO-1 are required for tight junction formation and function. It has been suggested that the cytoplasmic/nuclear relocalization of β-catenin and ZO-1 from the adhesions and tight junctions are common processes of the epithelial-mesenchymal transition associated with tumor invasion [35]. As shown in Figure 9, ALS significantly increased the expression level of ZO-1 in both cell lines. Compared to the control cells, there was a 2.1- and 3.1-fold increase in the expression level of ZO-1 when HT29 cells were treated with ALS at 1 and 5 μM, respectively ($p < 0.01$; Figure 9A,B). For Caco-2 cells, there was a 1.2-, 1.4-, and 4.5-fold increase in the expression level of ZO-1 when treated with ALS at 0.1, 1, and 5 μM respectively, compared to the control cells ($p < 0.01$; Figure 9A,B). In aggregate,

all these results demonstrate that ALS has a strongly inhibitory effect on EMT by upregulating the expression level of E-cadherin and ZO-1, and down-regulating the expression level of N-cadherin, slug, and TCF-8 in HT29 and Caco-2 cells.

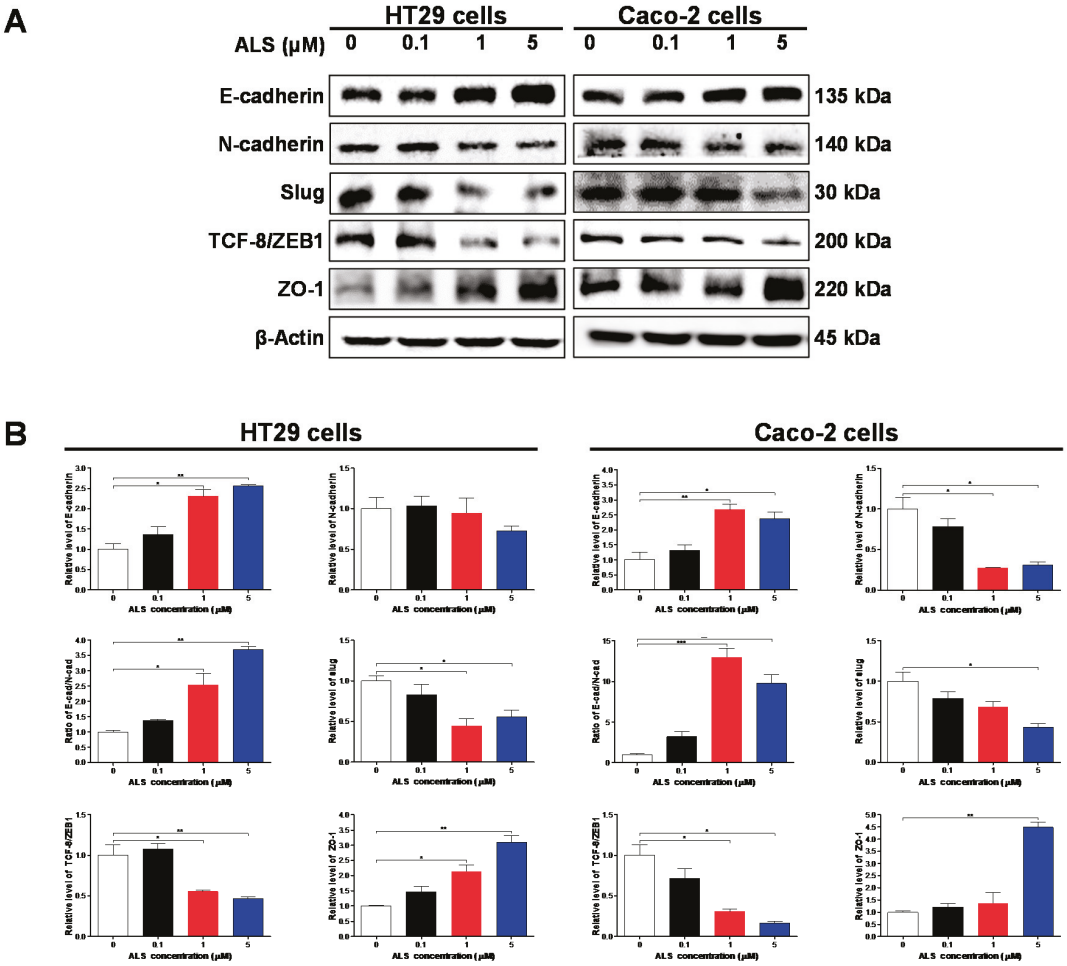

Figure 9. Effect of ALS on expression levels of epithelial to mesenchymal transition (EMT) associated markers in HT29 and Caco-2 cells. Cells were treated with ALS at concentrations of 0.1, 1, and 5 μM for 48 h and then protein samples were subject to Western blotting assay. (**A**) Representative blots showing the expression level of E-cadherin, N-cadherin, slug, TCF-8/ZEB1, and ZO-1 in HT29 and Caco-2 cells determined by Western blotting assay; (**B**) Bar graphs showing the expression level of E-cadherin, N-cadherin, slug, TCF-8/ZEB1, and ZO-1, and the ratio of E-cadherin over N-cadherin in HT29 and Caco-2 cells. β-Actin was used as the internal control. Data represent as the mean ± SD of three independent experiments. * $p < 0.05$, ** $p < 0.01$, and *** $p < 0.001$ by one-way ANOVA.

3. Discussion

Due to the high mortality and morbidity resulted from CRC worldwide, CRC places a substantial heavy burden on individual and society [36]. It requires novel therapeutic agent with more therapeutic efficacy and less severe side effects. In particular, patients with advanced stages of CRC often suffer from the recurrence, metastasis, and complications, and frequently display poor therapeutic outcome, despite the application of various therapeutic strategies, including potentially curable surgery, chemotherapy, selective radiotherapy and other forms of treatment. Recently, compelling evidence indicates that AURKA can act as a novel and promising antineoplastic target; its selective inhibitor, ALS, is a small molecule which has demonstrated the potent anticancer

effect in the treatment of various types of cancer in preclinical and clinical studies [15–17,19–22,37]. In the present study, a potent anti-proliferative effect of ALS was observed in HT29 and Caco-2 cells. We have found that ALS exerts a remarkable inducing effect on cell cycle arrest in G_2/M phase and markedly promotes apoptosis and autophagy in concentration- and time-dependent manners in both cell lines with the involvement of multiple signaling pathways, including mitochondrial pathway, death receptor signaling pathway, PI3K/Akt/mTOR, p38 MAPK, and AMPK signaling pathways. Moreover, the inhibitory effect of ALS on the EMT may also contribute to its antitumor potential.

The cell cycle regulatory proteins, which have been found involved in proliferation of tumor cells, including the cyclins, the cyclin dependent kinases (CDKs), their downstream substrates, the CDK inhibitors (CKIs), and the tumor suppressor proteins (e.g., p53 and Rb). Activated CDK1 (CDC2) bound to cyclin B1 promotes entry into M-phase in cell cycle. So it is pivotal to maintain the activity of the cyclin B1-CDC2 (CDK1) complex in promoting G_2/M transition process. There are many upstream regulators modifying the activity of the cyclin B1-CDC2 (CDK1) complex. p53 is a critical tumor suppressor protein and a positive regulator of cell cycle arrest. Normally, the G_2/M DNA damage or chromosomal instability promote the phosphorylation of p53 and accelerates its dissociation from MDM2 and MDM4. Consequently, the transcriptional ability of p53 is activated. The p53 downstream-regulated genes including 14-3-3, p21, GADD45, and WIP1 ultimately serve to inactivate the Cyclin B1-CDC2 complex and suppress the entry into G_2/M transition. AURKA is localized at the mitotic spindle and centrosome, where it interacts with many functional proteins/substrates, including PP1, p53, Cdh-1, TPX-2, RasGAP, and Ajuba. It was reported that in the absence of hyperactivation of AURAK, the crosstalk of AURKA with p53 caused tumorigenesis transformation of cells by counteracting the p53 mediated tumor suppression [38]. In our work, we detected a potent effect of ALS on G_2/M phase cell cycle arrest in HT29 and Caco-2 cells, and we found that the active form of p-AURKA at Thr288 was significantly suppressed by ALS. There was an increase in expression level of p53 and p21 and a decrease in expression level of cyclinB1 and CDC2 which were observed as well. Collectively, these results indicate that ALS-induced G_2/M cell cycle arrest may be attributed to its inhibitory effect on the interaction of AURKA and p53, however, this explanation needs to be further verified for CRC treatment.

On the other hand, due to the lack of p53 expression in Caco-2 cells, we, therefore, examined the upstream molecules regulating the cyclin B1-CDC2 (CDK1) complex. PLK1 could be activated by the concerted function of AURKA and the cofactor Bora [39]. CDC25 that can be activated by PLK1 and inactivated by Chk kinases through phosphorylation, is a positive regulator of CDC2 by removal of phosphates at Thr14 and Tyr15 [40–42]. In addition, PLK1 can phosphorylate cyclin B1 at Ser133 resulting in a rapid nuclear import of cyclin B1, which promotes the mitosis entry [43]. In the present study, we found a significant increase in the level of p-CDC25C (Ser216), total cyclinB1, and p-CDC2 (Tyr 15), but a decline in the level of PLK1, p-cyclinB1 (Ser133), suggesting that the PLK1-CDC25C-cyclinB1 and CDC2 complex axis is involved in ALS-induced G_2/M cell cycle arrest in Caco-2 cells. Also, we also found that ALS induced cell cycle arrest in G_2/M phase in gastric cancer cells [19], pancreatic cancer cells [21], osteosarcoma cells [22], breast cancer cells [44], and ovarian cancer cells [20].

Apoptosis is a distinct genetic and biochemical pathway of cell death necessary for cell growth, development and maintenance of homeostasis in metazoans. There are two specific pathways activating cell apoptosis, including intrinsic and extrinsic death pathway [45,46]. In this study, cytochrome c was released from mitochondria after ALS treatment, which might be caused by the increased expression level of Bax and decreased expression level of Bcl-2 and Bcl-xl. Subsequently, caspase 9 was activated with the elevated level of cleaved caspase 9, which in turn cleaved caspase 3 and PARP and ultimately induced apoptosis. The expression level of PUMA, which acted as one of pro-apoptotic members of Bcl-2 family, was increased in a concentration-dependent manner. These data indicate that ALS induces mitochondria-dependent apoptosis of HT29 cells. For Caco-2 cells, a decrease in the expression level of Bax and increased expression level of Bcl-2 were observed

after ALS treatment, which suggests that mitochondrial pathway might be not involved in the ALS-induced apoptosis. Then, we found a significant increase in the expression level of RIP and the p-FADD/FADD ratio, which might initiate the death receptor signaling pathway. Consequently, caspase cascades was activated, including activated caspase-8 and cleaved caspase-3. Therefore, ALS induces apoptosis of Caco-2 cells via death receptor signaling pathway. Additionally, in comparison to previous studies on the apoptosis inducing effect of ALS, it showed that ALS induced mitochondria-dependent apoptosis cell death in gastric cancer cells [19], pancreatic cancer cells [21], osteosarcoma cells [22], breast cancer cells [44], and ovarian cancer cells [20], showing the most potent cancer cell killing effect in pancreatic cancer cell lines PANC-1 and BxPC-3 [21].

Autophagy is a cellular process of catabolic degradation in which damaged, dysfunctional, or superfluous organelles and proteins are sequestered, engulfed, and recycled to maintain cellular metabolism, viability and homeostasis [25]. Autophagy is generally induced by the deprivation of nutrient or stress. The mTOR kinase, which is activated by signaling pathway originating from growth factors and nutrient availability but inhibited in response to starvation, plays a critical role in regulating autophagy progression. Suppression of mTOR is required for induction of autophagy by limiting the inhibitory effect on the ULK1 kinase complex [47]. There are diverse signaling pathways implicated in the regulation of mTOR signaling, including positive regulation of mTOR (PI3K/Akt and p38 MAPK signaling) suppressing autophagy and negative regulation of mTOR (AMPK and p53 signaling) promoting autophagy [48–50]. The role of autophagy in tumorigenesis is controversial. Under certain circumstances, autophagy suppresses tumorigenesis by increasing programmed cell death [51]. However, in other cases, autophagy provides cancer cells with a rescue mechanism to sustain cell viability [52]. The present study showed a remarkable autophagy-inducing effect of ALS on HT29 and Caco-2 cells. The underlying mechanism of this autophagy-inducing effect may be ascribed to the inhibition of PI3K/Akt/mTOR pathway and activation of AMPK in both cell lines. Interestingly, there is a differential alteration in the modification of p38 MAPK signaling pathway. This phenomenon may be associated with the existence of four isoforms of p38 MAPK (p38α, p38β, p38γ, and p38δ), which differ in their tissue distribution profile, upstream regulators and downstream targets in a cell type- and stimulus-dependent manner in the mammals [49]. In addition, HT29 cells do not have mutations in the *p53* gene, while Caco-2 cells have a mutated *p53* gene without *p53* expression. These different characteristics may also contribute to the differential alteration in the regulation of p38 MAPK signaling pathway. On the other hand, the previous studies showed that ALS inhibited PI3K/Akt/mTOR, p38 MAPK, or Erk1/2 signaling pathways while activating AMPK signaling pathway, contributing to the pro-autophagic effects of ALS in gastric cancer cells [19], pancreatic cancer cells [21], osteosarcoma cells [22], breast cancer cells [44], and ovarian cancer cells [19–21].

Furthermore, autophagy and apoptosis are highly conserved and tightly regulated processes that play essential roles in development, tissue homeostasis and disease [53]. Generally, the two biological processes involved in similar regulatory pathways and even share initiator and effector molecules, which indicates a perplexing crosstalk. Accumulating evidence suggests that autophagy and apoptosis can cooperate in a balanced interplay to allow cells to decide which route to take, thus influencing differentially the fate of the cell. Our study showed a crosstalk between apoptosis and autophagy by using rapamycin (a mTOR inhibitor and autophagy inducer), WM (a PI3K inhibitor and autophagy blocker), MK2206 (a selective inhibitor of Akt and autophagy inducer), and SB202190 (a selective p38 MAPK inhibitor and autophagy inducer). Similar regulatory effect of the autophagy inducer SB202190 on the ALS-induced apoptosis were observed, whereas differential influence of other chemical modulators on apoptosis and autophagy were present in both HT29 and Caco-2 cells. It can be speculated that several important molecules or pathways coordinated and mediated the complex interplay between autophagy and apoptosis, including TOR kinase pathway, p53, beclin 1, and Akt. Herein, ALS can induce apoptosis and autophagy in a coordinated manner in HT29 and Caco-2 cells.

Additionally, EMT is a cellular process in epithelial cells changing their adhesive repertoire, polarized arrange and cytoskeletal organization, and acquiring mesenchymal characteristics and migratory and invasive properties [54]. When it comes to cancer cells, EMT represents the conversion of fully differentiated epithelial cells into poorly differentiated and invasive mesenchymal cells [55]. EMT involves numerous distinct genetic and epigenetic alterations, including the decline in expression of epithelial markers, such as E-cadherin, ZO-1, claudins, occludins, β-catenin, and cytokeratins, and the elevation in expression of mesenchymal markers, such as N-cadherin, vimentin, TCF-8/ZEB-1, and slug [56]. The present study showed an increase in the expression level of E-cadherin and a decrease in the expression level of N-cadherin in HT29 and Caco-2 cells, with an elevated ratio of E-cadherin over N-cadherin, which demonstrate that the "cadherin switch" was closed and EMT was suppressed. We also found a significant alteration in the expression of ZO-1, TCF-8/ZEB-1, and slug. The down-regulation of epithelial cell-cell adhesion molecule E-cadherin and the up-regulation of mesenchymal cell-cell adhesion molecule N-cadherin expression, which is called the "cadherin switch", is a major hallmark of EMT in cancer cells [57–59]. Taken together, the findings suggest that inhibitory effect on EMT contributing to the beneficial effects of ALS in HT29 and Caco-2 cells.

In conclusion, in the present study, we have explored the anticancer effect of ALS and the potential molecular mechanisms for its cancer cell killing effect *in vitro*. The mechanism of actions of ALS includes the inhibition of cell proliferation, cell cycle arrest, activation of the mitochondria-dependent and death receptor-dependent apoptosis, and induction of autophagy in human HT29 and Caco-2 cells. Suppression of PI3K/Akt/mTOR and activation of AMPK signaling pathways are involved in the autophagy-inducing effect of ALS in HT29 and Caco-2 cells. In addition, the inhibitory effect on EMT contributes to the anticancer activity of ALS (Figure 10). In aggregate, ALS may represent a new targeted therapeutic agent that can kill CRC cells. However, more studies are warranted to fully delineate the underlying anticancer mechanism and the interaction of other potential targets of ALS in the treatment of colorectal cancer.

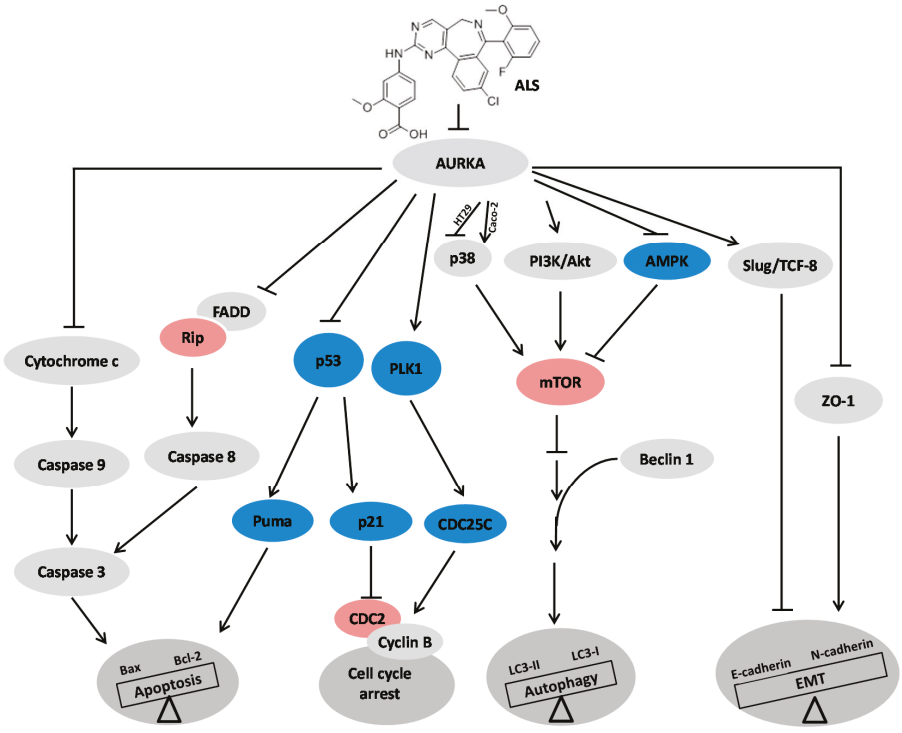

Figure 10. Schematic mechanism underlies the cancer cell killing effect of ALS in HT29 and Caco-2 cells.

4. Materials and Methods

4.1. Chemicals and Reagents

ALS was bought from Selleckchem Inc. (Houston, TX, USA). DMSO, $^{13}C_6$-L-lysine, L-lysine, $^{13}C_6$,$^{15}N_4$-L-arginine, L-arginine, fetal bovine serum (FBS), dialyzed FBS, ammonium persulfate, propidium iodide (PI), ribonuclease (RNase A), protease and phosphatase inhibitor cocktails, MTT, bovine serum albumin, ethylenediaminetetraacetic acid (EDTA), and Dulbecco's phosphate buffered saline (PBS) were sourced from Sigma-Aldrich (St Louis, MO, USA). FASP™ protein digestion kit was obtained from Protein Discovery Inc. (Knoxville, TN, USA). 8-well chamber slide was purchased from Lab-Tek® Inc. (Hatfield, PA, USA). Dulbecco's Modified Eagle's Medium (DMEM) were sourced from Corning Cellgro Inc. (Herndon, VA, USA). 4′,6-Diamidino-2-phenylindole (DAPI), 5-(and 6)-chloromethyl-2′,7′-dichlorodihydrofluorescein diacetate (CM-H_2DCFDA), wortmannin (WM; a selective inhibitor of PI3K and a blocker of autophagosome formation), MK2206 (a selective inhibitor of Akt), and SB202190 (4-(4-fluorophenyl)-2-(4-hydroxyphenyl)-5-(4-pyridyl)-^1H-imidazole; a selective inhibitor of p38 MAPK used as an autophagy inducer) were obtained from InvivoGen Inc. (San Diego, CA, USA). Pierce™ bicinchoninic acid (BCA) protein assay kit, skim milk, radioimmunoprecipitation assay (RIPA) buffer, and Western blotting substrate were bought from Thermo Fisher Scientific Inc. (Waltham, MA, USA). The annexin V:PE (phycoerythrin) apoptosis detection kit was obtained from BD Biosciences Inc. (San Jose, CA, USA). Cyto-ID® Autophagy detection kit was bought from Enzo Life Sciences Inc. (Farmingdale, NY, USA). Primary antibodies against human CDC2, phospho(p)-CDC2 (Tyr15), cyclin B1, p-cyclin B1 (Ser133), p-CDC25C (Ser216), p53, p21 Waf1/Cip1, Bax, Bcl-2, Bcl-xl, PUMA, cytochrome c, cleaved caspase 9, cleaved caspase 3, cleaved PARP, p-FADD (Ser194), FADD, RIP, p-PI3K (Tyr458), PI3K, p-p38 MAPK (Thr180/Tyr182), p38 MAPK, p-Akt (Ser473), Akt, p-mTOR (Ser2448), mTOR, beclin 1, and LC3-I/II were all purchased from Cell Signaling Technology Inc. (Beverly, MA, USA). The antibody against human β-actin was purchased from Santa Cruz Biotechnology Inc. (Dallas, TX, USA). The polyvinylidene difluoride (PVDF) membrane was bought from EMD Millipore Inc. (Billerica, MA, USA).

4.2. Cell Lines and Cell Culture

The HT29 and Caco-2 cells are two well-recognized CRC cell lines and were obtained from American Type Culture Collection (Manassas, VA, USA). These cells were maintained in DMEM supplemented with 10% heat-inactivated FBS and 1% penicillin/streptomycin in a 5% CO_2/95% air humidified incubator at 37 °C. HT29 cells do not have mutations in the *p53* gene, while Caco-2 cells have a mutated *p53* gene without *p53* expression. ALS was dissolved in DMSO at a stock concentration of 100 mM and stored at −20 °C. The drug was freshly diluted with the final concentration of DMSO at 0.05% (volume per volume (v/v)). The control cells received 0.05% DMSO only.

For proteomic analysis, HT29 and Caco-2 cells were cultured in DMEM for SILAC (Sigma-Aldrich) with (heavy) or without (light) stable isotope labeled amino acids ($^{13}C_6$-L-lysine and $^{13}C_6$,$^{15}N_4$-L-arginine) and 10% dialyzed FBS. Cells were cultured in SILAC medium for six cell doubling times to achieve a high level (>98%) of labeled amino acid incorporation. Then, the cells were grown in "light" media were treated with 0.5% DMSO for 48 h to function as the negative control; cells grown in "heavy" media were treated with predetermined ALS for 48 h. All the experiments were performed three times independently. After ALS treatment, cell samples were harvested, lysated with hot lysis buffer (100 mM Tris base, 4% sodium dodecyl sulfate (SDS) and 100 mM dithiothreitol), and denatured for 5 min at 95 °C. Then, the samples were stored at −80 °C till further analysis.

4.3. Proteomic Response to ALS Treatment Analyzed by Stable Isotope Labeling by Amino Acids in Cell Culture (SILAC)-Based Approach

4.3.1. Digestion and Desalting SILAC Protein Samples

Prior to the quantitative proteomic analysis, the protein samples were subject to digestion and desalting which were performed using SILAC-based approach. Briefly, the thermal denatured cell lysate was sonicated, the supernatant was collected, and the protein concentration was determined. Subsequently, equal amount of heavy and light protein samples were combined to reach a total volume of 30–60 μL containing 300–600 μg protein. The combined samples were digested using FASP™ protein digestion kit according to the manufacturer's instruction. After the digestion, the resultant sample was acidified to pH of 3 and desalted using a C_{18} solid-phase extraction column to desalt. The desalted samples were concentrated and resuspended in 0.1% formic acid prior to liquid chromatography-tandem mass spectrometry (LC-MS/MS) analysis.

4.3.2. LC-MS/MS and Statistical Analysis

The concentrated samples (5 μL) were subject to the hybrid linear ion trap-Orbitrap (LTQ Orbitrap XL, Thermo Scientific Inc., Hudson, NH, USA). Peptide SILAC ratio was calculated using MaxQuant version 1.2.0.13 (Max Planck Institute of Biochemistry, Munich, Germany). The SILAC ratio was determined by averaging all peptide SILAC ratios from peptides identified of the same protein.

4.3.3. Pathway and Network Analysis

The protein IDs were identified using Scaffold 4.3.2 from Proteome Software Inc. (Portland, OR, USA) and the pathway and network were analyzed using Ingenuity Pathway Analysis (IPA, www.ingenuity.com) from QIAGEN (Redwood City, CA, USA) as previously described [60].

4.4. Cell Viability Assay

The MTT assay was used to determine the effect of ALS on the viability of HT29 and Caco-2 cells. HT29 and Caco-2 cells were seeded into 96-well plates at a density of 6000 (Caco-2) or 8000 (HT29) cells/well. After cells were incubated for 24 h at a volume of 100 μL complete culture medium, the HT29 and Caco-2 cells were treated with ALS at concentrations ranging from 0.1 to 100 μM for 24 or 48 h. Following the ALS treatment, 10 μL of MTT stock solution (5 mg/mL) was added to each well and cultured for another 4 h. Then the solution was carefully aspirated and 100 μL of DMSO was added into each well. The plate was shaken for 10 min for crystal dissolution. Then the cell viability was examined by reduction of MTT. The absorbance was measured and the IC_{50} values were determined as previously described [61].

4.5. Cell Cycle Distribution Analysis

The effect of ALS on cell cycle distribution was tested using PI as a DNA stain to determine DNA content by flow cytometry as previously described [21]. In brief, HT29 and Caco-2 cells were seeded into 60 mm Petri dishes for attaching overnight. When the cells reached ~75% confluence and were then treated with ALS at concentrations of 0.1, 1, and 5 μM for 24 h. In separate experiments, HT29 and Caco-2 cells were treated with 1.0 μM ALS for 4, 8, 12, 24, 48, or 72 h. The collected cells were fixed and stained, then subject to flow cytometry. A total of 10,000 events were analyzed.

4.6. Quantification of Cellular Apoptosis

Following the examination of the effect of ALS on cell growth, the effect of ALS on cell apoptosis was determined and the percentage of apoptotic cells was quantified using the annexin V:PE apoptosis detection kit after the cells were treated with ALS at different concentrations (0.1, 1,

and 5 μM) for 24 h. In separate experiments, cells were treated with 1 μM ALS for 4, 8, 12, 24, 48, or 72 h as previously described [61].

4.7. Quantification of Cellular Autophagy

To determine the effect of ALS on autophagy in HT29 and Caco-2 cells, cellular autophagy was examined using flow cytometry. Briefly, HT29 and Caco-2 cells were seeded into 60 mm Petri dishes for incubation overnight. The cells were treated with ALS at 0.1, 1, and 5 μM for 24 h when they reached ~75% confluence. Also, in separate experiments, HT29 and Caco-2 cells were treated with 1.0 μM ALS for 4, 8, 12, 24, 48, or 72 h as previously described [61].

4.8. Simultaneous Determination of Apoptosis and Autophagy Using Flow Cytometry

We further examined the two modes of programmed cell death simultaneously in order to investigate the potential crosstalk between ALS-induced apoptosis and autophagy. HT29 and Caco-2 cells were seeded into 60 mm Petri dishes. After incubation overnight, cells were pretreated with 10 μM WM (a PI3K inhibitor and autophagy blocker), 1 μM rapamycin (an mTOR inhibitor and autophagy inducer), 10 μM SB202190 (a selective inhibitor of p38 MAPK) or 1 μM MK2206 (a selective inhibitor of Akt) for 1 h, then co-treated with 5 μM ALS for further 24 h. At the end of treatment, the cells were trypsinized and centrifuged at 250× *g* for 5 min. The cells were divided into two samples of equal volume for detection of apoptosis and autophagy respectively. The subsequent steps follow the procedure mentioned above.

4.9. Confocal Fluorescence Microscopy

To further examine the cellular autophagy level, confocal microscopic examination was performed using a Cyto-ID® autophagy detection kit as previously described [61]. Briefly, HT29 and Caco-2 cells were seeded into an 8-well chamber slide at 30% confluence. The cells were treated with ALS at 0.1, 1, and 5 μM for 24 h. Next, cells were incubated with 100 μL of dual detection reagents and examined using a TCS SP2 laser scanning confocal microscope (Leica, Wetzlar, Germany) at wavelengths of 405/488 nm.

4.10. Western Blotting Analysis

Western blotting assays were used to examine the expression level of key regulators involved in cell cycle, apoptosis, autophagy, and EMT processes as previously described [61]. Briefly, HT29 and Caco-2 cells were collected and lysed after 48-h treatment with ALS at 0.1, 1, and 5 μM. The supernatant was collected and the protein concentrations were measured using a Pierce™ BCA protein assay kit. Thirty microgram proteins were subjected to Western blotting assay. Visualization was performed using an enhanced chemiluminescence kit (Thermal Scientific, Waltham, MA, USA) and the blots were analyzed using Image Lab 3.0 (BioRad, Hercules, CA, USA). Protein expression level was normalized to the matching densitometric value of the internal control β-actin.

4.11. Statistical Analysis

Data are expressed as the mean ± standard deviation (SD). Multiple comparisons were assessed by one-way analysis of variance (ANOVA) followed by Tukey's multiple comparison procedure. $p < 0.05$ was considered statistically significant. All the assays were performed in triplicate.

Supplementary Materials: Supplementary materials can be found at http://www.mdpi.com/1422-0067/17/1/41/s1.

Acknowledgments: The authors appreciate the financial support from the Startup Fund of the College of Pharmacy, University of South Florida, Tampa, Florida 33612, USA. Zhi-Wei Zhou is a holder of a postdoctoral scholarship from the College of Pharmacy, University of South Florida, Tampa, Florida 33612, USA.

Author Contributions: Bao-Jun Ren, Zhi-Wei Zhou, and Shu-Feng Zhou conceived and designed the experiments; Bao-Jun Ren performed the experiments; Da-Jian Zhu, Yong-Le Ju, Jin-Hao Wu, and Man-Zhao Ouyang analyzed the data; Xiao-Wu Chen and Shu-Feng Zhou contributed reagents/materials/analysis tools; Zhi-Wei Zhou and Shu-Feng Zhou wrote the paper.

Conflicts of Interest: The authors declare no conflict of interest.

References

1. Torre, L.A.; Bray, F.; Siegel, R.L.; Ferlay, J.; Lortet-Tieulent, J.; Jemal, A. Global cancer statistics, 2012. *Cancer J. Clin.* **2015**, *65*, 87–108. [CrossRef] [PubMed]
2. Siegel, R.; Desantis, C.; Jemal, A. Colorectal cancer statistics, 2014. *Cancer J. Clin.* **2014**, *64*, 104–117. [CrossRef] [PubMed]
3. Chen, W.; Zheng, R.; Zeng, H.; Zhang, S.; He, J. Annual report on status of cancer in China, 2011. *Chin. J. Cancer Res.* **2015**, *27*, 2–12. [CrossRef] [PubMed]
4. Society, A.C. Cancer facts and figures. Available online: http://www.cancer.org/acs/groups/content/@epidemiologysurveilance/documents/document/acspc-036845.pdf (accessed on 16 May 2013).
5. Chu, E. An update on the current and emerging targeted agents in metastatic colorectal cancer. *Clin. Colorectal Cancer* **2012**, *11*, 1–13. [CrossRef] [PubMed]
6. Lombardi, L.; Morelli, F.; Cinieri, S.; Santini, D.; Silvestris, N.; Fazio, N.; Orlando, L.; Tonini, G.; Colucci, G.; Maiello, E. Adjuvant colon cancer chemotherapy: Where we are and where we'll go. *Cancer Treat. Rev.* **2010**, *36* (Suppl. 3), S34–S41. [CrossRef]
7. Troiani, T.; Martinelli, E.; Orditura, M.; de Vita, F.; Ciardiello, F.; Morgillo, F. Beyond bevacizumab: New anti-VEGF strategies in colorectal cancer. *Expert Opin. Investig. Drugs* **2012**, *21*, 949–959. [CrossRef] [PubMed]
8. Nigg, E.A. Mitotic kinases as regulators of cell division and its checkpoints. *Nat. Rev. Mol. Cell Biol.* **2001**, *2*, 21–32. [CrossRef] [PubMed]
9. Bolanos-Garcia, V.M. Aurora kinases. *Int. J. Biochem. Cell Biol.* **2005**, *37*, 1572–1577. [CrossRef] [PubMed]
10. Gautschi, O.; Heighway, J.; Mack, P.C.; Purnell, P.R.; Lara, P.N., Jr.; Gandara, D.R. Aurora kinases as anticancer drug targets. *Clin. Cancer Res.* **2008**, *14*, 1639–1648. [CrossRef] [PubMed]
11. Dotan, E.; Meropol, N.J.; Zhu, F.; Zambito, F.; Bove, B.; Cai, K.Q.; Godwin, A.K.; Golemis, E.A.; Astsaturov, I.; Cohen, S.J. Relationship of increased aurora kinase A gene copy number, prognosis and response to chemotherapy in patients with metastatic colorectal cancer. *Br. J. Cancer* **2012**, *106*, 748–755. [CrossRef] [PubMed]
12. Baba, Y.; Nosho, K.; Shima, K.; Irahara, N.; Kure, S.; Toyoda, S.; Kirkner, G.J.; Goel, A.; Fuchs, C.S.; Ogino, S. Aurora-A expression is independently associated with chromosomal instability in colorectal cancer. *Neoplasia* **2009**, *11*, 418–425. [CrossRef] [PubMed]
13. Goos, J.A.; Coupe, V.M.; Diosdado, B.; Delis-Van Diemen, P.M.; Karga, C.; Belien, J.A.; Carvalho, B.; van den Tol, M.P.; Verheul, H.M.; Geldof, A.A.; *et al*. Aurora kinase A (AURKA) expression in colorectal cancer liver metastasis is associated with poor prognosis. *Br. J. Cancer* **2013**, *109*, 2445–2452. [CrossRef] [PubMed]
14. Cammareri, P.; Scopelliti, A.; Todaro, M.; Eterno, V.; Francescangeli, F.; Moyer, M.P.; Agrusa, A.; Dieli, F.; Zeuner, A.; Stassi, G. Aurora-a is essential for the tumorigenic capacity and chemoresistance of colorectal cancer stem cells. *Cancer Res.* **2010**, *70*, 4655–4665. [CrossRef] [PubMed]
15. Boss, D.S.; Beijnen, J.H.; Schellens, J.H. Clinical experience with aurora kinase inhibitors: A review. *Oncologist* **2009**, *14*, 780–793. [CrossRef] [PubMed]
16. Hong, X.; O'Donnell, J.P.; Salazar, C.R.; van Brocklyn, J.R.; Barnett, K.D.; Pearl, D.K.; deCarvalho, A.C.; Ecsedy, J.A.; Brown, S.L.; Mikkelsen, T.; *et al*. The selective Aurora-A kinase inhibitor MLN8237 (alisertib) potently inhibits proliferation of glioblastoma neurosphere tumor stem-like cells and potentiates the effects of temozolomide and ionizing radiation. *Cancer Chemother. Pharmacol.* **2014**, *73*, 983–990. [CrossRef] [PubMed]
17. Zhou, N.; Singh, K.; Mir, M.C.; Parker, Y.; Lindner, D.; Dreicer, R.; Ecsedy, J.A.; Zhang, Z.; Teh, B.T.; Almasan, A.; *et al*. The investigational Aurora kinase A inhibitor MLN8237 induces defects in cell viability and cell-cycle progression in malignant bladder cancer cells *in vitro* and *in vivo*. *Clin. Cancer Res.* **2013**, *19*, 1717–1728. [CrossRef] [PubMed]

18. Sehdev, V.; Peng, D.; Soutto, M.; Washington, M.K.; Revetta, F.; Ecsedy, J.; Zaika, A.; Rau, T.T.; Schneider-Stock, R.; Belkhiri, A.; *et al*. The Aurora kinase A inhibitor MLN8237 enhances cisplatin-induced cell death in esophageal adenocarcinoma cells. *Mol. Cancer Ther.* **2012**, *11*, 763–774. [CrossRef] [PubMed]
19. Yuan, C.X.; Zhou, Z.W.; Yang, Y.X.; He, Z.X.; Zhang, X.; Wang, D.; Yang, T.; Wang, N.J.; Zhao, R.J.; Zhou, S.F. Inhibition of mitotic Aurora kinase A by alisertib induces apoptosis and autophagy of human gastric cancer AGS and NCI-N78 cells. *Drug Des. Dev. Ther.* **2015**, *9*, 487–508.
20. Ding, Y.H.; Zhou, Z.W.; Ha, C.F.; Zhang, X.Y.; Pan, S.T.; He, Z.X.; Edelman, J.L.; Wang, D.; Yang, Y.X.; Zhang, X.; *et al*. Alisertib, an Aurora kinase A inhibitor, induces apoptosis and autophagy but inhibits epithelial to mesenchymal transition in human epithelial ovarian cancer cells. *Drug Des. Dev. Ther.* **2015**, *9*, 425–464.
21. Wang, F.; Li, H.; Yan, X.G.; Zhou, Z.W.; Yi, Z.G.; He, Z.X.; Pan, S.T.; Yang, Y.X.; Wang, Z.Z.; Zhang, X.; *et al*. Alisertib induces cell cycle arrest and autophagy and suppresses epithelial-to-mesenchymal transition involving PI3K/Akt/mTOR and sirtuin 1-mediated signaling pathways in human pancreatic cancer cells. *Drug Des. Dev. Ther.* **2015**, *9*, 575–601.
22. Niu, N.K.; Wang, Z.L.; Pan, S.T.; Ding, H.Q.; Au, G.H.; He, Z.X.; Zhou, Z.W.; Xiao, G.; Yang, Y.X.; Zhang, X.; *et al*. Pro-apoptotic and pro-autophagic effects of the Aurora kinase A inhibitor alisertib (MLN8237) on human osteosarcoma U-2 OS and MG-63 cells through the activation of mitochondria-mediated pathway and inhibition of p38 MAPK/PI3K/Akt/mTOR signaling pathway. *Drug Des. Dev. Ther.* **2015**, *9*, 1555–1584.
23. Gorgun, G.; Calabrese, E.; Hideshima, T.; Ecsedy, J.; Perrone, G.; Mani, M.; Ikeda, H.; Bianchi, G.; Hu, Y.; Cirstea, D.; *et al*. A novel Aurora-A kinase inhibitor MLN8237 induces cytotoxicity and cell-cycle arrest in multiple myeloma. *Blood* **2010**, *115*, 5202–5213. [CrossRef] [PubMed]
24. Cantley, L.C. The phosphoinositide 3-kinase pathway. *Science* **2002**, *296*, 1655–1657. [CrossRef] [PubMed]
25. Klionsky, D.J.; Emr, S.D. Autophagy as a regulated pathway of cellular degradation. *Science* **2000**, *290*, 1717–1721. [CrossRef] [PubMed]
26. Kim, J.; Klionsky, D.J. Autophagy, cytoplasm-to-vacuole targeting pathway, and pexophagy in yeast and mammalian cells. *Annu. Rev. Biochem.* **2000**, *69*, 303–342. [CrossRef] [PubMed]
27. Manning, B.D.; Cantley, L.C. AKT/PKB signaling: Navigating downstream. *Cell* **2007**, *129*, 1261–1274. [CrossRef] [PubMed]
28. Heras-Sandoval, D.; Perez-Rojas, J.M.; Hernandez-Damian, J.; Pedraza-Chaverri, J. The role of PI3K/AKT/mTOR pathway in the modulation of autophagy and the clearance of protein aggregates in neurodegeneration. *Cell Signal.* **2014**, *26*, 2694–2701. [CrossRef] [PubMed]
29. Lozy, F.; Karantza, V. Autophagy and cancer cell metabolism. *Semin. Cell Dev. Biol.* **2012**, *23*, 395–401. [CrossRef] [PubMed]
30. Mester, J.; Eng, C. When overgrowth bumps into cancer: The PTEN-opathies. *Am. J. Med. Genet. Part C Semin. Med. Genet.* **2013**, *163C*, 114–121. [CrossRef] [PubMed]
31. Shin, K.; Fogg, V.C.; Margolis, B. Tight junctions and cell polarity. *Annu. Rev. Cell Dev. Biol.* **2006**, *22*, 207–235. [CrossRef] [PubMed]
32. Heerboth, S.; Housman, G.; Leary, M.; Longacre, M.; Byler, S.; Lapinska, K.; Willbanks, A.; Sarkar, S. EMT and tumor metastasis. *Clin. Transl. Med.* **2015**, *4*, 6. [CrossRef] [PubMed]
33. Derksen, P.W.; Liu, X.; Saridin, F.; van der Gulden, H.; Zevenhoven, J.; Evers, B.; van Beijnum, J.R.; Griffioen, A.W.; Vink, J.; Krimpenfort, P.; *et al*. Somatic inactivation of E-cadherin and p53 in mice leads to metastatic lobular mammary carcinoma through induction of anoikis resistance and angiogenesis. *Cancer Cell* **2006**, *10*, 437–449. [CrossRef] [PubMed]
34. Nauseef, J.T.; Henry, M.D. Epithelial-to-mesenchymal transition in prostate cancer: Paradigm or puzzle? *Nat. Rev. Urol.* **2011**, *8*, 428–439. [CrossRef] [PubMed]
35. Polette, M.; Mestdagt, M.; Bindels, S.; Nawrocki-Raby, B.; Hunziker, W.; Foidart, J.M.; Birembaut, P.; Gilles, C. β-catenin and ZO-1: Shuttle molecules involved in tumor invasion-associated epithelial-mesenchymal transition processes. *Cells Tissues Organs* **2007**, *185*, 61–65. [CrossRef] [PubMed]
36. Ferlay, J.; Steliarova-Foucher, E.; Lortet-Tieulent, J.; Rosso, S.; Coebergh, J.W.; Comber, H.; Forman, D.; Bray, F. Cancer incidence and mortality patterns in Europe: Estimates for 40 countries in 2012. *Eur. J. Cancer* **2013**, *49*, 1374–1403. [CrossRef] [PubMed]

37. D'Assoro, A.B.; Liu, T.; Quatraro, C.; Amato, A.; Opyrchal, M.; Leontovich, A.; Ikeda, Y.; Ohmine, S.; Lingle, W.; Suman, V.; *et al*. The mitotic kinase Aurora—A promotes distant metastases by inducing epithelial-to-mesenchymal transition in ERα^+ breast cancer cells. *Oncogene* **2014**, *33*, 599–610. [CrossRef] [PubMed]
38. Chen, S.S.; Chang, P.C.; Cheng, Y.W.; Tang, F.M.; Lin, Y.S. Suppression of the STK15 oncogenic activity requires a transactivation-independent p53 function. *EMBO J.* **2002**, *21*, 4491–4499. [CrossRef] [PubMed]
39. Macurek, L.; Lindqvist, A.; Medema, R.H. Aurora-A and hBora join the game of Polo. *Cancer Res.* **2009**, *69*, 4555–4558. [CrossRef] [PubMed]
40. Hunter, T. Protein kinases and phosphatases: The yin and yang of protein phosphorylation and signaling. *Cell* **1995**, *80*, 225–236. [CrossRef]
41. Chow, J.P.; Siu, W.Y.; Ho, H.T.; Ma, K.H.; Ho, C.C.; Poon, R.Y. Differential contribution of inhibitory phosphorylation of CDC2 and CDK2 for unperturbed cell cycle control and DNA integrity checkpoints. *J. Biol. Chem.* **2003**, *278*, 40815–40828. [CrossRef] [PubMed]
42. Tyagi, A.; Singh, R.P.; Agarwal, C.; Siriwardana, S.; Sclafani, R.A.; Agarwal, R. Resveratrol causes CDC2-tyr15 phosphorylation via ATM/ATR-Chk1/2-CDC25C pathway as a central mechanism for S phase arrest in human ovarian carcinoma Ovcar-3 cells. *Carcinogenesis* **2005**, *26*, 1978–1987. [CrossRef] [PubMed]
43. Yuan, J.; Eckerdt, F.; Bereiter-Hahn, J.; Kurunci-Csacsko, E.; Kaufmann, M.; Strebhardt, K. Cooperative phosphorylation including the activity of polo-like kinase 1 regulates the subcellular localization of cyclin B1. *Oncogene* **2002**, *21*, 8282–8292. [CrossRef] [PubMed]
44. Li, J.P.; Yang, Y.X.; Liu, Q.L.; Pan, S.T.; He, Z.X.; Zhang, X.; Yang, T.; Chen, X.W.; Wang, D.; Qiu, J.X.; *et al*. The investigational Aurora kinase A inhibitor alisertib (MLN8237) induces cell cycle G_2/M arrest, apoptosis, and autophagy via p38 MAPK and Akt/mTOR signaling pathways in human breast cancer cells. *Drug Des. Dev. Ther.* **2015**, *9*, 1627–1652.
45. Danial, N.N.; Korsmeyer, S.J. Cell death: Critical control points. *Cell* **2004**, *116*, 205–219. [CrossRef]
46. Chinnaiyan, A.M.; O'Rourke, K.; Tewari, M.; Dixit, V.M. FADD, a novel death domain-containing protein, interacts with the death domain of fas and initiates apoptosis. *Cell* **1995**, *81*, 505–512. [CrossRef]
47. Jung, C.H.; Ro, S.H.; Cao, J.; Otto, N.M.; Kim, D.H. mTOR regulation of autophagy. *FEBS Lett.* **2010**, *584*, 1287–1295. [CrossRef] [PubMed]
48. Alers, S.; Loffler, A.S.; Wesselborg, S.; Stork, B. Role of AMPK-mTOR-Ulk1/2 in the regulation of autophagy: cross talk, shortcuts, and feedbacks. *Mol. Cell. Biol.* **2012**, *32*, 2–11. [CrossRef] [PubMed]
49. Tang, G.; Yue, Z.; Talloczy, Z.; Hagemann, T.; Cho, W.; Messing, A.; Sulzer, D.L.; Goldman, J.E. Autophagy induced by Alexander disease-mutant GFAP accumulation is regulated by p38/MAPK and mTOR signaling pathways. *Hum. Mol. Genet.* **2008**, *17*, 1540–1555. [CrossRef] [PubMed]
50. Mizushima, N.; Komatsu, M. Autophagy: Renovation of cells and tissues. *Cell* **2011**, *147*, 728–741. [CrossRef] [PubMed]
51. Mathew, R.; Kongara, S.; Beaudoin, B.; Karp, C.M.; Bray, K.; Degenhardt, K.; Chen, G.; Jin, S.; White, E. Autophagy suppresses tumor progression by limiting chromosomal instability. *Genes Dev.* **2007**, *21*, 1367–1381. [CrossRef] [PubMed]
52. Lum, J.J.; Bauer, D.E.; Kong, M.; Harris, M.H.; Li, C.; Lindsten, T.; Thompson, C.B. Growth factor regulation of autophagy and cell survival in the absence of apoptosis. *Cell* **2005**, *120*, 237–248. [CrossRef] [PubMed]
53. El-Khattouti, A.; Selimovic, D.; Haikel, Y.; Hassan, M. Crosstalk between apoptosis and autophagy: Molecular mechanisms and therapeutic strategies in cancer. *J. Cell Death* **2013**, *6*, 37–55. [PubMed]
54. Kalluri, R.; Weinberg, R.A. The basics of epithelial-mesenchymal transition. *J. Clin. Investig.* **2009**, *119*, 1420–1428. [CrossRef] [PubMed]
55. Nieto, M.A. The ins and outs of the epithelial to mesenchymal transition in health and disease. *Annu. Rev. Cell Dev. Biol.* **2011**, *27*, 347–376. [CrossRef] [PubMed]
56. Thiery, J.P.; Sleeman, J.P. Complex networks orchestrate epithelial-mesenchymal transitions. *Nat. Rev. Mol. Cell Biol.* **2006**, *7*, 131–142. [CrossRef] [PubMed]
57. Hulit, J.; Suyama, K.; Chung, S.; Keren, R.; Agiostratidou, G.; Shan, W.; Dong, X.; Williams, T.M.; Lisanti, M.P.; Knudsen, K.; *et al*. N-cadherin signaling potentiates mammary tumor metastasis via enhanced extracellular signal-regulated kinase activation. *Cancer Res.* **2007**, *67*, 3106–3116. [CrossRef] [PubMed]

58. Lehembre, F.; Yilmaz, M.; Wicki, A.; Schomber, T.; Strittmatter, K.; Ziegler, D.; Kren, A.; Went, P.; Derksen, P.W.; Berns, A.; *et al*. NCAM-induced focal adhesion assembly: A functional switch upon loss of E-cadherin. *EMBO J.* **2008**, *27*, 2603–2615. [CrossRef] [PubMed]
59. Aigner, K.; Dampier, B.; Descovich, L.; Mikula, M.; Sultan, A.; Schreiber, M.; Mikulits, W.; Brabletz, T.; Strand, D.; Obrist, P.; *et al*. The transcription factor ZEB1 (dEF1) promotes tumour cell dedifferentiation by repressing master regulators of epithelial polarity. *Oncogene* **2007**, *26*, 6979–6988. [CrossRef] [PubMed]
60. Harel, M.; Oren-Giladi, P.; Kaidar-Person, O.; Shaked, Y.; Geiger, T. Proteomics of microparticles with SILAC Quantification (PROMIS-Quan): A novel proteomic method for plasma biomarker quantification. *Mol. Cell. Proteom.* **2015**, *14*, 1127–1136. [CrossRef] [PubMed]
61. Zhou, Z.W.; Li, X.X.; He, Z.X.; Pan, S.T.; Yang, Y.; Zhang, X.; Chow, K.; Yang, T.; Qiu, J.X.; Zhou, Q.; *et al*. Induction of apoptosis and autophagy via sirtuin1- and PI3K/Akt/mTOR-mediated pathways by plumbagin in human prostate cancer cells. *Drug Des. Dev. Ther.* **2015**, *9*, 1511–1554. [CrossRef] [PubMed]



© 2015 by the authors; licensee MDPI, Basel, Switzerland. This article is an open access article distributed under the terms and conditions of the Creative Commons by Attribution (CC-BY) license (http://creativecommons.org/licenses/by/4.0/).

International Journal of
Molecular Sciences

MDPI

Review

Notch Signaling in Pancreatic Development

Xu-Yan Li [1,2], Wen-Jun Zhai [1] and Chun-Bo Teng [1,*]

Received: 22 November 2015; Accepted: 24 December 2015; Published: 30 December 2015
Academic Editor: William Chi-shing Cho

[1] College of Life Science, Northeast Forestry University, Harbin 150040, China; lxy0702@126.com (X.-Y.L.); makawada@163.com (W.-J.Z.)
[2] College of Life Sciences, Agriculture and Forestry, Qiqihar University, Qiqihar 161006, China
* Correspondence: chunboteng@nefu.edu.cn; Tel./Fax: +86-451-8219-1784

Abstract: The Notch signaling pathway plays a significant role in embryonic cell fate determination and adult tissue homeostasis. Various studies have demonstrated the deep involvement of Notch signaling in the development of the pancreas and the lateral inhibition of Notch signaling in pancreatic progenitor differentiation and maintenance. The targeted inactivation of the Notch pathway components promotes premature differentiation of the endocrine pancreas. However, there is still the contrary opinion that Notch signaling specifies the endocrine lineage. Here, we review the current knowledge of the Notch signaling pathway in pancreatic development and its crosstalk with the Wingless and INT-1 (Wnt) and fibroblast growth factor (FGF) pathways.

Keywords: pancreatic progenitor; Notch signaling; differentiation; maintenance

1. Introduction

Notch signaling is an evolutionarily conserved pathway for cell-cell communication and cell-fate determination during embryonic development and tissue homeostasis [1,2]; it includes canonical and non-canonical pathways. The former is initiated by ligand-receptor interactions between adjacent cells [3,4], which results in the activation of the *Hes1* gene by a complex consisting of the Notch intracellular domain (NICD), Rbp-Jκ family of nuclear proteins (Rbp-J (mammalian), Su(H) (*Drosophila*), and Lag-1 (*Caenorhabditis elegans*)), and the Mastermind co-activator. However, non-canonical Notch signaling broadly encompasses several modes of Notch activity that do not go through the Rbp-J and activation of the *Hes/Hey* genes [5,6]. Here, we review the role of the canonical pathway during pancreatic development. Notch-mediated lateral inhibition represents an important conserved mechanism that regulates cell differentiation, cell proliferation and cell survival in stem cells [7–9]. Abnormalities in Notch signaling have been linked to various syndromes and diseases, including developmental malformation, neurodegenerative diseases, metabolic disorders, and malignant disease [10–13].

Over the past two decades, numerous reports have revealed the pivotal role of Notch signaling in pancreatic specification, cell proliferation, differentiation and plasticity [9,14–16]. The first evidence of the involvement of the Notch signaling pathway in pancreatic development focused on its lateral inhibition role in controlling pancreatic fate decision. The activation of Notch signaling in pancreatic progenitors prevents their differentiation into the endocrine or exocrine cell lineage [17,18]. In contrast, the blockage of the Notch signaling pathway causes premature differentiation of the multipotent progenitor cells (MPCs) into endocrine cells [19,20]. A series of studies have revealed that Notch signaling functions as a negative regulator of the pro-endocrine factor neurogenin3 (*Ngn3*), and the formation of insulin-producing β-cells is significantly enhanced by induction of pro-endocrine factors or inhibition of Notch processing. However, recently, some researchers have disagreed with the notion that the Notch pathway is an inhibitor of endocrine cell differentiation. They have proposed that the

Notch pathway specifies the pancreatic progenitors differentiating towards endocrine lineage [21,22] or the inactivated Notch pathway promotes acinar cell differentiation [23–25]. Some recent findings have revealed that Notch signaling does not act through an on or off mode, but at a Notch level-dependent manner to regulate the quiescence, self-renewal and differentiation of pancreatic progenitor cells during pancreas development [22,26]. Studies on animal models of pancreatic regeneration and diseases have revealed that Notch signaling is involved in controlling the plasticity of terminally differentiated adult pancreatic cells [25,27,28]. During pancreatic development, the formation of islets of Langerhans is enhanced by specific transcription factors and regulated by multiple intercellular signaling pathways, including the Wingless and INT-1 (Wnt), fibroblast growth factor (FGF), Notch pathways, *etc.* [29–31]. These pathways independently or collaboratively perform regulatory functions at different time-points. This mini review summarizes the current knowledge of the roles of Notch signaling in pancreatic development, including pancreatic cell lineage commitment, pancreatic progenitor maintenance, and adult pancreatic cell plasticity, and it also discusses the crosstalk between the Notch and Wnt/FGF pathways.

2. An Outline of Pancreatic Development

The mammalian pancreas is derived from two independent ventral and dorsal buds and experiences three stages of transition [32,33]. In mice, the primary transition is marked by the specification and proliferation of pancreatic progenitors and the appearance of glucagon-producing cells during E9.5 and E12.5 [34,35]. The secondary transition is from E13.5 to E15.5, during which all five hormone-expressing endocrine lineages (α-, β-, δ-, ε-, and PP-cells) begin to emerge rapidly and amylase-expressing acinar cells arise from the extending tip epithelium [36,37]. The third transition occurs from E16.5 to E19. During this period, endocrine cells migrate and cluster into numerous islets, and acinar cells further expand [38]. The pancreatic buds contain undifferentiated progenitor cells, which contribute to all pancreatic cell lineages, the exocrine, ductal and endocrine cell lineages [39,40]. In the MPCs, Notch signaling is critical and essential for their proliferation and commitment [22,24] (Figure 1).

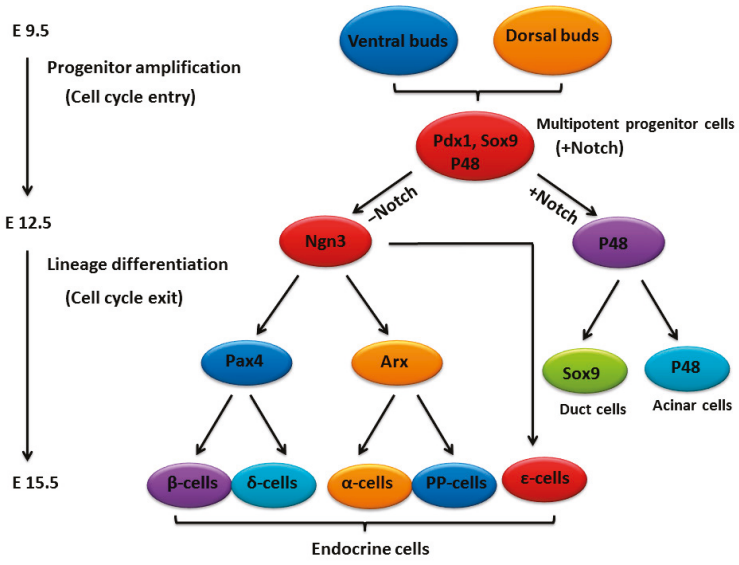

Figure 1. A schematic of pancreatic development.

Lineage-specific transcription factors control the differentiation of pancreatic progenitor cells towards a specific type [40,41]. Pancreatic cells arise from pancreatic duodenal homeobox 1 (Pdx1)-expressing progenitors (Figure 1). As pancreatic development proceeds, the *Pdx1* gene becomes progressively confined to endocrine β-cells, where it plays an essential role in the transcriptional

activation of the *insulin* gene [42]. The progenitors co-express sex-determining region Y (Sry) box 9 (Sox9) and pancreas specific transcription factor1a (Ptf1a, also known as P48) [43,44] (Figure 1). However, Sox9 expression is eventually limited to a subset of ductal and centroacinar cells (CACs) in adults, and Ptf1a is expressed solely in mature acinar cells [45,46] (Figure 1). The Basic Helix-Loop-Helix (bHLH) transcription factor Ngn3 drives MPCs towards the endocrine cell fate [47]. The specification of the endocrine subtypes is essentially under the control of the opposing actions of aristaless related homeobox (Arx) and paired box 4 (Pax4) acting downstream of Ngn3 [48] (Figure 1). *Ngn3*-null mice fail to generate pancreatic endocrine cells and lose the expression of islet transcription factors, including islet-1 (*Isl1*), NK2 homeobox 2 (*Nkx2.2*), paired box 4 (*Pax4*), paired box 6 (*Pax6*) and *NeuroD1*, which are all important for endocrine cell differentiation [49]. During the maturation of islet cells, the cell cycle regulatory proteins play a pivotal role in cell division and differentiation. Prior to and during the secondary transition, cyclin-dependent kinase 4 (Cdk4) and E2F transcription factor 1 (E2F1) promote β-cell development by activating Ngn3 to increase the numbers of endocrine precursors [50]. In the mouse embryonic pancreas, P21 protein (Cdc42/Rac)-activated kinase 3 (Pak3) acts downstream of Ngn3 to promote cell cycle exit and cell differentiation by repressing *cyclin D1* in $Ngn3^{+}$ endocrine progenitors [51]. The PTF1 complex initiates exocrine differentiation [52]. The PTF1 complex, which is composed of p64/HEB, p75/E2A and Ptf1a [52], directly binds to the promoter regions of the acinar digestive enzyme genes, and leads to acinar cell differentiation and cell cycle exit [46,53]. More interestingly, a recent study on the *Ptf1a* mutant zebrafish model has found that the down-regulation of Ptf1a induces acinar-to-endocrine fate conversion [54]. Using genetic loss- and gain-of-function approaches, Schaffer *et al.* [55], have demonstrated that the cross-repressive interactions between Nkx6 (Nkx6.1/Nkx6.2) and Ptf1a commit the fate of pancreatic progenitor cells. Nkx6 induces endocrine cell determination, however, Ptf1a promotes acinar cell specification.The cross-antagonistic switch between Nkx6 and Ptf1a is controlled by Notch signaling [55].

Growing evidence suggests that miRNAs play an important role in the embryonic development and physiological function of pancreas. Examples of these miRNAs include miR-7, miR-375, the miR17-92 cluster, miR-26 and miR-15 *et al.* [56]. *Dicer*-null mice display gross defects in all pancreatic lineages, especially the insulin-producing-cells. The endocrine defect in *Dicer*-null mice is associated with an increase in the expression of the Notch signaling target Hes1 [56]. miR-7 is dispensable for the maintenance of β-cell mass and functions [57]. miR-375 is required for normal pancreatic genesis and maintains α- and β-cell mass [58]. We have found that, during pancreatic progenitor cell differentiation, miR-375 inhibited pancreatic progenitor cell proliferation by targeting the Hippo signaling effector *Yap1* [59]. miR-375 also plays a role in regulating insulin secretion through targeting the myotrophin (*Mtpn*) and pyruvate dehydrogenase kinase (*Pdk1*) genes. miR-19b and miR-18a have been shown to directly act on *NeuroD1* and *Ptf1a* 3′ UTR, respectively [60,61]. These two miRNAs may contribute to the regulation of the differentiation and function of β-cells and acinar cells during pancreatic development. Pancreatic regeneration is accompanied by the high expression of miR-15a, miR-15b, miR-16 and miR-195, which can potentially bind to the *Ngn3* transcript [62].

The development of the pancreas depends on the spatio-temporal expression of a number of transcription factors and associated signaling pathways [63,64]. Studies on the transcriptional regulation of the pancreas have been reviewed extensively, and thus, not discussed in detail here.

3. An Overview of the Notch Signaling Cascade

Notch genes encode a single-pass transmembrane receptor family of molecules, including Notch1–4 in mammals [65]. Notch proteins contain a large Notch extracellular domain (NECD) composed of 29–36 tandem epidermal growth factor-like repeats, a short Notch transmembrane fragment (NTM), and a Notch intracellular domain (NICD) [66]. As part of the biosynthetic process of Notch, a Furin-like protease in the Golgi cuts nascent Notch proteins at the S1 cleavage site into two fragments [67,68], the NECD and non-NECD domains. Then, they conjugate non-covalently as a heterodimer and target to the cellular surface. The initiation of Notch signaling is trigged by the binding

of the NECD domain to type I transmembrane ligands (δ-like 1, 3, 4 (Dll1, 3, 4) and Serrate/Jagged1, 2 (Ser/Jag1, 2)) on adjacent cells. Then, the membrane-bound proteases are activated and continue to cleave the non-NECD domain into two domains, the NTM and NICD domains. This cleavage is catalyzed by A Disintegrin and Metalloprotease (ADAM)-family of metalloproteases at a luminal juxtamembrane site 2 (S2) and by a tetrameric γ-secretase complex at an intramembrane site 3 (S3) of non-NECD domain. After the transcriptionally activated NICD is released and translocates into the nucleus, it binds to Rbp-J [69]. Then, Rbp-J recruits the coactivator Mastermind-like (Maml) to activate downstream genes, including the Hairy enhance of split (*Hes*) and Hairy/enhancer of spit related with YRPW motif (*Hey*) families, nuclear factor-κB (*NF-κB*), vascular growth factor receptor (*VEGF*), *etc.* [70,71] (Figure 2). The *Hes* genes, which encode bHLH transcriptional repressors, play crucial roles in the fate choice and differentiation of stem cells, e.g., in the inner ear, neurons and pancreas development [72–74]. Activated Hes1 inhibits the expression of *Ngn3* by binding to the proximal promoter and specifically blocking promoter activity [75,76]. However, when Notch signaling is limited or nonexistent, Rbp-J recruits a corepressor (CoR) complex to repress the expression of the Notch target genes (Figure 2).

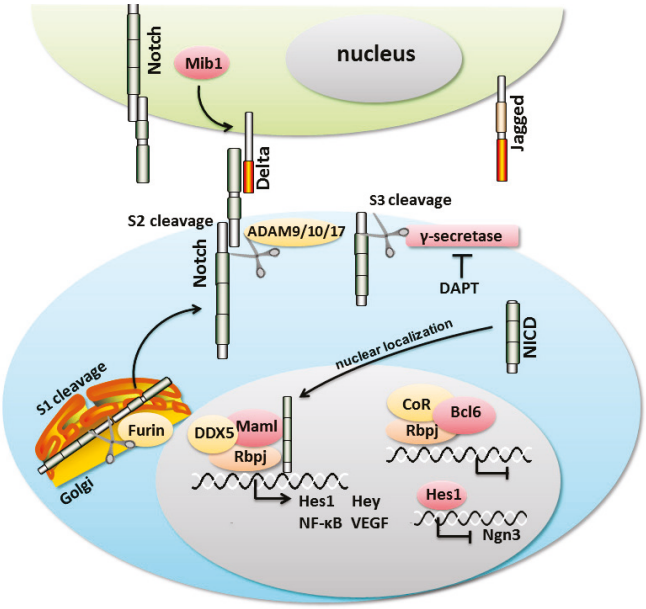

Figure 2. A schematic of Notch signaling during pancreatic development. Notch signaling is initiated by the binding of the ligands and receptors of two neighboring cells. Upon activation, Notch is cleaved, releasing the Notch intracellular domain (NICD). The NICD can subsequently translocate into the nucleus to transcriptionally activate Notch target genes. Hes1 inhibits the expression of *Ngn3* by blocking its promoter activity.

Several Notch-related regulators have also been found to function in normal organism development and tumorigenesis. In the left-right asymmetric development of *Xenopus*, the transcriptional repressor B cell leukemia/lymphoma 6 (Bcl6) competes with Maml to repress the Notch1 target genes [77]. Mind bomb1 (Mib1), which encodes an E3 ubiquitin ligase, promotes the internalization of Δ, which paradoxically increases the efficiency with which Δ activates Notch [78]. It is reported that Mib1 is required for the formation of pancreatic β-cells and the specification of neurons and glia in the spinal cord [79,80]. In neural progenitors, the multifunctional protein kinase Nemo-like kinase (NLK) negatively regulates the formation of the Rbp-J-NICD-Maml complex through the phosphorylation of Notch1 to fine-tune the timing of neuronal differentiation [81]. DEAD (Asp-Glu-Ala-Asp) box helicase5 (DDX5, also known as p68) is found to act as a component of the Mastermind-like1(Maml1) protein complex for transcriptional coactivation and is also a novel regulator

of oncogenic Notch signaling in T-ALL leukemic cells [82]. Several reports have shown that the Notch glycosylating enzyme Manic Fringe (Mfng) is expressed in Ngn3$^+$ cells, and the ectopic expression of Mfng is sufficient to induce chick endodermal cells to differentiate towards endocrine fate [83]. However, the deletion of *Mfng* in mice has no effect on pancreatic development, cell differentiation or function [84]. The glycosylation of the Notch receptors has been shown to prevent the binding of Jagged, thus inhibiting Jagged-mediated activation [85,86]. The ADAM family of metalloproteases have proteolytic activity and play a major role in the ectodomain shedding of proteins involved in paracrine signaling, cell adhesion and intracellular signaling [87–89]. During embryogenesis, ADAM9 and ADAM17 are expressed separately in insulin-producing β-cells and other islet cells, and ADAM10 is predominantly detectable in acinar cells [90]. ADAM10 and ADAM17 have been shown to cleave Notch at the S2 site, and ADAM9 and ADAM15 are also found to be involved in Notch signaling indirectly in neurons [91,92]. These ADAMs may play an essential role in the activation of Notch signaling during pancreatic development.

4. Notch Signaling Pathway in the Pancreas

4.1. Notch Signaling in Pancreatic Progenitor Cell Differentiation

Notch signaling is critical at multiple steps during pancreatic development [16,93]. The expression levels of the Notch ligand and receptor change during pancreatic development. Notch1 is the first expressed receptor in a subset of pancreatic epithelium cells at E9.5 and then is broadly expressed in the pancreatic epithelium at E14.5 [94]. Notch2 is strongly expressed at E11.5, and its expression is absolutely restricted to ductal cells at E15.5 [94]. Notch3 and Notch4 are expressed in the early pancreatic mesenchyme and then in the endothelial cells of the pancreas at E15.5 [94]. Dll1 is transiently expressed in the pancreatic duct epithelium between E9.5 and E11.5 [93,95], and Jag1 is the most abundant ligand during mid-gestation pancreatic development [96]. Recent studies have identified that CACs and terminal duct cells are unique locations of activated Notch signaling in the pancreas of adult mice and zebrafish [97,98]. In the adult pancreas, the reactivation of Notch is involved in phenotype modulation of adult rat exocrine cells and the proliferation of metaplastic exocrine cells during pancreas regeneration [99,100]. In the caerulein-induced pancreatitis mouse model, the expression of the exocrine genes disappeared in pancreatic exocrine cells, while genes normally associated with Notch components, such as *Notch1*, *Notch2*, *Hes1*, *Jag2*, and a low level of *Dll1* were induced [101].

During the secondary transition, Notch regulates endocrine differentiation via a lateral inhibition mechanism. The lateral inhibition model proposes that the onset of Ngn3 expression initiates endocrine differentiation and activates the Notch ligand Delta. Subsequently, Delta binds with Notch receptors in neighboring cells to initiate the Notch signaling cascade and release the NICD. The activated NICD enters the nucleus to activate the target gene *Hes1*, which inhibits the expression of Ngn3 [75,76]. Ultimately, the activated Notch pathway prevents adjacent cells from adopting an endocrine fate (Figure 3). Most early studies have shown that the inactivation of Notch signaling accelerates the premature differentiation of the endocrine pancreas [20]. In *Dll1*-deficient mice, Pdx1$^+$ progenitor cells within the pancreatic buds lacked expansion and differentiated prematurely into endocrine cells [93]. In zebrafish embryos, the inhibition of *Jagged* caused ectopic islet-cell differentiation [19]. The loss of *Rbp-J* at the initial stage of pancreatic development resulted in the rapid differentiation of α-and PP-cells and decreased numbers of Ngn3$^+$ cells [102]. Furthermore, *Rbp-J* KO mice exhibited insulin-deficient diabetes [20,102]. *Hes1*-deficient mice showed pancreatic hypoplasia, which is caused by the depletion of pancreatic epithelial progenitors from the accelerated differentiation of pancreatic endocrine cells [72,103]. A similar phenotype has been observed in mice that over-express *Ngn3* [104] or the intracellular form of *Notch3* (a repressor of Notch signaling) [105]. Conversely, the enforced activation of Notch signaling blocks pancreatic progenitors differentiation into the endocrine and exocrine cells. In chicken embryos, activated *Notch1* can block the expression of endocrine genes and

prevent endocrine differentiation [18]. The lentiviral-mediated activation of *Hes1* and intracellular domain of Notch (*Notch-IC*) in mouse dorsal pancreatic buds at E10.5 represses endocrine and exocrine differentiation [106]. Ectopic *Notch* activation in zebrafish embryos can inhibit acinar and β-cell differentiation [106]. When *Notch* was overexpressed in the E9.5 or E11.5 mouse embryonic pancreas, the differentiation of $Hes1^+$ cells was blocked; however, ectopic *Notch* activation at E15.5 does not perturb exocrine differentiation [107]. The sustained Notch1 signaling in Pdx1-NICD transgenic mice prevents the differentiation of pancreatic acinar and endocrine cells [17].

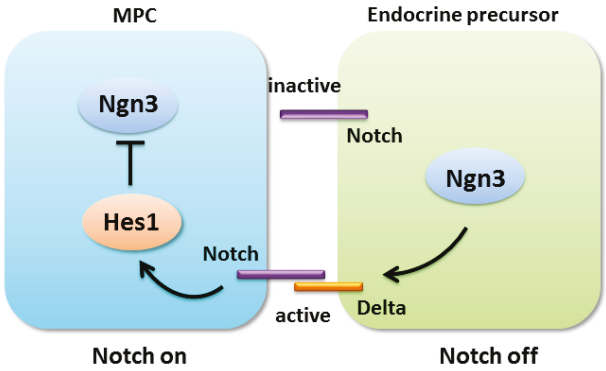

Figure 3. Notch-mediated lateral inhibition in pancreatic multipotent progenitor cell differentiation.

Furthermore, recent studies have implied that the Notch-mediated regulation of endocrine differentiation is more complex than the classical lateral inhibition model suggests. For example, E9.5 *Dll1* mutant mice show a dramatic decrease in their number of $Ngn3^+$ cells, which suggests that Dll1 is required for the continuous formation of $Ngn3^+$ endocrine precursors [21]. Shih *et al.* [22], demonstrated that Notch induces the expression of the *Ngn3* gene activator Sox9, which may provide further evidence that Notch initiates the endocrine lineage. Some current gene-targeting studies focused on the Notch signaling components found that inactivated Notch signaling promotes the differentiation or transdifferentiation of MPCs, CACs or adult duct cells to the acinar lineage, which suggests that Notch may specify the endocrine lineage. Zebrafish embryos that were injected with RNA encoding a dominant-negative Suppressor of Hairless showed accelerated exocrine cells compared with the controls [106]. Similarly, a study by Cras and his colleagues demonstrated that the deletion of presenilin1 (*Psen1*) and presenilin2 (*Psen2*) drives Ngn3-expressing cells to differentiate into acinar cells [108]. Once cultured in the presence of the γ-secretase inhibitor DAPT, mouse pancreatic progenitors differentiate into acinar cells [23]. When Notch signaling is suppressed through the mosaic overexpression of a Notch signaling antagonist, dominant-negative mastermind-like1 (dnMaml), the pancreatic progenitor cells subsequently differentiate into acinar cells [24]. The inactivation of *Mib1* in the endoderm causes a loss of endocrine cells and an increase in exocrine cells in the proximal domain, which suggested that Notch signalling is required to prompt MPCs to adopt an endocrine fate [79]. Upon *Rbp-J* deletion, mouse CACs undergo a rapid conversion to acinar cells [109]. In addition, the differentiation of acinar cells is accelerated by *Hes1* depletion but is suppressed by NICD induction in adult mouse Sox9-expressing cells [25].

The causal role of Notch signaling in the patterning of MPCs into endocrine cells has been evaluated in some studies in different aspects. Genetic interactions have suggested that γ-secretase and Notch2 act in a non-canonical mechanism to sequester Rbp-J away from Ptf1a, which secures mouse Ngn3-positive progenitor cells to the endocrine fate [108]. Afelik *et al.* [24], found that Notch signaling is required to establish a duct and endocrine identity through the activation of Nkx6.1, which is bound to Rbp-J. Some studies revealed that Notch does not function in an on-off mode, but that Notch signaling seems to act in a concentration-dependent manner [22,26,76]. A study by Shih *et al.* [22], proposed a model in which high Notch expression activates Hes1 and Sox9 expression, resulting in the

generation of pancreatic duct cells, while low Notch expression activates Sox9 but not Hes1, resulting in Ngn3 activation and endocrine differentiation. A study on the dynamic assessment of Notch signaling in the zebrafish intrapancreatic duct found that the proliferation and differentiation of MPCs are regulated by different levels of Notch signaling [26]. It has been reported that the hyperactivation of Notch signaling could convert the proliferative Notch-responsive MPCs to the quiescent state, hypo-activation of the Notch pathway induces the quiescent MPCs to the proliferative state, and strong down-regulation of Notch signaling promotes MPCs differentiate towards endocrine cells [26]. However, there are gaps in our understanding of the timing and extent of Notch ligand-receptor interactions and how this affects the behavior of MPCs. Therefore, there may be even more complexity in the Notch-mediated regulation of pancreatic development.

4.2. Notch Signaling in Pancreatic Progenitors Maintenance

The Notch signaling pathway has been found to maintain proliferation and prevent the precocious differentiation of pancreatic progenitor cells [18,110]. The activation of Notch at the "primary transition" maintains the pancreatic state, allowing the coordination of epithelial outgrowth and helping the pancreatic buds reach their destined size.

The transcription factor network is crucial for the maintenance and expansion of MPCs. Pdx1 and Ptf1a can form autoregulatory loops and feed-forward loop to retain and expand the progenitor cells during early pancreatic development [111]. The inactivation of Ptf1a in mice results in pancreatic hypoplasia, glucose intolerance and the transformation of pancreatic progenitors to a duodenal fate [112,113]. The expression of Pdx1 and Ptf1a is also regulated by fibroblast growth factor 10 (FGF10) and Notch signaling [111]. FGF10 signaling promotes the expansion of pancreatic epithelial cells through Sox9 and Hes1 activation [31,110,114,115]. Hes1 is reported to regulate the binary decision choice of pancreatic progenitors, cell cycle exist or self-renewal maintenance, through suppression of P57 and P27, which are cyclin-dependent kinase inhibitors [116,117] (Figure 4). In pancreatic progenitors, the inactivation of Hes1 could increase the expression of the *P57* gene, which leads to cell cycle arrest, early differentiation and the depletion of the progenitor pool [117]. Moreover, Sox9 promotes pancreatic progenitor expansion by modulating the FGF-receptor (FGFR), Notch and Wnt signal transduction [31,45,118]. It has been reported that the pancreas-specific *Sox9*-deficient progenitors exhibit reduced proliferation and a low level of Hes1 [45]. Sox9 cell-autonomously controls the expression of FGFR2b in pancreatic progenitors [31]. In isolated human islet-epithelial clusters, the knockdown of *Sox9* resulted in a decrease in pGSK3β, nuclear β-catenin and the Wnt signaling target gene *cyclin D1* [118]. Notch signaling also regulates Sox9 expression in the pancreas [22,25]. Notch positively regulates Sox9 expression in a Hes1-independent manner in the pancreatic duct cells of $Sox9^{CreERT2}$ mice [25]. The progenitor-intrinsic transcription factors Pdx1, Ptf1a and Sox9, as well as Notch, Wnt and FGF10 signaling, compose a complex network for the maintenance of MPCs.

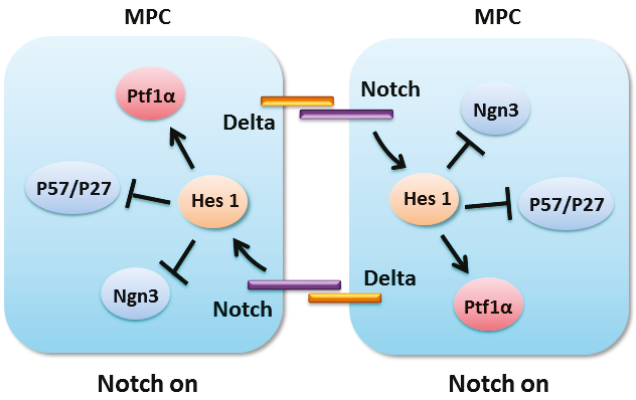

Figure 4. Notch signaling in the proliferation of pancreatic multipotent progenitor cells.

4.3. Notch Signaling in Adult Pancreatic Cell Plasticity

Because the components of the Notch signaling pathway are not normally expressed in terminally differentiated pancreatic cells, most mature cells lose their responsiveness to Notch signaling. However, in-depth studies have indicated that Notch signaling is involved in controlling the plasticity of adult, terminally differentiated pancreatic cells. Importantly, the dedifferentiation and transdifferentiation of terminally differentiated pancreatic cells are associated with Notch pathway reactivation during regeneration following pancreatitis [28,99,119], pancreatic neoplasia [120], and acino-ductal metaplasia [121,122]. For instance, when the pancreas is injured by pancreatitis, the exocrine acinar cells lose their differentiated characteristics and present acino-ductal metaplasia, which strongly upregulates the expression of the receptors Notch1 and 2 and the target genes *Hes1*, *Hey1*, and *Hey2* [27]. Adult pancreatic duct cells retain their plasticity to differentiate into endocrine or acinar cell types, which is controlled by Notch signaling and Sox9 cooperatively [25]. When dissociated adult human β-cells are cultured in serum-containing medium, the β-cells dedifferentiate, and they enter into the cell cycle, which correlates with the activation of the Notch pathway and the down-regulation of P57 [123]. When Hes1 expression was down-regulated by shRNA, the dedifferentiated β cells redifferentiate into insulin-expressing cells [124]. Notch signaling is also reported as a gatekeeper of acinar-to-β-cell conversion *in vitro* [100,125]. Baeyens *et al.* [100], found that the growth factor-induced conversion of adult acinar cells to β-cells is negatively regulated by activated Notch1, which has the ability to prevent the re-expression of the pro-endocrine transcription factor Ngn3. Notch re-expression is deeply associated with the modulation of the proliferation of metaplastic cells and possible plays an important role in pancreatic regeneration.

5. The Crosstalk between Notch Signaling and the Wingless and INT-1 (Wnt)/Fibroblast Growth Factor (FGF) Pathway in the Pancreas

5.1. Notch/Wnt Crosstalk

Notch and Wnt signaling are key pathways that control the expansion and differentiation of stem/progenitor cells during embryogenesis, tissue formation and maintenance in adult homeostasis [126]. The Wnt pathway inhibits the specification of the pancreas in the early endoderm, whereas the pathway promotes the growth of the dorsal and ventral primordial buds, specifically the proliferation of acinar cells [127]. In the developing mouse pancreatic epithelium, the deletion of *Wnt7b* leads to pancreatic hypoplasia because of the reduced proliferation of pancreatic progenitor cells [128]. The ectopic stabilization of *β-catenin* before E11.5 in mouse embryos prevents the proper differentiation and expansion of early pancreatic progenitor cells [129]. Ectopic expression of *β-catenin* in mouse embryos at E18.5 causes the gross enlargement of the exocrine pancreas, which results in a dramatic increase in pancreas organ size [129]. Conversely, in pancreas-specific *β-catenin* knockout mice, the pancreas almost completely lacks acinar cells [130]. Meanwhile, gain- and loss-of-function experiments have proved that the Wnt pathway is involved in β-cell growth and survival. The proliferation of mouse islet cells and β-cells increases when they are treated with Wnt3a [131,132]. Conditional activated β-catenin promotes the expansion of β-cells in mice [129]. However, the addition of the soluble Wnt inhibitor Fz8-cysteine-rich domain (Fz8-CRD) or the conditional knock-in of the Wnt inhibitor Axin impaired the proliferation of neonatal mouse β-cells [129,131]. Likewise, studies have found that the Wnt signaling pathway plays a role in regulating glucose-stimulated insulin secretion in mature β-cells and is involved in lipid metabolism and glucose homeostasis [133,134]. The knockout of the low-density lipoprotein receptor-related protein 5 (LRP5), which is a Wnt co-receptor, results in glucose intolerance in mice [133].

In the early pancreatic lineage commitment, there is a repressive crosstalk between Notch and Wnt signaling. Notch pathway promotes the lineage commitment and differentiation of pancreatic progenitors, whereas Wnt signaling maintains the stem cell state. The opposing activities of Notch and Wnt have also been found in the skin, mammary glands and intestinal stem cells [135–137].

Similarly, both pathways can act on the same cell during the development of sensory bristle and epidermal cells in *Drosophila* and *Xenopus* [138,139]. In recent years, genetic analysis and proposed mathematical models have explained the dynamics of the crosstalk between the Notch and Wnt pathways. Here, we will summarize the major findings concerning the molecular mechanisms of the interactions between the two signaling pathways. First, Dishevelled 2 (Dvl2) plays a dual role, acting as an activator of Wnt signaling and an inhibitor of Notch activity. Dvl2 blocks Notch signaling directly after interacting with the Notch carboxyl terminus, which results in the disruption of the lateral inhibition signal mediated by Notch in the sensory mother cells (SMCs) of *Drosophila* [138] (Figure 5). Collu *et al.* [139], found that Dvl2 binds and inhibits Rbp-J proteins in order to suppress the transcriptional activity of the Rbp-J-NICD-Maml transcriptional activator complex during *Xenopus* epidermal development (Figure 5). The crosstalk mechanism is conserved between vertebrates and invertebrates, as Dvl2 targets the unique and common pathway component, Rbp-J, a core player in conventional Notch signaling. The similar inhibition of Notch signaling by Dvl2 has been shown during the establishment of planar polarity in the *Drosophila* eye and leg epithelium [140,141]. The regulation of Notch signaling by the Wnt pathway is shown by the negative effect of Wnt on the Dvl2-mediated GSK3β activity. GSK3β stabilizes the Notch-IC by binding and phosphorylating Notch-IC in the embryonic fibroblasts and N2a cells [142], and GSK-3β inhibition leads to the degradation of Notch-IC mediated by the proteasome (Figure 5). Furthermore, Notch can directly interact with β-catenin. Notch regulates the stability and activity of Armadillo/β-catenin and negatively regulates β-catenin/TCF transcription in *Drosophila* [143]. In neural precursor cells and vascular progenitors, NICD inhibits β-catenin activity directly by forming a Notch/β-catenin/Rbp-J complex to prevent β-catenin from binding its target sites [144]. The protein complex may play a critical role in cell fate determination in various organs. Lastly, Wnt signaling inhibits Notch activity through Pygopus2 (Pygo2) to promote self-renewal and to prevent the premature differentiation of mammary stem cells (MaSCs) [145]. Pygo2, a histone methylation reader and a context-dependent Wnt/β-catenin coactivator, facilitates the binding of β-catenin to the Notch3 locus and maintains Notch3 in a bivalent chromatin structure in MaSCs [145]. The crosstalk between Wnt and Notch reinforces the balance among stem cells, progenitors and differentiated cells within a tissue, and these confirmed molecular interactions might occur in the pancreas.

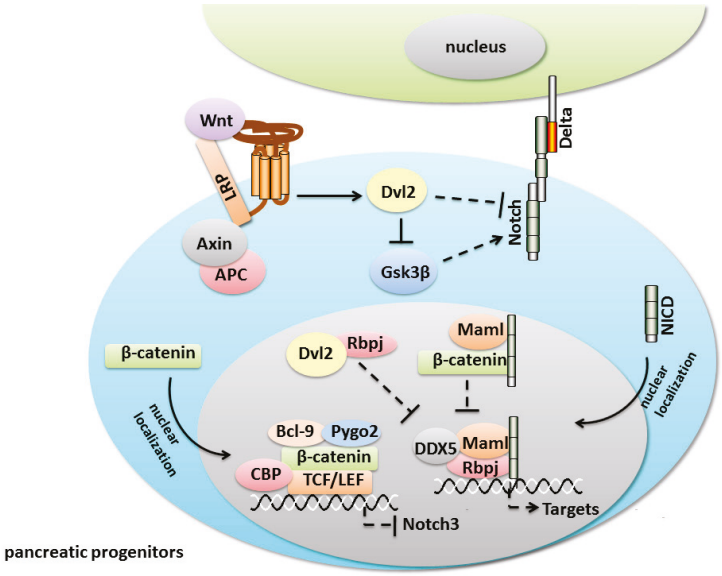

Figure 5. Inhibitory crosstalk between the Wingless and INT-1 (Wnt) and Notch pathways in pancreatic progenitor cells. The dashed lines signify that the mechanisms existing in the pancreas are unknown. The arrows represent activation whereas bar-headed lines represent inhibition.

5.2. Notch/FGF Crosstalk

FGF signaling from the pancreatic mesenchyme has been shown to play an essential role in pancreatic development and the pancreatic disease process. Studies using recombined models of embryonic tissues have shown that pancreatic buds can develop *in vitro* but will not undergo any growth or branching morphogenesis without the presence of the mesenchyme [146,147]. FGF10 signaling plays a crucial mitogenic role in driving the proliferation of pancreatic progenitor cells [64,148,149]. In *FGF10*$^{-/-}$ mouse embryos, the proliferation of Pdx1^{+} progenitor cells was reduced, but the growth, differentiation and branching morphogenesis of the pancreatic epithelia were arrested [148]. In mice, the persistent expression of *FGF10* mediated by the Ipf1/Pdx1 promoter increased the proliferation of pancreatic progenitor cells and arrested them in a pluripotent state [110]. Furthermore, the expression of Notch1 and Hes1 was maintained in the pancreatic epithelium, along with the reduction of Ngn3 [110]. The persistent expression of *FGF10* perturbs the expression of Suppressor enhancer lin12/Notch 1-like (Sel1l), which regulates pancreatic epithelial growth and differentiation by suppressing Notch signaling in mice [110,150]. The phenotype of mice with an overexpression of *FGF10* is similar to that of the mice with Notch overexpression described above. Thus, Notch signaling is a critical downstream effector of FGF pathway-induced embryonic pancreatic epithelial proliferation (Figure 6). FGF-stimulated progenitor cell maintenance via Notch signaling has been previously reported in several developmental contexts. During tracheal cell invagination in *Drosophila*, the FGF-like ligand Branchless activates the FGF-receptor, and the downstream MAPK signaling causes the upregulation of Δ [151]. Likewise, FGF10 is capable of maintaining the dental epithelial precursor pool via the stimulation of Hes1 in Fringe-dependent or Fringe-independent manners in the developing tooth [152]. However, whether the above mechanisms exist in the pancreas is unknown (Figure 6). Recently, mouse genetic studies have revealed that there is a FGF10/FGFR2b/Sox9 feed-forward loop in early pancreatic progenitors to maintain their proliferation [31] (Figure 6). Thus, Sox9 acts as the conduit between FGF10 and Notch in the proliferation of progenitors.

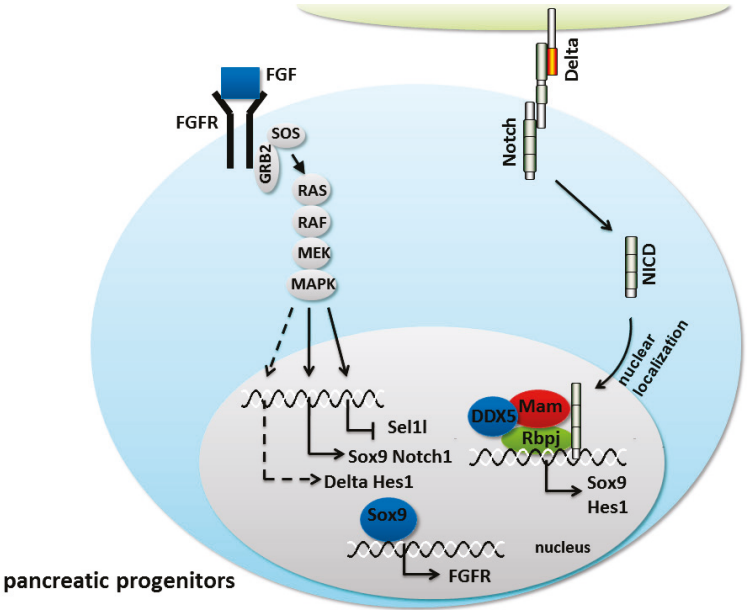

Figure 6. The crosstalk between the fibroblast growth factor (FGF) and Notch pathways in pancreatic progenitors. The dashed lines signify that the mechanisms existing in the pancreas are unknown. The arrows represent activation whereas bar-headed lines represent inhibition.

Classic culture explant experiments highlight the importance of the mesenchyme for exocrine pancreatic growth and differentiation [153,154]. In *Pdx1-FGF4* transgenic mice, the pancreas has degenerated ductal and destructive endocrine tissue [155]. However, the exact function of FGF signaling on β-cell development remains controversial. For example, studies on the *FGF10* knockout mice have suggested that FGF10 could directly and positively control the final number of β-cells [148,156,157]. Mice with attenuated FGFR1c have a decreased number of β-cells and develop diabetes. [158]. On the other hand, the overexpression of FGF10 in the pancreas inhibited endocrine fate by increasing Notch signaling in both mice and rats [110,159].

6. Conclusions and Future Perspective

The Notch pathway regulates cell fate and homeostasis during the development and postnatal life of self-renewing tissues. It not only plays important roles in the pancreas but also regulates self-renewal, lineage specification and differentiation of stem cells in other systems. Notch signaling functions at different time and at different levels during the development of the central nervous system (CNS). Initially, the Notch pathway enhances the neural precursor proliferation and represses their differentiation [160,161]. At later stages, Notch signaling promotes astrocyte differentiation and inhibits oligodendrocyte generation [162]. Notch signaling maintains self-renewal of the early muscle progenitors and regulates their differentiation during embryonic development and adulthood [163,164]. Studies with flies, nematodes, and vertebrates have revealed that Notch signaling is an evolutionarily conserved mechanism and specifies cell fates through local cell interactions in nearly all tissues [165–167]. However, there may be species- and tissue-specific differences in the precise roles of the Notch pathway in regulating stem cells and their fate. Notch signaling is an important player that operates sequentially and spatially to affect different aspects of pancreas formation. During early pancreatic development, distinct levels of Notch signaling at two different transition stages trigger the proliferation and differentiation of progenitors; strict control of the time and dosage of the Notch signaling components is necessary for proper organ homeostasis. We speculate that the Notch-mediated regulation of endocrine or exocrine differentiation may be more complex than we currently understand.

Acknowledgments: We apologize to the authors of those primary works that are not cited in this review due to space constraints. We are thankful to Yicheng Zhao and Delin Kong for their editing work on our manuscript and figures. This work was supported by the National Natural Science Foundation of China (No. 31472159, J1210053).

Author Contributions: Xu-Yan Li contributed to the drafting and editing of the manuscript. Wen-Jun Zhai participated in literature search. Chun-Bo Teng conceived the paper design, and supervised the writing, editing and proofreading of the paper. All authors have read and approved the final manuscript for publication.

Conflicts of Interest: The authors declare no conflict of interest.

References

1. Artavanis-Tsakonas, S.; Matsuno, K.; Fortini, M.E. Notch signaling. *Science* **1995**, *268*, 225–232. [CrossRef] [PubMed]
2. Bray, S. Notch signalling in drosophila: Three ways to use a pathway. *Semin. Cell Dev. Biol.* **1998**, *9*, 591–597. [CrossRef] [PubMed]
3. Buono, K.D.; Robinson, G.W.; Martin, C.; Shi, S.; Stanley, P.; Tanigaki, K.; Honjo, T.; Hennighausen, L. The canonical Notch/Rbp-j signaling pathway controls the balance of cell lineages in mammary epithelium during pregnancy. *Dev. Biol.* **2006**, *293*, 565–580. [CrossRef] [PubMed]
4. Kopan, R.; Ilagan, M.X. The canonical Notch signaling pathway: Unfolding the activation mechanism. *Cell* **2009**, *137*, 216–233. [CrossRef] [PubMed]
5. Yugawa, T.; Nishino, K.; Ohno, S.; Nakahara, T.; Fujita, M.; Goshima, N.; Umezawa, A.; Kiyono, T. Noncanonical Notch signaling limits self-renewal of human epithelial and induced pluripotent stem cells through rock activation. *Mol. Cell. Biol.* **2013**, *33*, 4434–4447. [CrossRef] [PubMed]

6. Layden, M.J.; Martindale, M.Q. Non-canonical Notch signaling represents an ancestral mechanism to regulate neural differentiation. *Evodevo* **2014**, *5*, 30. [CrossRef] [PubMed]
7. Pezeron, G.; Millen, K.; Boukhatmi, H.; Bray, S. Notch directly regulates the cell morphogenesis genes *Reck*, *talin* and *trio* in adult muscle progenitors. *J. Cell Sci.* **2014**, *127*, 4634–4644. [CrossRef] [PubMed]
8. De Back, W.; Zhou, J.X.; Brusch, L. On the role of lateral stabilization during early patterning in the pancreas. *J. R. Soc. Interface* **2013**, *10*, 20120766. [CrossRef] [PubMed]
9. Kim, W.; Shin, Y.K.; Kim, B.J.; Egan, J.M. Notch signaling in pancreatic endocrine cell and diabetes. *Biochem. Biophys. Res. Commun.* **2010**, *392*, 247–251. [CrossRef] [PubMed]
10. Le Caignec, C. Human diseases and Notch receptors. *Med. Sci.* **2011**, *27*, 593–595.
11. Polychronidou, E.; Vlachakis, D.; Vlamos, P.; Baumann, M.; Kossida, S. Notch signaling and ageing. *Adv. Exp. Med. Biol.* **2015**, *822*, 25–36. [PubMed]
12. Bi, P.; Kuang, S. Notch signaling as a novel regulator of metabolism. *Trends Endocrinol. Metab.* **2015**, *26*, 248–255. [CrossRef] [PubMed]
13. Grishina, I.B. Mini-review: Does Notch promote or suppress cancer? New findings and old controversies. *Am. J. Clin. Exp. Urol.* **2015**, *3*, 24–27. [PubMed]
14. Murtaugh, L.C.; Stanger, B.Z.; Kwan, K.M.; Melton, D.A. Notch signaling controls multiple steps of pancreatic differentiation. *Proc. Natl. Acad. Sci. USA* **2003**, *100*, 14920–14925. [CrossRef] [PubMed]
15. Greenwood, A.L.; Li, S.; Jones, K.; Melton, D.A. Notch signaling reveals developmental plasticity of pax4(+) pancreatic endocrine progenitors and shunts them to a duct fate. *Mech. Dev.* **2007**, *124*, 97–107. [CrossRef] [PubMed]
16. Afelik, S.; Jensen, J. Notch signaling in the pancreas: Patterning and cell fate specification. *Dev. Biol.* **2013**, *2*, 531–544. [CrossRef] [PubMed]
17. Hald, J.; Hjorth, J.P.; German, M.S.; Madsen, O.D.; Serup, P.; Jensen, J. Activated Notch1 prevents differentiation of pancreatic acinar cells and attenuate endocrine development. *Dev. Biol.* **2003**, *260*, 426–437. [CrossRef]
18. Ahnfelt-Ronne, J.; Hald, J.; Bodker, A.; Yassin, H.; Serup, P.; Hecksher-Sorensen, J. Preservation of proliferating pancreatic progenitor cells by δ-Notch signaling in the embryonic chicken pancreas. *BMC Dev. Biol.* **2007**, *7*, 63. [CrossRef] [PubMed]
19. Zecchin, E.; Filippi, A.; Biemar, F.; Tiso, N.; Pauls, S.; Ellertsdottir, E.; Gnugge, L.; Bortolussi, M.; Driever, W.; Argenton, F. Distinct *δ* and *jagged* genes control sequential segregation of pancreatic cell types from precursor pools in zebrafish. *Dev. Biol.* **2007**, *301*, 192–204. [CrossRef] [PubMed]
20. Nakhai, H.; Siveke, J.T.; Klein, B.; Mendoza-Torres, L.; Mazur, P.K.; Algul, H.; Radtke, F.; Strobl, L.; Zimber-Strobl, U.; Schmid, R.M. Conditional ablation of Notch signaling in pancreatic development. *Development* **2008**, *135*, 2757–2765. [CrossRef] [PubMed]
21. Ahnfelt-Ronne, J.; Jorgensen, M.C.; Klinck, R.; Jensen, J.N.; Fuchtbauer, E.M.; Deering, T.; MacDonald, R.J.; Wright, C.V.; Madsen, O.D.; Serup, P. Ptf1a-mediated control of Dll1 reveals an alternative to the lateral inhibition mechanism. *Development* **2012**, *139*, 33–45. [CrossRef] [PubMed]
22. Shih, H.P.; Kopp, J.L.; Sandhu, M.; Dubois, C.L.; Seymour, P.A.; Grapin-Botton, A.; Sander, M. A Notch-dependent molecular circuitry initiates pancreatic endocrine and ductal cell differentiation. *Development* **2012**, *139*, 2488–2499. [CrossRef] [PubMed]
23. Shimajiri, Y.; Kosaka, Y.; Scheel, D.W.; Lynn, F.C.; Kishimoto, N.; Wang, J.; Zhao, S.; German, M.S. A mouse model for monitoring islet cell genesis and developing therapies for diabetes. *Dis. Model. Mech.* **2011**, *4*, 268–276. [CrossRef] [PubMed]
24. Afelik, S.; Qu, X.; Hasrouni, E.; Bukys, M.A.; Deering, T.; Nieuwoudt, S.; Rogers, W.; Macdonald, R.J.; Jensen, J. Notch-mediated patterning and cell fate allocation of pancreatic progenitor cells. *Development* **2012**, *139*, 1744–1753. [CrossRef] [PubMed]
25. Hosokawa, S.; Furuyama, K.; Horiguchi, M.; Aoyama, Y.; Tsuboi, K.; Sakikubo, M.; Goto, T.; Hirata, K.; Tanabe, W.; Nakano, Y.; *et al*. Impact of Sox9 dosage and Hes1-mediated Notch signaling in controlling the plasticity of adult pancreatic duct cells in mice. *Sci. Rep.* **2015**, *5*, 8518. [CrossRef] [PubMed]
26. Ninov, N.; Borius, M.; Stainier, D.Y. Different levels of Notch signaling regulate quiescence, renewal and differentiation in pancreatic endocrine progenitors. *Development* **2012**, *139*, 1557–1567. [CrossRef] [PubMed]
27. Bhanot, U.; Kohntop, R.; Hasel, C.; Moller, P. Evidence of Notch pathway activation in the ectatic ducts of chronic pancreatitis. *J. Pathol.* **2008**, *214*, 312–319. [CrossRef] [PubMed]

28. Pinho, A.V.; Rooman, I.; Reichert, M.; de Medts, N.; Bouwens, L.; Rustgi, A.K.; Real, F.X. Adult pancreatic acinar cells dedifferentiate to an embryonic progenitor phenotype with concomitant activation of a senescence programme that is present in chronic pancreatitis. *Gut* **2011**, *60*, 958–966. [CrossRef] [PubMed]
29. Chetty, R.; Serra, S.; Salahshor, S.; Alsaad, K.; Shih, W.; Blaszyk, H.; Woodgett, J.R.; Tsao, M.S. Expression of wnt-signaling pathway proteins in intraductal papillary mucinous neoplasms of the pancreas: A tissue microarray analysis. *Hum. Pathol.* **2006**, *37*, 212–217. [CrossRef] [PubMed]
30. Lin, C.L.; Vuguin, P.M. Determinants of pancreatic islet development in mice and men: A focus on the role of transcription factors. *Horm. Res. Paediatr.* **2012**, *77*, 205–213. [CrossRef] [PubMed]
31. Seymour, P.A.; Shih, H.P.; Patel, N.A.; Freude, K.K.; Xie, R.; Lim, C.J.; Sander, M. A Sox9/FGF feed-forward loop maintains pancreatic organ identity. *Development* **2012**, *139*, 3363–3372. [CrossRef] [PubMed]
32. Wolfe-Coote, S.A.; Louw, J.; Poerstamper, H.M.; Du Toit, D.F. Do the pancreatic primordial buds in embryogenesis have the potential to produce all pancreatic endocrine cells? *Med. Hypotheses* **1990**, *31*, 313–317. [CrossRef]
33. Merino, P.L. Developmental biology of the pancreas. *Cell Biochem. Biophys.* **2004**, *40*, 127–142. [CrossRef]
34. Herrera, P.L. Adult insulin- and glucagon-producing cells differentiate from two independent cell lineages. *Development* **2000**, *127*, 2317–2322. [PubMed]
35. Teitelman, G.; Alpert, S.; Polak, J.M.; Martinez, A.; Hanahan, D. Precursor cells of mouse endocrine pancreas coexpress insulin, glucagon and the neuronal proteins tyrosine hydroxylase and neuropeptide y, but not pancreatic polypeptide. *Development* **1993**, *118*, 1031–1039. [PubMed]
36. Kemp, J.D.; Walther, B.T.; Rutter, W.J. Protein synthesis during the secondary developmental transition of the embryonic rat pancreas. *J. Biol. Chem.* **1972**, *247*, 3941–3952. [PubMed]
37. Wang, J.; Kilic, G.; Aydin, M.; Burke, Z.; Oliver, G.; Sosa-Pineda, B. Prox1 activity controls pancreas morphogenesis and participates in the production of "secondary transition" pancreatic endocrine cells. *Dev. Biol.* **2005**, *286*, 182–194. [CrossRef] [PubMed]
38. Bouwens, L.; Rooman, I. Regulation of pancreatic β-cell mass. *Physiol. Rev.* **2005**, *85*, 1255–1270. [CrossRef] [PubMed]
39. Offield, M.F.; Jetton, T.L.; Labosky, P.A.; Ray, M.; Stein, R.W.; Magnuson, M.A.; Hogan, B.L.; Wright, C.V. Pdx-1 is required for pancreatic outgrowth and differentiation of the rostral duodenum. *Development* **1996**, *122*, 983–995. [PubMed]
40. Arda, H.E.; Benitez, C.M.; Kim, S.K. Gene regulatory networks governing pancreas development. *Dev. Cell* **2013**, *25*, 5–13. [CrossRef] [PubMed]
41. Bonal, C.; Herrera, P.L. Genes controlling pancreas ontogeny. *Int. J. Dev. Biol.* **2008**, *52*, 823–835. [CrossRef] [PubMed]
42. Wu, H.; MacFarlane, W.M.; Tadayyon, M.; Arch, J.R.; James, R.F.; Docherty, K. Insulin stimulates pancreatic-duodenal homoeobox factor-1 (PDX1) DNA-binding activity and insulin promoter activity in pancreatic β cells. *Biochem. J.* **1999**, *344*, 813–818. [CrossRef] [PubMed]
43. Lynn, F.C.; Smith, S.B.; Wilson, M.E.; Yang, K.Y.; Nekrep, N.; German, M.S. Sox9 coordinates a transcriptional network in pancreatic progenitor cells. *Proc. Natl. Acad. Sci. USA* **2007**, *104*, 10500–10505. [CrossRef] [PubMed]
44. Hald, J.; Sprinkel, A.E.; Ray, M.; Serup, P.; Wright, C.; Madsen, O.D. Generation and characterization of Ptf1a antiserum and localization of Ptf1a in relation to Nkx6.1 and Pdx1 during the earliest stages of mouse pancreas development. *J. Histochem. Cytochem.* **2008**, *56*, 587–595. [CrossRef] [PubMed]
45. Seymour, P.A.; Freude, K.K.; Tran, M.N.; Mayes, E.E.; Jensen, J.; Kist, R.; Scherer, G.; Sander, M. Sox9 is required for maintenance of the pancreatic progenitor cell pool. *Proc. Natl. Acad. Sci. USA* **2007**, *104*, 1865–1870. [CrossRef] [PubMed]
46. Rodolosse, A.; Chalaux, E.; Adell, T.; Hagege, H.; Skoudy, A.; Real, F.X. Ptf1α/p48 transcription factor couples proliferation and differentiation in the exocrine pancreas [corrected]. *Gastroenterology* **2004**, *127*, 937–949. [CrossRef] [PubMed]
47. Gradwohl, G.; Dierich, A.; LeMeur, M.; Guillemot, F. *Neurogenin3* is required for the development of the four endocrine cell lineages of the pancreas. *Proc. Natl. Acad. Sci. USA* **2000**, *97*, 1607–1611. [CrossRef] [PubMed]
48. Beucher, A.; Gjernes, E.; Collin, C.; Courtney, M.; Meunier, A.; Collombat, P.; Gradwohl, G. The homeodomain-containing transcription factors Arx and Pax4 control enteroendocrine subtype specification in mice. *PLoS ONE* **2012**, *7*, e36449. [CrossRef] [PubMed]

49. Juhl, K.; Sarkar, S.A.; Wong, R.; Jensen, J.; Hutton, J.C. Mouse pancreatic endocrine cell transcriptome defined in the embryonic Ngn3-null mouse. *Diabetes* **2008**, *57*, 2755–2761. [CrossRef] [PubMed]
50. Kim, S.Y.; Rane, S.G. The Cdk4-E2F1 pathway regulates early pancreas development by targeting $PDX1^+$ progenitors and $Ngn3^+$ endocrine precursors. *Development* **2011**, *138*, 1903–1912. [CrossRef] [PubMed]
51. Piccand, J.; Meunier, A.; Merle, C.; Jia, Z.; Barnier, J.V.; Gradwohl, G. Pak3 promotes cell cycle exit and differentiation of β-cells in the embryonic pancreas and is necessary to maintain glucose homeostasis in adult mice. *Diabetes* **2014**, *63*, 203–215. [CrossRef] [PubMed]
52. Krapp, A.; Knofler, M.; Frutiger, S.; Hughes, G.J.; Hagenbuchle, O.; Wellauer, P.K. The p48 DNA-binding subunit of transcription factor Ptf1 is a new exocrine pancreas-specific basic helix-loop-helix protein. *EMBO J.* **1996**, *15*, 4317–4329. [PubMed]
53. Cockell, M.; Stevenson, B.J.; Strubin, M.; Hagenbuchle, O.; Wellauer, P.K. Identification of a cell-specific DNA-binding activity that interacts with a transcriptional activator of genes expressed in the acinar pancreas. *Mol. Cell. Biol.* **1989**, *9*, 2464–2476. [CrossRef] [PubMed]
54. Dong, P.D.; Provost, E.; Leach, S.D.; Stainier, D.Y. Graded levels of Ptf1a differentially regulate endocrine and exocrine fates in the developing pancreas. *Genes Dev.* **2008**, *22*, 1445–1450. [CrossRef] [PubMed]
55. Schaffer, A.E.; Freude, K.K.; Nelson, S.B.; Sander, M. Nkx6 transcription factors and Ptf1a function as antagonistic lineage determinants in multipotent pancreatic progenitors. *Dev. Cell* **2010**, *18*, 1022–1029. [CrossRef] [PubMed]
56. Lynn, F.C.; Skewes-Cox, P.; Kosaka, Y.; McManus, M.T.; Harfe, B.D.; German, M.S. Microrna expression is required for pancreatic islet cell genesis in the mouse. *Diabetes* **2007**, *56*, 2938–2945. [CrossRef] [PubMed]
57. Latreille, M.; Hausser, J.; Stutzer, I.; Zhang, Q.; Hastoy, B.; Gargani, S.; Kerr-Conte, J.; Pattou, F.; Zavolan, M.; Esguerra, J.L.; *et al*. Microrna-7a regulates pancreatic β cell function. *J. Clin. Investig.* **2014**, *124*, 2722–2735. [CrossRef] [PubMed]
58. Poy, M.N.; Hausser, J.; Trajkovski, M.; Braun, M.; Collins, S.; Rorsman, P.; Zavolan, M.; Stoffel, M. miR-375 maintains normal pancreatic α- and β-cell mass. *Proc. Natl. Acad. Sci. USA* **2009**, *106*, 5813–5818. [CrossRef] [PubMed]
59. Zhang, Z.W.; Men, T.; Feng, R.C.; Li, Y.C.; Zhou, D.; Teng, C.B. miR-375 inhibits proliferation of mouse pancreatic progenitor cells by targeting YAP1. *Cell. Physiol. Biochem.* **2013**, *32*, 1808–1817. [PubMed]
60. Zhang, Z.W.; Zhang, L.Q.; Ding, L.; Wang, F.; Sun, Y.J.; An, Y.; Zhao, Y.; Li, Y.H.; Teng, C.B. Microrna-19b downregulates insulin 1 through targeting transcription factor neurod1. *FEBS Lett.* **2011**, *585*, 2592–2598. [PubMed]
61. Yang, Y.; Ding, L.; An, Y.; Zhang, Z.W.; Lang, Y.; Tai, S.; Guo, F.; Teng, C.B. miR-18a regulates expression of the pancreatic transcription factor Ptf1a in pancreatic progenitor and acinar cells. *FEBS Lett.* **2012**, *586*, 422–427. [PubMed]
62. Joglekar, M.V.; Parekh, V.S.; Mehta, S.; Bhonde, R.R.; Hardikar, A.A. Microrna profiling of developing and regenerating pancreas reveal post-transcriptional regulation of neurogenin3. *Dev. Biol.* **2007**, *311*, 603–612. [PubMed]
63. Cano, D.A.; Soria, B.; Martin, F.; Rojas, A. Transcriptional control of mammalian pancreas organogenesis. *Cell. Mol. Life Sci.* **2014**, *71*, 2383–2402. [CrossRef] [PubMed]
64. Talavera-Adame, D.; Dafoe, D.C. Endothelium-derived essential signals involved in pancreas organogenesis. *World J. Exp. Med.* **2015**, *5*, 40–49. [CrossRef] [PubMed]
65. Fleming, R.J.; Purcell, K.; Artavanis-Tsakonas, S. The Notch receptor and its ligands. *Trends Cell Biol.* **1997**, *7*, 437–441. [CrossRef]
66. Bray, S. Notch. *Curr. Biol.* **2000**, *10*, R433–R435. [CrossRef]
67. Logeat, F.; Bessia, C.; Brou, C.; LeBail, O.; Jarriault, S.; Seidah, N.G.; Israel, A. The Notch1 receptor is cleaved constitutively by a furin-like convertase. *Proc. Natl. Acad. Sci. USA* **1998**, *95*, 8108–8112. [CrossRef] [PubMed]
68. Lake, R.J.; Grimm, L.M.; Veraksa, A.; Banos, A.; Artavanis-Tsakonas, S. *In vivo* analysis of the Notch receptor s1 cleavage. *PLoS ONE* **2009**, *4*, e6728. [CrossRef] [PubMed]
69. Lubman, O.Y.; Ilagan, M.X.; Kopan, R.; Barrick, D. Quantitative dissection of the Notch:CSL interaction: Insights into the Notch-mediated transcriptional switch. *J. Mol. Biol.* **2007**, *365*, 577–589. [CrossRef] [PubMed]
70. Bray, S.; Furriols, M. Notch pathway: Making sense of suppressor of hairless. *Curr. Biol.* **2001**, *11*, R217–R221. [CrossRef]
71. Bray, S.; Bernard, F. Notch targets and their regulation. *Curr. Top. Dev. Biol.* **2010**, *92*, 253–275. [PubMed]

72. Fukuda, A.; Kawaguchi, Y.; Furuyama, K.; Kodama, S.; Horiguchi, M.; Kuhara, T.; Koizumi, M.; Boyer, D.F.; Fujimoto, K.; Doi, R.; *et al*. Ectopic pancreas formation in *Hes1* -knockout mice reveals plasticity of endodermal progenitors of the gut, bile duct, and pancreas. *J. Clin. Investig.* **2006**, *116*, 1484–1493. [CrossRef] [PubMed]
73. Murai, K.; Philpott, A.; Jones, P.H. *Hes6* is required for the neurogenic activity of neurogenin and neurod. *PLoS ONE* **2011**, *6*, e27880. [CrossRef] [PubMed]
74. Petrovic, J.; Galvez, H.; Neves, J.; Abello, G.; Giraldez, F. Differential regulation of *Hes/Hey* genes during inner ear development. *Dev. Neurobiol.* **2015**, *75*, 703–720. [CrossRef] [PubMed]
75. Lee, J.C.; Smith, S.B.; Watada, H.; Lin, J.; Scheel, D.; Wang, J.; Mirmira, R.G.; German, M.S. Regulation of the pancreatic pro-endocrine gene *neurogenin3*. *Diabetes* **2001**, *50*, 928–936. [CrossRef] [PubMed]
76. Qu, X.; Afelik, S.; Jensen, J.N.; Bukys, M.A.; Kobberup, S.; Schmerr, M.; Xiao, F.; Nyeng, P.; Veronica Albertoni, M.; Grapin-Botton, A.; *et al*. Notch-mediated post-translational control of Ngn3 protein stability regulates pancreatic patterning and cell fate commitment. *Dev. Biol.* **2013**, *376*, 1–12. [CrossRef] [PubMed]
77. Sakano, D.; Kato, A.; Parikh, N.; McKnight, K.; Terry, D.; Stefanovic, B.; Kato, Y. *Bcl6* canalizes Notch-dependent transcription, excluding mastermind-like1 from selected target genes during left-right patterning. *Dev. Cell* **2010**, *18*, 450–462. [CrossRef] [PubMed]
78. Itoh, M.; Kim, C.H.; Palardy, G.; Oda, T.; Jiang, Y.J.; Maust, D.; Yeo, S.Y.; Lorick, K.; Wright, G.J.; Ariza-McNaughton, L.; *et al*. Mind bomb is a ubiquitin ligase that is essential for efficient activation of Notch signaling by δ. *Dev. Cell* **2003**, *4*, 67–82. [CrossRef]
79. Horn, S.; Kobberup, S.; Jorgensen, M.C.; Kalisz, M.; Klein, T.; Kageyama, R.; Gegg, M.; Lickert, H.; Lindner, J.; Magnuson, M.A.; *et al*. *Mind bomb 1* is required for pancreatic β-cell formation. *Proc. Natl. Acad. Sci. USA* **2012**, *109*, 7356–7361. [CrossRef] [PubMed]
80. Kang, K.; Lee, D.; Hong, S.; Park, S.G.; Song, M.R. The E3 ligase mind bomb-1 (Mib1) modulates δ-Notch signaling to control neurogenesis and gliogenesis in the developing spinal cord. *J. Biol. Chem.* **2013**, *288*, 2580–2592. [CrossRef] [PubMed]
81. Ishitani, T.; Hirao, T.; Suzuki, M.; Isoda, M.; Ishitani, S.; Harigaya, K.; Kitagawa, M.; Matsumoto, K.; Itoh, M. Nemo-like kinase suppresses Notch signalling by interfering with formation of the Notch active transcriptional complex. *Nat. Cell Biol.* **2010**, *12*, 278–285. [CrossRef] [PubMed]
82. Lin, S.; Tian, L.; Shen, H.; Gu, Y.; Li, J.L.; Chen, Z.; Sun, X.; You, M.J.; Wu, L. DDX5 is a positive regulator of oncogenic Notch1 signaling in T cell acute lymphoblastic leukemia. *Oncogene* **2013**, *32*, 4845–4853. [CrossRef] [PubMed]
83. Xu, Y.; Wang, S.; Zhang, J.; Zhao, A.; Stanger, B.Z.; Gu, G. The fringe molecules induce endocrine differentiation in embryonic endoderm by activating *cMyt1/cMyt3*. *Dev. Biol.* **2006**, *297*, 340–349. [CrossRef] [PubMed]
84. Svensson, P.; Bergqvist, I.; Norlin, S.; Edlund, H. Mfng is dispensable for mouse pancreas development and function. *Mol. Cell. Biol.* **2009**, *29*, 2129–2138. [CrossRef] [PubMed]
85. Rana, N.A.; Haltiwanger, R.S. Fringe benefits: Functional and structural impacts of *O*-glycosylation on the extracellular domain of Notch receptors. *Curr. Opin. Struct. Biol.* **2011**, *21*, 583–589. [CrossRef] [PubMed]
86. Takeuchi, H.; Haltiwanger, R.S. Significance of glycosylation in Notch signaling. *Biochem. Biophys. Res. Commun.* **2014**, *453*, 235–242. [CrossRef] [PubMed]
87. Blobel, C.P. Adams: Key components in egfr signalling and development. *Nat. Rev. Mol. Cell Biol.* **2005**, *6*, 32–43. [CrossRef] [PubMed]
88. Groot, A.J.; Vooijs, M.A. The role of adams in Notch signaling. *Adv. Exp. Med. Biol.* **2012**, *727*, 15–36. [PubMed]
89. Christian, L.M. The adam family: Insights into Notch proteolysis. *Fly* **2012**, *6*, 30–34. [CrossRef] [PubMed]
90. Asayesh, A.; Alanentalo, T.; Khoo, N.K.; Ahlgren, U. Developmental expression of metalloproteases ADAM 9, 10, and 17 becomes restricted to divergent pancreatic compartments. *Dev. Dny.* **2005**, *232*, 1105–1114. [CrossRef] [PubMed]
91. Dyczynska, E.; Sun, D.; Yi, H.; Sehara-Fujisawa, A.; Blobel, C.P.; Zolkiewska, A. Proteolytic processing of δ-like 1 by ADAM proteases. *J. Biol. Chem.* **2007**, *282*, 436–444. [CrossRef] [PubMed]

92. Tousseyn, T.; Thathiah, A.; Jorissen, E.; Raemaekers, T.; Konietzko, U.; Reiss, K.; Maes, E.; Snellinx, A.; Serneels, L.; Nyabi, O.; *et al*. ADAM10, the rate-limiting protease of regulated intramembrane proteolysis of Notch and other proteins, is processed by ADAMs-9, ADAMs-15, and the γ-secretase. *J. Biol. Chem.* **2009**, *284*, 11738–11747. [CrossRef] [PubMed]
93. Apelqvist, A.; Li, H.; Sommer, L.; Beatus, P.; Anderson, D.J.; Honjo, T.; Hrabe de Angelis, M.; Lendahl, U.; Edlund, H. Notch signalling controls pancreatic cell differentiation. *Nature* **1999**, *400*, 877–881. [PubMed]
94. Lammert, E.; Brown, J.; Melton, D.A. Notch gene expression during pancreatic organogenesis. *Mech. Dev.* **2000**, *94*, 199–203. [CrossRef]
95. Bettenhausen, B.; Hrabe de Angelis, M.; Simon, D.; Guenet, J.L.; Gossler, A. Transient and restricted expression during mouse embryogenesis of Dll1, a murine gene closely related to Drosophila δ. *Development* **1995**, *121*, 2407–2418. [PubMed]
96. Golson, M.L.; le Lay, J.; Gao, N.; Bramswig, N.; Loomes, K.M.; Oakey, R.; May, C.L.; White, P.; Kaestner, K.H. Jagged1 is a competitive inhibitor of Notch signaling in the embryonic pancreas. *Mech. Dev.* **2009**, *126*, 687–699. [CrossRef] [PubMed]
97. Parsons, M.J.; Pisharath, H.; Yusuff, S.; Moore, J.C.; Siekmann, A.F.; Lawson, N.; Leach, S.D. Notch-responsive cells initiate the secondary transition in larval zebrafish pancreas. *Mech. Dev.* **2009**, *126*, 898–912. [CrossRef] [PubMed]
98. Rovira, M.; Scott, S.G.; Liss, A.S.; Jensen, J.; Thayer, S.P.; Leach, S.D. Isolation and characterization of centroacinar/terminal ductal progenitor cells in adult mouse pancreas. *Proc. Natl. Acad. Sci. USA* **2010**, *107*, 75–80. [CrossRef] [PubMed]
99. Su, Y.; Buchler, P.; Gazdhar, A.; Giese, N.; Reber, H.A.; Hines, O.J.; Giese, T.; Buchler, M.W.; Friess, H. Pancreatic regeneration in chronic pancreatitis requires activation of the Notch signaling pathway. *J. Gastrointest. Surg.* **2006**, *10*, 1230–1241. [CrossRef] [PubMed]
100. Baeyens, L.; Bonne, S.; Bos, T.; Rooman, I.; Peleman, C.; Lahoutte, T.; German, M.; Heimberg, H.; Bouwens, L. Notch signaling as gatekeeper of rat acinar-to-β-cell conversion *in vitro*. *Gastroenterology* **2009**, *136*, 1750–1760. [CrossRef] [PubMed]
101. Jensen, J.N.; Cameron, E.; Garay, M.V.; Starkey, T.W.; Gianani, R.; Jensen, J. Recapitulation of elements of embryonic development in adult mouse pancreatic regeneration. *Gastroenterology* **2005**, *128*, 728–741. [CrossRef] [PubMed]
102. Fujikura, J.; Hosoda, K.; Iwakura, H.; Tomita, T.; Noguchi, M.; Masuzaki, H.; Tanigaki, K.; Yabe, D.; Honjo, T.; Nakao, K. Notch/Rbp-j signaling prevents premature endocrine and ductal cell differentiation in the pancreas. *Cell Matab.* **2006**, *3*, 59–65. [CrossRef] [PubMed]
103. Jensen, J.; Pedersen, E.E.; Galante, P.; Hald, J.; Heller, R.S.; Ishibashi, M.; Kageyama, R.; Guillemot, F.; Serup, P.; Madsen, O.D. Control of endodermal endocrine development by Hes-1. *Nat. Genet.* **2000**, *24*, 36–44. [PubMed]
104. Sommer, L.; Ma, Q.; Anderson, D.J. *Neurogenins*, a novel family of *atonal*-related bHLH transcription factors, are putative mammalian neuronal determination genes that reveal progenitor cell heterogeneity in the developing CNS and PNS. *Mol. Cell. Neurosci.* **1996**, *8*, 221–241. [CrossRef] [PubMed]
105. Beatus, P.; Lundkvist, J.; Oberg, C.; Lendahl, U. The Notch 3 intracellular domain represses Notch 1-mediated activation through hairy/enhancer of split (Hes) promoters. *Development* **1999**, *126*, 3925–3935. [PubMed]
106. Esni, F.; Ghosh, B.; Biankin, A.V.; Lin, J.W.; Albert, M.A.; Yu, X.; MacDonald, R.J.; Civin, C.I.; Real, F.X.; Pack, M.A.; *et al*. Notch inhibits Ptf1 function and acinar cell differentiation in developing mouse and zebrafish pancreas. *Development* **2004**, *131*, 4213–4224. [CrossRef] [PubMed]
107. Kopinke, D.; Brailsford, M.; Shea, J.E.; Leavitt, R.; Scaife, C.L.; Murtaugh, L.C. Lineage tracing reveals the dynamic contribution of Hes1^{+} cells to the developing and adult pancreas. *Development* **2011**, *138*, 431–441. [CrossRef] [PubMed]
108. Cras-Meneur, C.; Li, L.; Kopan, R.; Permutt, M.A. Presenilins, Notch dose control the fate of pancreatic endocrine progenitors during a narrow developmental window. *Genes Dev.* **2009**, *23*, 2088–2101. [CrossRef] [PubMed]
109. Kopinke, D.; Brailsford, M.; Pan, F.C.; Magnuson, M.A.; Wright, C.V.; Murtaugh, L.C. Ongoing Notch signaling maintains phenotypic fidelity in the adult exocrine pancreas. *Dev. Biol.* **2012**, *362*, 57–64. [CrossRef] [PubMed]

110. Hart, A.; Papadopoulou, S.; Edlund, H. FGF10 maintains Notch activation, stimulates proliferation, and blocks differentiation of pancreatic epithelial cells. *Dev. Dny.* **2003**, *228*, 185–193. [CrossRef] [PubMed]
111. Thompson, N.; Gesina, E.; Scheinert, P.; Bucher, P.; Grapin-Botton, A. RNA profiling and chromatin immunoprecipitation-sequencing reveal that Ptf1a stabilizes pancreas progenitor identity via the control of MNX1/HLXB9 and a network of other transcription factors. *Mol. Cell. Biol.* **2012**, *32*, 1189–1199. [CrossRef] [PubMed]
112. Kawaguchi, Y.; Cooper, B.; Gannon, M.; Ray, M.; MacDonald, R.J.; Wright, C.V. The role of the transcriptional regulator Ptf1a in converting intestinal to pancreatic progenitors. *Nat. Genet.* **2002**, *32*, 128–134. [CrossRef] [PubMed]
113. Fukuda, A.; Kawaguchi, Y.; Furuyama, K.; Kodama, S.; Horiguchi, M.; Kuhara, T.; Kawaguchi, M.; Terao, M.; Doi, R.; Wright, C.V.; *et al*. Reduction of *Ptf1a* gene dosage causes pancreatic hypoplasia and diabetes in mice. *Diabetes* **2008**, *57*, 2421–2431. [CrossRef] [PubMed]
114. Norgaard, G.A.; Jensen, J.N.; Jensen, J. FGF10 signaling maintains the pancreatic progenitor cell state revealing a novel role of Notch in organ development. *Dev. Biol.* **2003**, *264*, 323–338. [CrossRef] [PubMed]
115. Miralles, F.; Lamotte, L.; Couton, D.; Joshi, R.L. Interplay between FGF10 and Notch signalling is required for the self-renewal of pancreatic progenitors. *Int. J. Dev. Biol.* **2006**, *50*, 17–26. [CrossRef] [PubMed]
116. Murata, K.; Hattori, M.; Hirai, N.; Shinozuka, Y.; Hirata, H.; Kageyama, R.; Sakai, T.; Minato, N. Hes1 directly controls cell proliferation through the transcriptional repression of $p27^{kip1}$. *Mol. Cell. Biol.* **2005**, *25*, 4262–4271. [CrossRef] [PubMed]
117. Georgia, S.; Soliz, R.; Li, M.; Zhang, P.; Bhushan, A. P57 and Hes1 coordinate cell cycle exit with self-renewal of pancreatic progenitors. *Dev. Biol.* **2006**, *298*, 22–31. [CrossRef] [PubMed]
118. McDonald, E.; Li, J.; Krishnamurthy, M.; Fellows, G.F.; Goodyer, C.G.; Wang, R. Sox9 regulates endocrine cell differentiation during human fetal pancreas development. *Int. J. Biochem. Cell Biol.* **2012**, *44*, 72–83. [CrossRef] [PubMed]
119. Siveke, J.T.; Lubeseder-Martellato, C.; Lee, M.; Mazur, P.K.; Nakhai, H.; Radtke, F.; Schmid, R.M. Notch signaling is required for exocrine regeneration after acute pancreatitis. *Gastroenterology* **2008**, *134*, 544–555. [CrossRef] [PubMed]
120. De la, O.J.; Emerson, L.L.; Goodman, J.L.; Froebe, S.C.; Illum, B.E.; Curtis, A.B.; Murtaugh, L.C. Notch and Kras reprogram pancreatic acinar cells to ductal intraepithelial neoplasia. *Proc. Natl. Acad. Sci. USA* **2008**, *105*, 18907–18912. [CrossRef] [PubMed]
121. Rooman, I.; de Medts, N.; Baeyens, L.; Lardon, J.; de Breuck, S.; Heimberg, H.; Bouwens, L. Expression of the Notch signaling pathway and effect on exocrine cell proliferation in adult rat pancreas. *Am. J. Pathol.* **2006**, *169*, 1206–1214. [CrossRef] [PubMed]
122. Mukhi, S.; Brown, D.D. Transdifferentiation of tadpole pancreatic acinar cells to duct cells mediated by Notch and stromelysin-3. *Dev. Biol.* **2011**, *351*, 311–317. [CrossRef] [PubMed]
123. Bar, Y.; Russ, H.A.; Knoller, S.; Ouziel-Yahalom, L.; Efrat, S. Hes-1 is involved in adaptation of adult human β-cells to proliferation *in vitro*. *Diabetes* **2008**, *57*, 2413–2420. [CrossRef] [PubMed]
124. Bar, Y.; Russ, H.A.; Sintov, E.; Anker-Kitai, L.; Knoller, S.; Efrat, S. Redifferentiation of expanded human pancreatic β-cell-derived cells by inhibition of the Notch pathway. *J. Biol. Chem.* **2012**, *287*, 17269–17280. [CrossRef] [PubMed]
125. Minami, K.; Seino, S. Pancreatic acinar-to-β cell transdifferentiation *in vitro*. *Front. Biosci.* **2008**, *13*, 5824–5837. [CrossRef] [PubMed]
126. Pires-daSilva, A.; Sommer, R.J. The evolution of signalling pathways in animal development. *Nat. Rev. Genet.* **2003**, *4*, 39–49. [CrossRef] [PubMed]
127. Baumgartner, B.K.; Cash, G.; Hansen, H.; Ostler, S.; Murtaugh, L.C. Distinct requirements for β-catenin in pancreatic epithelial growth and patterning. *Dev. Biol.* **2014**, *391*, 89–98. [CrossRef] [PubMed]
128. Afelik, S.; Pool, B.; Schmerr, M.; Penton, C.; Jensen, J. Wnt7b is required for epithelial progenitor growth and operates during epithelial-to-mesenchymal signaling in pancreatic development. *Dev. Biol.* **2015**, *399*, 204–217. [CrossRef] [PubMed]
129. Heiser, P.W.; Lau, J.; Taketo, M.M.; Herrera, P.L.; Hebrok, M. Stabilization of β-catenin impacts pancreas growth. *Development* **2006**, *133*, 2023–2032. [CrossRef] [PubMed]
130. Murtaugh, L.C.; Law, A.C.; Dor, Y.; Melton, D.A. β-Catenin is essential for pancreatic acinar but not islet development. *Development* **2005**, *132*, 4663–4674. [CrossRef] [PubMed]

131. Rulifson, I.C.; Karnik, S.K.; Heiser, P.W.; ten Berge, D.; Chen, H.; Gu, X.; Taketo, M.M.; Nusse, R.; Hebrok, M.; Kim, S.K. Wnt signaling regulates pancreatic β cell proliferation. *Proc. Natl. Acad. Sci. USA* **2007**, *104*, 6247–6252. [CrossRef] [PubMed]
132. Gui, S.; Yuan, G.; Wang, L.; Zhou, L.; Xue, Y.; Yu, Y.; Zhang, J.; Zhang, M.; Yang, Y.; Wang, D.W. Wnt3a regulates proliferation, apoptosis and function of pancreatic NIT-1 β cells via activation of IRS2/PI3K signaling. *J. Cell. Biochem.* **2013**, *114*, 1488–1497. [CrossRef] [PubMed]
133. Fujino, T.; Asaba, H.; Kang, M.J.; Ikeda, Y.; Sone, H.; Takada, S.; Kim, D.H.; Ioka, R.X.; Ono, M.; Tomoyori, H.; *et al*. Low-density lipoprotein receptor-related protein 5 (LRP5) is essential for normal cholesterol metabolism and glucose-induced insulin secretion. *Proc. Natl. Acad. Sci. USA* **2003**, *100*, 229–234. [CrossRef] [PubMed]
134. Jin, T. The wnt signalling pathway and diabetes mellitus. *Diabetologia* **2008**, *51*, 1771–1780. [CrossRef] [PubMed]
135. Nusse, R.; Fuerer, C.; Ching, W.; Harnish, K.; Logan, C.; Zeng, A.; ten Berge, D.; Kalani, Y. Wnt signaling and stem cell control. *Cold Spring Harb. Symp. Quant. Biol.* **2008**, *73*, 59–66. [CrossRef] [PubMed]
136. Zeng, Y.A.; Nusse, R. Wnt proteins are self-renewal factors for mammary stem cells and promote their long-term expansion in culture. *Cell Stem Cell* **2010**, *6*, 568–577. [CrossRef] [PubMed]
137. Tian, H.; Biehs, B.; Chiu, C.; Siebel, C.W.; Wu, Y.; Costa, M.; de Sauvage, F.J.; Klein, O.D. Opposing activities of Notch and wnt signaling regulate intestinal stem cells and gut homeostasis. *Cell Rep.* **2015**, *11*, 33–42. [CrossRef] [PubMed]
138. Axelrod, J.D.; Matsuno, K.; Artavanis-Tsakonas, S.; Perrimon, N. Interaction between wingless and Notch signaling pathways mediated by dishevelled. *Science* **1996**, *271*, 1826–1832. [CrossRef] [PubMed]
139. Collu, G.M.; Hidalgo-Sastre, A.; Acar, A.; Bayston, L.; Gildea, C.; Leverentz, M.K.; Mills, C.G.; Owens, T.W.; Meurette, O.; Dorey, K.; *et al*. Dishevelled limits Notch signalling through inhibition of CSL. *Development* **2012**, *139*, 4405–4415. [CrossRef] [PubMed]
140. Strutt, D.; Johnson, R.; Cooper, K.; Bray, S. Asymmetric localization of frizzled and the determination of Notch-dependent cell fate in the drosophila eye. *Curr. Biol.* **2002**, *12*, 813–824. [CrossRef]
141. Capilla, A.; Johnson, R.; Daniels, M.; Benavente, M.; Bray, S.J.; Galindo, M.I. Planar cell polarity controls directional Notch signaling in the drosophila leg. *Development* **2012**, *139*, 2584–2593. [CrossRef] [PubMed]
142. Foltz, D.R.; Santiago, M.C.; Berechid, B.E.; Nye, J.S. Glycogen synthase kinase-3β modulates Notch signaling and stability. *Curr. Biol.* **2002**, *12*, 1006–1011. [CrossRef]
143. Hayward, P.; Brennan, K.; Sanders, P.; Balayo, T.; DasGupta, R.; Perrimon, N.; Martinez Arias, A. Notch modulates Wnt signalling by associating with Armadillo/β-catenin and regulating its transcriptional activity. *Development* **2005**, *132*, 1819–1830. [CrossRef] [PubMed]
144. Yamamizu, K.; Matsunaga, T.; Uosaki, H.; Fukushima, H.; Katayama, S.; Hiraoka-Kanie, M.; Mitani, K.; Yamashita, J.K. Convergence of Notch and β-catenin signaling induces arterial fate in vascular progenitors. *J. Cell Biol.* **2010**, *189*, 325–338. [CrossRef] [PubMed]
145. Gu, B.; Watanabe, K.; Sun, P.; Fallahi, M.; Dai, X. Chromatin effector Pygo2 mediates wnt-Notch crosstalk to suppress luminal/alveolar potential of mammary stem and basal cells. *Cell Stem Cell* **2013**, *13*, 48–61. [CrossRef] [PubMed]
146. Golosow, N.; Grobstein, C. Epitheliomesenchymal interaction in pancreatic morphogenesis. *Dev. Biol.* **1962**, *4*, 242–255. [CrossRef]
147. Shih, H.P.; Sander, M. Pancreas development *ex vivo*: Culturing embryonic pancreas explants on permeable culture inserts, with fibronectin-coated glass microwells, or embedded in three-dimensional matrigel. *Methods Mol. Biol.* **2014**, *1210*, 229–237. [PubMed]
148. Bhushan, A.; Itoh, N.; Kato, S.; Thiery, J.P.; Czernichow, P.; Bellusci, S.; Scharfmann, R. FGF10 is essential for maintaining the proliferative capacity of epithelial progenitor cells during early pancreatic organogenesis. *Development* **2001**, *128*, 5109–5117. [PubMed]
149. Ye, F.; Duvillie, B.; Scharfmann, R. Fibroblast growth factors 7 and 10 are expressed in the human embryonic pancreatic mesenchyme and promote the proliferation of embryonic pancreatic epithelial cells. *Diabetologia* **2005**, *48*, 277–281. [CrossRef] [PubMed]
150. Li, S.; Francisco, A.B.; Munroe, R.J.; Schimenti, J.C.; Long, Q. SEL1L deficiency impairs growth and differentiation of pancreatic epithelial cells. *BMC Dev. Biol.* **2010**, *10*, 19. [CrossRef] [PubMed]
151. Ikeya, T.; Hayashi, S. Interplay of Notch and FGF signaling restricts cell fate and mapk activation in the drosophila trachea. *Development* **1999**, *126*, 4455–4463. [PubMed]

152. Mustonen, T.; Tummers, M.; Mikami, T.; Itoh, N.; Zhang, N.; Gridley, T.; Thesleff, I. Lunatic fringe, FGF, and BMP regulate the Notch pathway during epithelial morphogenesis of teeth. *Dev. Biol.* **2002**, *248*, 281–293. [CrossRef] [PubMed]
153. Gittes, G.K.; Galante, P.E.; Hanahan, D.; Rutter, W.J.; Debase, H.T. Lineage-specific morphogenesis in the developing pancreas: Role of mesenchymal factors. *Development* **1996**, *122*, 439–447. [PubMed]
154. Blauer, M.; Sand, J.; Laukkarinen, J. Cryopreserved mouse pancreatic acinar cells from long-term explant outgrowth cultures maintain their secretory phenotype after thawing. *Pancreatology* **2013**, *13*, 610–614. [CrossRef] [PubMed]
155. Dichmann, D.S.; Miller, C.P.; Jensen, J.; Scott Heller, R.; Serup, P. Expression and misexpression of members of the FGF and TGFβ families of growth factors in the developing mouse pancreas. *Dev. Dyn.* **2003**, *226*, 663–674. [CrossRef] [PubMed]
156. Kobberup, S.; Schmerr, M.; Dang, M.L.; Nyeng, P.; Jensen, J.N.; MacDonald, R.J.; Jensen, J. Conditional control of the differentiation competence of pancreatic endocrine and ductal cells by FGF10. *Mech. Dev.* **2010**, *127*, 220–234. [CrossRef] [PubMed]
157. Duvillie, B.; Heinis, M.; Stetsyuk, V. *In vivo* and *in vitro* techniques to study pancreas development and islet cell function. *Endocr. Dev.* **2007**, *12*, 46–54. [PubMed]
158. Hart, A.W.; Baeza, N.; Apelqvist, A.; Edlund, H. Attenuation of FGF signalling in mouse β-cells leads to diabetes. *Nature* **2000**, *408*, 864–868. [PubMed]
159. Duvillie, B.; Attali, M.; Bounacer, A.; Ravassard, P.; Basmaciogullari, A.; Scharfmann, R. The mesenchyme controls the timing of pancreatic β-cell differentiation. *Diabetes* **2006**, *55*, 582–589. [CrossRef] [PubMed]
160. Chitnis, A.; Henrique, D.; Lewis, J.; Ish-Horowicz, D.; Kintner, C. Primary neurogenesis in xenopus embryos regulated by a homologue of the drosophila neurogenic gene δ. *Nature* **1995**, *375*, 761–766. [CrossRef] [PubMed]
161. Sakamoto, M.; Hirata, H.; Ohtsuka, T.; Bessho, Y.; Kageyama, R. The basic helix-loop-helix genes Hesr1/Hey1 and Hesr2/Hey2 regulate maintenance of neural precursor cells in the brain. *J. Biol. Chem.* **2003**, *278*, 44808–44815. [CrossRef] [PubMed]
162. Grandbarbe, L.; Bouissac, J.; Rand, M.; Hrabe de Angelis, M.; Artavanis-Tsakonas, S.; Mohier, E. δ-Notch signaling controls the generation of neurons/glia from neural stem cells in a stepwise process. *Development* **2003**, *130*, 1391–1402. [CrossRef] [PubMed]
163. Schuster-Gossler, K.; Cordes, R.; Gossler, A. Premature myogenic differentiation and depletion of progenitor cells cause severe muscle hypotrophy in δ1 mutants. *Proc. Natl. Acad. Sci. USA* **2007**, *104*, 537–542. [CrossRef] [PubMed]
164. Brohl, D.; Vasyutina, E.; Czajkowski, M.T.; Griger, J.; Rassek, C.; Rahn, H.P.; Purfurst, B.; Wende, H.; Birchmeier, C. Colonization of the satellite cell niche by skeletal muscle progenitor cells depends on Notch signals. *Dev. Cell* **2012**, *23*, 469–481. [CrossRef] [PubMed]
165. Skeath, J.B. At the nexus between pattern formation and cell-type specification: The generation of individual neuroblast fates in the drosophila embryonic central nervous system. *Bioessays* **1999**, *21*, 922–931. [CrossRef]
166. Sanalkumar, R.; Dhanesh, S.B.; James, J. Non-canonical activation of Notch signaling/target genes in vertebrates. *Cell. Mol. Life Sci.* **2010**, *67*, 2957–2968. [CrossRef] [PubMed]
167. Gazave, E.; Lapebie, P.; Richards, G.S.; Brunet, F.; Ereskovsky, A.V.; Degnan, B.M.; Borchiellini, C.; Vervoort, M.; Renard, E. Origin and evolution of the Notch signalling pathway: An overview from eukaryotic genomes. *BMC Evol. Biol.* **2009**, *9*, 249. [CrossRef] [PubMed]



© 2015 by the authors; licensee MDPI, Basel, Switzerland. This article is an open access article distributed under the terms and conditions of the Creative Commons by Attribution (CC-BY) license (http://creativecommons.org/licenses/by/4.0/).

International Journal of
Molecular Sciences

MDPI

Article

Identification of Serum Peptidome Signatures of Non-Small Cell Lung Cancer

Agnieszka Klupczynska [1], Agata Swiatly [1], Joanna Hajduk [1], Jan Matysiak [1], Wojciech Dyszkiewicz [2], Krystian Pawlak [2] and Zenon J. Kokot [1,*]

[1] Department of Inorganic and Analytical Chemistry, Poznan University of Medical Sciences, Grunwaldzka 6 Street, 60-780 Poznan, Poland; a.klupczynska@gmail.com (A.K.); agata_swiatly@wp.pl (A.S.); jo.hajduk@gmail.com (J.H.); jmatysiak@ump.edu.pl (J.M.)

[2] Department of Thoracic Surgery, Poznan University of Medical Sciences, Szamarzewskiego 62 Street, 60-569 Poznan, Poland; dyszkiewicz@wp.pl (W.D.); krystianp@hotmail.com (K.P.)

* Correspondence: zkokot@ump.edu.pl; Tel.: +48-61-854-6610

Academic Editor: William Chi-shing Cho
Received: 13 January 2016; Accepted: 14 March 2016; Published: 31 March 2016

Abstract: Due to high mortality rates of lung cancer, there is a need for identification of new, clinically useful markers, which improve detection of this tumor in early stage of disease. In the current study, serum peptide profiling was evaluated as a diagnostic tool for non-small cell lung cancer patients. The combination of the ZipTip technology with matrix-assisted laser desorption/ionization time-of-flight mass spectrometry (MALDI-TOF-MS) for the analysis of peptide pattern of cancer patients (n = 153) and control subjects (n = 63) was presented for the first time. Based on the observed significant differences between cancer patients and control subjects, the classification model was created, which allowed for accurate group discrimination. The model turned out to be robust enough to discriminate a new validation set of samples with satisfactory sensitivity and specificity. Two peptides from the diagnostic pattern for non-small cell lung cancer (NSCLC) were identified as fragments of C3 and fibrinogen α chain. Since ELISA test did not confirm significant differences in the expression of complement component C3, further study will involve a quantitative approach to prove clinical utility of the other proteins from the proposed multi-peptide cancer signature.

Keywords: peptide profiling; non-small cell lung cancer; MALDI-TOF-MS; ZipTip enrichment

1. Introduction

Lung cancer (LC) has been the leading cause of malignant tumor-related deaths for years [1,2]. Due to poor clinical manifestation and low effectiveness of diagnostic tools, LC is usually diagnosed at an advanced stage, which results in the highest mortality rates among all cancers, in both men and women. The prognosis of LC is generally poor and the overall five-year survival rate reaches only 15% [3]. Currently, the LC diagnosis is mainly based on the CT or PET/CT of the chest. A low-dose computed tomography was suggested as an additional screening tool, that can contribute to early LC detection. However, that technique is limited by a low specificity resulting in a large number of false positives [3–5].

Therefore, there is an urgent need for identification of new, clinically useful biological markers of LC that can enhance the current diagnostic capabilities. Biomarkers that can be used in a minimally invasive screening test would complement diagnostic imaging and have an immediate impact on better survival in LC patients. To identify potential LC biomarkers different strategies have been used. An increasing interest in searching for biomarkers of LC occurred in two rapidly expanding fields of science—proteomics and metabolomics. Both of them use different mass spectrometry techniques as an analytical tool for searching abnormalities in proteome and metabolome of LC patients.

A number of global metabolic profiling studies of non-small cell lung cancer (NSCLC) patients using gas chromatography-mass spectrometry [6–10] or liquid-chromatography-mass spectrometry [7,9,11,12] was presented. Mass spectrometry-based targeted metabolomic approach revealed altered levels of some plasma free amino acids in NSCLC subjects [13,14]. Another promising approach in discovery of candidate LC biomarkers represents proteomic research. The identification of differences in proteome between healthy and diseased individuals is a major aim of clinical proteomics [15,16]. Several proteins were proposed as the potential LC markers, among which the most extensively investigated are cytokeratin 19-fragments (CYFRA 21-1), neuron-specific enolase (NSE), carcinoembryonic antigen (CEA) and squamous cell carcinoma antigen (SCC) [17,18]. However, their clinical applicability in LC detection is limited. Although the concentration levels of CYFRA 21-1, CEA and SCC change along with the development of LC, they are characterized by insufficient sensitivity and specificity to be used as stand-alone diagnostic tests, whereas NSE is a useful prognostic factor only in the advanced stages of the disease [4,19]. Mass spectrometry was found to be the most powerful tool among the proteomic technologies. An overview of research focused on discovery of new diagnostic and prognostic markers of LC through mass spectrometry-based proteomic analyses has been published recently [20]. In searching for a noninvasive diagnostic tools in LC detection breath analysis was also tested. Among volatile organic compounds present in exhaled breath alcohols, aldehydes, ketones and hydrocarbons were found to be potential markers of LC [21]. Despite the encouraging data emerged from several studies none of the proposed biomarkers has reached clinical utility so far [22–24].

In proteomic and metabolomic research and the analysis of exhaled breath it was indicated that a panel of biomarkers has a higher discriminatory power in LC detection than a single compound alone [13,24–26]. The use of a single compound for cancer diagnosis has a higher risk of producing false-positive results caused by links with other disorders. Due to heterogeneity of LC a panel of markers seems to be more appropriate from the clinical point of view [27]. Therefore, it can be supposed that the study of a pattern of multiple compounds can lead to obtain many important diagnostic information simultaneously and provide enhanced sensitivity and specificity in patients' classification.

In searching for new cancer biomarkers, the expression pattern of multiple proteins has been investigated using diverse methods, such as an antibody microarray [28], surface-enhanced laser desorption/ionization time-of-flight mass spectrometry (SELDI-TOF-MS) [25] and matrix-assisted laser desorption/ionization time-of-flight mass spectrometry (MALDI-TOF-MS) [29–31]. The use of MALDI-TOF-MS profiling enables to obtain a whole pattern of low-molecular weight proteins occurring in human serum and was indicated as a promising strategy in several cancer research. This technology was found to be effective in discrimination of healthy individuals from patients with various tumors such as biliary tract cancer [32], gastric cancer [33], prostate cancer [34], ovarian cancer [16] and head and neck cancer [35]. Moreover, serum peptidome features were suggested to be useful in monitoring the toxicity of applied therapy in women with breast cancer [36].

Although the use of serum peptide profiling holds promise in diagnostics, there are several debate topics related to this approach. One of the most commonly discussed concern is a lack of reproducibility of obtained data across different published studies. It should be bear in mind that cancer-related biomarkers occur in blood at very low concentration levels in comparison to proteins such as albumin and immunoglobulins, which mask other compounds. Apart from high-abundant proteins, the presence of lipids and salts can also adversely affect the peptide pattern profiling [37–39]. A range of sample preparation techniques was developed to remove the abundant proteins and desalt samples. One of the most widely used depletion techniques in MALDI profiling studies is solid phase extraction. Taking into account that reproducibility of the MS profiling is highly dependent on sample preparation procedure in our study solid phase extraction using C18-ZipTip pipette tips based on reversed-phase chromatography was chosen as a sample pre-treatment method. To the best of our knowledge, this is the first research that presents the application of ZipTip technology for purifying the serum samples of LC patients. In this technique, the molecules are separated due to an adsorptive process based on their chemical properties and hydrophobic characteristics. The separation

is determined by hydrophobic interaction between the analytes in the mobile liquid phase and a solid stationary phase with immobilized hydrophobic ligand [40]. The ZipTip enrichment strategy was proved to be a reliable method for sample preparation in MS peptide profiling [38,39].

The goal of the present study was to determine serum peptide profiles of patients with NSCLC and matched healthy controls by MALDI-TOF-MS technology combined with C18-ZipTip packed tips. Patients with early stage NSCLC represented a significant part of the studied group, which is particularly valuable in terms of searching for early cancer biomarkers. The classification model obtained based on peptide pattern was verified using a validation set of samples. The selected discriminating peptide peaks were then identified using liquid chromatography-tandem mass spectrometry.

2. Results

2.1. Characteristics of the Study Participants

In the current study, serum peptide pattern profiling was evaluated as a diagnostic approach for NSCLC patients. The characteristics of cancer patients and the control group are summarized in Table 1. Histologically, 55.6% of tumors (n = 50) were diagnosed as squamous cell carcinomas and 44.4% of them (n = 40) as adenocarcinomas. The most often diagnosed grade of cancer differentiation was G2 (52.0%). According to TNM Classification for Lung Cancer the most common stages in the study group were as follows: IB (26.0%), IIA (26.0%) and IA (20.0%). Thus, patients with early stage NSCLC represented a significant part of the studied group. None of the patients had diagnosed NSCLC at IV stage. The study group and control group had similar percent of men and women. No statistically significant differences in age occurred between LC patients and controls (p = 0.2378).

Table 1. Characteristics of non-small cell lung cancer (NSCLC) patients and control subjects.

Characteristic	Training Set		Test Set		Total	
	NSCLC Patients	Controls	NSCLC Patients	Controls	NSCLC Patients	Controls
No. of Subjects	67	47	23	16	90	63
Sex						
Male	40 (59.7%)	31 (66.0%)	18 (78.3%)	10 (62.5%)	58 (64.4%)	41 (65.1%)
Female	27 (40.3%)	16 (34.0%)	5 (21.7)	6 (37.5%)	32 (35.6%)	22 (34.9%)
Age						
Mean (SD)	63 (6.5)	62 (8.5)	66 (8.0)	62 (10.0)	64 (6.9)	62 (8.7)
Range	48–86	43–78	53–81	45–77	48–86	43–78
Histological type						
Squamous cell carcinoma	39 (58.2%)		12 (52.2%)		50 (55.6%)	
Adenocarcinoma	28 (41.8%)		11 (47.8%)		40 (44.4%)	
Grade of cancer differentiation						
G1	1		1		2	
G2	31		12		43	
G2/3	6		2		8	
G3	23		6		29	
Unknown	6		2		8	
TNM stage						
IA	14		3		17	
IB	19		6		25	
IIA	14		5		19	
IIB	8		2		10	
IIIA	12		7		19	

2.2. Reproducibility Evaluation

Both application of ZipTips for sample pretreatment and the serum peptide profiling were proved to be reliable and reproducible technologies [38,39]. Nevertheless, we performed some additional experiments in order to check reproducibility of the whole applied procedure in our experimental conditions and to confirm that the variation in spectra shows biological differences in intensities of peptide ions rather than systematic variability. The intra-day reproducibility of the protein profiles was evaluated by analyzing samples spotted at three different target positions. Variability assessment was based on eight randomly selected peaks with low, medium and high peak area in a mass range of m/z 1–10 kDa. The coefficient of variation (CV) calculated for intra-day reproducibility varied from 2% to 10% (average CV = 6.9%) (Table S1). The inter-day reproducibility was evaluated using spectra obtained from the same samples but on three different days. The CV values ranged between 2% and 42% with an average inter-day variability of 20% (Table S2). It can be concluded that both intra-day and inter-day studies proved that the applied methodology yields a high quality results and is suitable for searching for cancer-related differences at peptidome level.

2.3. Serum Peptide Profiling

The current research involved the application of peptide profiling in serum samples collected from patients with diagnosed NSCLC and the matched control group. In total, 153 serum samples derived from cancer patients (n = 90) and healthy controls (n = 63) were subjected to C18 reversed-phase extraction using ZipTips and analyzed by MALDI-TOF-MS. The performed analyses allowed to detect 136 unique peaks. Univariate statistical analyses allowed to find peptides which were significantly different between the analyzed groups (Table 2). Their diagnostic efficiency was further examined by receiver operating characteristic (ROC) curve-based analyses. The area under the ROC curve (AUC) values above 0.75 confirmed high accuracy of peptide ions in discrimination between NSCLC patients and controls without cancer. Eight peptides of 1520.16, 1546.72, 1568.45, 1617.88, 2083.30, 4466.98, 4787.36, and 4803.17 Da had the most discriminative power with p-value < 0.00004 and AUC values ranging from 0.75 to 0.85 (Table 2).

Table 2. Intensities (mean ± SD) and results of the univariate statistical analyses of the most discriminating peptide ions determined in serum of non-small cell lung cancer patients (NSCLC) (n = 90) and control group (n = 63).

Mass (m/z)	NSCLC	Control Group	p-Value [1]	AUC [2]
1568.45	6.33 ± 4.27	2.75 ± 0.91	<0.000001	0.85
1546.72	54.19 ± 41.34	24.09 ± 14.03	0.00000386	0.78
1617.88	66.99 ± 48.77	29.24 ± 23.84	0.00000386	0.78
1520.16	13.56 ± 4.36	9.49 ± 4.28	0.00003860	0.78
4466.98	0.31 ± 0.19	0.51 ± 0.23	0.00002280	0.75
4803.17	0.29 ± 0.18	0.56 ± 0.34	0.00000975	0.77
4787.36	0.52 ± 0.48	1.21 ± 1.12	0.00001960	0.79
2083.30	1.07 ± 1.42	2.24 ± 2.57	0.00001960	0.76

[1] Calculated based on t-test or Wilcoxon test. [2] Area under the ROC curve.

The serum peptide patterns were also subjected to multivariate statistical analysis, which considers multiple variables simultaneously and takes into account correlations between variables. The classifications of the samples were tested using three different algorithms: genetic algorithm (GA), quick classifier (QC) and supervised neural network (SNN). The discrimination models were generated based on a training set containing the randomly assigned 67 NSCLC samples and 47 control samples. Two indicators of the model's performance, cross validation and recognition capability, were calculated (Table 3).

Table 3. List of peptide ions included to the generated classification models and diagnostic performances of the models.

	Non-Small Cell Lung Cancer [1]			Lung Adenocarcinoma			Lung Squamous Cell Carcinoma		
	Quick Classifier	**Supervised Neural Network**	**Genetic Algorithm**	**Quick Classifier**	**Supervised Neural Network**	**Genetic Algorithm**	**Quick Classifier**	**Supervised Neural Network**	**Genetic Algorithm**
Mass [Da]	1520.16	1546.72	1466.90	1568.45	1568.45	1450.94	1520.16	1546.72	2884.63
	1538.14	1617.88	1568.45	7923.94	1305.41	4626.52	1617.88		1527.52
	1546.72	1505.34	1450.94		5004.12	1546.72	1741.57		1520.16
	1568.45		1880.97		2755.6	1505.42	2884.63		1564.1
	1617.88		1617.88		2604.28	6630.86	4787.36		1546.72
	4466.98		1520.16		1450.94	1466.85			5808.48
	4680.61		1546.72		1628.01	9289.98			3882.95
	4803.17		5904.39		1741.49	1510.24			6589.21
	6528.67		6330.86		2673.89	6304.32			1078.16
			6432.69		2555.04	1021.00			5919.08
					1905.19				
					4787.36				
					2575.89				
					1888.66				
					1546.72				
Cross validation (%) [2]	75.54	47.87	71.89	84.31	86.35	74.71	69.51	60.64	74.66
Recognition capability (%) [2]	76.33	56.47	96.22	87.46	95.79	97.87	75.80	50.86	96.51
Specificity (%) [3]			64.40		66.70		-	-	86.70
Sensitivity (%) [3]			94.40		72.70		-	-	66.70

[1] Without division into histological types. [2] Calculated using a training set. [3] Calculated using a test set.

As can be seen in Table 3, among the three classification algorithms, the GA-based model showed the highest values of cross validation (71.89%) and recognition capability (96.22%). Due to the best efficiency in the discrimination between NSCLC group and the control group further statistical analyses were performed using only GA model. The GA-based classification model was composed of 10 peptides including four peaks selected earlier by univariate statistical tests (1520.16, 1546.72, 1568.45, and 1617.88 Da) (Table 3). The poor discriminatory ability of SNN model can result due to small number of peptide ions included into the model. In order to verify the classification capabilities of GA model, external validation was performed using a test set (Table 1). Based on analysis of new serum samples, it was indicated that the generated model discriminated the two studied classes with a sensitivity of 64.40% and a specificity of 94.40% (Table 3).

Additional statistical analyses were carried out for two main histological types of NSCLC, adenocarcinomas and squamous cell carcinomas separately. Characteristics of the classification models generated with regard to NSCLC subtypes are presented in Table 3. Despite some discrepancies existing between the generated models, it can be noticed that peptides of 1568.45 and 1450.94 Da were associated with adenocarcinomas, while peptide of 1520.16 Da was related to squamous cell carcinomas. Peptide of 1546.72 Da was found to have a high discriminative ability regardless the histological type of NSCLC.

2.4. Identification of Peptide Ions

The conducted statistical analyses allowed to select some ions from the whole peptide pattern occurring in human serum, which had the highest discriminatory abilities in LC detection. In order to identify chosen peptide ions (linear positive mode m/z 1520.16, 1546.72, 1568.45, and 1617.88 Da) additional experiments were carried out using LC-MALDI-TOF/TOF-MS/MS technique. Spectra were automatically recorded in the reflector mode in the mass range 700 to 3500 Da. As many peaks detected in the low mass range were presented in the close neighborhood, the identification of the chosen peaks by MALDI-TOF/TOF method seemed to be challenging. For this reason, we decided to extend the time of nLC gradient from our previous method [41]. This procedure allowed to obtain effective peptide separation and detection of all discriminative peaks. The MS analysis of signal m/z 1520.8456 showed the oxidation modification (16 Da) of signal 1504.8527, which is presented on the Figure 1A. The MS/MS fragmentation of precursor ion m/z 1520.8456 allow to identify complement C3 (CO3_HUMAN) protein with the peptide sequence of SPMYSIITPNILR with a significant score in the Mascot search. The MS/MS spectrum of peptide ion m/z 1520.8456 Da is shown in Figure S1.

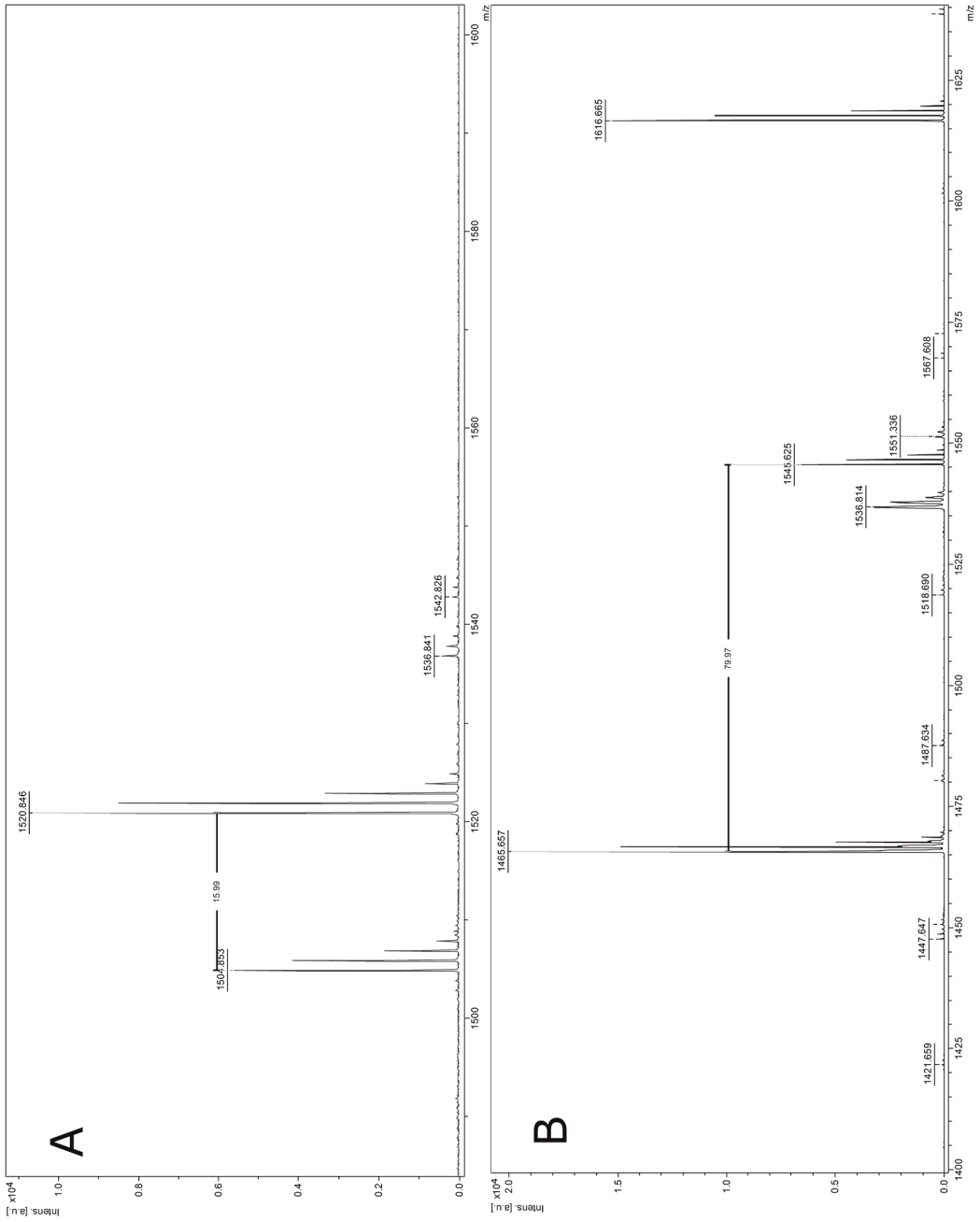

Figure 1. (**A**) Mass spectrum of m/z 1520.8456 with assigned oxidative modification of m/z signal 1504.853; (**B**) Mass spectrum of m/z 1545.6249 represent with assigned phosphorylation modification of m/z signal 1465.657.

The MS/MS analysis of signal m/z 1545.6249 resulted in identification of the following peptide sequence: DSGEGDFLAEGGGVR (Figure S2). The interpretation of MS spectrum of the peak 1545.6249 revealed the presence of phosphorylation modification (79.98 Da) of the m/z 1465.657 (Figure 1B). The matched sequence gave a significant score in the protein database to fibrinogen α chain (FIBA_HUMAN) protein. Analysis of m/z 1568.67 and 1616.67 failed, as the contamination of other neighborhood fragments were observed in the MS/MS spectrum. For this reason, m/z 1568.67 precursor with hypothetical peptide sequence DSCSRDGALLGCSLTA did not give any reliable identification. In the MS-BLAST search homology to Uncharacterized family 31 glucosidase KIAA1161 was found. The MS/MS fragmentation of m/z 1616.67 led to obtain AEIQGKMEDLPEQE peptide sequence. The structure contains additional unknown modifications, which may hinder its identification. Thus, the established sequence resulted with no significant hit in Mascot search. Therefore, further study involving the identification of both peptide ions of 1568.67 and 1616.67 Da should be done.

Validation of candidate protein markers identified based on MALDI-TOF-MS analysis should be performed using quantitative approaches such as an antibody-based technology or a mass spectrometry-based method. An enzyme-linked immunosorbent assay (ELISA) was used for verification of differences in the expression of complement component C3 in the analyzed serum samples. Despite in NSCLC group elevated concentration of complement C3 was observed compared to the control group (0.17 *vs.* 0.16 g/L) the difference was not statistically significant. Since ELISA test for determination of fibrinogen α chain in serum is not commercially available, future study will involve development of multiple reaction monitoring (MRM) method using triple quadrupole mass spectrometry, in which targeted measurements of the selected peptides are performed. Moreover, the MRM-based approach seems to be more reliable, because difference in the intensity of peptide ion derived from fibrinogen α chain can be also caused by cancer-specific exopeptidases.

3. Discussion

Despite a similar incidence to other malignant tumors, such as breast and prostate cancer, LC causes 4–5 times more deaths [2]. This discrepancy is partly associated with the fact that there are no satisfactory early diagnostic strategies for detection of lung malignant tumors. Hence, there is a need for identification of new, clinically useful markers, which improve detection of LC in its early stages. Identification of detectable abnormalities in low-molecular weight serum proteome is one of the strategies, which are now under intensive investigation. The aim of the study was to search for serum peptidome signatures of NSCLC patients and to assess their utility in the detection of that tumor. MALDI-TOF-MS is a high throughput technology that provide an opportunity to obtain polypeptide profiles which, combined with sophisticated bioinformatic tools, have a great impact on the acceleration of the work aimed at development of new diagnostic tests for cancer.

The combination of the ZipTip enrichment with MALDI-TOF-MS for the analysis of serum peptide spectra of LC patients was reported for the first time. There are few reports in the available literature, which present MALDI-TOF-MS analyses of blood proteome profiling in LC, however all of them are based on the usage of magnetic bead-based technologies for sample pretreatment [29–31]. It was indicated that the sample preparation procedure has a great influence on the obtained protein profiles [39]. Since the sample preparation method is an important issue and determines the success of the whole experiments, it also affects the discriminatory abilities of the peptide pattern in detection of cancer and other diseases. Consequently, the peptide ions proposed as candidate LC biomarkers are different when compare various studies. The discrepancies in the discriminatory peptides occurring in serum of LC patients can result not only from diverse analytical methodologies, but also from different histological type and clinical stage of cancer. In the presented study, 46.7% of the patients had NSCLC at stage I, whereas in the study of Musharraf *et al.* [31] subjects at stage III and IV were mainly analyzed. It can be supposed that patients with stage I represent more valuable group from the viewpoint of the development of a test for early LC detection. Shevchenko *et al.* [29] and Lin *et al.* [30] analyzed only

one subtype of NSCLC, squamous cell carcinomas and adenocarcinomas, respectively. In our research, these two most common NSCLC subtypes were involved and thus the findings may refer to a wider group of patients.

Based on our research, a number of low-molecular weight proteins were found to be differentially expressed in the serum samples of NSCLC patients compared to the control subjects. Some of the peptides were identified as discriminative based on both univariate and multivariate (GA) statistical analyses. These peptides include: 1520.16, 1546.72, 1568.45, and 1617.88 Da. As can be seen in Table 3, different algorithms used for generation of the classification models resulted in different peak selection. A lack of complete consistency in terms of peak selection to the generated models was not surprising, because the applied algorithms used various inclusion criteria for peptide ions, such as univariate sorting or prototype-based classification. Despite the apparent differences concerning peptide selection to the models, some shared traits between the generated models can be noticed. Two peptide ions of 1546.72 and 1617.88 Da were common to all three applied algorithms, which indicates their potential as NSCLC candidate biomarkers (Table 3). Moreover, some discrepancies in the results of multivariate analyses (GA, QC, and SNN) between two the most common histological types of NSCLC also existed. Nevertheless, it was found that peptides of 1568.45 and 1450.94 Da significantly correlated with adenocarcinomas, whereas peptide of 1520.16 Da was characteristic feature of squamous cell carcinomas. Based on Table 3, it can be concluded that peptide of 1546.72 Da had a high classification ability regardless the histological type of NSCLC. Our study confirmed the hypothesis that due to heterogeneity of NSCLC a panel of markers will have better performance in NSCLC detection than a single compound. It is worth noting that GA-based model for discrimination between NSCLC patients and controls consisted of peptides identified as characteristic traits of both adenocarcinomas and squamous cell carcinomas. This could explain the highest classification abilities of that model.

External validation was conducted to assess robustness of the generated classification models. This is an important step in data analysis, which enabled verification of the obtained preliminary results and discrimination of false positives from markers of high potential in clinical practice. The analysis of a new validation set of serum samples revealed satisfactory values of sensitivity and specificity for GA-based model (94.40% and 64.40%, respectively), proving the reliability of the model. Thus, only a combination of 10 peptide ions was robust enough to detect new set of NSCLC samples. Six of them were observed at higher intensity levels in NSCLC group (1466.90, 1568.45, 1617.88, 1520.16, 1546.72, and 5904.39 Da) and four of them were found significantly decreased in cancer patients (1450.94, 1880.97, 6330.86, and 6432.69 Da). This finding once more supports the assumption that a serum multi-peptide signature could be applied for detection of patients with NSCLC. The results of our studies should be confirmed by an analysis of additional set of serum samples. The sample size involved in the external validation procedure was 39, therefore further studies with greater number of samples should verify the obtained promising findings. Due to the fact that many serum proteins can be related to inflammatory processes, future studies should also include a set of samples collected from patients with inflammatory conditions as an additional control group.

Peptides of the highest discriminatory ability were subjected to further experiments with the aim of their identification as fragments of specific proteins. The LC-MS/MS analysis of m/z 1520.8456 peak led to identification of complement C3 (CO3_HUMAN) protein with the peptide sequence of SPMYSIITPNILR. In the current study, higher intensity of this peptide was found in NSCLC group. Complement C3 plays a key role in the activation of the complement system, which is an essential part of immune system and regulates many immunological and inflammatory processes. The interactions between complement and cancer turned out to be more complex than expected [42,43]. A number of studies indicate that cancer cells activate complement, which facilitates immune attack against tumor. However, recent findings on tumor-promoting activities of complement suggest its dual action in cancer. The role of complement proteins in chronic inflammation, angiogenesis, immunosuppression and cancer cell signaling has been extensively reviewed [42,43]. Complement activation by tumor cells was observed in both *in vitro* studies and physiological fluids from cancer patients [44–46]. Moreover,

significantly higher levels of complement components and activation fragments in plasma of LC patients were demonstrated [30,47,48]. High expression of complement regulatory proteins were associated with poor prognosis in colorectal and prostate tumors [49,50]. The results of our study should draw more attention to the possibility of use of complement-related proteins, especially C3, as new molecular cancer biomarkers. A more systematic analysis of abnormalities in the levels of complement components occurring in biofluids of cancer patients is needed, which can also contribute to better understanding of the dynamic interplay between cancer and complement.

The second protein, which was successfully identified as a NSCLC marker candidate in the current research is fibrinogen α chain (FIBA_HUMAN) protein. The peak of m/z 1545.6249, identified as a fragment of fibrinogen α chain, had a higher intensity in NSCLC patients compared to control subjects. Fibrinogen constitutes a major protein of human blood clotting and mediates platelet aggregation [51]. Fragments of fibrinogen α chain as well as fibrinopeptide A have been reported as markers of other tumor types, such as urothelial cancer [52], ovarian cancer [53], gastric cancer [54] and biliary tract cancer [32]. It was suggested that higher or lower intensities of various peptide ions in cancer can results not only from up- or downregulation of the parent proteins, but can originate from cancer-specific exoproteases as well. It was indicated that exopeptidase activities in particular overlapped with *ex vivo* coagulation can generate cancer-specific peptide fragments in serum [55,56]. Thus, those peptides may be treated as surrogate markers of cancer-derived proteases.

Since our results were obtained based on relative peptide intensities, new candidate protein biomarkers that are found using MALDI-TOF-MS analysis need verification and validation. For this purpose, two different quantitative analytical platforms: antibody-based technologies and mass spectrometry-based methods are used [57]. Since ELISA test did not show statistically significant differences in the expression of complement C3, further study will involve a quantitative approach to prove clinical utility of the other proteins from the proposed multi-component cancer signature.

4. Materials and Methods

4.1. Characteristics of the Study Participants

Serum samples were collected from ninety patients with a new diagnosis of LC, who were recruited in the Department of Thoracic Surgery, Poznan University of Medical Sciences. The criteria for the patient classification to the studied group were the following: diagnosis of NSCLC based on the histopathological examination of the biopsied or resected tissue specimens, there were no coexisting cancers, chemotherapy and/or radiotherapy and other cancer treatment were not used. Sixty-three healthy subjects, who underwent routine medical examination, without cancer and chronic metabolic diseases were enrolled to the control group. The control group was matched to the studied group in terms of age, sex and ethnic origin. Demographic and clinical profiles of the cancer patients and control individuals are presented in Table 1. The sera was collected in the same manner from LC patients and healthy subjects after an overnight fasting and stored –80 °C until analysis. The study was performed with full approval by the Local Ethical Committee of Poznan University of Medical Sciences, Poland (Decision No. 200/13) and in line with the Declaration of Helsinki. A written informed consent to use of serum samples in the study was received from all subjects.

4.2. Chemicals and Reagents

Ammonium acetate and trifluoroacetic acid (TFA) from Sigma Aldrich (St. Louis, MO, USA) were used. Ethanol, isopropanol, water, acetone and acetonitrile (ACN) were purchased from J.T. Baker (Center Valley, PA, USA). ClinProt standards, AnchorChip 800 μm target and α-cyano-4-hydroxycinnamic acid (HCCA) were from Bruker Daltonics (Bremen, Germany). Millipore Simplicity UV water purification system (Waters Corporation, Milford, MA, USA) was used to obtain deionized water. All used reagents were characterized by analytical grade or better.

4.3. Serum Samples Pretreatment

The solid phase extraction technique in the form of pipette tips pre-packed with hydrophobic phase was use as a sample pretreatment method. Prior MALDI-TOF-MS analyses, samples were diluted 1:5 using 0.1% TFA in water. In order to detect low molecular weight peptides depletion method using C18 ZipTip micropipette tips (Millipore, Bedford, MA, USA) was performed according to the manufacturer's instruction. The protocol includes 3 steps: binding of proteins and peptides, washing, and elution. Fifty percent ACN solution was used for elution of the samples fractions. The detailed procedure was described in our previous study [41].

4.4. MALDI-TOF-MS Analysis

After preconcentration and purification 1 μL of each eluent sample was mixed with 10 μL of HCCA matrix solution (0.3 g/L HCCA in ethanol:acetone, 2:1, v/v), which was prepared daily. For the MS profiling analysis, 1 μL of the mixture was spotted directly onto the MALDI plate (AnchorChip, Bruker Daltonics, Bremen, Germany). Before analysis the spots were dried in the room temperature. MS analyses were performed using MALDI-TOF mass spectrometer, UltrafleXtreme (Bruker Daltonics, Bremen, Germany). The instrument was operated in positive-ion linear mode. Peak m/z values or intensities were recorded in the mass range of 1–10 kDa. The following ion source settings were used for MALDI-TOF MS analysis: ion source 1, 25.09 kV; ion source 2, 23.80 kV. Other parameters were set at: lens, 6.40 kV; pulsed ion extraction, 260 ns; and matrix suppression mass cut off, m/z 700 Da. Two thousand shots with a laser power of 80% were collected per one spectrum. Each sample was spread into 3 spots and analyzed in triplicate. External calibration of the mass spectrometer was proceeded with a mixture containing of Peptide Calibration Standard and Protein Calibration Standard I (1:5, v/v). The analyses were performed with average mass deviation less than 100 ppm. The three representative samples were analyzed on 3 different spots during a day and during 3 different days in order to evaluate the inter-day and intra-day reproducibility of MS. Eight randomly selected peaks with low, medium and high abundance peak area in the mass range of m/z 1–10 kDa were marked for variability assessment. Calculation of CV values allowed to measure the variability of each MS peak area. For data collection and instrument control FlexControl 3.4 software (Bruker Daltonics, Bremen, Germany) was applied. The software allowed for automatic acquisition and processing of the obtained spectra.

4.5. LC-MS/MS Identification of Selected Ion Peptides

The sample was pretreated with C18 ZipTip micropipette tip. The obtained eluent was concentrated and separated using nano-liquid chromatography (EASY-nLC II, Bruker Daltonics). The set was consist of the trap column (NS-MP-10 BioSphere C18, NanoSeparations, Nieuwkoop, the Netherlands; 20 mm × 100 μm I.D., particle size 5 μm, pore size 120 Å) and column (Thermo Scientific Acclaim PepMap 100 C18, Thermo Scientific, Sunnyvale, CA, USA ; 150 mm × 75 μm I.D., particle size 3 μm, pore size 100 Å). The separation was performed by linear gradient of 2%–50% of ACN for 150 min (0.05% TFA water solution—mobile phase A, and 0.05% TFA 90% ACN—mobile phase B). The flow rate was 300 nL/min. The 2 μL of the sample was injected on the column. Sample collection was started in the 54 min of the running gradient. From this, 384 sample fractions directly mixed with matrix solution were automatically spotted onto an AnchorChip™ target with time intervals of 15 s by using fraction collector (Proteineer-fc II, Bruker Daltonics, Bremen, Germany). Matrix solution contained: 748 μL of mixture of acetonitrile and 0.1% TFA (95:5 v/v), 36 μL of HCCA saturated solution of 0.1% TFA and acetonitrile (90:10 v/v), 8 μL of 10% TFA and 8 μL of 100 mM ammonium phosphate monobasic. For control of the nano-LC system HyStar 3.2 software (Bruker Daltonics) was used. The obtained fractions were further analyzed using the MALDI-TOF/TOF instrument (UltrafleXtreme, Bruker Daltonics,). The Peptide Calibration Standard mixture (Bruker Daltonics) was used for the external calibration. For the MS-analysis the software WARP-LC (Bruker Daltonics,) was used to

establish a list of precursor ions. The chosen m/z (1520.8456, 1545.6249, 1568.67, and 1616.67) were subjected to MS/MS fragmentation mode. The identification of the proteins was conducted with settings for MS and MS/MS mode as previously described [41]. FlexControl 3.4, FlexAnalysis 3.4 and BioTools 3.2 (Bruker Daltonics) were used for the control of the mass spectrometer, acquisition, processing and evaluation of the data. The SwissProt database with Mascot 2.4.1 search engine (Matrix Science, London, UK) was used to analyze the results. Only searches restricted to "*Homo sapiens*" were taken into account. The peptide precursor mass tolerance was 50 ppm, while fragment mass tolerance 0.7 Da. Other search parameters for protein identification were as follows: monoisotopic mass, no enzyme used, peptide charge: +1.

4.6. Determination of Complement C3 by ELISA

A sandwich enzyme immunoassay (ELISA) kit was used for the quantitative measurement of complement C3. Assays were carried out as described in the manufacturer's manual (Cloud-Clone Corp., Houston, TX, USA). The test was validated for in vitro quantitative measurement of C3 in human serum within detection range 7.8–500 ng/mL.

4.7. Data Analysis

Each spectrum was analyzed using ClinProTools software (version 3.0; Bruker Daltonics). As each sample was measured in triplicate, the spectra grouping function was used to average the obtained data. Then, the spectra were processed with the following manner: normalization to the total ion current (TIC), recalibration using the prominent common m/z values, baseline "top hat" subtraction with the minimum baseline width set to 10%, smoothing, the signal-to-noise ratio $\geqslant$5, peak picking and peak calculation operation. Spectra were processed in the 1–10 kDa range. Peak intensity differences between the analyzed groups were evaluated using either a student t-test or Wilcoxon test (depending on variable distribution). In all tests, $p \leqslant 0.05$ was considered to indicate a statistically significant difference. Receiver operating characteristic (ROC) curve was calculated for each peak to show a graphical overview between sensitivity and specificity. The area under the ROC curve (AUC) enabled to compare discriminatory abilities of the serum peptide ions. In order to obtain discriminating models, 3 algorithms were used: genetic algorithm (GA), supervised neural network (SNN) and quick classifier (QC). The algorithms were used to integrate the best number of peaks in discrimination models. Determination of a common signature among the obtained spectra of each of the studied groups lead to proper classification of the test samples by the model [58]. GA imitates evolution in nature and selects a combination of variables that are the most significant for the class separation, while less capable are abandoned. The optimal class separation with high variance between classes is obtained by optimizing a cost function [59,60]. QC represents a univariate sorting algorithm. Generation of a QC model is based on storing the class averages of the peak areas together with p-values obtained from a *t*-test. First, the peak areas or intensities are sorted per peak and next a weighted average from all peaks need to be calculated [59,61]. SNN algorithm uses a prototype-based classification. The characteristic spectra of each study class, which are named prototypes, are identified. Then, they are considered as prototypical samples of that class from a proteomic point of view [59,61]. Two indicators of the model's performance, 20% leave one out cross validation (10 iterations) and recognition capability, were calculated for all three used algorithms. The cross validation values indicate the reliability of the generated model, whereas the recognition capability values show the model's capability of correct identification of the component spectra [62]. Sixty-seven samples from LC patients (29 adenocarcinomas and 38 squamous cell carcinomas) and 47 healthy control samples were randomly selected to a training set (Table 1). The rest of the samples, 23 LC samples (11 adenocarcinomas and 12 squamous cell carcinomas) and 16 control samples, were used as a test set. The aim of using the training set to build the model was to define spectra of the model classes in such a way that new spectra (the test set) might be classified afterwards. This external validation procedure was applied to the model of the best performance and enabled to calculate sensitivity and specificity values. Peptides of the highest discriminatory ability

were subjected to further experiments with the aim of their identification as fragments of specific proteins. The validation data concerning differential expression of identified proteins was analyzed using univariate statistical analyses by applying Statistica software (version 12.0; StatSoft Inc., Tulsa, OK, USA).

5. Conclusions

We used proteomic profiling strategy in searching of serum peptide signatures of NSCLC. The combination of the ZipTip technology with MALDI-TOF-MS for the analysis of serum peptide pattern of NSCLC patients was presented for the first time. Based on the observed significant differences between cancer patients and control subjects, the classification model was generated, which allowed for accurate group discrimination. The model turned out to be robust enough to discriminate new validation set of samples with satisfactory sensitivity and specificity. Two peptides from the diagnostic pattern for NSCLC were identified as fragments of C3 and fibrinogen α chain. There is a risk that the identified peptide ions may not be specific for NSCLC, but also represent tumor indicators in general. Therefore, further attempts are planned to identify other components of the developed classification model, which can be more specific for NSCLC. Since ELISA test did not confirm significant differences in the expression of complement component C3, further study will involve a quantitative approach to prove clinical utility of the other proteins from the proposed multi-peptide cancer signature.

Supplementary Materials: Supplementary materials can be found at http://www.mdpi.com/1422-0067/17/4/410/s1.

Acknowledgments: The project was supported by the Polish Ministry of Science and Higher Education (502-14-03307415-10356).

Author Contributions: Agnieszka Klupczynska, Agata Swiatly, Jan Matysiak and Zenon J. Kokot designed study. Wojciech Dyszkiewicz and Krystian Pawlak collected and characterized samples. Agnieszka Klupczynska, Agata Swiatly, Joanna Hajduk, and Jan Matysiak performed the experiments. Agnieszka Klupczynska, Agata Swiatly, Jan Matysiak and Wojciech Dyszkiewicz analyzed the data. Agnieszka Klupczynska, Agata Swiatly, Joanna Hajduk, Jan Matysiak, Wojciech Dyszkiewicz and Zenon J. Kokot wrote paper. All authors have read and approved the manuscript submitted.

Conflicts of Interest: The authors declare no conflict of interest.

Abbreviations

MALDI-TOF-MS	Matrix-assisted laser desorption/ionization time-of-flight mass spectrometry
LC	Lung cancer
NSCLC	Non-small cell lung cancer
ROC curve	Receiver operating characteristic curve
AUC	Area under the ROC curve
GA	Genetic algorithm
QC	Quick classifier
SNN	Supervised neural network
TFA	Trifluoroacetic acid
ACN	Acetonitrile
HCCA	α-Cyano-4-hydroxycinnamic acid

References and Notes

1. Jemal, A.; Bray, F.; Center, M.M.; Ferlay, J.; Ward, E.; Forman, D. Global cancer statistics: 2011. *CA Cancer J. Clin.* **2011**, *61*, 69–90. [CrossRef] [PubMed]
2. Siegel, R.L.; Miller, K.D.; Jemal, A. Cancer statistics, 2015. *CA Cancer J. Clin.* **2015**, *65*, 5–29. [CrossRef] [PubMed]

3. Subramaniam, S.; Thakur, R.K.; Yadav, V.K.; Nanda, R.; Chowdhury, S.; Agrawal, A. Lung cancer biomarkers: State of the art. *J. Carcinog.* **2013**, *12*, 3. [PubMed]
4. Patz, E.F.; Campa, M.J.; Gottlin, E.B.; Kusmartseva, I.; Xiang, R.G.; Herndon, J.E. Panel of serum biomarkers for the diagnosis of lung cancer. *J. Clin. Oncol.* **2007**, *25*, 5578–5583. [CrossRef] [PubMed]
5. Patz, E.F.; Pinsky, P.; Gatsonis, C.; Sicks, J.D.; Kramer, B.S.; Tammemägi, M.C.; Chiles, C.; Black, W.C.; Aberle, D.R. Overdiagnosis in low-dose computed tomography screening for lung cancer. *JAMA Intern. Med.* **2014**, *174*, 269–274. [CrossRef] [PubMed]
6. Hori, S.; Nishiumi, S.; Kobayashi, K.; Shinohara, M.; Hatakeyama, Y.; Kotani, Y.; Hatano, N.; Maniwa, Y.; Nishio, W.; Bamba, T.; *et al*. A metabolomic approach to lung cancer. *Lung Cancer* **2011**, *74*, 284–292. [CrossRef] [PubMed]
7. Mazzone, P.J.; Wang, X.F.; Beukemann, M.; Zhang, Q.; Seeley, M.; Mohney, R.; Holt, T.; Pappan, K.L. Metabolite profiles of the serum of patients with non-small cell carcinoma. *J. Thorac Oncol.* **2016**, *11*, 72–78. [CrossRef] [PubMed]
8. Musharraf, S.G.; Mazhar, S.; Choudhary, M.I.; Rizi, N.; Atta-ur-Rahman, A. Plasma metabolite profiling and chemometric analyses of lung cancer along with three controls through gas chromatography-mass spectrometry. *Sci. Rep.* **2015**, *5*, 8607. [CrossRef] [PubMed]
9. Chen, Y.; Ma, Z.; Li, A.; Li, H.; Wang, B.; Zhong, J.; Min, L.; Dai, L. Metabolomic profiling of human serum in lung cancer patients using liquid chromatography/hybrid quadrupole time-of-flight mass spectrometry and gas chromatography/mass spectrometry. *J. Cancer Res. Clin. Oncol.* **2015**, *141*, 705–718. [CrossRef] [PubMed]
10. Miyamoto, S.; Taylor, S.; Barupal, D.; Taguchi, A.; Wohlgemuth, G.; Wikoff, W.; Yoneda, K.; Gandara, D.; Hanash, S.; Kim, K.; *et al*. Systemic metabolomic changes in blood samples of lung cancer patients identified by gas chromatography time-of-flight mass spectrometry. *Metabolites* **2015**, *5*, 192–210. [CrossRef] [PubMed]
11. Li, Y.; Song, X.; Zhao, X.; Zou, L.; Xu, G. Serum metabolic profiling study of lung cancer using ultra high performance liquid chromatography/quadrupole time-of-flight mass spectrometry. *J. Chromatogr. B.* **2014**, *966*, 147–153. [CrossRef] [PubMed]
12. Chen, Y.; Ma, Z.; Min, L.; Li, H.; Wang, B.; Zhong, J.; Dai, L. Biomarker identification and pathway analysis by serum metabolomics of lung cancer. *Biomed. Res. Int.* **2015**, *2015*, 183624. [CrossRef] [PubMed]
13. Maeda, J.; Higashiyama, M.; Imaizumi, A.; Nakayama, T.; Yamamoto, H.; Daimon, T.; Yamakado, M.; Imamura, F.; Kodama, K. Possibility of multivariate function composed of plasma amino acid profiles as a novel screening index for non-small cell lung cancer: A case control study. *BMC Cancer* **2010**, *10*, 690. [CrossRef] [PubMed]
14. Shingyoji, M.; Iizasa, T.; Higashiyama, M.; Imamura, F.; Saruki, N.; Imaizumi, A.; Yamamoto, H.; Daimon, T.; Tochikubo, O.; Mitsushima, T.; *et al*. The significance and robustness of a plasma free amino acid (PFAA) profile-based multiplex function for detecting lung cancer. *BMC Cancer* **2013**, *13*, 77. [CrossRef] [PubMed]
15. Liotta, L.A.; Petricoin, E.F. Serum peptidome for cancer detection: Spinning biologic trash into diagnostic gold. *J. Clin. Investig.* **2006**, *116*, 26–30. [CrossRef] [PubMed]
16. Lopez, M.F.; Mikulskis, A.; Kuzdzal, S.; Golenko, E.; Petricoin, E.F.; Liotta, L.A.; Patton, W.F.; Whiteley, G.R.; Rosenblatt, K.; Gurnani, P.; *et al*. A novel, high-throughput workflow for discovery and identification of serum carrier protein-bound peptide biomarker candidates in ovarian cancer samples. *Clin. Chem.* **2007**, *53*, 1067–1074. [CrossRef] [PubMed]
17. Schneider, J. Tumor markers in detection of lung cancer. *Adv. Clin. Chem.* **2006**, *42*, 1–41. [PubMed]
18. Tas, F.; Aydiner, A.; Topuz, E.; Yasasever, V.; Karadeniz, A.; Saip, P. Utility of the serum tumor markers: CYFRA 21.1, carcinoembryonic antigen (CEA), and squamous cell carcinoma antigen (SCC) in squamous cell lung cancer. *J. Exp. Clin. Canc. Res.* **2000**, *19*, 477–481.
19. Kulpa, J.; Wojcik, E.; Reinfuss, M.; Kolodziejski, L. Carcinoembryonic antigen, squamous cell carcinoma antigen, CYFRA 21–1, and neuron-specific enolase in squamous cell lung cancer patients. *Clin. Chem.* **2002**, *48*, 1931–1937. [PubMed]
20. Indovina, P.; Marcelli, E.; Pentimalli, F.; Tanganelli, P.; Tarro, G.; Giordano, A. Mass spectrometry-based proteomics: The road to lung cancer biomarker discovery. *Mass Spectrom. Rev.* **2012**, *32*, 129–142. [CrossRef] [PubMed]
21. Bajtarevic, A.; Ager, C.; Pienz, M.; Klieber, M.; Schwarz, K.; Ligor, M.; Ligor, T.; Filipiak, W.; Denz, H.; Fiegl, M.; *et al*. Noninvasive detection of lung cancer by analysis of exhaled breath. *BMC Cancer* **2009**, *9*, 348. [CrossRef] [PubMed]

22. Peng, G.; Tisch, U.; Adams, O.; Hakim, M.; Shehada, N.; Broza, Y.Y.; Billan, S.; Abdah-Bortnyak, R.; Kuten, A.; Haick, H. Diagnosing lung cancer in exhaled breath using gold nanoparticles. *Nat. Nanotechnol.* **2009**, *4*, 669–673. [CrossRef] [PubMed]
23. Phillips, M.; Altorki, N.; Austin, J.H.M.; Cameron, R.B.; Cataneo, R.N.; Greenberg, J.; Kloss, R.; Maxfield, R.A.; Munawar, M.I.; Pass, H.I.; *et al*. Prediction of lung cancer using volatile biomarkers in breath. *Cancer Biomark.* **2007**, *3*, 95–109. [PubMed]
24. Poli, D.; Carbognani, P.; Corradi, M.; Goldoni, M.; Acampa, O.; Balbi, B.; Bianchi, L.; Rusca, M.; Mutti, A. Exhaled volatile organic compounds in patients with non-small cell lung cancer: Cross sectional and nested short-term follow-up study. *Respir. Res.* **2005**, *6*, 71. [CrossRef] [PubMed]
25. Yang, S.; Xiao, X.; Zhang, W.; Zhang, L.; Zhang, W.; Zhou, B.; Chen, G.; He, D. Application of serum SELDI proteomic patterns in diagnosis of lung cancer. *BMC Cancer* **2005**, *5*, 83. [CrossRef] [PubMed]
26. Hocker, J.R.; Peyton, M.D.; Lerner, M.R.; Mitchell, S.L.; Lightfoot, S.A.; Lander, T.J.; Bates-Albers, L.M.; Vu, N.T.; Hanas, R.J.; Kupiec, T.C.; *et al*. Serum discrimination of early-stage lung cancer patients using electrospray-ionization mass spectrometry. *Lung Cancer* **2011**, *74*, 206–211. [CrossRef] [PubMed]
27. Chen, Z.; Fillmore, C.M.; Hammerman, P.S.; Kim, C.F.; Wong, K.K. Non-small-cell lung cancers: A heterogeneous set of diseases. *Nat. Rev. Cancer* **2014**, *14*, 535–546. [CrossRef] [PubMed]
28. Han, M.K.; Oh, Y.H.; Kang, J.; Kim, Y.P.; Seo, S.; Kim, J.; Park, K.; Kim, H.S. Protein profiling in human sera for identification of potential lung cancer biomarkers using antibody microarray. *Proteomics* **2009**, *9*, 5544–5552. [CrossRef] [PubMed]
29. Shevchenko, V.E.; Arnotskaya, N.E.; Zaridze, D.G. Detection of lung cancer using plasma protein profiling by matrix-assisted laser desorption/ionization mass spectrometry. *Eur. J. Mass Spectrom.* **2010**, *16*, 539–549. [CrossRef] [PubMed]
30. Lin, X.L.; Yang, S.Y.; Du, J.; Tian, Y.X.; Bu, L.N.; Huo, S.F.; Wang, F.P.; Nan, Y.D. Detection of lung adenocarcinoma using magnetic beads based matrix-assisted laser desorption/ionization time-of-flight mass spectrometry serum protein profiling. *Chin. Med. J.* **2010**, *123*, 34–39. [PubMed]
31. Musharraf, S.G.; Hashmi, N.; Choudhary, M.I.; Rizvi, N.; Usman, A.; Atta-ur-Rahman, A. Comparison of plasma from healthy nonsmokers, smokers, and lung cancer patients: Pattern-based differentiation profiling of low molecular weight proteins and peptides by magnetic bead technology with MALDI-TOF MS. *Biomarkers* **2012**, *17*, 223–230. [CrossRef] [PubMed]
32. Sandanayake, N.S.; Camuzeaux, S.; Sinclair, J.; Blyuss, O.; Andreola, F.; Chapman, M.H.; Webster, G.J.; Smith, R.C.; Timms, J.F.; Pereira, S.P. Identification of potential serum peptide biomarkers of biliary tract cancer using MALDI MS profiling. *BMC Clin. Pathol.* **2014**, *14*, 7. [CrossRef] [PubMed]
33. Abramowicz, A.; Wojakowska, A.; Gdowicz-Klosok, A.; Polanska, J.; Rodziewicz, P.; Polanowski, P.; Namysl-Kaletka, A.; Pietrowska, M.; Wydmanski, J.; Widlak, P. Identification of serum proteome signatures of locally advanced and metastatic gastric cancer: A pilot study. *J. Transl. Med.* **2015**, *13*, 304. [CrossRef] [PubMed]
34. Fania, C.; Sogno, I.; Vasso, M.; Torretta, E.; Leone, R.; Bruno, A.; Consonni, P.; Albini, A.; Gelfi, C. A PSA-guided approach for a better diagnosis of prostatic adenocarcinoma based on MALDI profiling and peptide identification. *Clin. Chim. Acta* **2015**, *439*, 42–49. [CrossRef] [PubMed]
35. Wadsworth, J.T.; Somers, K.D.; Cazares, L.H.; Malik, G.; Adam, B.L.; Stack, B.C.; Wright, G.L.; Semmes, O.J. Serum protein profiles to identify head and neck cancer. *Clin. Cancer Res.* **2004**, *10*, 1625–1632. [CrossRef] [PubMed]
36. Pietrowska, M.; Polanska, J.; Marczak, L.; Behrendt, K.; Nowicka, E.; Stobiecki, M.; Polanski, A.; Tarnawski, R.; Widlak, P. Mass spectrometry-based analysis of therapy-related changes in serum proteome patterns of patients with early-stage breast cancer. *J. Transl. Med.* **2010**, *8*, 66. [CrossRef] [PubMed]
37. Liotta, L.A.; Petricoin, E.F. Mass spectrometry-based protein biomarker discovery: Solving the remaining challenges to reach the promise of clinical benefit. *Clin. Chem.* **2010**, *56*, 1641–1642. [CrossRef] [PubMed]
38. Tiss, A.; Smith, C.; Camuzeaux, S.; Kabir, M.; Gayther, S.; Menon, U.; Waterfield, M.; Timms, J.; Jacobs, I.; Cramer, R. Serum peptide profiling using MALDI mass spectrometry: Avoiding the pitfalls of coated magnetic beads using well-established ZipTip technology. *Proteomics* **2007**, *1*, 77–89. [CrossRef] [PubMed]
39. Hajduk, J.; Matysiak, J.; Kokot, P.; Nowicki, P.; Derezиński, P.; Kokot, Z.J. The application of fuzzy statistics and linear discriminant analysis as criteria for optimizing the preparation of plasma for matrix-assisted laser

desorption/ionization mass spectrometry peptide profiling. *Clin. Chim. Acta* **2015**, *448*, 174–181. [CrossRef] [PubMed]

40. Callesen, A.K.; Madsen, J.S.; Vach, W.; Kruse, T.A.; Mogensen, O.; Jensen, O.N. Serum protein profiling by solid phase extraction and mass spectrometry: A future diagnostics tool? *Proteomics* **2009**, *9*, 1428–1441. [CrossRef] [PubMed]
41. Hajduk, J.; Klupczynska, A.; Dereziński, P.; Matysiak, J.; Kokot, P.; Nowak, D.; Gajęcka, M.; Nowak-Markwitz, E.; Kokot, Z.J. A combined metabolomic and proteomic analysis of gestational diabetes mellitus. *Int. J. Mol. Sci.* **2015**, *16*, 30034–30045. [CrossRef] [PubMed]
42. Pio, R.; Ajona, D.; Lambris, J.D. Complement inhibition in cancer therapy. *Semin. Immunol.* **2013**, *25*, 54–64. [CrossRef] [PubMed]
43. Rutkowski, M.J.; Sughrue, M.E.; Kane, A.J.; Mills, S.A.; Parsa, A.T. Cancer and the complement cascade. *Mol. Cancer Res.* **2010**, *8*, 1453–1465. [CrossRef] [PubMed]
44. Maness, P.F.; Orengo, A. Serum complement levels in patients with digestive tract carcinomas and other neoplastic diseases. *Oncology* **1977**, *34*, 87–89. [CrossRef] [PubMed]
45. Ytting, H.; Jensenius, J.C.; Christensen, I.J.; Thiel, S.; Nielsen, H.J. Increased activity of the mannan-binding lectin complement activation pathway in patients with colorectal cancer. *Scand. J. Gastroenterol.* **2004**, *39*, 674–679. [CrossRef] [PubMed]
46. Markiewski, M.M.; DeAngelis, R.A.; Benencia, F.; Ricklin-Lichtsteiner, S.K.; Koutoulaki, A.; Gerard, C.; Coukos, G.; Lambris, J.D. Modulation of the antitumor immune response by complement. *Nat. Immunol.* **2008**, *9*, 1225–1235. [CrossRef] [PubMed]
47. Gmiński, J.; Mykała-Cieśla, J.; Machalski, M.; Drózdz, M.; Najda, J. Immunoglobulins and complement components in patients with lung cancer. *Tuberk. Toraks* **2004**, *30*, 39–44.
48. Corrales, L.; Ajona, D.; Rafail, S.; Lasarte, J.J.; Riezu-Boj, J.I.; Lambris, J.D.; Rouzaut, A.; Pajares, M.J.; Montuenga, L.M.; Pio, R. Anaphylatoxin C5a creates a favorable microenvironment for lung cancer progression. *J. Immunol.* **2012**, *189*, 4674–4683. [CrossRef] [PubMed]
49. Watson, N.F.; Durrant, L.G.; Madjd, Z.; Ellis, I.O.; Scholefield, J.H.; Spendlove, I. Expression of the membrane complement regulatory protein CD59 (protectin) is associated with reduced survival in colorectal cancer patients. *Cancer Immunol. Immunother.* **2006**, *55*, 973–980. [CrossRef] [PubMed]
50. Xu, C.; Jung, M.; Burkhardt, M.; Stephan, C.; Schnorr, D.; Loening, S.; Jung, K.; Dietel, M.; Kristiansen, G. Increased CD59 protein expression predicts a PSA relapse in patients after radical prostatectomy. *Prostate* **2005**, *62*, 224–232. [CrossRef] [PubMed]
51. Farrell, D.H.; Thiagarajan, P.; Chung, D.W.; Davie, E.W. Role of fibrinogen α and γ chain sites in platelet aggregation. *Proc. Natl. Acad. Sci. USA* **1992**, *89*, 10729–10732. [CrossRef] [PubMed]
52. Theodorescu, D.; Wittke, S.; Ross, M.M.; Walden, M.; Conaway, M.; Just, I.; Mischak, H.; Frierson, H.F. Discovery and validation of new protein biomarkers for urothelial cancer: A prospective analysis. *Lancet Oncol.* **2006**, *7*, 230–240. [CrossRef]
53. Bergen, H.R.; Vasmatzis, G.; Cliby, W.A.; Johnson, K.L.; Oberg, A.L.; Muddiman, D.C. Discovery of ovarian cancer biomarkers in serum using NanoLC electrospray ionization TOF and FT-ICR mass spectrometry. *Dis. Markers* **2004**, *19*, 239–249. [CrossRef]
54. Ebert, M.P.; Niemeyer, D.; Deininger, S.O.; Wex, T.; Knippig, C.; Hoffmann, J.; Sauer, J.; Albrecht, W.; Malfertheiner, P.; Röcken, C. Identification and confirmation of increased fibrinopeptide a serum protein levels in gastric cancer sera by magnet bead assisted MALDI-TOF mass spectrometry. *J. Proteome Res.* **2006**, *5*, 2152–2158. [CrossRef] [PubMed]
55. Villanueva, J.; Shaffer, D.R.; Philip, J.; Chaparro, C.A.; Erdjument-Bromage, H.; Olshen, A.B.; Fleisher, M.; Lilja, H.; Brogi, E.; Boyd, J.; *et al.* Differential exoprotease activities confer tumor-specific serum peptidome patterns. *J. Clin. Investig.* **2006**, *116*, 271–284. [CrossRef] [PubMed]
56. Villanueva, J.; Martorella, A.J.; Lawlor, K.; Philip, J.; Fleisher, M.; Robbins, R.J.; Tempst, P. Serum peptidome patterns that distinguish metastatic thyroid carcinoma from cancer-free controls are unbiased by gender and age. *Mol. Cell. Proteomics* **2006**, *5*, 1840–1852. [CrossRef] [PubMed]
57. Maes, E.; Mertens, I.; Valkenborg, D.; Pauwels, P.; Rolfo, C.; Baggerman, G. Proteomics in cancer research: Are we ready for clinical practice? *Crit. Rev. Oncol. Hematol.* **2015**, *96*, 437–448. [CrossRef] [PubMed]

58. Calderaro, A.; Arcangeletti, M.C.; Rodighiero, I.; Buttrini, M.; Gorrini, C.; Motta, F.; Germini, D.; Medici, M.C.; Chezzi, C.; de Conto, F. Matrix-assisted laser desorption/ionization time-of-flight (MALDI-TOF) mass spectrometry applied to virus identification. *Sci. Rep.* **2014**, *4*, 6803. [CrossRef] [PubMed]
59. Basics on data preparation, model generation and spectra classification. In *ClinProTools 3.0 User Manual*; Bruker Daltonics: Bremen, Germany, 2011; pp. 51–96.
60. Villanueva, J.; Lawlor, K.; Toledo-Crow, R.; Tempst, P. Automated serum peptide profiling. *Nat. Protoc.* **2006**, *1*, 880–891. [CrossRef] [PubMed]
61. Matysiak, J.; Światły, A.; Hajduk, J.; Matysiak, J.; Kokot, Z.J. Influence of honeybee sting on peptidome profile in human serum. *Toxins* **2015**, *7*, 1808–1820. [CrossRef] [PubMed]
62. Xiao, D.; Zhao, F.; Zhang, H.; Meng, F.; Zhang, J. Novel strategy for typing Mycoplasma pneumoniae isolates by use of matrix-assisted laser desorption ionization-time of flight mass spectrometry coupled with ClinProTools. *J. Clin. Microbiol.* **2014**, *52*, 3038–3043. [CrossRef] [PubMed]



© 2016 by the authors; licensee MDPI, Basel, Switzerland. This article is an open access article distributed under the terms and conditions of the Creative Commons by Attribution (CC-BY) license (http://creativecommons.org/licenses/by/4.0/).

International Journal of
Molecular Sciences

MDPI

Article

EIYMNVPV Motif is Essential for A1CF Nucleus Localization and A1CF (-8aa) Promotes Proliferation of MDA-MB-231 Cells via Up-Regulation of *IL-6*

Li Zhou [1,†], Jin Hao [1,†], Yue Yuan [1], Rui Peng [1], Honglian Wang [2], Dongsheng Ni [1], Yuping Gu [1], Liyuan Huang [1], Zhaomin Mao [1], Zhongshi Lyu [1], Yao Du [1], Zhicheng Liu [1], Yiman Li [1], Pan Ju [1], Yaoshui Long [1], Jianing Liu [1] and Qin Zhou [1,*]

1 The Division of Molecular Nephrology and the Creative Training Center for Undergraduates, The M.O.E. Key Laboratory of Laboratory Medical Diagnostics, the College of Laboratory Medicine, Chongqing Medical University, Chongqing 400016, China; shmily525520@sina.com (L.Z.); lanyxiu@163.com (J.H.); yyokyy1126@hotmail.com (Y.Y.); pengrui911@foxmail.com (R.P.); cqmunds@163.com (D.N.); guyupinglittle@sina.com (Y.G.); lyhuang0603@sina.com (L.H.); mao1204086118@163.com (Z.M.); Zhongshilyu@163.com (Z.L.); duyao_steve@163.com (Y.D.); liuzhicheng323@163.com (Z.L.); 18715854036@sina.cn (Y.L.); 18883936591@163.com (P.J.); lys960110@sina.com (Y.L.); keithljn@sina.cn (J.L.)

2 Laboratory of Organ Fibrosis Prophylaxis and Treatment by Combine Traditional Chinese and Western Medicine, Research Center of Combine Traditional Chinese and Western Medicine, Affiliated Traditional Medicine Hospital of Sichuan Medical University, Luzhou 646000, China; hackie_wang@126.com

* Correspondence: zhouqin@cqmu.edu.cn; Tel.: +86-23-6848-5688

† These authors contributed equally to this work.

Academic Editors: William Chi-shing Cho and Sanjay K. Srivastava
Received: 5 January 2016; Accepted: 20 May 2016; Published: 25 May 2016

Abstract: Apobec-1 complementation factor (A1CF) is a heterogeneous nuclear ribonucleoprotein (hnRNP) and mediates apolipoprotein-B mRNA editing. A1CF can promote the regeneration of the liver by post-transcriptionally stabilizing Interleukin-6 (*IL-6*) mRNA. It also contains two transcriptional variants-A1CF64 and A1CF65, distinguished by the appearance of a 24-nucleotide motif which contributes to the corresponding eight-amino acid motif of EIYMNVPV. For the first time, we demonstrated that the EIYMNVPV motif was essential for A1CF nucleus localization, A1CF deficient of the EIYMNVPV motif, A1CF (-8aa) showed cytoplasm distribution. More importantly, we found that A1CF (-8aa), but not its full-length counterpart, can promote proliferation of MDA-MB-231 cells accompanied with increased level of *IL-6* mRNA. Furthermore, silencing of *IL-6* attenuated A1CF (-8aa)-induced proliferation in MDA-MB-231 cells. In conclusion, notably, these findings suggest that A1CF (-8aa) promoted proliferation of MDA-MB-231 cells *in vitro* viewing *IL-6* as a target. Thus, the EIYMNVPV motif could be developed as a potential target for basal-like breast cancer therapy.

Keywords: Apobec-1 complementation factor (A1CF); EIYMNVPV motif; Interleukin-6 (*IL-6*); nucleus localization; proliferation; MDA-MB-231 cells

1. Introduction

Apobec-1 complementation factor (A1CF), also known as ACF, is the RNA binding subunit of a minimal core protein complex for apolipoprotein-B (apoB) mRNA edition [1–3]. Coordinated with APOBEC-1, A1CF regulates site-specific C to U edition of apoB mRNA, leadings to the truncated isoform apoB48, rather than apoB100. During this process, A1CF recognizes an AU-rich motif (mooring sequences) on apoB mRNA and guides APOBEC-1, the cytosine deaminase, to localize to the right site to edit [1,4–8]. However, the binding of A1CF to RNA may not be restricted to mooring sequence. It was reported that A1CF can promote liver regeneration after hepatectomy by binding *IL-6* mRNA at

the AU-rich region of 3′-UTR, which shows no typical mooring sequence, to stabilize its expression [9]. Furthermore, germ-line deletion of *A1CF* directly resulted in embryonic lethality due to the defect of early embryo implant [10]. Knockdown of *A1CF* decreased proliferation in rat hepatoma cells [11]. In addition, A1CF contains three non-identical RNA recognition motifs (RRM) in its N-terminus and a unique C-terminal auxiliary domain, which are required for complementing activity, RNA binding and apoB mRNA editing [12]. Dance *et al.* demonstrated that the A1CF exon 11 is alternatively spliced to include or exclude 24 nucleotides at exon 12, leading to two variants, ACF65 and ACF64. Both variants are equivalent for apoB mRNA edition in cells [13]. In order to highlight the structure characters of the two variants, we designate the one excluding EIYMNVPV motif (A1CF64) as A1CF (-8aa), and the other including the EIYMNVPV motif (A1CF65) as A1CF. Fossat *et al.* reported that RBM47 interacted with APOBEC1 and A1CF and also took part in the C to U RNA edition. Furthermore, RBM47 can replace A1CF to complement APOBEC1's RNA edition *in vitro* [14]. Given the important role of RBM47 in progression of breast cancer, and similar structure, function between RBM47 and A1CF [15], we hypothesize that A1CF (-8aa) or A1CF may also play a biological role in breast cancer.

Breast cancer is one of the most common malignancies in women with multifactorial etiology. In recent years, the treatments of breast cancer focus on the identification of cytokines as prognostic factors, including several interleukins (IL-1, IL-6, IL-10), transforming growth factor-β (TGF-β), tumor necrosis factor-a (TNF-a) and so on [16]. Among them, IL-6 is a secreted multifunctional cytokine and mainly functions in the host immune defense and the modulation of growth and differentiation in various malignancies [17–22]. It has been reported that IL-6 is involved in stimulating proliferation in many cancers, such as colorectal cancer, prostate cancer, intestinal disease, and so forth [23–25]. Meanwhile, recent studies have identified IL-6 as a prognostic factor in the treatment of breast cancer. There existed a reduction in proliferation following *IL-6* knockdown on basal-like breast cancer cells including MDA-MB-231 and Hs578T cells [21,26]. Most importantly, it was confirmed that A1CF could bind to an unstable AU-rich region in *IL-6* at its 3′-UTR to functionally regulate *IL-6* mRNA stability at posttranscriptional level [9,11]. However, whether *IL-6* is a downstream effector of A1CF (-8aa) or A1CF in breast cancer progression remained unclear.

In this study, we demonstrated that the EIYMNVPV motif is essential for the nuclear localization of A1CF in MDCK cells and MDA-MB-231 cells. A1CF (-8aa), but not A1CF, could promote the proliferation of MDA-MB-231cells via upregulating *IL-6*, However, A1CF (-8aa)-mediated proliferation can be inhibited by silence of *IL-6*.

2. Results

2.1. Bioinformatics Analysis of A1CF

To show the characteristic of A1CF, we respectively analyzed the evolution tree and the conservation of A1CF among mammal species using MEGA5 software (http://www.megasoftware.net/), clustalW multiple sequence alignment software, and NCBI blast. The DNA sequences similarity rates among species had been shown on the right side of the evolution tree mainly ranging from 78% to 92% in relation to *Homo sapiens*, except that *Caenohabditis elegans* displayed the similarity of 47% (Figure 1A). Furthermore, the transcript variants of A1CF encoding the longest protein sequences were employed to do a comparative analysis of amino acids based on the DNAssist software among *Homo sapiens*, *Mus musculus*, *Gallus gallus*, *Xenopus laevis*, and *Danio rerio*. As descripted in Figure 1B, the results of alignment revealed a high conservation among them. Moreover, functional motif analysis prediction suggested that mus-A1CF contains three non-identical RNA recognition motifs (RRM) on the N terminus, a double-strand RNA binding motif (dsRBM) on C terminus, and a nucleus localization signal (Figure 1C), which is in accordance with the results in *Homo sapiens* reported by Valerie Blanc *et al.* [27]. All of the results further indicate that A1CF is highly conservative.

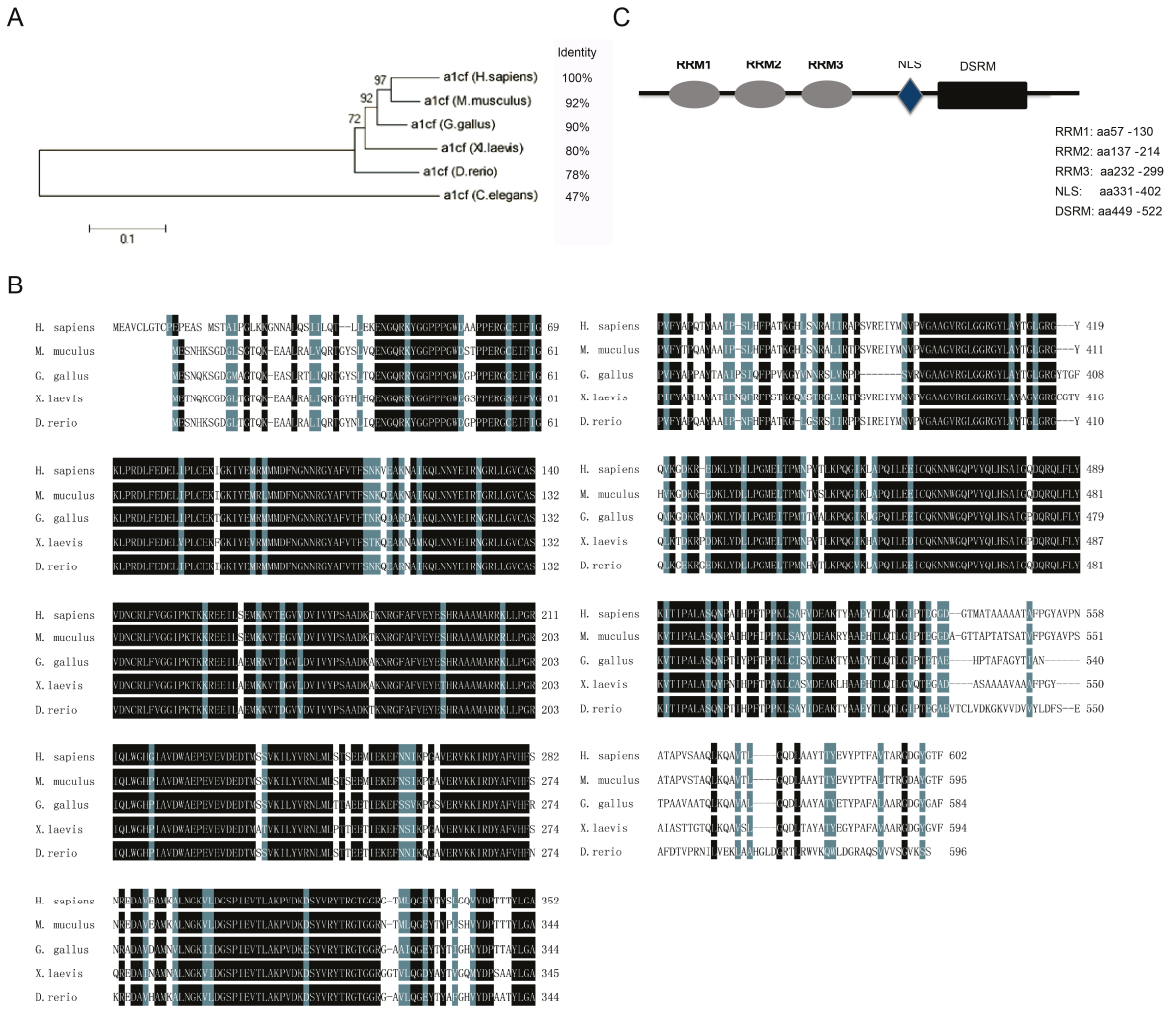

Figure 1. A1CF is conservative on evolution via bioinformatics analysis. (**A**) High conservation of A1CF across species in the schematic diagram of phylogenetic analysis. The similarity of amino acids sequences among species was shown as percentage; (**B**) Amino acids sequences alignment of A1CF among *Homo sapiens*, *Mus musculus*, *Gallus gallus*, *Xenopus laevis*, and *Denio rerio*. The identical amino acids were shaded in black and the similar amino acids were in grey; and (**C**) the predicted protein structure of *mus-A1CF* on the net. It contains three non-identical RRM on the N terminus, a nucleus localization signal, and a dsRBM on its C terminus, RRM, RNA recognition motif. ASN, A1CF specific nuclear signal. DSRM, double-strand RNA binding motif.

2.2. The Deletion of the EIYMNVPV Motif by Alternative Splicing is Conserved Across Species

Previous study has indicated that A1CF is alternatively spliced to include or exclude a 24-nucleotide motif in humans [13]. For mouse A1CF, this alternative splice takes place in the 5′ terminus of exon 9 (Figure 2A). To figure out whether this kind of special splice event happens in other evolutionarily lower-ordered species, we compared the corresponding mRNA region of A1CF transcripts from *H. sapiens* (*Homo sapiens*), *M. musculus* (*Mus musculus*), *G. gallus* (*Gallus gallus*) and *D. rerio* (*Denio rerio*). As shown in Figure 2B, transcript deficient of EIYMNVPV (A1CF (-8aa)) can be found from chicken and zebrafish. Further analysis show that there exist an alternative splice acceptor site in the anterior region of exon 9 (asterisk in Figure 2B). In conclusion, these data demonstrate that the alternative splice event leading to the A1CF (-8aa) isoform is evolutionarily conserved, which implies its biological importance.

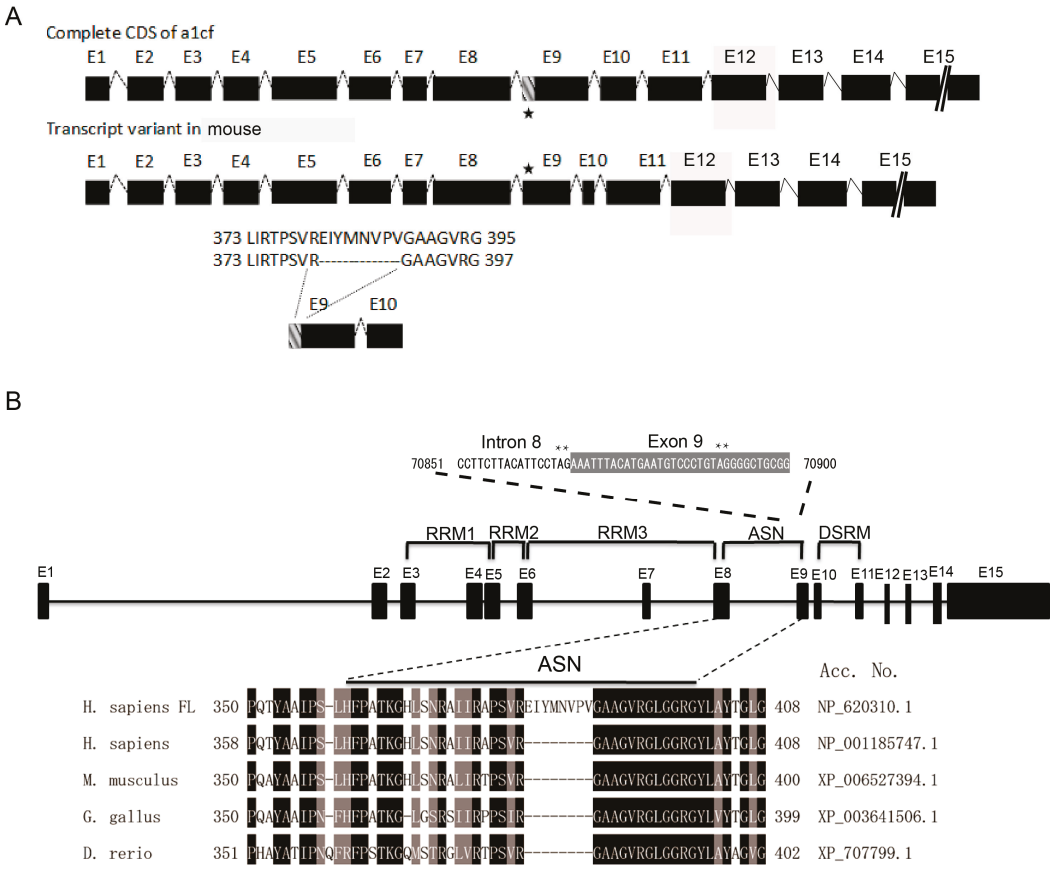

Figure 2. The conservation analysis of the EIYMNVPV motif deficiency (**A**) exon pattern of mouse *a1cf* transcript and its alternatively-spliced variant *A1CF (-8aa)*.An alternative splice in exon 9 results in a deletion of the EIYMNVPV motif. As the pentagram shows, this alternative splice takes place in the 5′ terminus of exon 9; and (**B**) the conservation of the EIYMNVPV motif deficiency among *H. sapiens*, *M. musculus*, *G. gallus*, and *D. rerio*. Human full length A1CF (FL) was used for comparison with A1CF (-8aa) from human, mouse, chicken, and zebrafish respectively, the asterisks represent an alternative splice acceptor site in the anterior region of exon 9. The identical amino acids were shaded in black and the similar amino acids were in grey.

2.3. EIYMNVPV Motif is Essential for A1CF Nucleus Localization

As is displayed in Figure 2B, the EIYMNVPV motif was located at the 381–388 aa region. However, it was reported that there existed a novel nuclear location signal, termed A1CF-specific nuclear signal (ASN), at the 331–402 aa region, which is indispensable for A1CF nucleus localization (Figure 2B) [27]. Therefore, it remains a concern that whether the absence of EIYMNVPV would impair the nuclear translocation ability of A1CF. To address this question, A1CF and A1CF (-8aa) were cloned, respectively, into proper vectors to express GFP-fused or Flag tag-labeled recombinant protein and the subcellular distribution was checked. As shown in Figure 3A, A1CF-EGFP fusion protein presented nuclear distribution in MDCK cells, while A1CF (-8aa)-EGFP was located in cytoplasm. However, the control protein, EGFP, demonstrated both cytoplasm and nuclear expression. To confirm the influence of the 8aa motif on A1CF subcellular distribution, the small sized flag tag was used to label A1CF protein to exclude the influence of EGFP on A1CF distribution. Similarly, in MDA-MB-231 cells, Flag-A1CF was located in nuclear. However, Flag-A1CF (-8aa) was restricted in cytoplasm (Figure 3B). Collectively, our findings demonstrated that the EIYMNVPV motif physiologically caused by alternative splicing played a critical role in A1CF nucleus localization.

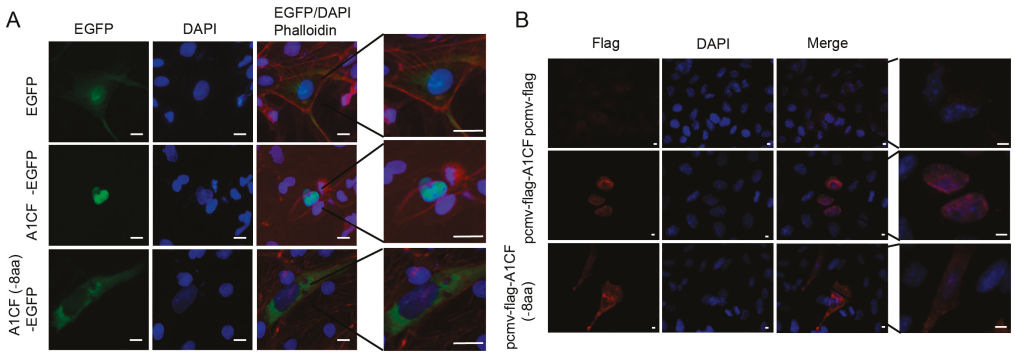

Figure 3. EIYMNVPV motif plays a vital role in A1CF nucleus localization. (**A**) Subcellular distribution of A1CF (-8aa)-EGFP and A1CF-EGFP in MDCK cells with the immunofluorescence technique. Green represents A1CF-EGFP, A1CF (-8aa)-EGFP, or EGFP (null vector); blue stains the nucleus; red is responsible for Phallodin; scale bar represents 10 μm, the scale bar of the sub Figure on the right: 10 μm; and (**B**) fluorescence immunostaining to show the subcellular distribution of Flag-A1CF (-8aa) and Flag-A1CF in MDA-MB-231 cells. Red is responsible for pcmv-flag-A1CF (-8aa), pcmv-flag-A1CF, and pcmv-flag, blue stains the nucleus; scale bar: 49 μm, the scale bar of the sub Figure on the right: 2 μm.

2.4. A1CF (-8aa) Promotes Proliferation of MDA-MB-231 Cells

To uncover the biological significance of A1CF (-8aa), we firstly investigate the expression pattern of *A1CF* and *A1CF (-8aa)* in MDA-MB-231 cells, a breast tumor cell line. Semi-quantitative PCR was used to analyze the relative expression abundance of *A1CF* and *A1CF (-8aa)*. As shown in Figure 4a, the predominant transcript isoform is A1cf, while weak expression of *A1CF (-8aa)* can be observed. Quantitative analysis indicated that A1CF showed twice the expression than that of *A1CF (-8aa)*. As is reported, RBM47 could replace A1CF, and regulate APOBEC1-mediating mRNA editing *in vitro* [14]. Additionally, it participates in the breast cancer progression via modulating mRNA stability [15]. To verify the possible correlation between A1CF (-8aa) and basal-like breast cancer cells, we respectively transfected MDA-MB-231 cells with *A1CF (-8aa)*, *A1CF* and control vector for 36 h. The 5-Ethynyl-20-deoxyuridine (EdU) and the expression of PCNA were examined to evaluate the proliferation effect of A1CF (-8aa) and A1CF on MDA-MB-231 cells. PCNA plays an important role in DNA synthesis, DNA repair, cell cycle progression and cell proliferation [28,29]. As Figure 4B displayed, the ratio of proliferative cells was increased in MDA-MB-231 cells treated with *A1CF (-8aa)*. In line with the EdU incorporation assay, PCNA, a marker for proliferation, showed increased expression in A1CF (-8aa)-transfected cells but not in A1CF-transfected cells as detected by Western blot (Figure 4C). All in all, the above findings indicated that A1CF (-8aa) rather than A1CF promote the proliferation of MDA-MB-231 cells.

2.5. IL-6 Was Involved in A1CF (-8aa)-Promoted Proliferation of MDA-MB-231 Cells

It has been reported that A1CF can promote liver regeneration via *IL-6* by stabilizing *IL-6* mRNA [9]. Furthermore, IL-6 has been proved to play a vital role in breast cancer progression and prognosis. To unravel whether IL-6 mediates A1CF (-8aa)-promoted proliferation, we first checked whether A1CF (-8aa) could enhanced the expression of IL-6. As illustrated in Figure 5A and B, expression level of both mRNA and protein of IL-6 increased in MDA-MB-231 cells transfected with A1CF (-8aa), but not in cells transfected with A1CF. To further clarify the effect of *IL-6* in A1CF (-8aa)-mediated proliferation, RNA silence was used to knockdown IL-6. Three siRNA oligos were designed to screen the siRNA showing best expression silence of IL-6. As determined by western blot in Figure 5C, siRNA1 demonstrated best gene silence efficiency (more than 50% compared with control group). Thus, siRNA1 was used for downstream investigation. Transfection of IL-6 siRNA alone can downregulate the expression of PCNA in MDA-MB-231 cells (Figure 5D). Most importantly, knockdown of IL-6 can reverse the increased expression of PCNA stimulated by A1CF

(-8aa) (Figure 5E). In accordance with decreased expression of PCNA, IL-6 knockdown can also rescue enhanced proliferating cell proportion induced by A1CF (-8aa) as determined by EdU incorporation assay (Figure 5F).

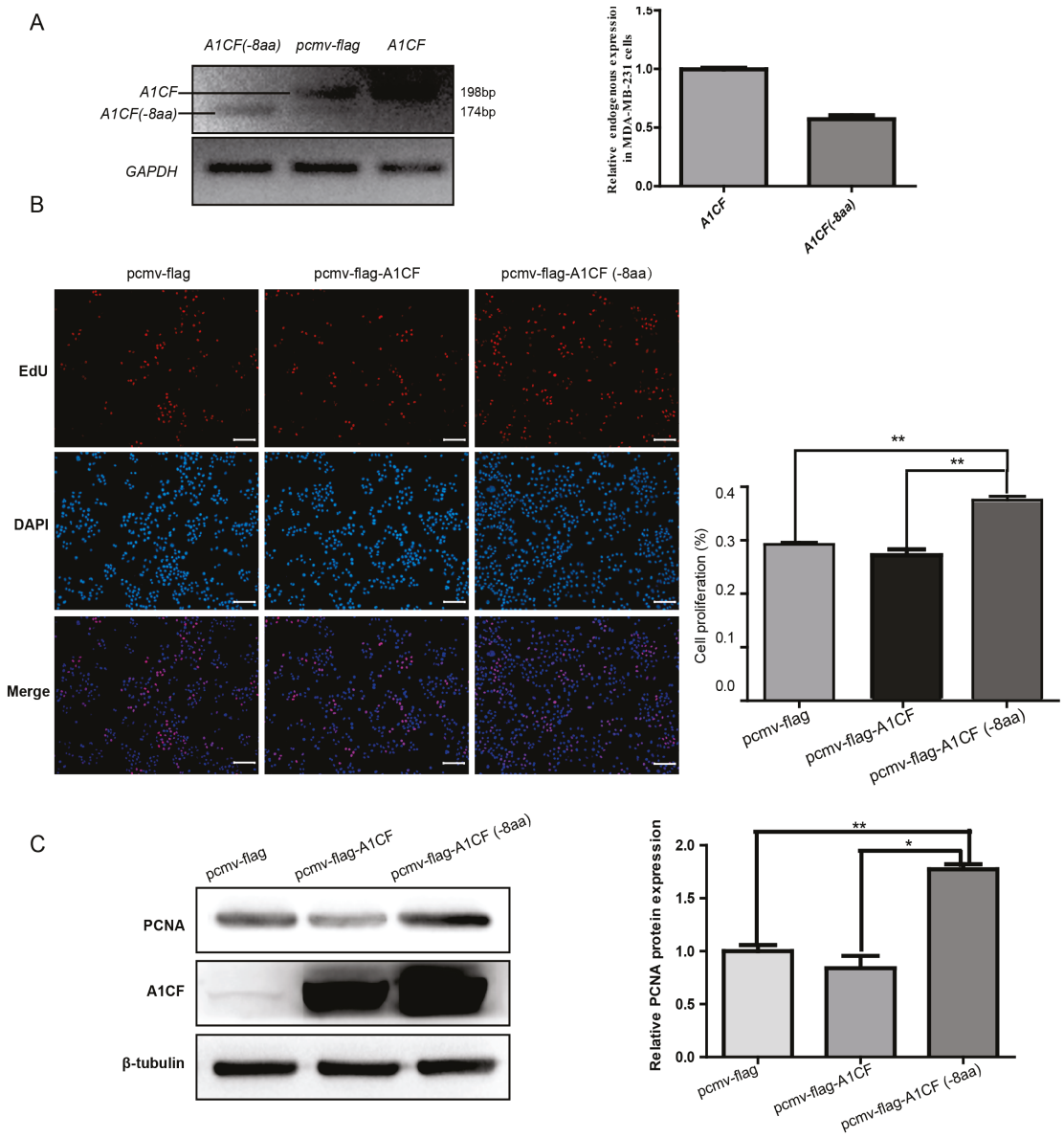

Figure 4. Ectopic expression of *A1CF (-8aa)* promotes the proliferation of MDA-MB-231 cells accompanied by upregulated *IL-6*. (**A**) RT-PCR to detect the endogenous and enforced expression of *A1CF (-8aa)* and *A1CF* expression in MDA-MB-231 cells, *GAPDH* was used as internal control. Cells transfected with pcmv-flag-A1CF and pcmv-flag-A1CF (-8aa) were used as positive control; (**B**) cell proliferation was checked by EdU incorporation assay. Proliferating cells were labeled with EdU (red), with nuclear stained DAPI (blue), scale bar: 100 μm. Statistic graph of the EdU staining was given on the right. Data were representative of three independent experiments, and error bars represent the standard deviation from the mean. ** $p \leqslant 0.01$; and (**C**) MDA-MB-231 cells were transfected with pCMV-flag-A1CF or pCMV-flag-A1CF (-8aa) followed by Western blot to detect the expression of PCNA and A1CF. β-Tubulin was used as loading control. The statistic result was displayed on the right, and revealed that ectopic expression of *A1CF (-8aa)* resulted in a gain of proliferation marker (PCNA) compared with *A1CF* and negative control. * $p \leqslant 0.05$; ** $p \leqslant 0.01$.

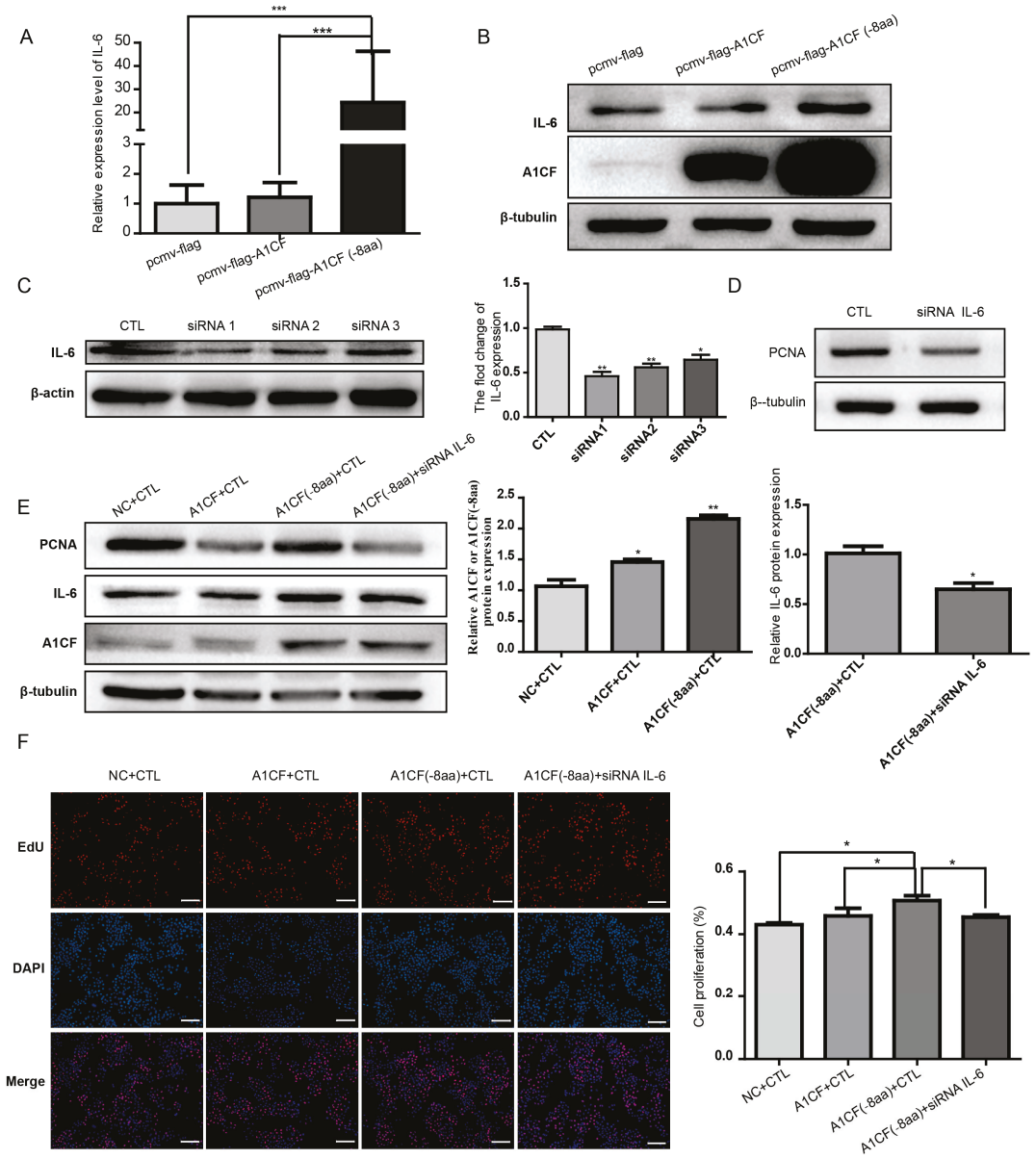

Figure 5. Silencing *IL-6* could attenuate the A1CF (-8aa)-induced proliferation of MDA-MB-231 cells. MDA-MB-231 cells were transfected with pCMV-flag-A1CF or pCMV-flag-A1CF (-8aa) or blank vector. Real-time PCR was performed to detect the RNA level of *IL-6* (**A**) and Western blot to detect the protein level of IL6 and A1CF (**B**); β-tubulin was used as loading control in (**B**); (**C**) the knockdown efficiency of *IL-6* siRNAs was detected by Western blot analysis. β-Actin was taken as loading control. Statistical results are shown on the right; (**D**) the expression of PCNA decreased after *IL-6* siRNA treatment as determined by Western blot. β-Tubulin was taken as internal control; (**E**) Western blot is used to show that the expression of *IL-6* and PCNA declined in cells co-transfected with *A1CF (-8aa)* and *IL-6* siRNA compared with controls. The right statistic data quantified the over-expression and silence efficiency of A1CF and *IL-6*, respectively; and (**F**) rescue assay of cell proliferation by *IL-6* siRNA as determined by EdU assay. Proliferating cells were labeled with EdU (red), and cell nuclei were stained with DAPI (blue), scale bar: 100 μm. The statistical graph is shown on the right. All of the data were representatives of three independent assays, and error bars were on behalf of the standard deviation from the mean. * $p < 0.05$; ** $p < 0.01$; *** $p < 0.001$.

3. Discussion

A series of research findings from Nicholas' group validated the vital role of A1CF for survival, as its deficiency will cause early embryo lethality in development, impaired liver regeneration after hepatectomy, and increased apoptosis of liver cancer cell [10,11]. A1CF is an hnRNP protein with shuttling ability between nuclear and cytoplasm. Yet now, the reported clear biological functions are direct participation in post-transcriptional RNA edition and mRNA stabilization. RNA edition is believed to be a nuclear event. However, A1CF stabilizes *IL-6* mRNA by binding to its AU-rich region should take place in cytoplasm. Blanc *et al.* first identified the nuclear translocation signal of A1CF. Although existence of the alternative transcript encoding A1CF (-8aa), also A1CF64, has been verified years ago, no biological significance has yet been found. Here, for the first time, we reported that the deleted 8aa, EIYMNVPV, was just localized in the internal region of A1CF nuclear translocation signal. Furthermore, functionally, we proved that absence of 8aa abrogated the nuclear localization ability of A1CF. Moreover, we further validated that A1CF (-8aa) but not A1CF contributed to the proliferation of breast cancer cells, thus again firstly uncovering the biological significance of A1CF (-8aa). Given the high-degree conservation of the alternative spliced transcript encoding A1CF (-8aa) across species, A1CF (-8aa)-regulated cell proliferation may have vital roles in varies of aspects. Still, more data are needed to verified the role of A1CF (-8aa) in cell proliferation and survival in other cell lines in addition to breast cancer cells.

Breast cancer is the one of the most common tumors in women with multifactorial etiology. And almost all of the existing strategies for breast cancer treatment are unsatisfactory, impressing the urgent and quite important mechanism research [16]. IL-6 and its downstream signal network (IL-6/IL-6R/gp130) are reported to play important roles in breast cancer. IL-6 was widely expressed in breast cancer and was involved in growth, metastasis of cancer cells, and renewal of cancer stem cells. Thus, IL-6 has already been one of the therapy targets and markers for disease prognosis [30]. In this study, we found that A1CF (-8aa) can promote proliferation of breast cancer cells mostly likely by stabilizing the mRNA of *IL-6*. These findings implicated a role of A1CF in *IL-6* signaling-mediated progress of breast cancer. However, before validation of the role of A1CF in breast cancer, more studies are required to address the prevalence of A1CF (-8aa) in breast cancer and whether blocking A1CF (-8aa) or the corresponding alternative splice event can help cancer therapy.

4. Materials and Methods

4.1. Plasmid Construction

For synthesis of *A1CF (-8aa)* and *A1CF in vitro*, the *A1CF (-8aa)* and *A1CF* fragment were cloned from cDNA by PCR with following primers: *pcmv-flag-A1CF* (F1: 5′-GGATCCACTAGTTCTATGG AATCAAATCACAAATCC-3′; R1: 5′-CACCCGGGATCCTCTGTTAGAAGGTTCCATATGCATCG-3′); *pEGFP-N1-A1CF* (F2: 5′-GATCTCGAGCTCAAGATGGAATCAAATCACAAATCC-3′; R2: 5′-TTCTGC AGTCGACGGGTTAGAAGGTTCCATATGCATCG-3′); Amplified fragment of *A1CF* was inserted into the pcmv-flag at the site of XbaI and pEGFP-N1 at the site of HindIII and XhoI, respectively. Then, plasmids of *pcmv-flag-A1CF (-8aa)* and *pEGFP-N1-A1CF (-8aa)* were separately amplified with the method of point mutation from mature plasmids of *pcmv-flag-A1CF* and *pEGFP-N1-A1CF*, with the primers: *A1CF (-8aa)* (F: 5′-AGGGACATTCATGTAAATTT CTCTGACAGA AGGGGTCCTG-3′; R: 5′-TACATGAATGTCCCTGTAG GGGCTGCGGG GGTGAGAGGA-3′). Finally, all the plasmids were verified by sequencing.

4.2. Cell Culture and Transfection

MDCK cells and MDA-MB-231 cells, as described previously [31,32], were respectively cultured in Dulbecco's Modified Eagle Medium (DMEM) and RPMI-1640, supplemented with 10% fetal bovine serum (FBS, *vol*/*vol*, GIBCO,BRL Co., Ltd., Grand Island, NY, USA) and 0.1% penicillin/streptomycin (Invitrogen, Grand Island, NY, USA). All the cell lines were cultured at 37 °C with 5% CO_2. For some

experiments, cells was transiently transfected with overexpression plasmids of *A1CF (-8aa)*, *A1CF*, negative control, or *IL-6*-siRNA (50 nM) by using Lipofectamine 2000 reagent (Invitrogen, Grand Island, NY, USA) according to the manufacturer's instructions. Then the cells were received at different time point, RNA or protein was extracted from those cells and stored at −80 °C for subsequent analyses. *IL-6*-siRNA duplexes sequences are as follows:

siRNA1:sense5′-GCAGACCCAAGAUACCCUA-3′, antisense 3′-UAGGGUAUCUUGGGUCUGC-5′;
siRNA2: sense5′-GGUCUGGCAUGUGACCAUU-3′, antisense3′-AAUGGUCACAUGCCAGACC-5′;
siRNA3:sense5′-GGGUGAUAGUGACAGUGAA-3′, antisense3′-UUCACUGUCACUAUCACCC-5′.

4.3. RNA Extraction, RT-PCR, Quantitative RT-PCR (qPCR)

Total RNA was extracted from the breast cancer cells with Trizol reagent (Ambion, Austin, TX, USA) on the basis of the manufacturer's protocol. Adding 1 mL Trizol, and placing at 22 °C for 5 min. After extracting using chloroform and precipitating with isopropanol, we washed the RNA twice using 75% ethanol, and finally dissolved in RNase-free water. The concentration was determined by NanoDrop2000 spectrophotometer (Thermo, Waltham, MA, USA). Subsequently the RNA was reversely transcribed by transcription kit (RevertAid First Strand cDNA Synthesis. Fermentas) following the instruction. QPCR reactions were performed by UltraSYBR Mixture (CWBIO, Beijing, China), and each sample includes three pair of repetitions. To calculate the relative abundance of mRNA compared with 18 s, we employed the comparative cycle threshold (*C*t) method. Then the RT-PCR and qPCR primer sequences were as follows:

has-A1CF (-8aa)/A1CF (F: GCCAAGTTTATGATCCCACC; R: CAGTCCTCT CACTCCCGCA);
hsa-IL-6 (F: GCCACTCACCTCTTCAGAACG; R: CAGTGCCTCTTTGCTG CTTTC).

4.4. Protein Extraction and Western Blot Analysis

Proteins were extracted from breast cancer cells with RIPA lysis buffer containing 20 mmol/L (pH 7.5) Tris–HCl, 150 mM NaCl, 1% EDTA, 1% TritonX-100, and 2.5 mM sodium pyrophosphate, supplemented with 1 mM PMSF. Equal amounts of the 30 μg proteins from each extract were separated in 10% SDS-PAGE gel, and then electrophoretically transferred to a PVDF membrane for 50 min in the 300 mA electrical flow. After blocking with 5% free-fat milk in TBST for 1 h at RT, PVDF membranes were incubated with anti-A1CF rabbit pAb (1:1000, ab99955, abcam, Cambridge, MA, USA), anti-IL6 rabbit pAb (1:500, WL01678, Wanleibio, Shenyang, China), anti-PCNA rabbit pAb (1:500, WL01804, Wanleibio, Shenyang, China), and anti-β-Tubulin Mouse mAb (1:2000, HC101-01, Transgen, Beijing, China) overnight at 4 °C, and then incubated with corresponding secondary antibody: horseradish peroxidase-conjugated goat anti-mouse IgG (1:2000, SA00001-1, Proteintech, Wuhan, China) or goat anti-rabbit IgG (1:3000, SA00001-2, Proteintech, Wuhan, China). Finally, the protein bands were visualized with Western blot chemiluminescent HRP substrate reagent (Millipore Corporation, Billerica, MA, USA).

4.5. Immunofluorescence

Firstly, MAD-MB-231 cells were grown on the glass coverslips. The cells were fixed with pre-chilled acetone for 15 min, after transiently transfected with *A1CF (-8aa)*, *A1CF*, or null vector for 36 h. Subsequently, cells were, respectively, permeabilized with 1% Triton X-100 (diluted in PBS) for 20 min and blocked with 5% BSA (diluted in PBS) for 1 hour at room temperature. For immunofluorescence staining, the rabbit polyclonal antibody against EGFP (1:1000, ab99955, abcam) and monoclonal anti-flag® M2 antibody produced in mouse (1:1000, F1804, Sigma, Ronkonkoma, NY, USA) were used to probe A1CF overnight at 4 °C, At the meantime, we detected rabbit IgG by the goat anti rabbit IgG-CFL 488 (Santa Cruz Biotechnology, Santa Cruz, CA, USA; 1:2000). In regard to F-actin cytoskeleton staining, MDCK cells were incubated with rhodamine-labeled phalloidin (Sigma; 1:1000)

overnight at 4 °C. Finally, nuclei were stained with DAPI (Santa Cruz Biotechnology; 1:5000) for 5 min at room temperature. All of the departments were rinsed with 1× PBS for three times, subsequently, and were softly washed with water. To view under fluorescence microscope, we immobilized the coverslips on the glass slides with 50% glycerol in PBS. At the same time, we took relevant pictures with a SPOT Diagnostic (Sterling Heights, MI, USA) CCD camera. Eventually, immunofluorescent images were performed by using Adobe Photoshop CS3.

4.6. 5-Ethynyl-20-Deoxyuridine (EdU) Assays

Simply, breast cancer cells were seeded into 24-well plates. Twelve hours later, cells were, respectively, transfected with 500 ng plasmids of *A1CF (-8aa)*, *A1CF*, and null vector. After 36 h transfection, the proliferation of cells was determined via EdU DNA proliferation and detection kit (RiboBio, Guangzhou, China) based on the manufacturer's instructions.

4.7. Statistical Analysis

All of the experiments were performed in three independent assays, and error bars represented the standard deviation from the mean. Unpaired two-tailed Student's test was applied to test differences by statistical software GraphPad Prism 5 (GraphPad, Inc., La Jolla, CA, USA), and p-values of less than 0.05 were regarded statistically significant. Significant differences were indicated for $p < 0.05$ (*), $p < 0.01$ (**) or $p < 0.001$ (***).

5. Conclusions

Taken together, our present study demonstrates, for the first time, that the EIYMNVPV motif is required for A1CF nucleus localization, and A1CF (-8aa) and A1CF are, respectively, located in the cytoplasm and the nucleus. Additionally, based on the detection of EDU and PCNA, A1CF (-8aa) promotes cell proliferation via upregulating the expression of *IL-6* in basal-like breast cancer cells (MAD-MB-231). Therefore, the EIYMNVPV motif or A1CF (-8aa) might be an underlying gene therapeutic target for breast cancer.

Acknowledgments: This work was supported by grant from the National Natural Science Foundation of China (Grant No. 81572076 and Grant No. 31271563) to Qin Zhou; and the National Basic Research Program of China (No. 2011CB944002) to Qin Zhou.

Author Contributions: Li Zhou, Honglian Wang and Qin Zhou conceived and designed the experiments; Li Zhou, Liyuan Huang, Yuping Gu, Yao Du and Rui Peng performed the experiments; Zhaomin Mao and Zhongshi Lyu analyzed the data; Jin Hao, Dongsheng Ni, Yiman Li, Pan Ju, Yaoshui Long, Jianing Liu and Zhicheng Liu contributed reagents/materials/analysis tools; Li Zhou and Qin Zhou wrote the paper, Yue Yuan and Rui Peng read and approved the paper.

Conflicts of Interest: The authors declare no conflict of interest.

Abbreviations

dsRBM	Double strand RNA binding motif
PCNA	Proliferating cell nuclear antigen
A1CF	Apobec-1 complementation factor
cDNA	Complementary DNA
qPCR	Quantitative reverse-transcription polymerase chain reaction
RRM	RNA recognition motifs
apoB	Apolipoprotein-B
EdU	5-Ethynyl-20-Deoxyuridine
IL-6	Interleukin-6

References

1. Lellek, H.; Kirsten, R.; Diehl, I.; Apostel, F.; Buck, F.; Greeve, J. Purification and molecular cloning of a novel essential component of the apolipoprotein B mRNA editing enzyme-complex. *J. Boil. Chem.* **2000**, *275*, 19848–19856. [CrossRef] [PubMed]
2. Maris, C.; Masse, J.; Chester, A.; Navaratnam, N.; Allain, F.H. NMR structure of the apoB mRNA stem-loop and its interaction with the C to U sediting APOBEC1 complementary factor. *RNA* **2005**, *11*, 173–186. [CrossRef] [PubMed]
3. Mehta, A.; Kinter, M.T.; Sherman, N.E.; Driscoll, D.M. Molecular cloning of apobec-1 complementation factor, a novel RNA-binding protein involved in the editing of apolipoprotein B mRNA. *Mol. Cell. Biol.* **2000**, *20*, 1846–1854. [CrossRef] [PubMed]
4. Teng, B.; Burant, C.F.; Davidson, N.O. Molecular cloning of an apolipoprotein B messenger RNA editing protein. *Science* **1993**, *260*, 1816–1819. [CrossRef] [PubMed]
5. Backus, J.W.; Smith, H.C. Apolipoprotein B mRNA sequences 3′ of the editing site are necessary and sufficient for editing and editosome assembly. *Nucleic Acids Res.* **1991**, *19*, 6781–6786. [CrossRef] [PubMed]
6. Chester, A.; Scott, J.; Anant, S.; Navaratnam, N. RNA editing: Cytidine to uridine conversion in apolipoprotein B mRNA. *Biochim. Biophys. Acta* **2000**, *1494*, 1–13. [CrossRef]
7. Shah, R.R.; Knott, T.J.; Legros, J.E.; Navaratnam, N.; Greeve, J.C.; Scott, J. Sequence requirements for the editing of apolipoprotein B mRNA. *J. Boil. Chem.* **1991**, *266*, 16301–16304.
8. Smith, H.C.; Sowden, M.P. Base-modification mRNA editing through deamination—The good, the bad and the unregulated. *Trends Genet. TIG* **1996**, *12*, 418–424. [CrossRef]
9. Paschoud, S.; Dogar, A.M.; Kuntz, C.; Grisoni-Neupert, B.; Richman, L.; Kuhn, L.C. Destabilization of interleukin-6 mRNA requires a putative RNA stem-loop structure, an AU-rich element, and the RNA-binding protein AUF1. *Mol. Cell. Biol.* **2006**, *26*, 8228–8241. [CrossRef] [PubMed]
10. Blanc, V.; Henderson, J.O.; Newberry, E.P.; Kennedy, S.; Luo, J.; Davidson, N.O. Targeted deletion of the murine apobec-1 complementation factor (*acf*) gene results in embryonic lethality. *Mol. Cell. Biol.* **2005**, *25*, 7260–7269. [CrossRef] [PubMed]
11. Blanc, V.; Sessa, K.J.; Kennedy, S.; Luo, J.; Davidson, N.O. Apobec-1 complementation factor modulates liver regeneration by post-transcriptional regulation of interleukin-6 mRNA stability. *J. Boil. Chem.* **2010**, *285*, 19184–19192. [CrossRef] [PubMed]
12. Mehta, A.; Driscoll, D.M. Identification of domains in apobec-1 complementation factor required for RNA binding and apolipoprotein-B mRNA editing. *RNA* **2002**, *8*, 69–82. [CrossRef] [PubMed]
13. Dance, G.S.; Sowden, M.P.; Cartegni, L.; Cooper, E.; Krainer, A.R.; Smith, H.C. Two proteins essential for apolipoprotein B mRNA editing are expressed from a single gene through alternative splicing. *J. Boil. Chem.* **2002**, *277*, 12703–12709. [CrossRef] [PubMed]
14. Fossat, N.; Tourle, K.; Radziewic, T.; Barratt, K.; Liebhold, D.; Studdert, J.B.; Power, M.; Jones, V.; Loebel, D.A.; Tam, P.P. C to U RNA editing mediated by APOBEC1 requires RNA-binding protein RBM47. *EMBO Rep.* **2014**, *15*, 903–910. [CrossRef] [PubMed]
15. Vanharanta, S.; Marney, C.B.; Shu, W.; Valiente, M.; Zou, Y.; Mele, A.; Darnell, R.B.; Massague, J. Loss of the multifunctional RNA-binding protein RBM47 as a source of selectable metastatic traits in breast cancer. *eLife* **2014**, *3*. [CrossRef] [PubMed]
16. Knupfer, H.; Preiss, R. Significance of interleukin-6 (IL-6) in breast cancer (review). *Breast Cancer Res. Treat.* **2007**, *102*, 129–135. [CrossRef] [PubMed]
17. Ara, T.; Declerck, Y.A. Interleukin-6 in bone metastasis and cancer progression. *Eur. J. Cancer* **2010**, *46*, 1223–1231. [CrossRef] [PubMed]
18. Chang, Q.; Daly, L.; Bromberg, J. The IL-6 feed-forward loop: A driver of tumorigenesis. *Semin. Immunol.* **2014**, *26*, 48–53. [CrossRef] [PubMed]
19. Chomarat, P.; Banchereau, J.; Davoust, J.; Palucka, A.K. IL-6 switches the differentiation of monocytes from dendritic cells to macrophages. *Nat. Immunol.* **2000**, *1*, 510–514. [CrossRef] [PubMed]
20. Guo, Y.; Xu, F.; Lu, T.; Duan, Z.; Zhang, Z. Interleukin-6 signaling pathway in targeted therapy for cancer. *Cancer Treat. Rev.* **2012**, *38*, 904–910. [CrossRef] [PubMed]

21. Itou, J.; Tanaka, S.; Sato, F.; Akiyama, R.; Kawakami, Y.; Toi, M. An optical labeling-based proliferation assay system reveals the paracrine effect of interleukin-6 in breast cancer. *Biochim. Biophys. Acta* **2015**, *1853*, 27–40. [CrossRef] [PubMed]
22. Yadav, A.; Kumar, B.; Datta, J.; Teknos, T.N.; Kumar, P. IL-6 promotes head and neck tumor metastasis by inducing epithelial-mesenchymal transition via the JAK-STAT3-SNAIL signaling pathway. *Mol. Cancer Res. MCR* **2011**, *9*, 1658–1667. [CrossRef] [PubMed]
23. Nguyen, D.P.; Li, J.; Tewari, A.K. Inflammation and prostate cancer: The role of interleukin 6 (IL-6). *BJU Int.* **2014**, *113*, 986–992. [CrossRef] [PubMed]
24. Waldner, M.J.; Neurath, M.F. Master regulator of intestinal disease: IL-6 in chronic inflammation and cancer development. *Semin. Immunol.* **2014**, *26*, 75–79. [CrossRef] [PubMed]
25. Wang, S.W.; Sun, Y.M. The IL-6/JAK/STAT3 pathway: Potential therapeutic strategies in treating colorectal cancer (Review). *Int. J. Oncol.* **2014**, *44*, 1032–1040. [PubMed]
26. Lin, S.; Gan, Z.; Han, K.; Yao, Y.; Min, D. Interleukin-6 as a prognostic marker for breast cancer: A meta-analysis. *Tumori* **2015**, *101*, 535–541. [CrossRef] [PubMed]
27. Blanc, V.; Kennedy, S.; Davidson, N.O. A novel nuclear localization signal in the auxiliary domain of apobec-1 complementation factor regulates nucleocytoplasmic import and shuttling. *J. Boil. Chem.* **2003**, *278*, 41198–41204. [CrossRef] [PubMed]
28. Chiang, C.P.; Lang, M.J.; Liu, B.Y.; Wang, J.T.; Leu, J.S.; Hahn, L.J.; Kuo, M.Y. Expression of proliferating cell nuclear antigen (PCNA) in oral submucous fibrosis, oral epithelial hyperkeratosis and oral epithelial dysplasia in Taiwan. *Oral Oncol.* **2000**, *36*, 353–359. [CrossRef]
29. Srinivasan, M.; Jewell, S.D. Quantitative estimation of PCNA, c-myc, EGFR and TGF-α in oral submucous fibrosis—An immunohistochemical study. *Oral Oncol.* **2001**, *37*, 461–467. [CrossRef]
30. Heo, T.H.; Wahler, J.; Suh, N. Potential therapeutic implications of IL-6/IL-6R/gp130-targeting agents in breast cancer. *Oncotarget* **2016**. [CrossRef] [PubMed]
31. Ayub, A.; Yip, W.K.; Seow, H.F. Dual treatments targeting IGF-1R, PI3K, mTORC or MEK synergize to inhibit cell growth, induce apoptosis, and arrest cell cycle at G1 phase in MDA-MB-231 cell line. *Biomed. Pharmacother.* **2015**, *75*, 40–50. [CrossRef] [PubMed]
32. Nakahara, S.; Tsutsumi, K.; Zuinen, T.; Ohta, Y. FilGAP, a Rho-ROCK-regulated GAP for Rac, controls adherens junctions in MDCK cells. *J. Cell Sci.* **2015**, *128*, 2047–2056. [CrossRef] [PubMed]



© 2016 by the authors; licensee MDPI, Basel, Switzerland. This article is an open access article distributed under the terms and conditions of the Creative Commons Attribution (CC-BY) license (http://creativecommons.org/licenses/by/4.0/).

MDPI AG
Grosspeteranlage 5
4052 Basel
Switzerland
Tel.: +41 61 683 77 34

International Journal of Molecular Sciences Editorial Office
E-mail: ijms@mdpi.com
www.mdpi.com/journal/ijms



Disclaimer/Publisher's Note: The title and front matter of this reprint are at the discretion of the Guest Editor. The publisher is not responsible for their content or any associated concerns. The statements, opinions and data contained in all individual articles are solely those of the individual Editor and contributors and not of MDPI. MDPI disclaims responsibility for any injury to people or property resulting from any ideas, methods, instructions or products referred to in the content.





Academic Open
Access Publishing

mdpi.com

ISBN 978-3-7258-8374-5